

WCAP-16996-NP  
Revision 0

November 2010

**Realistic LOCA Evaluation  
Methodology Applied to the  
Full Spectrum of Break Sizes  
(FULL SPECTRUM LOCA  
Methodology)**

**Volume II, Part 3  
WCOBRA/TRAC-TF2  
Assessment**



**Westinghouse**

## 21 ROSA-IV TEST SIMULATIONS

### 21.1 INTRODUCTION

The Rig-of-Safety Assessment Number 4 (ROSA-IV) program conducted a series of experiments to investigate the thermal-hydraulic behavior of a Westinghouse-designed four-loop PWR during small break LOCAs and operational transients using the Large Scale Test Facility (LSTF). A number of phenomena that are of interest to FSLOCA were investigated in ROSA-IV test facility. Tests were well documented and many test reports are available in open literature or via the library of the Japan Atomic Energy Agency (JAEA), former JAERI.

The ROSA-IV LSTF is discussed in Section 21.2, and the WCOBRA/TRAC-TF2 model of the facility used for analysis of the full spectrum of breaks considered is presented in Section 21.3.

Sections 21.4 through 21.9 describe the simulations of a number of ROSA tests using WCOBRA/TRAC-TF2. The following test series were selected for the assessment of the WCOBRA/TRAC-TF2 code and the FSLOCA methodology. SB-CL-01, SB-CL-02, SB-CL-03, SB-CL-05, SB-CL-14, SB-CL-12, SB-CL-15, SB-CL-16, SB-CL-18, and ST-NC-02. SB-CL-18 is a 5% cold leg break test which is considered to be the reference transient and is the international standard problem No. 26. SB-CL-01, SB-CL-02, and SB-CL-03 are 2.5% cold leg break tests with the break located at side, bottom and top. SB-CL-12, SB-CL-15, and SB-CL-16 studied the same break orientation effect but at 0.5% break size. SB-CL-14 is a 10% break test. SB-CL-12, SB-CL-01, SB-CL-18, and SB-CL-14 form a break size sensitivity study covering a break range of 0.5% to 10%. SB-CL-05 is another 5% cold leg break test and it is the only test with the high-head safety injection (SI) activated. Comparison of SB-CL-05 and SB-CL-18 investigated the impact of having the pumped SI throughout the transient. Finally, ST-NC-02 is the 2% power natural circulation test.

Table 21.1-1 shows the list of tests used for the validation work. It contains relevant reports and articles related to the ROSA-IV LSTF and the different test considered herein.

The analysis of the different tests is presented as follows in Section 21.4 to 21.9. First, the reference transient, SB-CL-18, is discussed in Section 21.4. Section 21.5 documents the simulation of another 5% break test (SB-CL-05) which was conducted with actuation of pumped safety injection (SI). The results of the simulation of the 10% break test SB-CL-14 (intermediate break size) are documented in Section 21.6. The effect of break orientation is discussed in Section 21.7, using simulation results from the top/side/bottom 0.5% (SB-CL-16/12/15) and 2.5% (SB-CL-03/01/02) cold leg break tests. In Section 21.8, a break spectrum study is documented, using the simulation results of the 0.5% (SB-CL-12), 2.5% (SB-CL-01), 5% (SB-CL-18) and 10% (SB-CL-14) break tests. Finally, the simulation of ST-NC-02, a 2% power natural circulation test is documented in Section 21.9.

Section 21.10 discusses the capability of the code to calculate counter-current flow at the upper core plate (UCP), in the vicinity of the hot leg elbow and steam generator inlet nozzle, and the steam generator U-tube bundle. The results presented in that section are based on the code calculation of the different break test, described in the previous sections 21.4 through 21.9.

Sections 21.11 contain results of various sensitivity calculation performed with selected ROSA-IV test that are needed to support conclusions made in other sections of the Topical report.

## 21.2 TEST FACILITY DESCRIPTION

The LSTF is a 1/48 volume scale representation of a Westinghouse four-loop 3423 MWt Pressurizer Water Reactor (PWR). Figure 21.2-1 is a schematic diagram of the facility. The LSTF consists of two equal volume loops, A and B, with a pressurizer attached to the hot leg of loop A. Table 21.2-1 compares the major design characteristics of the LSTF and the PWR. The core simulator contains 16 square 7x7 and 8 semi-crescent heater rod assemblies. The heater rods are 9.5 mm (0.374 inches) in diameter and 3.66 m (12 feet) in length. To simulate possible effects of non-uniform radial power distribution there are low, average and high power assemblies. The core utilizes chopped cosine axial power distribution.

The maximum power in the facility at steady state is 10 MW, which is equivalent to 14 percent of the scaled steady state core power of the reference PWR.

The secondary coolant system consists of two steam generators, main and auxiliary feed water pumps, and condensing system. The height of the LSTF steam generator is the same as in the reference PWR. The downcomer of each steam generator consists of four pipes located outside the steam generator vessel. The pipes are sized to provide a representative volume and width of a typical steam generator downcomer. Each steam generator contains 141 U-tubes with 19.6 mm (0.772 inches) inside diameter (ID) and 25.4 mm (1.0 inches) outside diameter (OD). Primary and secondary steam separators are included in each steam generator vessel.

The LSTF Emergency Core Cooling System (ECCS) consists of a high pressure charging system, a high pressure injection system, a low pressure injection system, an accumulator system, and a residual heat removal system.

A detailed description of the facility is available in the Japan Atomic Energy Research Institute (JAERI) documents (JAERI-M 84-237, 1985 and JAERI-M 98-113, 1989).

### 21.2.1 Important Physical Phenomena and Scaling Considerations

The ROSA-IV LSTF is designed to conduct tests which provide important information regarding the behavior of a Westinghouse PWR during small break LOCA transient. The scaling, relative to the typical 4-loop PWR, is such that the tests conducted can reproduce realistically the most important small break thermo-hydraulic phenomena. Since it is practically impossible to design a small test facility that can reproduce all aspects of the behavior of a complex system like a PWR, proper scaling can be achieved for only few key small break LOCA phenomena.

The key scaling ratios of the ROSA-IV LSTF against typical PWR are presented in Table 21.2-1.

At steady state conditions the core simulator power is 10 MW, which is 14% of the 1:48 scaled power of the reference PWR, resulting in 1:342 power ratio at steady state conditions. The core flow ratio at steady

state is 1:342 in order to achieve initial primary side temperatures representative of PWR. Under these conditions the steady state power-to-volume (power density) ratio is approximately 1:7.

Preserving power-to-volume ratio of 1:1 assures that the time scale of the simulated transient phenomena is prototypical of the PWR. To achieve this ratio during the important phases of the small break LOCA transient, the power of the LSTF core simulator is actively controlled and follows a predefined power-vs-time curve which assures that beyond 30 seconds after reactor trip the simulated decay heat is scaled 1:48 to that of the representative PWR. In the small break tests, immediately after the break the pump speed is briefly increased and then follows a predefined coastdown curve, which assures that fluid velocities typical of PWR are achieved during the initial phase of the transient.

Since the elevations of the major components of LSTF are full-scale and match those of the real PWR the height scaling ratio is 1:1. Preserving the same height and characteristic elevations assures that the natural circulation phenomena important to core cooling and the general system behavior are adequately simulated in the tests. Preserving the bottom elevation of the cross-over legs is of great importance to observing the effects of a realistic depth of core uncovering related to the loop seal clearance phenomenon.

Preservation of the same core height and fuel bundle geometry characteristics (square lattice, rod diameter, pitch, etc.) assures that important phenomena that might occur in the core during the different phases of the accident are simulated in a realistic manner. Some of these are void generation & distribution and related rod heatup during loop seal clearance, level swell and rod heatup during boiloff, etc.

With the height key elevations preserved the same as the PWR, the scaling of each steam generator (volume and flow area ratios of 1:24 and U-tube surface area 1:25) assures that important thermo-hydraulic phenomena like primary-to-secondary heat transfer, natural circulation, reflux condensation and counter-current flow are simulated in a realistic manner. Note that one LSTF steam generator represents two PWR steam generators; therefore the total SG surface area scaling ratio is actually 1:48.

The diameter of the hot and cold leg pipes is large enough to allow the establishment of all possible flow regimes of significance that may develop in the real plant. This also allows to investigate effects of break orientation on the SBLOCA transient.

The hot and cold legs, with a diameter of 207 mm (8.15 inches), are sized to conserve volume scaling and the ratio of length to the square root of the pipe diameter ( $L/\sqrt{D}$ ) of the reference PWR. The ( $L/\sqrt{D}$ ) ratio is in essence a Froude number and the 1:1 scaling relative to PWR assures that flow regime transition would be manifested properly during the various tests, performed with the ROSA-IV LSTF.

The goal of preserving hot leg  $L/\sqrt{D} = 1$  and volume ratio of 24 results in a hot leg flow area ratio of 12.68. Thus the flow area of the LSTF hot leg (and cold leg as well) is essentially twice the 1:24 scaled PWR hot leg area. This scaling distortion would create conditions where easier flow stratification in the hot and cold legs will be simulated during the tests compared to a real PWR small break transient.

As seen in Table 21.2-1, the scaling ratio of the upper core plate flow area is approximately 1:45, which is very close to the PWR/LSTF volume and power ratio of 1:48. This similarity creates the preconditions to

simulate realistic fluid velocities and counter-current flow at the upper core plate during the SBLOCA tests.

[

] <sup>a,c</sup>

### 21.3 DESCRIPTION OF WCOBRA/TRAC-TF2 MODEL FOR ROSA/LSTF-IV

[

] <sup>a,c</sup>

Figure 21.3-1 shows the WCOBRA/TRAC-TF2 noding of the LSTF pressure vessel. Figures 21.3-2 through 22.3-6 show the transverse channel connections in each of the vessel sections. Figure 21.3-7 shows the core simulator map of the LSTF. The vessel is modeled [

] <sup>a,c</sup>

The upper plenum modeling of the LSTF facility includes [

] <sup>a,c</sup>

[

] <sup>a,c</sup>

The piping outside the LSTF pressure vessel is modeled by using 1-D components. Figure 21.3-8 shows the general 1-D loop noding diagram of the LSTF and Figure 21.3-9 provides more detail in the noding of the hot leg, steam generator and the loop seal regions.

Each hot leg, including the elbow at the inlet of the steam generator, is modeled [ ] <sup>a,c</sup>

As seen from Figure 21.3-8 and the more detailed Figure 21.3-9, primary flow enters the steam generator [

] <sup>a,c</sup>

The steam generator secondary side includes sufficient detail to model recirculation in the downcomer and separation in the vapor dome region. [

] <sup>a,c</sup>

During steady state simulation, and prior to reactor trip, steam leaving the generators passes through a TEE component and VALVE component to a constant pressure BREAK. At reactor trip, the main steam isolation valve (MSIV) is closed and flow goes through a VALVE component representing the main steam safety valve (MSSV) to a second BREAK component that provides a constant pressure boundary condition at the MSSV setpoint pressure.

Figure 21.3-9 shows the loop seal nodalization. Flow from the steam generator outlet passes through [

] <sup>a,c</sup>

The safety injection system is shown in Figure 21.3-8. Combined high pressure safety injection plus charging flows to each loop are modeled [

] <sup>a,c</sup> accumulator setpoint of 4.51 MPa (654.1 psia). VALVE Components 216

and 226 are isolation valves. The combined safety injections from the pumps and accumulators enter each of the cold legs through the side pipes of TEE Components 15 and 25 to loops A and B respectively.

## **21.4 SIMULATION OF SB-CL-18, 5-PERCENT COLD LEG SIDE BREAK**

### **21.4.1 Description of the SB-CL-18 Test Boundary and Initial Conditions**

Experiments as part of ROSA-IV (LSTF-IV) were conducted for several different break areas. Test SB-CL-18 simulated a 5-percent cold leg break, which corresponds to approximately a 6-inch break in a PWR. The break was located in loop B and had a horizontal orientation. Unlike test SB-CL-05, HHSI and LHSI safety injection were not modeled in this test. The experimental results are available in the test data report JAERI-M 89-027 (Kumamaru, et al., 1989). This test is also known as International Standard Problem No. 26 of OECD/NEA/CSNI.

For each of the break test simulations, verification that the WCOBRA/TRAC-TF2 model of the LSTF-IV adequately represented the facility was accomplished through a full-power, 300-seconds steady state simulation. Table 21.4-1 summarizes initial conditions achieved at for the SB-CL-18 test the end of the 300 seconds steady state calculation. At the end of this 300-seconds simulation, predicted and measured system parameters were compared to ensure reasonably good agreement.

The operational setpoints for this test are the same as the standard set implemented for all ROSA-IV tests, provided in Table 21.2-2. As described in the test report (Reference 13), the high-pressure charging and high-pressure injection were not actuated for this test, since they were assumed to fail. Low-pressure safety injection did not occur since the test was terminated before the cut-off pressure of 1.29 MPa was reached. Auxiliary feed water was not actuated as well.

The core power was scrammed once the primary pressure decreased below 12.97 MPa (1881.1 psia). The core decay heat was simulated following a pre-programmed curve, which accounts for actinides and delayed neutron effects and gives a slower decrease than the ANS standard. The decay heat curve implemented during the test and used in the SB-CL-18 simulations is provided in Table 21.4-2.

On the LSTF, the initial conditions prior to the initiation of the test are established at pump speeds (respectively fluid velocities) that are much lower than those existing at the PWR at steady state conditions. This was done so that, with the reduced core power at the LSTF, the initial cold leg and hot leg temperatures are preserved similar to PWR. Immediately following the break, the pump speed was increased to achieve loop flow rates similar to the reference PWR. Loss of offsite power is assumed and the reactor coolant pumps are tripped to begin coastdown coincident with reactor scram. In the transient simulation, the pumps followed a coastdown curve consistent with the test. The main feed water was stopped, and the secondary sides of the two steam generators were isolated by closure of their main steam isolation valves (MSIV) coincident with reactor trip.

## 21.4.2 Steady State Calibration and Transient Calculation Procedures

### Steady State Calculation

In the SB-CL-18 test simulation first a steady state calculation is performed (in this case 300 seconds) in order to achieve the desired primary and secondary side conditions, according to those measured at the test. The initial steady state conditions achieved for the SB-CL-18 test are presented in Table 21.4-1.

### Transient Calculation Procedure

The WCOBRA/TRAC-TF2 simulation of the LSTF-IV 5-percent cold leg break test SB-CL-18 is initiated by [

] <sup>a,c</sup>

Depending on the break size being simulated, the appropriate set of HRM1PM, HRM2PM and HRMOFD multipliers is used, in accordance with the break modeling described in Section 12.5.4.

### Transient Acceptance Criteria

The primary acceptance criterion for the simulations of the ROSA-IV test documented herein is achieving the best possible consistency with the available test data. Particular attention is given to the accurate prediction of key transient phenomena like system depressurization, timing and magnitude of loop seal clearance, boiloff, etc. [

] <sup>a,c</sup>

### 21.4.3 Results and Conclusions From the SB-CL-18 Simulation

In this test, the primary system rapidly depressurized and equilibrated at a pressure slightly higher than the steam generator secondary pressure, at approximately 8.3 MPa (~1200 psia), until the loop seal cleared at about 140 seconds, (see DPE080-LSA in Figure 21.4.3 and DPE220-LSB in Figure 21.4-4).

After loop seal clearance, the break quality changed from a low quality mixture to primarily vapor and the primary system continued to depressurize.

As the primary system continued to drain, liquid is redistributed among the different regions; the core and downcomer, the upper plenum, hot legs and steam generator uphill and downhill side, and the uphill and downhill sides of the loop seal piping. A manometric (hydrostatic) balance is established between the liquid present in these regions during the transient. Prior to the loop seal clearance, the core collapsed level became depressed nearly to the bottom of the core, while liquid remained in the uphill side of the loop seal. At this time, the heater rods heated up rapidly. While most of the liquid had drained from the steam generator tubes, some of it remained in the steam generators' inlet plenums and the bottom of the uphill side. After steam slipped through the loop seals, the core level recovered and most of the water was pushed out of both loop seals through the cold legs and into the downcomer.

Test SB-CL-18 had a core depression during loop seal clearance that was considerably below the elevation of the bottom of the loop seal piping. Osakabe (Osakabe et al., 1987) attributed this to a significant liquid holdup in the uphill side of steam generator tubes. During this core level depression, the cladding temperature increased by approximately 190K (342°F) reaching a maximum cladding temperature of approximately 740K (872°F). After loop seal clearance, the core level recovered quickly and the rods were quenched.

Figures 21.4-1 through 22.4-20 compare predicted and measured results for the 5-percent cold leg break test SB-CL-18. Figure 21.4-1 compares predicted and measured primary system pressure. [

] <sup>a,c</sup>

Break flow is compared in Figure 21.4-2. Early in the transient, flow out of the break is sub-cooled single-phase liquid. [

] <sup>a,c</sup>

Figures 21.4-3 and 21.4-4 show a comparison of the calculated and measured loop seal differential pressures. In the test, loop seal venting occurs at approximately 140 seconds. [

] <sup>a,c</sup> The test data and calculations also show that after the loop seals clear, steam venting is established through both cross-over legs.

As the loop seals vent, the collapsed liquid level in the core is depressed. Figure 21.4-5 compares calculated and measured inner vessel differential pressure, which is an indicator of the inner vessel collapsed level. [

] <sup>a,c</sup>

Core heat-up occurs during the loop seal clearance period as the core is temporarily uncovered. Figure 21.4-6 compares the PCT predicted by WCOBRA/TRAC-TF2 to the maximum cladding heat-up observed in the data. [

] <sup>a,c</sup>

The depth of core uncover during the loop seal clearance period depends upon the manometric balance between the core and downcomer, and the sum of pressure drops through the loop and uphill side of the loop seal piping. An important static head exists on the uphill side of the steam generator tubes, where water condensed in the tubes collects because of CCFL and flooding in the steam generator up-hill tubes. Figures 21.4-7 and 22.4-8 show collapsed liquid levels in the uphill steam generator tubes for SG-A and SG-B respectively. [

] <sup>a,c</sup>

Figures 21.4-11 and 22.4-12 show a comparison of the calculated and measured differential pressures across the two steam generators. From those two figures, it is evident that during the loop seal clearance period the code calculates steam generator resistance [

] <sup>a,c</sup>

There is a good agreement between the calculated and measured resistance across the hot legs from the upper plenum up to the SG inlet plenums, as evident from Figures 21.4-15 and 22.4-16.

Figures 21.4-13 and 22.4-14 show the calculated and measured collapsed liquid levels in the steam generator inlet plenums. [

] <sup>a,c</sup>

[

] <sup>a,c</sup>

[

] <sup>a,c</sup>

Figures 21.4-19 and 22.4-20 show the calculated and measured accumulator injection flows. The calculated initiation of the accumulator injection is consistent with the test, and the turn-around of the boil-off PCT occurs at about the same time as that observed in the test, Figure 21.4-6. [

] <sup>a,c</sup>

## **21.5 SI-INJECTION SENSITIVITY STUDY: SIMULATION OF SB-CL-05, 5-PERCENT COLD LEG SIDE BREAK**

### **21.5.1 Description of the Boundary and Initial Conditions**

Test SB-CL-05 simulated a 5-percent cold leg break (equivalent to a 6-inch break in a PWR). The test is one of the earliest of the ROSA-IV series. In terms of initial conditions, break size and decay heat curve this test is equivalent to the 5% break SB-CL-18, which is documented in the previous section. However, the SB-CL-05 test was conducted with charging and high-pressure injection available.

As in the SB-CL-18 test, the break was located in loop B and had a horizontal orientation. Safety injection flow rates corresponding to a single failure in the safety injection system were assumed. Experimental results are discussed by Kawaji (Kawaji, et al., 1986) and Tasaka (Tasaka, et al., 1988).

The operational setpoints for this test are the same as implemented in all ROSA-IV break tests, as listed in Table 21.2-2.

[

] <sup>a,c</sup>

[

] <sup>a,c</sup>

### 21.5.2 Results and Conclusions from the SB-CL-05 Simulation

Table 21.5-2 summarizes the observed (data) and predicted results for the 5-percent cold leg test SB-CL-05.

[

<sup>a,c</sup> The results from the simulation are presented in the following Figures 21.5-1 through 21.5-21. In these figures, the WCOBRA/TRAC-TF2 calculations are compared to measured SB-CL-05 test parameters.

As intended, the core power (Figure 21.5-1) and pump speed (Figure 21.5-2) were modeled to be consistent with the measurements. [

] <sup>a,c</sup>

Figure 21.5-4 shows the calculated break flow compared against that measured by the high-range flow meter (FE560A-BU).

The break flow prediction is similar to the one observed in the SB-CL-18 test simulations. Early in the transient, flow out of the break is sub-cooled, that is, single-phase liquid. [

] <sup>a,c</sup>

[

] <sup>a,c</sup>

The pressurizer pressure is fairly consistent with the measured (Figure 21.5-6). There is somewhat small mismatch which seems consistent with the break flow mismatch trend.

[

] <sup>a,c</sup>

[

] <sup>a,c</sup>

[

] <sup>a,c</sup>

## 21.6 SIMULATION OF THE 10% SIDE BREAK TEST SB-CL-14

One of the integral shakedown tests performed in the LSTF is a 10-percent cold leg break, which was the maximum break size for the facility design. This is a relatively large break size, corresponding to approximately a 9-inch break in a PWR, which could be considered more of an intermediate break as opposed to a small break LOCA. This break size is considered in order to test the code capabilities and expand the break spectrum to include intermediate break sizes as well.

[

] <sup>a,c</sup>

### 21.6.1 Description of the Boundary and Initial Conditions

The initial conditions for the 10% break test SB-CL-14 are summarized in Table 21.6-2.

The operational setpoints for this 10-percent break are the consistent with the standard set used in all ROSA-IV tests, as summarized in Table 21.2-2. The charging and the high-pressure injection were not actuated in this test. The low-pressure injection system was active in this test, but was not modeled in the simulation, since during the test the injection initiated 862 seconds after the break, well beyond the period of interest in this calculation.

The break was located in loop B, the loop without the pressurizer, and was oriented horizontally from the middle of the cold leg. The 10% break size was simulated by using a break orifice with diameter of 31.9 mm (1.256 inch). The break was initiated by opening of a fast acting air operated valve that directed the break flow into the catch tank.

As mentioned earlier, this test used a realistic decay heat curve, as documented in Table 21.6-1. Initiated by the reactor scram signal, the core power was controlled by a test sequence controller according to the curve in Table 21.6-1.

The pump speed was controlled by the sequence controller to follow a preprogrammed coastdown curve. The pump speed was initially increased but then, triggered by the reactor scram signal, a coastdown was initiated at 13.2 seconds which followed a predefined curve.

## 21.6.2 Results and Conclusions for the SB-CL-14 Simulation

Table 21.6-3 summarizes the predicted and measured chronology of events for the 10-percent cold leg test.

Figures 21.6-1 and 21.6-2 show a comparison of the modeled vs. measured pump speed for the two pumps. [

] <sup>a,c</sup>

The break flow comparison is shown in Figure 21.6-5. Figure 21.6-5(b) presents the test break flow as calculated from the measured level in the catch tank. [

] <sup>a,c</sup>

[

] <sup>a,c</sup>

## 21.7 BREAK ORIENTATION STUDY: SIMULATION OF TOP/SIDE/BOTTOM 0.5% (SB-CL-16/12/15) AND 2.5% (SB-CL-03/01/02) COLD LEG BREAKS

[

<sup>a,c</sup> The purpose of the study, presented in this section, is to assess the ability of the WCOBRA/TRAC-TF2 code to predict break orientation effects.

### 21.7.1 Description of the Boundary and Initial Conditions

[

] <sup>a,c</sup>

### 21.7.2 Discussion of Results

In LSTF, the break unit can be configured such that the break orientation effect can be studied. Two sets of three experiments were conducted in the LSTF to investigate the effect of break orientation. The first three tests (SB-CL-01, -02, and -03; side, bottom and top respectively), simulated a 2.5 % break in the cold leg, which approximates a 3 inch break in a PWR. The second three tests (SB-CL-12, -15 and -16) simulated a 0.5% break in the cold leg. In this section these two sets of break orientation studies will be discussed.

#### 21.7.2.1 2.5% Tests

In these experiments, the break was oriented at the side, bottom, and top of the loop B cold leg. Experimental results are summarized in the data report by Koizumi (Koizumi, et al., 1988). The test results showed that break orientation had only a small effect on system parameters such as pressure and core collapsed liquid level. Figure 21.7-1 shows the break geometry and orientation for these tests. Together with 0.5% break orientation tests, which will be discussed later in this section, these tests provide a useful means of evaluating the break flow model in WCOBRA/TRAC-TF2 for the effects of vapor pull through and liquid entrainment near the break orifice.

#### Boundary Conditions

Operational setpoints for the 2.5 % cold leg break tests were the same as those implemented in all ROSA-IV small break tests, shown in Table 21.2-2, with the following two exceptions. [

] <sup>a,c</sup>

[

] <sup>a,c</sup>

**Pressure**

[

] <sup>a,c</sup>

**Break Flow**

[

] <sup>a,c</sup>

[ ]<sup>a,c</sup>

### Core Collapsed Liquid Level

[

] <sup>a,c</sup>

### Core Heat-up

[

] <sup>a,c</sup>

### 21.7.2.2 0.5% Breaks

Break orientation study was also conducted with the 0.5% break tests SB-CL-12, 15 and 16 (side, bottom and top respectively). Figure 21.7-11 shows the break unit used in these tests. Unlike the SB-CL-01/02/03

tests, in these tests there is no break offtake pipe and the break hole (orifice) is located right at the cold leg wall.

As the 2.5% break tests, these three tests were conducted, and modeled, using the same JAERI (full conservative) decay heat curve, Table 21.7-1.

#### **Liquid Level in Broken Cold Leg**

[

] <sup>a,c</sup>

#### **Core Collapsed Level**

[

] <sup>a,c</sup>

#### **Break Flow**

[

] <sup>a,c</sup>

[ ]<sup>a,c</sup>

### 21.7.3 Conclusions

Comparison between the test data and the simulation runs performed using WCOBRA/TRAC-TF2 show that the break orientation effects exhibit similar trends in terms of the break flow, loop seal clearing timing, core depression, and the beginning of boil-off heat-up. [ ]<sup>a,c</sup>

## 21.8 BREAK SPECTRUM STUDY

The break spectrum study presented herein is compiled from simulations results of cold leg side break tests, documented in the previous sections. These are the 0.5% break (SB-CL-12), 2.5% break (SB-CL-01), 5% break (SB-CL-18), and 10% break test (SB-CL-14). The results of the break spectrum study are presented in Figures 21.8-1 through 21.8-5.

Figure 21.8-1 compares the calculated break flows. As seen from that figure, the initial value of the break flows are proportional to the break size. Larger break size results in a greater inventory loss at the beginning of the transient, and thus the initial depressurization rate is higher for the larger breaks, which is evident on the system pressure comparison provided on Figure 21.8-2. After the initial fast depressurization, a period of primary system pressure hold-up is observed at about 8 MPa, which is slightly above the secondary side pressure. The length of this holdup period depends on the break size with the smallest break having the longest hold-up period. During this period, the steam generators are a heat sink and remove heat from the primary side by natural circulation. The length of pressure hold-up (and natural circulation) period is decreasing with the increase of the break size, with the 10% size break exhibiting almost no pressure holdup.

Figures 21.8-3(a) and (b) and Figure 22.8-4 show the cross-over leg vapor flows and the core collapsed liquid levels respectively. Results in these figures show a correlation between the clearing of the loop seal (characterized by spike in loop vapor flow, Figure 21.8-3) and the depression of the core collapsed liquid level (Figure 21.8-4). As seen from those figures, the bigger the break size is, the sooner the loop seals are cleared. The smallest break size (0.5%) clears only one of the loop seals very late – about 1750 seconds into the transient.

And finally, Figures 21.8-5(a) and (b) show the calculated differential pressures in the upflow side of the steam generator U-tubes. The calculation results show that the smallest break size, which has the longest natural circulation period, retains liquid in the U-tubes much longer than the larger breaks.

## 21.9 SIMULATION OF ST-NC-02, 2% POWER NATURAL CIRCULATION TEST

### 21.9.1 Natural Circulation Phenomena

The natural circulation is an important phenomenon and effective mechanism of heat removal from the primary to the secondary side of the steam generators during a small break LOCA.

One important phenomenon that might influence the severity of small break LOCA transients is liquid holdup in the steam generator U-tubes. This holdup phenomenon was first identified experimentally in a Semiscale small break LOCA experiment (Leonard, 1982). It has since been duplicated in other facilities such as ROSA (Osakabe, et al., 1987) and has been discussed extensively in the open literature (Leonard, 1983 and Loomis, 1985a).

The liquid present in the steam generator tubes as a function of total system inventory is an important phenomenon in small break LOCA performance. During the initial phase of natural circulation, the system inventory is sufficient to maintain enough (two-phase bubbly) fluid present in both the uphill and downhill sides the steam generator U-tubes. At this stage, the interfacial drag is big enough to prevent draining of the SG tubes by gravity, and there is a continuous single-phase to bubbly flow established in the entire region of the steam generator tubes. As the primary system inventory is further depleted, voids are first developed at the top of the U-tubes, which then collapse and give way to a cyclic "fill-and-dump" phenomenon. The hydrostatic balance between the uphill and downhill side of the steam generator tubes becomes unstable and the fluid drains from the steam generator tubes – first the downhill side and later the uphill side.

In the later stages of natural circulation, when the inventory is depleted enough to expose the steam generator tubes to steam coming from the core, the liquid holdup that is caused by the condensation of that steam – a phenomenon called "reflux condensation." This holdup may not be able to drain by gravity back through the hot leg into the upper plenum if it is impeded by high upward steam flow rates; the pressure drop induced by this holdup affects the hydrostatic head balances throughout the RCS.

### 21.9.2 Description of the ST-NC-02 Natural Circulation Test

JAERI-M-88-215 (Reference 11) documents results of simulations of the ST-NC-02 test with RELAP5/MOD2, and contains a fair amount of detail related to the initialization and execution of the ST-NC-02 natural circulation test and RELAP5/MOD2 simulation results.

Unfortunately, JAERI did not issue the anticipated official Test Report for the ST-NC-02 natural circulation test (listed as Reference [1] in JAERI-M-88-215).

References 8, 9, 10 and 12 present additional analyses of the ST-NC-02 test and provide valuable information that cannot be easily found in (or inferred from) JAERI-M-88-215.

As described in Section 2.2 of JAERI-M-88-215, the first stage of the experiment was performed at the LSTF nominal conditions: full power (10MW), pumps on, temperature increase across the core as in the actual plant.

The second stage was designed to study the natural circulation at 100% primary side inventory. The core power was reduced down to 1.42 MW (this is 2% power of the reference PWR) and was kept at that level for the rest of the entire experiment. The pumps were turned off and the secondary side pressure was reduced to 6.6 MPa and kept constant until the end of the experiment. Figure 4 of Reference 9 (reproduced here as Figure 21.9-1) illustrates the measured evolution of the primary side pressure and loop flow and sheds some light on the timing of the different stages of the experiment. As seen from that figure, at the end of the second stage of the experiment, when the pressurizer pressure was established at 12.2 MPa, the pressurizer surge line valve was closed and the pressurizer isolated prior to the drain of the primary side inventory.

During the rest of the experiment, the primary side water inventory was reduced step-wise by bleeding through the drain line at the bottom of the vessel. The drain valve at the bottom was closed when certain inventory reduction was reached and kept closed for some time until intermediate steady state primary pressure and loop flow was achieved at that inventory level.

As described in JAERI-M-88-215, constant secondary side water level was maintained throughout the experiment. Unfortunately, there is no ST-NC-02 test report that documents in detail the test execution, and Section 2.2 of JAERI-M-88-215 does not explain how the secondary side pressure reduction was achieved and maintained at 6.6 MPa. Most likely, the feed water flow rate was adjusted to keep the constant steam generator level and balance the primary-to-secondary side heat transfer at the reduced secondary side pressure. JAERI-M-88-215 (pg. 6) also states that feedwater temperature fluctuation of 30K has been observed throughout the draindown phase of the test as well. Since the test simulated the natural circulation at different primary side inventory levels, safety injection was not modeled by isolating the accumulators.

As seen on Figure 21.9-1, the duration of the experiment was almost 10 hours (35000 sec). Due to computational (CPU) time constraints, it is not reasonable to try and replicate the test in real time length. Moreover, as seen on that figure, the quasi-steady states at different stages could be achieved for time periods shorter than the ones implemented through the experiment, especially those of Stage 1 and 2. Therefore, shorter time periods are used to achieve the desired quasi-steady state conditions at each stage.

### 21.9.3 Description of the Test Simulation and Boundary and Initial Conditions

The system initial conditions achieved for the ST-NC-02 simulation are presented in Table 21.9-1. The test simulation followed the procedure implemented during the real test, except that shorter time periods were simulated to achieve a quasi-steady state during each drain period. The length of the individual drain periods and the drain flows used in the simulation were estimated from the information available in Figure 21.9-1 (Figure 4 of Reference 8). The accumulators were isolated by closing the accumulator isolation valves. Prior to the beginning of the draining, the pressurizer was isolated by closing the PRZ isolation valve.

The following steps were implemented for the simulation of the natural circulation test ST-NC-02:

[

] <sup>a,c</sup>

[

] <sup>a,c</sup>

#### 21.9.4 Results and Conclusions

The results of the simulation of the ST-NC-02 natural circulation test (2% core power) are presented in Figure 21.9-2 through Figure 21.9-14.

Figure 21.9-2 compares the measured primary system loop circulation flow against the calculated by the code. During the single-phase natural circulation (primary side inventory from 100% to 90%) the circulation flow is predicted fairly well. [

] <sup>a,c</sup>

[

] <sup>a,c</sup>

The comparison of the downcomer differential pressures, Figure 21.9-7, shows a good prediction of the amount of liquid in the downcomer.

[

] <sup>a,c</sup>

The following major conclusions are made with respect to the ability of the code to calculate primary-to-secondary side heat transfer.

- For purely reflux condensation conditions in the steam generators, the code calculates overall effective heat transfer coefficient (normalized for the outside SG surface area) of around [ ] <sup>a,c</sup>. This value is determined from Figure 21.9-9 for system inventories when the steam generators are drained and the entire surface of the U-tubes is exposed for the steam to condense [ ] <sup>a,c</sup>. The calculated value is [ ] <sup>a,c</sup> than the average minimum reflux heat transfer coefficient of 1.7 kW/m<sup>2</sup>K, measured on the LSTF post-natural circulation test ST-SG-02 (Figure 14, Reference 8), therefore the code tends to under-predict the heat transfer during reflux conditions.
- [ ]

] <sup>a,c</sup>

- The power is removed effectively to the steam generator secondary side even though one of the steam generators remains plugged for a prolonged time.

Based on the results documented in this section, it is concluded that when used with WCOBRA/TRAC-TF2, the ROSA-IV LSTF model developed for the purpose of the FSLOCA methodology produces simulation results that are in general consistent with those observed on the ST-NC-02 experiment.

## **21.10 COUNTER-CURRENT FLOW (CCFL) RESULTS AND EVALUATION**

The counter-current flow limiting phenomenon is a process where liquid flow (usually directed downward by the force of gravity) is restricted by vapor flowing in opposite (usually upward) direction, due to interfacial drag forces. With increasing vapor velocity, at some point the downward flow of liquid becomes unstable, stagnates and is eventually reversed so that co-current flow is established. The boundary between the stable counter-current flow and the unstable co-current flow configuration is generally recognized as the so called Counter-current Flow Limit (CCFL).

The importance of CCFL at different locations of the primary side during the different periods of the LOCA transient and its PIRT ranking is discussed in Section 2.

The liquid in the uphill and downhill SG risers drains to the hot leg and loop seal, respectively; CCFL is possible at the U-tube inlet, SG plenum inlet, and in the hot leg elbow. The potential for CCFL in these locations and the impact of CCFL predictions on the transient dictate that a high (H) ranking is assigned for the loop seal clearing period.

During the steam generator reflux phase of the small break LOCA, steam leaving the core enters the SG and condenses forming a liquid film inside the U-tubes. The liquid draining from the steam generator tubes is then accumulated in the inlet plenum. Counter-current flow at the inlet of the U-tubes can affect the maximum reflux condensation.

The liquid draining from the SG through the hot legs and into the upper plenum collects above the upper core plate (UCP). Water draining from the upper plenum region, or falling back after entrainment from the core, can contribute to core cooling. The amount of water that can drain may be limited by counter-current flow limitation phenomena at the upper core plate, wherein the steam upflow is sufficient to limit or prevent draining.

Validation of the code capability to model CCFL in different regions of the primary system of PWR is presented in Section 19. However, the large scale experiments considered therein are designed primarily for conditions developing in Large Break LOCA accidents. The purpose of the discussions included in this section is to complement the CCFL discussions in Section 19 and expand the CCFL considerations into the intermediate and small break LOCA space.

### **21.10.1 CCFL in the Steam Generator U-tubes**

Counter-current flow in the steam generator U-tubes develops during the later stage of the two-phase natural circulation and continues into the reflux condensation phase of the Small Break LOCA transient. It is an important phenomenon since it is the major factor that controls the draining of the steam generator tubes especially during the reflood condensation phase.

One of the most widely used correlations to describe counter-current flow and flooding in U-tubes is a Wallis-type correlation in its general form  $(j_g^*)^{1/2} + m \times (j_f^*)^{1/2} = C$ , where  $m = 0.8-10$  and  $C = 0.7 - 1.0$  are empirically determined constants. In the case of turbulent flow  $m$  is close to 1.0.

[

$$\left[ \quad \quad \quad \right]^{a,c} \quad \quad \quad \left[ \quad \quad \quad \right]^{a,c} \quad \quad \quad (21.10-1)$$

[

The calculated counter-current flow calculated in the simulation of the natural circulation test ST-NC-02 is presented in Figure 21.10.1-5. The results show no violations of the flooding line in the counter-current flow calculated during reflux conditions in the steam generators.

**21.10.2 CCFL in the Vicinity of the Hot Leg Elbow (Steam Generator Inlet)**

Counter-current flow in the hot leg (HL), including the vicinity of the elbow and the inlet of the steam generator plenum, can develop during the period of two-phase natural circulation and is especially important during the subsequent reflux condensation phase. [

$$\left[ \quad \quad \quad \right]^{a,c} \quad \quad \quad \left[ \quad \quad \quad \right]^{a,c} \quad \quad \quad (21.10-2)$$

The counter-current flow calculation results, presented in Figures 21.10.2-1 through 21.10.2-4, are extracted for the hot leg elbow and steam generator inlet locations from different ROSA-IV test simulations documented in the previous subsections. In these figures, the calculated counter-current conditions (points) are plotted against the two limiting flooding lines, [

]<sup>a,c</sup> In each of the figures, both the SG plenum inlet plenum and hot leg elbow counter-current flows are compared against Equation 21.10-2.

Figure 21.10.2-1 shows results extracted from the simulation of the 10% cold leg side break test SB-CL-14. The calculated counter-current flow points are mostly clustered around the lower flooding limit. No violations of the higher flooding limit were identified in any of the two locations.

Figure 21.10.2-2 shows the results extracted from the simulation of the 5% cold leg side break test SB-CL-18. [

]<sup>a,c</sup>

The results of the counter-current flow calculations, extracted from the simulations of the 2.5% break test SB-CL-01, Figure 21.10.2-3, and the 0.5% break test SB-CL-12, Figure 21.10.2-4, further confirm the conservative bias of the code with respect to counter-current flow at the hot leg and the steam generator inlet. [

]<sup>a,c</sup>

### 21.10.3 CCFL at the Upper Core Plate (UCP)

Counter-current flow limitation at the upper core plate is an important phenomenon during both large-break and small-break loss-of coolant accidents. Steam-water counter-current flow condition at the top of UCP might occur during different phases of the LOCA accidents.

In large-break accidents CCFL can occur during the reflood phase when water is accumulated above the UCP as a result of de-entrainment or direct SI injection in the upper plenum. If the flow of vapor generated in the core is high enough, it may impede the penetration of the water accumulated in the upper plenum and reduce the effectiveness of the core cooling. Validation of the capability of the code to calculate CCFL in large break LOCA conditions is presented in Section 19.4, [

]<sup>a,c</sup>.

In Small-break LOCA, the accumulation of water in the upper plenum occurs primarily as a result of the draining of the hot legs and upflow side of the steam generators during the later stages of the two-phase natural circulation period. Pool of water accumulated above the UCP can still exist during the reflux condensation period maintained by steam condensing on the surface of the steam generator U-tubes and draining back into the upper plenum. Irrespective of how the pool of water above the UCP is formed and maintained during the accident, the nature of the CCFL phenomenon is in essence similar in both Large-break and Small-break LOCA scenarios. [

] <sup>a,c</sup>

The results of calculated counter-current flow at the UCP, presented in this section, are extracted from the ROSA-IV LSTF simulations for the individual CCFL channels that are modeled in the [

1 and 21.3.3. [

] <sup>a,c</sup> region of the UCP, Figures 21.3-] <sup>a,c</sup>

Figure 21.10.3-1 shows calculated counter-current flow at the peripheral (low-power) CCFL Channel 72, extracted from the simulation of the SB-CL-18 test. Figures 21.10.3-2 and 21.10.3-3 show the counter-current flow calculated at the inner average and hot channel respectively.

[

] <sup>a,c</sup>

Figures 21.10.3-4 through 21.10.3-6 show counter-current flow results that were extracted from other ROSA-IV test simulations documented in the previous sections. The CCFL results shown in these figures include all instances where counter-current flow is calculated to occur at the top of the CCFL channels.

Figure 21.10.3-4 shows counter-current flow points extracted from the simulation of the 10% break test SB-CL-14; [

] <sup>a,c</sup>

In summary, the results presented in this section show that with the current ROSA-IV LSTF model, the code (WCOBRA/TRAC-TF2) calculates counter-current flow at the top of the UCP channels which is, for the most part, conservative with respect to the draining of the liquid pool that might exist above the upper core plate. This is especially true for the periods of significant core uncover that occur during loop seal clearance and core boiloff.

#### 21.10.4 Effects of Calculated CCFL on ROSA-IV SB-CL-18 Transient Simulation

The discussion, presented in the previous three subsections, is focused on the calculated counter-current flow at three key locations of the ROSA-IV LSTF: steam generator U-tubes inlet, the hot leg elbow region and the upper core plate. The calculated counter-current flow at these three locations is benchmarked against flooding correlations established from available experimental data (Glaeser, Kukita and Hsieh).

[

] <sup>a,c</sup>

#### Steam Generator U-tube and Inlet Plenum Draining

Figure 21.10.4-1 shows the calculated and measured differential pressures in the uphill side of the U-tubes steam generator A (SGA). The periods of calculated counter-current flow conditions at the U-tube inlet and the HL elbow are also shown in the figure to facilitate the discussion herein.

[

] <sup>a,c</sup>

Figure 21.10.4-2 shows the calculated and measured collapsed liquid level (CLL) in the inlet plenum of SGA. The periods of calculated counter-current flow conditions at the U-tube inlet and the HL elbow are also shown in that figure. [

] <sup>a,c</sup>

[

] <sup>a,c</sup>

Similar observations and conclusions can be made based on the draining of the U-tubes and inlet plenum of Steam Generator B (SGB), presented in Figures 21.10.4-3 and 21.10.4-4.

As seen in Figure 21.10.4-4, for Steam Generator B (SGB) the test measurements indicated a sudden drop of the inlet plenum CLL between 130 and 170 seconds followed by a second CLL holdup at about 0.5 meters. [

] <sup>a,c</sup>

In summary, the simulation results indicate that with the adopted ROSA model the code calculation is biased in a conservative direction with regards to the draining of the steam generator U-tubes and inlet plenum. This is largely due to the conservative counter-current flow conditions calculated at the hot leg elbow region.

### Upper Plenum Draining

[

] <sup>a,c</sup>

Figure 21.10.4-8 shows a comparison of the calculated and measured differential pressures in the upper plenum for the 5% side break test SB-CL-18. Figure 21.10.4-9 shows the calculated and measured inner vessel differential pressures for the same test. The measured differential pressures shown in these two figures are indicators of the collapsed liquid levels in the upper plenum and the inner vessel region respectively.

The almost complete draining of the upper plenum, measured at the test between 125 and 160 seconds (Figure 21.10.4-8) is related to the significant core uncover due to the loop seal clearance depression (Figure 21.10.4-9). The fast recovery of the upper plenum level between 160 and 170 seconds is caused by both the recovery of the core inventory and the draining of the steam generators, especially the draining surge from the inlet plenum of SGB, seen in Figure 21.10.4-4. Relatively constant liquid level is measured in the upper plenum until 330 seconds maintained by the gradual draining of the steam generator inlet plenums and the hot legs. As the system inventory is further depleted, due to the steam discharged through the break, the upper plenum drains completely by 400 seconds.

[

] <sup>a,c</sup>

Figure 21.10.4-10 shows the calculated mixture flow at the inlet of the two hot legs as well as the total hot leg flow (negative is flow going into the upper plenum). This figure provides information regarding the amount of fluid being delivered into (or removed from) the upper plenum through the hot legs.

[

] <sup>a,c</sup>

Figure 21.10.4-11 shows the calculated counter-current flow at the peripheral UCP jet Channel 73 (top of CCFL Channel 72). The result shown in Figure 21.10.4-11 are very similar to those reported in Figure 21.10.3-1, with the exception that the selected periods of interest are presented separately to better illustrate the calculated counter-current flow during the different phases of upper plenum draining. [

] <sup>a,c</sup>

Figures 21.10.4-12 through 21.10.4-14 show a comparison of measured and calculated rod cladding temperatures at the 7.33-ft elevation in the core. The period of interest is between 124 and 260 seconds [

[

] <sup>a,c</sup>

Figure 21.10.4-12 shows the calculated and measured cladding temperatures of the low power rods. As seen in this figure, the test measurements show that only 4 out of 15 rods heated up briefly during the loop seal clearance period. The heatup of these (low power) rods was brief and did not exceed more than 40K. According to the measurements, the majority of the high-power rods heated up during the loop seal clearance period, Figure 21.10.4-13. Only 5 out of 13 rods in the inner average power region experienced

heatup, according to Figure 21.10.4-14. In summary, the rod temperature measurements at the 7.33-ft elevation show that during the period of interest the peripheral (low power) region of the core simulator received and retained most of the fluid that was draining from the upper plenum.

[

] <sup>a,c</sup>

The evaluation presented in this section further supports the previously made conclusions with regards to CCFL at the steam generator U-tube inlet, the hot leg elbow region and the upper core plate. It also shows that, with the adopted vessel modeling approach, the results of the SB-CL-18 test simulation are consistent with those observed in the test, with a conservative bias with regards to the draining of the upper plenum.

## 21.11 BYPASS SENSITIVITY CALCULATIONS

This section documents results from various simulations of ROSA-IV tests performed with different modeling variations. These sensitivity calculations are needed to provide a basis for the treatment of the modeling uncertainty within the FSLOCA Methodology.

### 21.11.1 Hot Leg Nozzle Gap Modeling Sensitivity with the SB-CL-18 Test

The ROSA-IV LSTF vessel model, used in the different break simulations documented in Section 21, models explicitly a bypass line that exists in the LSTF and connects the hot leg outlet nozzle to the downcomer. The purpose of this bypass line is to simulate the effect of the hot leg nozzle gap that would open during the LOCA transient and create a bypass flow between the upper plenum and the downcomer in addition to the spray nozzle bypass.

The goal of this sensitivity calculation is to investigate the effect of a modeling approach where the bypass flow through the hot leg nozzle gap is lumped together with the spray nozzle and the HL-to-DC flow link is not explicitly modeled. The calculations with the revised "lumped" bypass modeling are performed and tested with the SB-CL-18 test.

Figures 21.11.1-1 through 21.11.1-7 compare the simulation results with the lumped bypass modeling approach against the simulation results of the SB-CL-18 documented in the previous Section 21.4. In each of the figures, the reference SB-CL-18 simulation results are at the top, while the simulation results obtained with the lumped bypass model are at the bottom.

[

] <sup>a,c</sup>

[

] <sup>a,c</sup>

### 21.11.2 SB-CL-18 Simulation Without Hot Leg Nozzle Bypass Flow

In this calculation, the (spray) bypass flow is tuned to [ ] <sup>a,c</sup> of the total core flow. This is a case, where the [ ] <sup>a,c</sup> HL-to-DC gap bypass (modeled in the reference SB-CL-18 simulation in Section 21.4) is eliminated by blocking the HL-to-DC Gaps 21 and 22. The results of this sensitivity calculation are intended to provide a basis for judgment whether modeling HL-to-DC bypass flow has a big effect on the transient calculation. Establishing a direction of conservatism can support making a decision whether to model HL-to-DC bypass in addition to the spray nozzle bypass or not.

[

] <sup>a,c</sup>

The reduced bypass leads to earlier loop seal clearance (Figures 21.11.2-1 and 21.11.2-2) with deeper core and lower plenum depression (Figures 21.11.2-3 and 21.11.2-5). As a result the loop seal clearance PCT tends to increase (Figure 21.11.2-7). Also, due to the reduced vessel venting capability, the boiloff tends to occur earlier leading to a higher boiloff PCT as well, as seen in Figure 21.11.2-7.

[

] <sup>a,c</sup>

### 21.11.3 Spray Nozzle Bypass Ranging Sensitivity with the SB-CL-18 Test

During the steady state tune-up procedure, the bypass flow through the spray nozzle is adjusted to be within [ ] <sup>a,c</sup> the desired value, established for each plant. The purpose of this sensitivity is to investigate if ranging the spray bypass at the extreme ends of the [ ] <sup>a,c</sup> steady state acceptance criterion will have significant effect on the transient.

The results of the sensitivity are presented in Figures 21.11.3-1 through 21.11.3-7. The top figure on each page is the high [ ] <sup>a,c</sup> bypass case and the bottom is the lower [ ] <sup>a,c</sup> bypass case. The comparison of the calculation results, provided in this section shows that ranging the spray nozzle bypass [ ] <sup>a,c</sup> of the desired steady state value has a small effect on the SB-CL-18 transient results.

Consistent with the trend established with the [ ] <sup>a,c</sup> bypass sensitivity presented in the previous Section 21.11.2, the loop seal clearance PCT is predicted to occur a little earlier with the smaller bypass case and the calculated boiloff PCT excursion is similar, Figure 21.11.3-7. In summary, ranging of the spray bypass [ ] <sup>a,c</sup> of the desired steady state value does not appear to have significant effect on the SBLOCA transient and would not require ranging of this parameter as part of the uncertainty treatment.

## 21.12 SUB-COOLED BREAK DISCHARGE COEFFICIENT (CD1) SENSITIVITY

Two simulations of the SB-CL-18 test were performed implementing a sub-cooled break discharge coefficients (CD1) at high and low values. The extreme values of CD1 were set at [ ]<sup>a,c</sup> of the reference CD1 [ ]<sup>a,c</sup>, used in the simulation of the SB-CL-18 test, presented in Section 21.4 – [ ]<sup>a,c</sup>. It is acknowledged that the CD1 range considered [ ]<sup>a,c</sup> is smaller than the CD1 standard deviation [ ]<sup>a,c</sup> established from the validation of the critical flow model, Section 12. However, it is sufficient to provide sensitivity results to illustrate the importance of this parameter and support the decision on how to address it within the uncertainty treatment approach established for the FSLOCA methodology, Section 29.

Figures 21.12-1 through 21.12-19 show a comparison of the SB-CL-18 simulation results using the two extreme values of CD1. [ ]

[ ]<sup>a,c</sup> For each of the simulations, the SB-CL-18 test measurements are presented in the figures as well.

Obviously, the effect of the extreme CD1 variation manifests from the very early stages of the transient. This higher CD1 coefficient results in a visibly higher peak of the break flow (Figure 21.12-1). The increased loss of inventory with the higher CD1 results in earlier transition to two-phase discharge, Figure 21.12-2, and earlier loop seal clearance (Figures 21.12-3 and 21.12-4). The system depressurization is visibly affected during the period between 25 and 75 seconds (Figure 21.12-5).

The draining of the uphill side of the steam generator tubes occurs visibly earlier in the simulation with the higher CD1 coefficient (Figures 21.12-6 to 21.12-9). With the higher CD1, the draining of the steam generator inlet plenums (Figures 21.12-10 and 21.12-11) and the hot legs (Figures 21.12-12 and 21.12-13) is predicted to occur relatively earlier as well. The calculated differential pressures in the different regions of the test facility is consistent with the expected effect of the inventory lost, which is dependent on the value of CD1 (see Figures 21.12-14 through 21.12-17).

[ ]

] <sup>a,c</sup>

As a result of the greater inventory loss with the higher CD1, the accumulator injection is predicted to occur earlier than the case with low CD1, see Figure 21.12-19.

## 21.13 TWO-PHASE BREAK DISCHARGE COEFFICIENT (CD2) SENSITIVITY

The effect of the two-phase break discharge coefficient (CD2) on the small break LOCA transient is shown by comparison of two simulations of the SB-CL-18 test. [ ]

] <sup>a,c</sup>

The results of the two simulations are presented in Figures 21.13-1 through 21.13-19. [ ]

] <sup>a,c</sup>

Since the sub-cooled discharge coefficient used in the two simulations was the same, the initial break flow until the time when transition to two-phase flow occurred was not affected, Figure 21.13-1. There is a difference in the calculated break flow (Figure 21.13-1) during the transition from sub-cooled to two-phase, [

] <sup>a,c</sup>

The system depressurization rate is visibly affected by the CD2 coefficient during the period of the transient following loop seal clearance, Figure 21.13-5. The case with higher CD2 resulted in faster system depressurization after the loop seals cleared. As a result, the earlier accumulator injection calculated in the simulation with higher CD2 coefficient, Figure 21.13-19.

The draining of the steam generator U-tubes and inlet and outlet plenums is not affected by CD2 as well, Figures 21.13-6 through 21.13-11.

[

] <sup>a,c</sup>

## 21.14 BROKEN LOOP PUMP RESISTANCE SENSITIVITY CALCULATION

This sensitivity calculation is performed to support a discussion in Section 29, which is related to the ranging of the broken loop pump resistance (KP). The approach on KP ranging is considered to be applicable to both small and large break LOCA scenarios. The sensitivity performed herein is not sensitivity on KP; it simply looks at the effect on the simulation results when the resistance at zero pump velocity is shifted by a certain amount. In this case, the homologous curve point at zero pump speed is modified so that the resistance for both pumps is reduced by 50% from the one used in the SB-CL-18 simulation in Section 21.4.

Figures 21.14-1 through 21.14-10 show comparison of SB-CL-18 simulation with 50% reduced locked rotor resistance to the SB-CL-18 simulation in Section 21.4. The simulations with the 50% reduced locked rotor resistance are shown in the bottom figures on each page. Except for the slightly different

pump differential pressure after the pumps are locked at about 260 seconds, Figure 21.14-1, no major differences are observed in the comparison of the rest of the simulation results.

## 21.15 YDRAG SENSITIVITY CALCULATIONS

This sensitivity is performed to investigate the effect of the variation of YDRAG in the core channels on the transient calculation results. The YDRAG multiplier in the core region is set at extreme minimum [ ]<sup>a,c</sup> and maximum [ ]<sup>a,c</sup> values.

The results of the YDRAG sensitivity are presented in Figures 21.15-1 through 21.15-6.

The loop seal clearance is not affected visibly by the variation of the core YDRAG parameter, Figures 21.15-1 and 21.14-2.

[

, ]<sup>a,c</sup>

In summary, the sensitivity shows that using a lower YDRAG multiplier in the core channels results in earlier boiloff and more severe PCT excursion.

## 21.16 HS\_SLUG SENSITIVITY CALCULATIONS

### 21.16.1 HS\_SLUG Sensitivity with 0.5% Side Break Test SB-CL-16

An HS\_SLUG sensitivity calculations were performed with the 0.5% side cold leg break test SB-CL-16. In these calculations, the HS\_SLUG multiplier was set at the maximum [ ]<sup>a,c</sup> and minimum [ ]<sup>a,c</sup> values. The results of these calculations are shown in Figures 21.16.1-1 through 21.16.1-10.

As seen in Figure 21.16.1-1, the break discharge flow was not affected much by the HS\_SLUG variation. The timing of the transition from sub-cooled to two-phase and later to pure steam break flow was not affected much as well. As a result, the predicted system pressure response remains unaffected, as seen in Figure 21.16.1-2.

An asymmetry is observed in the calculated draining of the steam generators, Figure 21.16.1-3. However, if we ignore the asymmetry, the timing when the steam generators are completely drained is similar.

The calculated loop seal clearance in the individual cross-over legs, Figures 21.16.1-4 and 21.16.1-5, shows that an asymmetry exists in the calculated differential pressures (SG outlet to bottom), Figures 21.16.1-4(a) and 21.16.1-5(a). This asymmetry can be related to the calculated asymmetry in the steam generator draining, mentioned above. The HS\_SLUG variation does not affect the loop seal clearance. In both cases, loop A does not clear completely, Figure 21.16.1-4(b), and the timing of the calculated clearance of Loop B is practically the same, Figure 21.16.1-5(b).

The calculated downcomer differential pressures, Figure 21.16.1-6, and upper plenum differential pressures, Figure 21.16.1-7, are not affected by the HS\_SLUG variation as well.

Asymmetry is observed in the calculated hot leg differential pressures, Figure 21.16.1-8, which can be related to the calculated asymmetrical draining of the steam generators, Figure 21.16.1-3.

The asymmetrical steam generator and loop seal clearance behavior, caused by the HS\_SLUG variation, does not however affect the calculated core uncover, Figure 21.16.1-9, and the related rod heatup, Figure 21.16.1-10.

### **21.16.2 HS\_SLUG Sensitivity with 5% Top Break test SB-CL-18**

Two simulations of the 5% side break test SB-CL-18 test were performed with setting the HS\_SLUG multiplier at its maximum [ ]<sup>a,c</sup> and minimum [ ]<sup>a,c</sup> values. The results of these simulations are shown in Figures 21.16.2-1 through 21.16.2-10.

The break flow, Figure 21.16.2-1, and system pressure response, Figure 21.16.2-2, are not affected by the HS\_SLUG variation. The calculated steam generator draining is very similar, Figure 21.16.2-3.

Minor asymmetry is observed in the calculated differential pressures in the cross-over legs (bottom to pump inlet), Figures 21.16.2-4(b) and 21.16.2-5(b), however the timing of the loop seal clearance is however almost identical.

The calculated downcomer and upper plenum differential pressures are not much affected by the HS\_SLUG variation, Figures 21.16.2-6 and 21.16.2-8.

Asymmetry is calculated in the draining of the hot legs, Figure 21.16.2-8, however the calculated pressure drop is very similar.

Finally, the calculated core uncover, Figure 21.16.2-9, and rod heatup, Figure 21.16.2-10, show that the overall effect of the HS\_SLUG variation is small.

### **21.16.3 HS\_SLUG Sensitivity with 10% Side Break Test SB-CL-14**

Two simulations of the 10% side break test SB-CL-14 test were performed with setting the HS\_SLUG multiplier at its maximum [ ]<sup>a,c</sup> and minimum [ ]<sup>a,c</sup> values. The results of these simulations are shown in Figures 21.16.3-1 through 21.16.3-10.

The break flow, Figure 21.16.3-1, and system pressure response, Figure 21.16.3-2, are not affected by the HS\_SLUG variation. The calculated steam generator draining is almost identical, Figure 21.16.3-3.

The calculated downcomer and upper plenum differential pressures are not much affected by the HS\_SLUG variation, Figures 21.16.3-6 and 21.16.3-8.

Some delay is calculated in the draining of the hot legs, Figure 21.16.2-8, however the calculated pressure drop is very similar, independent on the HS\_SLUG multiplier used.

For the 10% break size the calculated timing of the loop seal clearance is however almost identical, Figures 21.16.3-4 and 21.16.3-5. [

] <sup>a,c</sup>

#### 21.16.4 Conclusion Regarding the HS\_SLUG Sensitivity Simulations

Based on the results from the HS\_SLUG sensitivity calculations presented herein, it can be concluded that the effect of the HS\_SLUG ranging would have minimal effect on the Small Break LOCA transient. The effect of the HS\_SLUG multiplier appears to have greater effect on the bigger 10% break size simulation, where the vapor velocities are higher and the importance of interfacial drag is greater.

#### 21.17 KCOSI SENSITIVITY CALCULATIONS

This section presents the results of two simulations of the 5% side break test SB-CL-05 (reference case documented in Section 21.5), performed with setting the cold leg condensation multiplier KCOSI at high [ ] <sup>a,c</sup> and low [ ] <sup>a,c</sup> values. The results of the sensitivity are presented in Figures 21.17-1 through 21.17-12.

With KCOSI multiplier set at maximum the code calculates increased liquid present at the SI injection node of the intact cold leg, Figure 21.17-1(a). At the broken cold leg SI injection node the liquid content does not seem to be affected by the KCOSI variation in the intact cold leg, Figure 21.17-1(b). This is explained by the fact that, in this sensitivity, the COSI model is turned off in the broken cold leg to be consistent with the modeling approach adopted for the PWR simulations, Section 26. The only exception is a temporary increase of the liquid fraction calculated for the [ ] <sup>a,c</sup> case (Figure 21.17-1(b)) between 210 and 240 second.

[

] <sup>a,c</sup>

[

] a,c

## 21.18 MSSV SETPOINT SENSITIVITY CALCULATION

A sensitivity calculation is performed with the 0.5% side break test SB-CL-15 to provide a basis for assessing the effect of increased main steam safety valve (MSSV) setpoint on the SBLOCA transient. The 0.5% break was selected for this sensitivity since with this break size the loss of inventory is the lowest, the holdup of the primary system pressure above the secondary side pressure is for a longer period of time, and the effect of the increase of the MSSV setpoint would be greater.

For the purpose of the sensitivity study, the steam generator MSSV pressure setpoints were increased arbitrarily, as follows.

MSSV Open @ 9.37 MPa (old value 8.0 MPa)  
MSSV Close @ 8.5 MPa (old value 7.8 MPa)

With the setpoints selected above, the average MSSV setpoint is increased by 1.035 MPa (150 psi).

The calculation results from this sensitivity are compared to the results of the SB-CL-15 simulation, performed for the break orientation studies in Section 21.7.

Figure 21.18-1 compares the calculated pressurizer and steam generator secondary side pressures from the two simulations. As seen, the increase of the MSSV setpoint results in an increased primary system pressure during the prolonged period when the steam generator acts as a heat sink. The cyclical behavior of the secondary side pressure affects the primary side pressure in a similar way, through the primary-to-secondary side heat transfer feedback mechanism. The greater amplitude of the calculated pressure oscillations in the high MSSV setpoint case is due to the greater difference between the Open and Close pressure setpoints of the MSSV, implemented for that case.

The comparison of the calculated break flows, Figure 21.18-2, shows that the increased secondary side pressure (high MSSV setpoint) results in an increased inventory loss through the break.

With the MSSV setpoint increased, the calculated steam generator draining is asymmetrical, with steam generator B draining earlier, Figure 21.18-3. The increased loss of inventory through the break results in earlier draining of the upper plenum, Figure 21.18-4, and hot legs as well, Figure 21.18-5.

Figure 21.18-6, shows a comparison of the calculated differential pressures from the bottom of the cross-over leg to the pump inlet for the two loops. As seen in that figure, with the increase of the MSSV the loop seal clearance is calculated to occur earlier with loop A being cleared as well.

The calculated loop flows, Figure 21.18-7, are similar. However, the frequency of the flow oscillations for the high MSSV case is lower, consistent with the lower frequency oscillations of the system pressure for that case.

As a result of the faster inventory loss with increased MSSV setpoint, the loop seal clearance uncover of the core occurs earlier, as well as the boiloff, Figure 21.18-8. Consequently, in the case of increased MSSV setpoint the calculated rod heatup is more severe, as seen in Figure 21.18-9.

## 21.19 CONCLUSIONS

The analysis of the results of the various ROSA-IV LSTF test simulations presented in this section demonstrates that WCOBRA-TRAC-TF2 is capable of simulating with sufficient accuracy the key thermal-hydraulic phenomena that might occur during PWR small break LOCA accident. The major conclusions from the analysis of the test simulations with the ROSA-IV LSTF model presented in this section are summarized below.

- [

- 

- 

- 

]a,c

• [

] <sup>a,c</sup>

- The break orientation studies in Section 21.7 show results which are consistent with the observed in the tests. [

] <sup>a,c</sup>

- The various sensitivity studies show results that are consistent with the expected effect of the parameter being ranged in these small break LOCA test simulations.

## 21.20 REFERENCES

1. Asaka, et al., "Results of 0.5% Cold-Leg Small-Break LOCA Experiments at ROSA-IV/LSTF: Effect of Break Orientation," *Experimental Thermal and Fluid Science*, 3, 588-596, 1990.
2. JAERI-M 84-237, 1985, "ROSA-IV Large Scale Test Facility (LSTF) System Description."
3. Kawaji, M., et al., 1986, "ROSA-IV/LSTF 5% Cold Leg Break LOCA Experiment Data Report, Run SB-CL-05," JAERI-memo 61-056.
4. Koizumi, Y., et al., 1987, "ROSA-IV/LSTF 2.5% Cold Leg Break LOCA Experiment Data Report for Runs SB-CL-01, 02 and 03," JAERI-memo 62-399.
5. Koizumi, Y., et al., 1988, "Investigation of Break Orientation Effect During Cold Leg Small-Break LOCA at ROSA-IV LSTF," *Journal of Nuclear Science and Technology*, 25.
6. Koizumi, Y. and Tasaka, K., 1988, "Quick Look Report for ROSA-IV/LSTF 10% Cold Leg Break LOCA Test, SB-CL-14," JAERI-memo 63-262.
7. Osakabe, M., et al., 1987, "Core Liquid Level Depression due to Manometric Effect during PWR Small Break LOCA," *Journal of Nuclear Science and Technology*, 24.
8. Tasaka, K., et al., 1988, "The Results of 5% Small Break LOCA Tests and Natural Recirculation Tests at the ROSA-IV LSTF," *Nuclear Engineering and Design*, 108.
9. Y. Kukita, et al., "Nonuniform Steam Generator U-Tube Flow Distribution During Natural Circulation Tests in ROSA-IV Large Scale Test Facility," *Nuclear Science and Engineering: Vol. 99* (1988).
10. H. Stumpf, et al., "Reverse Primary-Side Flow in Steam Generators During Natural Circulation Cooling," *ASME Heat Transfer Division (HTD)*, Vol. 92.

11. JAERI-M 88-215, "Post-Test Analysis with RELAP5/MOD2 of ROSA-IV/LSTF Natural Circulation Test ST-NC-02," October 1988.
12. Yonomoto, T., "ROSA/LSTF Experiments of PWR Natural Circulation and Validation of RELAP5/MOD3.3, IAEA-TECDOC-1149, Proceedings of 1998 IAEA Technical Meeting on Experimental Test and Qualification of Analytical Methods to Address Thermohydraulic Phenomena in Advanced Water Cooled Reactors."
13. Kumamaru, et.al., 1989, "ROSA-IV/LSTF 5% Cold Leg Break LOCA Experiment, Run SB-CL-18 Data Report," JAERI-M 89-027.
14. Koizumi, Y. and Tasaka, K., 1988, "Quick Look Report for ROSA-IV/LSTF 0.5% Cold Leg Break LOCA Tests, SB-CL-15 and SB-CL-16," JAERI-memo 63-344.
15. H. Glaeser, et.al., 1993, "The Contribution of UPPTF Experiments to Resolve Some Scale-up Uncertainties in Countercurrent Two Phase Flow," Nuclear Engineering and Design, 145 (63-84)
16. Y. Kukita., et al., 1991, "Summary of ROSA-IV LSTF First-phase Test Program – Integral Simulation of PWR Small-break LOCAs and Transients," Nuclear Engineering and Design, 131 101-111.
17. JAERI-M 89-113, "Supplemental Description of ROSA-IV/LSTF with No.1 Simulated Fuel-Rod Assembly," September 1989.
18. N. Zuber, "Problems in Modeling of Small Break LOCA," NUREG-0724, 1980.
19. Hsieh, C., et al., 1980, "Countercurrent Air/Water and Steam/Water Flow above a Perforated Plate," NUREG/CR-1808.

<b>Table 21.1-1 Selected ROSA-IV Test Series Description and Related Technical Reports</b>				
<b>Run ID</b>	<b>Date</b>	<b>Break</b>	<b>Condition</b>	<b>JAERI-Report/Article</b>
SB-CL-01	5/30/85	2.5% CL	Cold Leg w/o HPI (Orifice in branch pipe)	<u>memo-62-399</u> (87-11, Koizumi), <u>JNST 25-9</u> ('88, Koizumi), 13th WRSM, JNST 24-2 ('87)
SB-CL-05	6/26/85	5% CL	Cold Leg w/HPI, w/AFW (Orifice in branch pipe)	<u>memo-61-056</u> (86-3, Kawaji), <u>memo-61-411</u> ('86, Chauliac,RELAP5), JNST 24-2 ('87, Osakabe), <u>JNST 25-3</u> ( '88, Osakabe), San Siego ('86-2, Osakabe), 14th WRSM ('87 Tas)
SB-CL-02	7/18/85	2.5% CL	Cold Leg w/o HPI, bottom break (orifice in branch pipe)	<u>memo-62-399</u> ('87-11, Koizumi), <u>JNST 25-9</u> ('88, Koizumi, break orient)
SB-CL-03	8/8/85	2.5% CL	Cold Leg w/o HPI, top break (orifice in branch pipe)	<u>memo-62-399</u> ('87-11, Koizumi), <u>JNST 25-9</u> ('88, Koizumi, break orient)
ST-NC/SG-02	12/4/85	2% power nat. circ.	Reflux to core uncov. Then stepwise secondary level drop.	<u>memo-63-040</u> ('88, Yonomoto), 14th WRSM ('87), <u>Nucl.Eng.Des. (WRSM)</u> <u>('88, Tas)</u> , 24th Nat.Heat Transf. ( '87, Kukita), <u>Nucl.Sci.Eng.</u> ('88, Kukita), <u>NURETH4</u> ('89, Kukita), AESJ ( '89-Fall,Nakamura), <u>JAERI-M88-215</u> ( '88-10, Chauliac,RELAP5), <u>ASME-HTD92</u> (pp. 103-109, '88, Stumpf), <u>Session 3 Phenomena 6</u> (Yonomoto, OECD mtg., 2006)
SB-CL-14	8/28/86	10% CL	Cold Leg w/o HPI, side break (orifice in branch pipe) Realistic (low) power curve used in the test.	JAERI-memo 63-262 ('88, Koizumi)
SB-CL-12	7/29/87	0.5% CL	Cold leg w/o HPI, w/o AFW, <b>side break</b> (orifice flush w/cold leg wall)	<u>memo-63-026</u> ('88-2, Asaka), Seoul ( '88, Tasaka), <u>Nucl.Engrg.Des.</u> ('90, <u>Seoul, Tas-Kukita</u> ), <u>memo-01-375</u> ( '89, Clement, CATHARE), AESJ-Fall ( '88, Bk orientation, CATHARE), <u>Nucl.Engrg.Des.</u> 122, pp. 255-262 ('90, <u>Kukita</u> )

**Table 21.1-1 Selected ROSA-IV Test Series Description and Related Technical Reports**  
(cont.)

Run ID	Date	Break	Condition	JAERI-Report/Article
SB-CL-15	1/26/88	0.5% CL	Cold leg w/o HPI, w/o AFW, <b>bottom break</b>  (orifice flush w/cold leg wall)	<u>memo-63-344</u> ('88-9, Koizumi, comb. w/SB-CL-16), AESJ-Fall ('88, break orientation, CATHARE), memo-01-375 ('89, Cle, CATHARE), AESJ ('90-4, RELAP, secondary depressurization effects), CSNI Spec. Mtg. on Intentional System Depressurization ('89, Kukita), NURETH4 ('89, Asaka, break orient), <u>Exp. Fluid Thermal Sci.</u> ('90, Asaka, NURETH4)
SB-CL-16	3/2/88	0.5% CL	Cold leg w/o HPI, w/o AFW, <b>top break</b>  (orifice flush w/ cold leg wall)	memo-63-344 ('88-2, Koizumi, comb. w/SB-CL-15), AESJ Fall ('88, break orientation, CATHARE), memo-01-375 ('89, Clement, CATHARE), NURETH4 ('89, Asaka), <u>Exp. Fluid Thermal Sci.</u> ('90, Asaka)
SB-CL-18	5/25/88	5% CL	Cold leg w/o HPI, w/o AFW, <b>side break</b> (orifice in branch pipe), JAERI-old power. Repeat of SB-CL-08 w/improved SG $\Delta P$ measurements. <b>This is CSNI ISP-26.</b>	<b><u>JAERI-M89-027</u></b> ('89-3, Kumamaru), <b><u>BE2000 (2000, Glaeser, ISP26 Uncertainty Methods Study)</u></b>

<b>Table 21.2-1 Major Design Characteristics of LSTF and PWR</b>			
<b>Characteristic</b>	<b>LSTF</b>	<b>PWR</b>	<b>PWR/LSTF</b>
Pressure, MPa (psia)	15.5 (2250)	15.5 (2250)	1
Temperature, K (°F)	598 (617)	598 (617)	1
Number of fuel rods	1064	50,952	48
Core height, m (ft)	3.66 (12)	3.66 (12)	1
Total Primary Fluid volume, m <sup>3</sup> (ft <sup>3</sup> )	7.23 (255.3)	374 (12,254.2)	48
Vessel Fluid Volume, m <sup>3</sup> (ft <sup>3</sup> )	2.675 (94.47)	131.7 (4650.9)	49.24
Core Volume, m <sup>3</sup> (ft <sup>3</sup> )	0.4078 (14.4)	17.5 (618.0)	42.91
Upper Plenum Volume (incl. end box), m <sup>3</sup> (ft <sup>3</sup> )	0.5472 (19.32)	28.4 (1002.9)	51.9
Lower Plenum Volume, m <sup>3</sup> (ft <sup>3</sup> )	0.5802 (20.49)	29.62 (1046.0)	51.05
Core power, MW	10	3423(t)	342 <sup>(2)</sup>
Power density, kW/m <sup>3</sup> (kW/ft <sup>3</sup> )	1383 (39.17)	9152.4 (279.33)	7.1
Core inlet flow, kg/sec (lbm/sec)	48.8 (97.6)	16700 (33,400)	342
Core Flow Area, m <sup>2</sup> (ft <sup>2</sup> )	0.1134 (1.22)	4.75 (51.13) <sup>(1)</sup>	41.9
Upper Core Plate Area, m <sup>2</sup> (ft <sup>2</sup> )	0.066 (0.71)	2.94 (31.65) <sup>(1)</sup>	44.5
Upper Plenum Area, m <sup>2</sup> (ft <sup>2</sup> )	0.159 (1.71)	6.92 (74.48) <sup>(1)</sup>	43.5
Downcomer gap, m (in.)	0.053 (2.09)	0.26 (10.24)	4.9
<b>Hot leg</b>			
Diameter (D), m (ft)	0.207 (0.679)	0.737 (2.418)	3.56
Length (L), m (ft)	3.69 (12.1)	6.99 (22.93)	1.89
L/√D, m <sup>1/2</sup> (ft <sup>1/2</sup> )	8.14 (14.68)	8.14 (14.68)	1.0
Volume $\left(\frac{\pi}{4} D^2 L\right)$ , m <sup>3</sup> (ft <sup>3</sup> )	0.124 (4.38)	2.98 (105.2)	24.0
Area $\left(\frac{\pi}{4} D^2\right)$ , m <sup>2</sup> (ft <sup>2</sup> )	0.03365 (0.362)	0.4266 (4.59)	12.68
Number of loops	2	4	2
Number of tubes in steam generator	141	3382	24.0
Total Inner Surface Area of U-tubes, m <sup>2</sup> (ft <sup>2</sup> )	171 (1840.6)	4214 (45359.1)	25
Length of steam generator tube (average), m (ft)	20.2 (66.3)	20.2 (66.3)	1.0

a,c

<b>Table 21.2-2 Standard Operational Setpoints of the ROSA-IV Large Scale Test Facility</b>	
<b>Event</b>	<b>Setpoint</b>
Reactor scram signal, MPa (psia)	12.97 (1881.1)
Initiation of RCP coastdown	With reactor scram
Safety injection signal, MPa (psia)	12.27 (1779.6)
High pressure charging <sup>(1)</sup>	12 s after safety injection signal
Safety injection	17 s after safety injection signal
High pressure injection cutoff, MPa (psia) <sup>(2)</sup>	10.7 (1551.9)
Low pressure injection cutoff, MPa (psia) <sup>(3)</sup>	1.29 (187.1)
Accumulator injection, MPa (psia)	4.51 (654.1)
Main feedwater termination	With reactor scram
Turbine throttle valve closure	With reactor scram
Auxiliary feedwater initiation <sup>(4)</sup>	28 s after reactor scram
<b>Notes:</b>	
1. High-pressure charging was not actuated during the SB-CL-18 and SB-CL-14.	
2. High-pressure injection was not actuated during the SB-CL-18 test and SB-CL-14.	
3. The SB-CL-18 test was terminated prior to the actuation of low-pressure injection.	
4. Auxiliary feedwater was not actuated during the SB-CL-18 test.	

<b>Parameter</b>	<b>Target (Measured)</b>	<b>a,c</b>
Pressurizer pressure, MPa (psia)	15.5 (2248)	
Hot leg fluid temperature, K (°F)	599 (619)	
Cold leg fluid temperature, K (°F)	564(555)	
Core power, MW (MBTU/hr)	10	
Core inlet flow rate, kg/sec (lbm/s)	48.7 (107.3)	
HL-to-DC Leakage Flow Rate, kg/sec (% core flow)	0.124 (0.25%)	
DC-to-UH Bypass Flow Rate, kg/sec/sec (% core flow)	0.146 (0.3%)	
Pressurizer water level, m (ft)	2.6 (8.5)	
Pump speed, rad/sec (rpm) For Pump A For Pump B	80.5 (769) 83.3 (796)	
Hot leg $\Delta P$ , kPa (psi) For Loop A For Loop B	3.62 (0.53) 3.50 (0.50)	
Steam generator inlet to outlet, kPa (psi) For Loop A For Loop B	1.35 (0.19) 1.46 (0.21)	
Cross-Over Leg Down $\Delta P$ , kPa (psi) For Loop A For Loop B	-45.3 (-6.57) N/A	
Cross-Over Leg Up $\Delta P$ , kPa (psi) For Loop A For Loop B	26.6 (3.86) 26.6 (3.86)	
Downcomer $\Delta P$ , kPa (psi)	61.5 (8.92)	
Downcomer to upper plenum $\Delta P$ , kPa (psi)	2.65 (0.38)	
Lower Plenum $\Delta P$ , kPa (psi)	12.9 (1.87)	
Core $\Delta P$ (including lower core plate), kPa (psi)	33.2 (4.8)	
Upper Plenum $\Delta P$ , kPa (psi)	13.5 (1.96)	
Steam generator secondary pressure, MPa (psia)	7.35 (1066)	
Steam generator secondary level, m (ft)	10.6 (34.8)	
Steam generator feedwater temperature, K (°F)	494 (429.5)	
Steam generator feedwater flow rate, kg/sec (lbm/s)	2.7 (5.95)	
Steam generator secondary circulation flow, kg/sec (lbm/s)	16.5 (36.3)	

<b>Test Time</b>	<b>WC/T Time</b>	<b>Test Power</b>	<b>Normalized Power</b>
<b>sec</b>	<b>sec</b>	<b>MW</b>	<b>-</b>
<b>(1)</b>	<b>(2)</b>	<b>(3)</b>	<b>(4)</b>
0	300.0	10.022	1.00000
46.6	346.6	10.025	1.00030
57.6	357.6	8.8175	0.87981
77.6	377.6	7.2675	0.72516
97.6	397.6	6.0925	0.60791
117.6	417.6	5.1775	0.51661
167.6	467.6	3.6325	0.36245
217.6	517.6	2.8650	0.28587
417.6	717.6	1.7925	0.17886
617.6	917.6	1.5800	0.15765
817.6	1117.6	1.5100	0.15067
899.6	1199.6	1.4750	0.14718











<b>Table 21.7-1 JAERI (Full Conservative) Decay Heat Curve</b>		
<b>Time After Rx Trip</b>	<b>Test Power</b>	<b>Normalized Power</b>
<b>sec</b>	<b>MW</b>	<b>-</b>
<b>(1)</b>	<b>(2)</b>	<b>(3)</b>
-	10.000	1.00000
0	10.000	1.00000
29	10.000	1.00000
40	8.912	0.89120
60	7.344	0.73440
80	6.128	0.61280
100	5.200	0.52000
150	3.632	0.36320
200	2.848	0.28480
400	1.776	0.17760
600	1.568	0.15680
800	1.488	0.14880
1000	1.424	0.14240
1500	1.280	0.12800
2000	1.200	0.12000
4000	0.992	0.09920

Parameter	End of Stage 1 <small>a.c.</small>		End of Stage 2 (Prior to Drain) <small>a.c.</small>	
	Target		Target	
Core Power, MW	10.0		1.42	
Pressurizer Pressure, MPa	15.47 ±0.06		12.2	
Hot Leg Temperature, K	598 ±5		N/A	
Cold Leg Temperature, K	565 ±5		N/A	
Pump Speed, rad/sec (rpm)	85.8/86.1 (819/822)		0.00/0.00	
Total Loop Flow Rate, kg/sec	51.0 (±0.6)		11.4	
DC-to-UH Bypass Flow Rate, % total core (kg/sec)	0.9% (0.46)		N/A	
Core Inlet Flow Rate, kg/sec	50.54		N/A	
SG Secondary Pressure, MPa	7.38/7.42 (±0.03)		6.5	
SG Steam Flow Rate, kg/sec	2.6 (±0.1)		N/A	

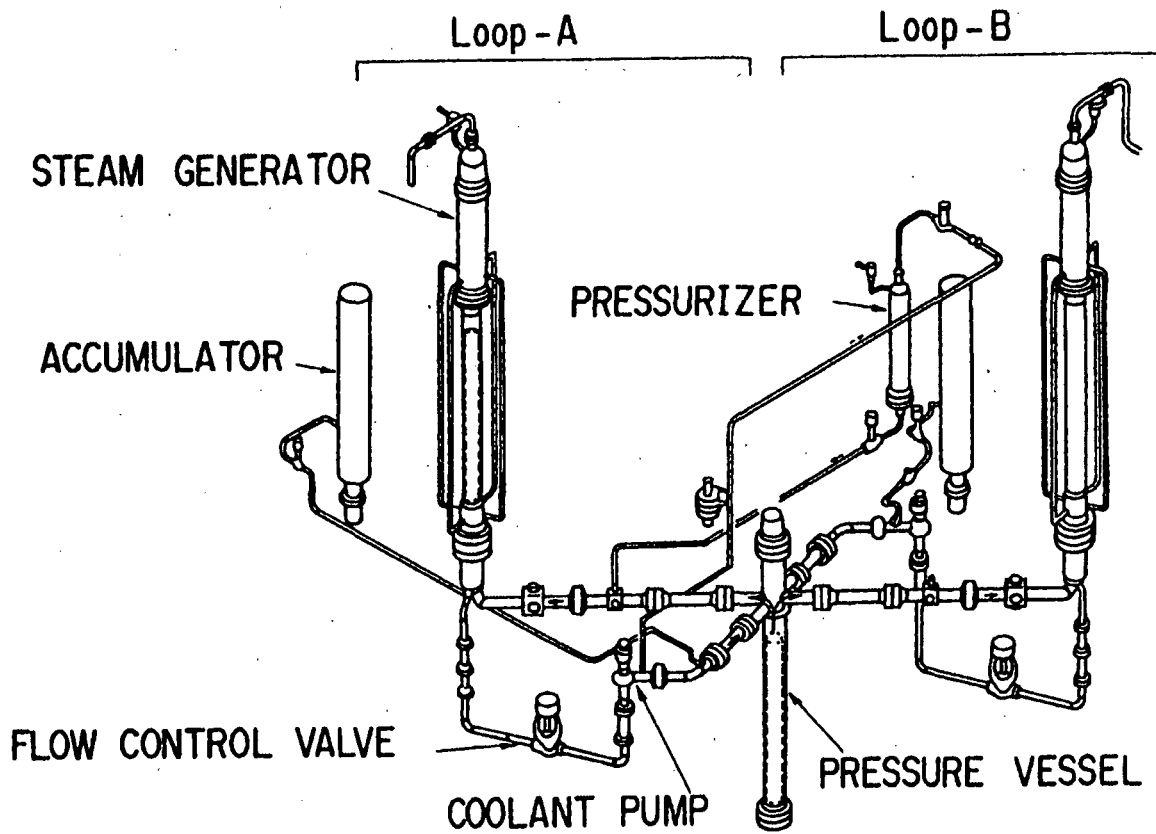
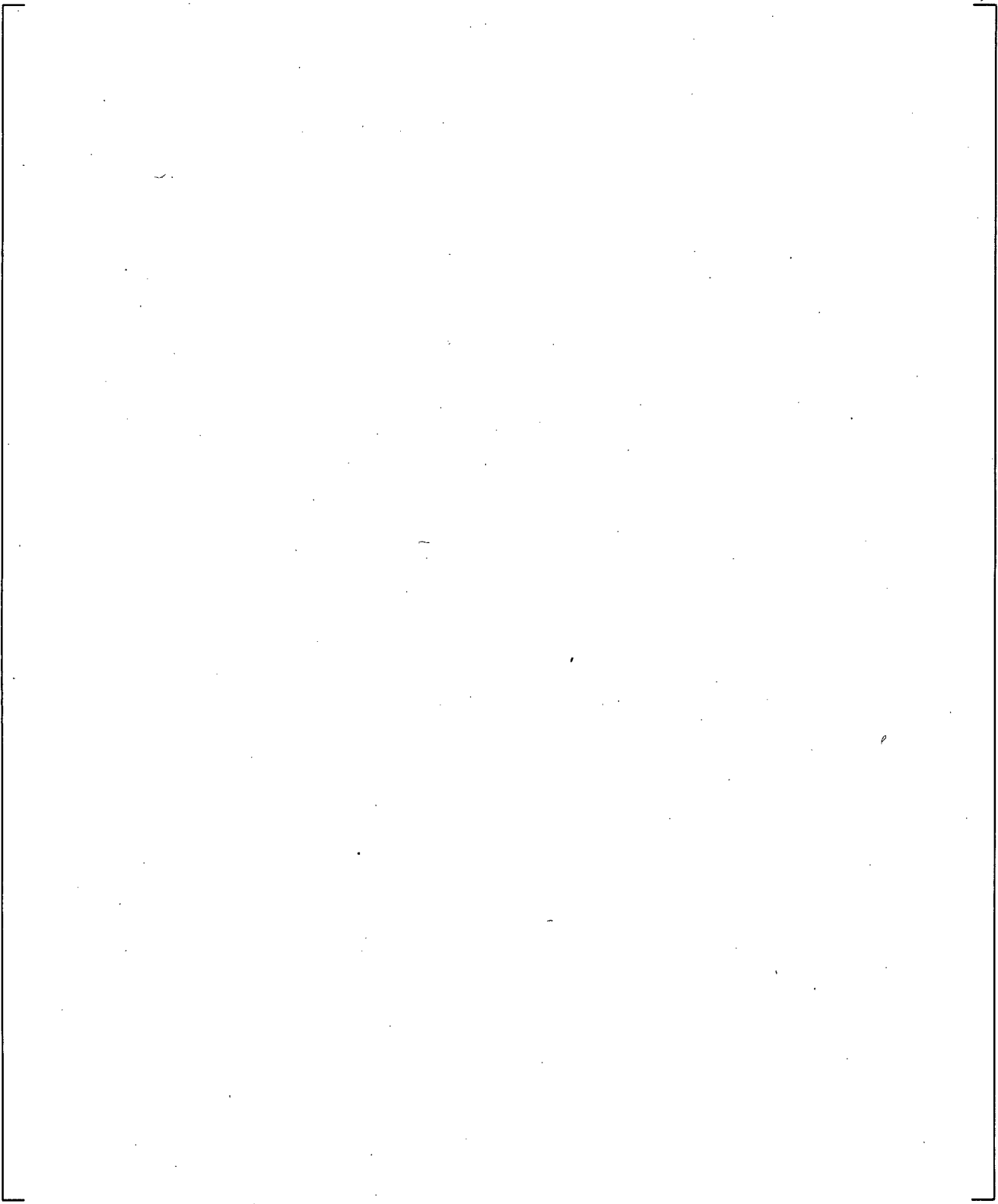
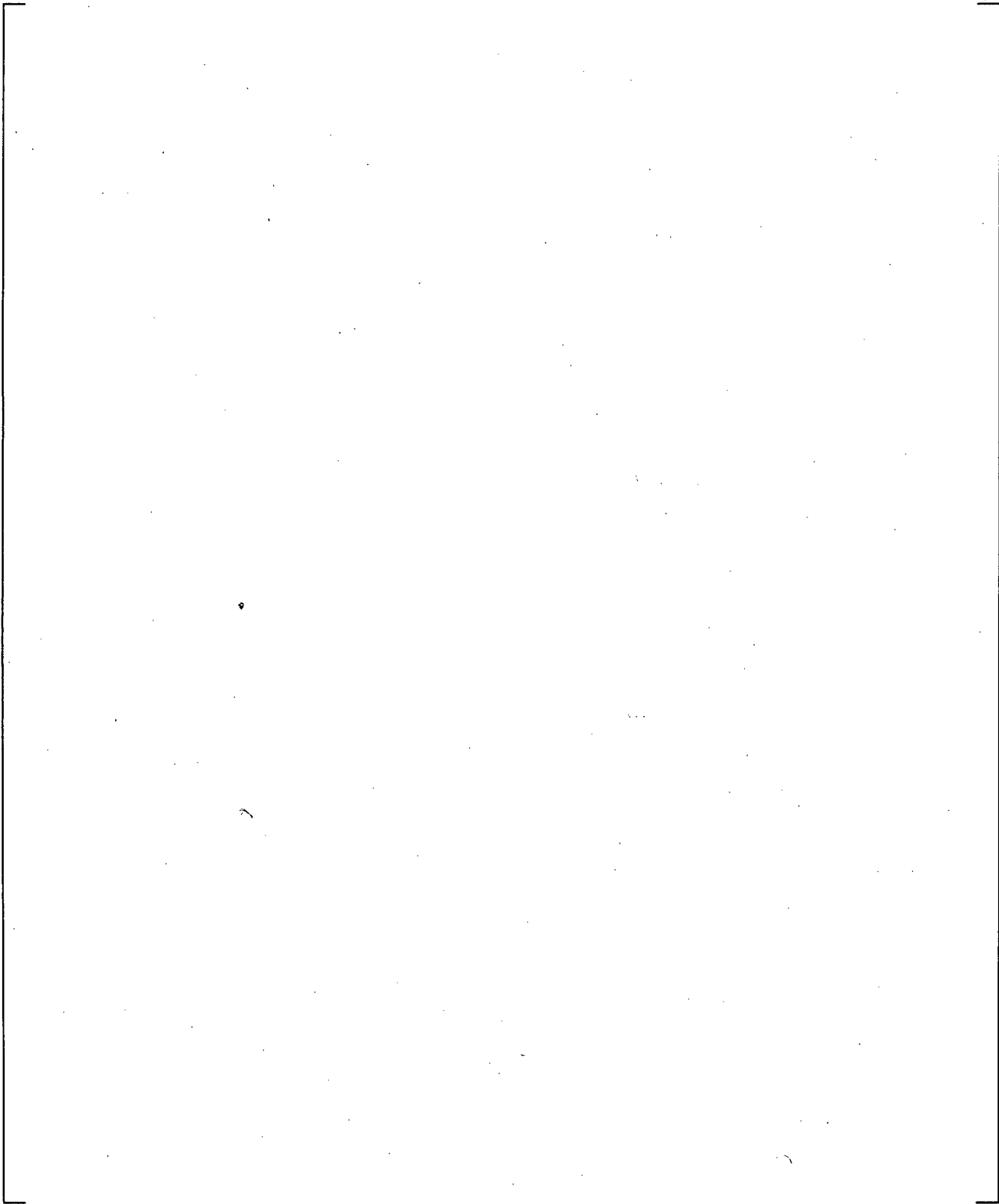


Figure 21.2-1 Schematic Diagram of LSTF

a,c



**Figure 21.3-1 WCOBRA/TRAC-TF2 Model of LSTF Pressure Vessel**



**Figure 21.3-2 LSTF Pressure Vessel Sections 1 and 2**

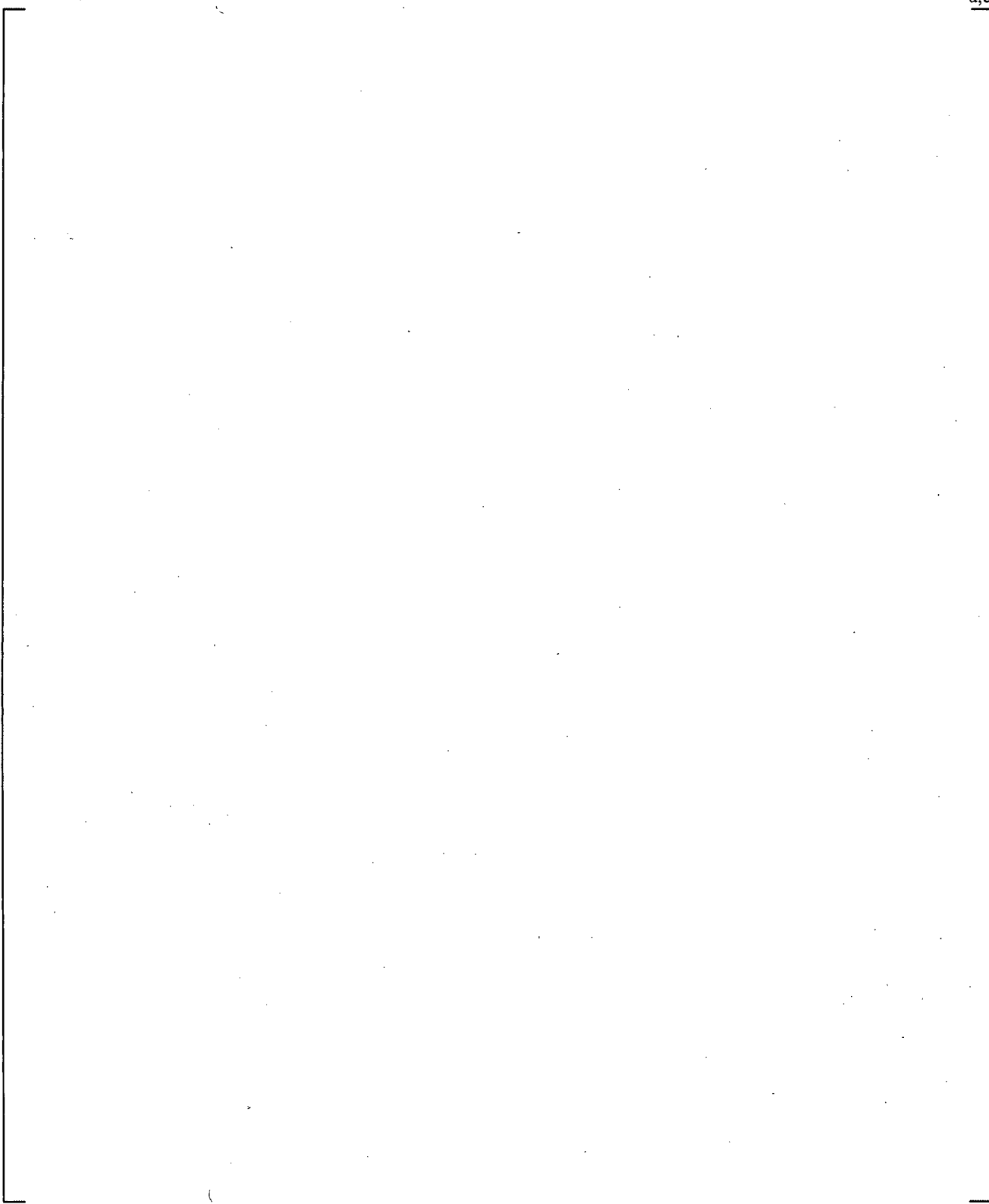


**Figure 21.3-3 LSTF Pressure Vessel Sections 3 and 4**

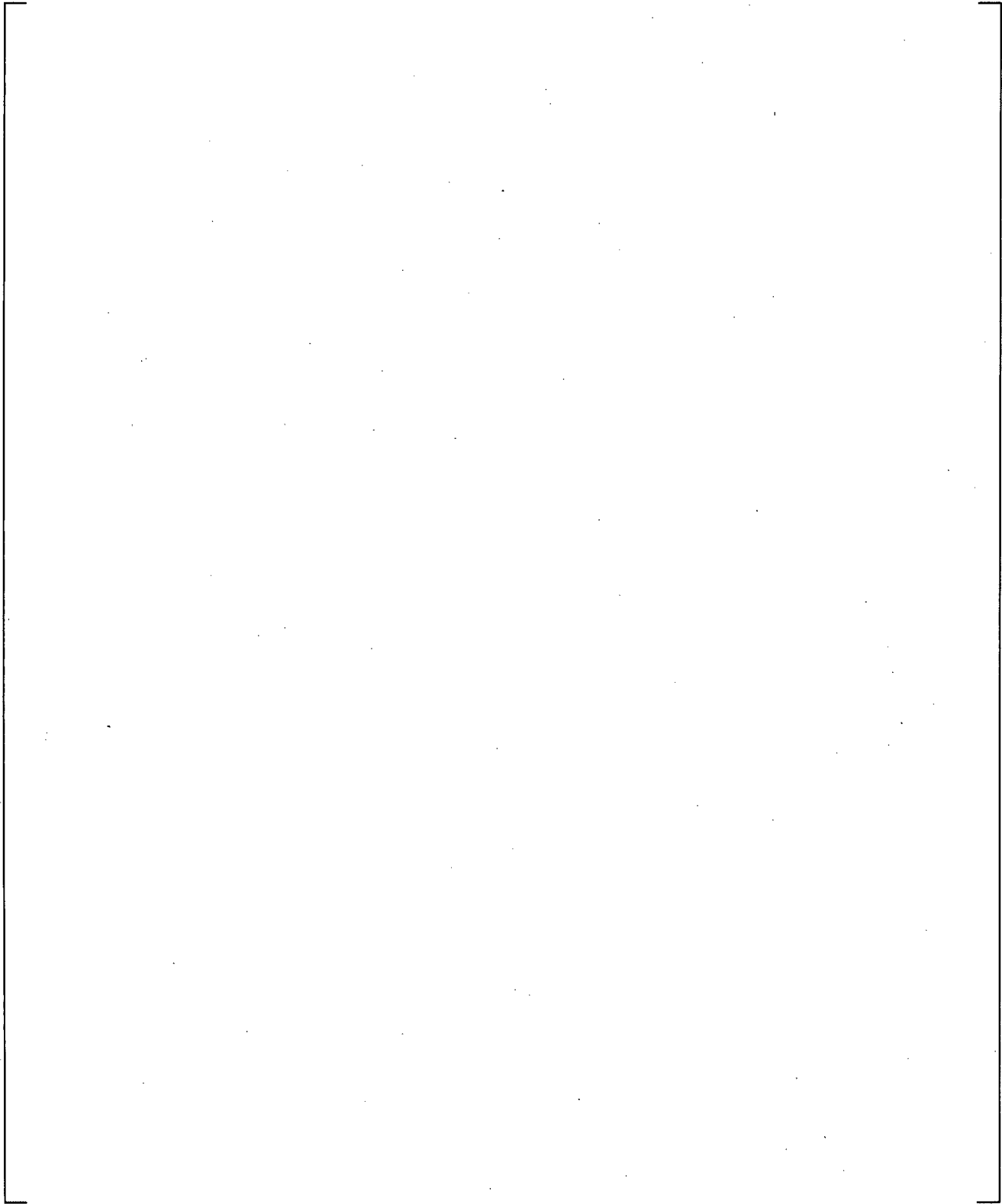


**Figure 21.3-4 LSTF Pressure Vessel Sections 5 and 6**

a,c

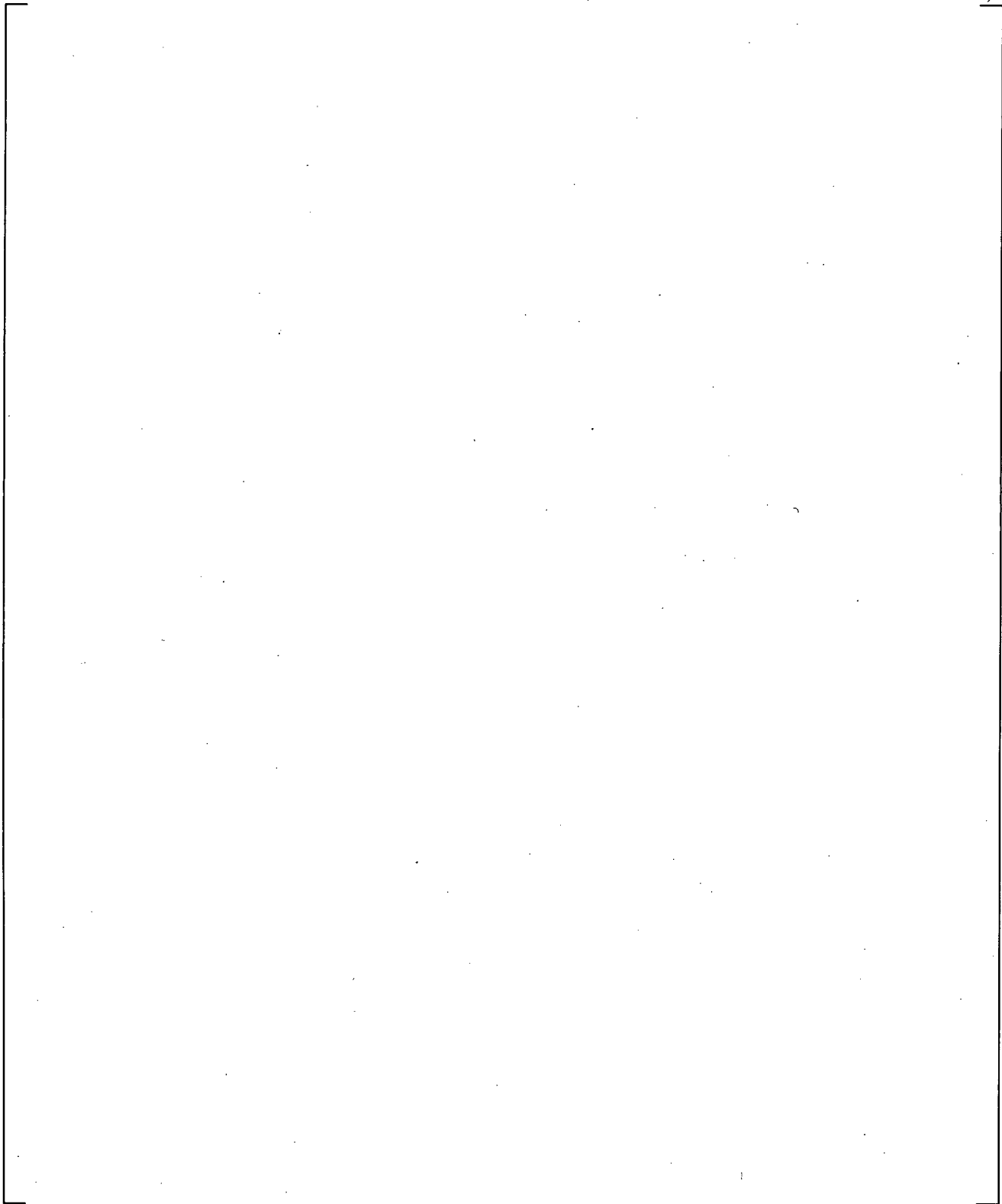


**Figure 21.3-5 LSTF Pressure Vessel Sections 7 and 8**

**Figure 21.3-6 LSTF Pressure Vessel Sections 9 and 10**

a,c

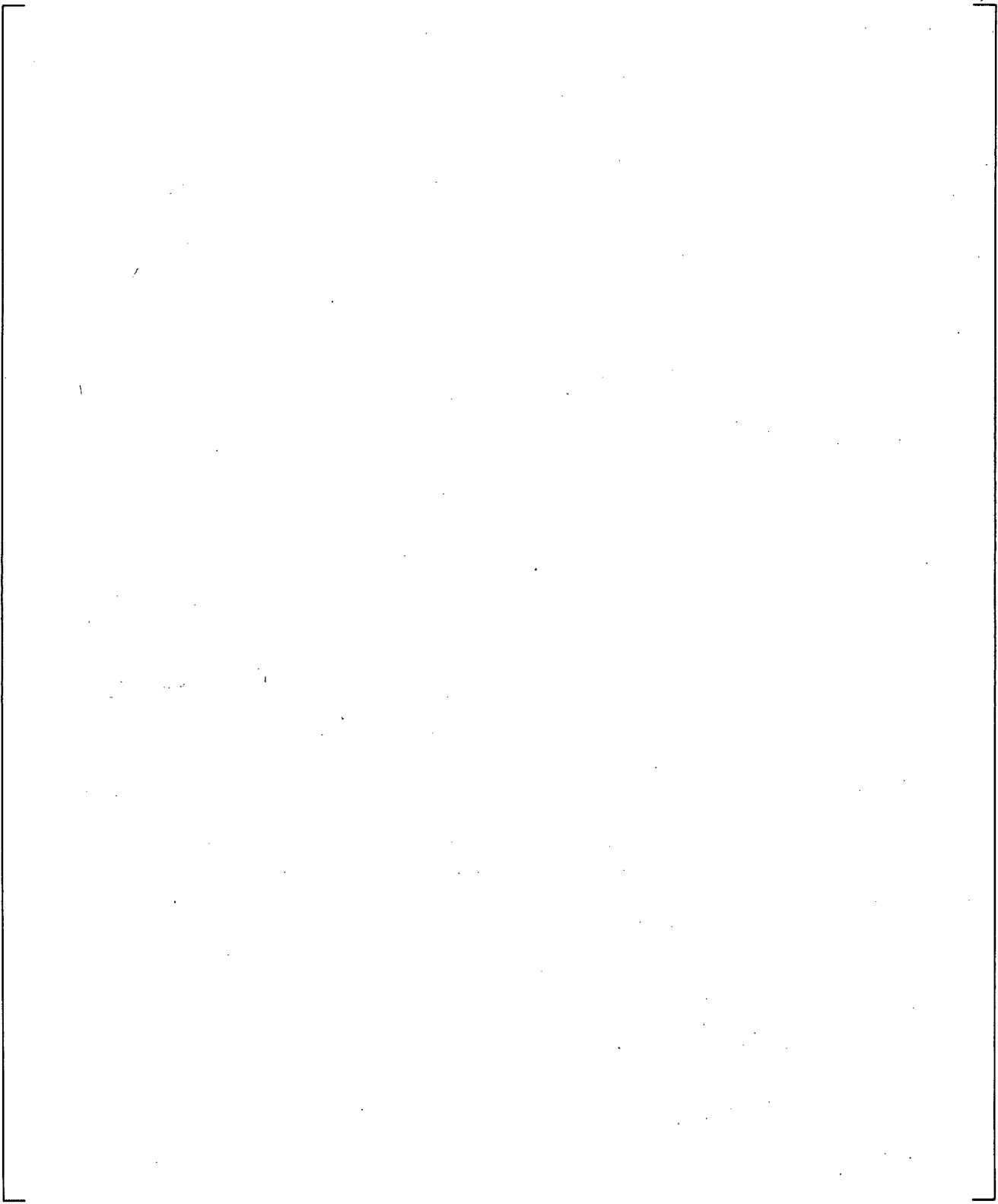


**Figure 21.3-7 ROSA-IV LSTF Core Simulator Map**

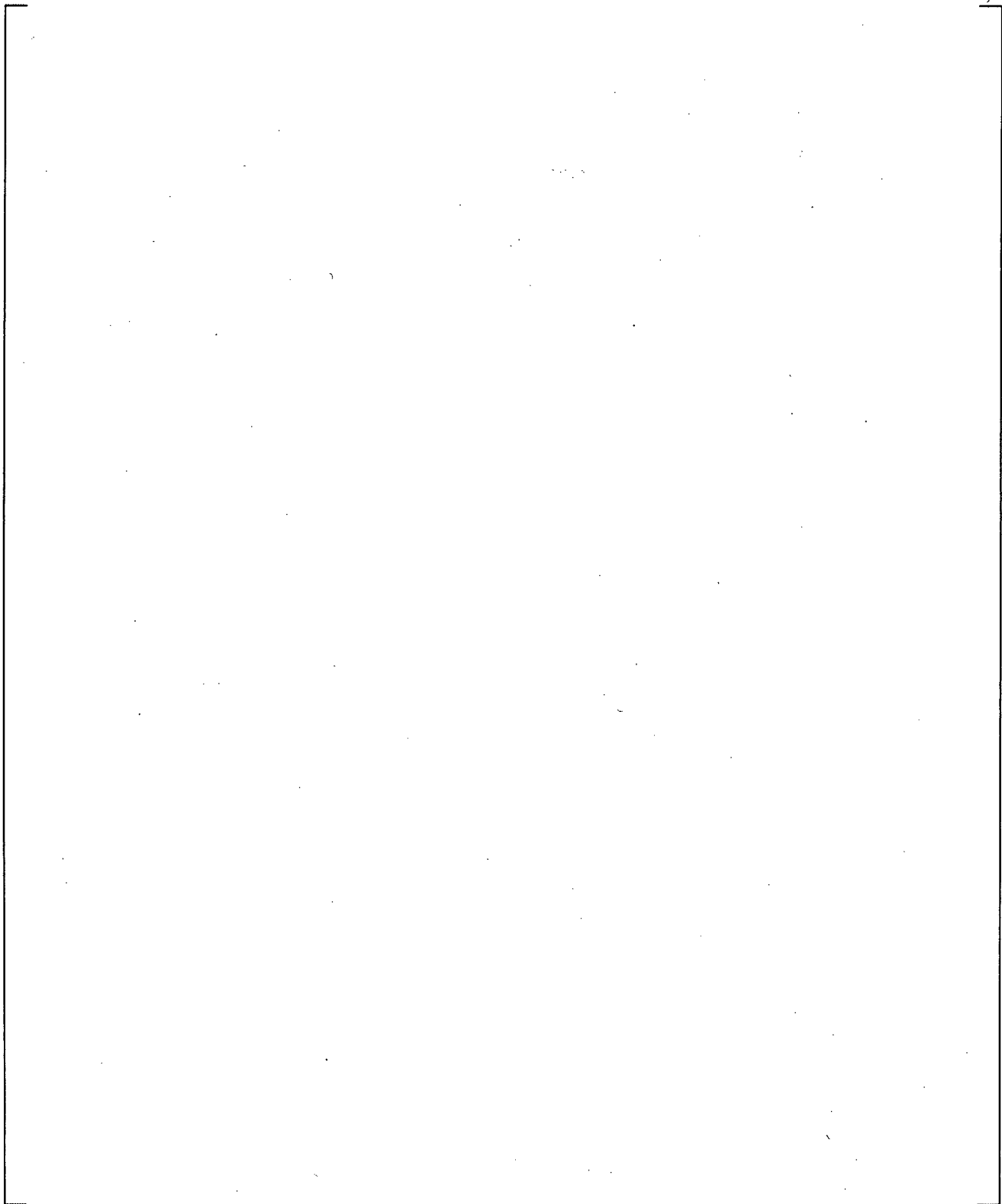


**Figure 21.3-8 WCOBRA/TRAC-TF2 Loop Noding Diagram of LSTF**

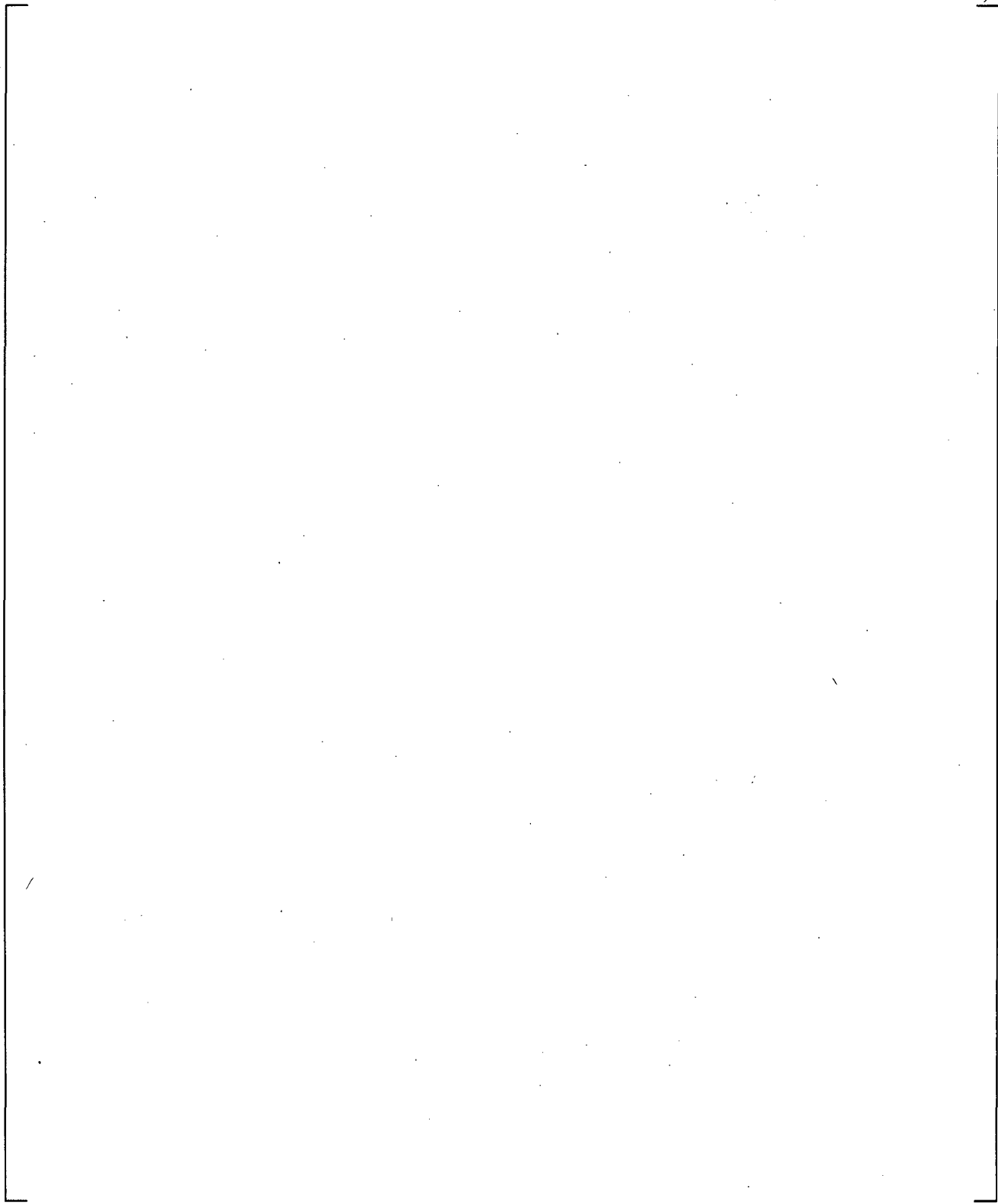


**Figure 21.3-9 Hot Leg (Including Pressurizer), Steam Generator and Cross-Over Leg Noding**

a,c

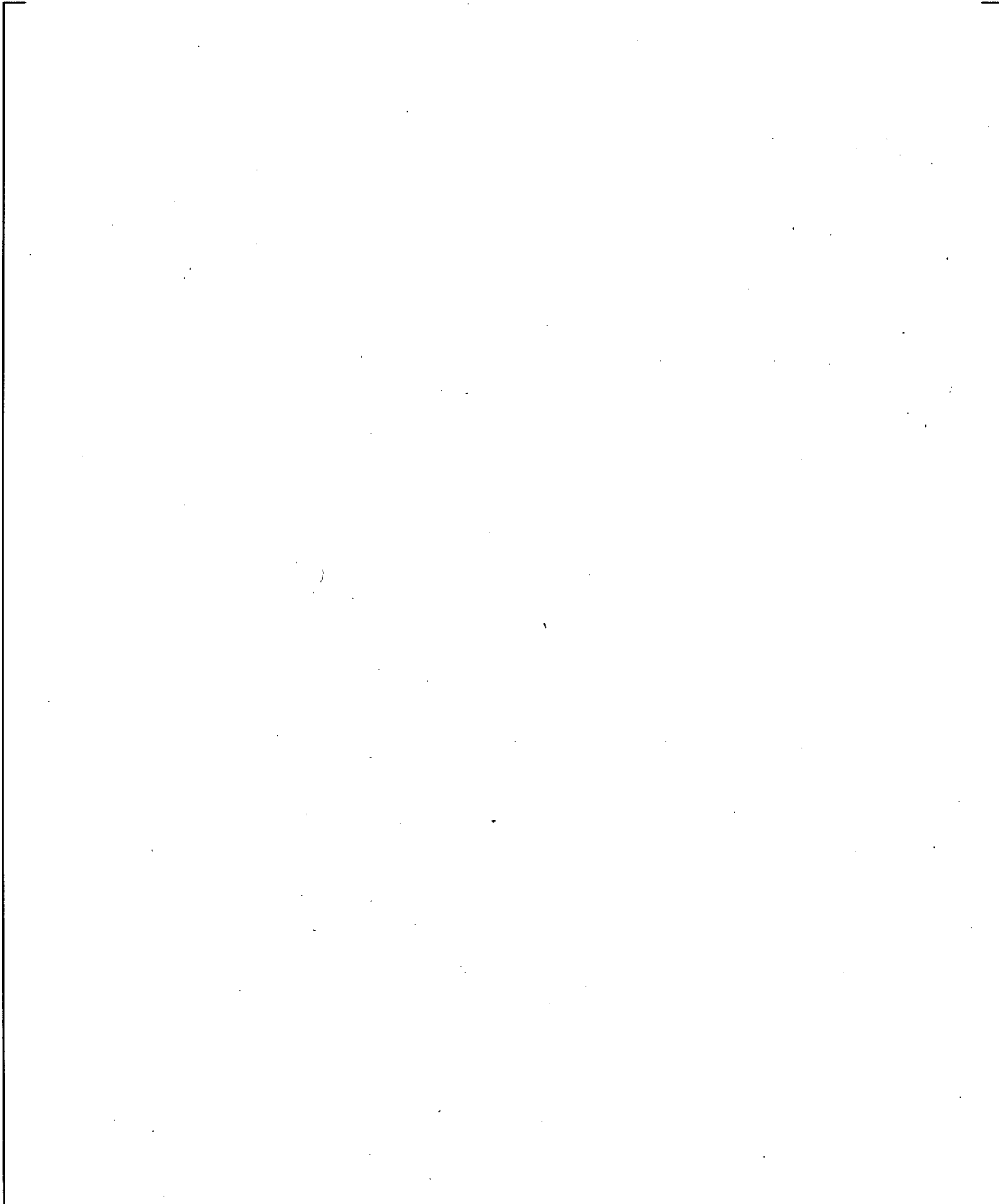


**Figure 21.4-1 Pressurizer Pressure**

a,c



**Figure 21.4-2 Break Flows**

a,c

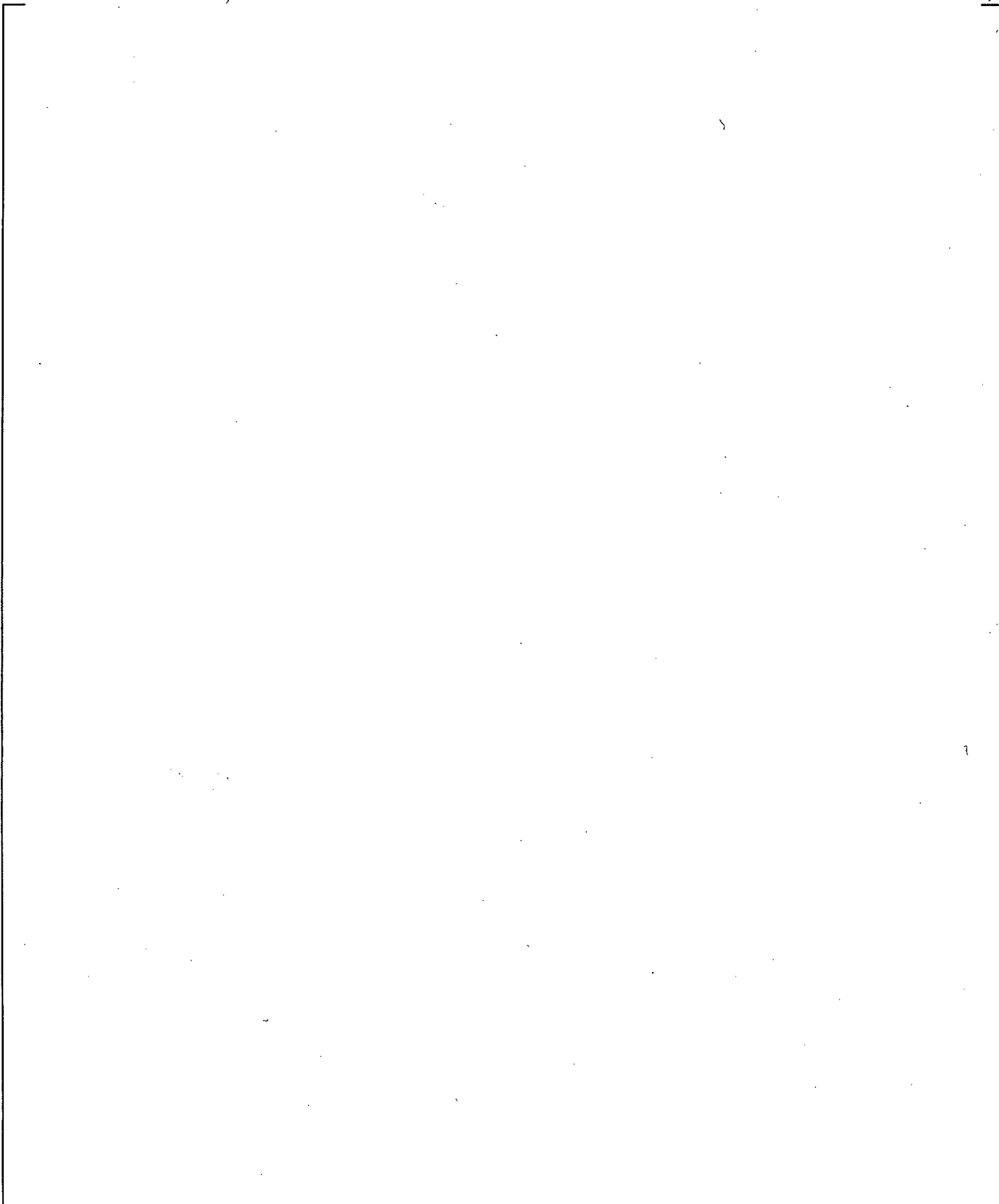


**Figure 21.4-3 Cross-Over Leg A Differential Pressures**

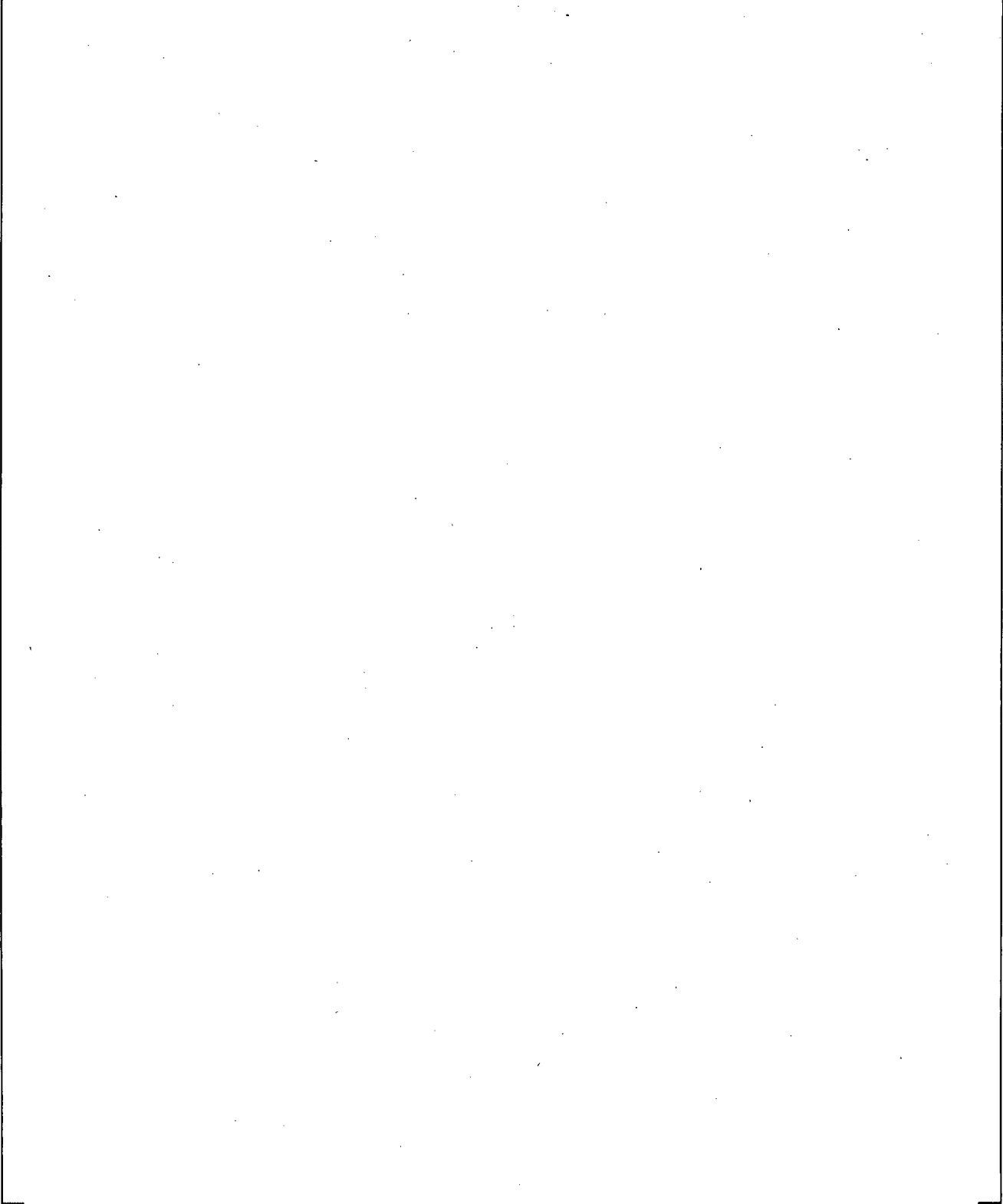


**Figure 21.4-4 Cross-Over Leg B Differential Pressures**

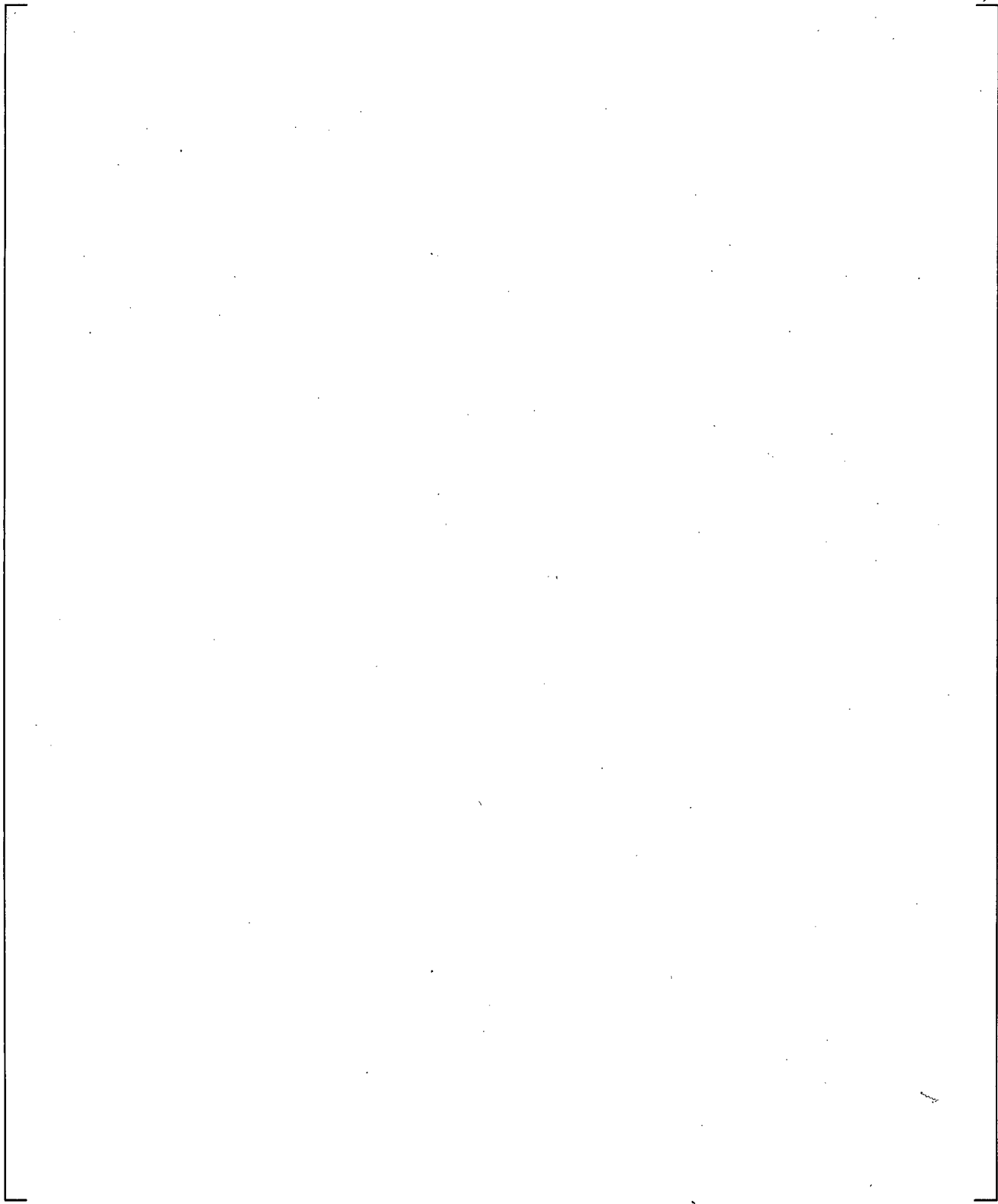


**Figure 21.4-5 Inner Vessel Differential Pressures**

a,c

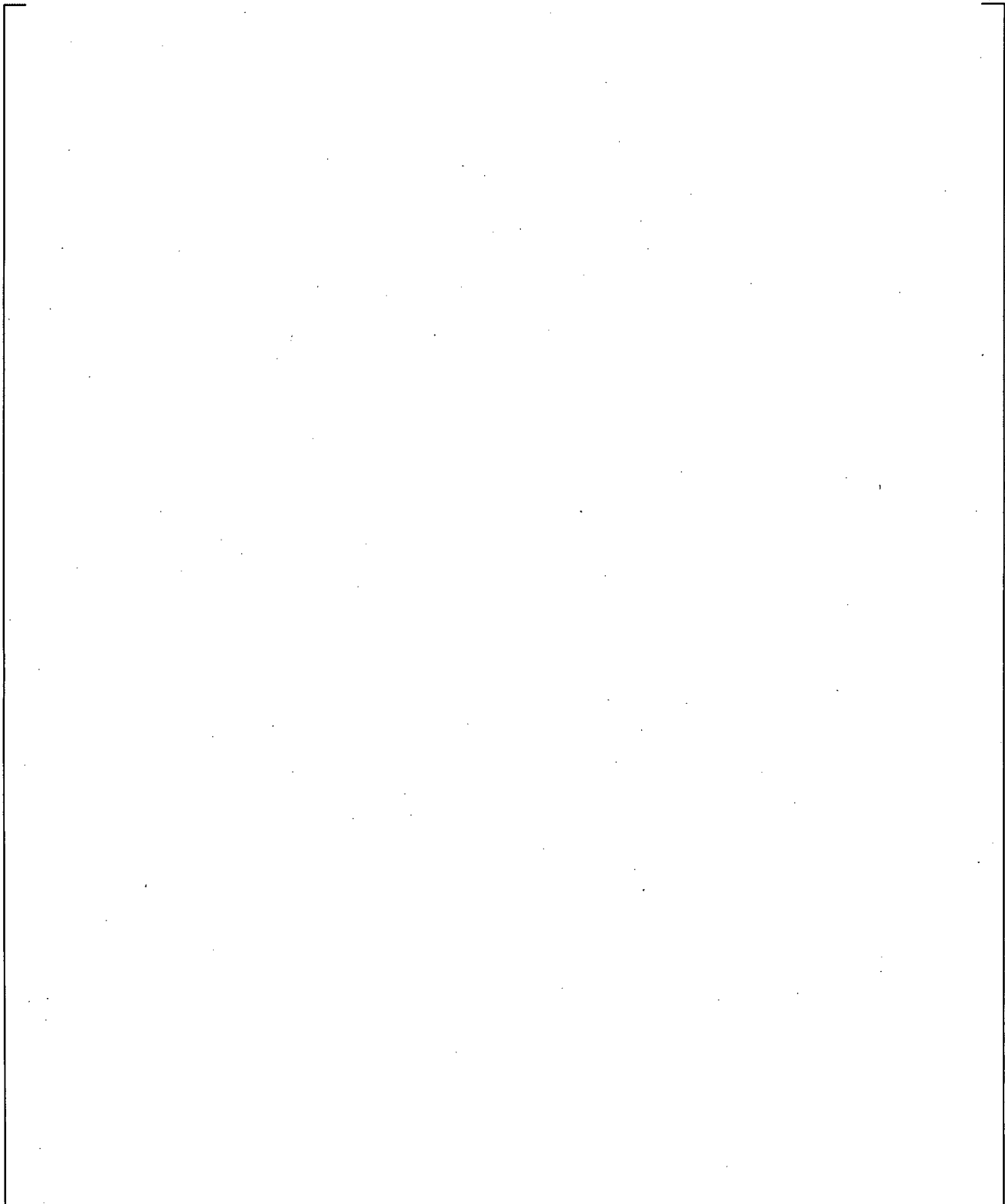


**Figure 21.4-6 Calculated and Measured Peak Cladding Temperatures**

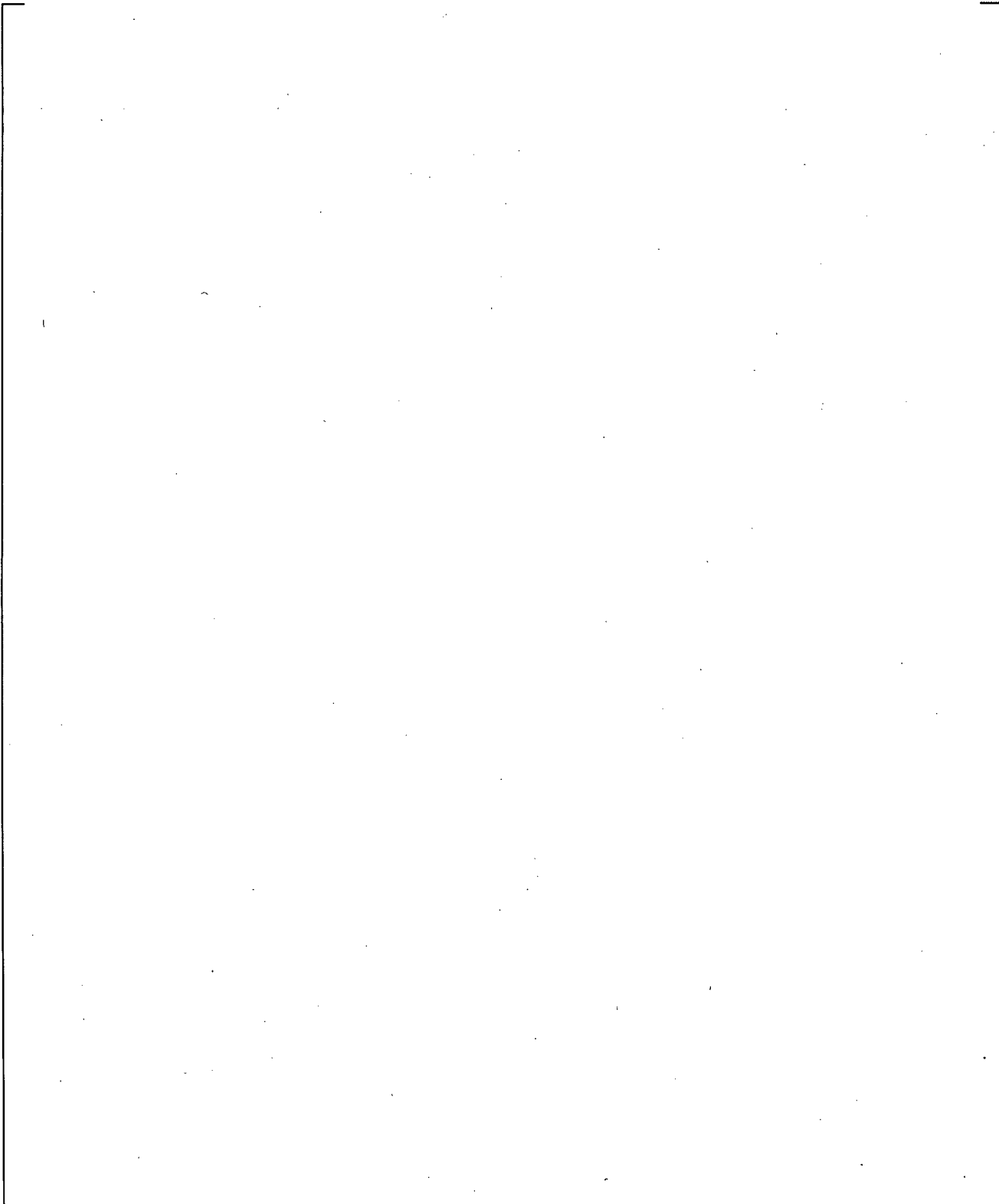


**Figure 21.4-7 SG-A U-tube Upflow Side Differential Pressures**

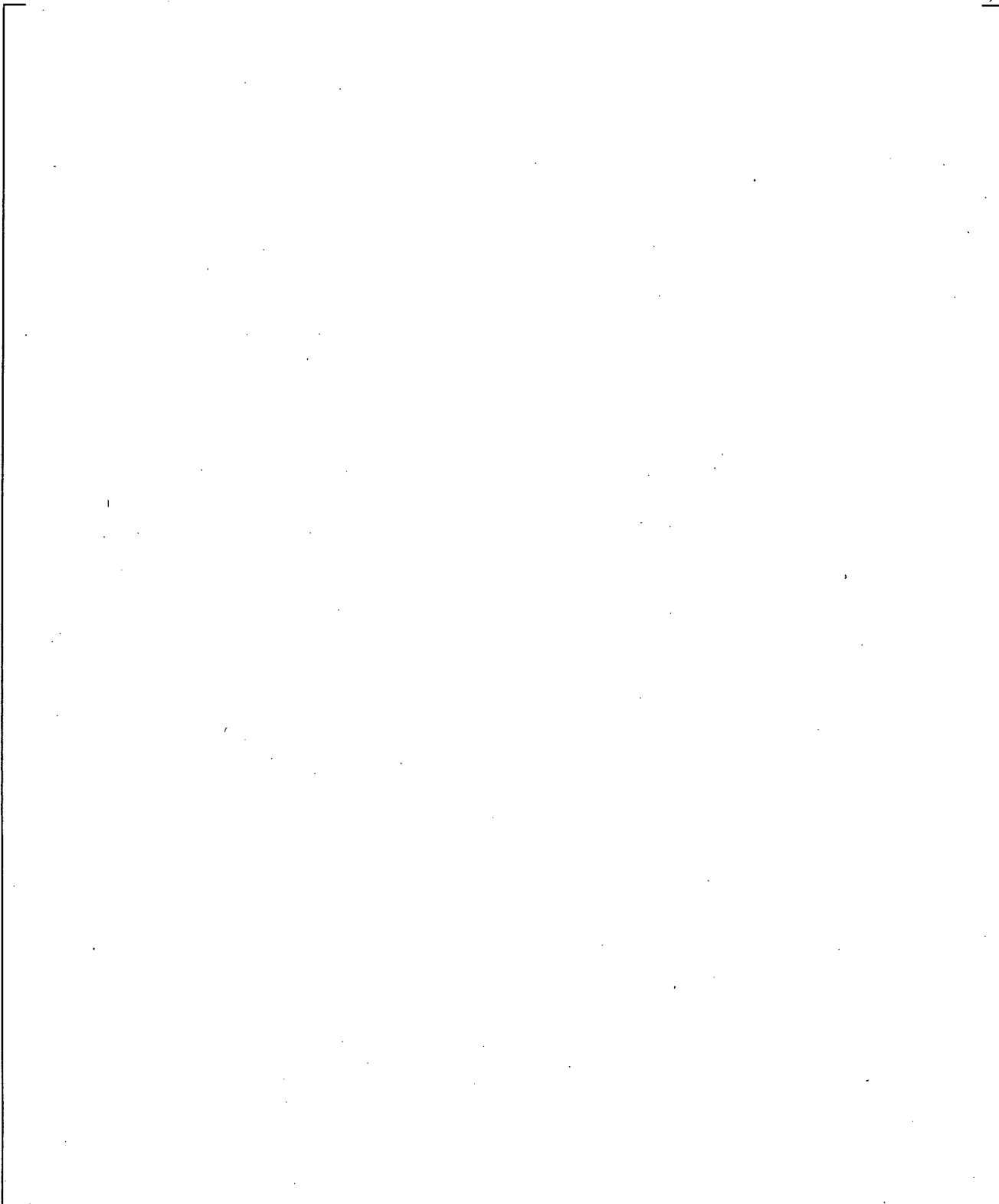


**Figure 21.4-8 SG-B U-tube Upflow Side Differential Pressures**

a,c

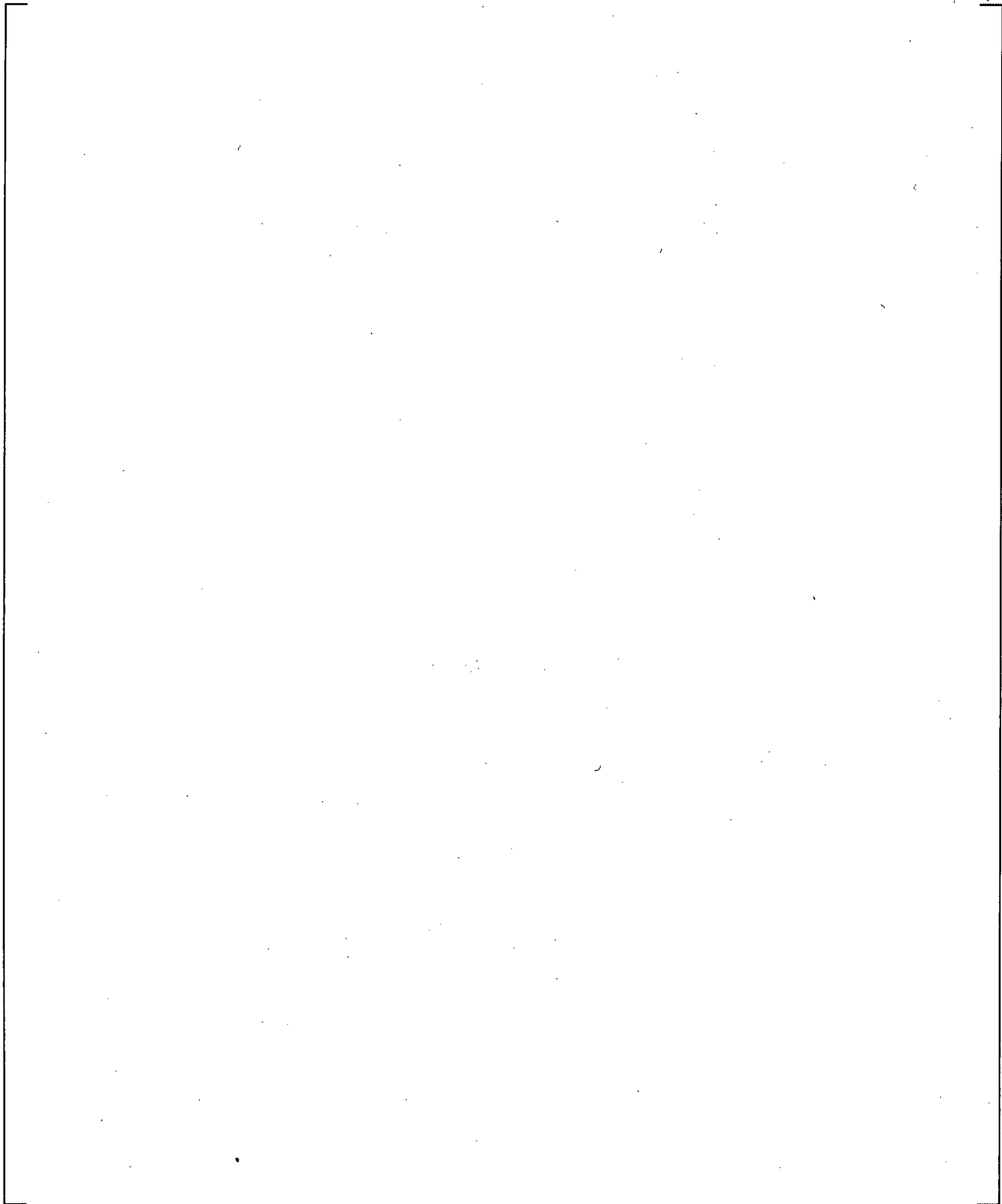


**Figure 21.4-9 SG-A U-tube Downflow Side Differential Pressures**

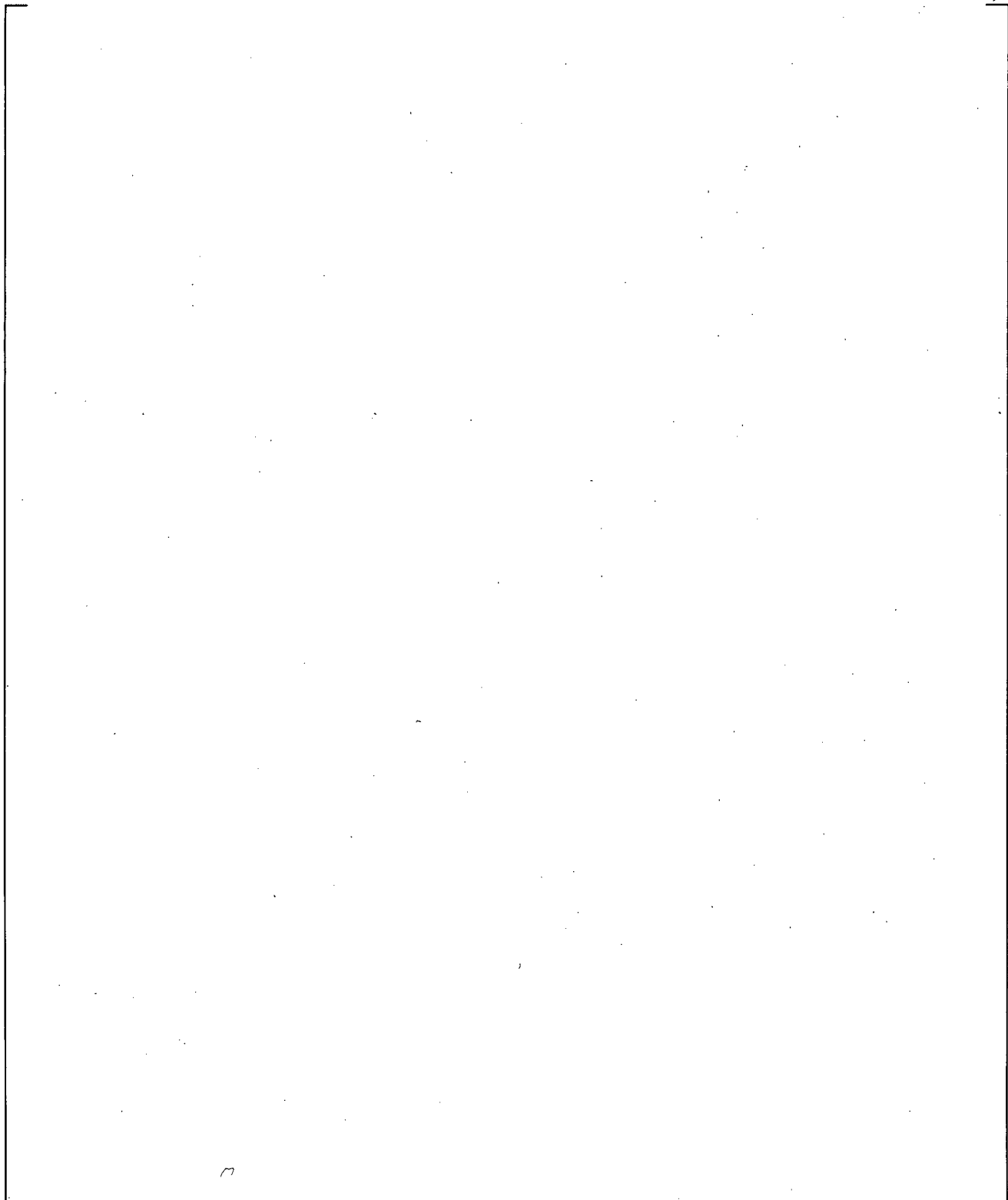


**Figure 21.4-10 SG-B U-tube Downflow Side Differential Pressures**

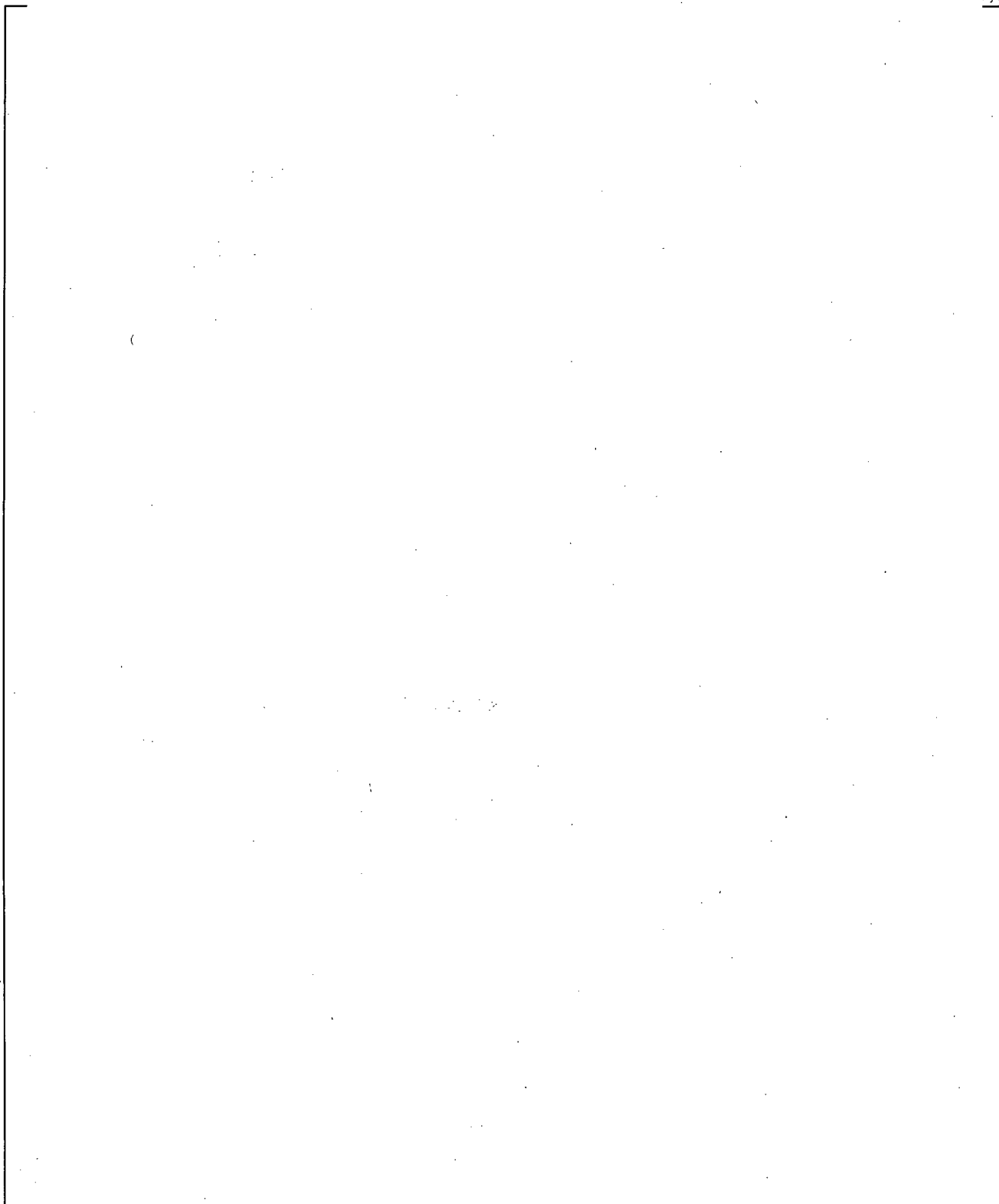


**Figure 21.4-11 SG-A Inlet-to-Outlet Differential Pressures**

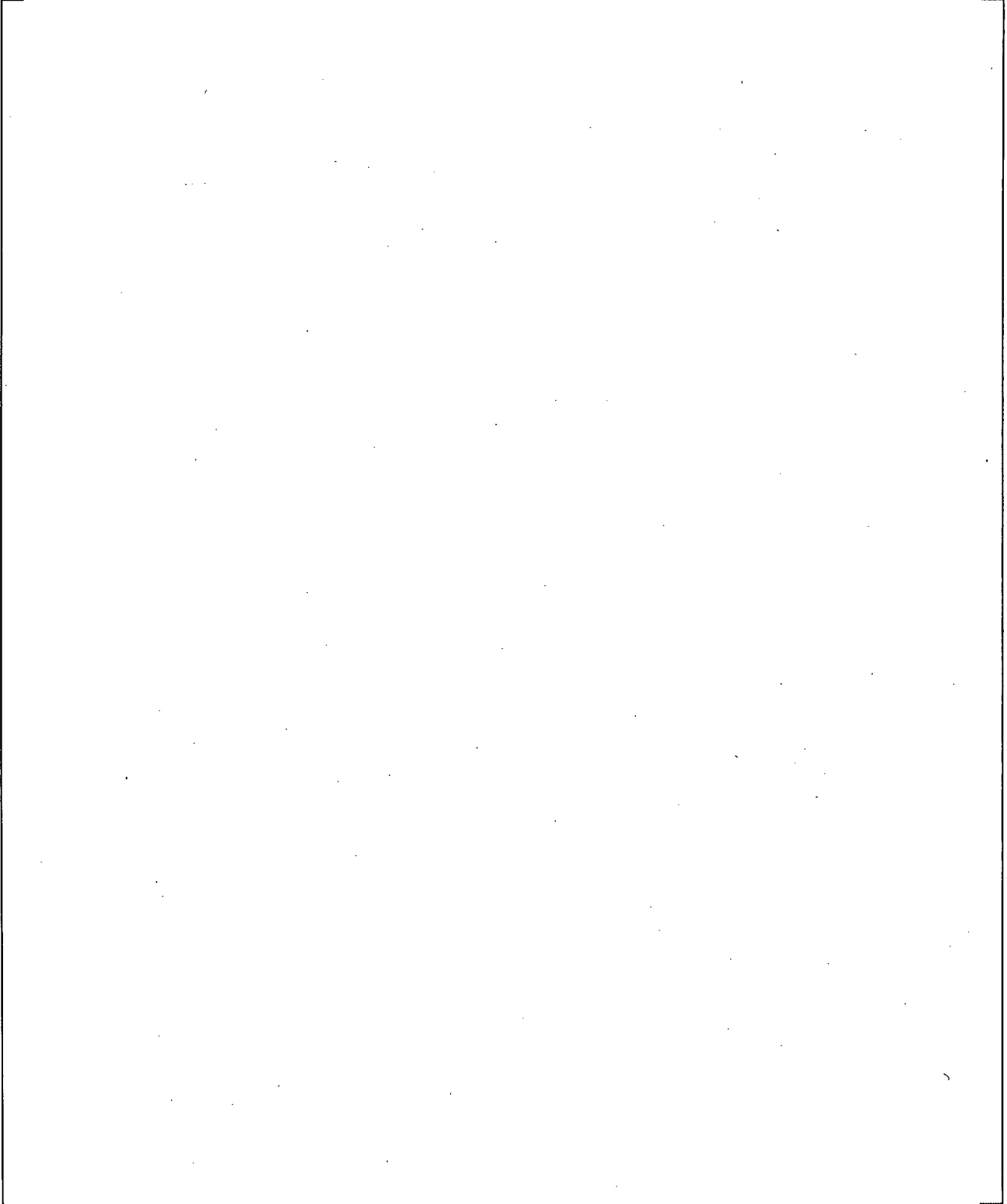


**Figure 21.4-12 SG-B Inlet-to-Outlet Differential Pressures**

a,c

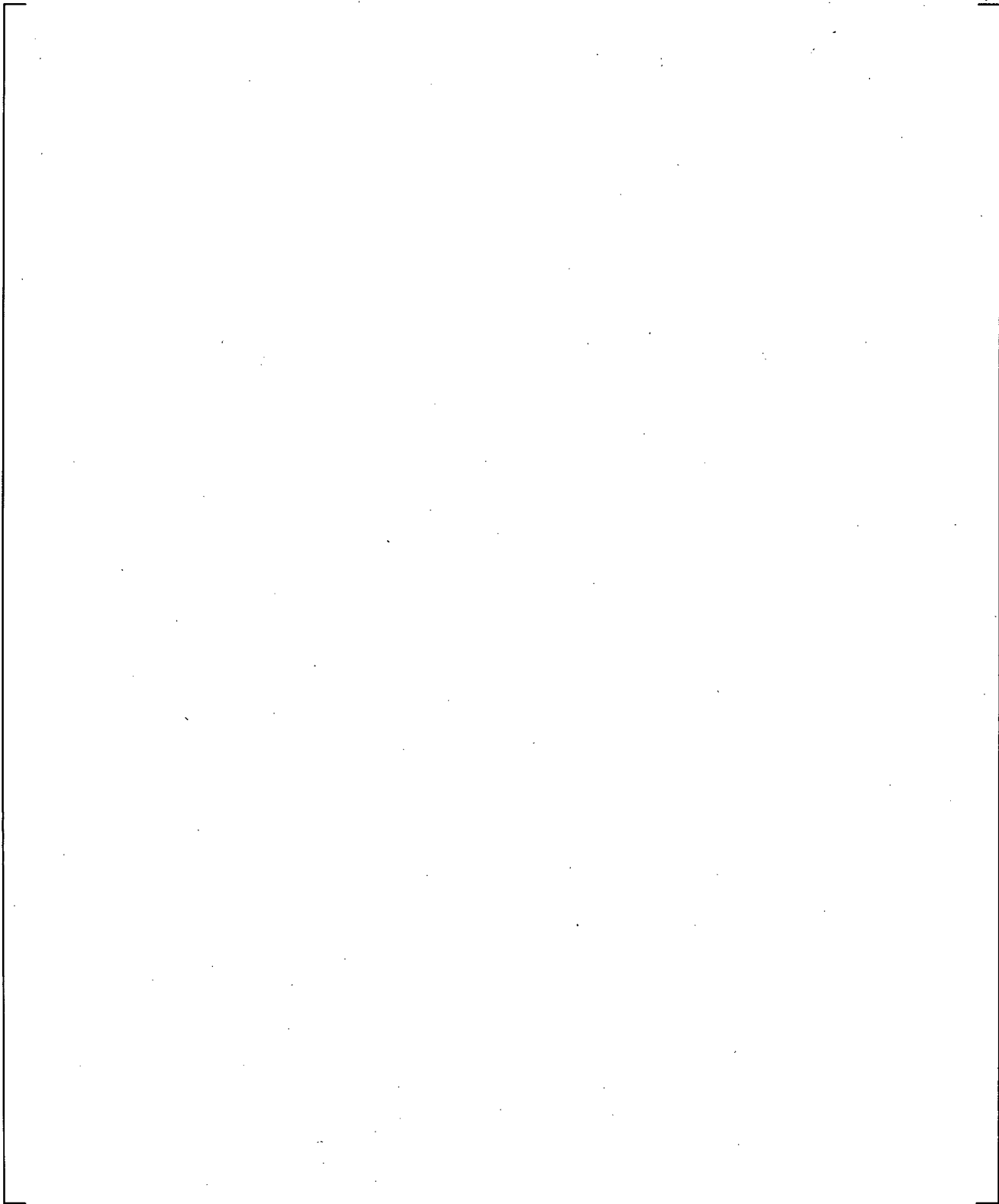


**Figure 21.4-13 SG-A Inlet Plenum Collapsed Liquid Levels**

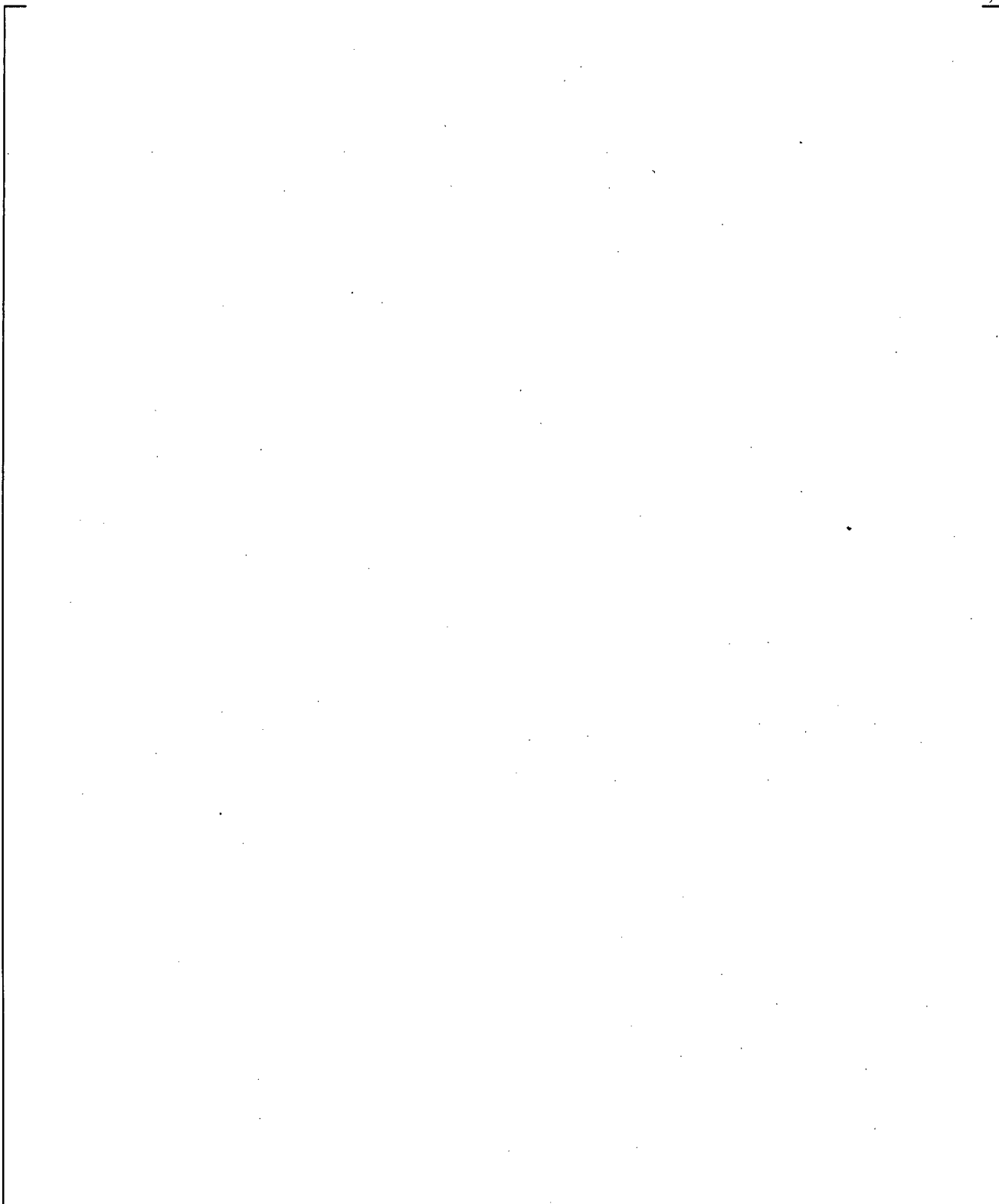


**Figure 21.4-14 SG-B Inlet Plenum Collapsed Liquid Levels**

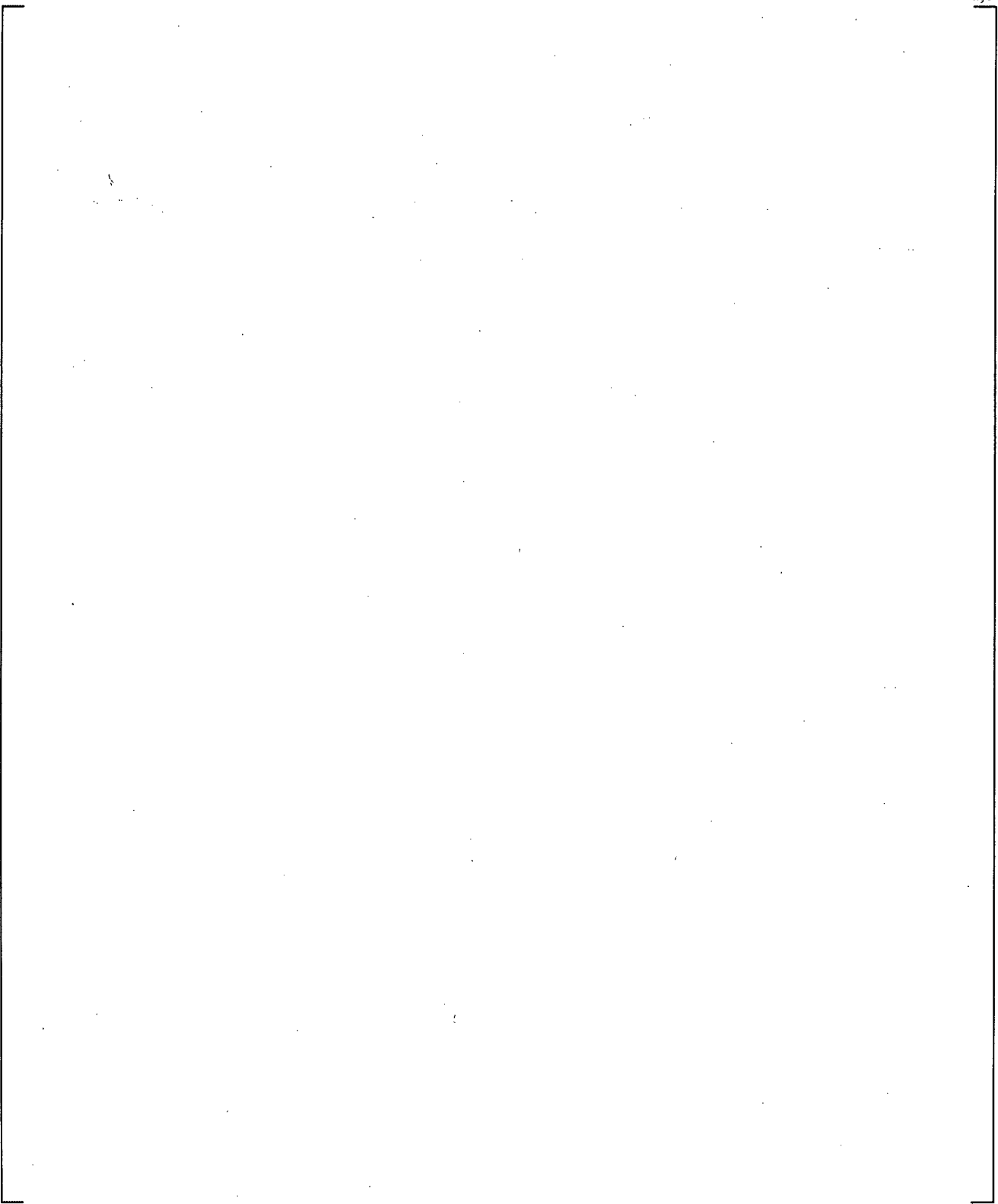


**Figure 21.4-15 Upper Plenum to SG-A Inlet Differential Pressures**

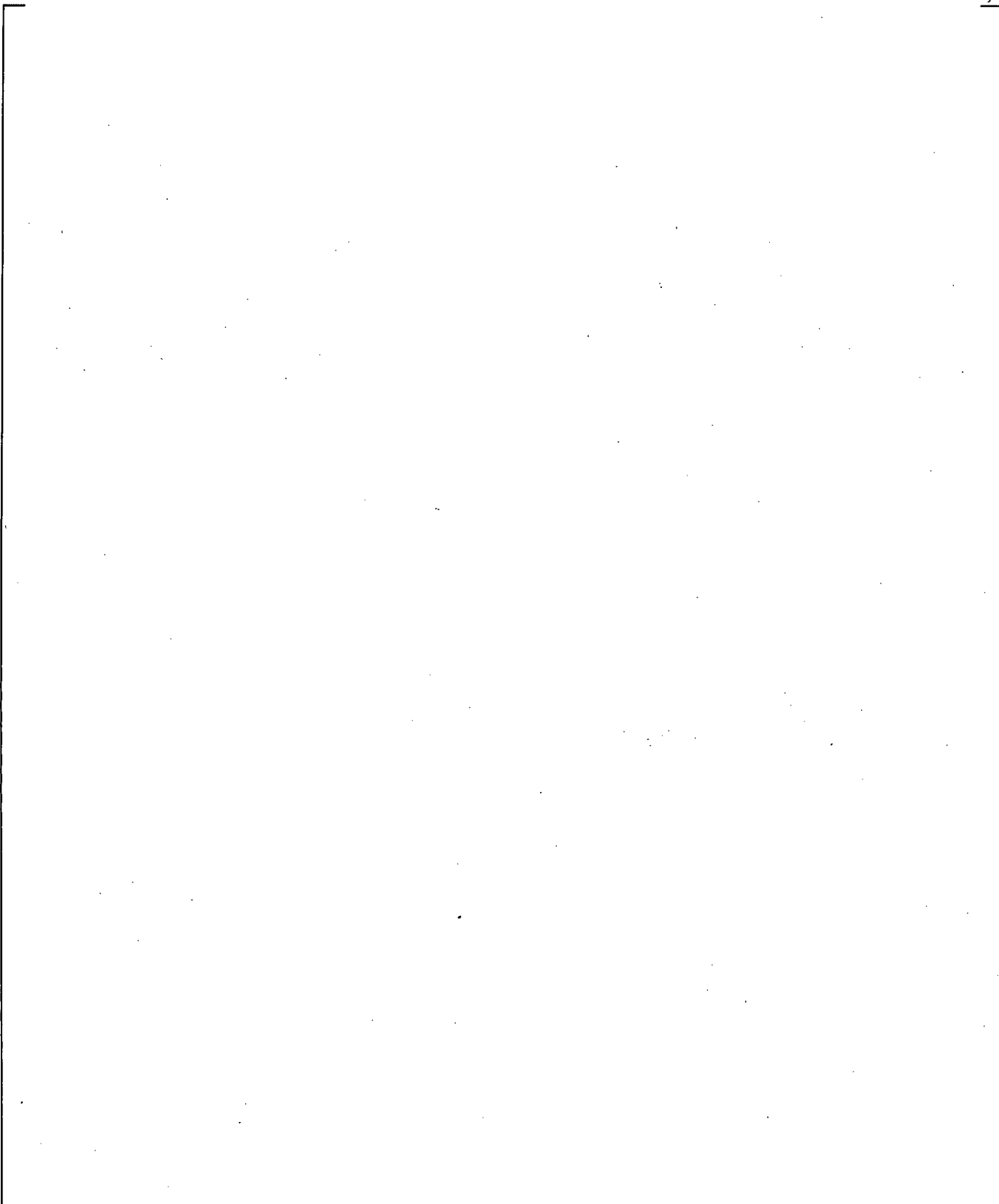


**Figure 21.4-16 Upper Plenum to SG-B Inlet Differential Pressures**

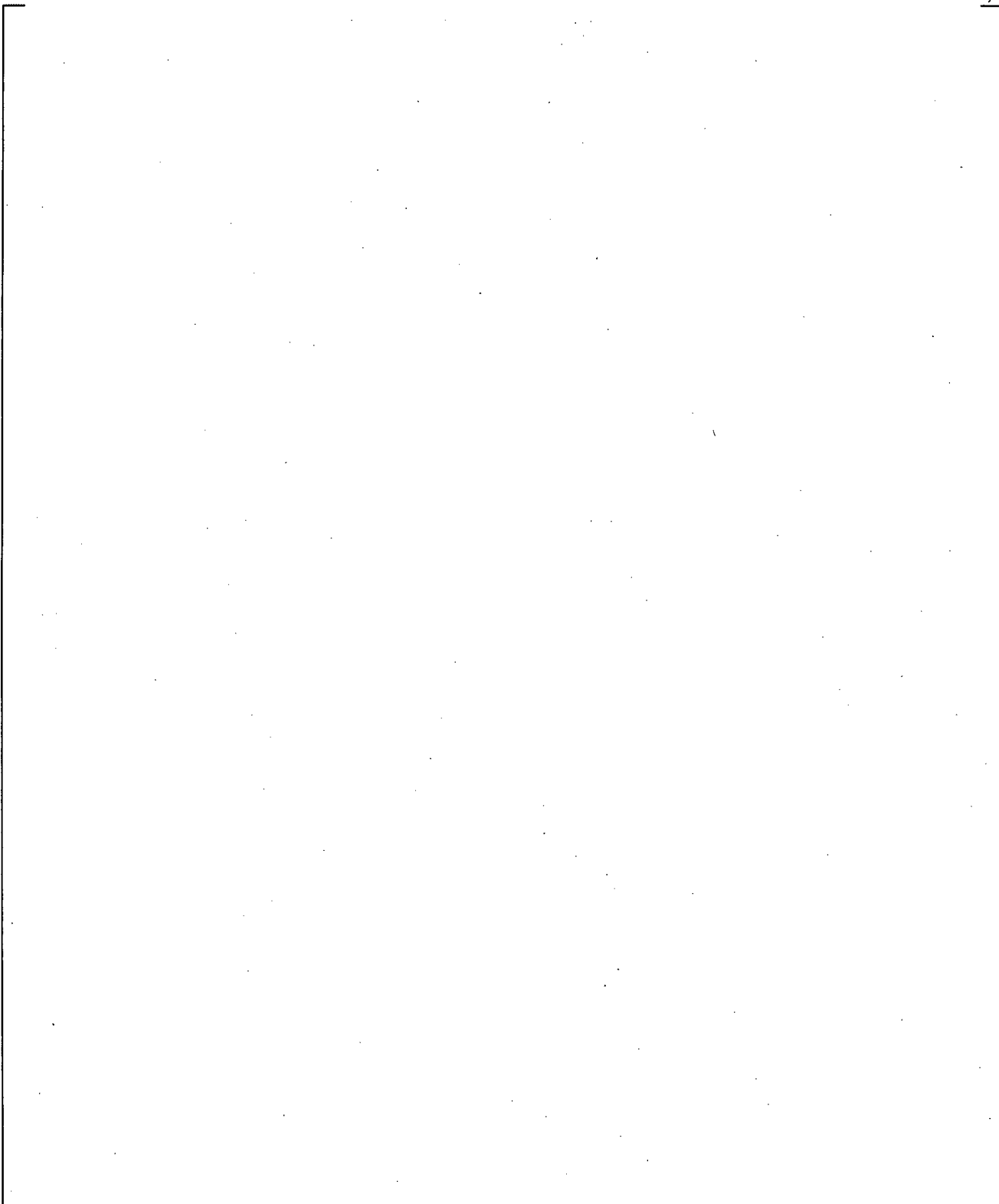


**Figure 21.4-17 Upper Plenum Differential Pressures**

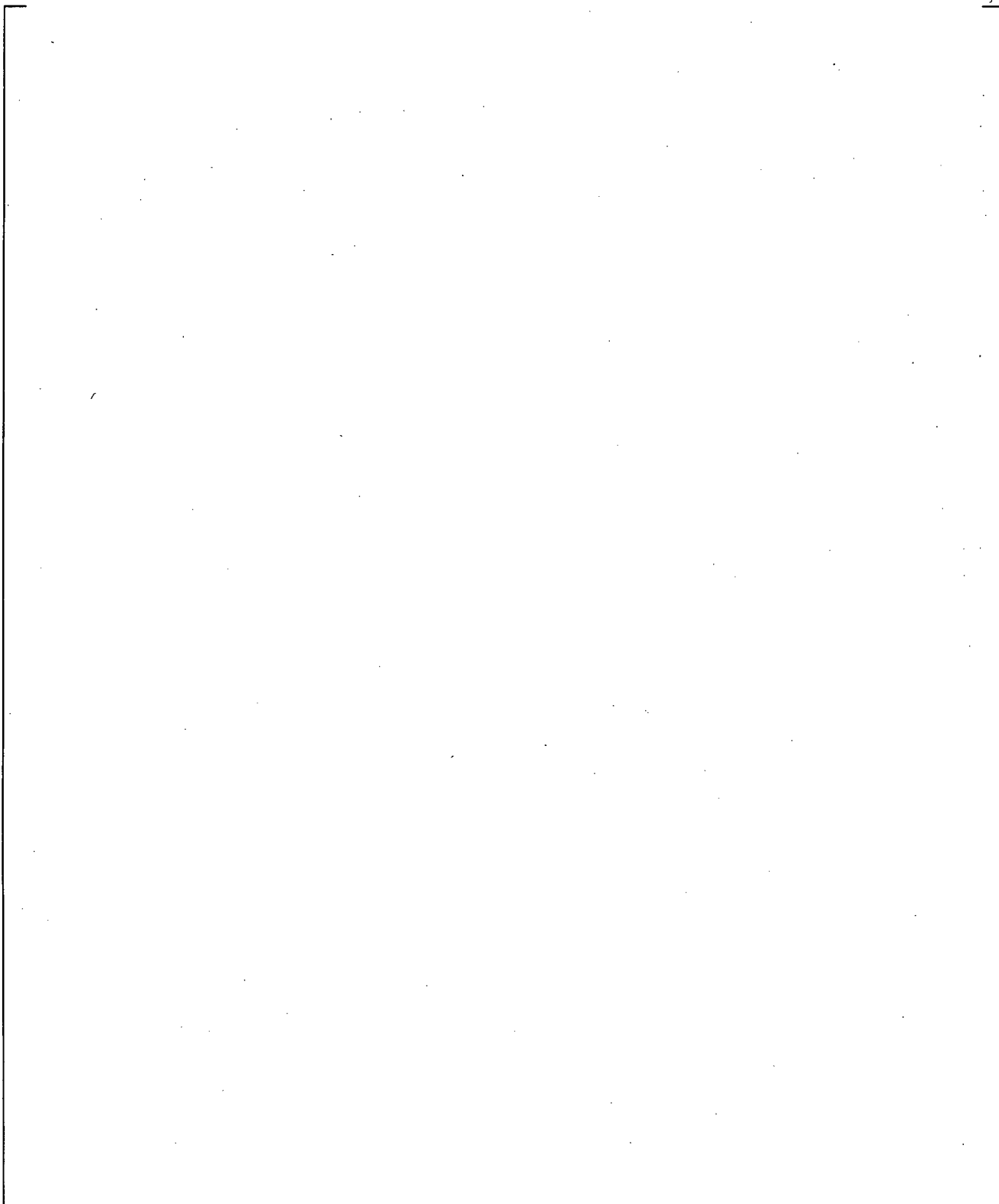


**Figure 21.4-18 Downcomer Differential Pressures**

a,c

**Figure 21.4-19 Comparison of Calculated and Measured Accumulator Injection Flows Loop A**

a,c

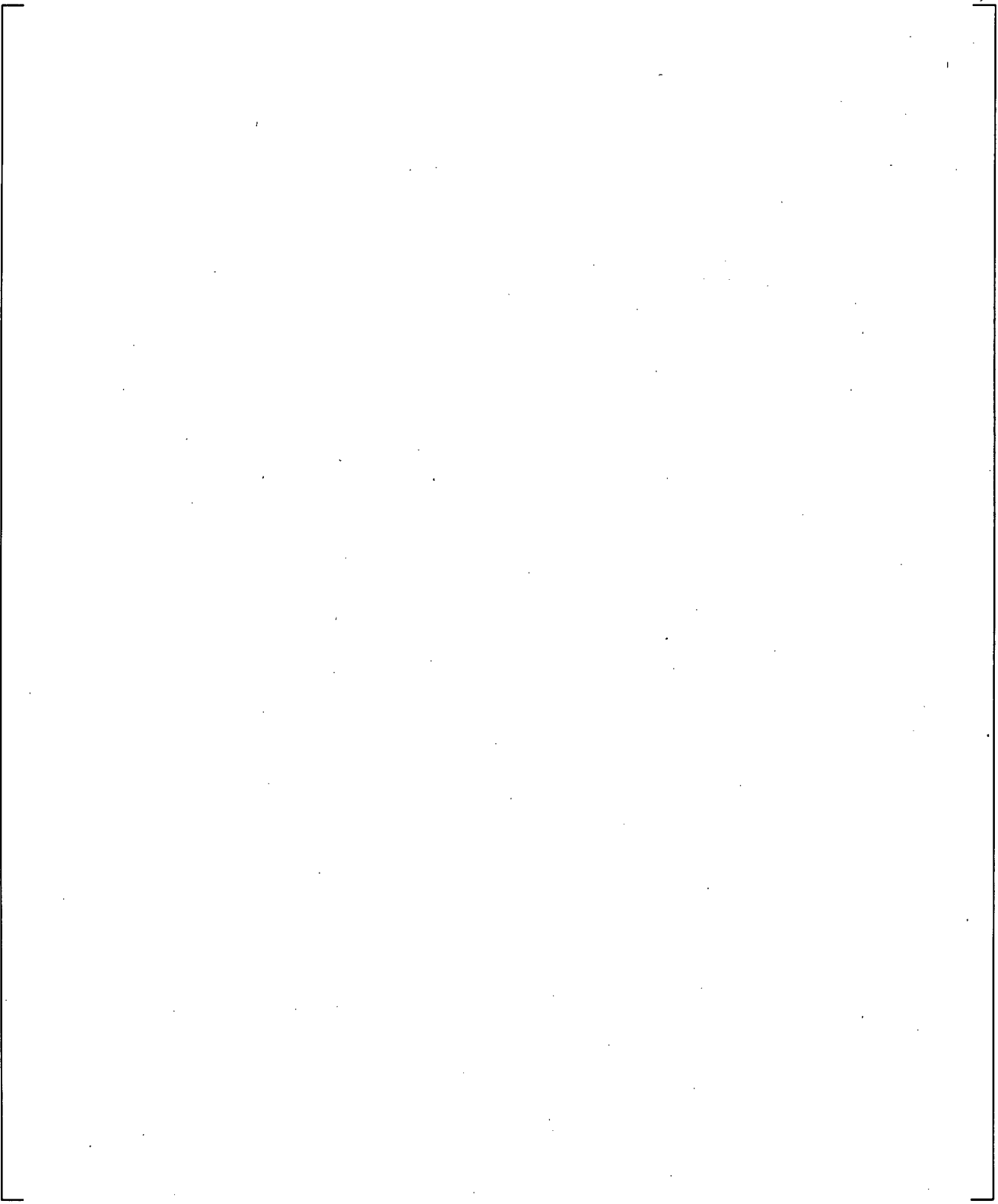


**Figure 21.4-20 Comparison of Calculated and Measured Accumulator Injection Flows Loop**

a,c

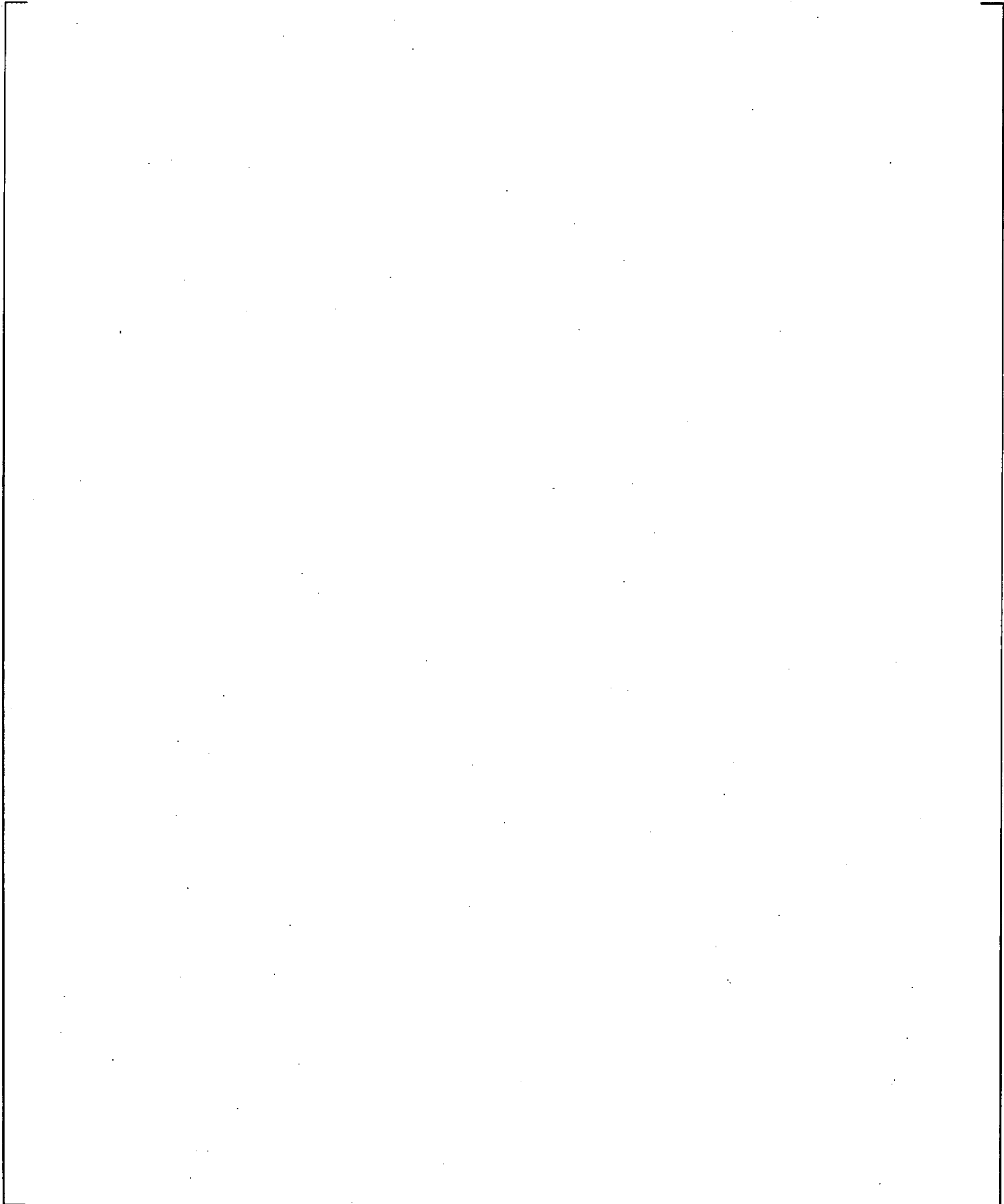


**Figure 21.5-1 Core Power**

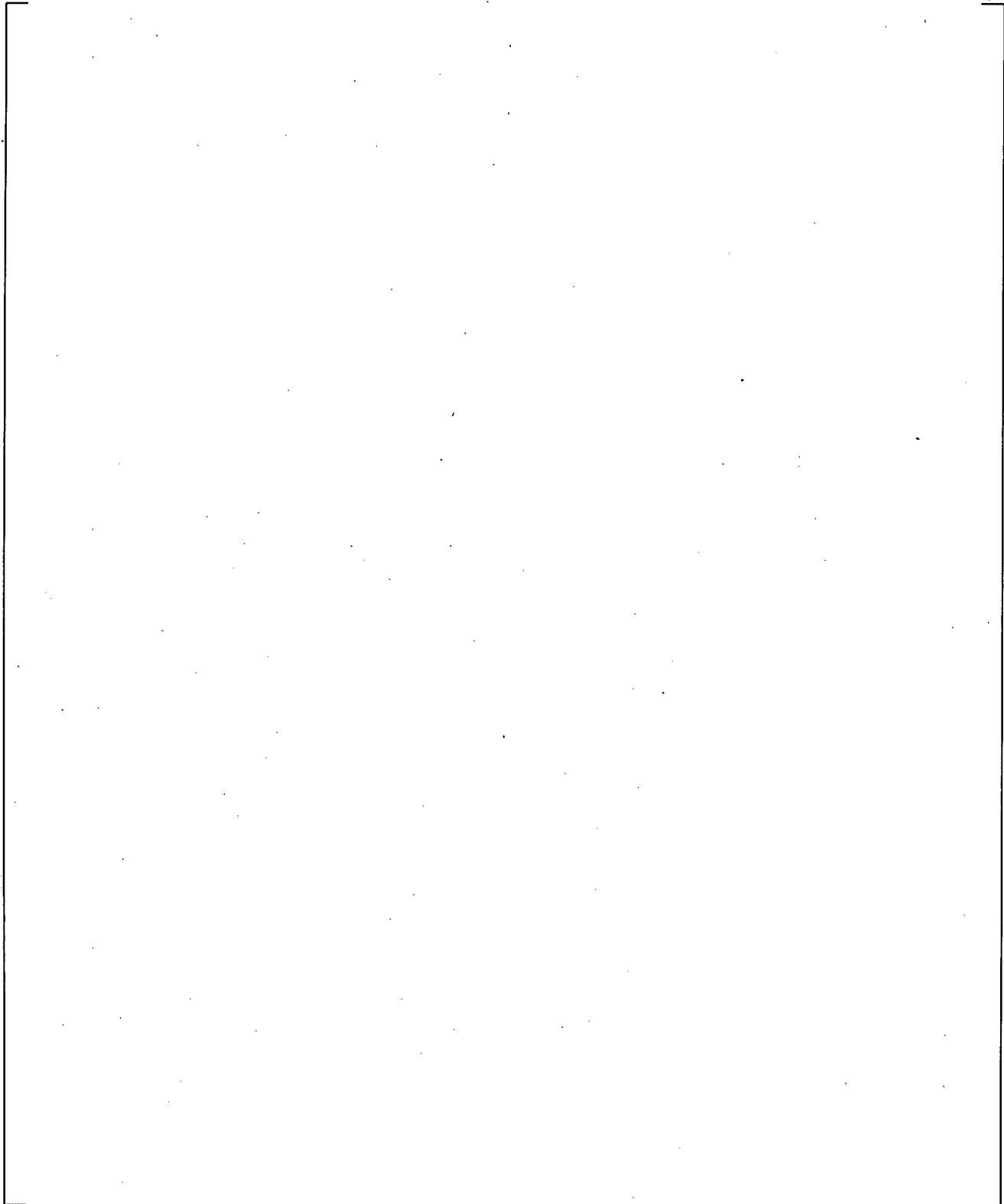


**Figure 21.5-2 Pump Speed**

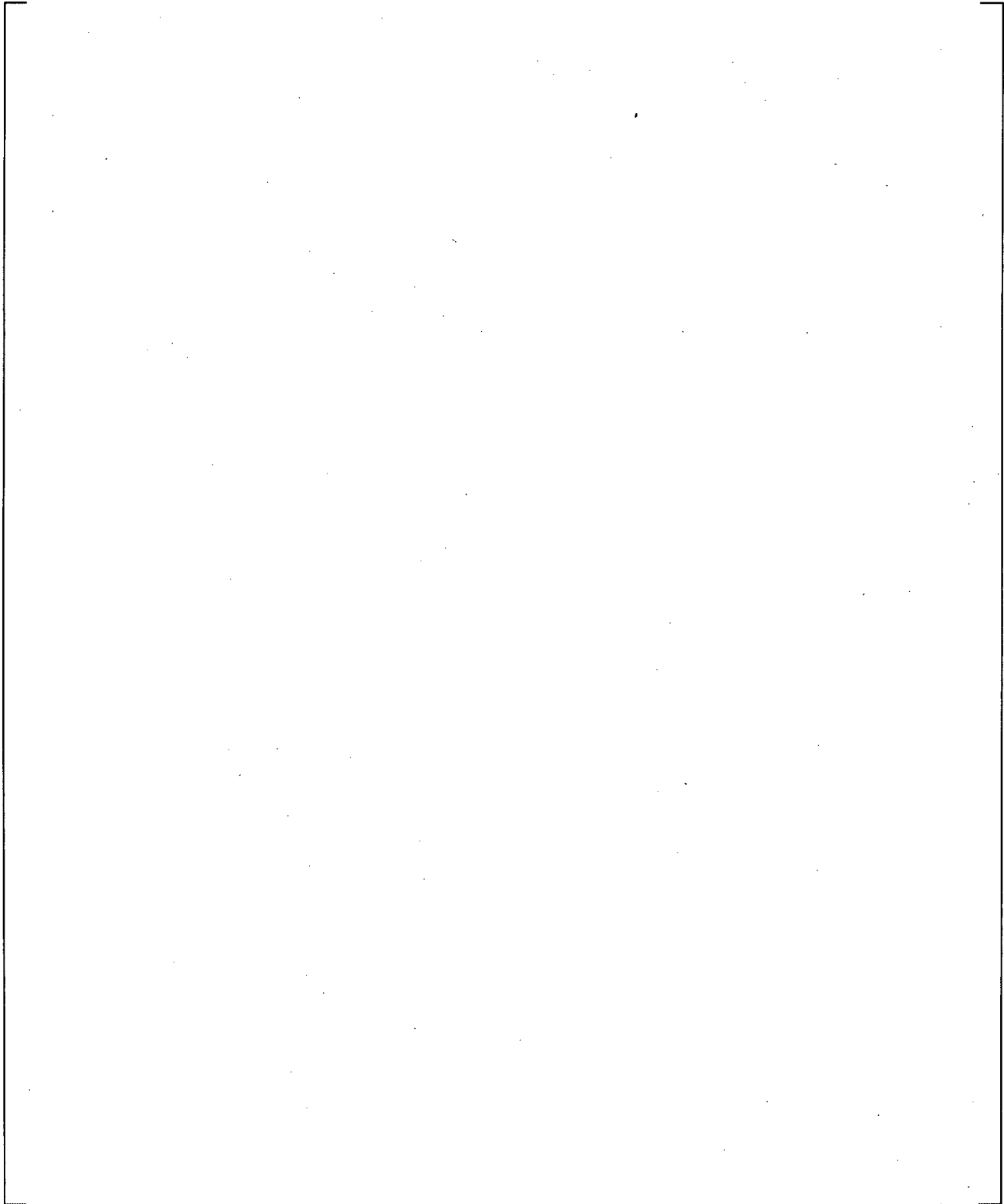


**Figure 21.5-3 Loop Flow Rates**

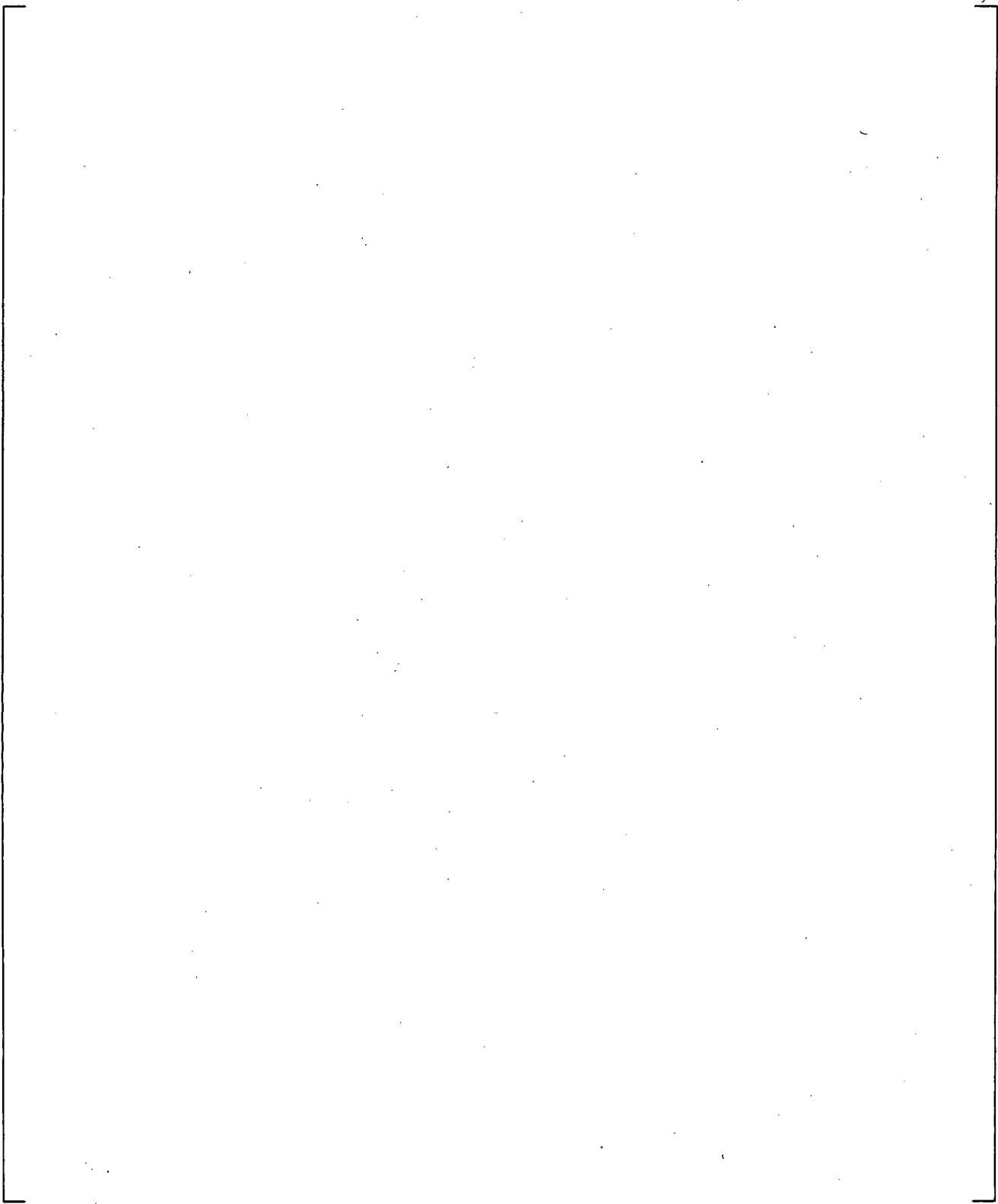


**Figure 21.5-4 Break Flows**

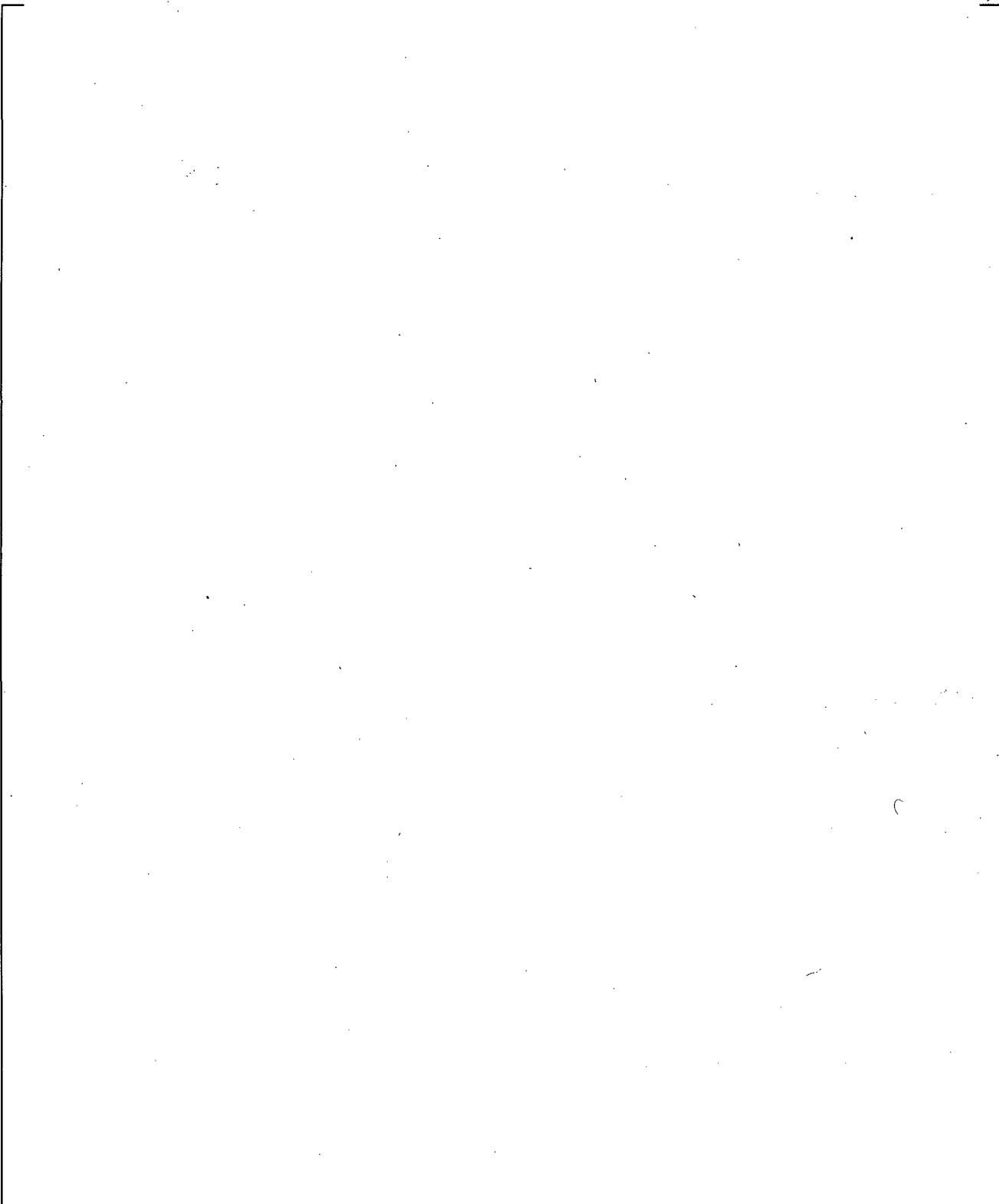


**Figure 21.5-5 Calculated Break Spool Void Fraction**

Note: This location is in the side pipe of the broken TEE#26, upstream the break orifice location.

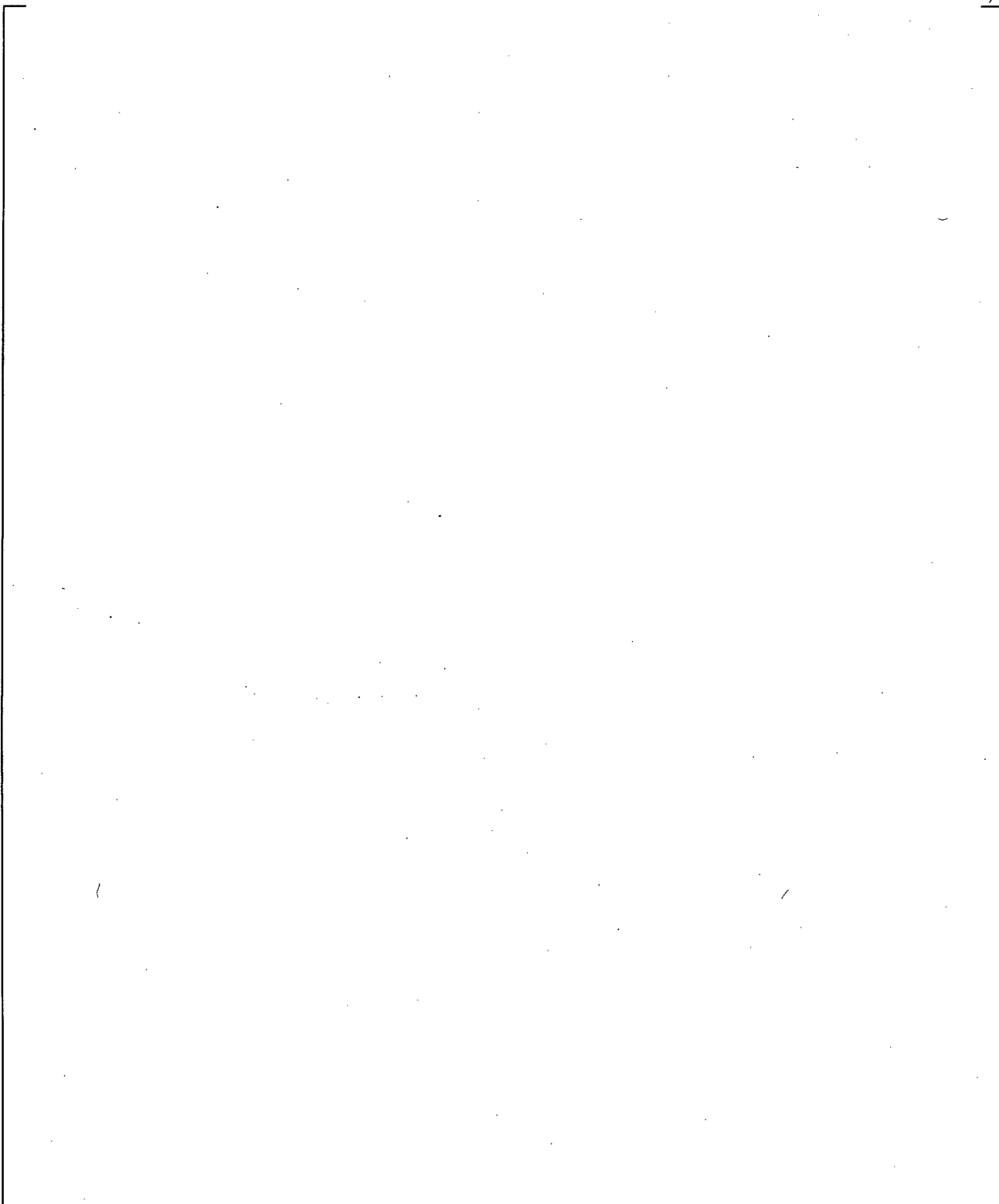


**Figure 21.5-6 Pressurizer Pressures**

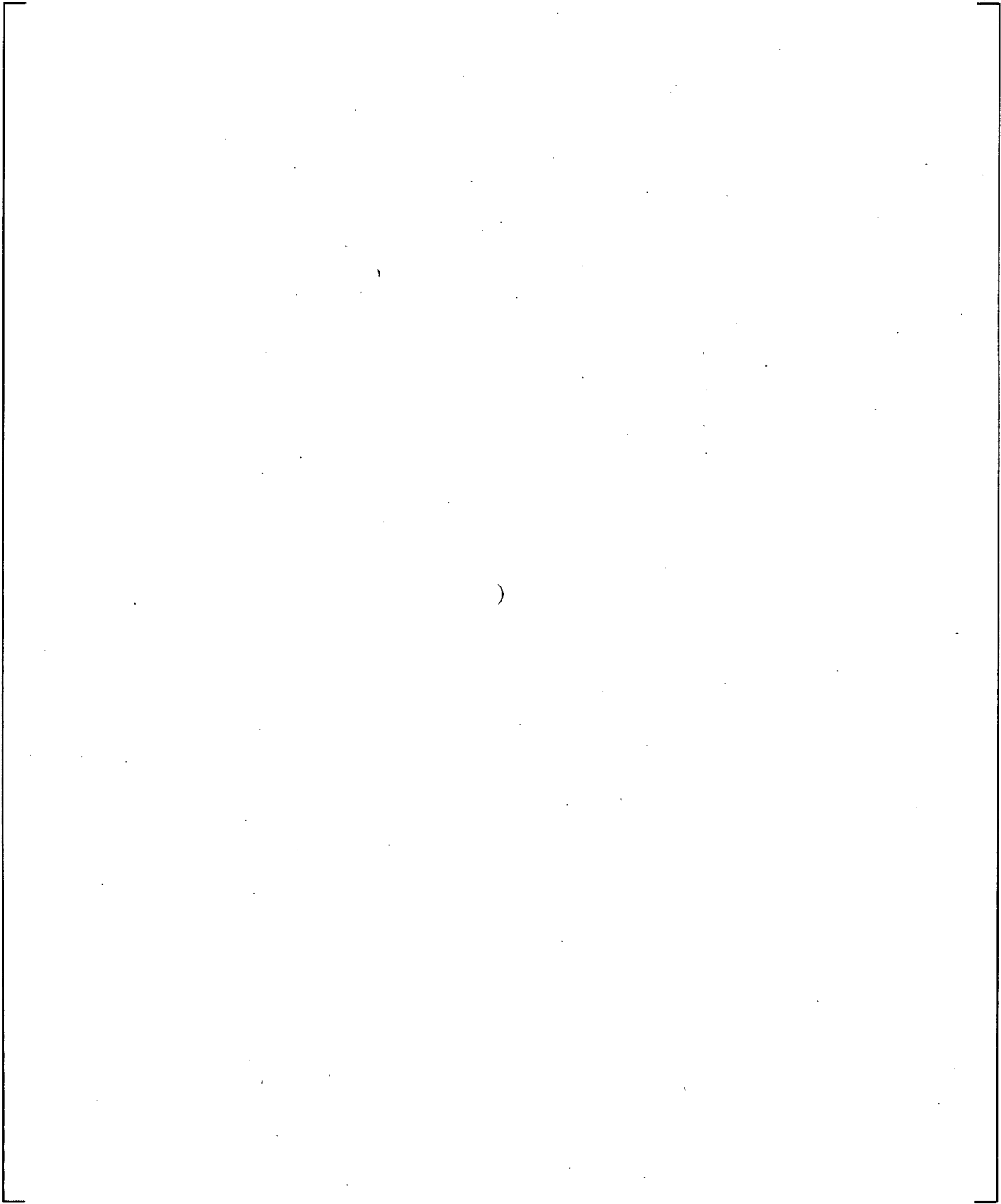


**Figure 21.5-7 Steam Generator Secondary Side Pressures**

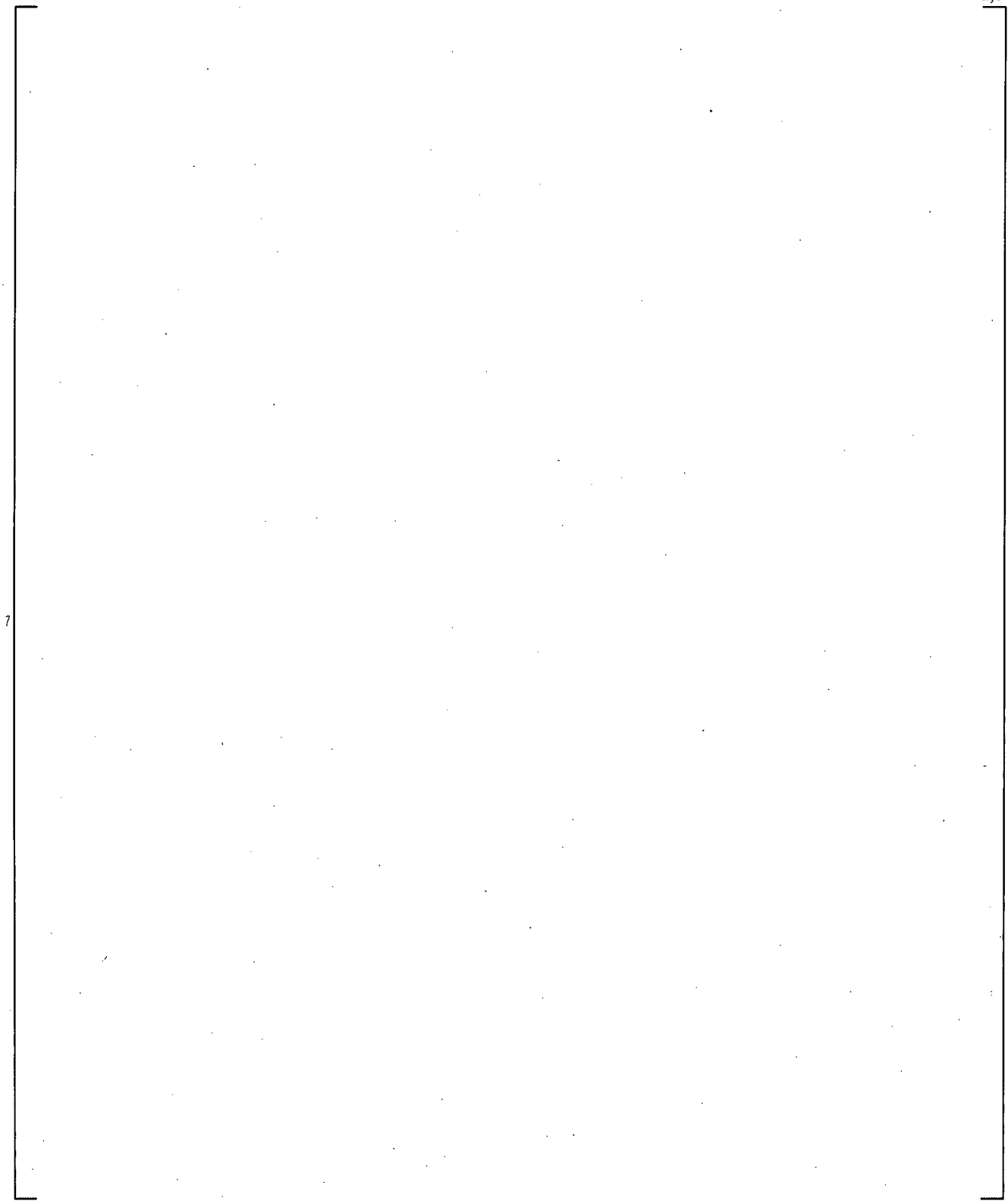


**Figure 21.5-8 Steam Generator SGA U-tube Differential Pressures**

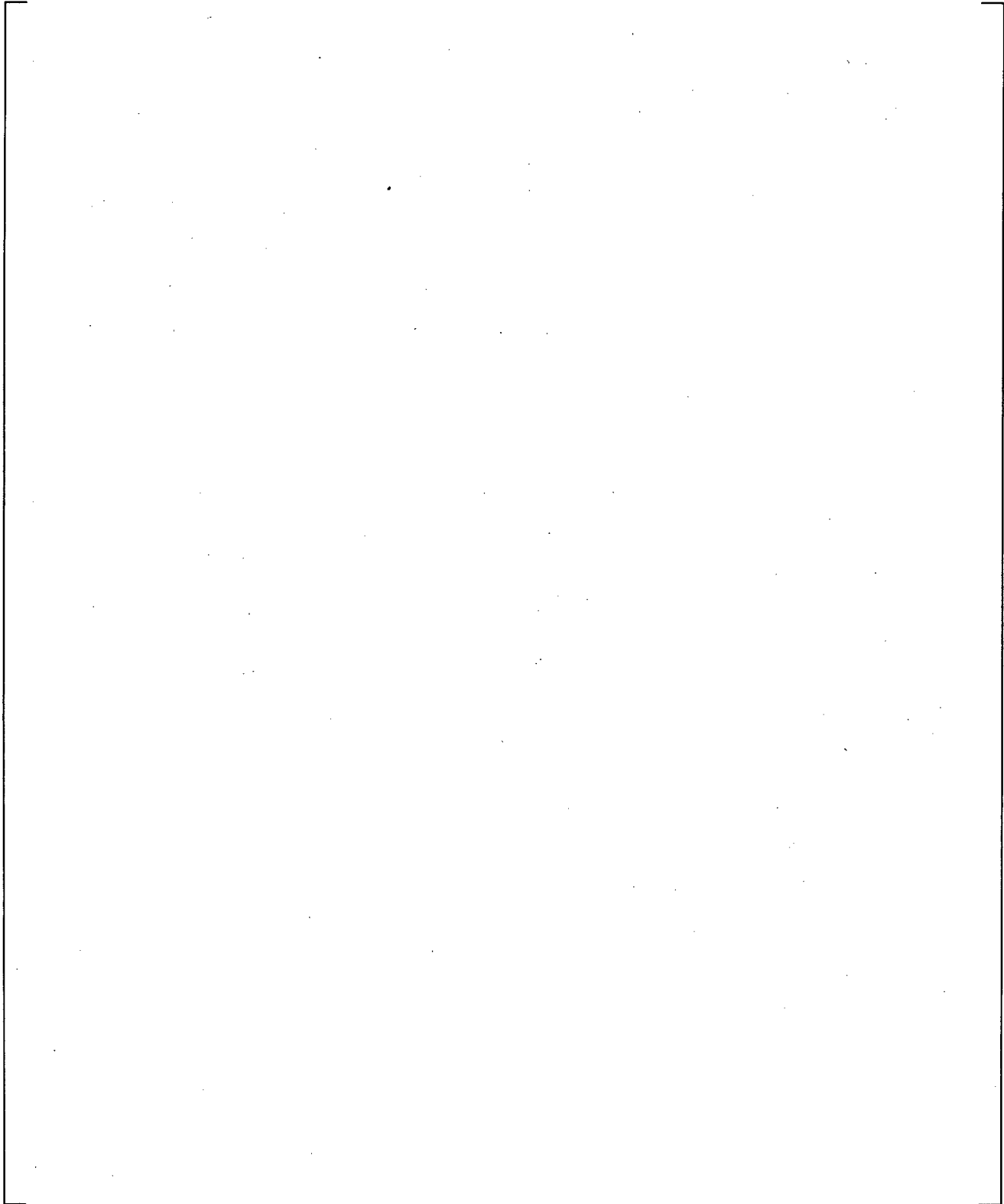


**Figure 21.5-9 Steam Generator SGB U-tube Differential Pressures**

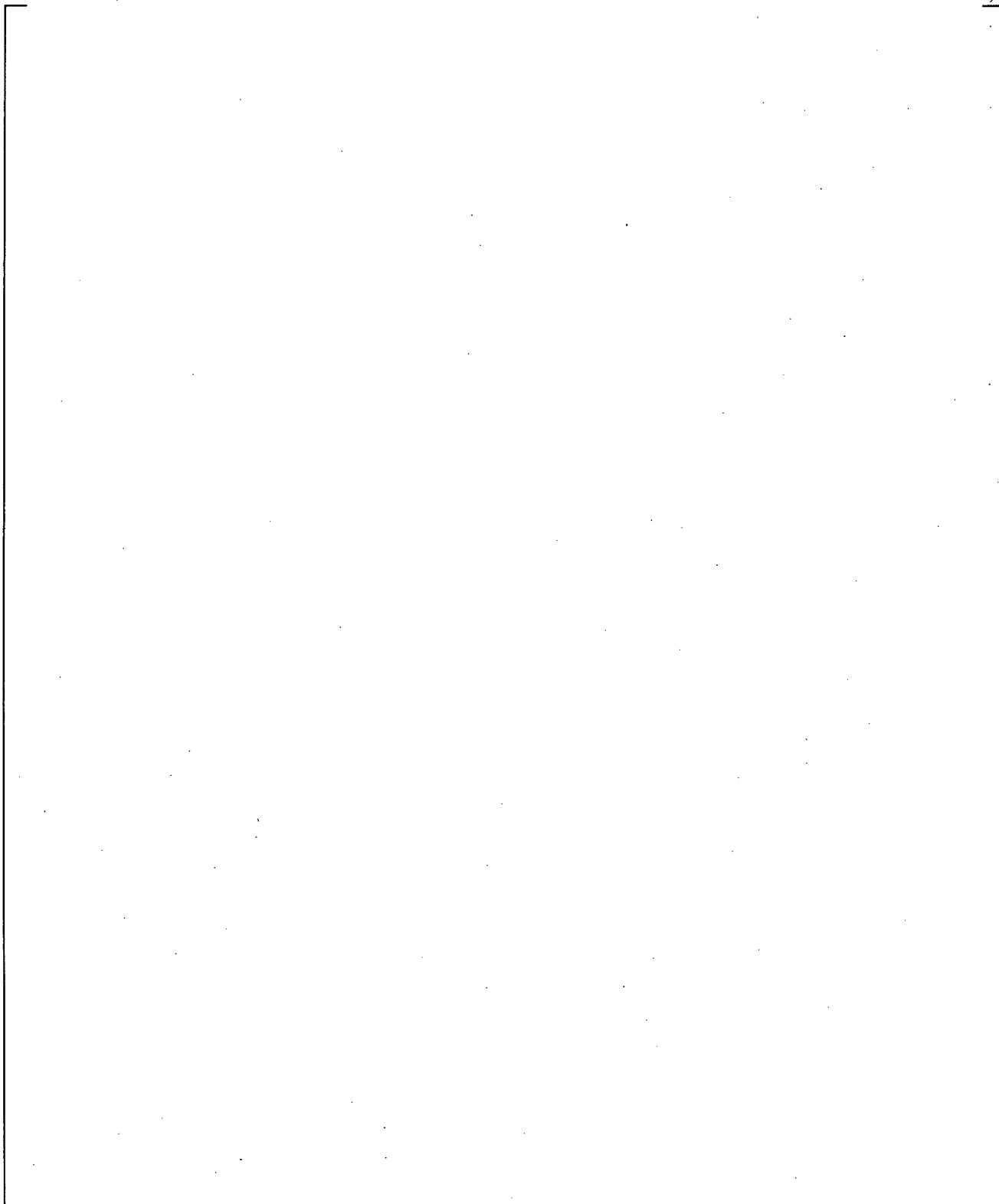


**Figure 21.5-10 Cross-Over Leg A Differential Pressures**

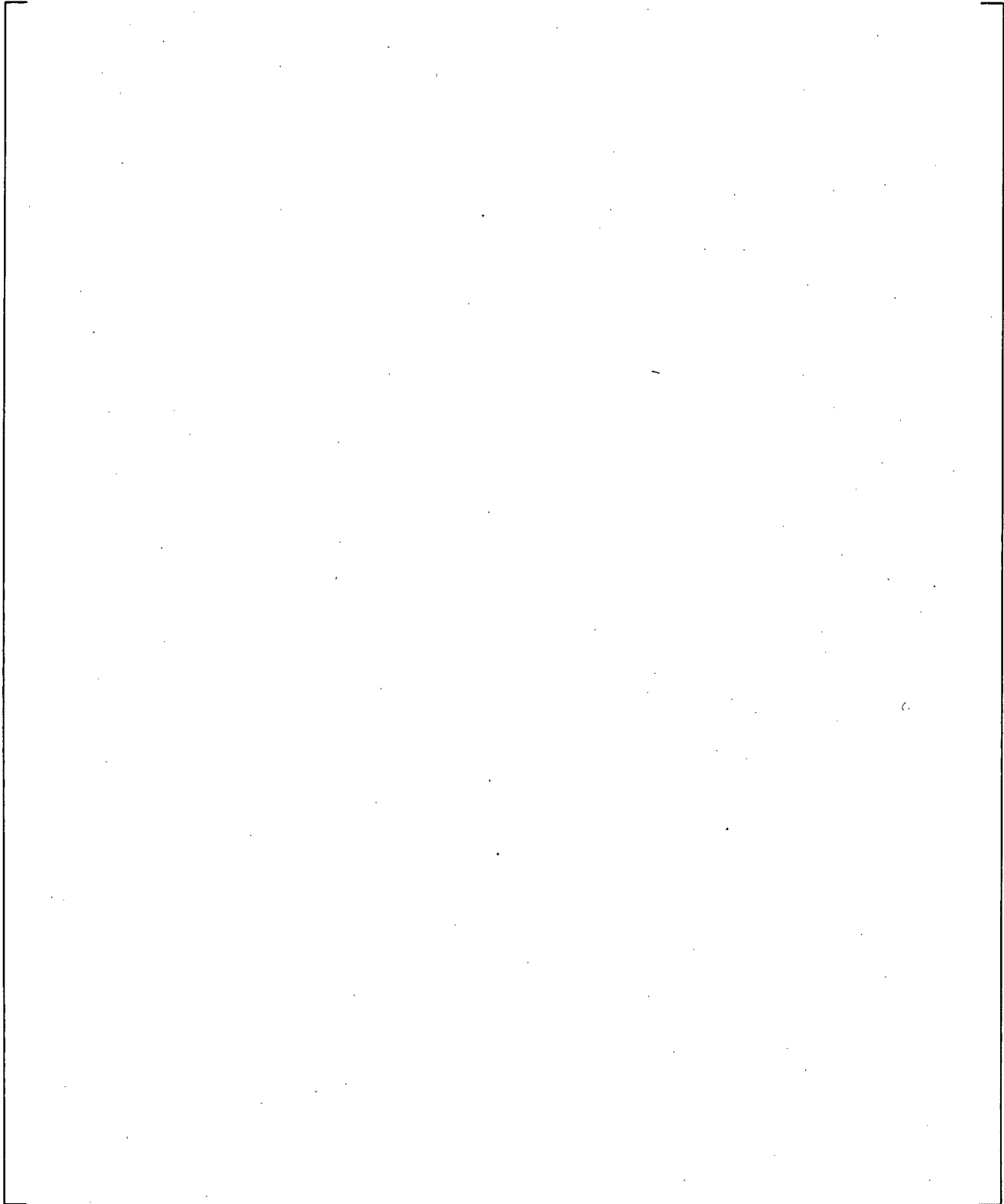


**Figure 21.5-11 Cross-Over Leg B Differential Pressures**

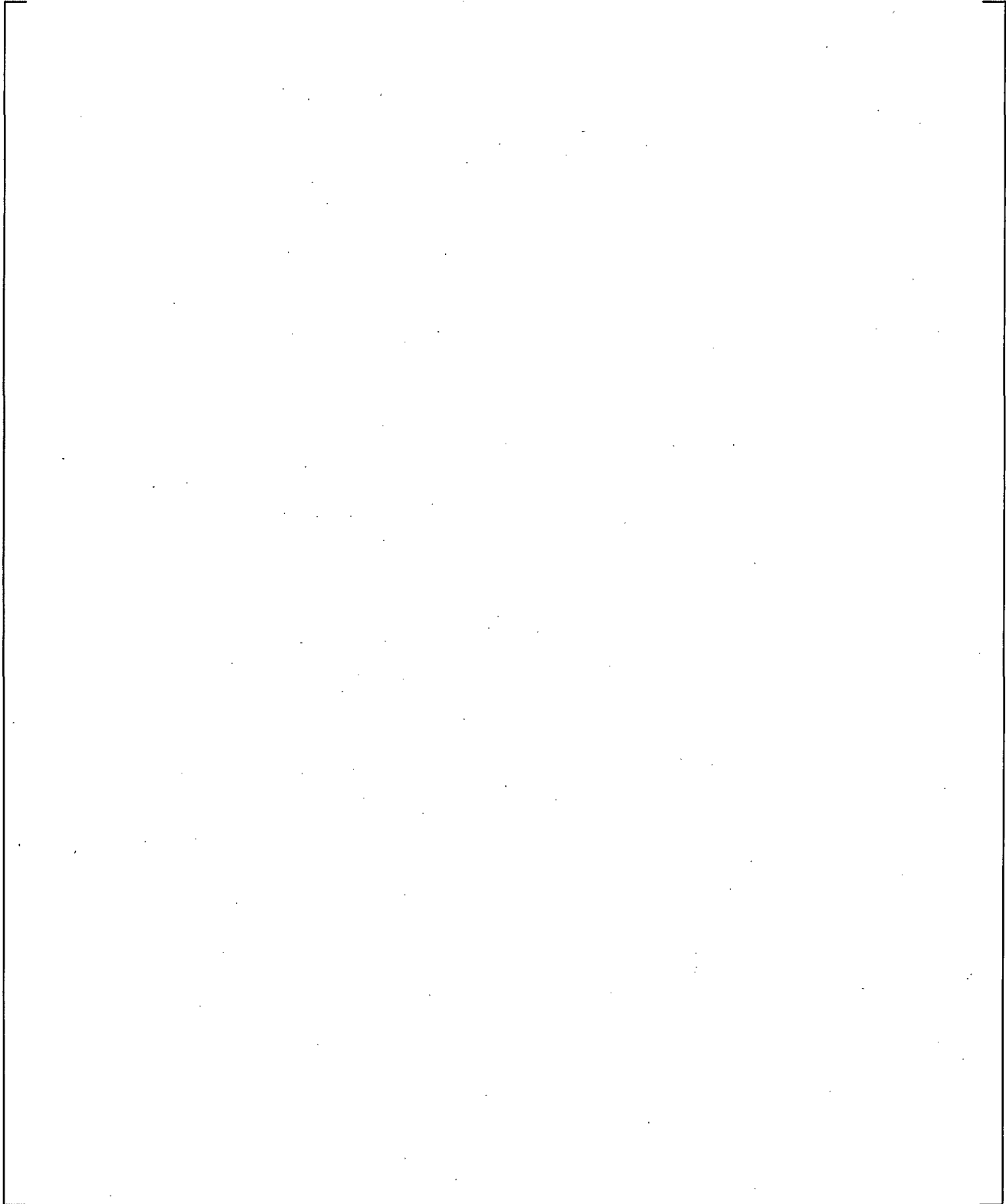


**Figure 21.5-12 Upper Plenum Differential Pressures**

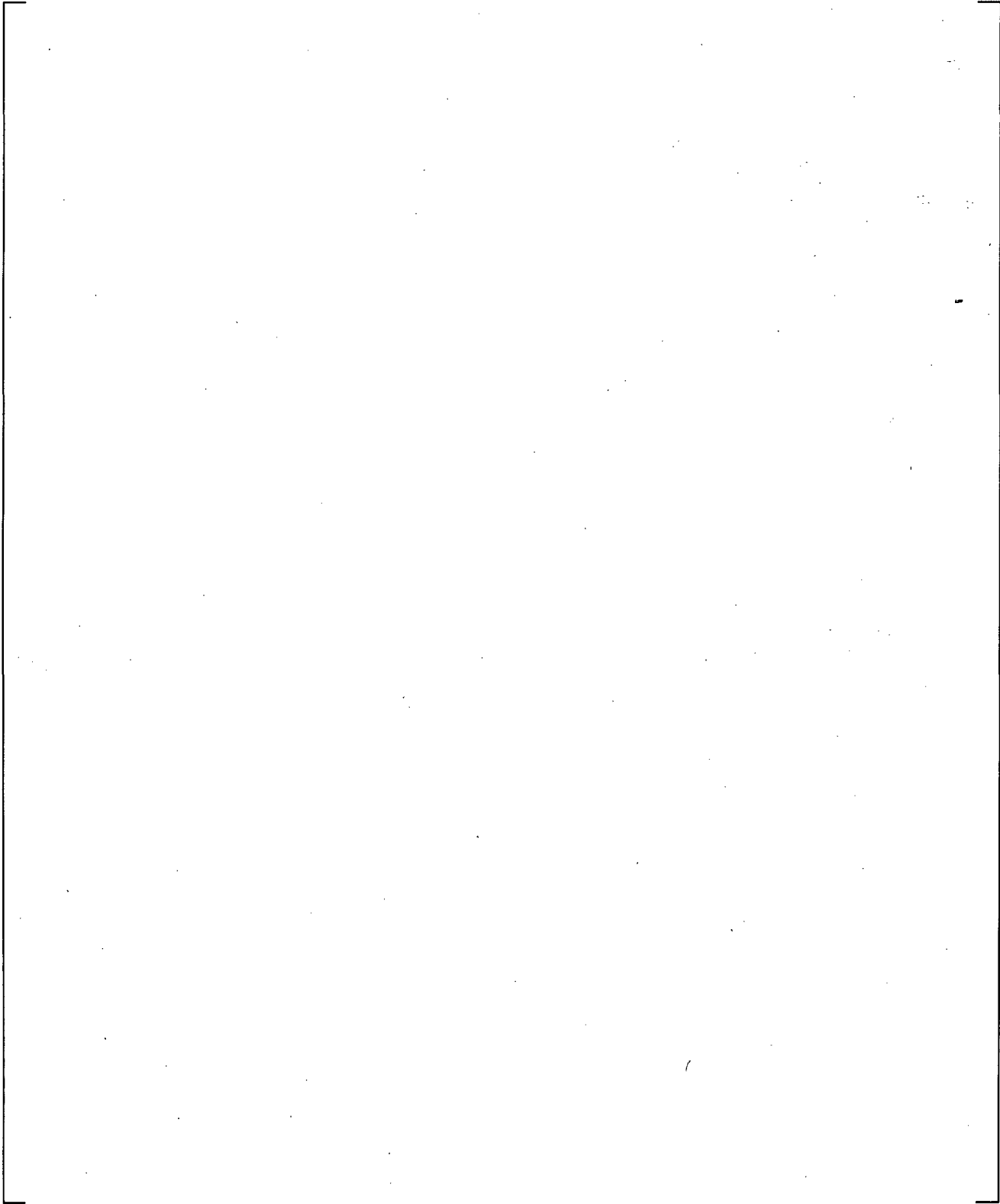


**Figure 21.5-13 Upper Plenum to SGA Inlet Differential Pressures**

a,c

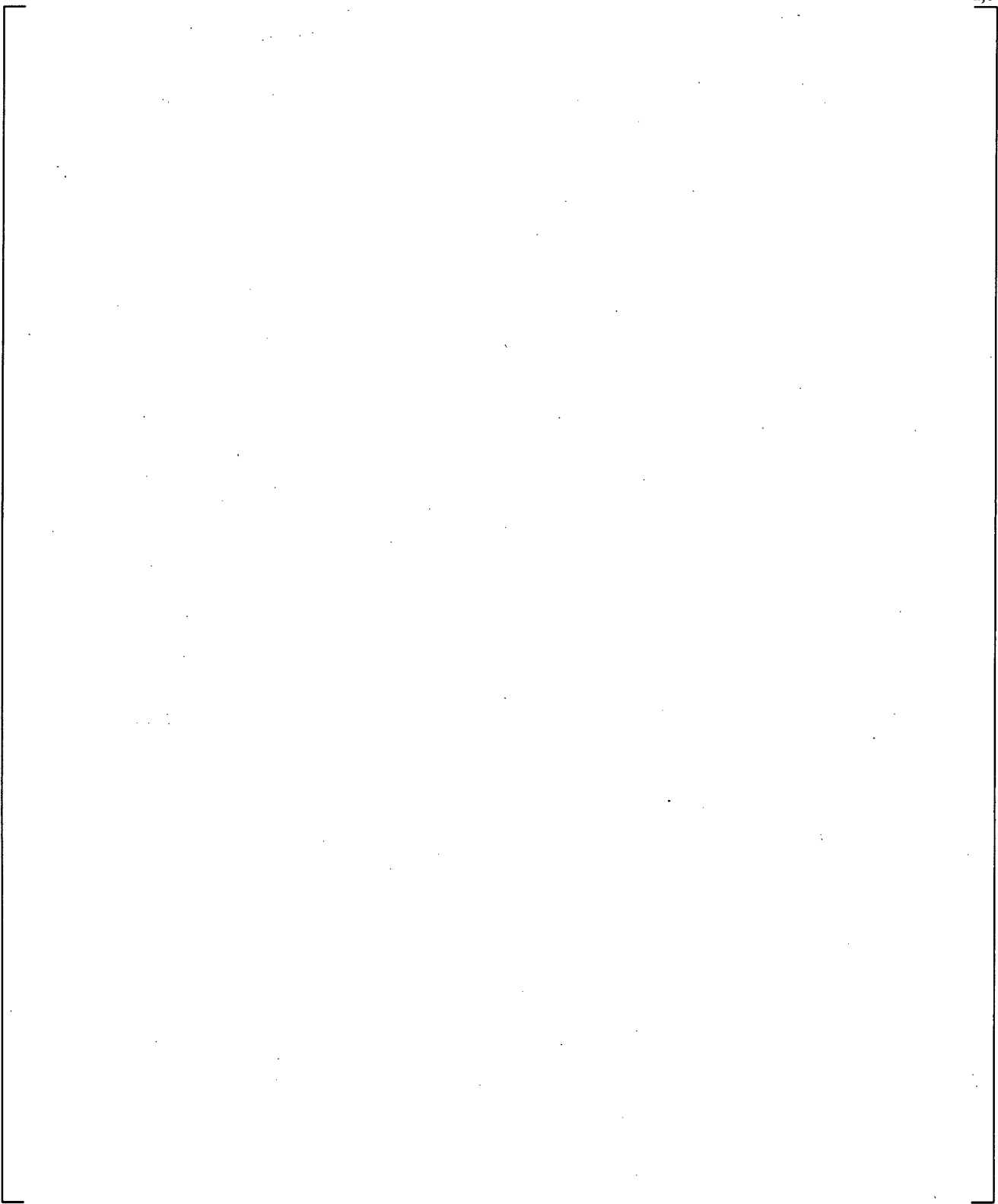


**Figure 21.5-14 Upper Plenum to SGB Inlet Differential Pressures**

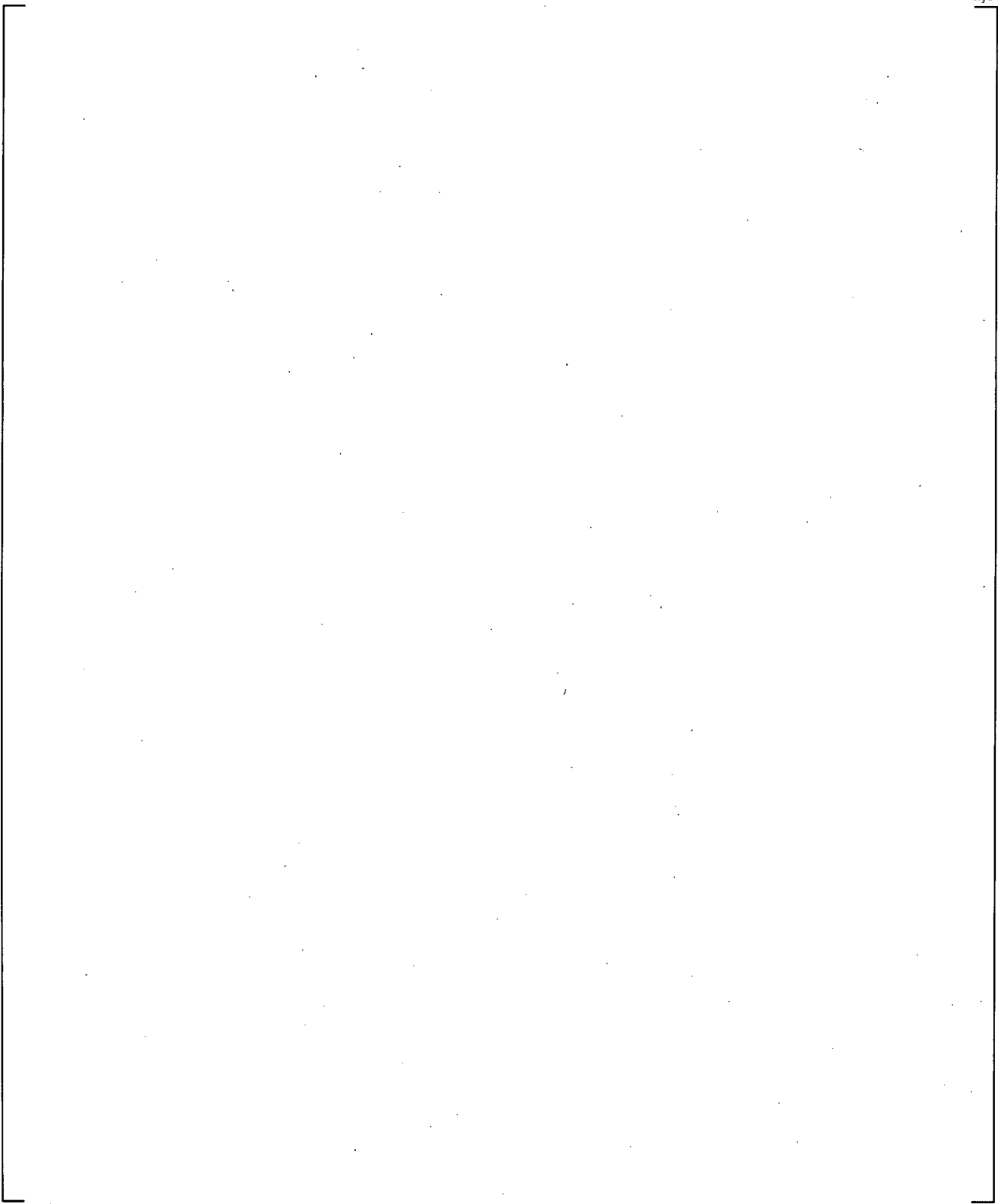


**Figure 21.5-15 Downcomer Differential Pressures**

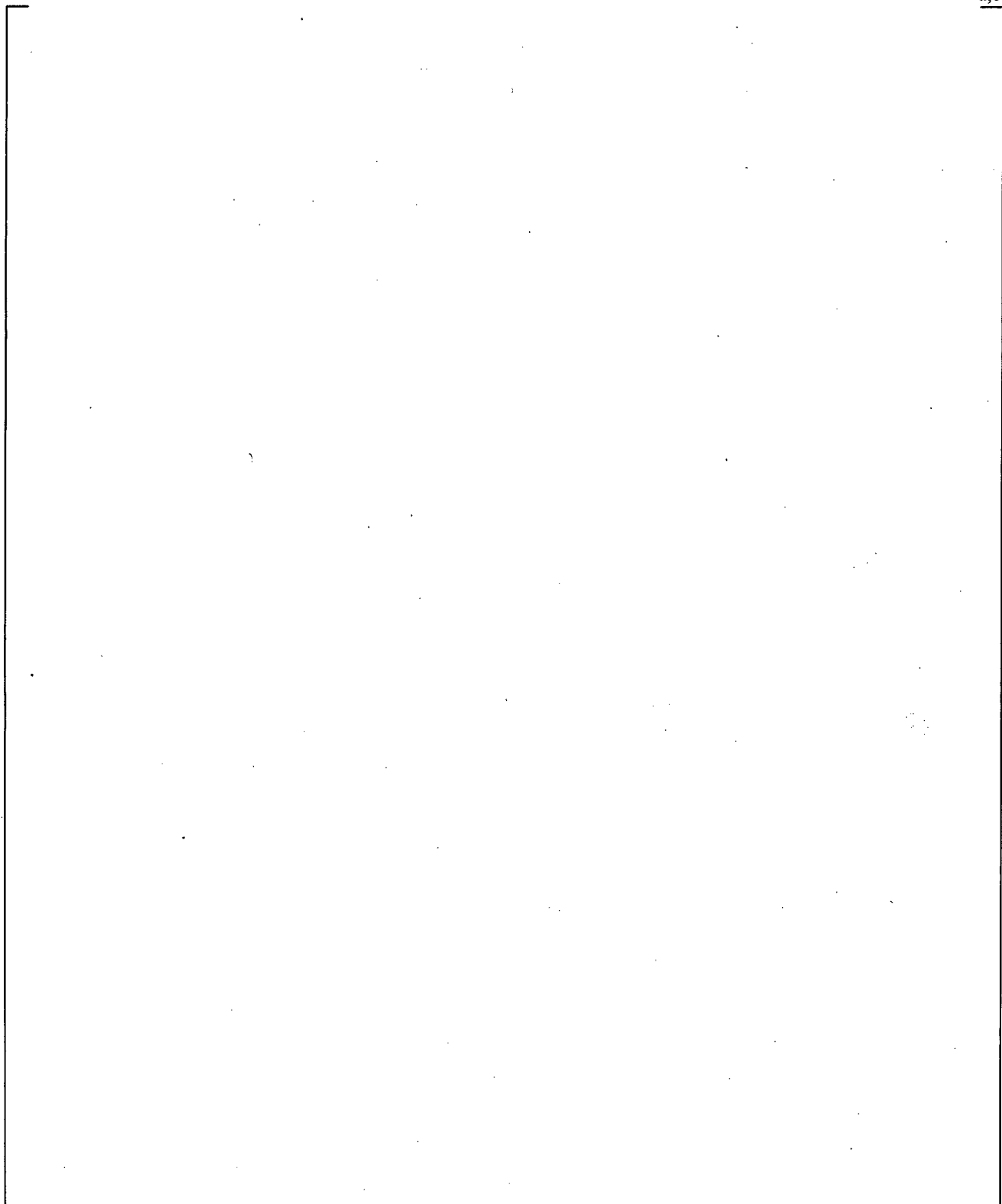


**Figure 21.5-16 Core Differential Pressures**

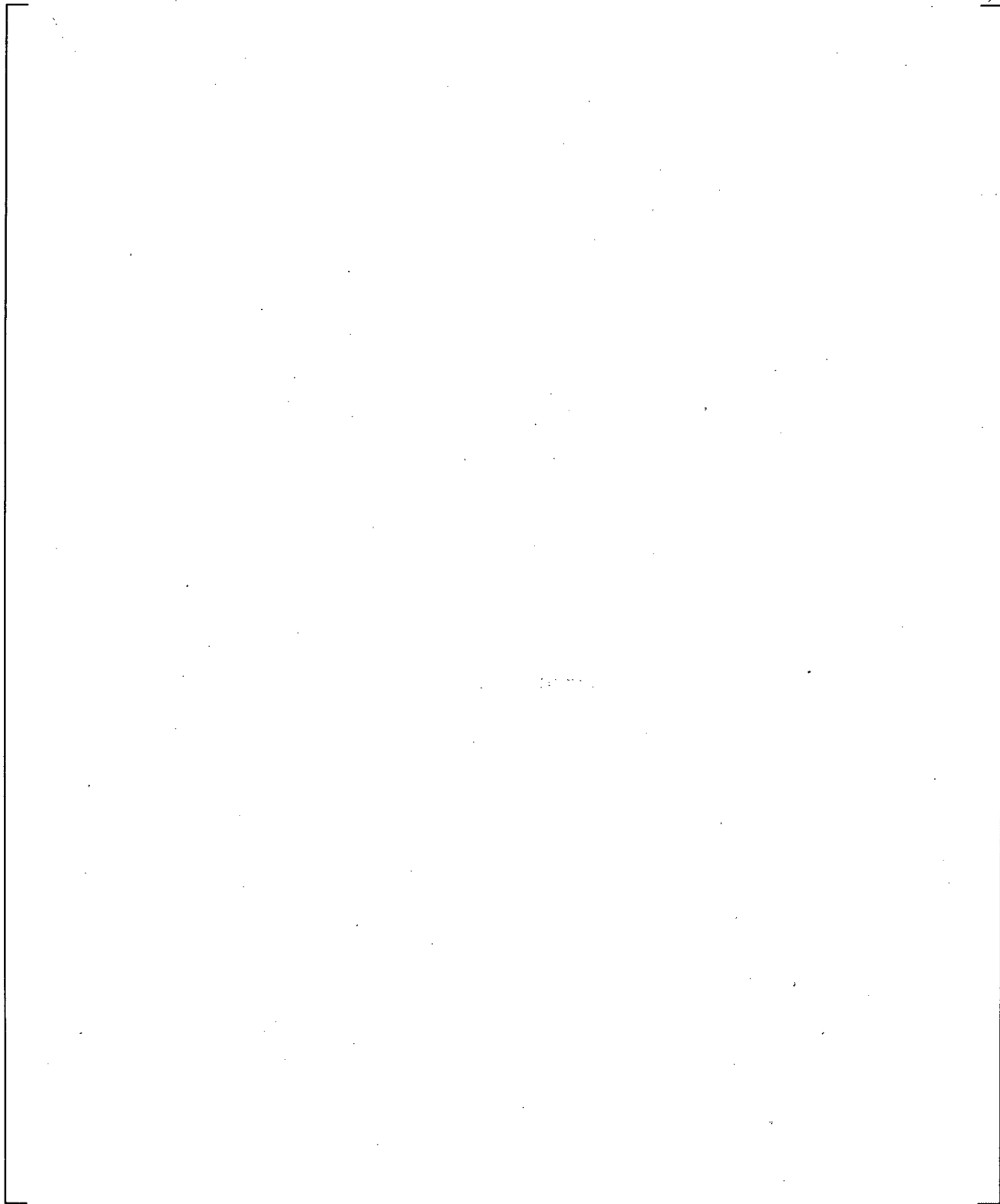


**Figure 21.5-17 Core Differential Pressures for SB-CL-05 and SB-CL-18**

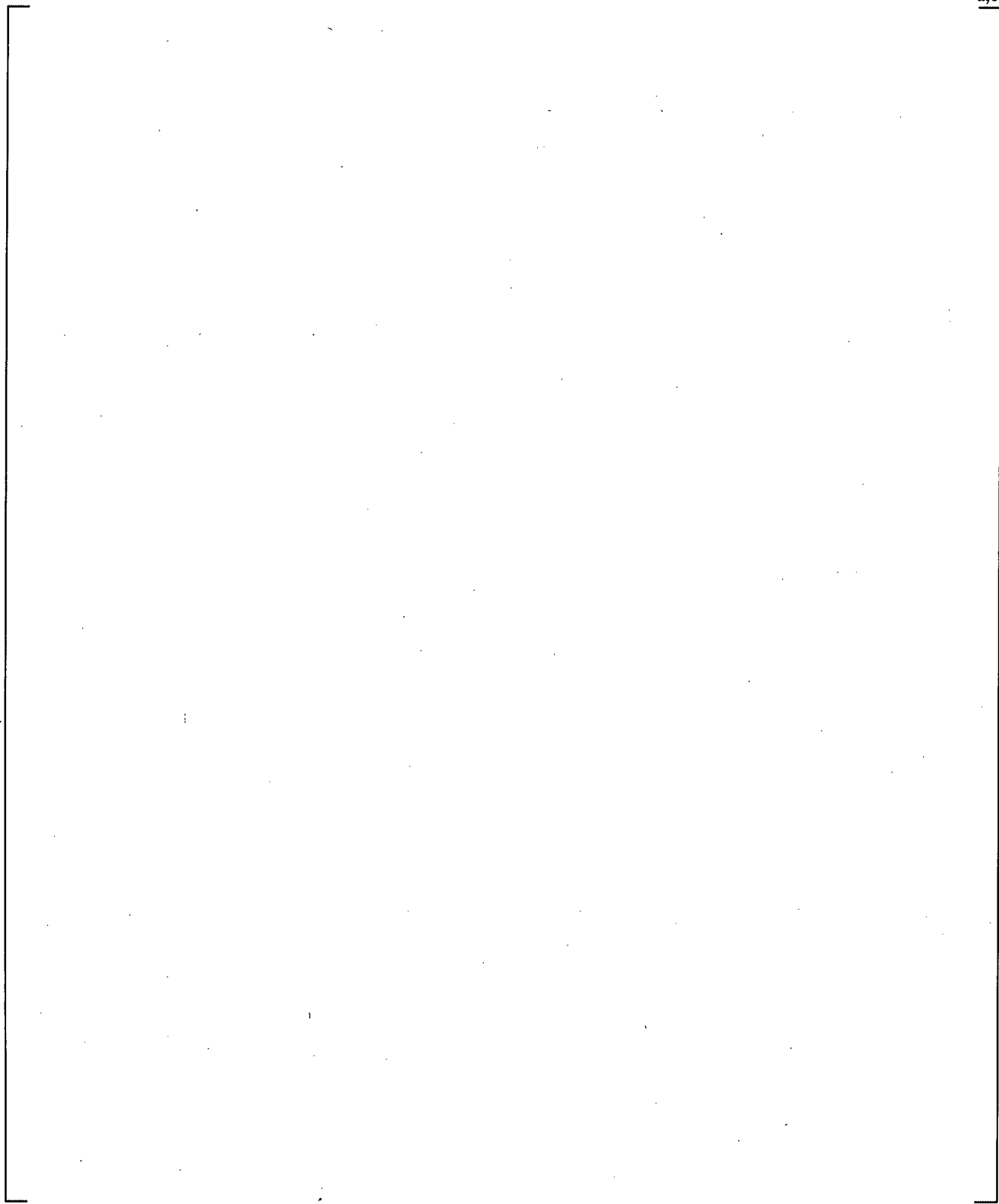


**Figure 21.5-18 Cold Leg A Pumped ECCS Injection Flows (CLA)**

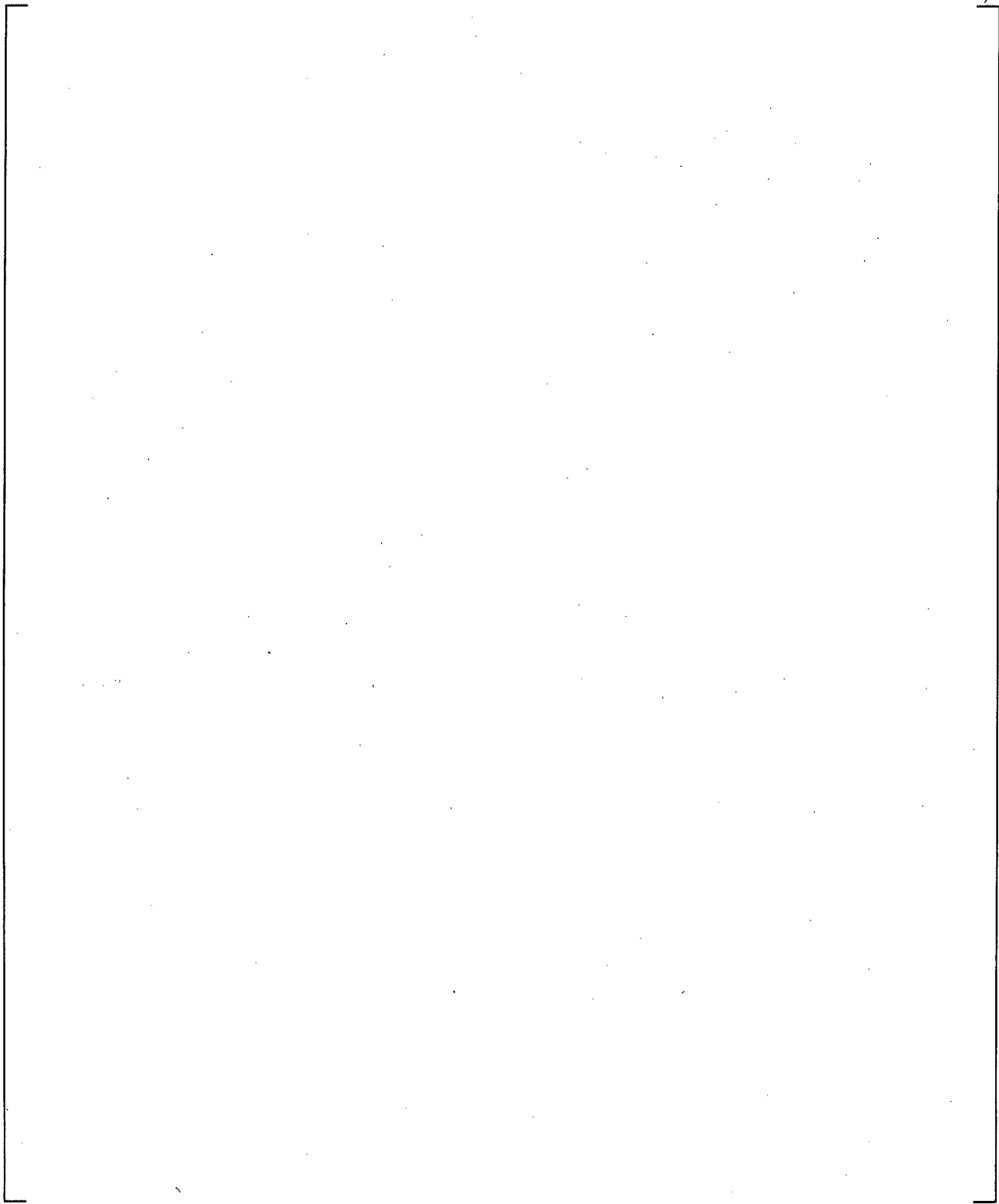


**Figure 21.5-19 Total Pumped ECCS Injection Flows (CLA plus CLB)**

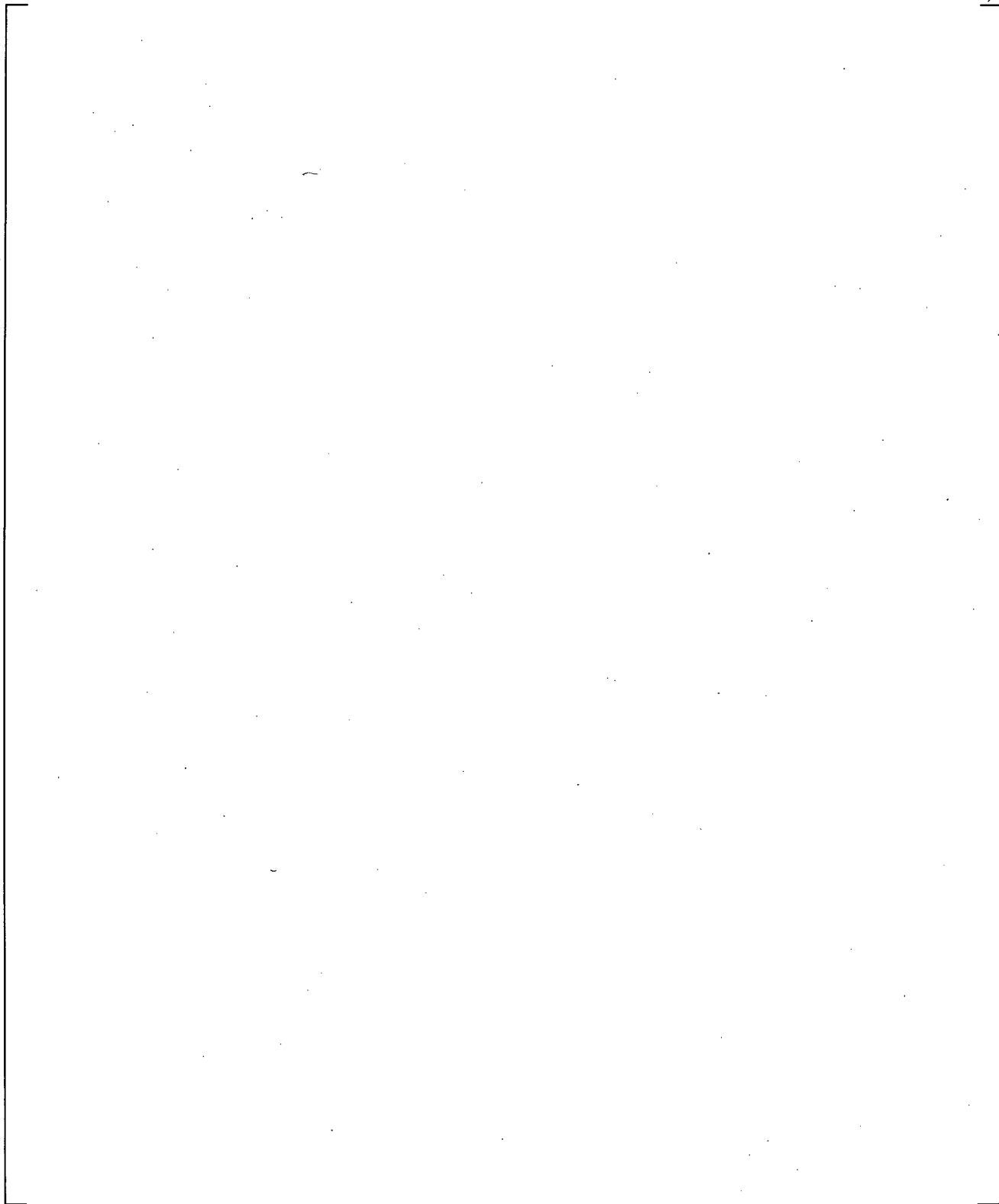
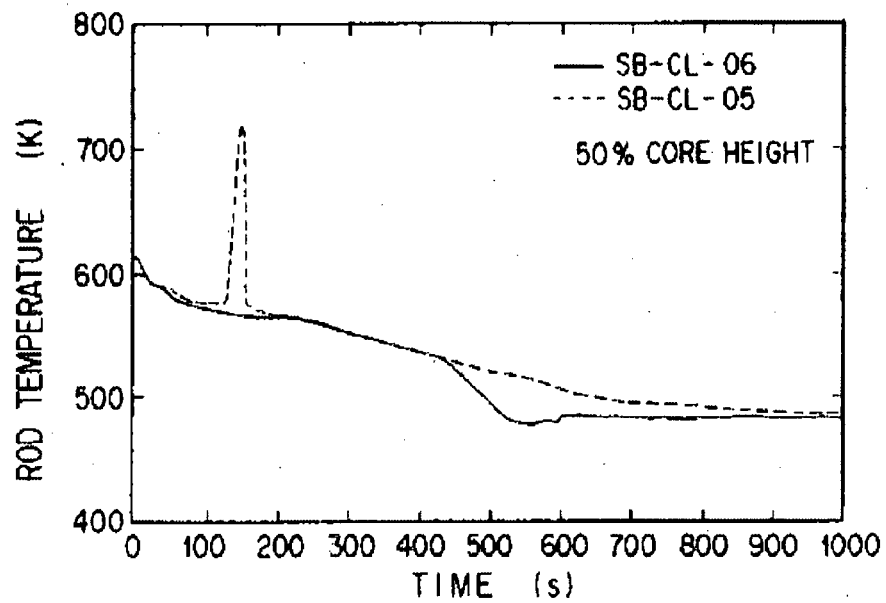


**Figure 21.5-20 Accumulator Hot (ACH) Liquid Level**



(b) Extract from Fig.6 of Reference 8 (Tasaka, et.al.)

Figure 21.5-21 Calculated and Measured Peak Cladding Temperatures

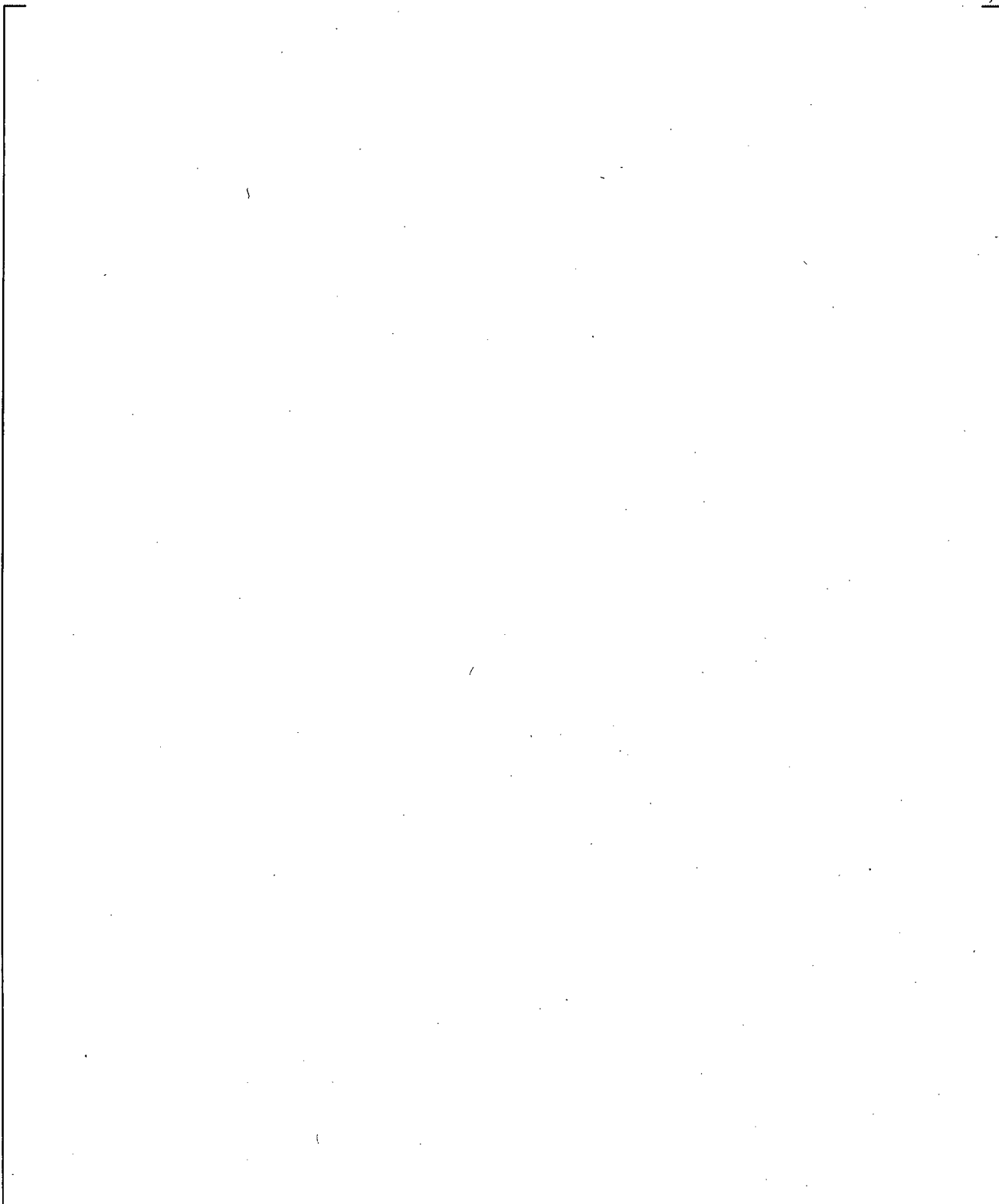
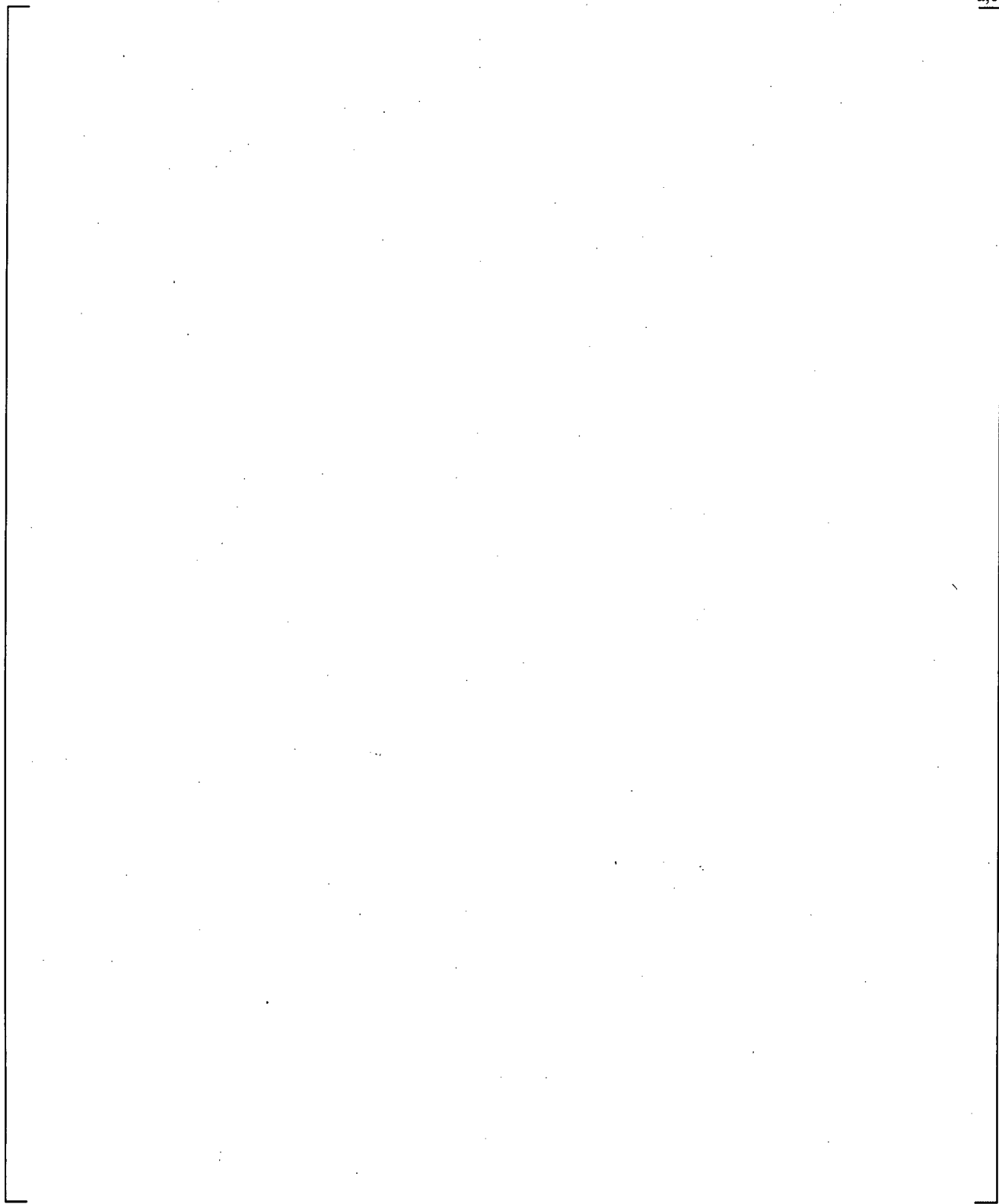


**Figure 21.6-1 Loop-A Pump Speed Comparison**

Note: 1 Hz=30 rpm=3.1415 rad/sec

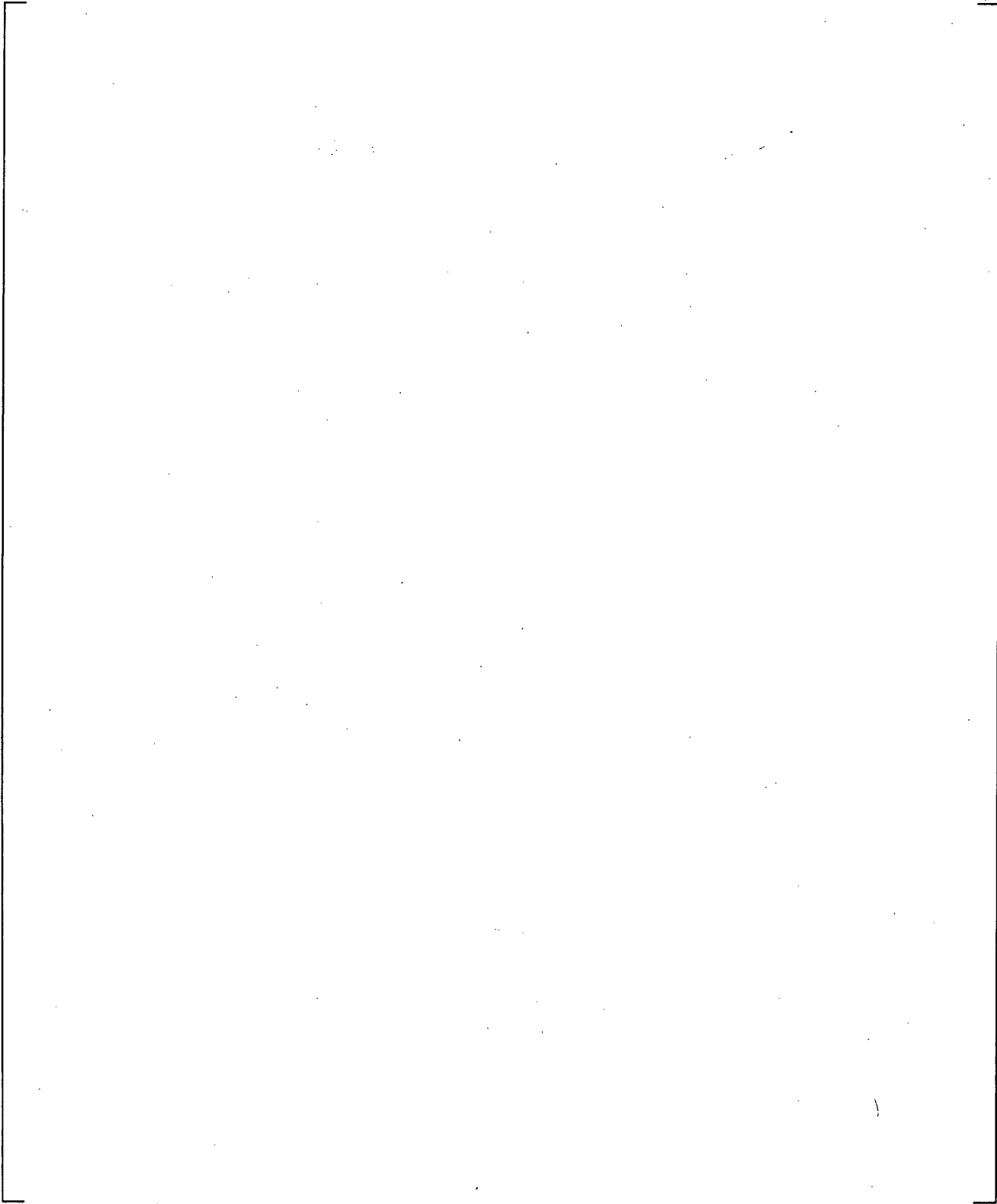
**Figure 21.6-2 Loop-B Pump Speed Comparison**

Note: 1 Hz=30 rpm=3.1415 rad/sec

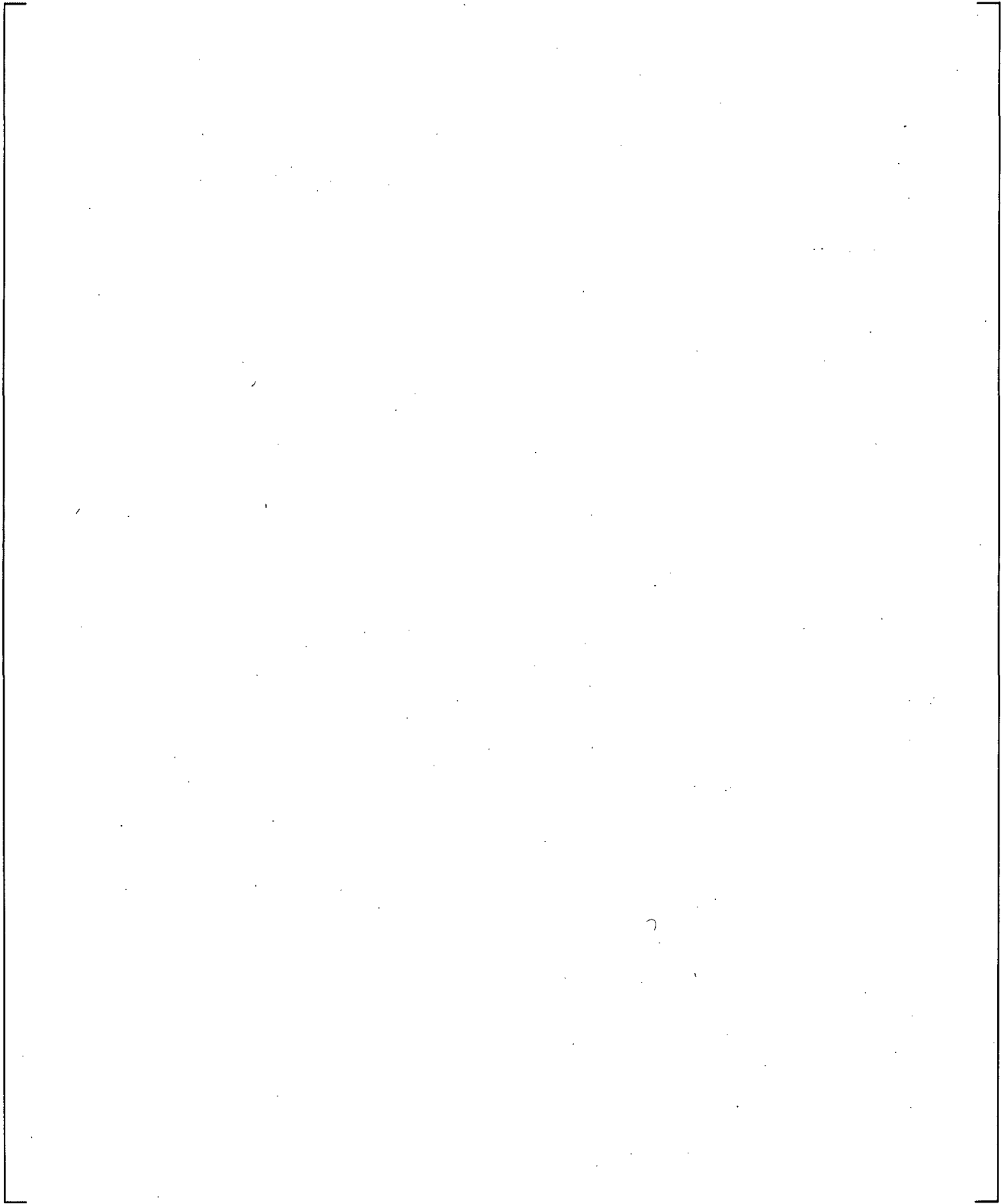


**Figure 21.6-3 Comparison of Loop-A Flow Rates**

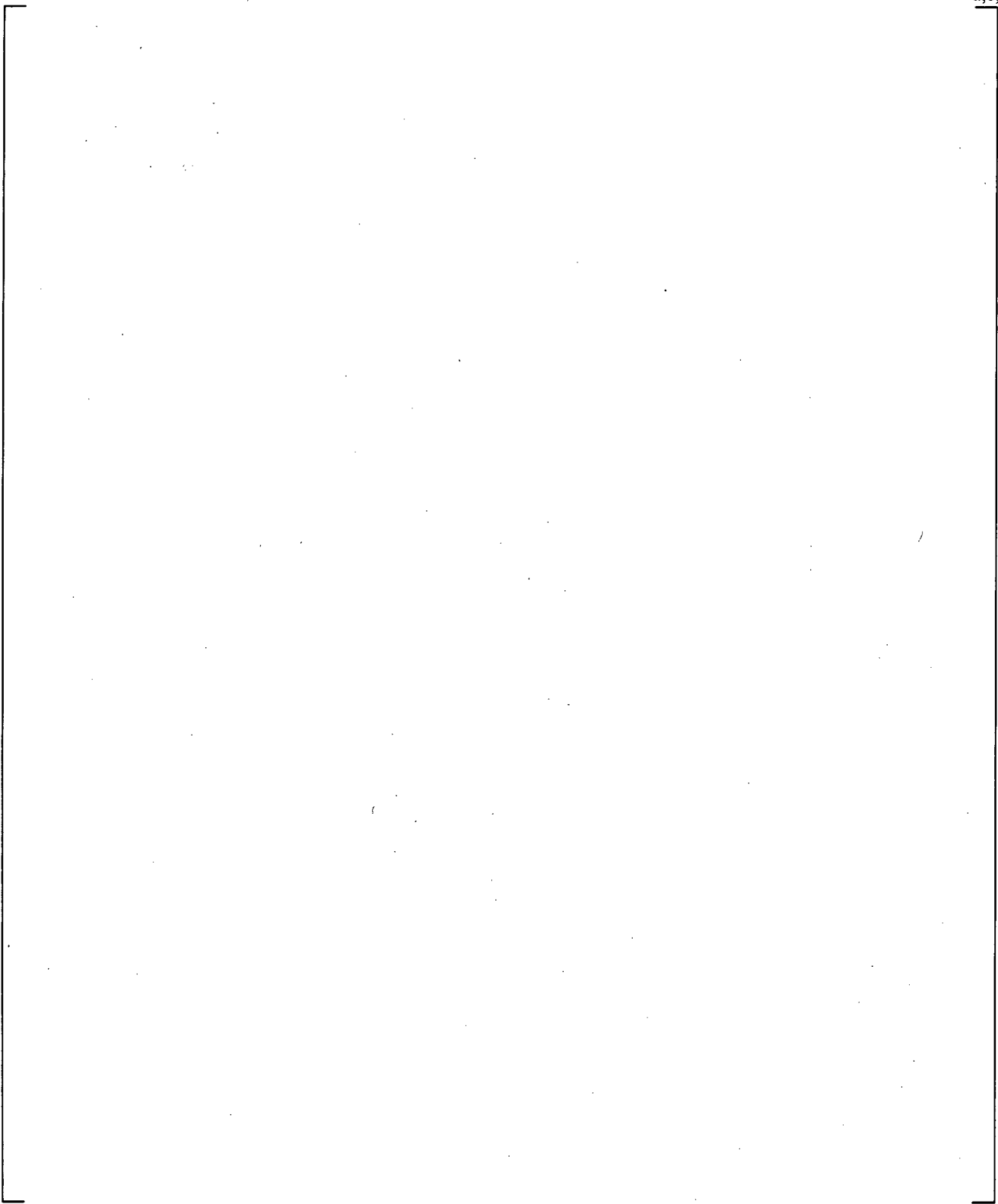
a,c,e



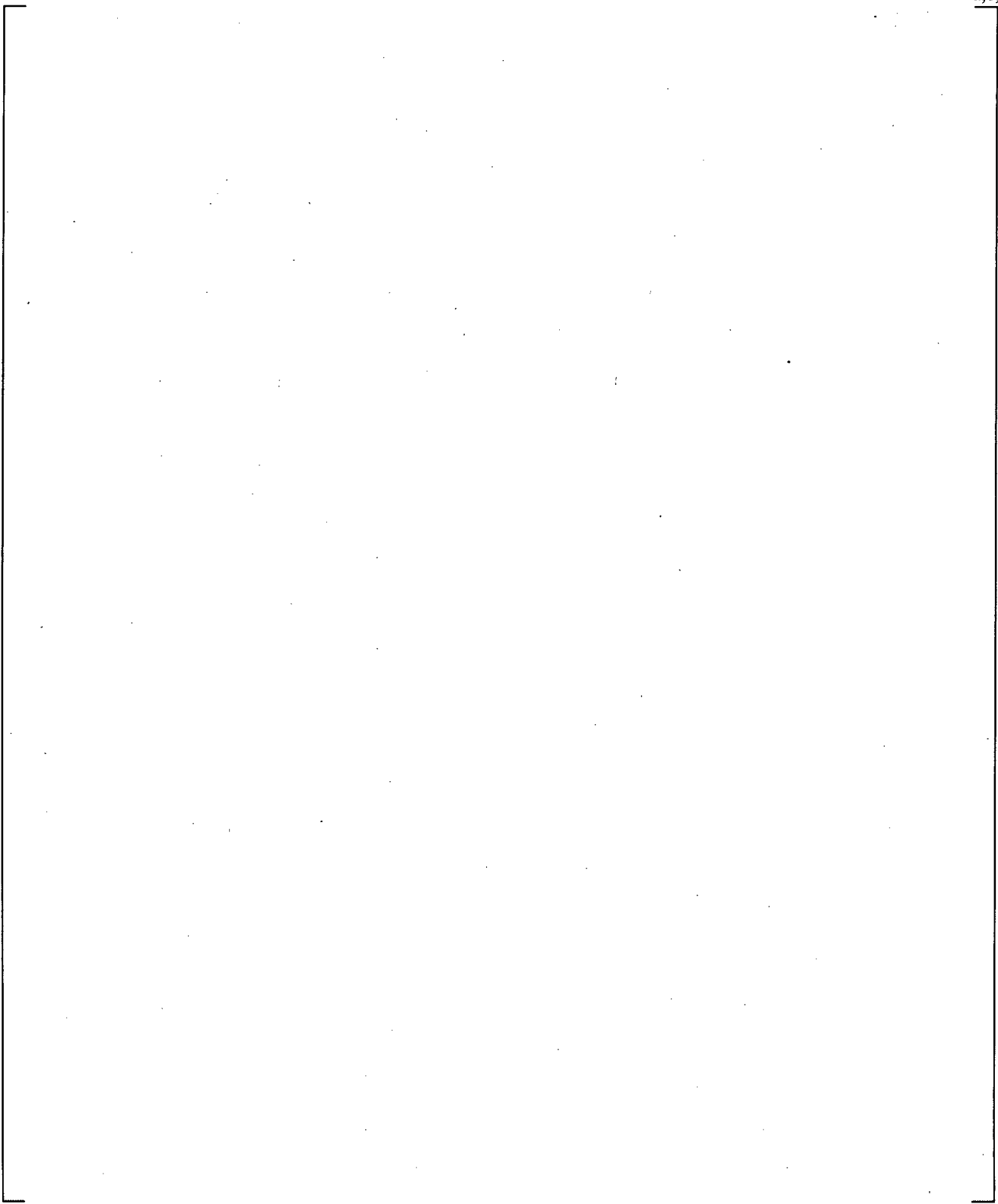
**Figure 21.6-4 Comparison of Loop-B Flow Rates**



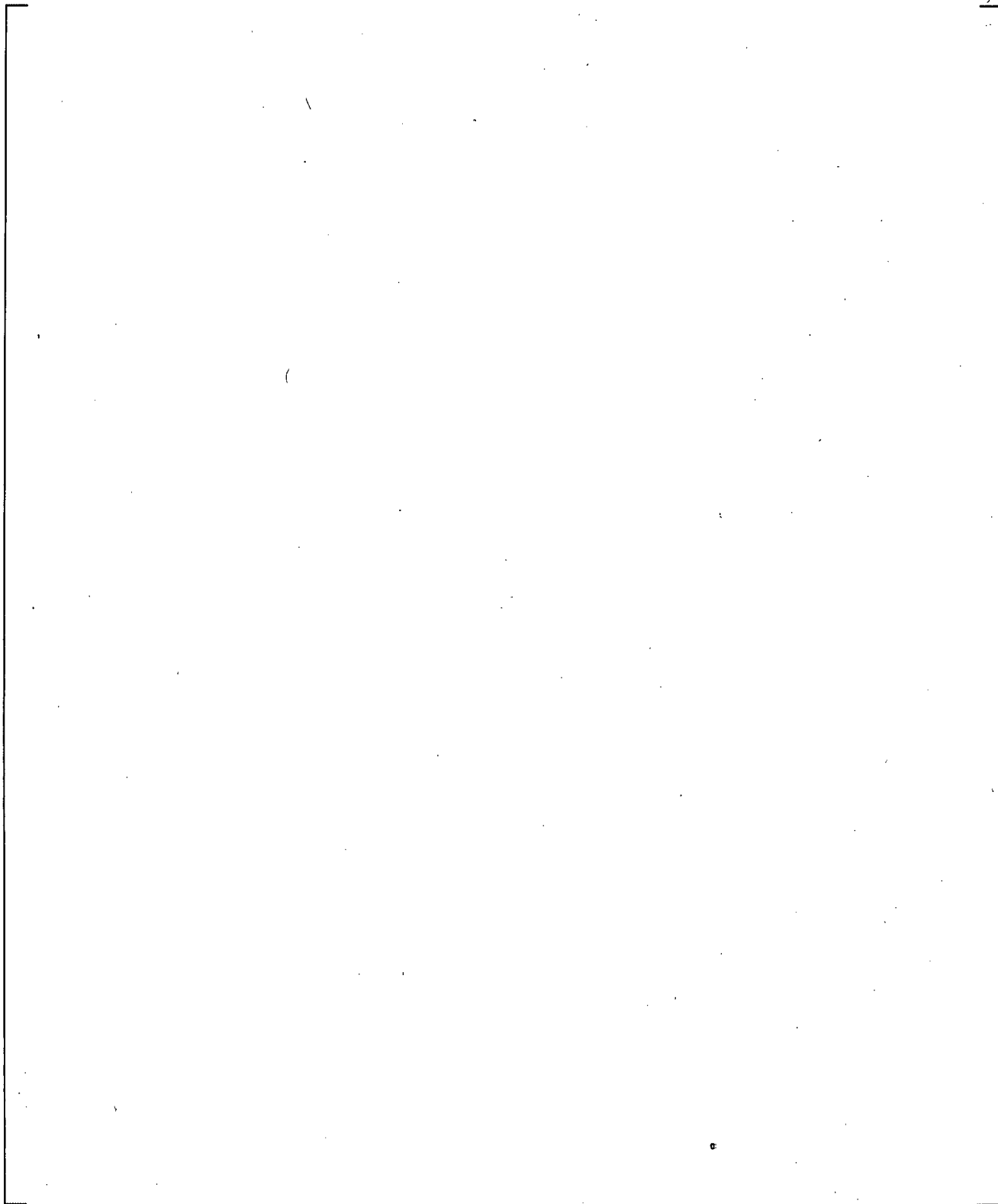
**Figure 21.6-5 Comparison of Break Flows**



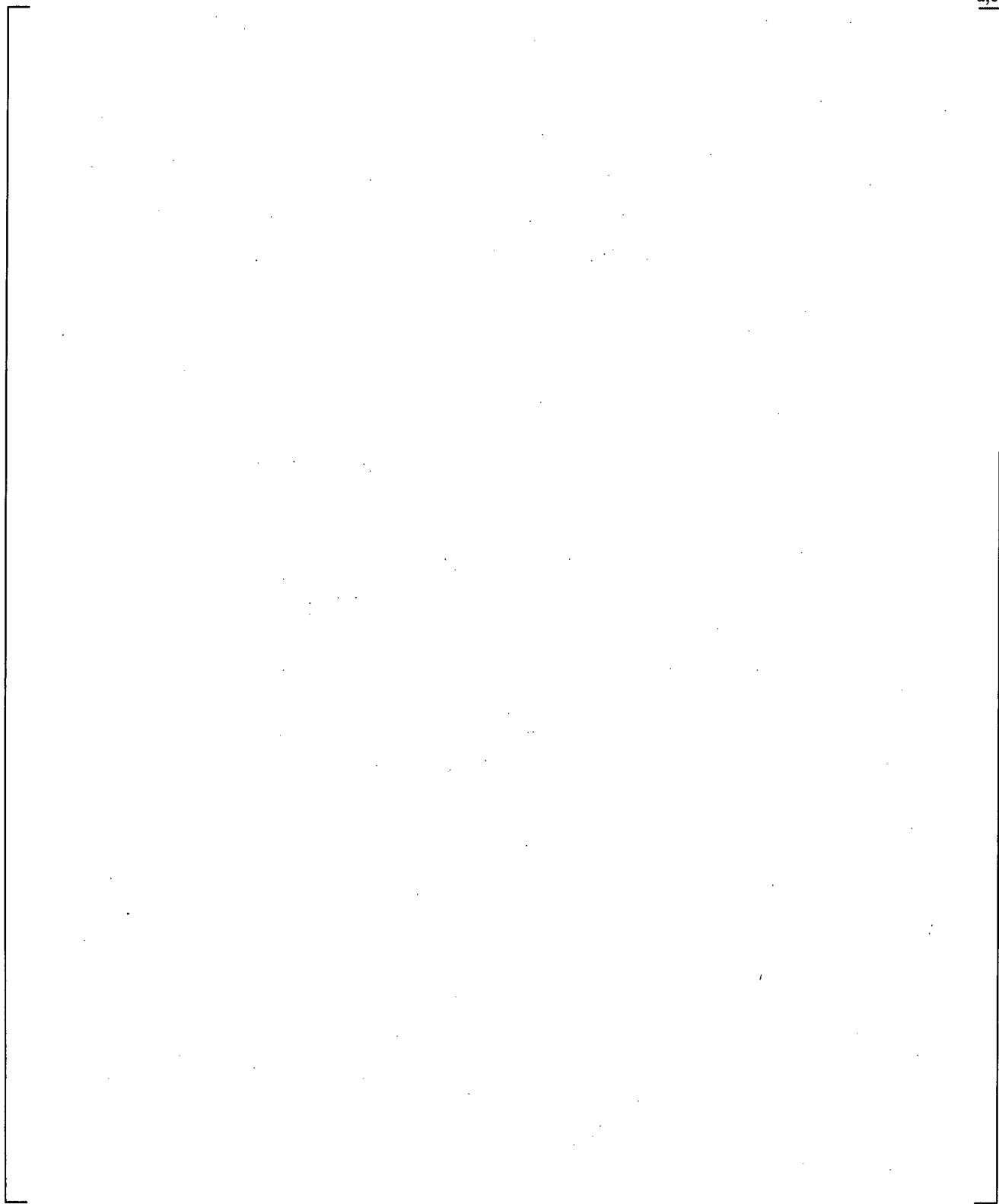
**Figure 21.6-6 Comparison of Fluid Density in the Break Spool**



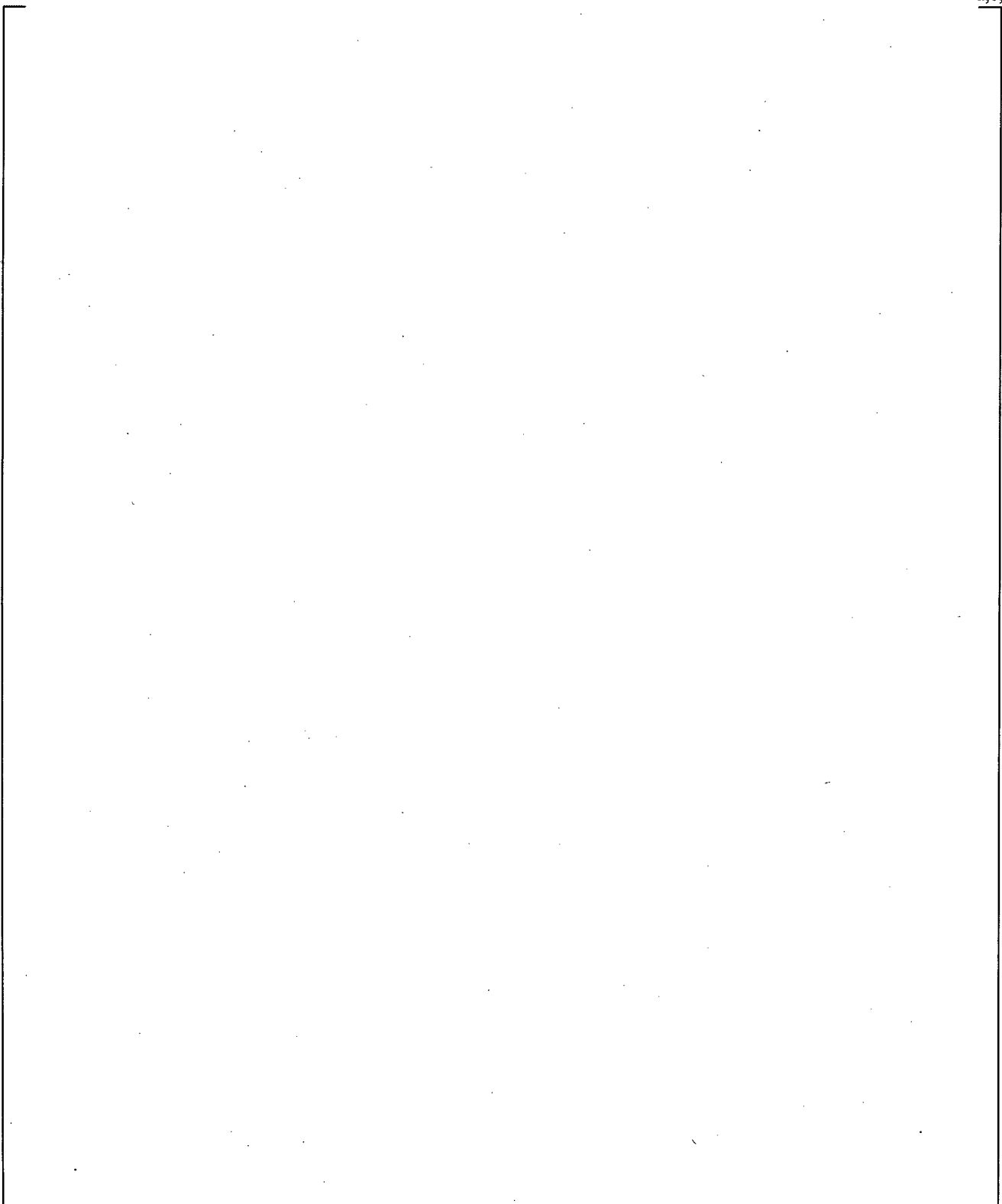
**Figure 21.6-7 Comparison of Loop-B Cross-Over Leg Differential Pressures**



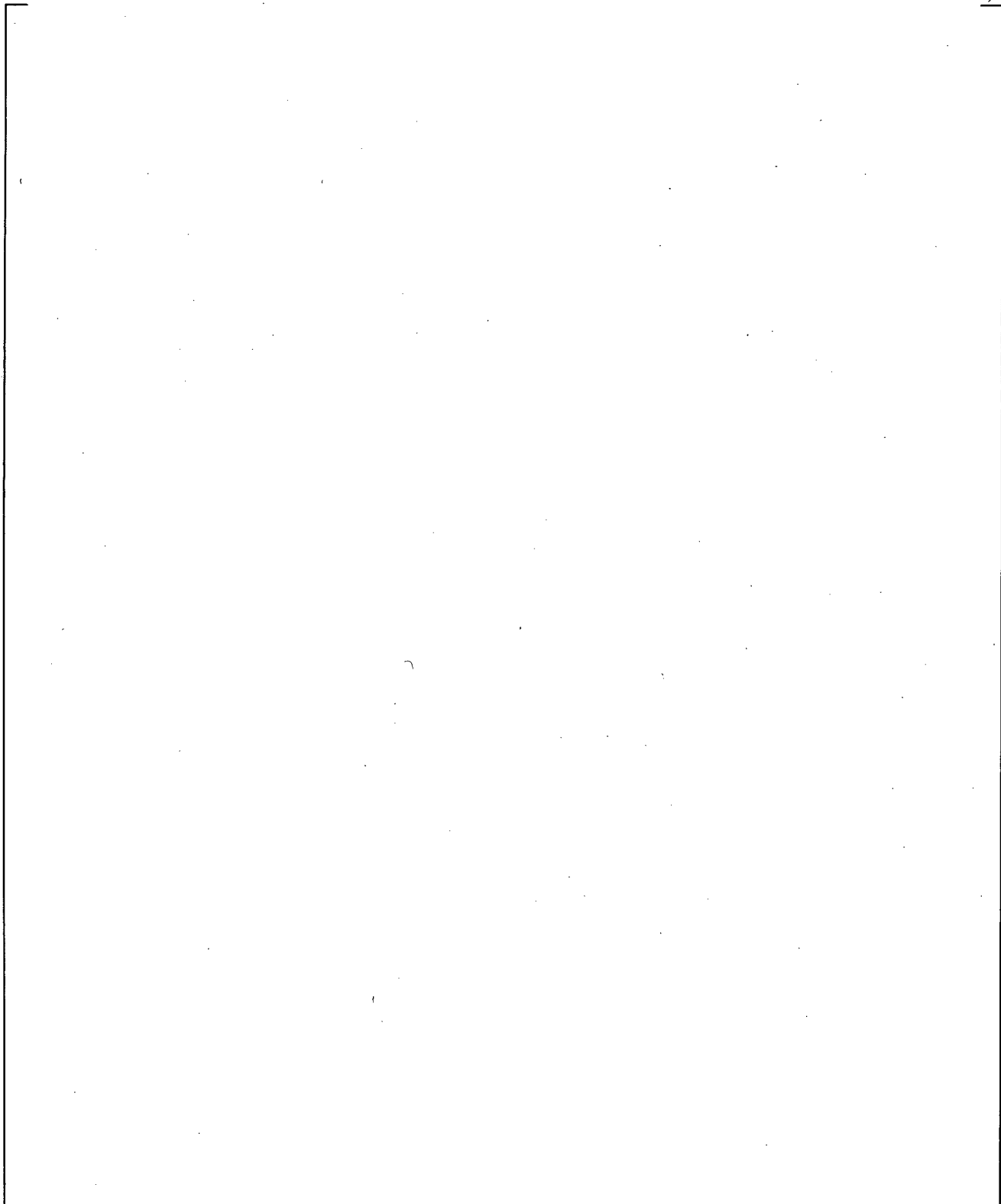
**Figure 21.6-8 Comparison of System Pressures**



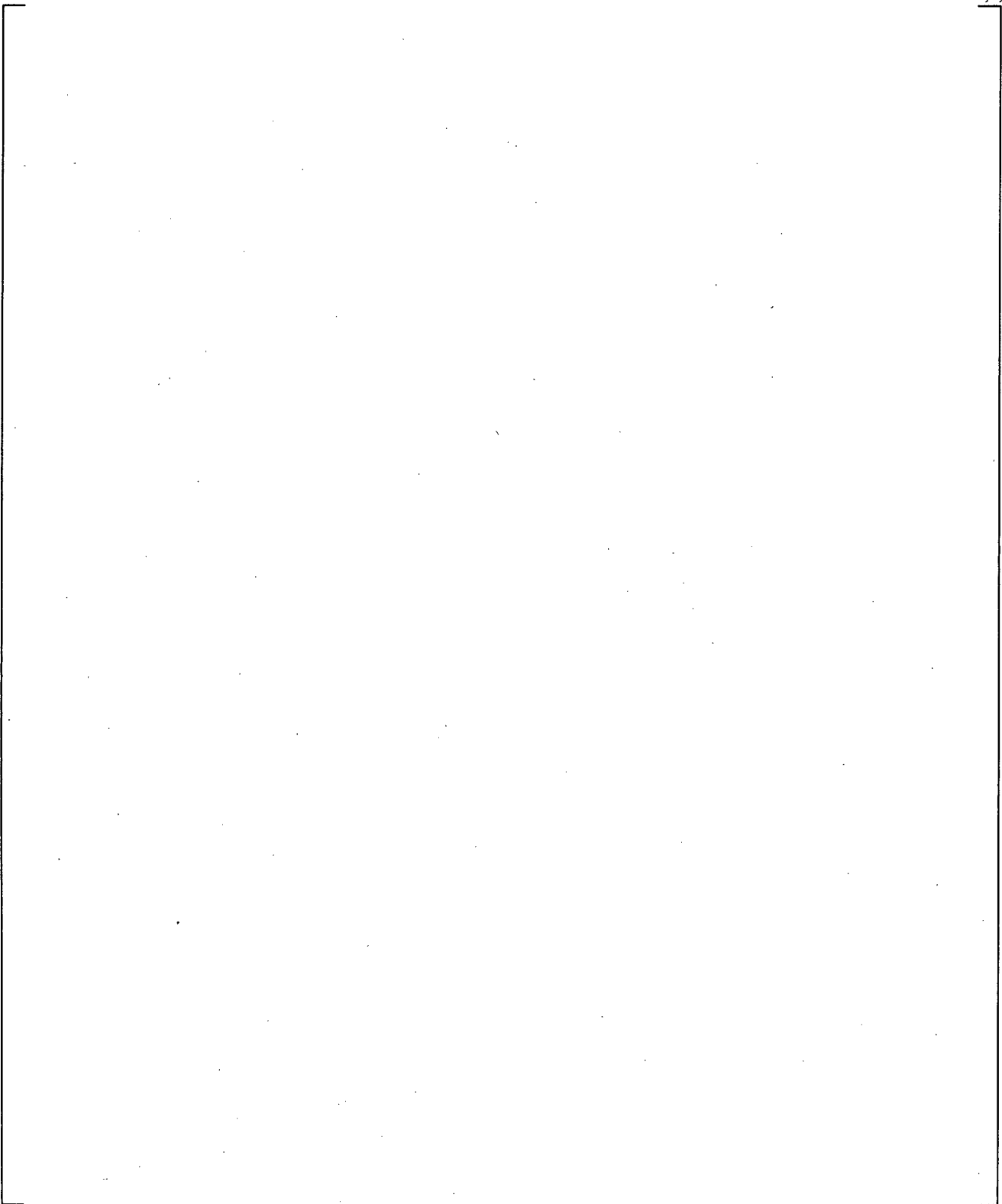
**Figure 21.6-9 Comparison of SG-A U-tube Inlet-to-top Differential Pressures**



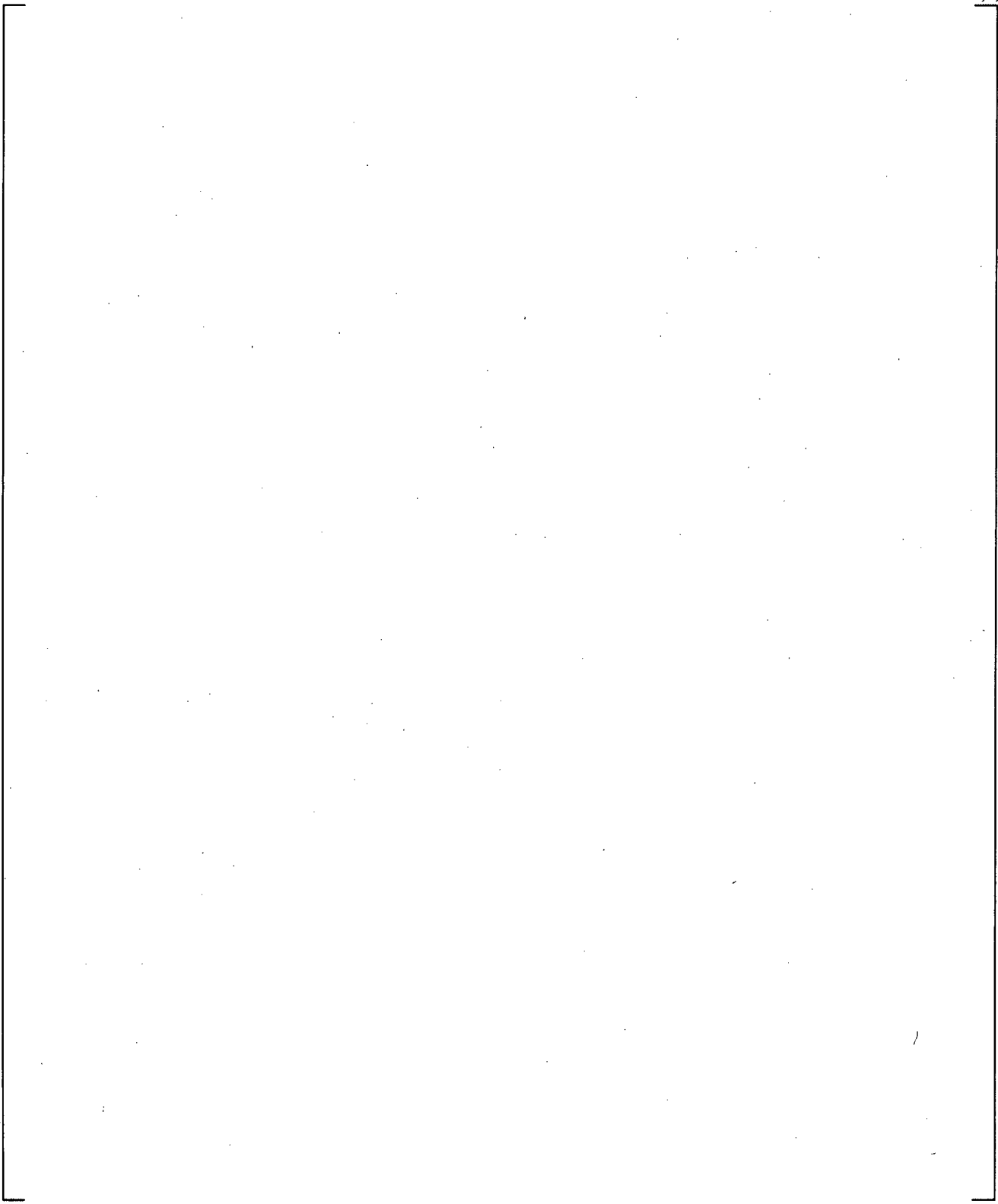
**Figure 21.6-10 Comparison of SG-B U-tube Inlet-to-top Differential Pressures**



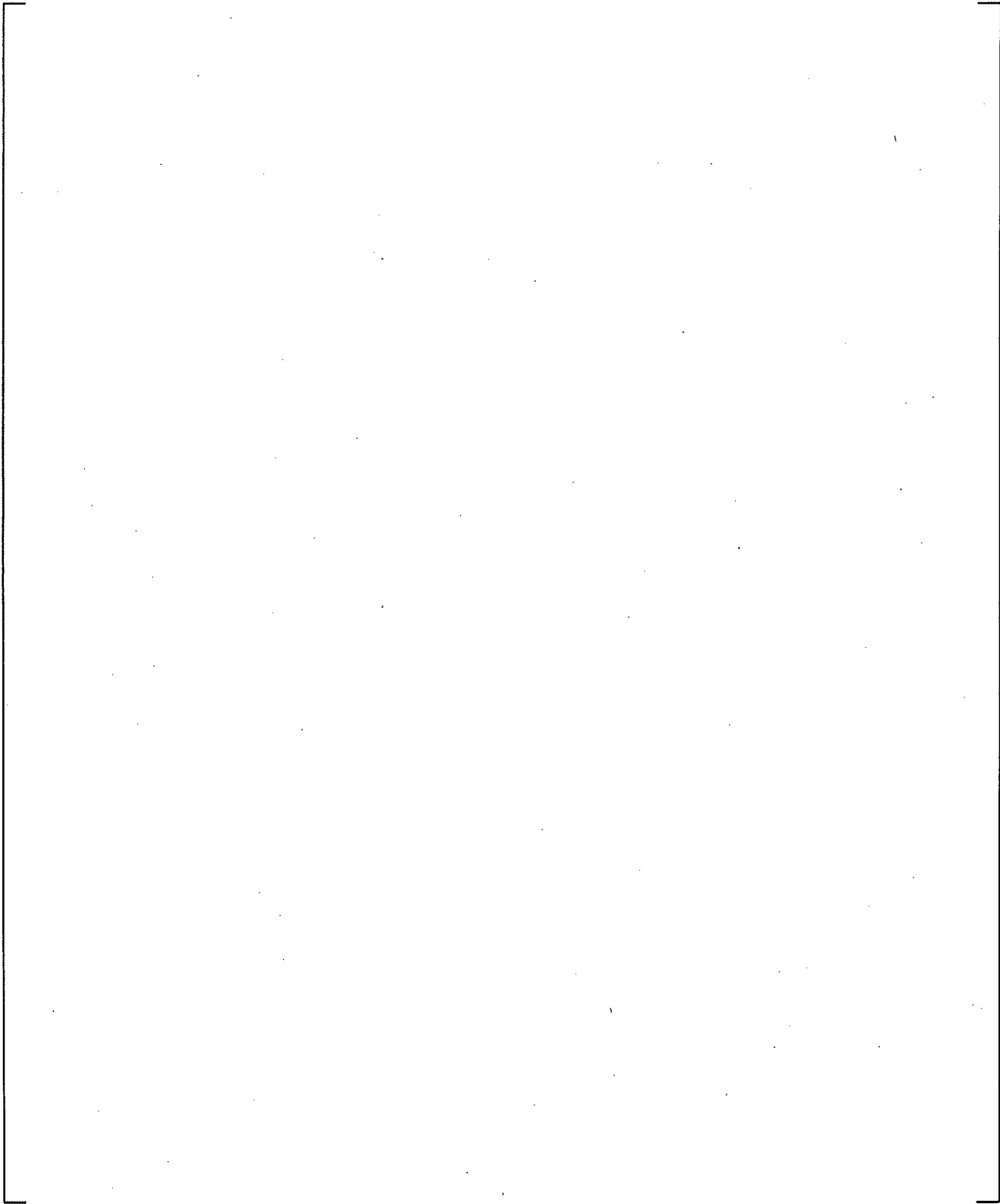
**Figure 21.6-11 Comparison of SG-A U-tube Outlet-to-top Differential Pressures**



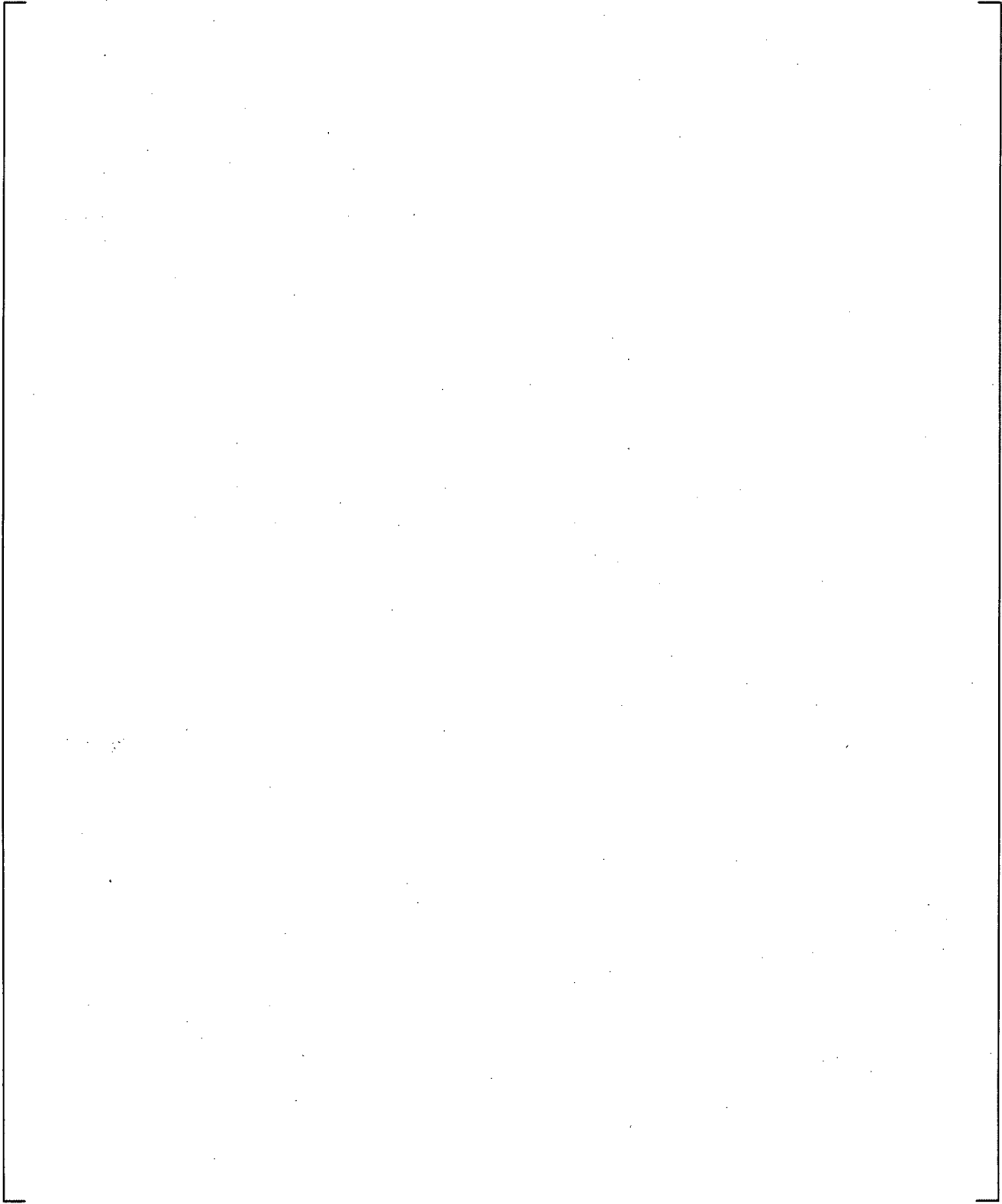
**Figure 21.6-12 Comparison of SG-B U-tube Outlet-to-top Differential Pressures**



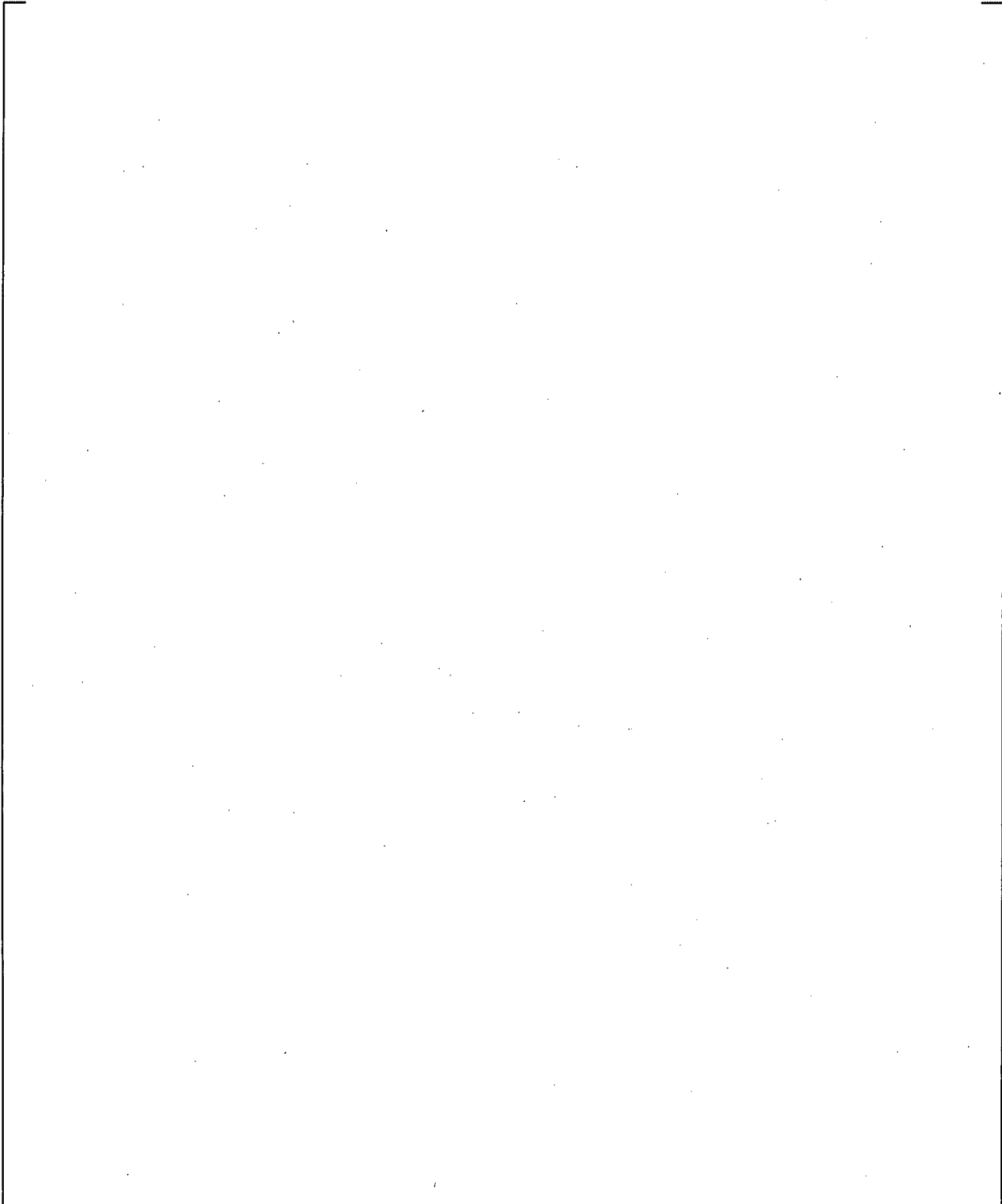
**Figure 21.6-13 Comparison of SG\_A Inlet Plenum Draining**



**Figure 21.6-14 Comparison of Core Collapsed Liquid Levels**



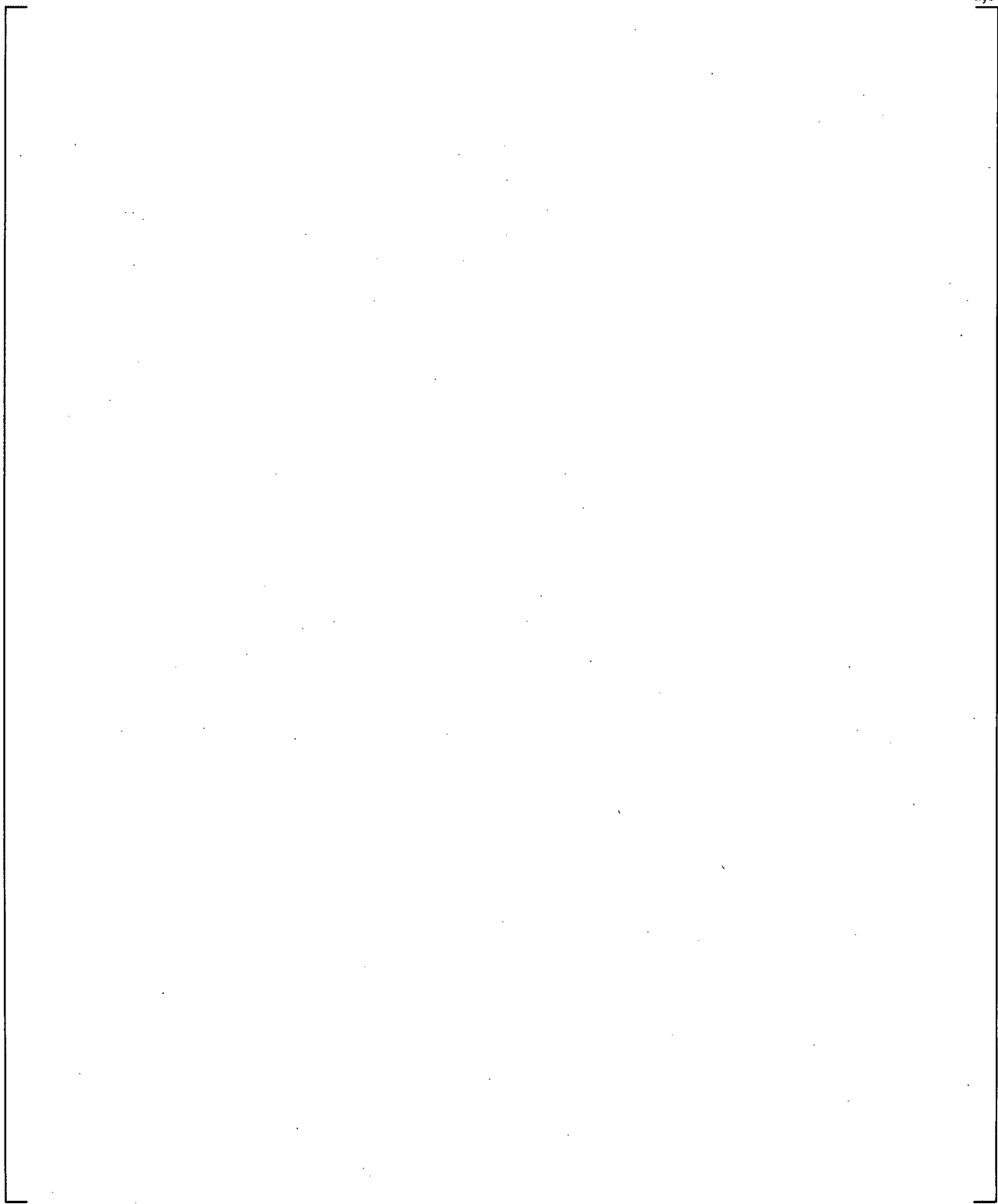
**Figure 21.6-15 Calculated Accumulator Injection Flows**



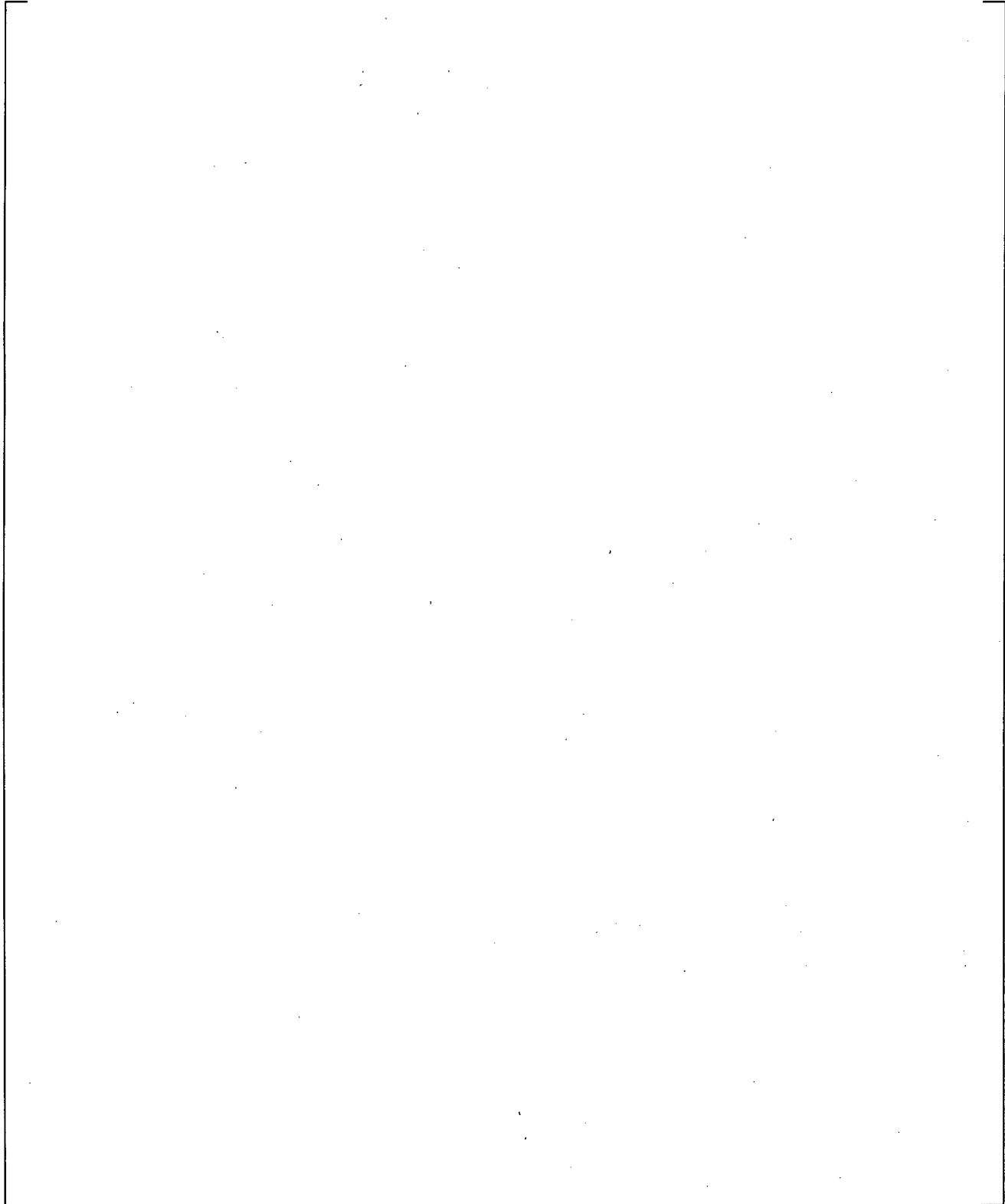
**Figure 21.6-16 High Power Rod (Rod 1) Cladding Temperature**

e

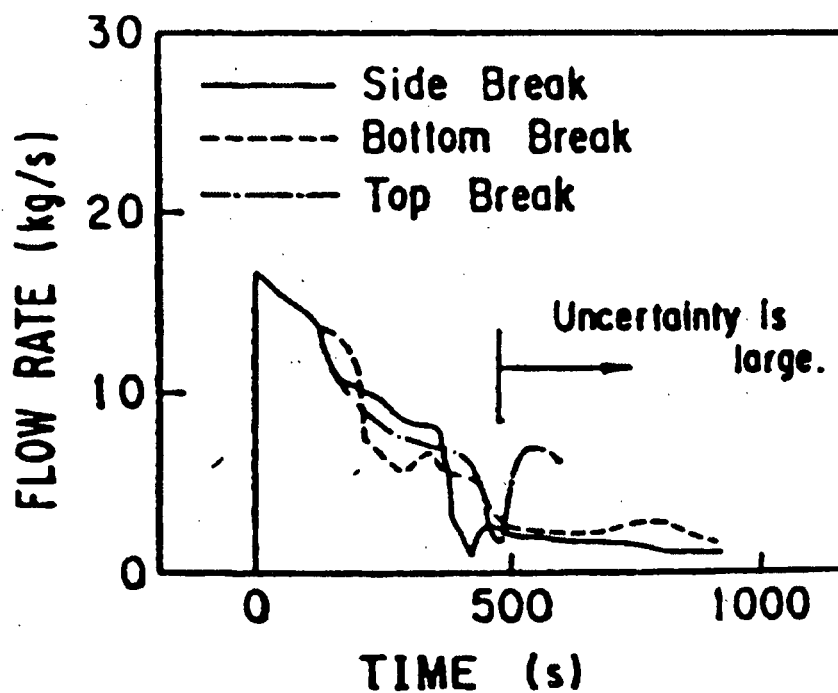
**Figure 21.7-1 Break Unit Configuration used in 2.5% Cold Leg Break Tests, SB-CL-01, 02, and 03 (Koizumi, et al., 1987)**



**Figure 21.7-2 WCOBRA/TRAC-TF2 Nodalization of LSTF Break Unit**

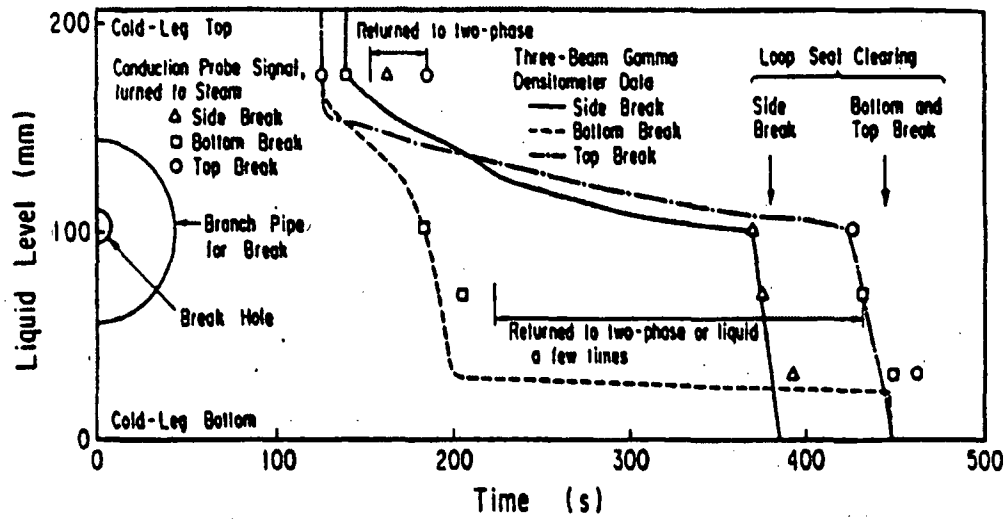


**Figure 21.7-3 Comparison of Predicted and Measured Primary System Pressure (ROSA-IV 2.5-Percent Cold Leg Break)**



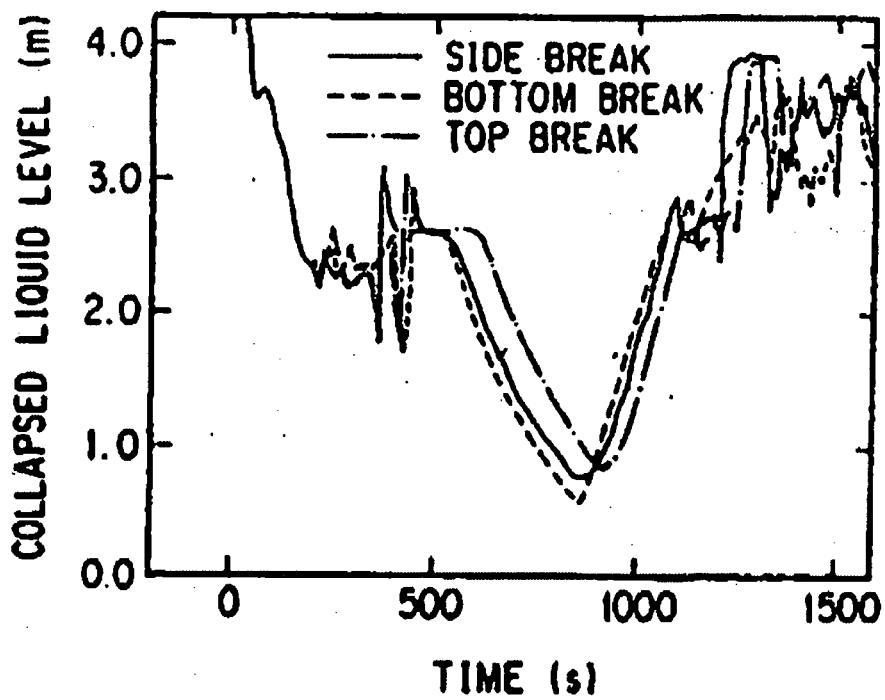
(b) Reported in Reference 5

Figure 21.7-4 Comparison of Predicted and Measured Break Flow rates  
(ROSA-IV 2.5-Percent Cold Leg Break)



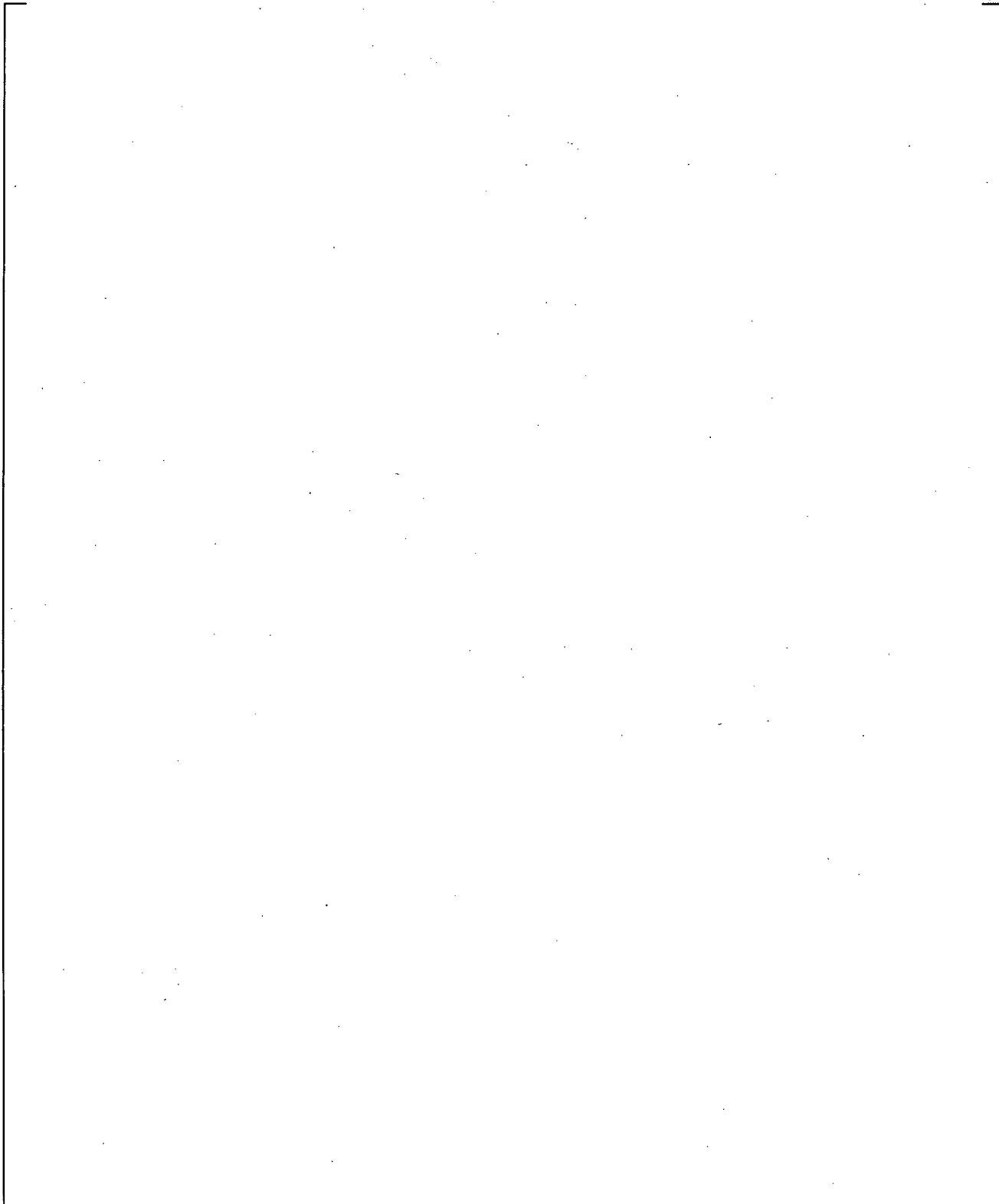
(b) Reported in Reference 5

Figure 21.7-5 Comparison of Predicted and Measured Mixture Levels in Broken Cold Leg (ROSA-IV 2.5-Percent Cold Leg Break Runs)



(b) Reported in Reference 5

Figure 21.7-6 Comparison of Predicted and Measured Core Collapsed Liquid Levels (ROSA-IV 2.5-Percent Cold Leg Break Runs)



**Figure 21.7-7** Cladding Temperature of B-20 Rod at Position 7 (8.67-ft Elevation) for Side, Bottom, and Top Break Experiments

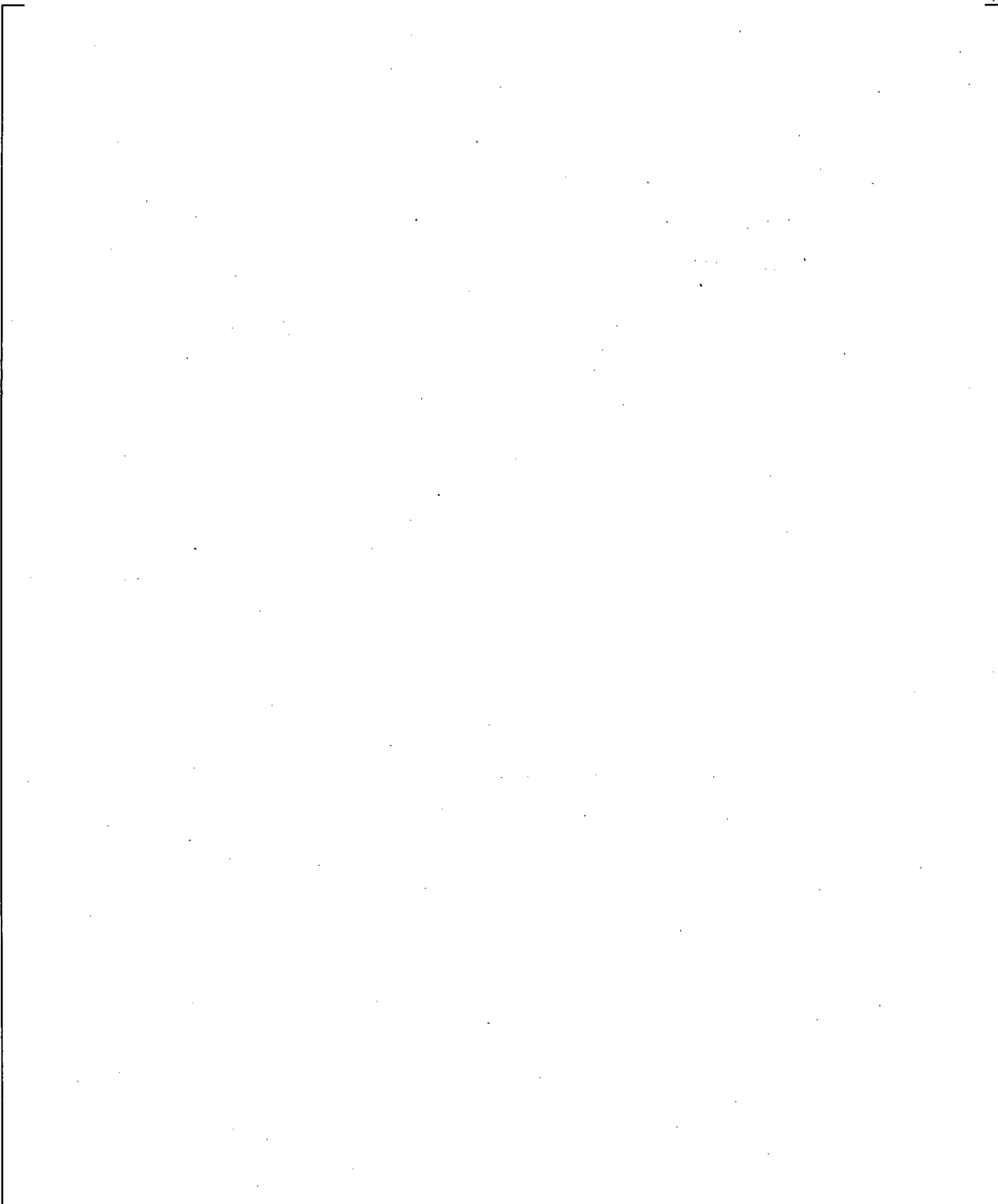


**Figure 21.7-8 Predicted and Measured Differential Pressures in SGA Uphill Side**

Note: The observed draining of the steam generator U-tubes for the SB-CL-02 (bottom) and SB-CL-03 (top) tests were very similar, according to the test data provided in Reference 4.

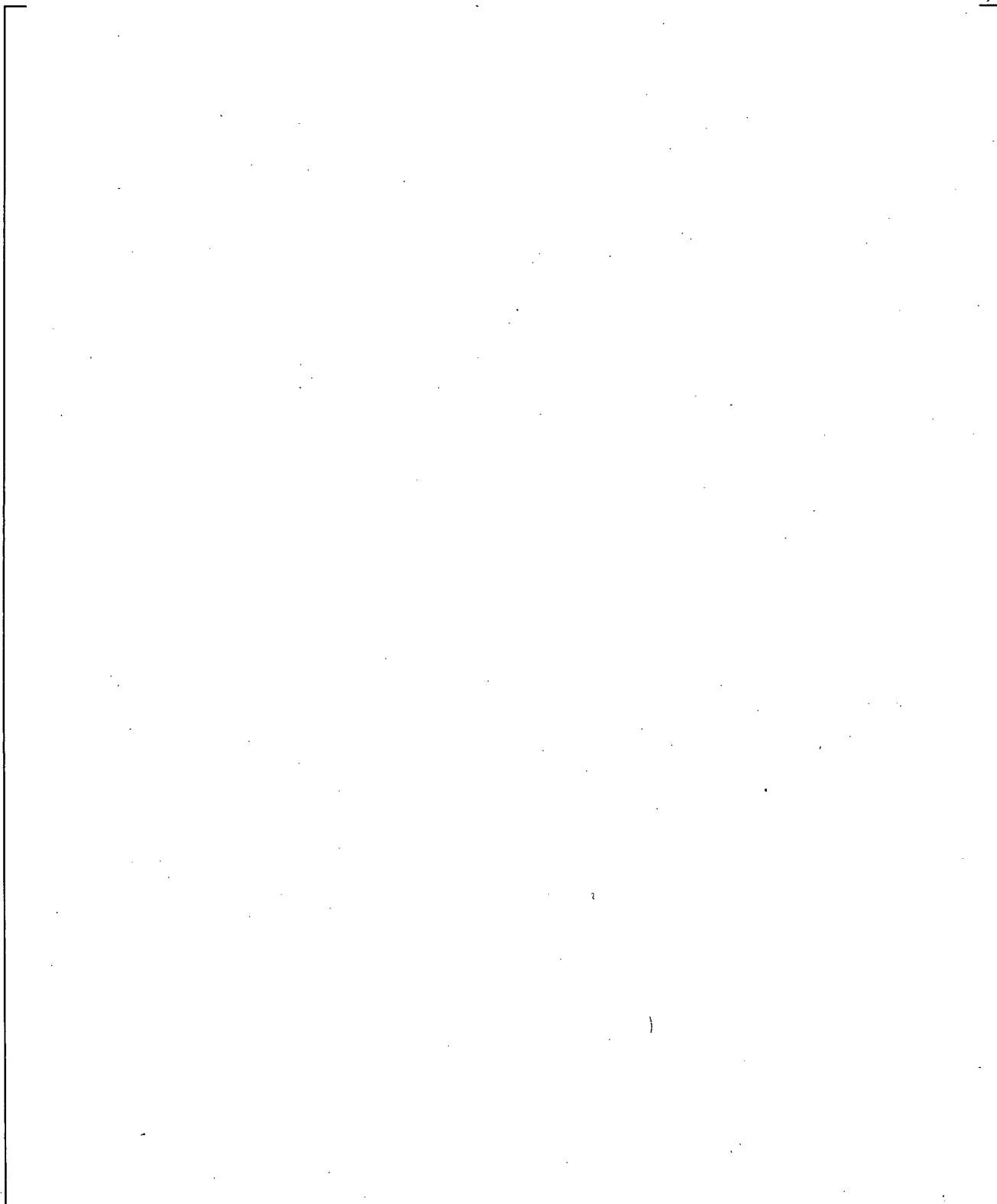


**Figure 21.7-9 Predicted and Measured Differential Pressures in SGB Uphill Side**

Note: The observed draining of the steam generator U-tubes for the SB-CL-02 (bottom) and SB-CL-03 (top) tests were very similar, according to the test data provided in Reference 4.

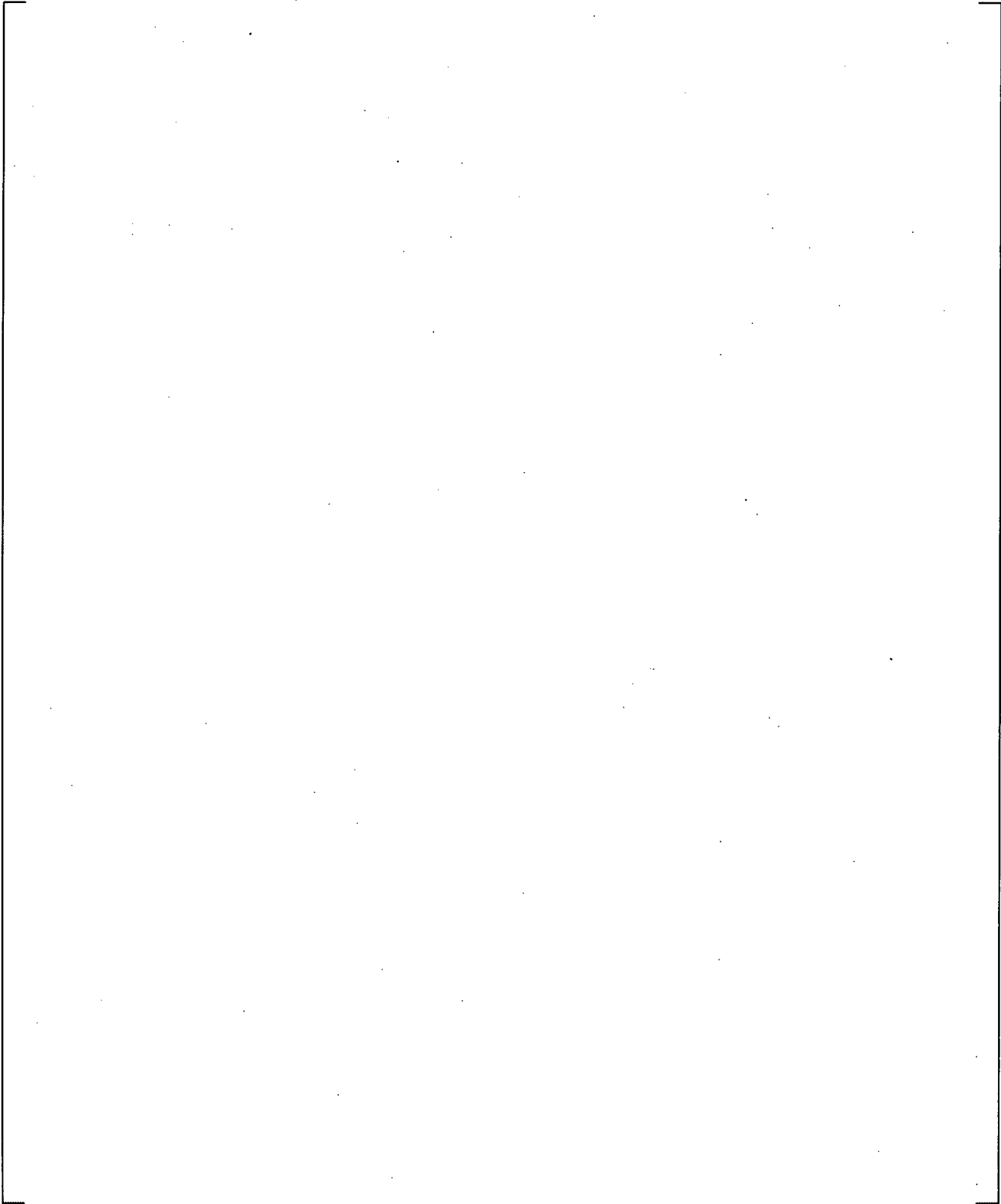


**Figure 21.7-10 Calculated Accumulator Injection Flows**

e

**Figure 21.7-11 Break Unit Configuration used in the 0.5% Break Tests, SB-CL-12, -15, and -16**

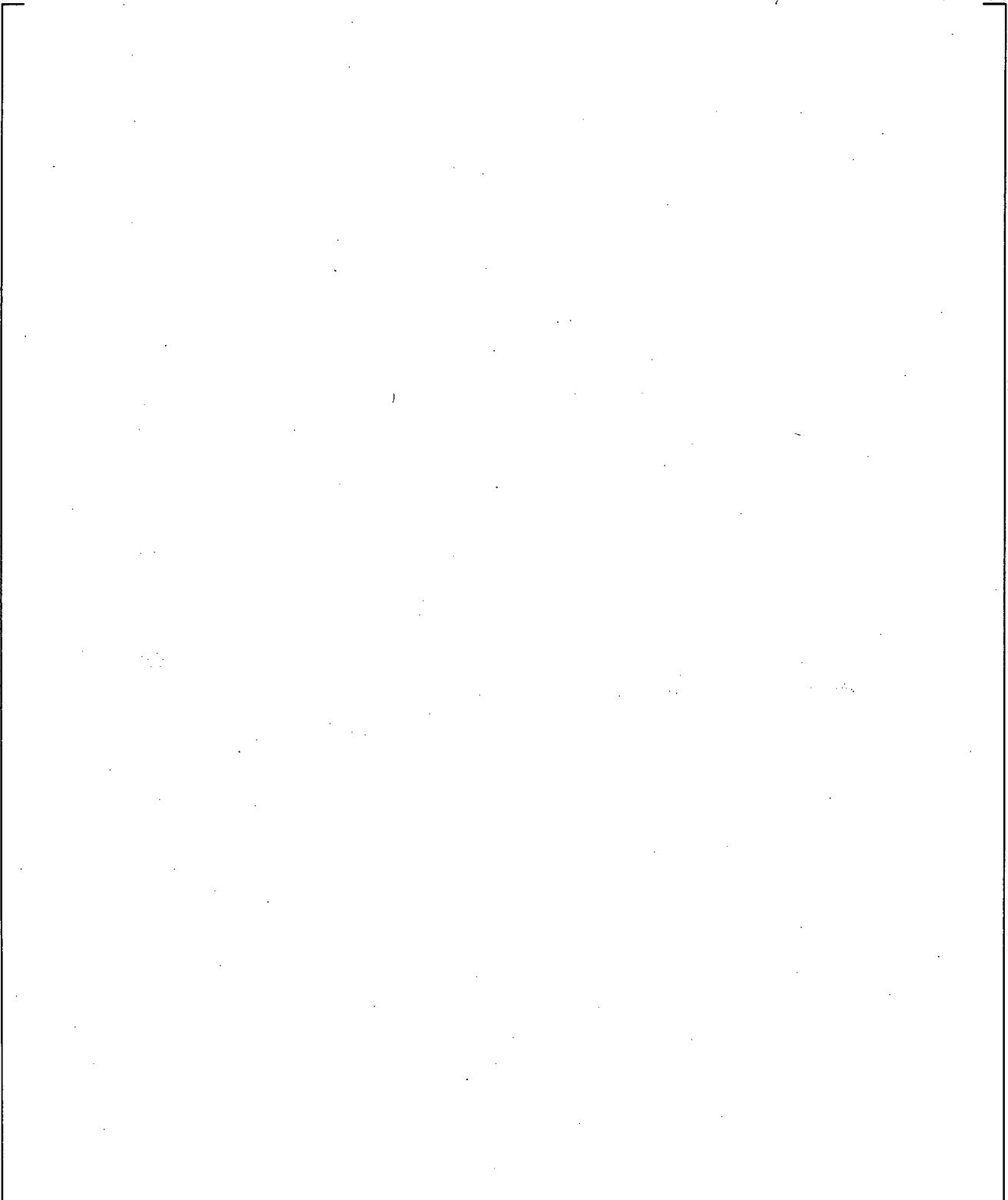


**Figure 21.7-12 Comparison of Predicted and Measured Broken Cold Leg Liquid Levels, ROSA 0.5-Percent Cold Leg Break Runs**

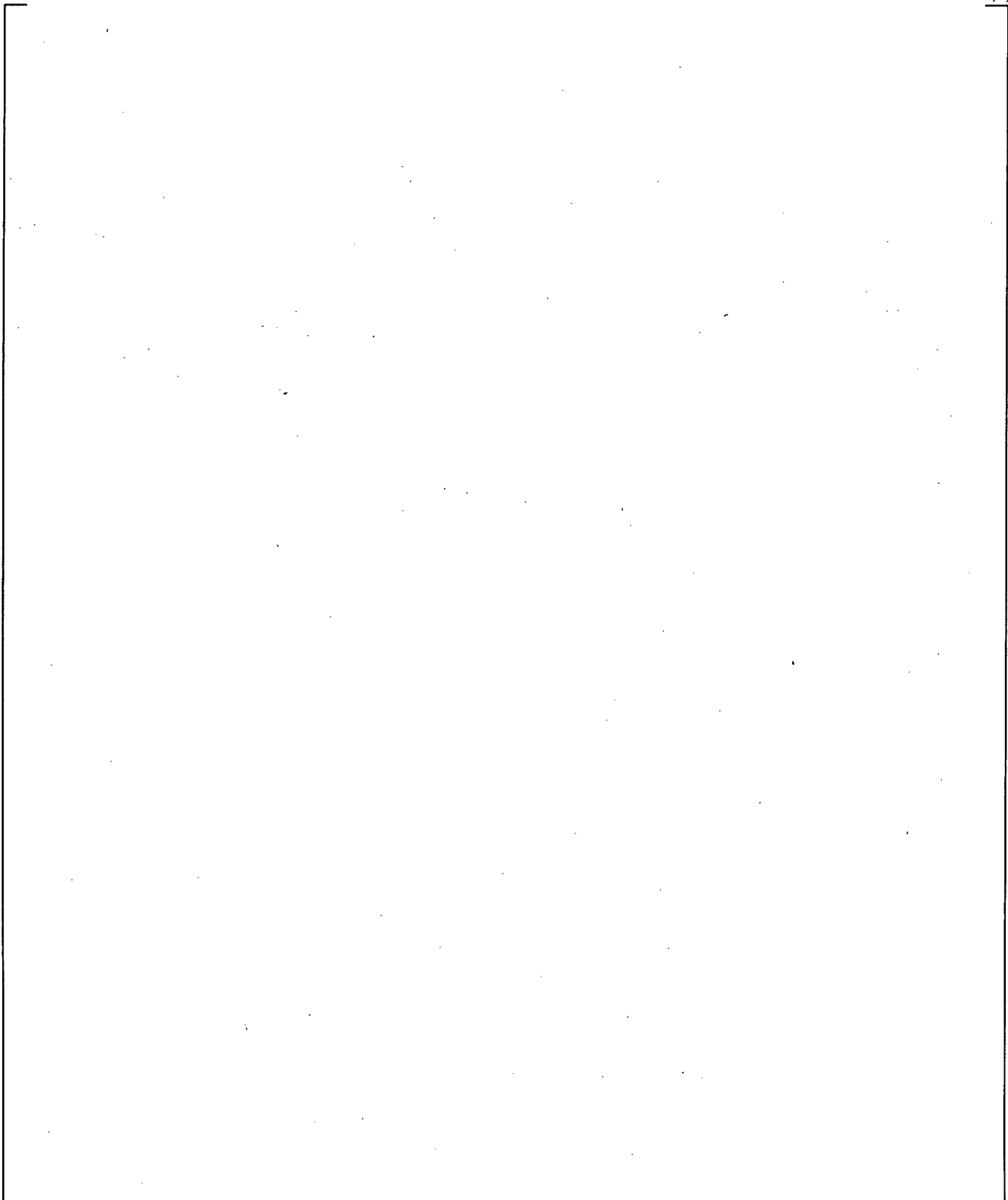


**Figure 21.7-13 Comparison of Predicted and Measured Core Collapsed Liquid Levels, ROSA 0.5-Percent Cold Leg Break Runs**

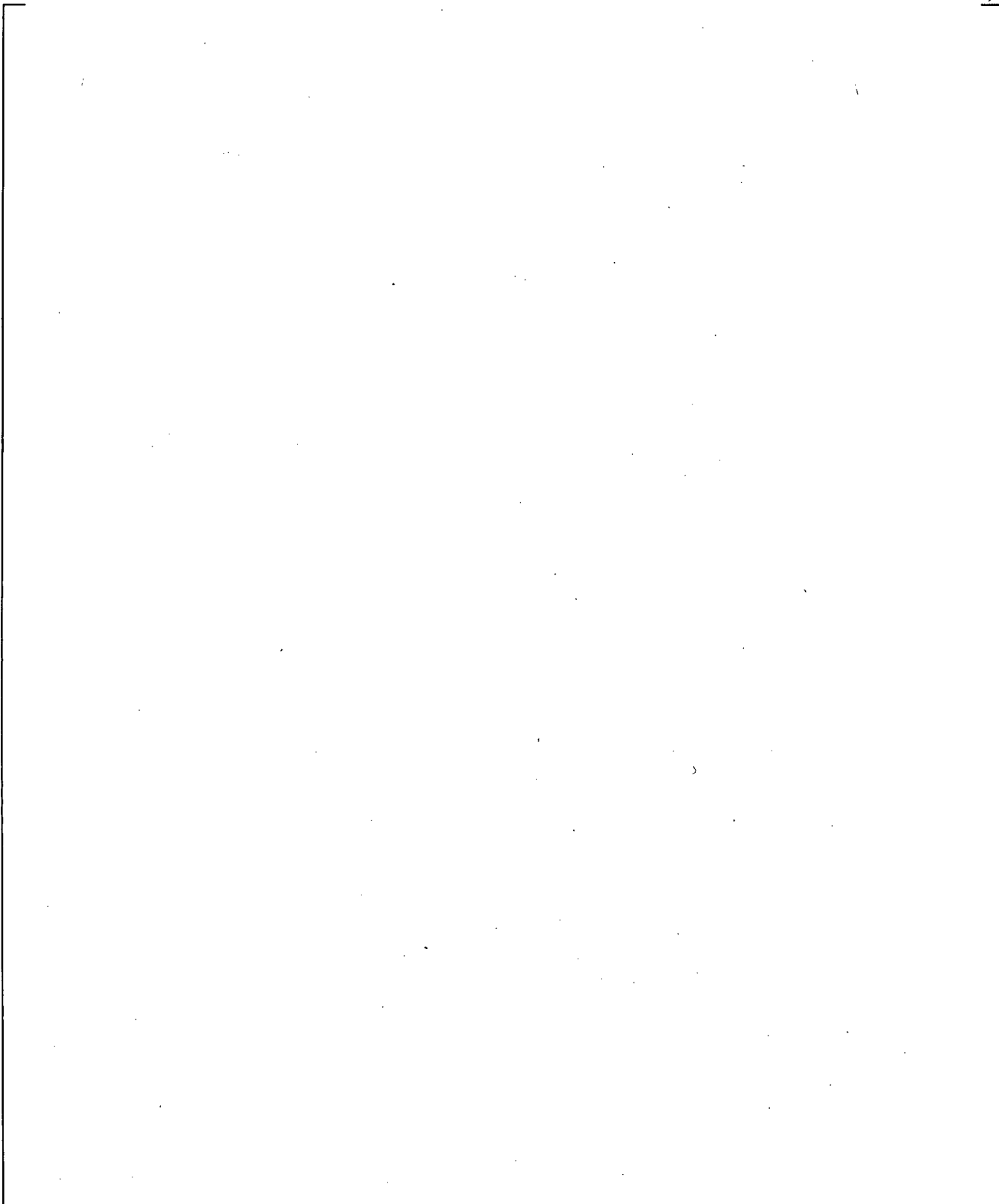


**Figure 21.7-14 Comparison of Predicted and Measured Integrated Break Flows, ROSA  
0.5-Percent Cold Leg Break Runs**

a,c

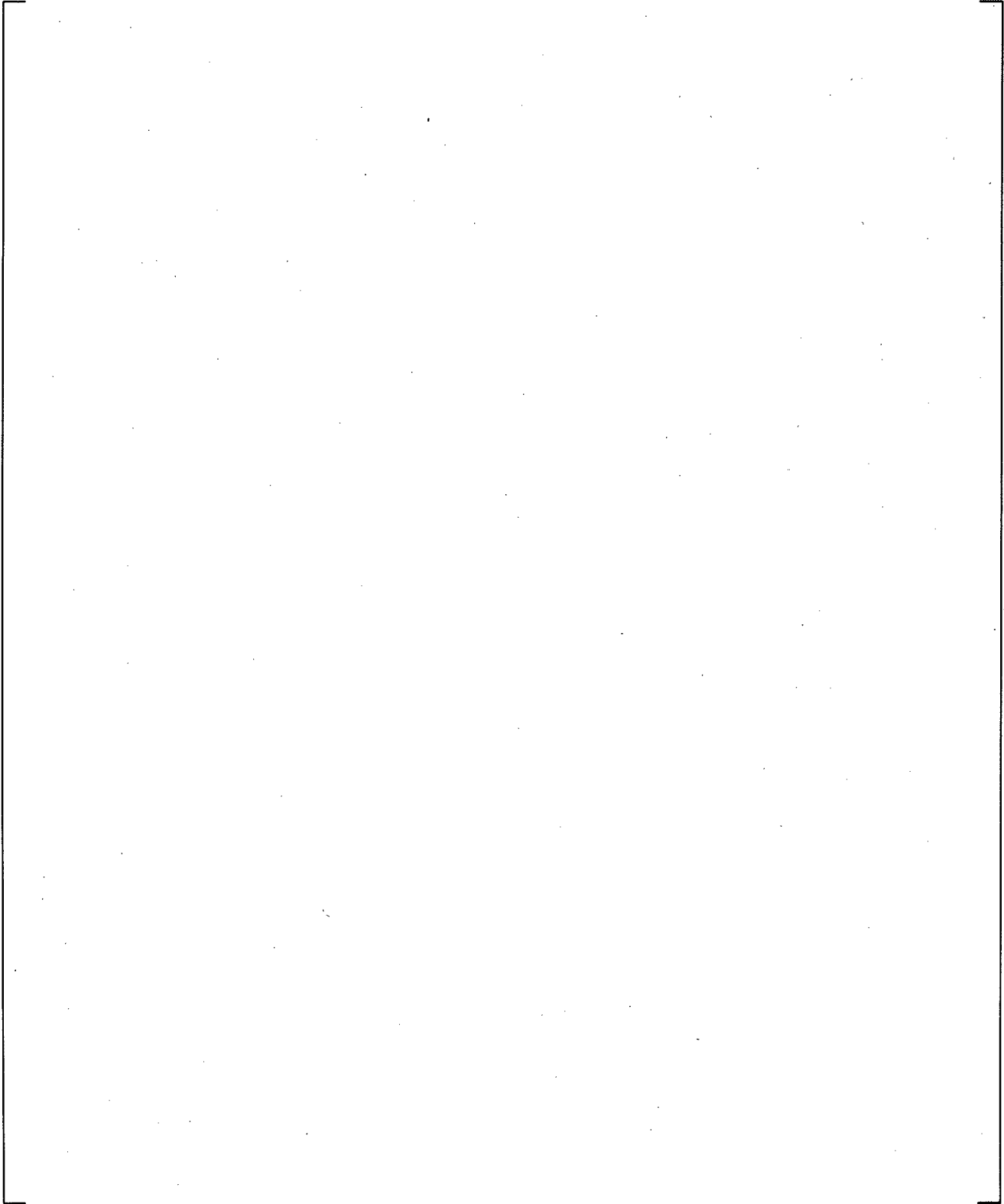


**Figure 21.8-1 Break Flow Comparison**

a,c

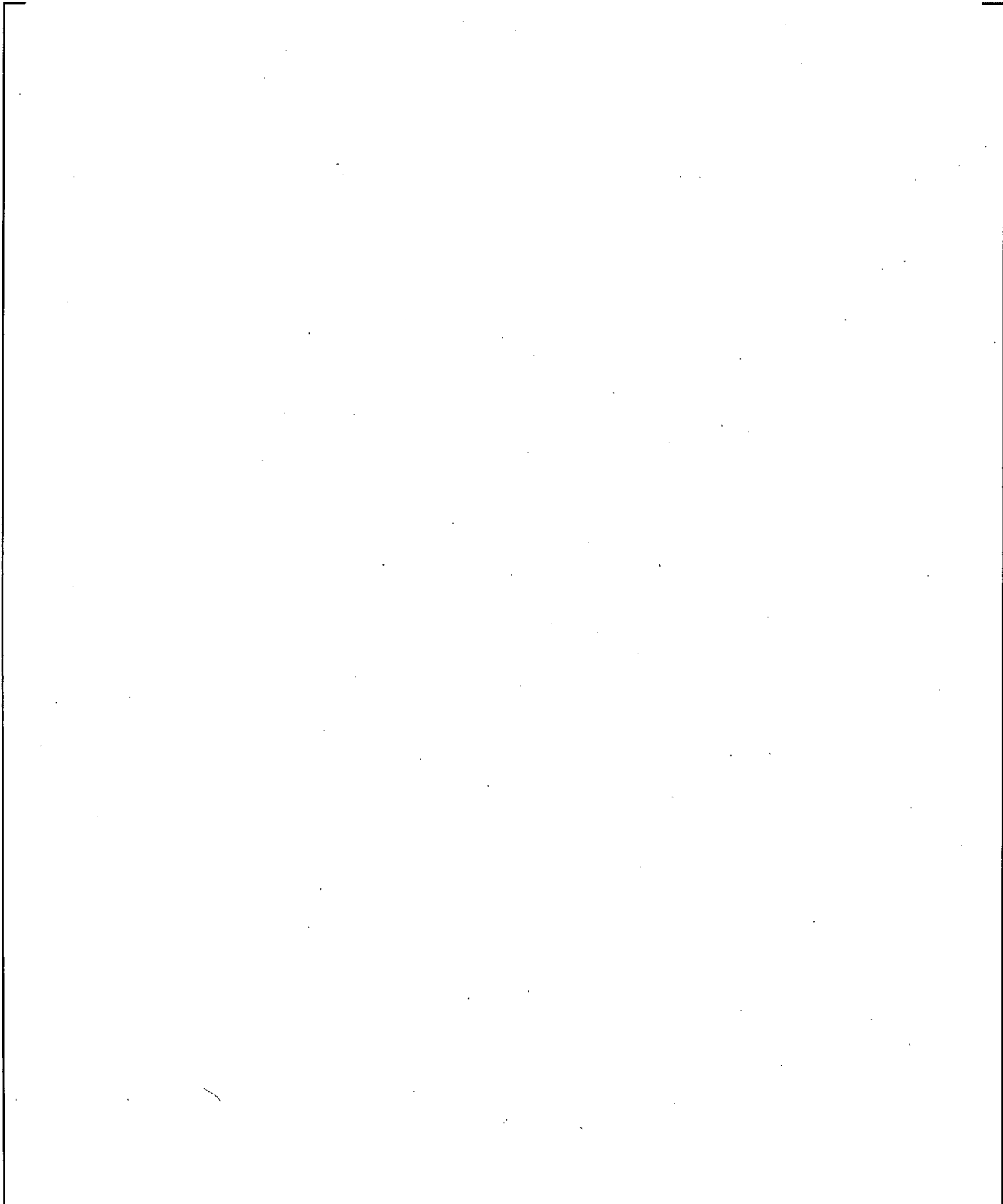


**Figure 21.8-2 System Pressure Comparison**

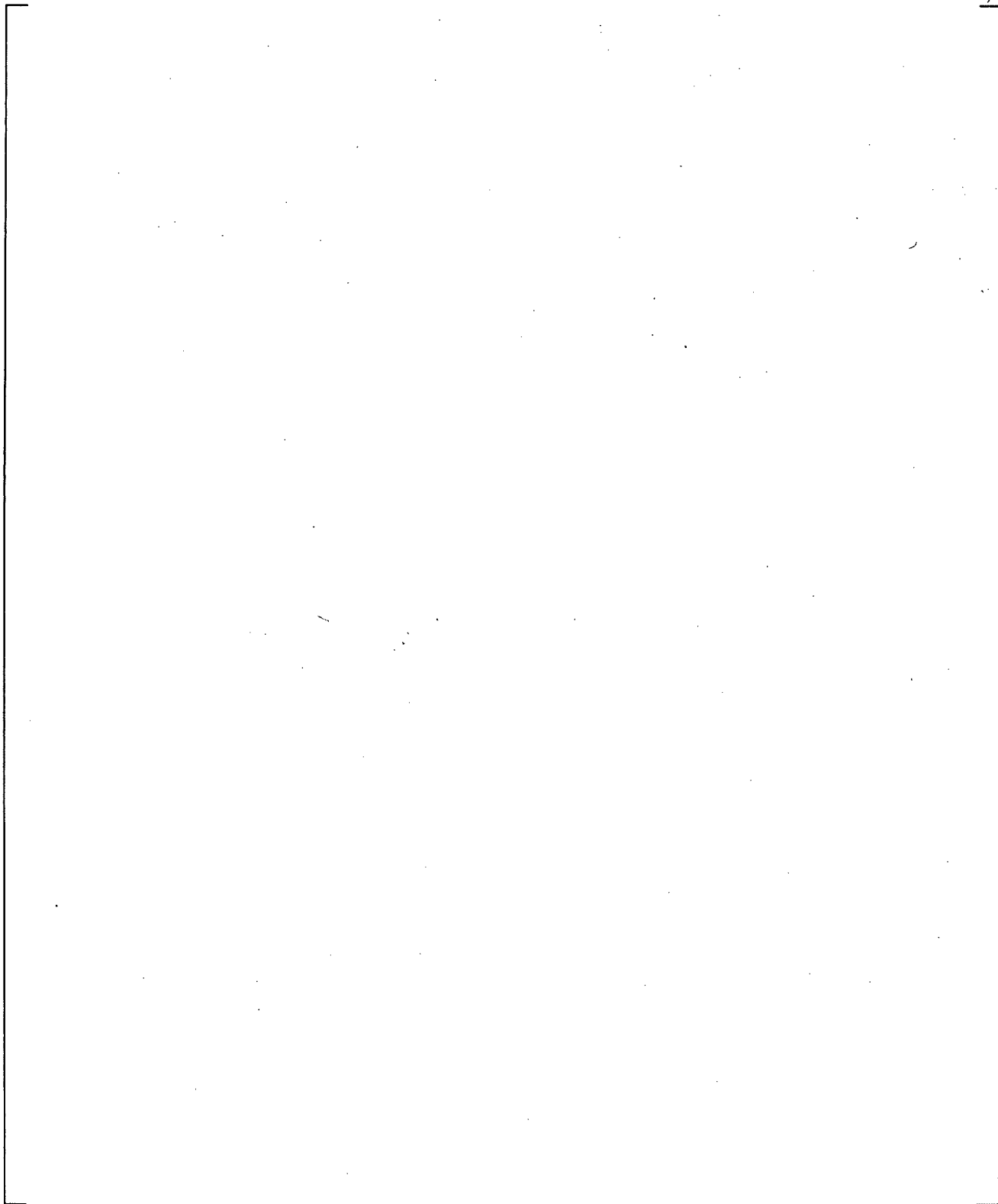


**Figure 21.8-3(a) Cross-over Leg A Vapor Flows**

**Figure 21.8-3(b) Cross-over Leg B Vapor Flows**

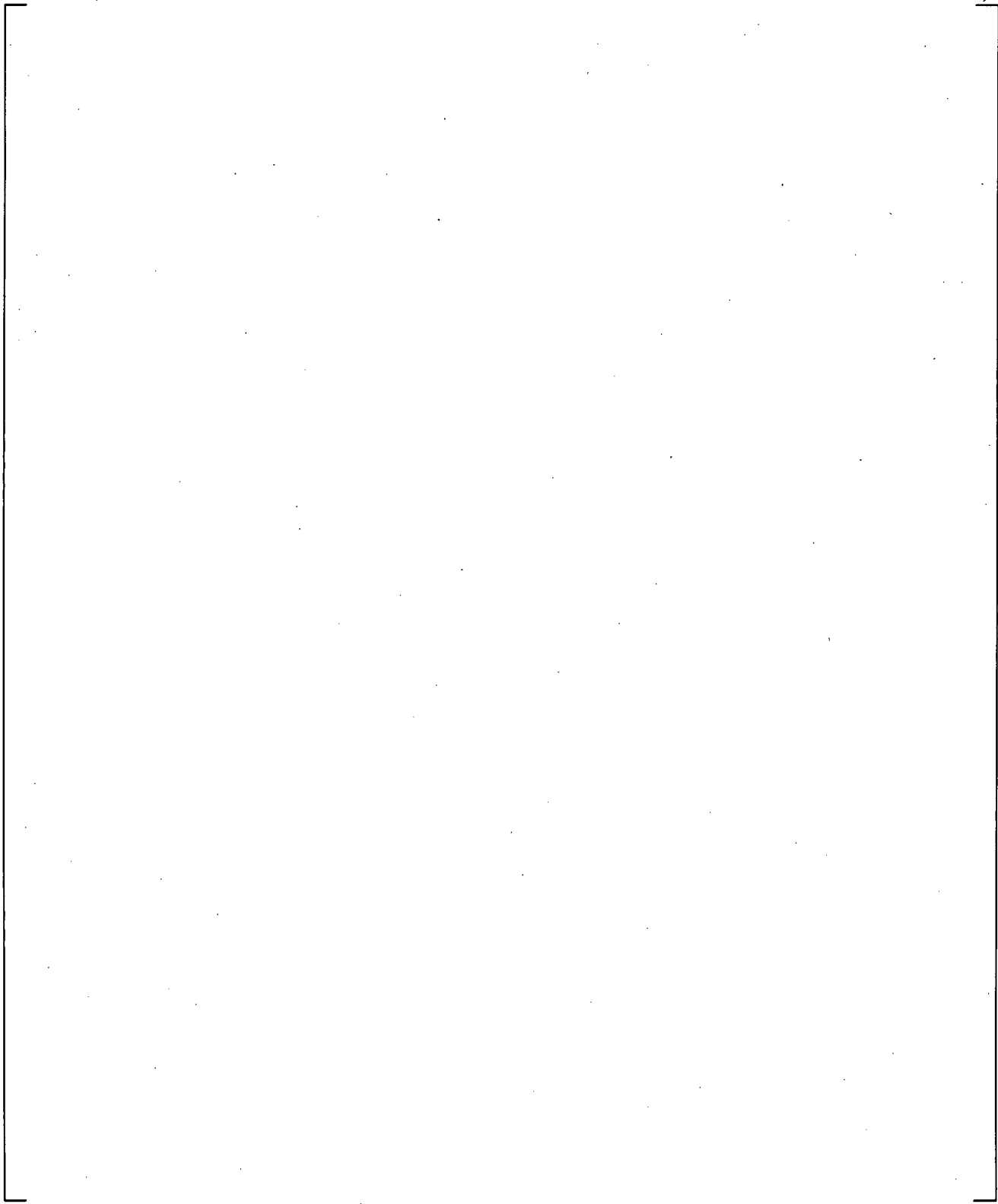


**Figure 21.8-4 Core Collapsed Levels**

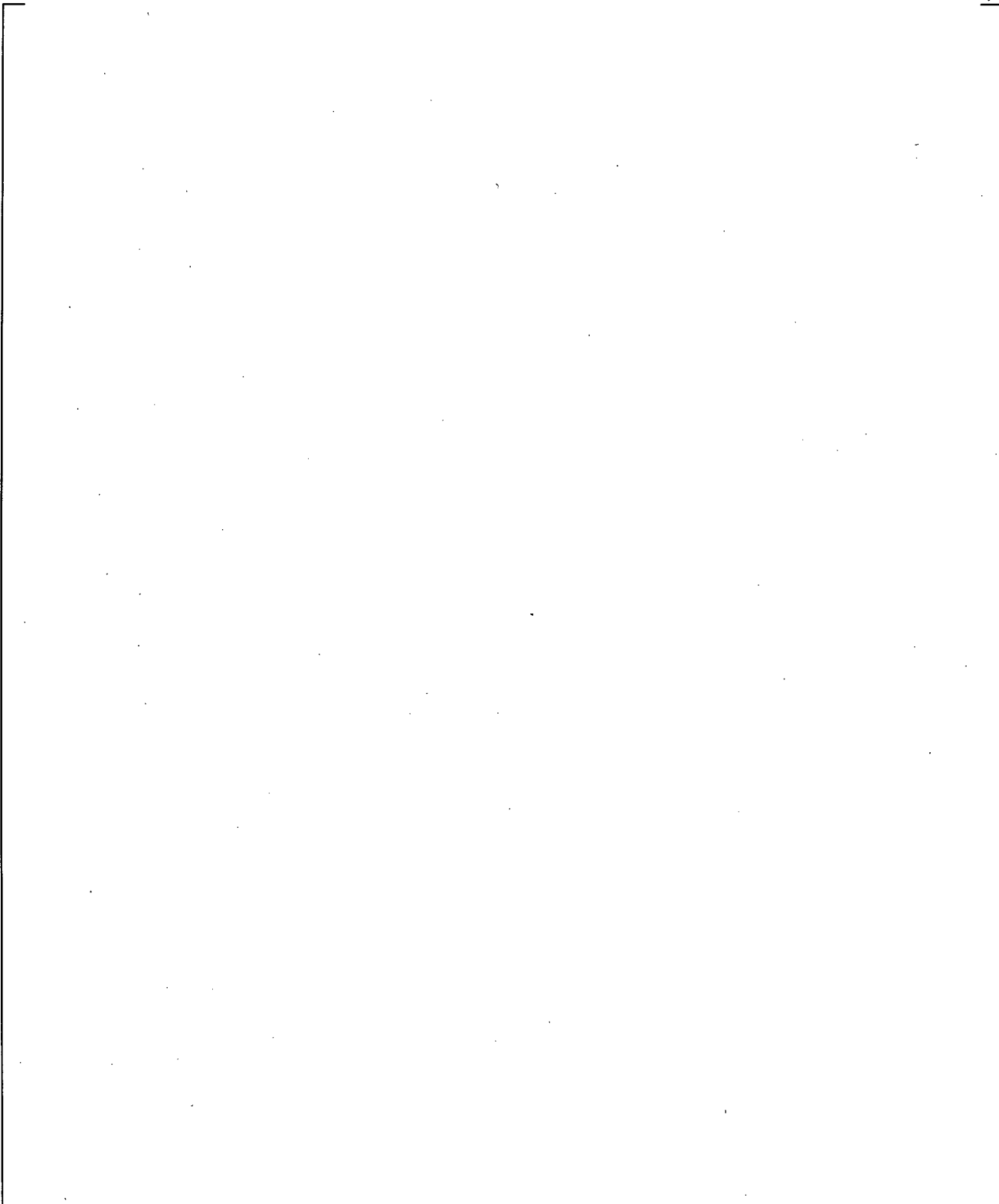


**Figure 21.8-5(a) Steam Generator A U-tubes Upflow Differential Pressures**

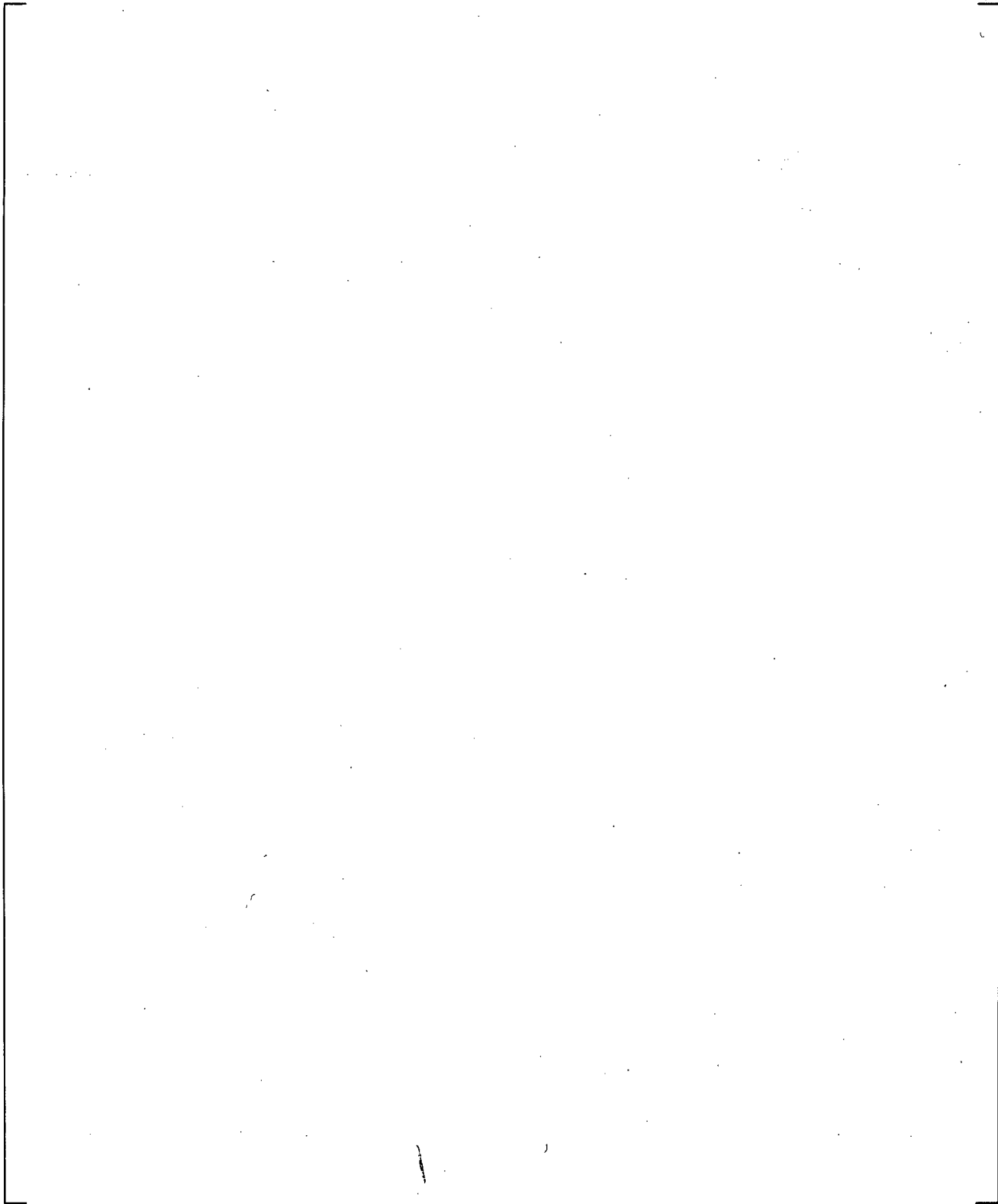


**Figure 21.8-5(b) Steam Generator B U-tubes Upflow Differential Pressures**

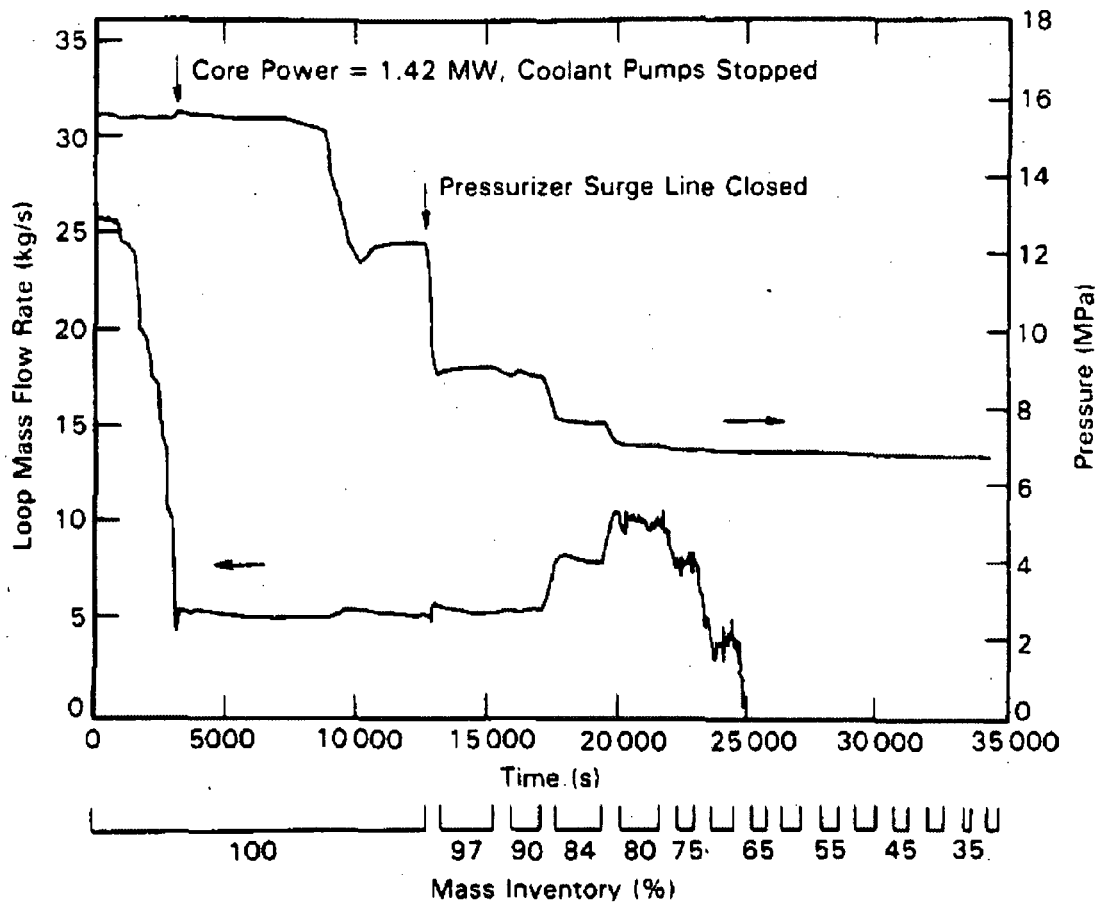
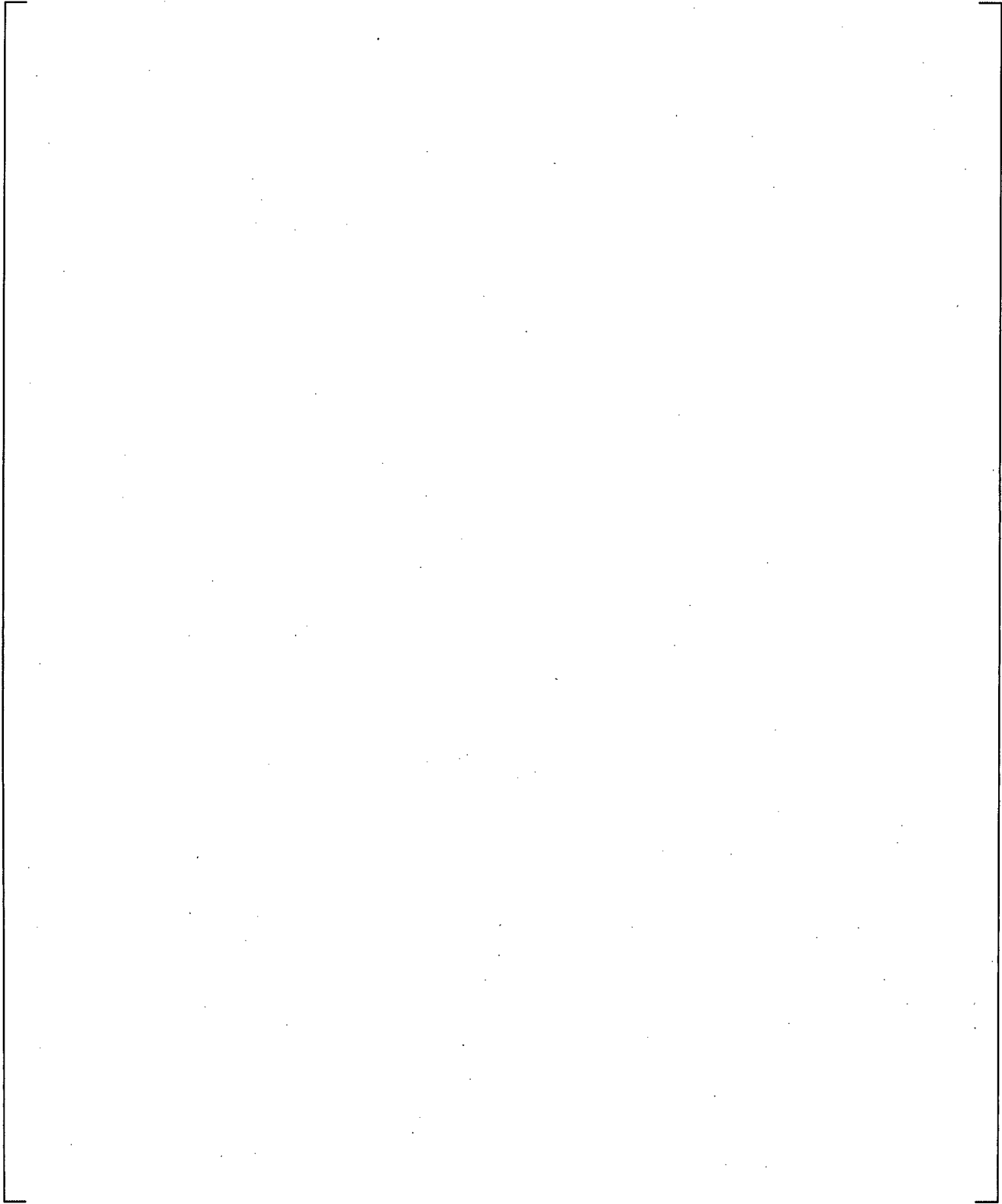
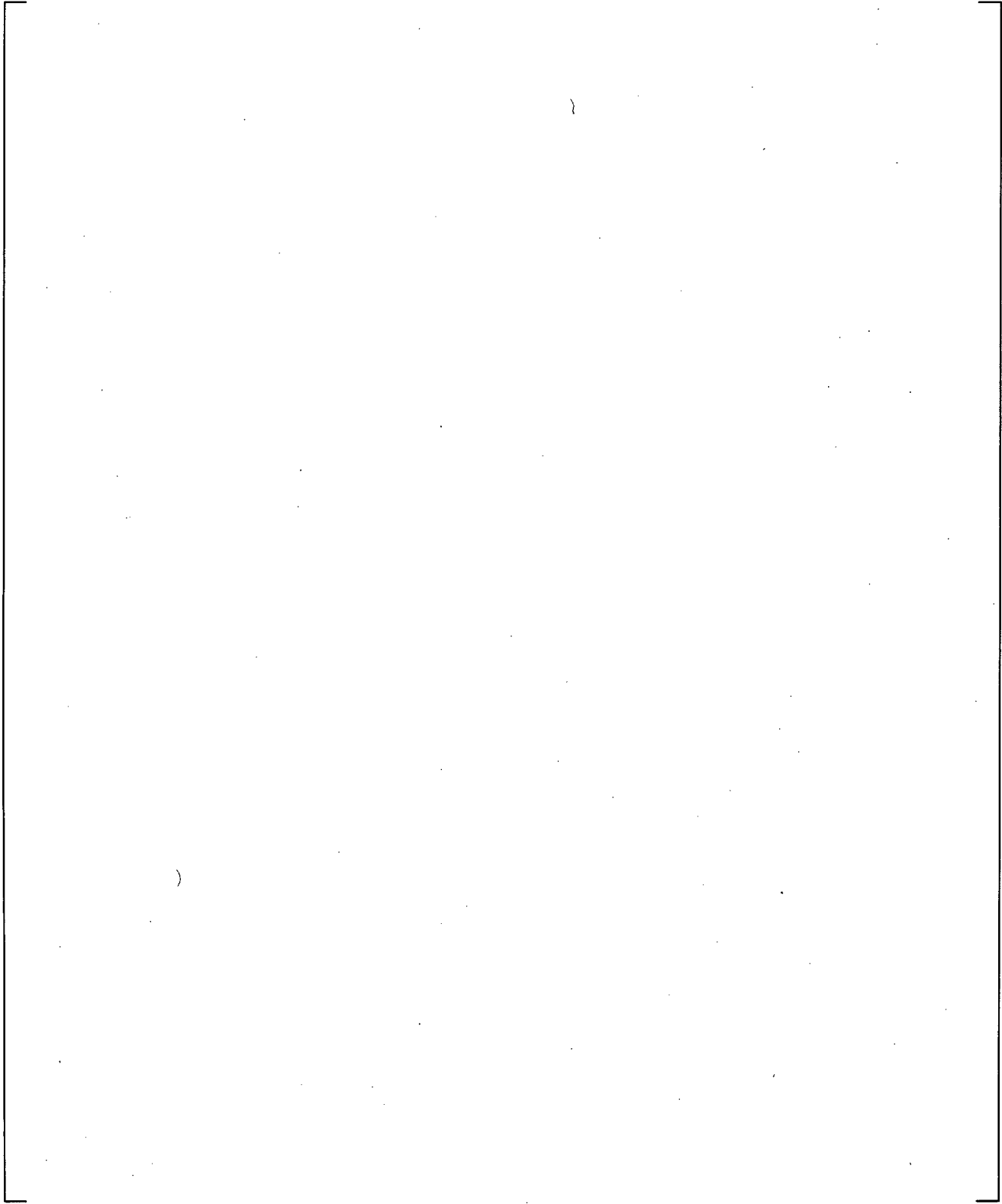


Fig. 4. Primary pressure and loop flow rate during 2% core power natural circulation test.

Figure 21.9-1 ST-NC-02 Primary Pressure and Loop Flow Rate (Figure taken from Reference 9) (Y. Kikuta, et.al., "Nonuniform Steam Generator U-Tube Flow Distribution During Natural Circulation Tests in ROSA-IV Large Scale Test Facility," 1988.)



**Figure 21.9-2 Primary Side Circulation Flow as a Function of Primary Side Inventory**



**Figure 21.9-3 ST-NC-02 Primary and Secondary System Pressures**

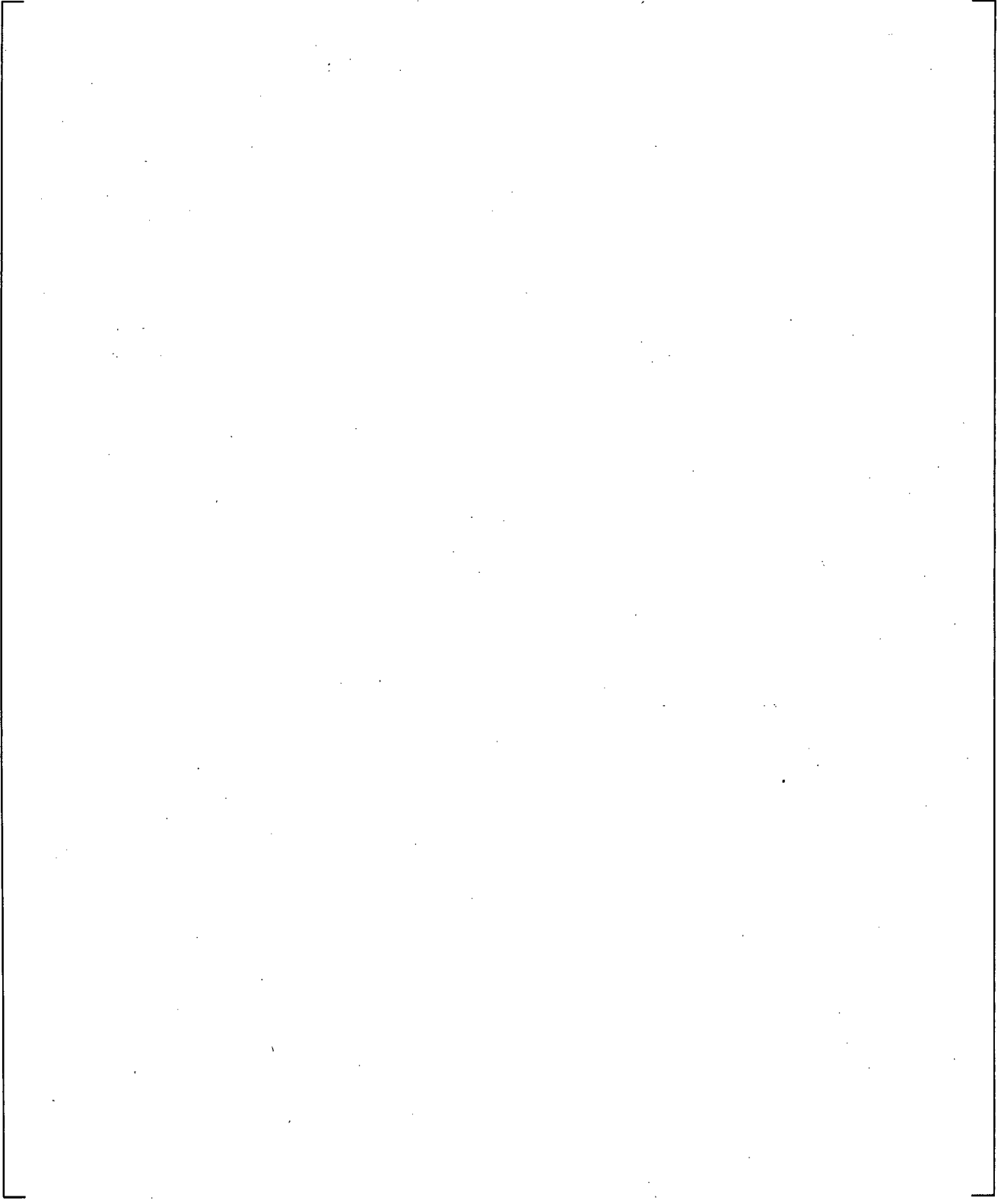


**Figure 21.9-4 Steam Generator U-tube Upflow Side Differential Pressures**

a,c

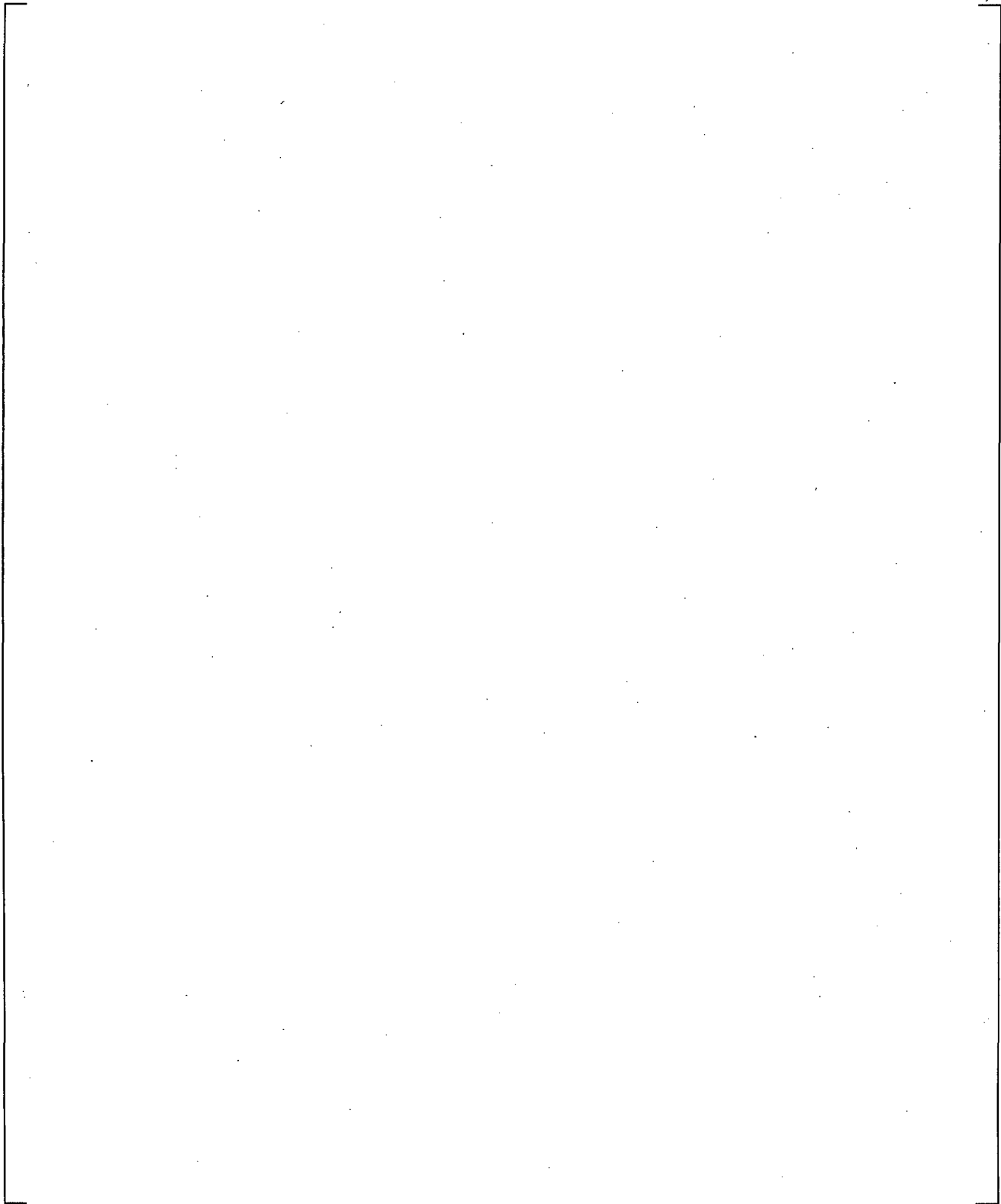


**Figure 21.9-5 Core Differential Pressure**

a,c

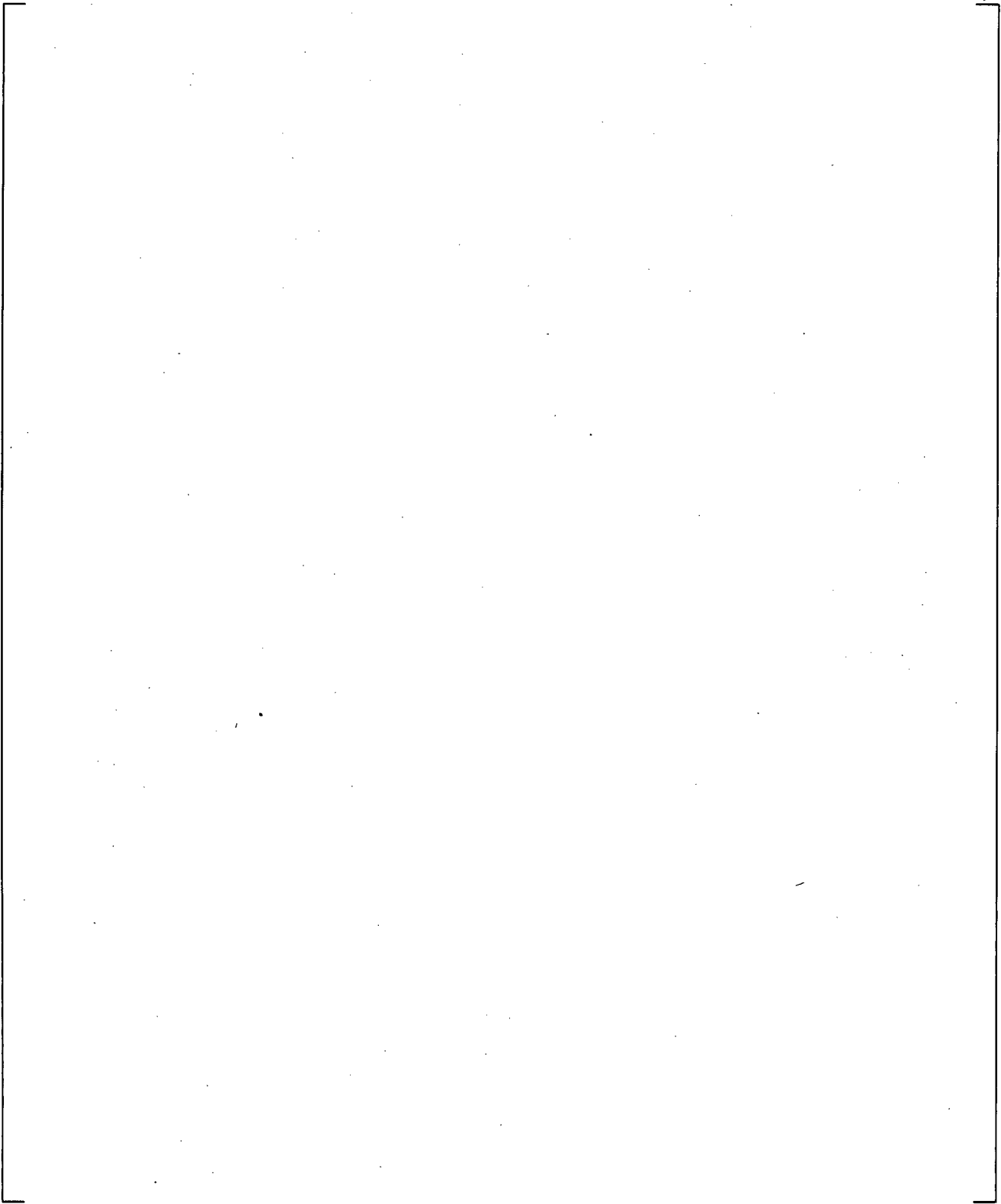


**Figure 21.9-6 Upper Plenum Differential Pressure**

a,c

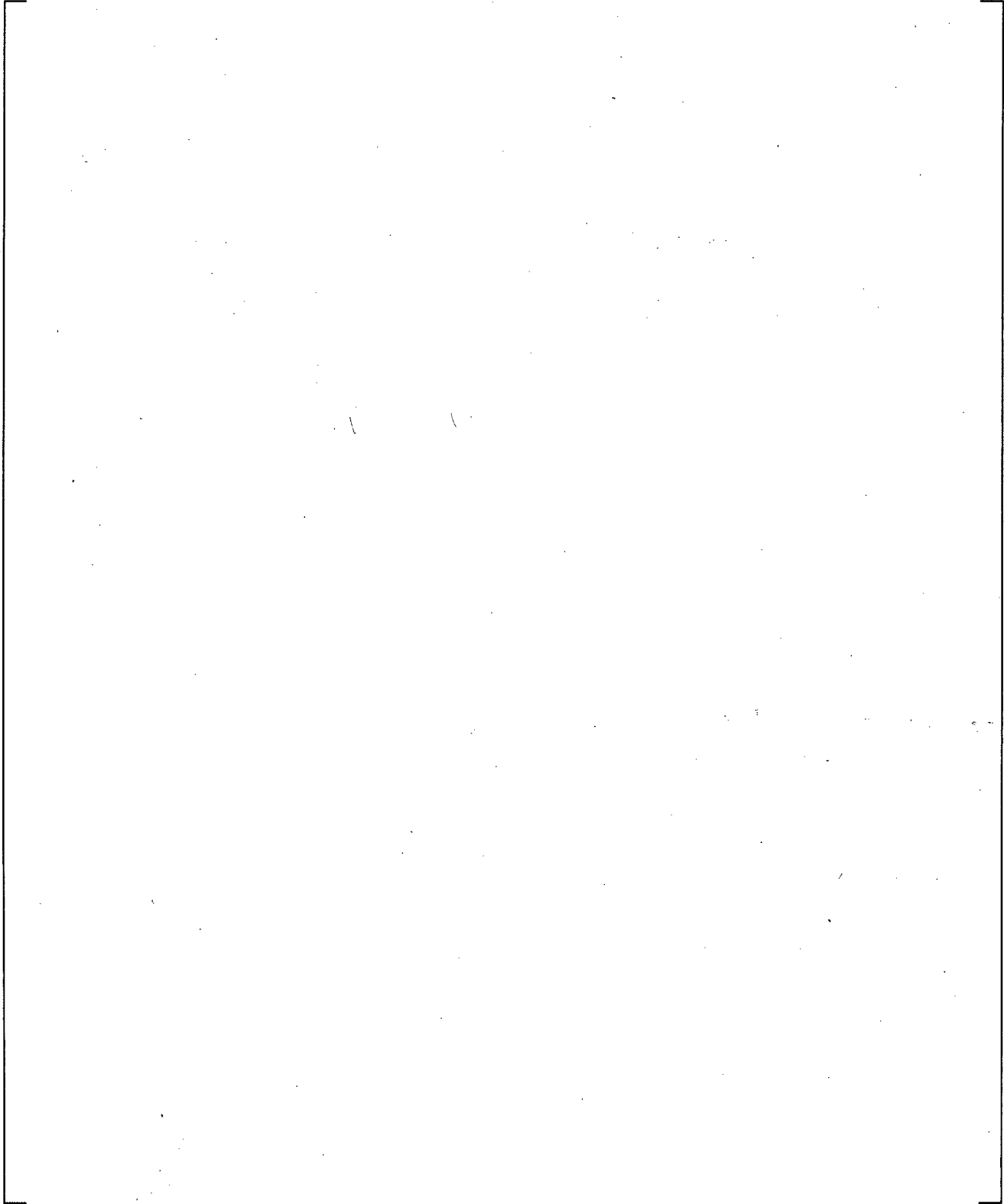


**Figure 21.9-7 Downcomer Differential Pressure**

a,c

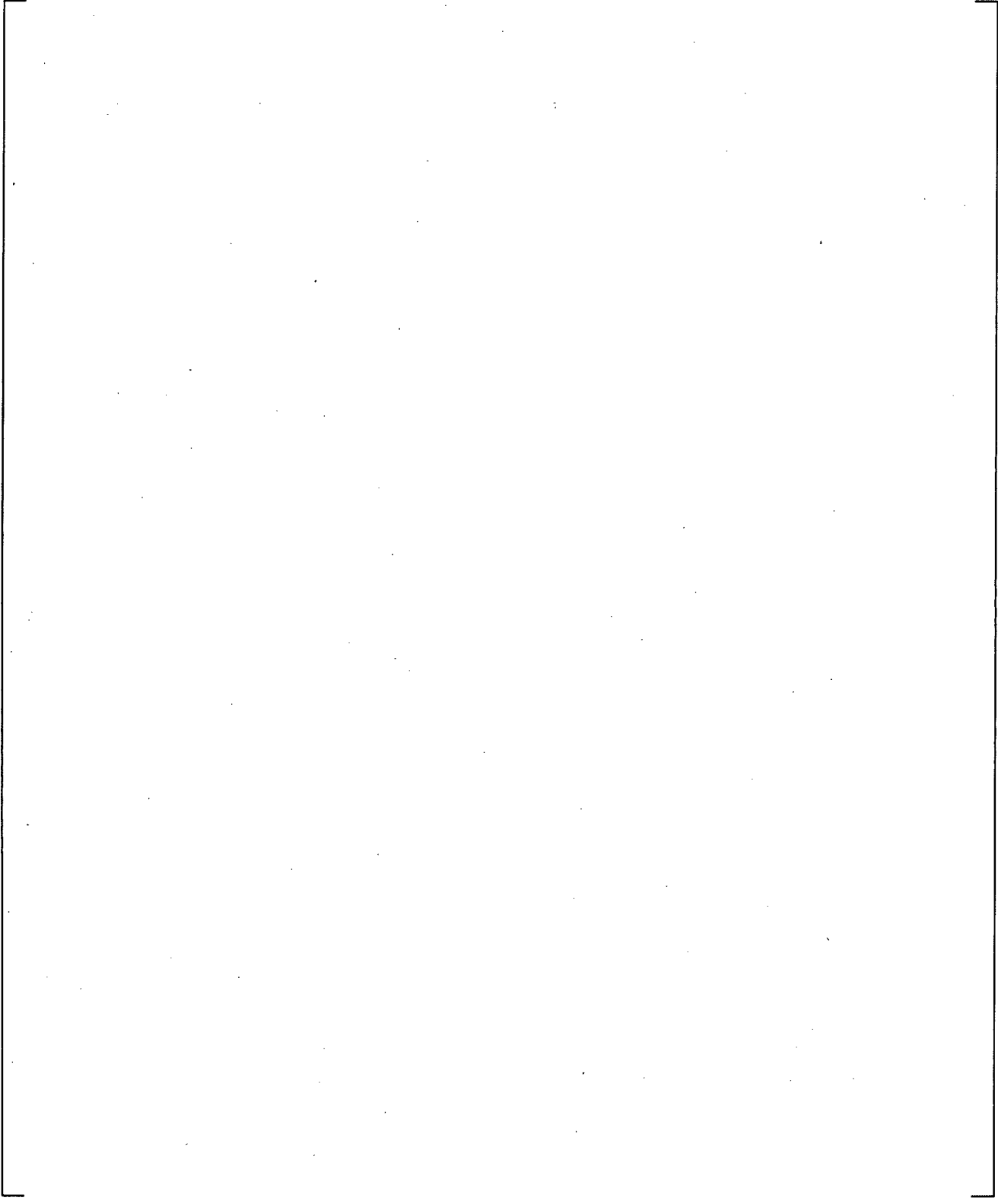


**Figure 21.9-8 Downcomer-to-Upper Plenum Differential Pressure**

**Figure 21.9-9 SG Primary-to-Secondary Side Heat Transfer Coefficients**

Note: The SG heat transfer coefficient is calculated as  $h_{SG} = \frac{Q_{SG,OUT}}{(FA_{SG,OUT} \times \Delta T_{SG})}$

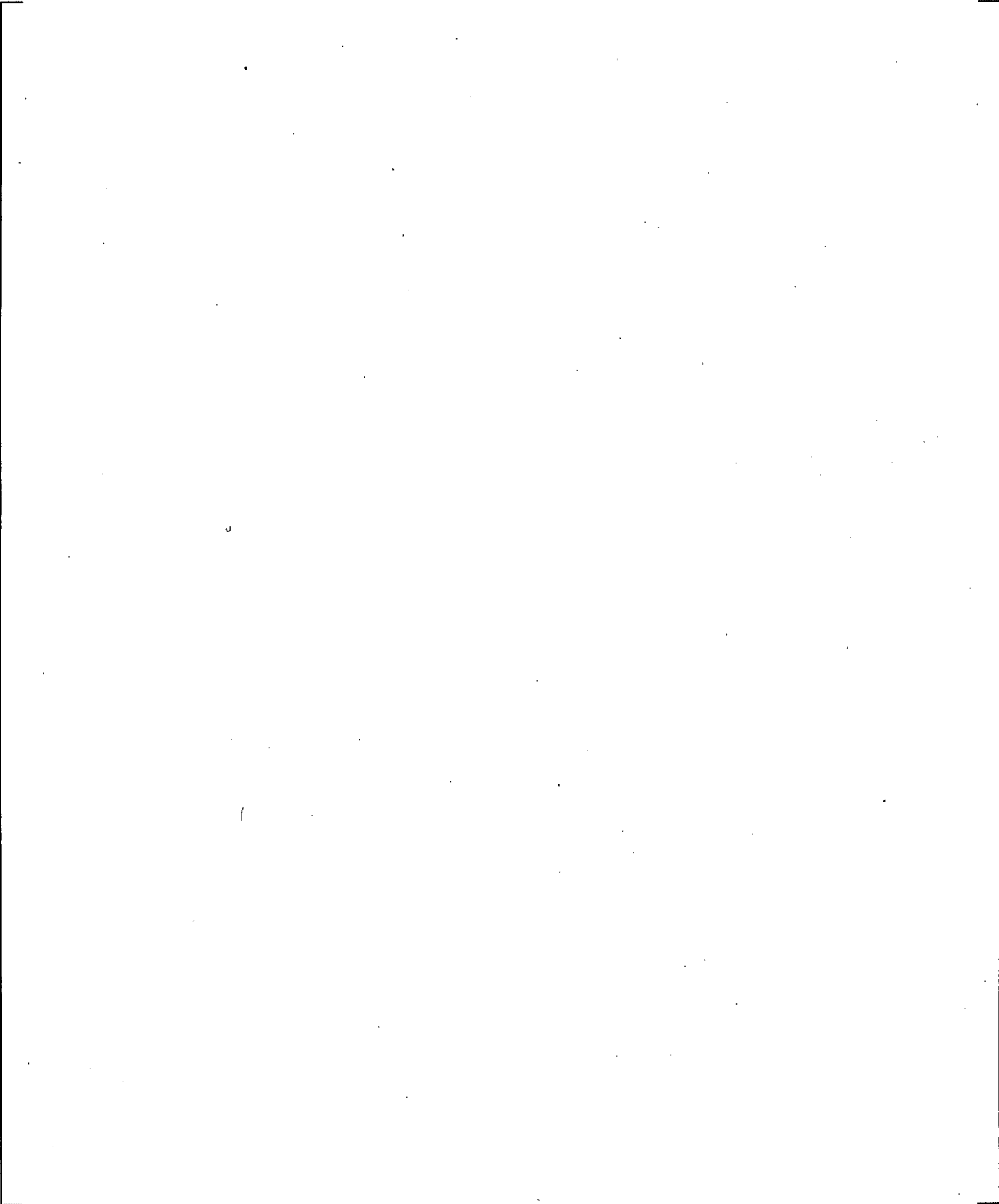


**Figure 21.9-10 Steam Generator Primary-to-Secondary Side Temperature Difference**

a,c

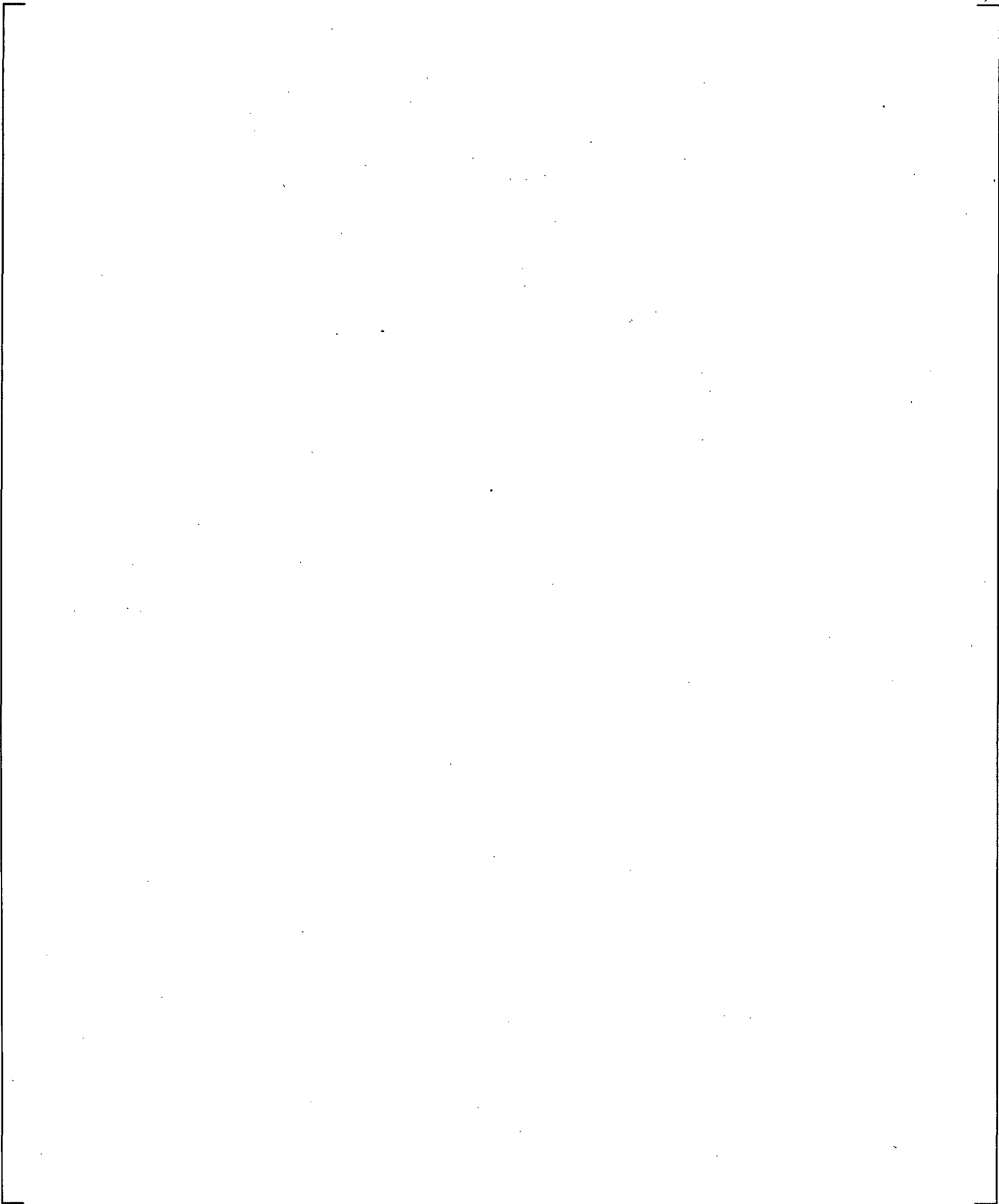


**Figure 21.9-11 Steam Generator SGA U-tube Uphill Void Fraction**

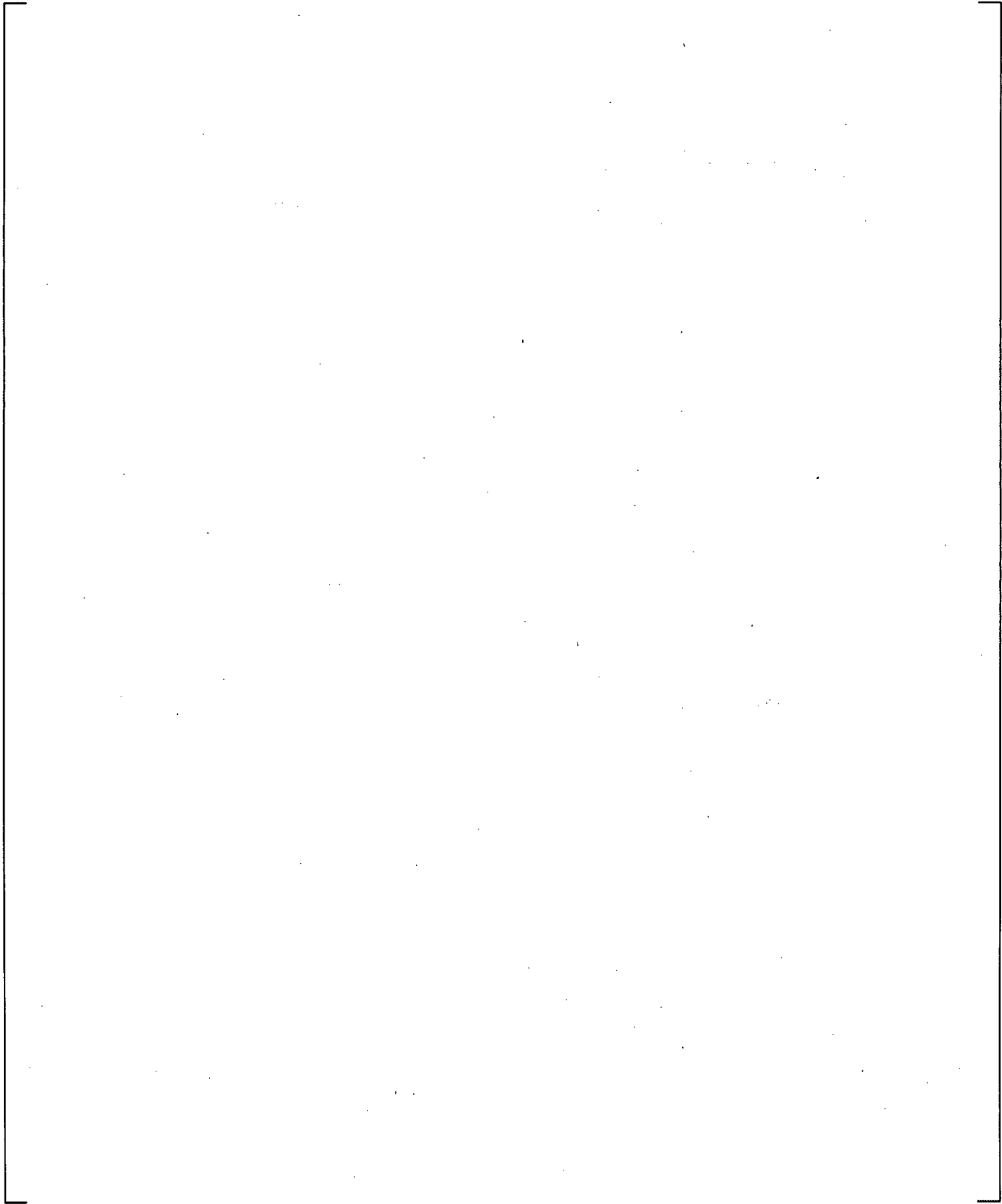


**Figure 21.9-12 Steam Generator SGA U-tube Downhill Void Fraction**

a,c

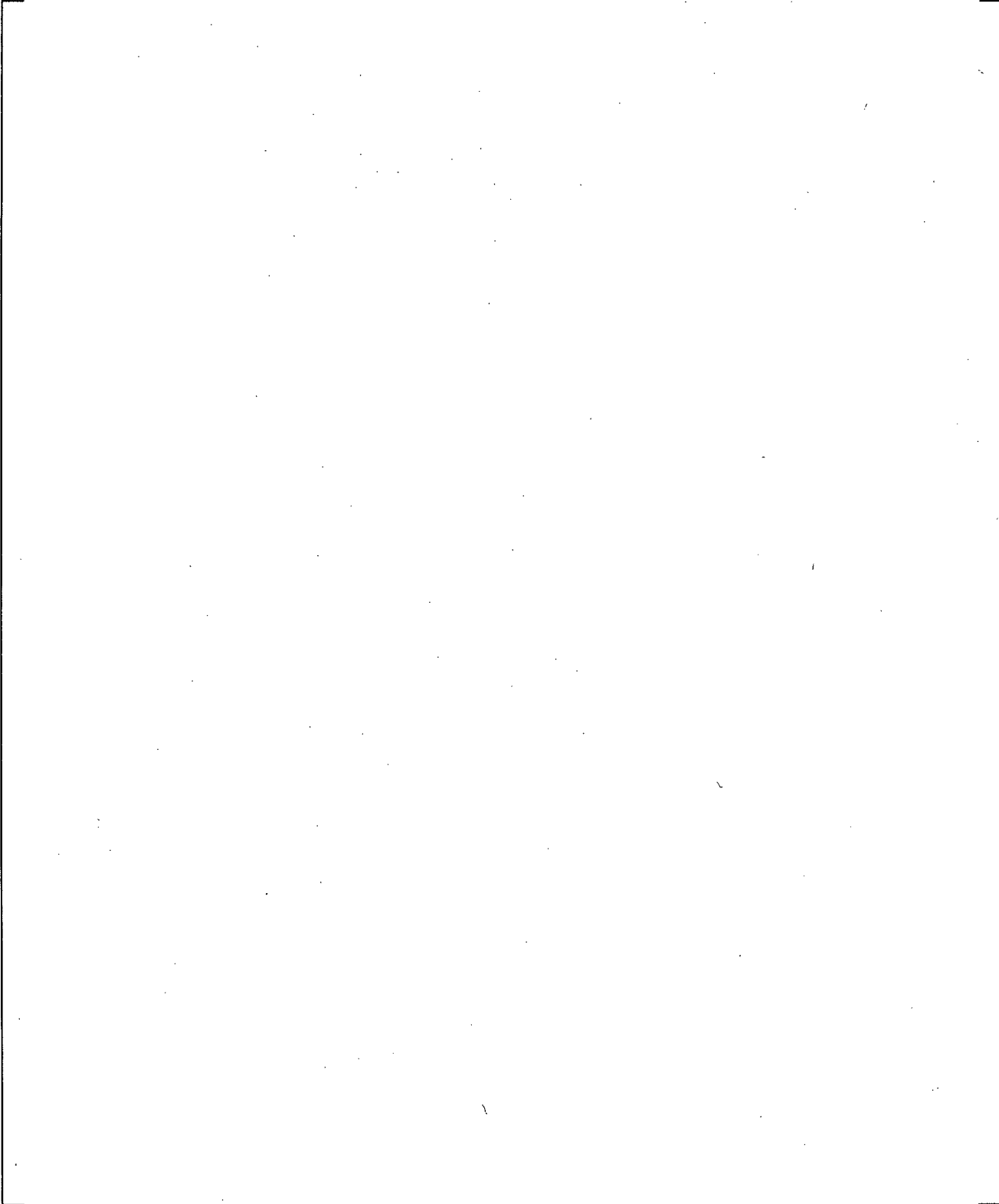


**Figure 21.9-13 Steam Generator SGB U-tube Uphill Void Fraction**

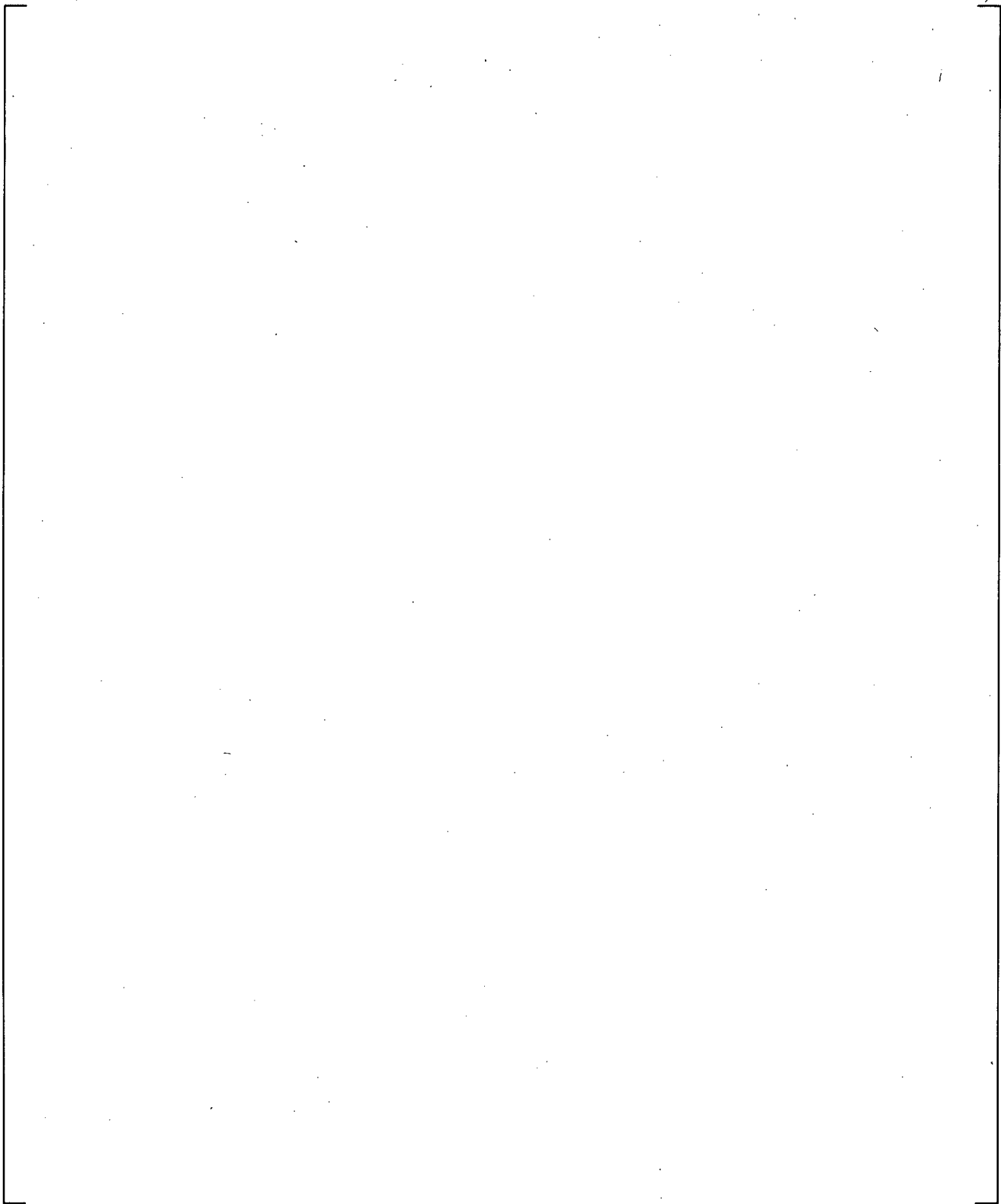


**Figure 21.9-14 Steam Generator SGB U-tube Downhill Void Fraction**

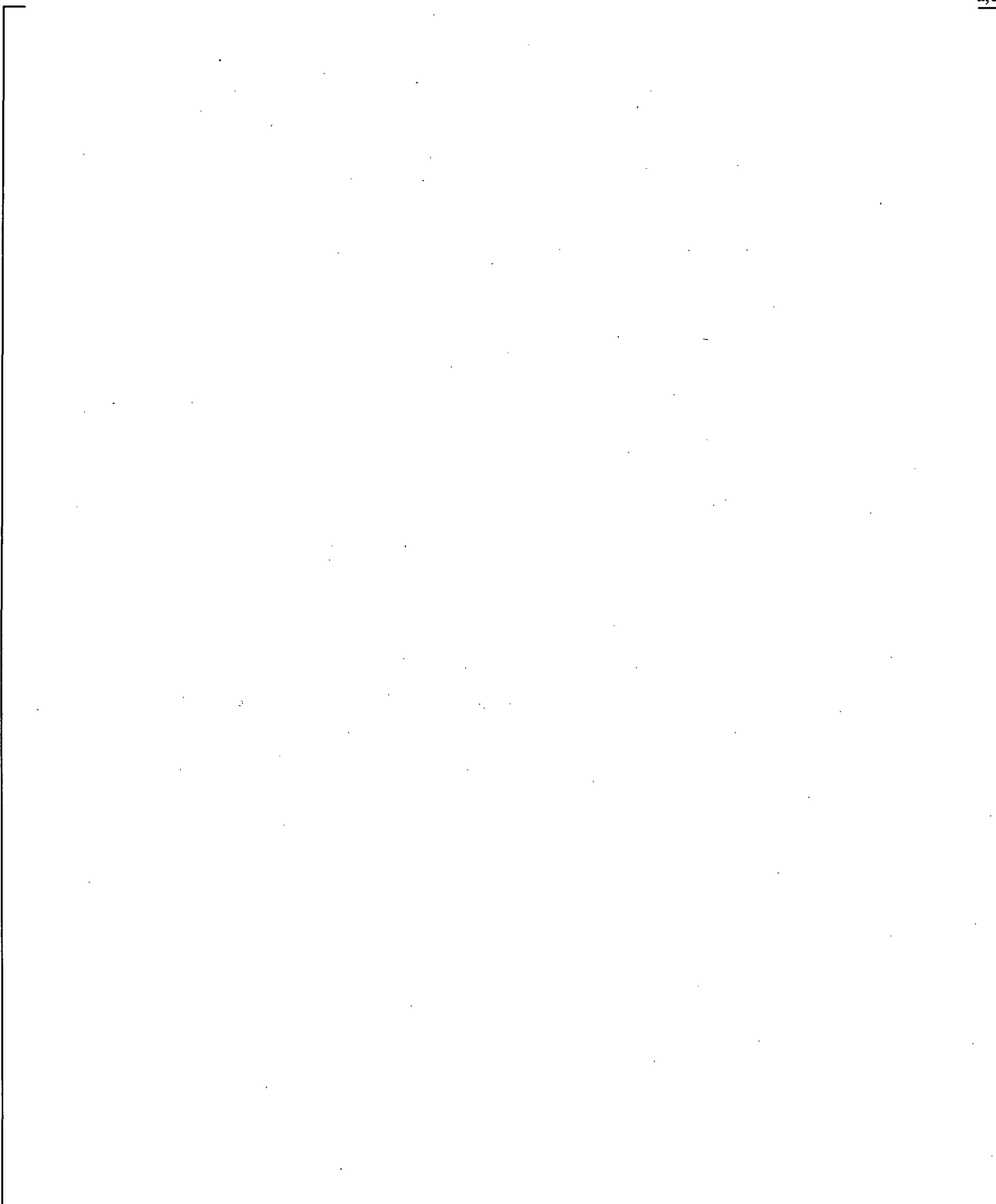


**Figure 21.10.1-1** Calculated Counter-current Flow at the Inlet of Steam Generator U-tubes  
(Simulation of 10% Break Test SB-CL-14)

**Figure 21.10.1-2** Calculated Counter-current Flow at the Inlet of Steam Generator U-tubes  
(Simulation of 5% Break Test SB-CL-18)

**Figure 21.10.1-3** Calculated Counter-current Flow at the Inlet of Steam Generator U-tubes  
(Simulation of 2.5% Break Test SB-CL-01)

**Figure 21.10.1-4** Calculated Counter-current Flow at the Inlet of Steam Generator U-tubes  
(Simulation of 0.5% Break Test SB-CL-12)

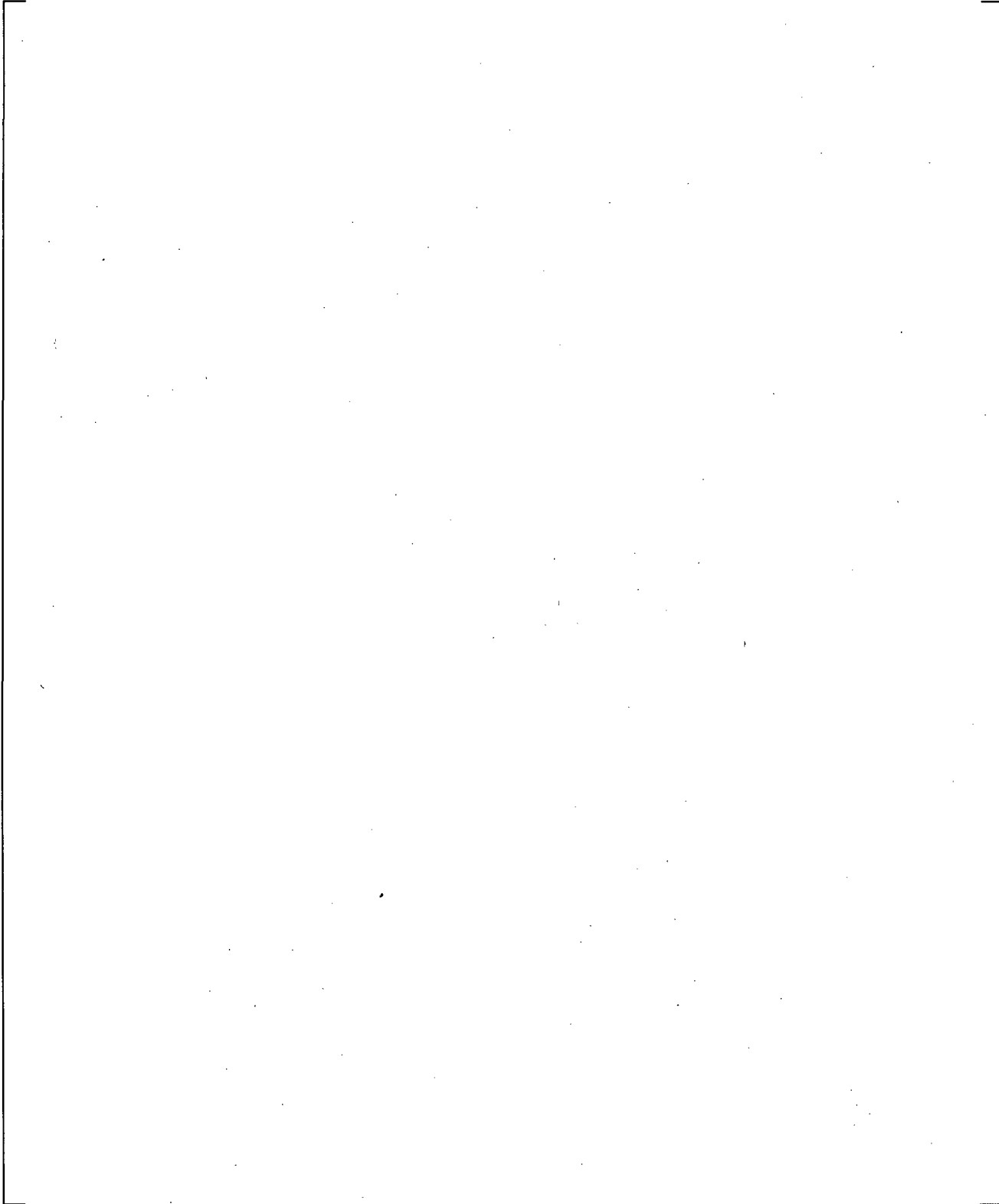


**Figure 21.10.1-5** Calculated Counter-current Flow at the Inlet of Steam Generator U-tubes  
(Simulation of the Natural Circulation Test SB-CL-12)

**Figure 21.10.2-1** Calculated Counter-current Flow at the Hot Leg Elbows and SG Inlets  
(Simulation of 10% Break Test SB-CL-14)

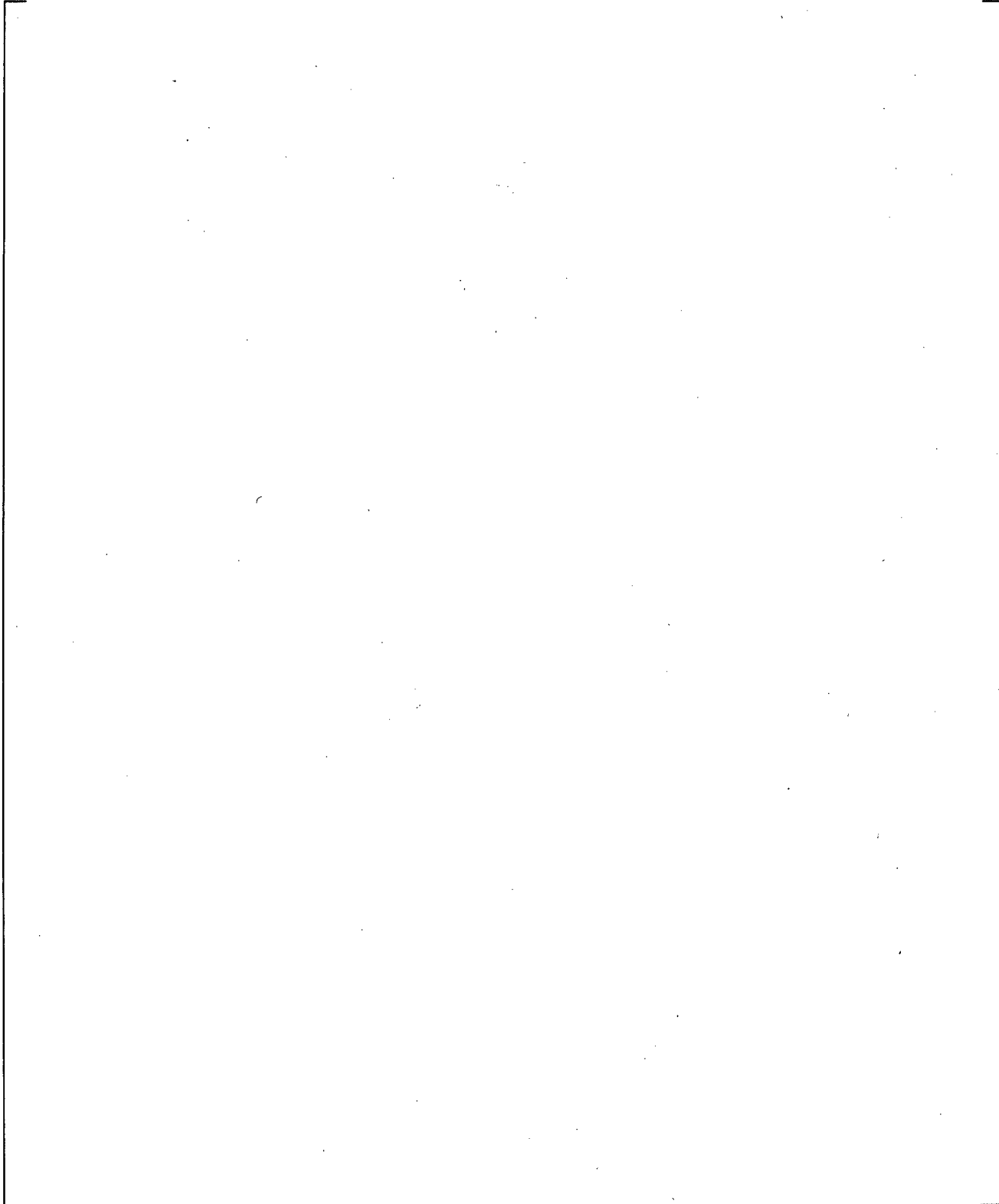


**Figure 21.10.2-2** Calculated Counter-current Flow at the Hot Leg Elbows and SG Inlets  
(Simulation of 5% Break Test SB-CL-18)

**Figure 21.10.2-3** Calculated Counter-current Flow at the Hot Leg Elbows and SG Inlets  
(Simulation of 2.5% Break Test SB-CL-01)

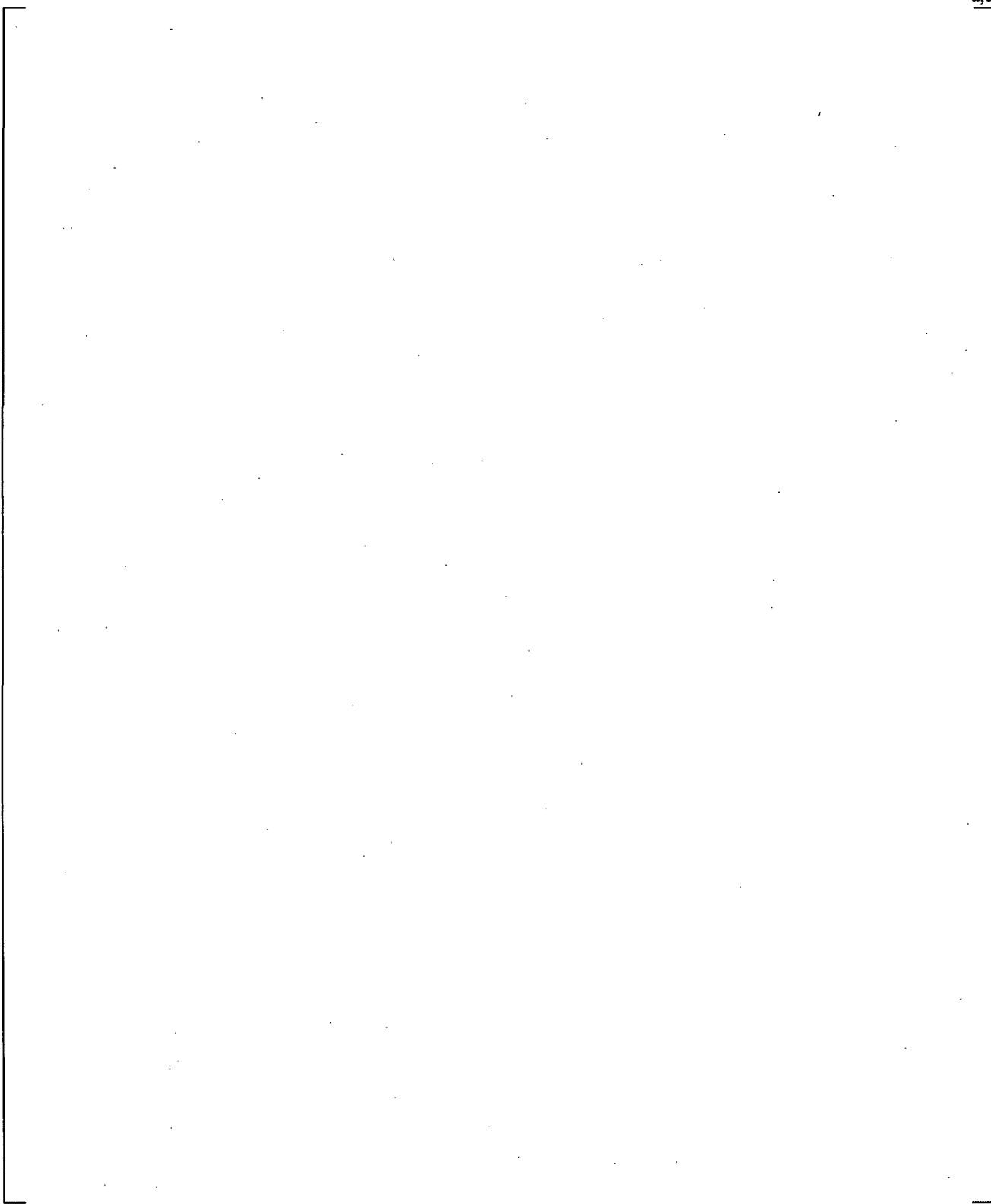


**Figure 21.10.2-4** Calculated Counter-current Flow at the Hot Leg Elbows and SG Inlets  
Simulation of 0.5% Break Test SB-CL-12)

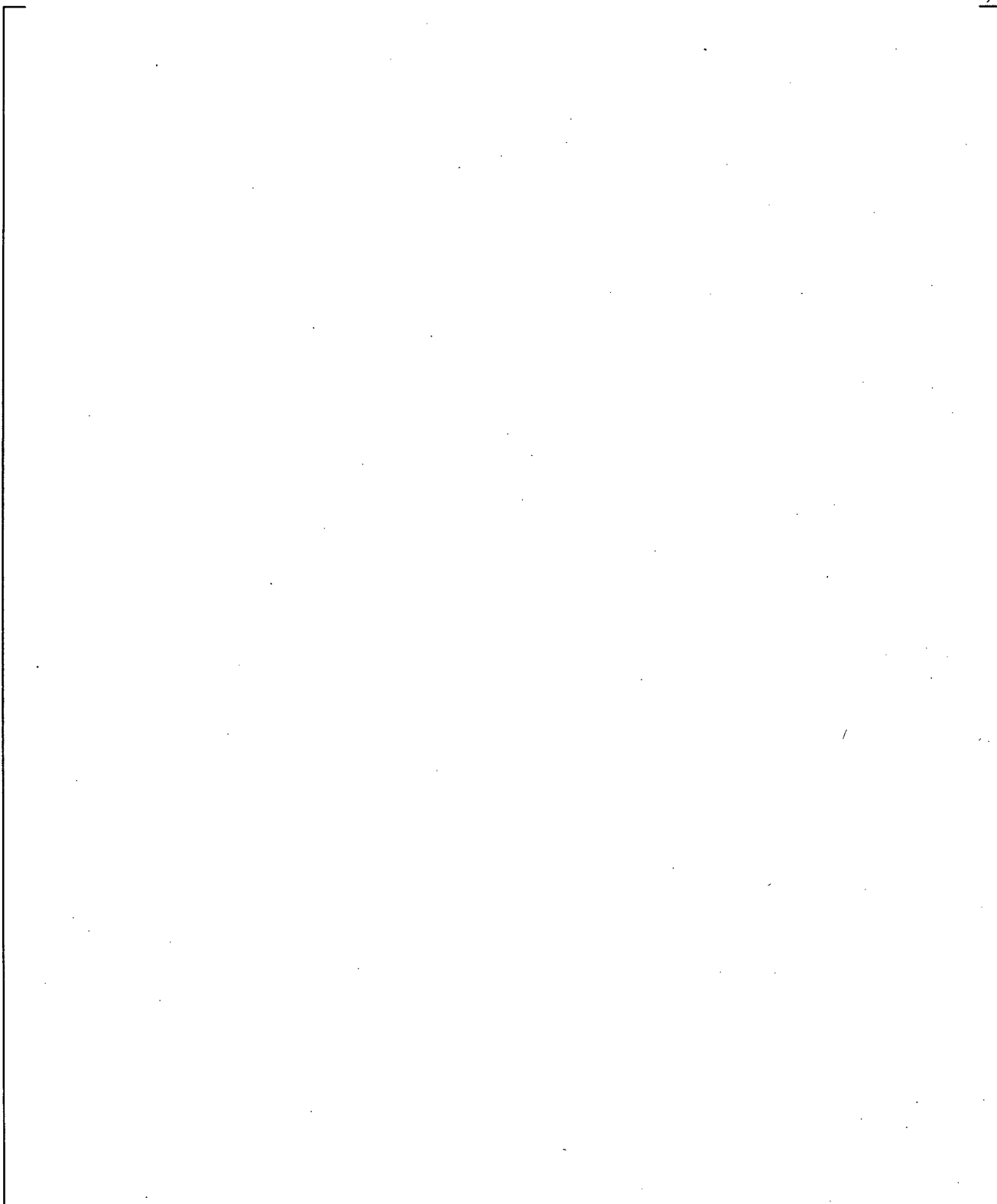


**Figure 21.10.3-1** Calculated Counter-current Flow Conditions at the Top of the Peripheral CCFL Channel 72

a,c

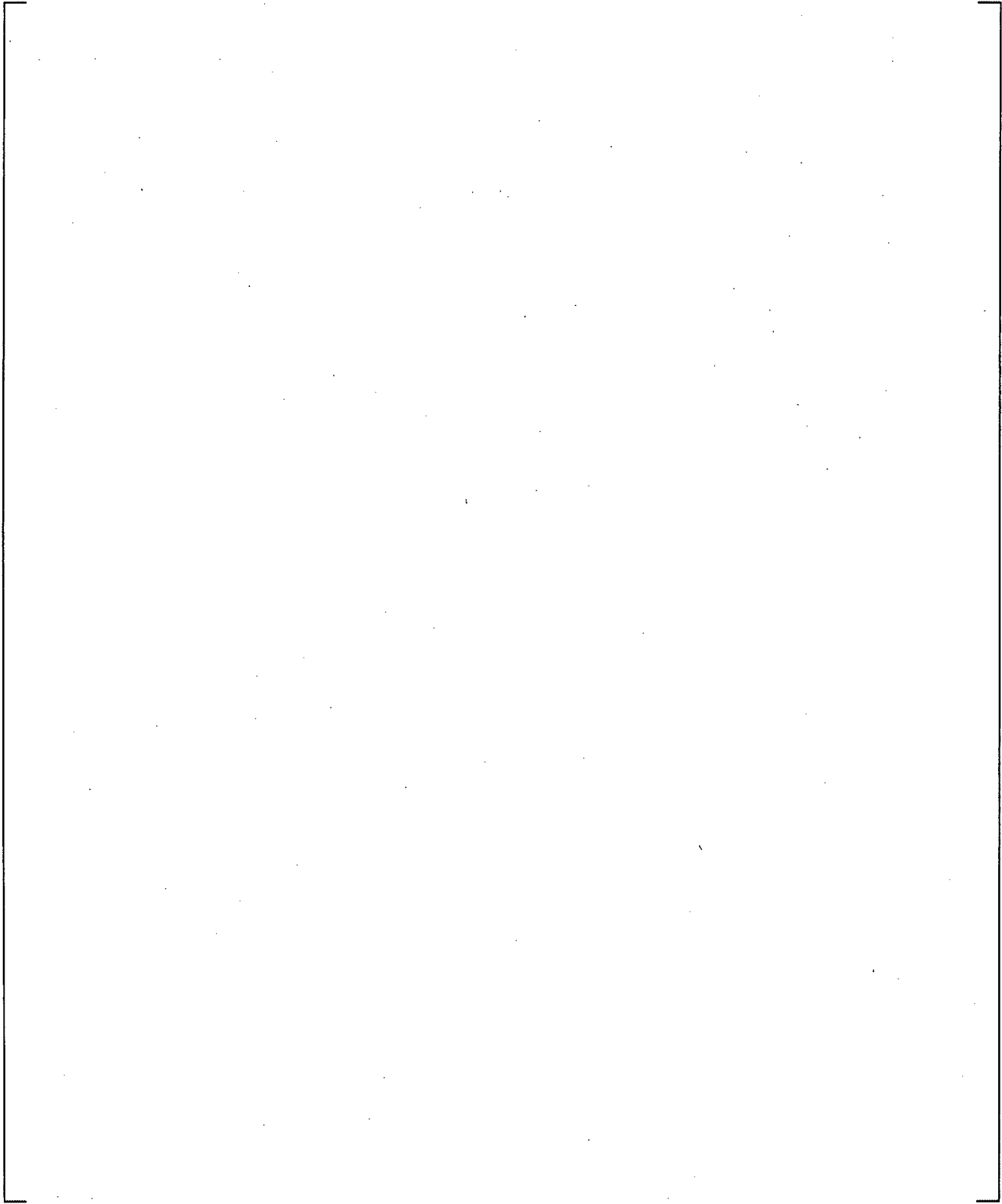


**Figure 21.10.3-2** Calculated Counter-current Flow Conditions at the Top of the Inner Average CCFL Channel 14

a,c

**Figure 21.10.3-3** Calculated Counter-current Flow Conditions at the Top of the Inner Hot CCFL Channel 11

**Figure 21.10.3-4 Calculated UCP Counter-current Flow Conditions (10% Break Test SB-CL-14).**

**Figure 21.10.3-5 . Calculated UCP Counter-current Flow Conditions (2.5% Break Test SB-CL-01)**

a,c

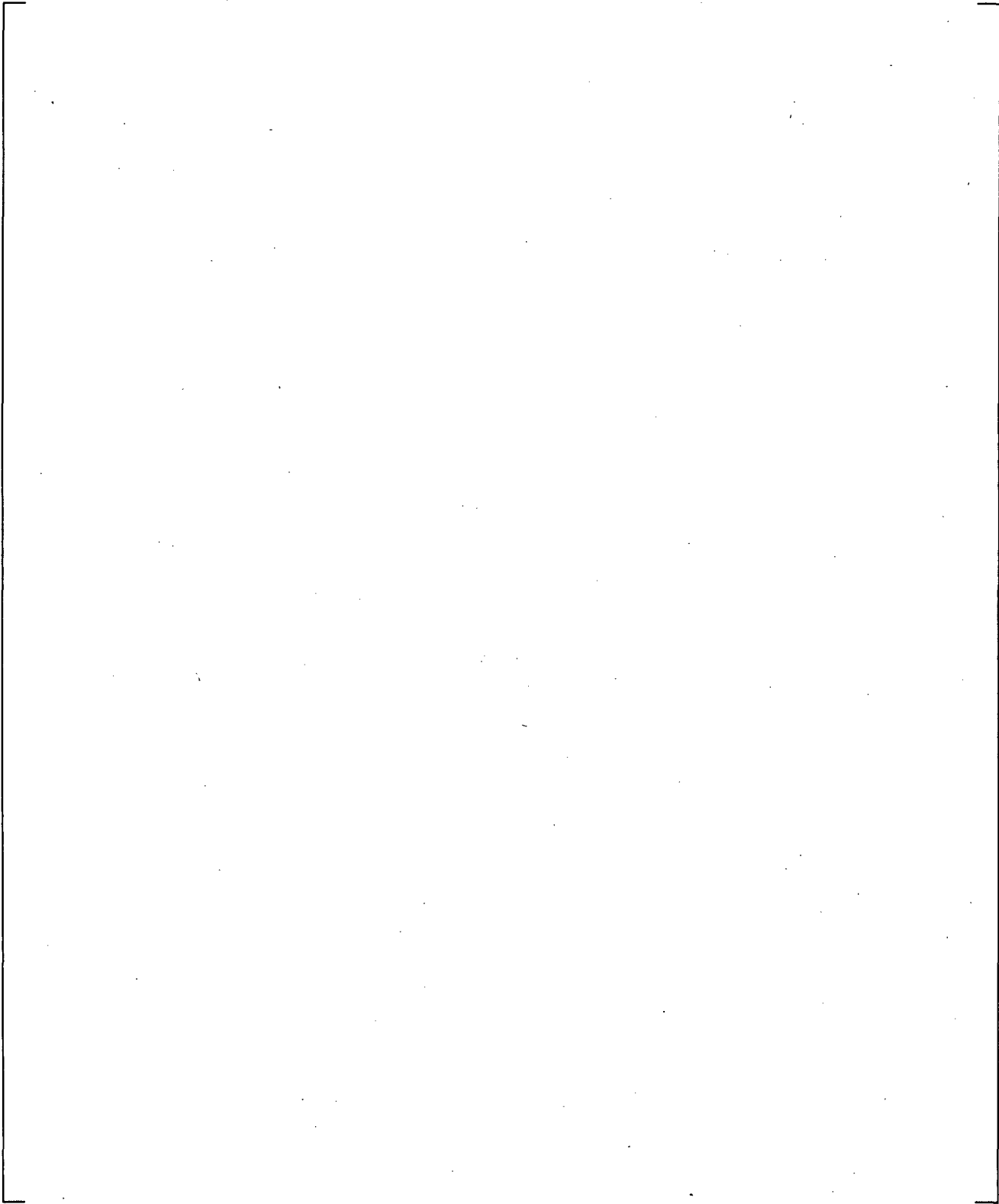


**Figure 21.10.3-6 Calculated UCP Counter-current Flow Conditions (0.5% Break Test SB-CL-12)**

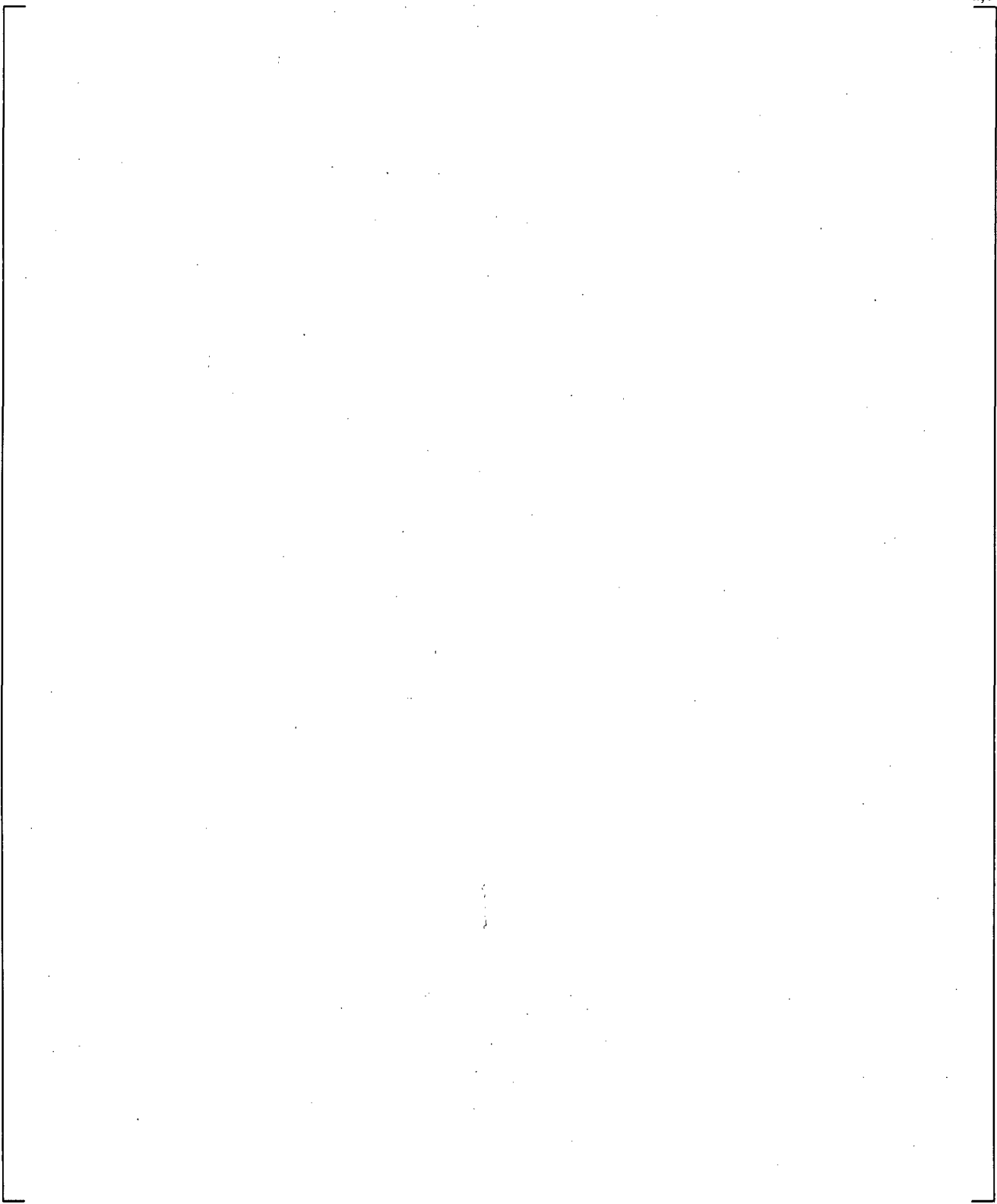


**Figure 21.10.4-1 Counter-current Flow Periods in Relation to the Steam Generator A Uphill Side Differential Pressure**

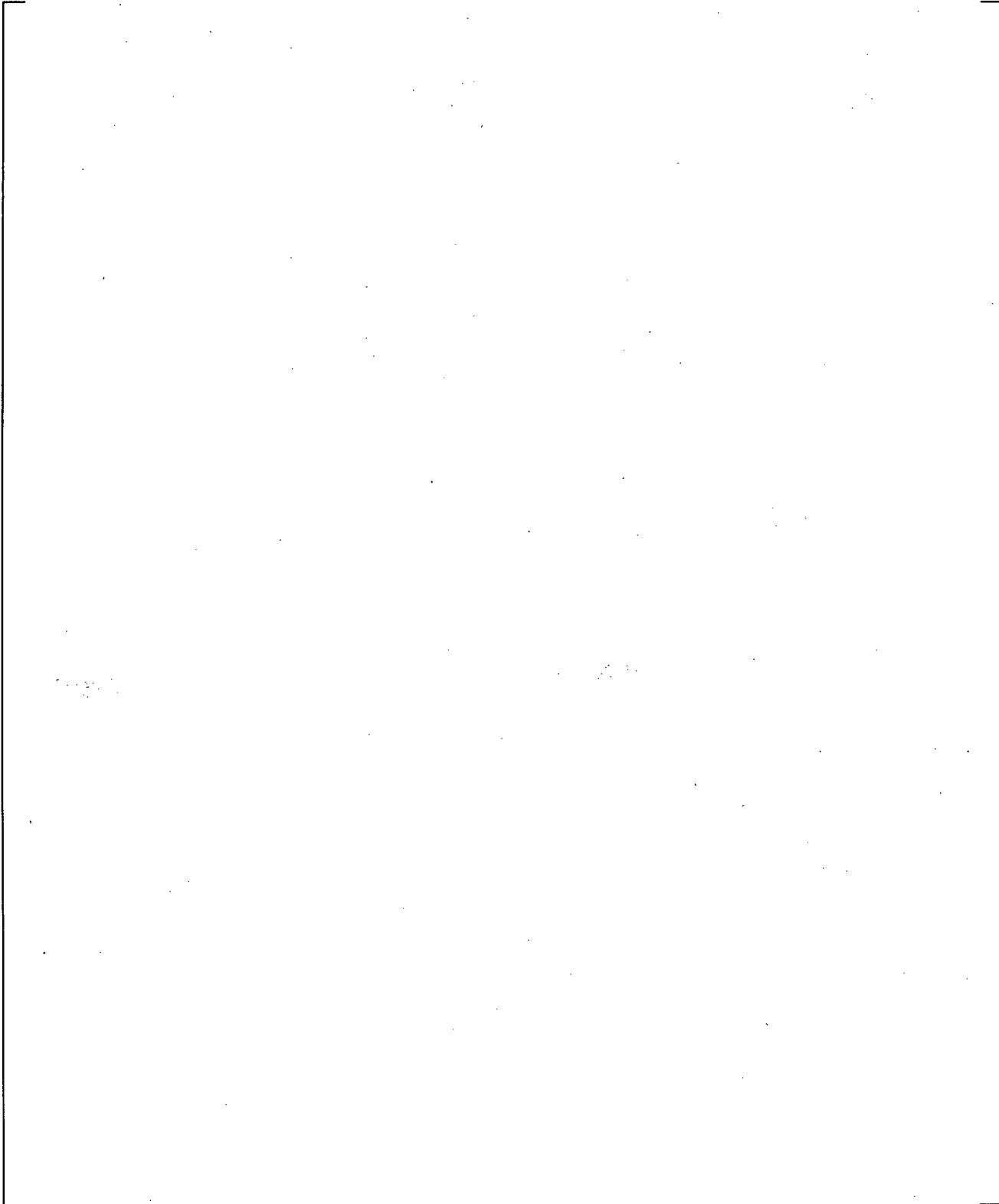


**Figure 21.10.4-2 Counter-current Flow Periods in Relation to the Steam Generator A Inlet Plenum Collapsed Level**

a,c

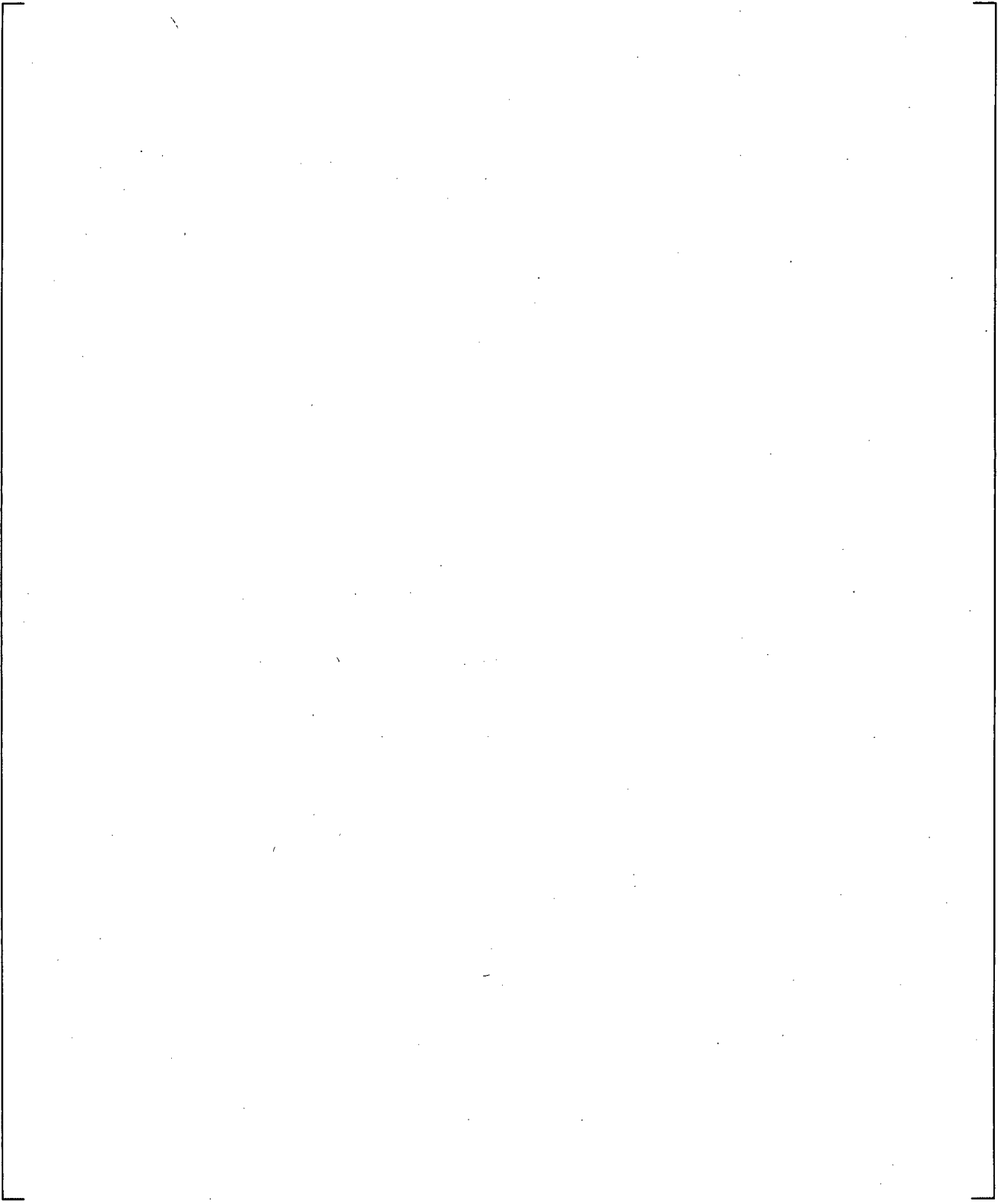


**Figure 21.10.4-3 Counter-current Flow Periods in Relation to the Steam Generator B Uphill Side Differential Pressure**

a,c

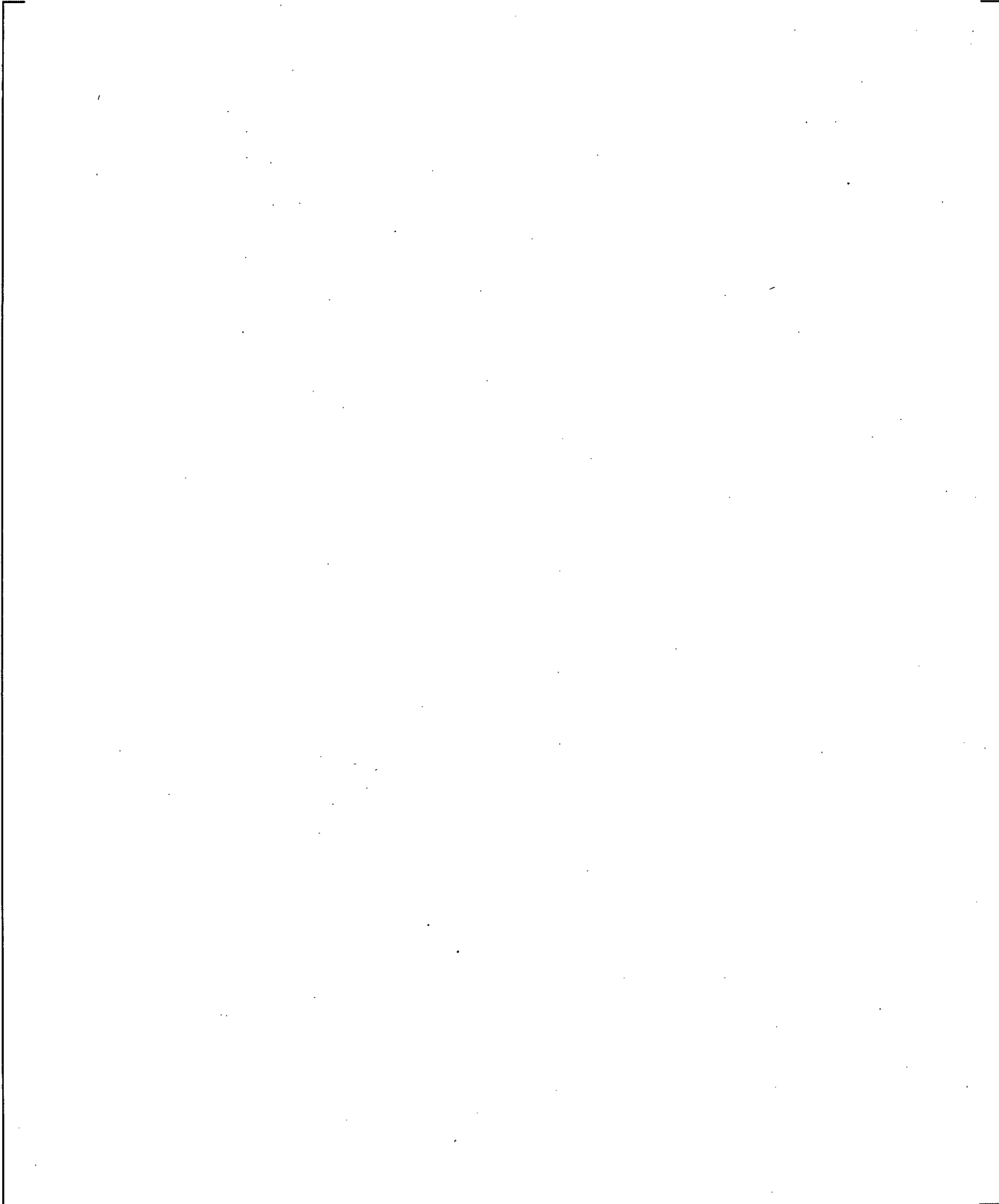


**Figure 21.10.4-4 Counter-current Flow Periods in Relation to the Steam Generator B Inlet Plenum Collapsed Level**

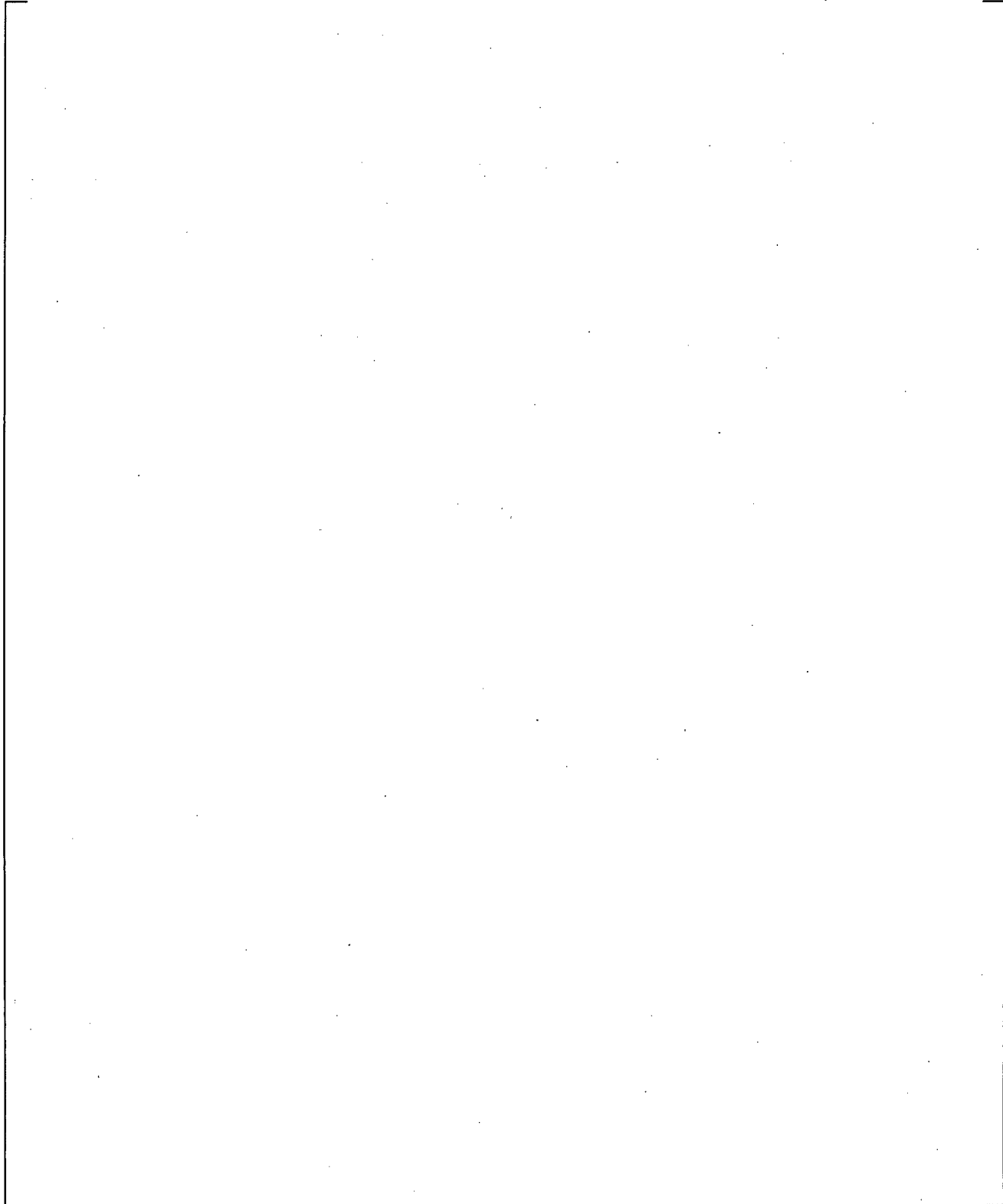


**Figure 21.10.4-5** Calculated Velocities at Upper Core Plate Outer Jet Channel 73 (top of peripheral CCFL Channel 72)

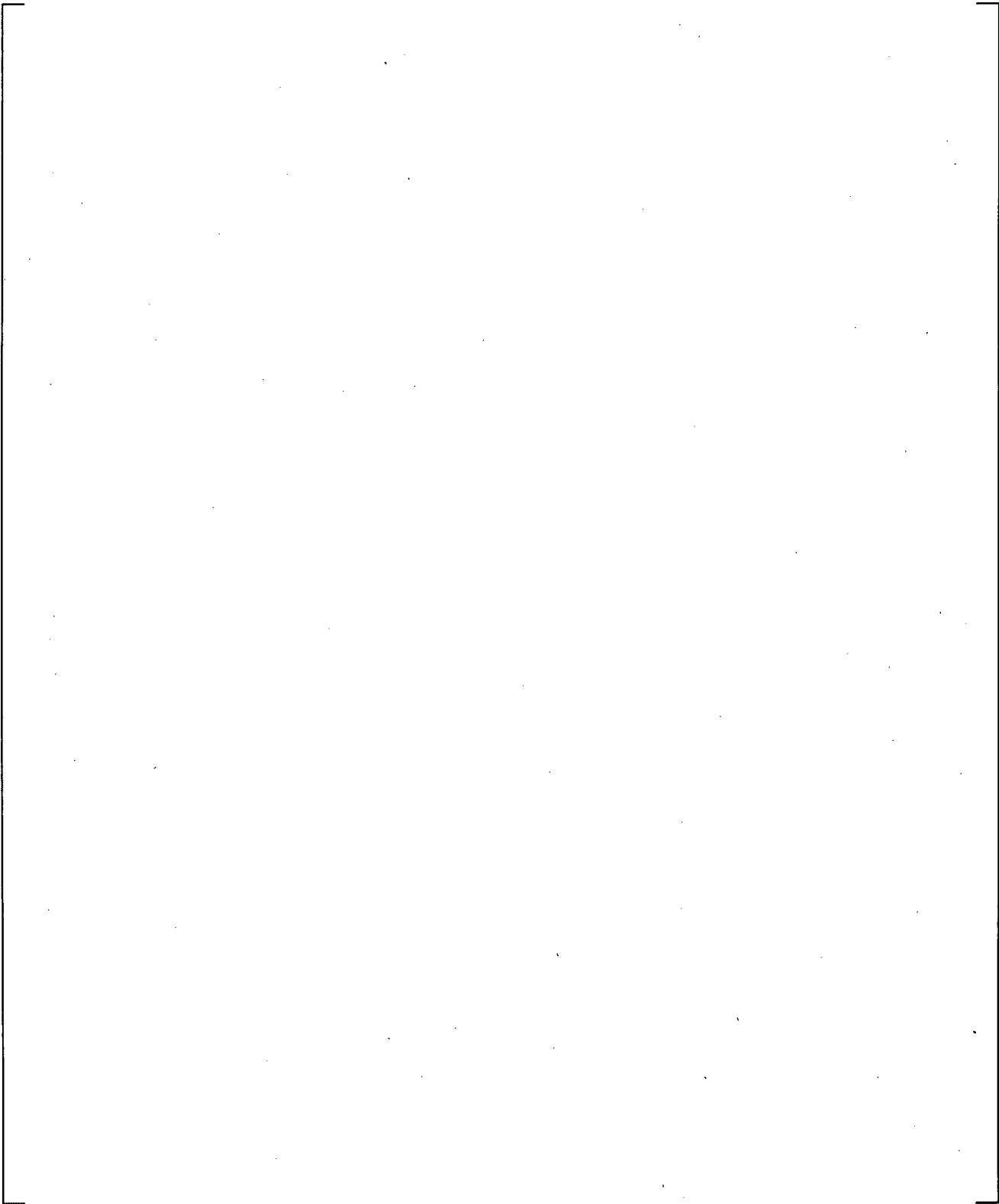


**Figure 21.10.4-6** Calculated Velocities at Upper Core Plate Average Jet Channel 20 (top of CCFL Channel 14)

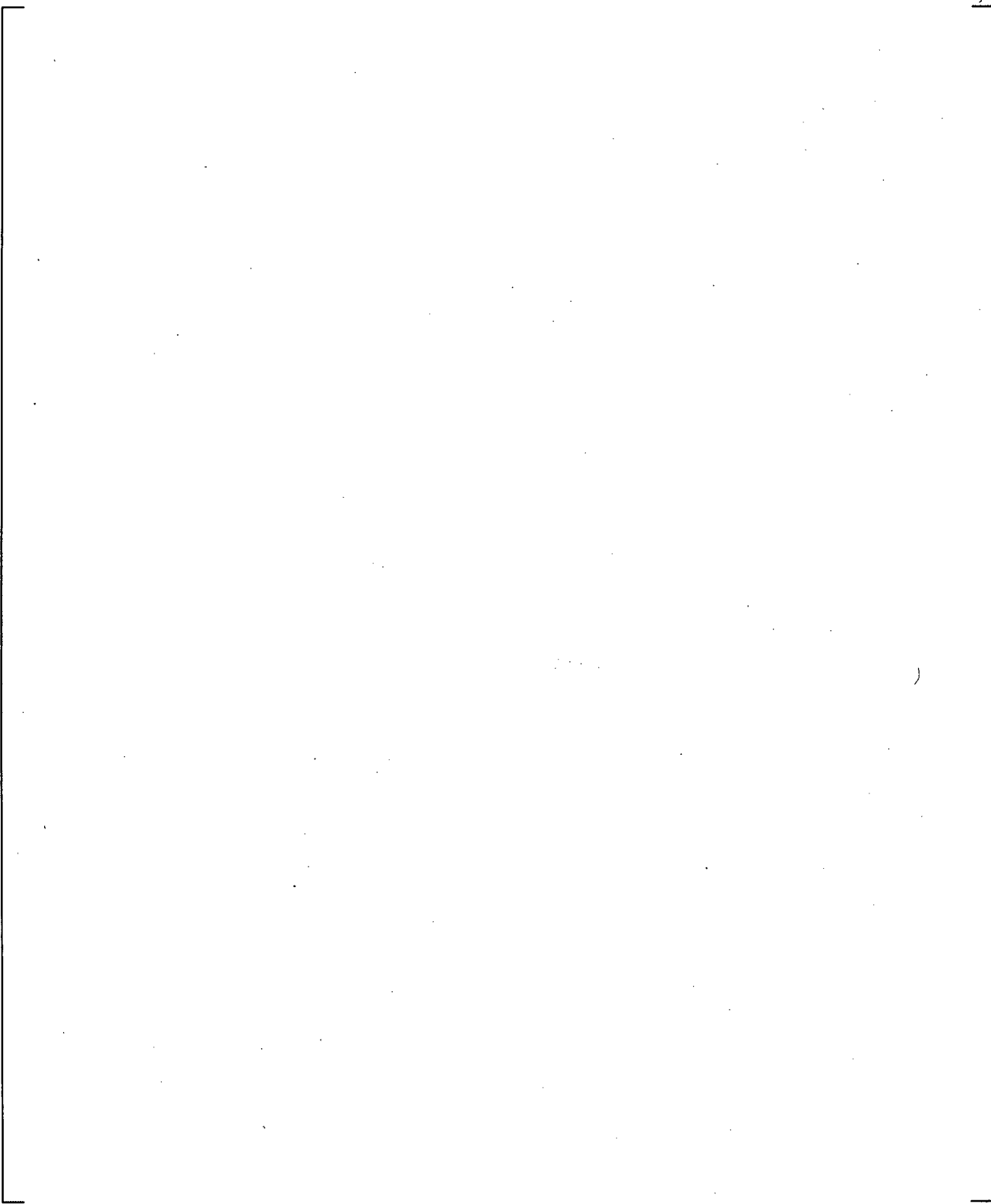


**Figure 21.10.4-7** Calculated Velocities at Upper Core Plate Hot Jet Channel 19 (top of CCFL Channel 14)

a,c

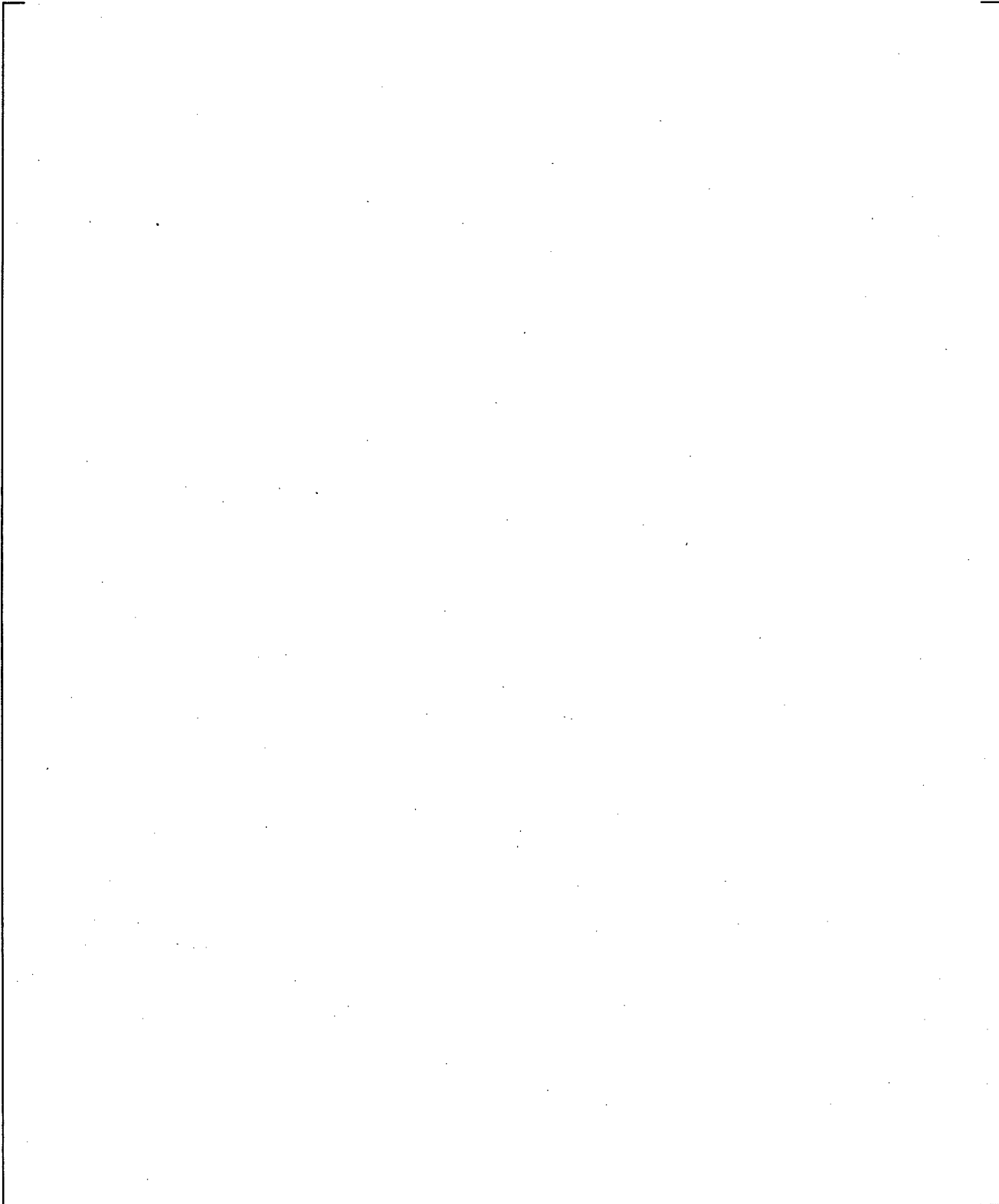


**Figure 21.10.4-8 Counter-current Flow Periods in Relation to the Liquid Pool Level above UCP**

a,c

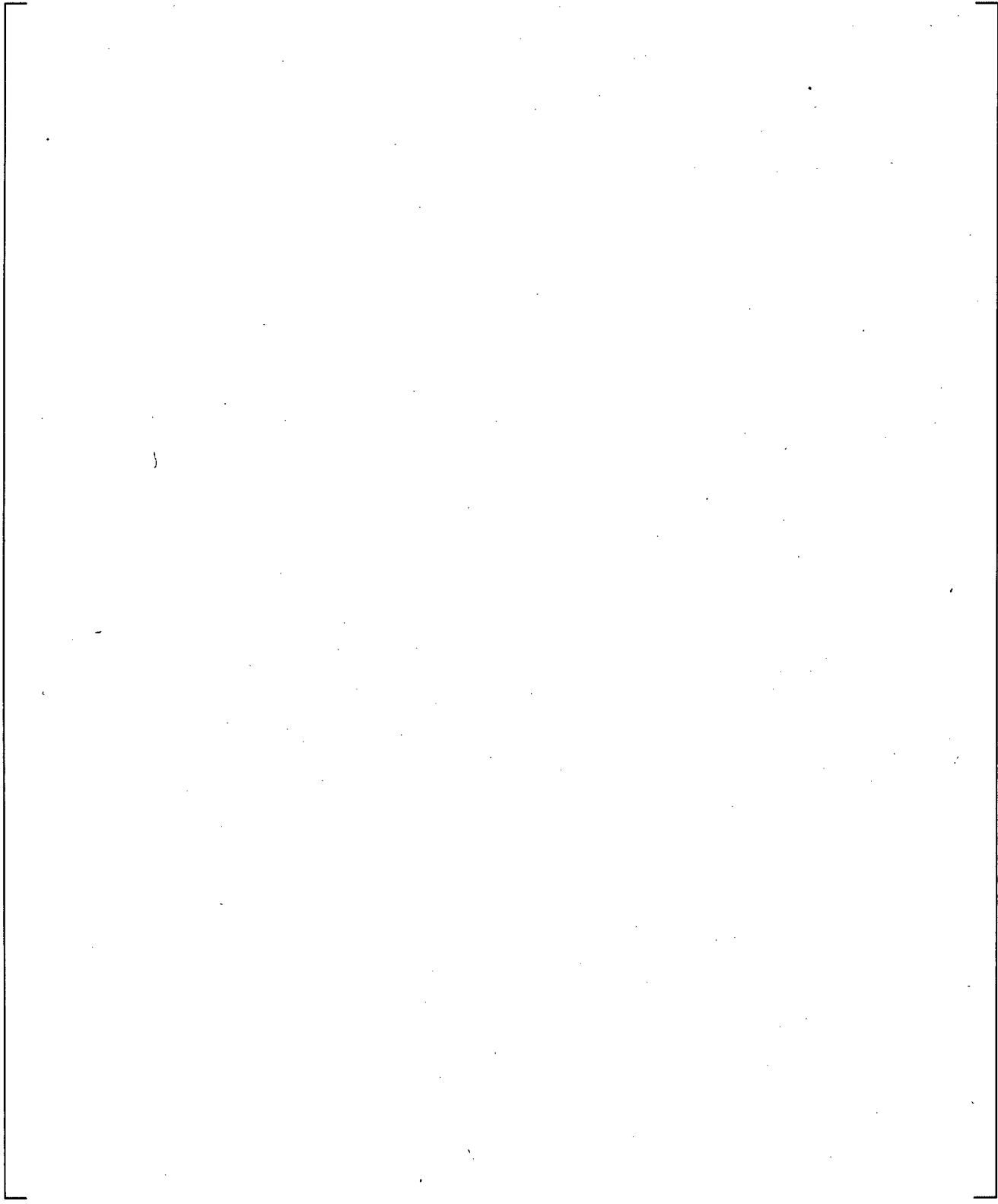


**Figure 21.10.4-9 Counter-current Flow Periods in Relation to the Inner Vessel Level**

a,c

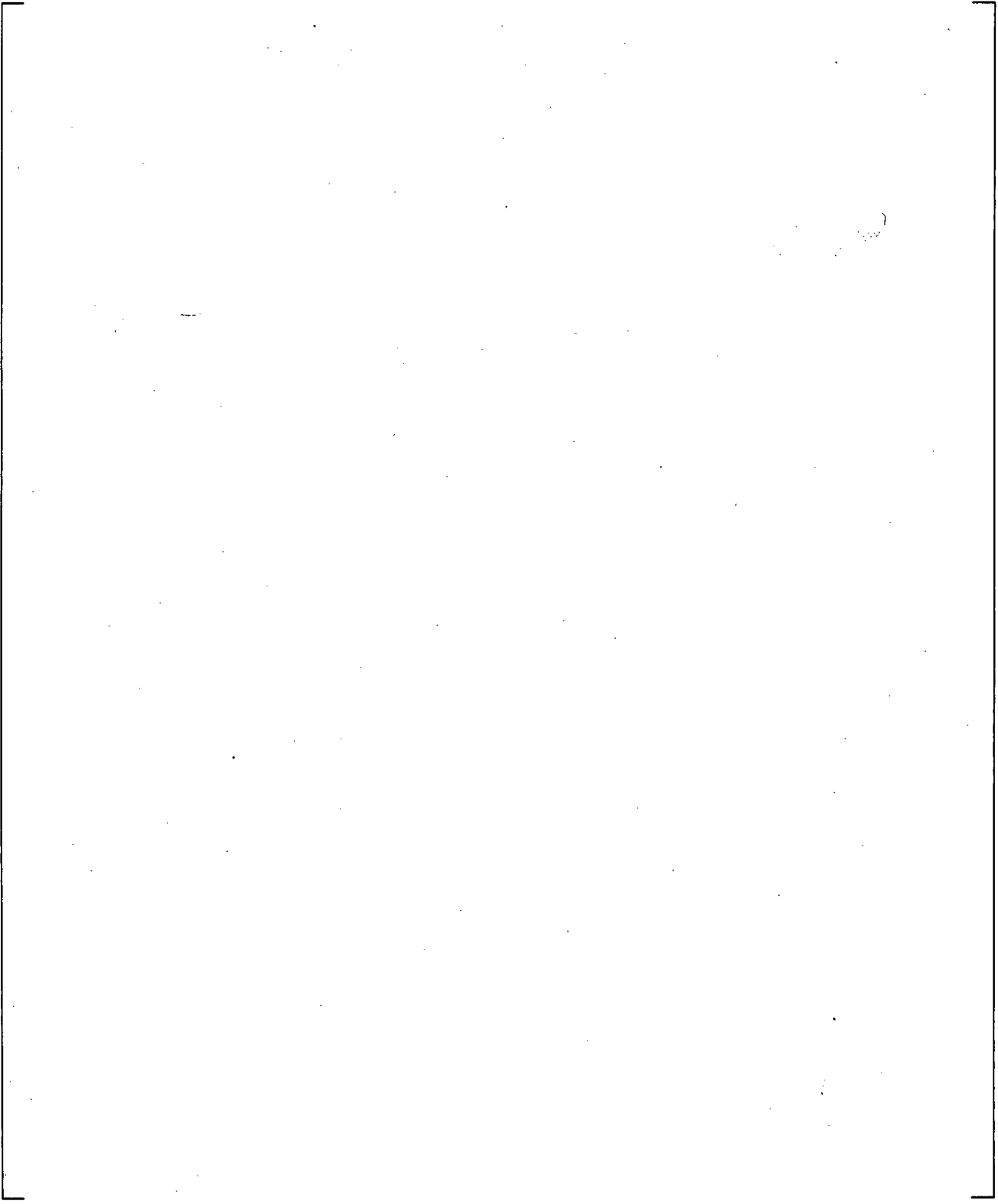


**Figure 21.10.4-10 Calculated Hot Leg Flow Rates**

a,c

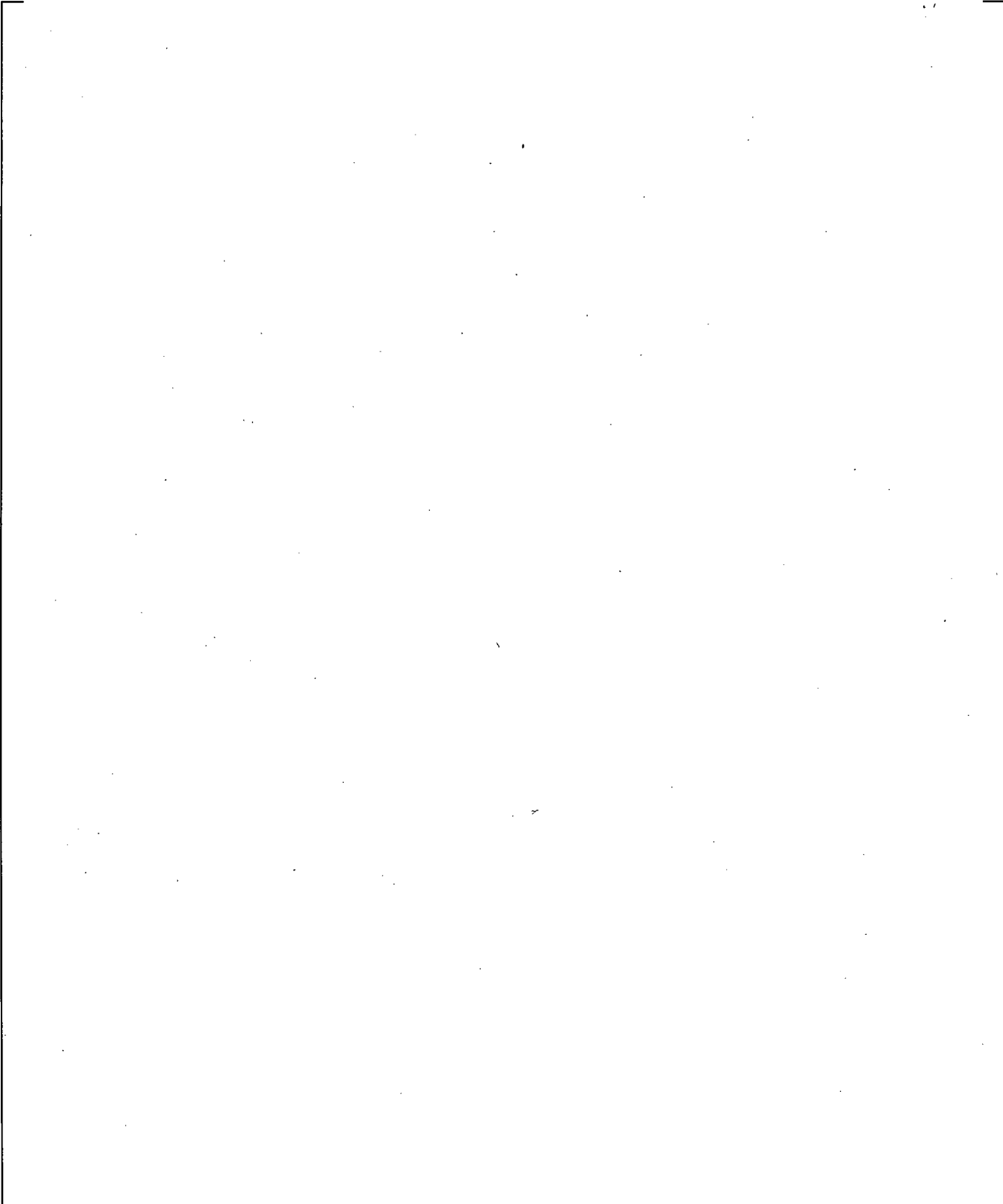


**Figure 21.10.4-11 Calculated CCFL at UCP Outer Jet Channel 73**

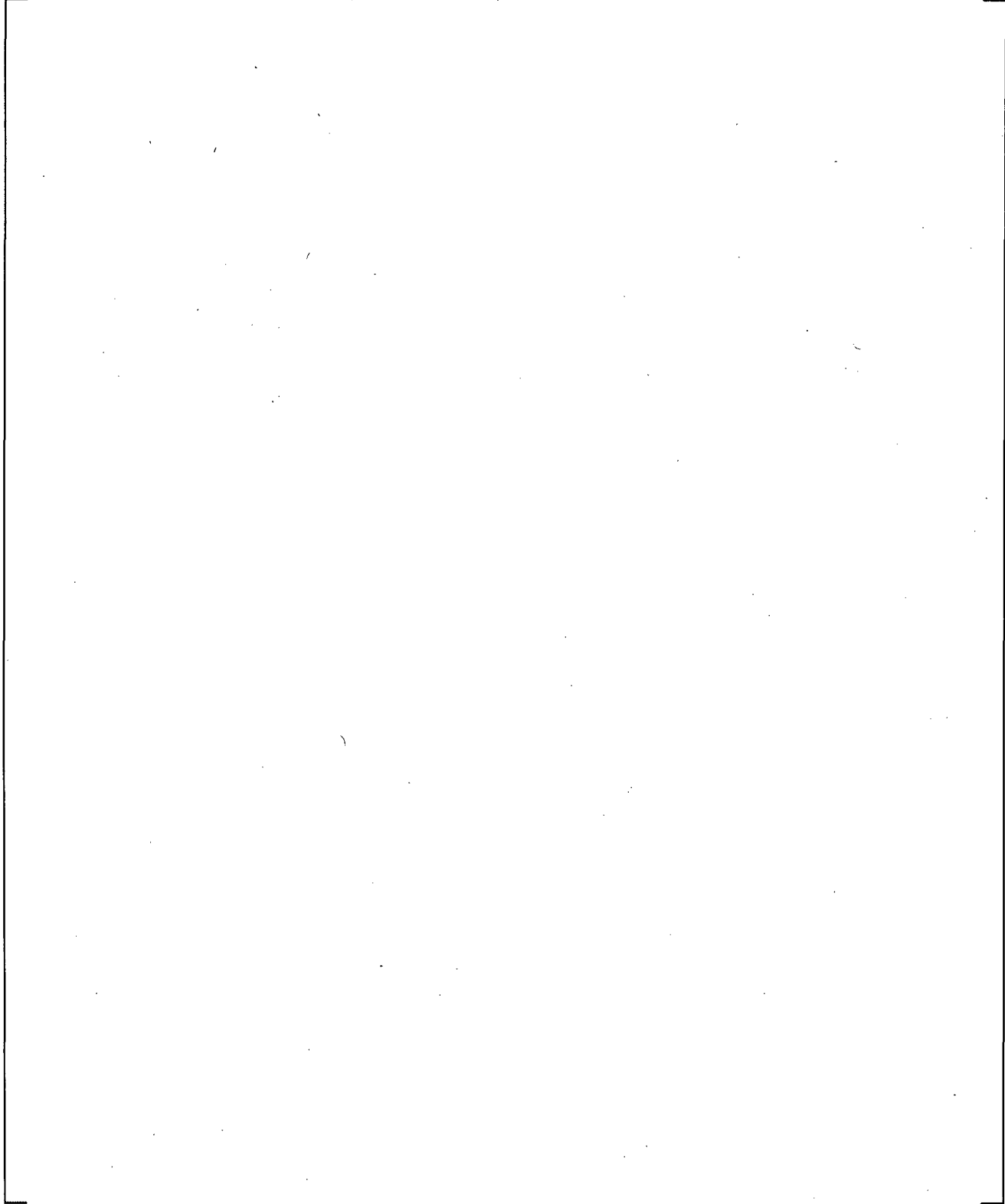


**Figure 21.10.4-12** Calculated and Measured Cladding Temperatures of Low Power Rods at 7.33-ft Elevation

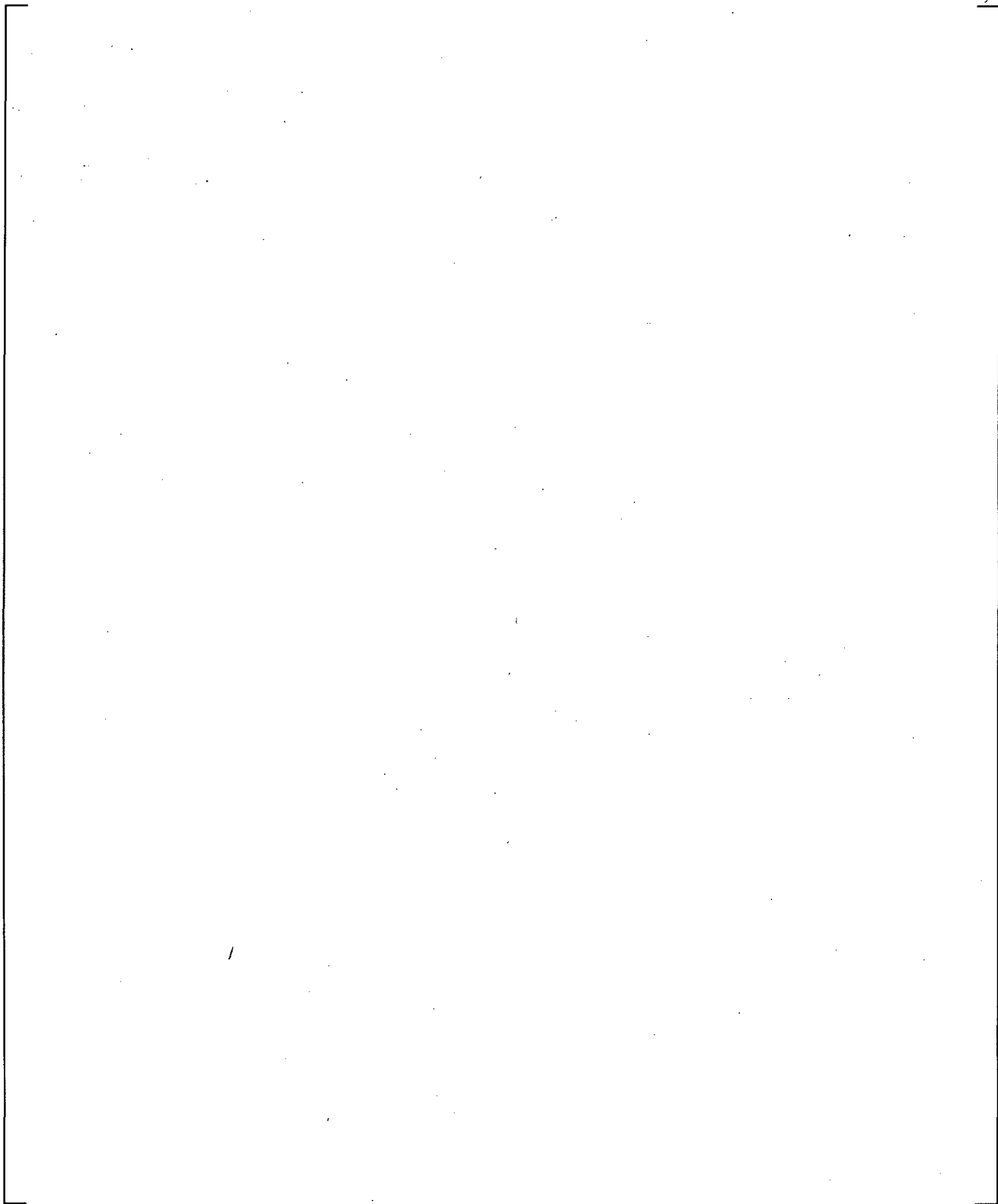


**Figure 21.10.4-12** Calculated and Measured Cladding Temperatures of Low Power Rods at 7.33-ft Elevation

a,c

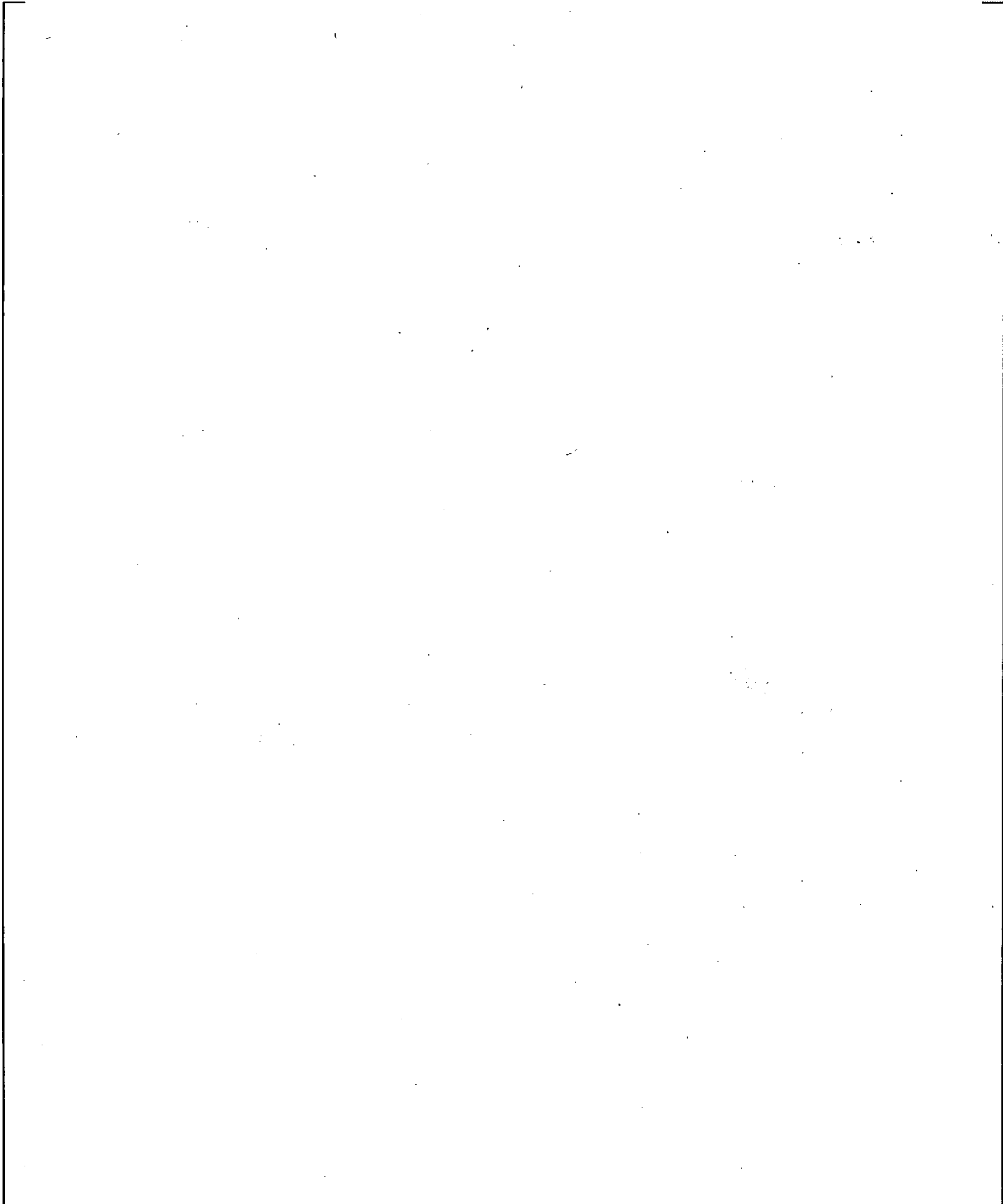


**Figure 21.10.4-13 . Calculated and Measured Cladding Temperatures of High Power Rods at 7.33-ft Elevation**

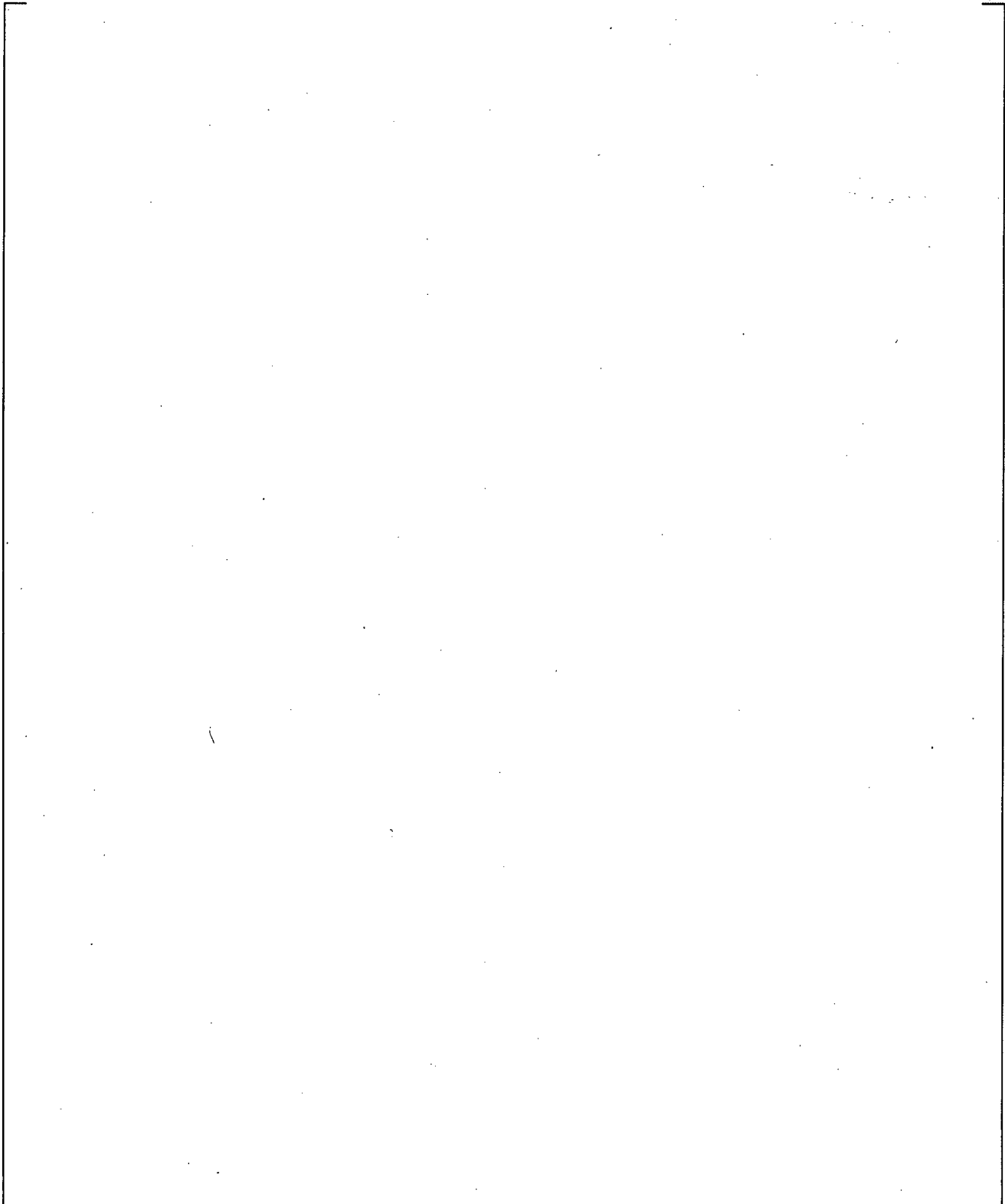


**Figure 21.10.4-13 Calculated and Measured Cladding Temperatures of High Power Rods at 7.33-ft Elevation**

**Figure 21.10.4-14 Calculated and Measured Cladding Temperatures of Average Power Rods at 7.33-ft Elevation**

a,c

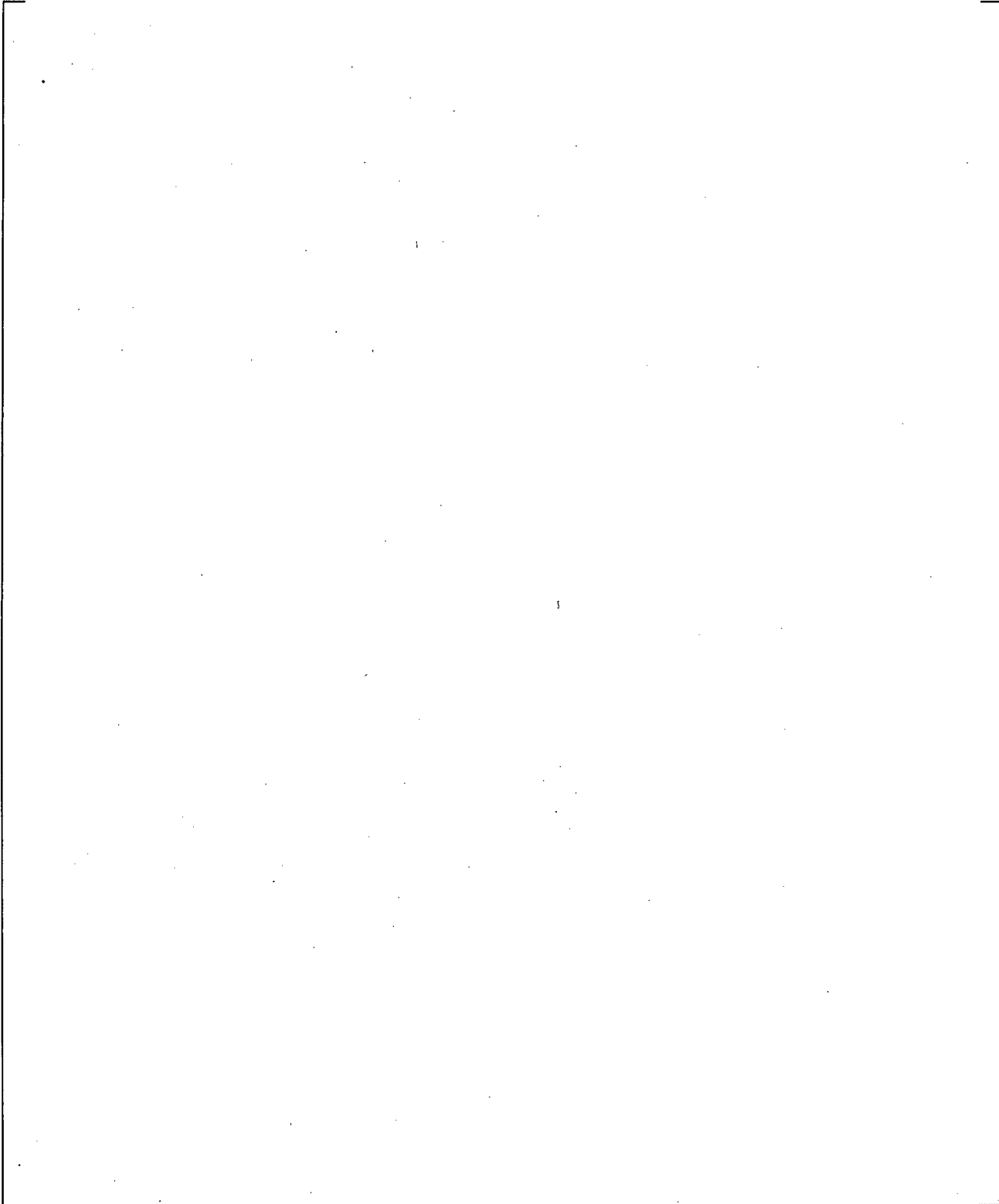


**Figure 21.10.4-14** Calculated and Measured Cladding Temperatures of Average Power Rods at 7.33-ft Elevation

a,c

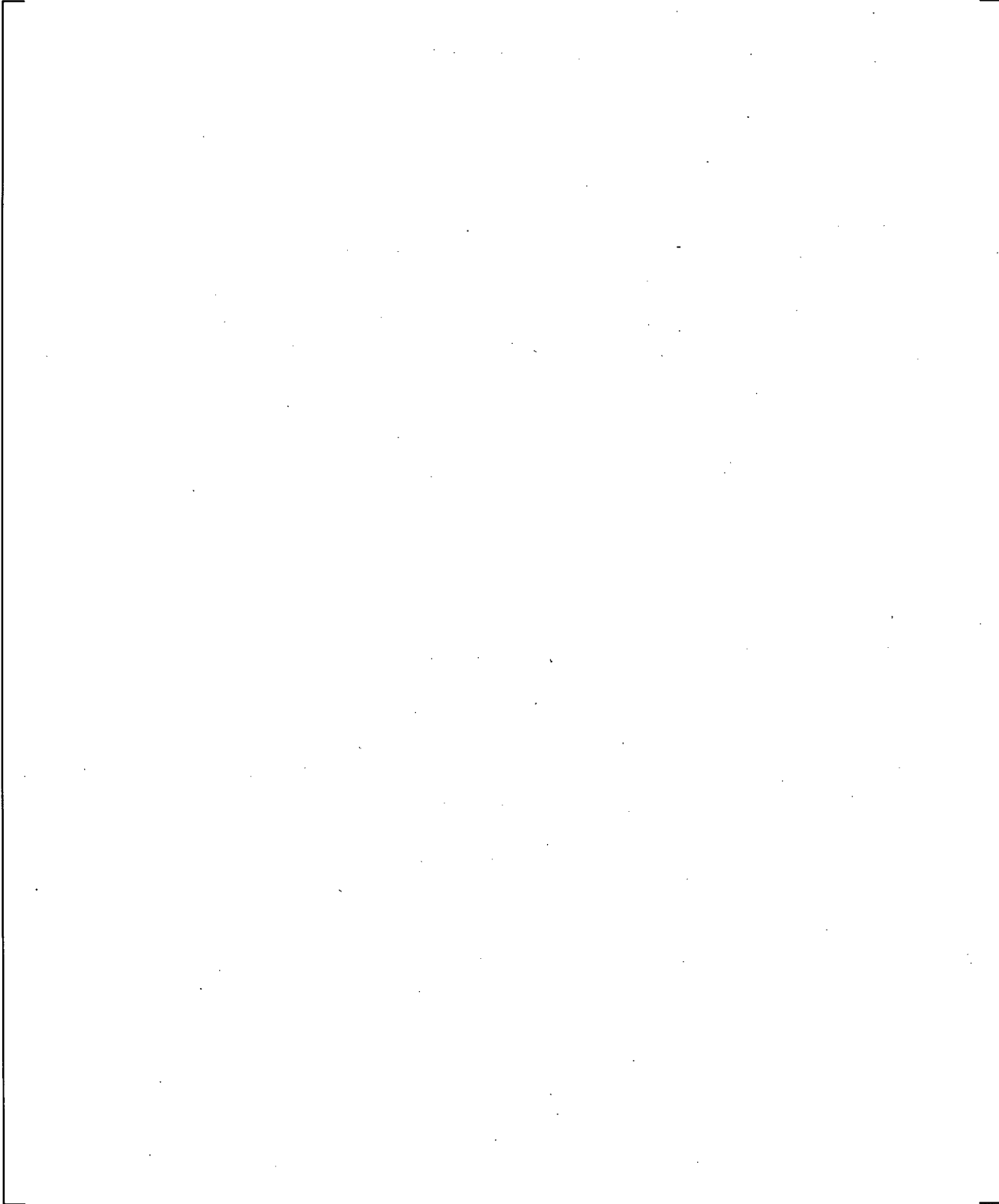


**Figure 21.11.1-1 SB-CL-18 Cross-Over Leg A Differential Pressures**

a,c

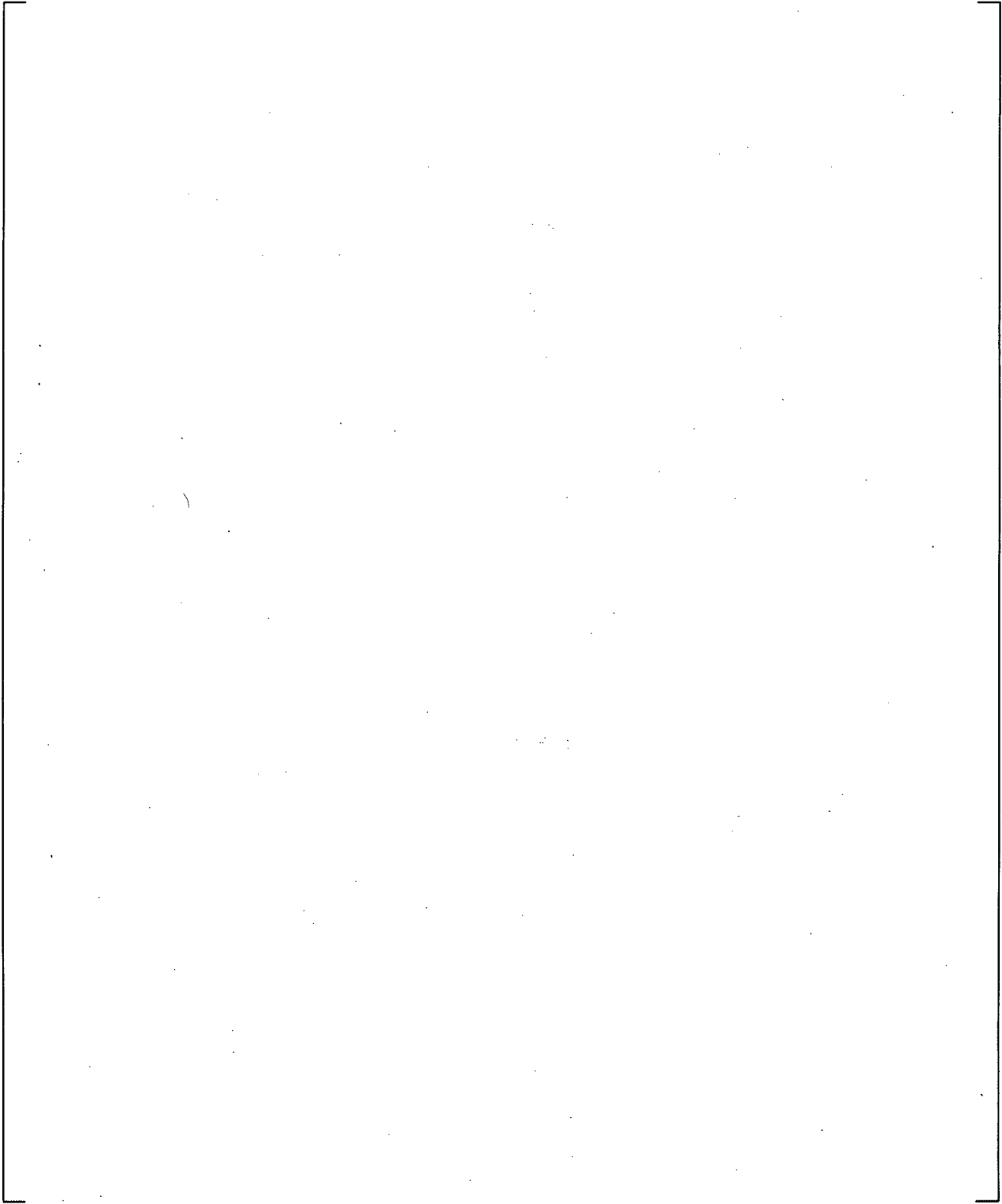


**Figure 21.11.1-2 SB-CL-18 Cross-Over Leg B Differential Pressures**

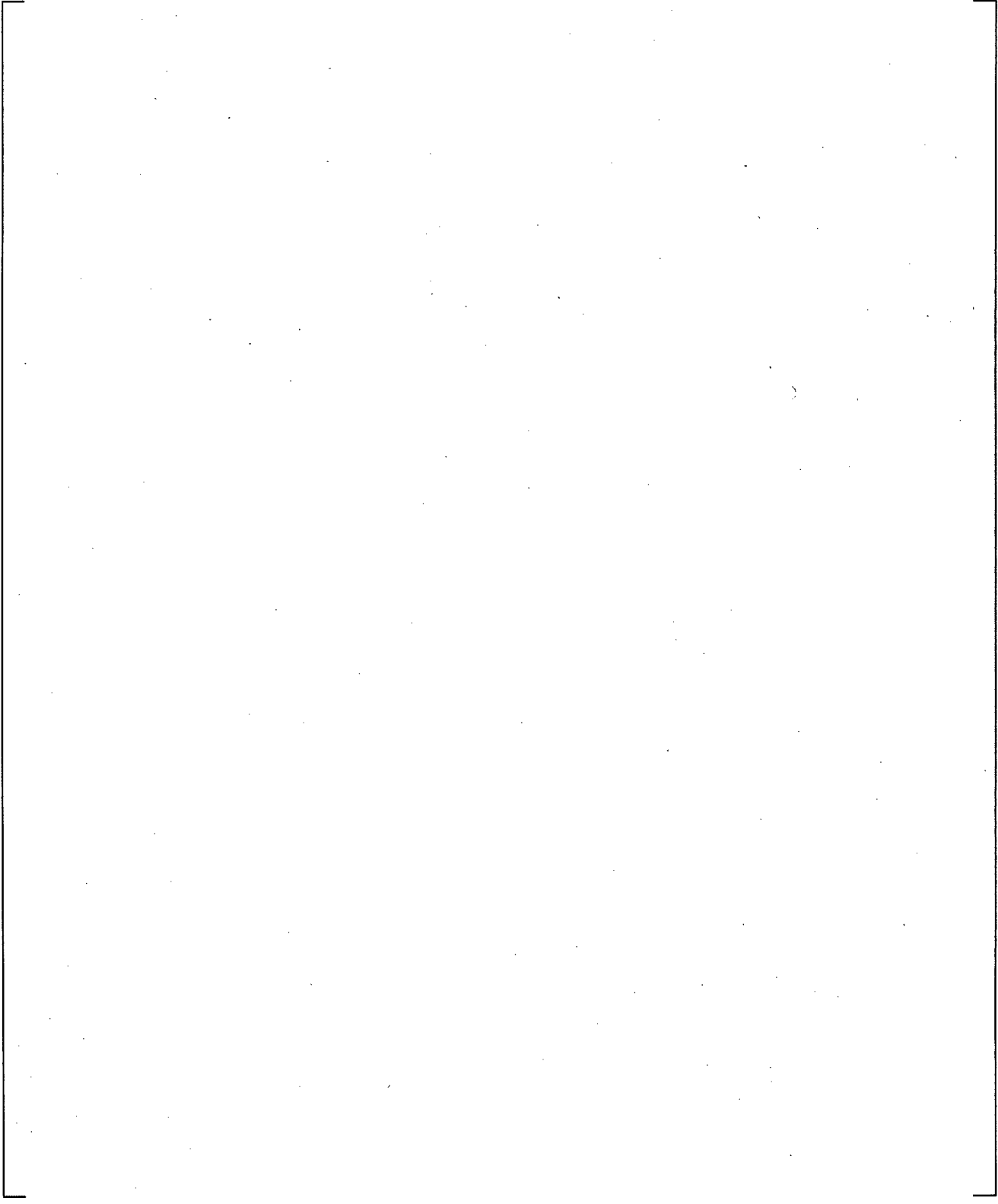


**Figure 21.11.1-3 Inner Vessel Differential Pressures (LP+Core+UCP)**

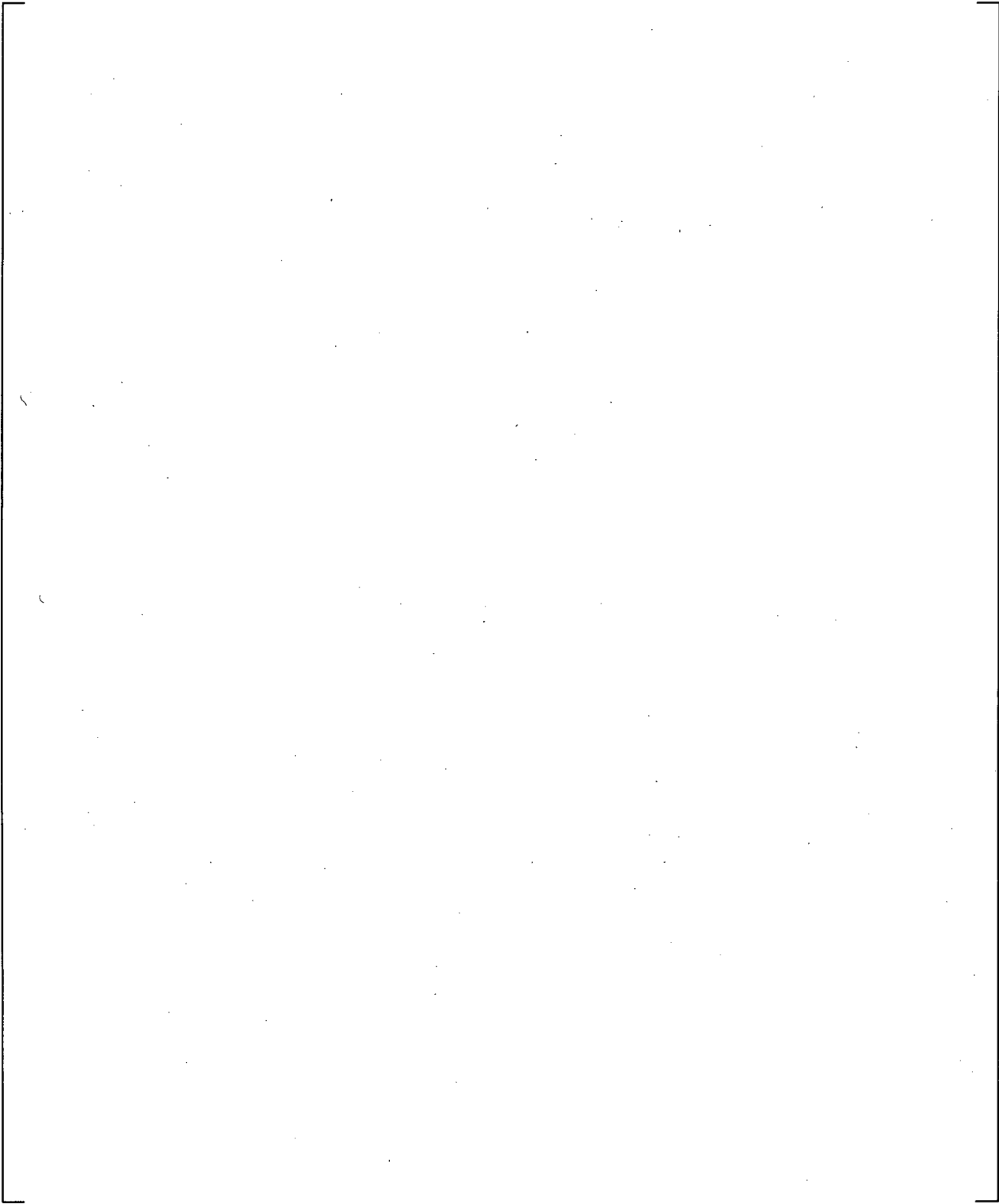


**Figure 21.11.1-4 Downcomer Differential Pressures**

a,c

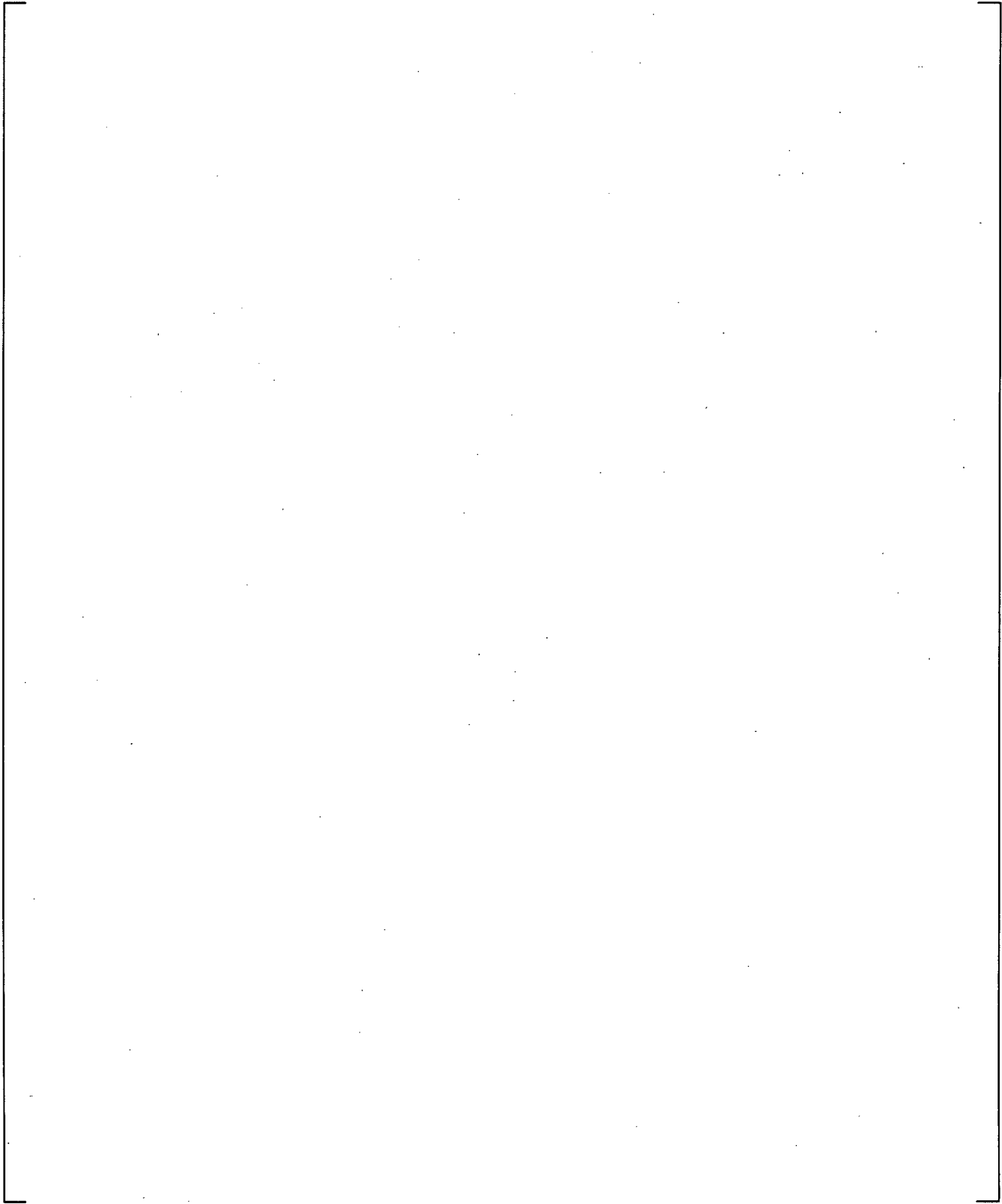


**Figure 21.11.1-5 Lower Plenum Differential Pressures**

a,c

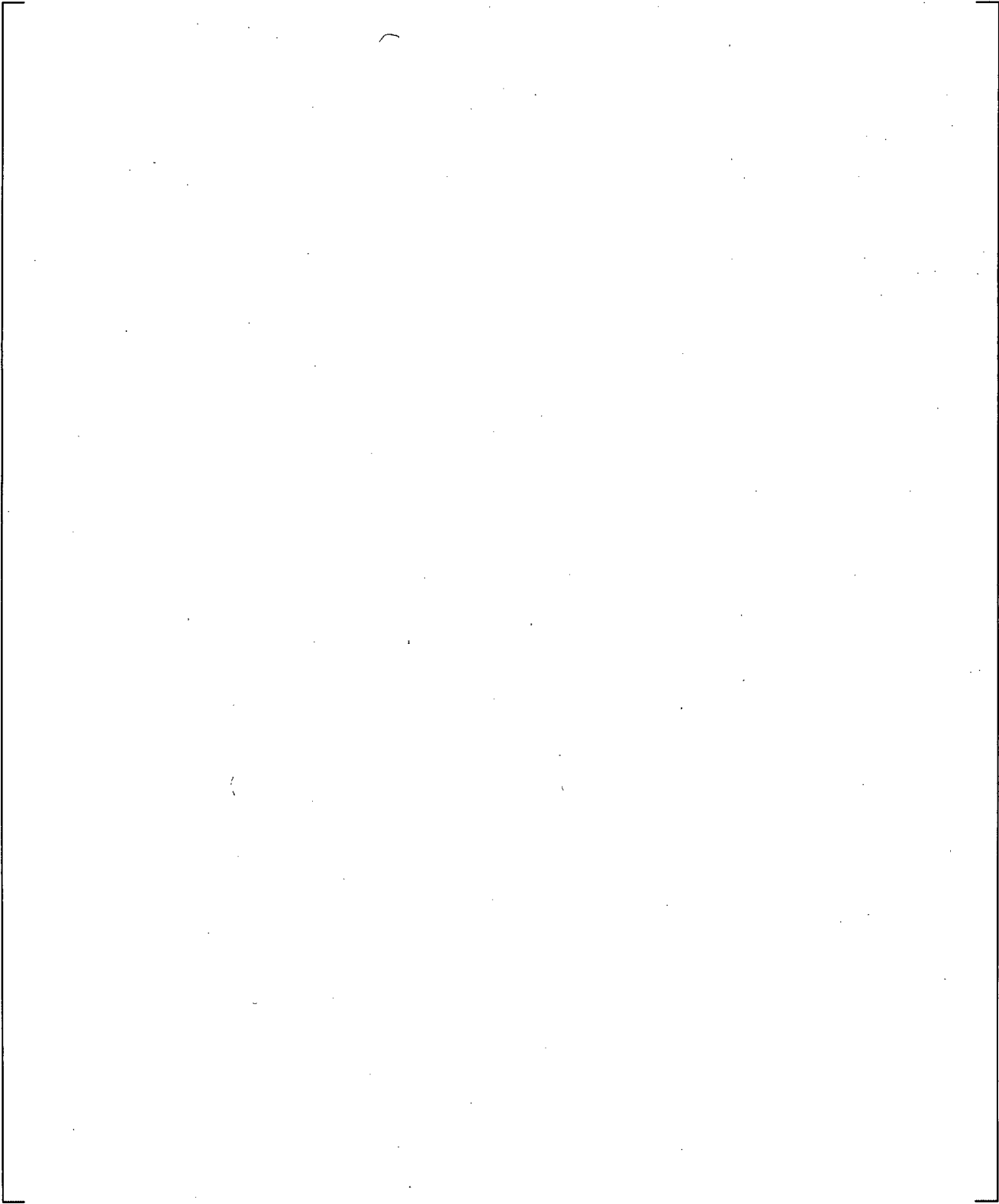


**Figure 21.11.1-6 Upper Plenum Differential Pressures**

a,c

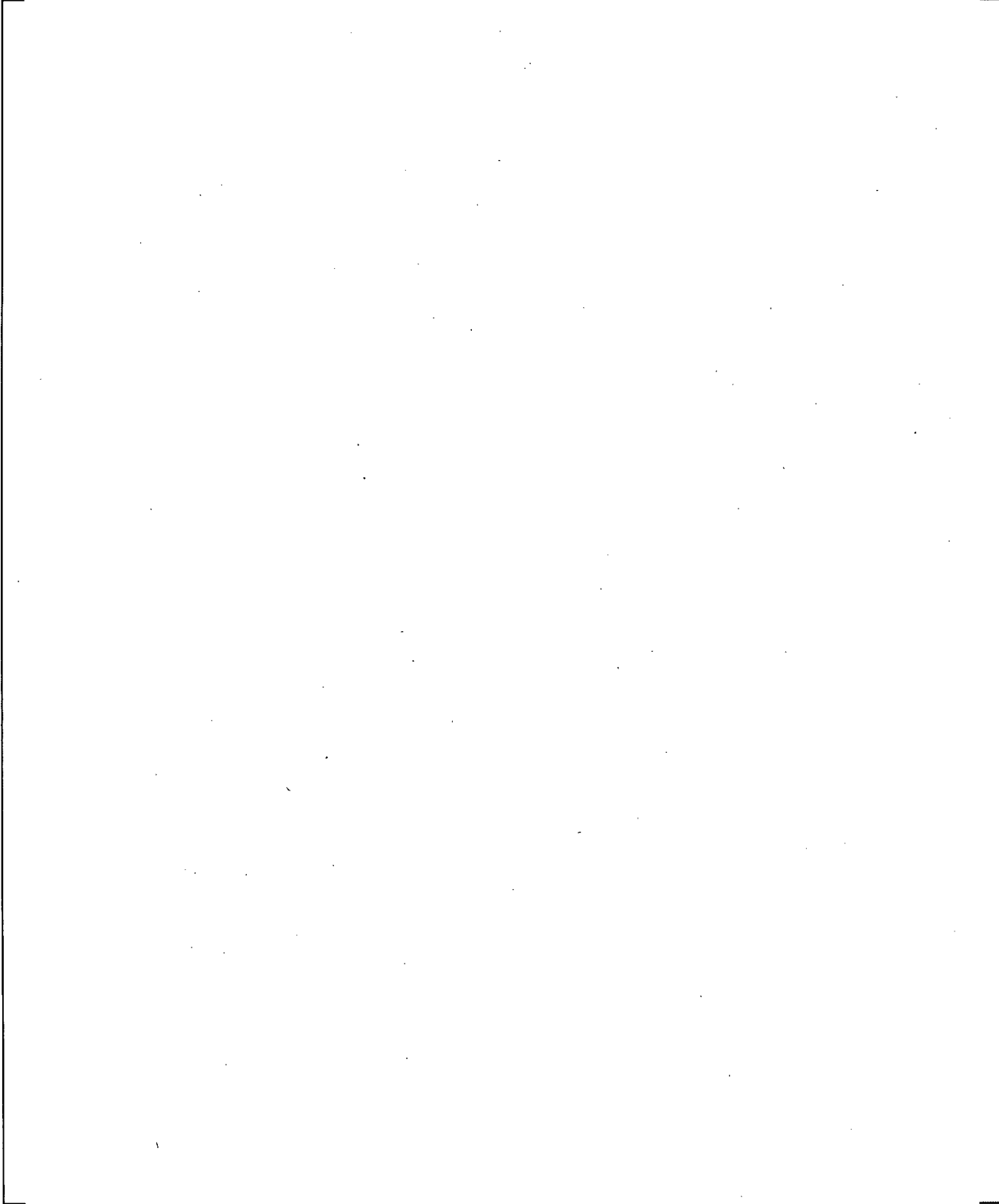


**Figure 21.11.1-7 Peak Cladding Temperatures**

a,c

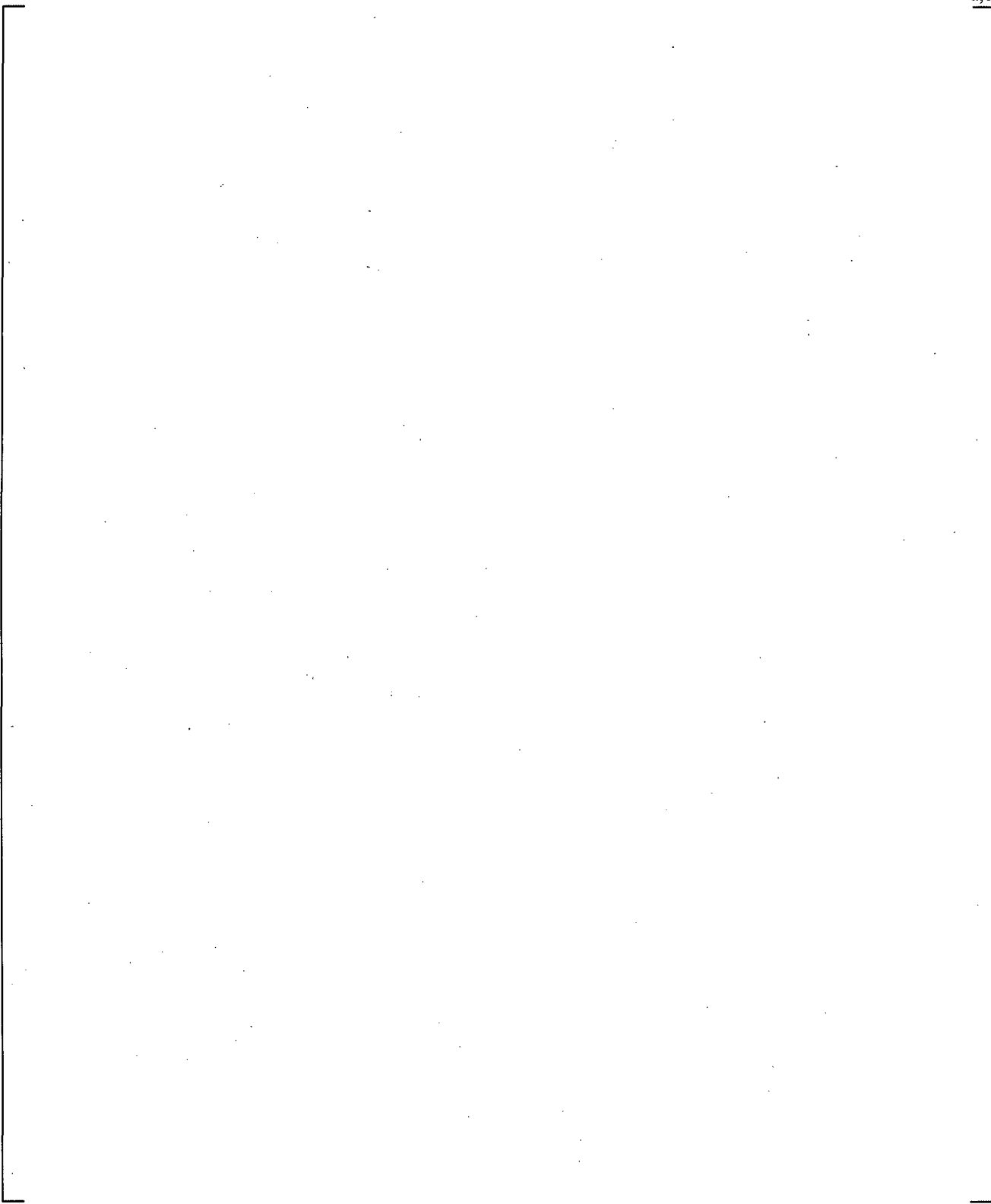


**Figure 21.11.2-1 SB-CL-18 Cross-Over Leg A Differential Pressures**

a,c

**Figure 21.11.2-2 SB-CL-18 Cross-Over Leg B Differential Pressures**

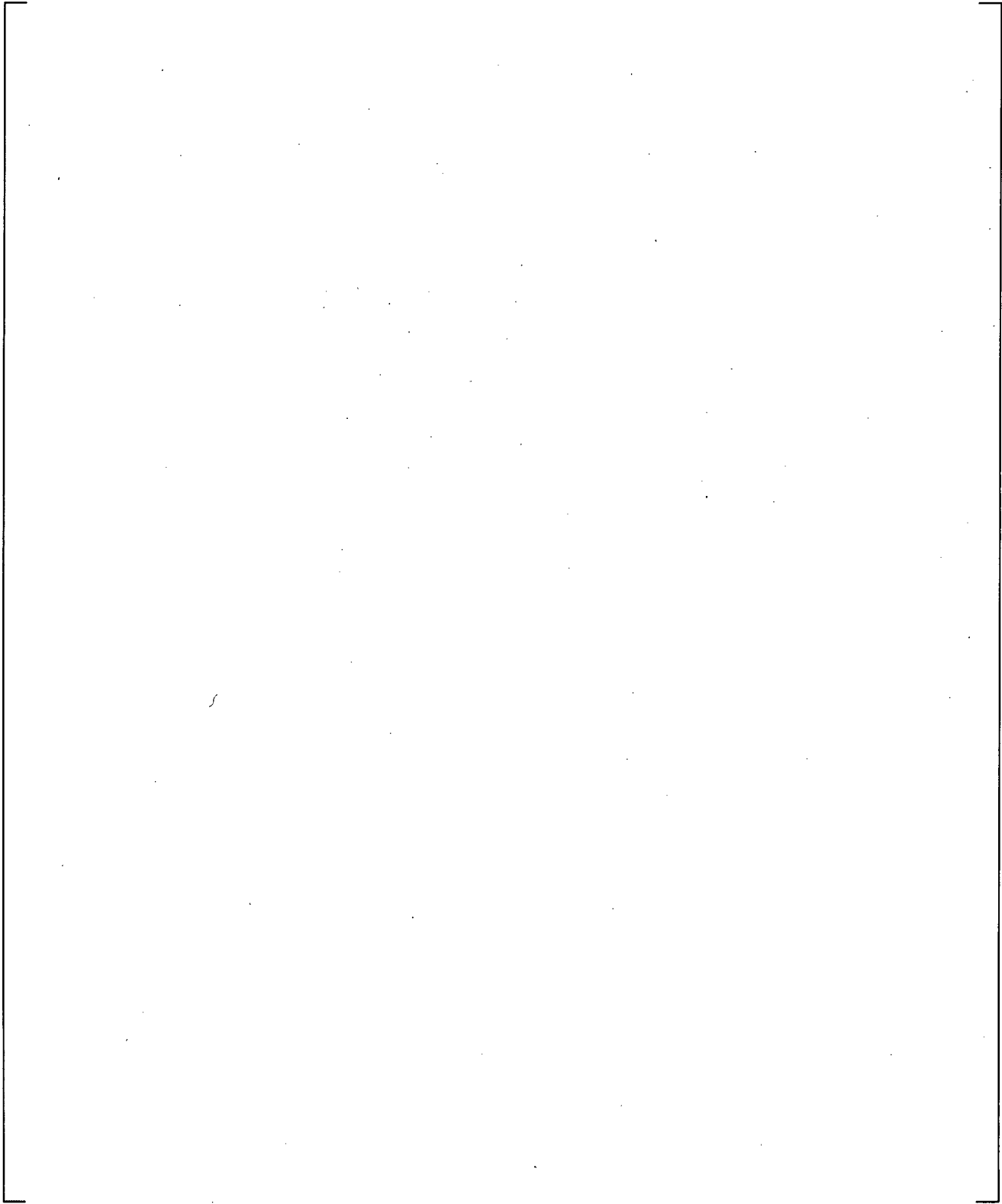


**Figure 21.11.2-3 Inner Vessel Differential Pressures (LP+Core+UCP)**

a,c

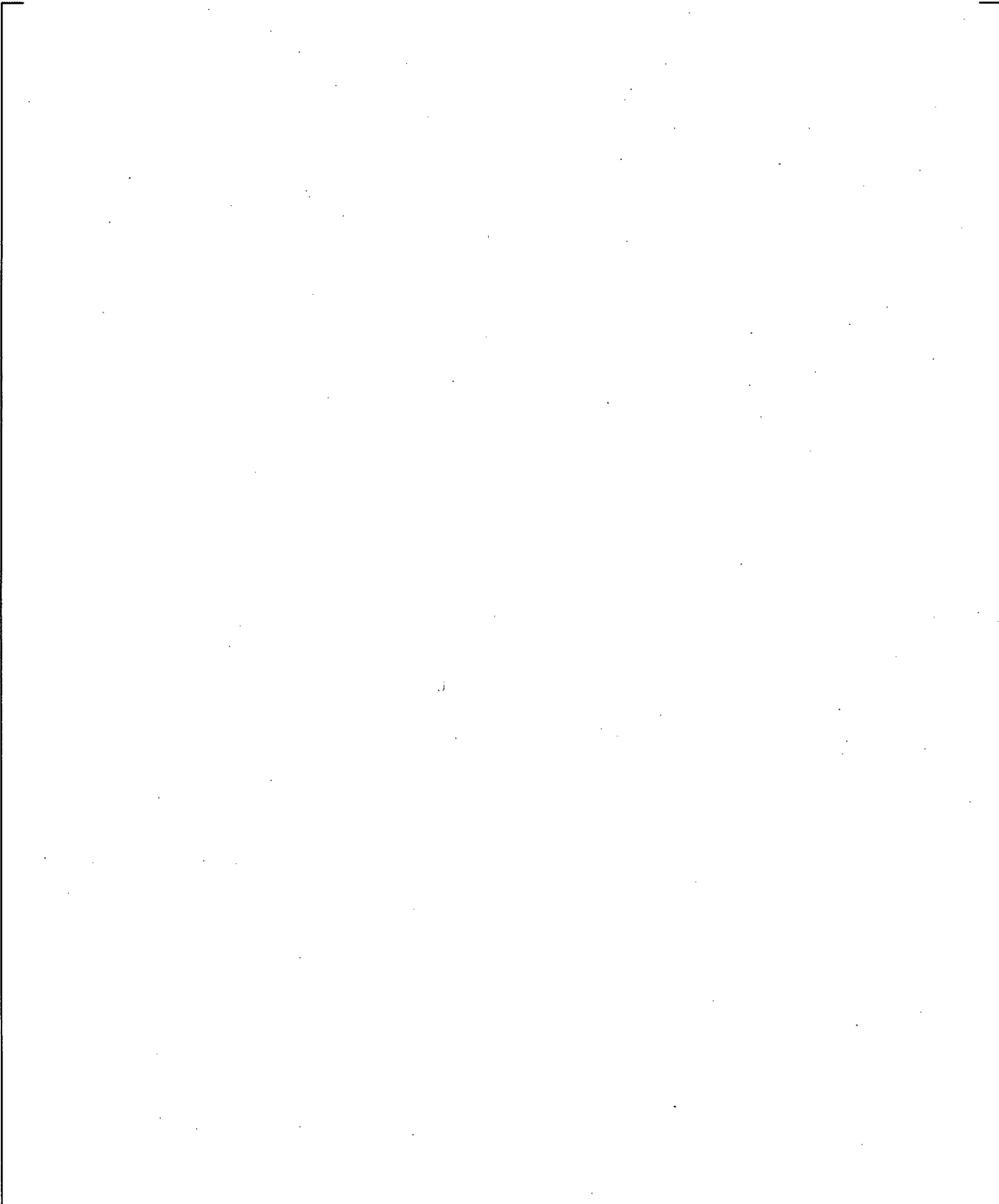


**Figure 21.11.2-4 Downcomer Differential Pressures**

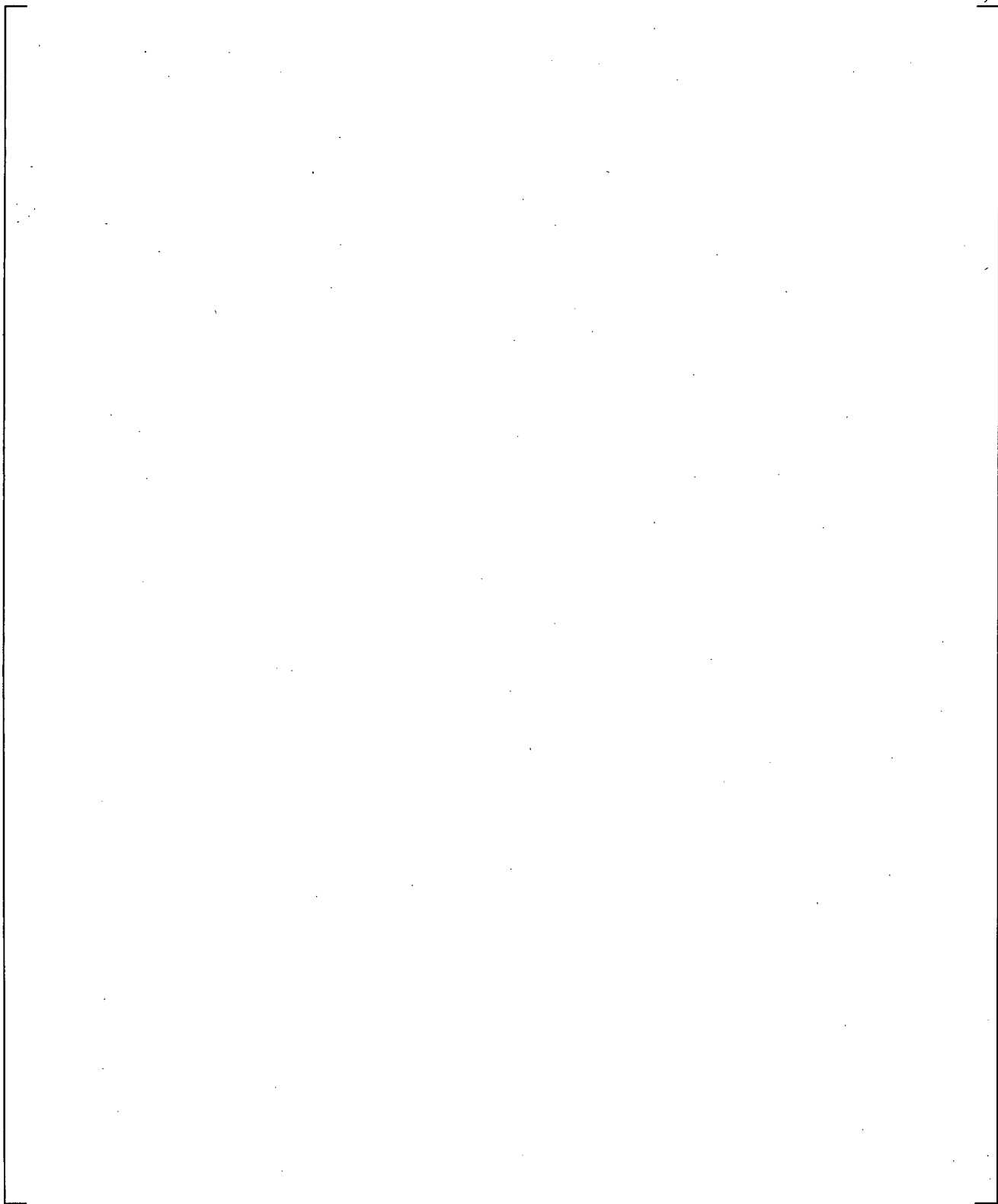


**Figure 21.11.2-5 Lower Plenum Differential Pressures**

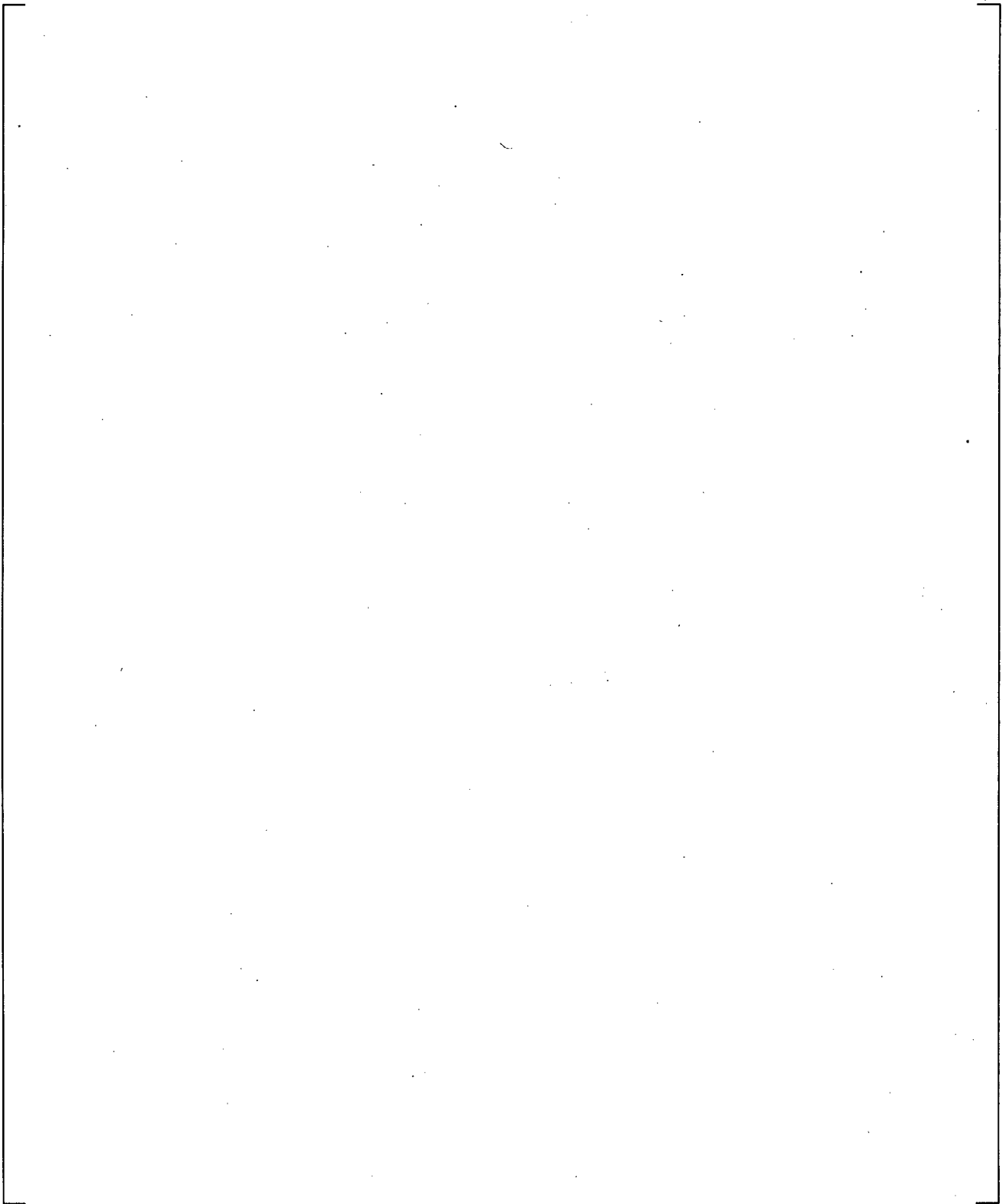


**Figure 21.11.2-6 Upper Plenum Differential Pressures**

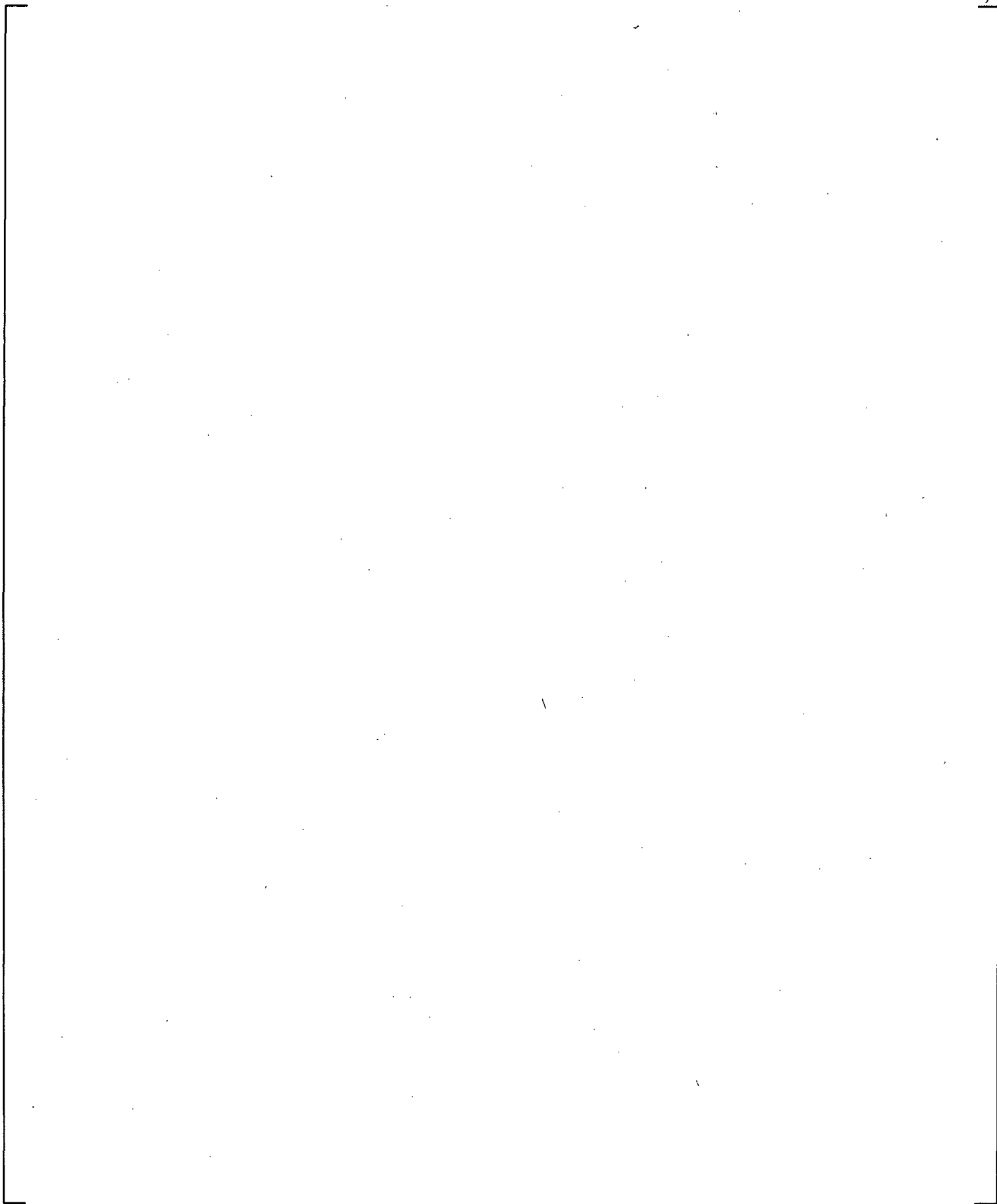


**Figure 21.11.2-7 Peak Cladding Temperatures**

a,c

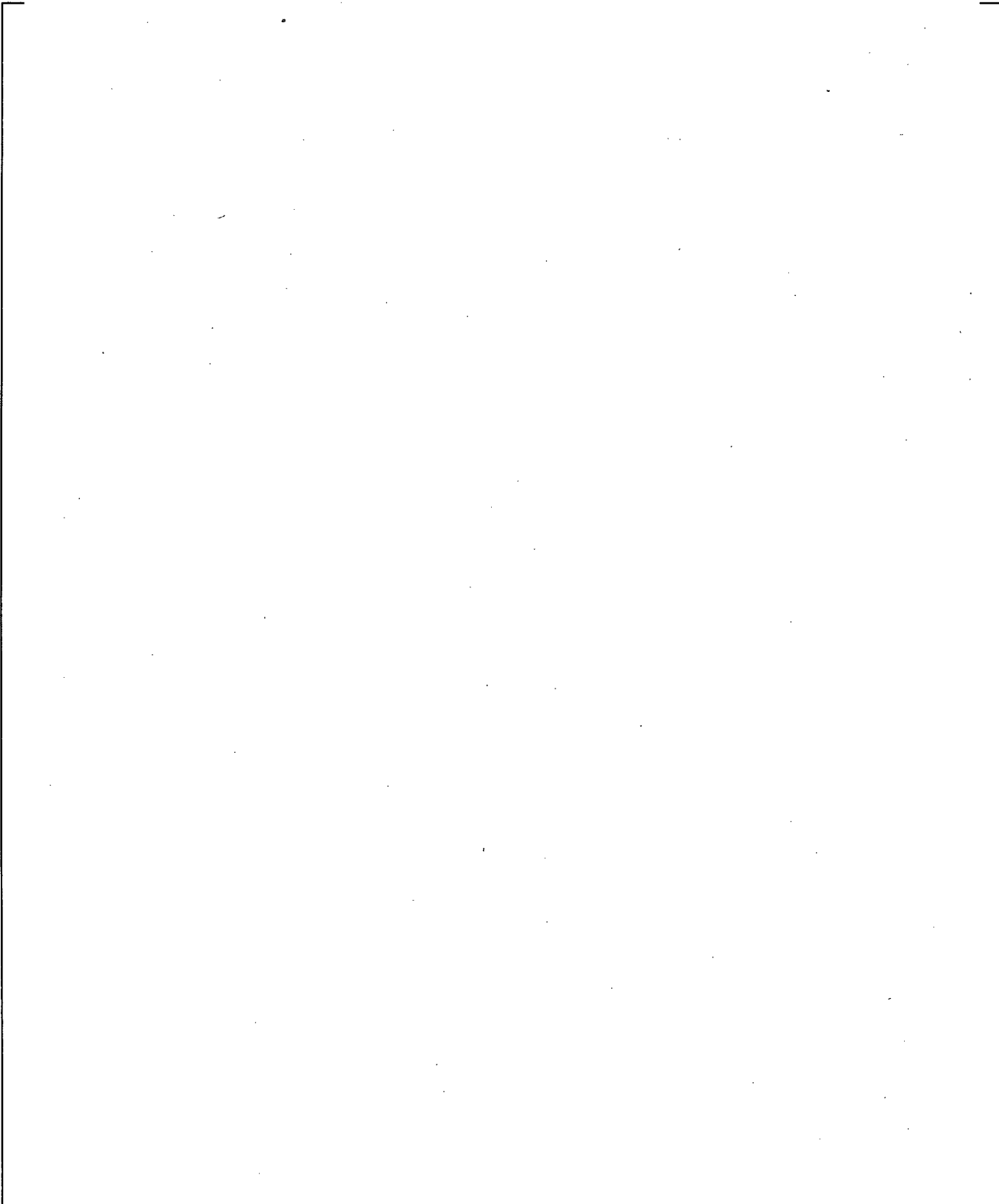


**Figure 21.11.3-1 SB-CL-18 Cross-Over Leg A Differential Pressures**

a,c

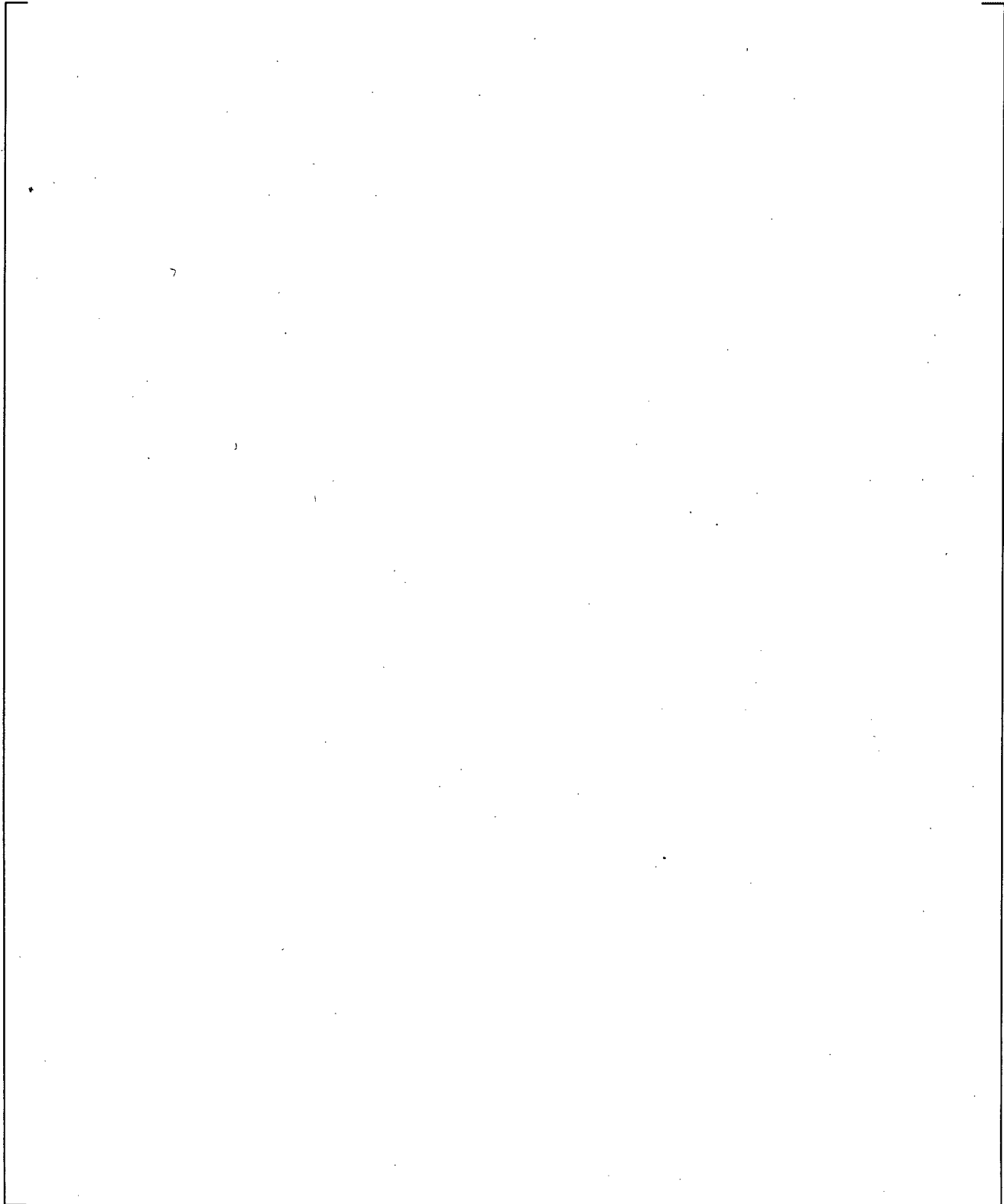


**Figure 21.11.3-2 SB-CL-18 Cross-Over Leg B Differential Pressures**

a,c

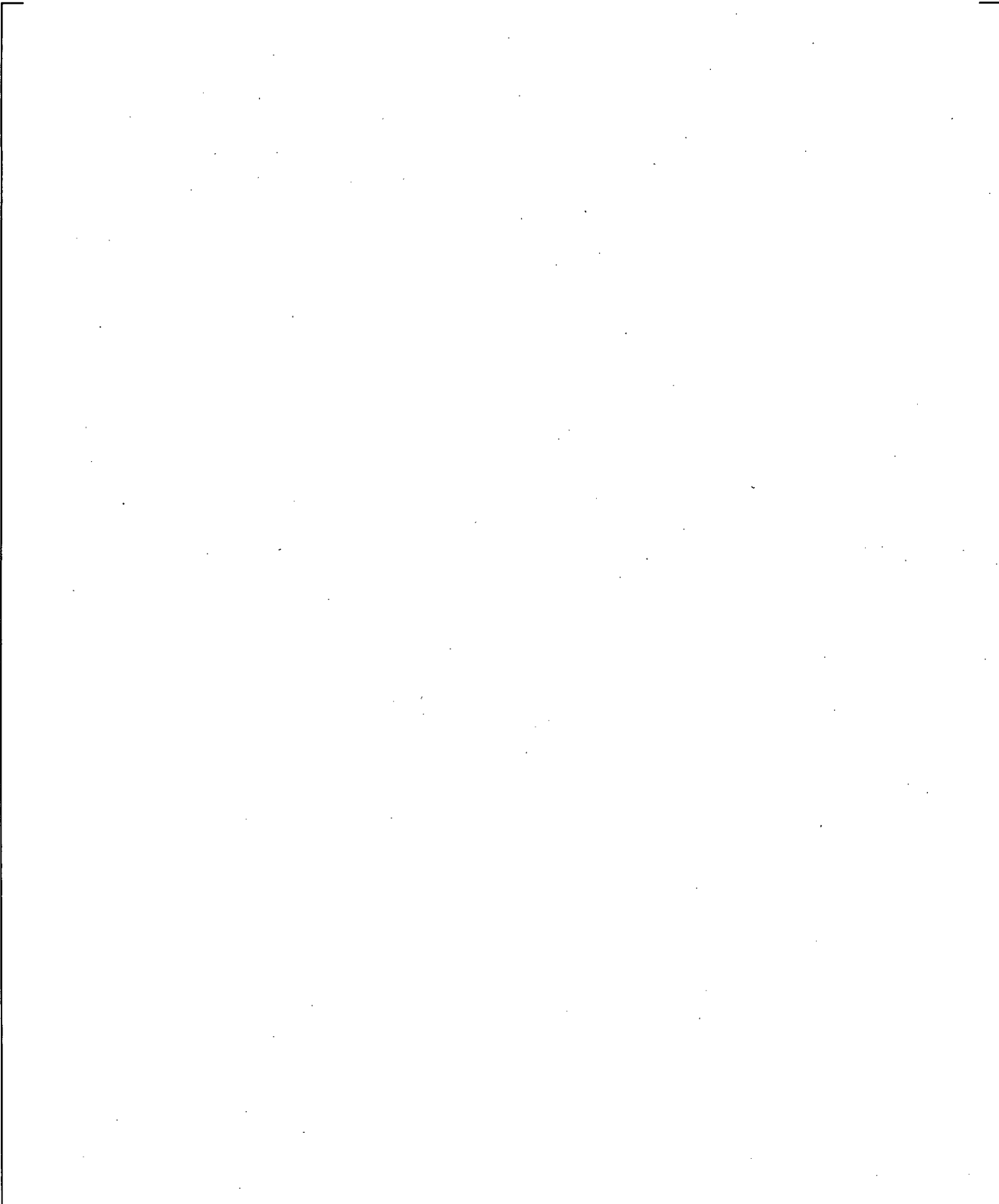


**Figure 21.11.3-3 Inner Vessel Differential Pressures (LP+Core+UCP)**

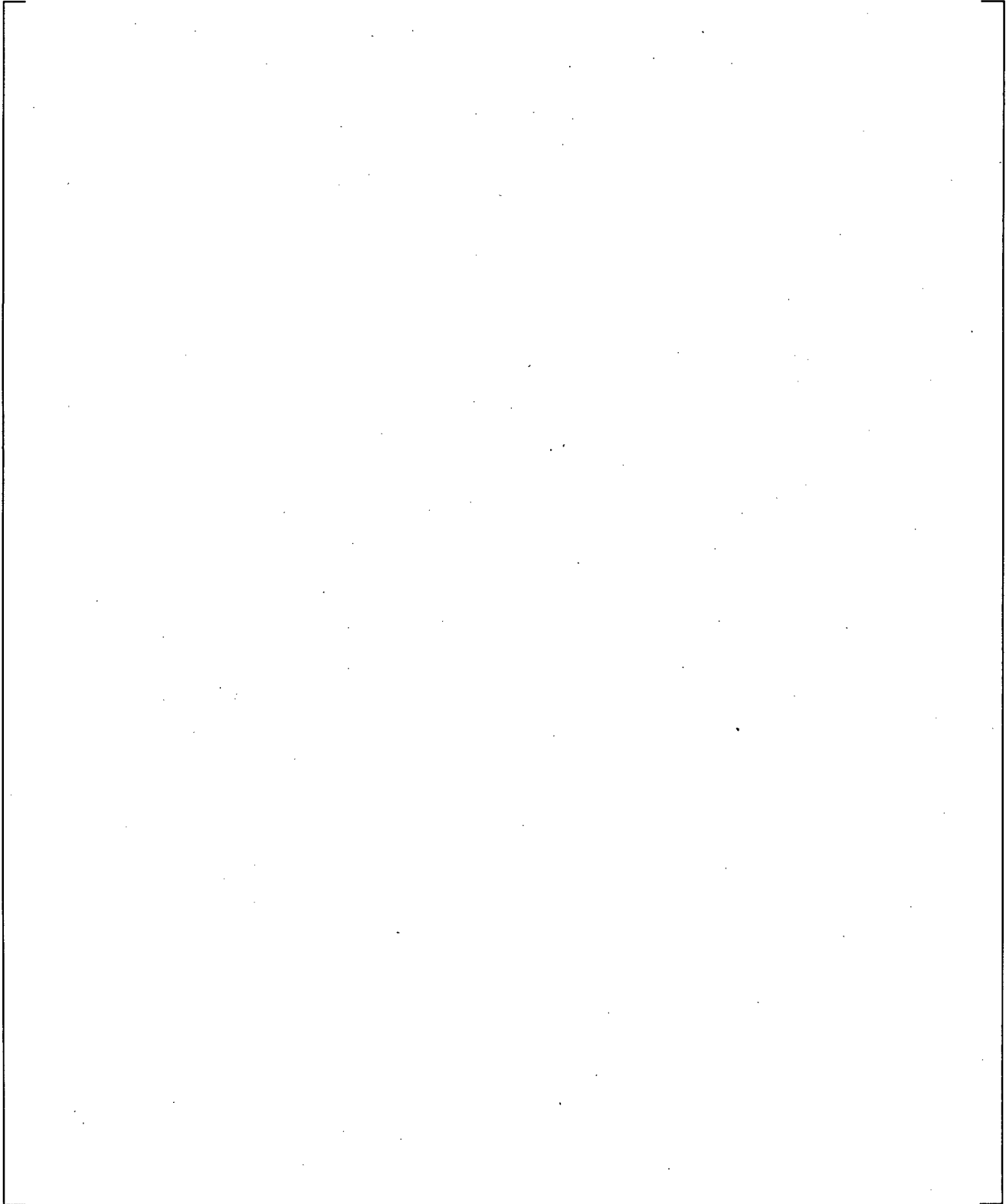


**Figure 21.11.3-4 Downcomer Differential Pressures**

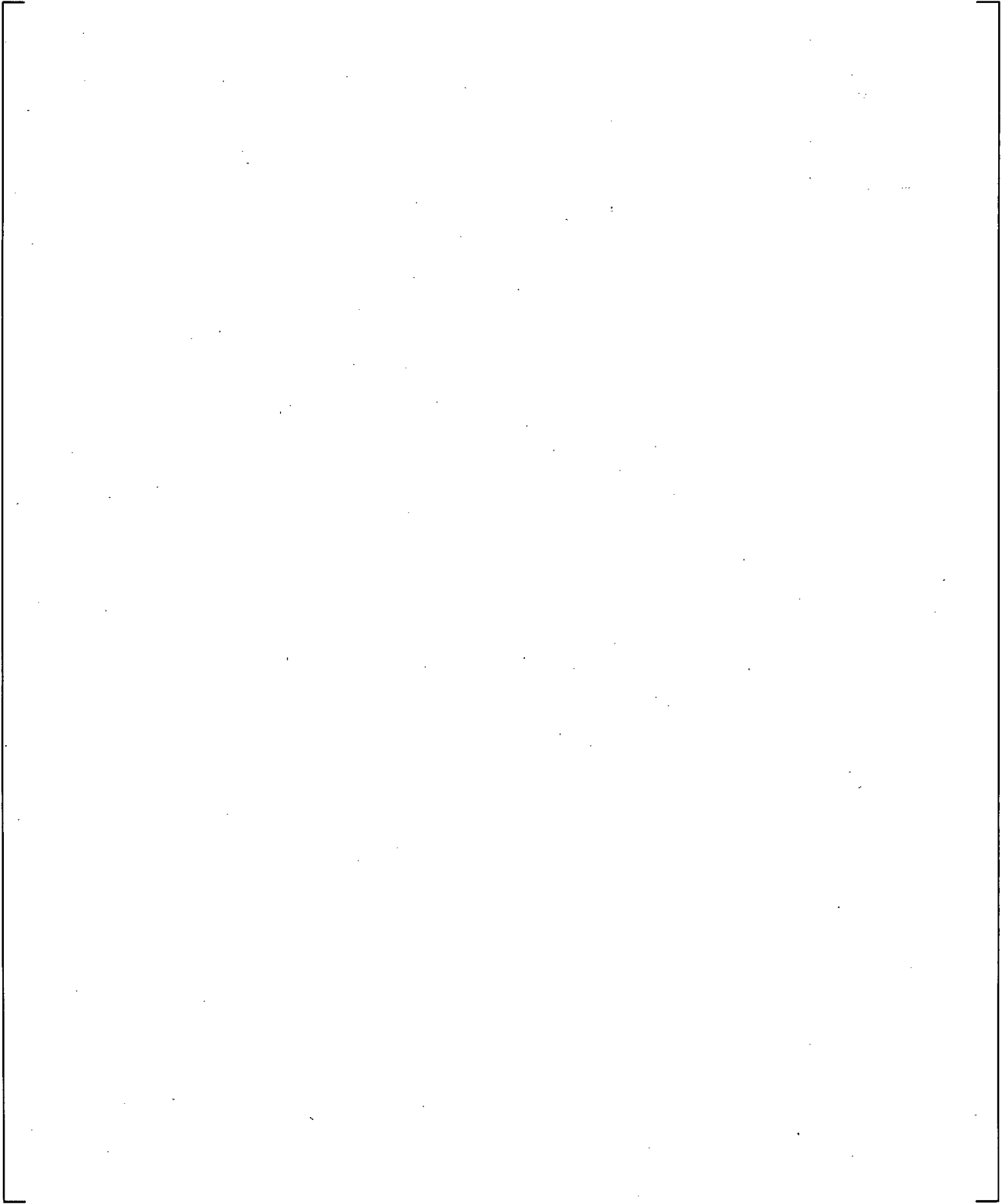


**Figure 21.11.3-5 Lower Plenum Differential Pressures**

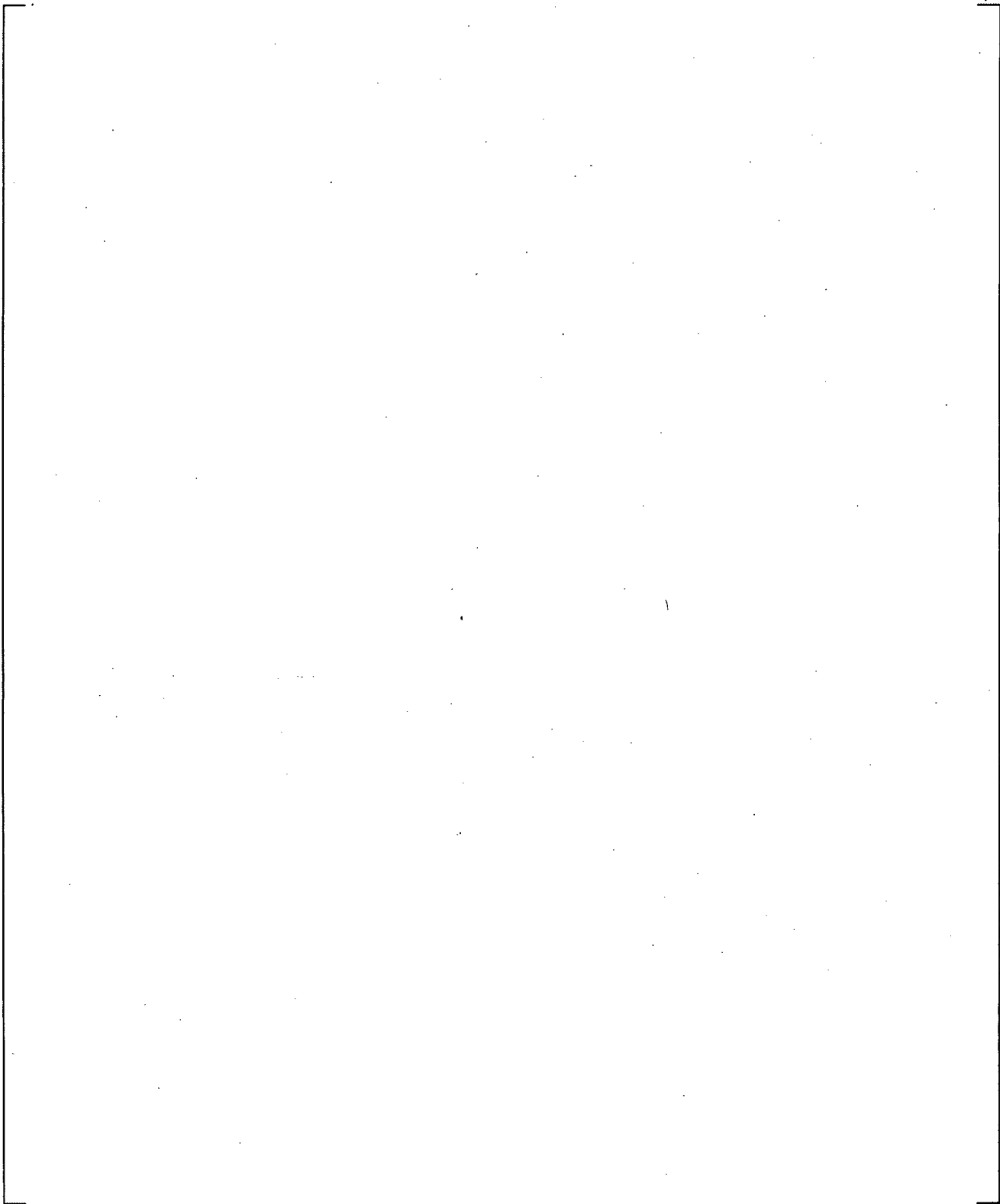


**Figure 21.11.3-6 Upper Plenum Differential Pressures**

a,c

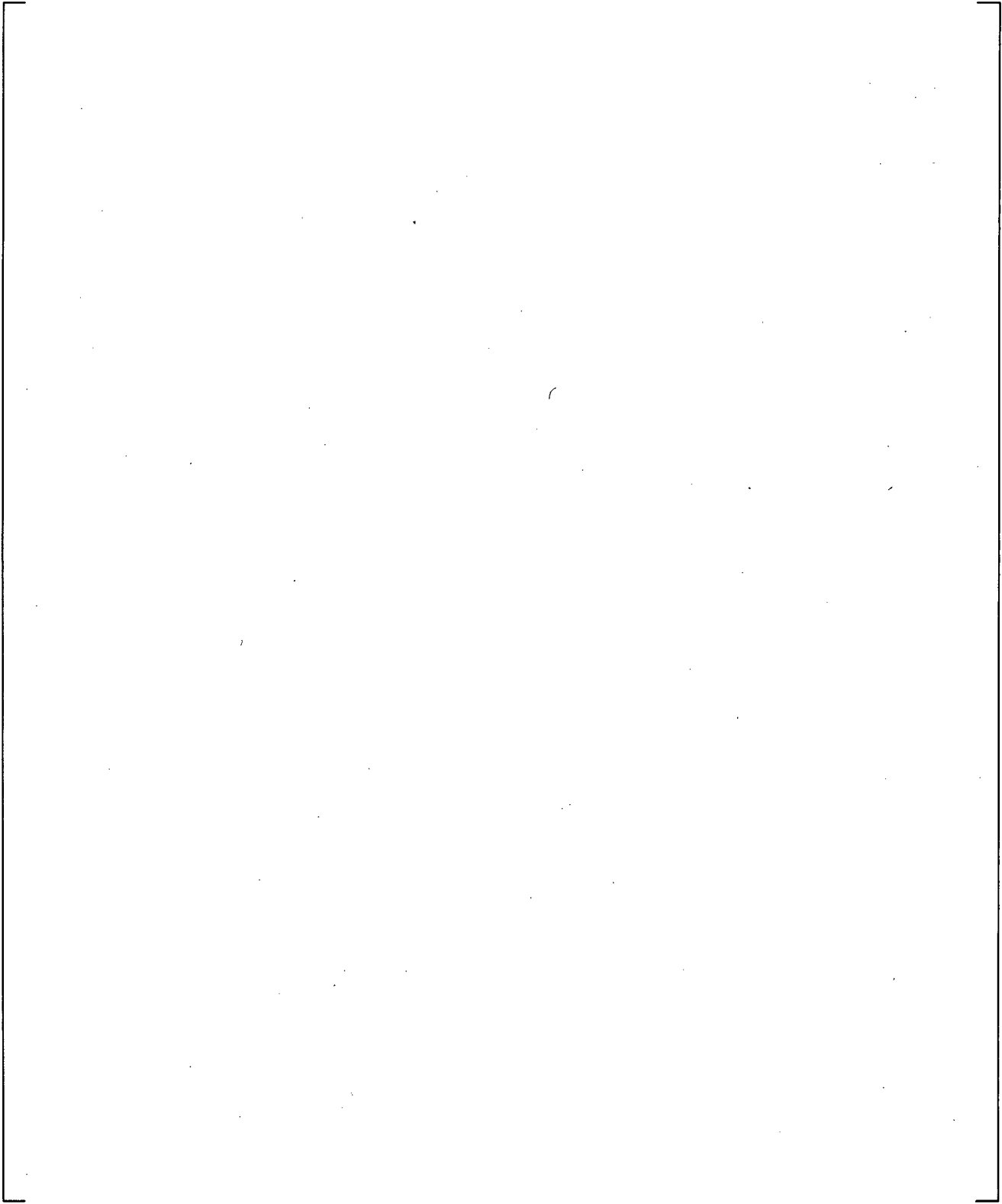


**Figure 21.11.3-7 Peak Cladding Temperatures**

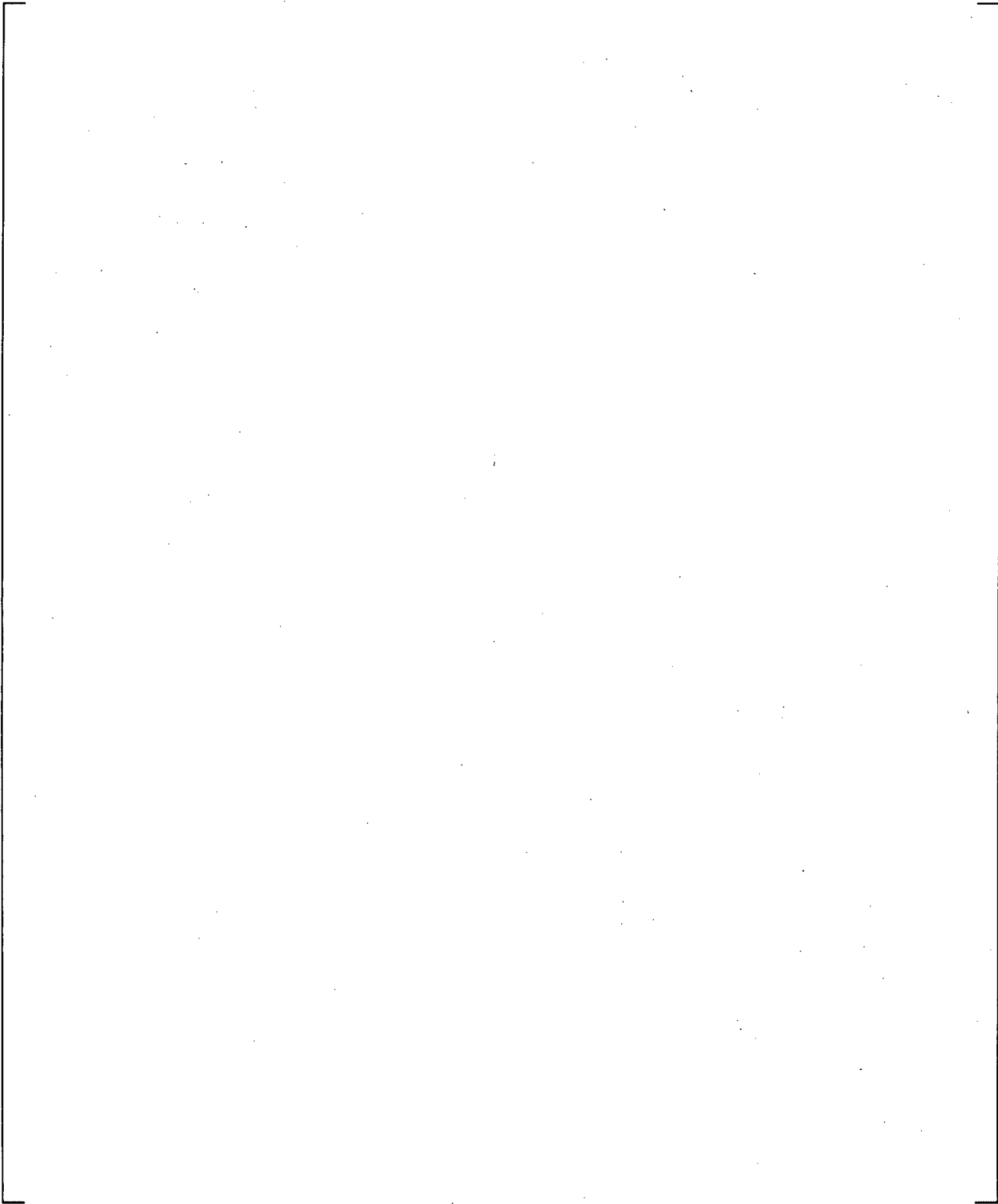


**Figure 21.12-1 Break Flows**

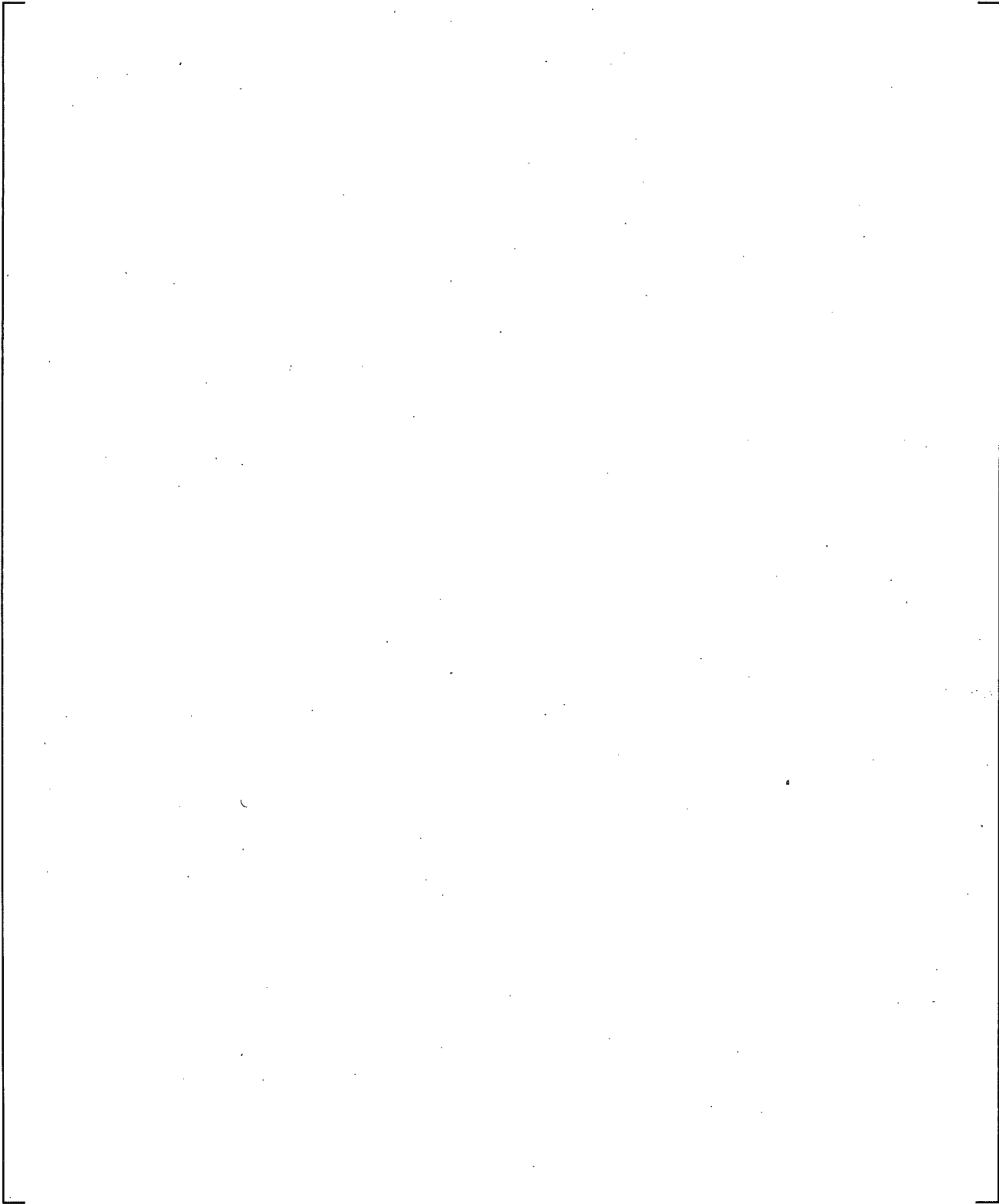


**Figure 21.12-2 Calculated Break Void Fraction**

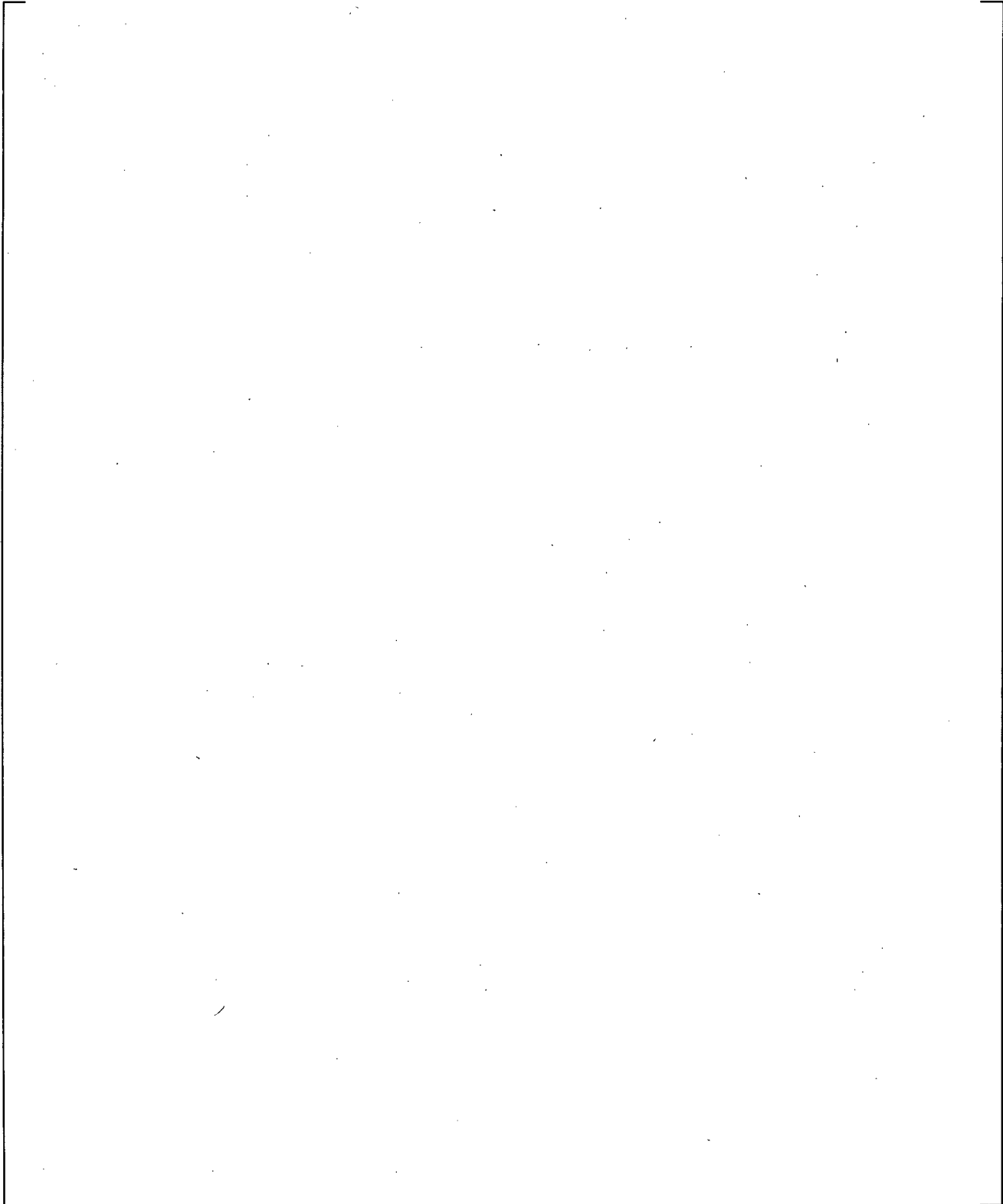


**Figure 21.12-3 Cross-Over Leg A Differential Pressures**

a,c

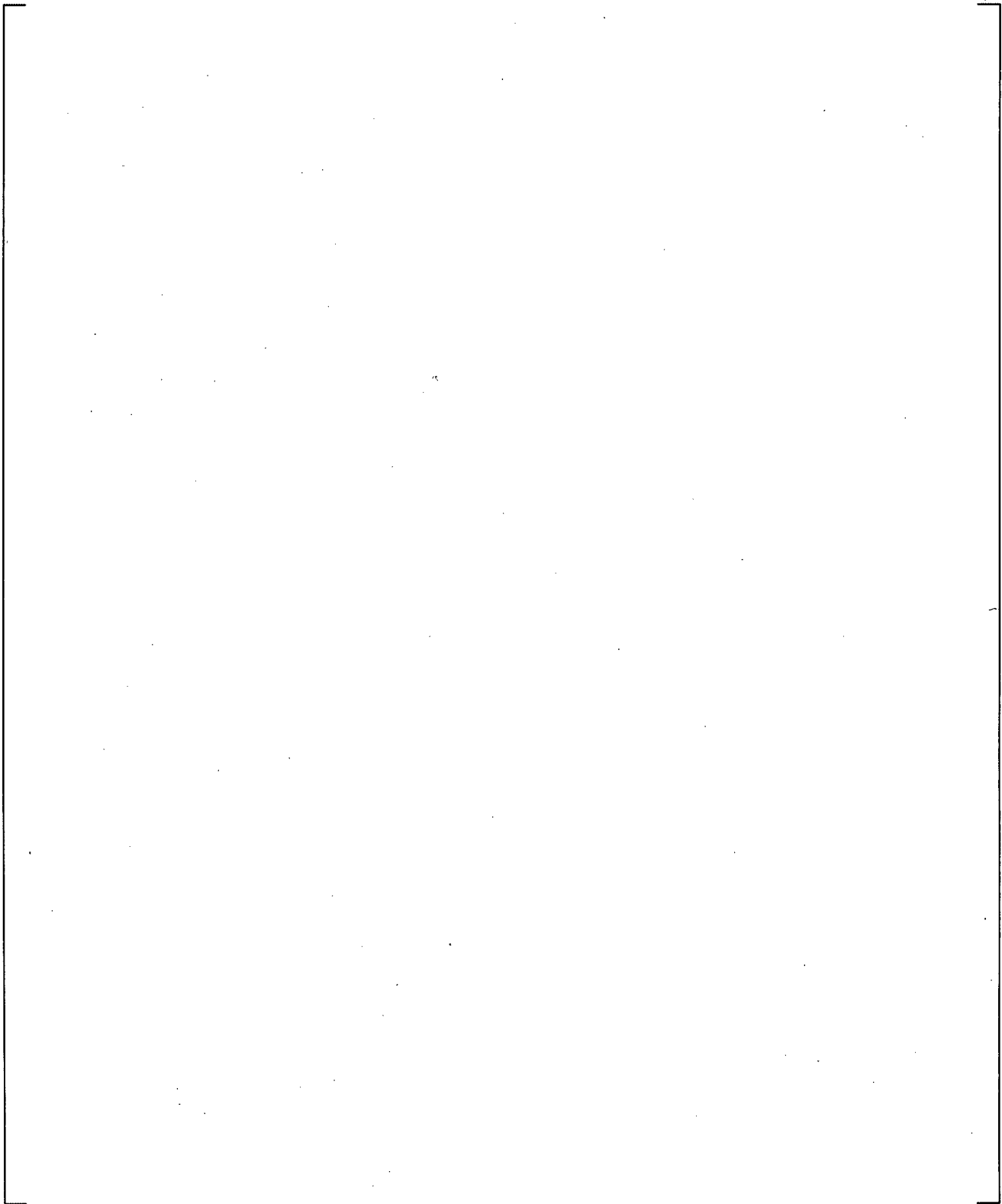


**Figure 21.12-4 Cross-Over Leg B Differential Pressures**

a,c

**Figure 21.12-5 Pressurizer Pressures**

a,c

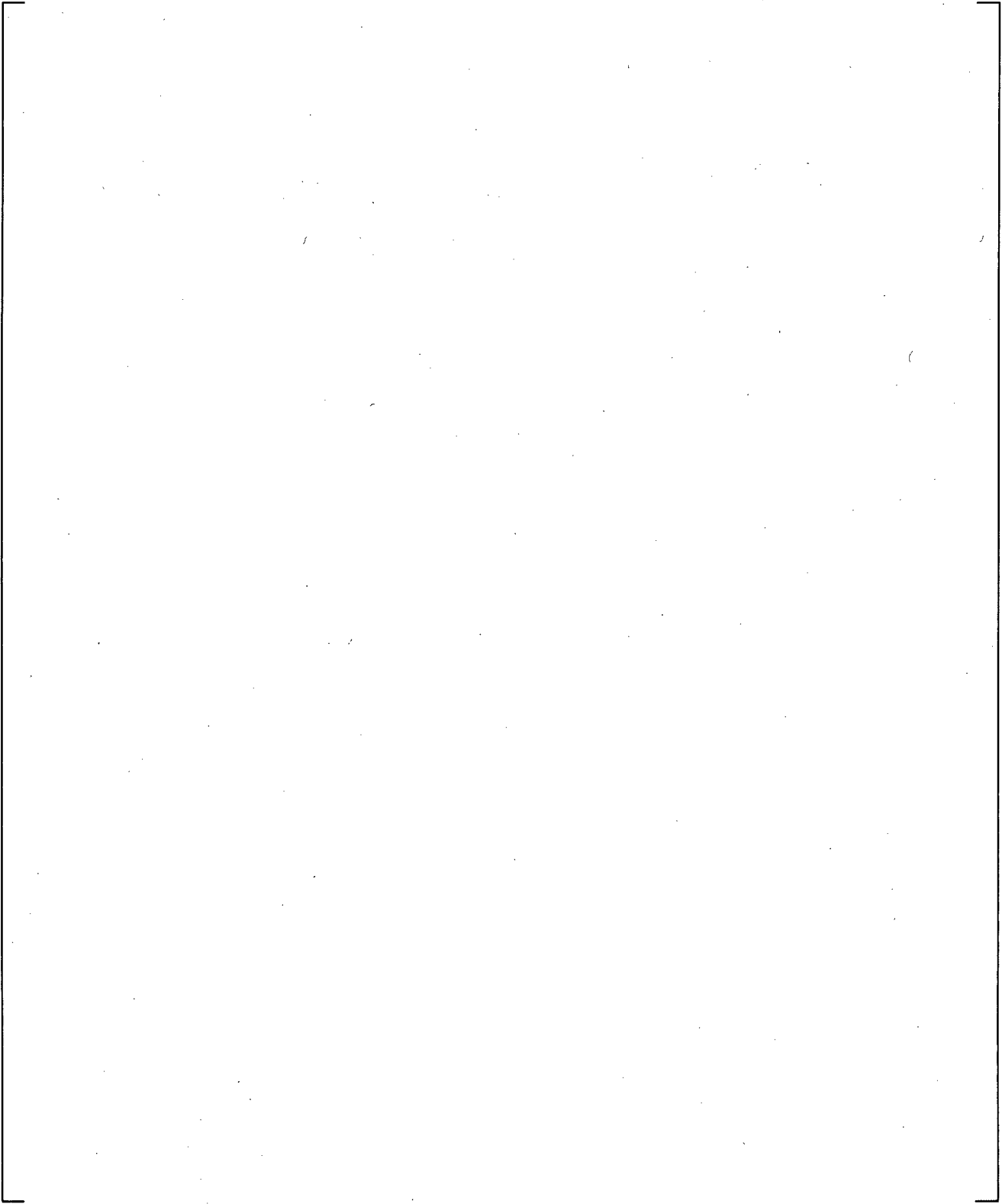


**Figure 21.12-6 SGA U-tubes Inlet-to-Top Differential Pressure**

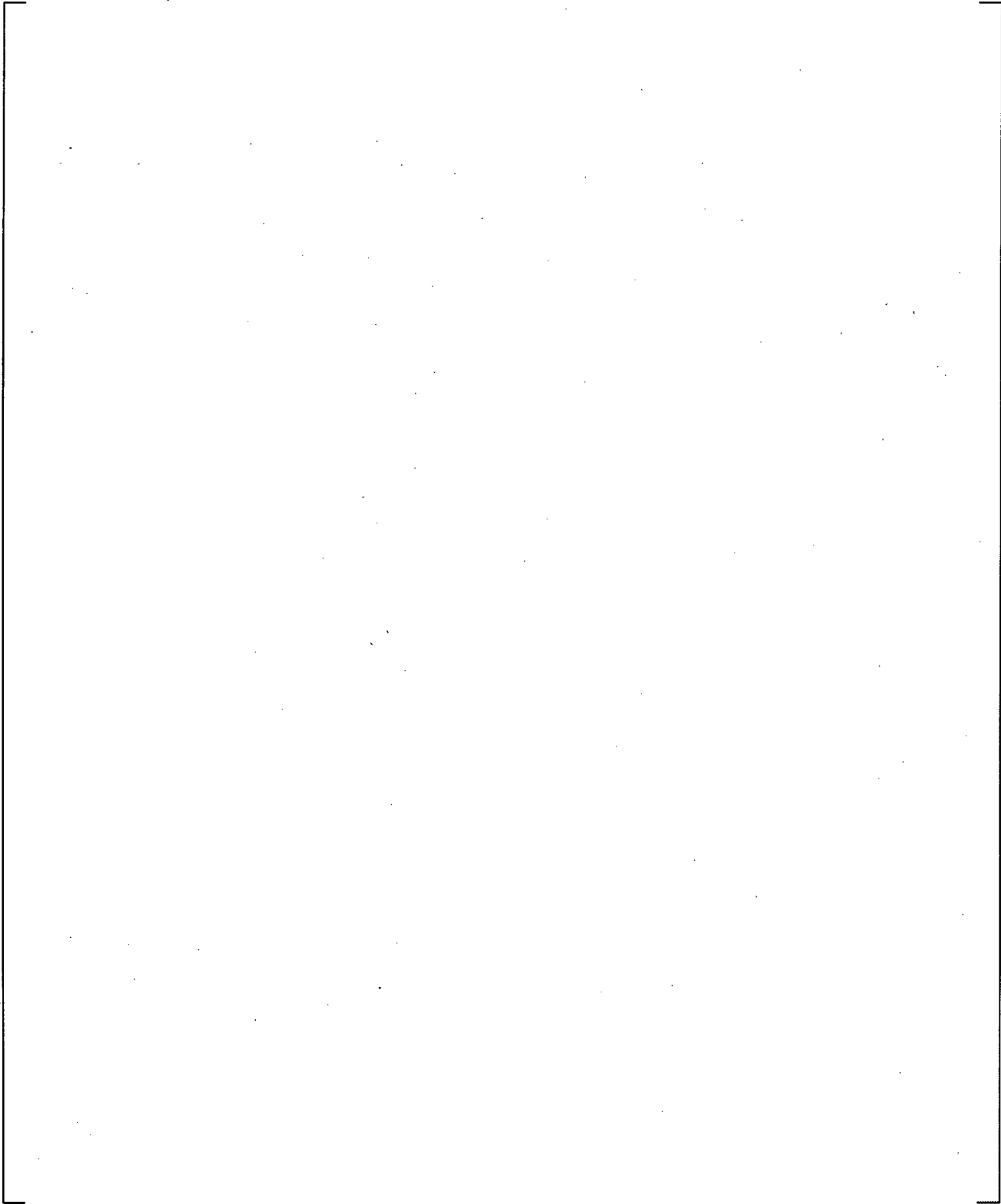


**Figure 21.12-7 SGB U-tubes Inlet-to-Top Differential Pressures**

a,c

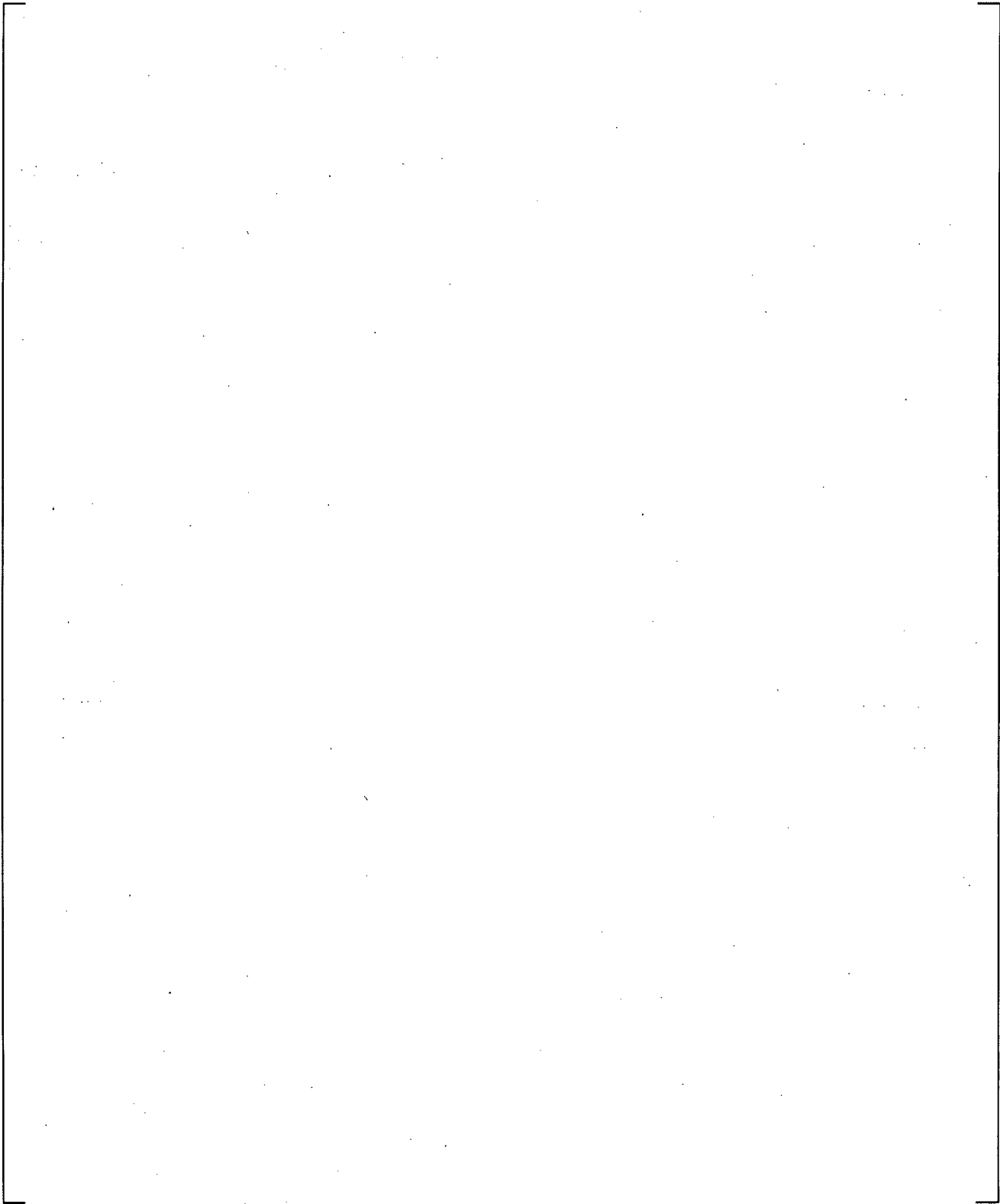


**Figure 21.12-8 SGA U-tubes Outlet-to-Top Differential Pressures**

a,c

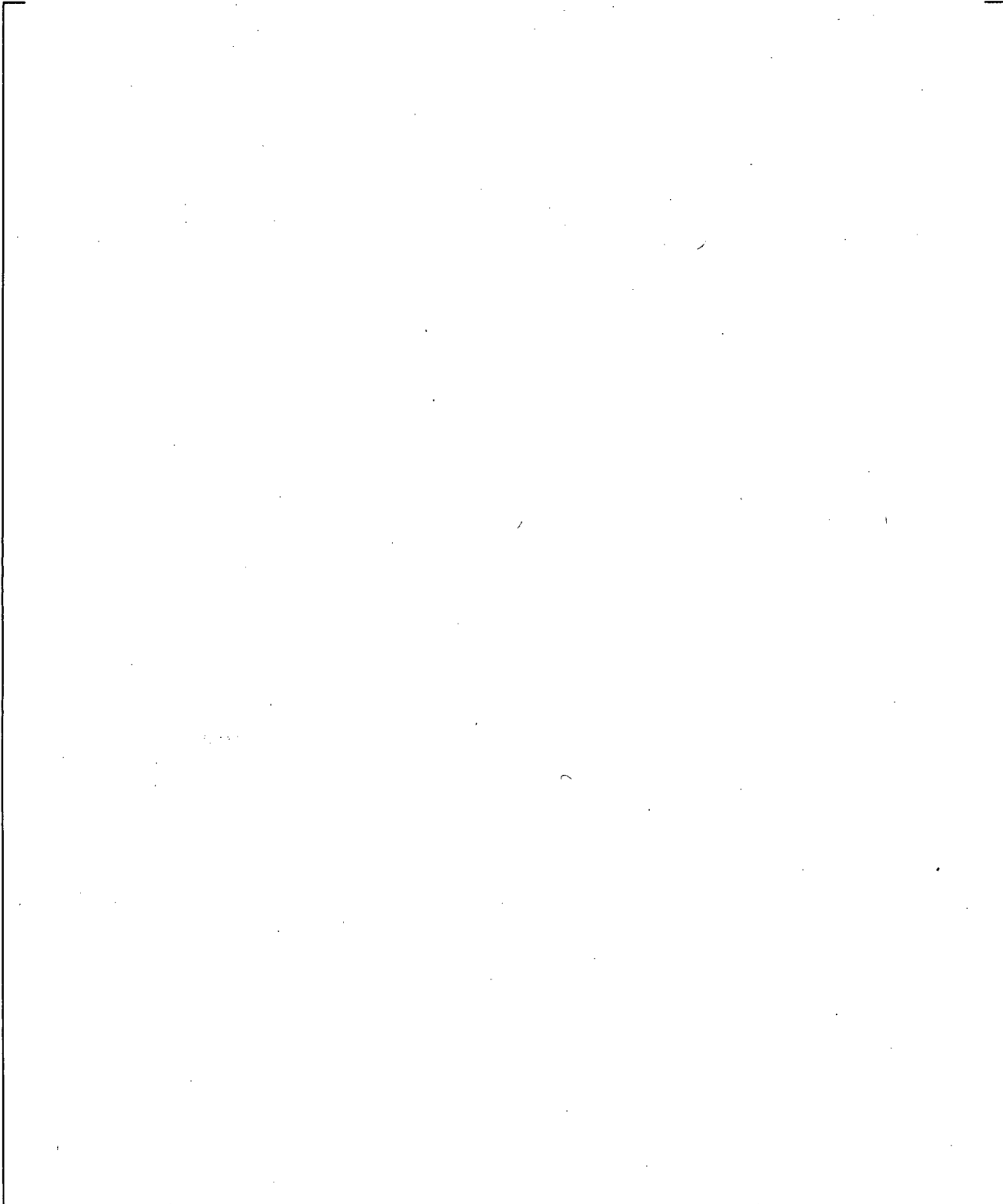


**Figure 21.12-9 SGB U-tube Outlet-to-Top Differential Pressures**

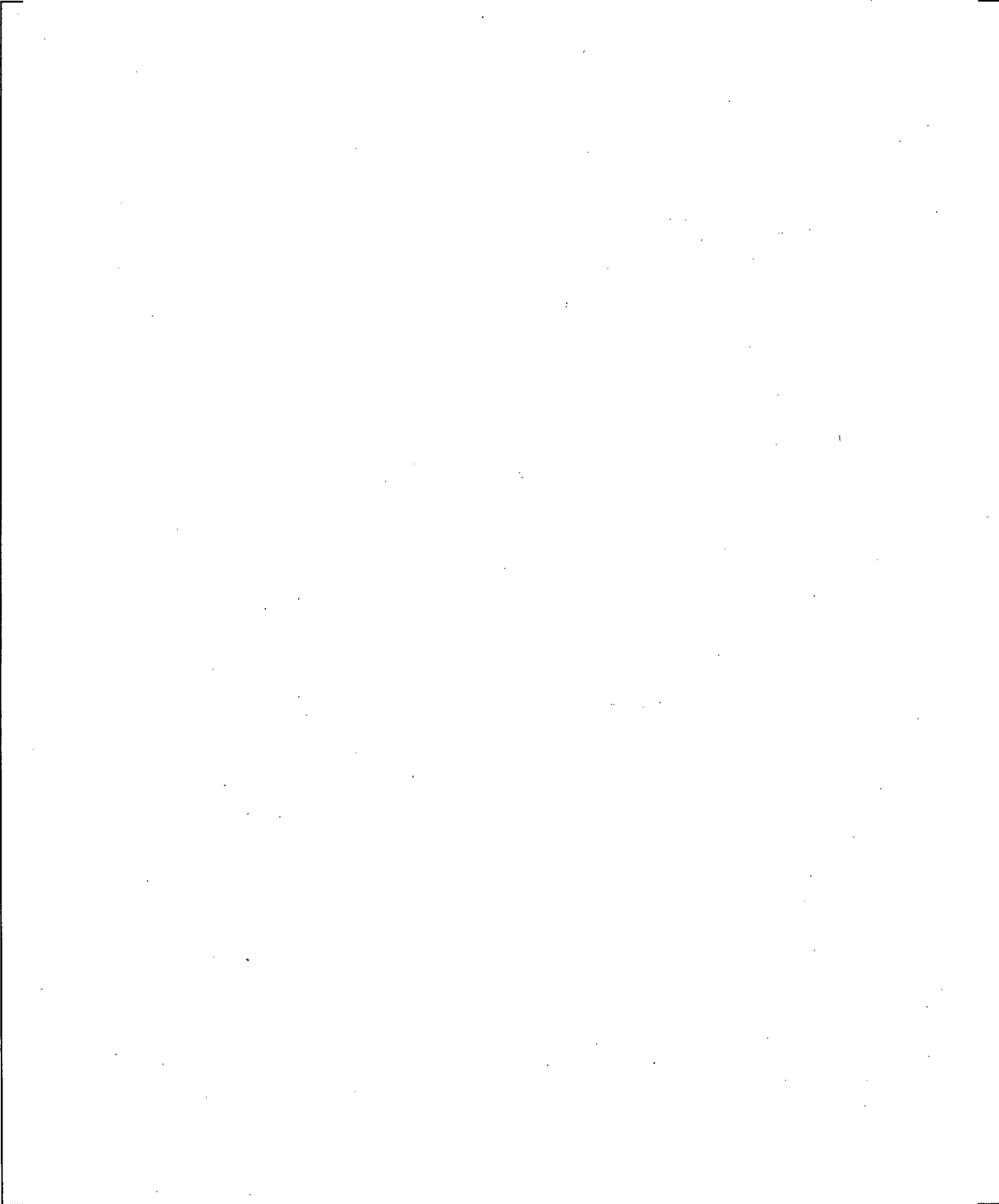


**Figure 21.12-10 SGA Inlet Plenum Collapsed Liquid Levels**

a,c

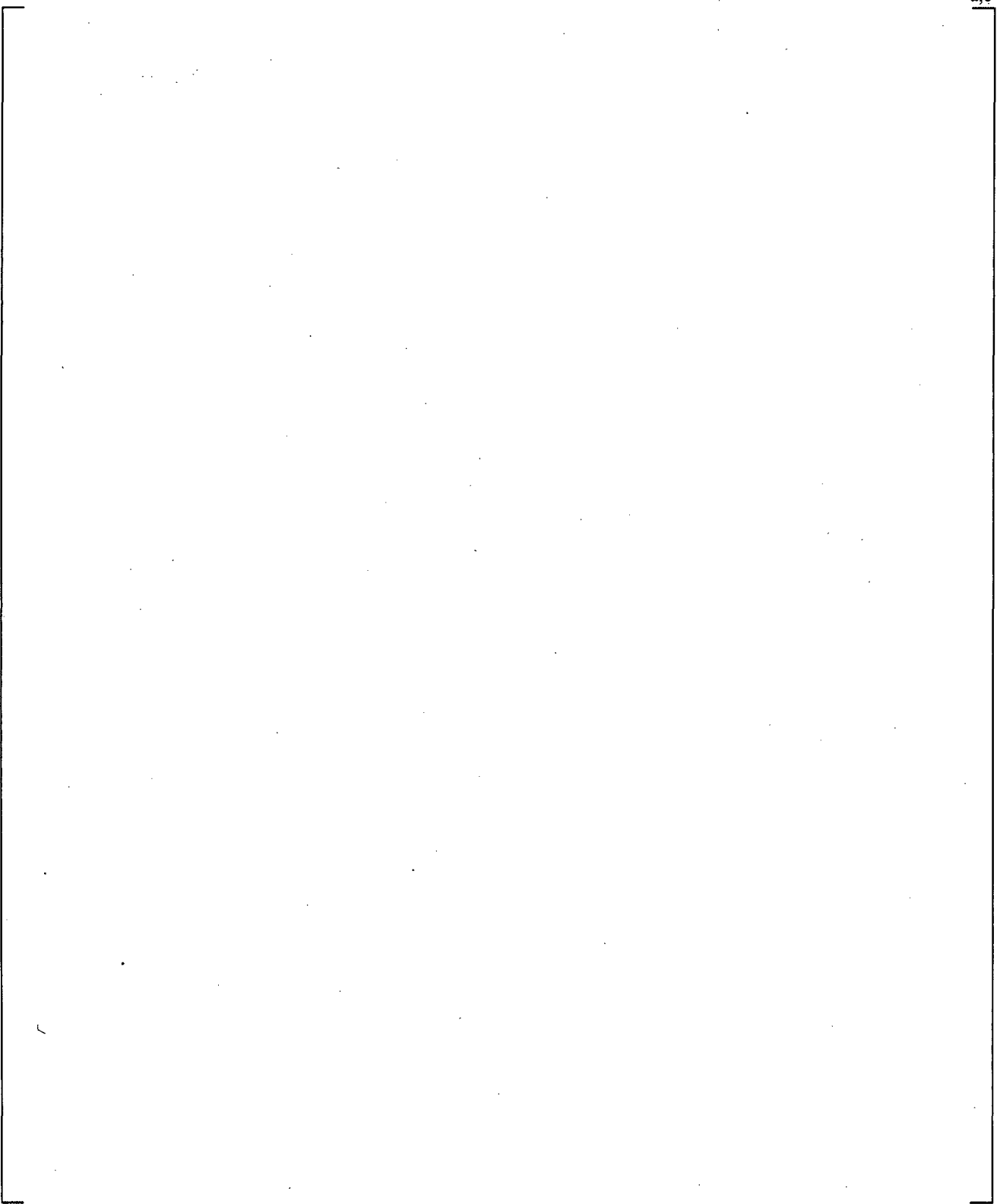


**Figure 21.12-11 SGB Inlet Plenum Collapsed Liquid Levels**

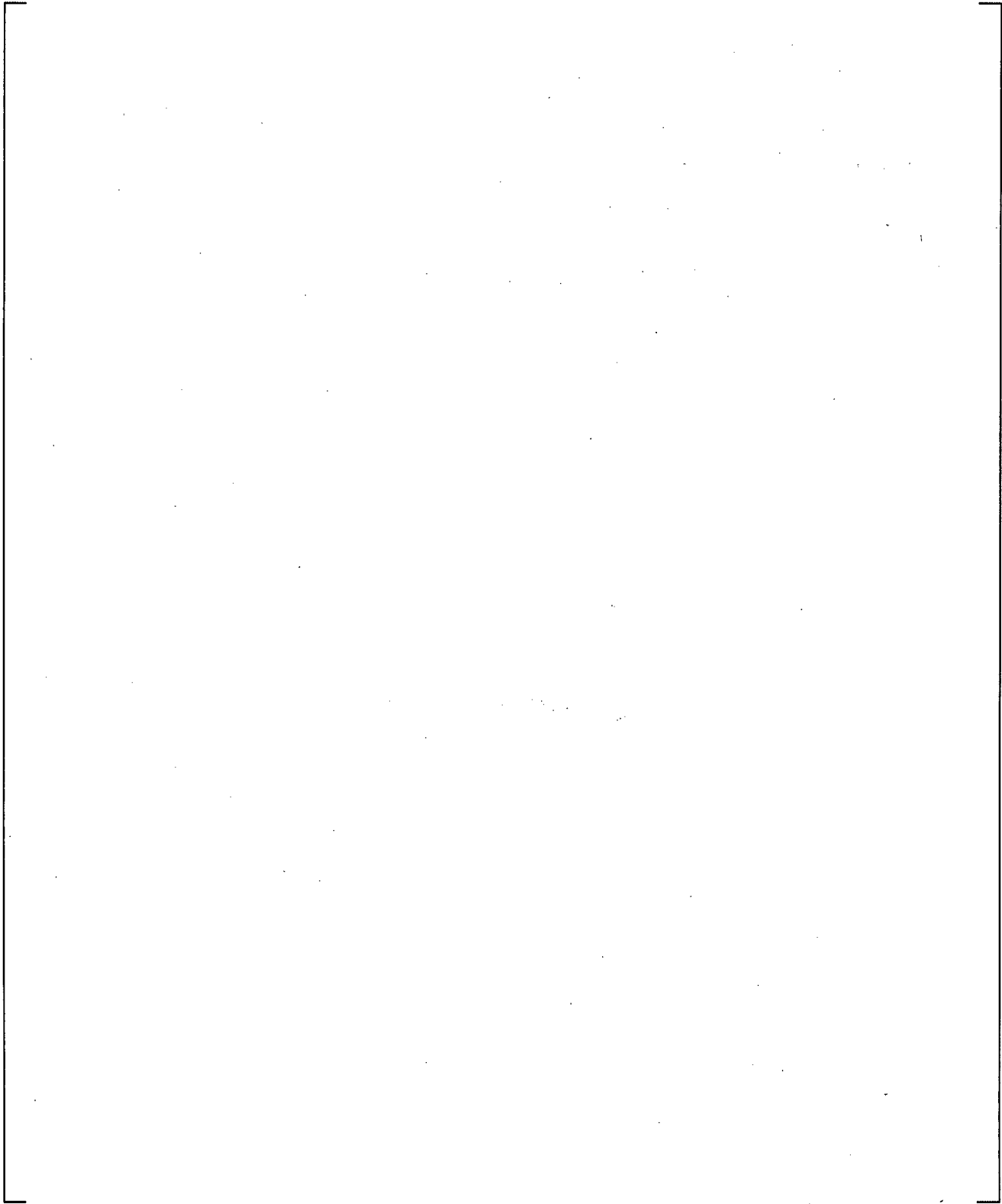


**Figure 21.12-12 Upper Plenum to SGA Inlet Differential Pressures**

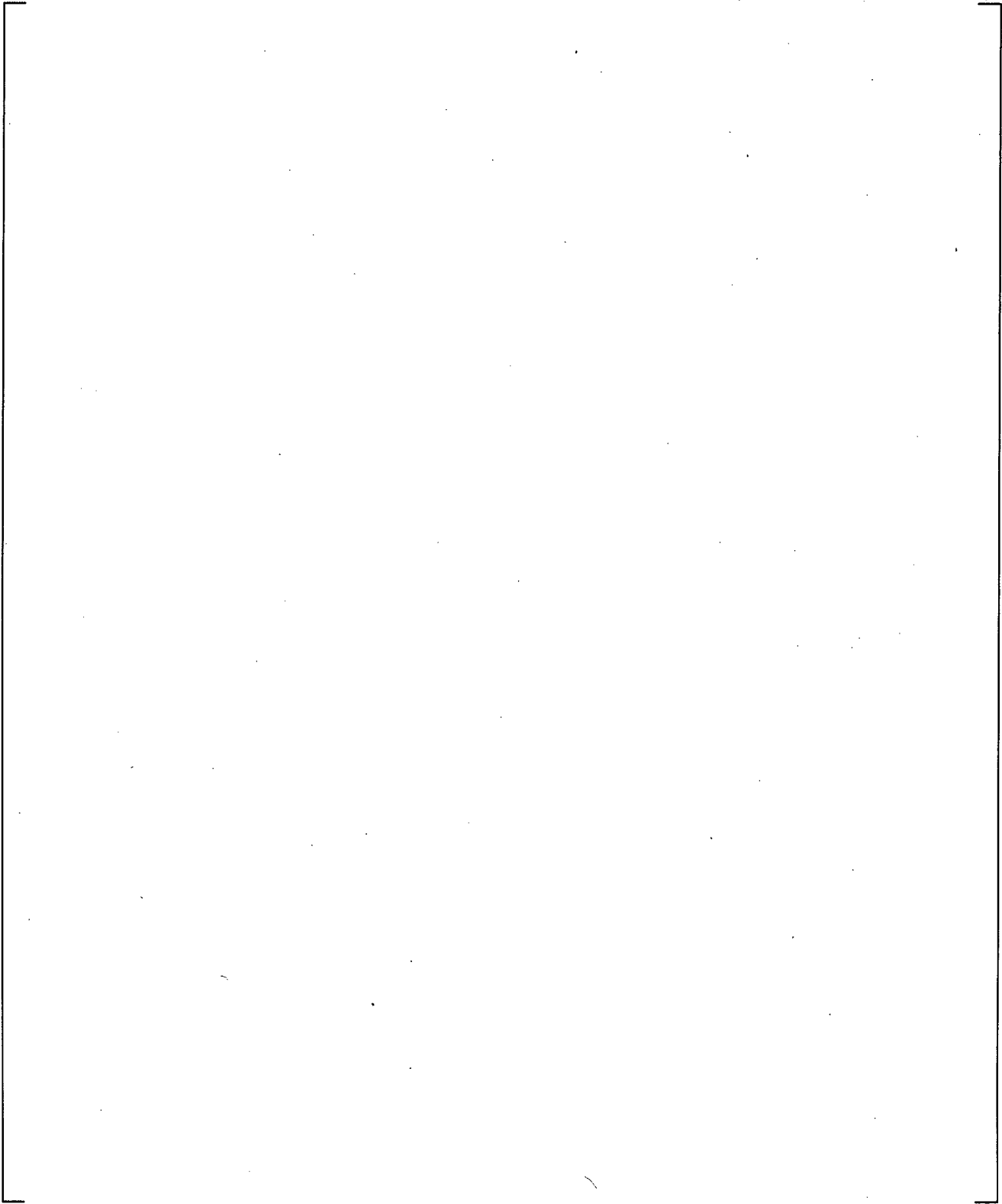


**Figure 21.12-13 Upper Plenum to SGB Inlet Differential Pressures**

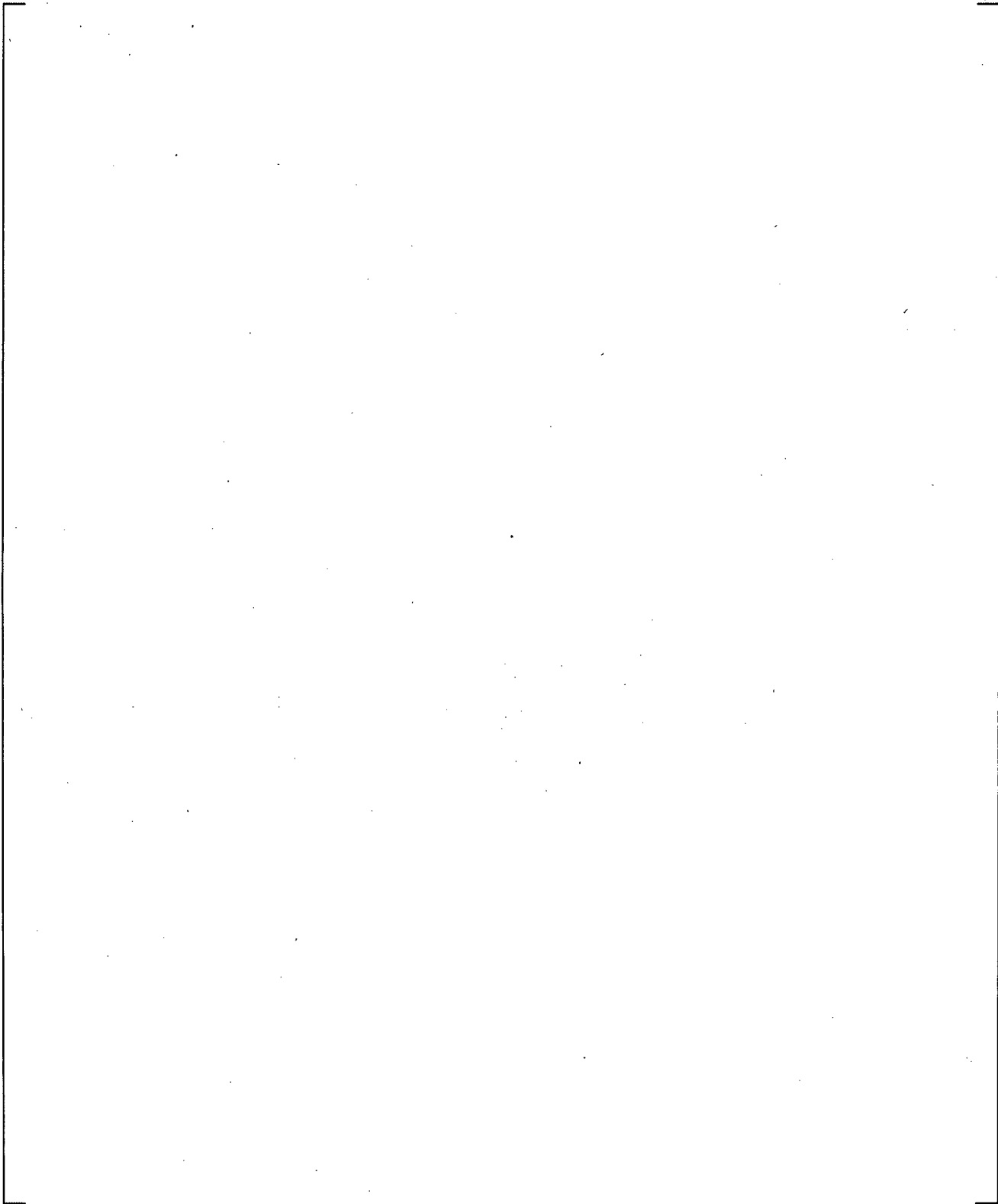


**Figure 21.12-14 Downcomer Differential Pressures**

a,c

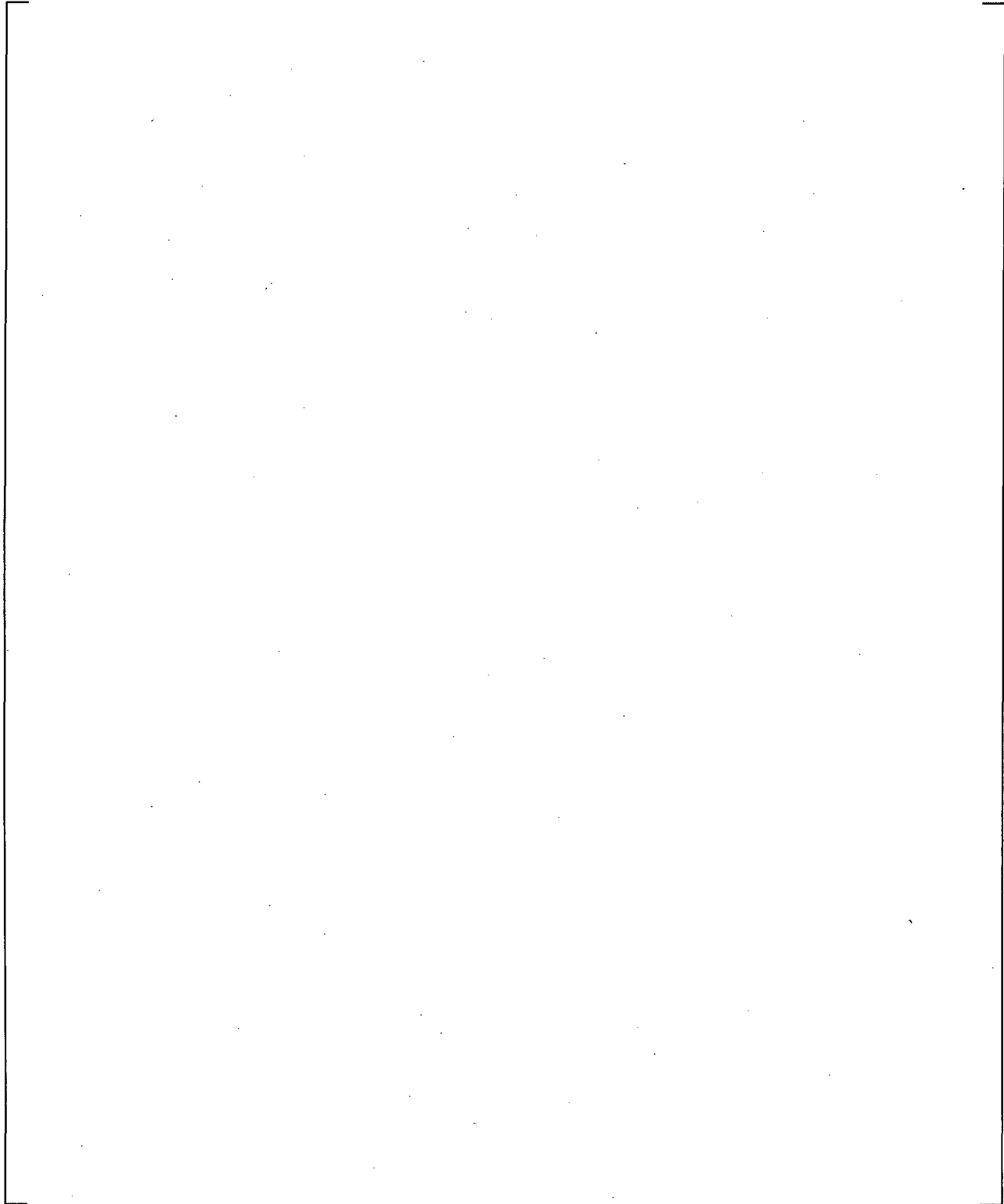


**Figure 21.12-15 Upper Plenum Differential Pressures**

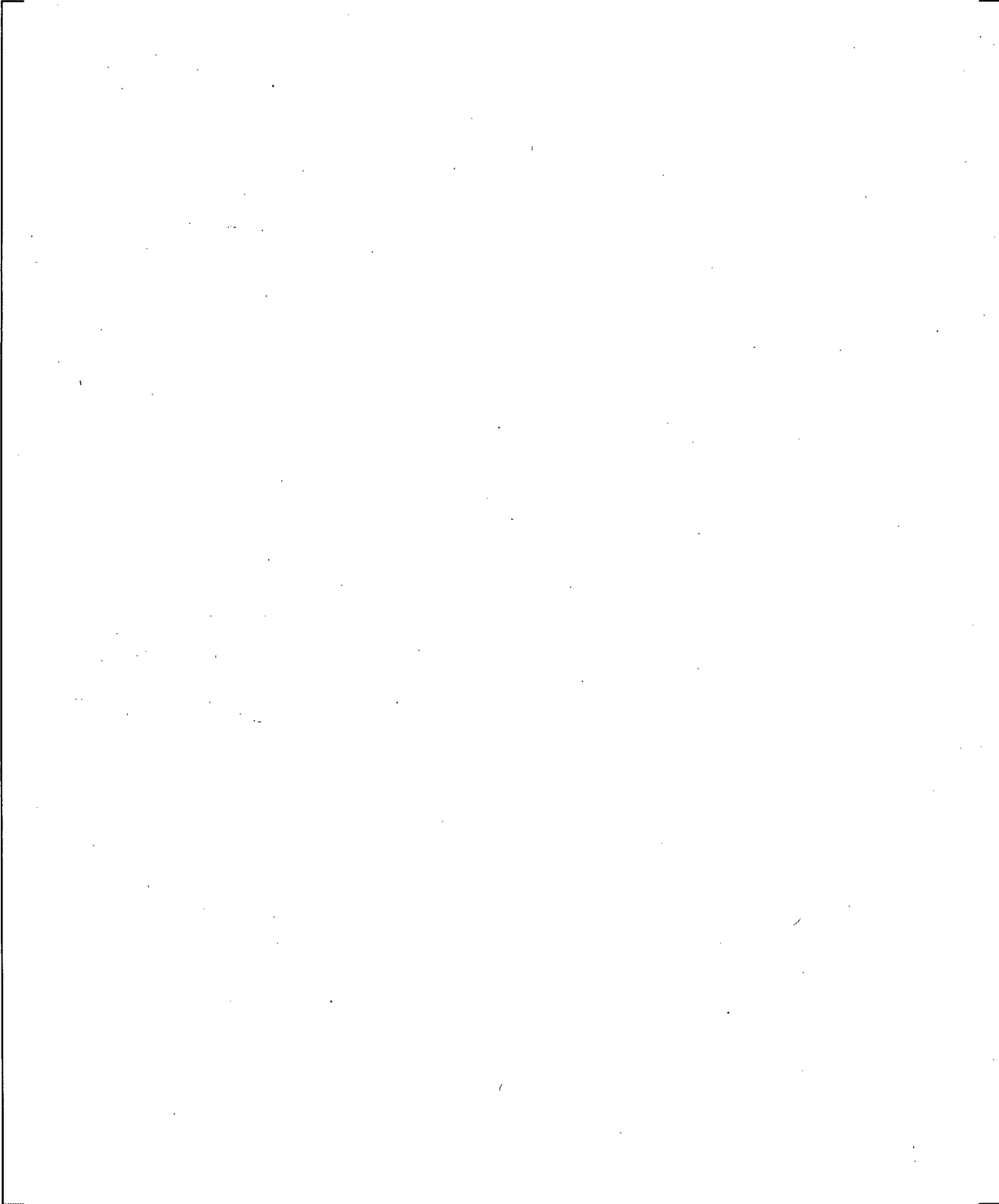


**Figure 21.12-16 Inner Vessel (LP+Core+UP) Differential Pressures**

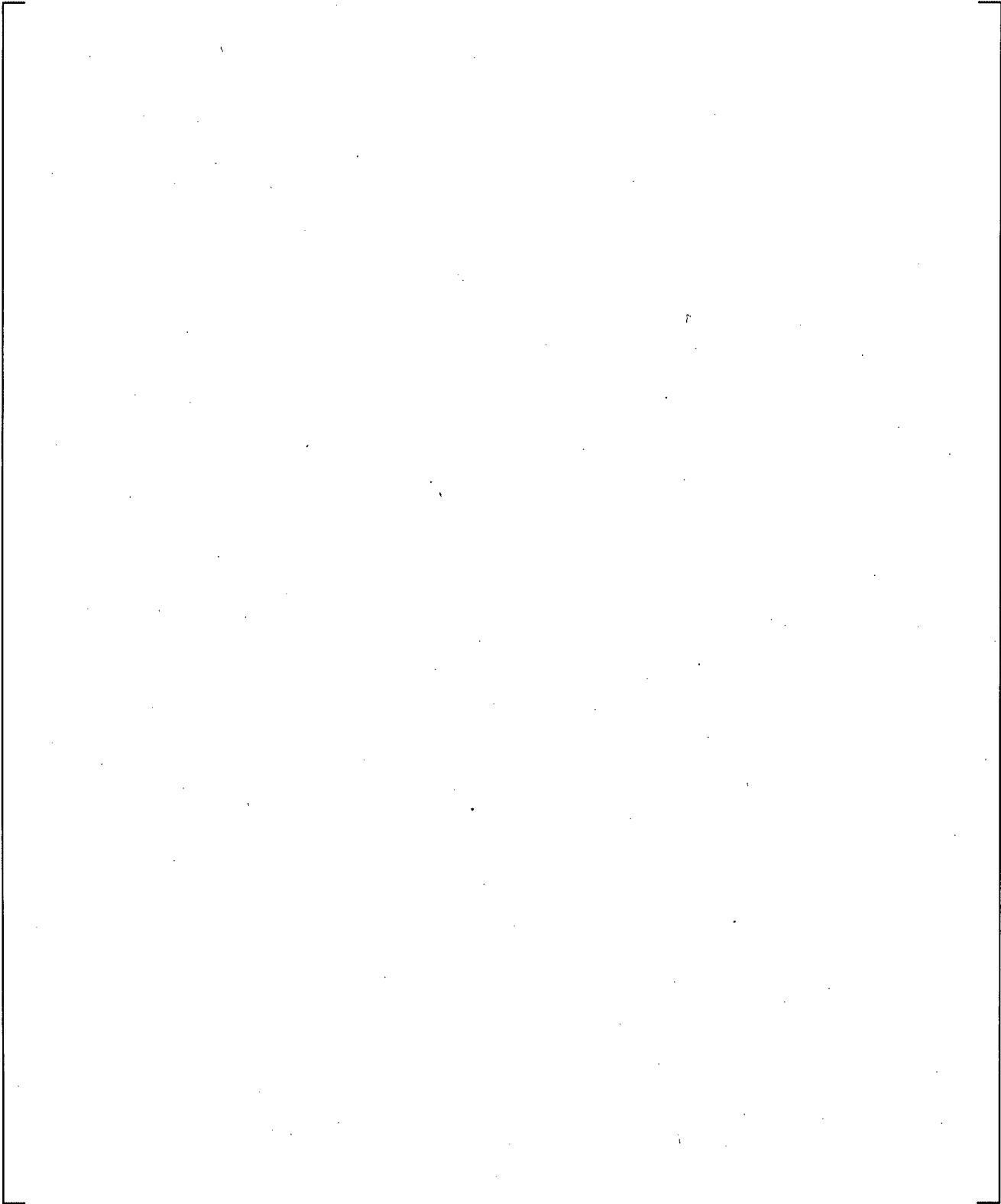


**Figure 21.12-17 Lower Plenum Differential Pressures**

a,c

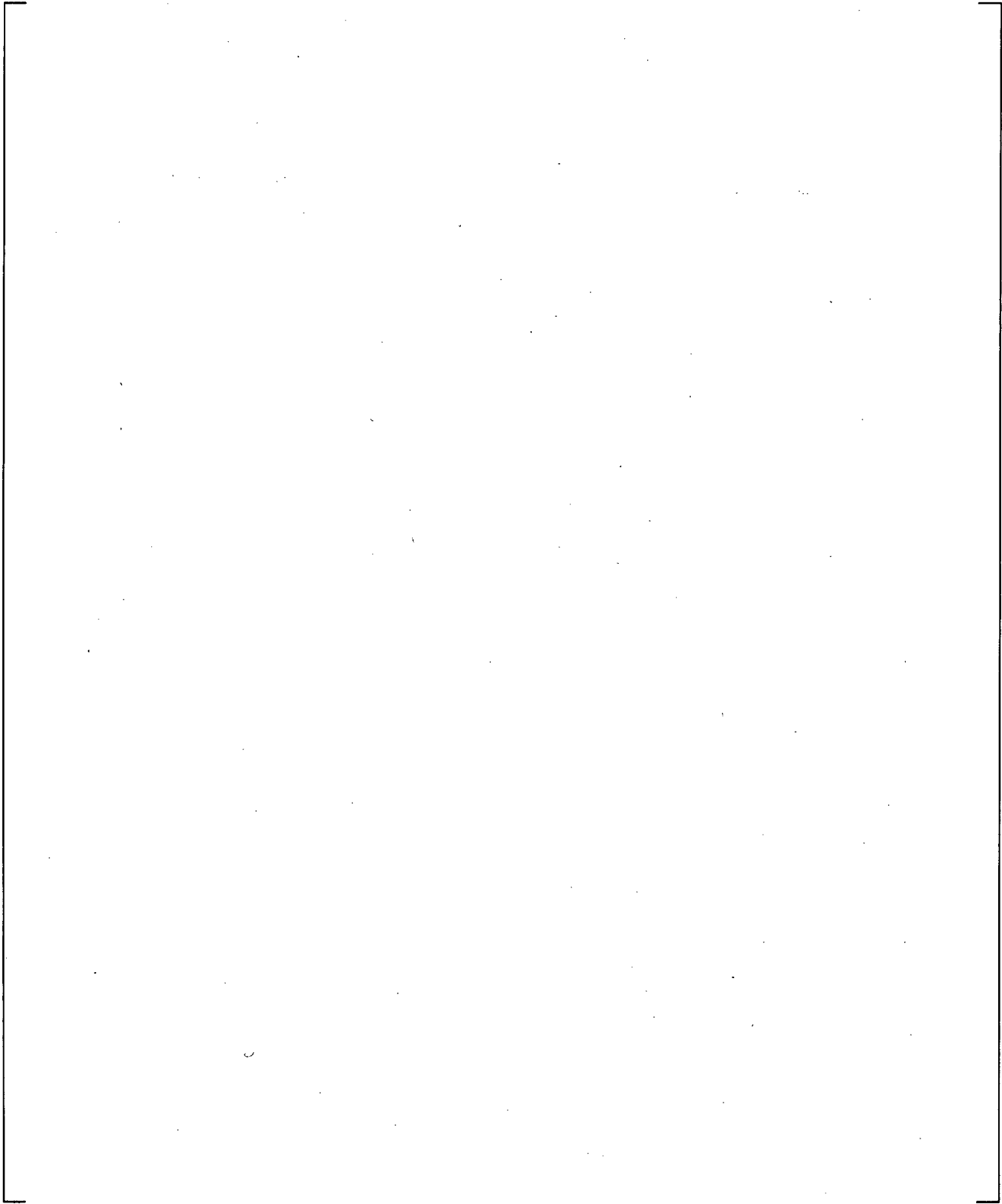


**Figure 21.12-18 Peak Cladding Temperatures**

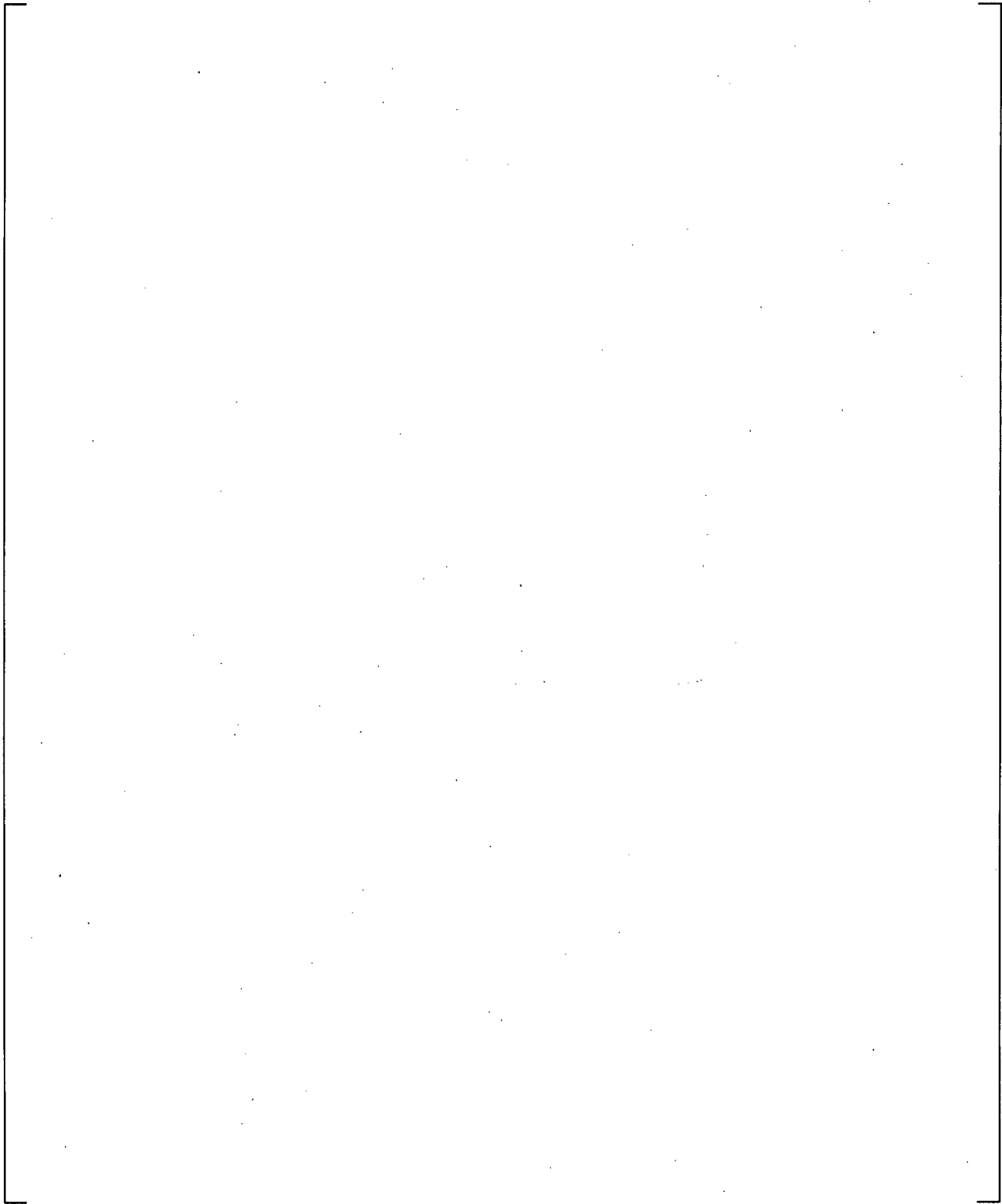


**Figure 21.12-19 Accumulator A Injection Flows**

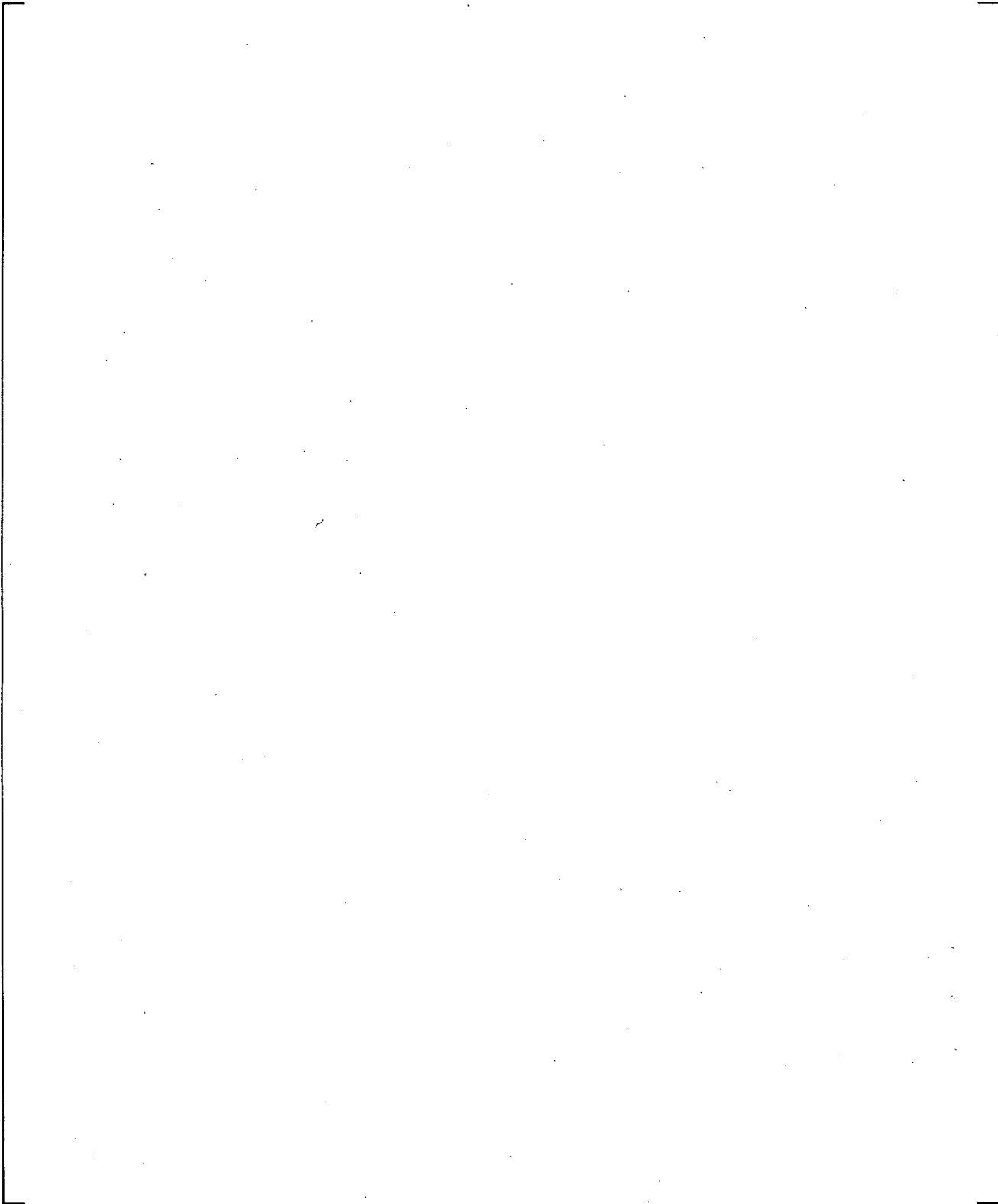


**Figure 21.13-1 Break Flows**

a,c

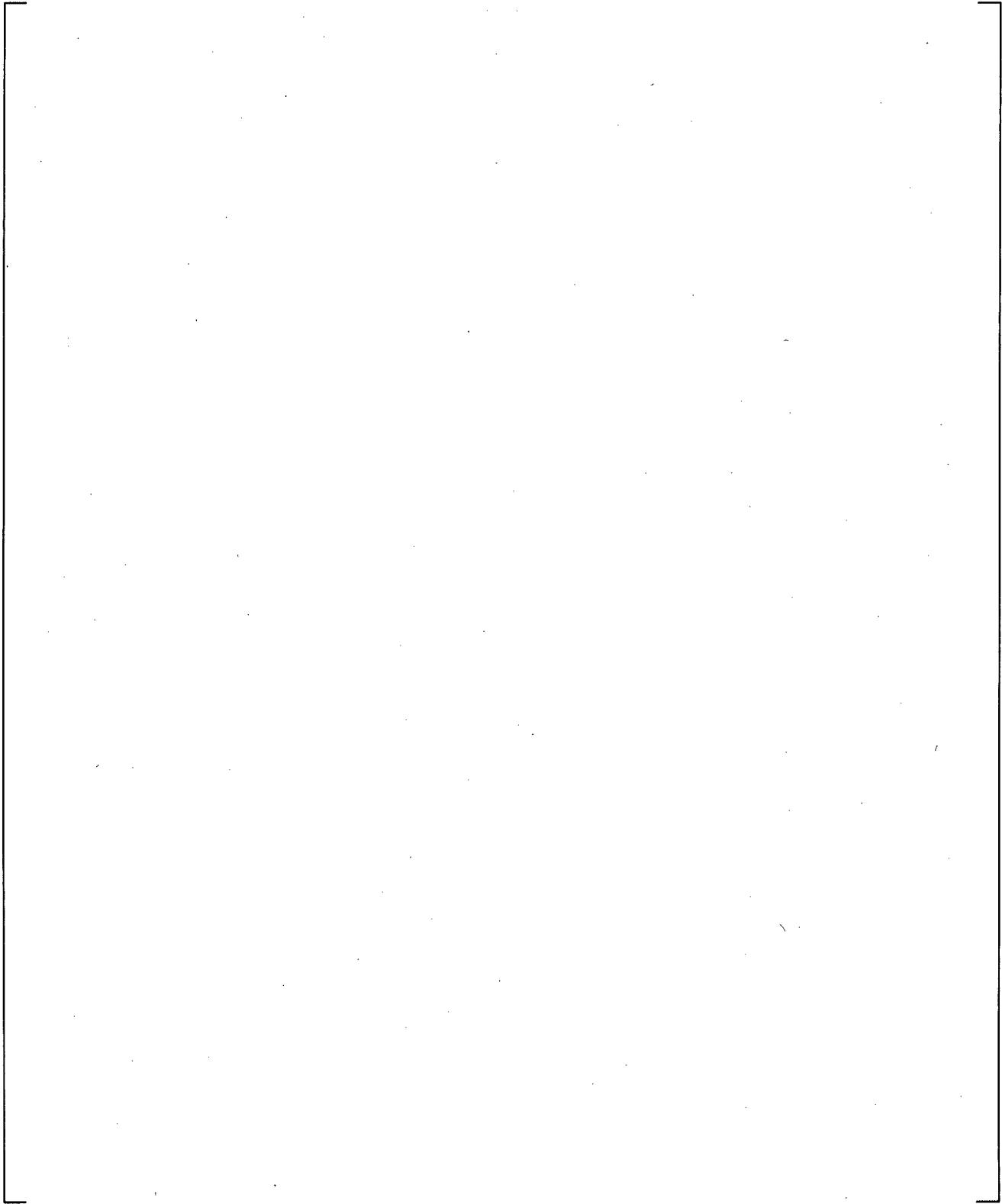


**Figure 21.13-2 Calculated Break Void Fraction**

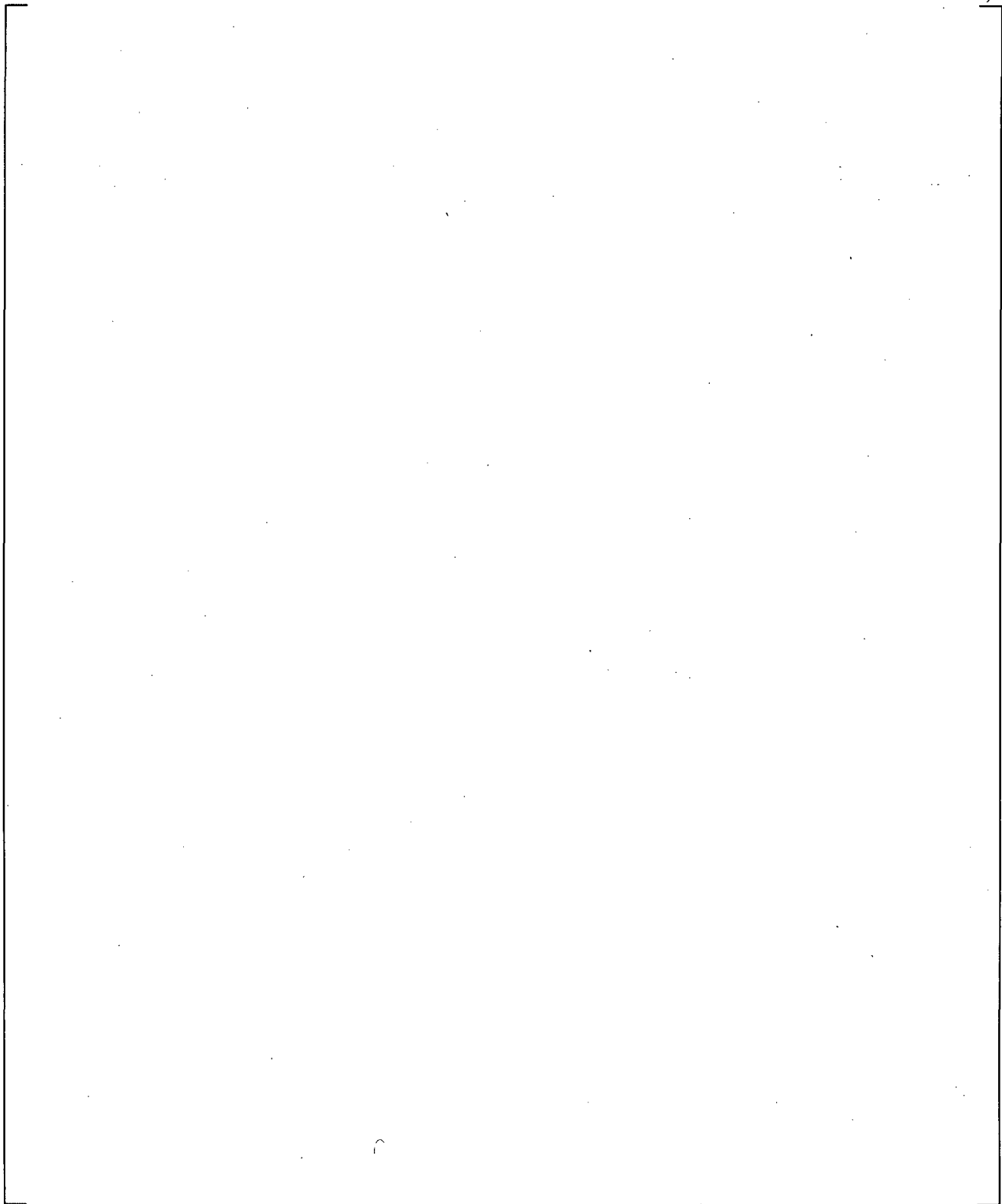


**Figure 21.13-3 Cross-Over Leg A Differential Pressures**

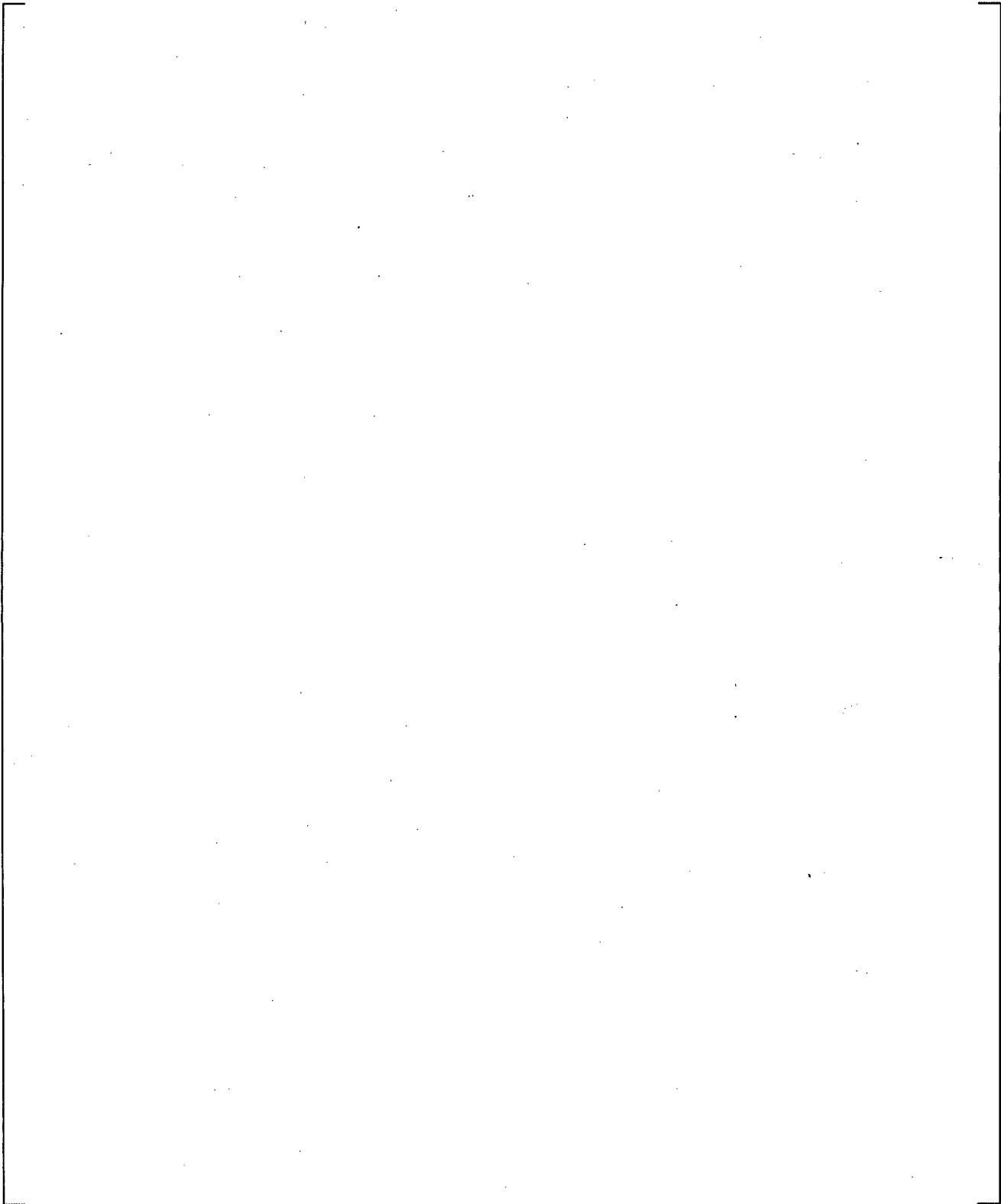


**Figure 21.13-4 Cross-Over Leg B Differential Pressures**

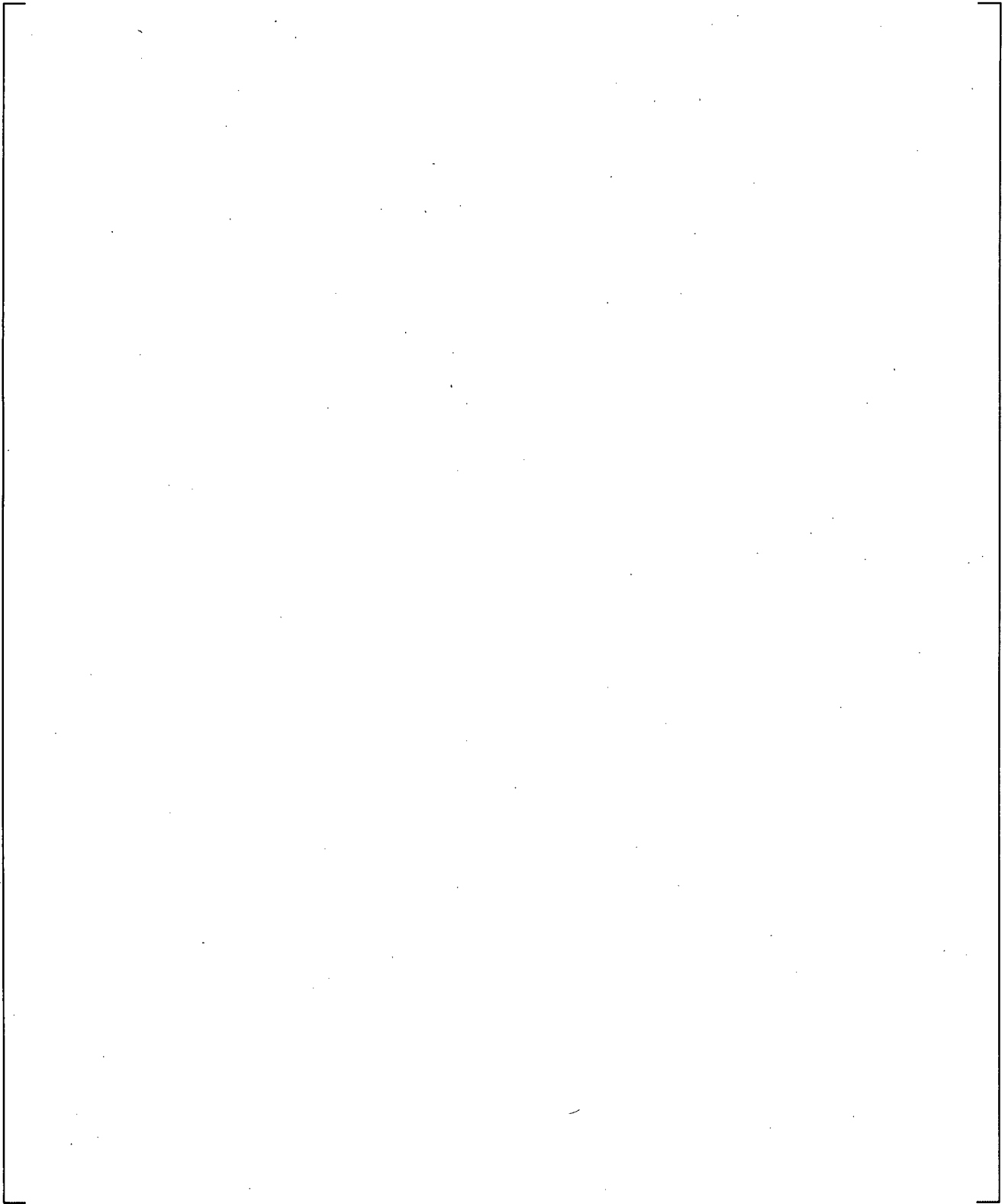


**Figure 21.13-5 Pressurizer Pressures**

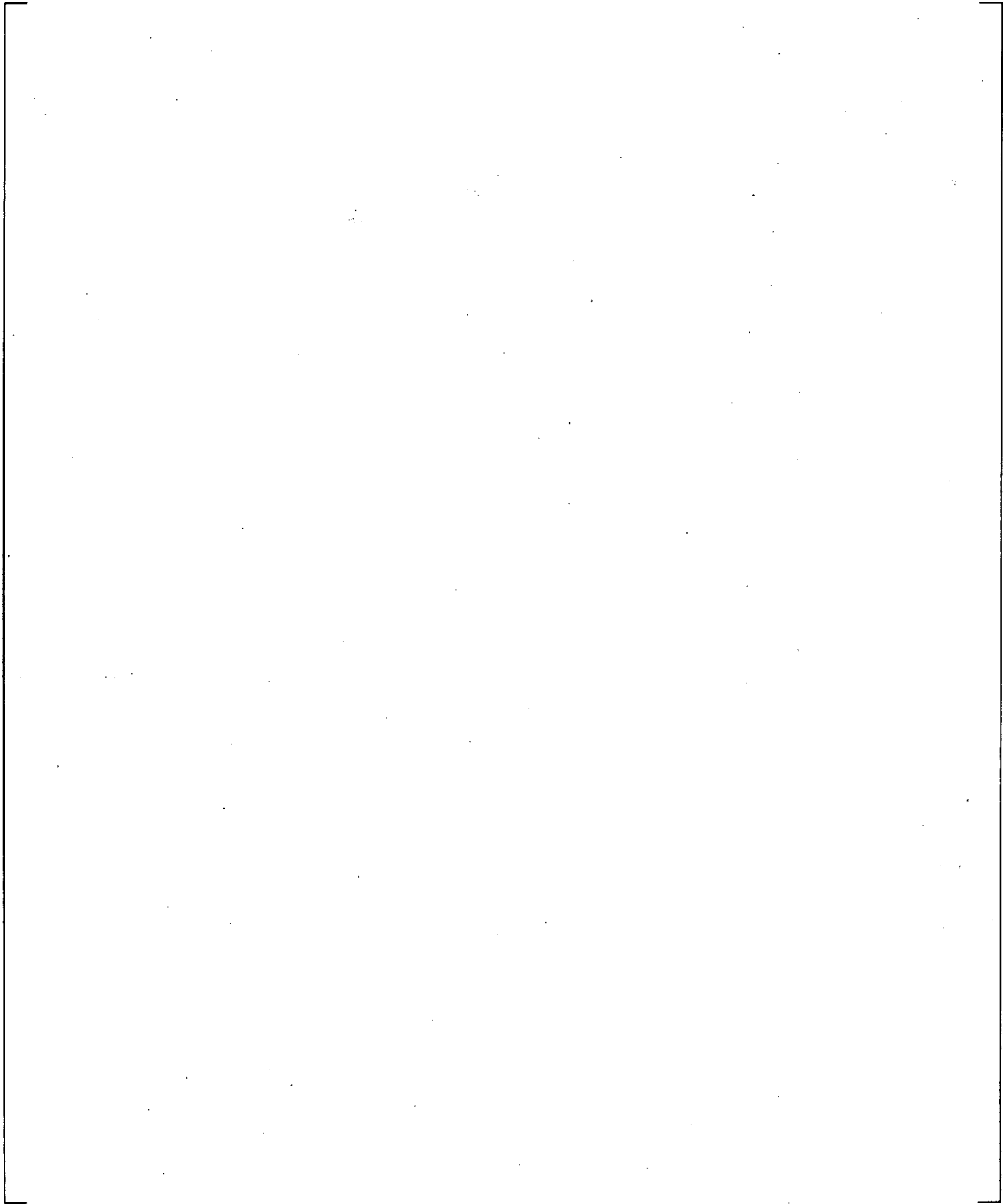


**Figure 21.13-6 SGA U-tubes Inlet-to-Top Differential Pressure**

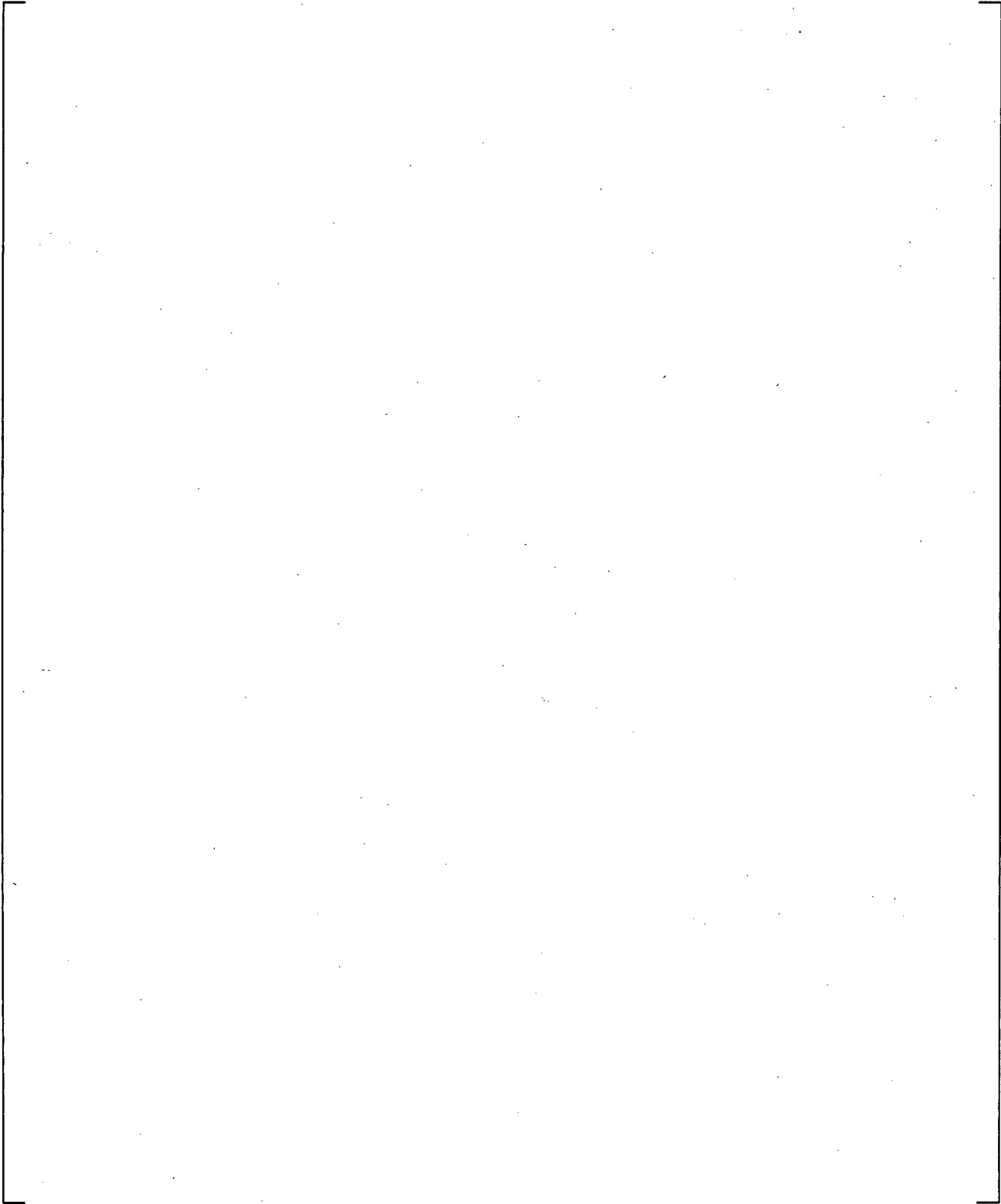


**Figure 21.13-7 SGB U-tubes Inlet-to-Top Differential Pressures**

a,c

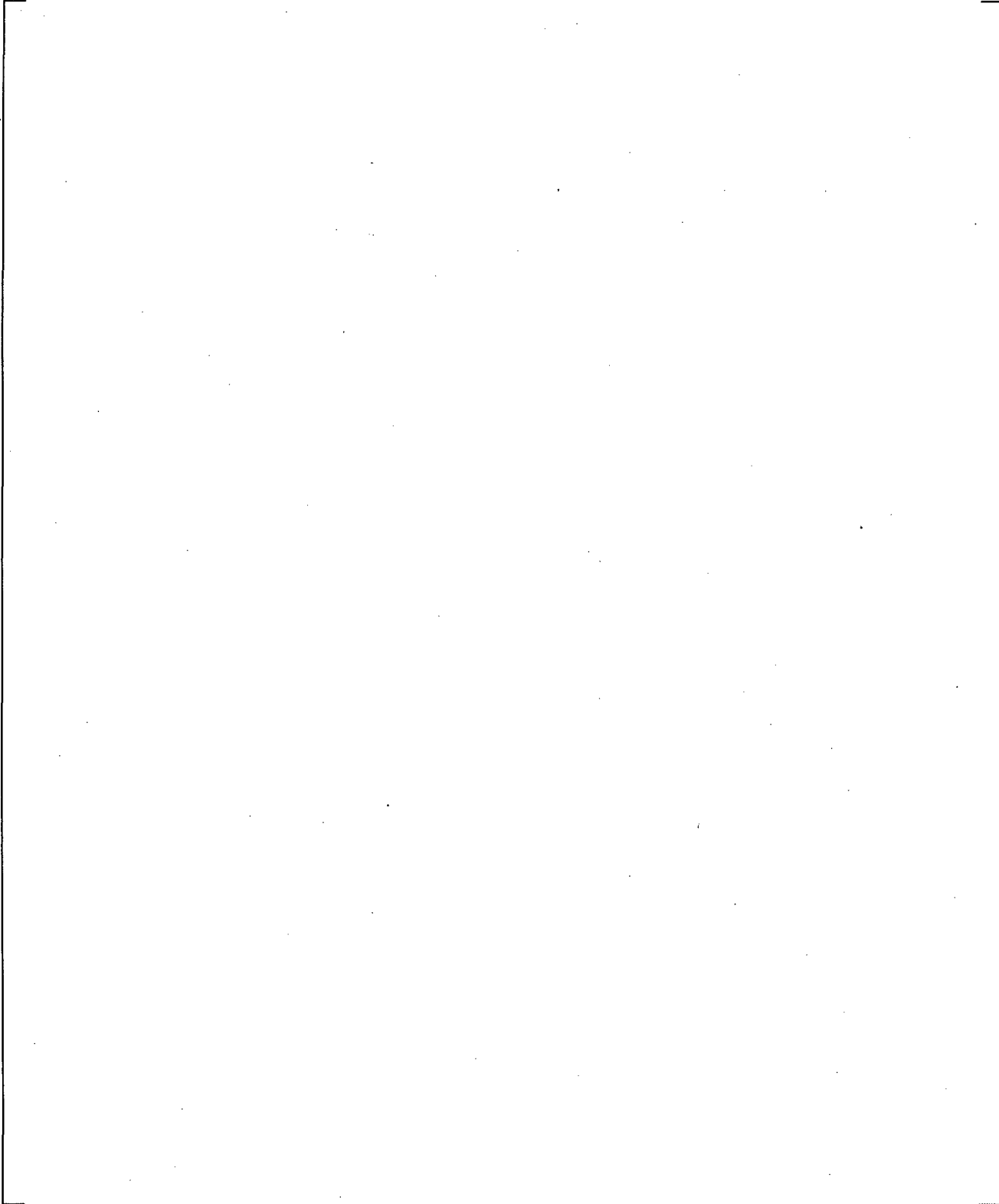


**Figure 21.13-8 SGA U-tubes Outlet-to-Top Differential Pressures**

a,c

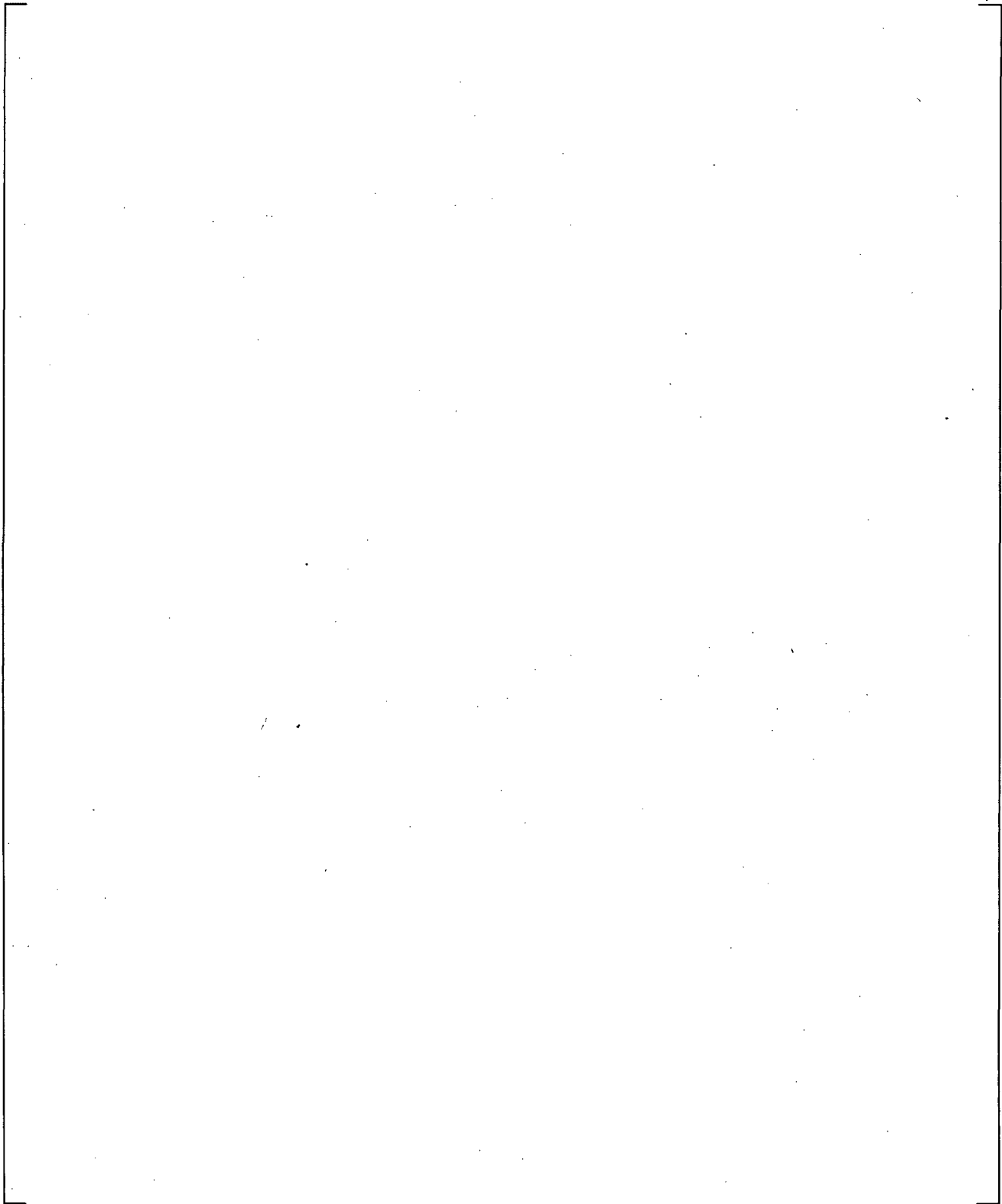


**Figure 21.13-9 SGB U-tube Outlet-to-Top Differential Pressures**

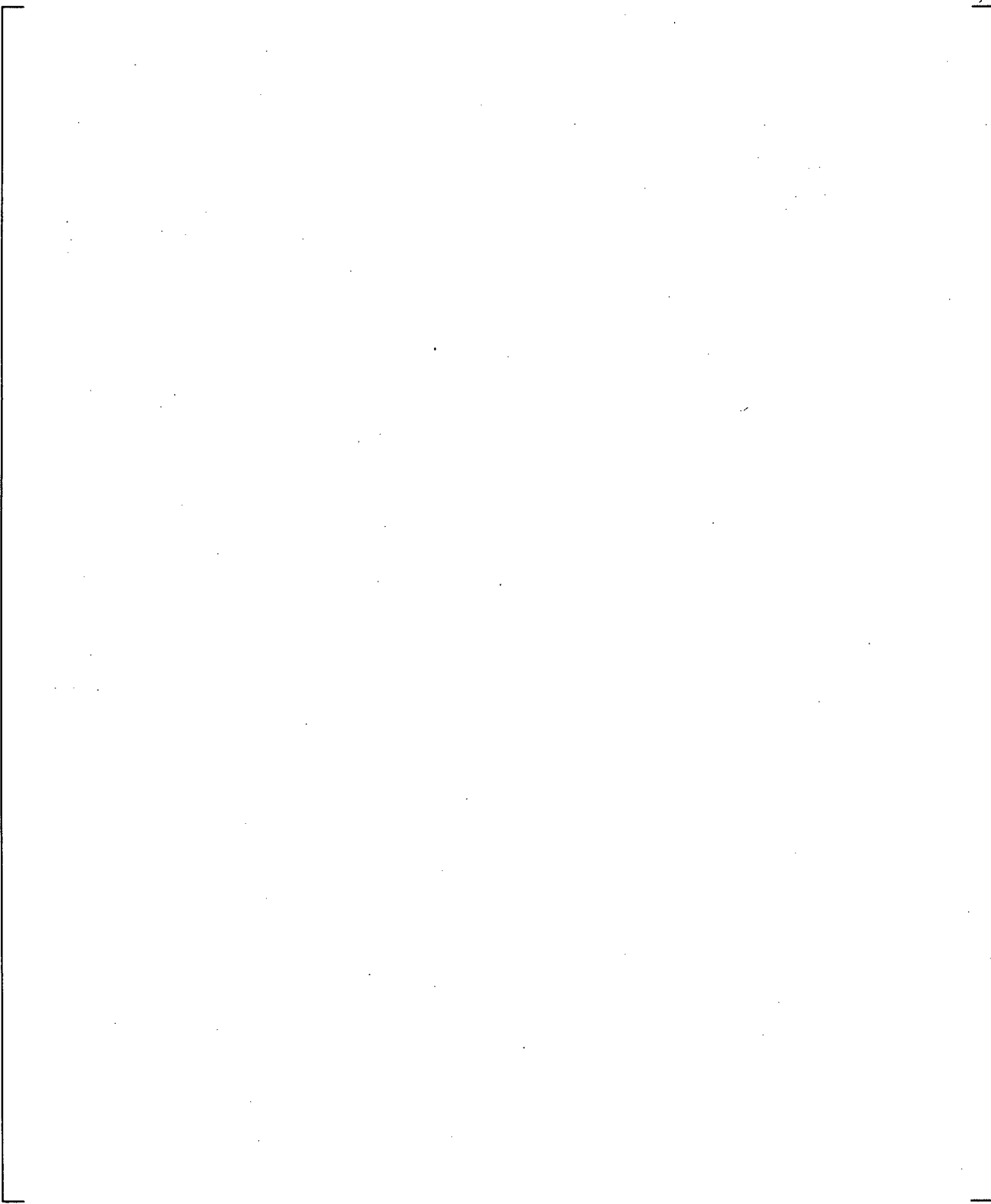


**Figure 21.13-10 SGA Inlet Plenum Collapsed Liquid Levels**

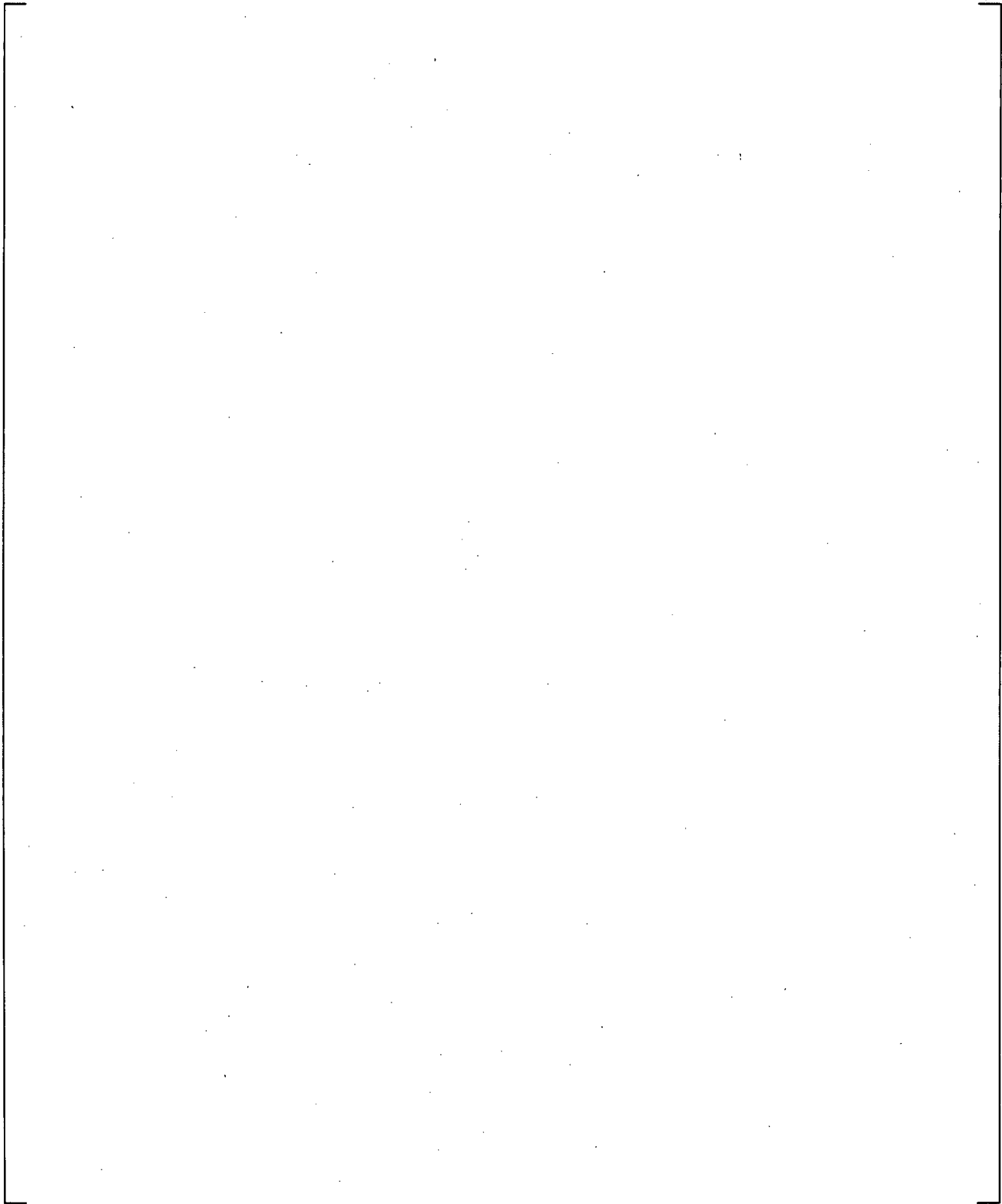


**Figure 21.13-11 SGB Inlet Plenum Collapsed Liquid Levels**

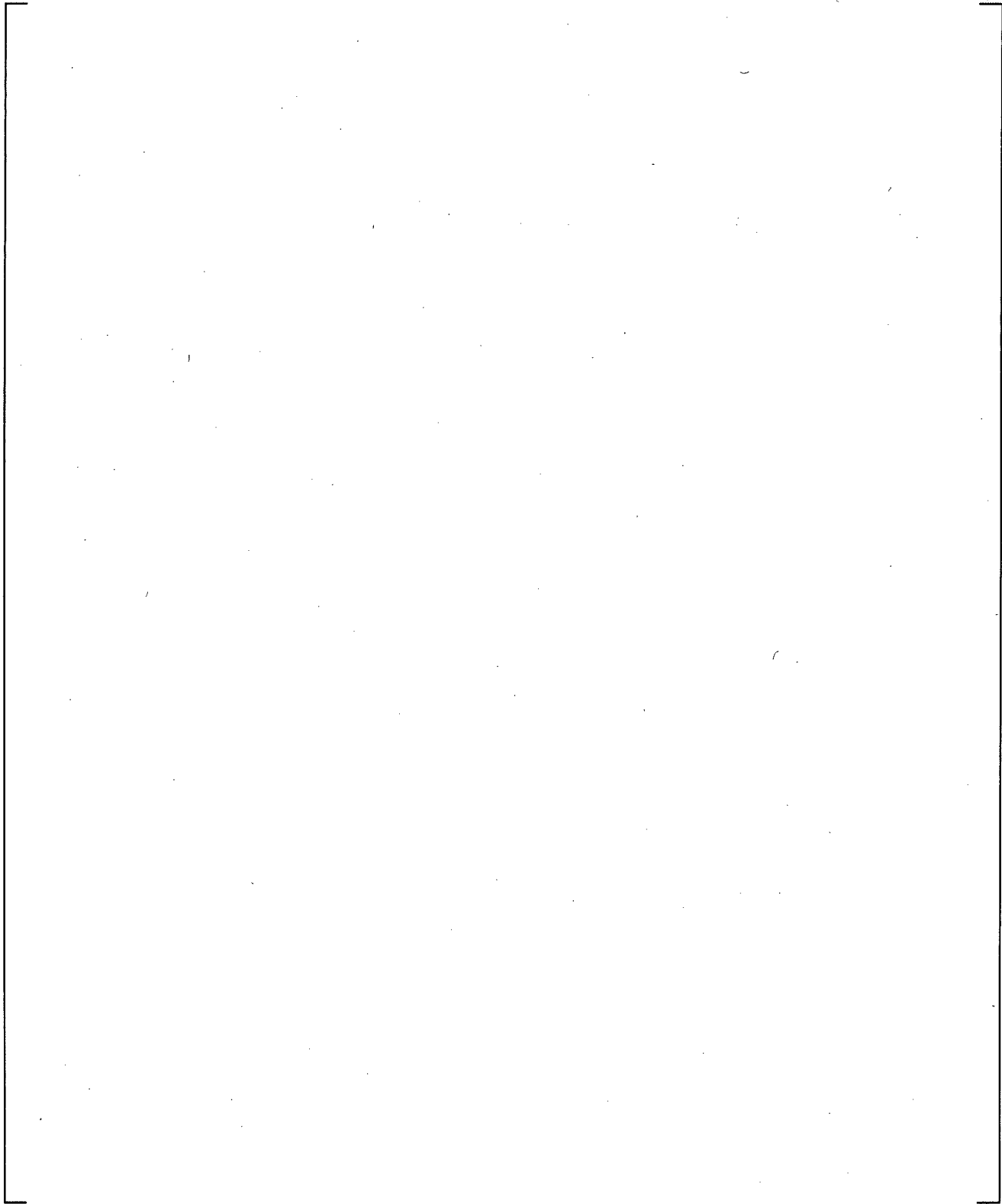


**Figure 21.13-12 Upper Plenum to SGA Inlet Differential Pressures**

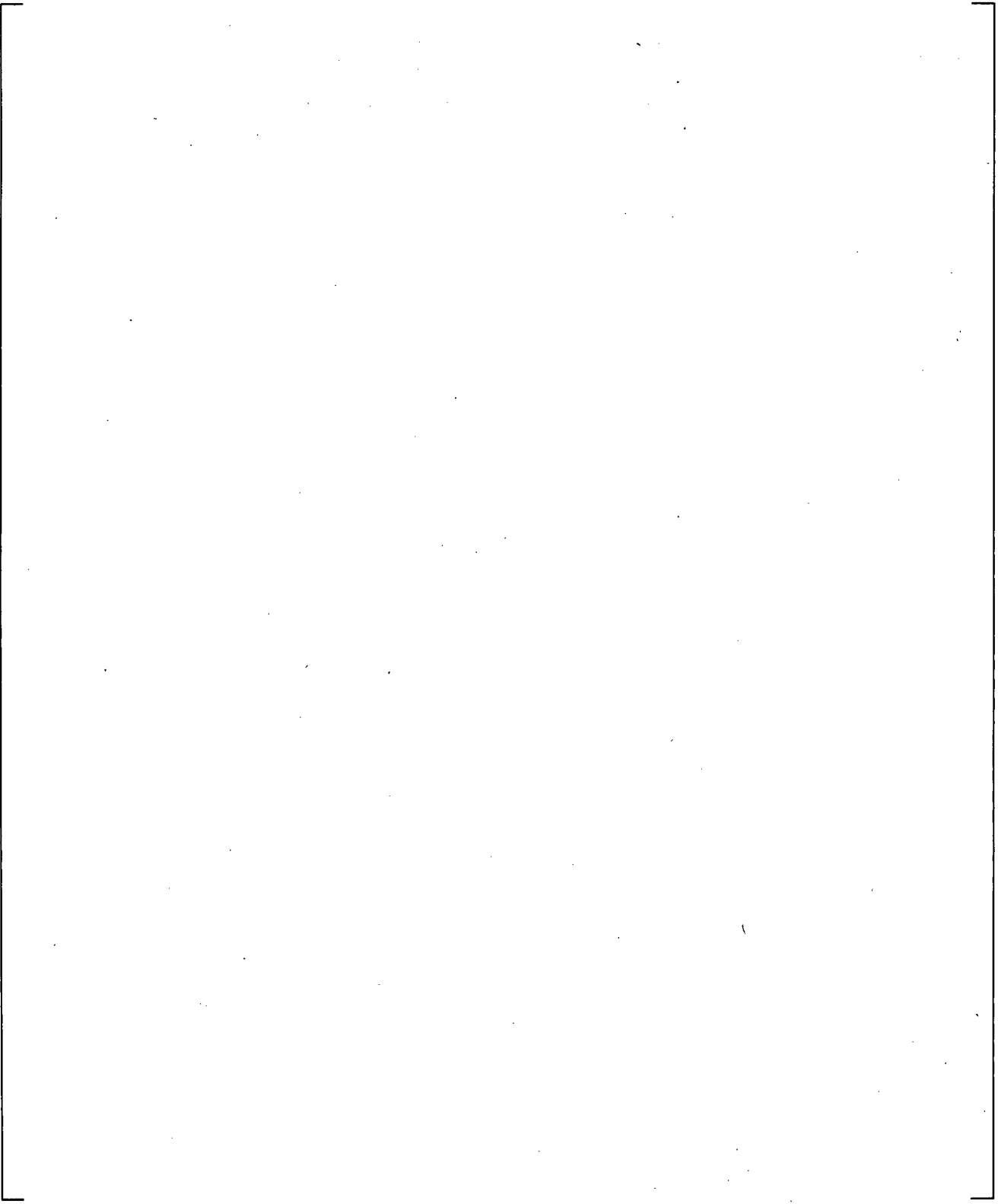


**Figure 21.13-13 Upper Plenum to SGB Inlet Differential Pressures**

a,c

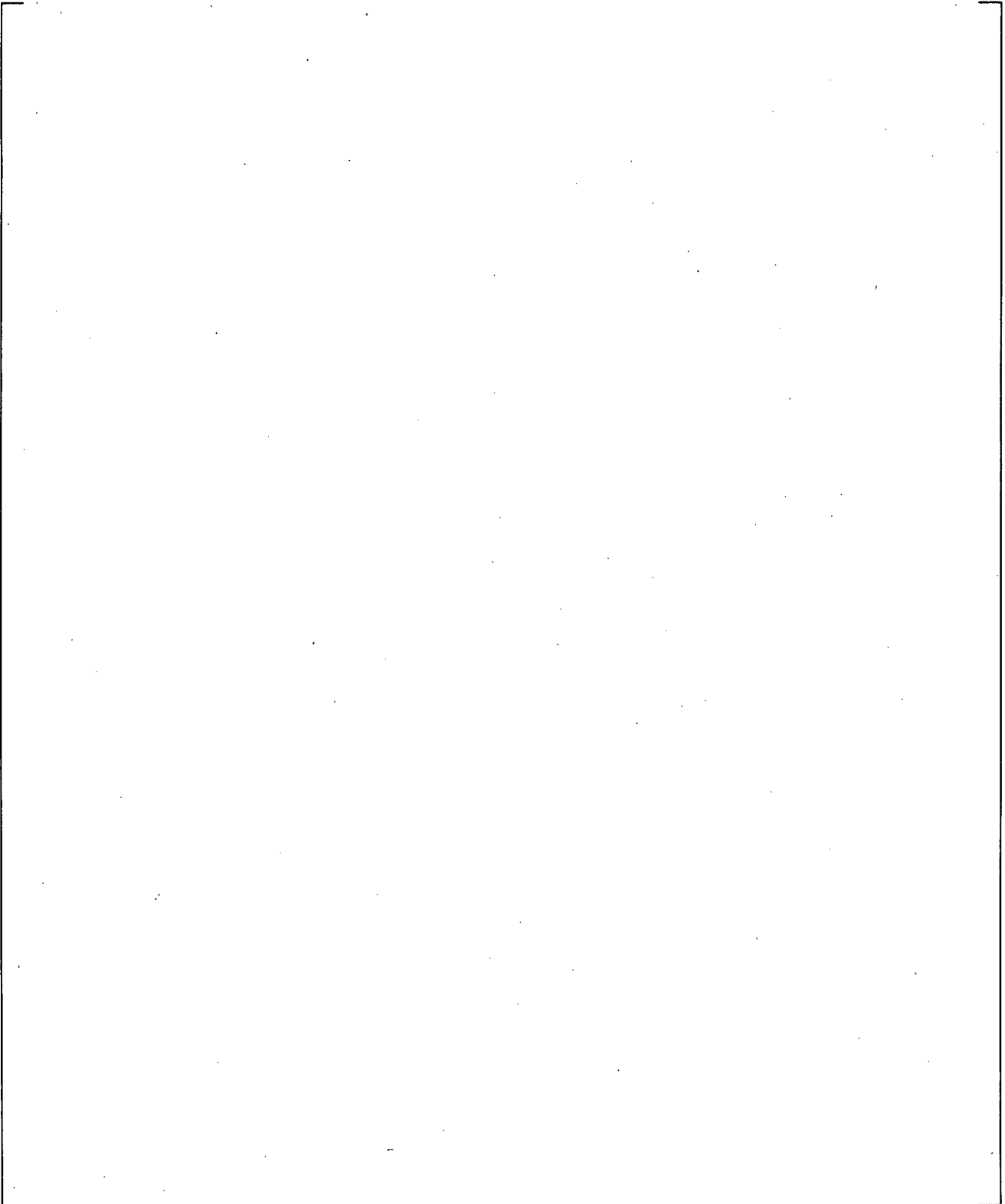


**Figure 21.13-14 Downcomer Differential Pressures**

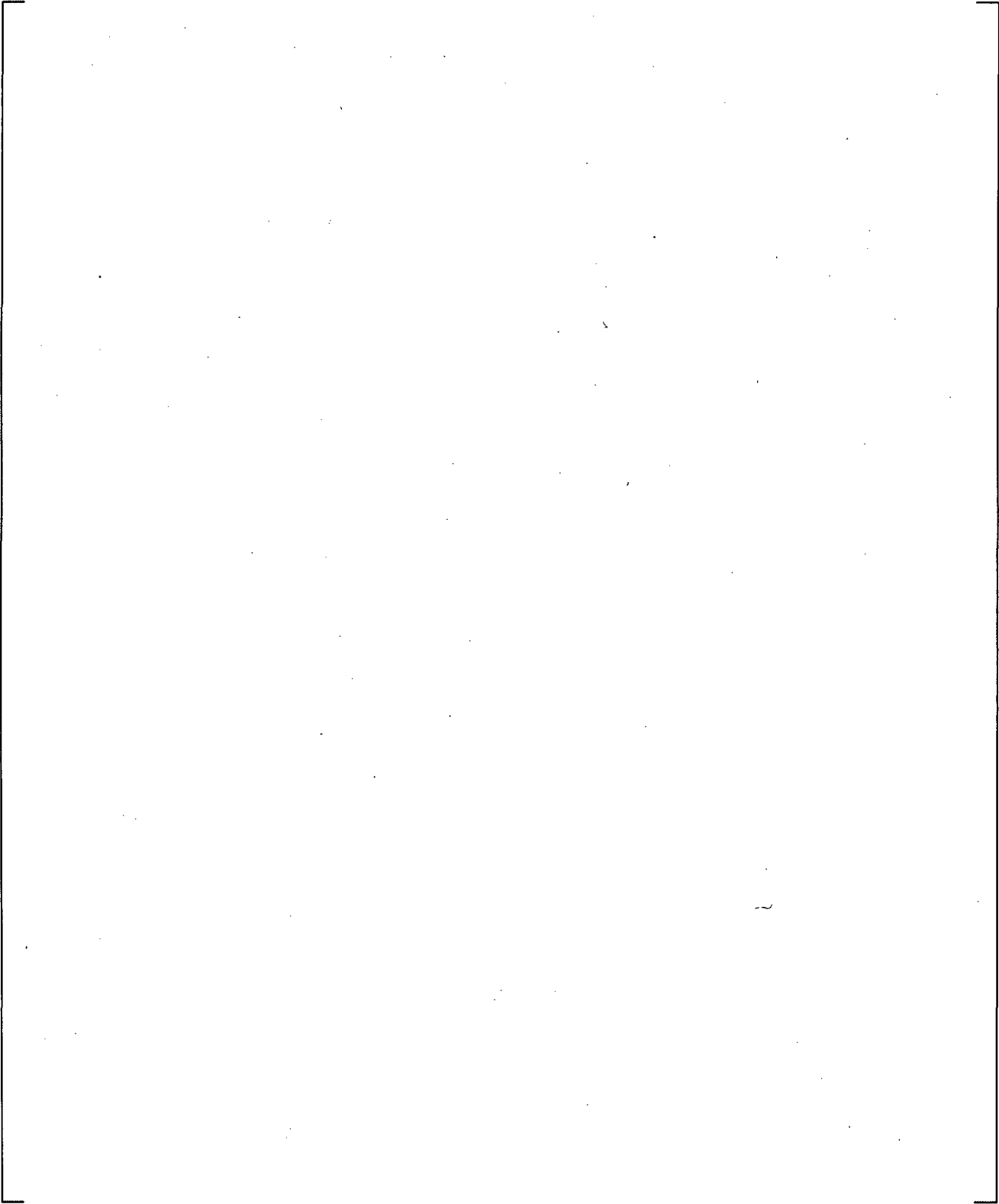


**Figure 21.13-15 Upper Plenum Differential Pressures**

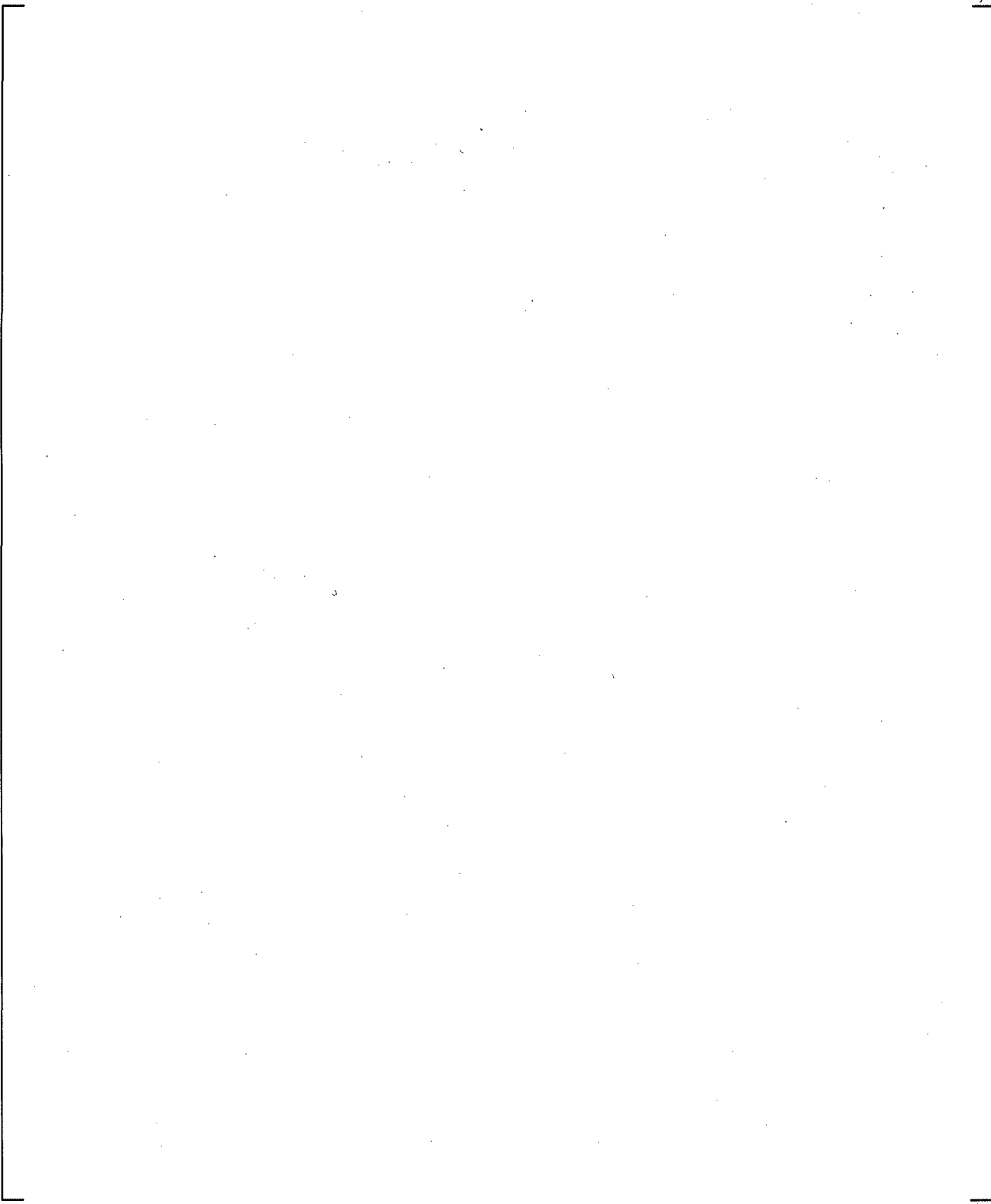


**Figure 21.13-16 Inner Vessel (LP+Core+UP) Differential Pressures**

a,c

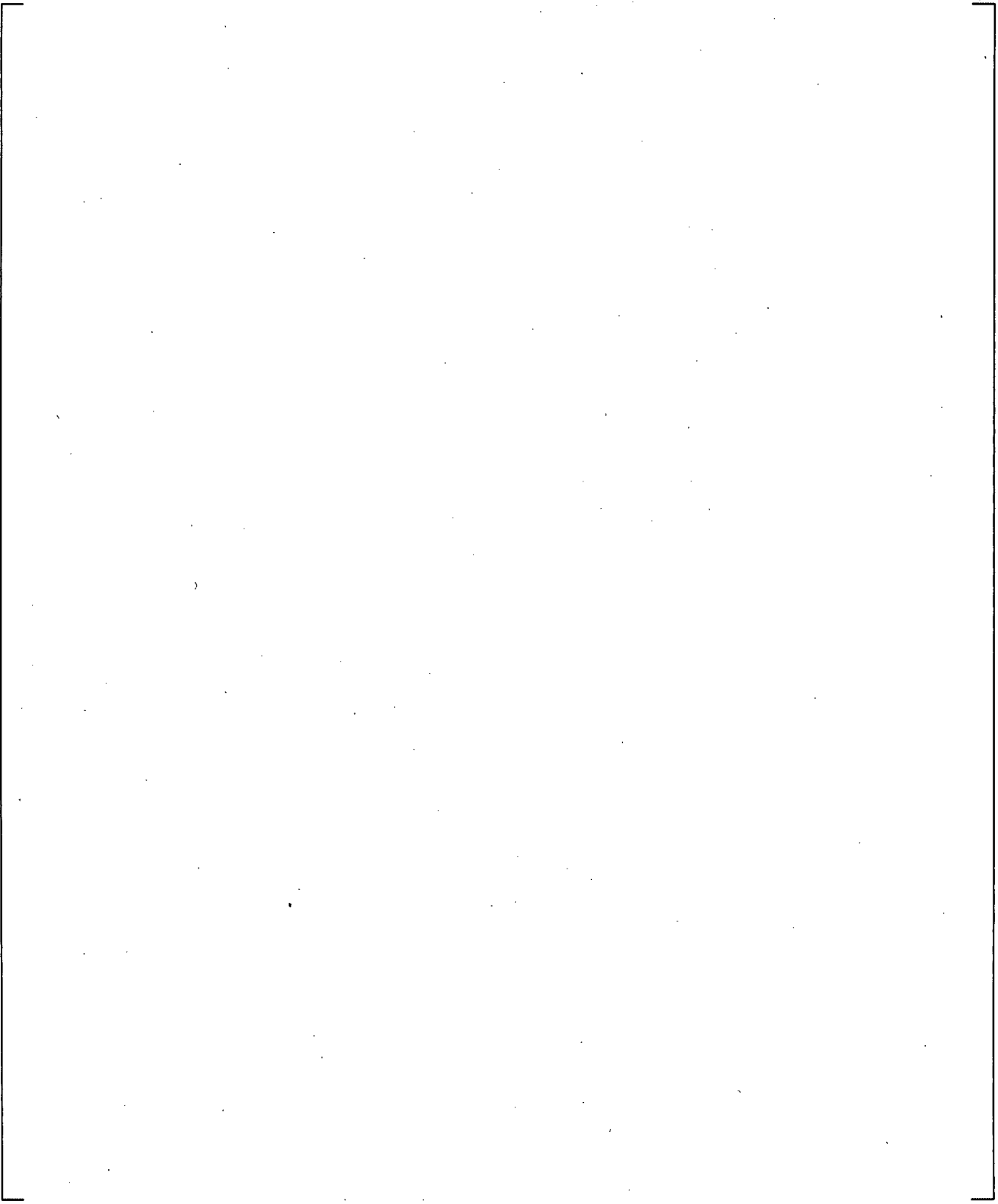


**Figure 21.13-17 Lower Plenum Differential Pressures**

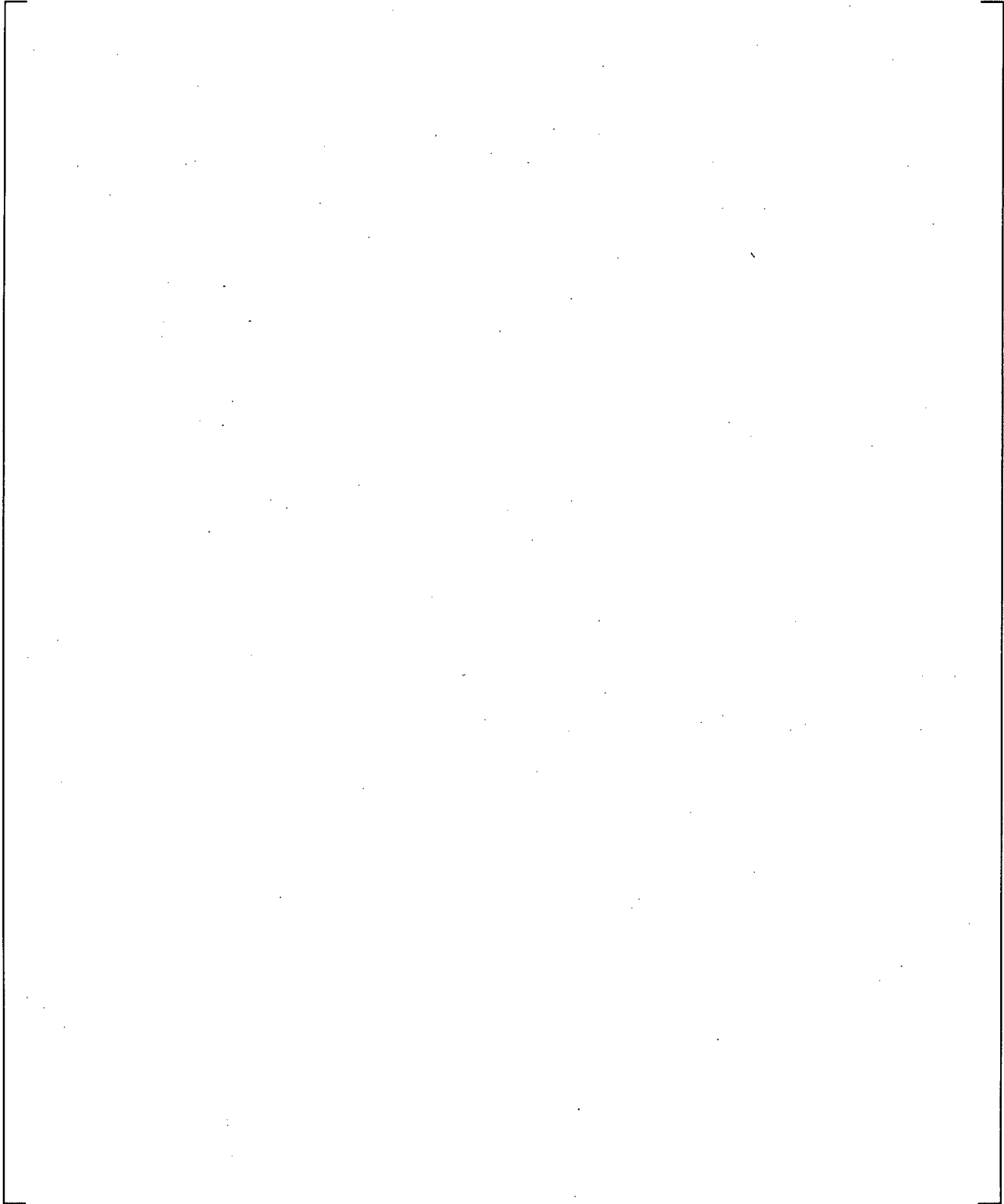


**Figure 21.13-18 Peak Cladding Temperatures**

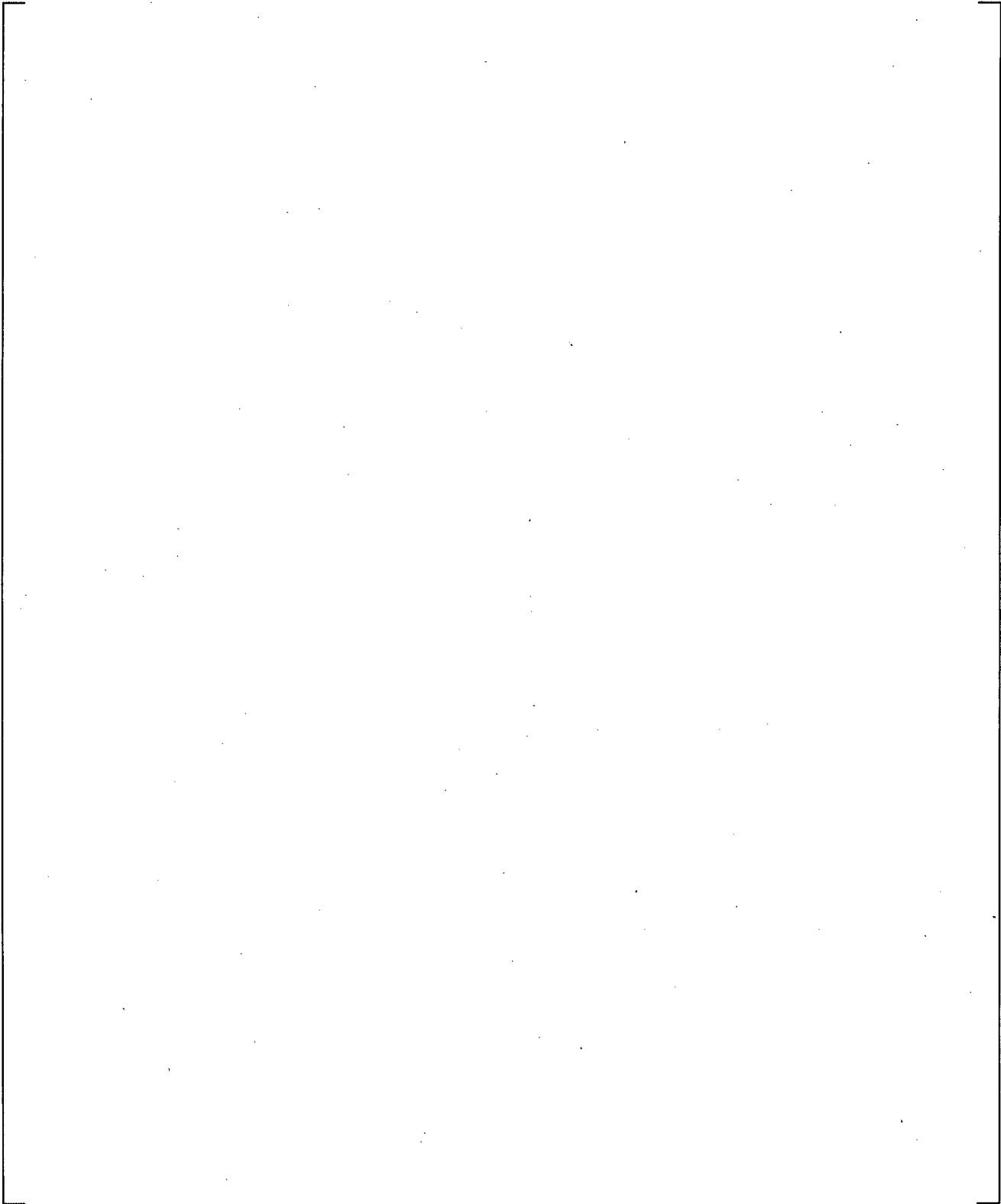


**Figure 21.13-19 Accumulator A Injection Flows**

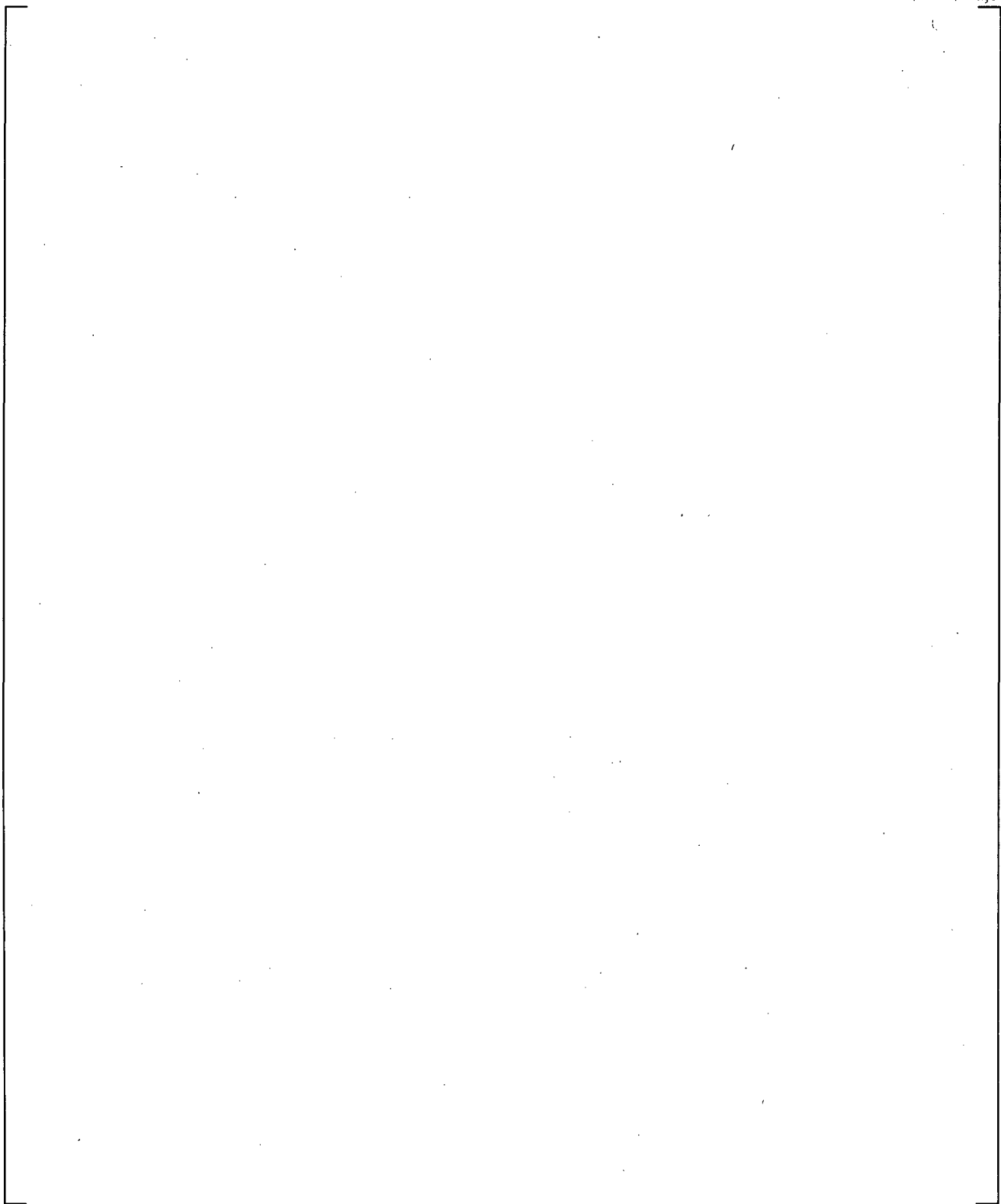


**Figure 21.14-1 Pump A Differential Pressures**

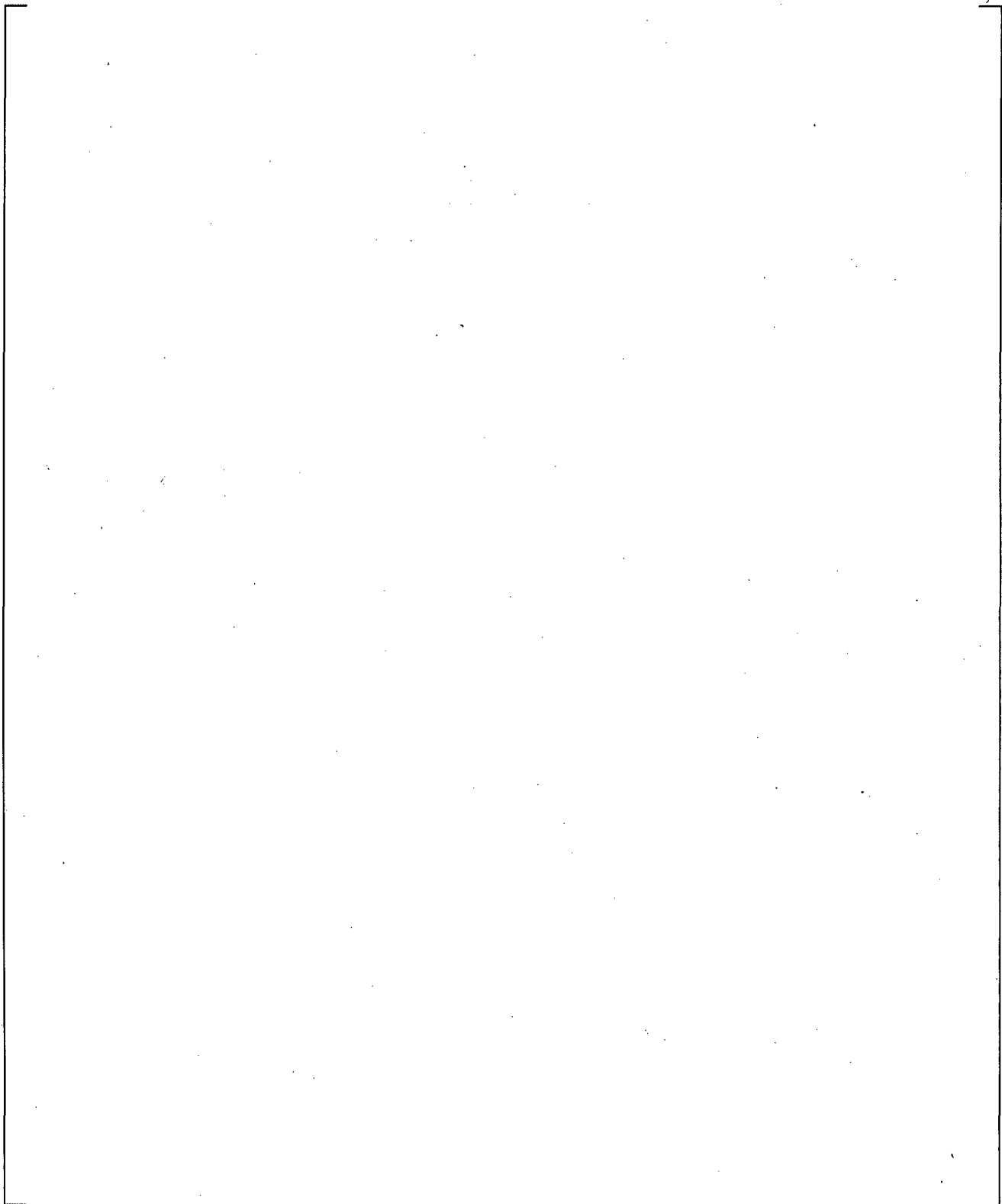


**Figure 21.14-2 SB-CL-18 Cross-Over Leg A Differential Pressures**

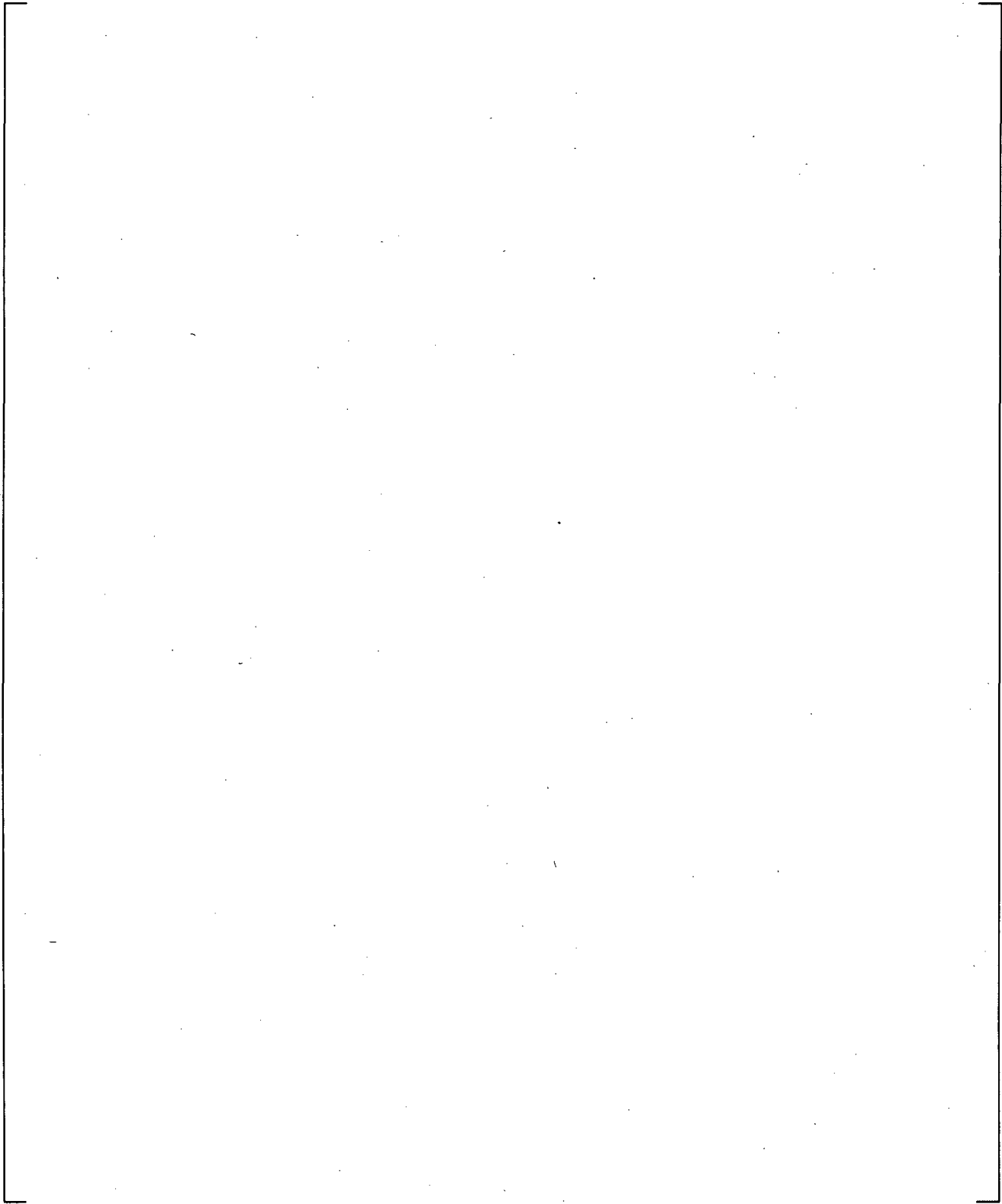


**Figure 21.14-3 SB-CL-18 Cross-Over Leg B Differential Pressures**

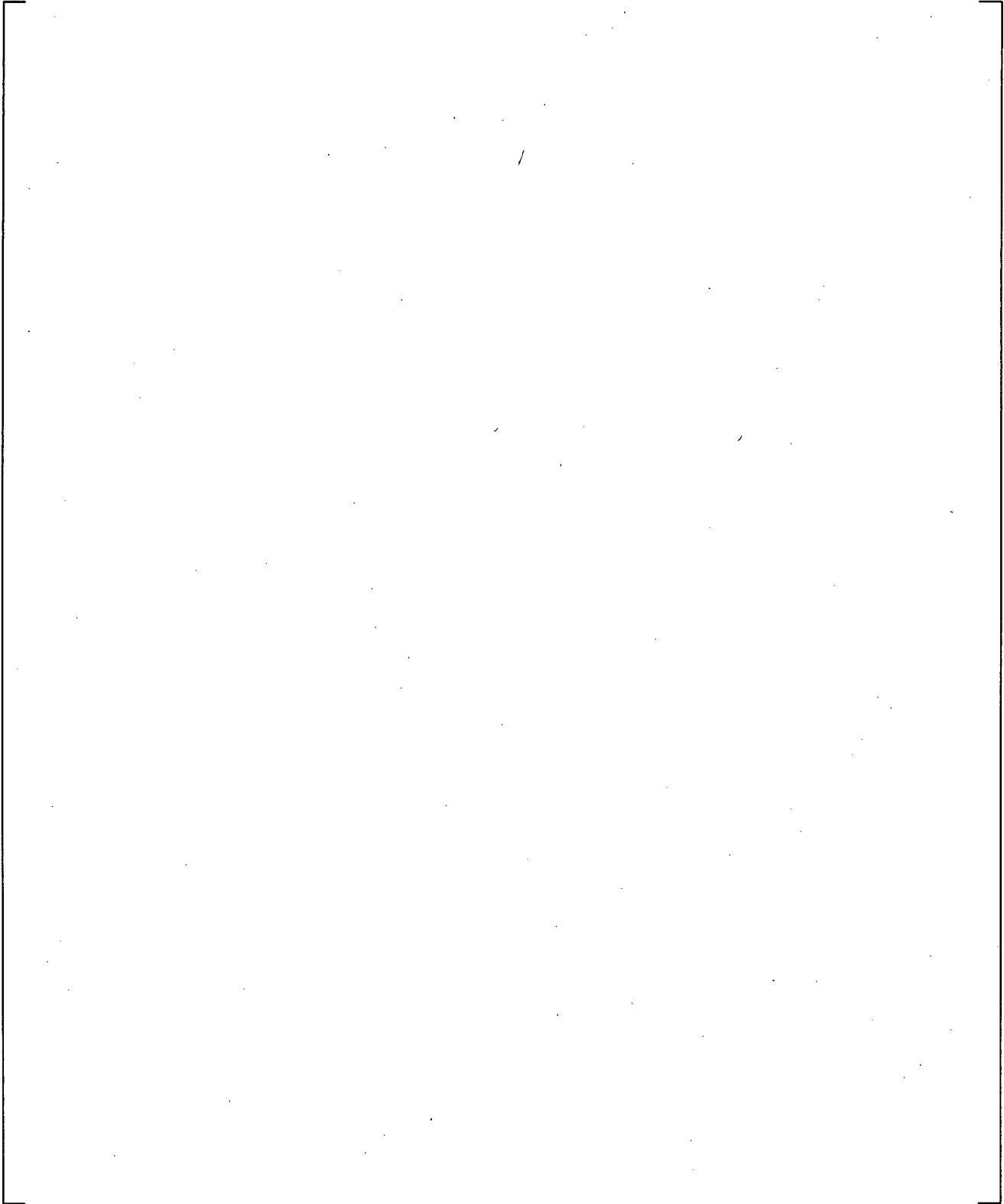


**Figure 21.14-4 Inner Vessel Differential Pressures (LP+Core+UCP)**

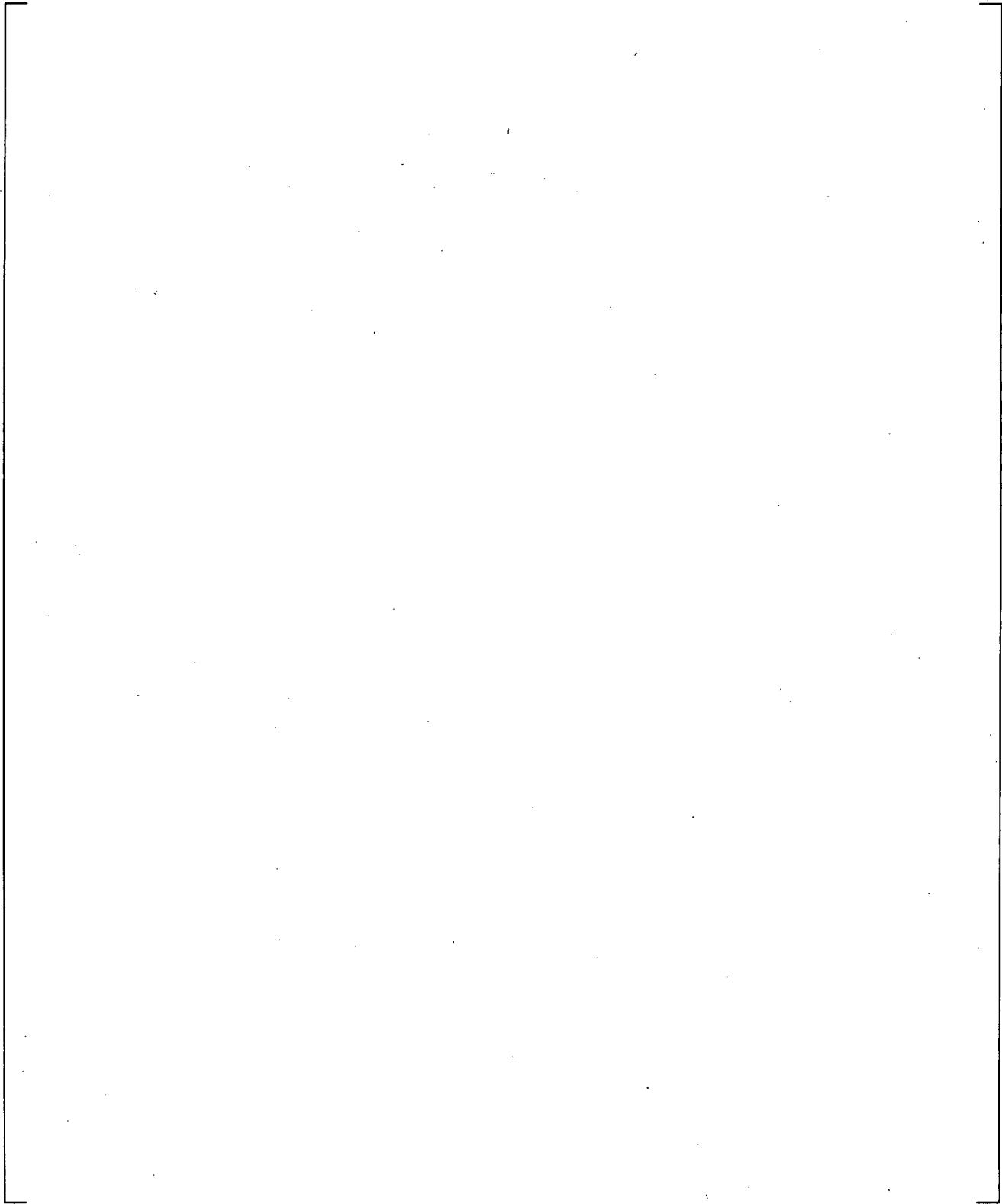


**Figure 21.14-5 Downcomer Differential Pressures**

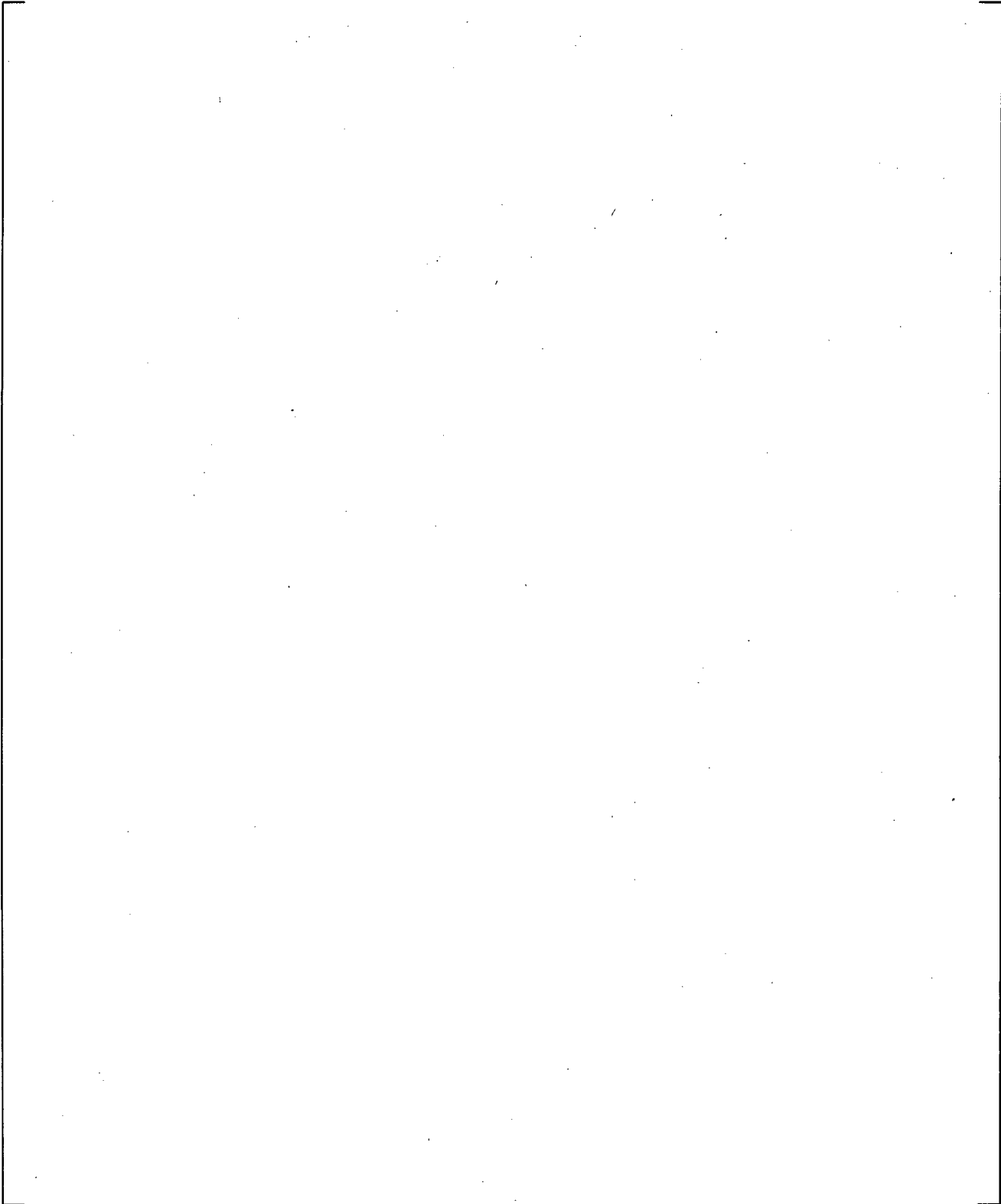


**Figure 21.14-6 Lower Plenum Differential Pressures**

a,c

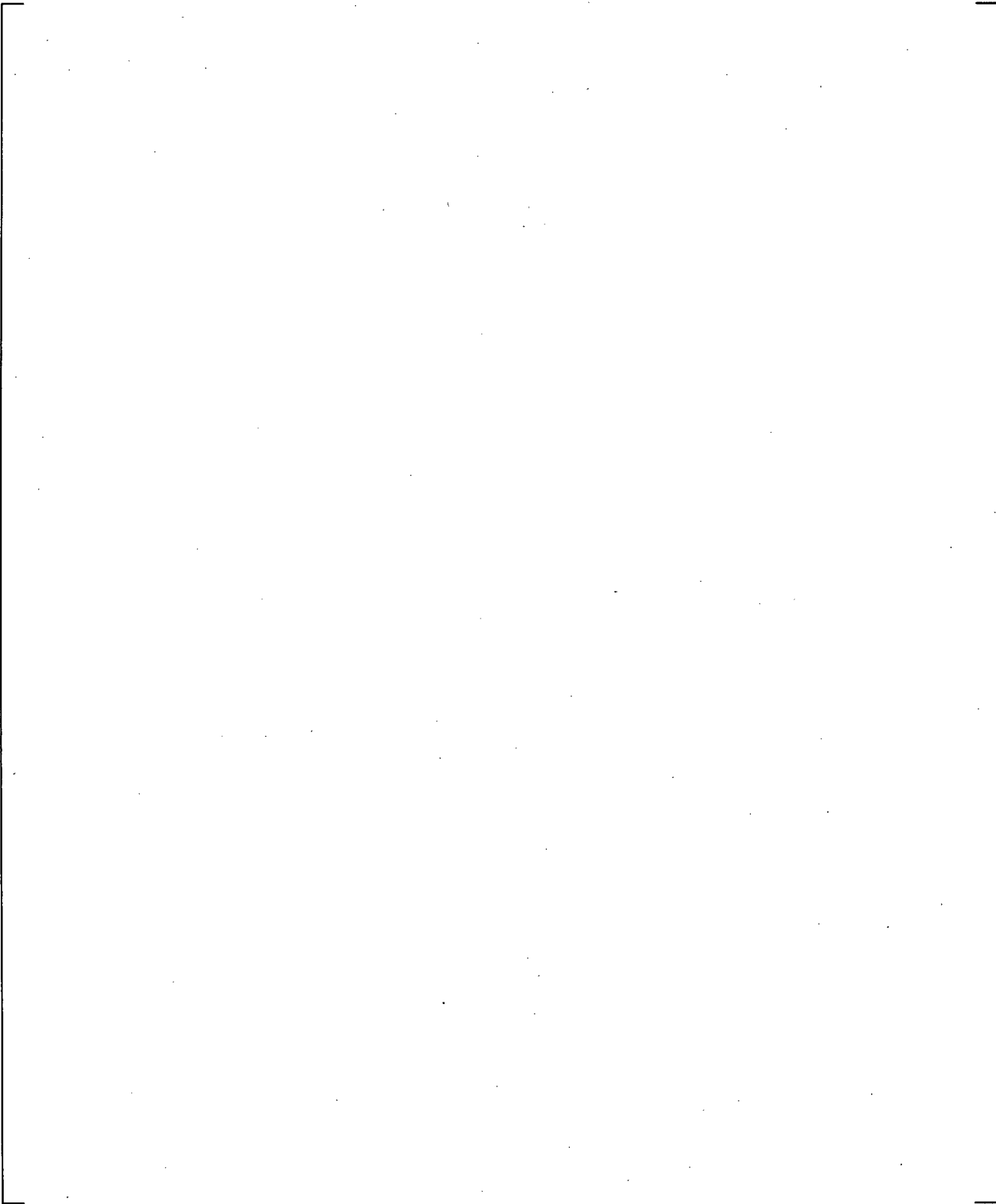


**Figure 21.14-7 Upper Plenum Differential Pressures**

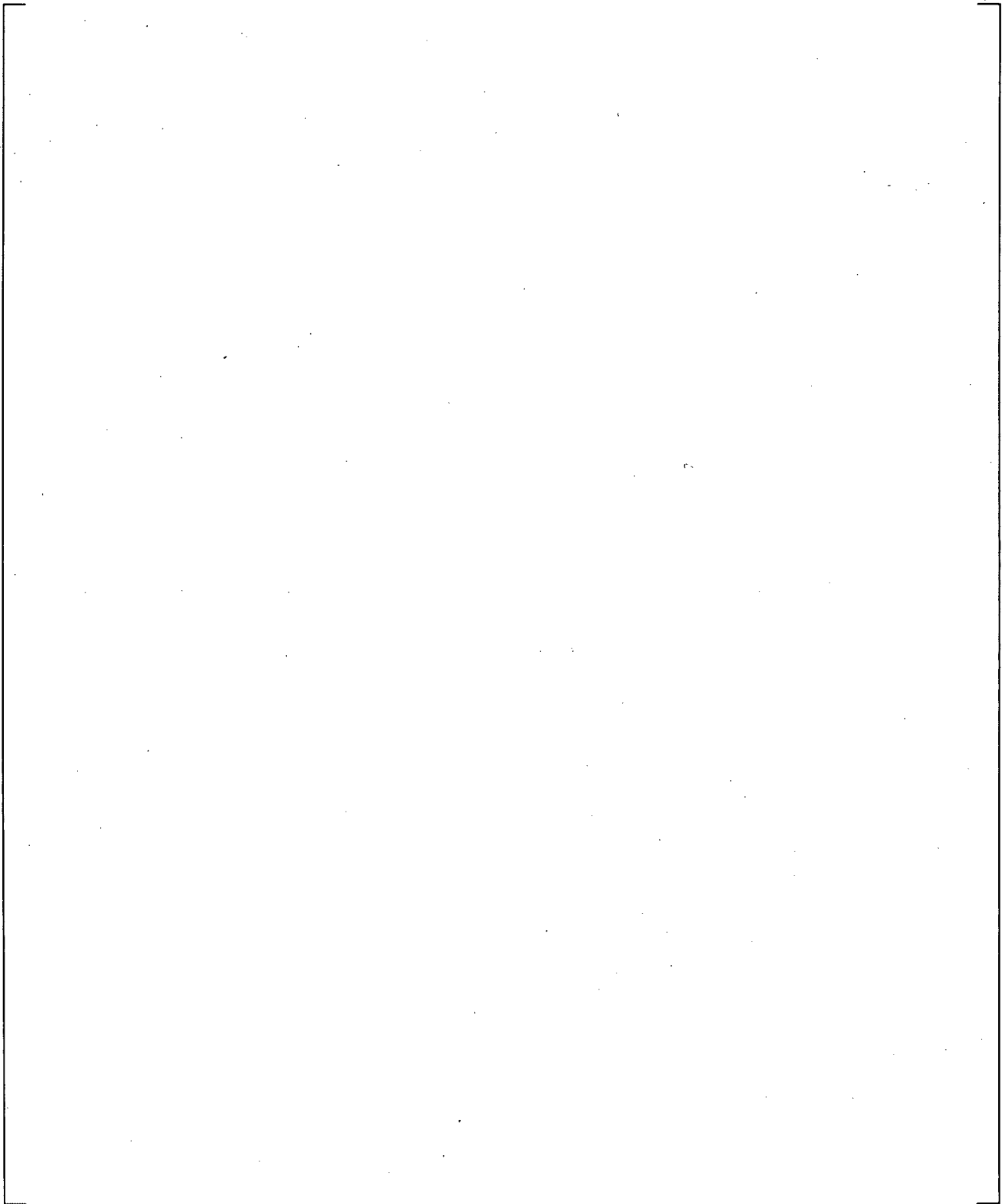


**Figure 21.14-8 Hot Leg A Differential Pressures**

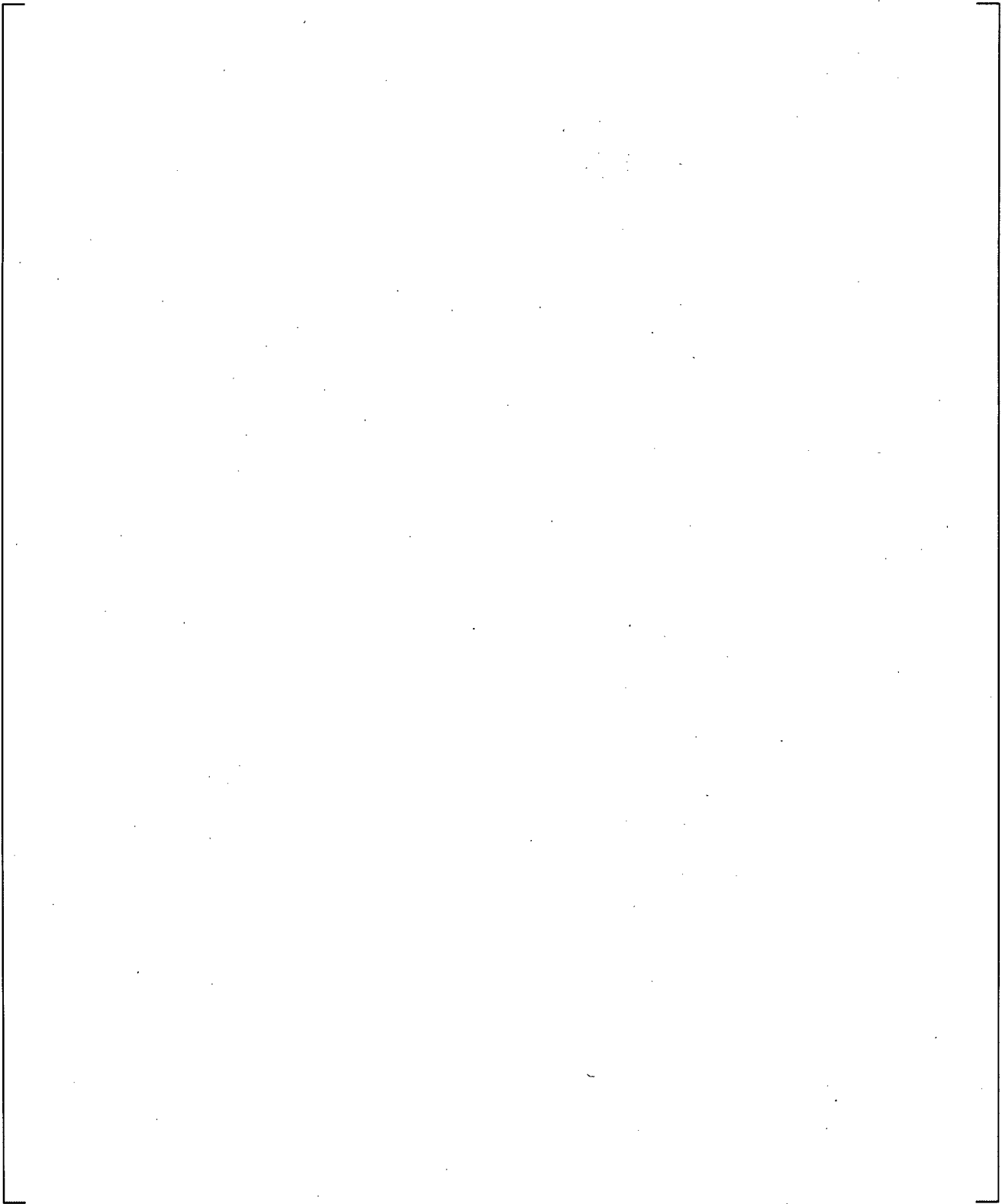


**Figure 21.14-9 Hot Leg B Differential Pressures**

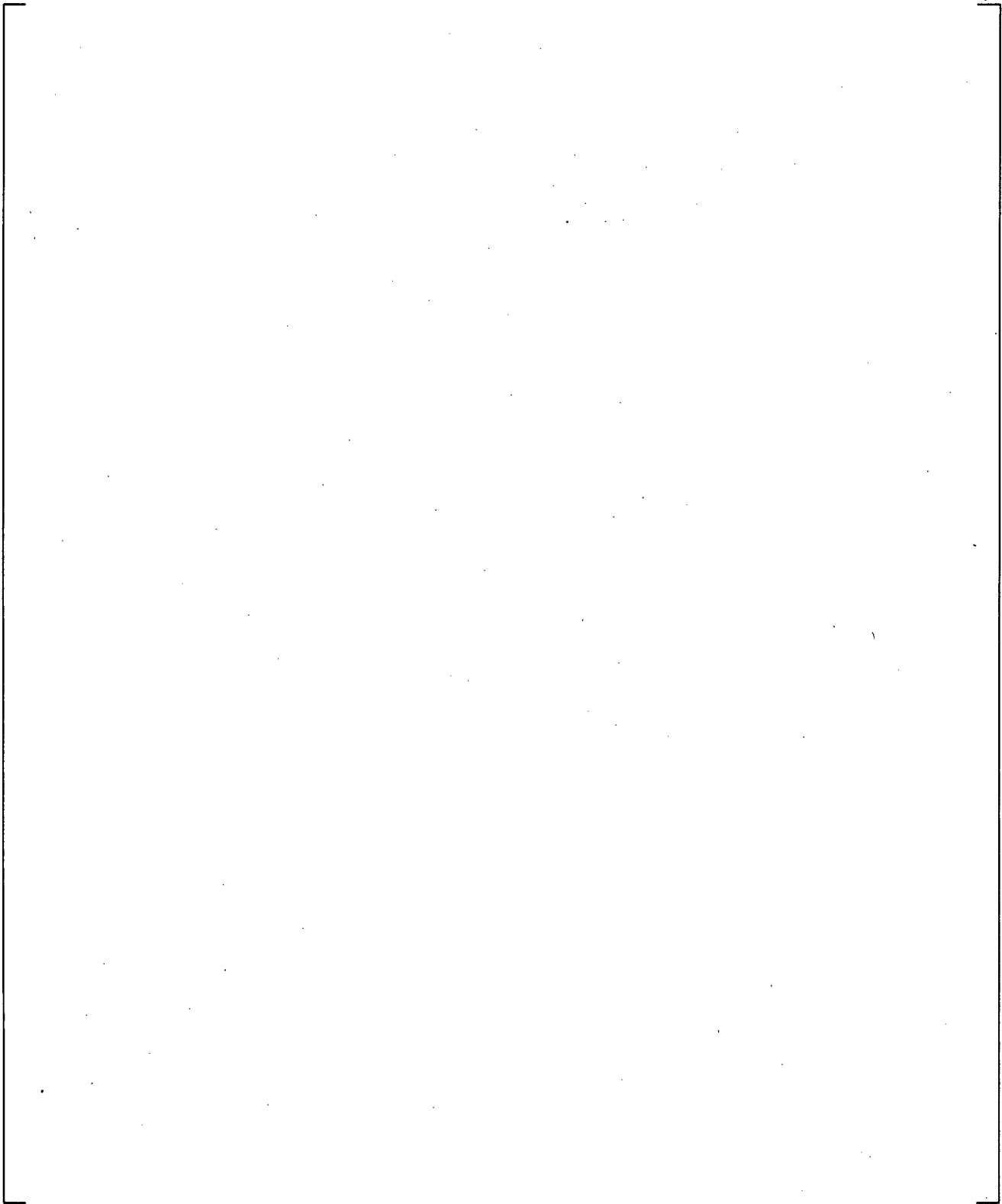


**Figure 21.14-10 Peak Cladding Temperatures**

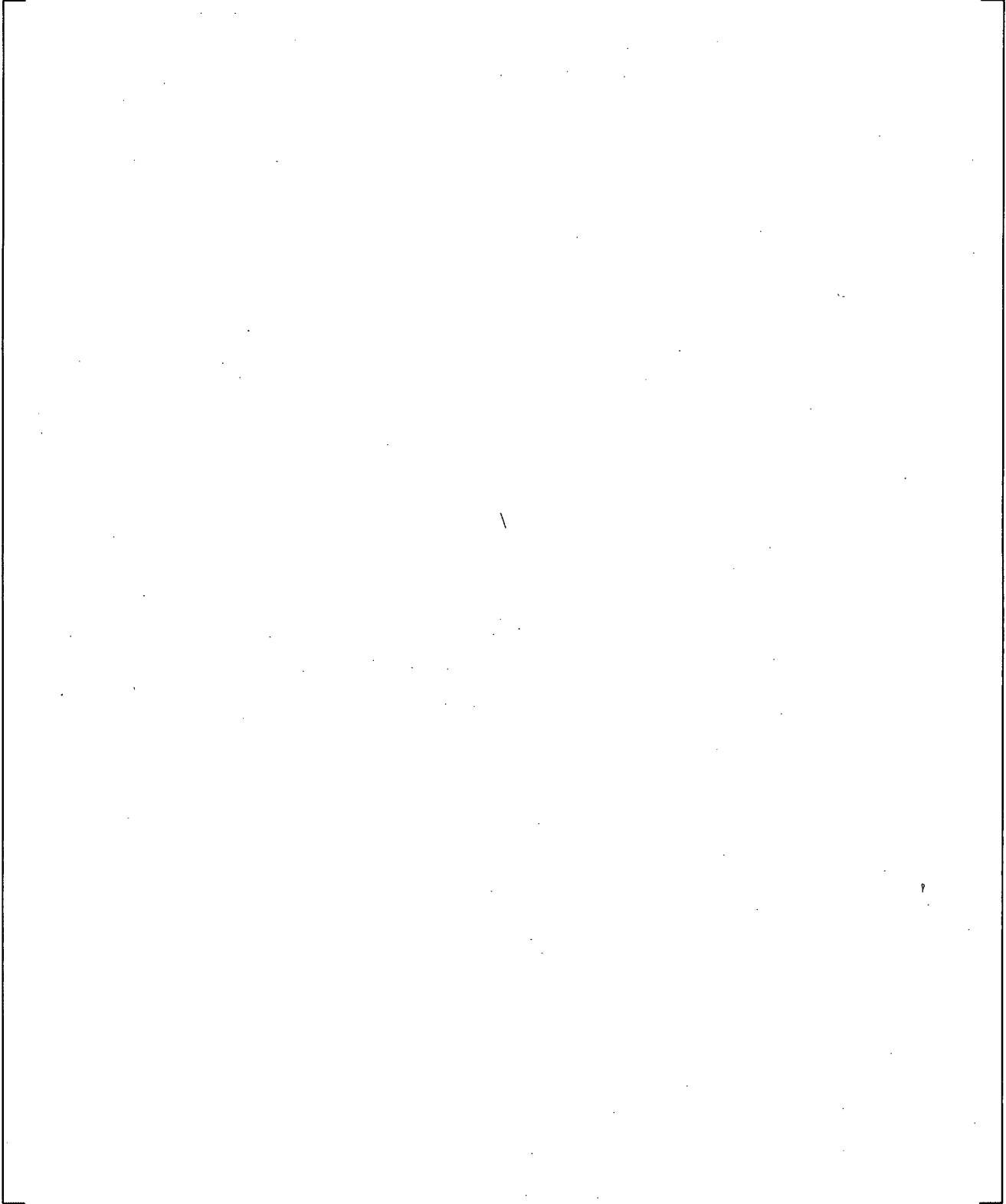


**Figure 21.15-1 SB-CL-18 Cross-Over Leg A Differential Pressures**

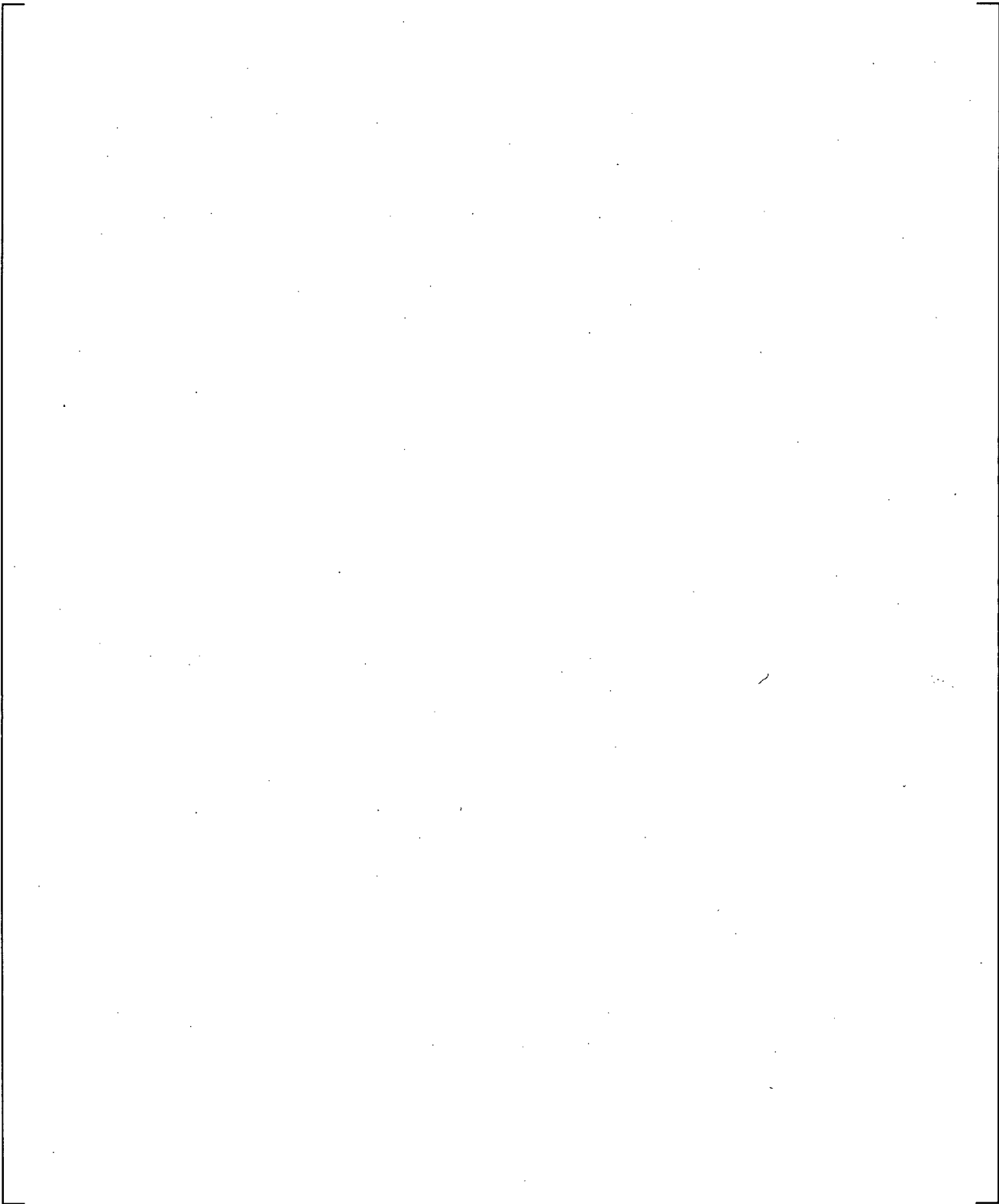


**Figure 21.15-2 SB-CL-18 Cross-Over Leg B Differential Pressures**

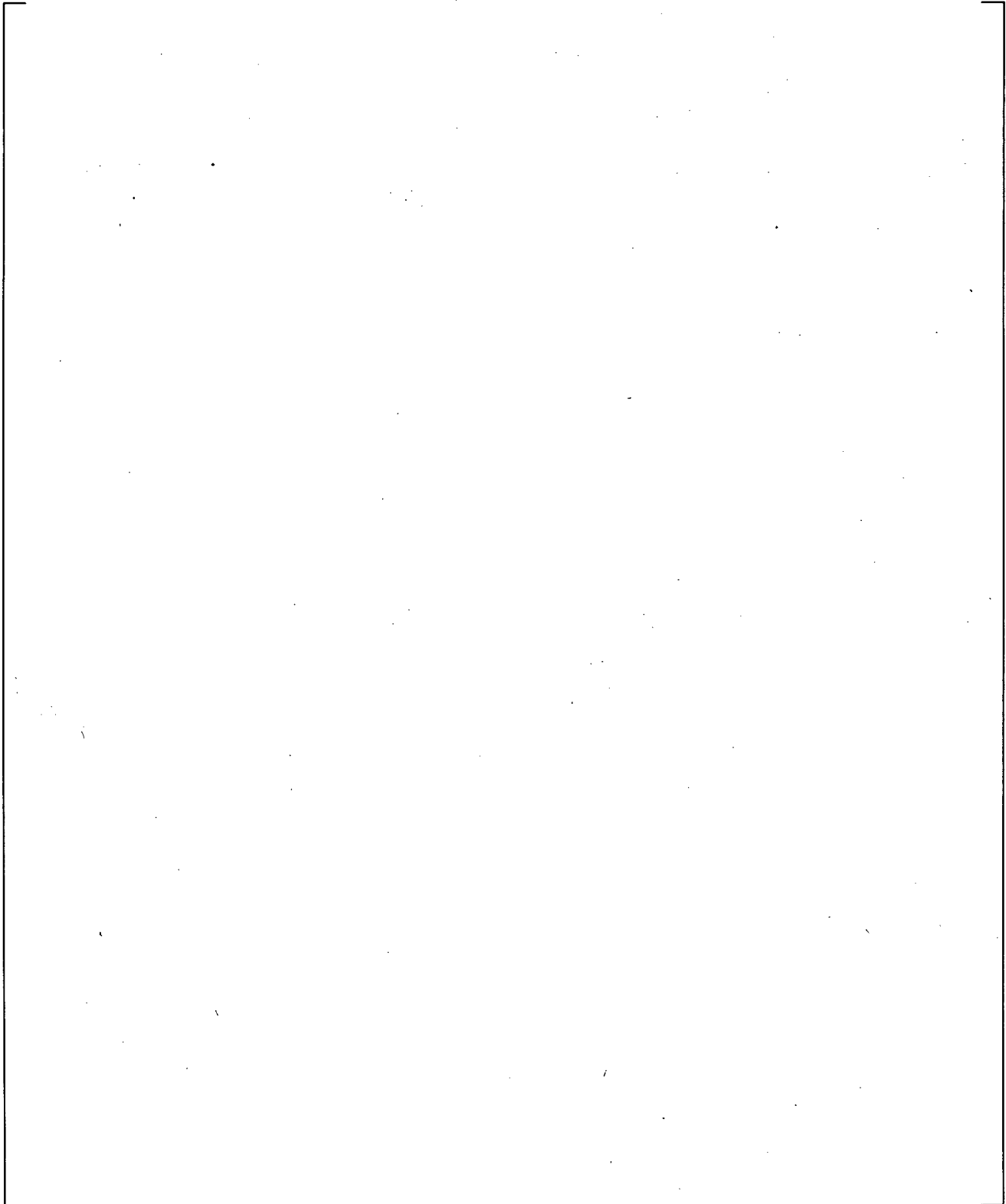


**Figure 21.15-3 Inner Vessel Differential Pressures (LP+Core+UCP)**

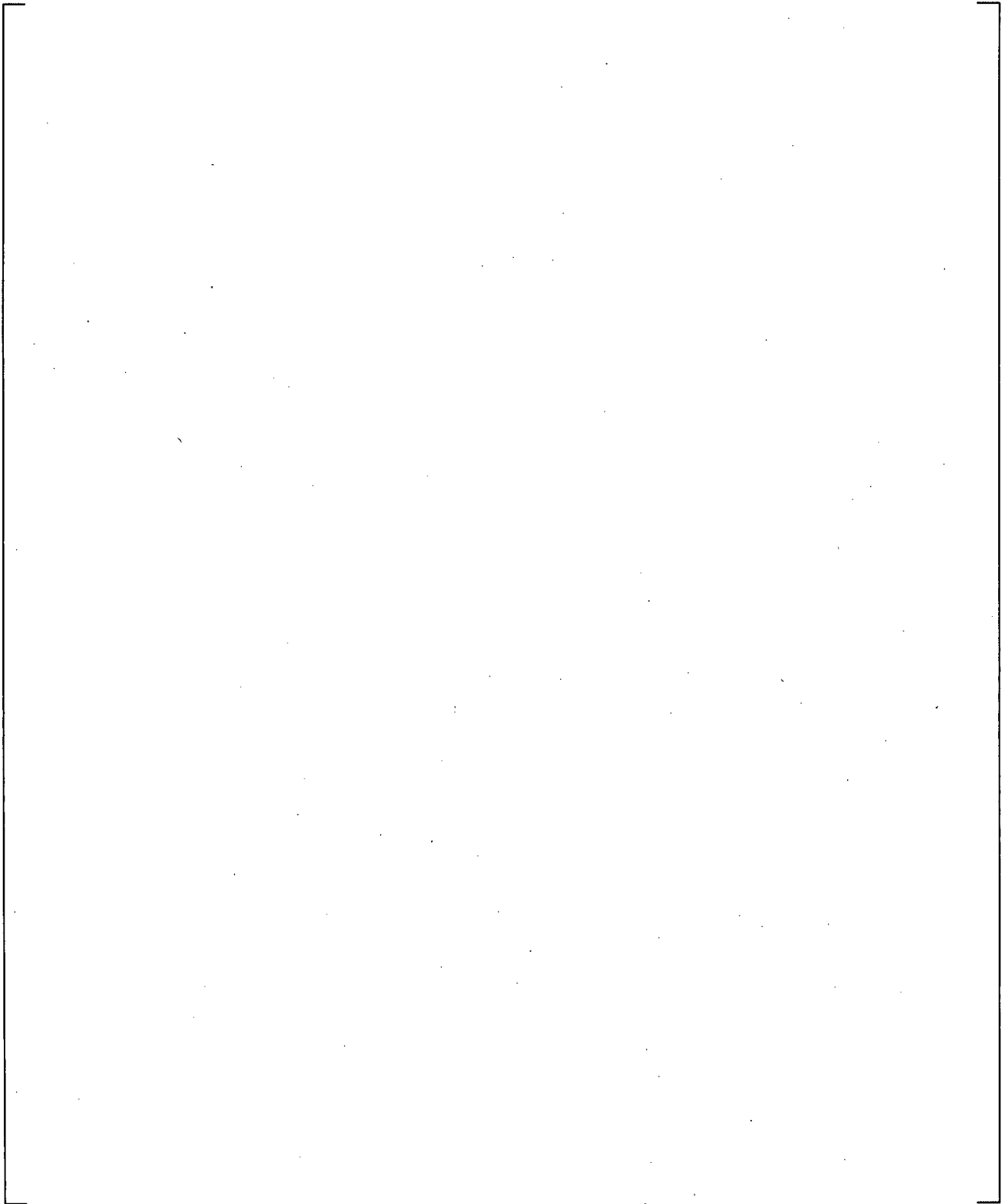


**Figure 21.15-4 Upper Plenum Differential Pressures**

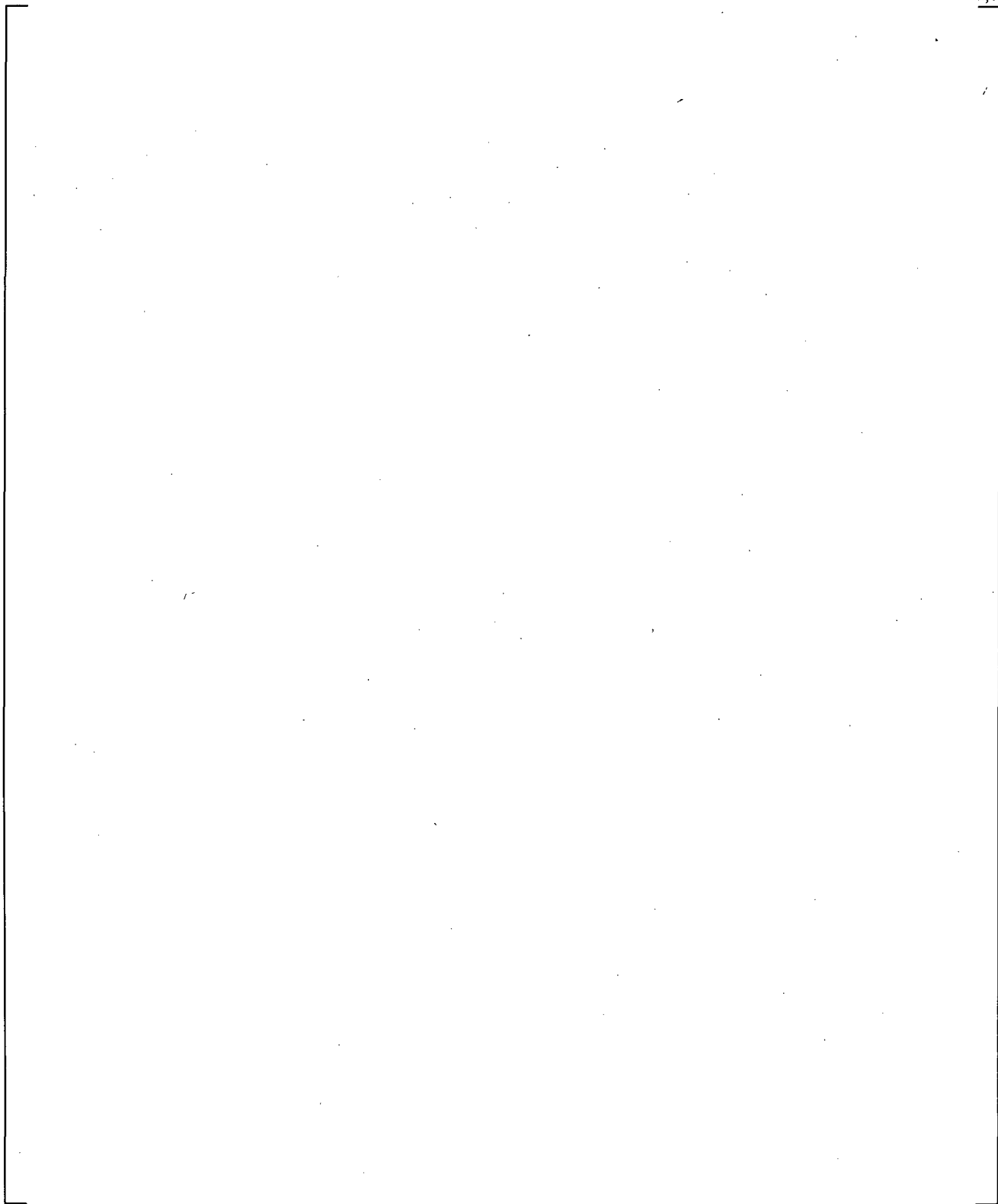


**Figure 21.15-5 Downcomer Differential Pressures**

a,c

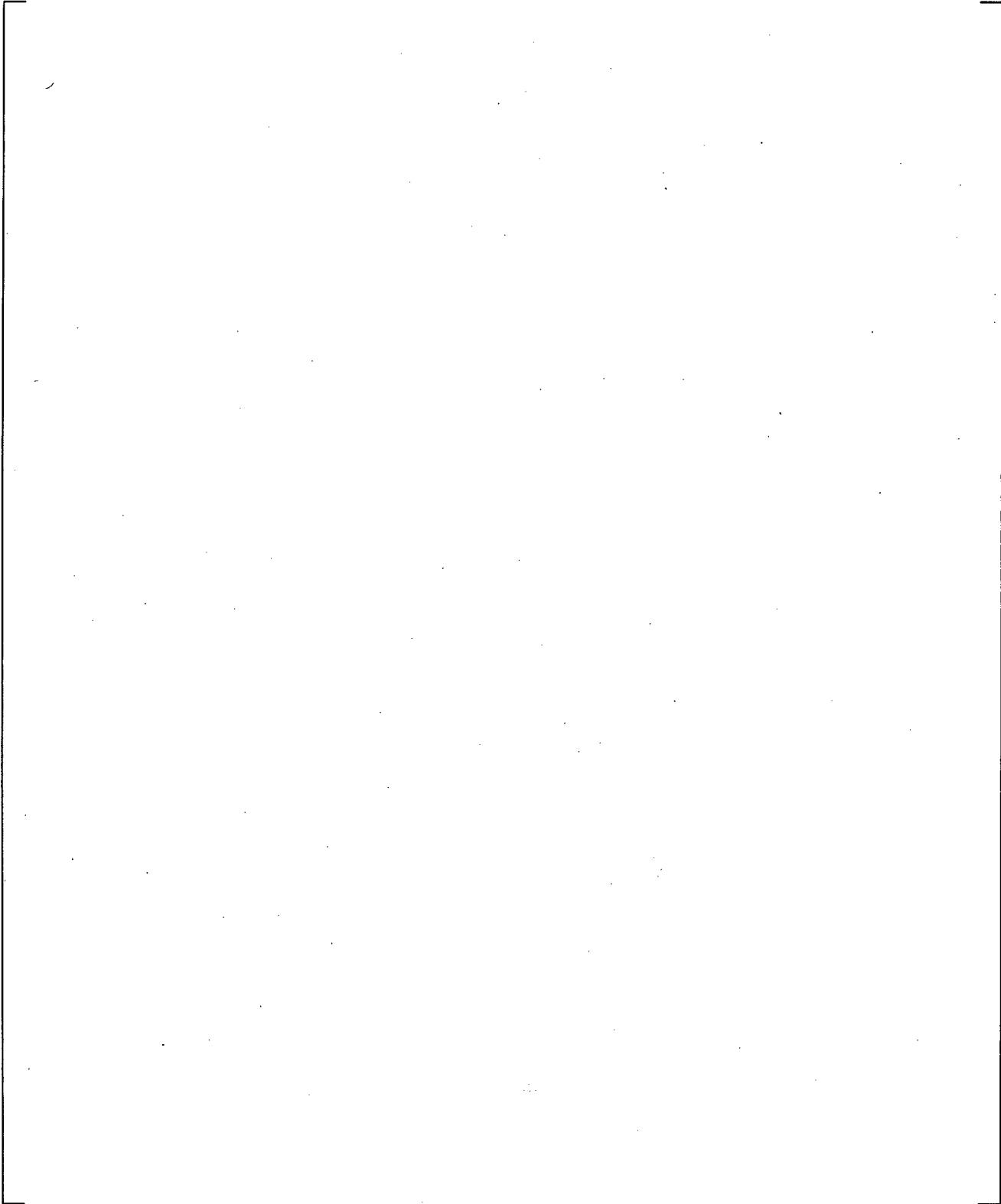


**Figure 21.15-6 Peak Cladding Temperatures**

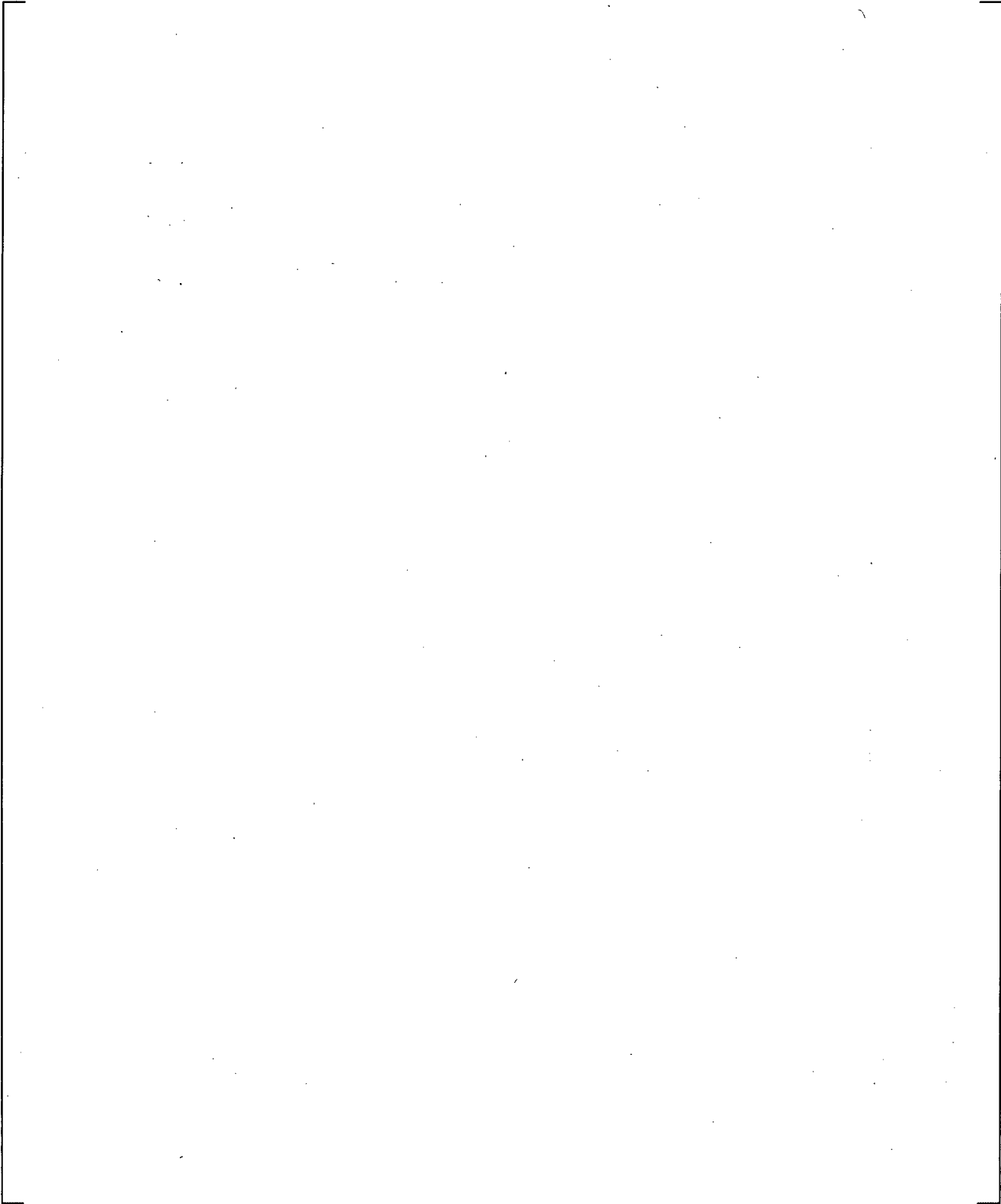


**Figure 21.16.1-1 Calculated Break Flow Rates**

**Figure 21.16.1-2 Calculated Pressurizer and Steam Generator Secondary Pressures**

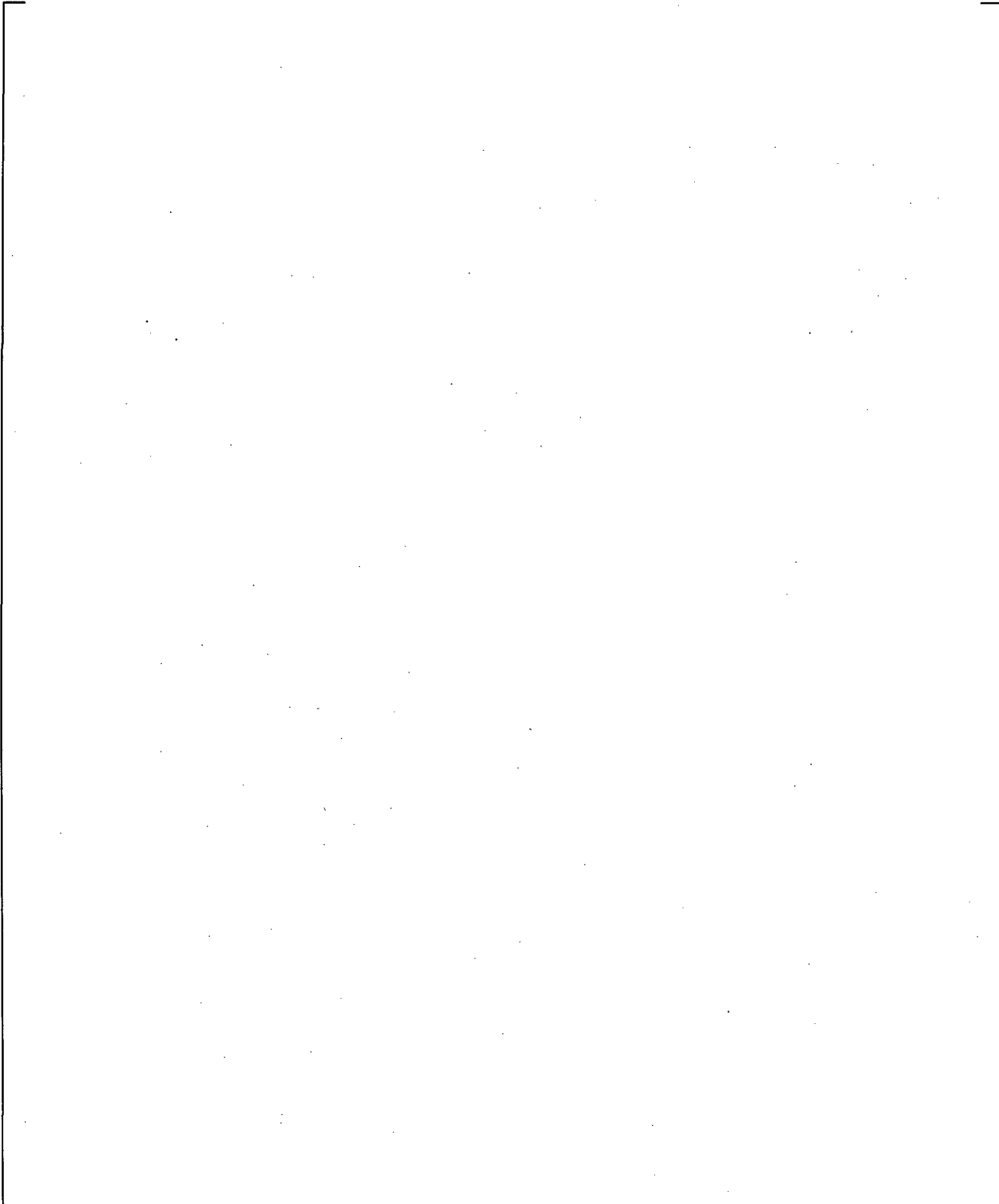


**Figure 21.16.1-3 Calculated Steam Generator U-tube Uphill Side Differential Pressures**

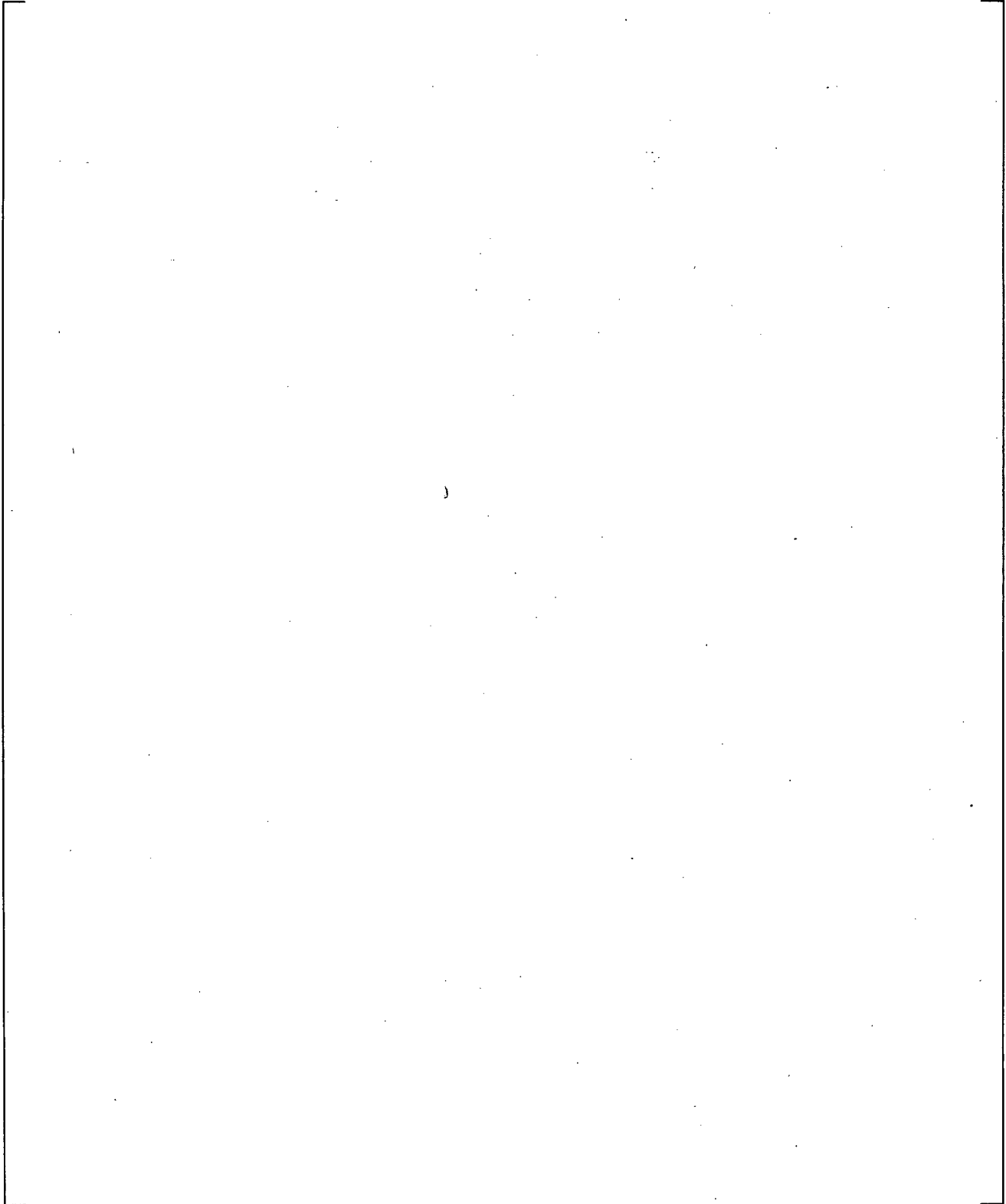


**Figure 21.16.1-4 Calculated Cross-Over Leg A Differential Pressures**

a,c

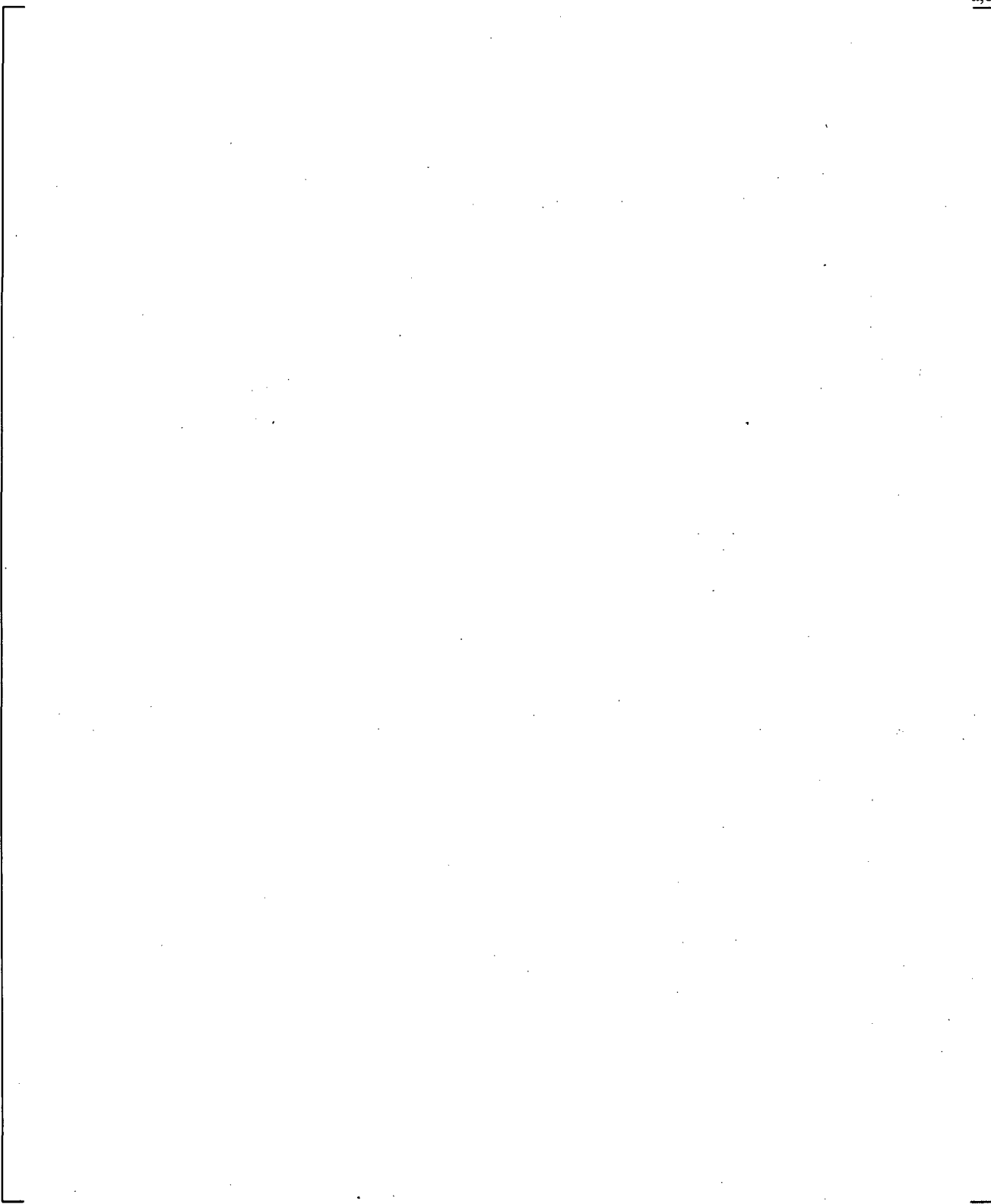


**Figure 21.16.1-5 Calculated Cross-Over Leg B Differential Pressures**

a,c

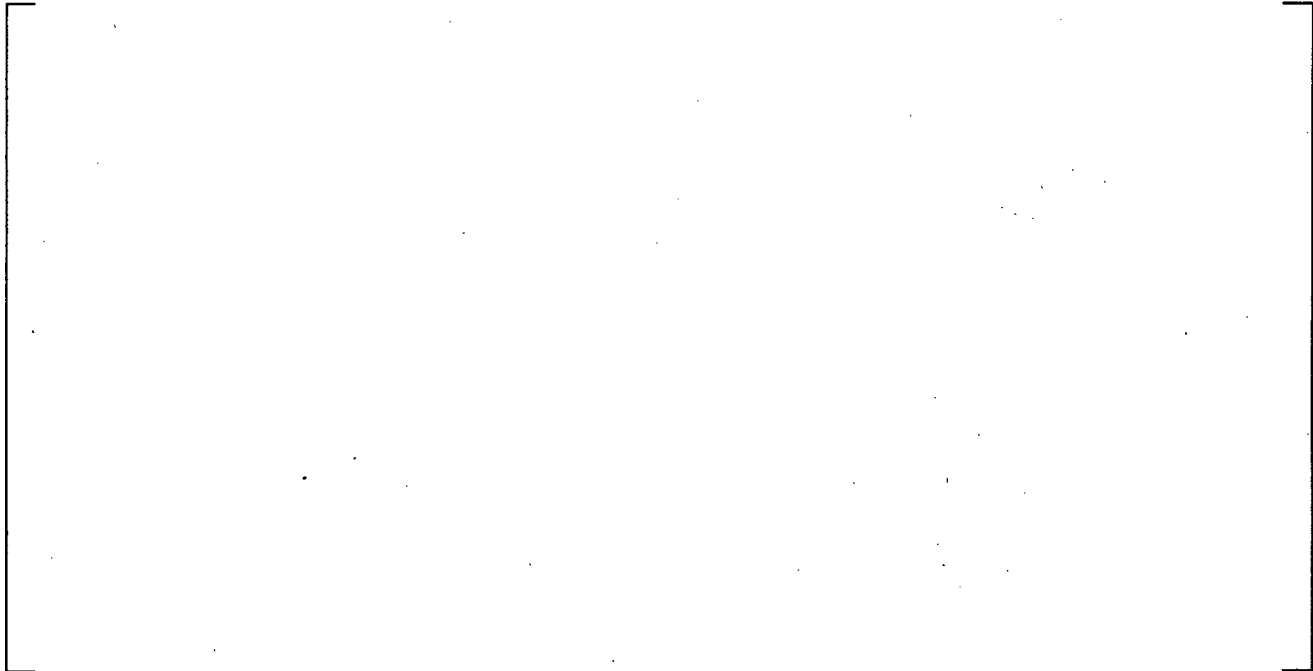


**Figure 21.16.1-6 Calculated Downcomer Differential Pressures**

a,c



**Figure 21.16.1-7 Calculated Upper Plenum Differential Pressures**

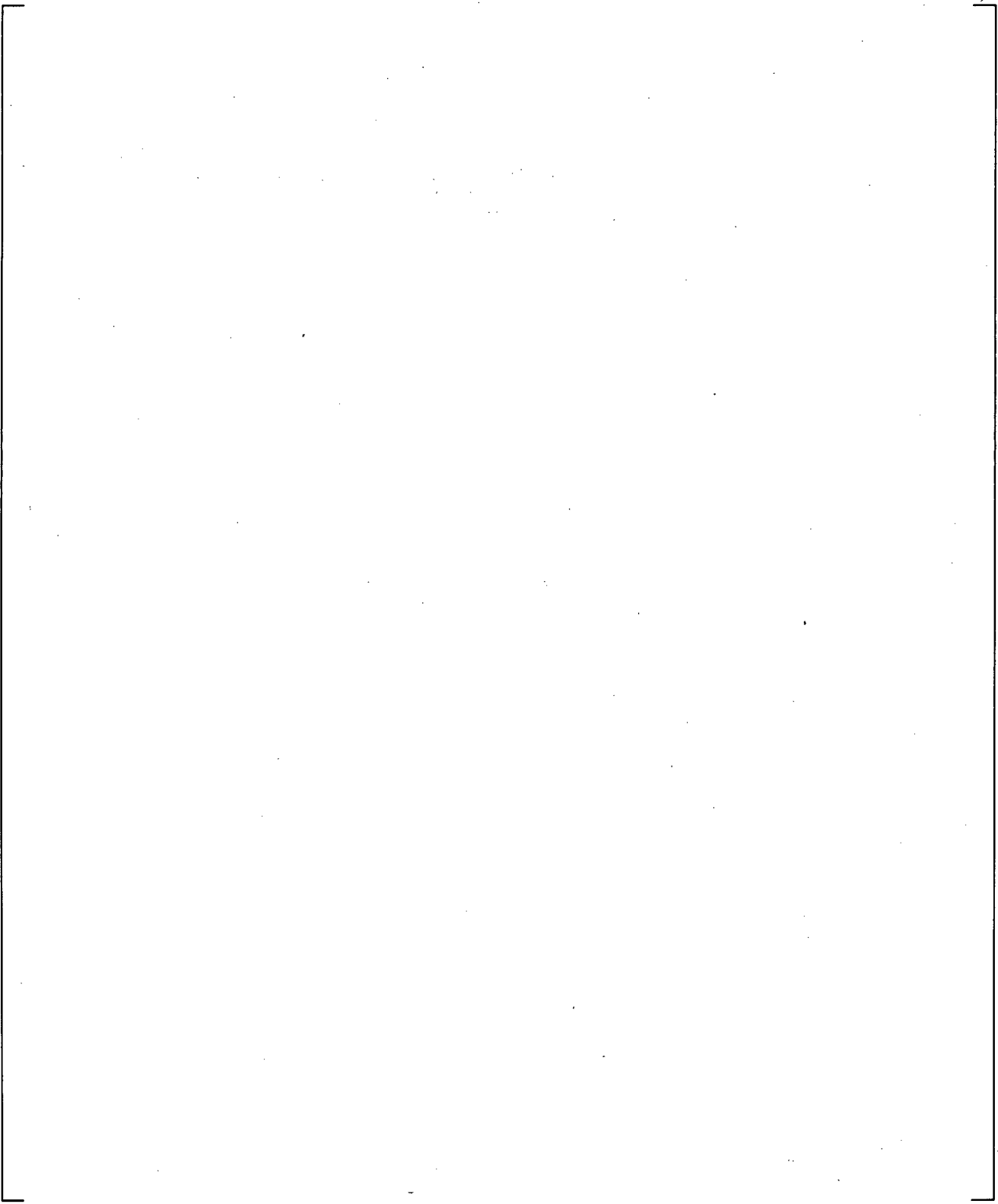


**Figure 21.16.1-8 Calculated Hot Leg Differential Pressures**

a,c



**Figure 21.16.1-9 Calculated Core Differential Pressures**

a,c



**Figure 21.16.1-10 Calculated Peak Cladding Temperatures**

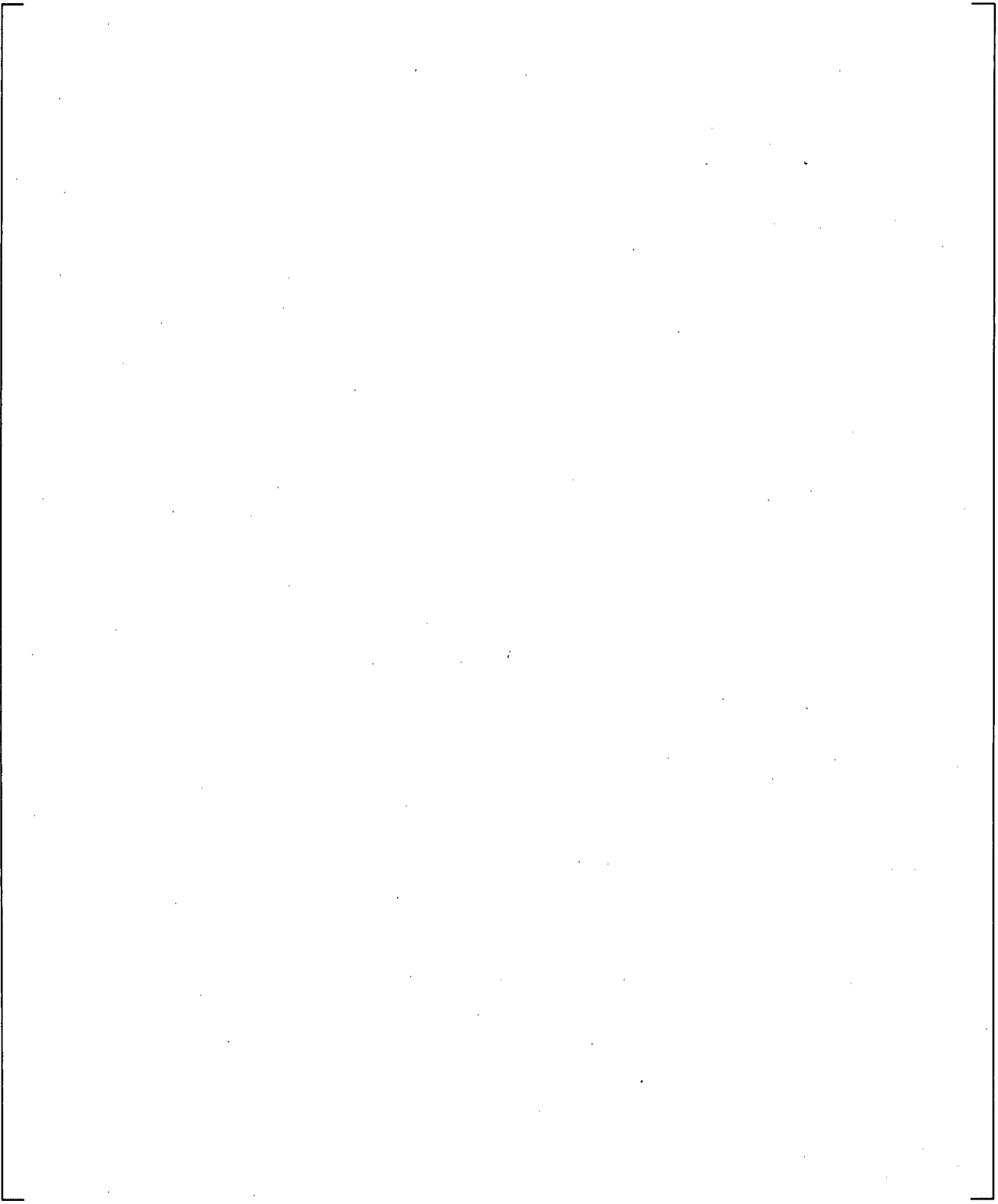


**Figure 21.16.2-1 Calculated Break Flow Rates**

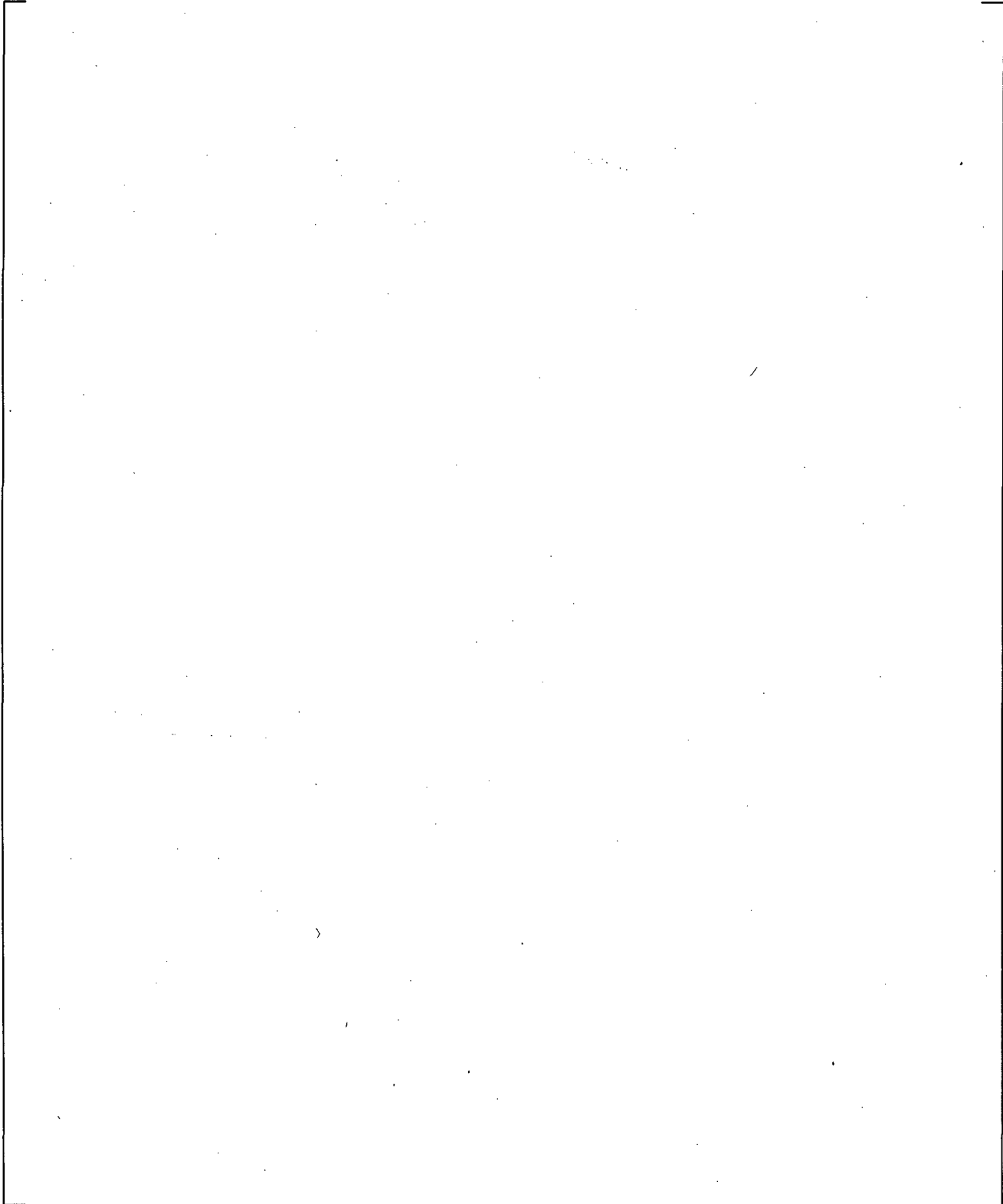


**Figure 21.16.2-2 Calculated Pressurizer and Steam Generator Secondary Pressures**

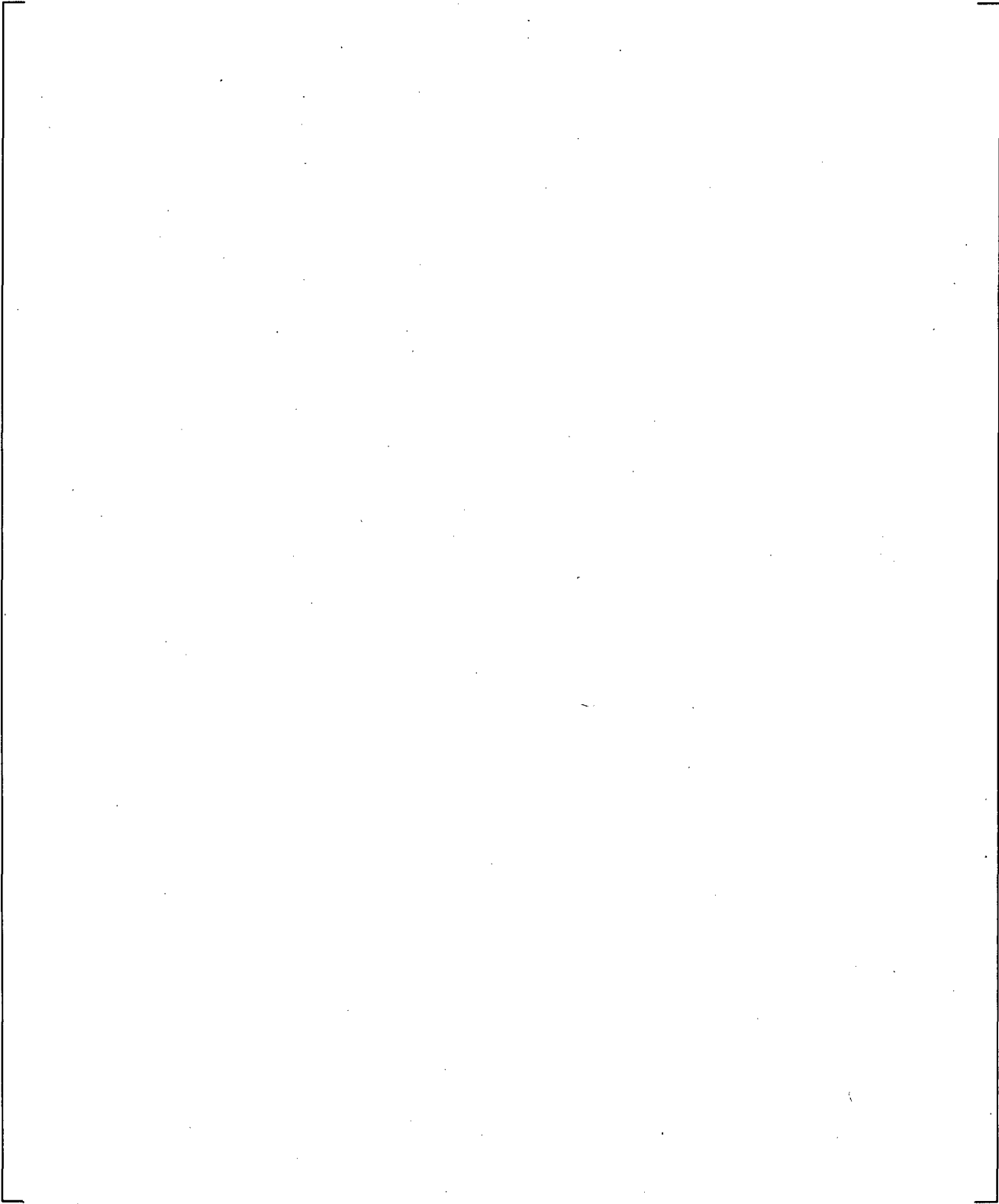


**Figure 21.16.2-3 Calculated Steam Generator U-tube Uphill Side Differential Pressures**

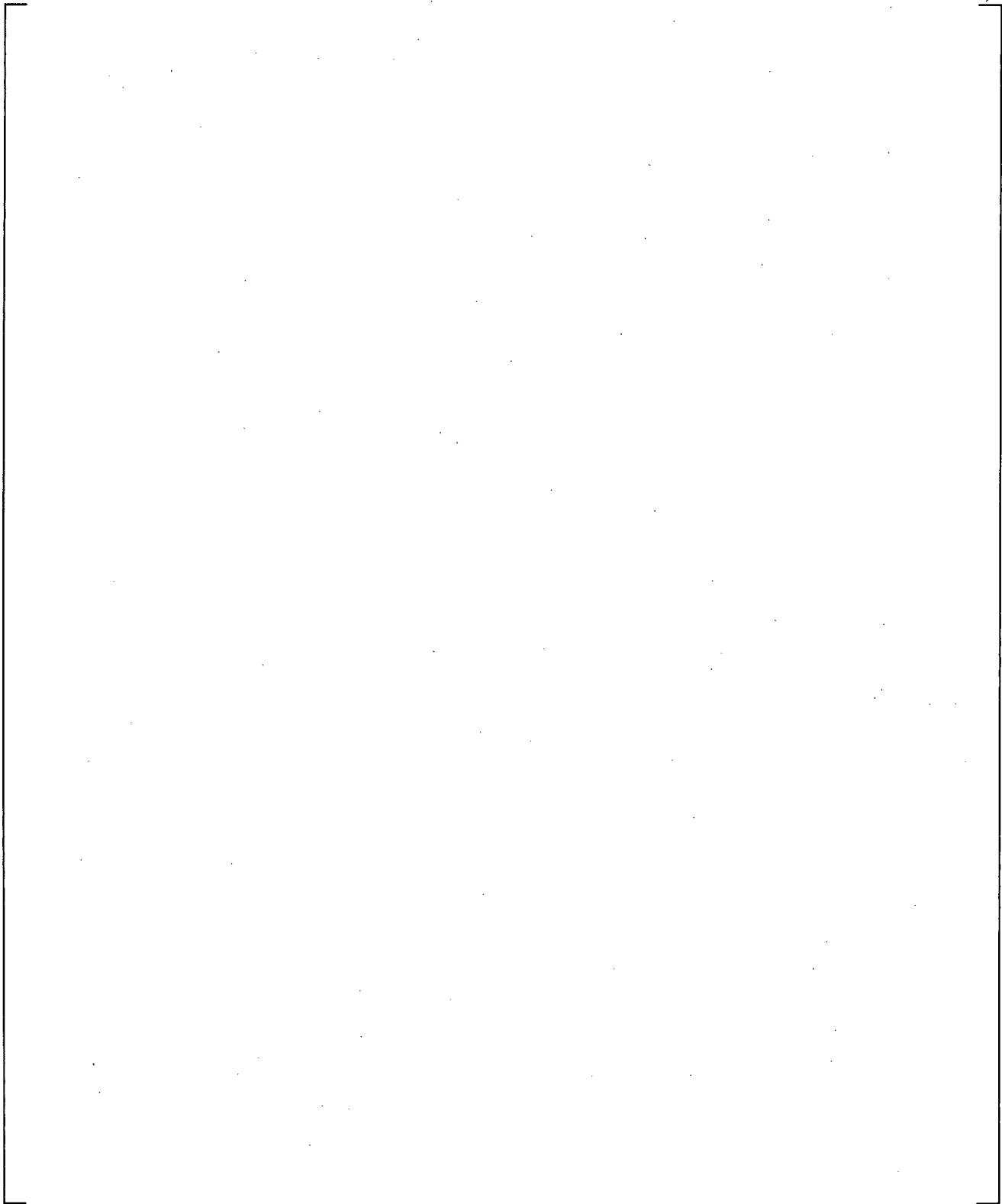


**Figure 21.16.2-4 Calculated Cross-Over Leg A Differential Pressures**

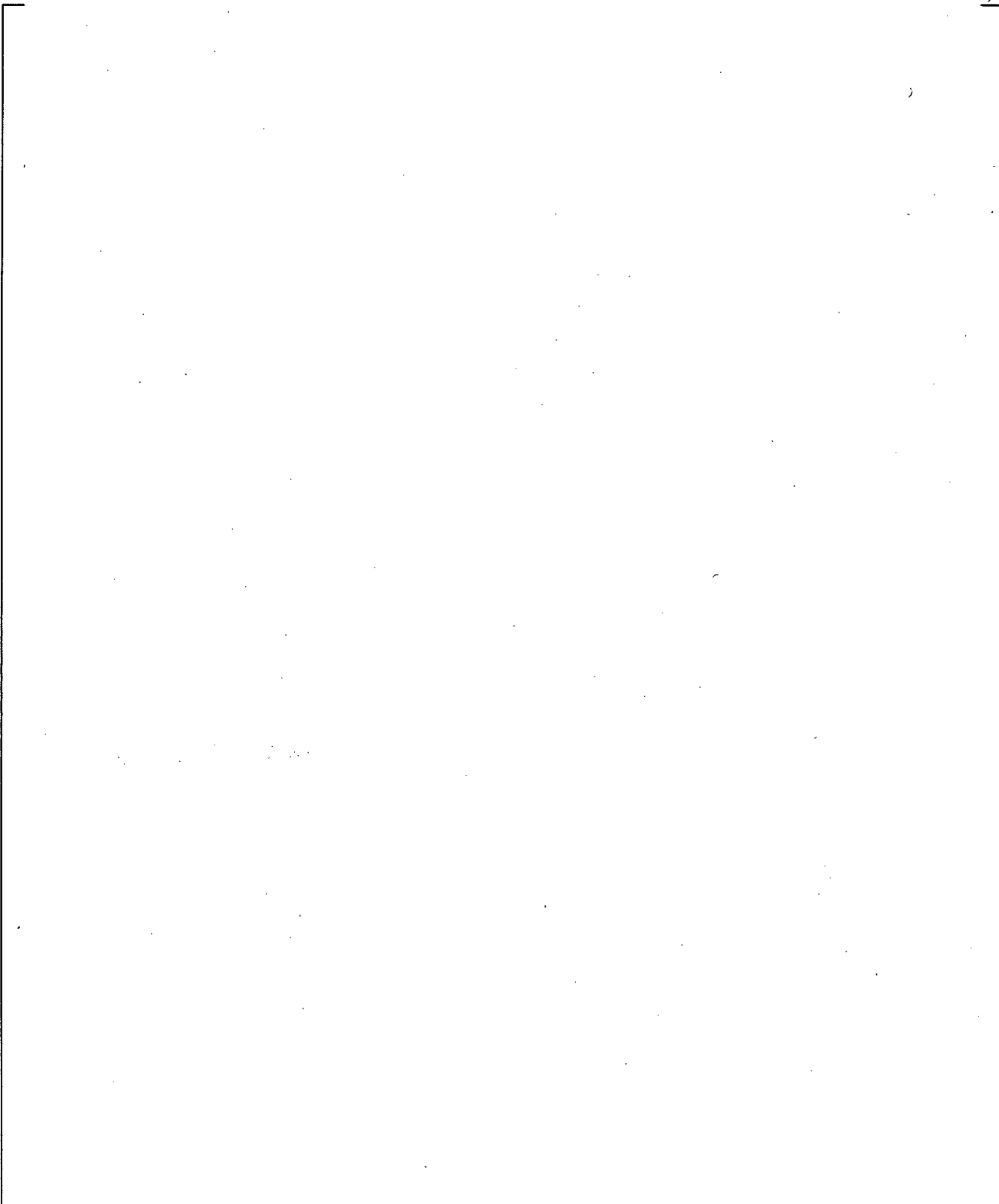


**Figure 21.16.2-5 Calculated Cross-Over Leg B Differential Pressures**

a,c

**Figure 21.16.2-6 Calculated Downcomer Differential Pressures**

a,c

**Figure 21.16.2-7 Calculated Upper Plenum Differential Pressures**

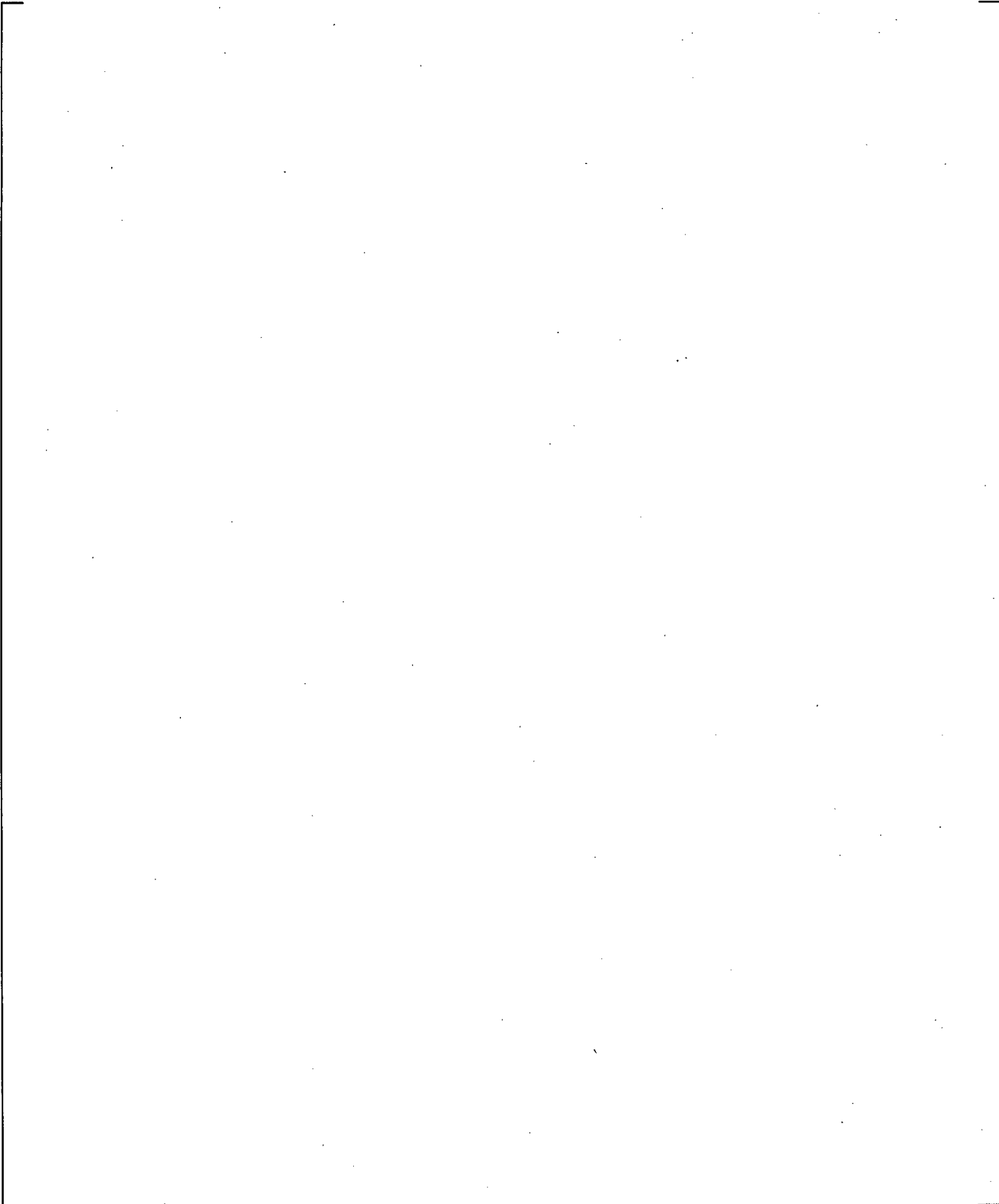


**Figure 21.16.2-8 Calculated Hot Leg Differential Pressures**

a,c



**Figure 21.16.2-9 Calculated Core Differential Pressures**

a,c

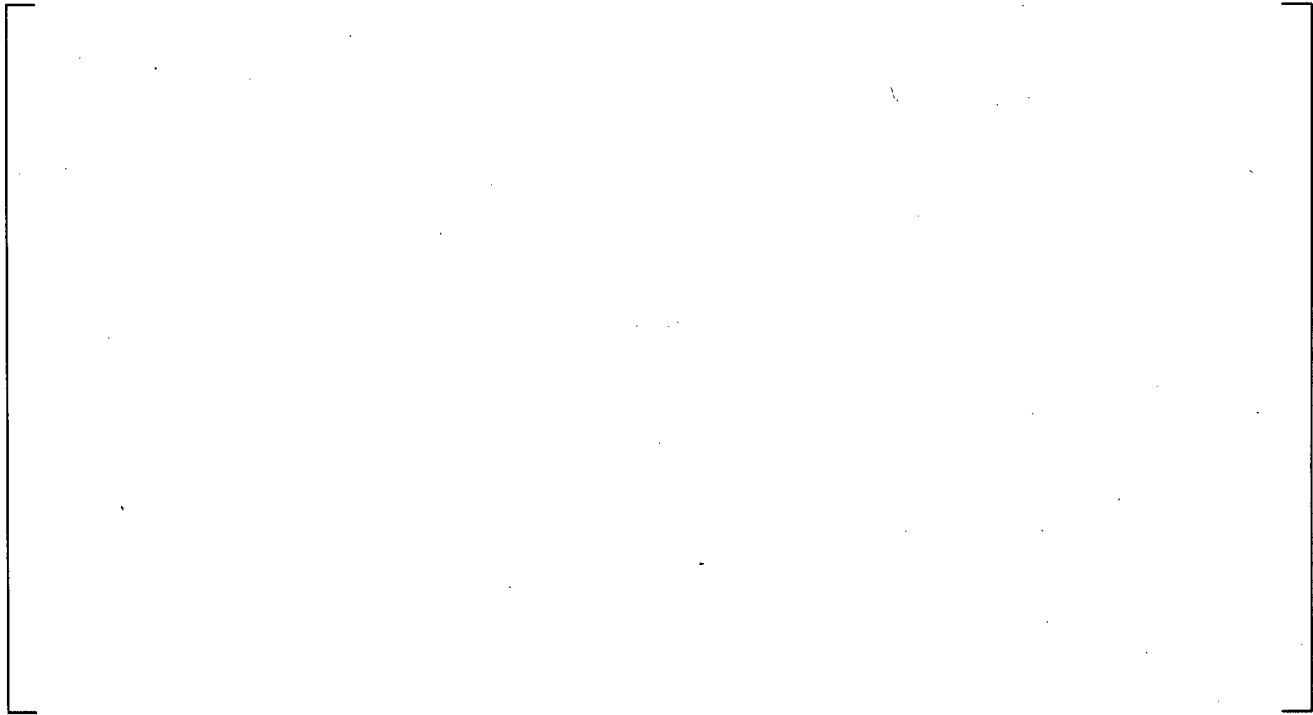


**Figure 21.16.2-10 Calculated Peak Cladding Temperatures**

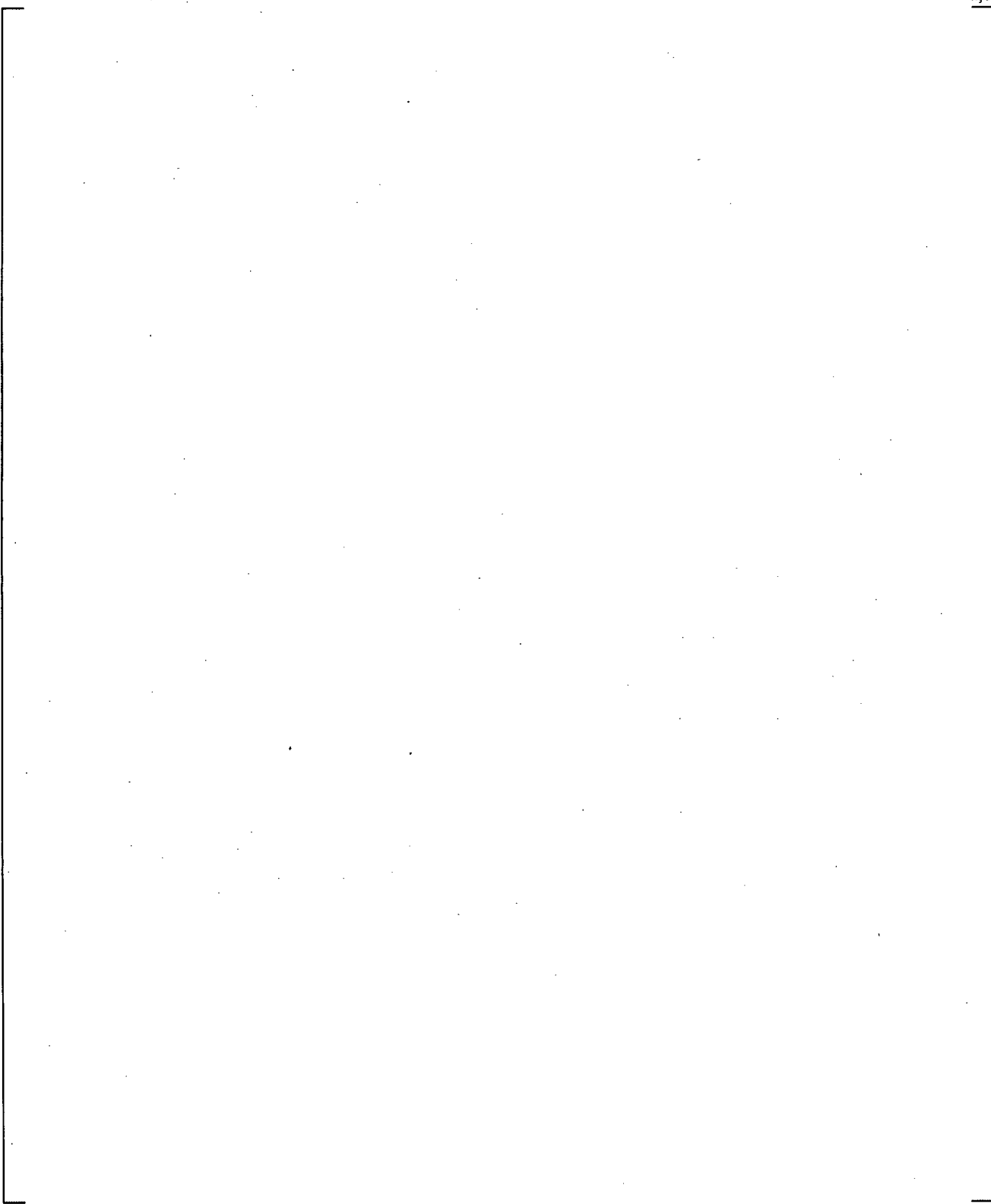


**Figure 21.16.3-1 Calculated Break Flow Rates**

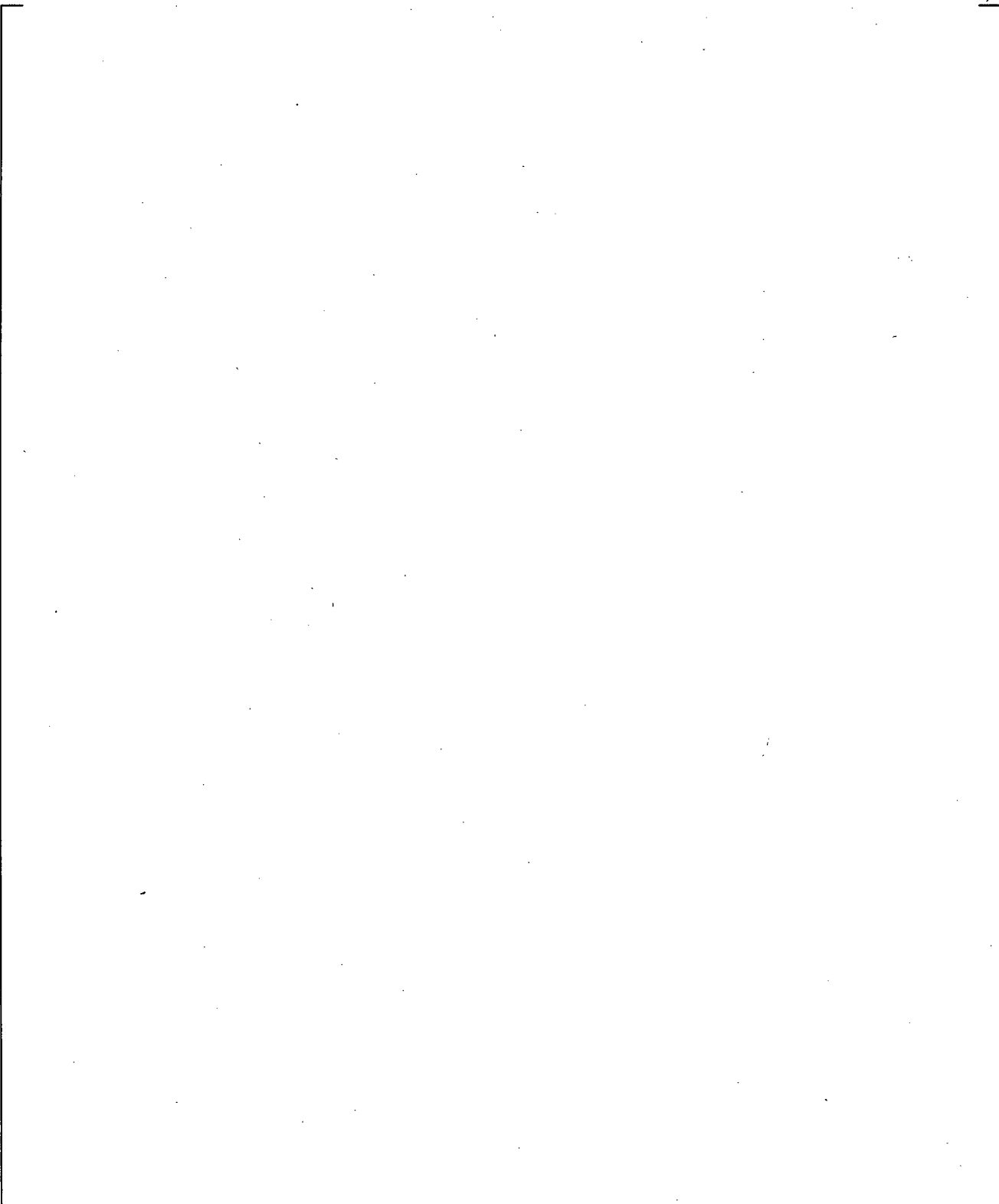


**Figure 21.16.3-2 Calculated Pressurizer and Steam Generator Secondary Pressures**

a,c

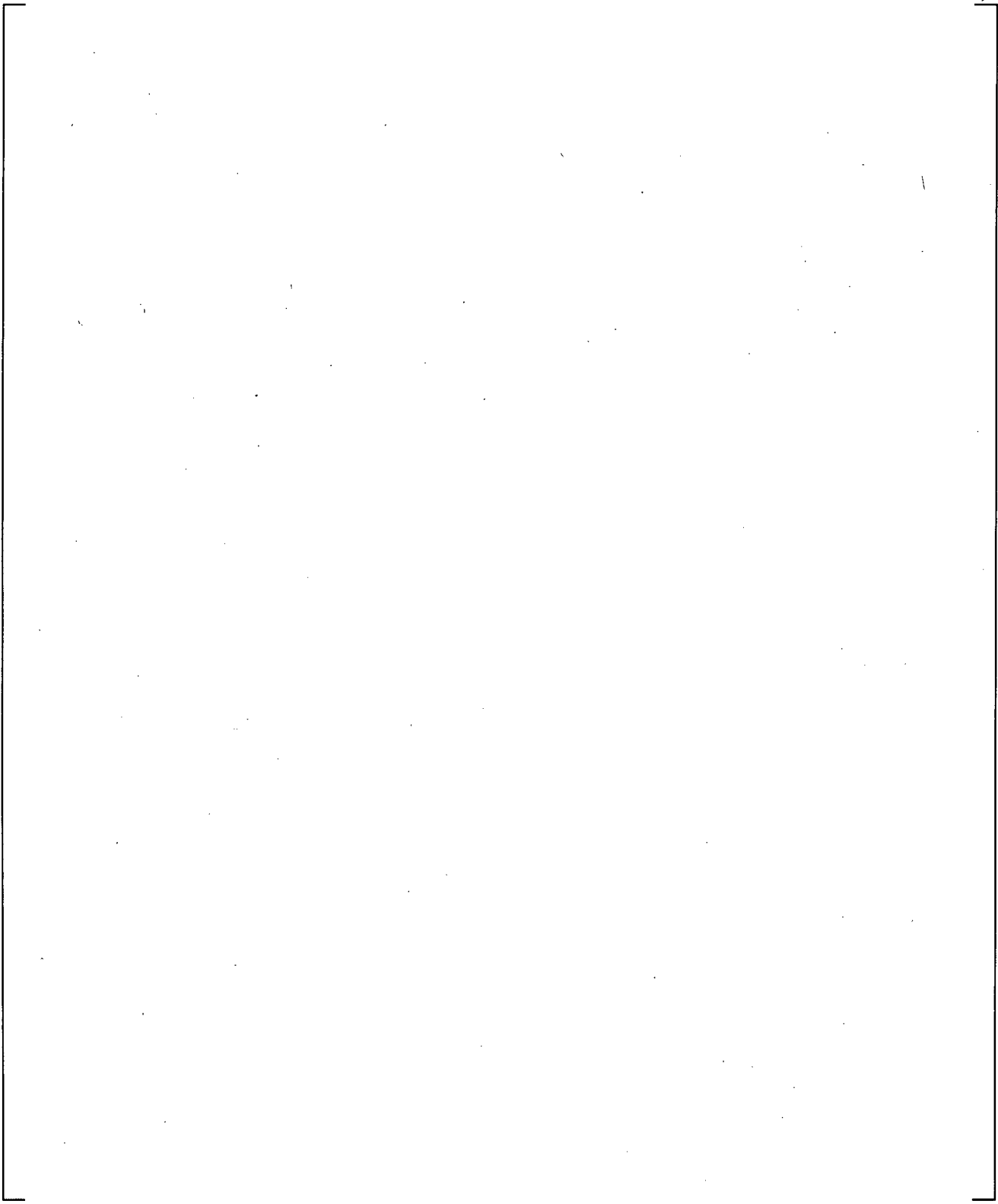


**Figure 21.16.3-3 Calculated Steam Generator U-tube Uphill Side Differential Pressures**

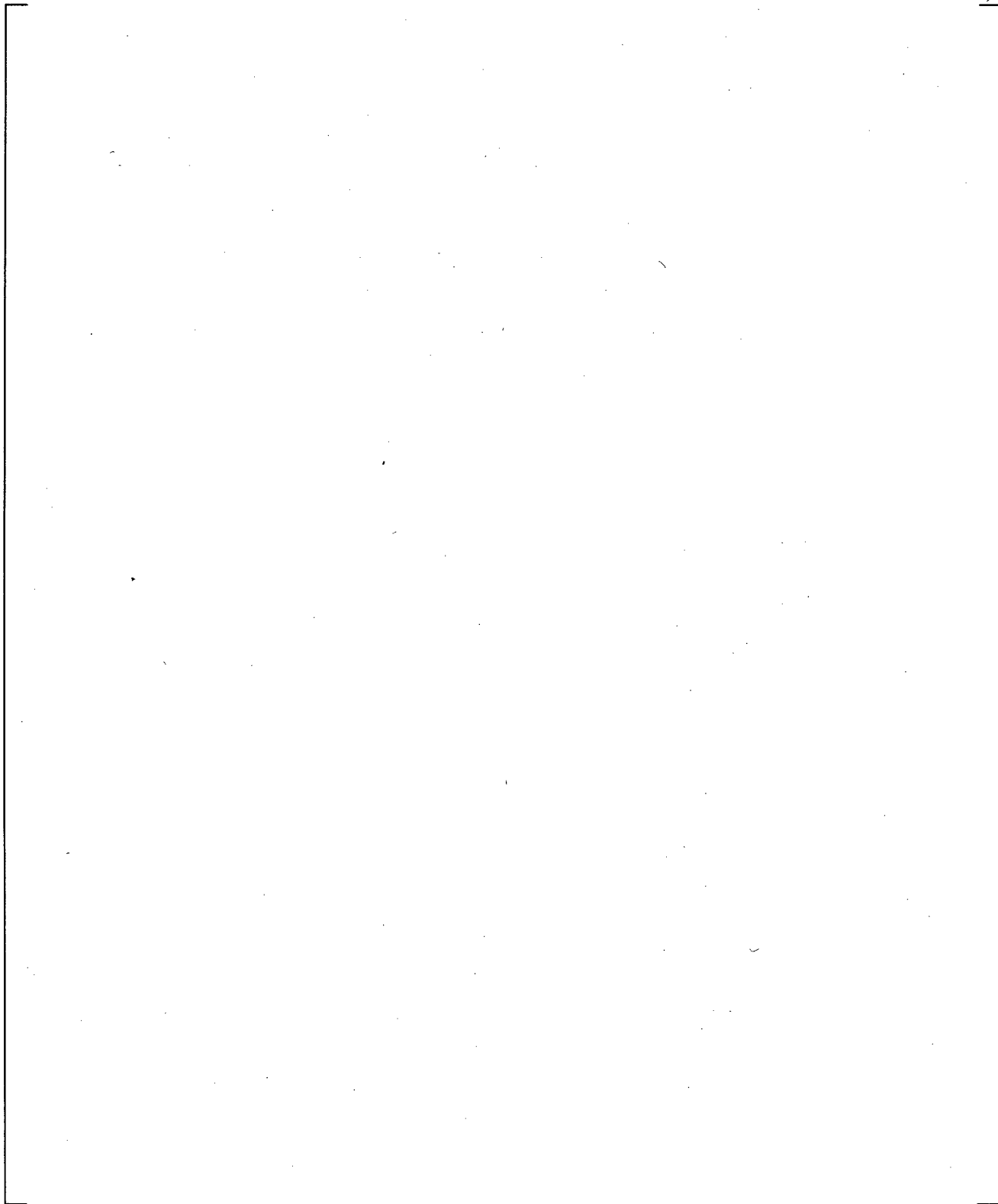


**Figure 21.16.3-4 Calculated Cross-Over Leg A Differential Pressures**

a,c

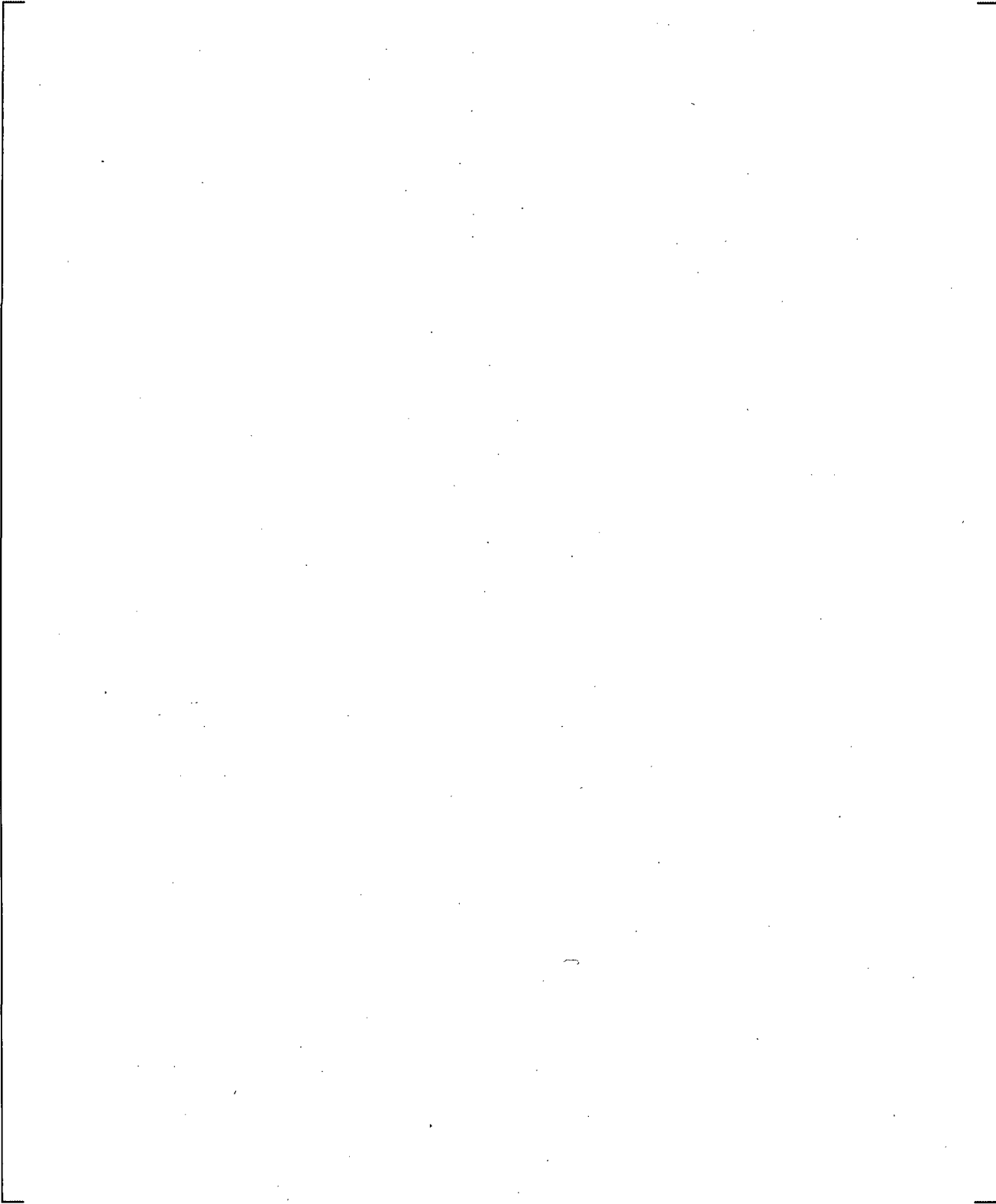


**Figure 21.16.3-5 Calculated Cross-Over Leg B Differential Pressures**

a,c



**Figure 21.16.3-6 Calculated Downcomer Differential Pressures**

a,c



**Figure 21.16.3-7 Calculated Upper Plenum Differential Pressures**

a,c

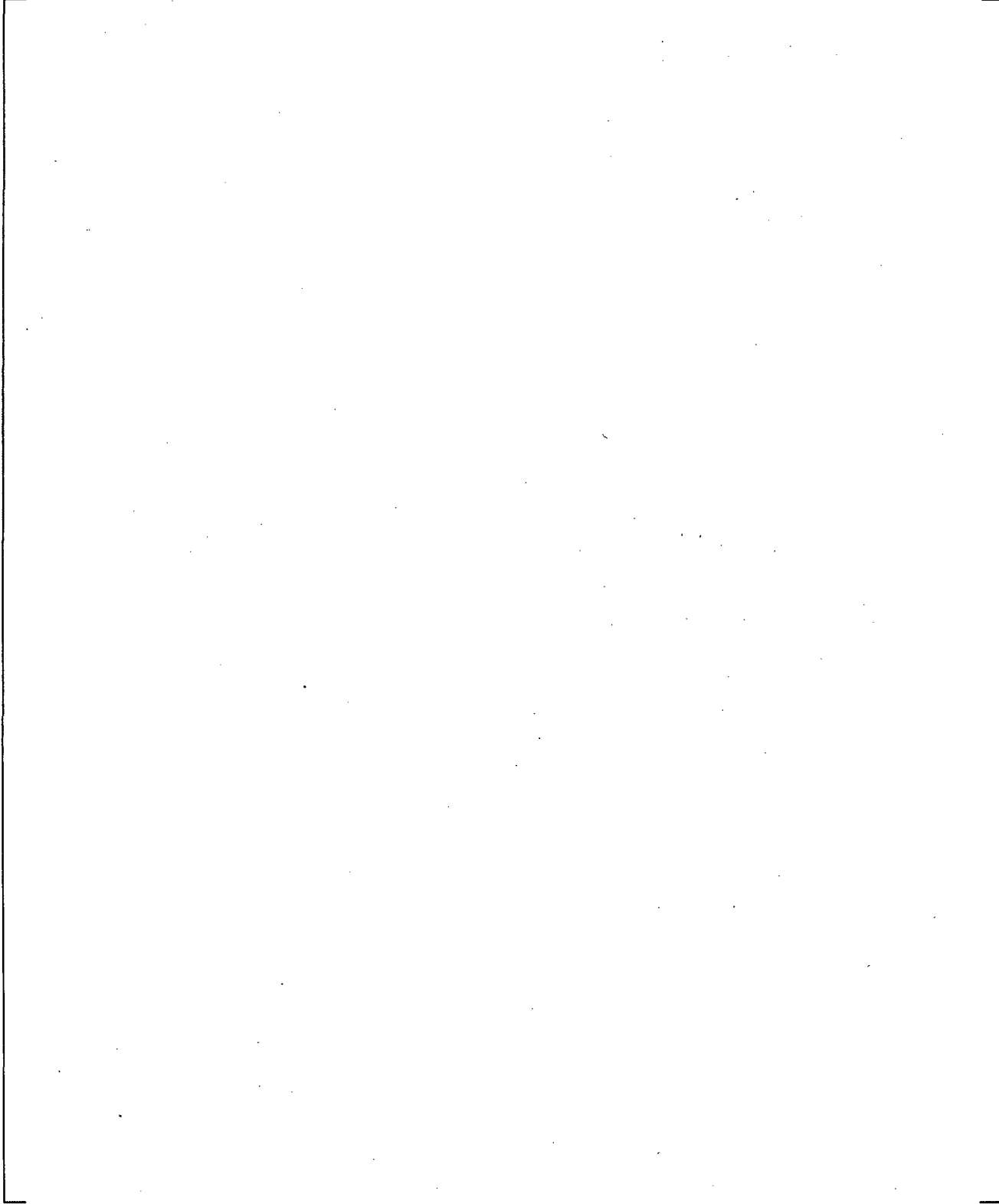


**Figure 21.16.3-8 Calculated Hot Leg Differential Pressures**

a,c

**Figure 21.16.3-9 Calculated Core Differential Pressures**

a,c

**Figure 21.16.3-10 Calculated Peak Cladding Temperatures**

a,c

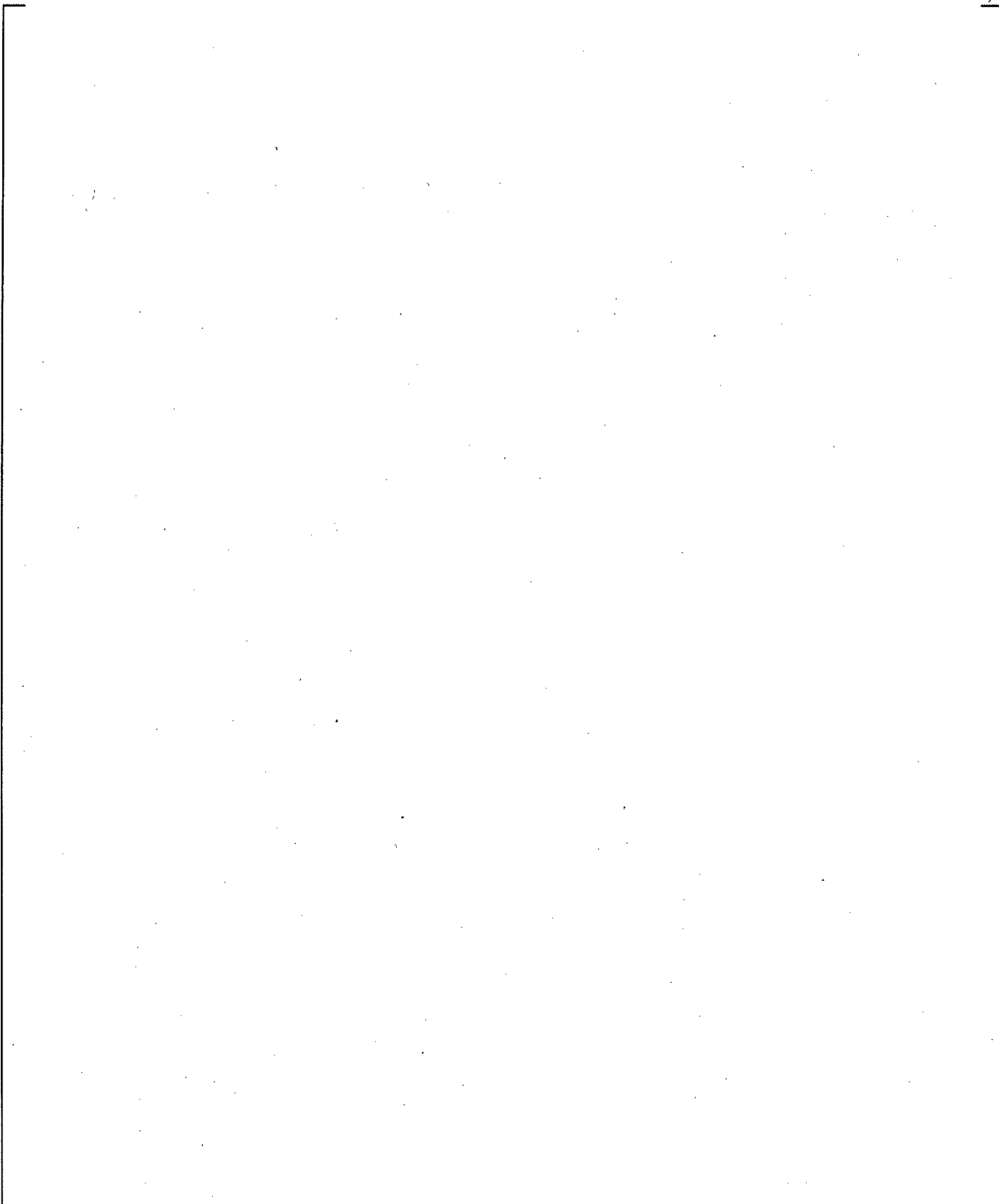


**Figure 21.17-1 Cold Leg Void Fractions at the SI Injection Nodes**

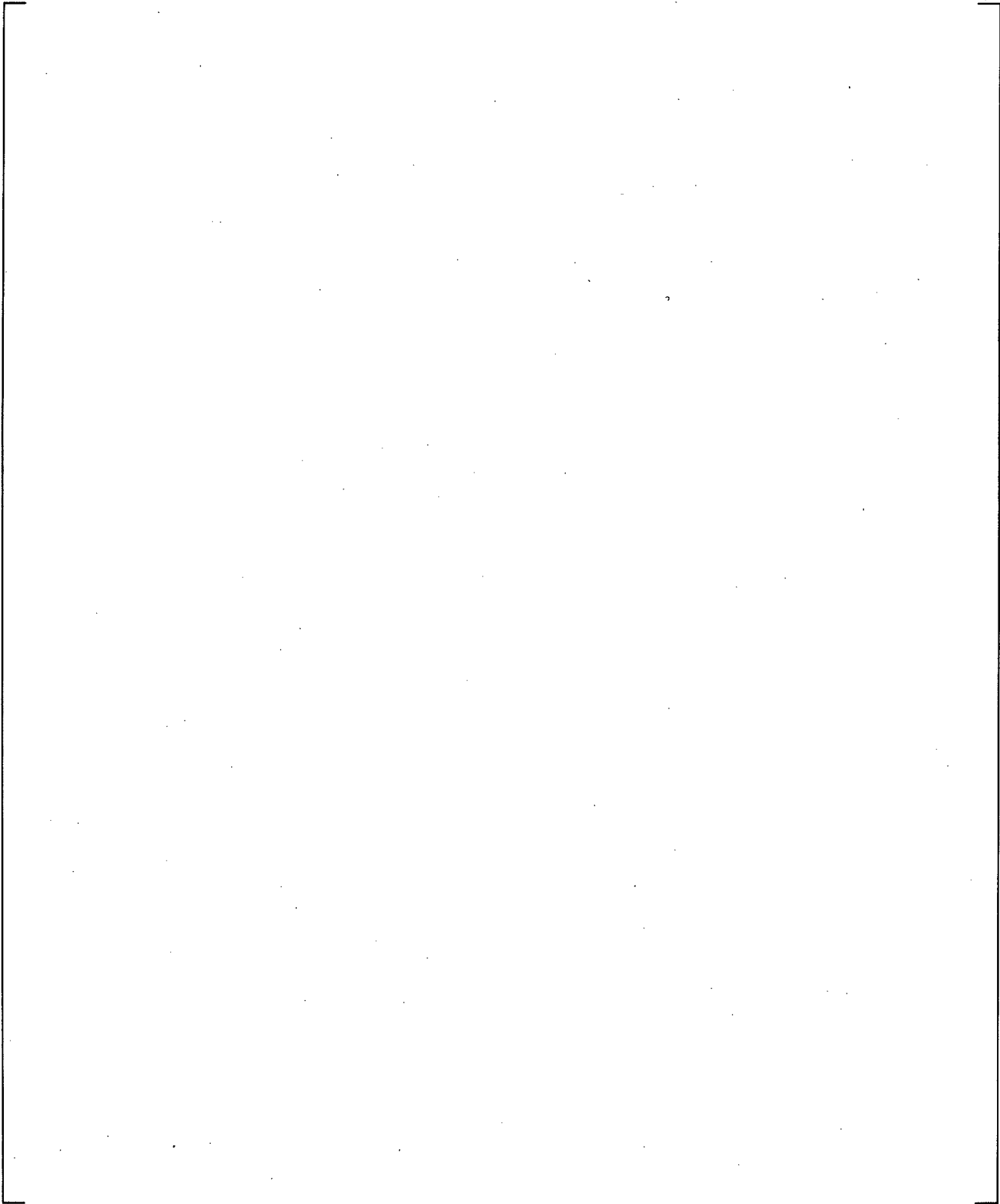


**Figure 21.17-2 Mixture Flow at the Broken Cold Leg Nozzle (interface with the vessel)**

Note: Negative is flow from the vessel into the cold leg.

**Figure 21.17-3 Total SI Condensation Heat Rate at Cold Leg Injection Node in CLA**

Note: With COSI model turned off, CSIQTOT is not calculated in the SI injection node of the broken cold leg.

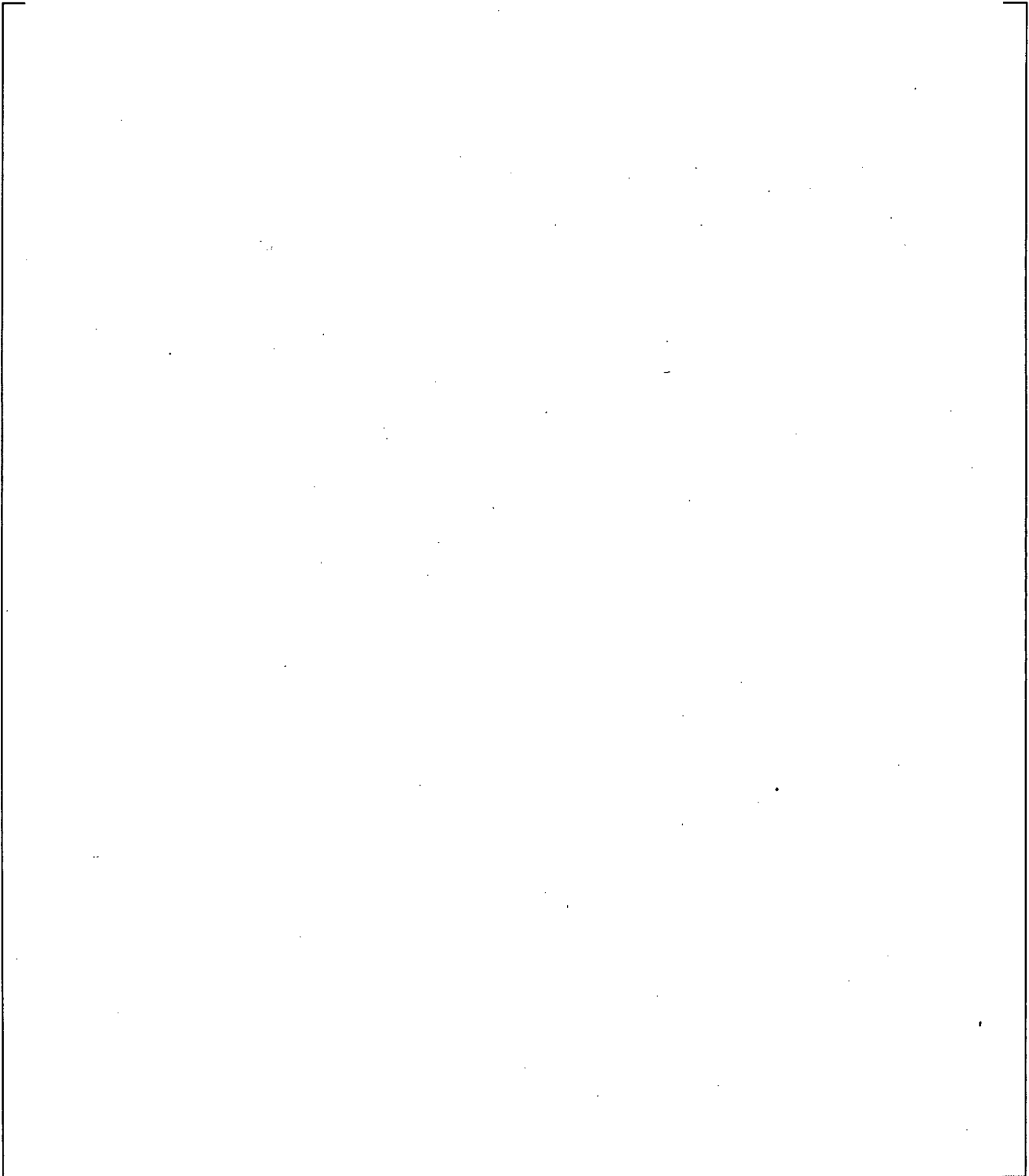


**Figure 21.17-4 Cold Leg Fluid Temperatures at SI Injection Nodes**

Note: The temperature of the pumped SI delivered into the cold legs is ~310K (98 F)

a,c

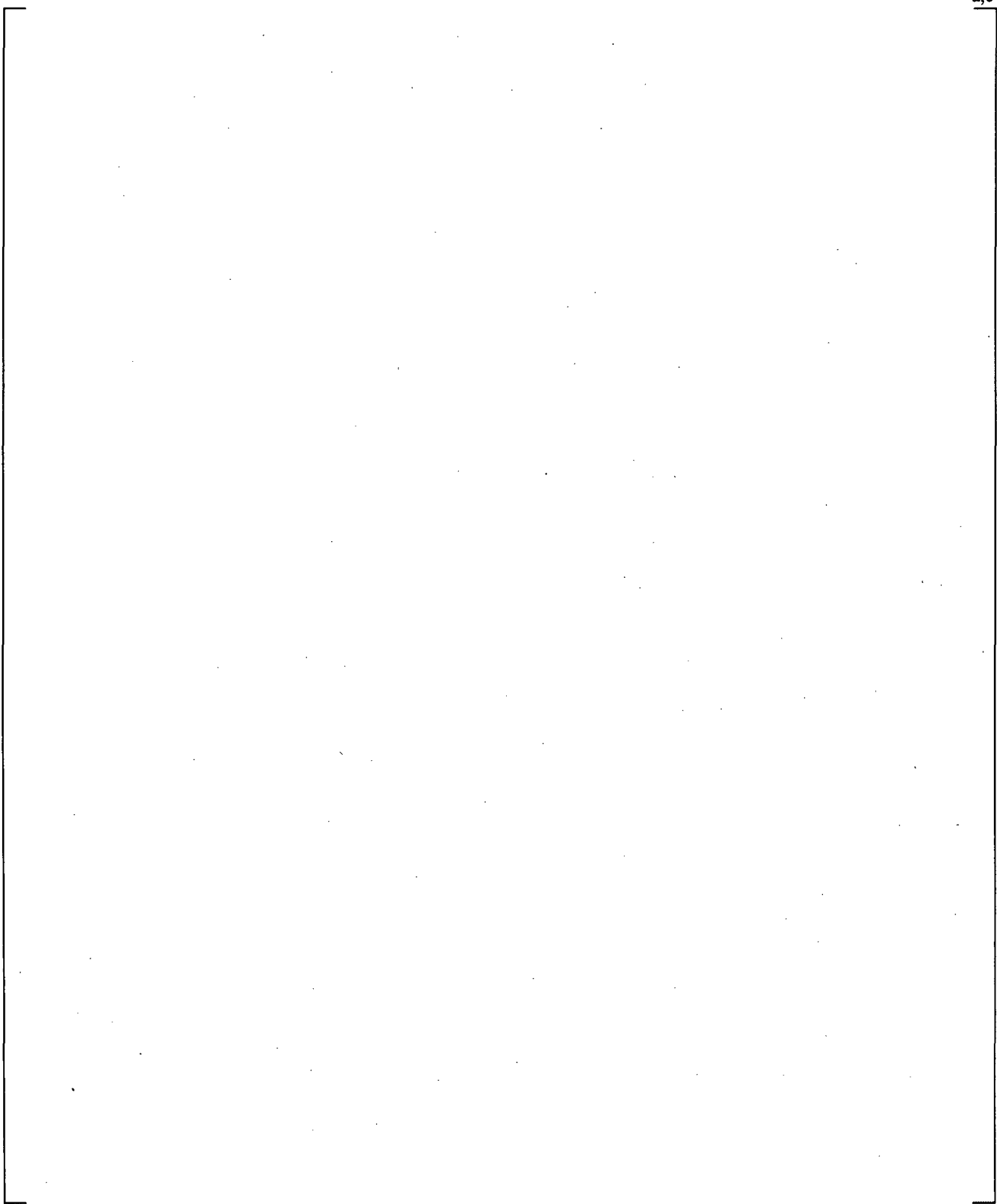


**Figure 21.17-5 Cold Leg Pressures at SI Injection Nodes**

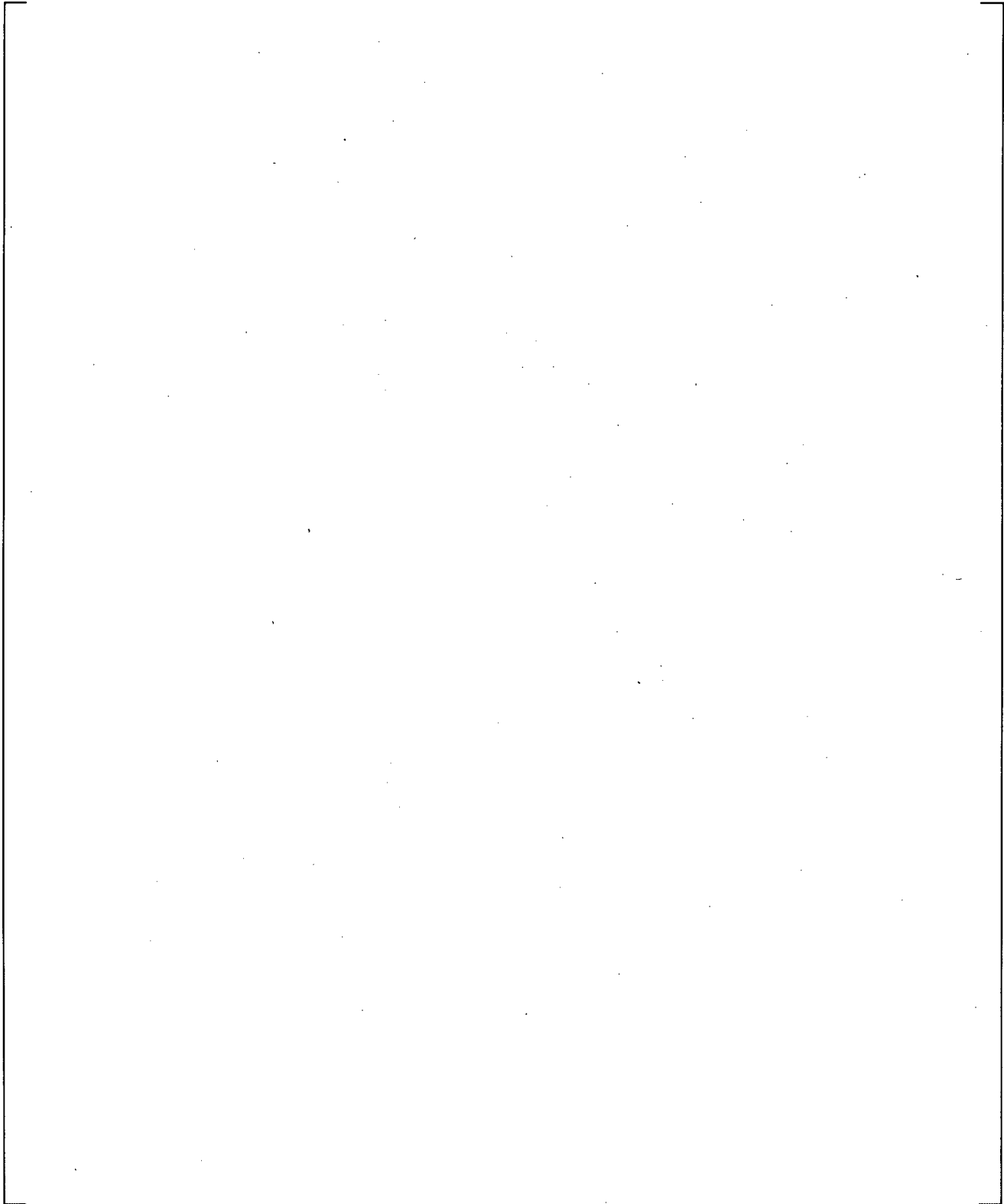


**Figure 21.17-6 Accumulator Injection Flows**

a,c



**Figure 21.17-7 Broken Cold Leg Void at Break Off-take Node**

a,c



**Figure 21.17-8 Break Void Fractions**

a,c

**Figure 21.17-9 Fluid Temperatures at the Break**

a,c

**Figure 21.17-10 Break Flow Rates**

a,c

**Figure 21.17-11 Integrated Break Flows**

a,c

**Figure 21.17-12 Integrated Break Flow Difference (KCOSI\_low-KCOSI\_high)**

a,c

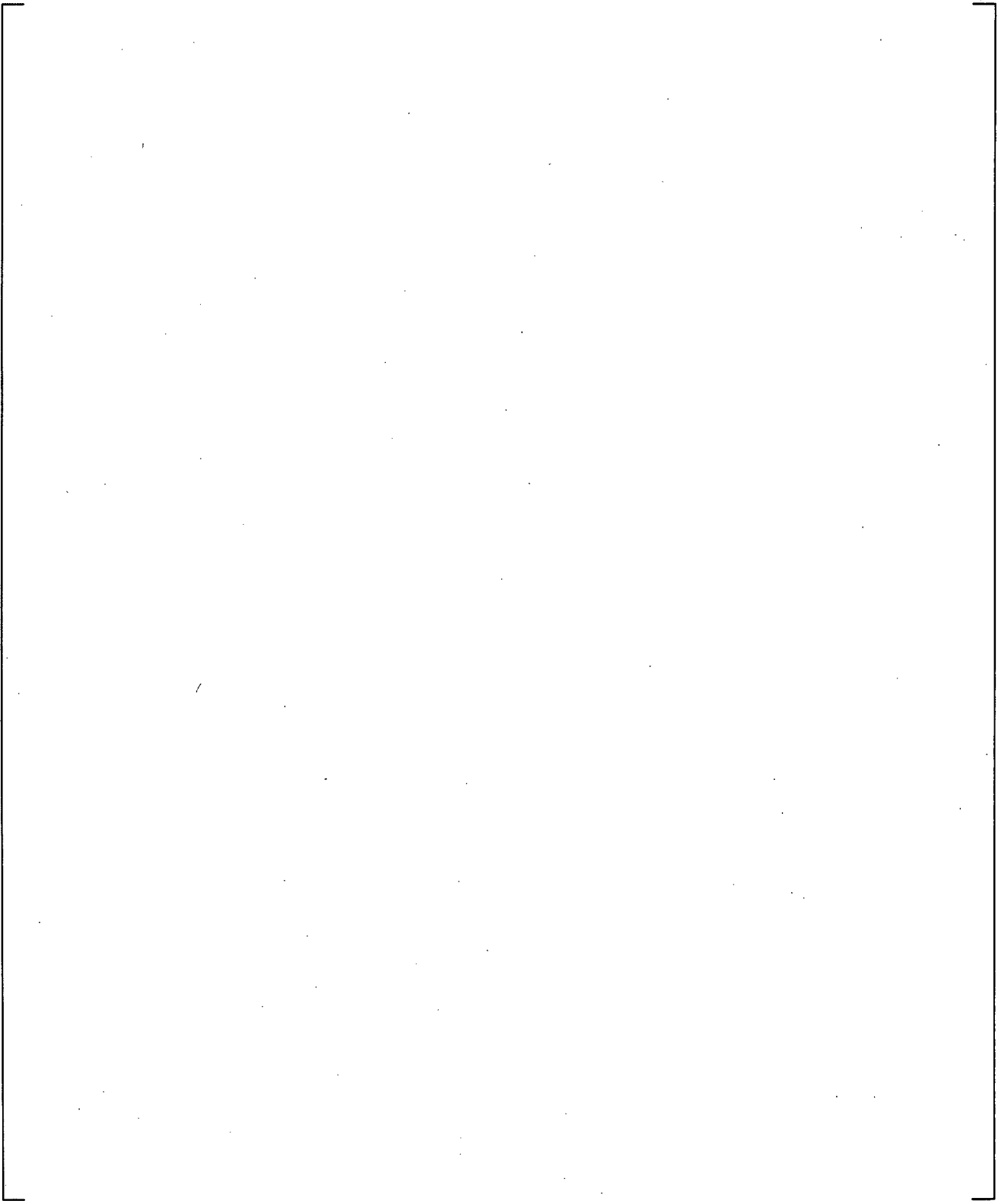


**Figure 21.18-1 Calculated Primary and Steam Generator Secondary Pressures**

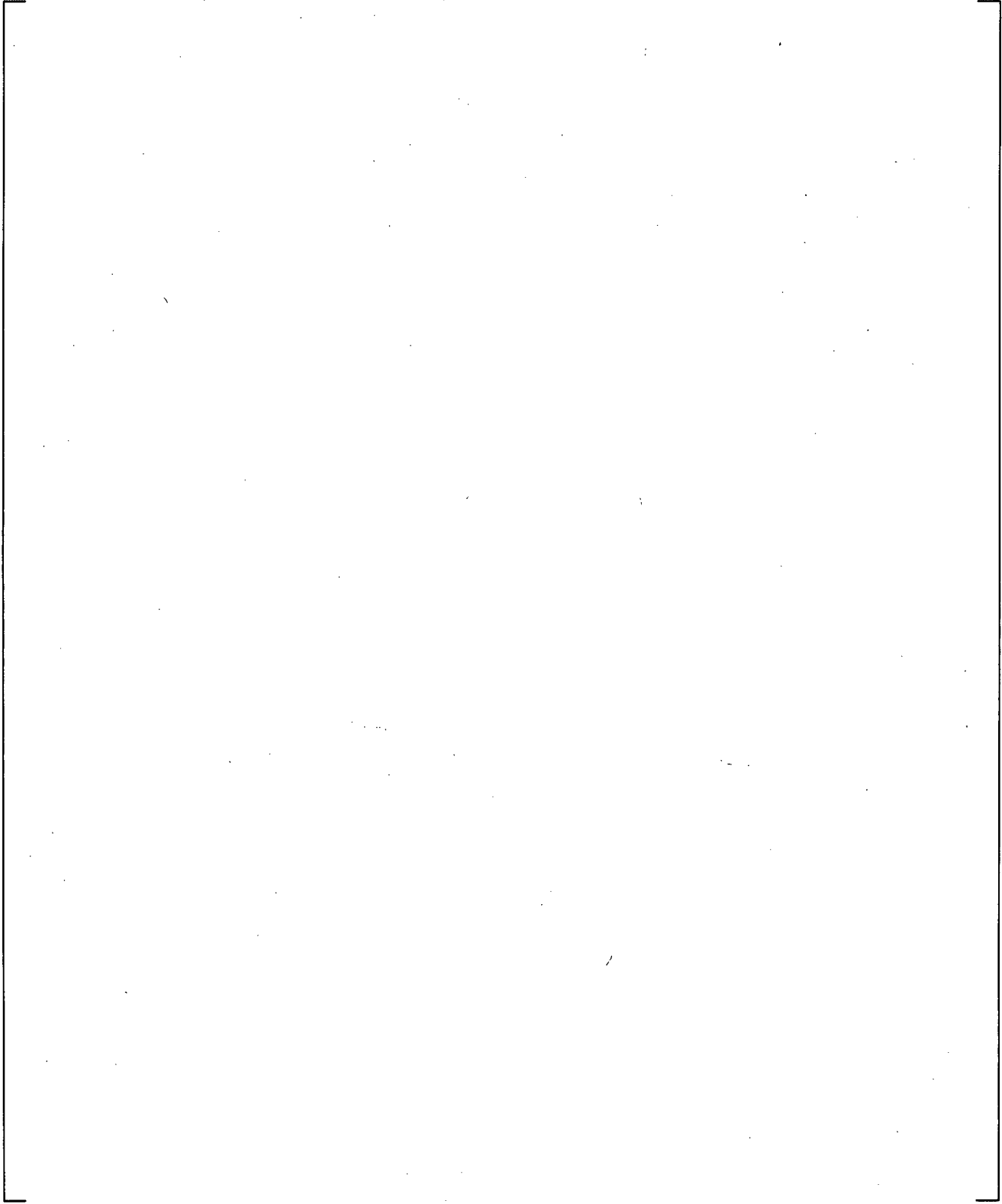


**Figure 21.18-2 Calculated Break Flows**

a,c

v

**Figure 21.18-3 Calculated Draining of Steam Generator U-tubes Uphill Side**

a,c

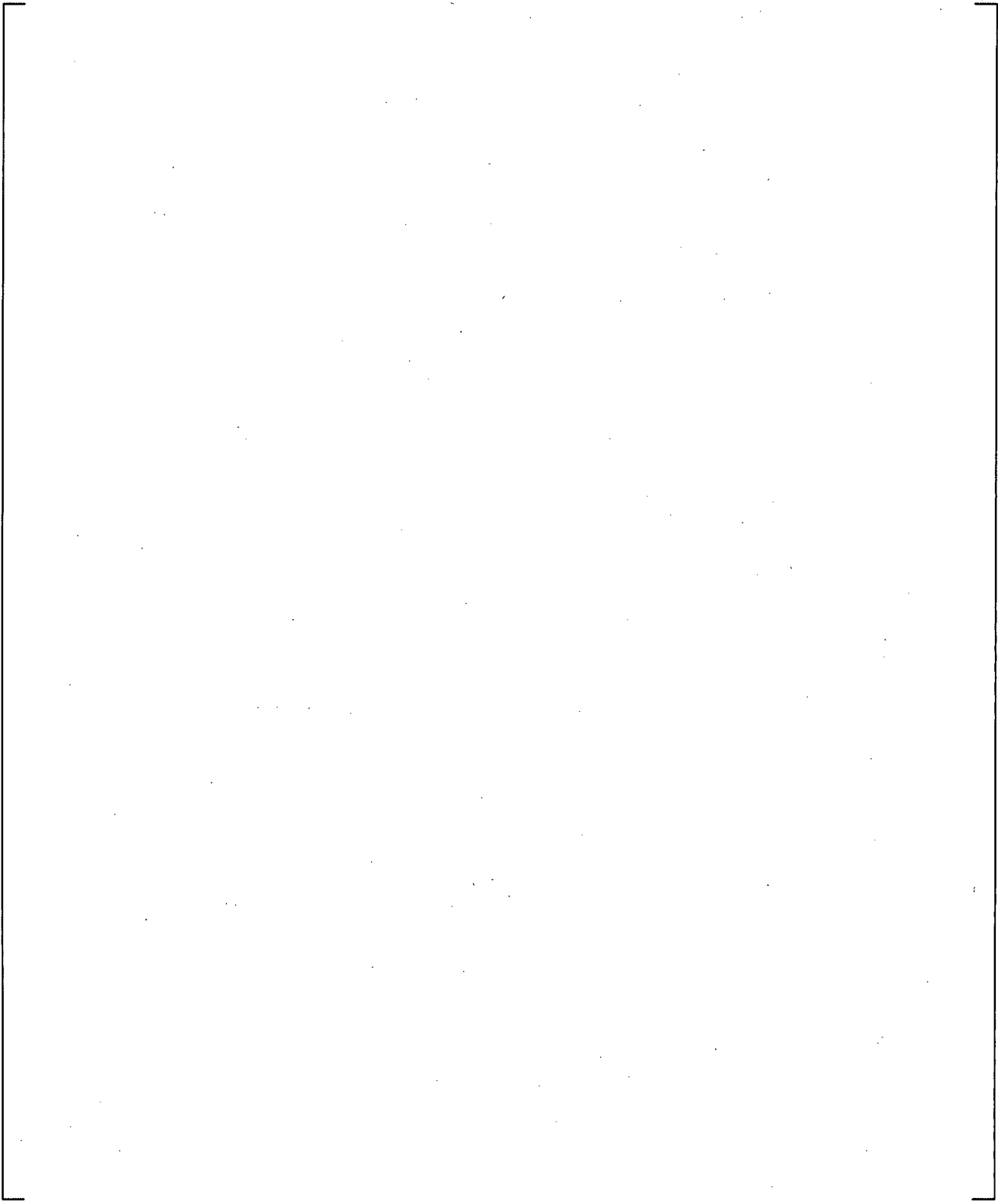


**Figure 21.18-4 Calculated Upper Plenum Differential Pressures**

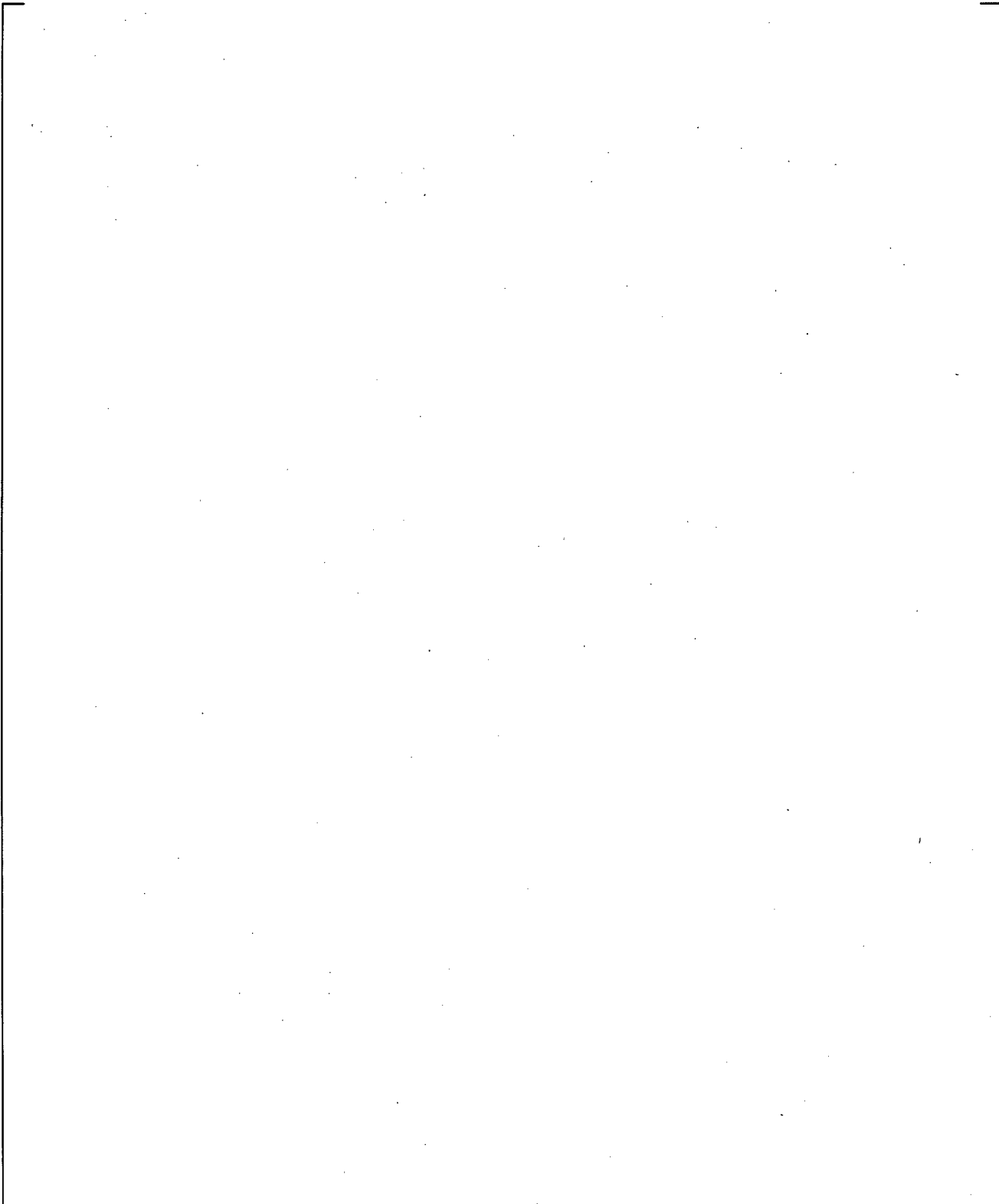


**Figure 21.18-5 Calculated Upper Plenum to Steam Generator Inlet Differential Pressures**

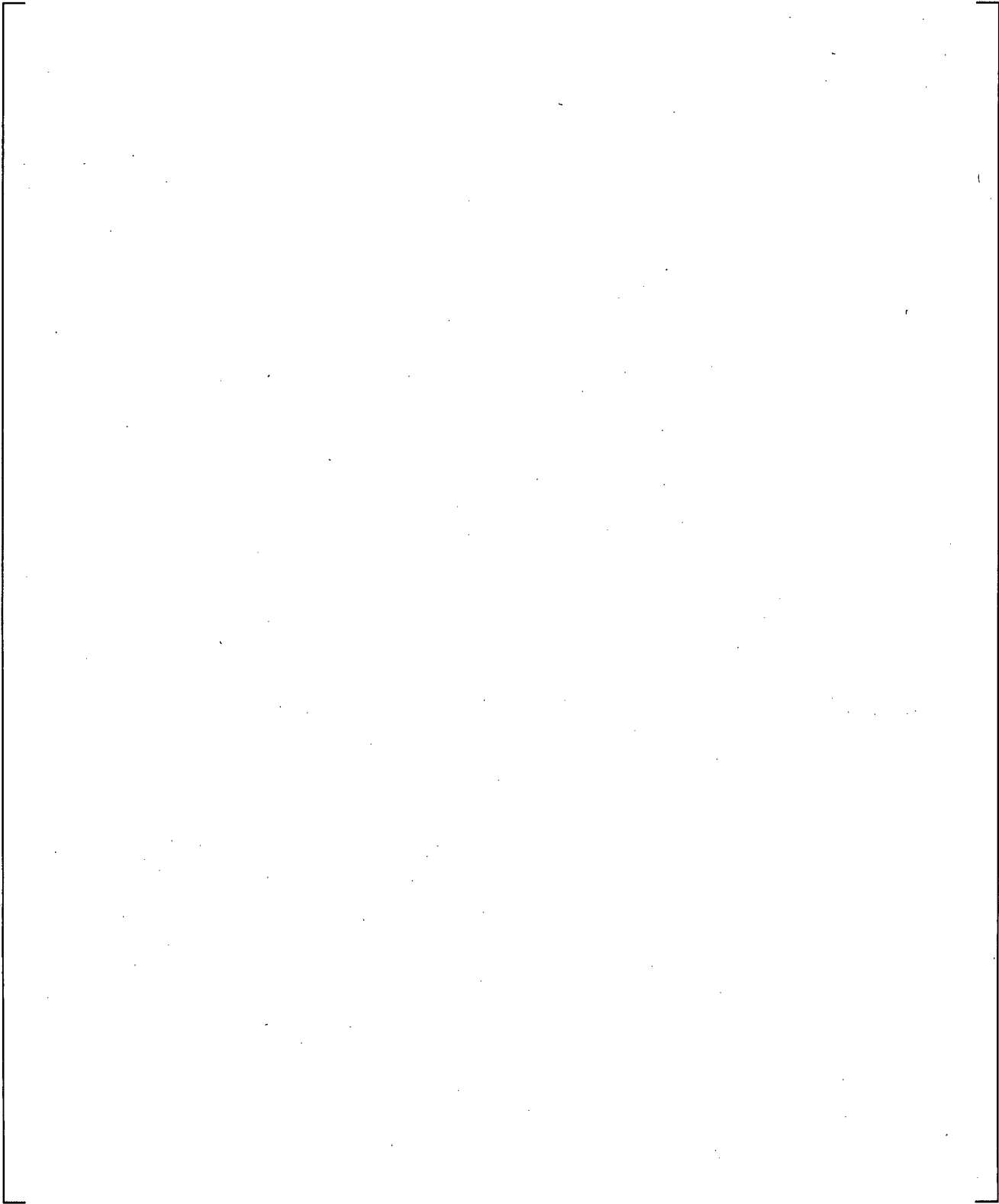


**Figure 21.18-6 Calculated Cross-Over Leg Differential Pressures (Bottom-to-Pump Inlet)**

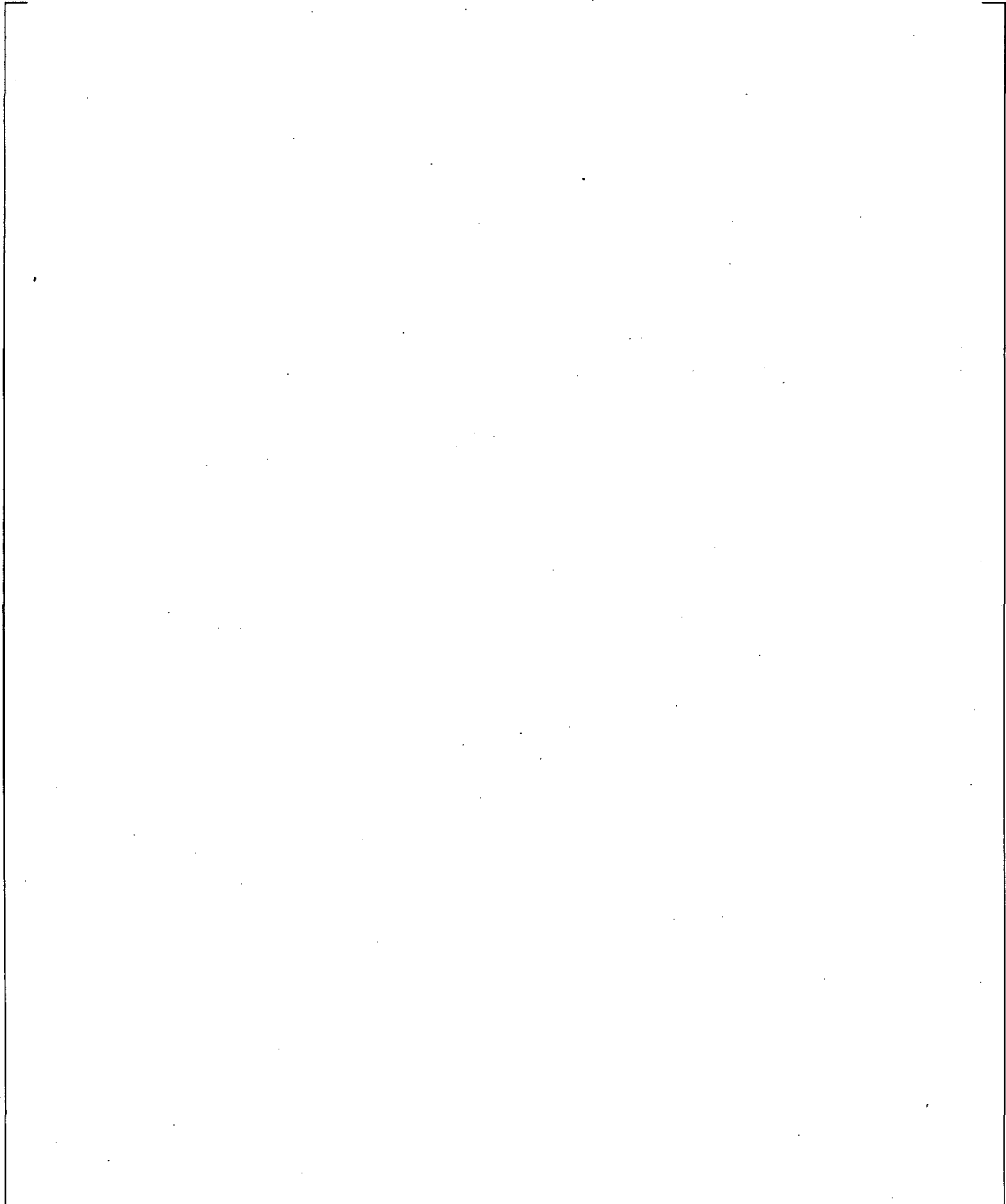


**Figure 21.18-7 Calculated Loop Flow Rates**

a,c



**Figure 21.18-8 Calculated Core Differential Pressures**

a,c



**Figure 21.18-9 Calculated Peak Cladding Temperatures**

## 22 LOSS-OF-FLUID TEST (LOFT) INTEGRAL TEST

### 22.1 INTRODUCTION

The LOFT loss-of-coolant experiments have been widely used for validation of PWR computer models due to the relatively large scale of the facility (1:55 volume scaling of a commercial four-loop PWR) and the use of a nuclear core designed to have the same physical, chemical, and metallurgical properties as a PWR core (Reeder, 1978). The large scale of the facility enables multidimensional effects which allow assessment of the ability of the code to predict these effects. Also, because LOFT is the only integral facility to use a nuclear core, the experiments are considered to be an essential part of the validation package for any PWR computer model.

The LOFT facility is designed to provide thermal-hydraulic data representative of a large rupture of a main coolant pipe. A large amount of thermal and hydraulic data is available from the tests performed on the LOFT facility which allow the assessment of the key processes in a postulated LOCA event covering a full spectrum (or range) of break sizes from small to large breaks. As such, LOFT represents a unique set of tests, which can be used to assess the performance of WCOBRA/TRAC-TF2 in a simulation of LOCA over a wide spectrum of pipe break sizes.

The LOFT facility contains a number of atypicalities relative to a large-scale PWR for large and small break LOCA simulations. Nevertheless, the facility remains a valuable benchmark for model assessment, provided the atypicalities are recognized and do not overshadow the thermal-hydraulic behavior of interest. In general, LOFT fluid volumes were scaled according to the ratio of LOFT core power to PWR core power of a large plant. If practical, flow areas were scaled by the same ratio. A more detailed LOFT scaling discussion is provided in Section 22.2.2.

Four LOFT large break tests were simulated with WCOBRA/TRAC-TF2: L2-2, L2-3, L2-5, and LB-1. Tests L2-2 (McCormick, 1979) and L2-3 (Prassinis, 1979) were low and intermediate power tests in which the reactor coolant pumps were allowed to continue operating under the inertia of the flywheels. Tests L2-5 (Bayless, 1982) and LB-1 (Adams, 1984) were intermediate and high power tests in which the pumps were tripped and the pump flywheels disconnected. These four experiments are used to assess the code's ability to predict the following quantities:

1. Reactor power decay
2. ECC bypass
3. Reactor coolant pump behavior
4. Break flow rate
5. Fuel rod cladding temperature
6. Core and loop flow distribution

To complete the assessment across the break spectrum, the WCOBRA/TRAC-TF2 simulations of one LOFT small break test L3-1 and one LOFT intermediate break test L5-1 are performed. LOFT L3-1 simulates a 4-inch equivalent diameter pipe break, while L5-1 is a 14-inch accumulator line break. The breaks are located at the centerline of the inactive loop cold leg. The L3-1 and L5-1 experiments are of interest for model validation due to the influence of accumulator injection on the primary system response in both tests.

The LOFT facility and the tests chosen for simulation are described in Section 22.2 and Section 22.3, respectively. The WCOBRA/TRAC-TF2 models of the facility used for the analysis of the chosen tests are presented subsequently in Section 22.4. Sections 22.5, 22.6 and 22.7 provide a brief description of the calculated results in comparison to the available test data for simulated large, small and intermediate break tests, respectively. Particularly for the LOFT large break simulations, a more detailed analysis of the simulation results including the assessment of compensating error is further provided in Section 24.

## 22.2 LOFT FACILITY AND SCALING

### 22.2.1 LOFT Facility Description

The following text describing the LOFT facility is summarized from NUREG/CR-1145 (Bayless, et al., 1980) and NUREG/CR-2398 (Jarrell and Divine, 1981) with additional information from NUREG/CR-0247 (Reeder, 1978).

The LOFT facility (operated by EG&G Idaho Inc. for the Department of Energy) was designed to represent a 1/60 scale (by volume) of a four loop PWR. Figure 22-1 (Bayless, et al., 1980) illustrates the layout of the LOFT facility. LOFT consists of five major components: the reactor vessel, the active loop, the inactive loop, the blowdown suppression system, and the emergency core cooling system (ECCS). A reflood assist bypass line (RABL) was also included in the inactive loop to provide additional safeguards capability in an emergency.

The LOFT reactor vessel is similar to a PWR reactor vessel in that it includes a nuclear core and an integral annular downcomer. However, the LOFT downcomer contains large metal filler blocks not found in a standard PWR downcomer to maintain volume scaling. Also, the LOFT vessel does not have an upper head typical of a PWR vessel. Figure 22-2 (Reeder, 1978) illustrates the LOFT reactor vessel and shows the various flow paths that are available for coolant that enters through the vessel inlet nozzle. The main flow path is around the distributor annulus, down the downcomer, through the core, and out the outlet nozzles. There are alternate paths which do not direct the coolant through the core, particularly through the thimble tubes and the inactive loop; these are termed core bypass paths and amount to approximately 5 percent of the total initial reactor vessel flow.

The 5.5-foot core used in LOFT is designed to have the same physical, chemical, and metallurgical properties as those in a PWR. It is also designed to provide thermal-hydraulic relationships, mechanical responses, and fission product releases during the LOCA and emergency core cooling (ECC) recovery, which are representative of a PWR. Figure 22-3 (Bayless, et al., 1980) shows a cross-sectional layout of the LOFT core.

The LOFT nuclear core consists of nine fuel assemblies designed for a thermal output of 50 MW. Two basic fuel assembly configurations are used in LOFT. As shown in Figure 22-3 (Bayless, et al., 1980), five assemblies have a 15×15 square cross section with fuel pins and guide tubes in locations typical of those in PWR fuel assembly structures. The remaining four assemblies have a triangular cross section, with 12 fuel pins along each side that represents a portion of the square cross-sectional design. The square assemblies have 225 pin locations, 21 of which are occupied by guide tubes except for the center assembly; the center guide tube is not installed to allow for additional instrumentation. The

triangular assemblies have 78 pin locations, 8 of which are occupied by guide-tubes. In all, the nine LOFT fuel assemblies contain 1,300 fuel rods, 136 guide tubes, and 1 open hole for instrumentation.

The LOFT facility has one active loop that is similar to a PWR main coolant loop in that it includes a hot leg, an active steam generator (inverted U-tube and shell design), pump suction piping, and a cold leg. However, the LOFT active loop uses two coolant pumps in parallel, rather than a single coolant pump typical of a PWR loop, and the LOFT steam generator tubes are not full height. The steam generator simulates the response of three out of four steam generators in the unbroken loops of a PWR during a large break LOCA. The steam flow control valve motion is electronically controlled as a function of secondary pressure after reactor trip. The LOFT secondary side steam flow is controlled on a pressure hysteresis following steam generator trip: since the secondary side steam flow control valve is not positioned in the same way each time it closes, the secondary side steam leakage varies from test to test.

The LOFT inactive loop contains a hot leg, a steam generator simulator to represent the steam generator resistance, a reactor coolant pump (RCP) simulator to represent the pump resistance, and a cold leg. The hot and cold legs are connected on one side to the reactor vessel, and on the other side to the quick-opening blowdown valves of the blowdown suppression system. The hot and cold legs are also connected to each other by the Reflood Assist Bypass Line (RABL), normally closed during the simulated LOCA event. This provides additional safeguards capability by allowing steam generated in the core to be vented directly to the break in an emergency.

The LOFT blowdown suppression system consists of header pipes from the quick-opening blowdown valves in the inactive loop, connected to a blowdown suppression tank with a spray system for steam condensation. This system provides the backpressure to the RCS for the simulated LOCA event and, therefore, approximates the containment response during a postulated LOCA.

The LOFT ECCS consists of two accumulators; a high-pressure injection system (HPIS), consisting of two high-pressure injection pumps and a low-pressure injection system (LPIS), consisting of two low-pressure injection pumps. Generally, only one of each is active during a given experiment.

### **22.2.2 LOFT Scaling Consideration**

The scaling discussion of the LOFT test facility in this section is summarized from NUREG/CR-3005 (Nalezny, 1985) and McPherson (1979).

The 55 MW LOFT was scaled to simulate the behavior of a 1000 MWe commercial PWR at reduced size but full pressure. It was designed with the power-volume scaling to ensure that the important features of the PWR during the postulated LOCA be properly simulated, e.g., the energy distribution process during the saturated blowdown, the primary concern during a PWR LOCA, is distorted at minimum. The similar thermal-hydraulic phenomena are expected to occur in both the LOFT and PWR systems in the same time scale as the power-volume scaling preserves the time scale.

The LOFT nuclear core is 5.5 ft (1.68 m) long and 2 ft (0.61 m) in diameter. It provides reasonable axial and radial power profiles with fuel assemblies which are geometric and full-scaled (except length) replicas of their commercial PWR counterparts, and allows extensive instrumentation and radial flow

effects. The core height of LOFT is reduced by a factor of about 2 compared to the full length of a typical PWR.

Based on the scaling method, each component volume in the LOFT system was designed to be proportional to its counterpart in a PWR to the extent that is practical.

Table 22-1 shows the comparison of the subsystem volume, power, core length and core surface area per unit primary coolant system volume of the LOFT to a commercial PWR.

### 22.3 LOFT TEST DESCRIPTION

LOFT L2-2, L2-3, L2-5 and LB-1 were designed to represent double-ended cold leg pipe breaks (200%) in a full-scale PWR. LOFT L3-1 was configured to simulate a PWR Loss of Coolant Accident (LOCA) caused by a cold leg small break equivalent to a 4-inch pipe rupture (2.5%) and LOFT 5-1 represents an intermediate break PWR LOCA caused by a 14-inch accumulator injection line rupture (25%).

The configuration and size of the breaks were modeled following the layout and the diameter of the break orifices located at the inactive/broken loop in the test facility, as shown in Figure 22-11(a), Figure 22-11(b) and Figure 22-11(c). In the four large break tests simulated, two break orifices, one at the broken cold leg and one at the broken hot leg, were connected to the blowdown suppression tank that simulated the condition of a PWR containment in the test through two Quick Opening Blowdown Valves (QOBV). In LOFT L3-1 and L5-1 tests, broken loop hot leg was blocked during the break transient and only one break orifice located at the broken cold leg was connected to the suppression tank through the QOBV.

Besides the different break sizes, the six LOFT tests feature different operating conditions in their steady states and transients, and the detail of which will be discussed in Sections 22.5.1, 22.6.1 and 22.7.1 for the large, small and intermediate break tests, respectively.

Each test began when the quick-opening blowdown valve connecting the inactive cold leg to the blowdown suppression system was opened (or in tests simulating the double-ended cold leg break, both quick-opening blowdown valves connecting the inactive cold leg and hot leg, respectively, to the blowdown suppression system were opened), simulating a pipe break.

The thermal-hydraulic responses of the reactor coolant system and the reactor core following a large break event are inertially dominated, whereas small break transients are hydrostatically controlled. For the intermediate break sizes, the transient process after the break could be similar to a prolonged transient process typical of a large break transient without severe ECCS bypass, or to a quicker small break transient process without an extended natural circulation phase.

The LOFT L2 series and LB-1 tests simulated the postulated large break LOCA events of a PWR. During the blowdown period of the transient, the initial reversed core flow occurred before the break flows became two-phase and the vessel fluid in the lower plenum and downcomer started to flash. This reversed core flow resulted in departure from the nuclear boiling (DNB) and rapid heatup of the core. At the end of the subcooled blowdown period, the core was rewetted in the L2-2 and L2-3 tests. As the decay heat in the core is large enough to keep drying out the core before the ECCS water entered the core from the

bottom, the cladding temperature rose again during the reflood period of the transient before the bottom-up quenching due to ECCS water occurred.

The LOFT small break test L3-1 exhibited the typical small break transient phases of the rapid initial blowdown, the quasi-equilibrium natural circulation, the loop seal clearance and the boiloff. L3-1 did not experience any core dryout and fuel rod heatup. The primary system pressure fell rapidly until the subcooled break flow ends. At this time, the primary system pressure was still higher than the steam generator secondary side pressure, and the natural circulation occurred and the measured pressure then decreased more slowly until the loop seal clears and the depressurization rate increased again. The scaled HPIS and LPIS safety injection were initiated by the low primary system pressure. The test was terminated once the accumulator water was injected.

The transient processes observed in the LOFT intermediate break test L5-1 is similar to the L3-1 in shorter time period and consisted of the depressurization process at different rates; however L5-1 shows core dryout and fuel rod heatup during the boiloff portion of the transient from the high to low elevations of the core. Initially, the depressurization rate was the highest due to the high single phase break flow. As the flow to break became two-phase, the depressurization rate decreases with the decreased break flow. A relatively stable RCS pressure was still noticed before the primary pressure 'cross' the steam generator secondary side pressure, similar to small break quasi-equilibrium natural circulation period. Finally, the RCS pressure decreased at higher rate again until the end of the transient marked by the quenched core by the accumulator injection.

## 22.4 WCOBRA/TRAC-TF2 LOFT MODEL

### 22.4.1 General Modeling Considerations

A WCOBRA/TRAC-TF2 model of the LOFT test facility consists of three major regions: the vessel, the active loop, and the inactive loop.

Section 26.1.1 describes the general noding guideline, hereafter referred to as guideline, in order to set specific relationship between the noding used for the PWR, and that used for the validation experiments. The application of these guidelines is explained below for LOFT:

1. Vessel
  - a. Lower Plenum – The LOFT lower plenum region (bottom of vessel to bottom of core) is shorter than the PWR (Table 22-3). However, noding guidelines in the Section 26.1.1 require cell boundaries at the bottom of the barrel and at the core inlet, and axial and lateral cells where the flow changes direction at the bottom of the lower plenum. Therefore in this region, there are [ ]<sup>a,c</sup> axial levels and lateral channels interior and exterior to the core barrel, similar to the PWR. This results in cell axial dimensions approximately [ ]<sup>a,c</sup>.
  - b. Core – The guidelines, as well as the need to properly simulate grid locations, result in cell boundaries at each grid location, with a cell boundary in between. This results in [ ]<sup>a,c</sup> axial cells in the shorter LOFT core, as opposed to [ ]<sup>a,c</sup> in the PWR core. [ ]<sup>a,c</sup>

] <sup>a,c</sup> In the lateral direction, guidelines have been applied in a manner similar to the PWR; [

] <sup>a,c</sup>

In LOFT, the basic structures described above also exist. Consequently, channels in the core representing fuel channels below each specific upper plenum structure type are defined, similar to the PWR.

In addition, guidelines have been applied to simulate the hot assembly in the center of the core:

- c. Downcomer – In the axial direction, the noding in the downcomer is controlled by noding requirements in the core and upper plenum. Recall that in WCOBRA/TRAC-TF2, cell axial dimensions are laterally uniform at each axial location. This results in several additional cells in the downcomer beyond what is required by a simple application of the noding guidelines. This additional detail is probably desirable in view of the complex processes occurring in the downcomer during blowdown. The downcomer is divided into [ ] <sup>a,c</sup> azimuthal channels. This is consistent with the number of loops involved and the noding philosophy of [ ] <sup>a,c</sup> downcomer channels per cold leg entrance nozzle.
- d. CCFL Region – [

] <sup>a,c</sup>

- e. Upper Plenum – Noding guidelines require at least [ ] <sup>a,c</sup> axial cells between the bottom of the upper plenum, and the elevation of the hot legs (a change in flow direction), and an additional [ ] <sup>a,c</sup> from the hot leg elevation to the top of the upper plenum. Since the LOFT axial dimension from the bottom of the upper plenum to the hot leg is roughly twice that of the PWR, [ ] <sup>a,c</sup>. This results in [ ] <sup>a,c</sup> axial cells in LOFT, as opposed to [ ] <sup>a,c</sup> used in the PWR. [

] <sup>a,c</sup>

## 2. Intact Loop

- a. Hot Leg – The LOFT hot leg is approximately the same length as the PWR (Table 22-3). Consequently, application of guidelines should result in the same number of cells, and due to other WCOBRA/TRAC-TF2 modeling restrictions, a total of [ ]<sup>a,c</sup> cells is specified.
- b. Steam Generator – The LOFT steam generator plena and tubes are substantially shorter than the PWR. Consistency with guidelines requires short and cells to be employed to represent the inlet and outlet plena. [ ]<sup>a,c</sup>
- c. Crossover Leg – The special nature of the LOFT crossover legs with the dual RCS pumps requires [ ]<sup>a,c</sup> noding in this region, compared with the PWR. In general, the LOFT crossover leg cell lengths are about half the PWR value.
- d. Pump – The LOFT pumps are approximately the same length as the PWR. Applying guidelines, the LOFT pump model contains the same number of cells as the PWR model.
- e. Cold Leg – The LOFT cold leg is shorter than the PWR cold leg. Application of guidelines results in a compromise to preserve the cell length to the extent possible.
- f. Pressurizer – The LOFT pressurizer is substantially shorter than the PWR. Application of guidelines controls the choice of noding size here, with the number of cells in LOFT chosen to be the same as that of PWR.

### 22.4.2 WCOBRA/TRAC-TF2 Vessel Model of the LOFT Facility

A diagram of the vessel model is shown in Figure 22-4 and the section views are shown in Figure 22-5, Figure 22-6 and Figure 22-7.

The vessel model contains [ ]<sup>a,c</sup> azimuthal channels at each elevation of the downcomer. The downcomer annulus extends to the bottom of the lower plenum. The cylinder inside the downcomer annulus represents the inner part of the lower plenum, core region, and the upper plenum. Channel numbers are enclosed by squares in the figure. Channels are laterally connected to one another by gaps represented by circles in each figure. [ ]

] <sup>a,c</sup>

[

] <sup>a,c</sup>

The hydraulic loss at the inlet nozzle/downcomer junction is modeled at the last cell of the cold leg pipe component (using the same calibrated value specific to the LOFT facility geometry). The friction and hydraulic losses inside the vessel are modeled so that the losses for the vertical flow are divided and distributed at appropriate cell locations. For lateral flow, hydraulic loss is applied by wall-friction factors applied to gaps between the cells. [

] <sup>a,c</sup> Hydraulic losses between core channels are similarly taken into account.

The metal structures in the vessel are composed of lower and upper support plates plus many other structures. The metal structures are divided into sections in accordance with the interfacing hydraulic channels. Unheated conductors are used to model the metal structures by conserving the metal mass and heat transfer area associated with each fluid channel.

[

] <sup>a,c</sup>

Normalized axial distributions of the power generation rates in the HA, GT, and SC channels are assumed approximately equal, and are represented by a single table describing the axial profile with the data pairs of power and elevation.

The fine mesh rezoning option of the fuel rod model is used, allowing for finer resolution of heat transfer in the region of a quench front.

For the calculation of gap conductance, the same dynamic gap-conductance model as used in the PWR is employed. This model accounts for thermal and elastic expansion of the fuel and cladding. Fuel relocation, conductivity degradation, and other factors affecting the gap conductance are taken into account by specifying the size of the gap width to attain the desired initial fuel temperature, using data obtained from the same fuel design codes used in the PWR calculations.

The WCOBRA/TRAC-TF2 point kinetics and decay heat models are used to predict the LOFT reactor power during the transient. The gamma redistribution model used for the PWR was not used, since it assumes a PWR core geometry. A constant value of [ ] <sup>a,c</sup> percent was used as the fraction of the local power in both the hot rod and hot assembly rod redistributed to the average channel. Detailed PWR calculations indicate redistribution values slightly higher for the hot rod (about 4 percent) and lower for the hot assembly rod (about 2 percent). It is noted that for the simulation of the smaller break tests (L3-1 and L5-1) the core power as a function of time for the LOFT small break LOCEs is supplied as a boundary condition to WCOBRA/TRAC-TF2, based on Figure 21 of NUREG CR-1145 (Bayless, et al., 1980) for L3-1 and for L5-1. Use of these best-estimate curves in place of the WCOBRA/TRAC-TF2

kinetics and decay heat models ensures that the thermal-hydraulic predictions are not influenced by known differences in core power behavior between the code modeling and the experiments.

The experimenters identified that about 5% leakage occurred between the upper plenum and downcomer in the LOFT reactor vessel hot leg nozzle region. This leakage is modeled in the gaps 68 through 71 as shown in Figure 22-4.

### 22.4.3 WCOBRA/TRAC-TF2 Loop Model of the LOFT Facility

#### 22.4.3.1 Active Loop Model

The active loop is modeled with TEE, PUMP and PIPE components, as shown in Figure 22-9. The hot leg is modeled by [

] <sup>a,c</sup>. The crossover leg is modeled by [

] <sup>a,c</sup>. The cold leg is modeled by [

] <sup>a,c</sup>

The pressurizer is modeled with [ ] <sup>a,c</sup> cells; [

] <sup>a,c</sup>

In the LOFT model, the active loop steam generator is modeled [

] <sup>a,c</sup>

The heat transfer between the primary side of the U-tubes [ ] <sup>a,c</sup> and the secondary side [ ] <sup>a,c</sup> is modeled through the [ ] <sup>a,c</sup>

Figure 22-10 illustrates the active loop steam generator modeling for the WCOBRA/TRAC-TF2 simulations of the LOFT tests.

It is noted that the LOFT steam control valve operates on a pressure hysteresis following steam generator trip and is, therefore, different from the PWR. For L3-1 a non-trivial amount of leakage through this valve affected the experimental results. [

] <sup>a,c</sup>

In the LOFT model, the active loop pump suction piping is modeled [ <sup>a,c</sup>. The pump volume is 3.5 cubic feet and is represented by [ <sup>a,c</sup>. The pumps are modeled using single- and two-phase hydraulic characteristics obtained from the Semiscale pump (Reeder, 1978). This data is compared with PWR data in Section 20.2. Pump rated characteristics are: the rated torque ( $T_R = 369$  ft-lbf), the rated density ( $\rho_R = 38.31$  lbm/ft<sup>3</sup>), the rated speed ( $N_R = 3530$  rpm); the rated flow rate ( $Q_R = 5117$  gpm); and the rated pump head ( $H_R = 315$  lb<sub>f</sub>-ft/lbm). The pump coastdown for all LOFT tests is supplied to WCOBRA/TRAC-TF2 as a boundary condition, based on the test information (for example, Figures 59 and 60 of NUREG/CR-1145 (Bayless, et al., 1980) for L3-1). Use of these experimentally obtained curves in place of the WCOBRA/TRAC-TF2 pump coastdown calculations ensures that the thermal-hydraulic predictions are not influenced by the known differences in RCP behavior among the various LOFT experiments.

The piping layout of the crossover leg from the steam generator outlet to the RCP inlets in the LOFT facility is very unique and different from the PWR loop seal piping. The crossover leg is modeled by [ <sup>a,c</sup> as shown in Figure 22-9.

In the LOFT model, the active loop cold leg was modeled [ <sup>a,c</sup>. Figure 22-9 illustrates the active loop cold leg modeling for the WCOBRA/TRAC-TF2 LOFT simulations.

The LOFT pumped injection enters the cold leg at a location near the reactor vessel, while the PWR injection point is typically further upstream. This results in distortion between the flow regimes observed in the LOFT cold leg and the flow regimes observed in a PWR cold leg and must be considered before using LOFT cold leg behavior to draw conclusions regarding the PWR small break model.

In the LOFT model, the accumulator and ECCSs were modeled using: [

] <sup>a,c</sup> Water injection rates and timing from HPIS and LPIS are determined by the test procedure, so these injection systems are jointly modeled by one flow rate boundary condition. In all LOFT simulations, the accumulators were active and injected when the predicted RCS pressure achieved the accumulator pressure value. The non-condensable nitrogen was expelled when the tank emptied of liquid in all the simulations reported herein.

The heat losses occurred in the LOFT coolant loops during the test are neglected in the LOFT LOCE simulations.

### 22.4.3.2 Broken Loop Model

[

] <sup>a,c</sup>

The broken cold leg hydraulic losses are calculated [

] <sup>a,c</sup>. Modeled also are the approximate liquid temperature distributions measured during steady-state operation.

The broken hot leg is composed of piping, and steam generator and pump simulators. The steam generator and pump simulator hydraulic resistances are calculated by the code using the natural geometry input of these components. The pipeline (RABL) connecting the broken hot leg and cold leg is modeled (Figure 22-12).

For small breaks (L3-1 and L5-1), the inactive loop modeling as illustrated in Figure 22-12 includes a zero FILL, while the large break tests (L2-2, L2-3, L2-5 and LB1) a BREAK is instead used for Component #10: this difference is due to the different test procedure for large and small breaks. For the large breaks, both ends of the broken loop (Components # 10 and #30) were opened, simulating a 'double-ended' rupture. However, for small break tests, the valves connected to the hot leg in the broken loop were kept closed: to be consistent with the actual test configuration, BREAK 10 is therefore replaced with a zero FILL component.

The RABL connecting the inactive loop hot and cold legs was designed to remain closed during the experiments. During testing, although possible leakage through the RABL was reported, the information available was not sufficient to quantify the RABL line model in the input for specific test simulations, and thus the RABL line was modeled to [ ] <sup>a,c</sup>.

[ ]<sup>a,c</sup>

## 22.5 LARGE BREAK LOFT SIMULATIONS USING WCOBRA/TRAC-TF2

### 22.5.1 Large Break LOFT Tests Description

The LOFT experiments L2-2, L2-3, L2-5, and LB-1 were designed to represent double-ended pipe breaks of the cold leg in a full-scale PWR. The differences between these three tests were in their power levels and whether the reactor coolant pumps were tripped or not, as shown in Table 22-2. In addition to the differences listed in Table 22-2, LB-1 was run with a much lower accumulator water volume than the other three large break tests.

The tests began when the quick-opening blowdown valves connecting the inactive hot leg and cold leg to the blowdown suppression system were opened, simulating a pipe break.

After the break occurred, the primary system in each of the four experiments depressurized and mass depletion caused the core to uncover. ECCS flow was injected into the intact loop cold leg at low RCS pressure. During the blowdown portion of the transient, the cladding temperature increased due to departure from nucleate boiling (DNB). Later, some of the fuel rods cooled as rewet occurred in the two tests L2-2 and L2-3 where the primary coolant pumps coasted down and their flywheels were not disconnected instantly after the break. Near the end of the blowdown transient, decay heat in the core was large enough to dry out the core and consequently, the cladding temperature rose during the reflood portion of the transient until the fuel rods again quenched as ECCS water entered the core from the bottom. Figure 22-13 shows a typical time history of the cladding temperature.

### 22.5.2 Steady-State Calculations

The methods for setting up the LOFT model initial conditions were similar to those used in the PWR. In particular, the hot assembly power and fuel stored energy were input as best-estimate representations of actual core conditions (radial power distribution). Measured data (axial power distribution) were used to obtain estimates of peak and average linear heat rates for each region. The initial fuel stored energy (fuel temperature) was obtained from the same fuel design code used for the PWR, using LOFT specific burnup conditions and core power. Table 22-4 summarizes input hot assembly conditions for Test L2-5, as an example. Prior to simulating any of the transients, WCOBRA/TRAC-TF2 steady-state simulations were performed. The steady-state simulations resulted in favorable comparisons with the initial conditions as can be seen in Table 22-5, and the reactor vessel and active loop pressure drops were calibrated to approximate values published for the four large break tests, as available. The steady-states achieved are considered acceptable for simulation of the LOFT large break transients, as stable thermal-hydraulic states of the system are asymptotically achieved and match the initial test conditions within their measurement uncertainties.

### 22.5.3 Transient Calculations

The simulation of the break transients were initiated by restarting the calculation from the steady-state simulation and opening the break. In the WCOBRA/TRAC-TF2 model, the valve opening time of 30 milliseconds is simulated by linearly reducing the break pressure over 30 milliseconds to the suppression tank header pressure, which is available from test data.

The sequence of events for these analyses are compared to the sequence of events observed in the experiments in Tables 22-6 through 22-7. The measured end of bypass time was estimated from the core level plots, if available from the data reports, as shown in Figure 22-30c, Figure 22-31c and Figure 22-32c for Tests L2-2, L2-3 and L2-5, respectively.

The transient results of the calculation are compared to the measured test data in Figures 22-14 through 22-42 (in the figures, the instrument used for comparison is indicated; if data was extracted from the data reports, the figures used are indicated). The system pressure transient is shown in Figure 22-14 through Figure 22-17. [

] <sup>a,c</sup>

The broken hot leg flow rates for each test are shown in Figure 22-18 to Figure 22-21. The broken cold leg flow rates are shown in Figure 22-22 to Figure 22-25. [

] <sup>a,c</sup>] <sup>a,c</sup>

Figure 22-30a, Figure 22-31a, Figure 22-32a and Figure 22-33a compare measured and predicted volumetric flow rate from the accumulator in Tests L2-2, L2-3, L2-5 and LB-1, respectively. [

] <sup>a,c</sup>

[

] <sup>a,c</sup>

The comparisons in Figure 22-30a, Figure 22-31a, Figure 22-32a and Figure 22-33a are intended for the accumulator liquid injections (from 0 to about 40 seconds) before the nitrogen starts to flow through the test flow meters, since there was unknown uncertainties associated with the flow meter reading when it measured two-phase flow. The time when nitrogen starts to be discharged from the accumulator tank can be estimated based on the void fraction at the exit of the accumulator tank (void fraction of the discharge line adjoining the bottom of the accumulator tank is co-plotted in Figure 22-30a, Figure 22-31a, Figure 22-32a and Figure 22-33a for Tests L2-2, L2-3, L2-5 and LB-1, respectively.

[

Figure 22-30e, Figure 22-31e and Figure 22-32e show the predicted and measured core liquid levels of L2-2, L2-3 and L2-5, respectively. [

] <sup>a,c</sup>

Figure 22-30b, Figure 22-31b, Figure 22-32b and Figure 22-33b present predicted accumulator water level during L2-2, L2-3, L2-5 and LB-1 tests, respectively. [

] <sup>a,c</sup>

Figure 22-34 through Figure 22-37 show the measured and predicted peak cladding temperatures in the hot assembly region. [

] <sup>a,c</sup>

[

] <sup>a,c</sup>

The occurrence of CHF due to the reversed core flow [

for tests L2-2, L2-3, L2-5 and LB-1, respectively.

] <sup>a,c</sup>, as shown in Tables 22-6 through 22-7

[

] <sup>a,c</sup>

Figure 22-41 shows that the predicted fluid temperature [

] <sup>a,c</sup>

Figure 22-43 compares the predicted pressure difference across the intact loop pump for Test L2-5. [

] <sup>a,c</sup>

Figure 22-44 compares the fuel temperature for Test L2-5. [

] <sup>a,c</sup>

[

] <sup>a,c</sup>

Figure 22-45 compares the measured nuclear power with the predicted value, normalized to the initial power. [

] <sup>a,c</sup>

#### 22.5.4 Conclusions

The WCOBRA/TRAC-TF2 computer code [

] <sup>a,c</sup>

### 22.6 SMALL BREAK LOFT SIMULATION USING WCOBRA/TRAC-TF2

#### 22.6.1 Small Break LOFT Test Description

The LOFT L3-1 test is a simulated small break LOCA test that has a 4-inch equivalent break in the inactive loop cold leg. The reactor was tripped 2 seconds prior to opening the blowdown valve to initiate the break when the control rods were signaled to reach the bottom of the core. In the test, only the blowdown valve in the inactive loop cold leg was opened, with the one in the inactive loop hot leg remained closed throughout the test transient. This unique physical arrangement of the inactive loop means that L3-1 is atypical of a full-scale PWR layout in a postulated small break accident scenario.

The initial conditions prior to the break transient in test L3-1 are detailed in Table 22-10. After the blowdown, the reactor coolant pumps were tripped and the pumps began to coast down under the influence of a flywheel system. Upon receipt of the reactor trip signal, the feed water pump tripped off and the main feed water isolation valve shut. The electronically controlled steam generator steam control valve started to ramping shut after the blowdown at 5% position/second. The scaled emergency core coolant injection was directed to the intact loop cold leg through the use of a high pressure safety injection (HPSI) pump, accumulator and a low pressure safety injection (LPSI) pump. The accumulator initiated injection at about 634 seconds, and HPSI flow and LPSI flow were initiated at about 5 and 4240 seconds after the rupture, respectively. The secondary coolant system (SCS) auxiliary feed pump was operated from about 75 to 1875 seconds to deliver cold water at 70°F to the SG. The simulation transient was terminated approximately at the end of the accumulator liquid injection, which is 2000 seconds after the break occurs.

There was no observed core dryout and heatup in test L3-1 before the termination of the test and simulation transients.

### 22.6.2 Steady-State Calculations

Prior to the transient simulations, a 200-second steady-state was run to ensure stable system states that match what were reported prior to break initiation in the test. As in the test, the break valves are closed during the steady state with trivial leakage through the RABL connecting the inactive loop cold and hot leg [ ]<sup>a,c</sup>. Consequently, the inactive loop initial temperatures at the components close to the break orifice are barely changed from their initial values during the steady state run due to the limited amount of circulation in the dead ends before the break valve.

The pressurizer component sets the primary system pressure. Pump speed is varied to obtain the desired primary system flow. Secondary system pressure is varied to obtain active loop hot and cold leg temperatures within specified limits. The average linear heat generation rate is set to obtain the correct core power.

The initial conditions prior to the break transient are listed in Table 22-10, which shows the comparison of the measured conditions in the test (Bayless, et al., 1980) and the conditions achieved at the end of the WCOBRA/TRAC-TF2 steady state calculation. The steady state results are deemed as acceptable initial conditions to the subsequent transient simulation of test L3-1.

### 22.6.3 Transient Calculations

The L3-1 sequence of events is compared in Table 22-11 between the test (Bayless, et al., 1980) and prediction. [ ]<sup>a,c</sup>

The comparisons of the important system parameters representative of the thermal-hydraulic responses of the system during the test transient are generated between the calculation and the measurement in Figure 22-46 through Figure 22-51. As there were no core dryout and rod heatup observed and predicted in this test, the key parameters to compare are primary system pressure, break flows, steam generator secondary side pressure, accumulator injection and its influence on the primary system pressure.

A comparison of the calculated and measured primary coolant system pressure, as seen in Figure 22-46, shows that [ ]<sup>a,c</sup>

[

] <sup>a,c</sup>

The comparison of the steam generator (SG) secondary side pressure is shown in Figure 22-47. [

] <sup>a,c</sup>

A comparison of the measured inactive loop mass flow rate and the calculated break mass flow rate is shown in Figure 22-48. [

] <sup>a,c</sup>

[ ]<sup>a,c</sup>

In Figure 22-53 and Figure 22-54, the comparisons of the two WCOBRA/TRAC-TF2 simulation runs and the test data are made. [ ]

] <sup>a,c</sup>

The accumulator liquid level and pressure are shown in Figure 22-49 and Figure 22-50, respectively. [ ]

] <sup>a,c</sup>

#### 22.6.4 Conclusions

The WCOBRA/TRAC-TF2 computer code [ ]

] <sup>a,c</sup>

### 22.7 INTERMEDIATE BREAK LOFT SIMULATIONS USING WCOBRA/TRAC-TF2

#### 22.7.1 Intermediate Break LOFT Tests Description

The LOFT L5-1 test is a simulated intermediate break LOCA test that has a 14-inch equivalent break in the inactive loop cold leg. The size of the break simulates a single 14-in accumulator injection line in a commercial PWR.

Similar to test L3-1, the quick-opening blowdown valve in the inactive loop hot leg remained closed throughout the test L5-1 and the one in the inactive loop cold leg was opened to initiate the break transient. A low-pressure scram followed at 0.17 seconds, and the emergency core cooling system HPIS started at 0.4 seconds. Power to the primary coolant system (PCS) pumps motor-generator sets was manually tripped at 4.0 seconds; coastdown was complete at 19.3 seconds. The secondary coolant system main feed pump was tripped on reactor scram coincident with the steam generator control valve beginning to ramp close; the valve was fully closed at 12.1 seconds.

The L5-1 break transient started from the initial conditions that are detailed in Table 22-12. Saturation pressure was reached in the upper plenum at 0.2 seconds and in the broken loop cold leg at 10.5 seconds. Fuel cladding thermal excursion began at about 110 seconds as the PCS continued to blowdown. A

maximum fuel cladding temperature of 833°F (718 K) was reached at 198 seconds before the reactor core was recovered by scaled flow from the accumulator (commencing at 186 seconds) and LPIS (commencing at 201 seconds). The transient was terminated at 213 seconds following its initiation when all monitored core thermocouples indicated at or below saturation temperature.

### 22.7.2 Steady-State Calculations

Prior to the transient simulations, a 200-second steady-state was run to ensure stable system states that match what were reported prior to break initiation in the test. The same as in the test, both break valves are closed during the steady state with trivial leakage through the RABL connecting the inactive loop cold and hot leg [ ]<sup>a,c</sup>. Consequently, the inactive loop initial temperatures at the components close to the break orifice are barely changed from their initial guesses during the steady state run due to the limited amount of circulation in the dead ends before the break valve.

The initial conditions prior to the break transient are listed in Table 22-12, which shows the comparison of the measured conditions in the test (Jarrell and Divine, 1981) and the asymptotically achieved conditions at the end of the WCOBRA/TRAC-TF2 steady state run. The steady state results are deemed as acceptable initial conditions to the subsequent transient simulation of test L5-1.

### 22.7.3 Transient Calculations

The sequence of events in test L5-1 is compared in Table 22-13 between the test (Jarrell and Divine, 1981) and prediction. [ ]<sup>a,c</sup>

Figure 22-55 through Figure 22-59 show the comparisons of the test to the simulation transient results resulted from the input model in which the models are set at their nominal values. [ ]<sup>a,c</sup>

The steam generator secondary side pressure and RCS pressure are shown in Figure 22-57. [ ]<sup>a,c</sup>

The comparison of the predicted hot assembly fuel rod cladding temperatures against the data is shown in Figure 22-58. [ ]<sup>a,c</sup>

[

]a,c

[

] <sup>a,c</sup>

#### 22.7.4 Conclusions

The WCOBRA/TRAC-TF2 input model of the LOFT L5-1 is consistent with those used for LOFT LB and SB test simulations, except the test specific components, such as break orifice in the broken (inactive) loop, the HPIS and LPIS, Pump coastdown tables, etc. [

] <sup>a,c</sup>

#### 22.8 REFERENCES

1. Adams, J. P., 1979, "Quick-Look Report on LOFT Nuclear Experiment L3-1," EGG-LOFT-5057.
2. Adams, J. P. and Birchley, J. C., 1983, "Quick Look Report on OECD LOFT Experiment LP-LB-1," OECD LOFT-TR-3504.
3. Bajorek, S. M., et al., 1998, "Code Qualification Document for Best Estimate LOCA Analysis – Volume III: Hydrodynamics, Components, and Integral Validation," WCAP-12945-P-A, Vol. 3.
4. Bayless, P. D., et al., 1980, "Experiment Data Report for LOFT Nuclear Small Break Experiment L3-1," NUREG CR-1145/EGG-2007.
5. Bayless, P. D. and Divine, J. M., 1982, "Experiment Data Report for LOFT Large-Break Loss-of-Coolant Experiment L2-5," NUREG/CR-2826.
6. Condie, K. G., et al., 1981, "Four-Inch Equivalent Break Loss-of-Coolant Experiments: Posttest Analysis of LOFT Experiments L3-1, L3-5 (Pumps Off), and L3-6 (Pumps On)," EGG-LOFT-5480.
7. Czapary, L. S., 1980, "LOFT L3-1 Preliminary Comparison Report," EGG-CAAP-5255.
8. Dao, L. T. L. and Carpenter, J. M., 1980, "Experiment Data Report for LOFT Nuclear Small Break Experiment L3-5/L-35A," NUREG CR-1695/EGG-2060.
9. Gillas, D. L. and Carpenter, J. M., 1980, "Experiment Data Report for LOFT Nuclear Small Break Experiment L3-7," NUREG CR-1570/EGG-2049.
10. Grush, W. H., 1980, "Cold Leg Warmup Line and RABVs Flows During Experiment L3-1," Kau – 208-80.

11. Jarrell, Donald B. and Divine Janice M., 1981, "Experiment Data Report for LOFT Intermediate Break Experiment L5-1 and Severe Core Transient Experiment L8-2," NUREG/CR-2398.
12. "LOFT Experiment Operating Specification" 1978, Volume 2, NE-L2 Series, EOS Vol. 2, Rev. 2.
13. McCormick-Barger, M., 1979, "Experiment Data Report for LOFT Power Ascension Test L2-2," NUREG/CR-0492.
14. McPherson, G. D., 1979, "The LOFT Facility and Test Program," Presentation at GRS-Fachgespräch, Munich, Germany.
15. Nalezny, C. L., 1985, "Summary of the Nuclear Regulatory Commission's LOFT Program Research Findings," NUREG/CR-3005.
16. Prassinis, P. G. et al., 1979, "Experiment Data Report for LOFT Power Ascension Experiment L2-3," NUREG/CR-0792.
17. Reeder, D. L., 1978, "LOFT System and Test Description (5.5-ft. Nuclear Core 1 LOCEs)," NUREG CR-0247/TREE-1208.
18. Russell, M. L., 1983, "Loss-of-Fluid Findings in Pressurized-Water-Reactor Core's Thermal Hydraulic Behavior," EGG-M-08882.
19. Tolman, E. L., Driskell, W. E. and Carboneau, M. L., 1981, "Comparison of Nuclear and Electric Heater Rod Responses for Large Break PWR LOCA Conditions," EGG-LOFT-5529.
20. "Westinghouse Large Break LOCA Best-Estimate Methodology," 1987, WCAP 10924, Volume 2.

	<b>LOFT</b>	<b>PWR</b>
<b>Volumes (ft<sup>3</sup>)</b>		
Total PCS	272	12240
Reactor Vessel (% of Primary Coolant Volume)	34	38
Intact Loop (% of Primary Coolant Volume, including pressurizer)	48	51
Broken Loop (% of Primary Coolant Volume)	18	11
<b>Power (MWt)</b>	55	3400
<b>Length of Active Core (ft)</b>	5.5	12
<b>Ratios</b>		
Volume/Power (ft <sup>3</sup> /MWt)	5.0	3.6
Break Area/Primary Coolant Volume (ft <sup>-1</sup> ×10 <sup>4</sup> )	6.6	6.7
Core Surface Area/Primary Coolant Volume (ft <sup>-1</sup> )	3.5	4.5
PWR Volume/Volume	47	1

<b>Test</b>	<b>Peak Power</b>	<b>Reactor Coolant Pump</b>	<b>Equivalent Pipe Break Size</b>
	(kW/ft)		
L2-2	8.04	Coastdown	Double-ended Cold Leg (200%)
L2-3	11.89	Coastdown	Double-ended Cold Leg (200%)
L2-5	12.20	Tripped at Reactor Scram (Flywheel disconnected)	Double-ended Cold Leg (200%)
LB-1	15.80	Same as L2-5	Double-ended Cold Leg (200%)
L3-1	15.76	Coastdown	4.0 inch Cold Leg (2.5%)
L5-1	14.02	Coastdown <sup>(1)</sup>	14.0 inch Accumulator Line (25%)
PWR	13-17	Both Conditions Analyzed	All Break Sizes Analyzed

**Note:**  
1. The pumps began to coast down after being manually tripped at 4 s after the break.

**Table 22-3 LOFT/PWR Axial Noding Ratio Comparison**


a,c

**Table 22-4 LOFT L2-5 Hot Assembly Fuel Initial Conditions**

Parameter	Value	Comments

a,c

	L2-2		L2-3		L2-5		LB-1	
<b>Parameter</b>	<b>Measured Data<sup>(1)</sup></b>	<b>Analysis Result</b>	<b>Measured Data</b>	<b>Analysis Result</b>	<b>Measured Data</b>	<b>Analysis Result</b>	<b>Measured Data</b>	<b>Analysis Result</b>
Active loop Pressure (psia) <sup>(2)</sup>	2265.5	2265.7	2184.0 ±4.4	2184.2	2166.9 ±8.7	2167.2	2152.0 ±16.0	2151.9
SG Secondary Pressure (psia)	921.0	887.3	896.3 ±11.6	897.8	848.4 ±9.0	835.9	—	779.8
Active Loop Flow (lbm/s)	428.1	427.4	438.7 ±13.9	440.3	424.2 ±17.2	424.0	674.2 ±5.7	674.0
SG Secondary Flow (lbm/s)	27.9	27.9	43.0 ±0.9	41.4	42.1 ±0.88	42.1	—	54
Vessel Bypass Flow (% of loop flow)	5.0	4.9	5.0	4.8	5	4.8	—	1.9
Pressurizer Level (ft)	3.573	3.54	3.90 ±0.03	3.90	3.74 ±0.1	3.74	—	3.42
Active Loop Hot Leg Temperature (°F)	585.1	586.9	607.6 ±3.2	609.3	601.8 ±7.2	603.1	595.3 ±1.8	595.1
Active Loop Cold Leg Temperature (°F)	544.2	543.6	549.6 ±3.2	550.6	542.2 ±7.2	541.8	542.2 ±1.8	541.6
Inactive Loop Hot Leg Temperature (°F)	550.5	549.9	558.2 ±3.2	556.8	556 ±7.7	551.4	—	546.8
Inactive Loop Cold Leg Temperature (°F)	539.3	542.0	538.7 ±3.2	538.7	538.1 ±7.6	538.0	—	541.9

**Notes:**

1. Measurement uncertainties were not given in test report (McCormick-Barger, 1979), the steady state is considered acceptable referring to the measurement uncertainties in L2-3 test.
2. Pressurizer pressures were given in L2-2, L2-3 and LB-1 test reports (McCormick-Barger, 1979; Prassinis, 1979 and Adams, 1984); hot leg pressures were given in L2-5 test report (Bayless, 1982).

Table 22-6 [ ] <sup>a,c</sup>		

a,c

Table 22-7 [ ] <sup>a,c</sup>		

a,c

Table 22-8 [ ] <sup>a,c</sup>		

a,c

Table 22-9 [ ] <sup>a,c</sup>		

a,c





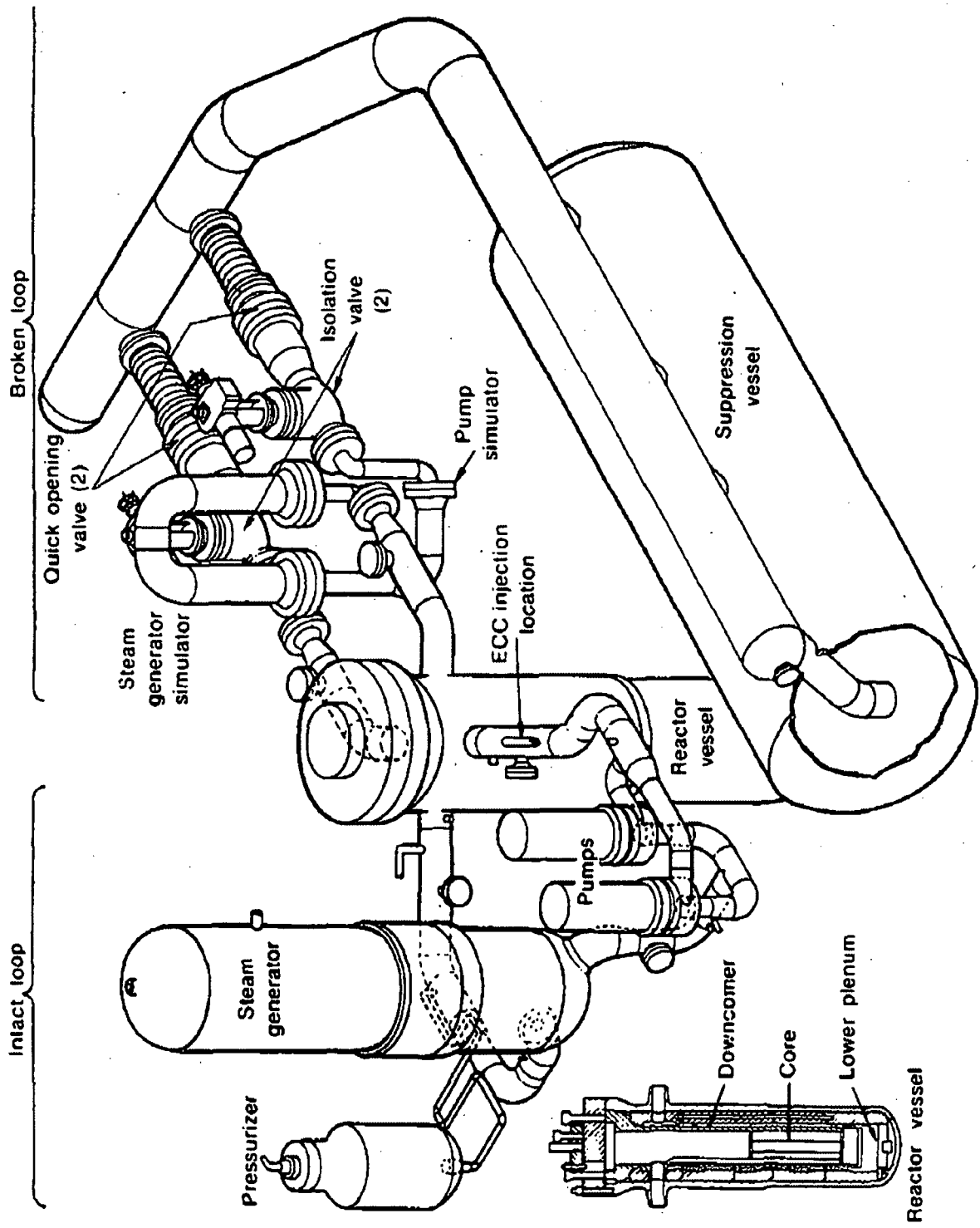


Figure 22-1 Schematic of LOFT Facility

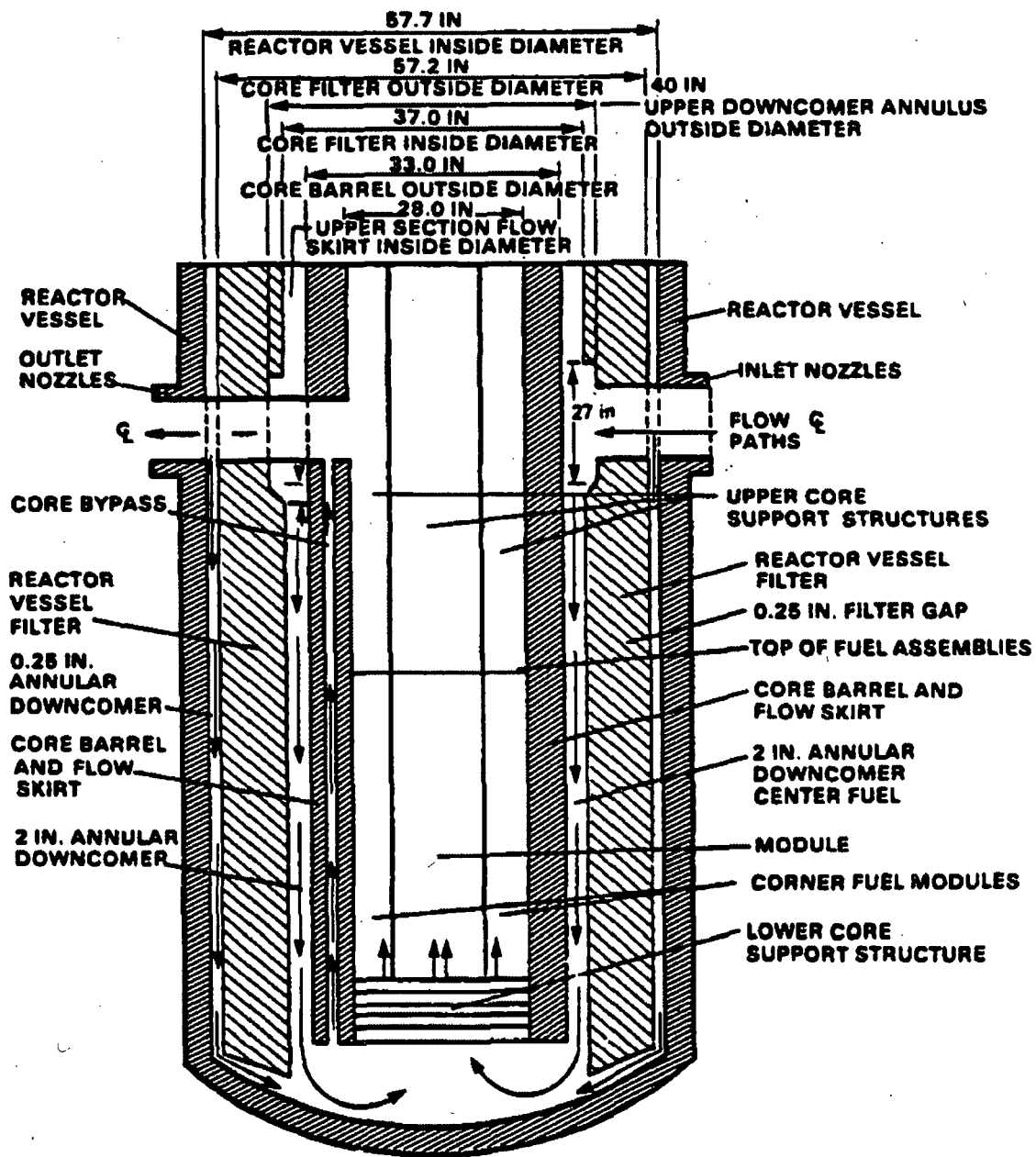


Figure 22-2 LOFT Reactor Vessel Diagram with Flow Paths

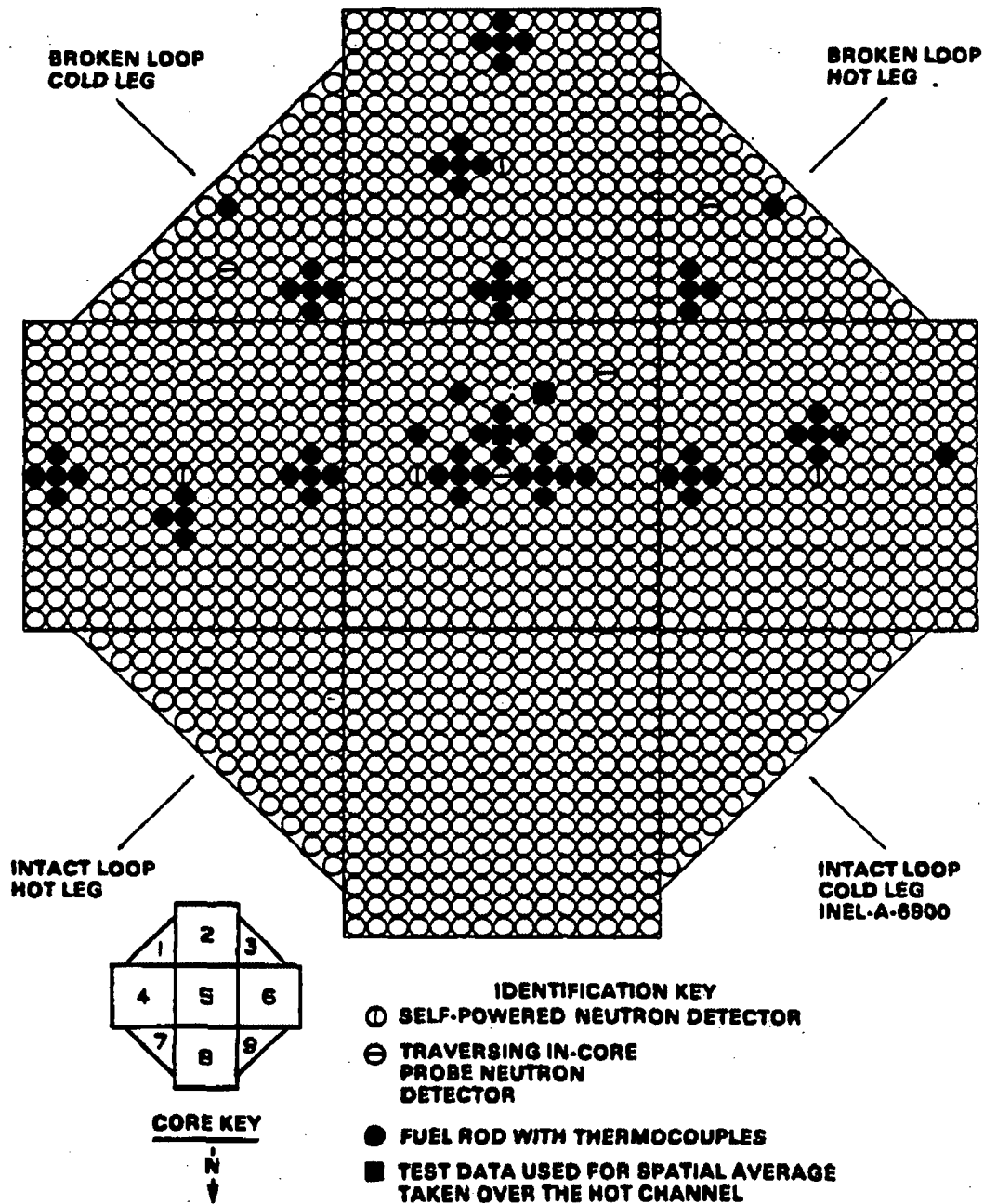
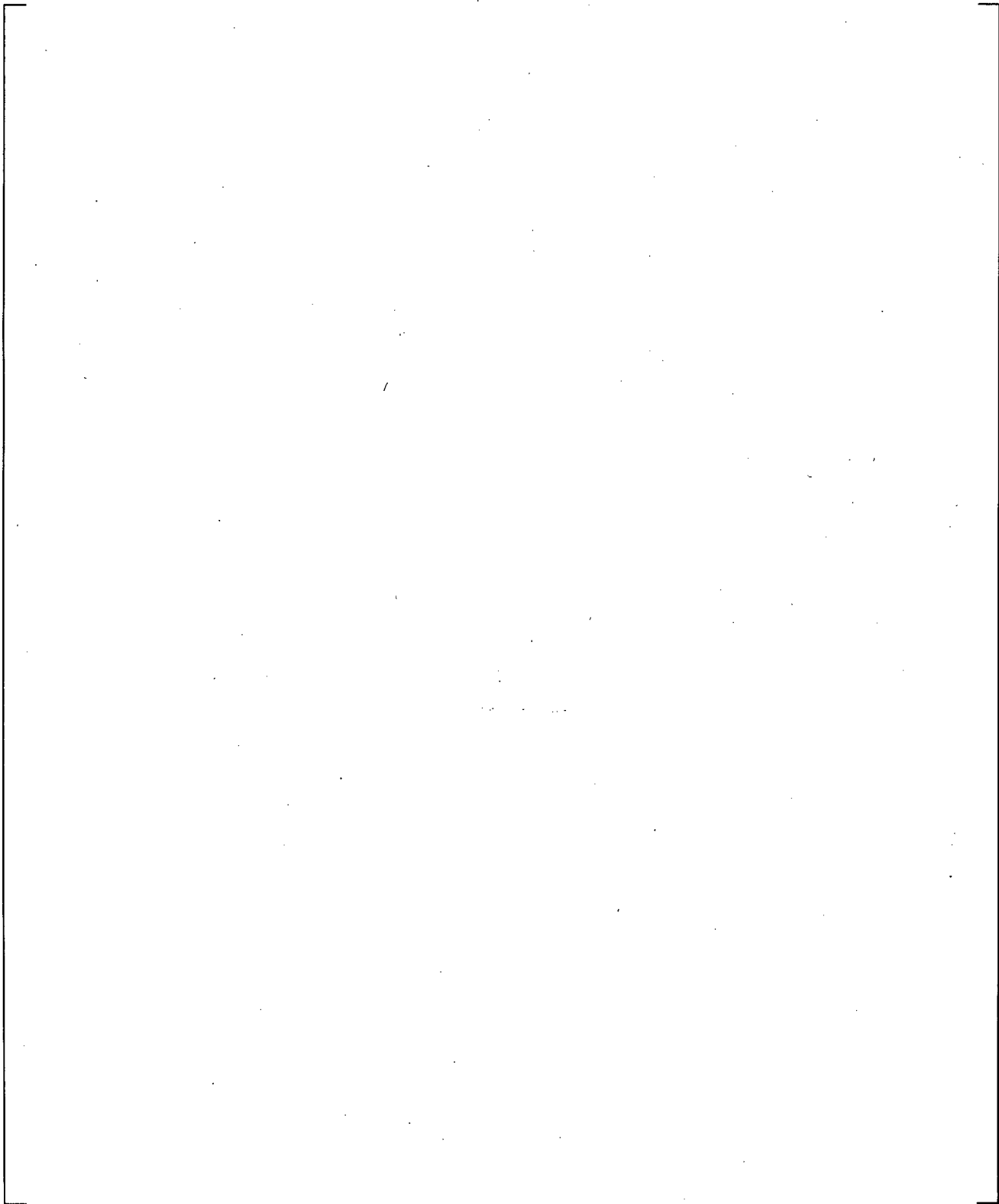
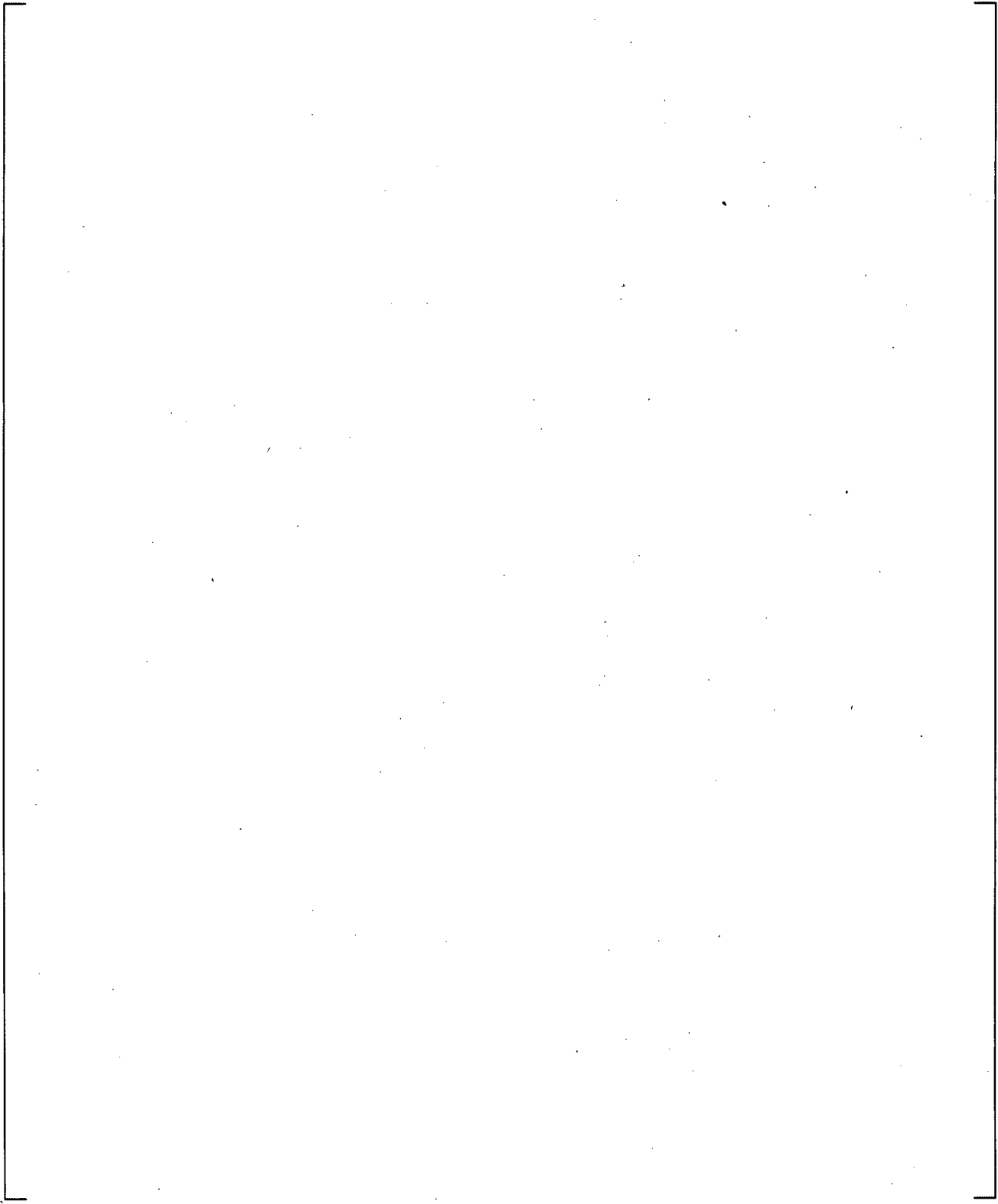


Figure 22-3 LOFT Reactor Core and Arrangement of Incore Instrumentation



**Figure 22-4 LOFT WCOBRA/TRAC-TF2 Vessel Model**

a,c



**Figure 22-5 Section Views of LOFT WCOBRA/TRAC-TF2 Vessel Model**

a,c

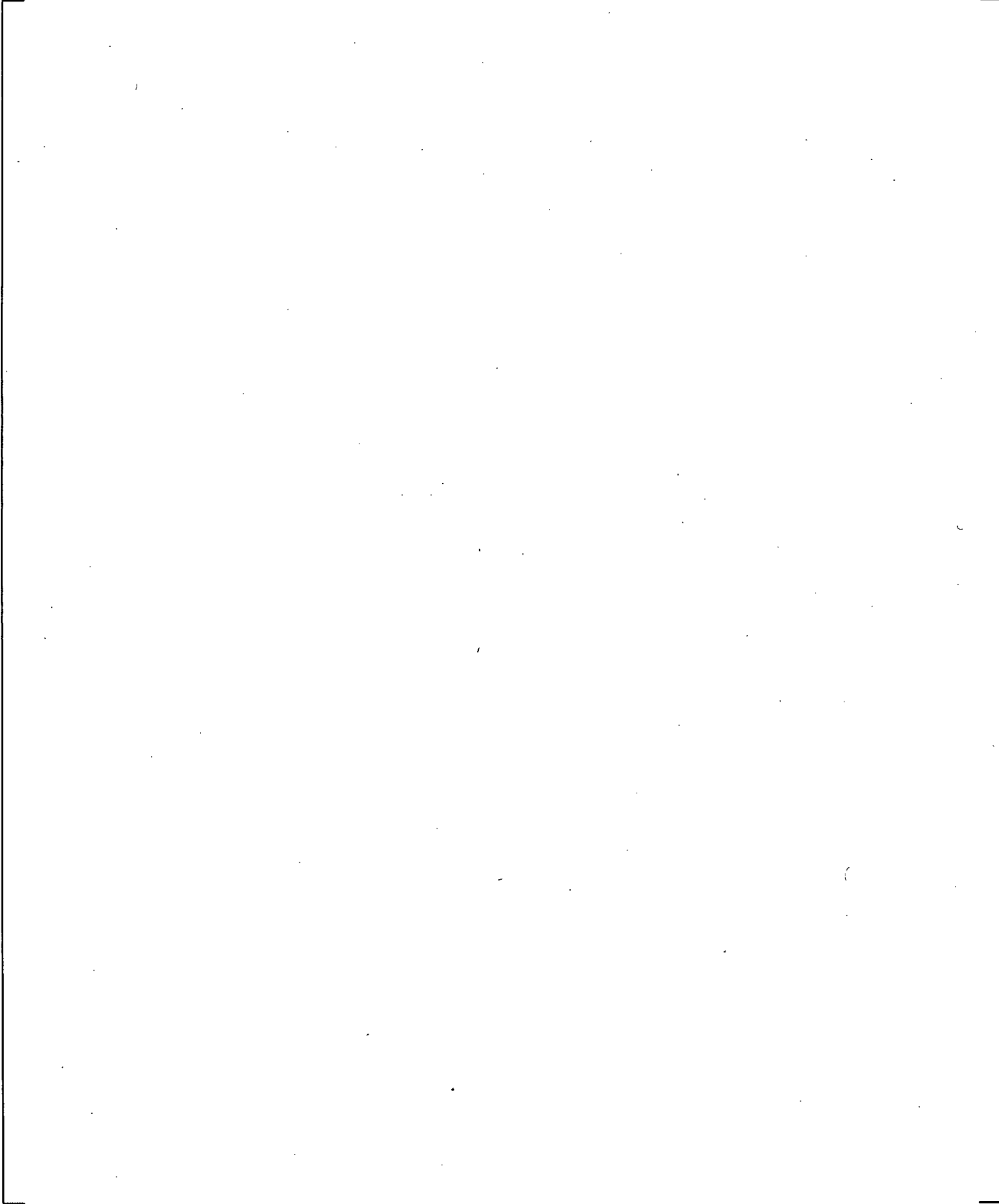


**Figure 22-6 Section Views of LOFT WCOBRA/TRAC-TF2 Vessel Model**

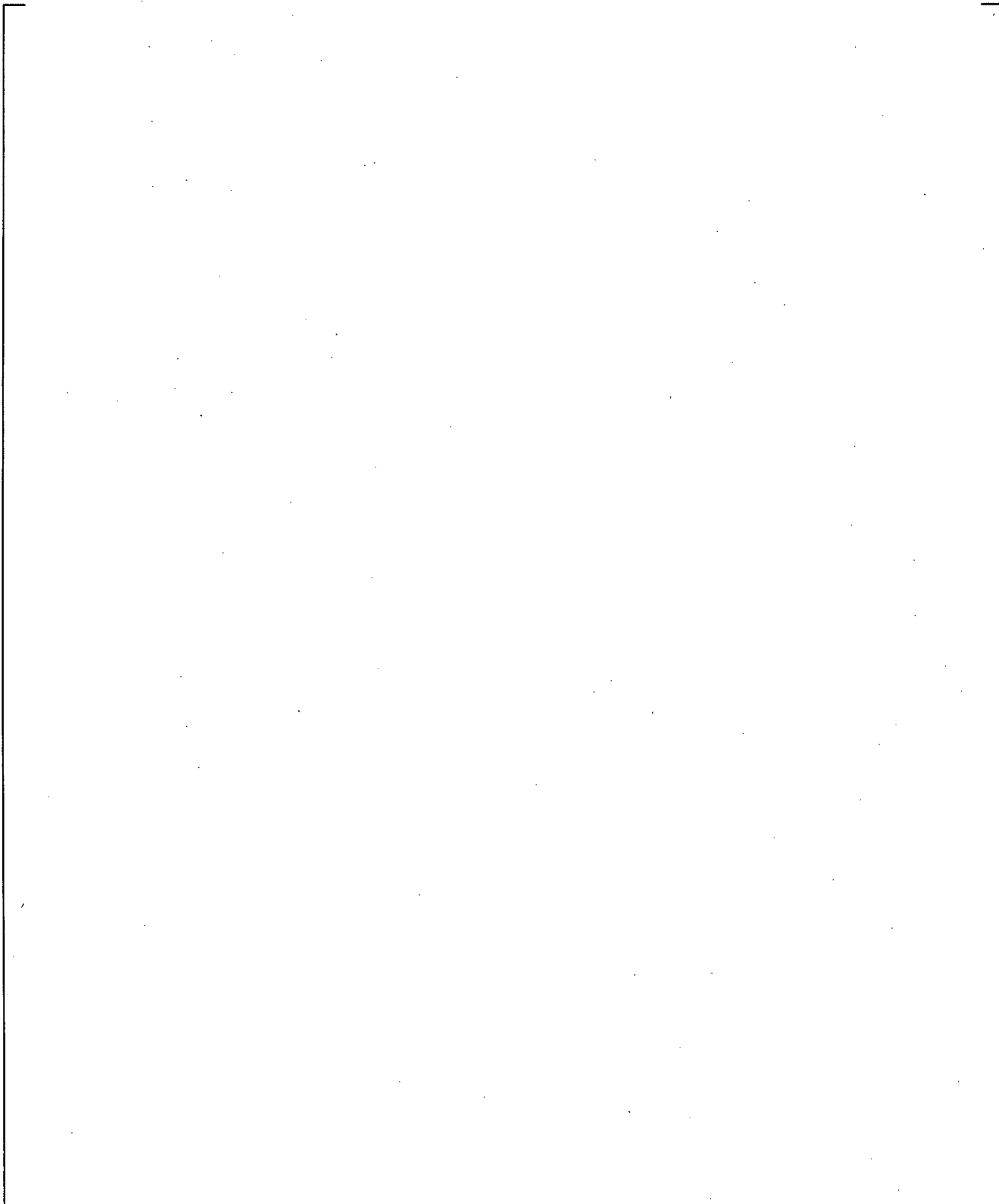


**Figure 22-7 Section Views of LOFT WCOBRA/TRAC-TF2 Vessel Model**

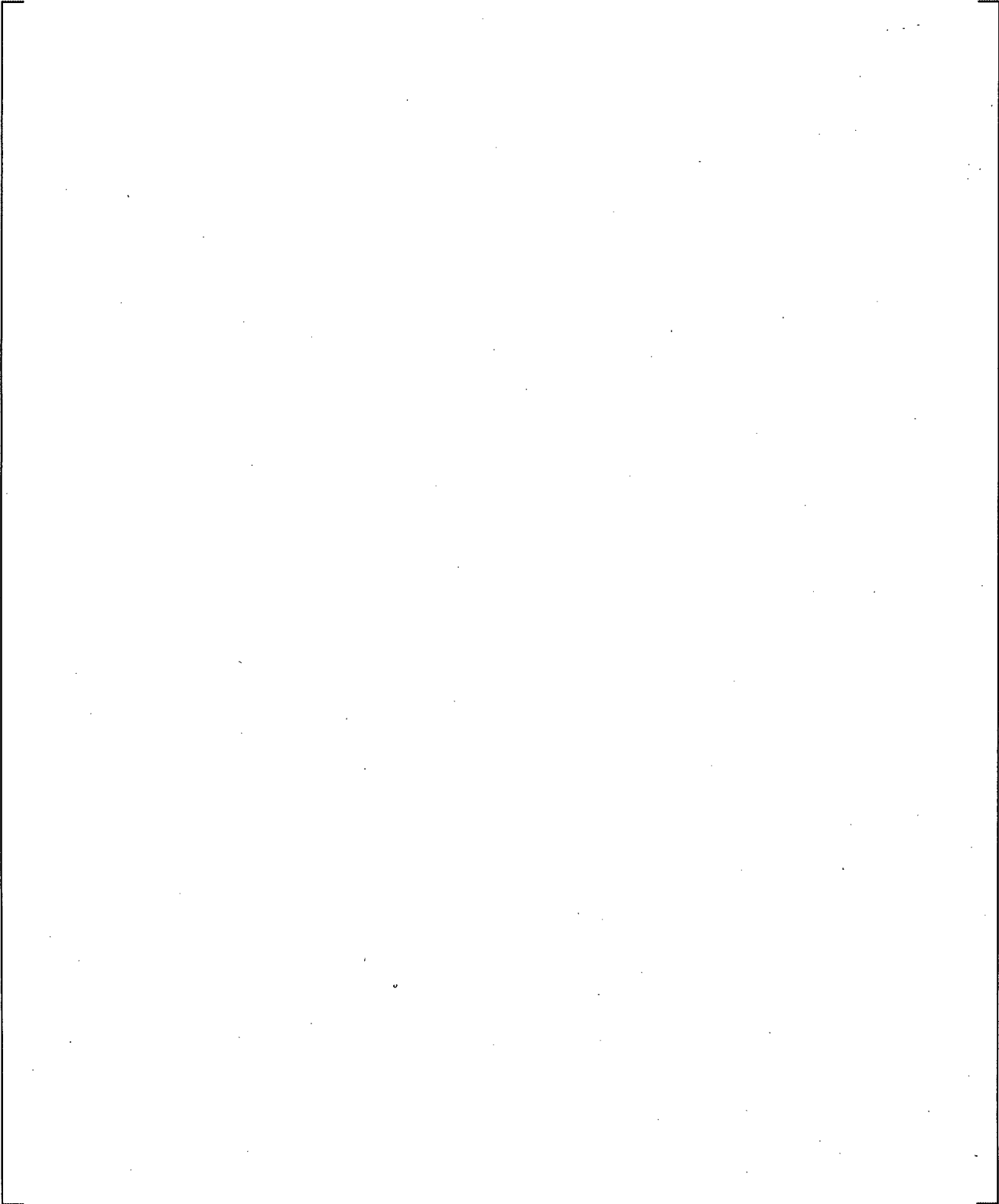


**Figure 22-8 Arrangement of WCOBRA/TRAC Core Channels**

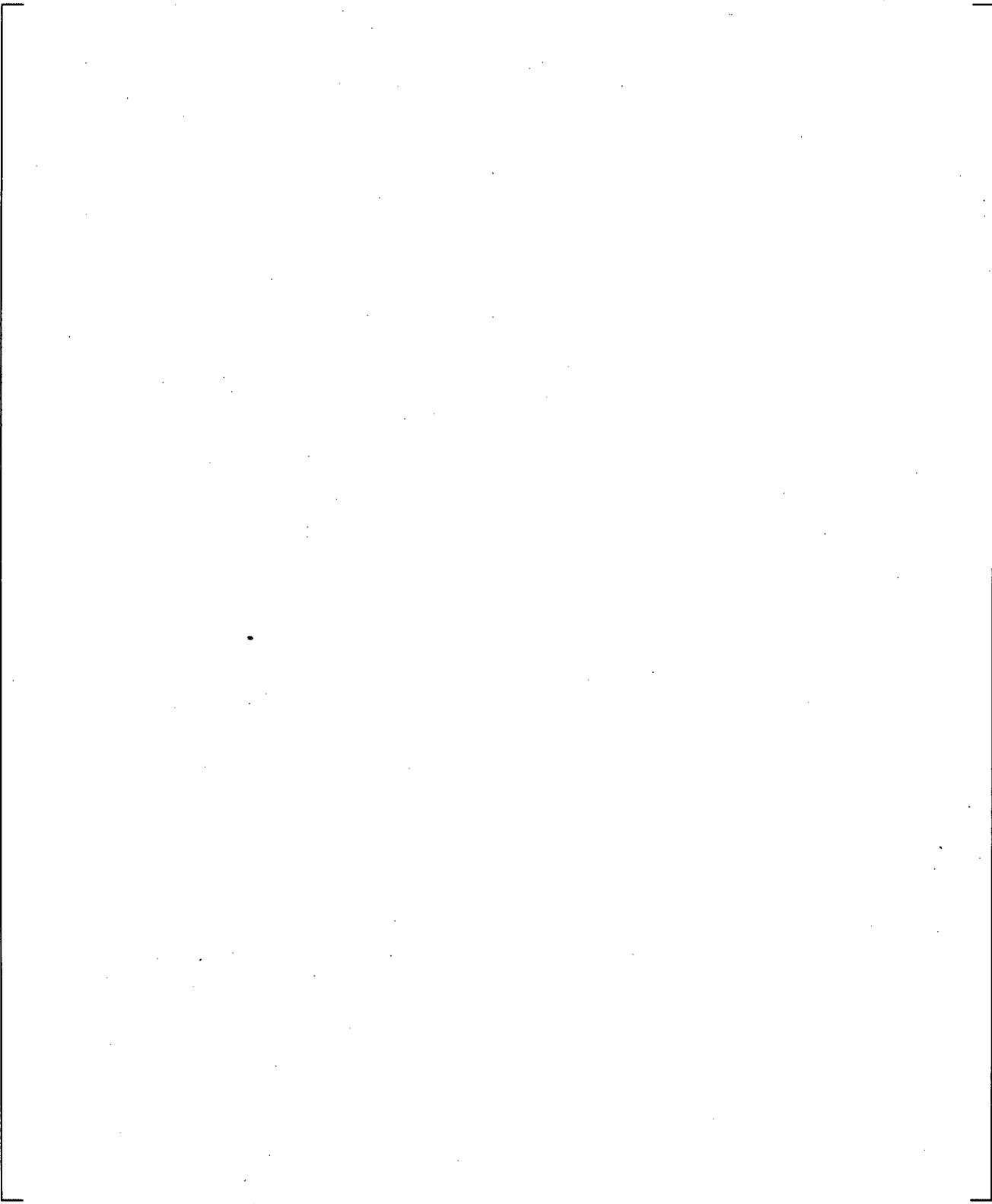


**Figure 22-9 LOFT Intact Loop WCOBRA/TRAC-TF2 Model**

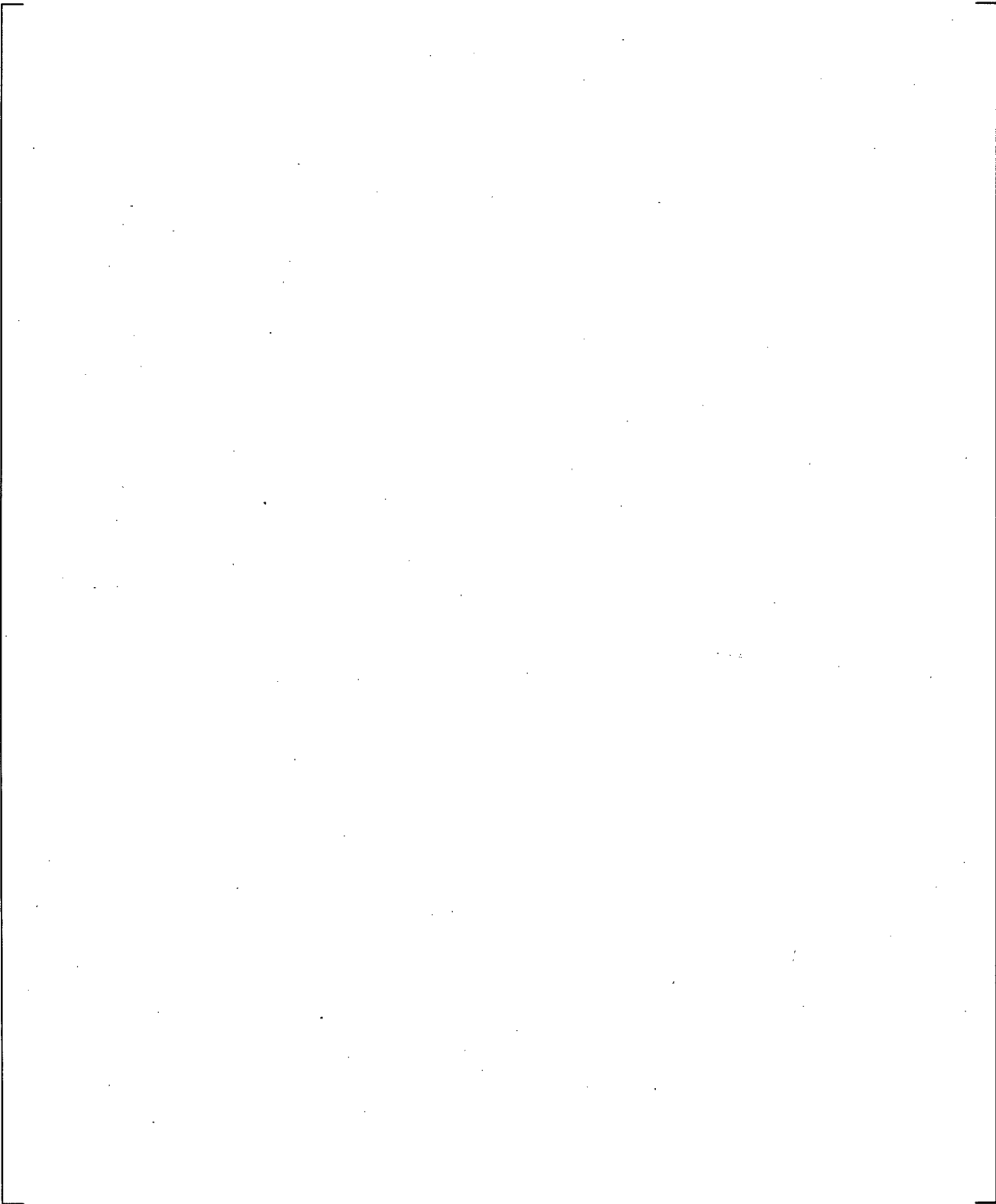
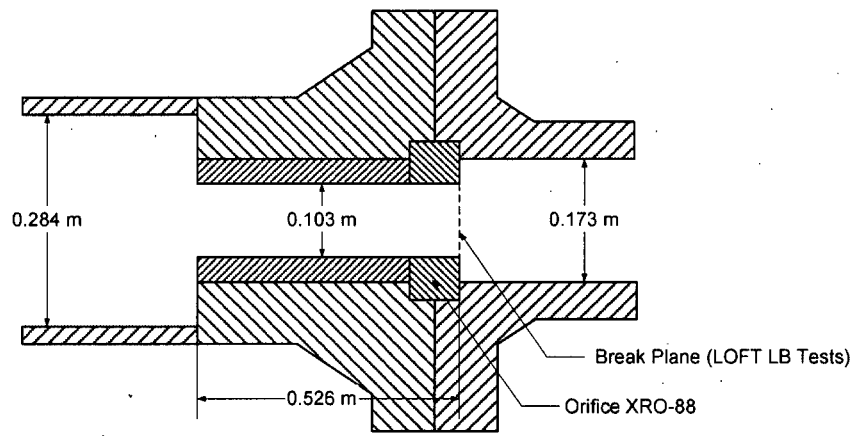


**Figure 22-10 LOFT Active Loop Steam Generator WCOBRA/TRAC-TF2 Model**



a,c

**Figure 22-11(a) Inactive (Broken) Loop Break Orifice and Cold Leg Modeling – LOFT Large Break**

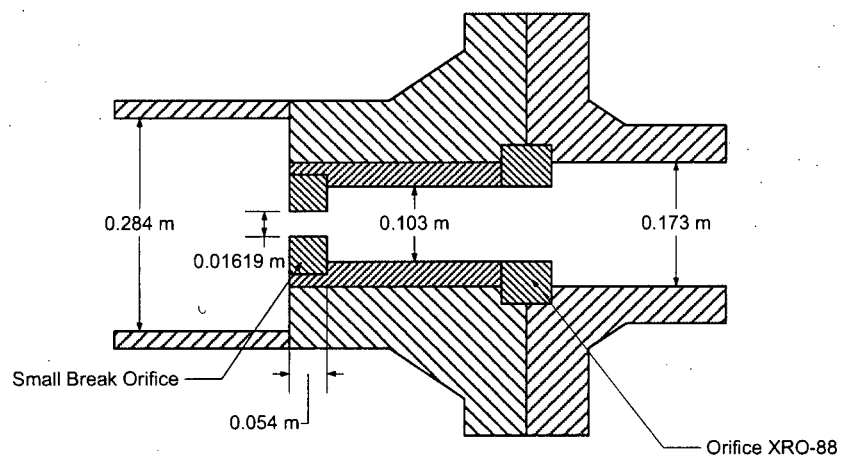


**Figure 22-11(b) Inactive (Broken) Loop Break Orifice and Cold Leg Modeling – LOFT Small Break**

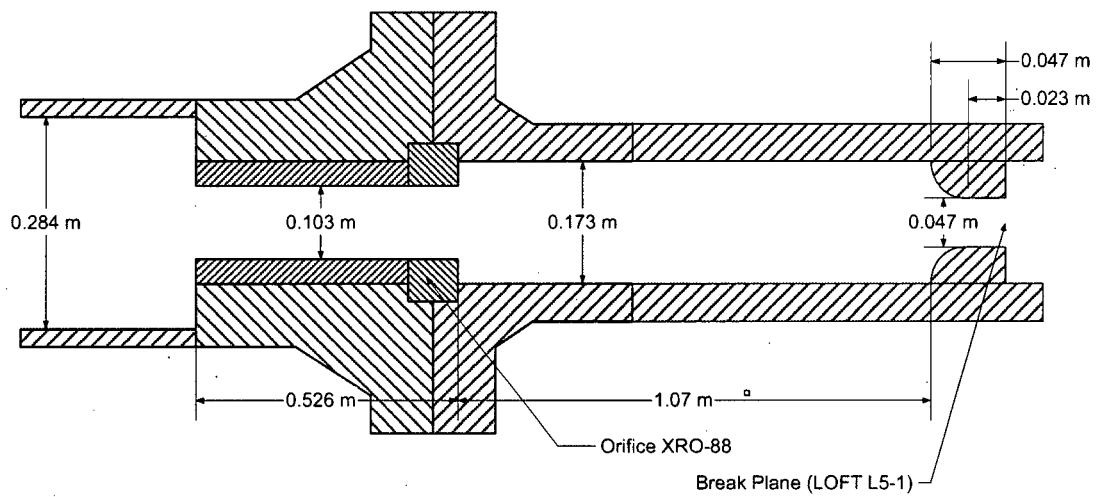
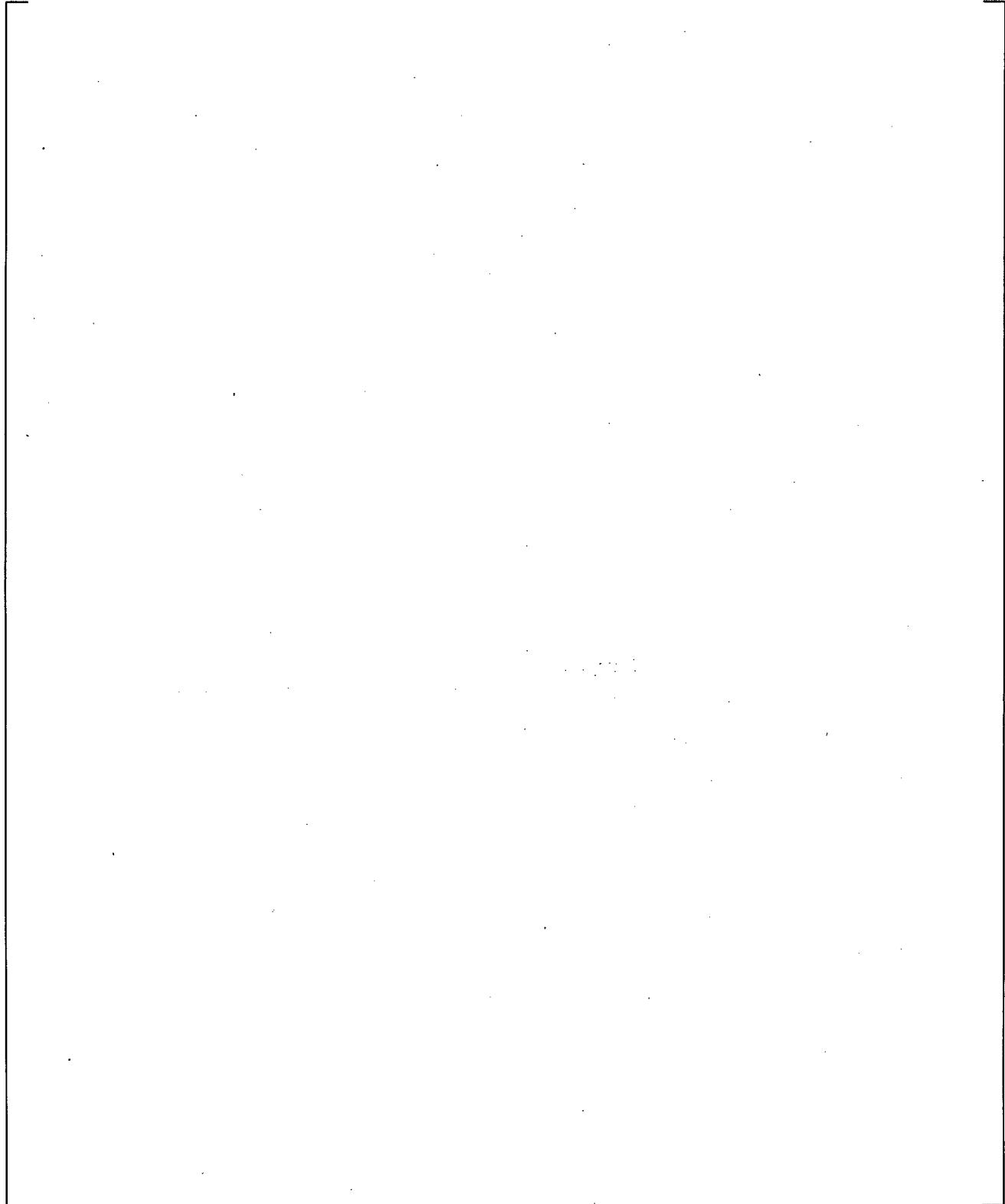


Figure 22-11c) Inactive (Broken) Loop Break Orifice (Gillas and Carpenter, 1980) and Cold Leg Modeling – LOFT Intermediate Break



**Figure 22-12 LOFT Inactive (Broken) Loop Hot Leg WCOBRA/TRAC-TF2 Model**

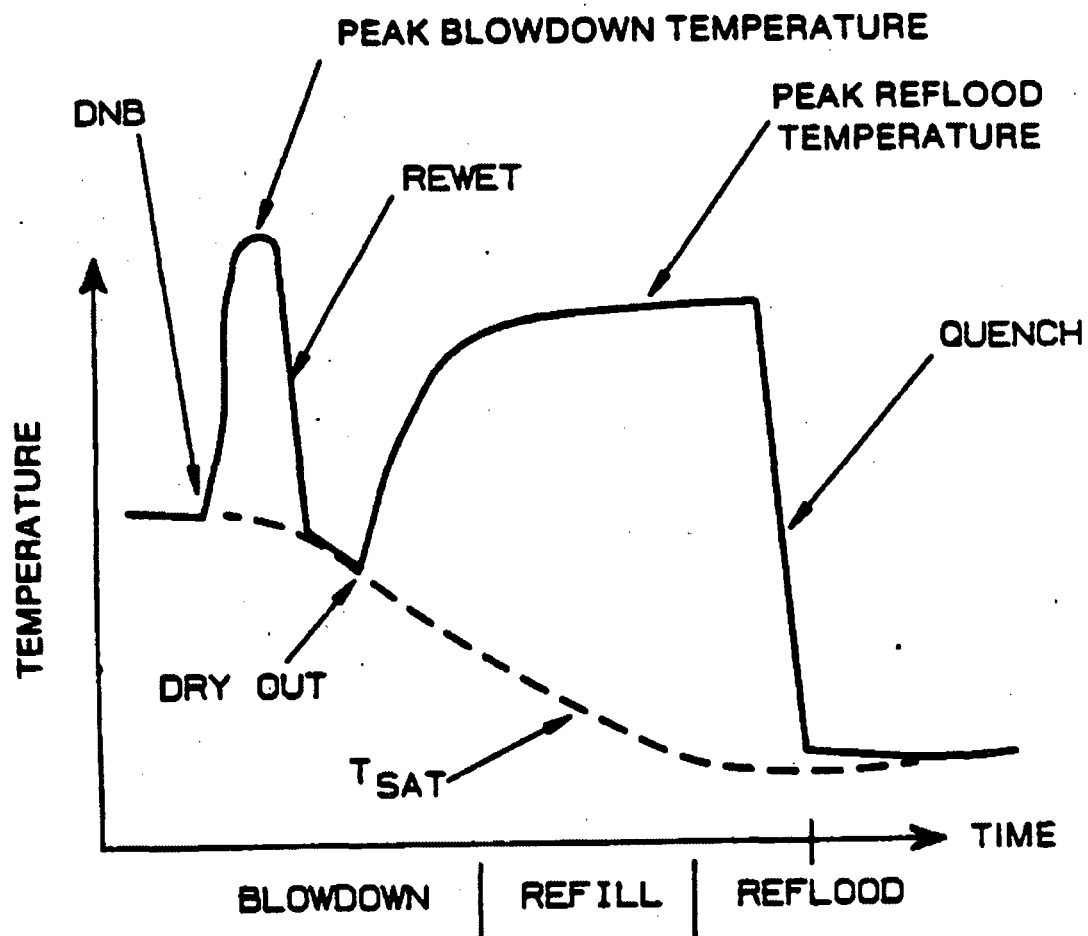
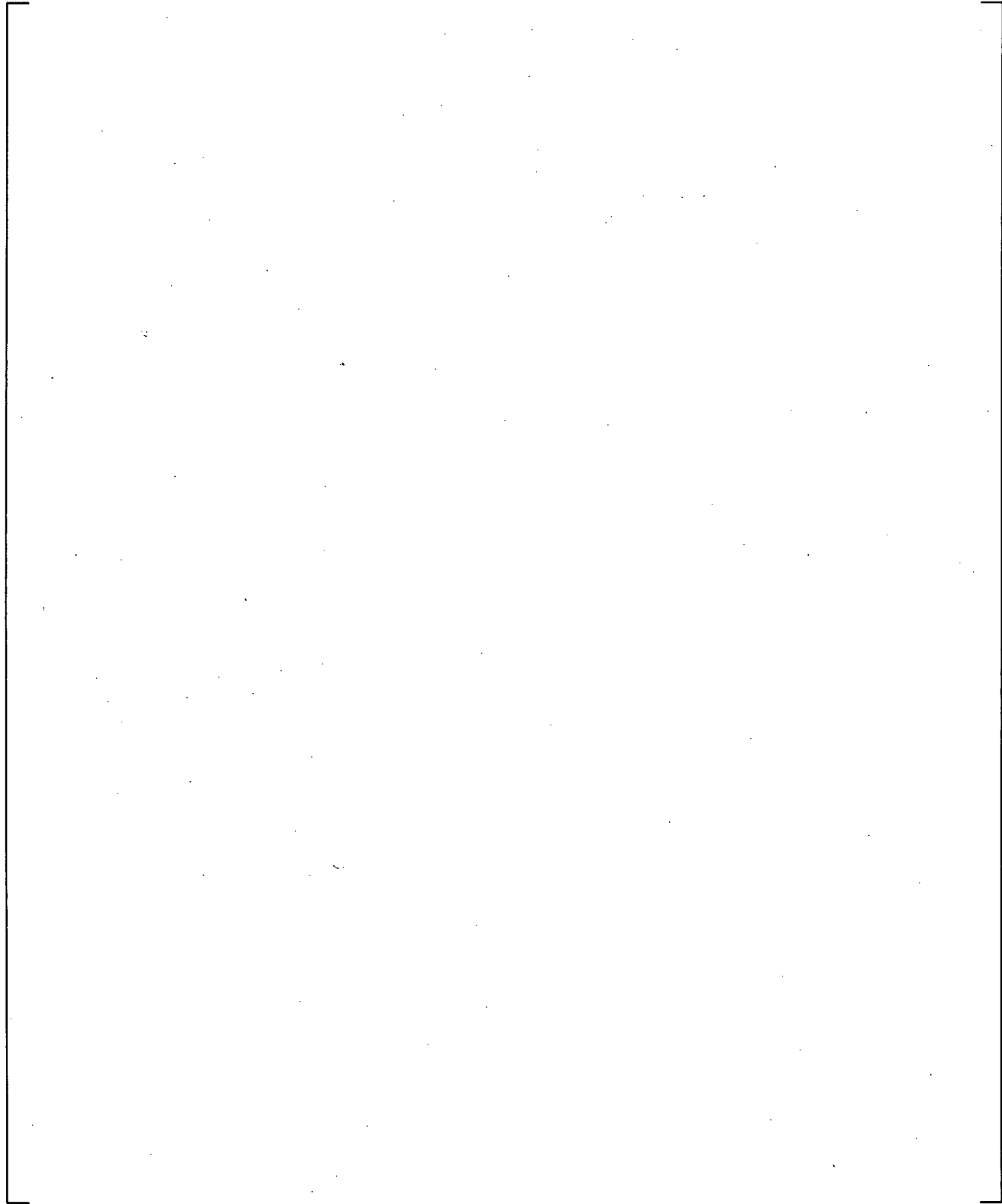
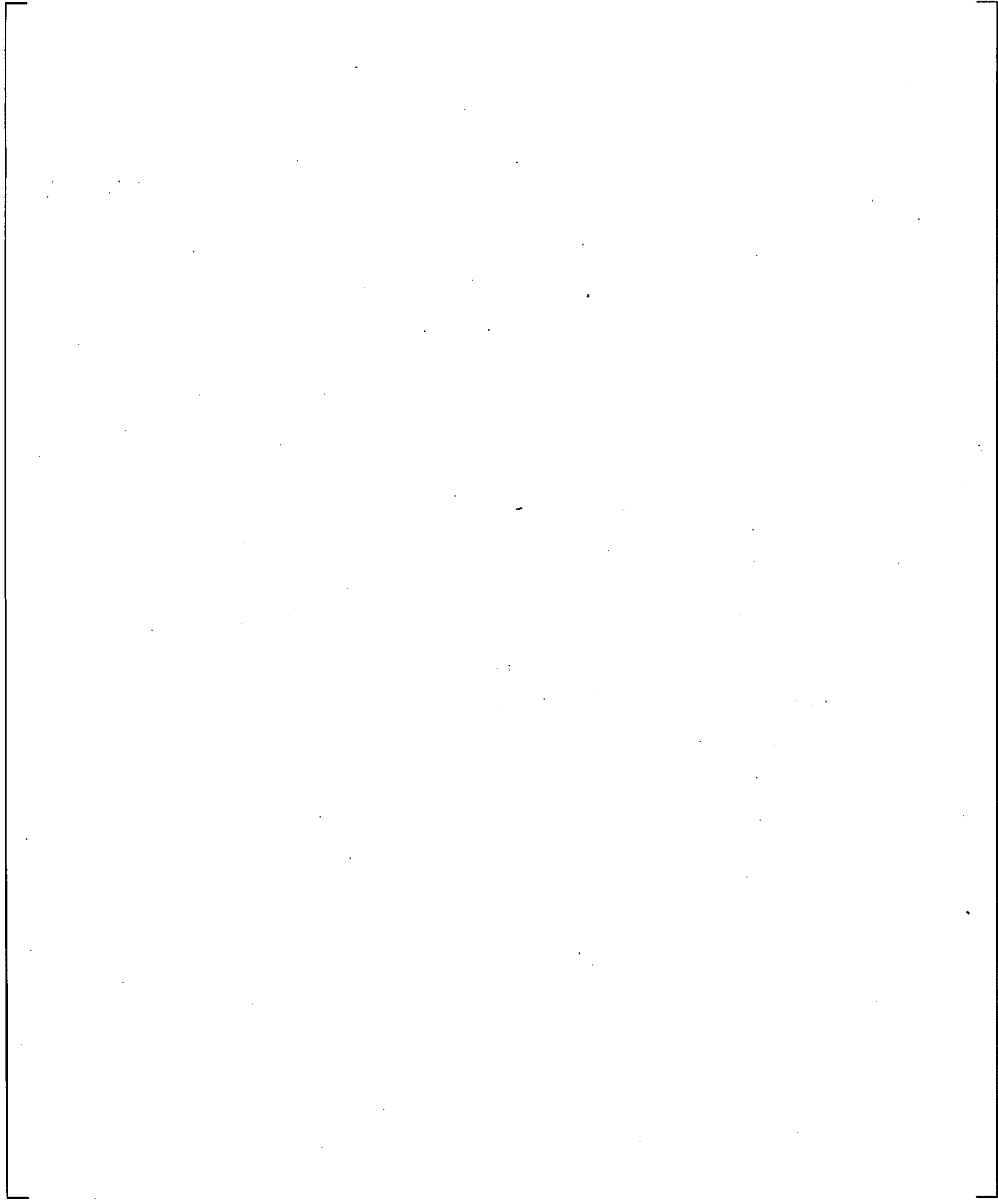


Figure 22-13 Typical Time History of Cladding Temperature during a LOFT Large break Test Transient



**Figure 22-14 Predicted (Component 500) and Measured (PE-PC-005) Pressure, Test L2-2**



**Figure 22-15 Predicted (Component 500) and Measured (PE-PC-005) Pressure, Test L2-3**

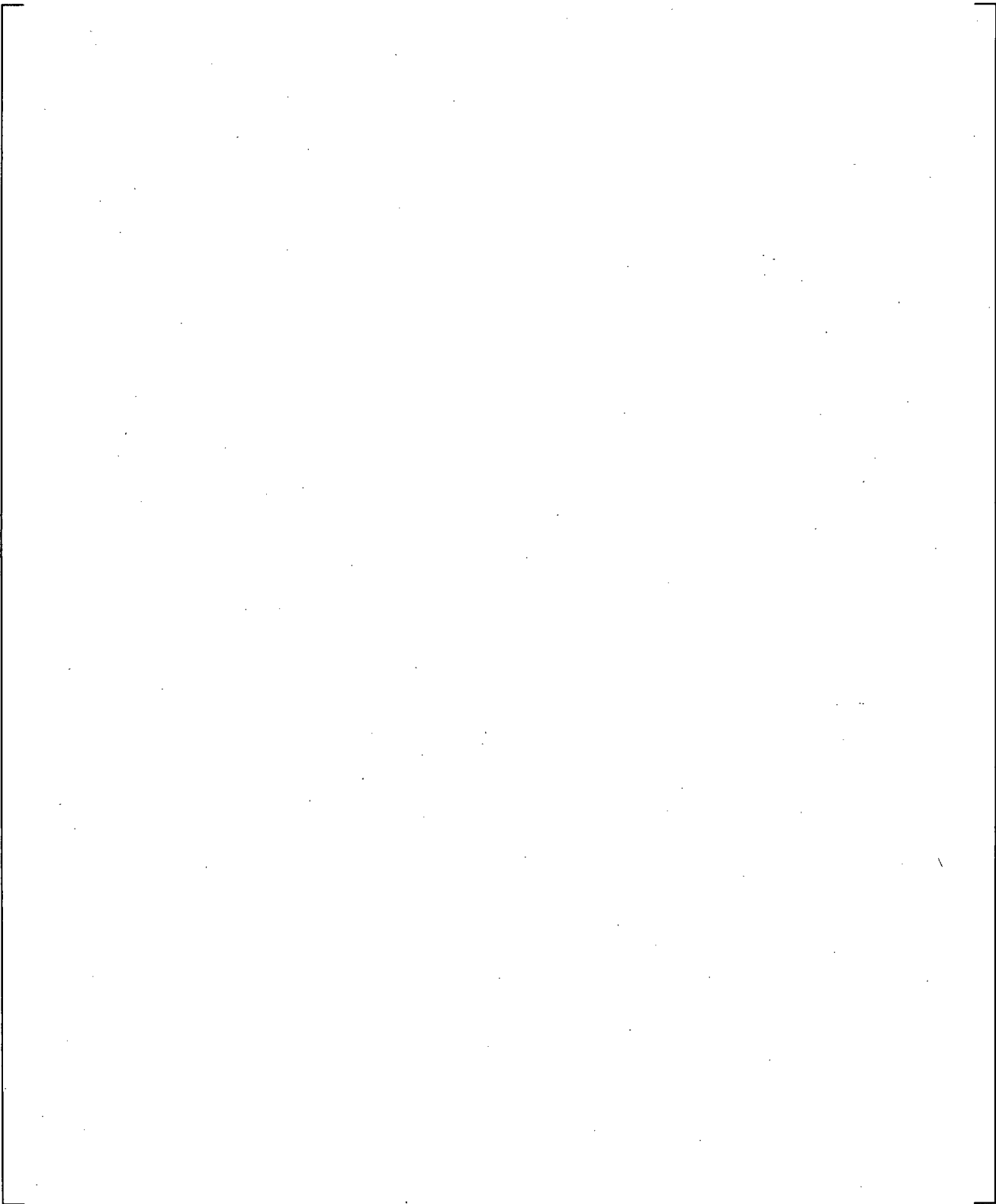


**Figure 22-16 Predicted (Component 500) and Measured (PE-PC-005) Pressure, Test L2-5**

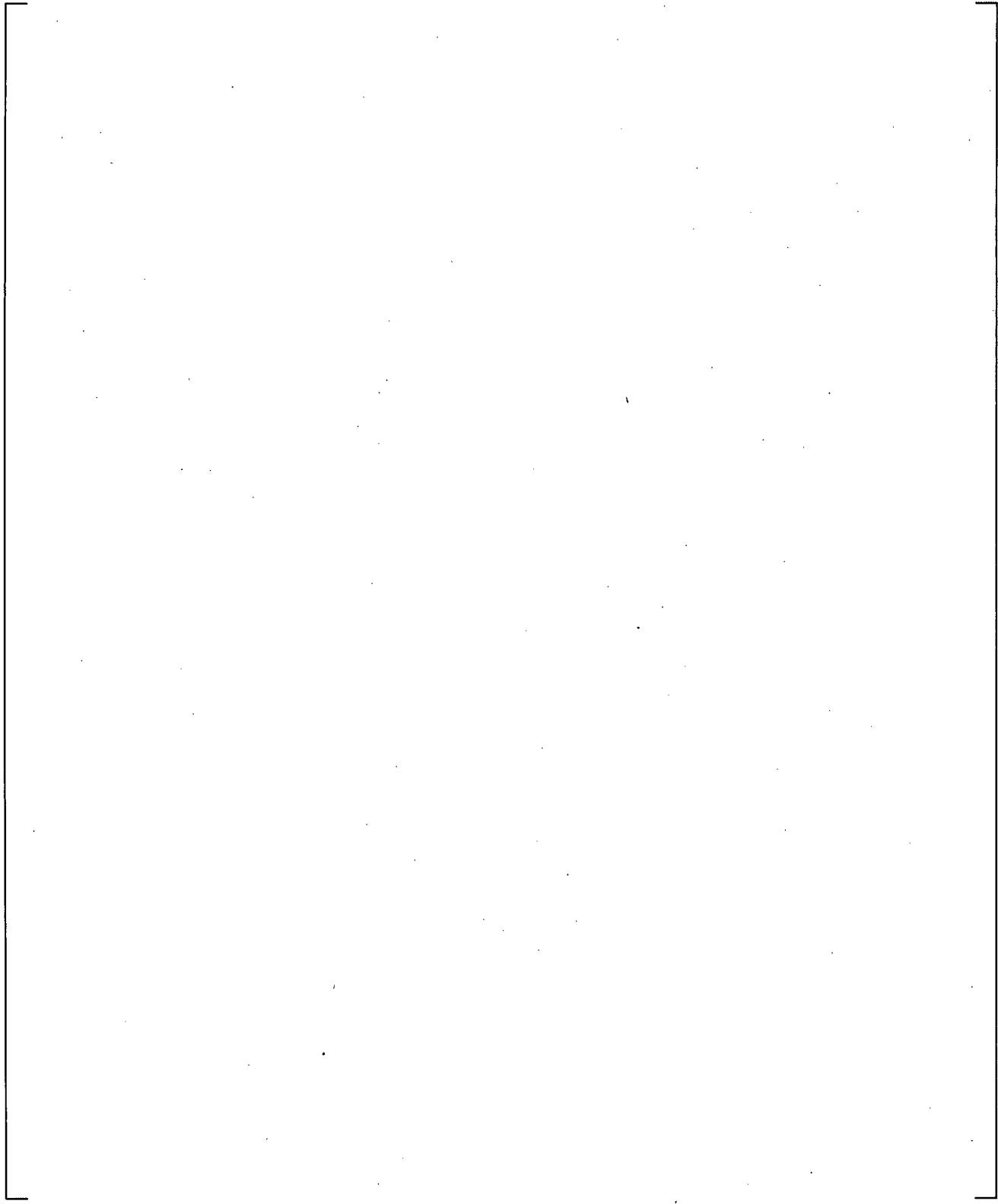


**Figure 22-17 Predicted (Component 500) and Measured (PE-PC-005) Pressure, Test LB-1**

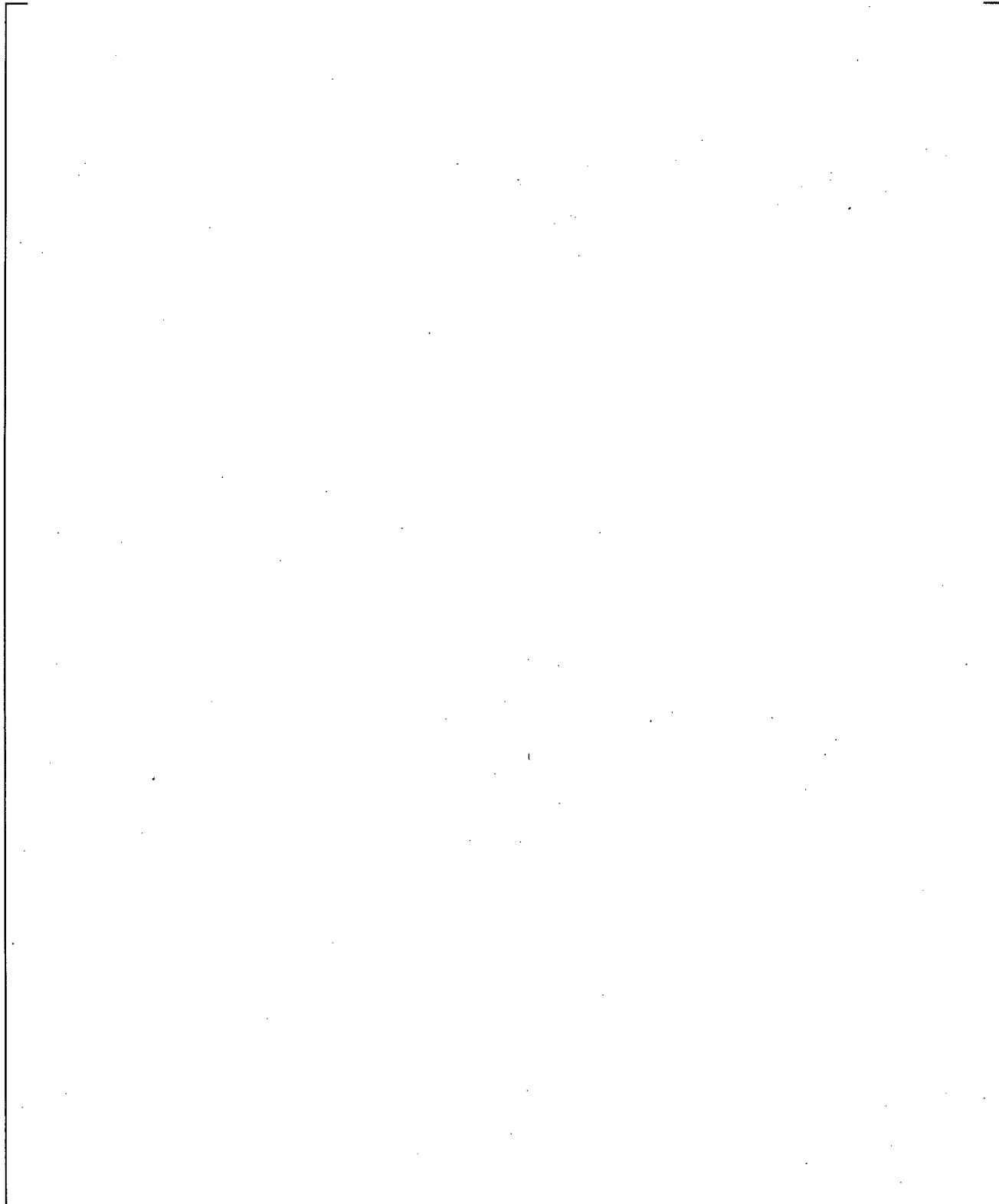


**Figure 22-18 Predicted (Component 900) and Measured (FR-BL-216) Mass Flow Rate in Broken Hot Leg, Test L2-2**

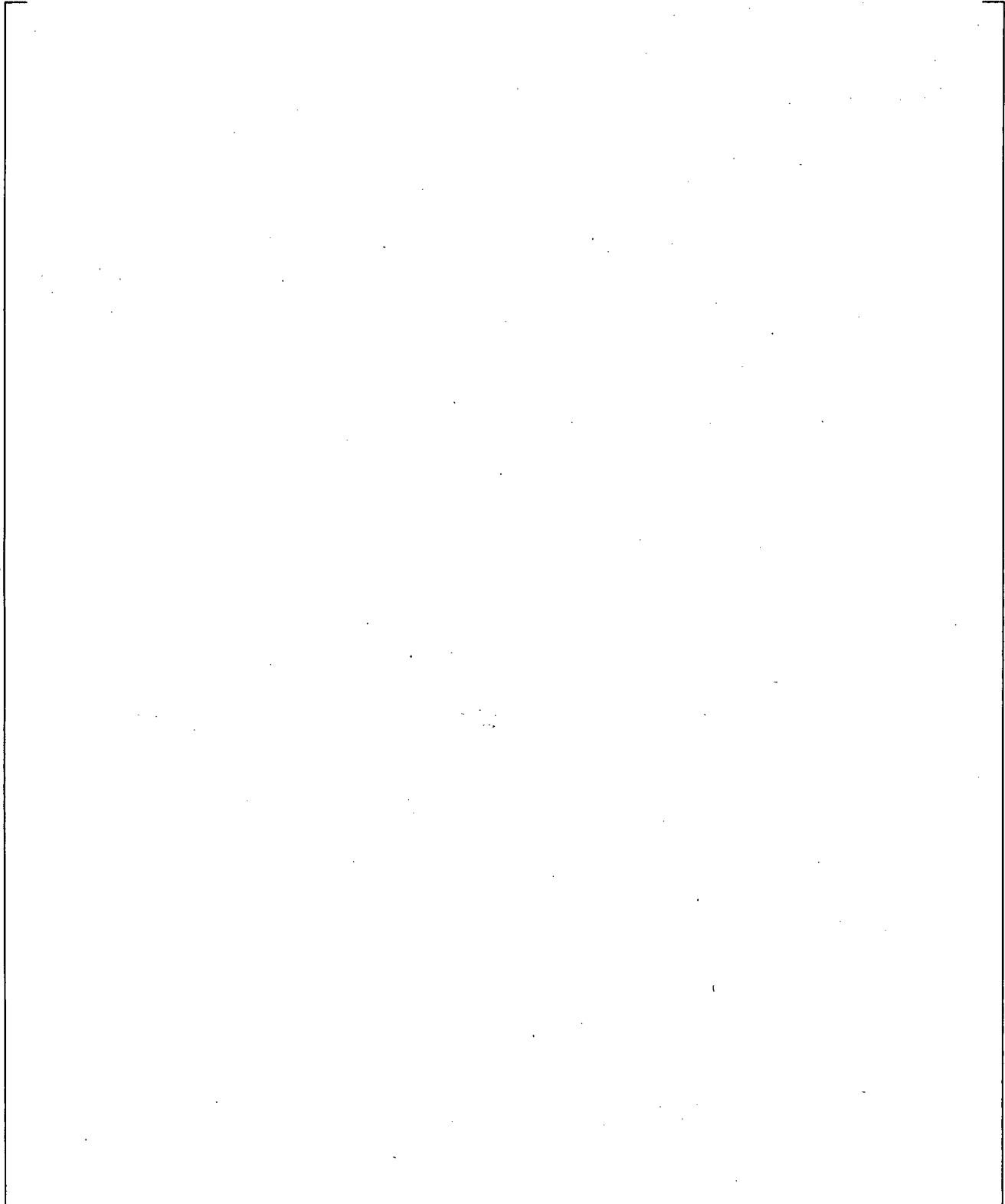


**Figure 22-19 Predicted (Component 900) and Measured (FR-BL-116) Mass Flow Rate in Broken Hot Leg, Test L2-3**

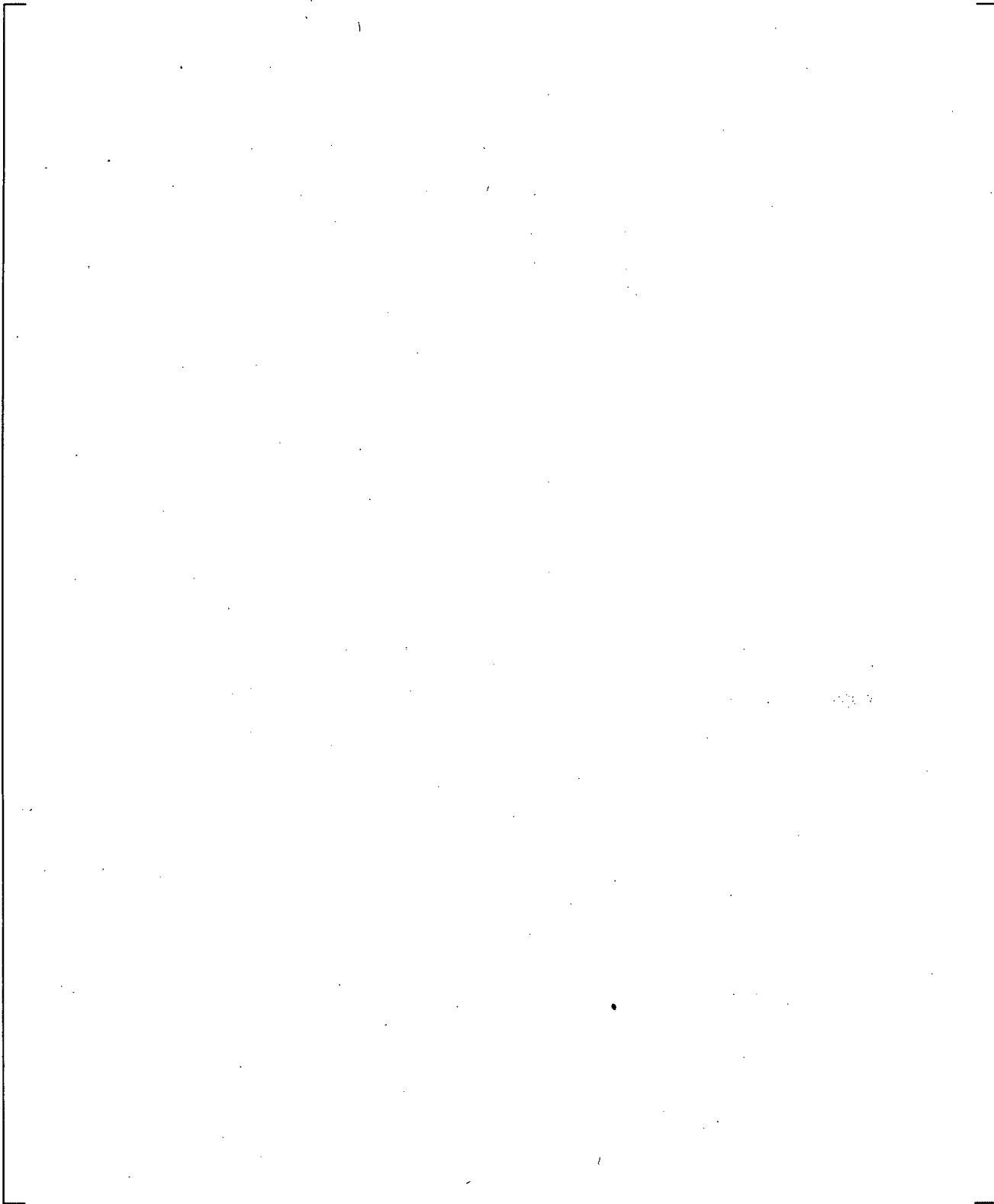


**Figure 22-20 Predicted (Component 900) and Measured (FR-BL-002) Mass Flow Rate in Broken Hot Leg, Test L2-5**

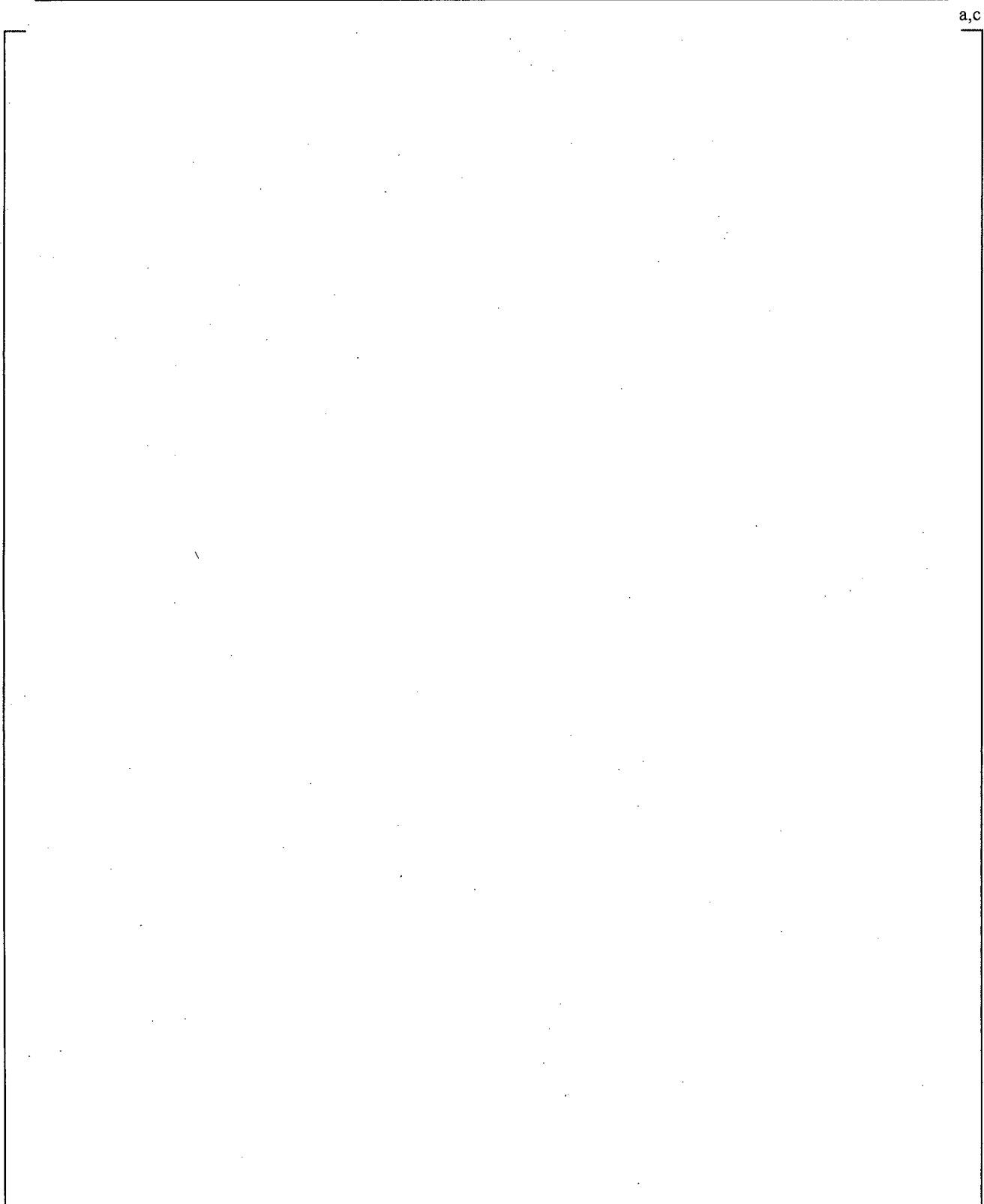


**Figure 22-21 Predicted (Component 900) and Measured (FR-BL-205) Mass Flow Rate in Broken Hot Leg, Test LB-1**

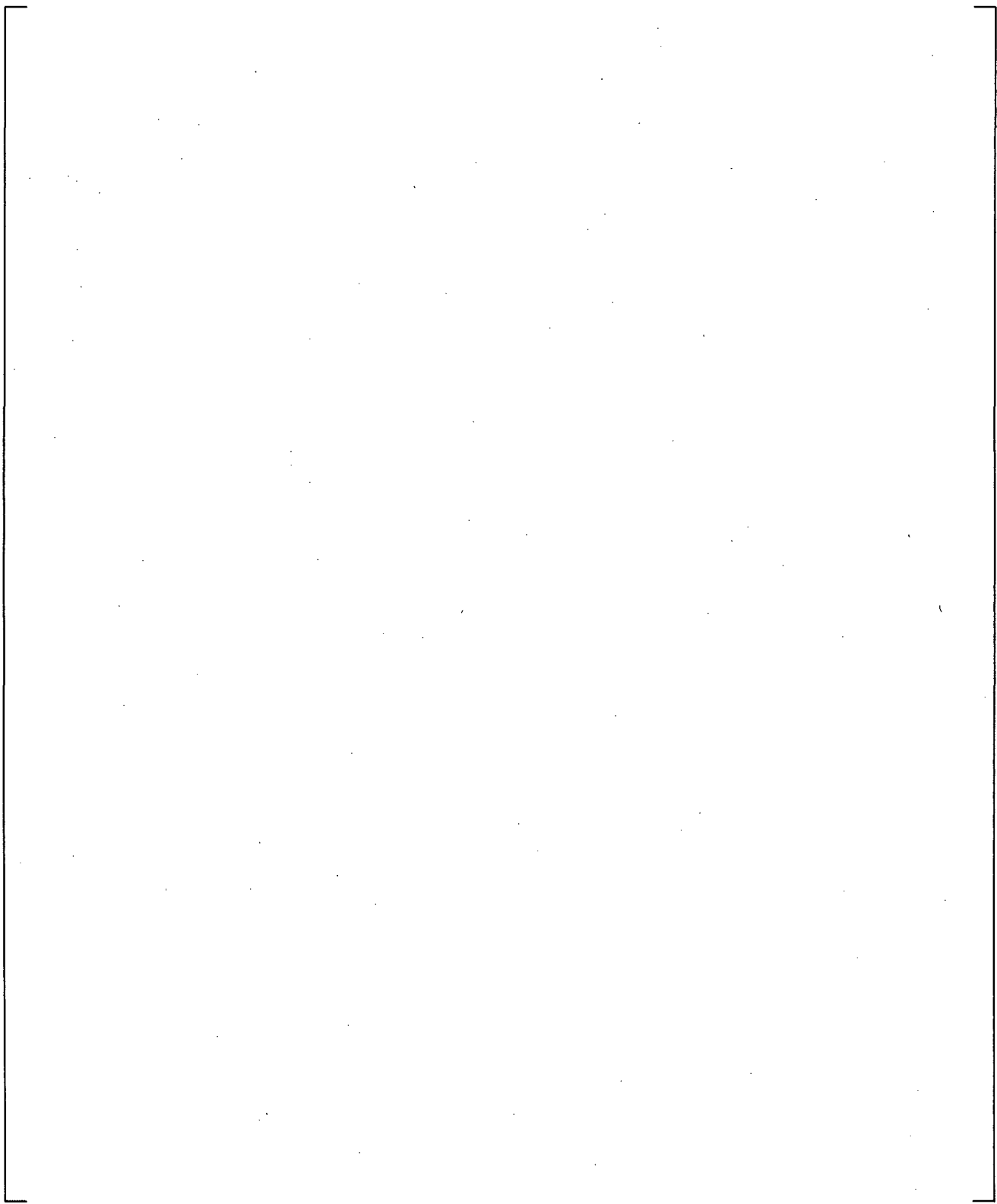


**Figure 22-22 Predicted (Component 96) and Measured (FR-BL-116) Mass Flow Rate in Broken Cold Leg, Test L2-2**

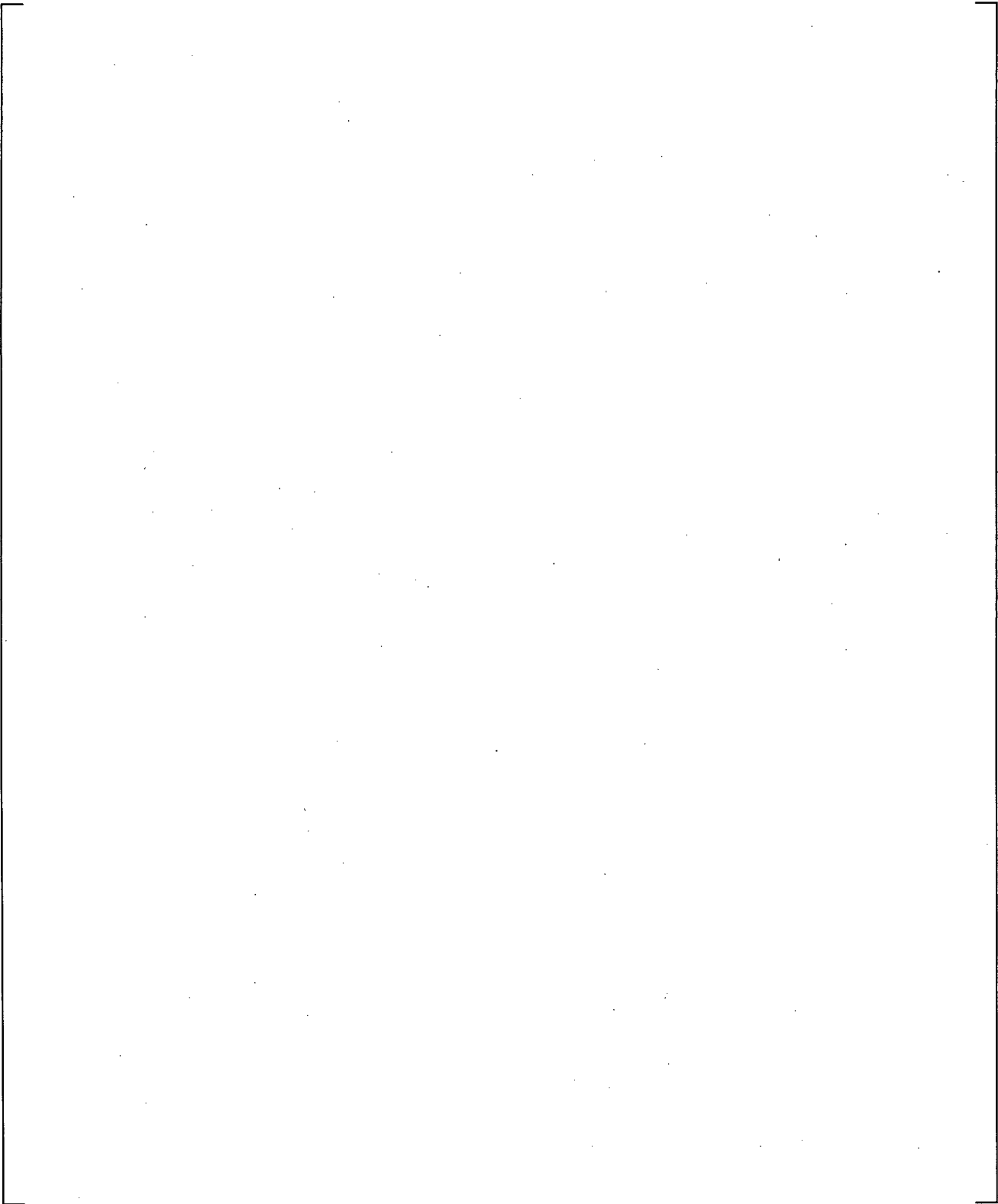


**Figure 22-23 Predicted (Component 96) and Measured (FR-BL-216) Mass Flow Rate in Broken Cold Leg, Test L2-3**

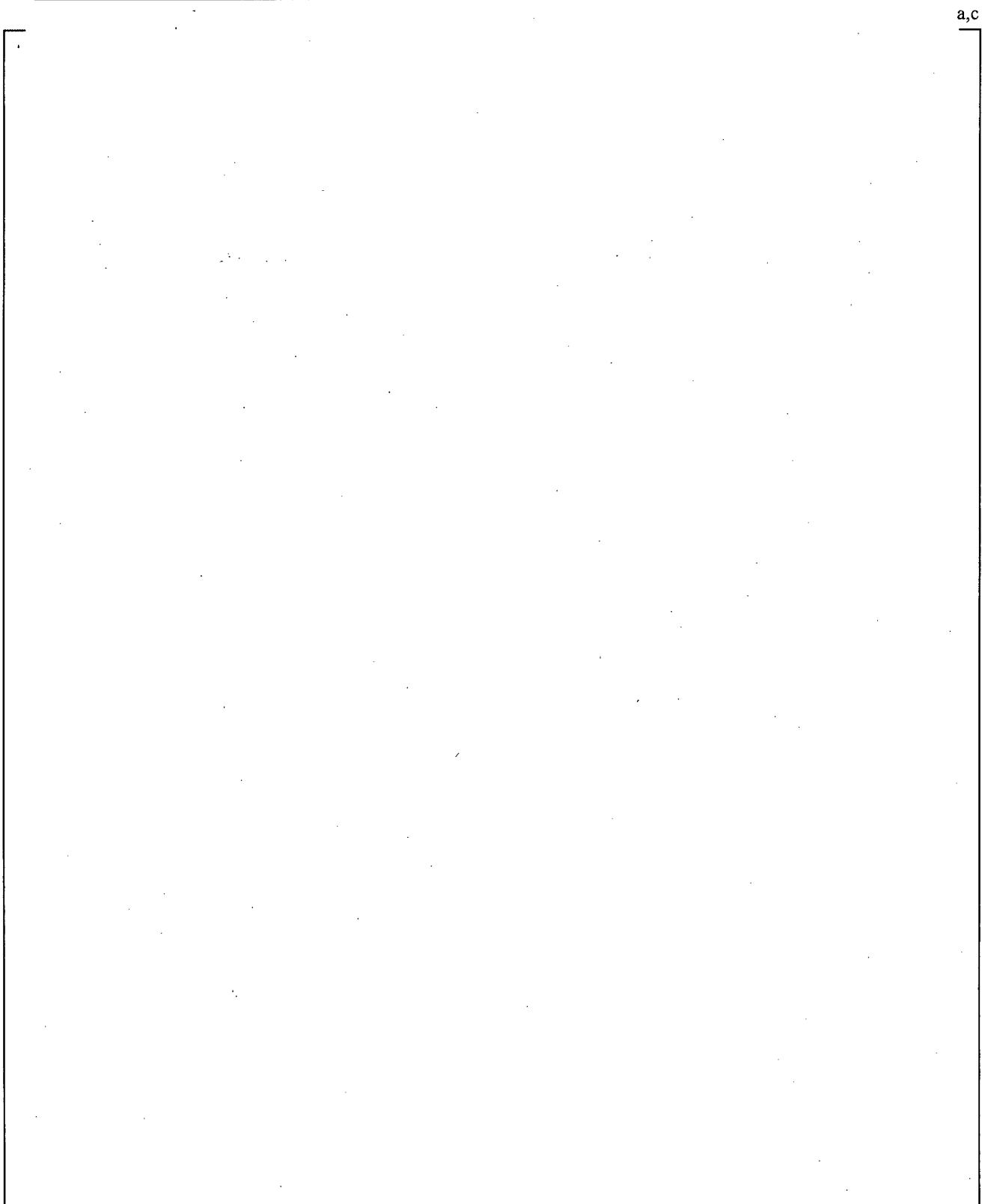


**Figure 22-24 Predicted (Component 96) and Measured (FR-BL-001) Mass Flow Rate in Broken Cold Leg, Test L2-5**

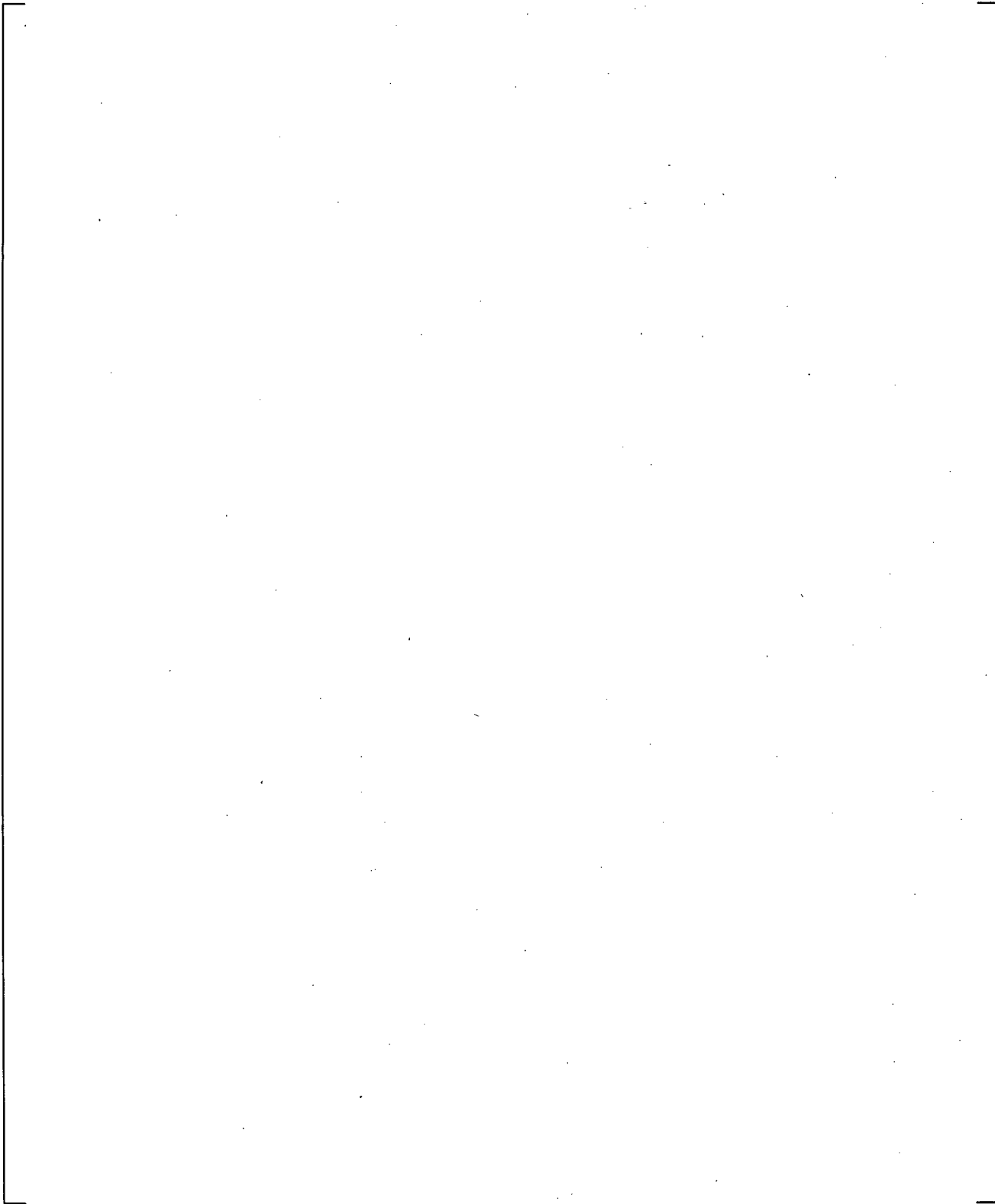


**Figure 22-25 Predicted (Component 96) and Measured (FR-BL-105) Mass Flow Rate in Broken Cold Leg, Test LB-1**

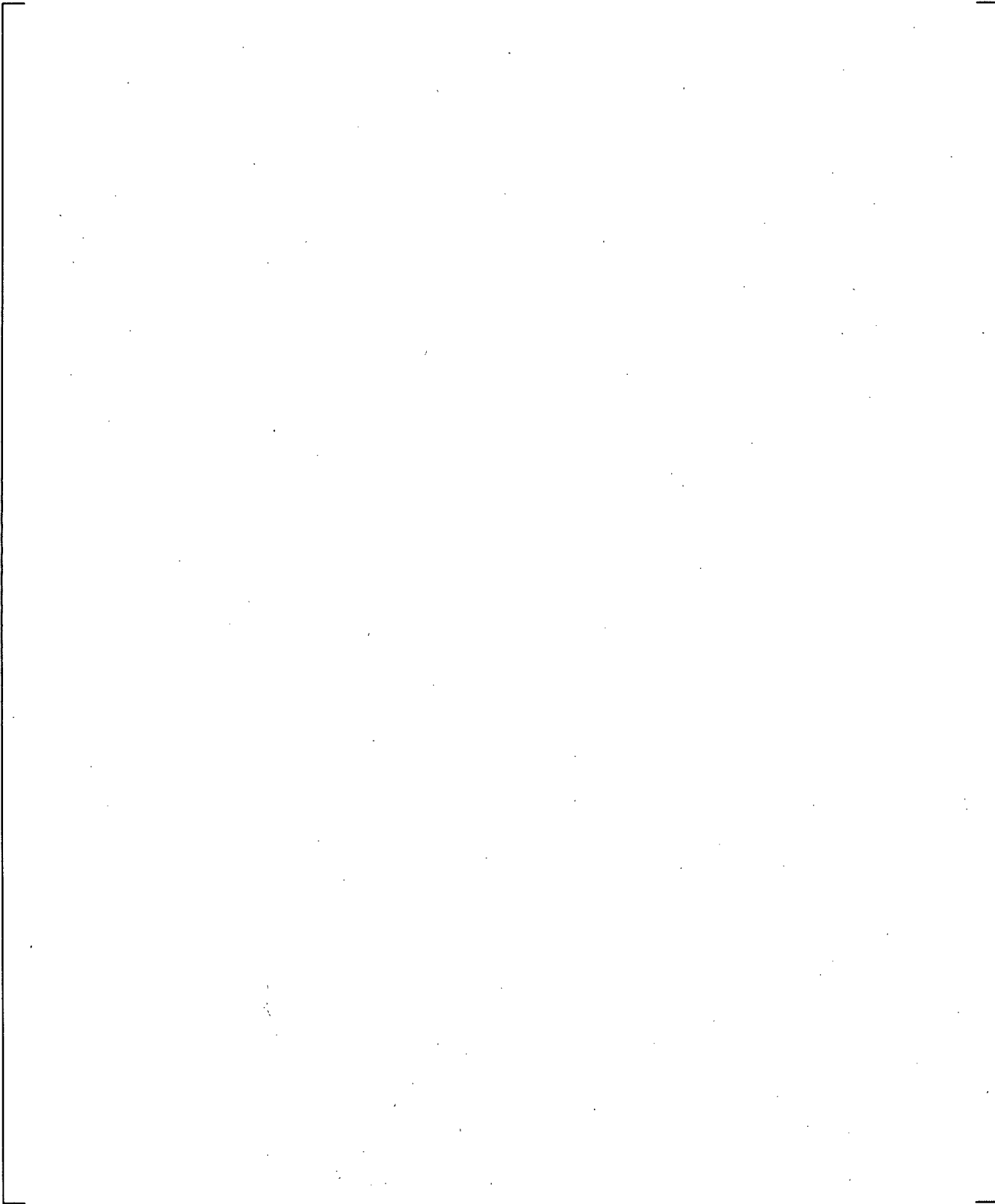


**Figure 22-26 Predicted (Component 300) and Measured (FT-P139-27) Mass Flow Rate in Intact Hot Leg, Test L2-2**

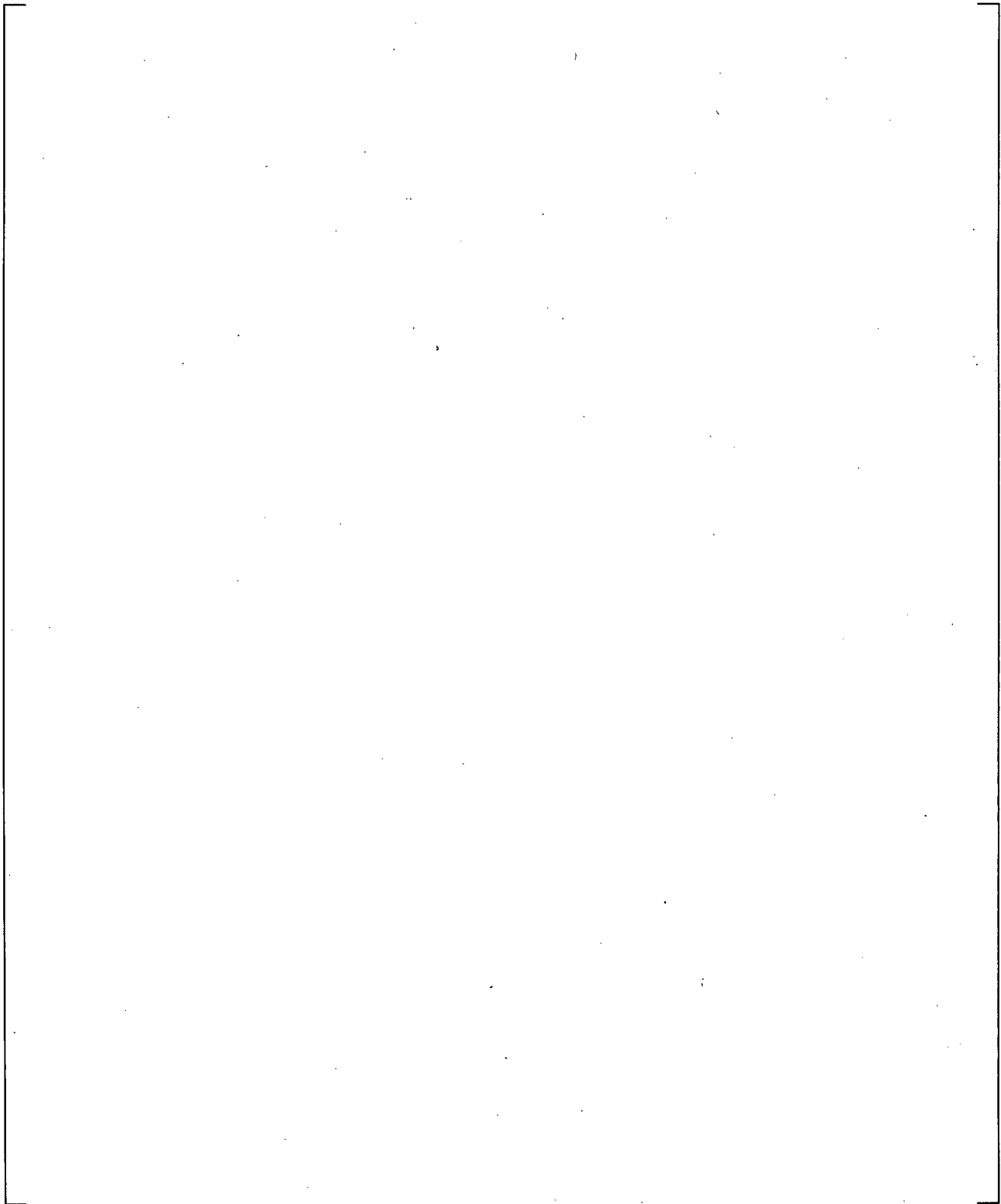


**Figure 22-27 Predicted (Component 300) and Measured (Figures 69, 78, Prassinos, et. al, 1979) Mass Flow Rate in Intact Hot Leg, Test L2-3**

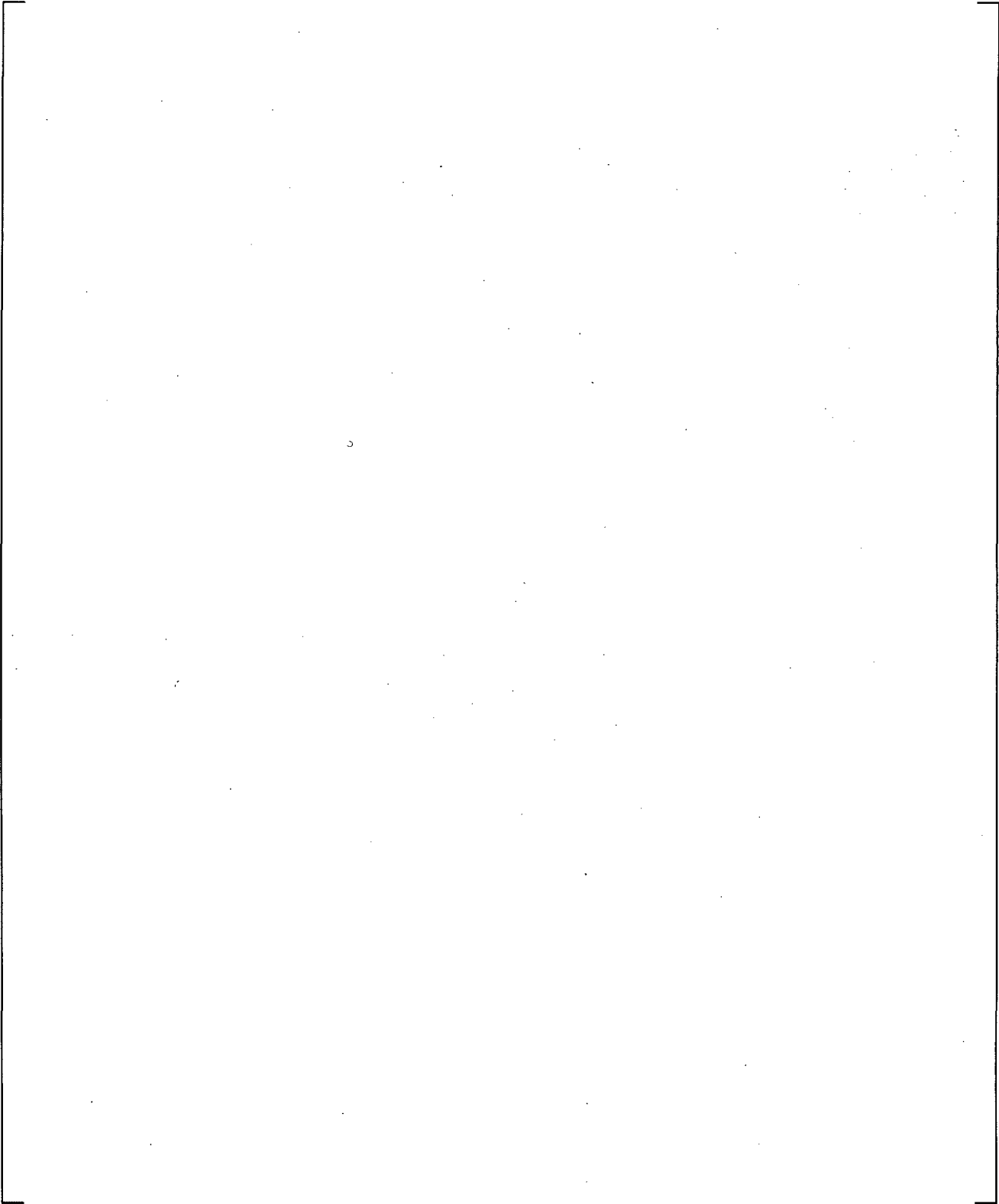


**Figure 22-28 Predicted (Component 300) and Measured (FR-PC-201) Mass Flow Rate in Intact Hot Leg, Test L2-5**

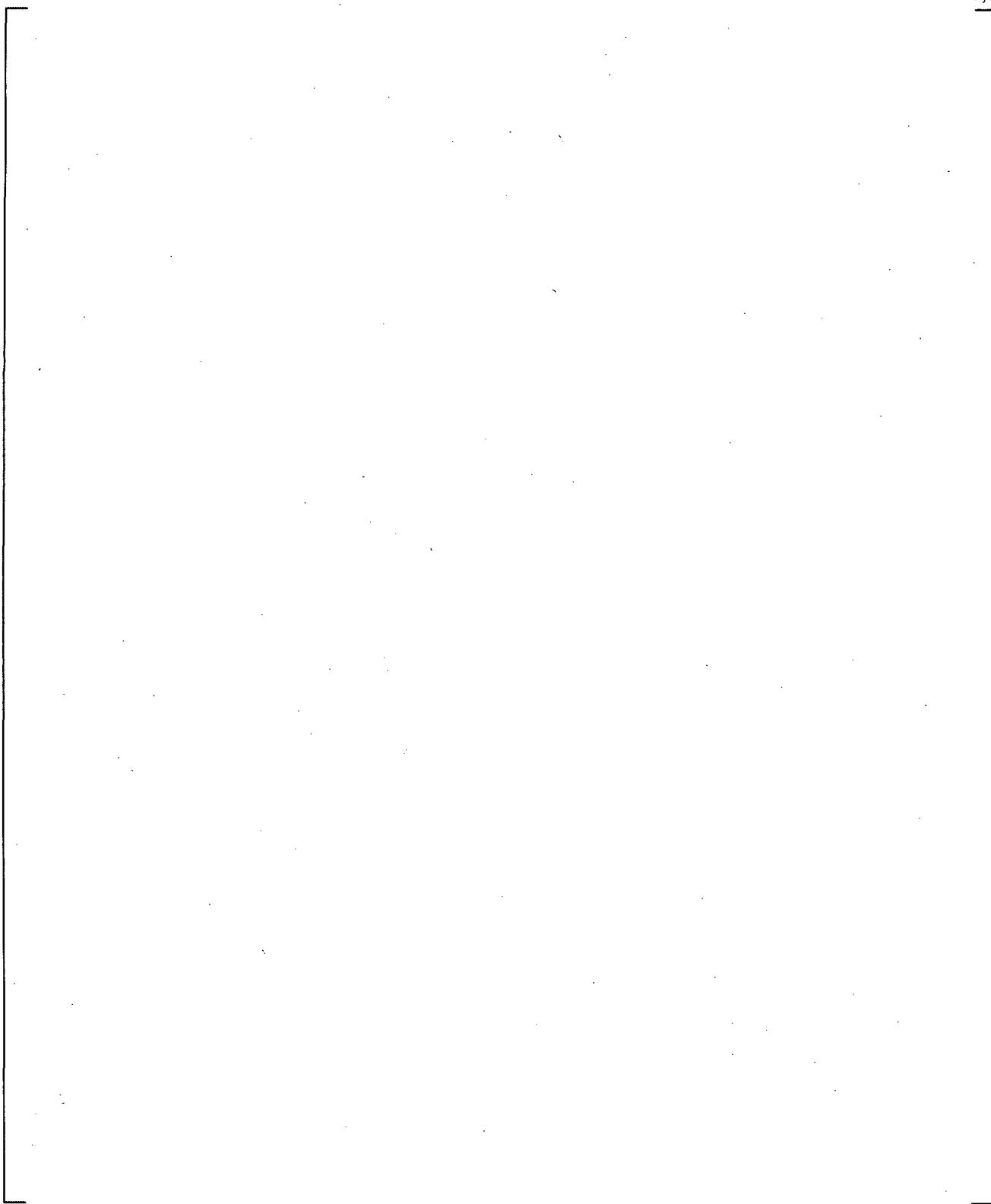


**Figure 22-29 Predicted (Component 810) and Measured (FR-PC-105) Mass Flow Rate in Intact Cold Leg, Test LB-1**

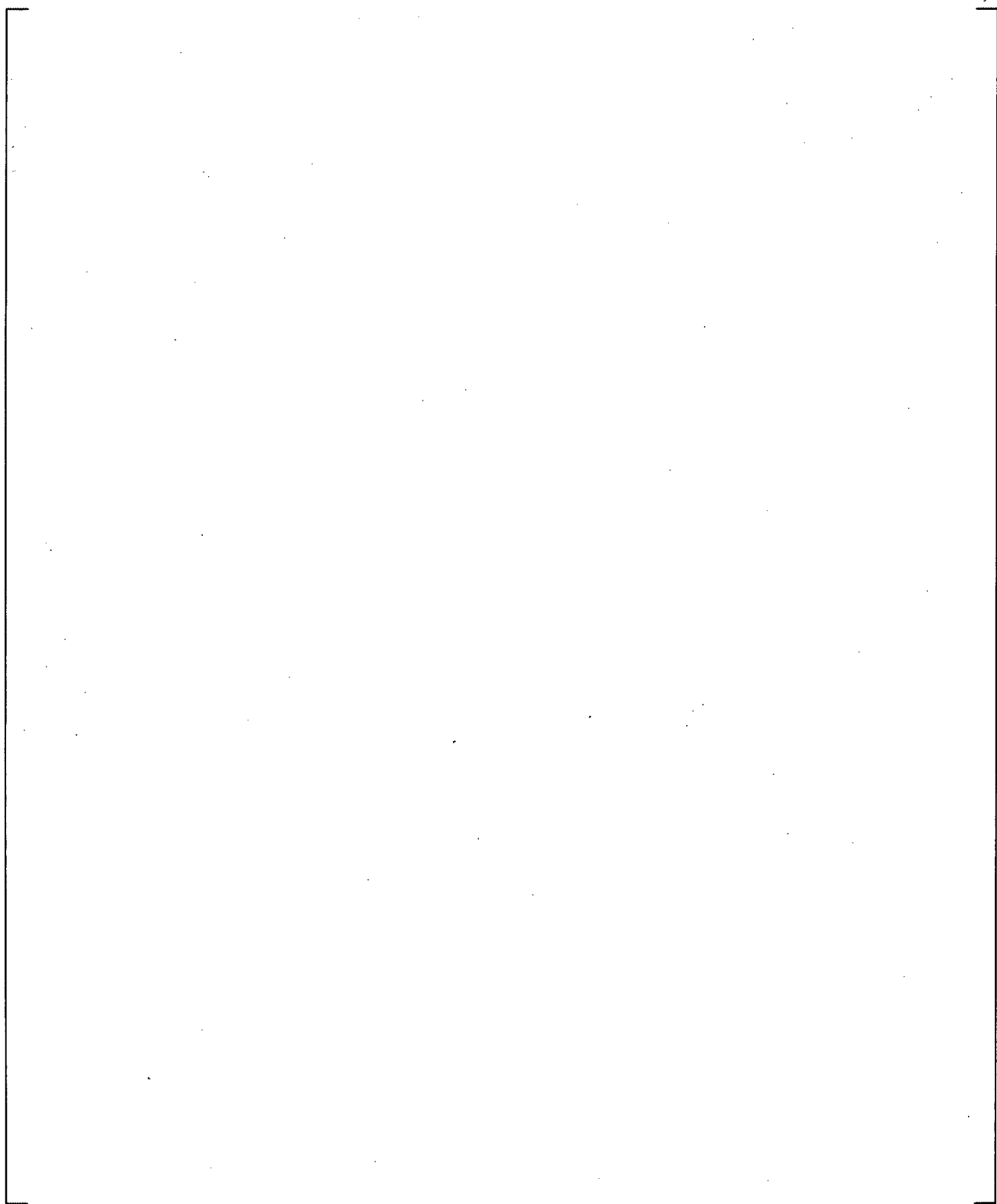


**Figure 22-30a Predicted (Component 840) and Measured (FT-P120-36) Volumetric Flow Rate and Predicted (Component 840) Void Fraction from Accumulator, Test L2-2**

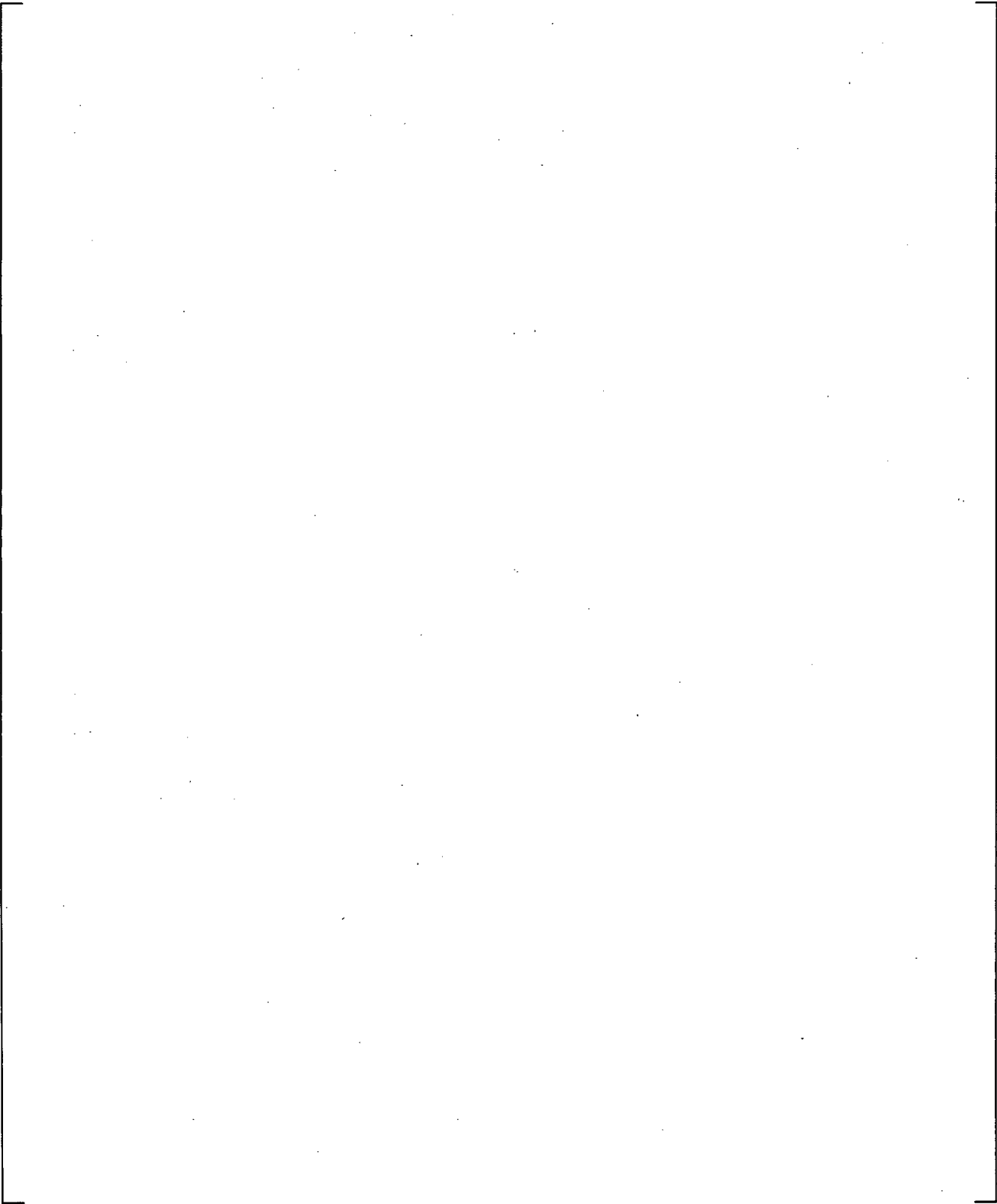


**Figure 22-30b Predicted (Component 850) and Measured (LIT-P120-087) Liquid Level in Accumulator, Test L2-2**

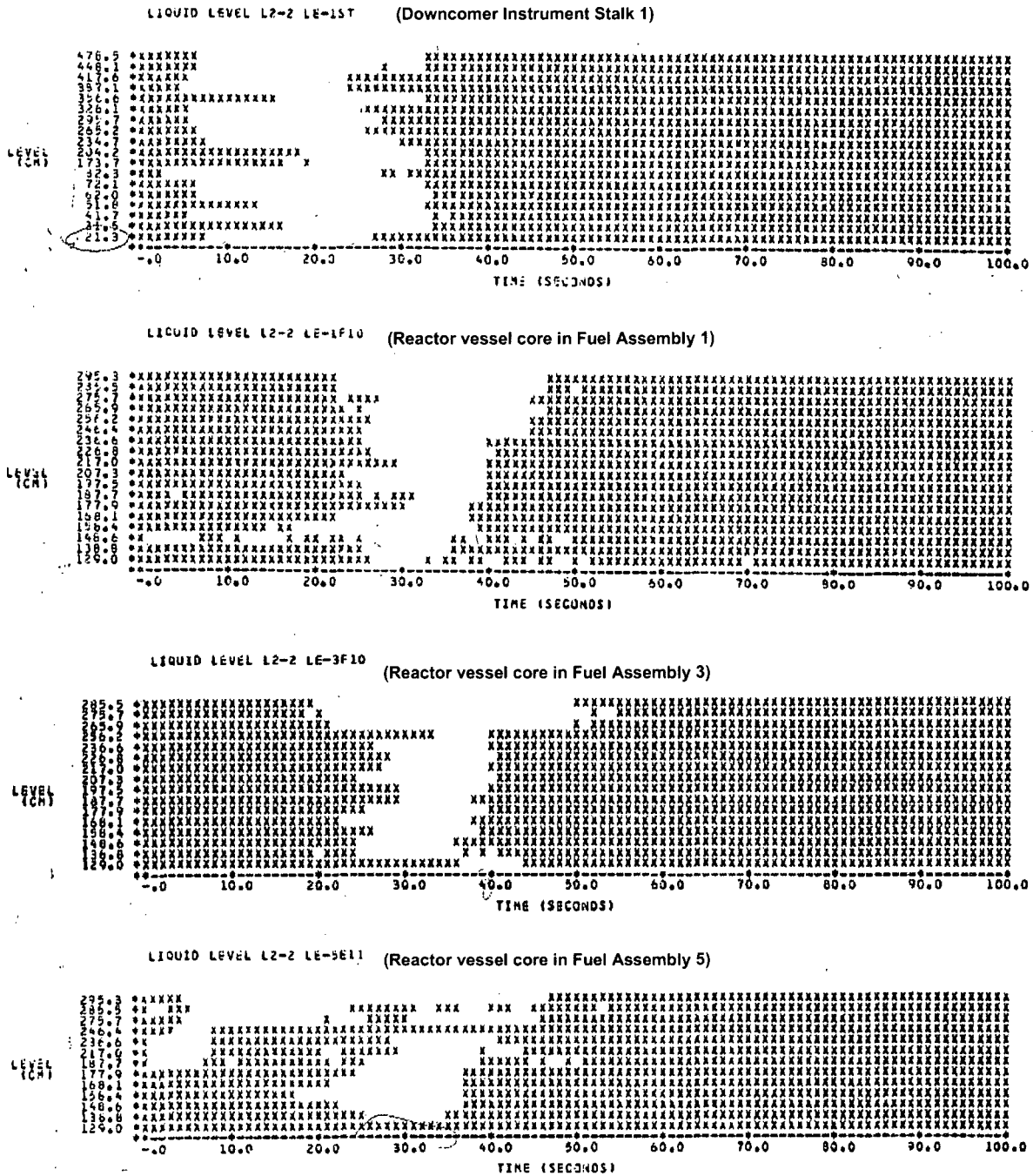
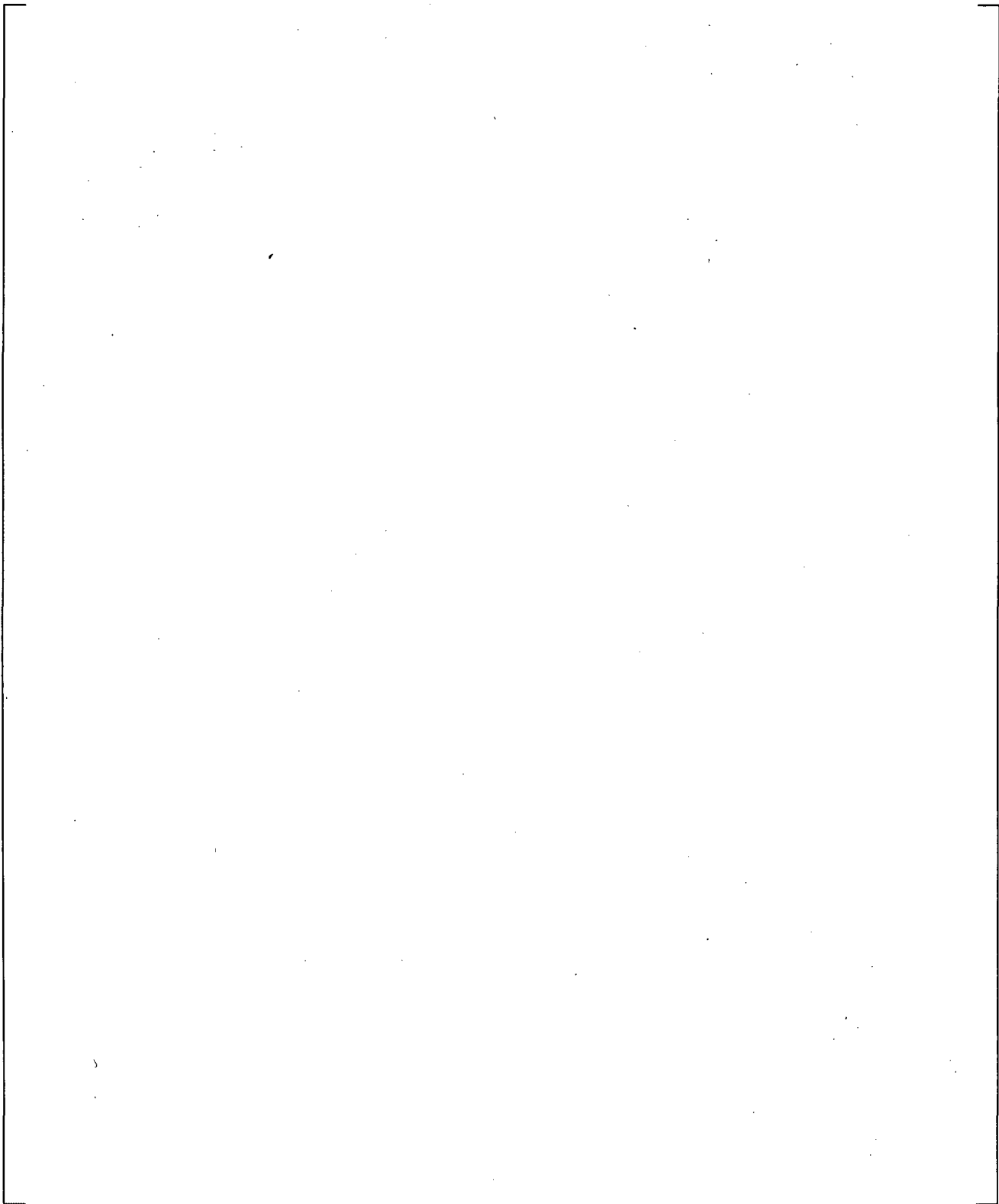
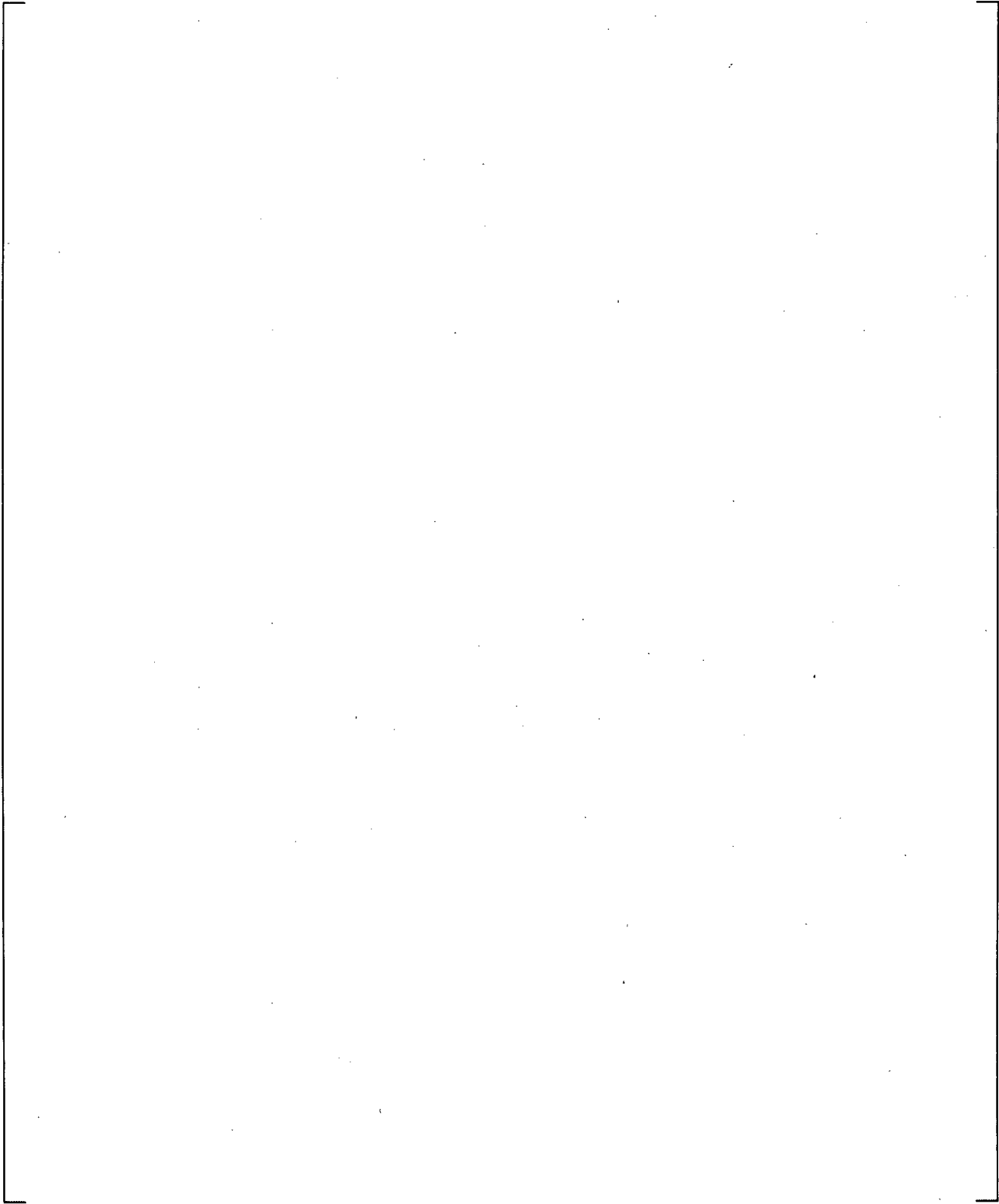


Figure 22-30c Measured Liquid Levels in Downcomer and Core Regions, Test L2-2



**Figure 22-30d Predicted Liquid Levels in Downcomer and Core Region, Test L2-2**



**Figure 22-30e Predicted and Measured Liquid Levels in Core Regions, Test L2-2**

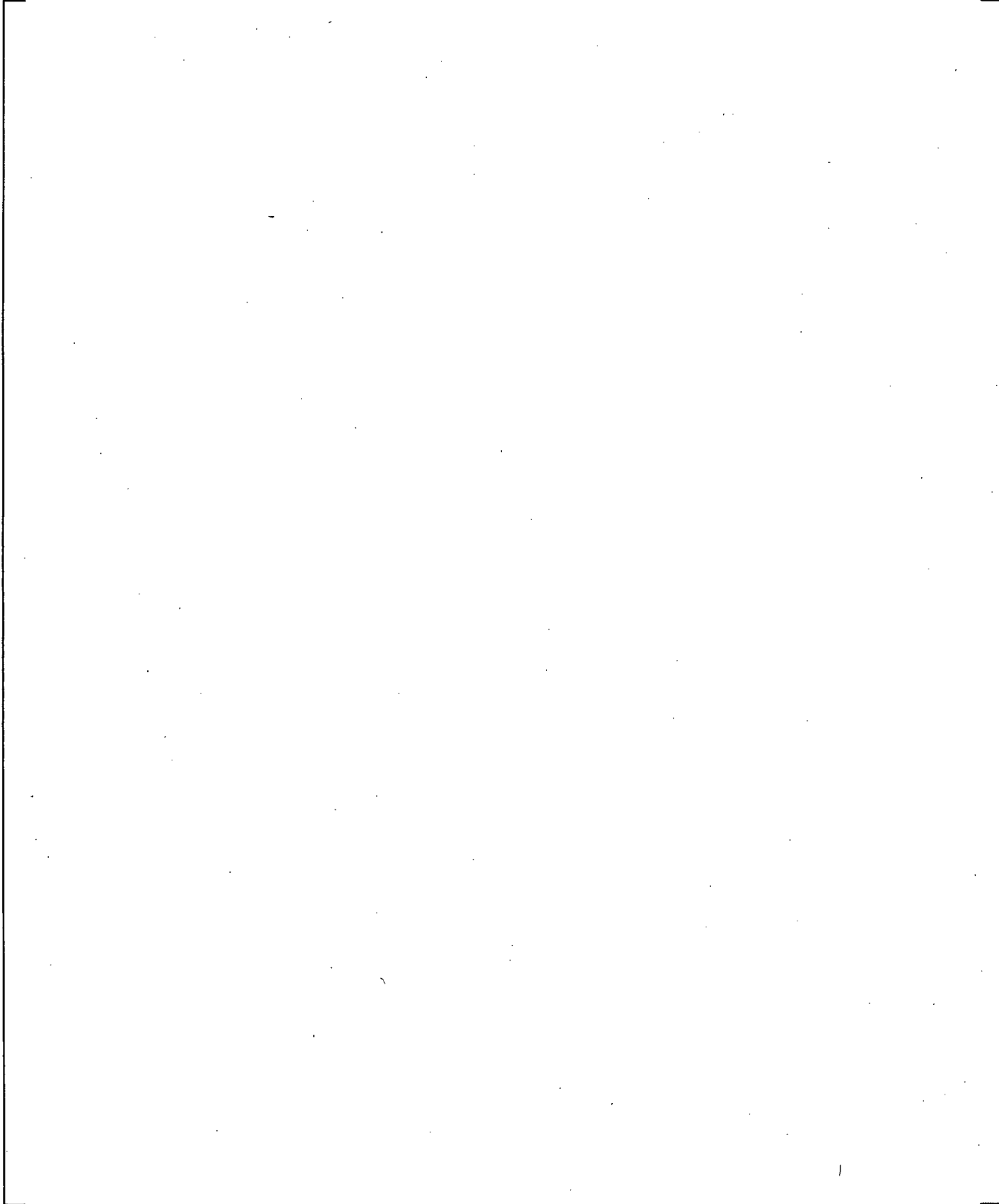


**Figure 22-31a Predicted (Component 840) and Measured (FT-P120-36) Volumetric Flow Rate and Predicted (Component 840) Void Fraction from Accumulator, Test L2-3**

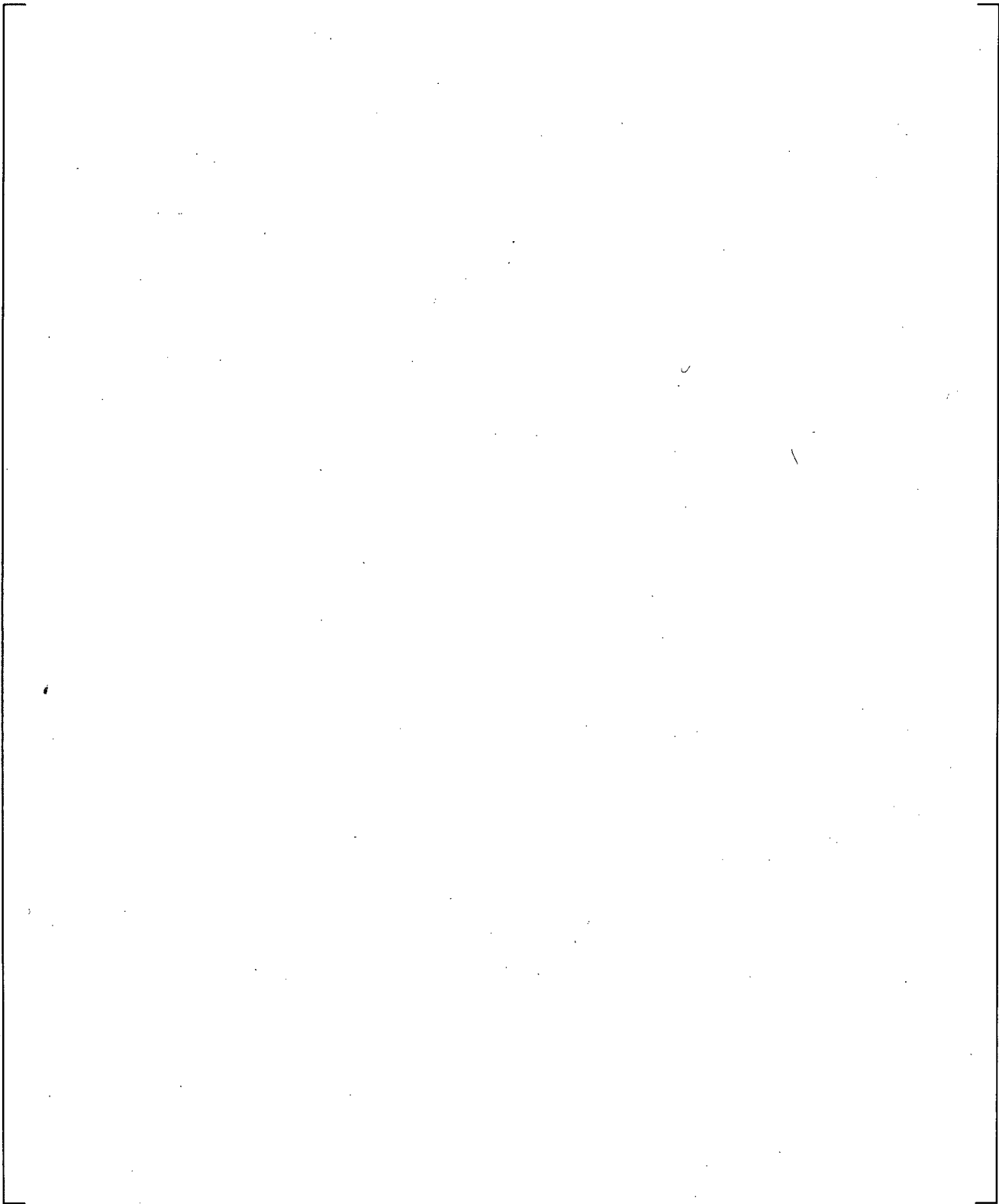


**Figure 22-31b Predicted (Component 850) and Measured (LIT-P120-084) Liquid Level in Accumulator, Test L2-3**

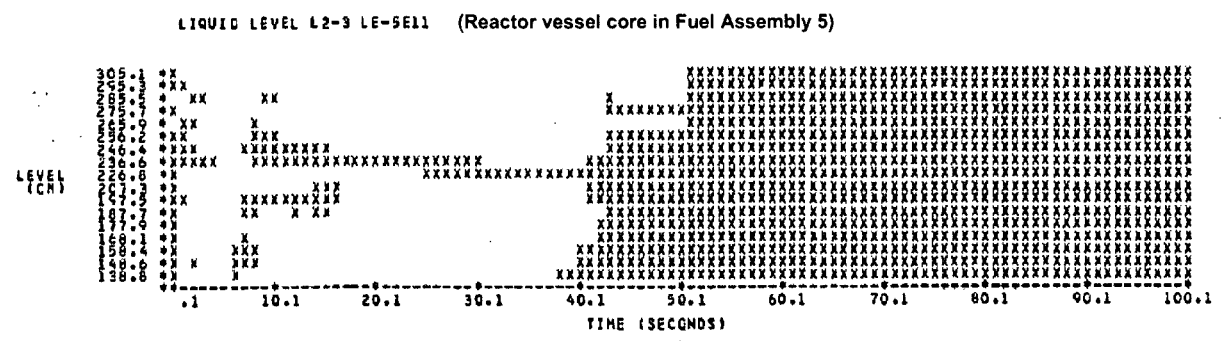
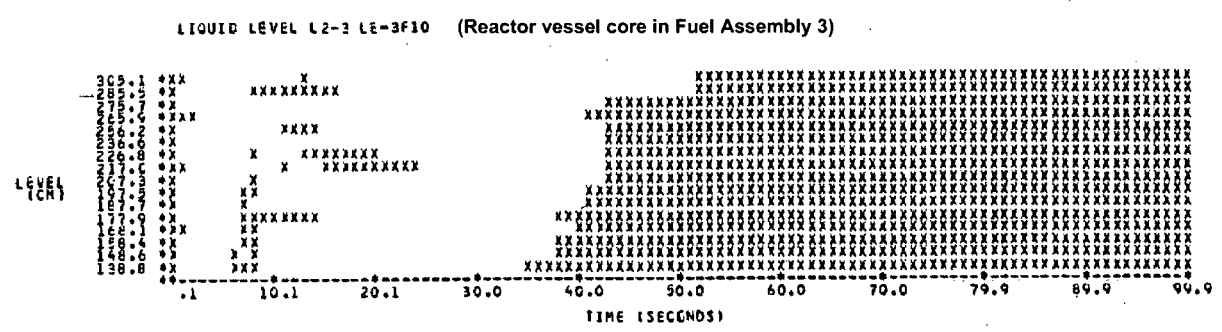
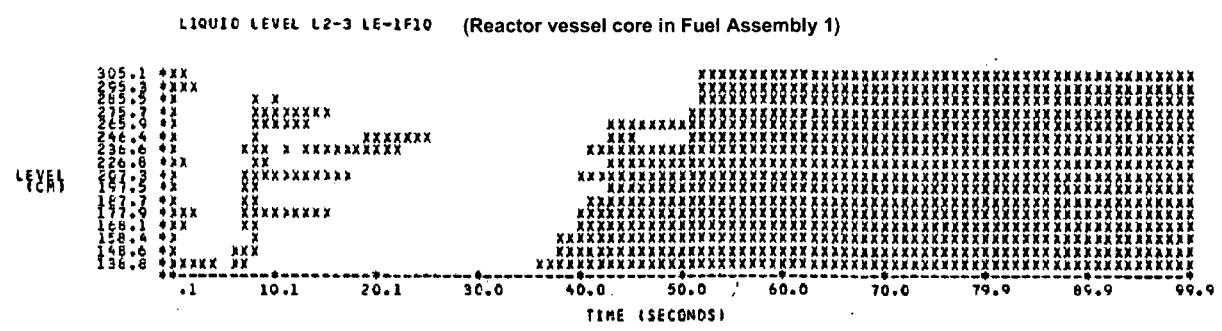
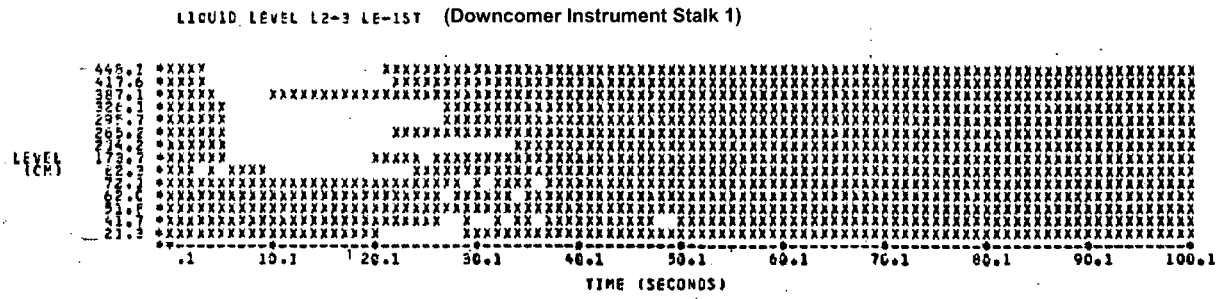
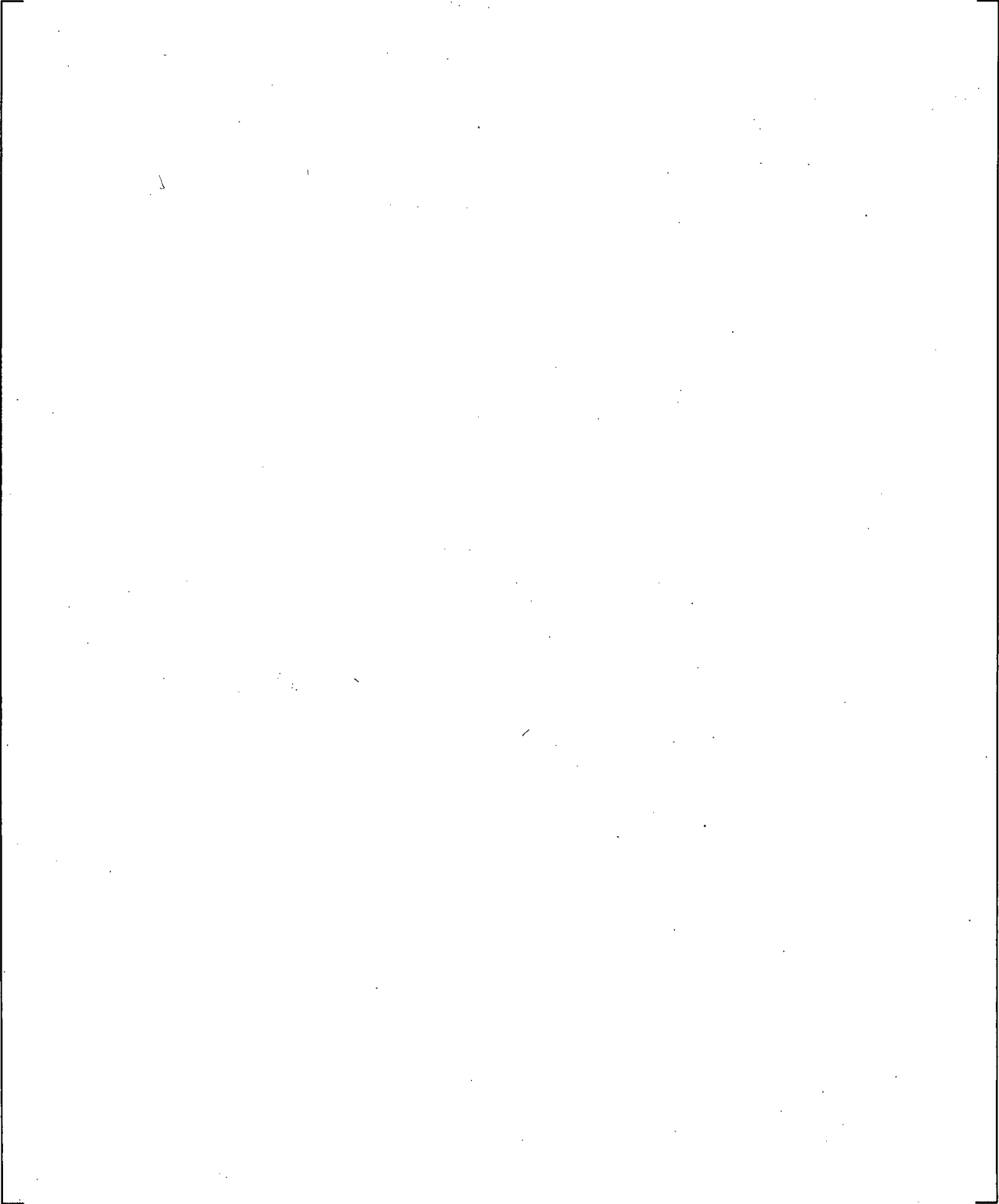
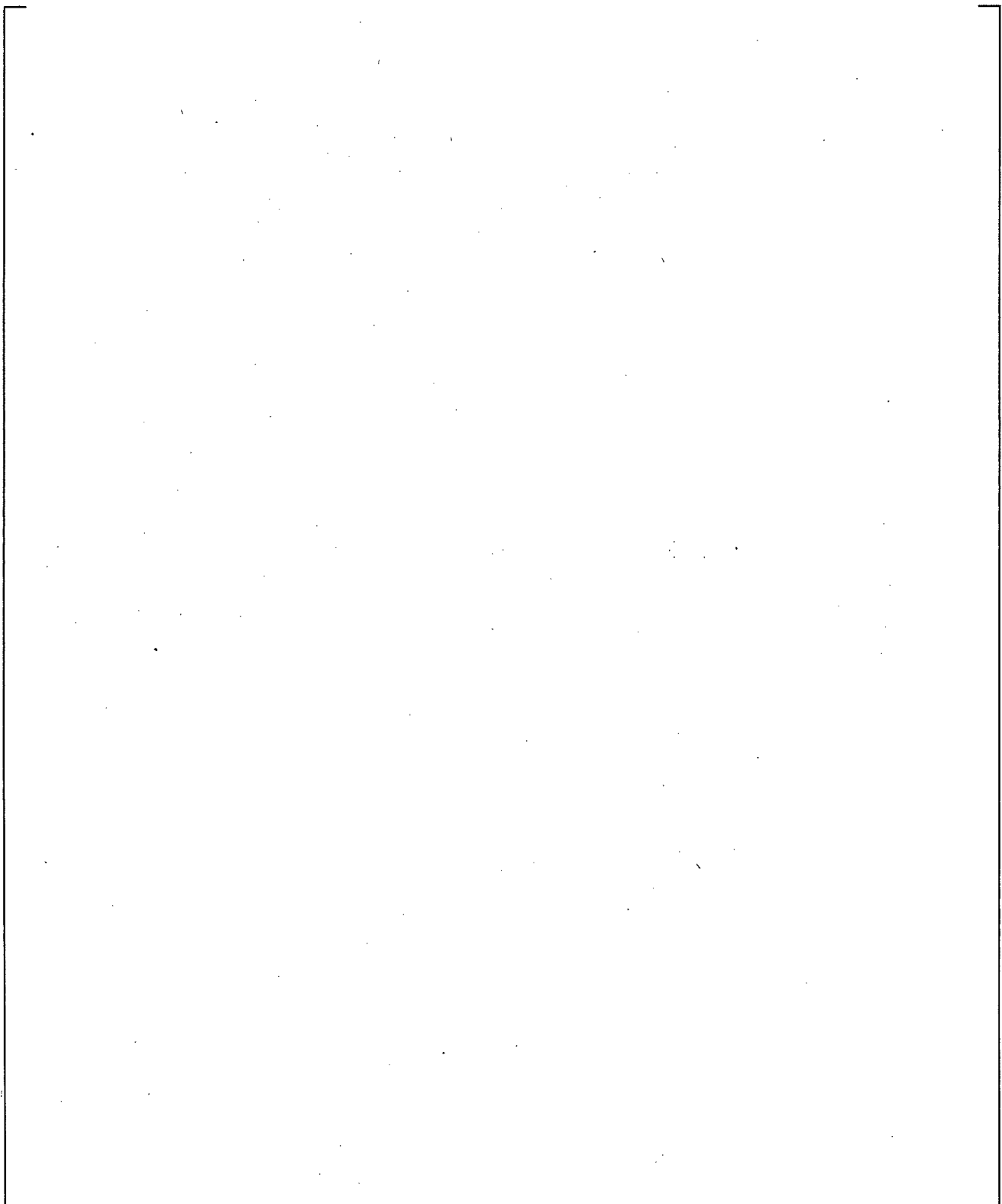


Figure 22-31c Measured Liquid Levels in Downcomer and Core Regions, Test L2-3



**Figure 22-31d Predicted Liquid Levels in Downcomer and Vessel Core Regions, Test L2-3**



**Figure 22-31e Predicted Liquid Levels in Downcomer and Vessel Core Regions, Test L2-3**

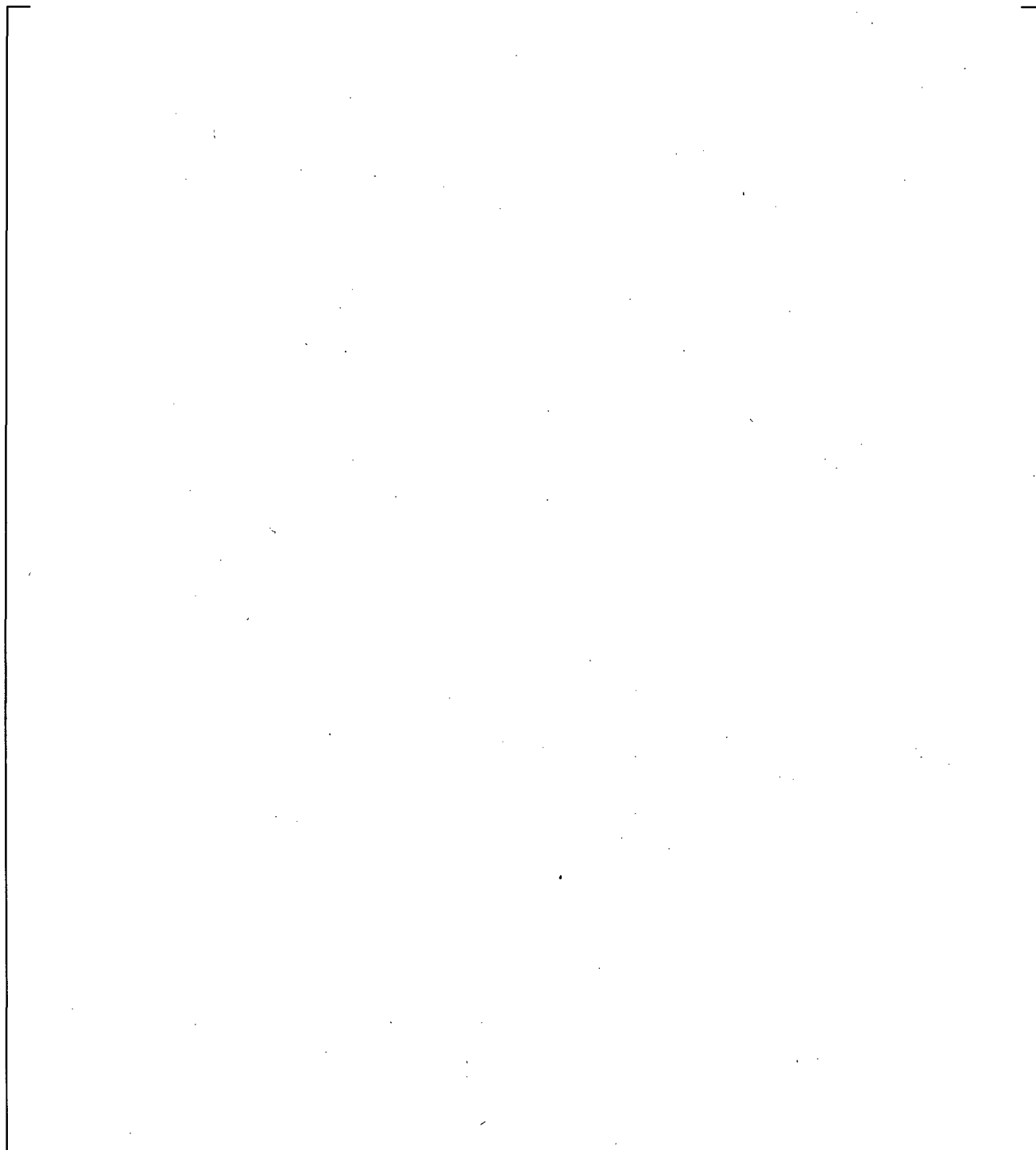


**Figure 22-32a Predicted (Component 850) Accumulator Volumetric Flow Rate and Void Fraction<sup>1</sup>, Test L2-5**

1. Measured data are not available from test report (Bayless, 1982).

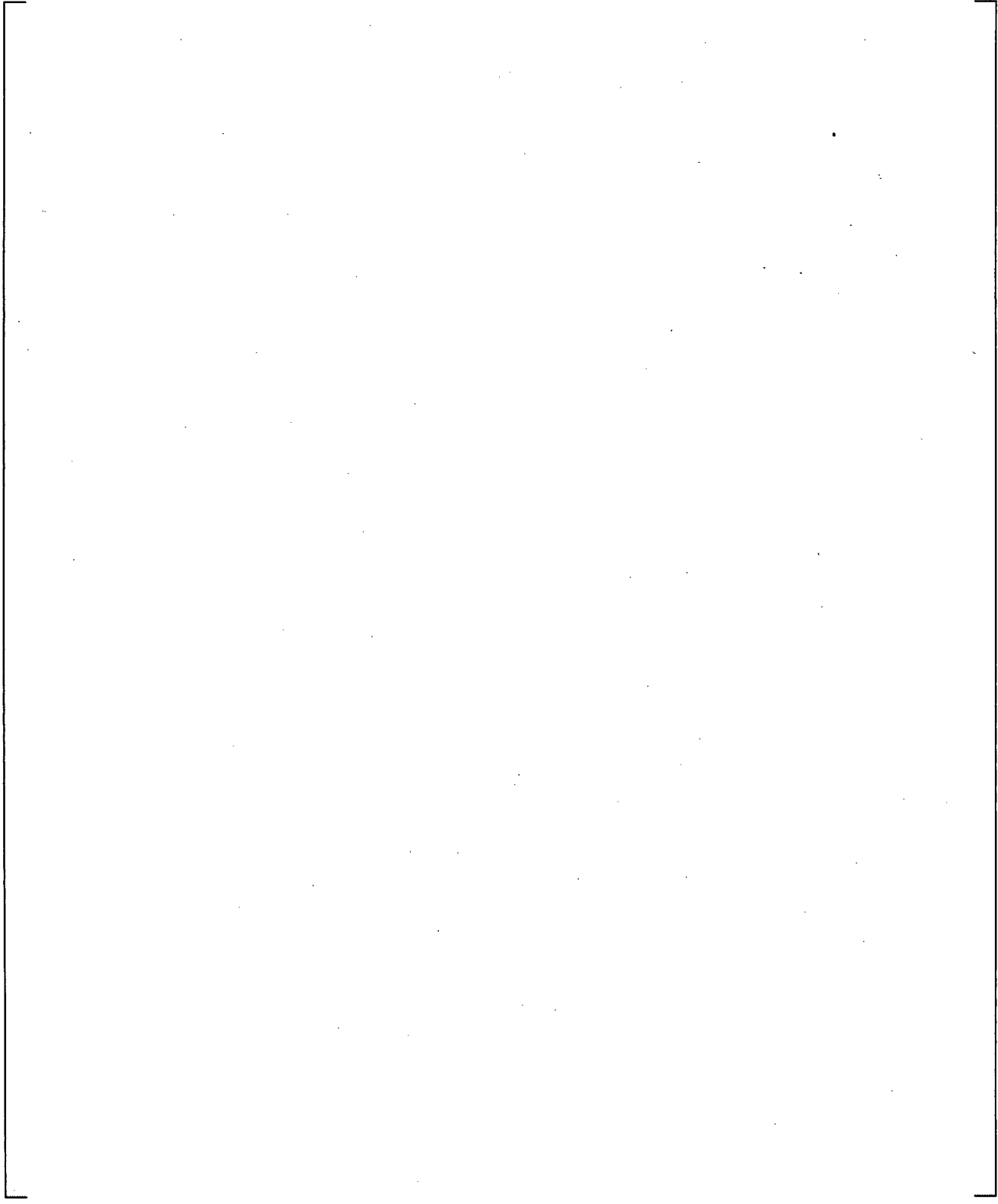


**Figure 22-32b Predicted (Component 850) and Measured Accumulator Water Level, Test L2-5**

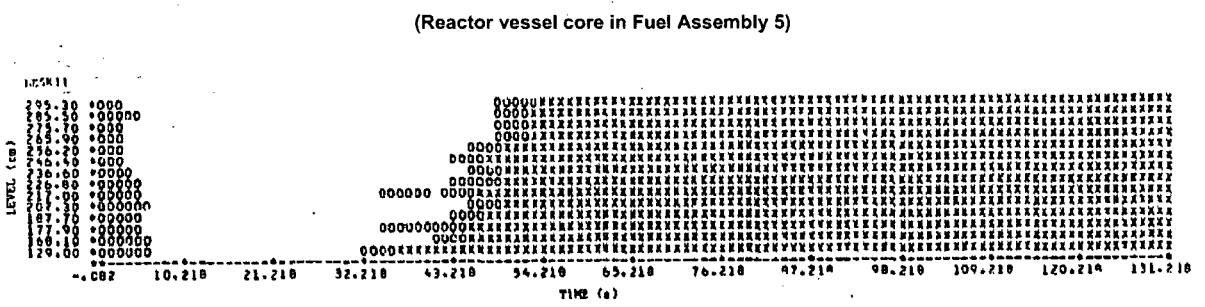
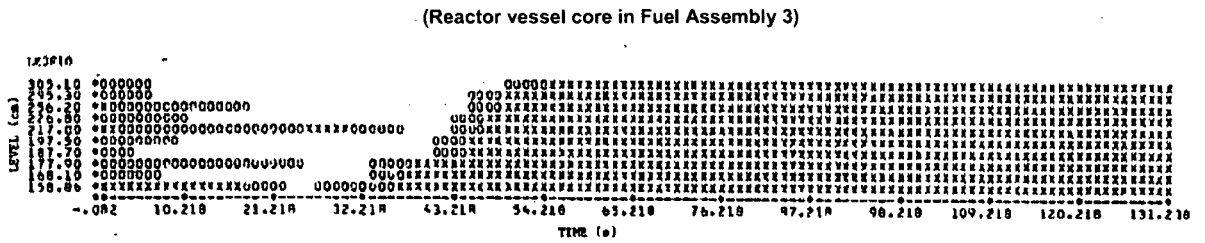
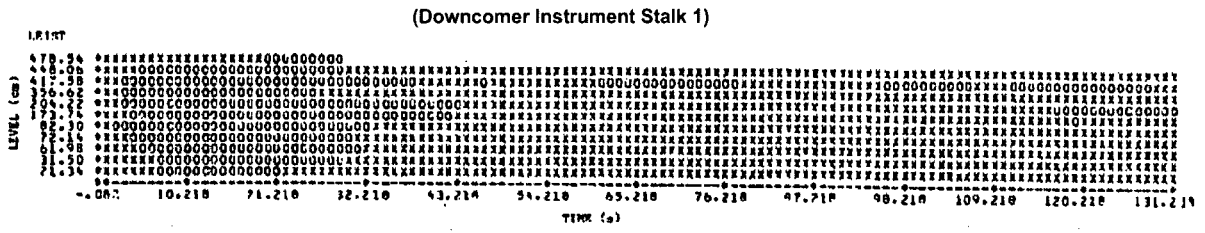
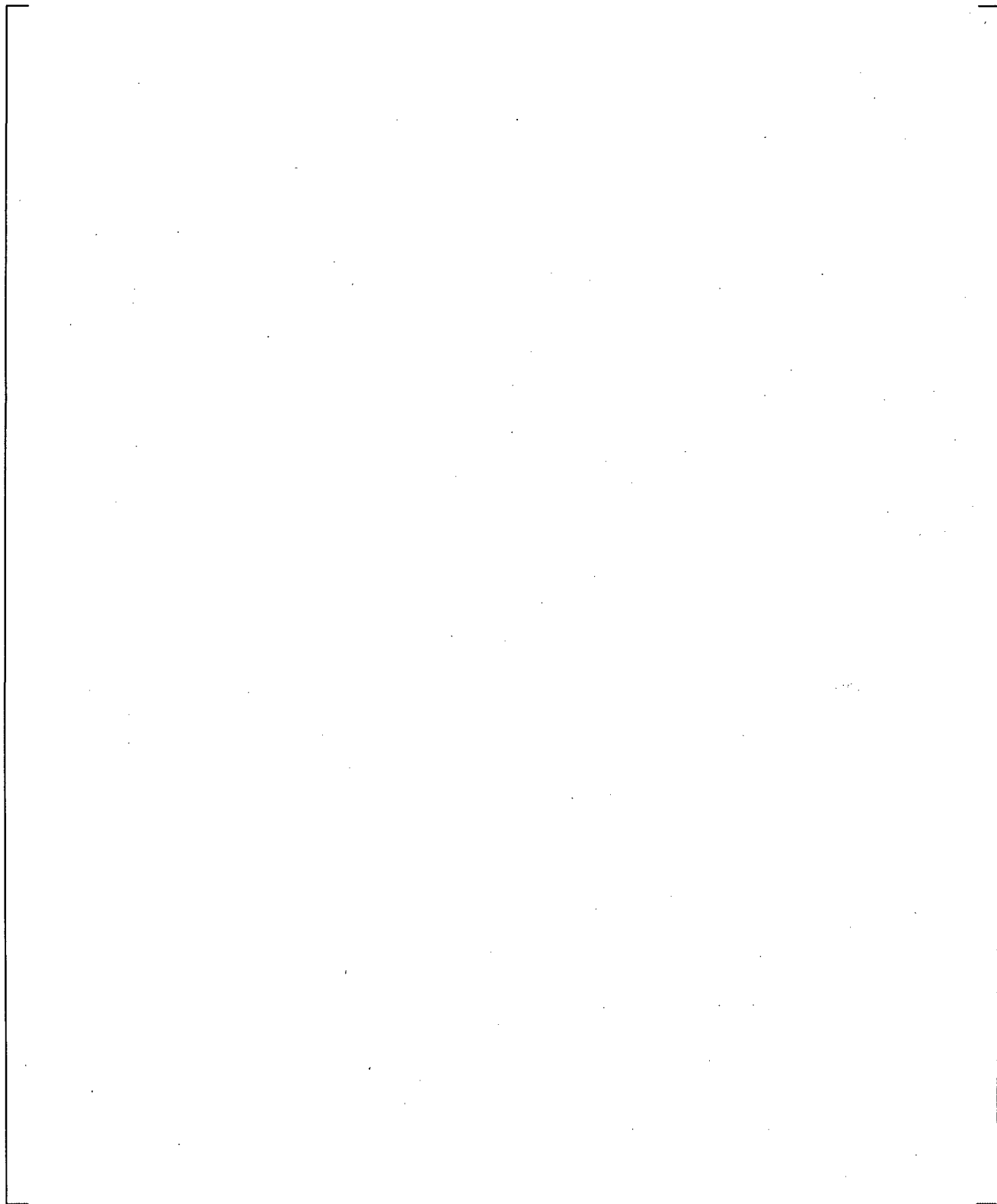
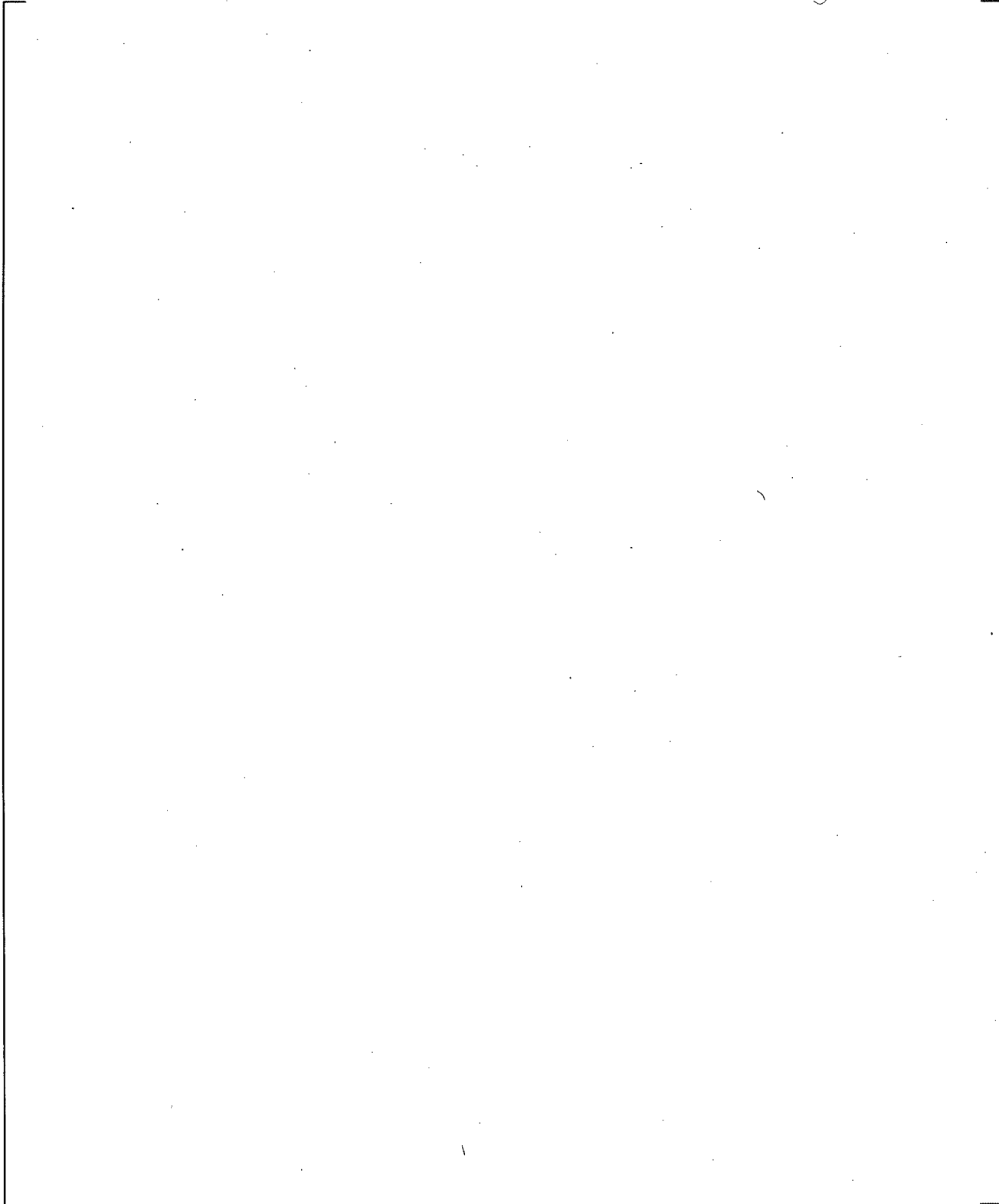


Figure 22-32c Measured Liquid Levels in Downcomer and Core Regions, Test L2-5



**Figure 22-32d Predicted Liquid Levels in Downcomer and Vessel Core Regions, Test L2-5**



**Figure 22-32e Predicted and Measured Liquid Levels in Vessel Core Regions, Test L2-5**

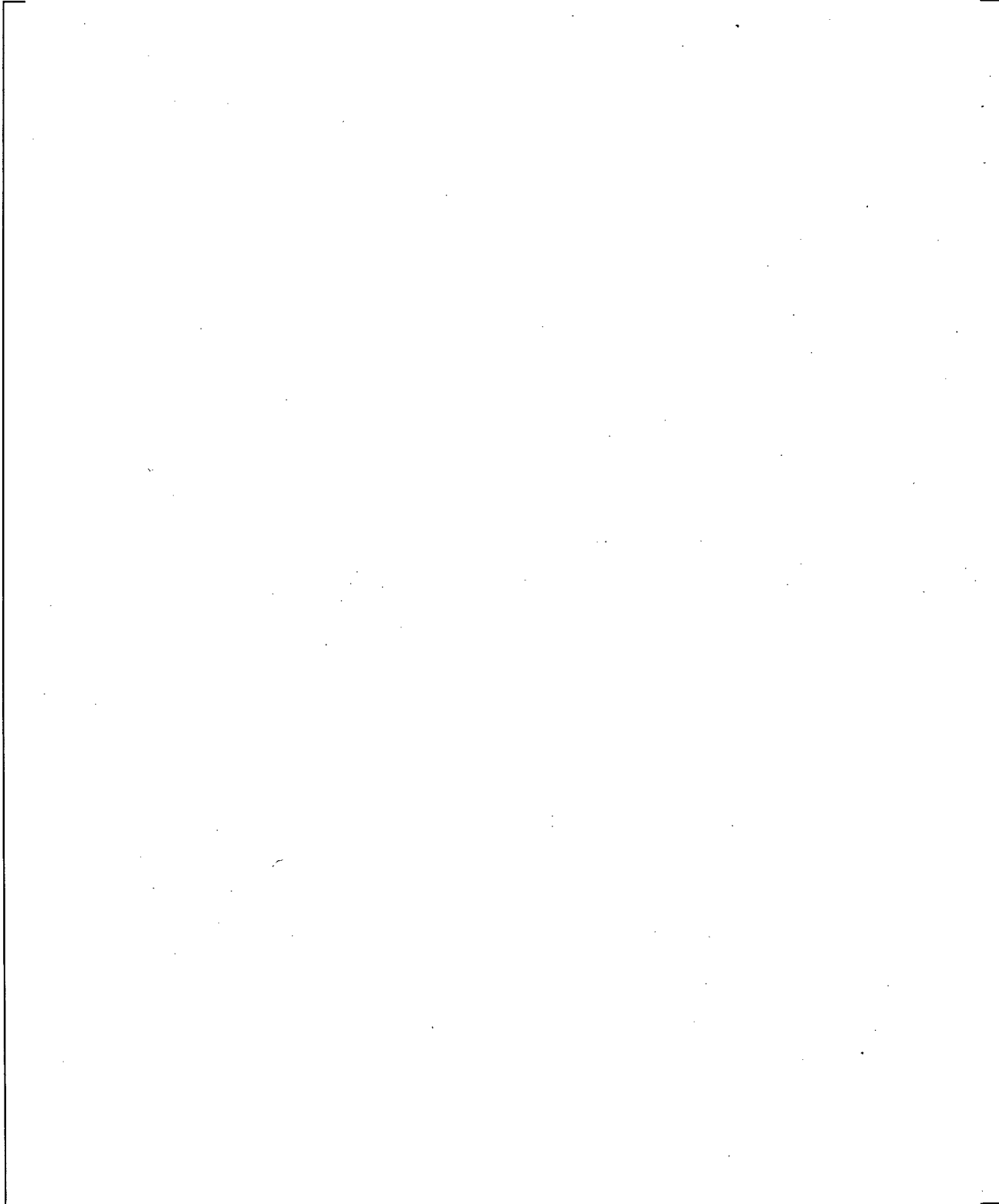


**Figure 22-33a Predicted (Component 840) and Measured (FT-P120-36-1) Volumetric Flow Rate and Predicted (Component 840) Void Fraction from Accumulator, Test LB-1**

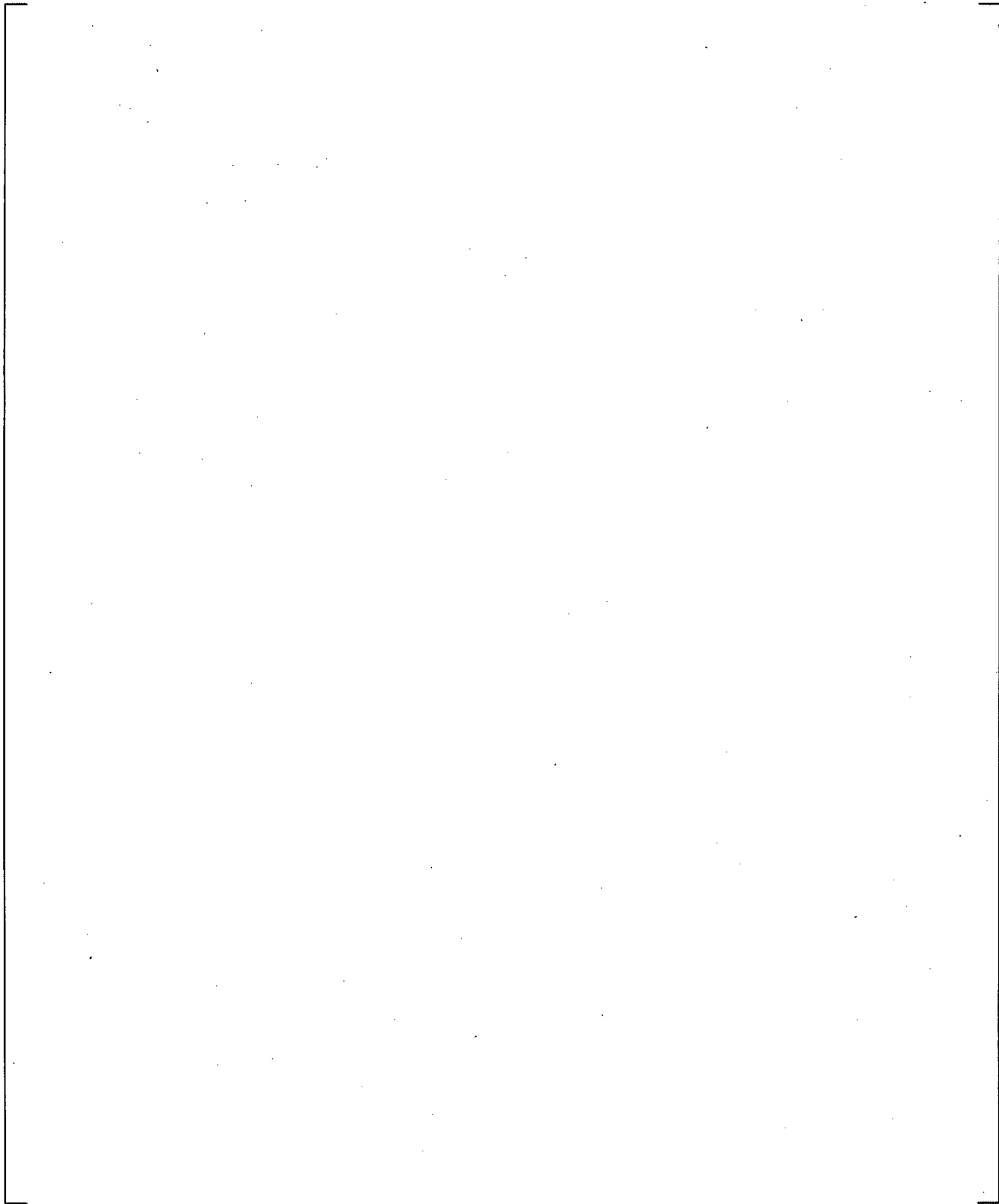


**Figure 22-33b Predicted (Component 850) and Measured (LIT-P120-044, LIT-P120-087) Accumulator Water Level, Test LB-1**

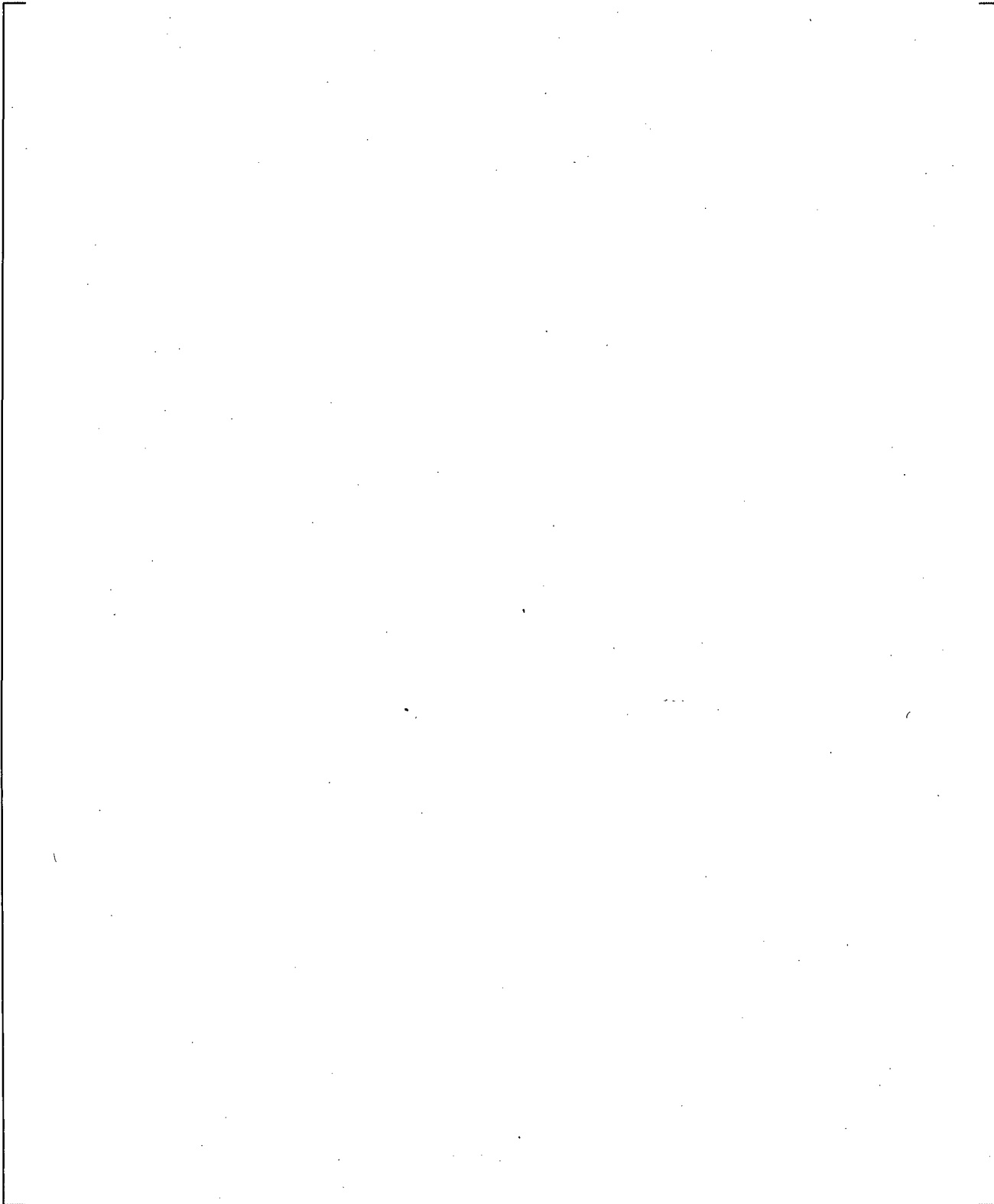


**Figure 22-33c Predicted Liquid Levels in Downcomer and Vessel Core Regions, Test LB-1**



**Figure 22-33e Predicted Liquid Level in Vessel Core Regions and Measured Vessel Lower Plenum Fluid Temperature, Test LB-1**

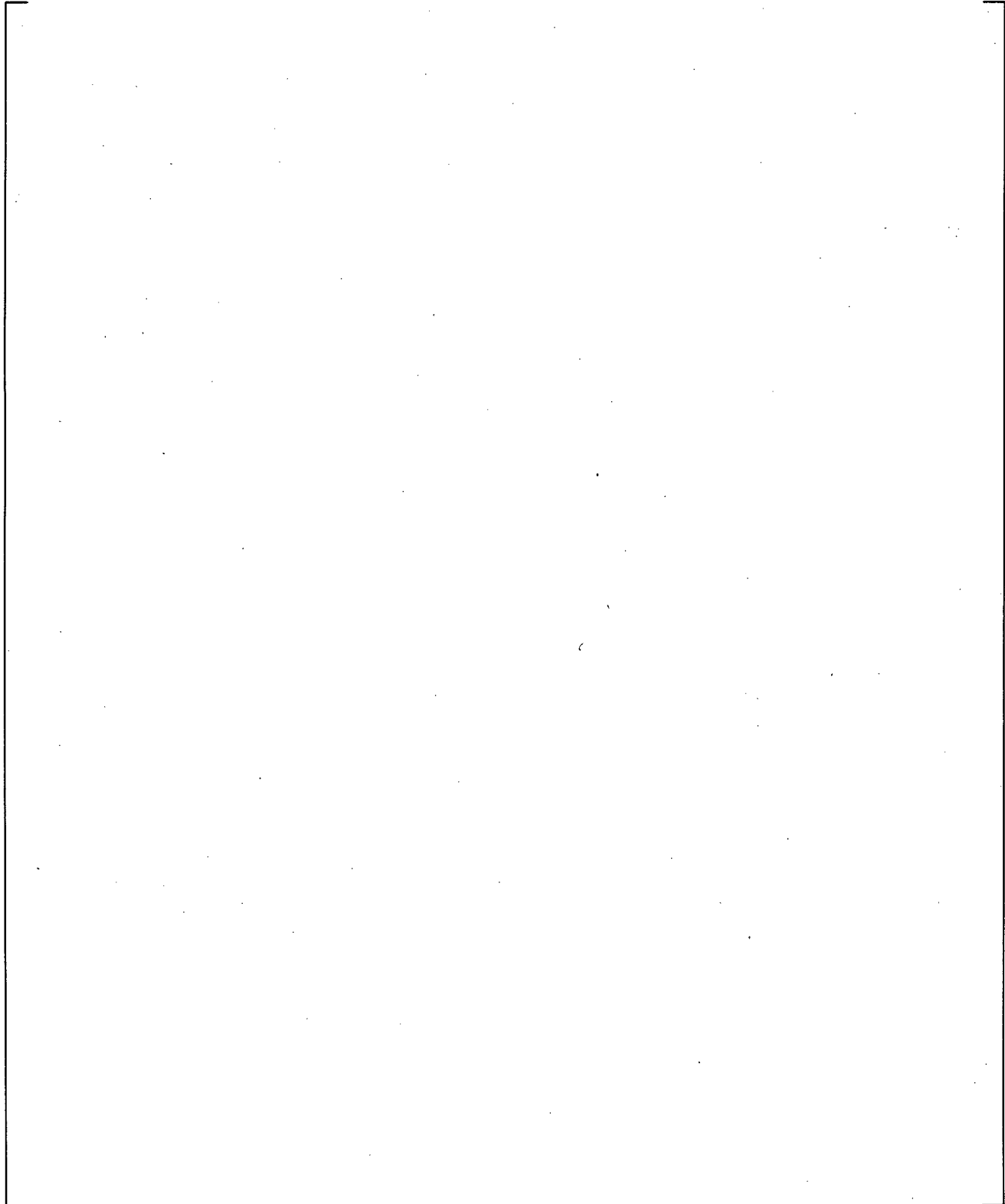


**Figure 22-34** Predicted (2.72 ft) and Measured Cladding Temperature in the Hot Channel, Test L2-2

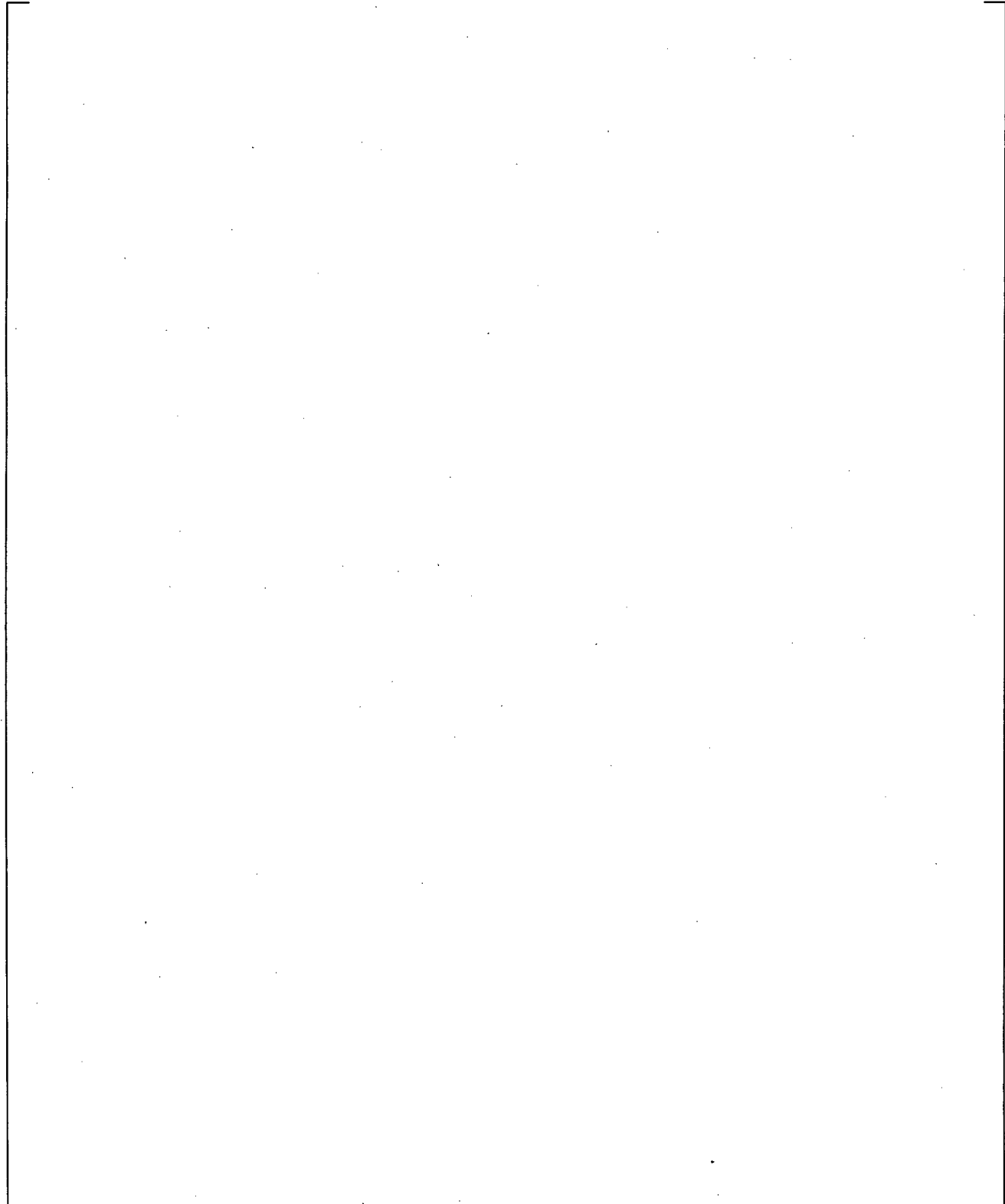


**Figure 22-35 Predicted (2.79 ft) and Measured Cladding Temperature in the Hot Channel, Test L2-3**

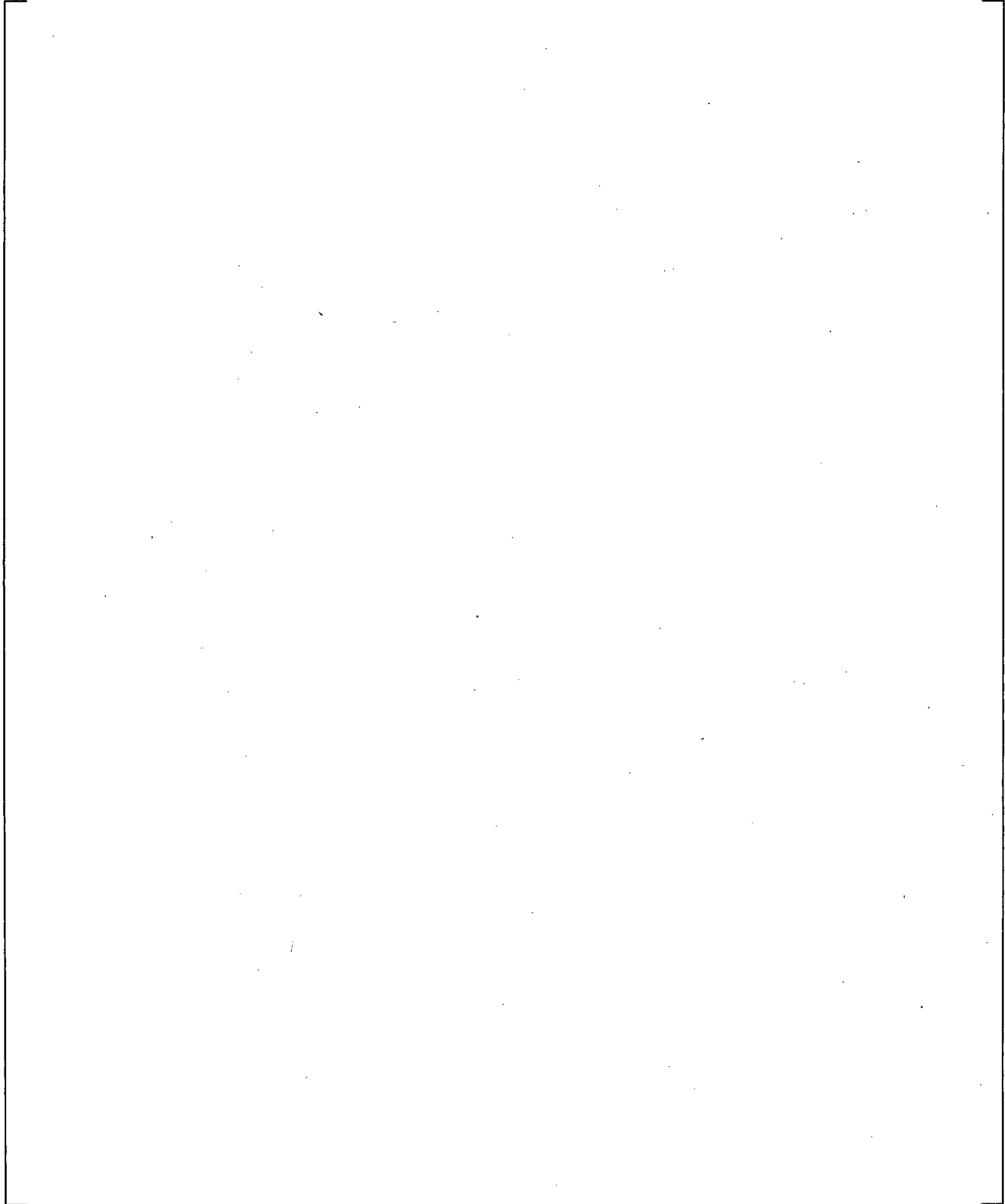


**Figure 22-36 Predicted (1.54 ft) and Measured Cladding Temperature in the Hot Channel, Test L2-5**

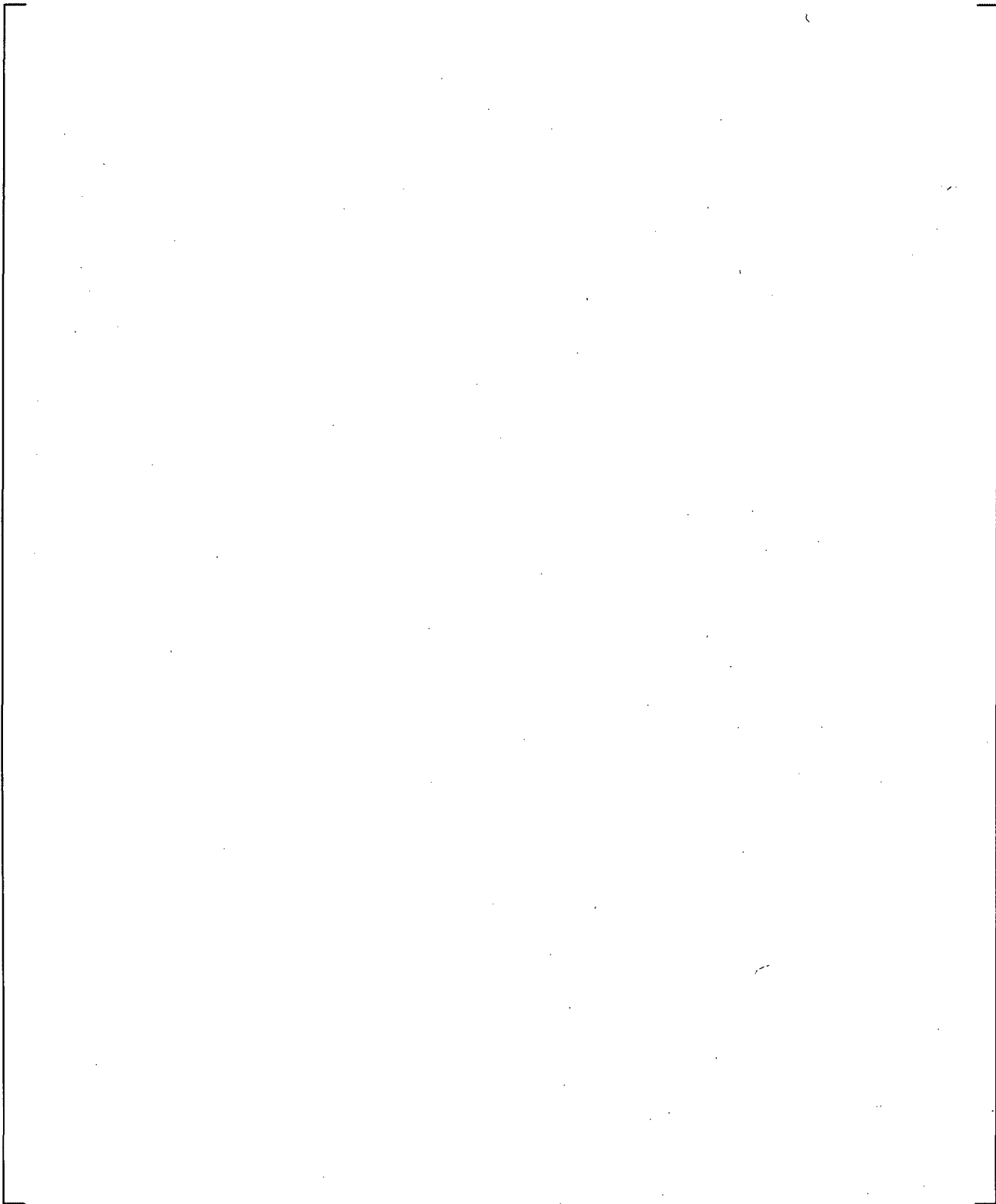


**Figure 22-37 Predicted (2.79 ft) and Measured Cladding Temperature in Hot Channel, Test LB-1**

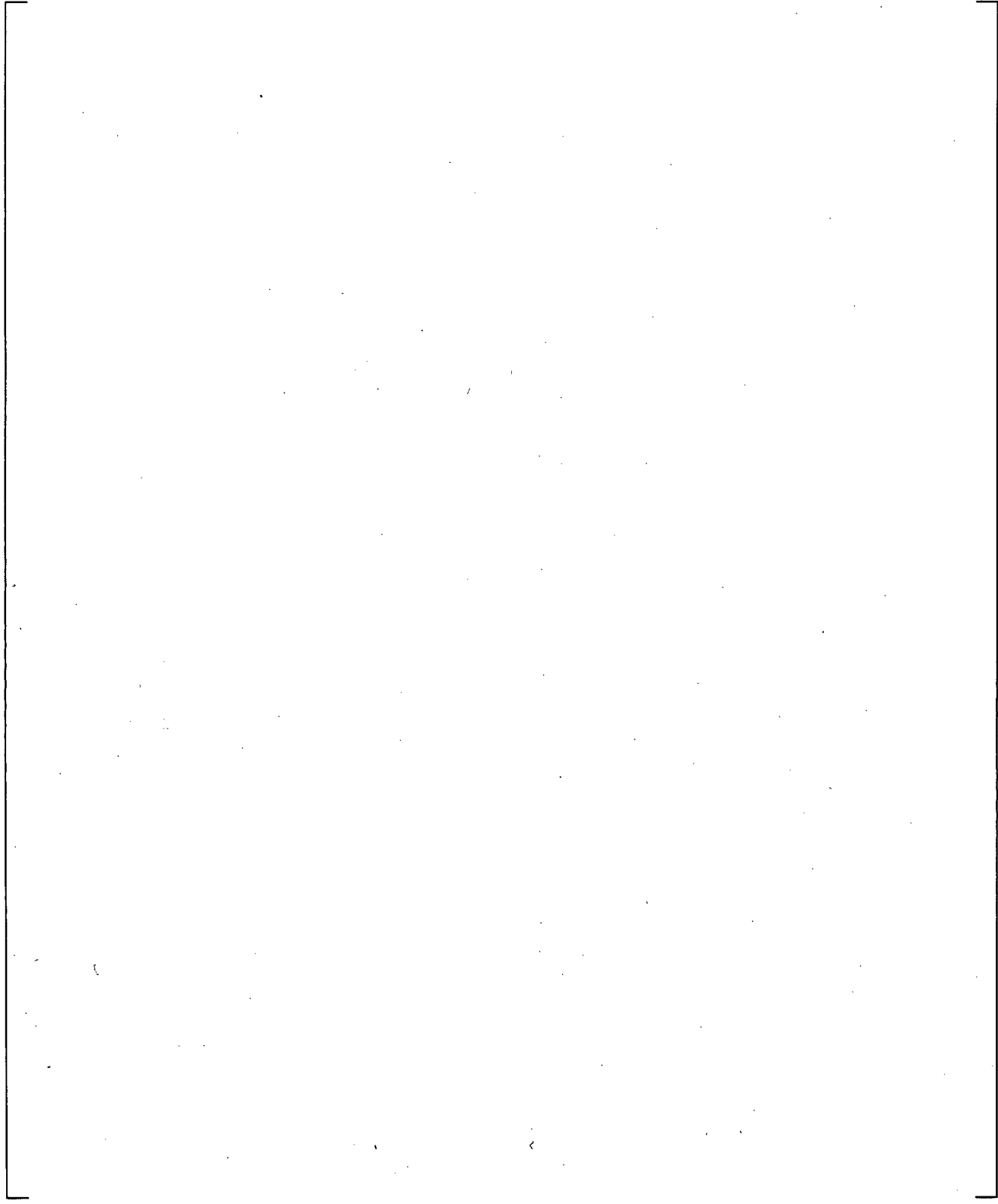


**Figure 22-38 Impact of Critical Flow Model Uncertainties on PCS Pressure, Test L2-3**

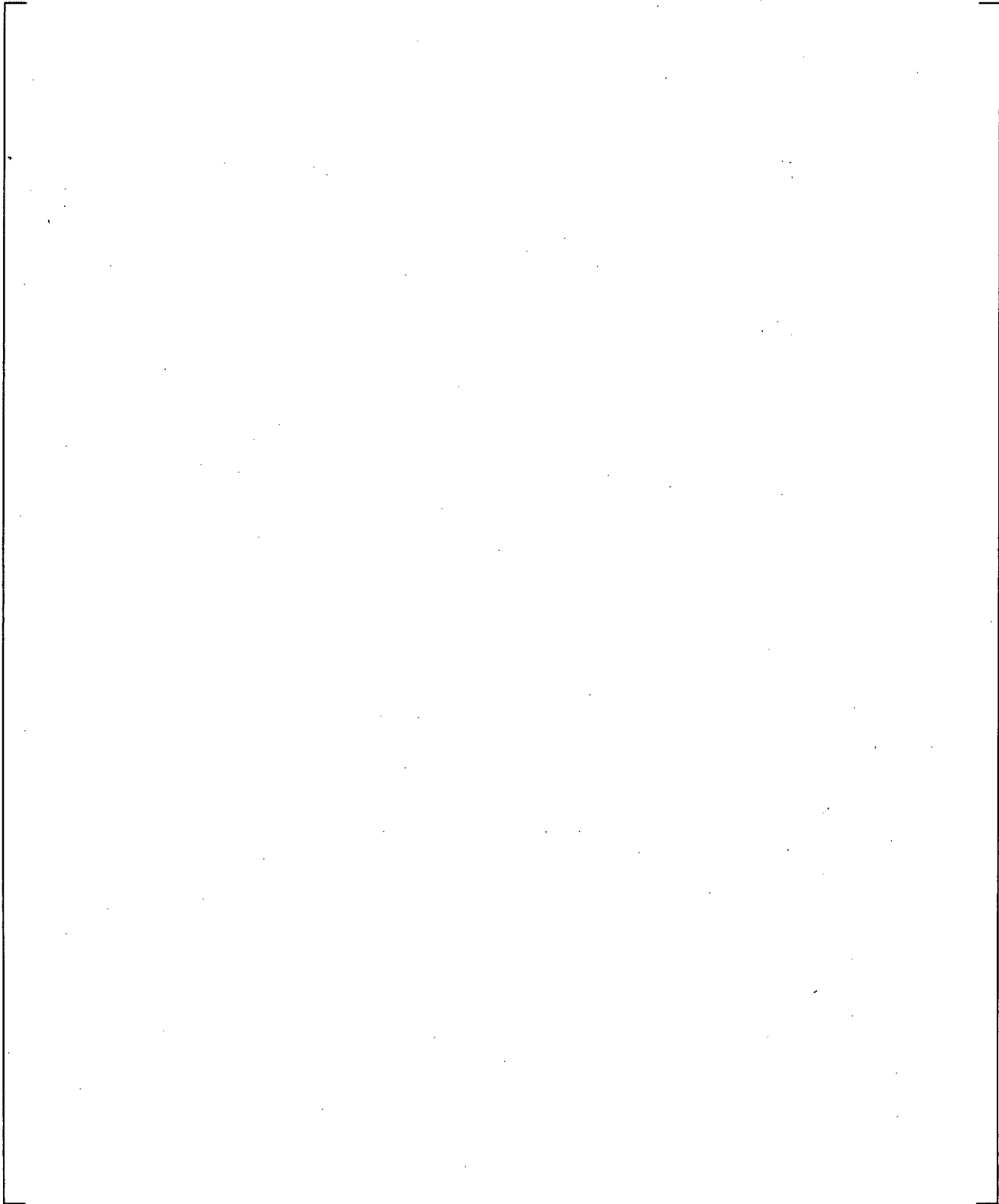


**Figure 22-39 Impact of Critical Flow Model Uncertainties on Cold Leg Break Flow, Test L2-3**

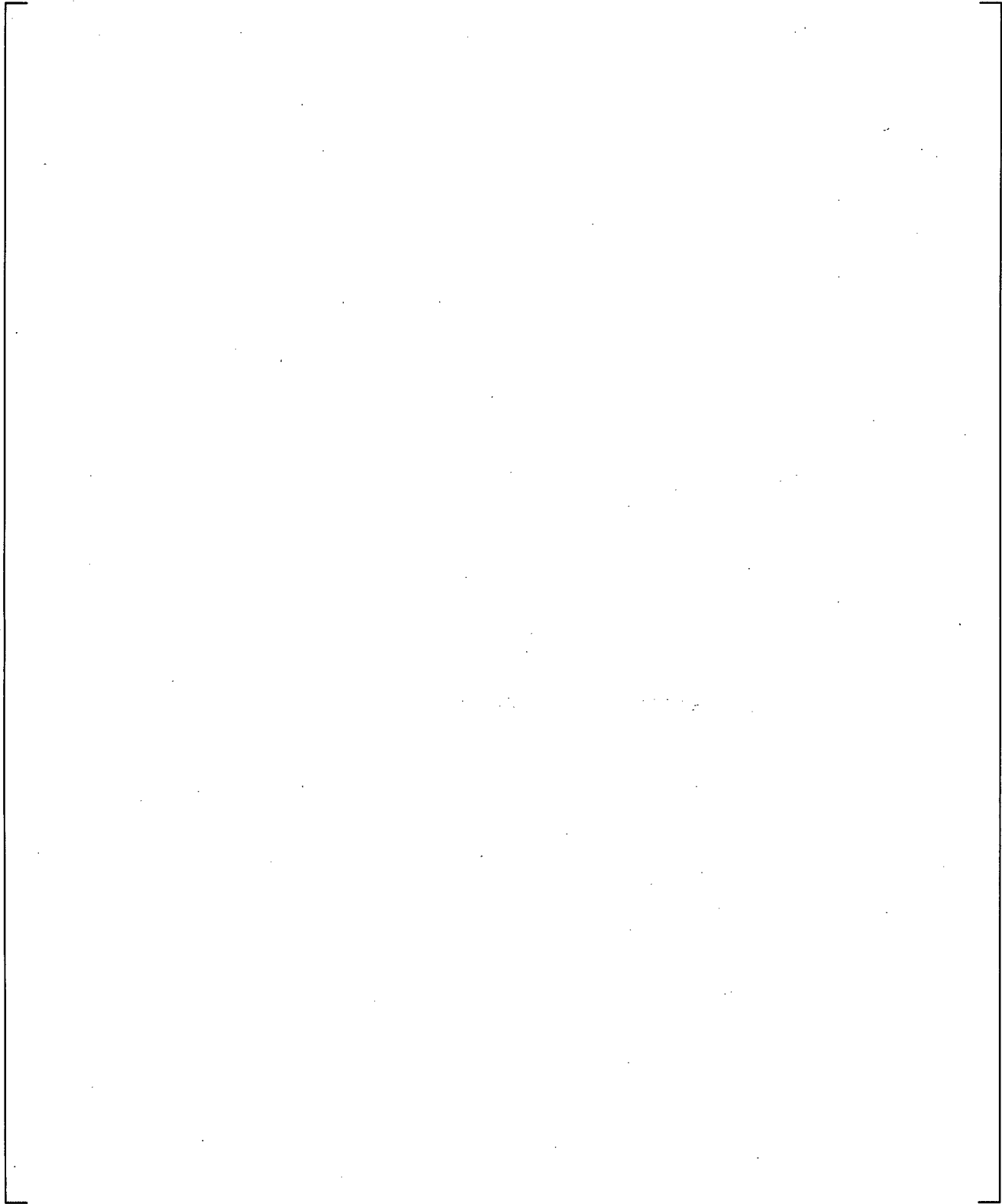


**Figure 22-40 Impact of Critical Flow Model Uncertainties on Cladding Temperature, Test L2-3**

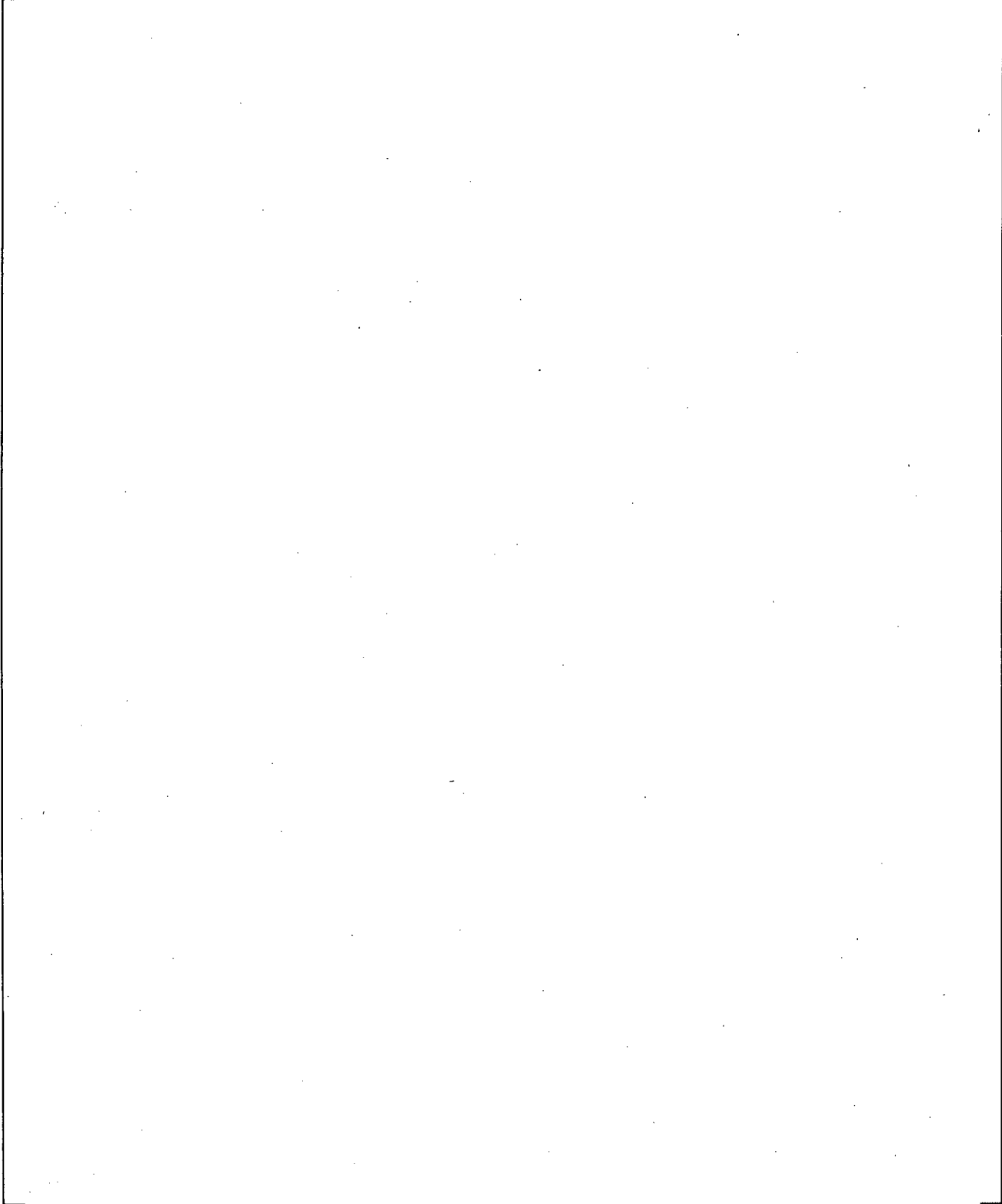


**Figure 22-41 Predicted (Component 810) and Measured Fluid Temperatures in Intact Cold Leg, Test L2-5**

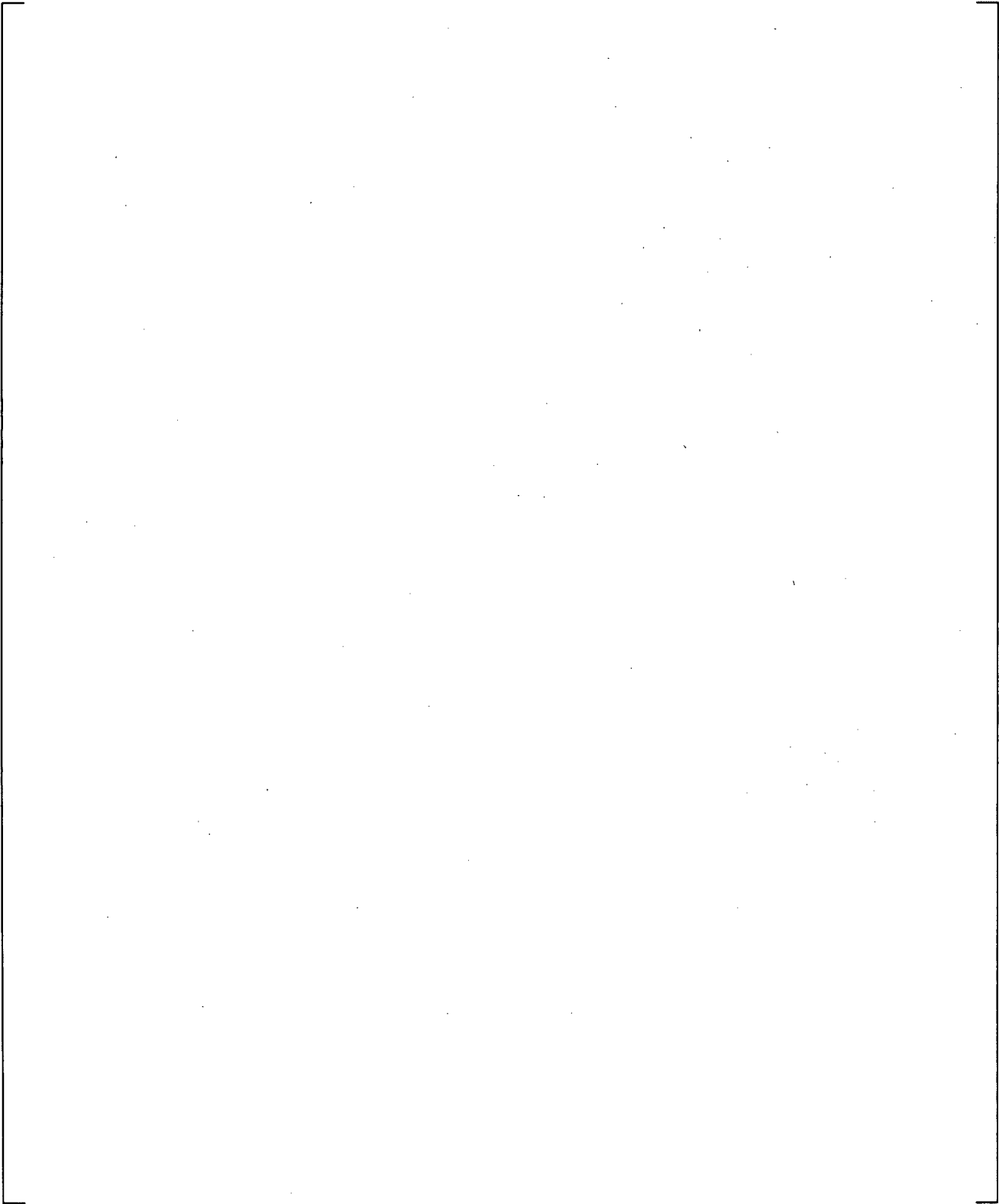


**Figure 22-42 Predicted and Measured Inlet and Outlet Fluid Temperature in Intact Loop Steam Generator, Test L2-5**

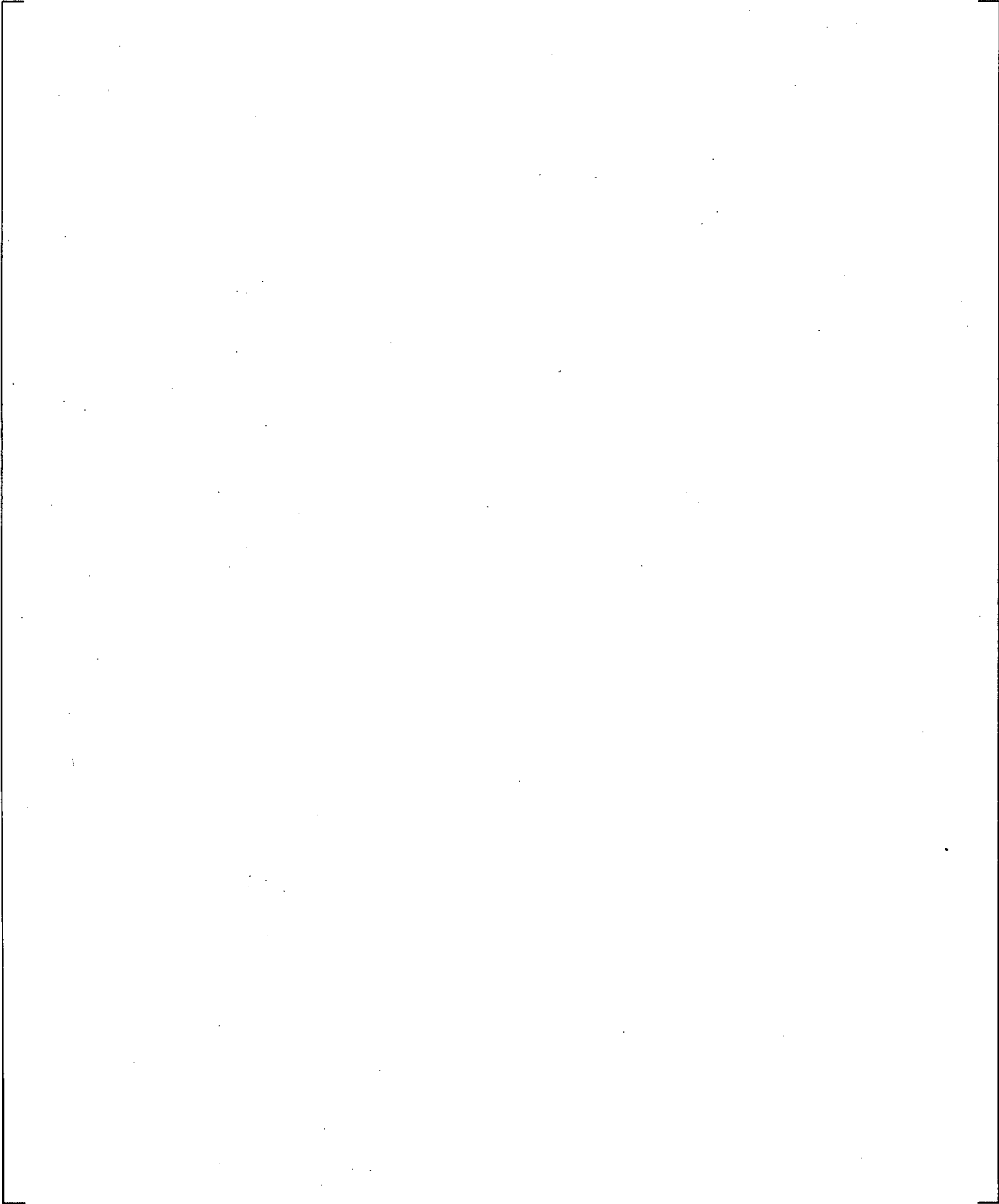


**Figure 22-43 Predicted (Component 600) Pressure Difference Across Intact Loop Pump, Test L2-5**

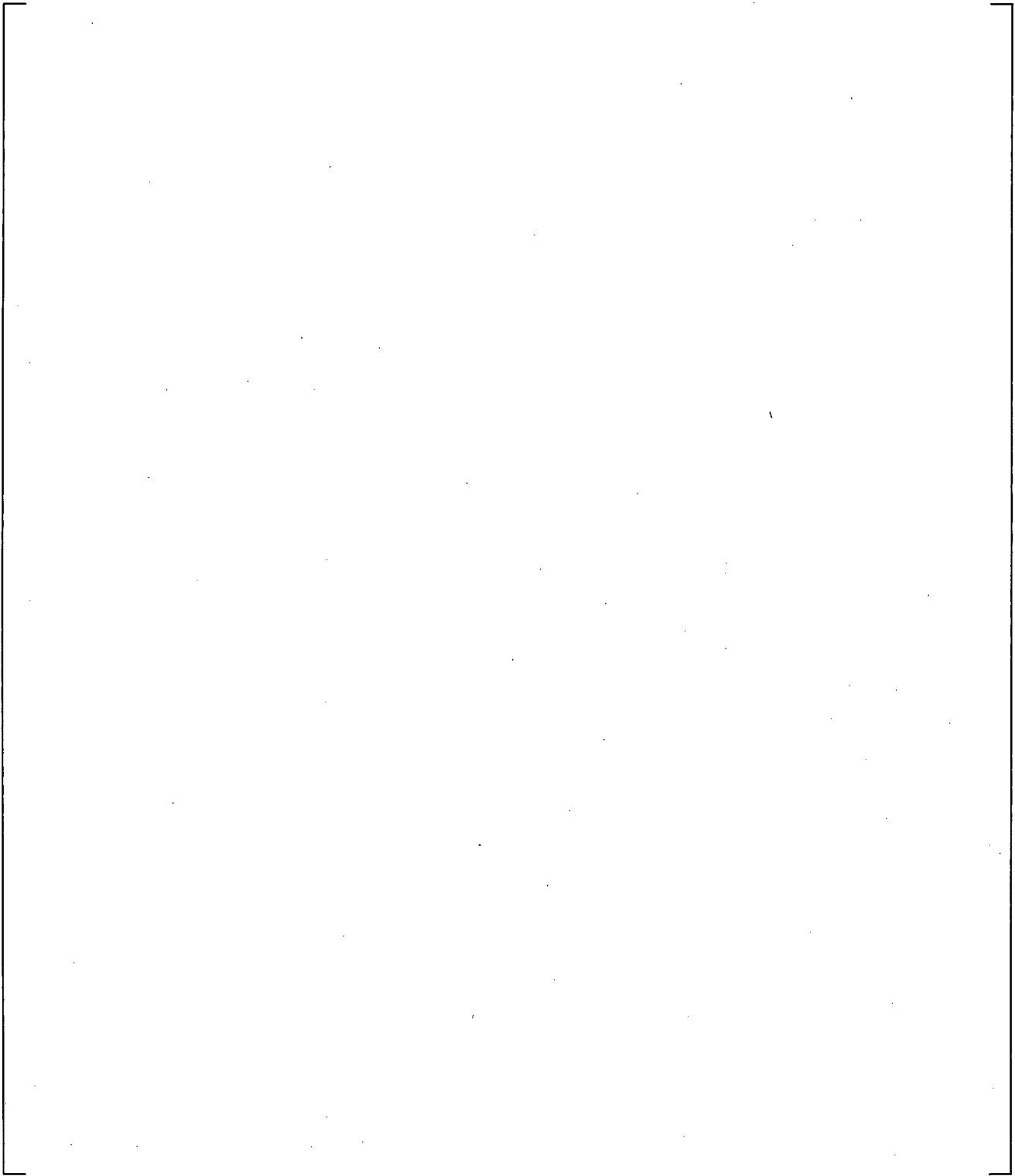


**Figure 22-44 Predicted (Rod 1 at 2.18 ft.<sup>1</sup>) and Measured Centerline Fuel Temperature, Test LB-1**

1. 2.18 ft. from the bottom of the fuel rod.

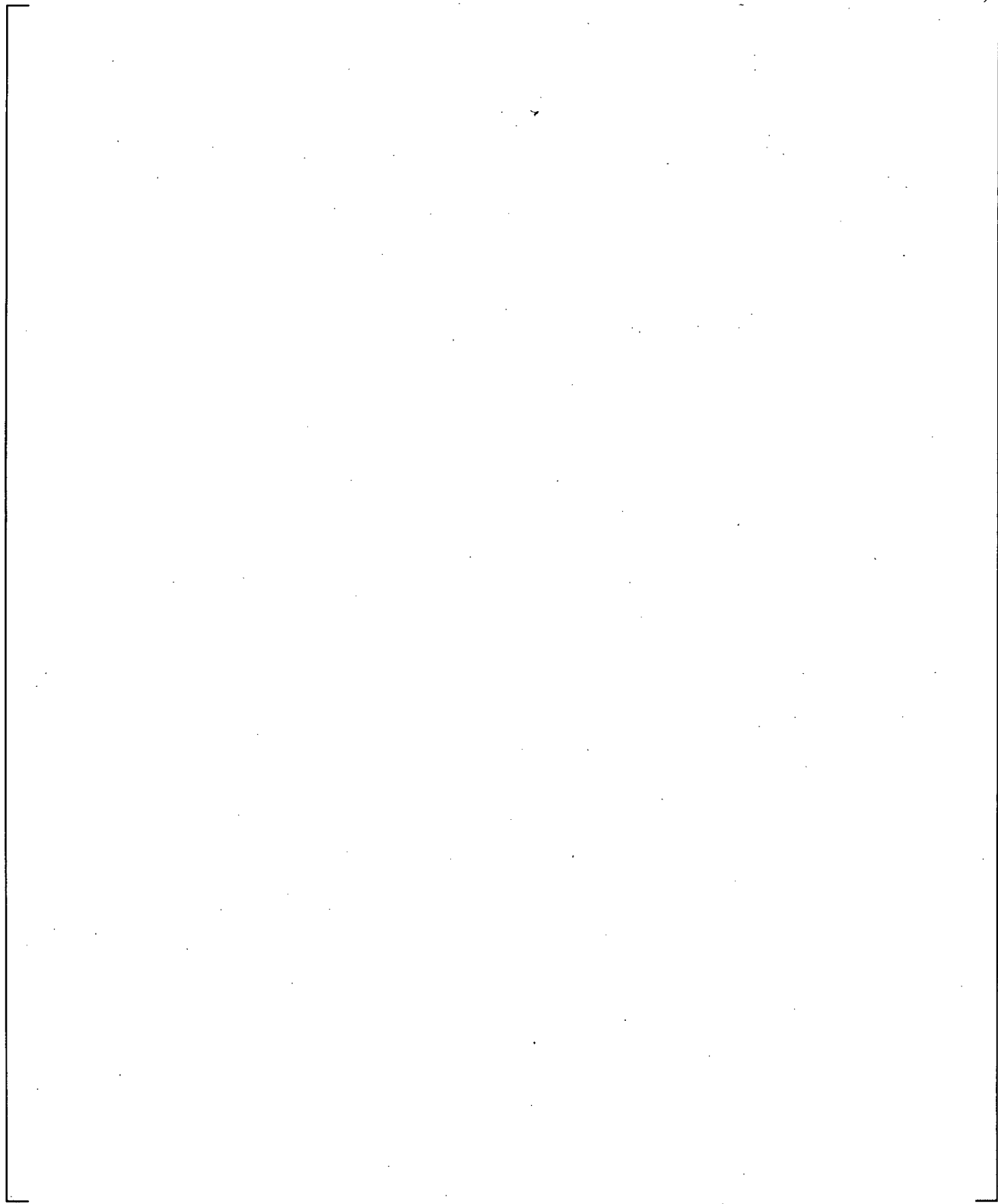


**Figure 22-45 Predicted and Measured Core Power, Test L2-5**

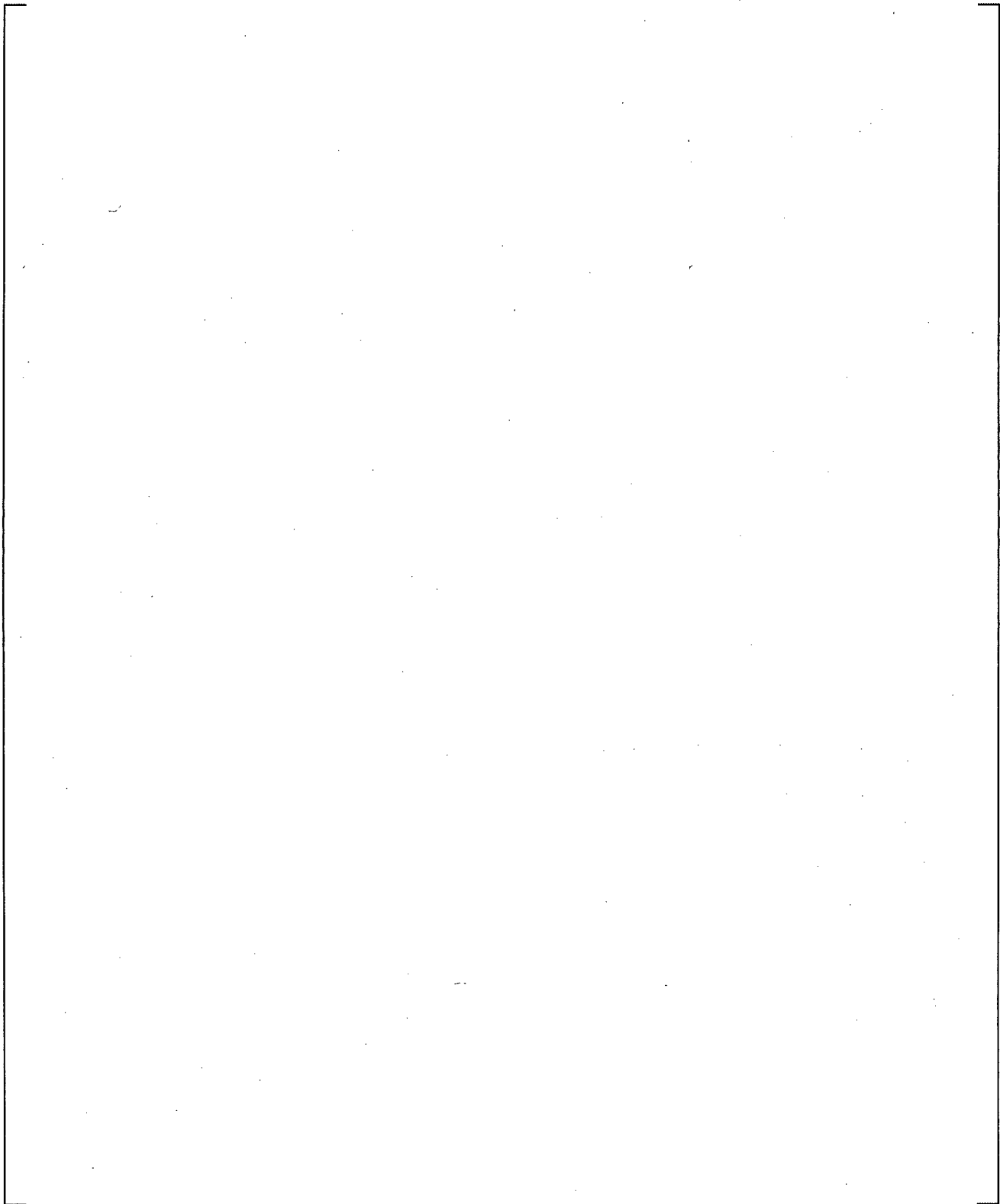


**Figure 22-46 Predicted and Measured Primary System Pressure, Test L3-1**

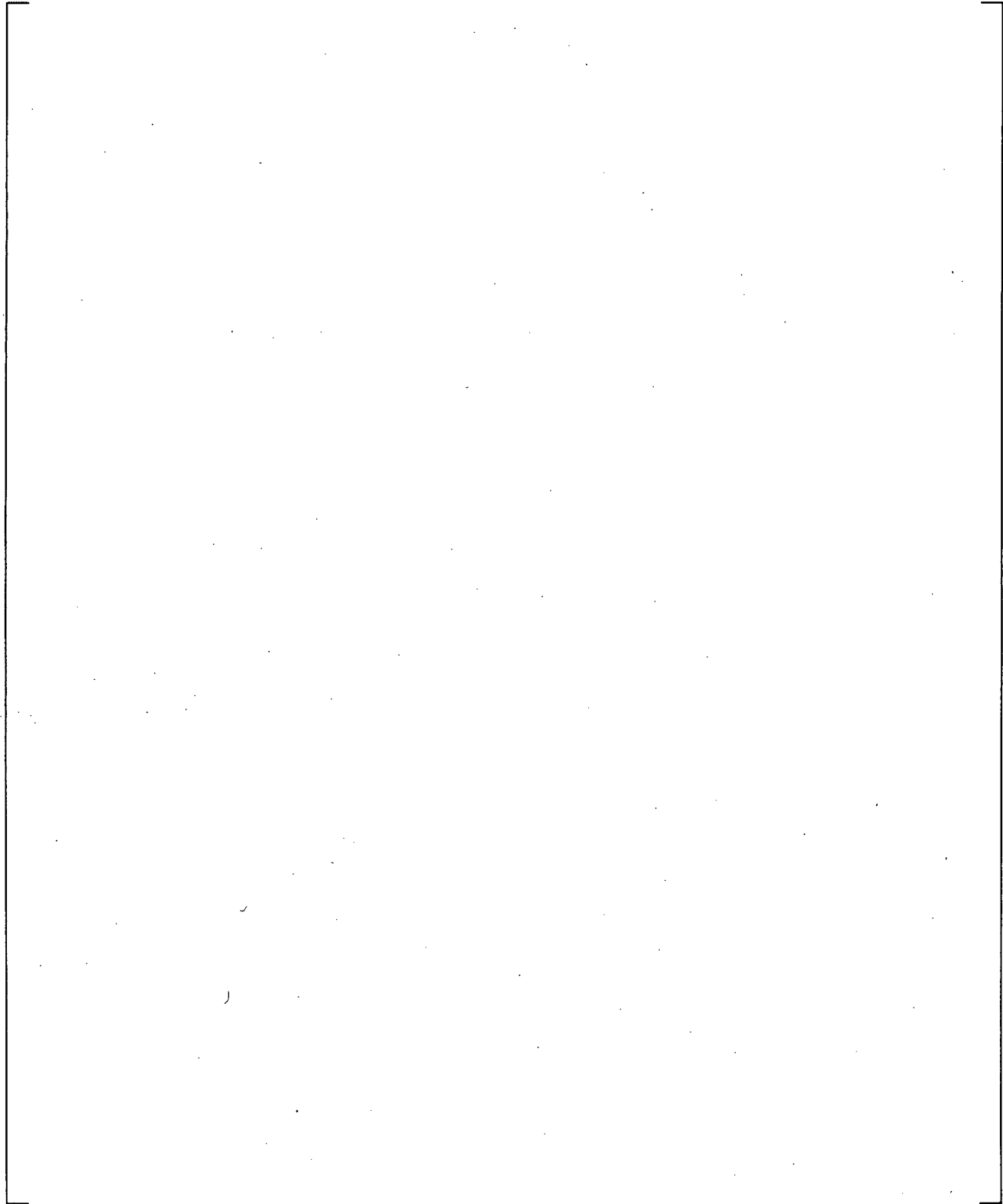


**Figure 22-47 Predicted and Measured Steam Generator Secondary Side Pressure, Test L3-1**

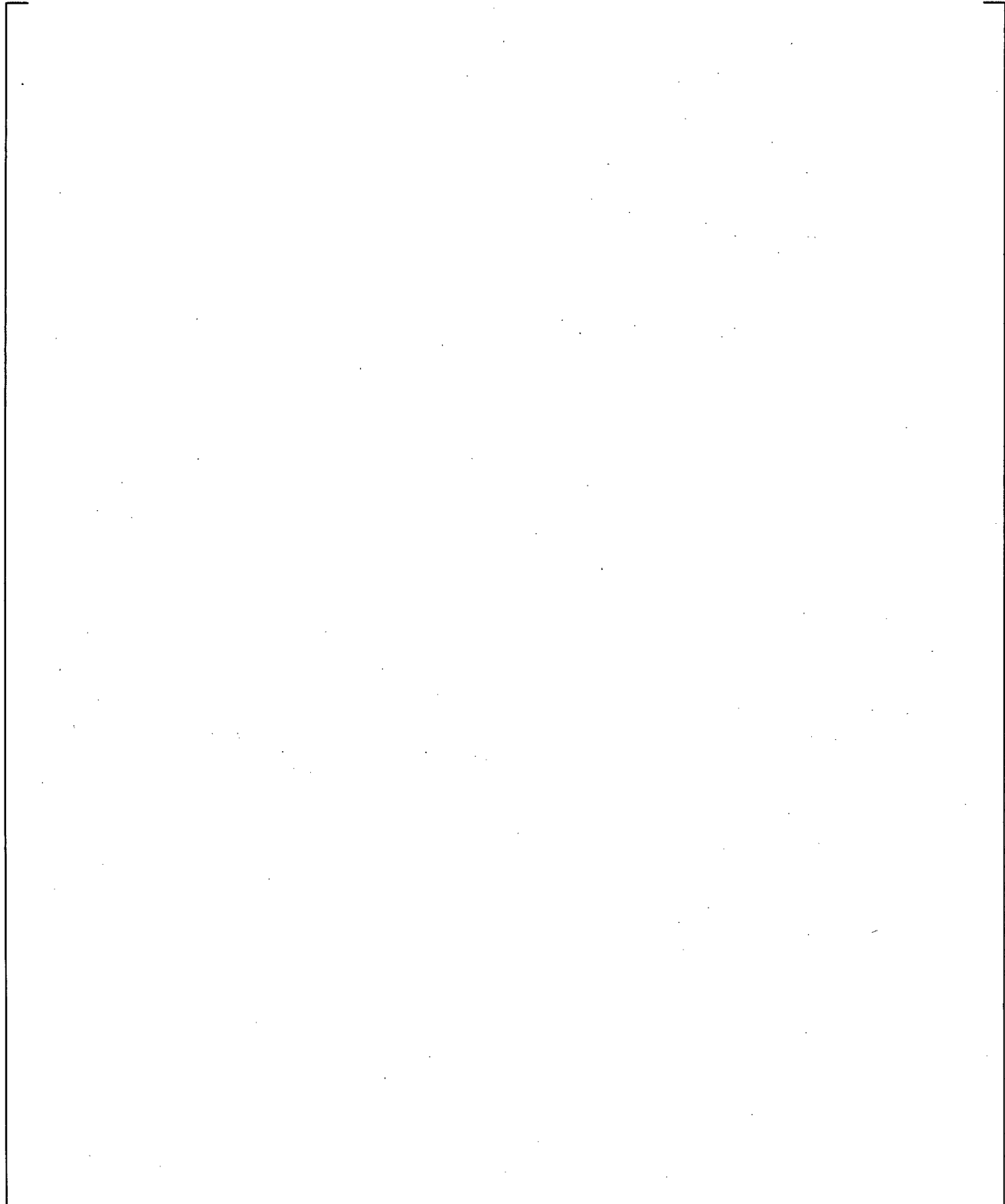


**Figure 22-48 Predicted and Measured Cold Leg Break Flow and Void Fraction Before the Break, Test L3-1**

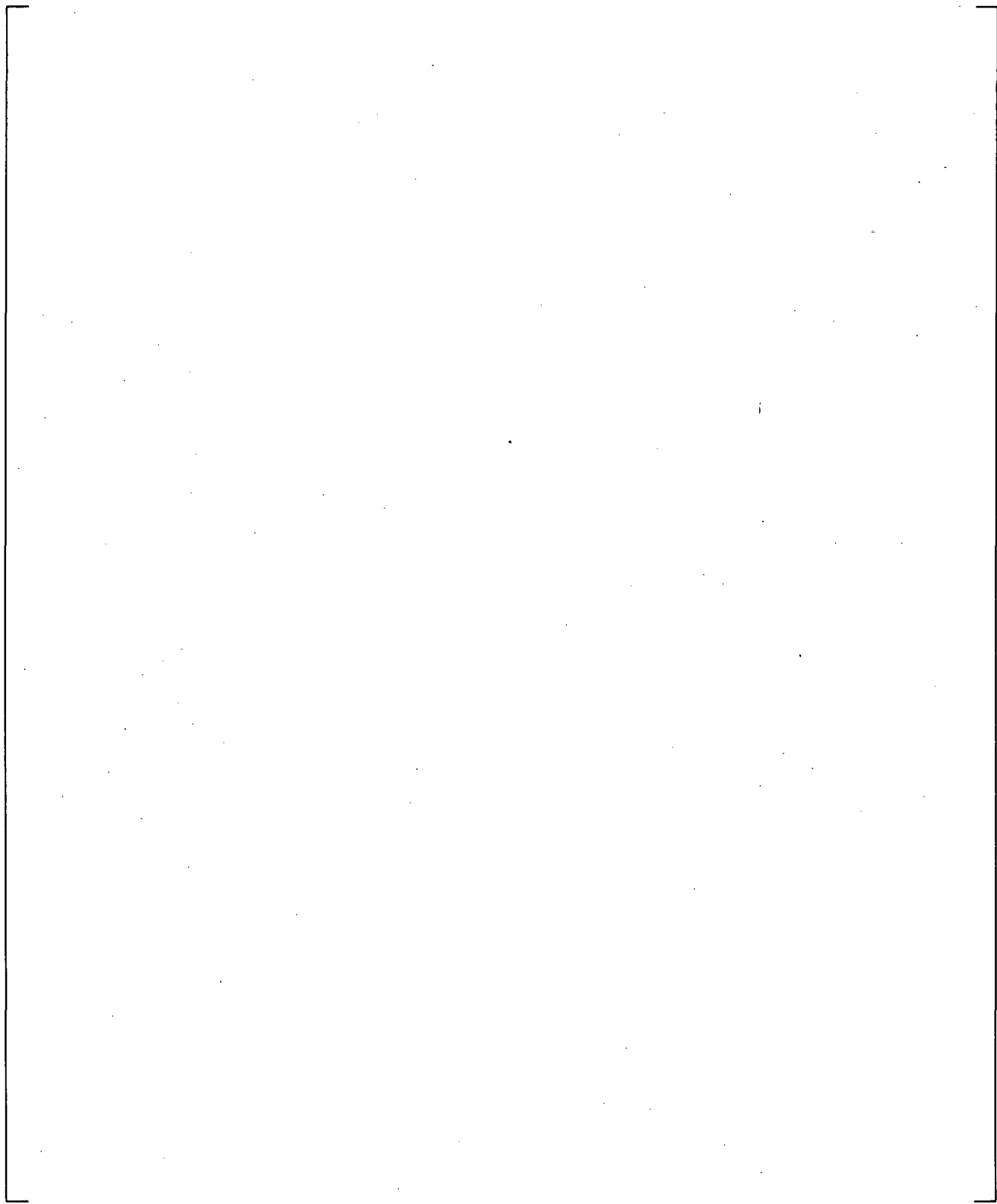


**Figure 22-49 Predicted and Measured Accumulator Liquid Level, Test L3-1**

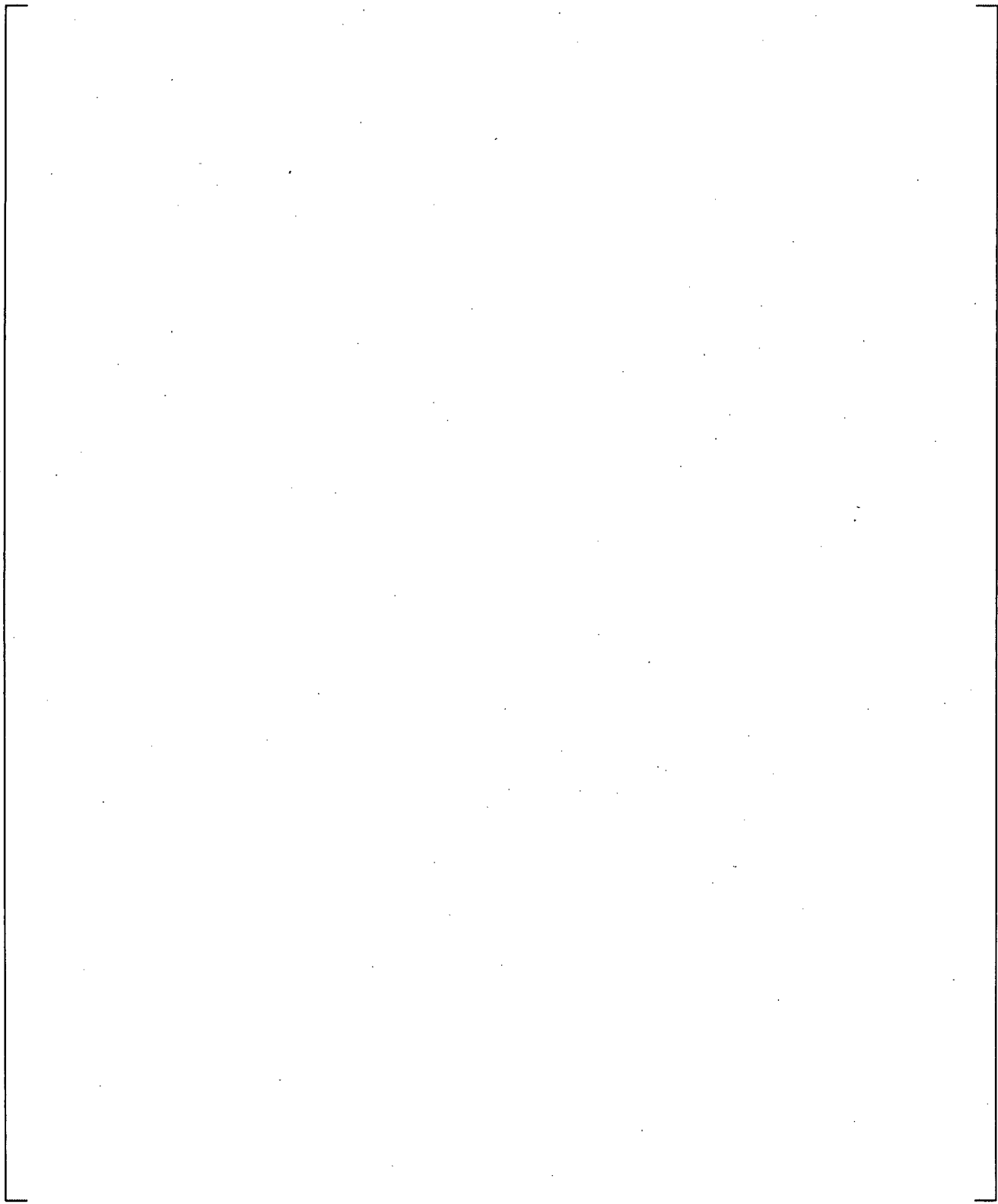


**Figure 22-50 Predicted and Measured Accumulator Pressure, Test L3-1**

## LOFT L31 TEST RESULTS PRIMARY & SECONDARY PRESSURE

<p>--- P</p> <p>--- P</p>	<p>72</p> <p>85</p>	<p>0</p> <p>0</p>	<p>0</p> <p>0</p>	<p>PE-PC-006 (TEST)</p> <p>PT-P004-010A (TEST)</p>
---------------------------	---------------------	-------------------	-------------------	--

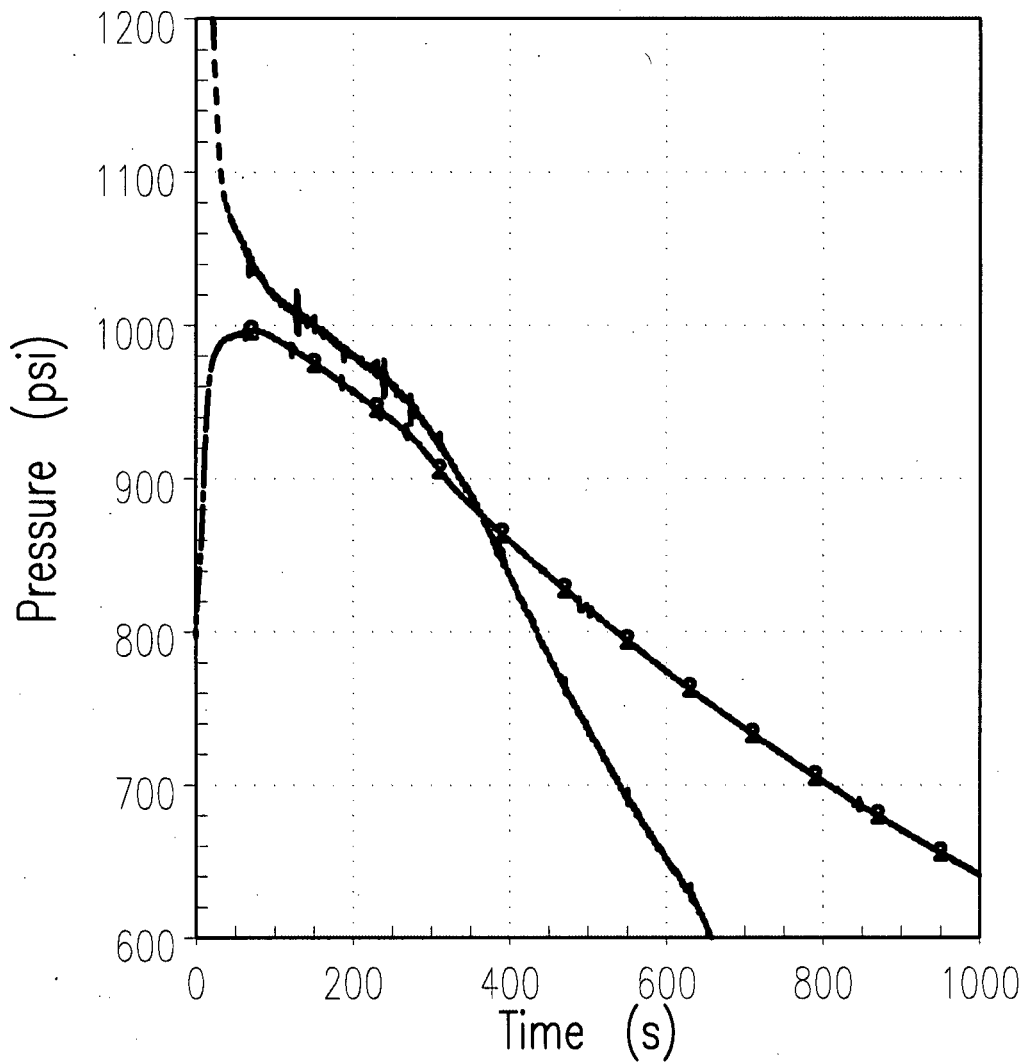
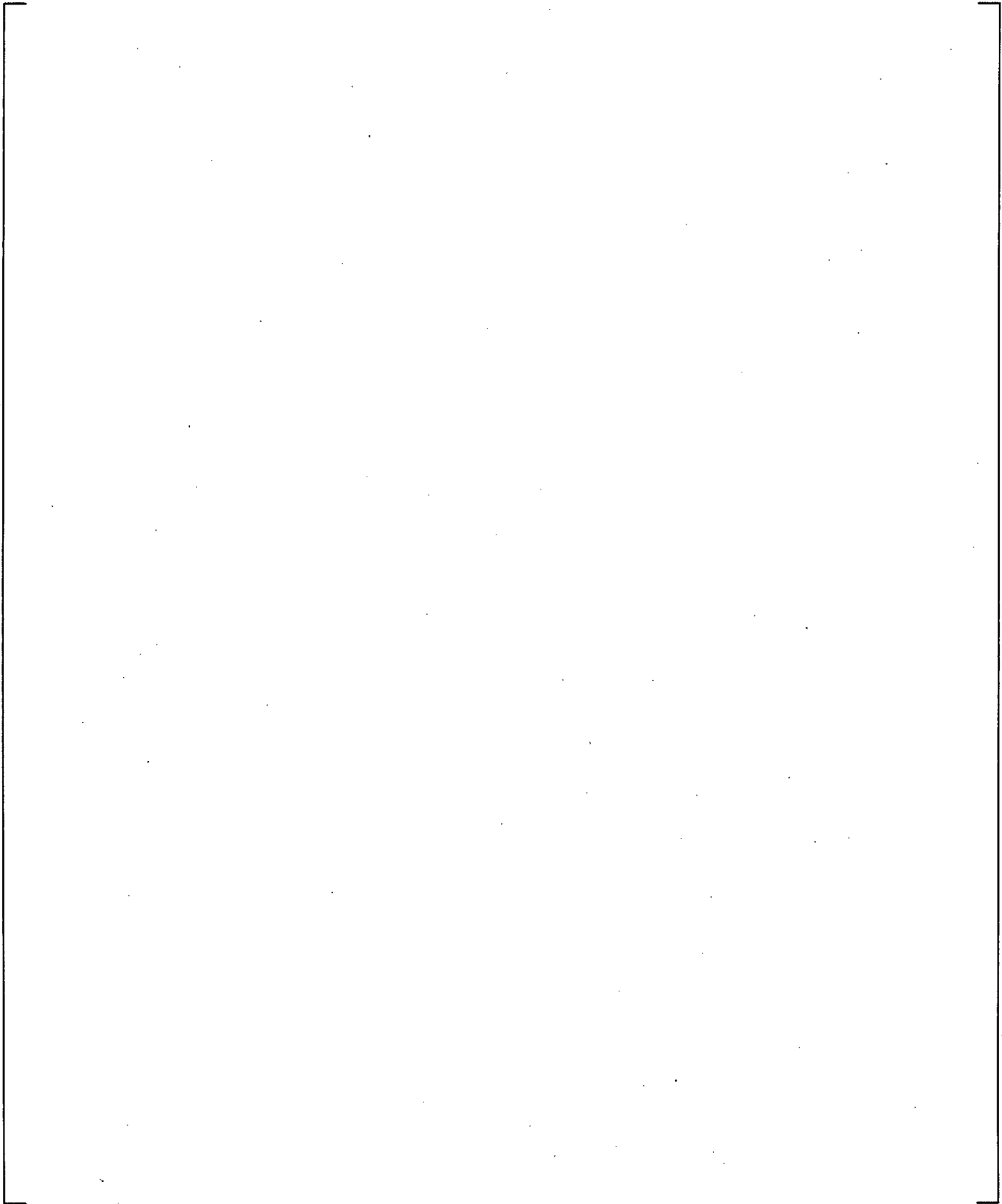
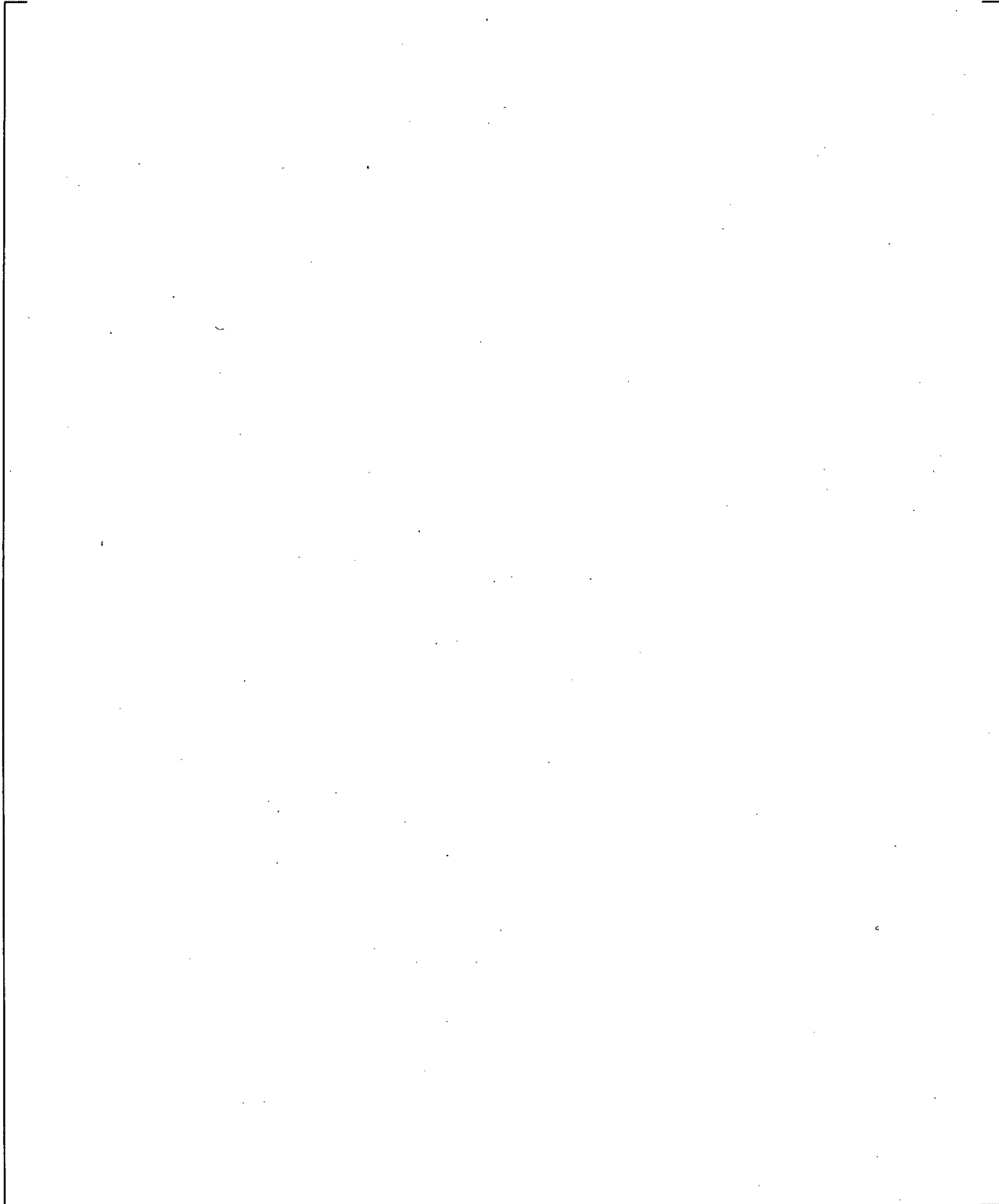


Figure 22-51 Measured Primary and SG Secondary Pressure, Test L3-1



**Figure 22-52 Impact of SG Secondary Side Pressure on Primary Pressure, Test L3-1**



**Figure 22-53 Impact of Critical Flow Model Uncertainties on Primary Pressure, Test L3-1**

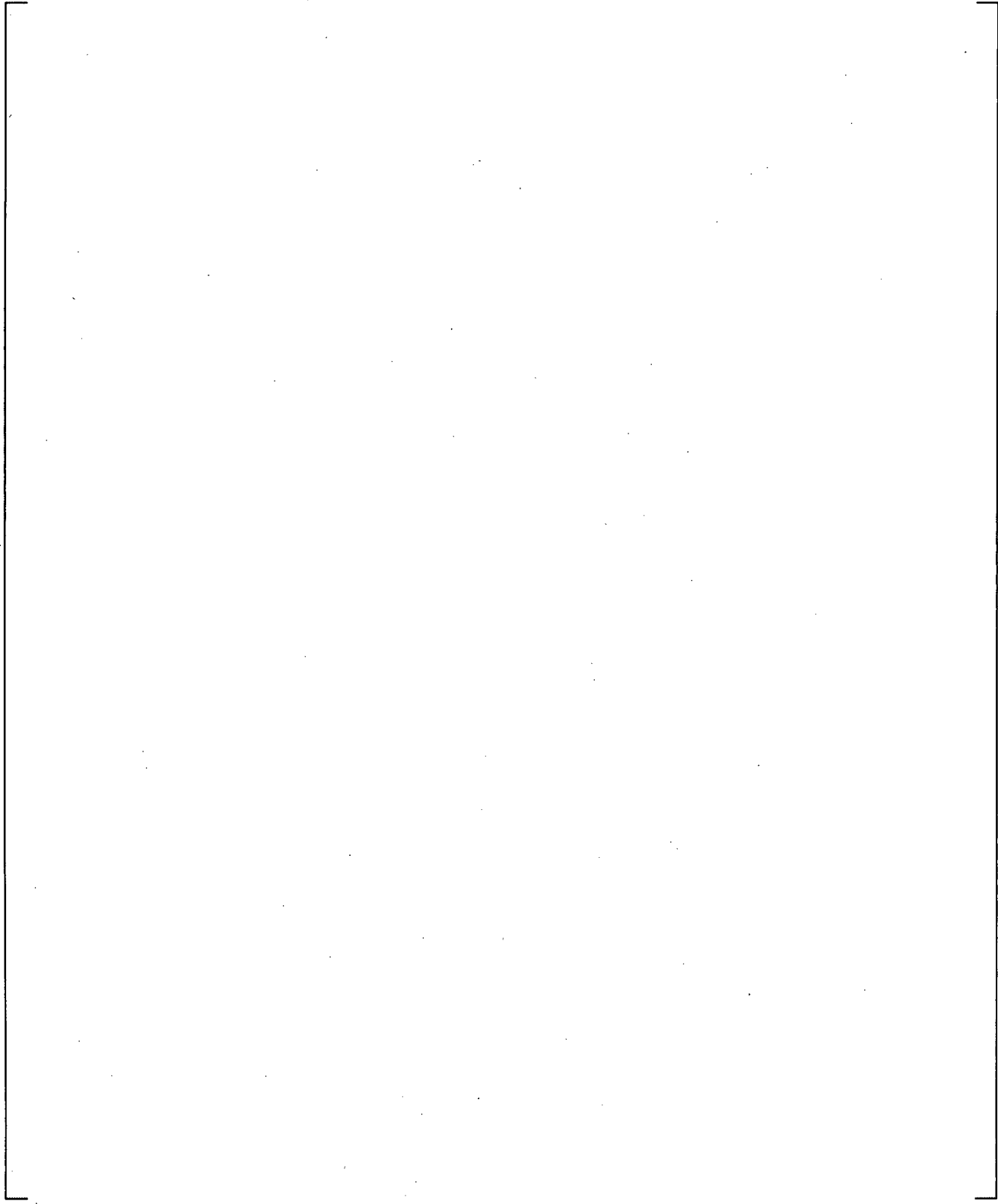


**Figure 22-54 Impact of Critical Flow Model Uncertainties on Break Flow, Test L3-1**

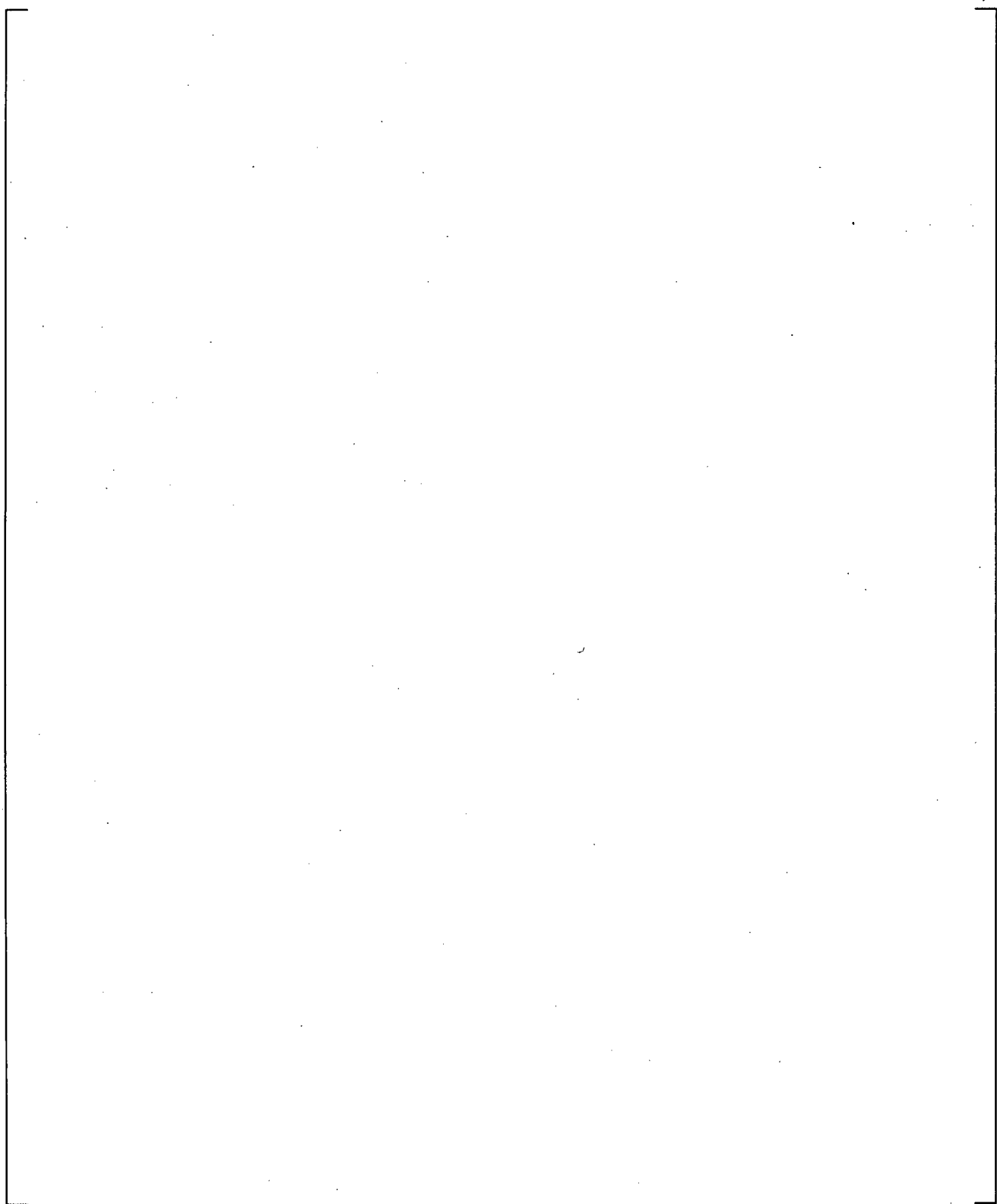


**Figure 22-55 Predicted and Measured Primary System Pressure, Test L5-1**

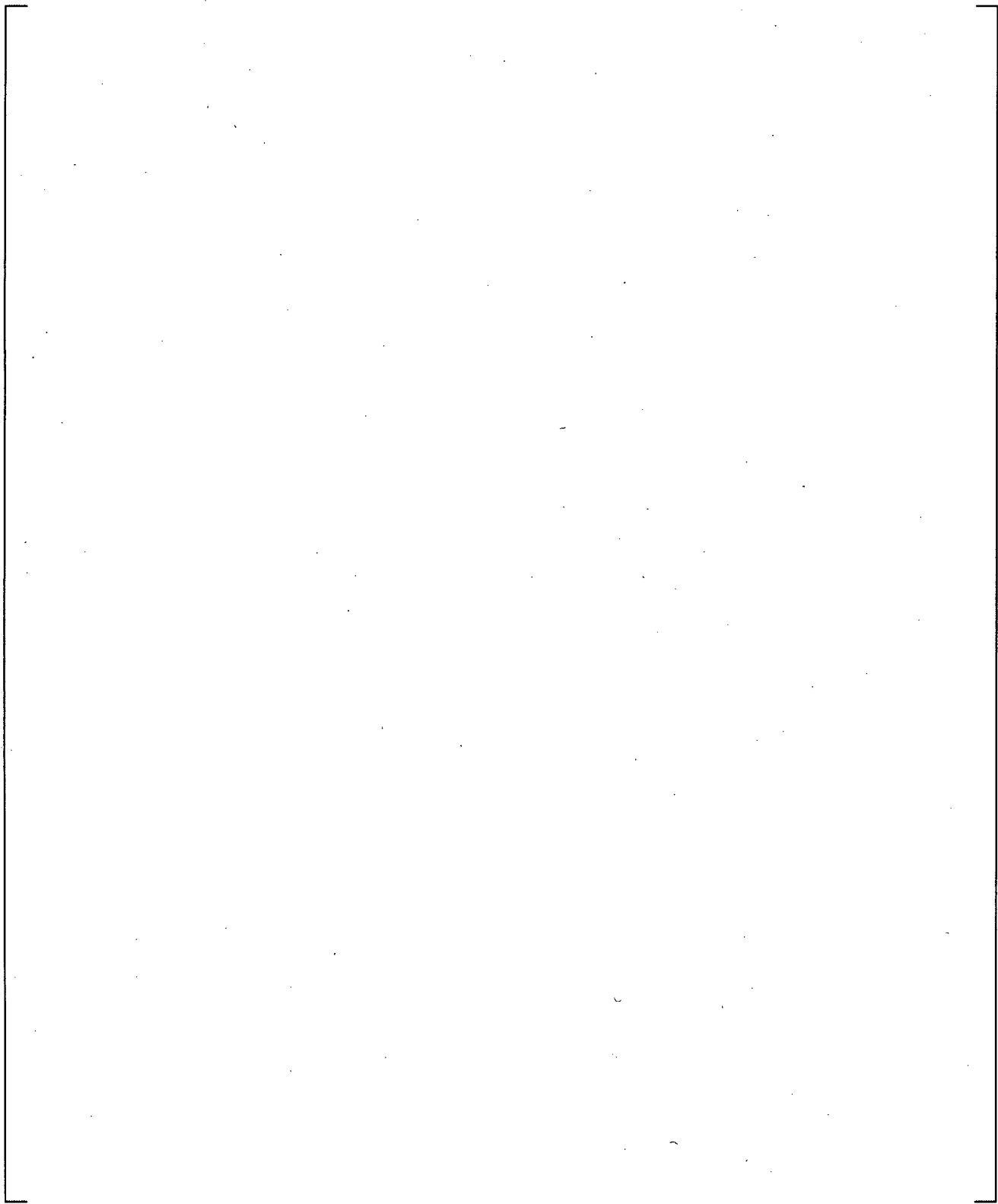


**Figure 22-56 Predicted and Measured Cold Leg Break Flow and Break Upstream Void Fraction, Test L5-1**

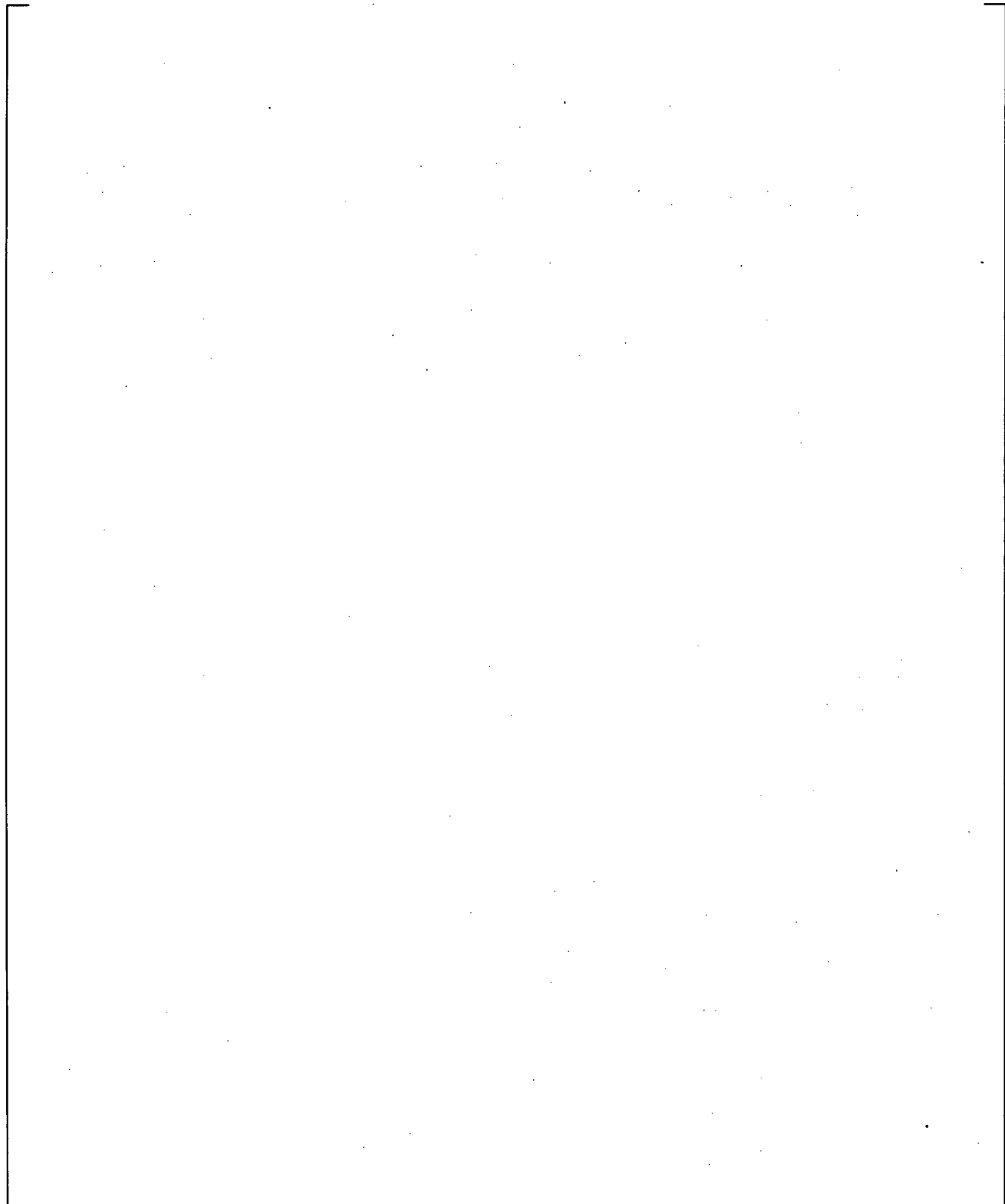


**Figure 22-57 Predicted and Measured Primary and Steam Generator Secondary Side Pressure, Test L5-1**

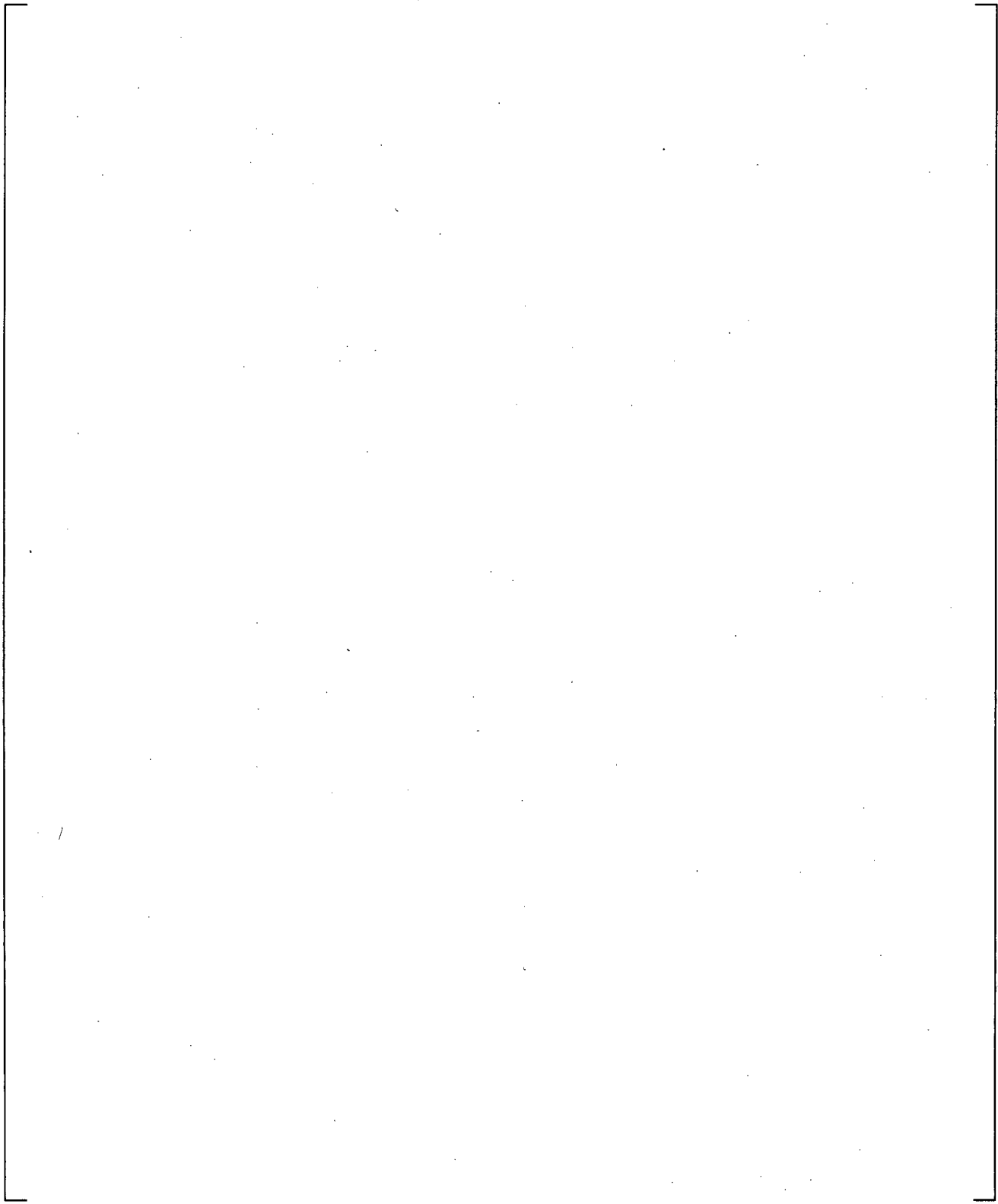


**Figure 22-58 Predicted and Measured Hot Assembly Cladding Temperature, Test L5-1**

a,c

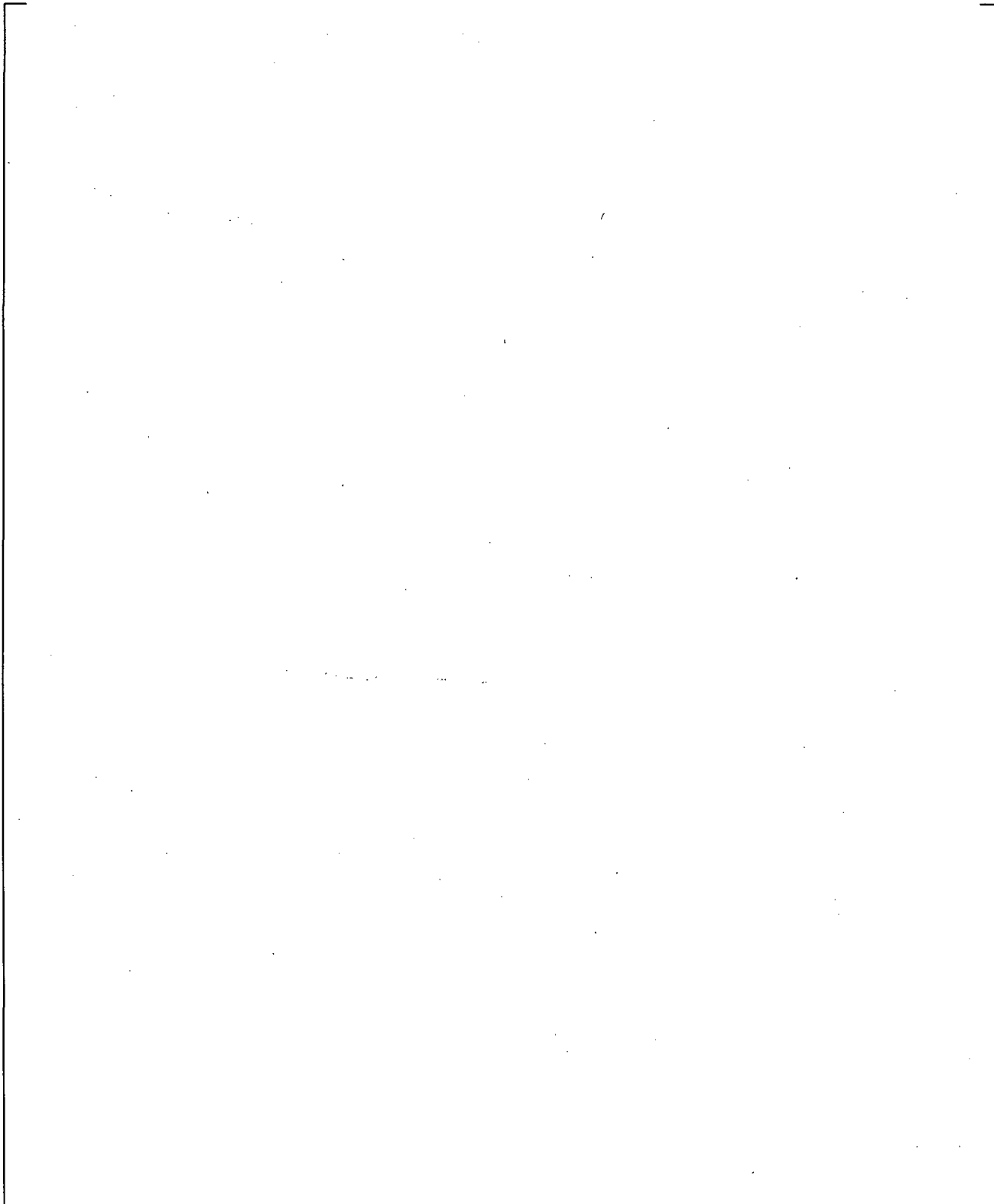


**Figure 22-59 Predicted and Measured Accumulator Liquid Level, Test L5-1**

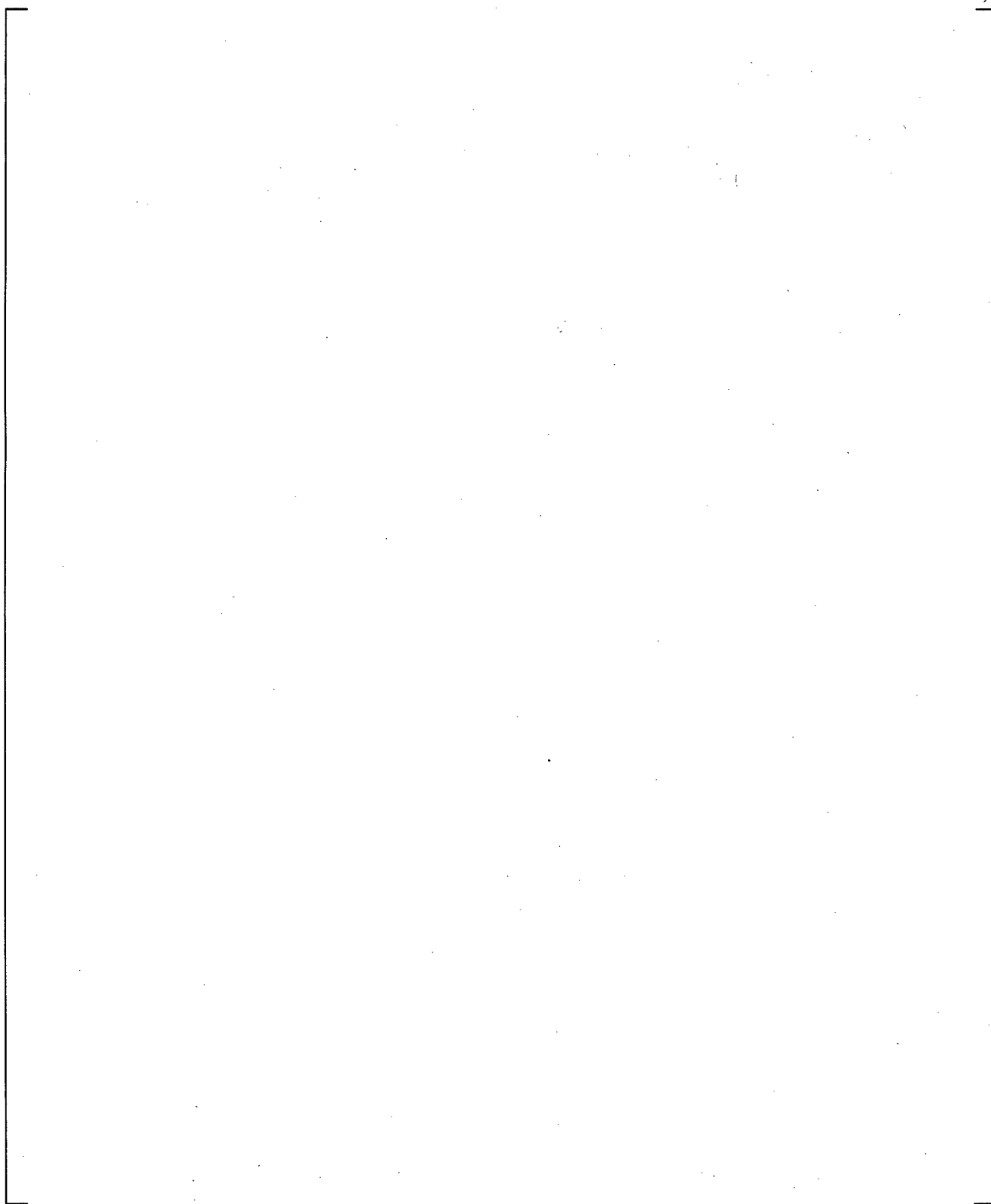


**Figure 22-60 Impact of Critical Flow Model Uncertainties on Primary Pressure, Test L5-1**

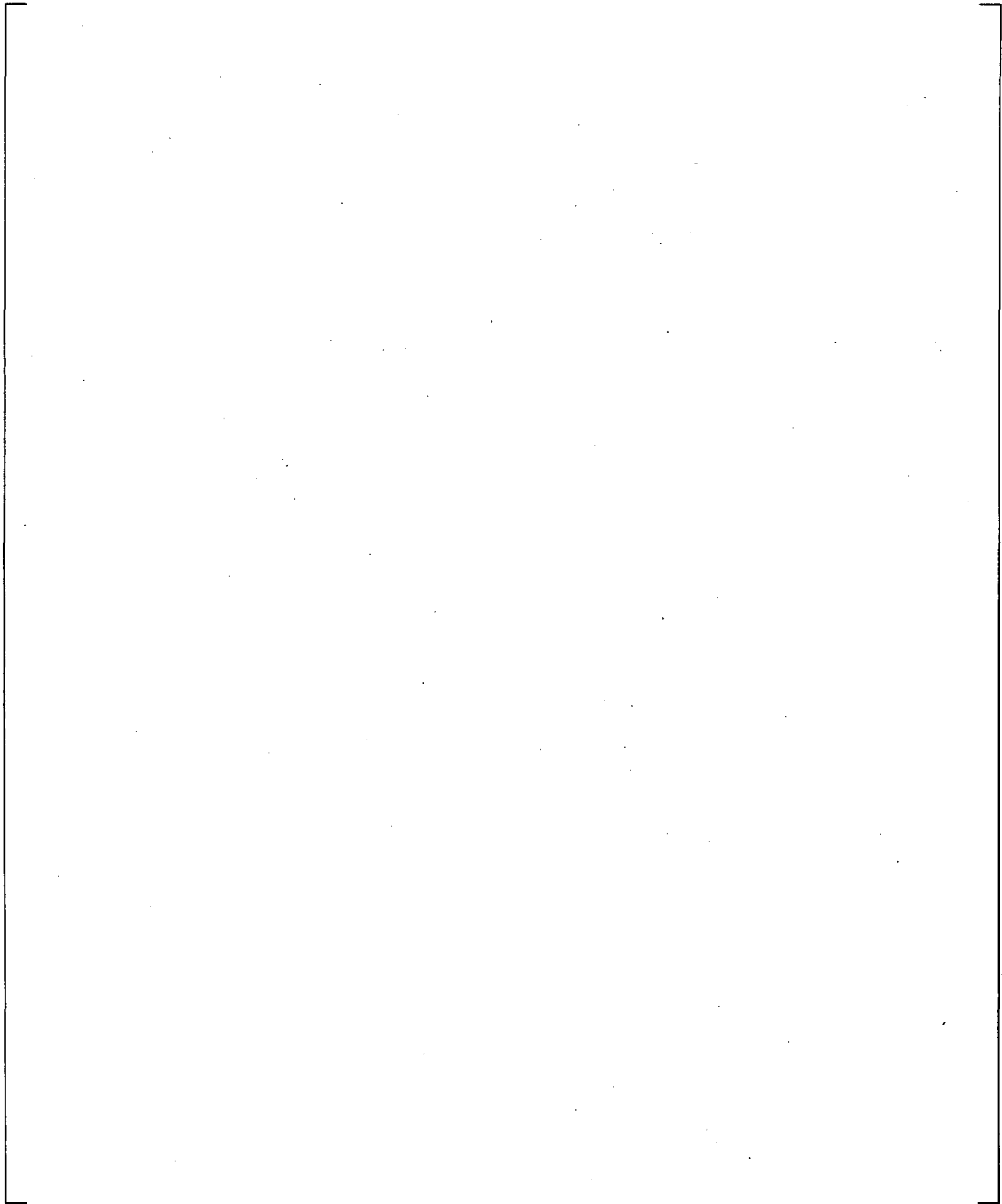


**Figure 22-61 Impact of Critical Flow Model Uncertainties on Break Flow, Test L5-1**

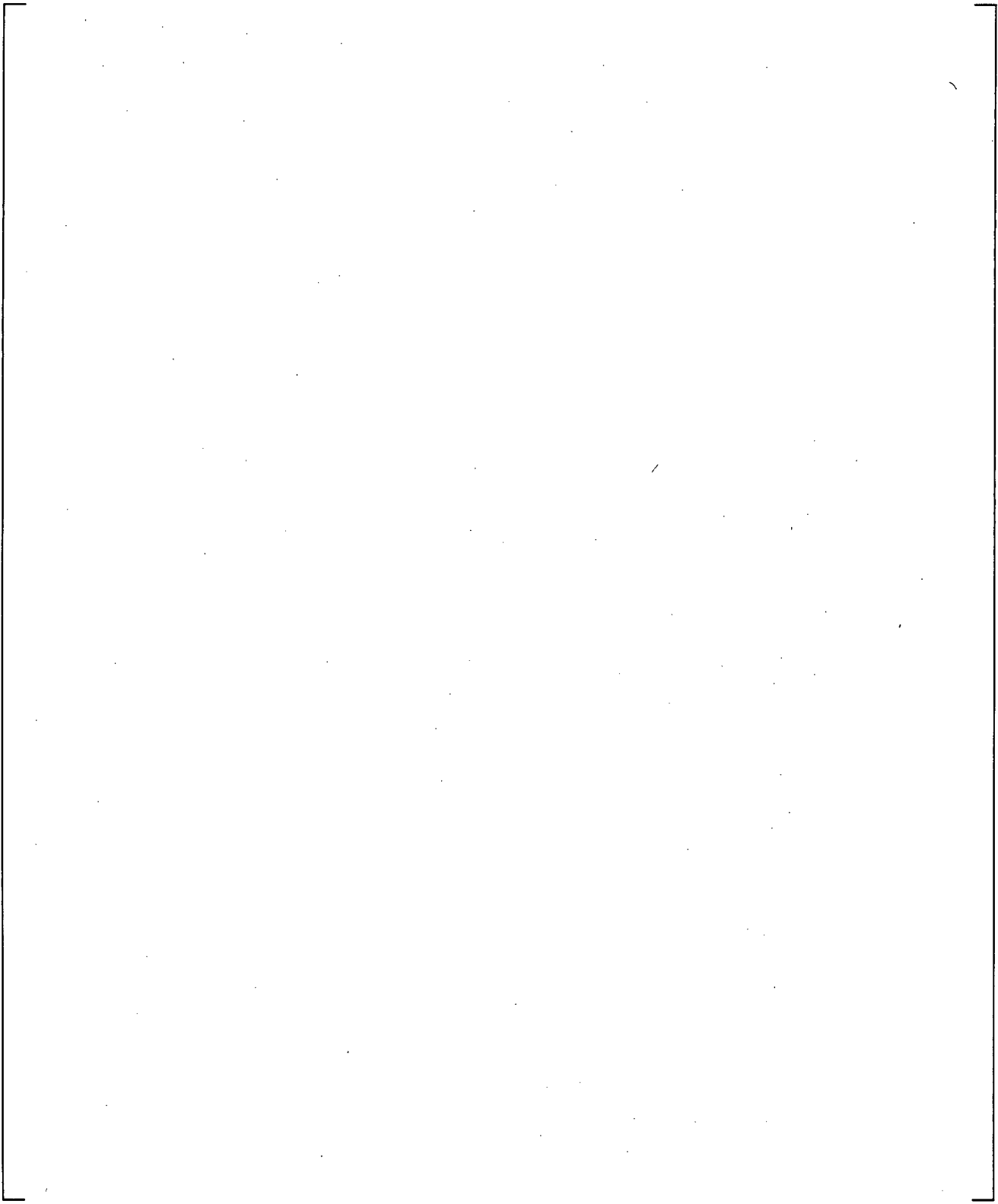


**Figure 22-62 Impact of Critical Flow Model Uncertainties on Cladding Temperature, Test L5-1**

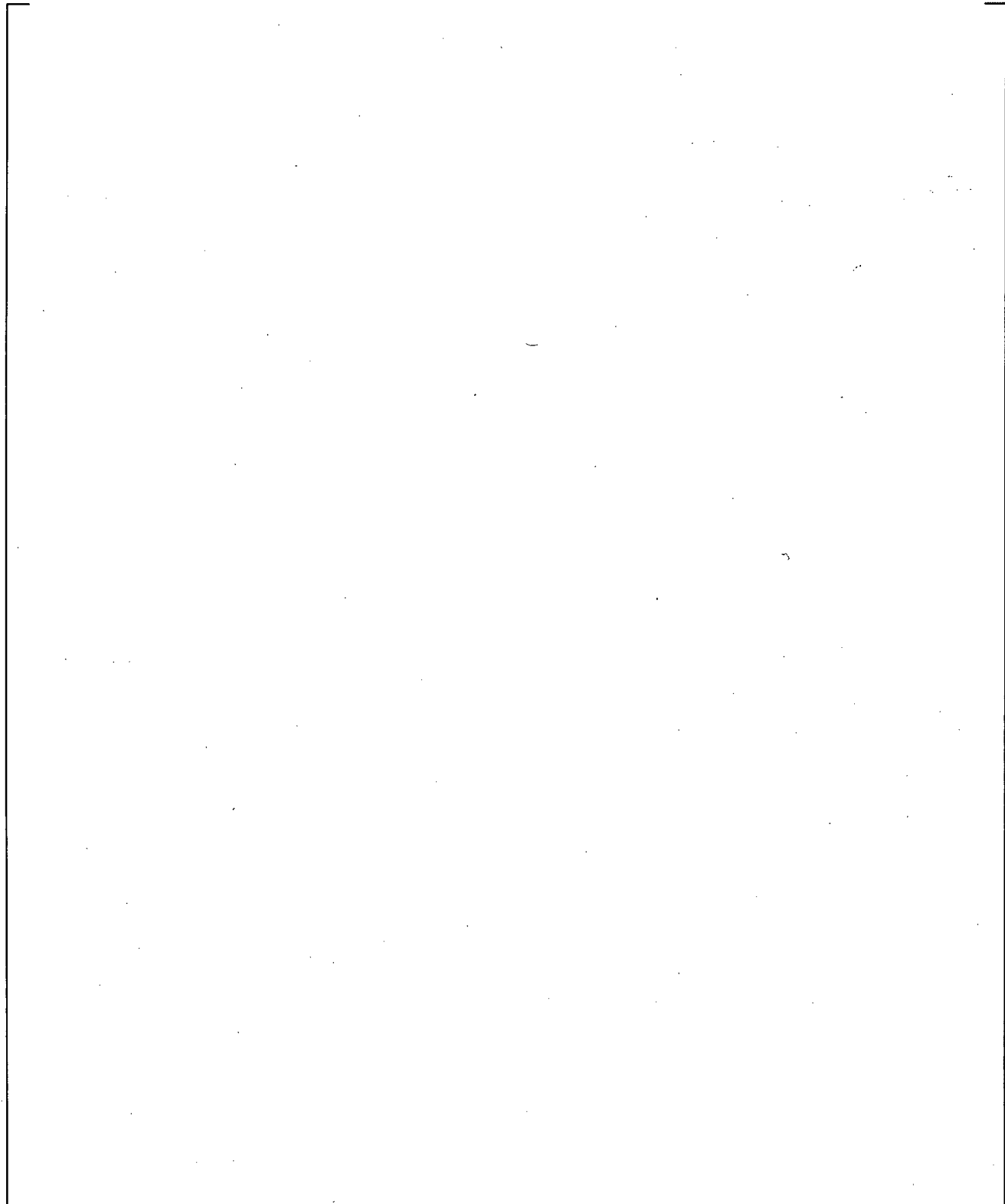


**Figure 22-63**    **Impact of Horizontal Stratification in the Intact Hot Leg on Cladding Temperature, Test L5-1**

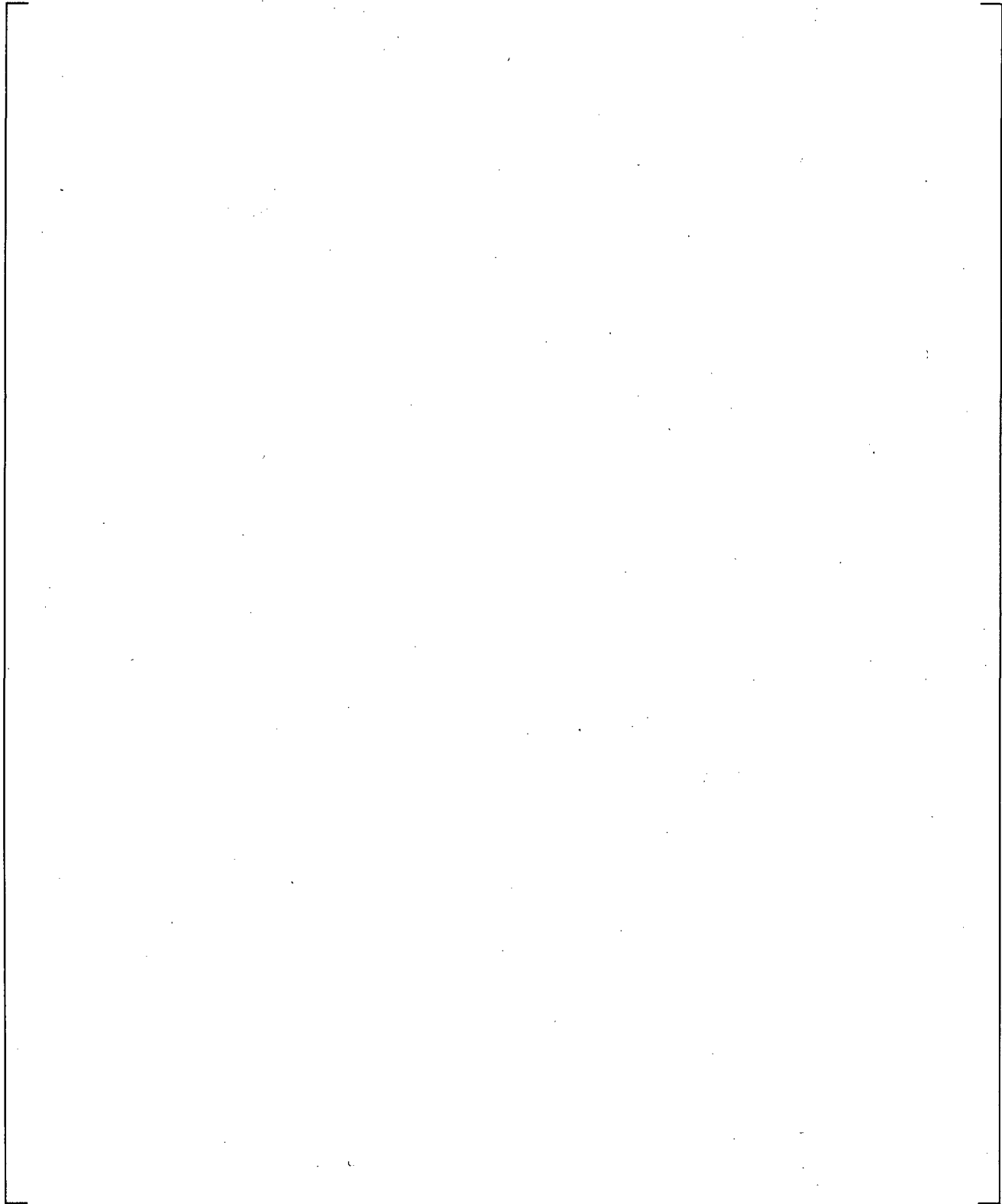


**Figure 22-64 Impact of Horizontal Stratification in the Intact Hot Leg on Break Flow, Test L5-1**

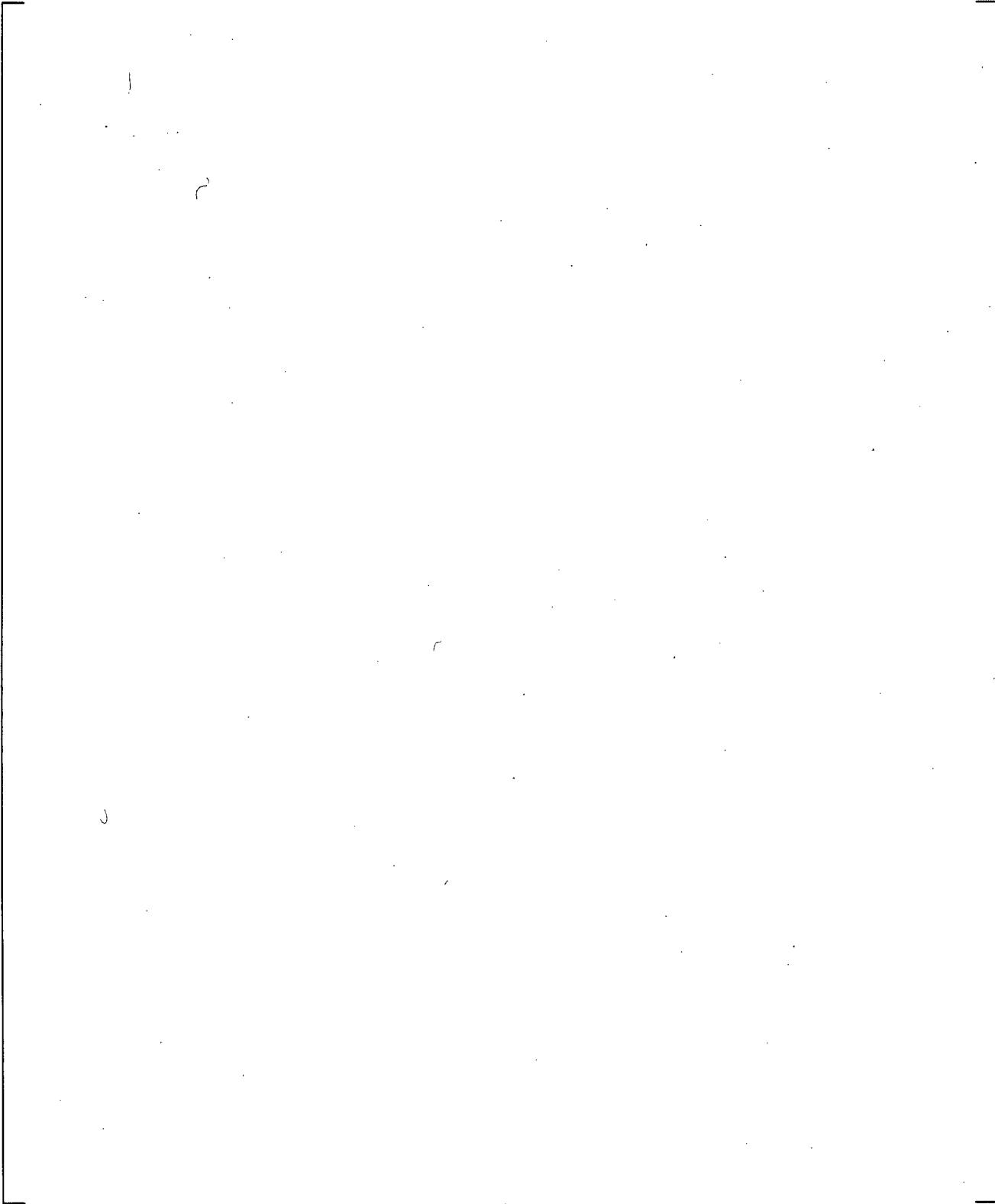


**Figure 22-65 Impact of Horizontal Stratification in the Intact Hot Leg on Cladding Temperature, Test L5-1**

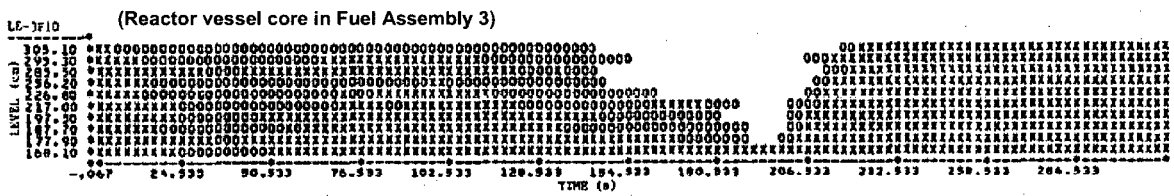
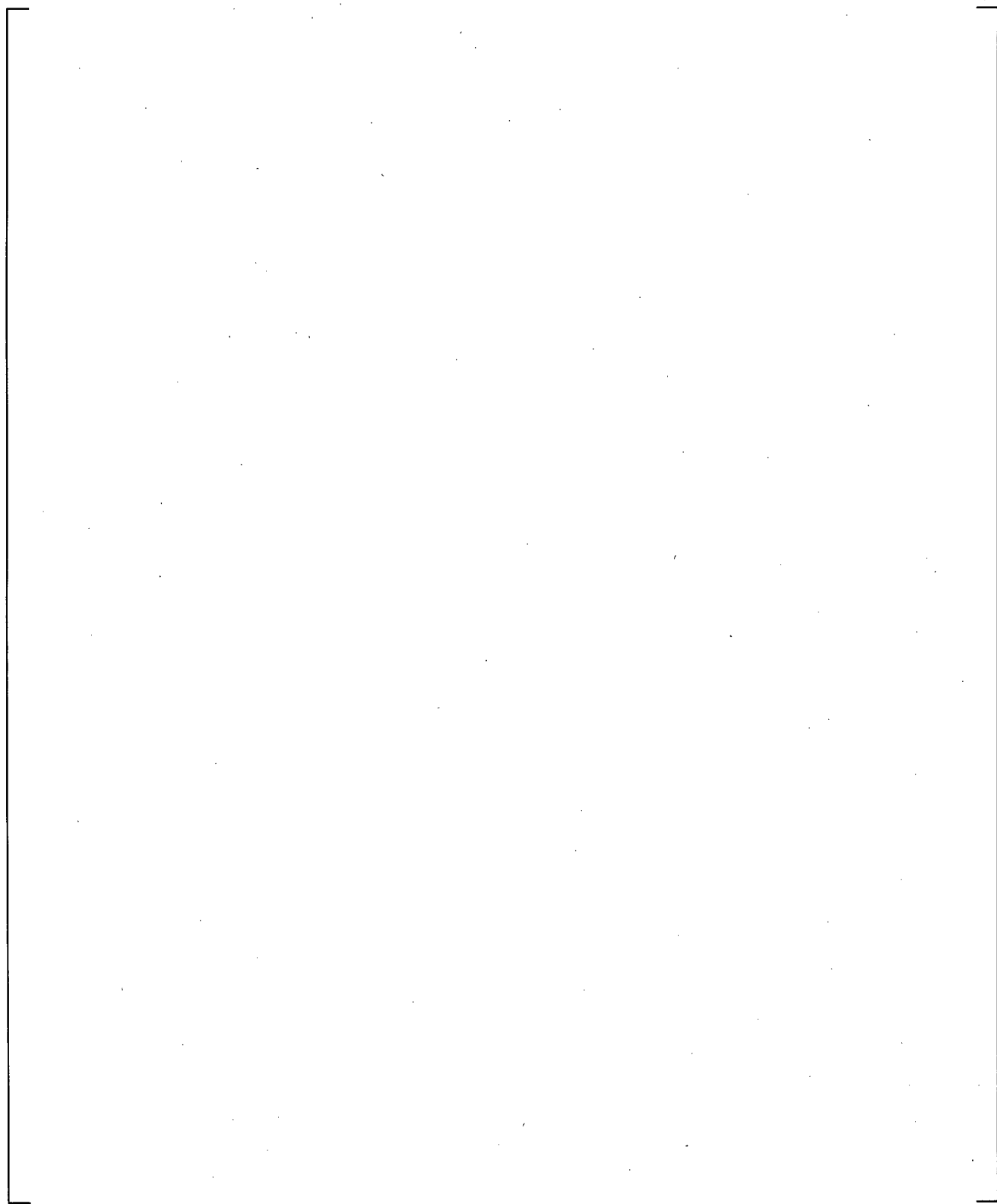


Figure 22-66 Measured Liquid Levels in Reactor Vessel Core Region, Test L5-1

a,c

Figure 22-67 Predicted Liquid Levels in Upper Plenum and Vessel Core Regions (Base Case), Test L5-1



**Figure 22-68** Predicted Liquid Levels in Upper Plenum and Vessel Core Regions  
(with HS\_SLUG=0.1) for Test L5-1

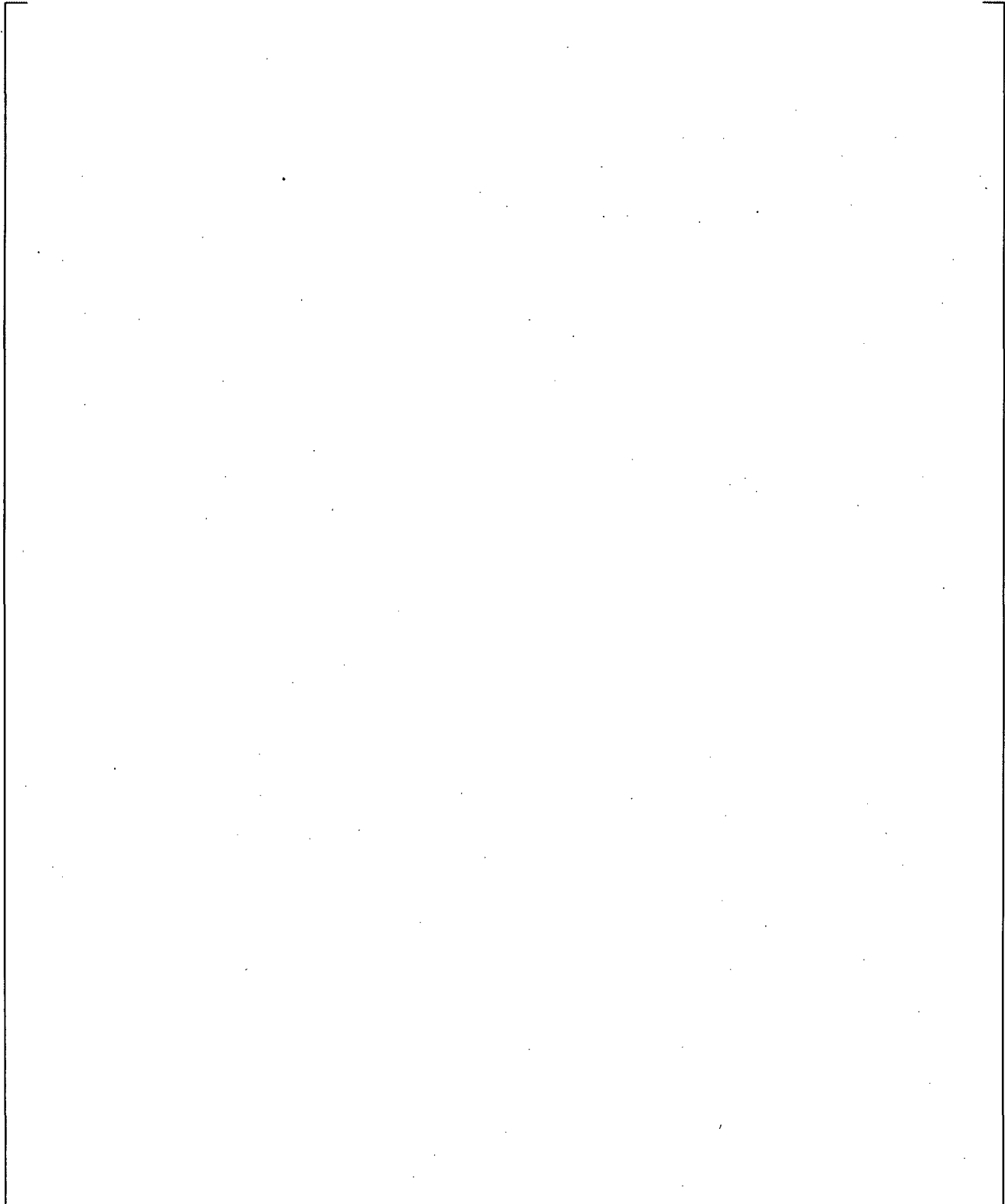


**Figure 22-69** Predicted Flow Regime and Liquid Flow Rate in the Hot Leg for both the Base case and Sensitivity case (with HS\_LUG=0.1) for Test L5-1

## 23 ADDITIONAL VALIDATION AND NUMERICAL PROBLEMS

Sections 12 through 20 provide the validation basis of WCOBRA/TRAC-TF2 against the critical phenomena identified in the PIRT documented in Section 1. Sections 21 and 22 provide information on the analysis of two series of integral effect tests, ROSA and LOFT, covering the whole spectrum of postulated break sizes.

This final assessment Section documents additional validation, and in particular some numerical thought problems, and has two key objectives:

1. Complete the validation basis documented in Sections 12 through 22, with the evaluation of critical issues that have not been addressed in previous Sections. In essence, some specific limitations of the previous validation are analyzed and completed herein.
2. Use a series of numerical problems, for which an analytical solution can be developed, to verify that not only WCOBRA/TRAC-TF2 correctly predicts the complex physical phenomena analyzed in previous sections, but is also capable of providing physically sound solutions to some standard problems, thus verifying the overall code robustness and quality. Consistent with Regulatory Guide 1.203, these numerical problems are performed “to illustrate fundamental calculational device capability.”

To achieve these objectives, the following analyses are documented in this Section.

- Section 23.1 Additional Validation
  - Section 23.1.1 GE Blowdown – The level swell analysis documented in Section 13 relies mostly on steady state tests. The objective of the GE Blowdown analysis is to assess WCOBRA/TRAC-TF2 in a dynamic, blowdown transient. This Section will demonstrate that the WCOBRA/TRAC-TF2 level swell prediction remains adequate in these conditions.
  - Section 23.1.2 Semiscale – The Level Swell and Boiloff analyses documented in Section 13 are all characterized by relatively low clad temperature. Selected Semiscale boiloff tests are analyzed herein to verify the WCOBRA/TRAC-TF2 prediction of level swell and post-CHF heat transfer when clad temperatures are high.
- Section 23.2 Numerical Test Problems
  - Section 23.2.1 1D PIPE Manometer Problem with Non-Condensable Gases
  - Section 23.2.2 3D VESSEL Manometer Problem with Non-Condensable Gases
  - Section 23.2.3 1D PIPE Steam Expulsion Test
  - Section 23.2.4 3D VESSEL Steam Expulsion Test
  - Section 23.2.5 1D PIPE Fill and Drain Test
  - Section 23.2.6 3D VESSEL Fill and Drain Test
  - Section 23.2.7 Condensation Test

## 23.1 ADDITIONAL VALIDATION

### 23.1.1 GE Vessel Blowdown Tests

#### 23.1.1.1 Introduction

Early in a LOCA, voids are generated in the primary reactor coolant system (RCS) by flashing and boiling in the core. During the blowdown phase, depressurization is rapid and flashing can play an important role. Flashing in the core and upper plenum can re-distribute fluid in the RCS, which can lead to uncertainty in loop seal clearing time (for smaller break sizes) and analysis results. [

] <sup>a,c</sup>

The void distribution in the reactor vessel during the blowdown phase depends on several processes; the interfacial drag between the vapor and liquid (film), wall drag, the bubble rise velocity and bubble size, the entrainment of droplets at the two-phase interface, the transition point between bubbly and other vertical flow regimes, and the rate of system depressurization. The rate of depressurization depends on the break flow rate.

The GE Vessel Blowdown Facility is designed to study basic phenomena such as void fraction distribution and transient liquid-vapor level swell during blowdown. Several top-break blowdown tests were conducted using different-sized orifice plates to vary the blowdown transient. The tests also varied the open area of the resistance plate at the vessel mid-plane. [

] <sup>a,c</sup>

A description of all the tests performed is given in NUREG/CR-1899 (Findlay and Sozzi, 1981).

#### 23.1.1.2 GE Blowdown Test Facility Description

The blowdown tests were performed in a cylindrical carbon steel vessel. The vessel was a two-piece unit that could be separated at a pair of flanges located near the center of the vessel. The cylindrical portion of the vessel was constructed from Schedule 80 pipe, 12 feet long with an inside diameter of 1 foot. Elliptical heads were welded onto the ends of the pipe to create the vessel. The total vessel volume was 10 cubic feet, and the total height was 14 feet. There were five calorimetric heater rods, 1 inch in diameter and 2 feet high, in the bottom of the vessel to heat the water. The steam exhaust was located at the 13-foot elevation with an orifice that was captured in a flange. The orifices used to control the tank blowdown rate were plates with the prescribed hole machined without a chamfer. The orifice was located close to the vessel in a 2-inch Schedule 80 pipe. Figure 23.1.1-1 is a scaled drawing that shows the vessel, its penetrations, the blowdown line, and a suppression pool where the blowdown effluent was discharged.

A 3/4-inch thick perforated plate (containing 109 holes, 9/16-inch diameter), designed to provide an internal flow restriction, was installed between the main vessel flanges at the mid-elevation during some

of the tests. The resistance of the plate was varied by plugging a selected number of holes. Orifice plates with different flow areas were used in the blowdown line to limit the blowdown flow rate and vary the vessel depressurization rate.

Figure 23.1.1-2 shows the instrumentation arrangement used to measure three basic parameters: pressures, pressure differences, and temperatures. Vessel pressure and differential pressures were measured using strain-gauge pressure transducers, and temperatures were measured using Iron-Constantan thermocouples. The transient void fraction and the mixture level were calculated from differential pressure measurements.

#### **23.1.1.3 Test Matrix for GE Blowdown Simulations**

Table 23.1.1-1 lists the seven experiments in the test series. All seven of the tests were simulated with WCOBRA/TRAC-TF2, and none were excluded. These tests span a range of orifice diameters from 3/8 of an inch to 1 inch, and a variety of different flow restrictions at the midpoint of the vessel.

#### **23.1.1.4 Test Procedure for GE Blowdown Simulations**

The vessel was initially filled with demineralized water and boiled at atmospheric pressure for approximately 30 minutes to liberate any dissolved gas in the supply water. A vent at the top of the vessel was then closed, and the water was heated to establish the initial conditions (which were a nominal pressure of 1000 psia and 545°F). Actual initial conditions for each test are given in the test matrix in Table 23.1.1-1. With the facility initially heated and pressurized, several top-break blowdown tests were conducted.

#### **23.1.1.5 WCOBRA/TRAC-TF2 Model for GE Vessel Blowdown Tests**

The WCOBRA/TRAC-TF2 model of the GE Vessel Blowdown Facility is shown in Figure 23.1.1-3. [

] <sup>a,c</sup>

#### **23.1.1.6 Simulation of GE Vessel Blowdown Tests**

The primary figure of merit for these simulations is the ability of the WCOBRA/TRAC-TF2 code to predict the void distribution in the vessel for these simulations. The results of the WCOBRA/TRAC-TF2 simulations of the Vessel Blowdown Tests are summarized and compared to the experimental data in

Table 23.1.1-2. The ability of the code to predict the void fraction trends in each of the simulations was assessed in the first column of the table. The specific void fraction prediction at six elevations (see Figure 23.1.1-3) in the vessel was then assessed against the test data in the remaining table columns.

[

] <sup>a,c</sup>

### 23.1.1.7 Effect of Interfacial Drag Multiplier

The simulations of the GE Vessel Blowdown Tests were also run with WCOBRA/TRAC-TF2 to investigate the impact of the interfacial drag multiplier (YDRAG) on the prediction of the two-phase level and pressure. [

] <sup>a,c</sup>

] <sup>a,c</sup> to the experimental data for each of the GE blowdown tests. [

] <sup>a,c</sup> The experimental data is presented as dashed black lines, with both the nominal and upper/lower bound uncertainties presented. It can be seen from these plots that [

] <sup>a,c</sup>

### 23.1.1.8 Summary and Conclusions

The results of the GE Vessel Blowdown Test simulations tend to confirm that [

] <sup>a,c</sup>

### 23.1.1.9 References

1. Findlay, J. A. and Sozzi, G. L., 1981, BWR Refill-Reflood Program B Model Qualification Task Plan, NUREG/CR-1899.



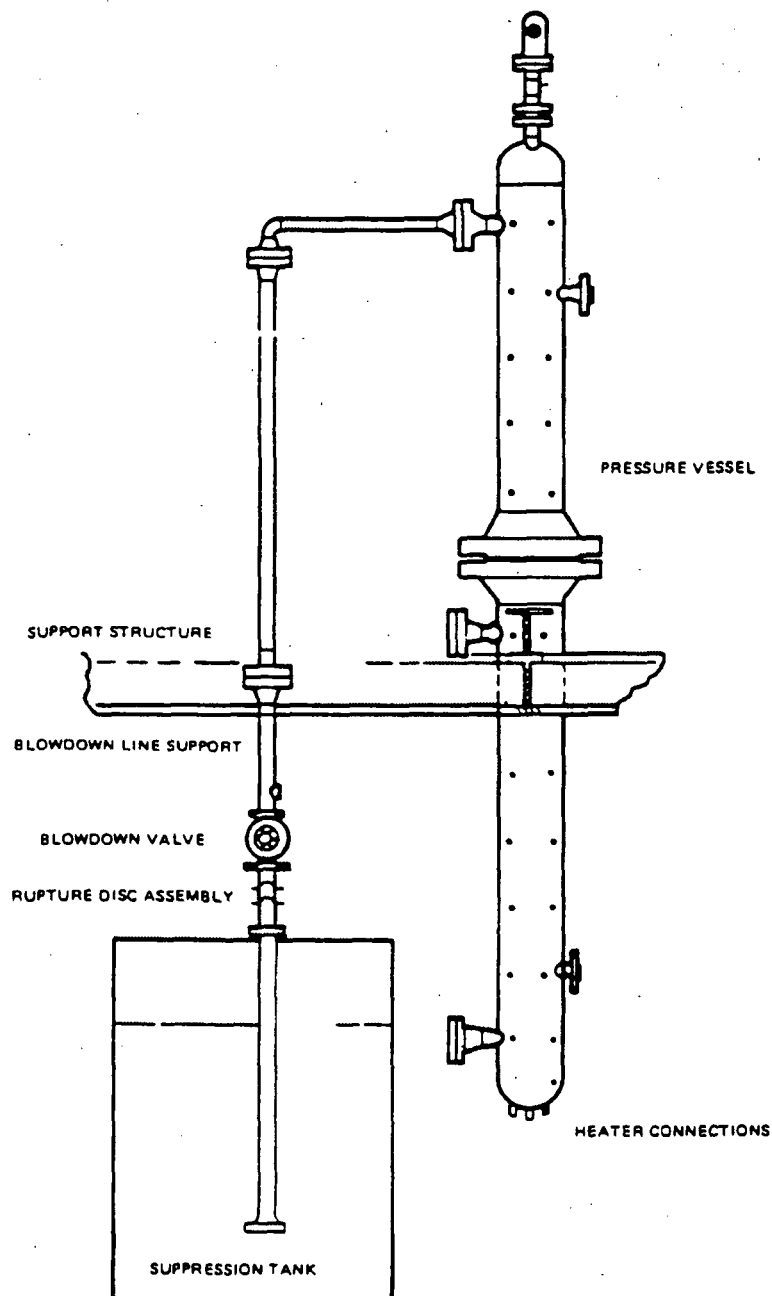


Figure 23.1.1-1 Small Blowdown Vessel

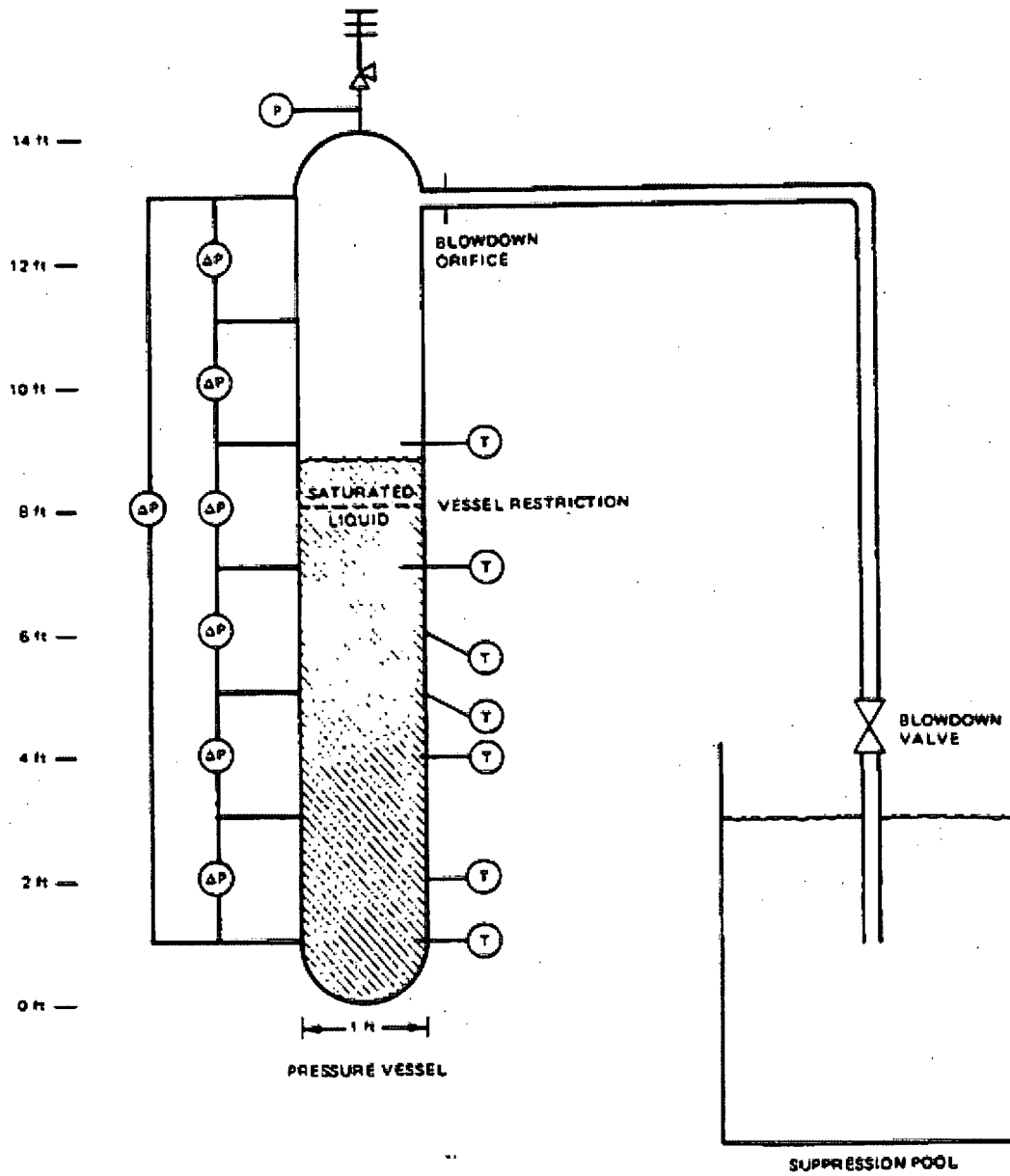
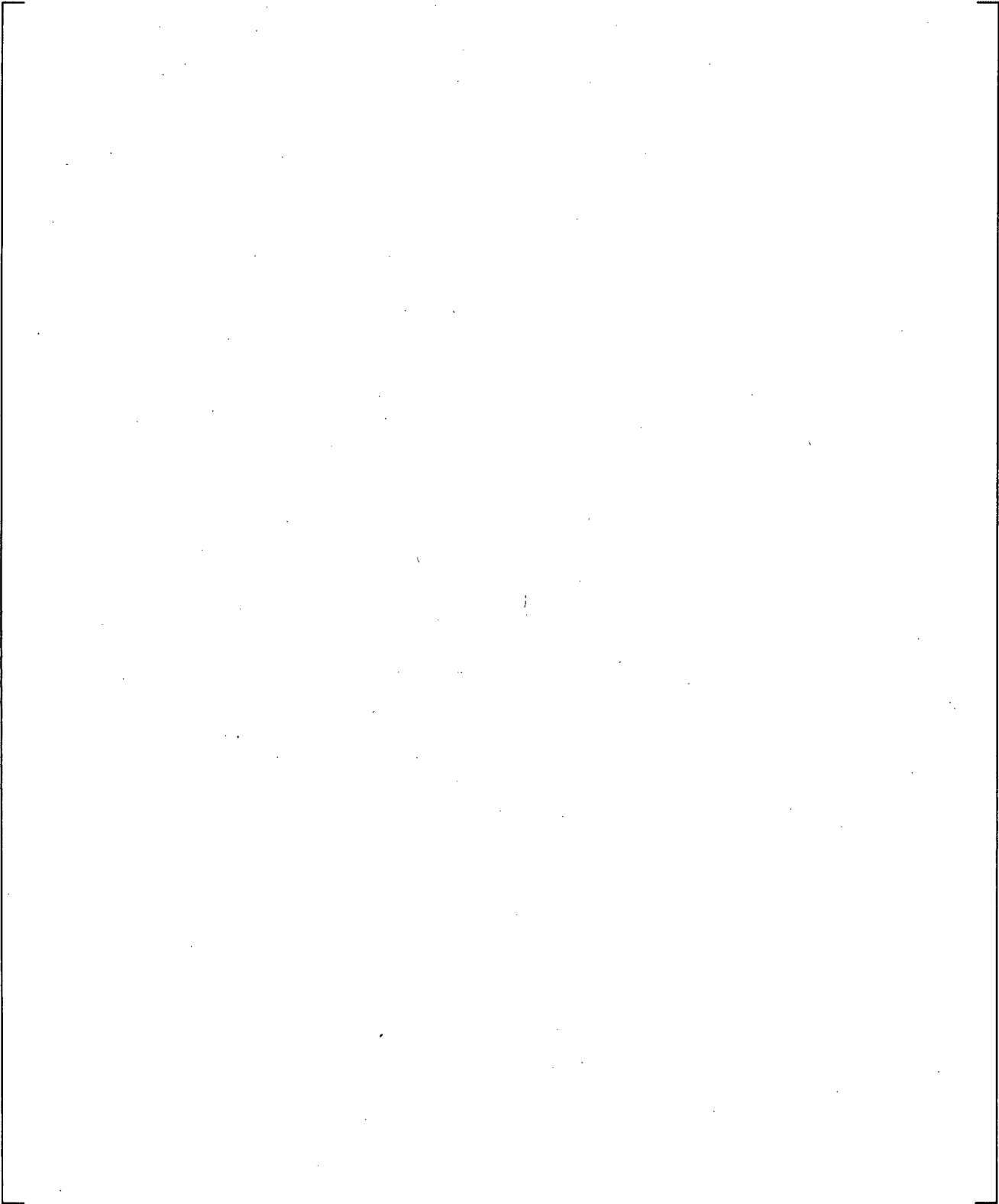
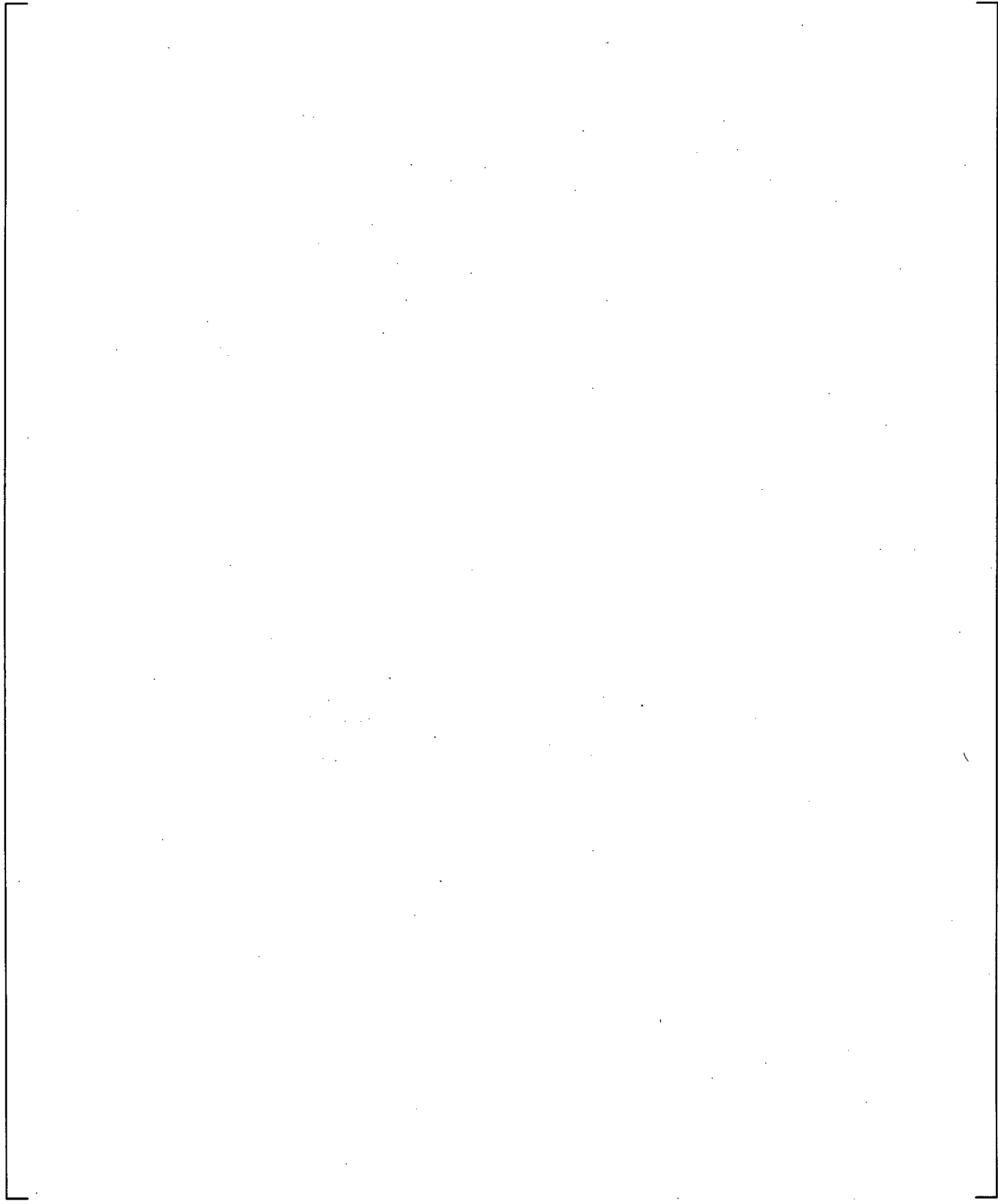


Figure 23.1.1-2 Small Blowdown Vessel Instrumentation



**Figure 23.1.1-3 WCOBRA/TRAC-TF2 Model of the GE Vessel Blowdown Facility**



**Figure 23.1.1-4 Comparison of Predicted and Measured Void Fraction at Level 1, Test 8-21-1**

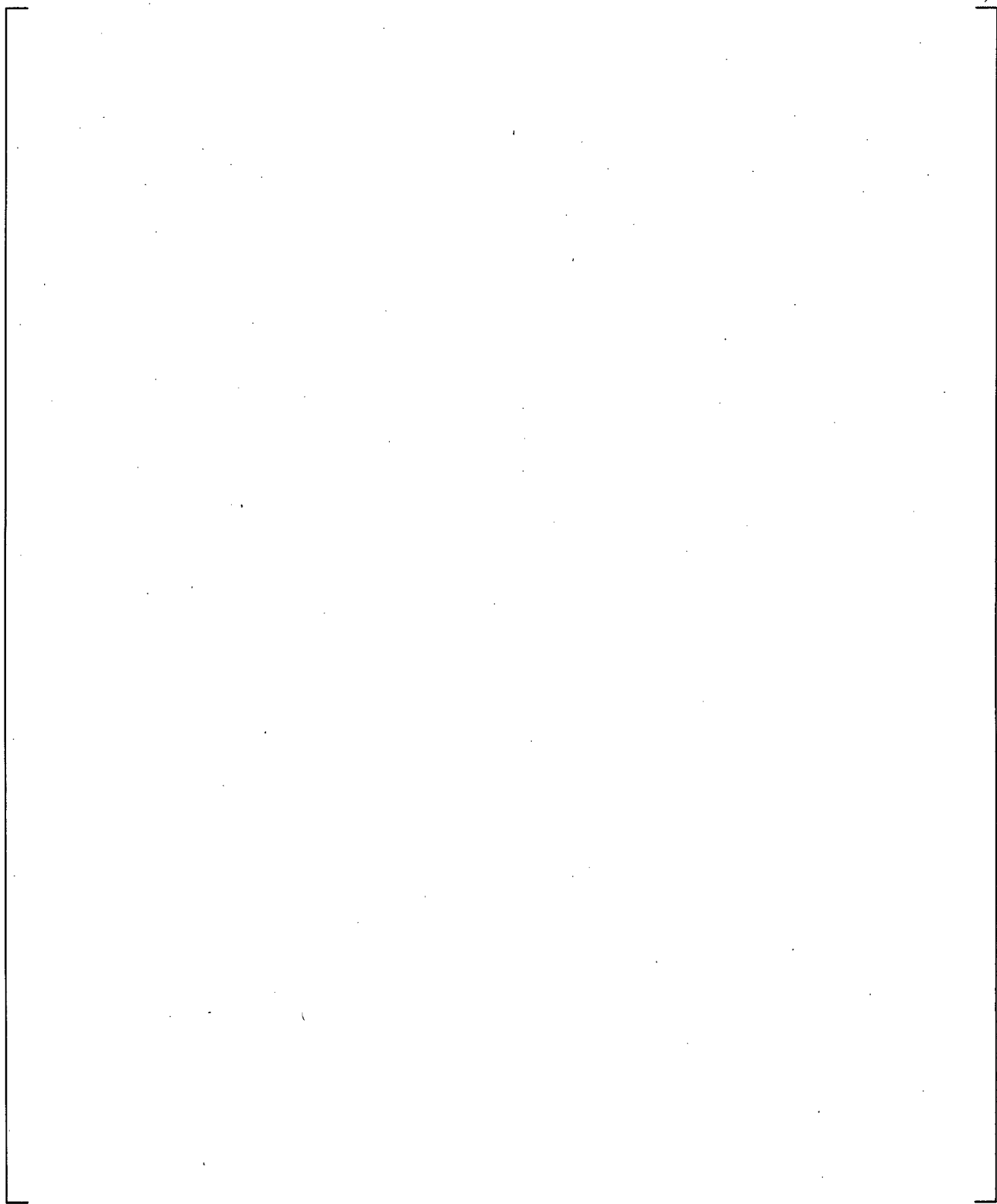


**Figure 23.1.1-5 Comparison of Predicted and Measured Void Fraction at Level 2, Test 8-21-1**

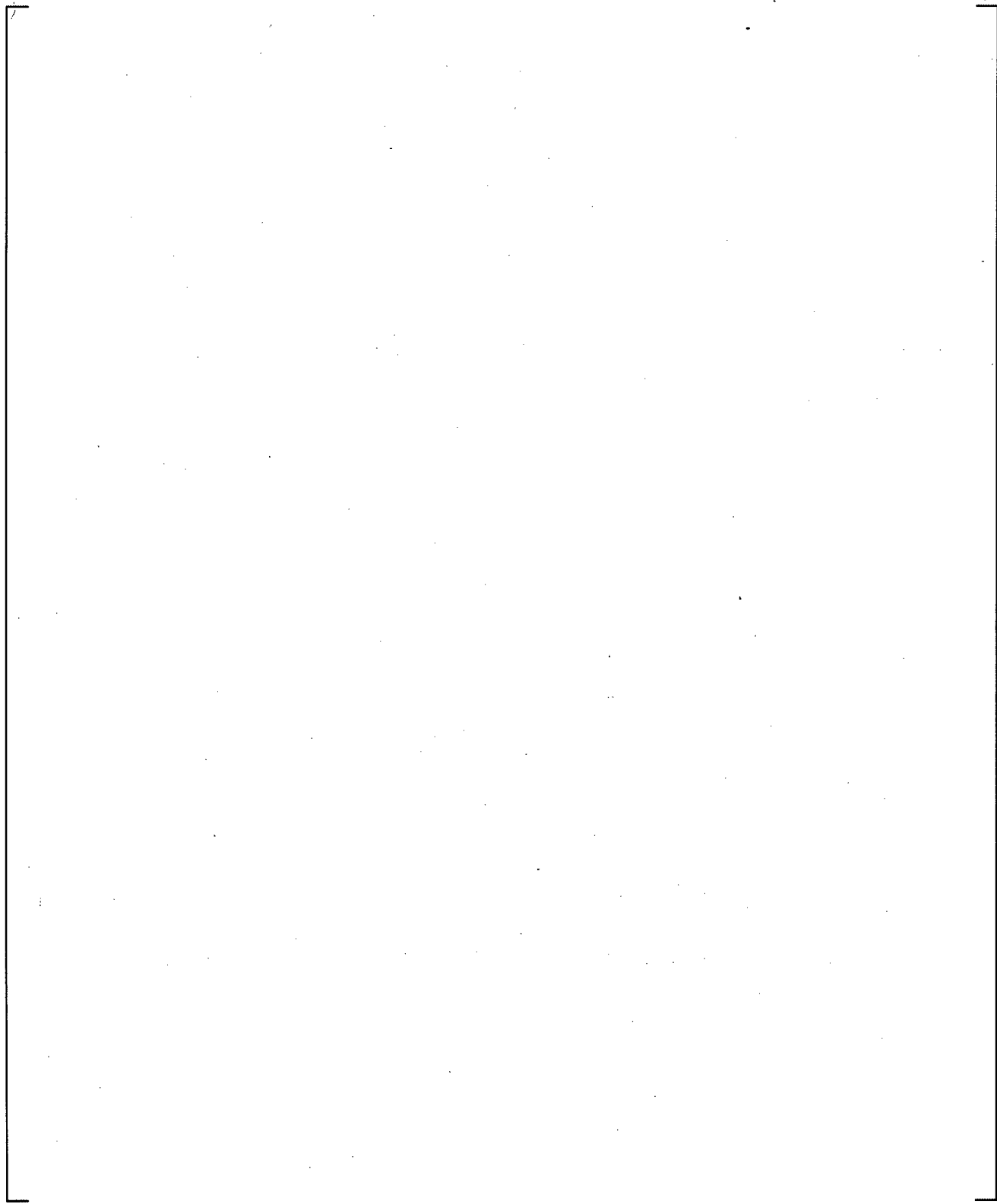


**Figure 23.1.1-6 Comparison of Predicted and Measured Void Fraction at Level 3, Test 8-21-1**

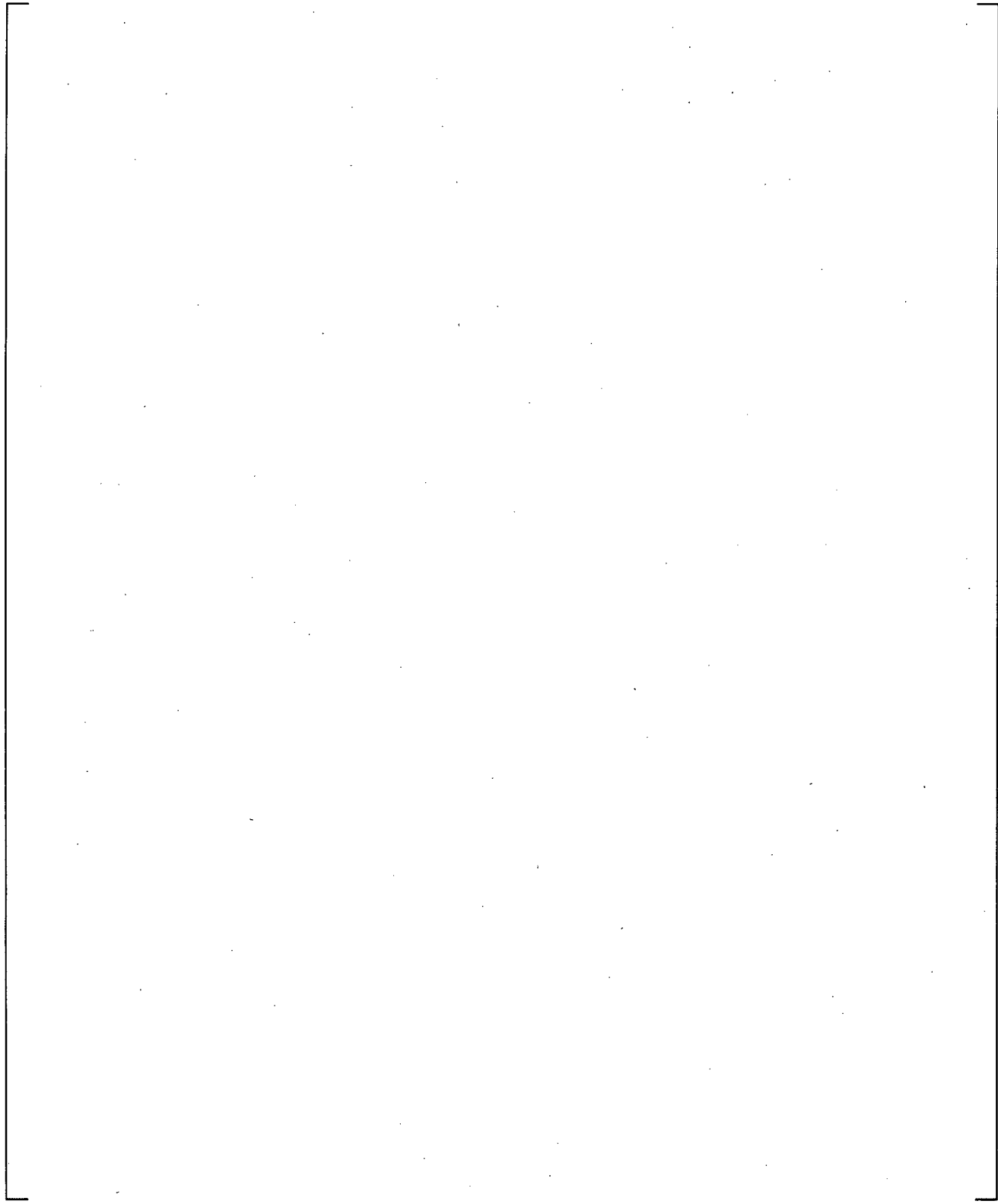


**Figure 23.1.1-7 Comparison of Predicted and Measured Void Fraction at Level 4, Test 8-21-1**

a,c

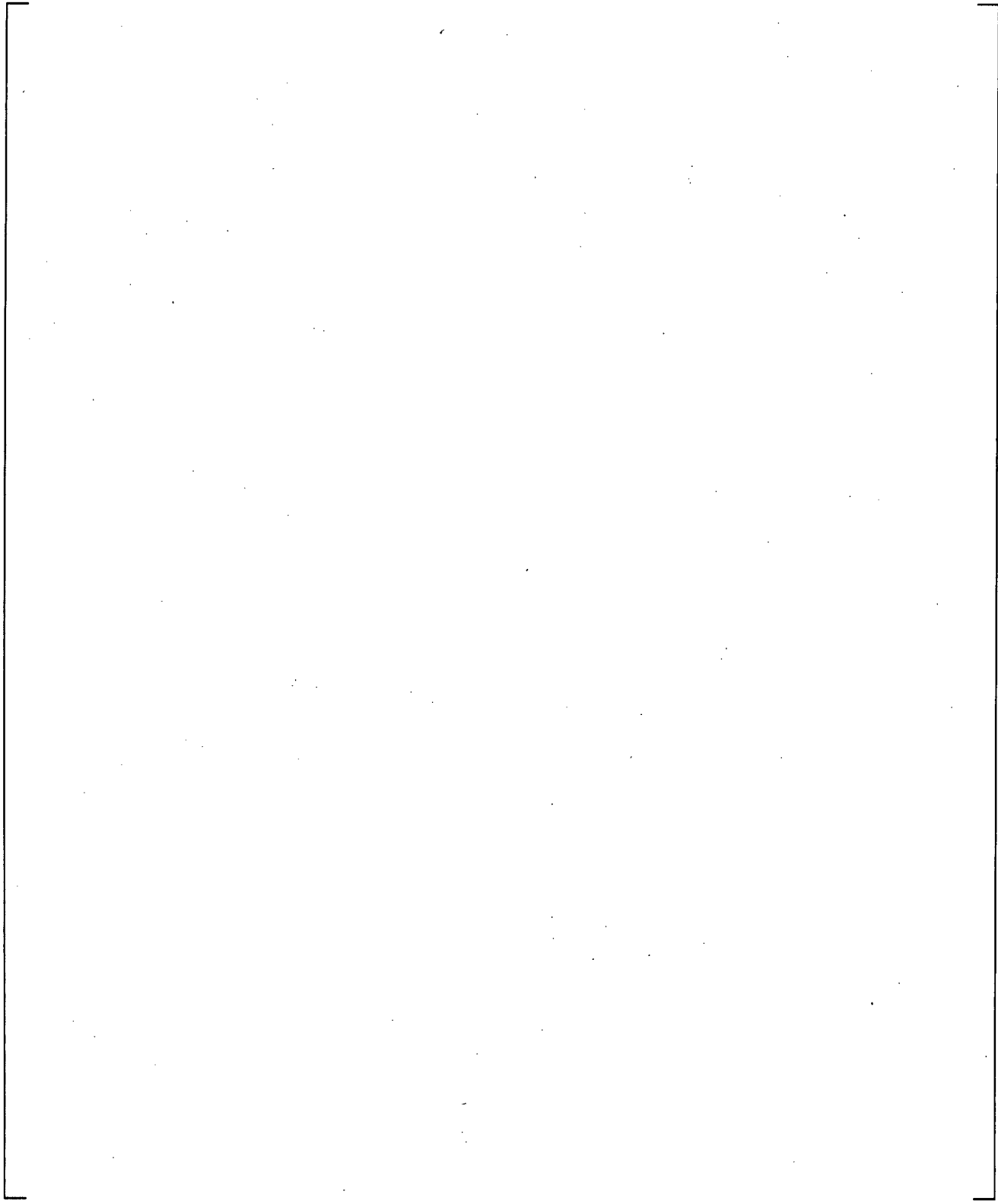


**Figure 23.1.1-8 Comparison of Predicted and Measured Void Fraction at Level 5, Test 8-21-1**

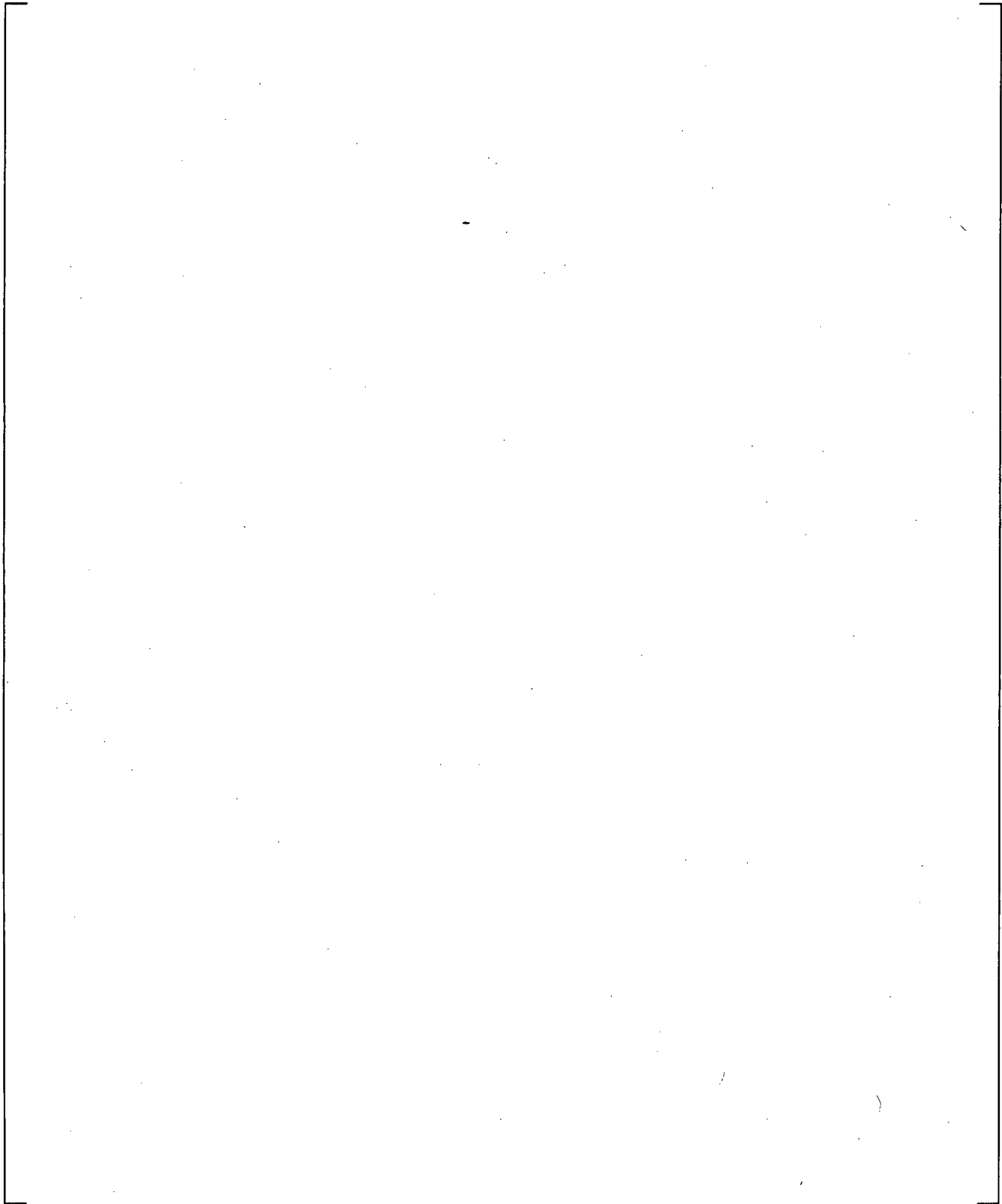


**Figure 23.1.1-9 Comparison of Predicted and Measured Void Fraction at Level 6, Test 8-21-1**

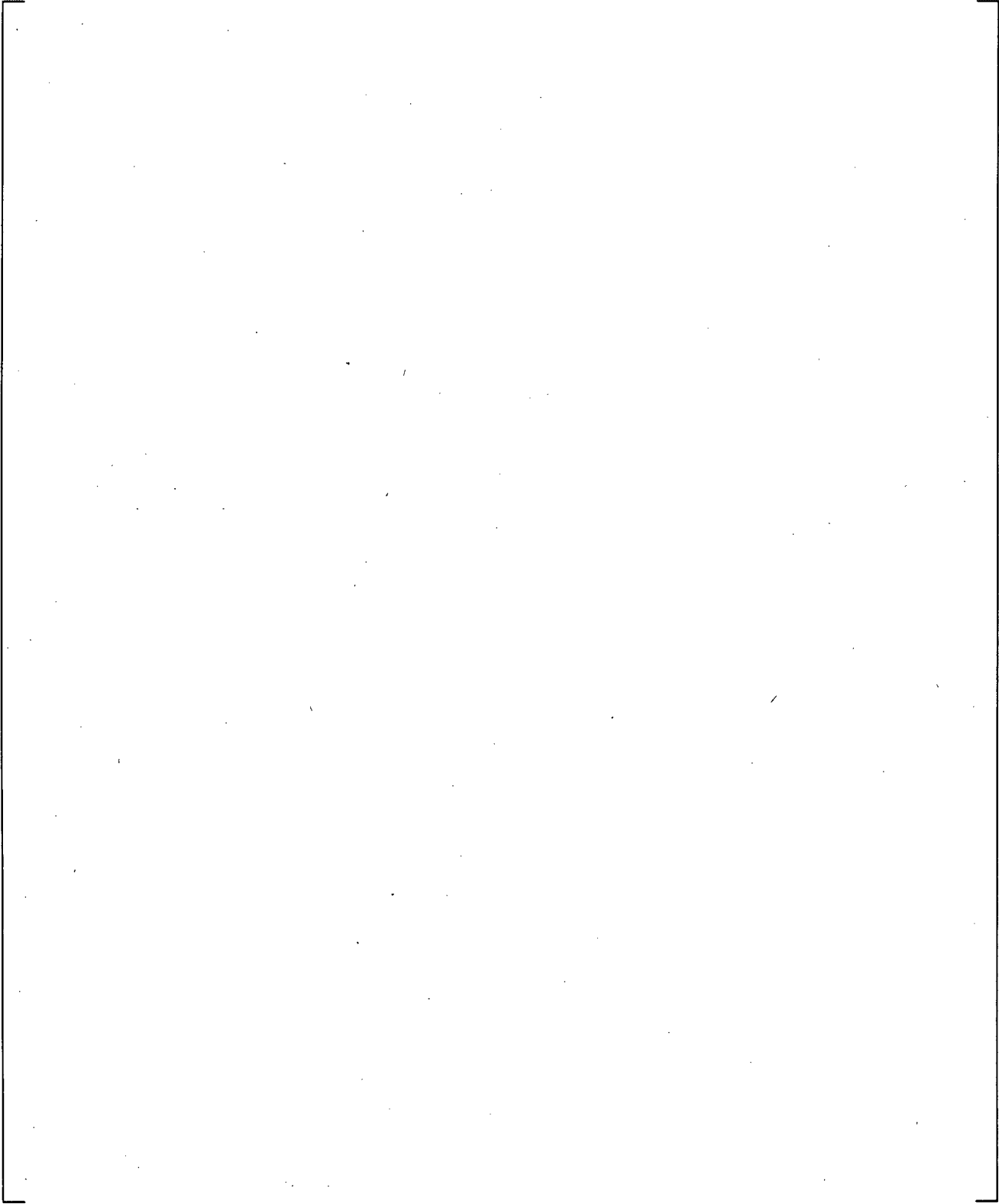


**Figure 23.1.1-10 Comparison of Predicted and Measured Void Fraction at Level 1, Test 8-25-1**

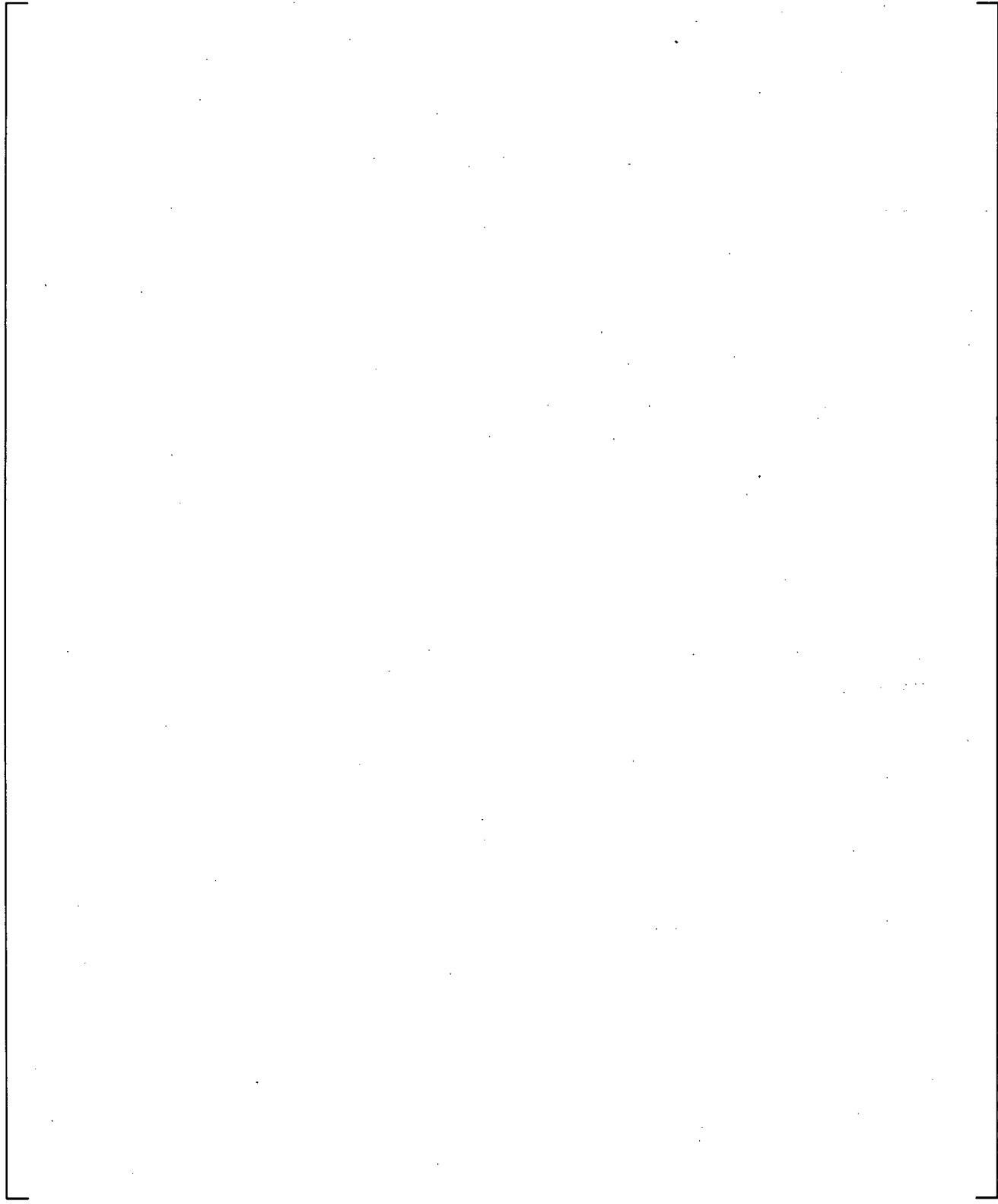


**Figure 23.1.1-11 Comparison of Predicted and Measured Void Fraction at Level 2, Test 8-25-1**

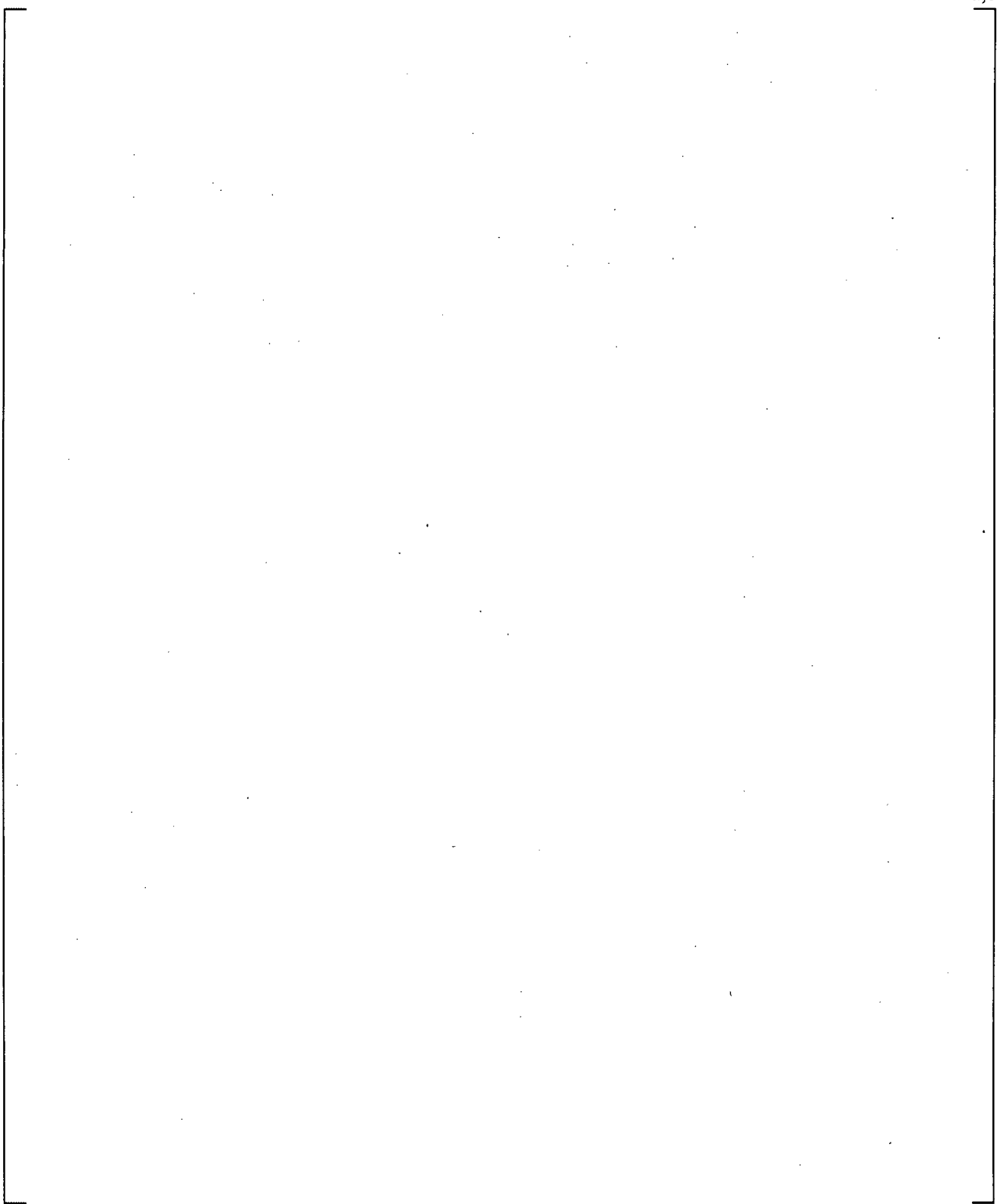


**Figure 23.1.1-12 Comparison of Predicted and Measured Void Fraction at Level 3, Test 8-25-1**

a,c

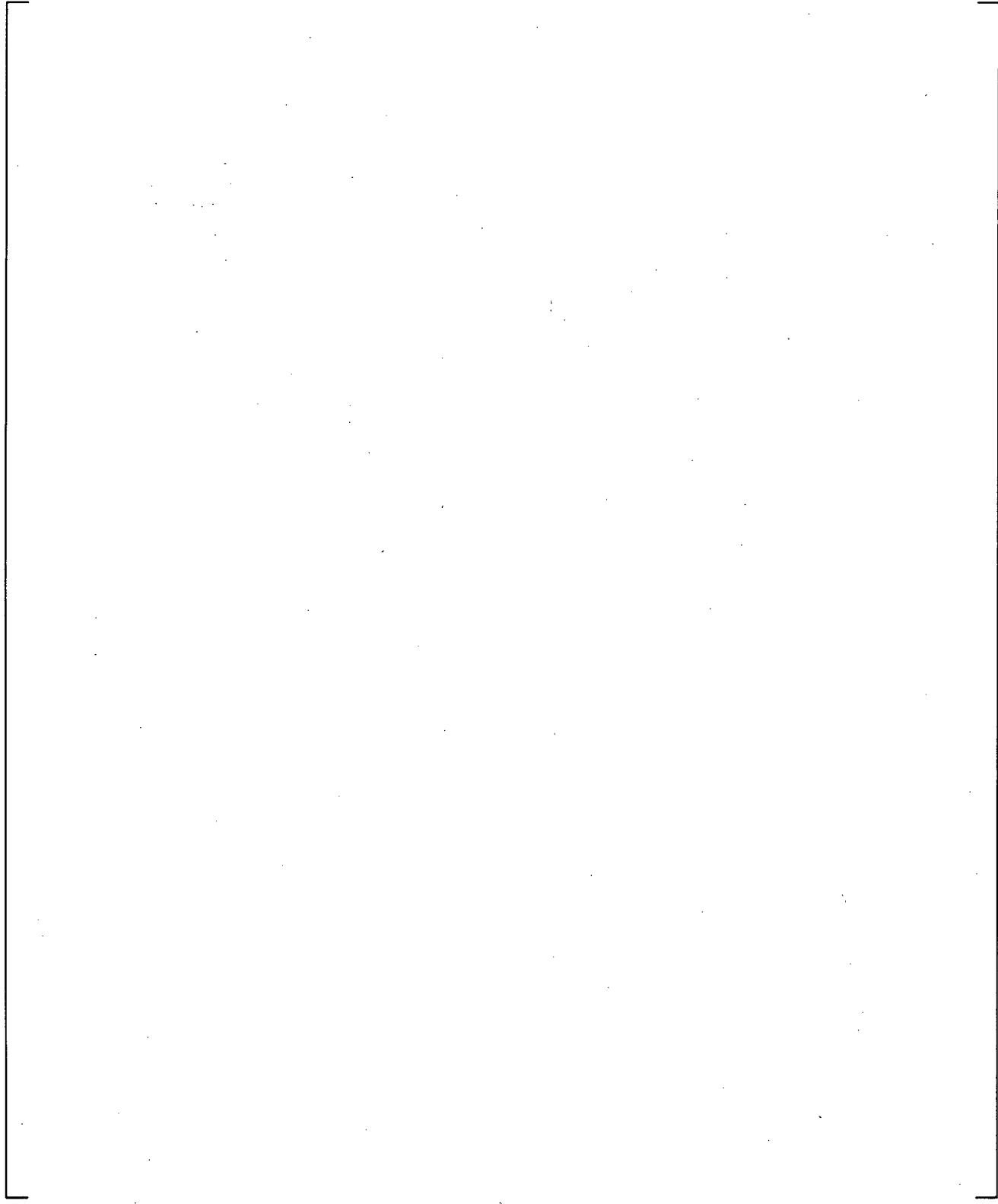


**Figure 23.1.1-13 Comparison of Predicted and Measured Void Fraction at Level 4, Test 8-25-1**

a,c

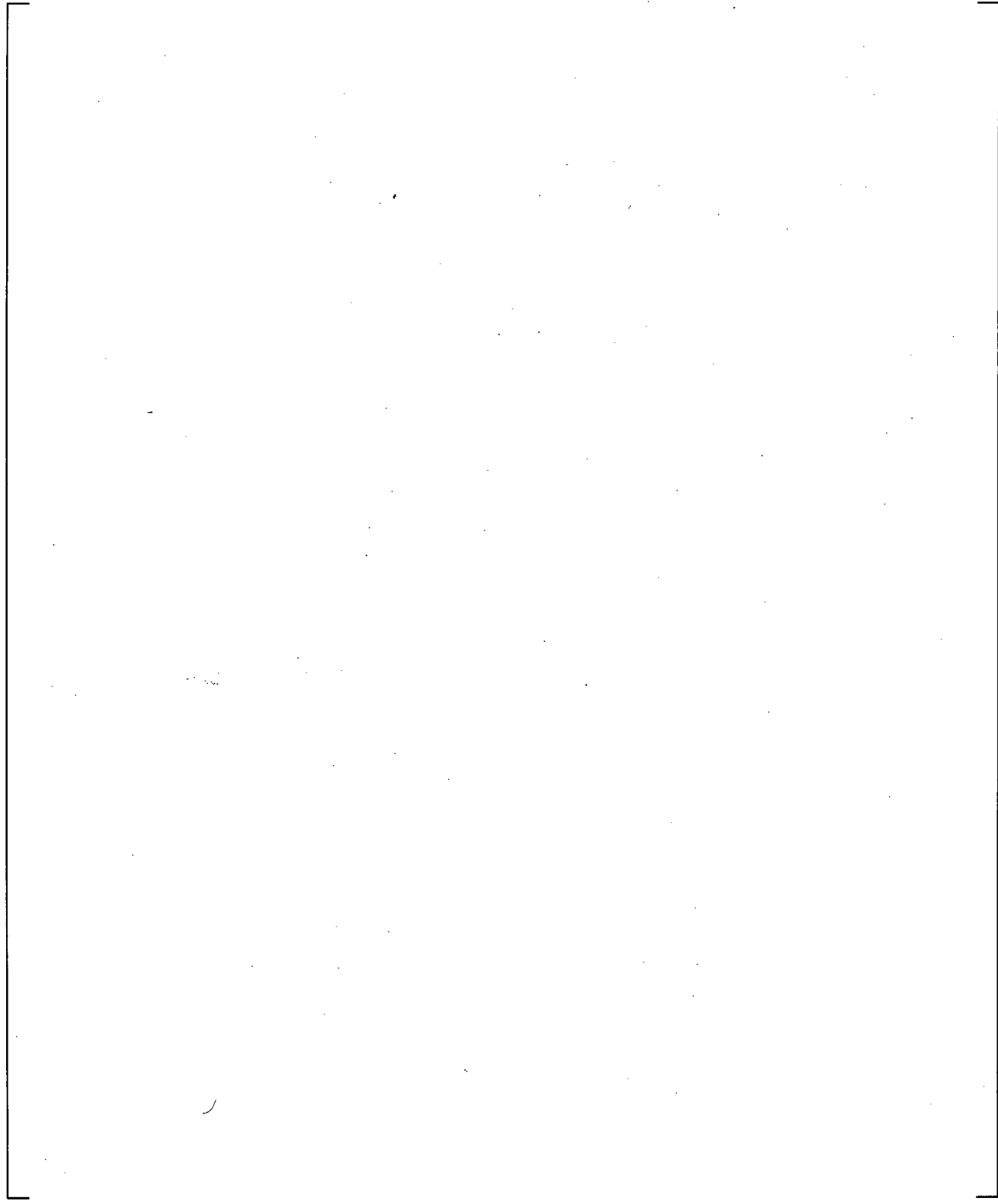


**Figure 23.1.1-14 Comparison of Predicted and Measured Void Fraction at Level 5, Test 8-25-1**

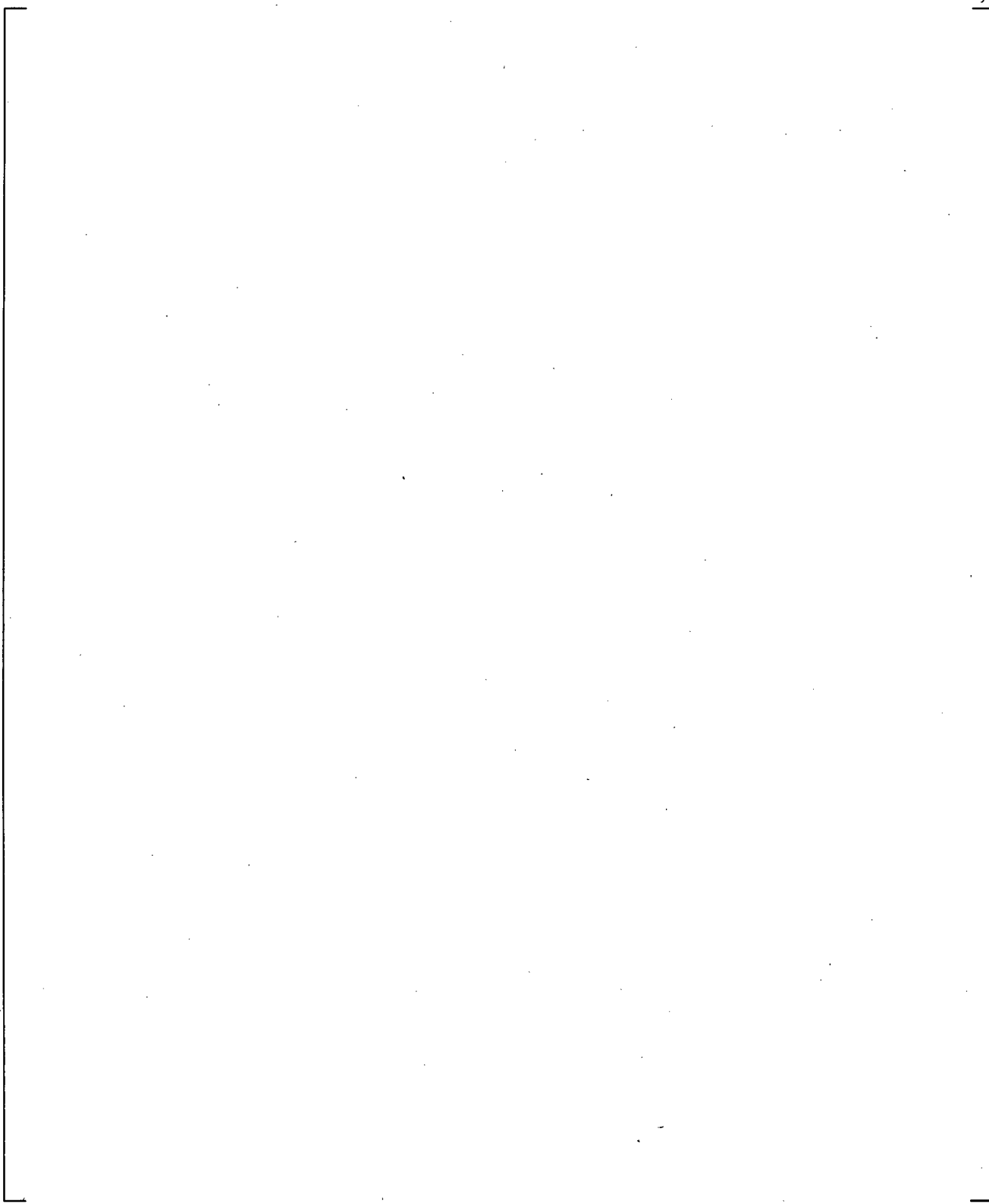


**Figure 23.1.1-15 Comparison of Predicted and Measured Void Fraction at Level 6, Test 8-25-1**

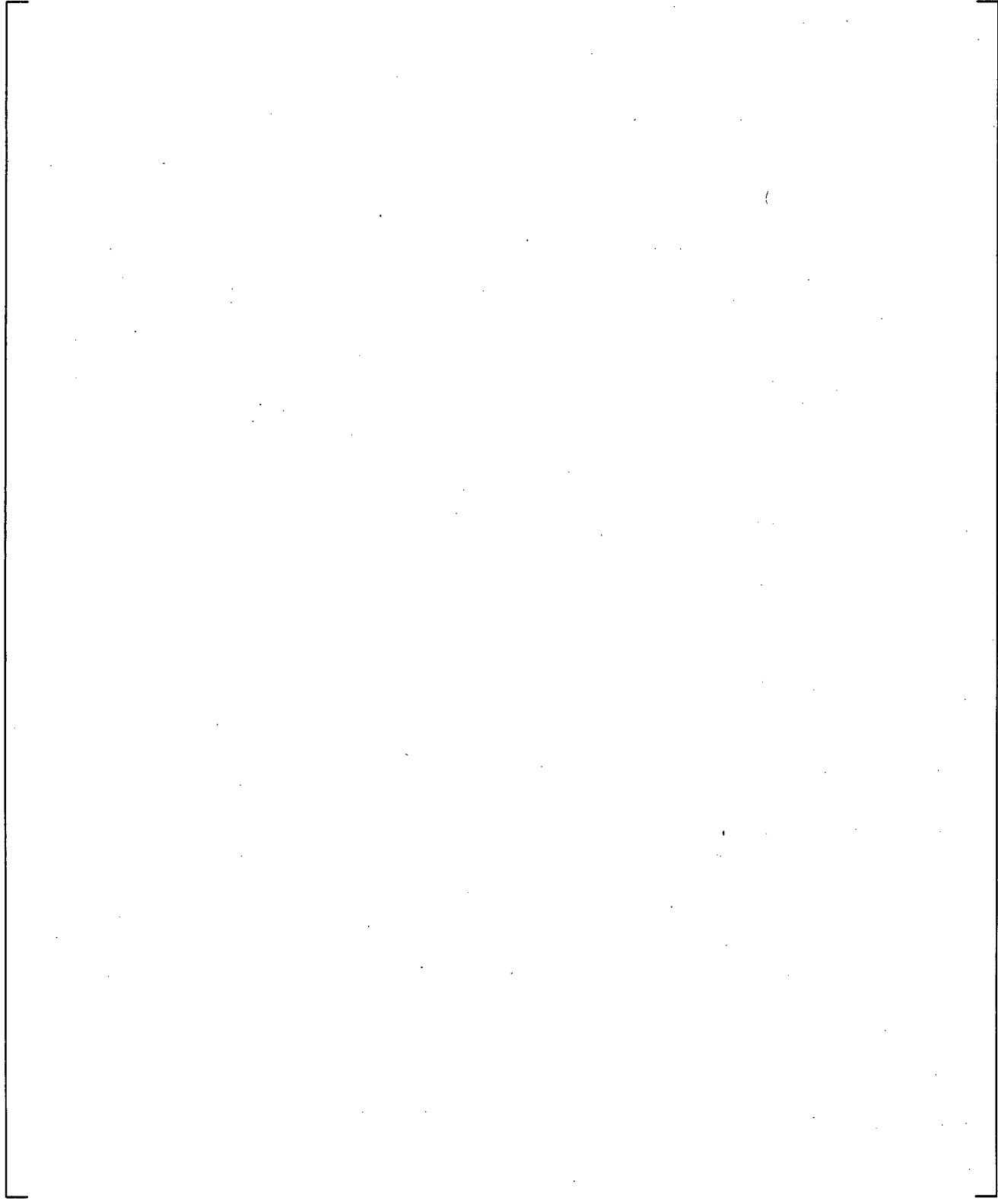


**Figure 23.1.1-16 Comparison of Predicted and Measured Void Fraction at Level 1, Test 8-28-1**

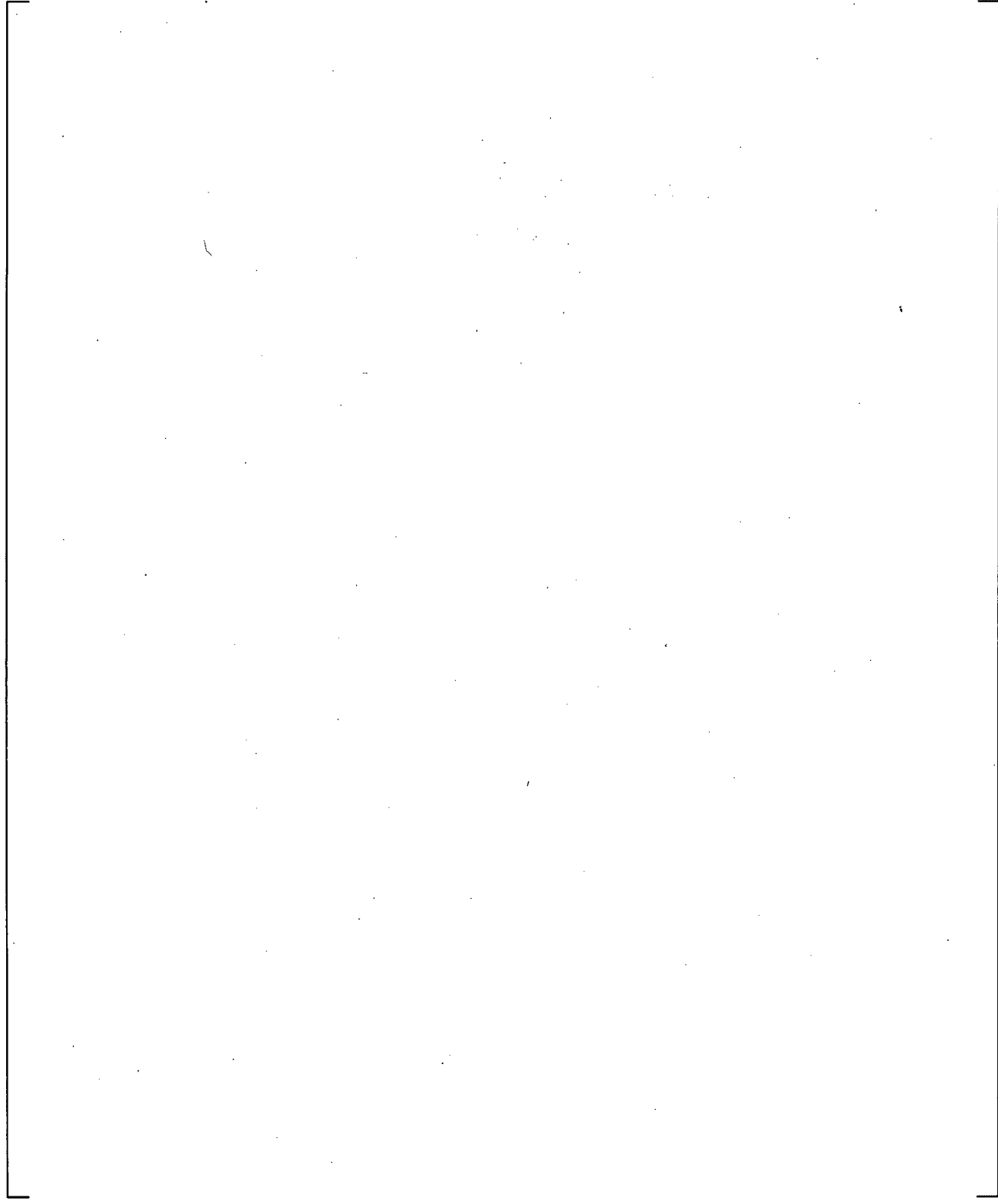


**Figure 23.1.1-17 Comparison of Predicted and Measured Void Fraction at Level 2, Test 8-28-1**

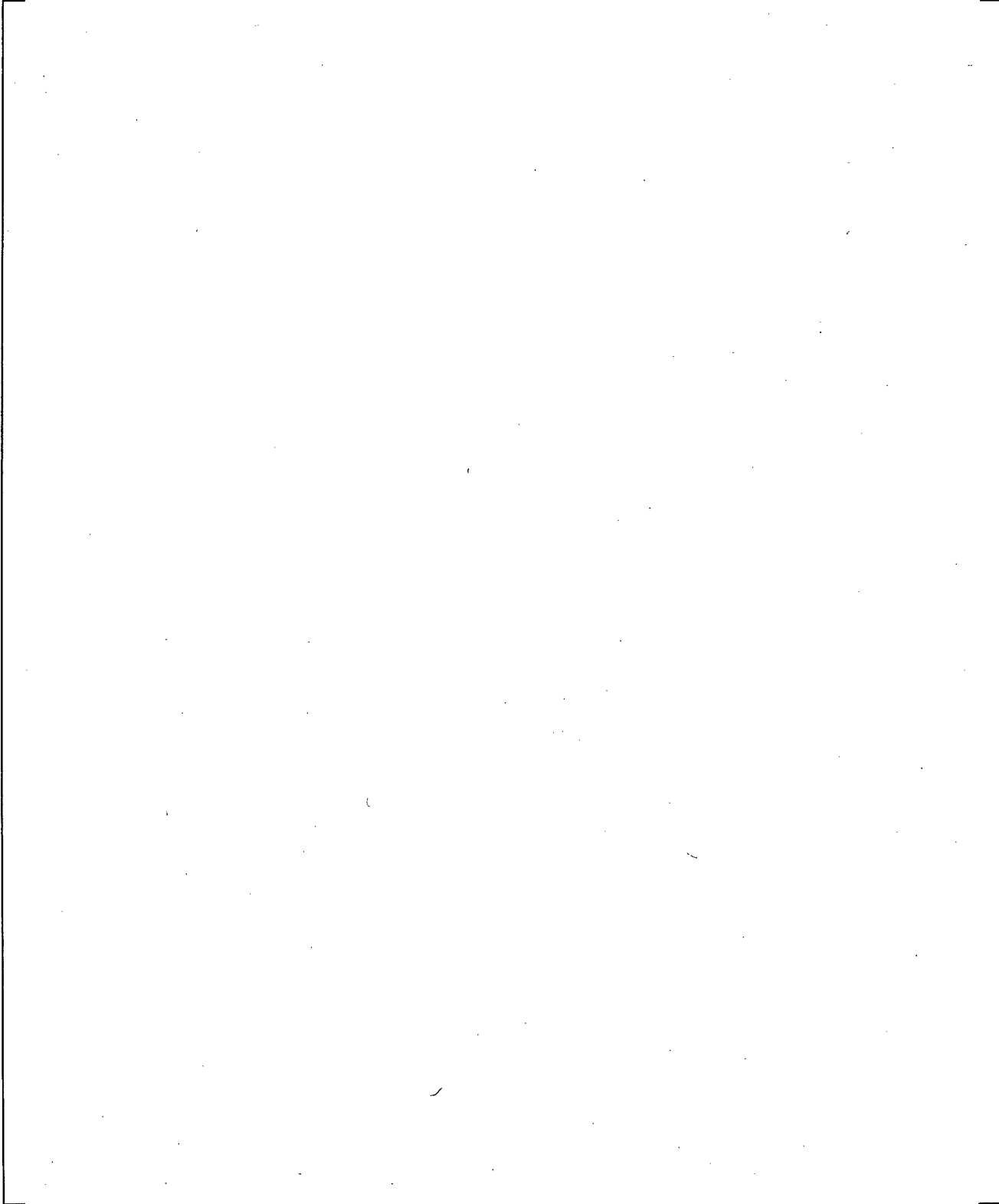


**Figure 23.1.1-18 Comparison of Predicted and Measured Void Fraction at Level 3, Test 8-28-1**

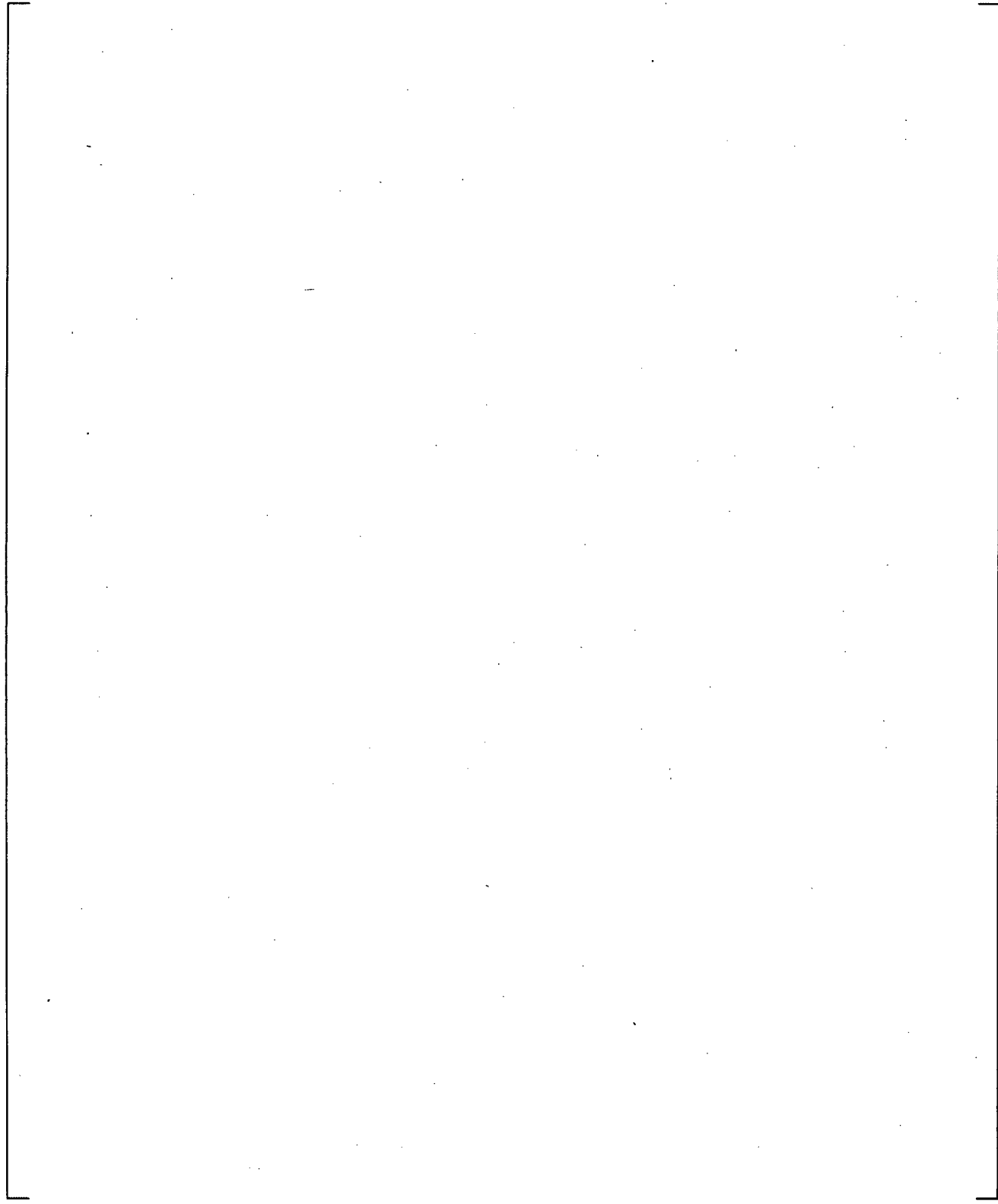


**Figure 23.1.1-19 Comparison of Predicted and Measured Void Fraction at Level 4, Test 8-28-1**

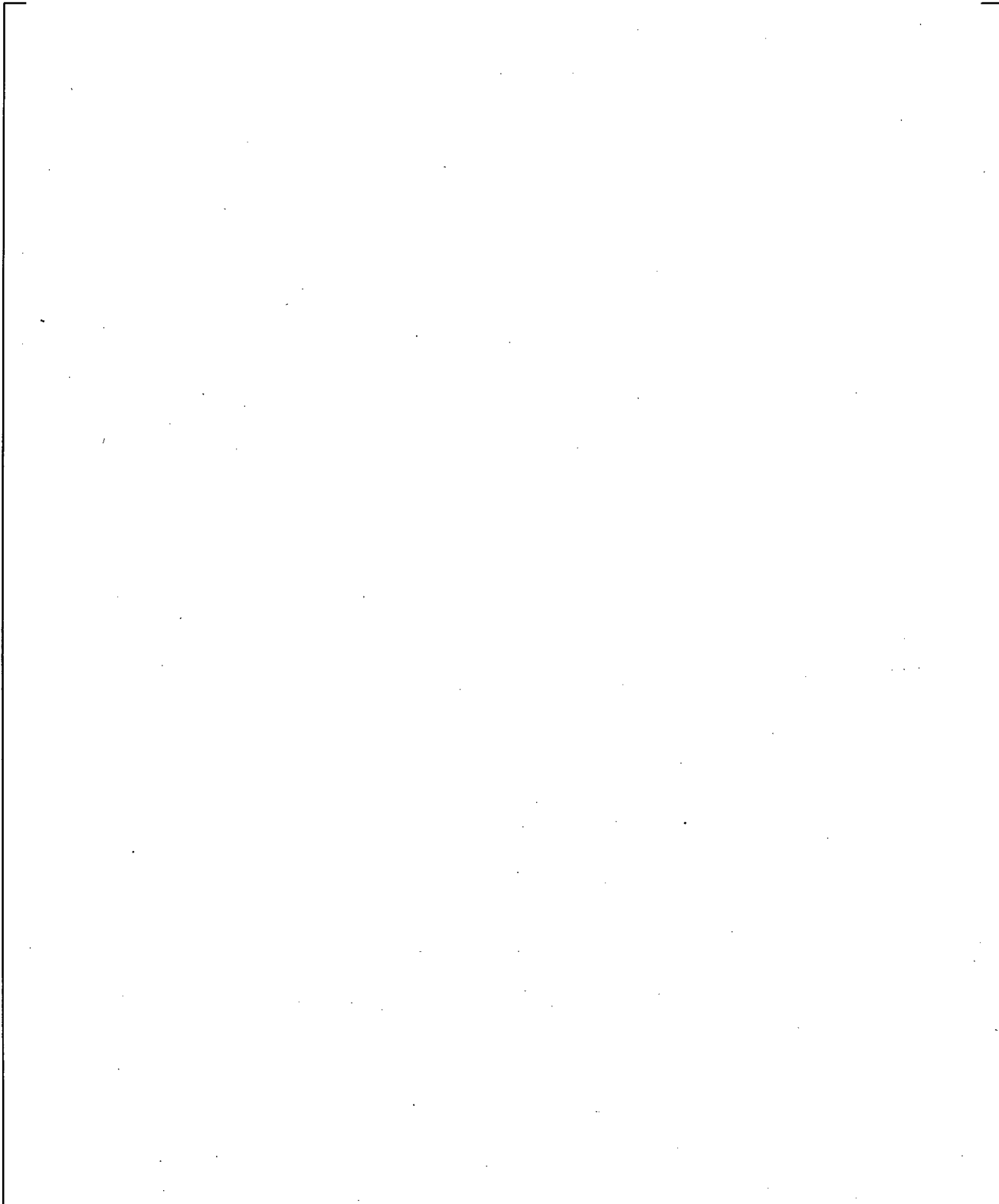


**Figure 23.1.1-20 Comparison of Predicted and Measured Void Fraction at Level 5, Test 8-28-1**

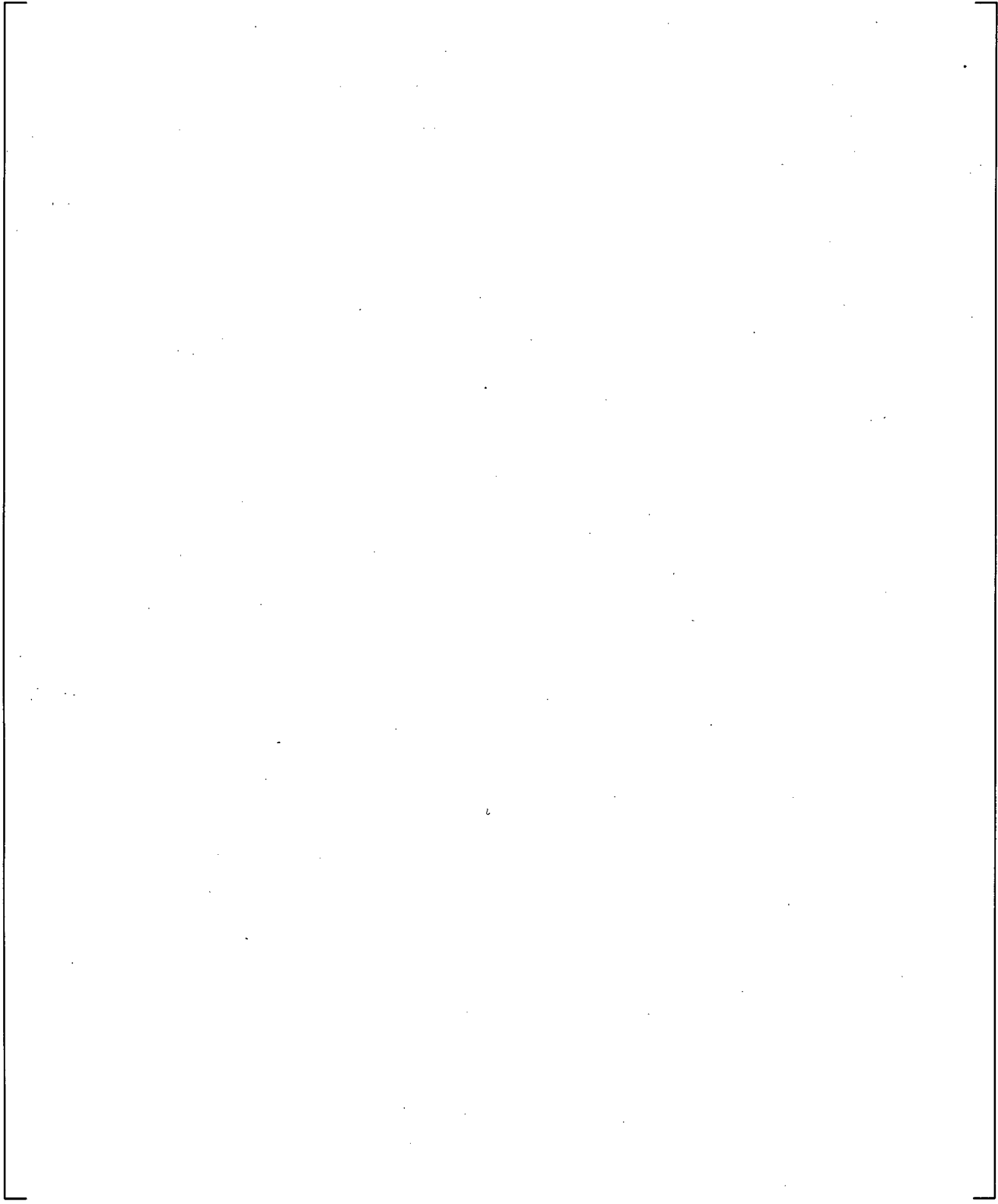


**Figure 23.1.1-21 Comparison of Predicted and Measured Void Fraction at Level 6, Test 8-28-1**

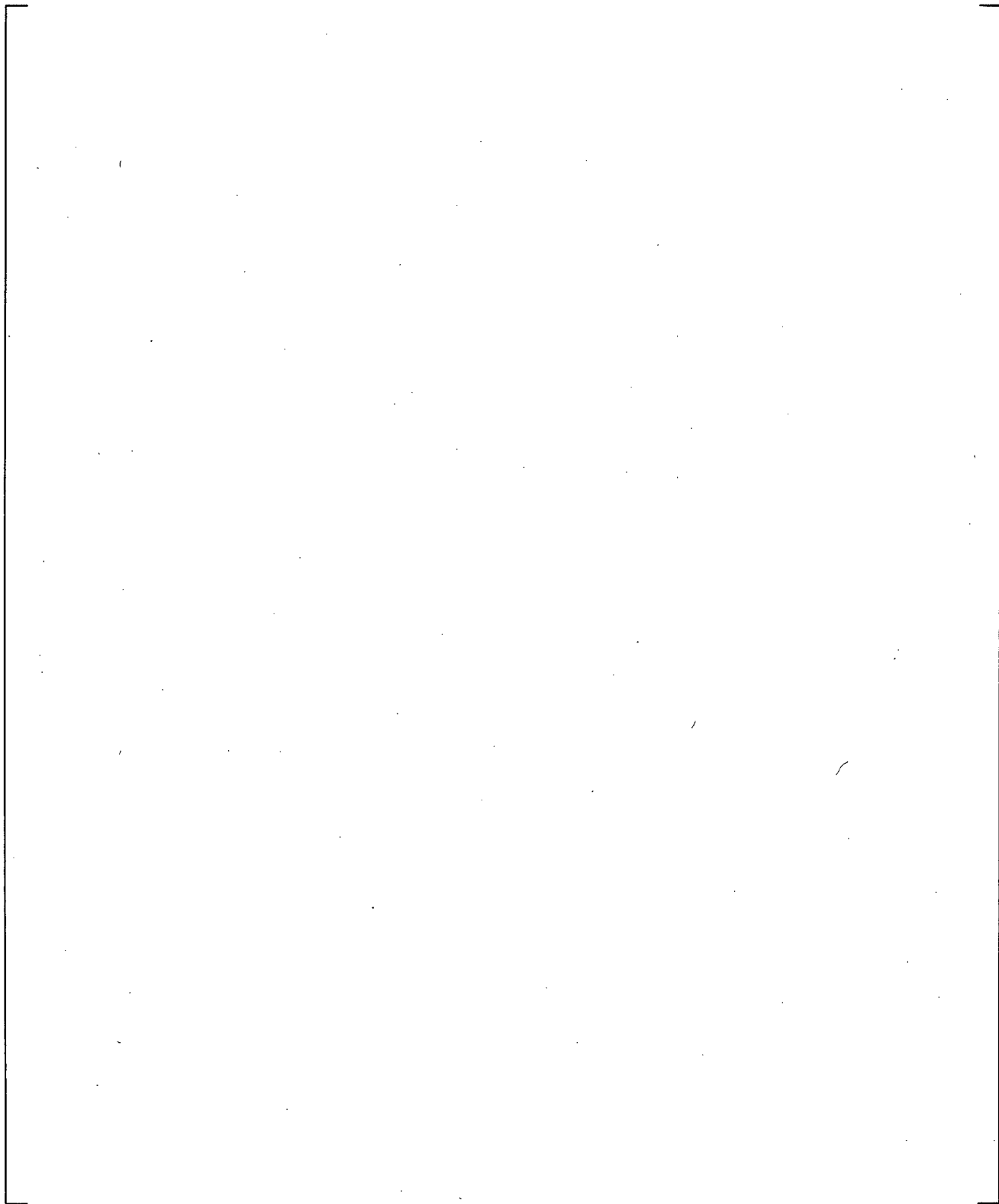


**Figure 23.1.1-22 Comparison of Predicted and Measured Void Fraction at Level 1, Test 9-1-1**

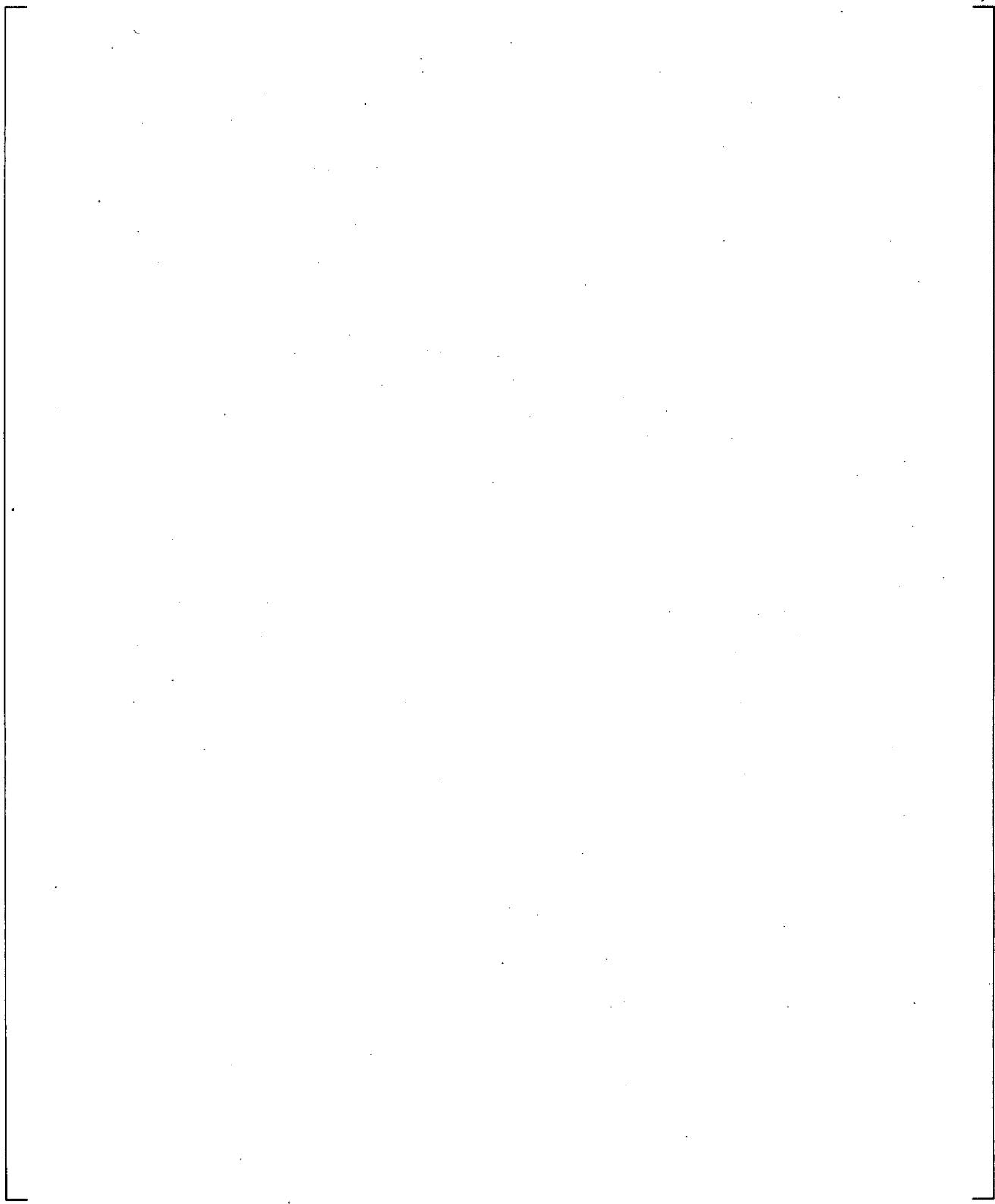


**Figure 23.1.1-23 Comparison of Predicted and Measured Void Fraction at Level 2, Test 9-1-1**

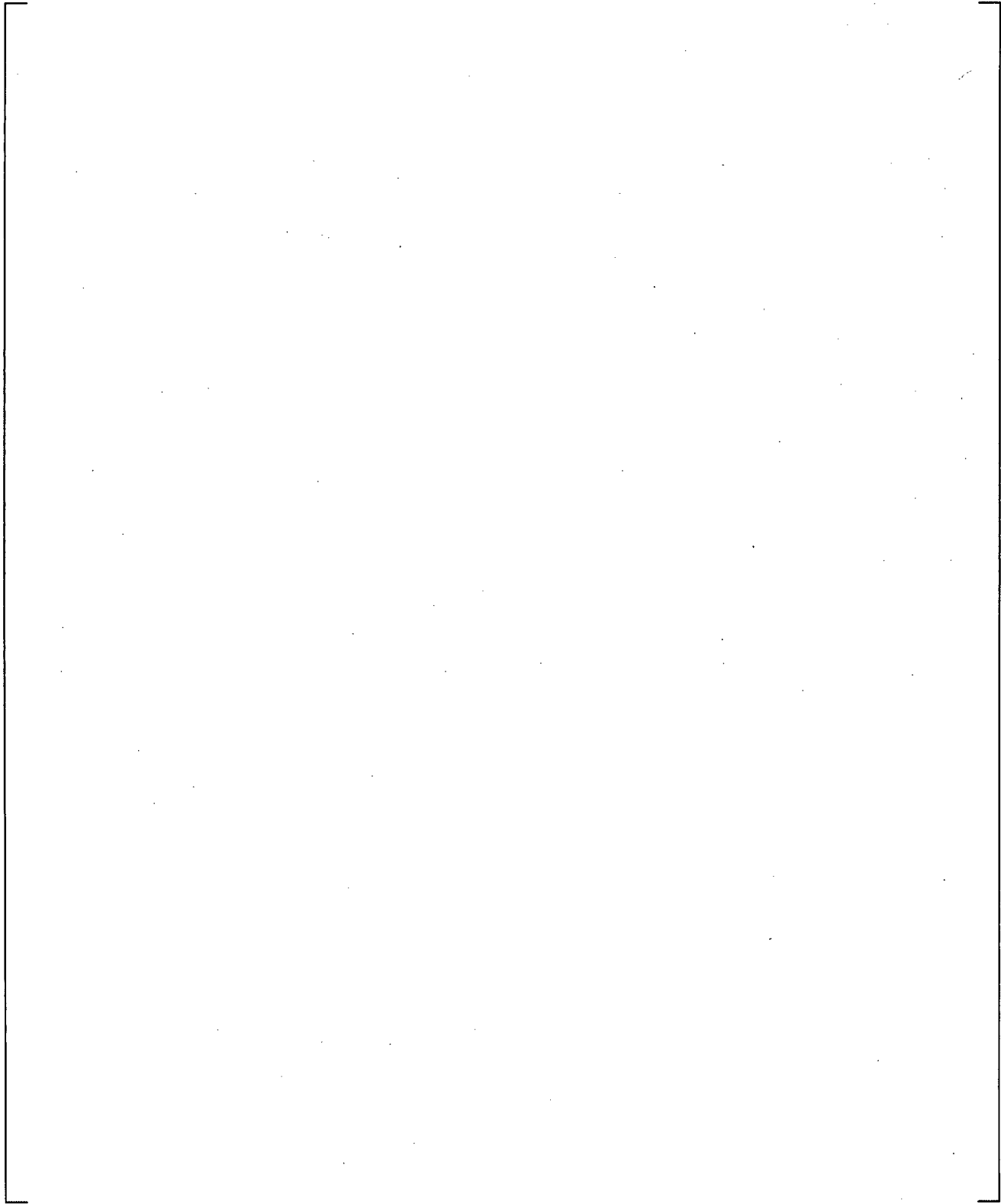


**Figure 23.1.1-24 Comparison of Predicted and Measured Void Fraction at Level 3, Test 9-1-1**

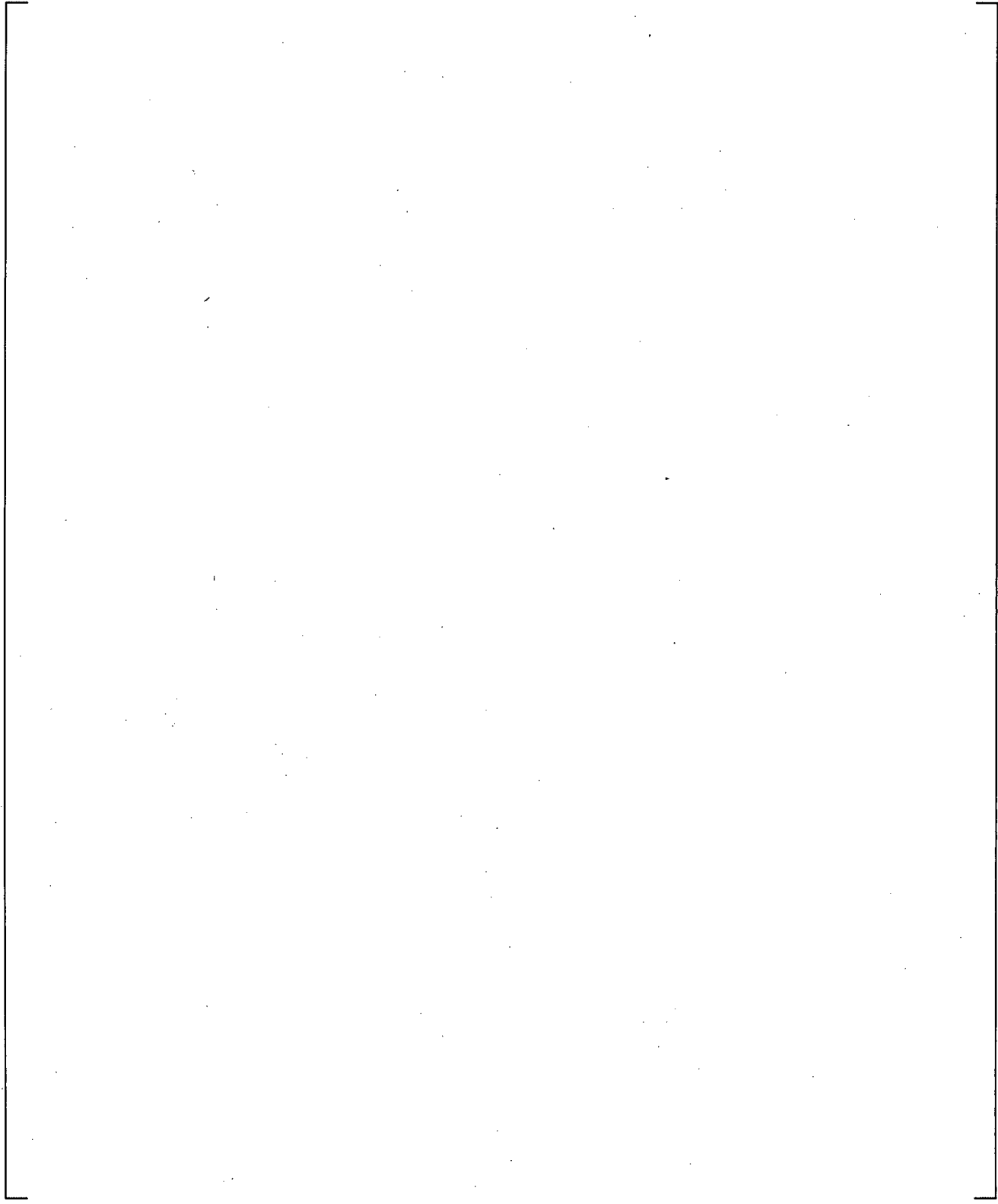


**Figure 23.1.1-25 Comparison of Predicted and Measured Void Fraction at Level 4, Test 9-1-1**

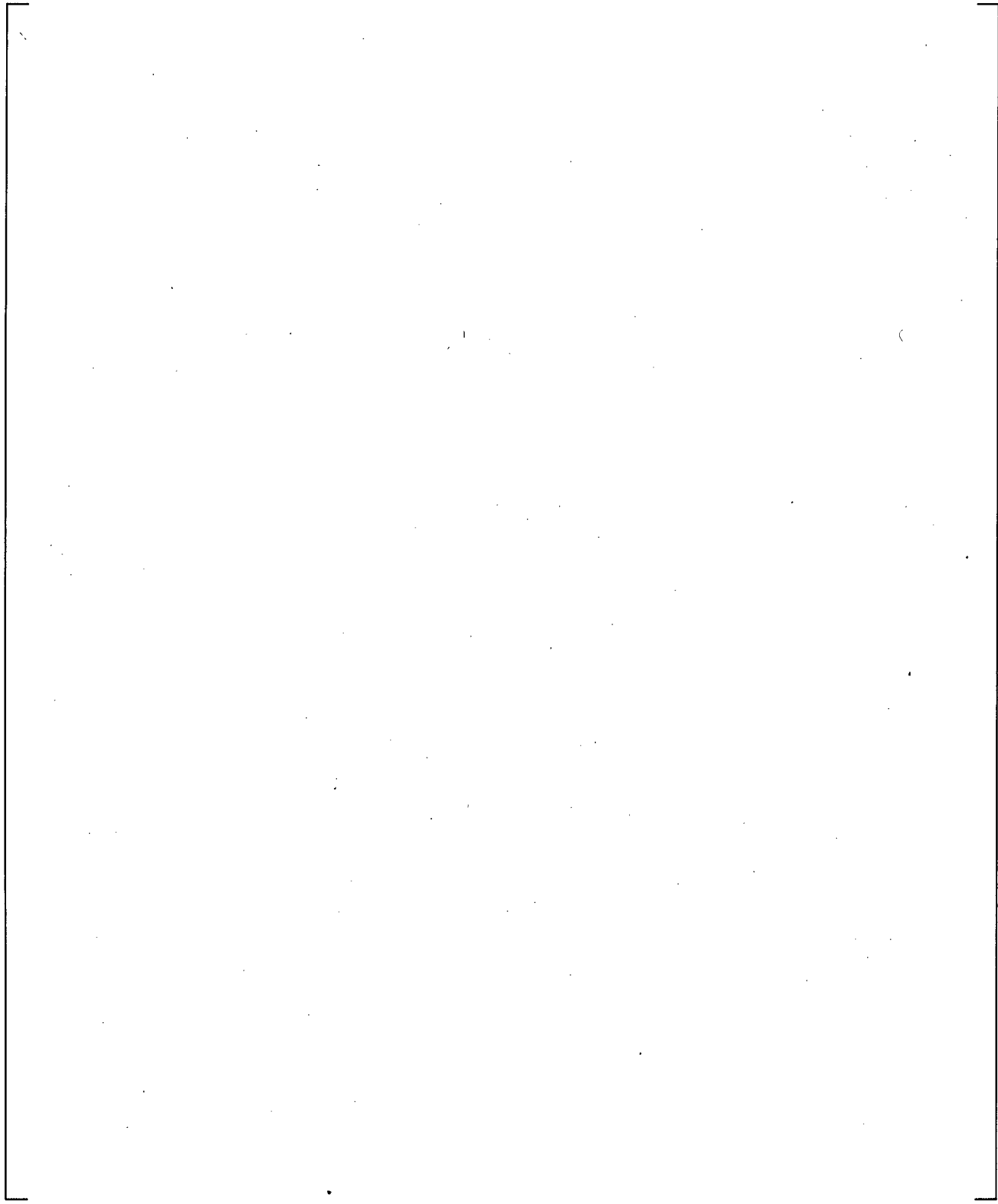


**Figure 23.1.1-26 Comparison of Predicted and Measured Void Fraction at Level 5, Test 9-1-1**

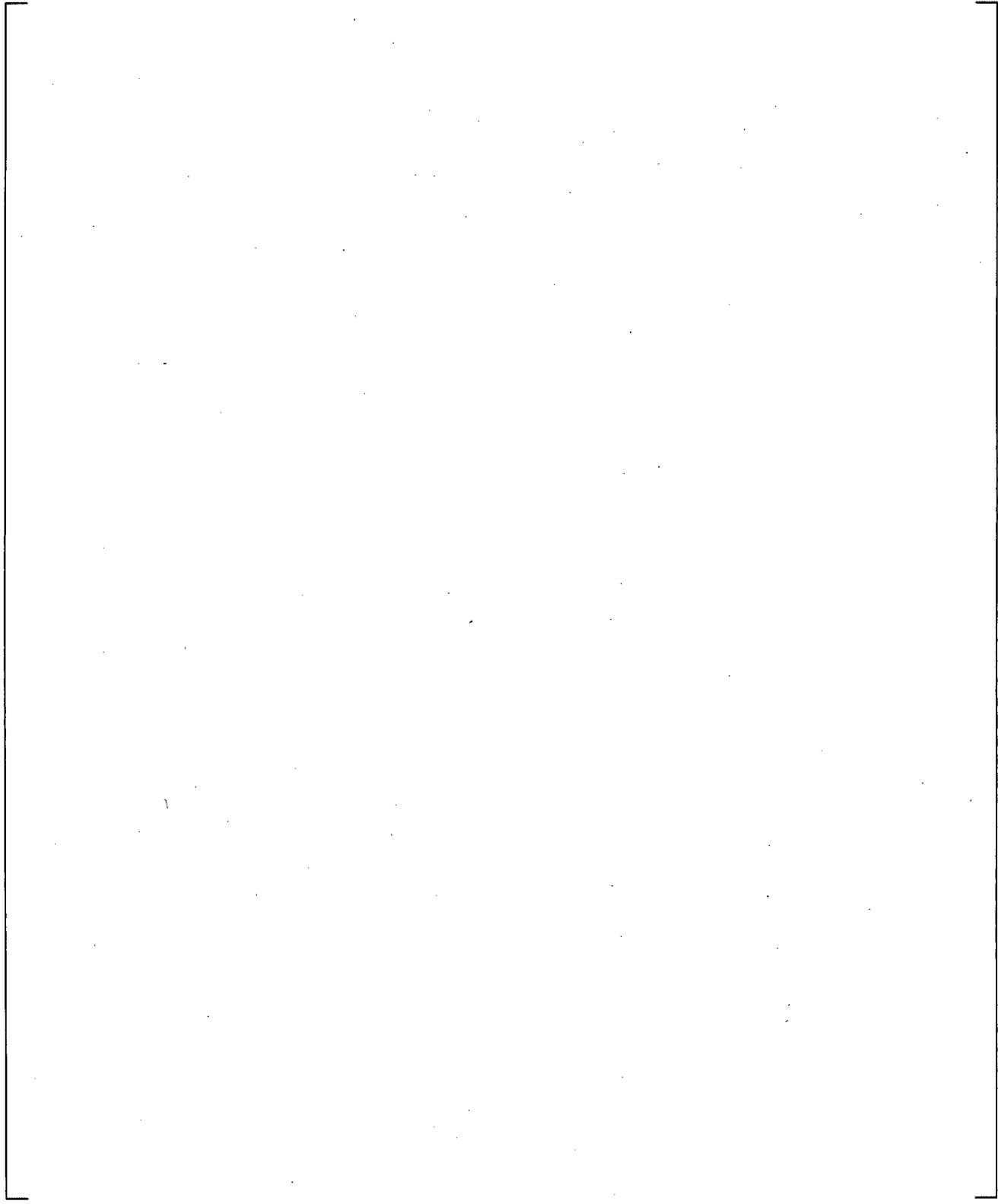


**Figure 23.1.1-27 Comparison of Predicted and Measured Void Fraction at Level 6, Test 9-1-1**

a,c

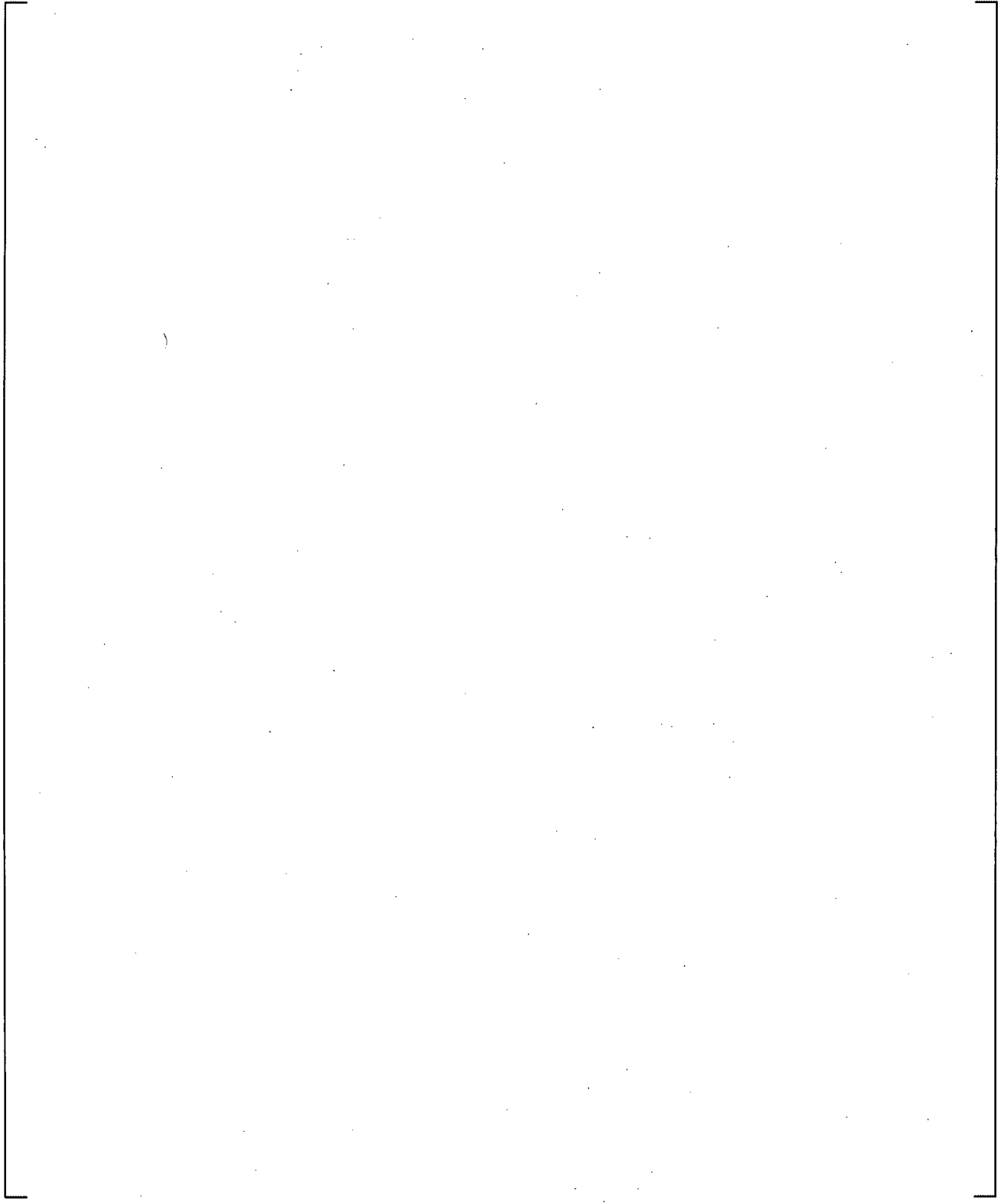


**Figure 23.1.1-28 Comparison of Predicted and Measured Void Fraction at Level 1, Test 9-15-1**

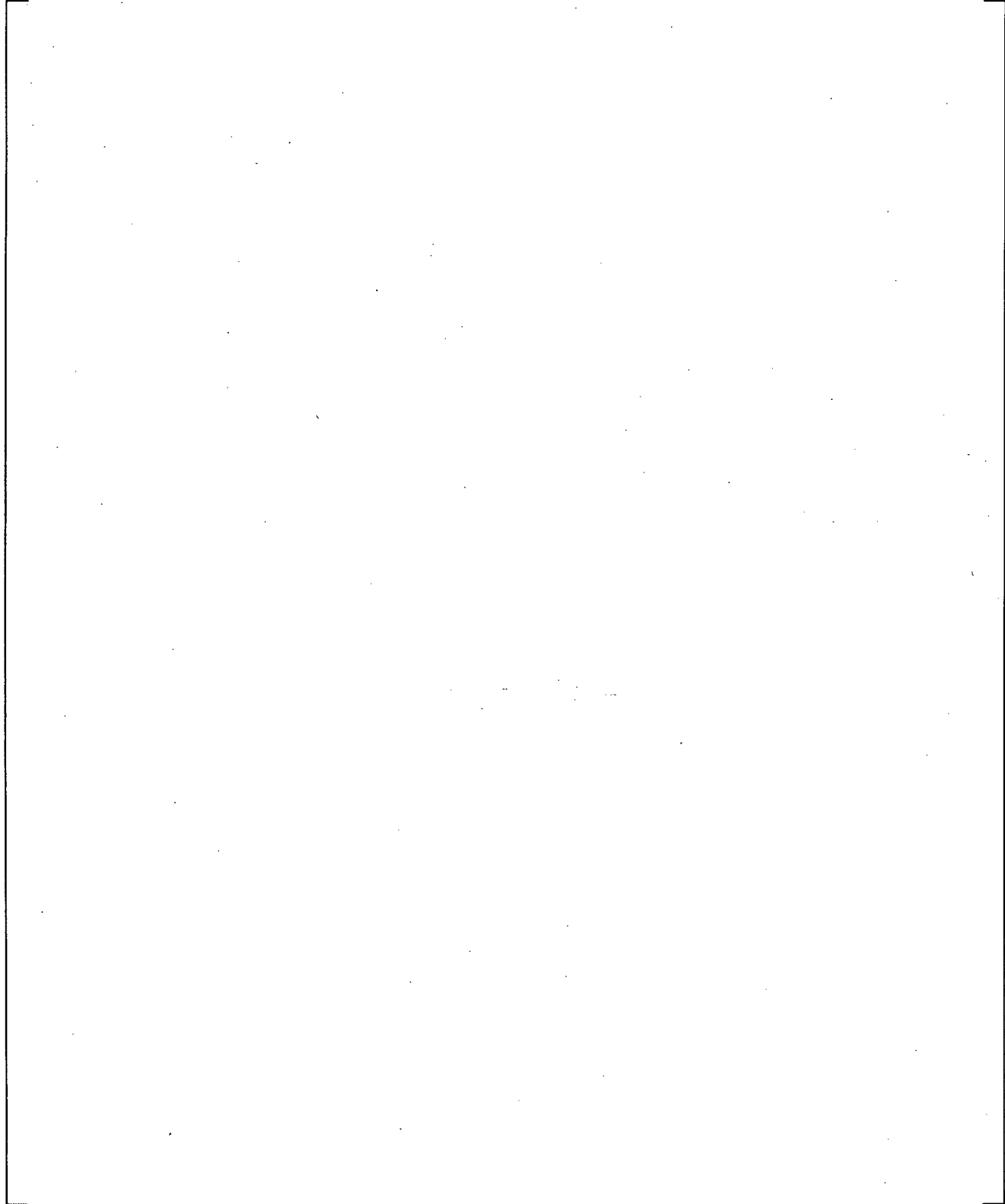


**Figure 23.1.1-29 Comparison of Predicted and Measured Void Fraction at Level 2, Test 9-15-1**

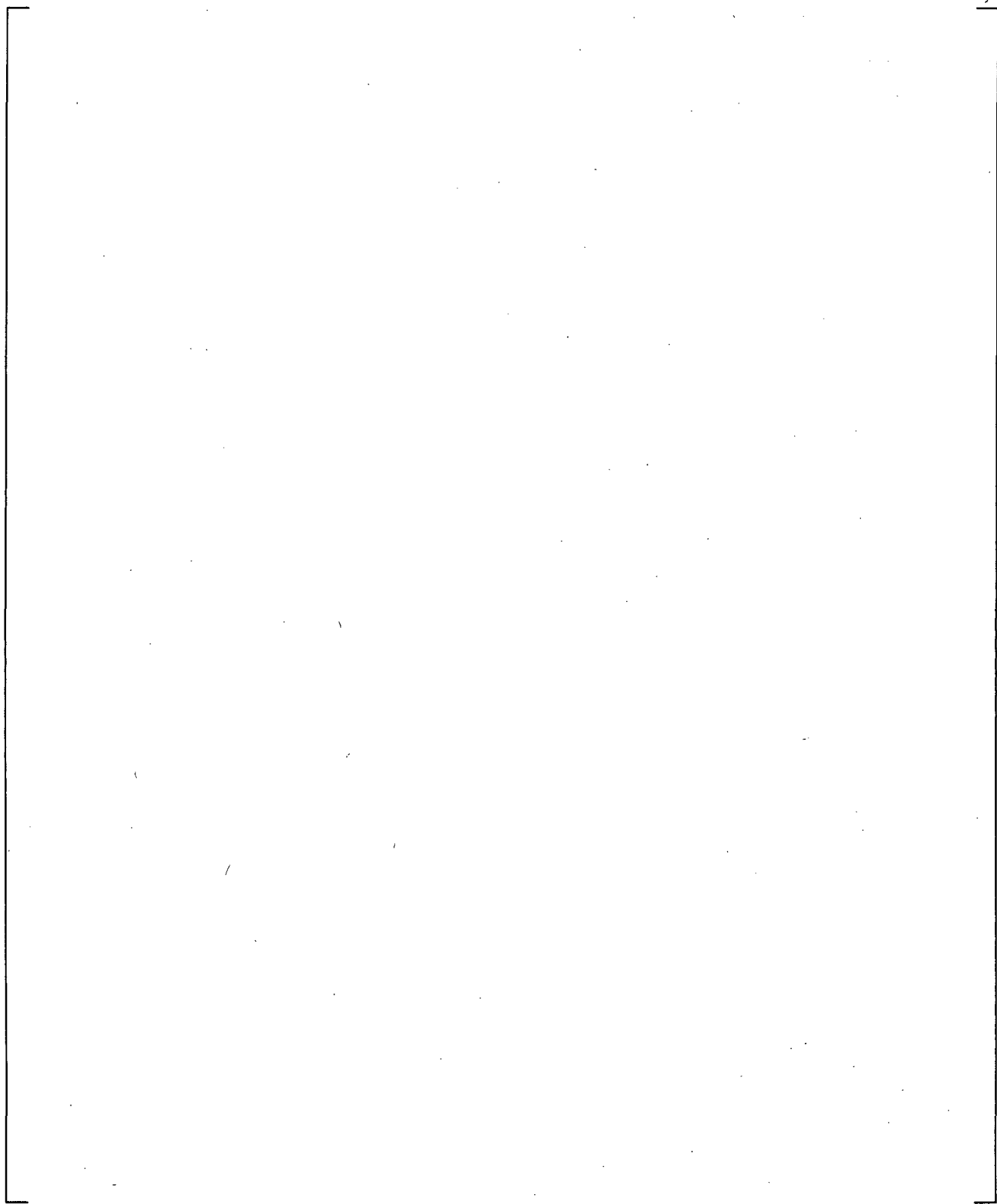


**Figure 23.1.1-30 Comparison of Predicted and Measured Void Fraction at Level 3, Test 9-15-1**

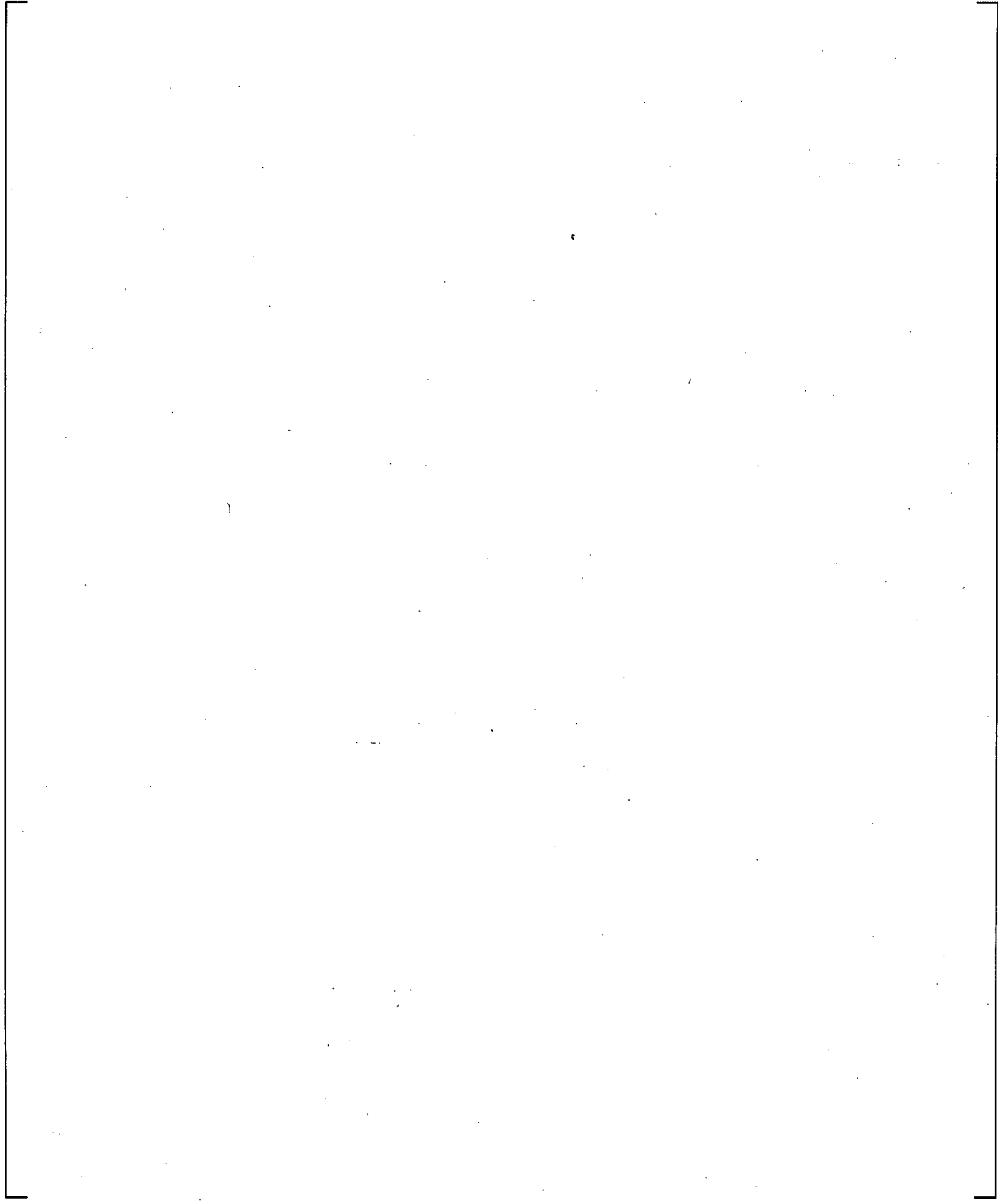


**Figure 23.1.1-31 Comparison of Predicted and Measured Void Fraction at Level 4, Test 9-15-1**

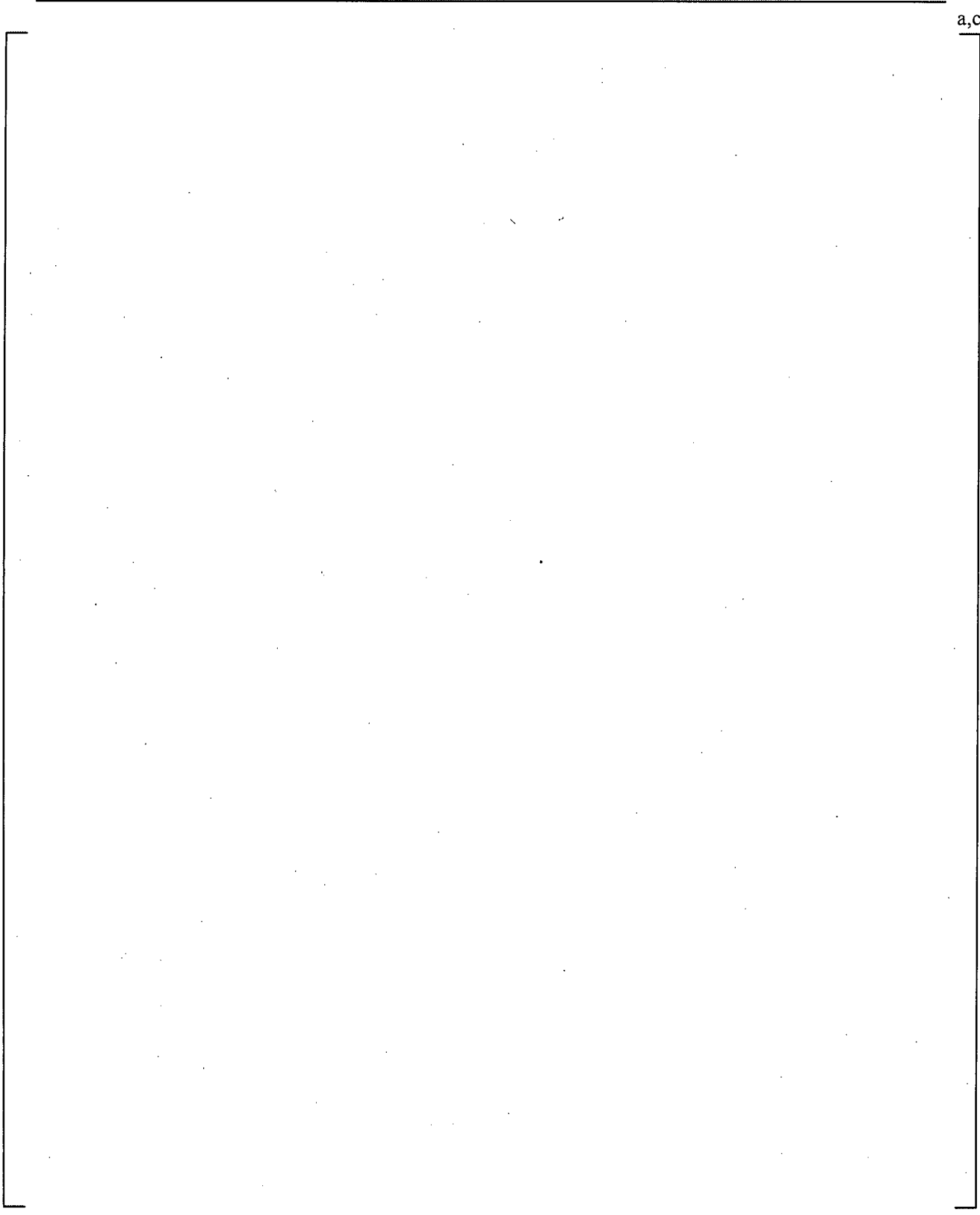


**Figure 23.1.1-32 Comparison of Predicted and Measured Void Fraction at Level 5, Test 9-15-1**

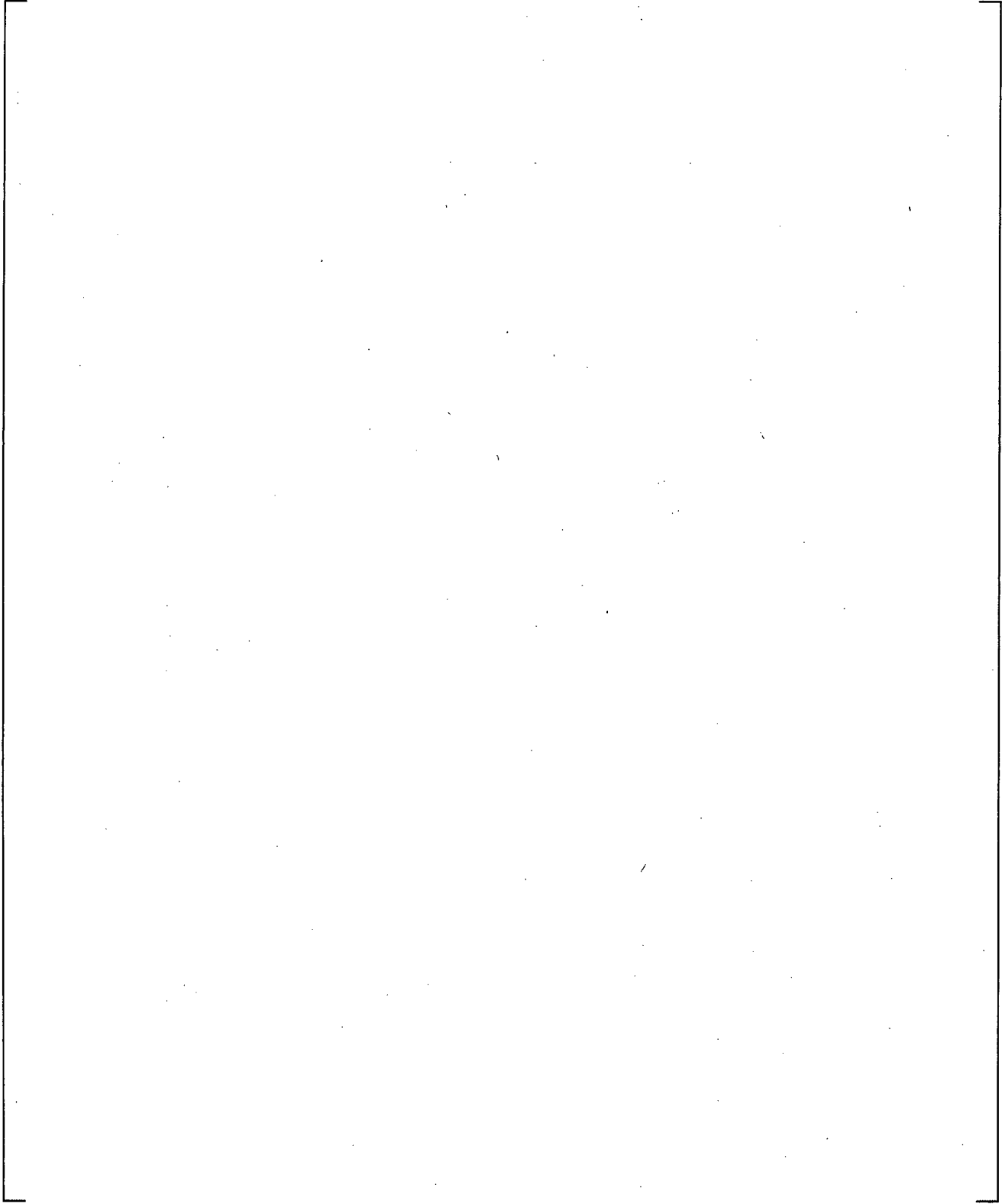


**Figure 23.1.1-33 Comparison of Predicted and Measured Void Fraction at Level 6, Test 9-15-1**

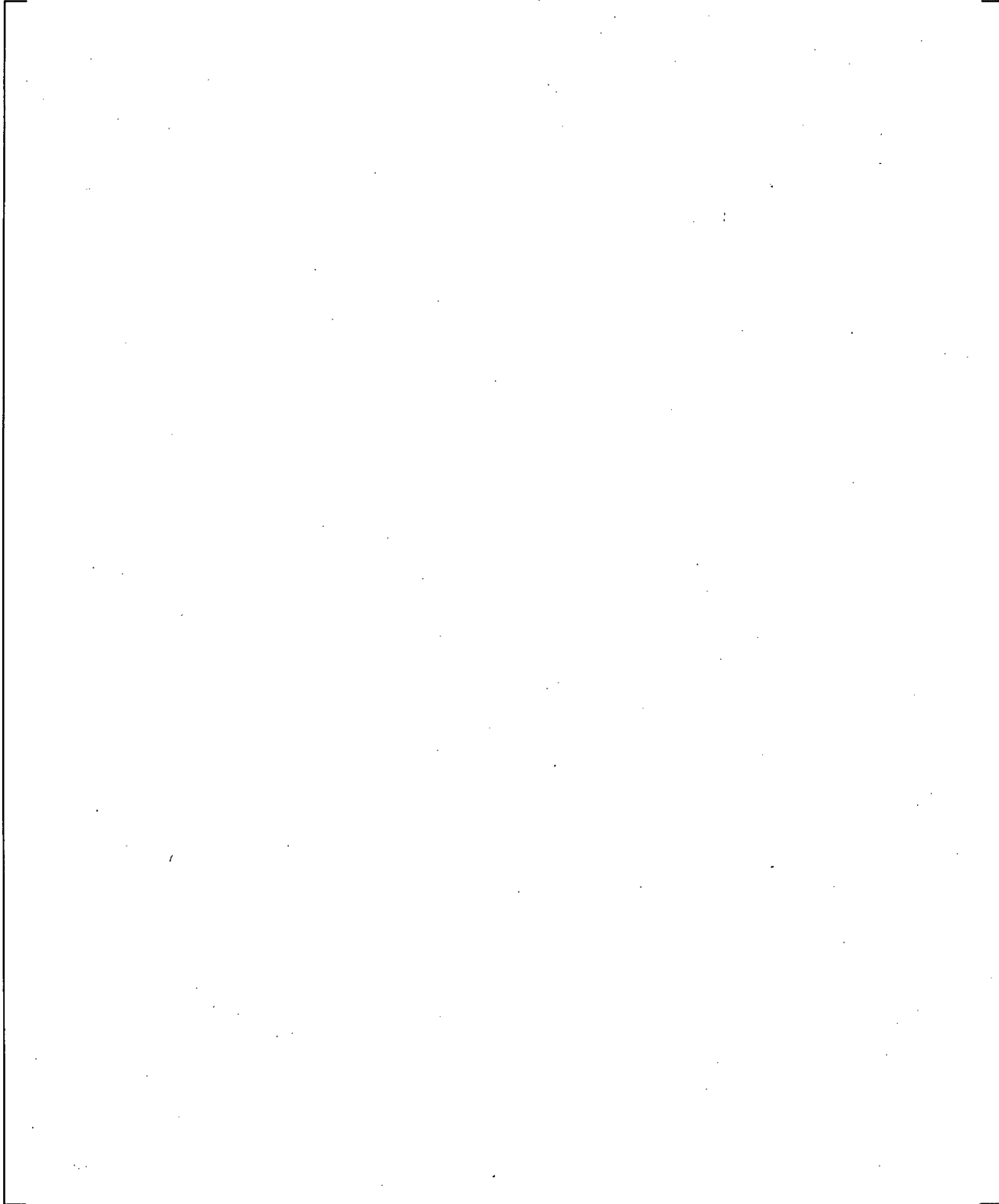


**Figure 23.1.1-34 Comparison of Predicted and Measured Void Fraction at Level 1, Test 1004-3**

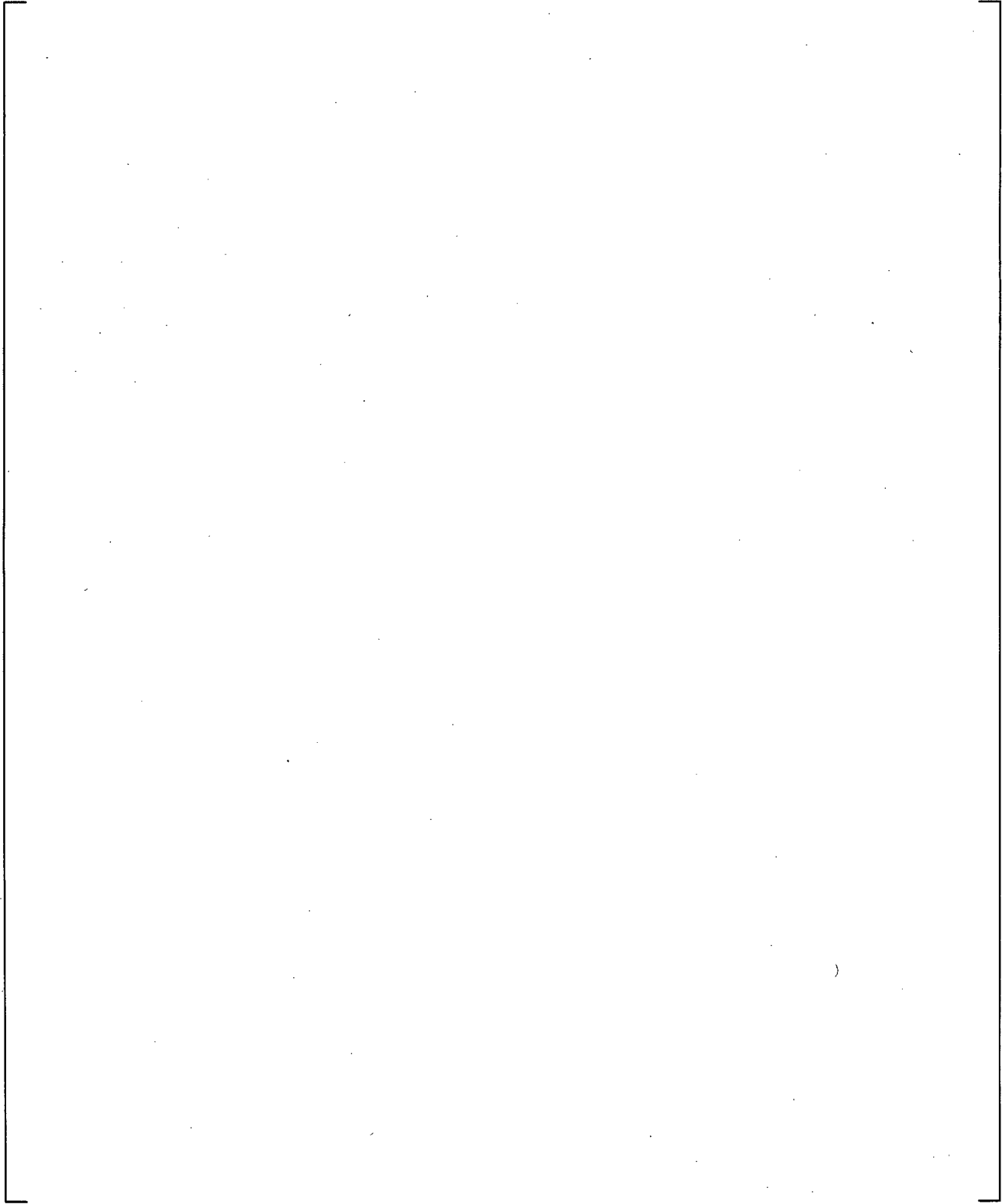


**Figure 23.1.1-35 Comparison of Predicted and Measured Void Fraction at Level 2, Test 1004-3**

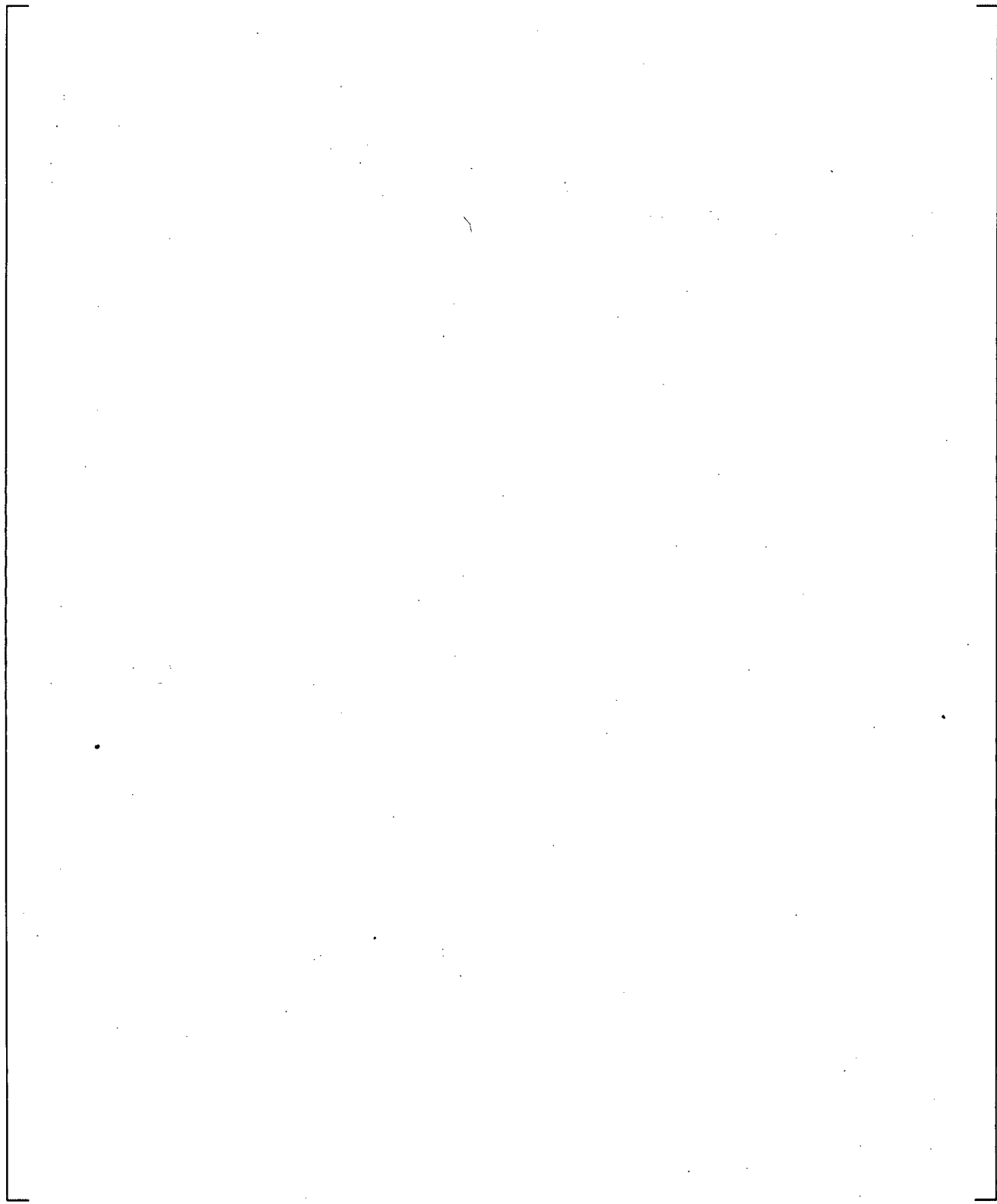


**Figure 23.1.1-36 Comparison of Predicted and Measured Void Fraction at Level 3, Test 1004-3**

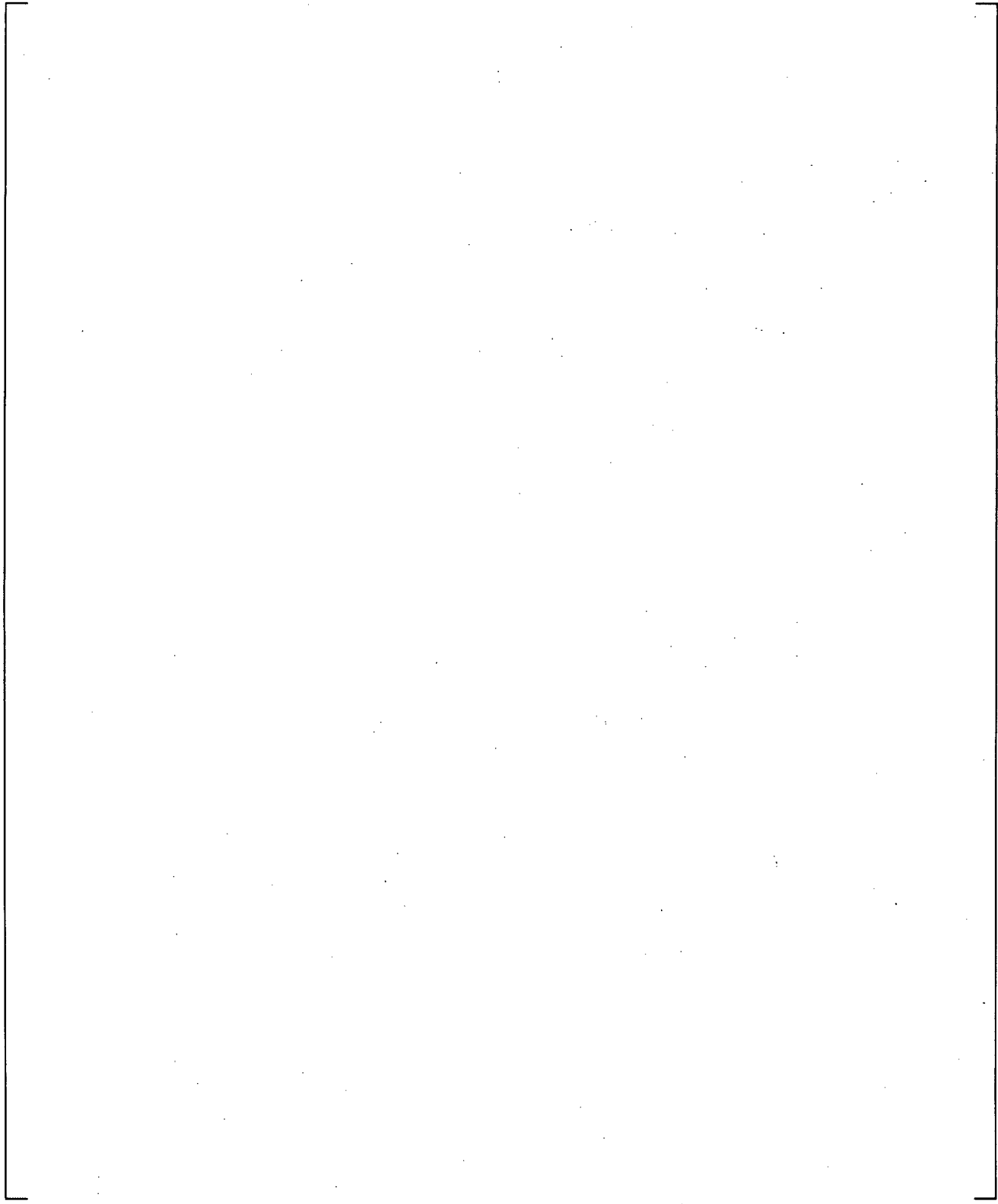


**Figure 23.1.1-37 Comparison of Predicted and Measured Void Fraction at Level 4, Test 1004-3**

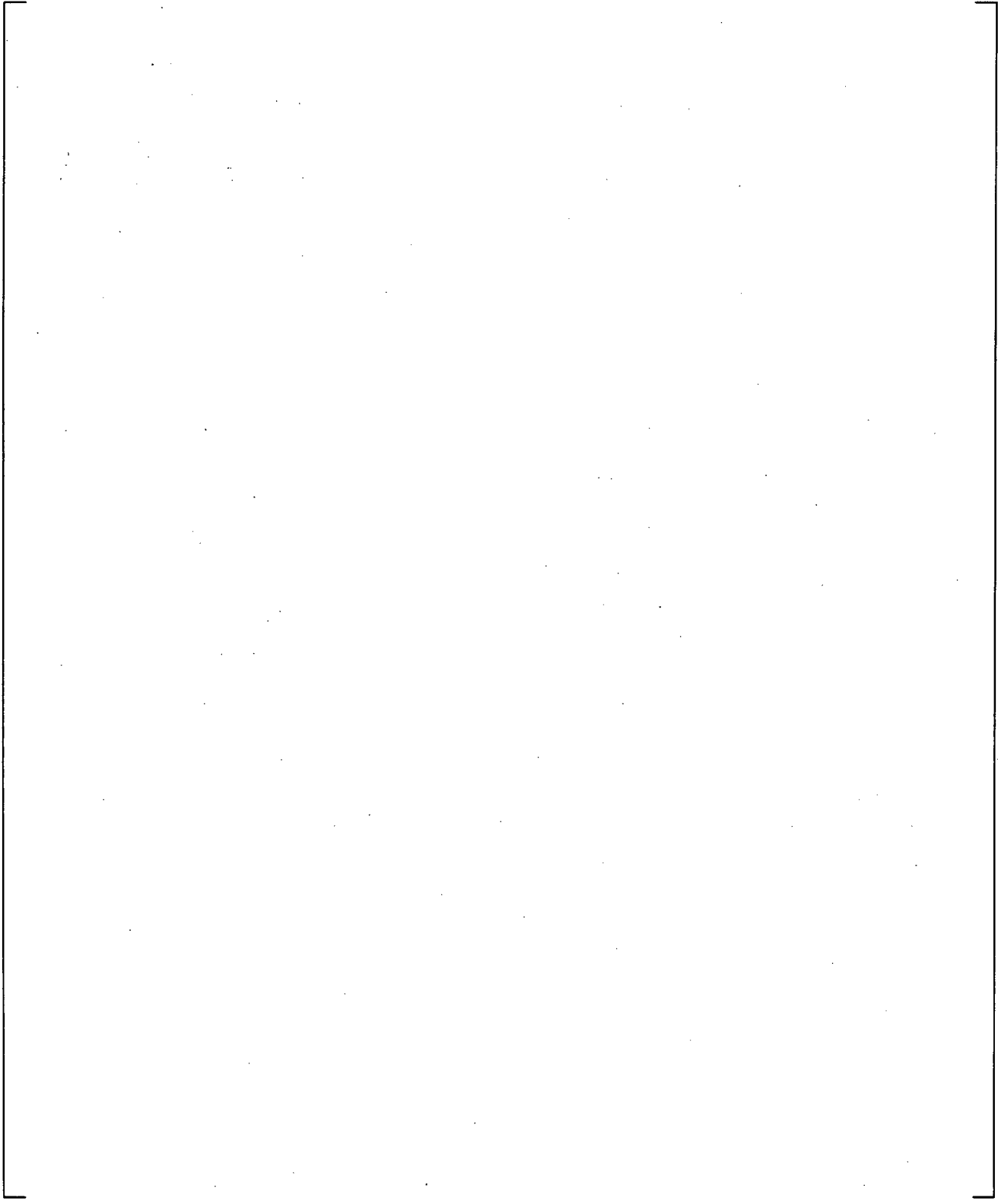


**Figure 23.1.1-38 Comparison of Predicted and Measured Void Fraction at Level 5, Test 1004-3**

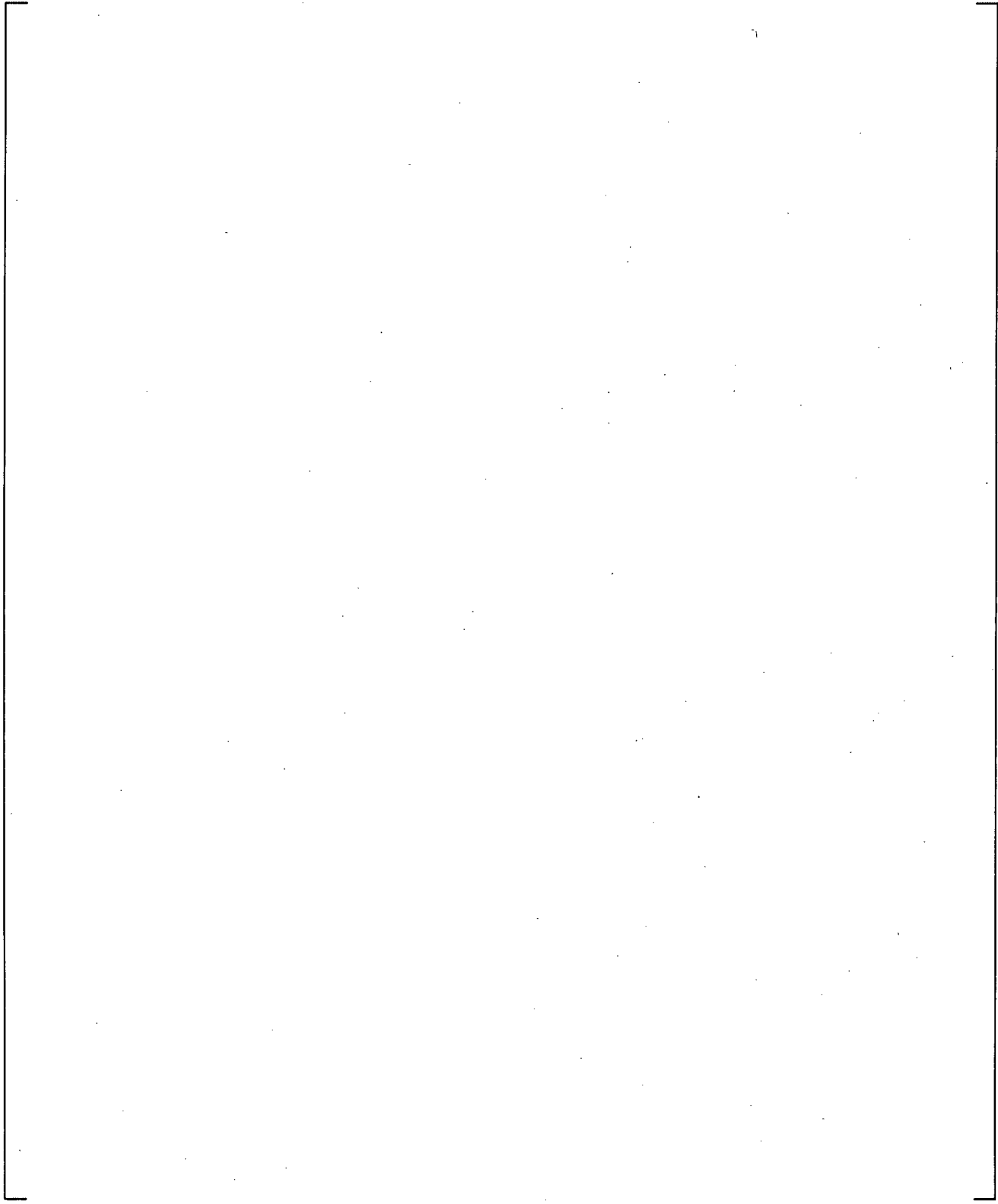


**Figure 23.1.1-39 Comparison of Predicted and Measured Void Fraction at Level 6, Test 1004-3**

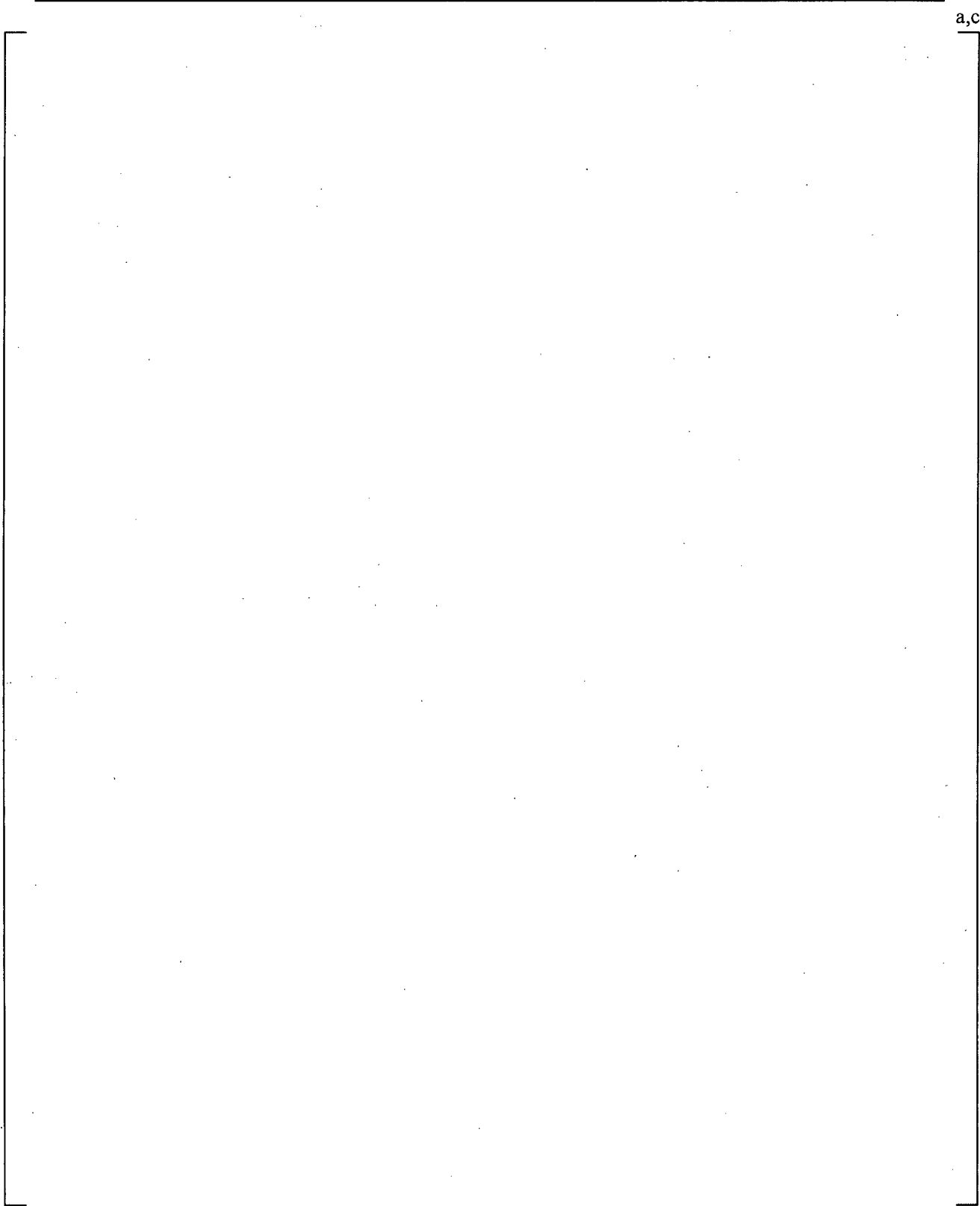


**Figure 23.1.1-40 Comparison of Predicted and Measured Void Fraction at Level 1, Test 1004-2**

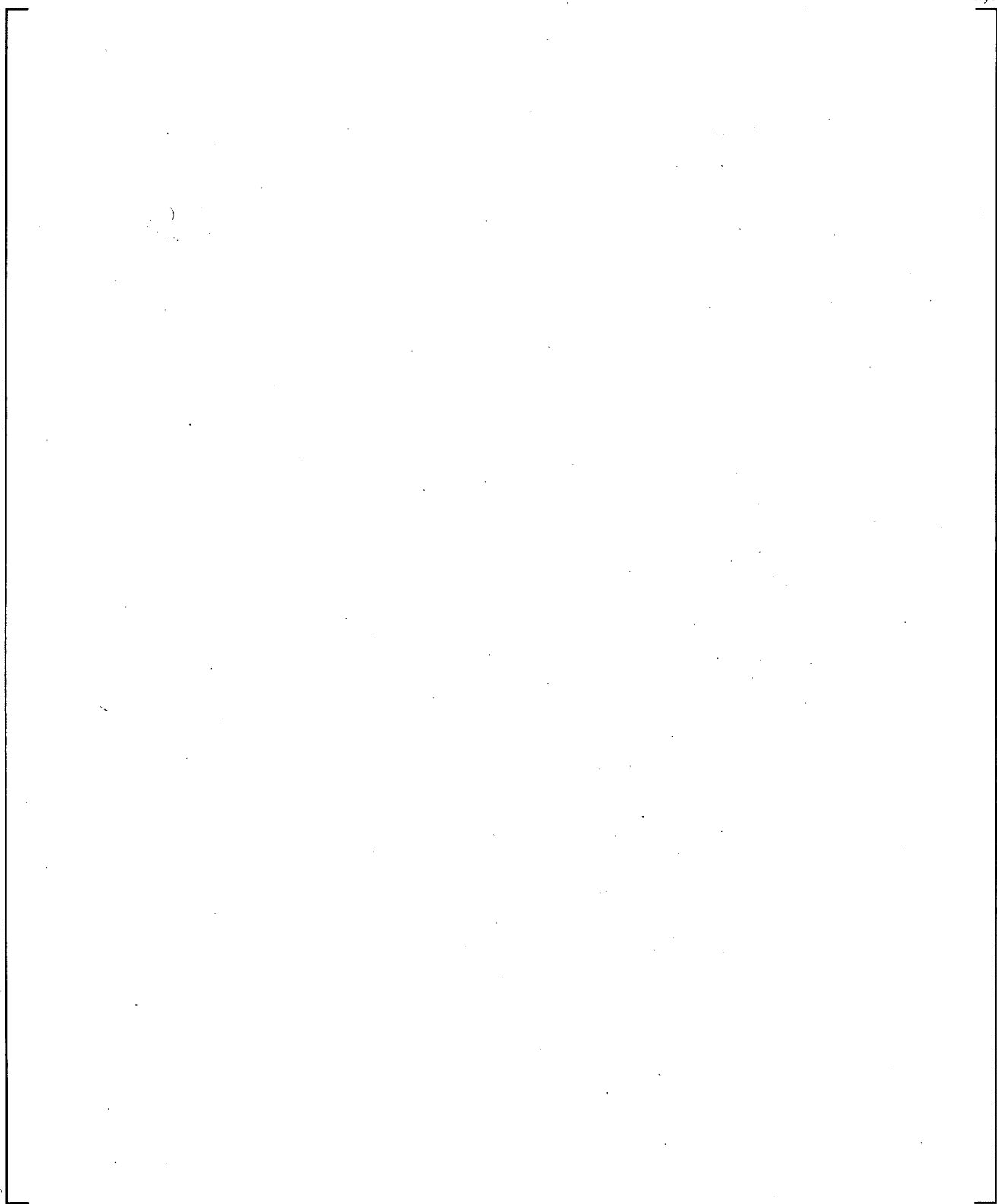


**Figure 23.1.1-41 Comparison of Predicted and Measured Void Fraction at Level 2, Test 1004-2**

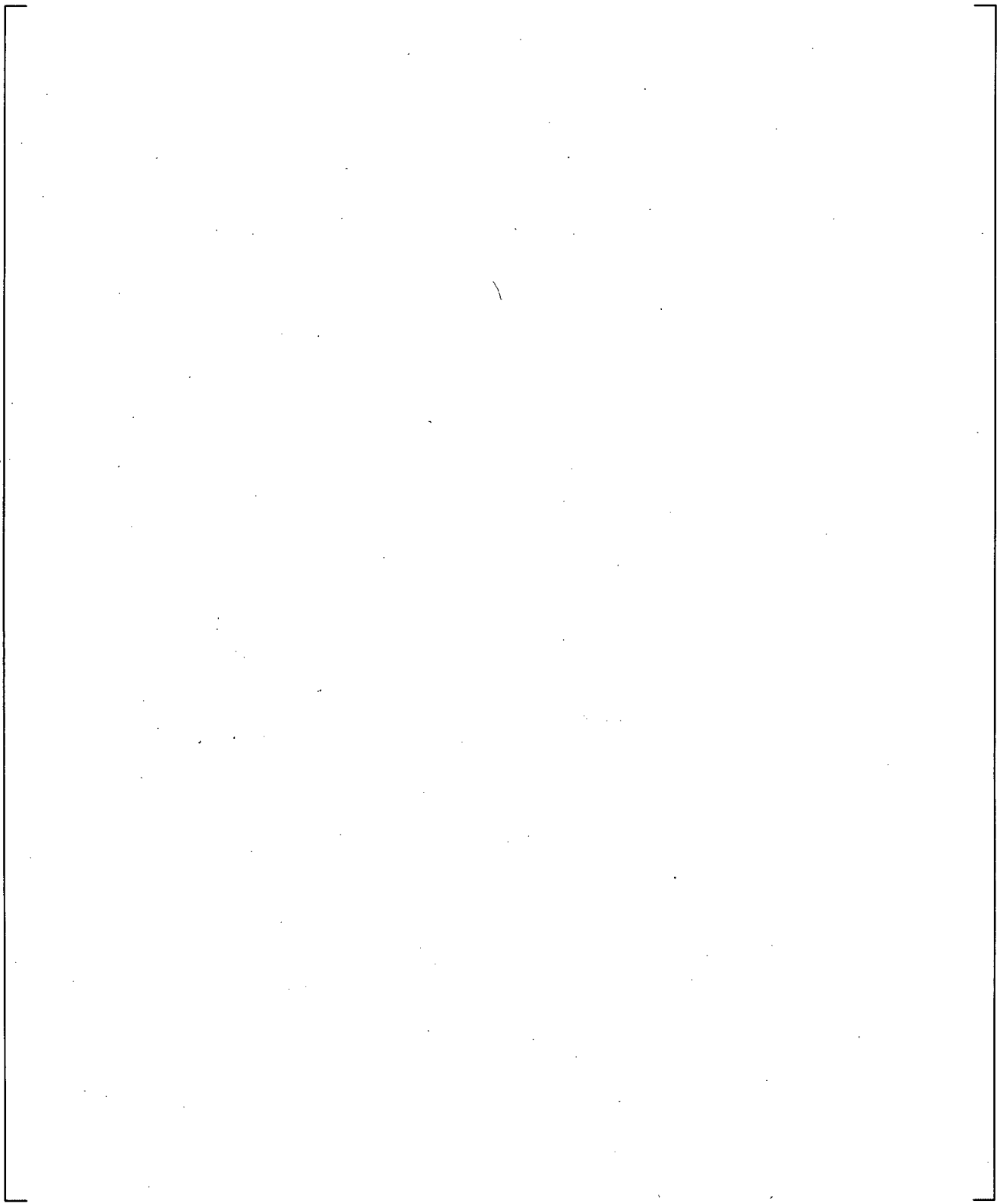


**Figure 23.1.1-42 Comparison of Predicted and Measured Void Fraction at Level 3, Test 1004-2**

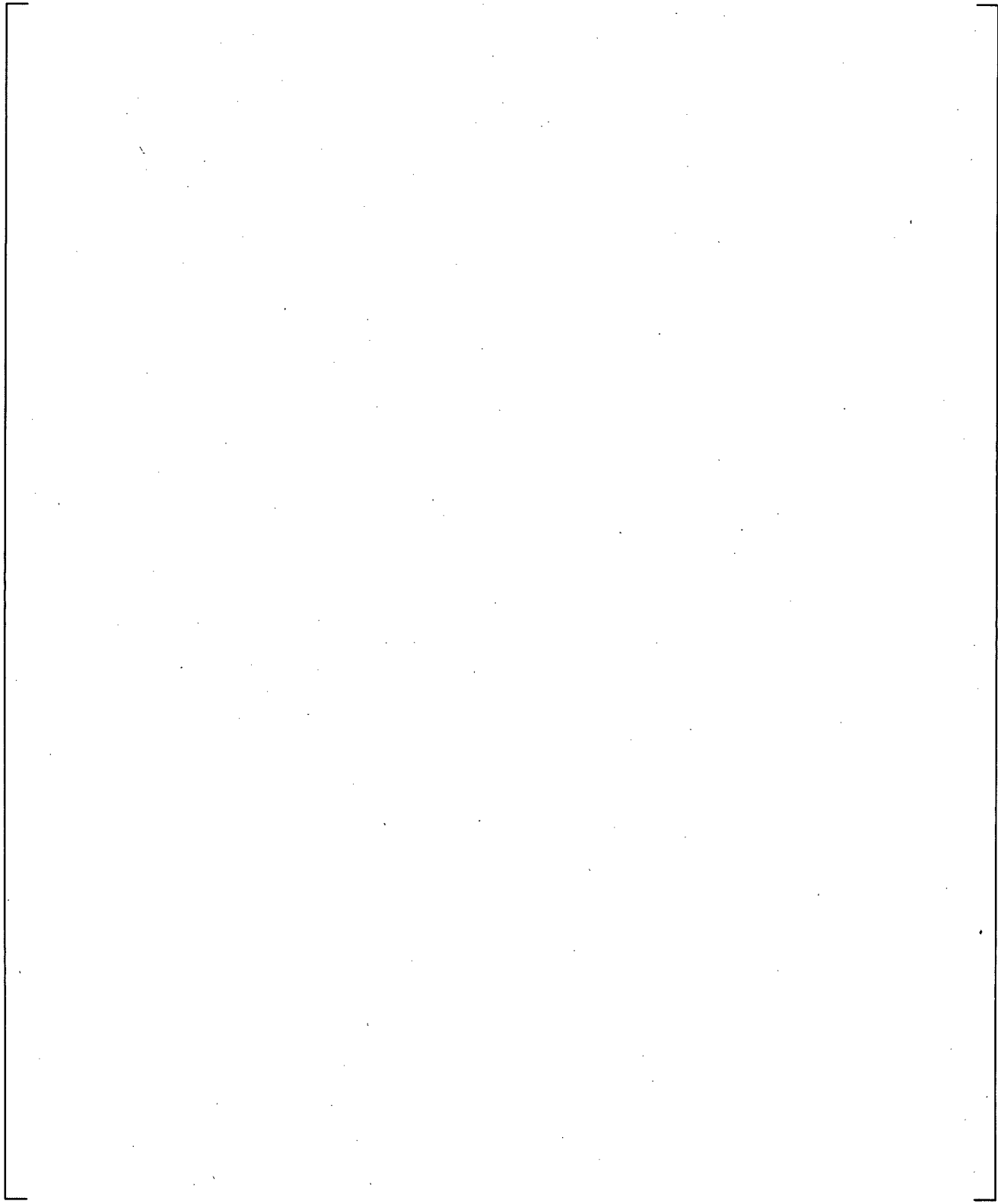


**Figure 23.1.1-43 Comparison of Predicted and Measured Void Fraction at Level 4, Test 1004-2**

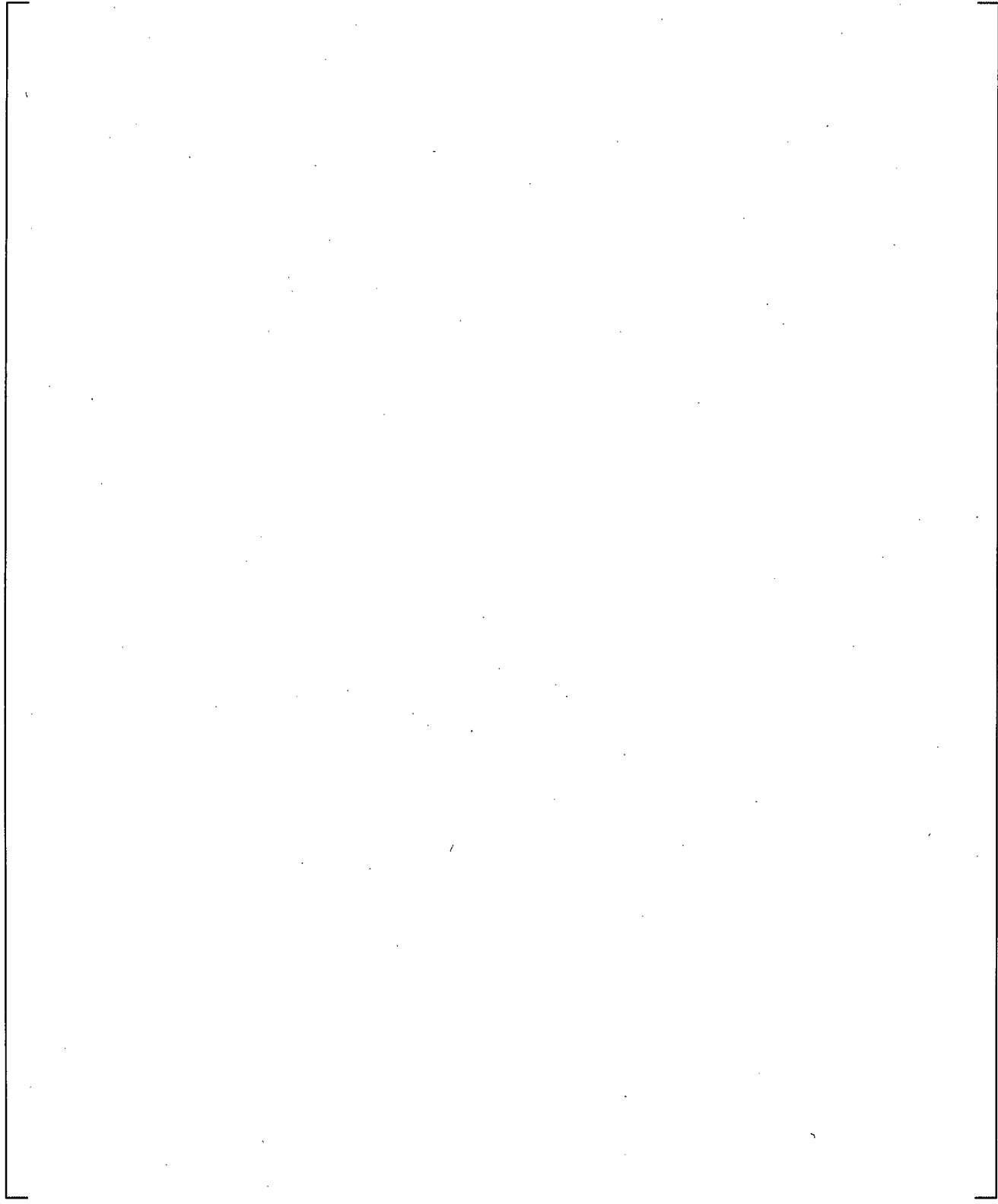


**Figure 23.1.1-44 Comparison of Predicted and Measured Void Fraction at Level 5, Test 1004-2**

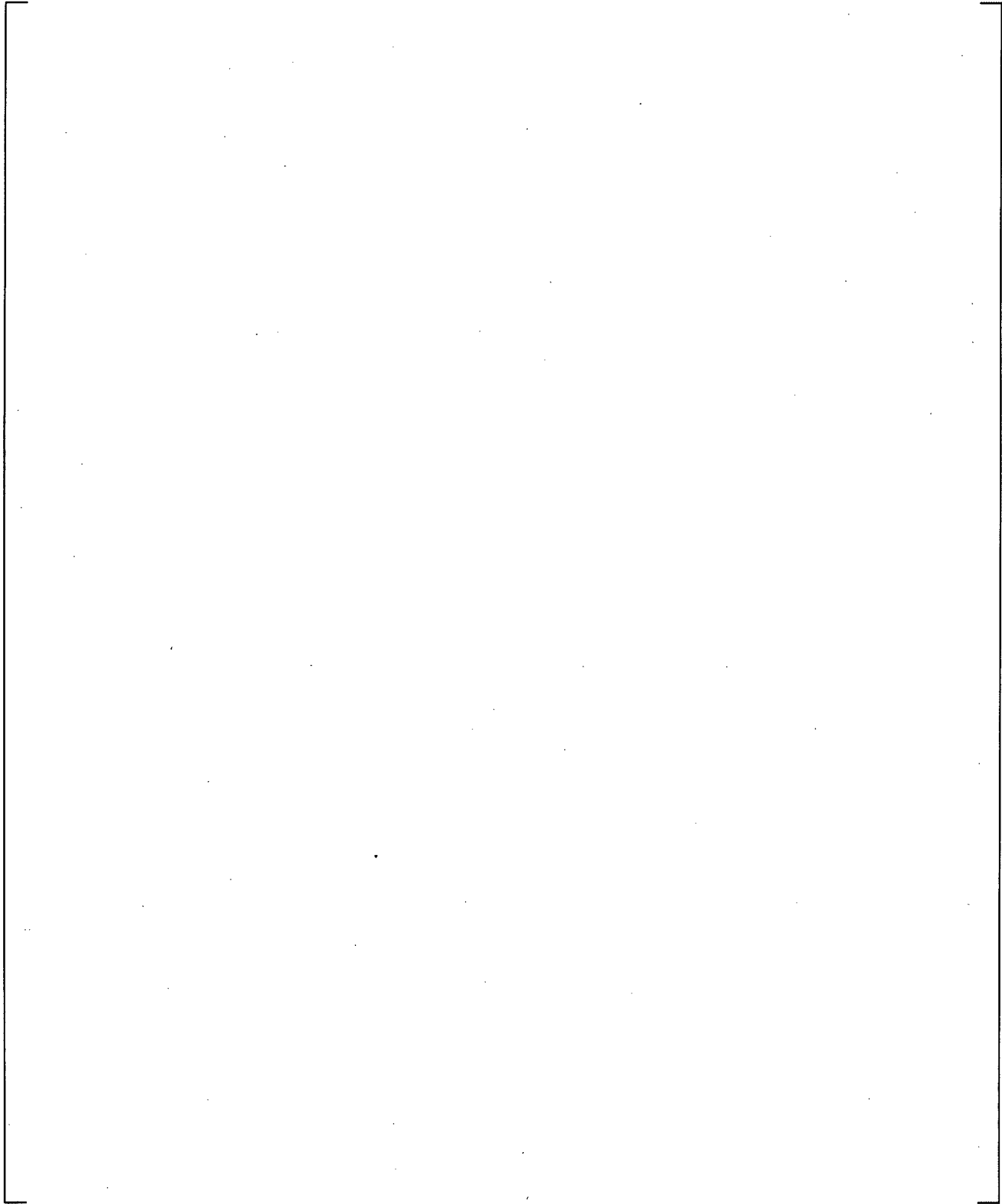


**Figure 23.1.1-45 Comparison of Predicted and Measured Void Fraction at Level 6, Test 1004-2**

## 23.1.2 Semiscale Tests

### 23.1.2.1 Introduction

The FSLOCA PIRT in Section 2 of this document [

] <sup>a,c</sup> The Semiscale simulation study in this section provides further assessment of the code's capability in predicting the void distribution and the post-CHF heater rod temperature excursion in a prolonged boiloff transient with unusually high cladding temperature attained.

As a portion of the Semiscale Mod-3 experimental program conducted by EG&G Inc. under the sponsorship of the US NRC, Semiscale Tests S-07-10 and S-07-10D (Sackett and Clegg, 1980) feature deep core uncover and high heater rod temperature due to manually delayed ECCS injection. In these two tests, the core was almost completely uncovered and the peak heater rod temperature was as high as 1145 K before the ECCS injection, providing a valuable database in assessing the WCOBRA/TRAC-TF2 code covering extreme conditions, and complementing the validation documented in Sections 13 and 15.

Semiscale test S-07-10D is a repeat of S-07-10, which was designated as a United States Standard Problem Small Break Experiment (SBE) (Shimeck, 1980). Both tests simulated a 10% cold leg break. The difference between them is that the steam generator in S-07-10 was isolated at 17 s into the transient, while it was allowed to blowdown throughout the transient in S-07-10D.

This section assesses the important phenomena occurring in the Semiscale S-07-10D test and the performance of WCOBRA/TRAC-TF2 in predicting two-phase mixture level swell and post-CHF heat transfer.

### 23.1.2.2 Semiscale Test Facility Description

The Semiscale Mod-3 facility is a small-scale model of the primary system of a four loop PWR. The system includes equivalent elevations and component layout (including steam generators, vessel, pumps, pressurizer, and loop piping) at 1:1705.5 volumetric scaling. One intact loop is scaled to simulate the three intact loops, while a broken loop simulates the single loop in which a break is postulated to occur. Geometric similarity is maintained between a PWR and Mod-3, most notably in the design of a 25 rod, full-length (3.66 m), electrically heated core, full length upper head and upper plenum, component layout, and relative elevations of various components. The scaling philosophy followed in the design of the Mod-3 system (modified volume scaling) is intended to preserve the most important first order effects for small break LOCA transients.

The Semiscale Mod-3 system consists of a pressure vessel with simulated reactor internals, including a 25 rod core with electrically heated rods and an external downcomer assembly; an intact loop with a pressurizer, steam generator, and pump; and a broken loop with a steam generator, pump, and rupture assembly. The system has an emergency core cooling system (ECCS) with the high and low pressure coolant injection pumps for each loop, an accumulator for the intact loop and a pressure suppression system with header and suppression tank.

Figure 23.1.2-1 provides an isometric of the Semiscale Mod-3 facility, as configured for Tests S-07-10 and S-07-10D. The tests had a communicative break simulator configuration with the break nozzle located in the broken loop cold leg between the pump and the vessel. The break size was  $0.223 \text{ cm}^2$ , which is volumetrically scaled to represent 10% of the area of a cold leg pipe in a PWR. For the broken loop, a sharp edged pipe orifice with a length-to-diameter ratio of 0.27 was used to represent an orifice-like break.

Figure 23.1.2-2 is a plan view of the 25-rod Mod-3 core for Test S-07-10D which shows the location of the unpowered rods, their orientation with respect to the remainder of the system, and the distribution of the internal cladding thermocouples monitored during each test. Internally heated electric rods with a heated length of 3.66 m and an outside diameter of 1.072 cm were used to geometrically simulate PWR nuclear rods. Figure 23.1.2-3 shows the step cosine axial power profile for the rods with a 1.55 peak to average power factor. The relative location of in-core instrumentation (gamma dosimeters and core inlet drag screen) and grid spacers are provided in Figure 23.1.2-4.

For the S-07-10D test, the 5x5 core was configured with the 9 center rods operating at an initial maximum linear heat generation rate (MLHGR) of 46.7 kW/m and the 13 peripheral rods at an initial MLHGR of 30.9 kW/m with A1, A3, and A4 unpowered. The total core power for the test was  $1.94 \pm 0.1 \text{ MW}$ .

### 23.1.2.3 Semiscale Test S-07-10D Description

The Semiscale Mod-3 small break test S-07-10D was conducted to assist the US NRC licensing staff in evaluating the acceptability of small break licensing models used by pressurized water reactor vendors. The test simulated a 10% cold leg break in which no emergency core coolant was injected until elevated core heater rod temperatures were achieved. The broken loop steam generator secondary side was allowed to blow down to investigate the effect of secondary side conditions on primary behavior.

Test S-07-10D was conducted from initial conditions of 15.73 MPa (2281.5 psia) pressurizer pressure, and core inlet temperature of 556 K (541.1°F), with a core power level of 1.94 MW. The simulated small break with a break area of  $0.223 \text{ cm}^2$  ( $0.0346 \text{ in.}^2$ ) was located on the centerline of the broken loop cold leg between the pump and the vessel and was scaled to represent 10% of the area of a cold leg pipe in a PWR.

After initiation of the blowdown, power to the electrically heated core was reduced to simulate the predicted heat flux response of nuclear fuel rods during a LOCA. The intact and broken loop circulation pumps continued to operate until 1 s after the pressurizer pressure reached 12.41 MPa (1800 psia) approximately 10 s after initiation of blowdown. At this time, and for the next 60 s, the pumps followed a predetermined profile after which power was tripped and pumps were allowed to coast down.

Table 23.1.2-1 provides the conditions in the Semiscale Mod-3 system for S-07-10D test at initiation of blowdown. Tables 23.1.2-2 and 23.1.2-3 provide the sequence of operational procedures and events relative to rupture.

In Test S-07-10D, the coolant injection systems were arranged to discharge into the cold leg of the intact loop. The high pressure and low pressure injection pumps were started at 460 seconds and 560 seconds after blowdown initiation at a flow rate of 0.059 L/s and 0.135 L/s, respectively, and continued for the

duration of the test. Intact loop accumulator coolant injection started 458 seconds after blowdown initiation and continued for 23 seconds. The total volume of coolant injected into the system was 0.028 m<sup>3</sup>. Nitrogen was not discharged into the system.

The Semiscale S-07-10D was well equipped with sufficient instruments to measure the test system thermal hydraulic response in a simulated small break LOCA transient of a PWR. The performance of the system during the test was monitored by 268 detectors. A digital data acquisition system recorded data for Test S-07-10D at an effective sample rate of 28.75 points per second per channel for the first 100 seconds and then 9.58 points per second per channel for the remainder of the test.

#### 23.1.2.4 WCOBRA/TRAC-TF2 Model for Semiscale Boiloff Tests

The WCOBRA/TRAC-TF2 simulation of the Semiscale test documented herein focuses only on the boiloff transient period after the loop seals are cleared in both loops and therefore consists of a simplified model with just a VESSEL component with the boundary conditions defining the mass flow between the downcomer and vessel, and BREAK components connected to the hot legs to simulate the depressurization based on the test measurement.

The Semiscale vessel noding diagram is provided in Figure 23.1.2-5 [

]<sup>a,c</sup> the hot leg back pressure, lower plenum feed temperature, core collapsed liquid level, and heater rod power decay, provided in Figures 23.1.2-6 through 23.1.2-9, respectively.

Figure 23.1.2-10 provides the Density Measurement recorded over time for the S-07-10D test, which shows complete core uncovering – vapor density at the core entrance.

#### 23.1.2.5 Simulation of Semiscale Boiloff Tests

The objective of the Semiscale S-07-10D simulation with WCOBRA/TRAC-TF2 is to assess the two-phase mixture level swell and post-CHF heat transfer models in the code. To assess these two phenomena, the heater rod temperature response and core void fraction calculated by WCOBRA/TRAC-TF2 during the boiloff transient are compared with the test data at elevations where test measurements are available.

Figures 23.1.2-11 through 23.1.2-24 provide the comparison of the predicted and measured clad temperature at various elevations, from top to bottom of the core. [

] <sup>a,c</sup>

Also, the heatup transient above the dryout point shows that the WCOBRA/TRAC-TF2 predicted [

] <sup>a,c</sup>

Figures 23.1.2-26 to 23.1.2-32 provide the predicted and measured void fraction at different elevations; [

] <sup>a,c</sup>

The overall results of the simulation are summarized in Figure 23.1.2-33 which provides the heater rod dryout history during the boiloff transient compared with the test, for both the high and low power rods. [

] <sup>a,c</sup>

### 23.1.2.6 Summary and Conclusions

As discussed in Section 23.1.2.5, the Semiscale S-7-10D test has been evaluated in this section [

] <sup>a,c</sup>

The simulation with WCOBRA/TRAC-TF2 of the S-7-10D test has shown that:

[

•

•

] <sup>a,c</sup>

As such, it is concluded that the WCOBRA/TRAC-TF2 is capable of predicting the level swell and post-CHF heat transfer satisfactorily.

### 23.1.2.7 References

1. Sackett, Kenneth E. and Clegg, L. Bruce, 1980, "Experiment Data Report for Semiscale MOD-3 Small Break Test S-07-10D (Baseline Test Series)," prepared for the U.S. Nuclear Regulatory Commission under Department of Energy Contract No. DE-AC07-76IDO1570.
2. Shimeck, D.J., 1980, "Analysis of Semiscale MOD-3 Small Break Test S-07-10 and S-07-10D," prepared for the U.S. Nuclear Regulatory Commission under Department of Energy Contract No. DE-AC07-761DO1570.

<b>Table 23.1.2-1 Initial Conditions and ECC Requirements S-07-10D Test</b>		
<b>Configuration</b>	<b>Specified</b>	<b>S-07-10D Actual<sup>(1)</sup></b>
Break Size	0.223 cm <sup>2</sup> (10%)	0.223 cm <sup>2</sup> (10%)
Break Type	Communicative	Communicative
Break Location	Cold Leg	Cold Leg
Break Orientation	Side of pipe	Side of pipe
Pressurizer Location	Intact loop	Intact loop
<b>Initial Conditions</b>	<b>Specified</b>	<b>S-07-10D Actual</b>
Core Power	1.94 MW	1.925 MW
Nominal System Pressure	15.7 MPa	15.73 MPa
Intact Loop Cold Leg Fluid Temperature	556 K	556 K
Broken Loop Cold Leg Fluid Temperature	556 K	558 K
Intact Loop Core Delta T	35 K	37 K
Broken Loop Core Delta T	35 K	33 K
Core Inlet Flow	9.77 kg/s	9.7 kg/s
Intact Loop Cold Leg Flow	Note 2	10 L/s
Broken Loop Cold Leg Flow	Note 2	3.2 L/s
Intact Loop Steam Generator Liquid Level (above top of tube sheets)	295 ±5 cm	Note 3
Broken Loop Steam Generator Liquid Level (above top of tube sheets)	998 ±5 cm	978 cm
<b>ECC Parameters</b>		
Intact Loop Accumulator		
Location	Cold Leg	Cold Leg
System Pressure at actuation	None	1600 kPa
Tank Pressure at actuation	None	3100 kPa
Liquid Volume	0.045 m <sup>3</sup>	0.045 m <sup>3</sup>
Gas Volume	0.025 m <sup>3</sup>	0.025 m <sup>3</sup>
Line resistance	10675 s <sup>2</sup> /m <sup>3</sup> -cm <sup>2</sup>	Same
Temperature	300 K	300 K
<b>Intact Loop High Pressure Injection (HPI)</b>		
Location	Cold Leg	
Actuation Pressure	None	1600 kPa

<b>Table 23.1.2-1 Initial Conditions and ECC Requirements S-07-10D Test (cont.)</b>		
Injection Rate (average)	0.062 kg/s	0.075 kg/s
Temperature	300 K	300 K
<b>Intact Loop Low Pressure Injection (LPI)</b>		
Location	Cold Leg	
Actuation Pressure	none	2100 kPa
Injection Rate (average)	0.16 kg/s	0.11 kg/s
Temperature	300 K	300 K
PSS Tank Pressure	Pressure range over time	
<b>Notes:</b>		
1. Measured initial conditions are taken from digital acquisition system read just prior to blowdown initiation.		
2. Flow is not specified since it must be adjusted to achieve the required differential pressure across the core.		
3. Level detector erratic prior to blowdown initiation. Liquid level not available.		

<b>Table 23.1.2-2 Sequence of Operational Procedures for Test S-07-10D</b>		
<b>Event</b>	<b>Specified Time (s)</b>	<b>Actual Time (s)</b>
Rupture	0.0	0.0
Initiate PSS tank pressure reduction	50	50
Enable accumulator and HPIS injection	When on-line monitors indicate high core temperatures	460
Enable LPIS injection	When on-line monitors indicate high core temperatures	560
Terminate Test		748

<b>Table 23.1.2-3 Sequence of Events for Test S-07-10D</b>	
	<b>S-07-10D Time in Seconds</b>
Blowdown Initiated	0
Pressurizer Pressure = 12.41 MPa	6.9
Begin core power decay	7.7
Intact loop steam generator feedwater closed	
Broken loop steam generator feedwater closed	
Upper plenum fluid saturates	8.0
Intact loop steam generator steam valve closed	21
Broken loop steam generator steam valve closed	
Pressurizer empties	20
Entire system saturated, system pressure = 7.1 MPa	27
Upper plenum liquid level reaches intact loop hot leg	42
Pressure suppression system pressure reduction begins	52
Intact loop pump suction blows out	85
Liquid from cold legs drains to vessel and pump suction resulting in two-phase mixture at break	65 to 90
Power to pumps terminated	69.7
Pumps stop	79
Top of support tubes uncovered in upper head	80
Pressure suppression system tank pressure reduction finished	160
Broken loop pump suction swept out	N/A
First dryouts indicated in upper regions of the core	268 – 300
Dryout of core peak power zone from top down	268 – 300
Core completely void	435
Fallback turns over and/or rewets thermocouples progressively from upper to mid core	N/A
Accumulator Injection begins	460
HPIS injection begins	
ECC water reaches bottom of core	467
Accumulator flow falls to zero as accumulator “floats” on the system	482
System repressurized due to steam generation	
Core peak power zone quenched	488 to 498
LPIS injection initiated	560
Entire core quenched	525
Test terminated	748

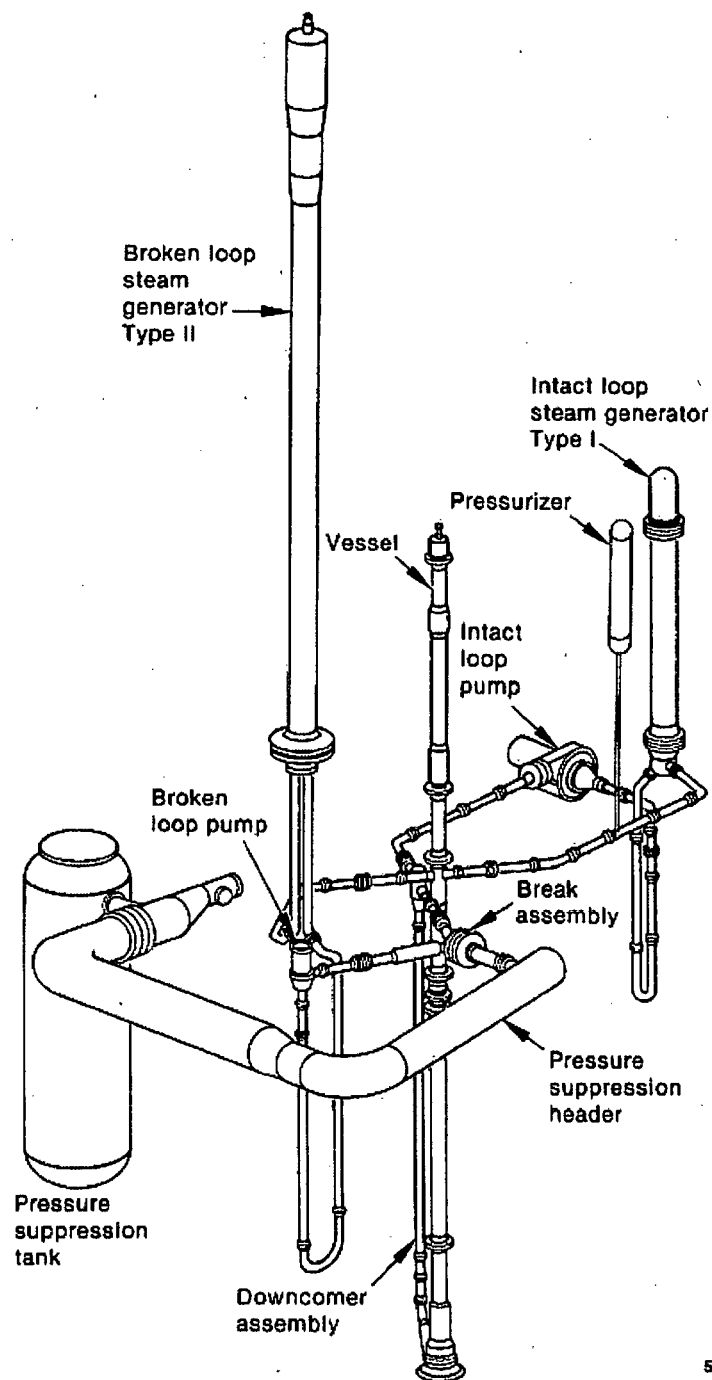


Figure 23.1.2-1 Semiscale Mod-3 Facility Overview

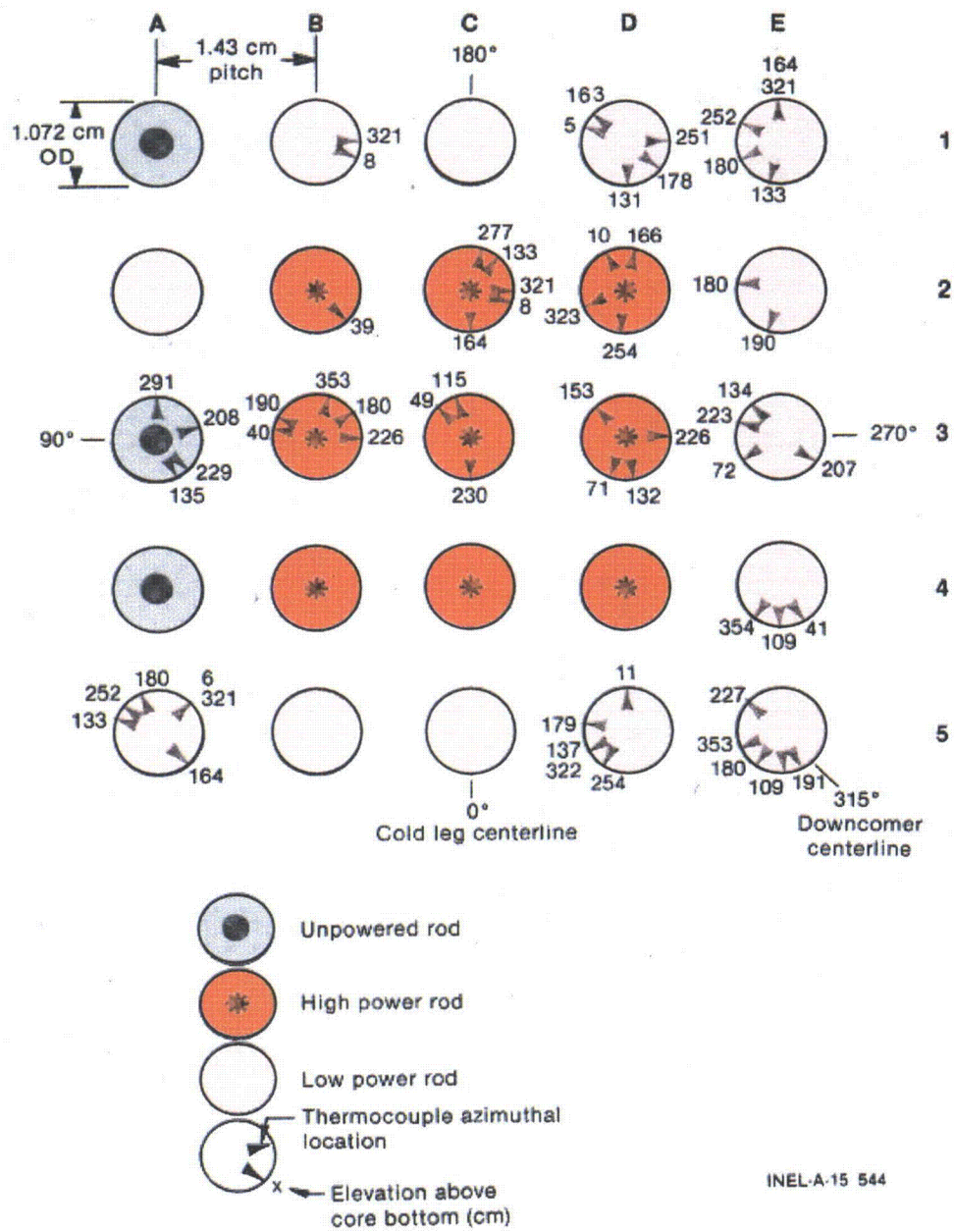


Figure 23.1.2-2 Plan View of Semiscale Mod-3 Core for S-07-10D Test

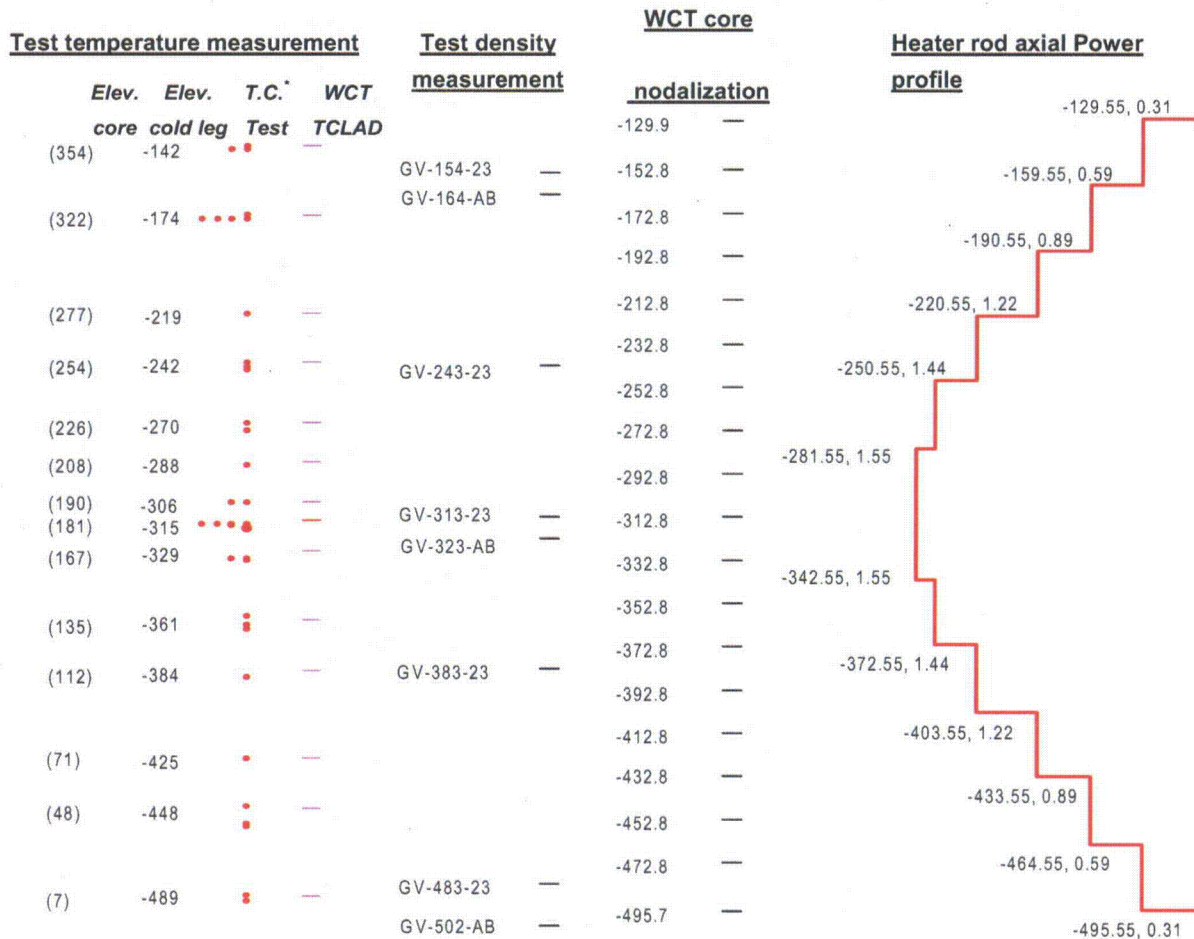


Figure 23.1.2-3 Semiscale S-07-10D Test Axial Power Profile in Relation to Vessel Instrumentation

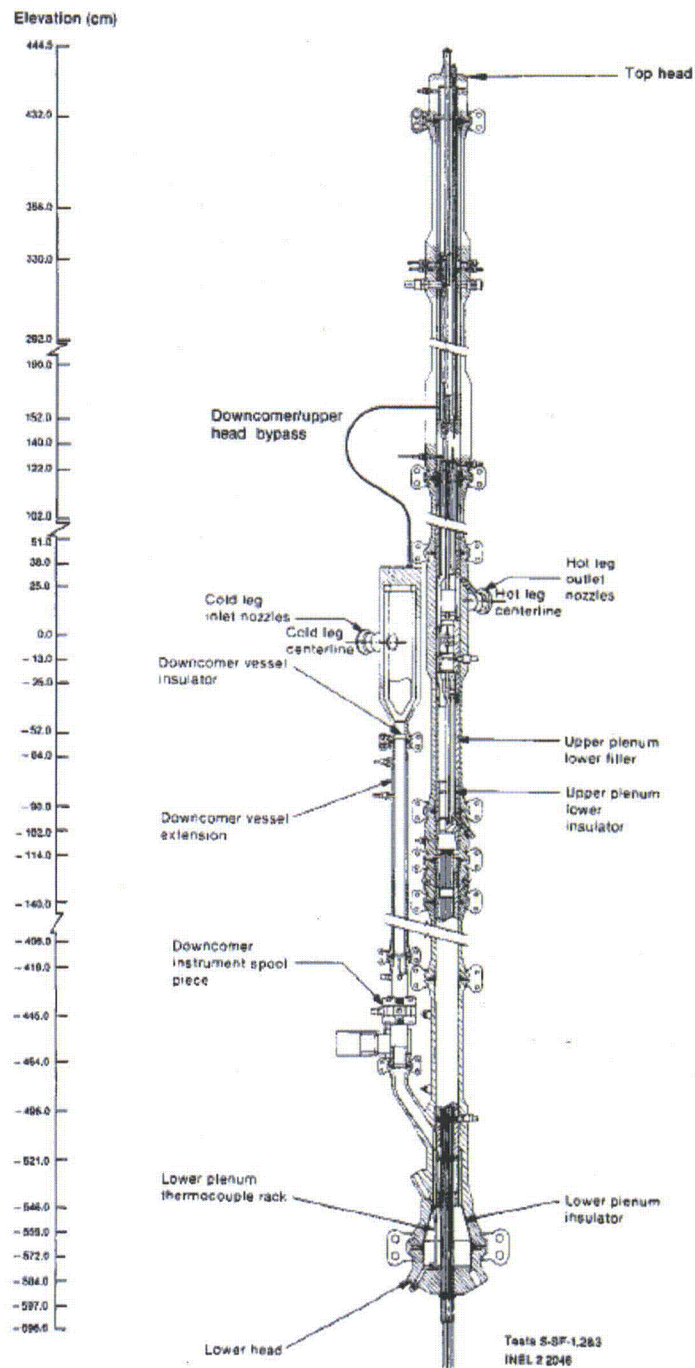
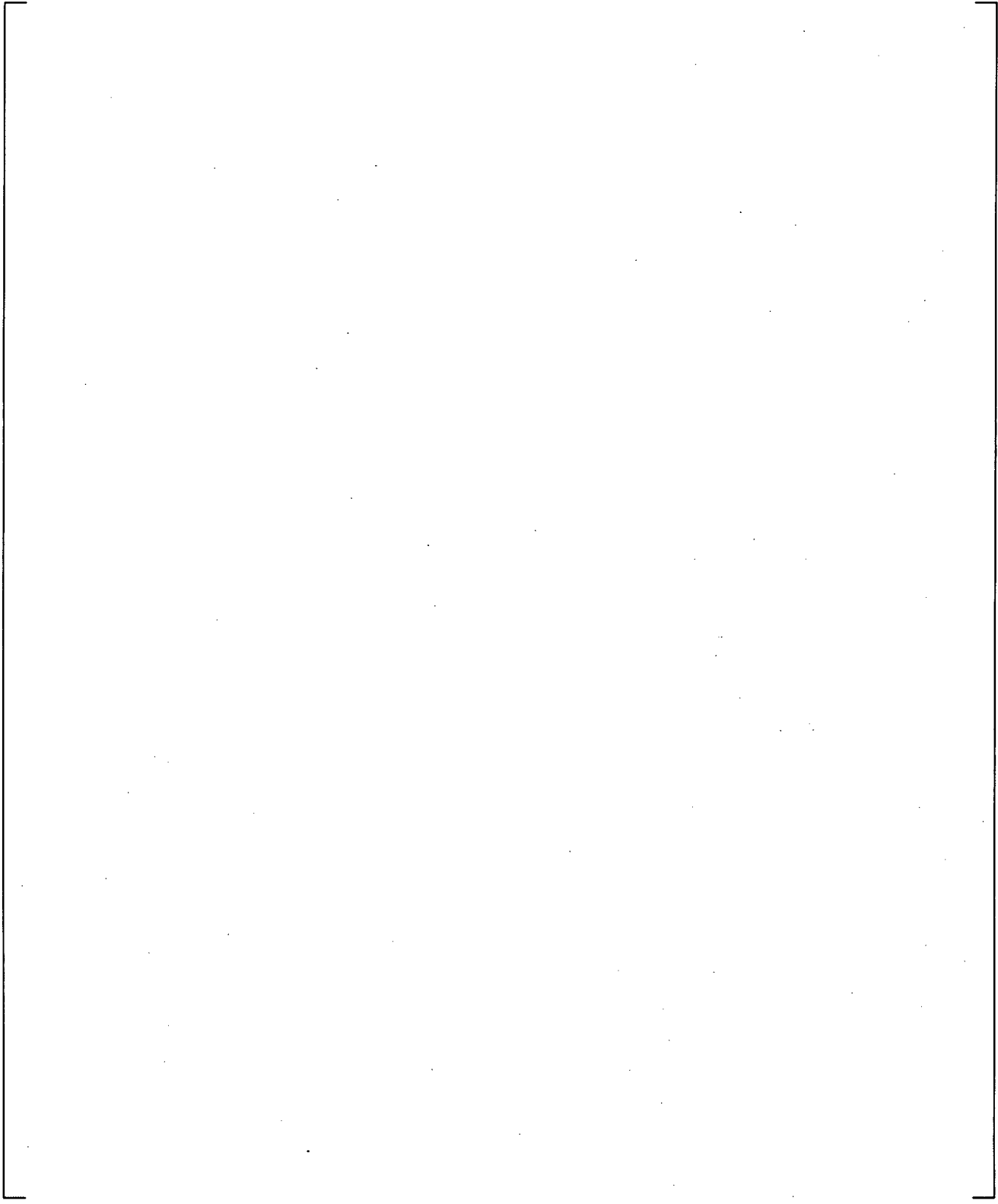


Figure 23.1.2-4

Semiscale Mod-3 Pressure Vessel and Downcomer – Cross Section Showing Instrumentation



**Figure 23.1.2-5 WCOBRA/TRAC-TF2 Semiscale Mod 3 Vessel Model**

**Semiscale S-07-10D Test - Upper plenum pressure**  
*(PV-13 : in vessel hot leg extension, 13 cm below cold leg centerline)*

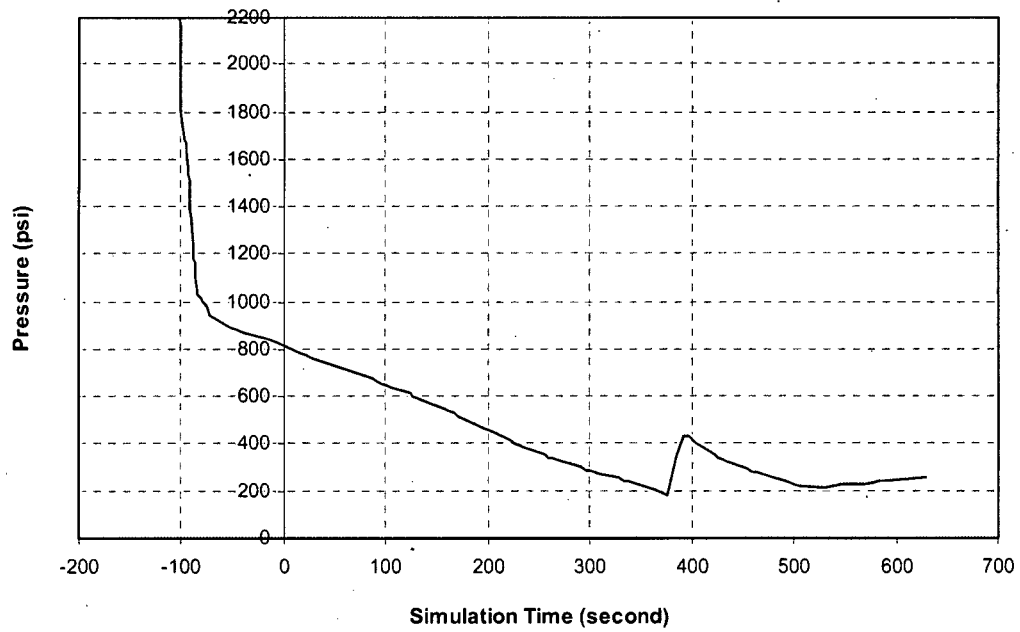


**Figure 23.1.2-6 Semiscale S-07-10D Test Upper Plenum Pressure (Hot Leg Backpressure)**

**Semiscale S-07-10D Test - Lower plenum fluid temperature**  
*(TFV-572W : in vessel lower plenum, -572 cm below cold leg centerline)*

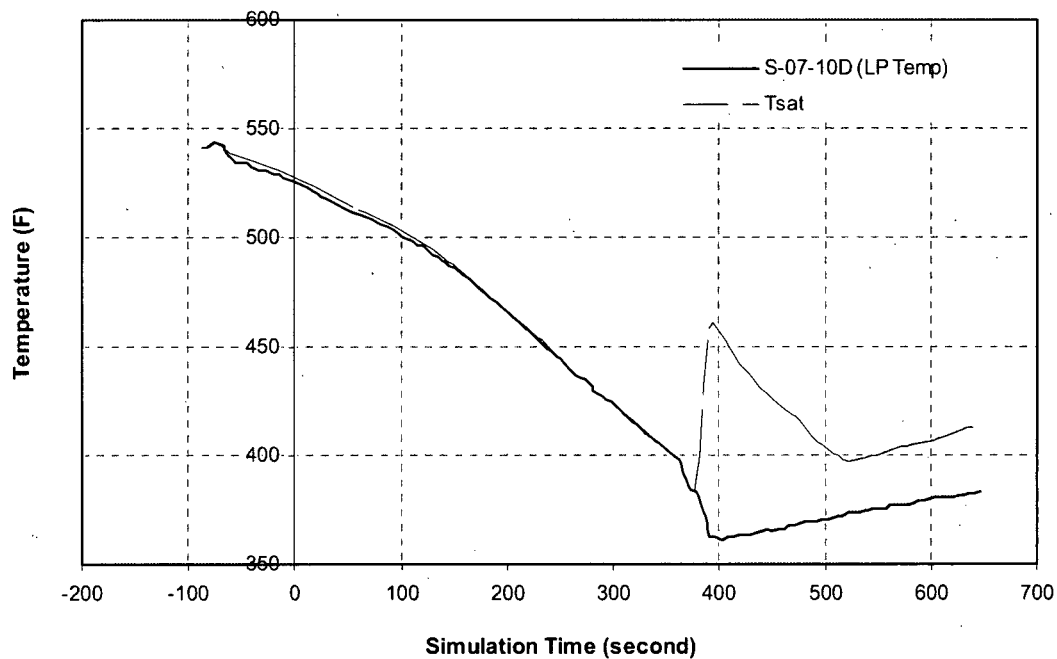


**Figure 23.1.2-7 Semiscale S-07-10D Test Lower Plenum Fluid Temperature**

Semiscale S-07-10D Test - Core power decay

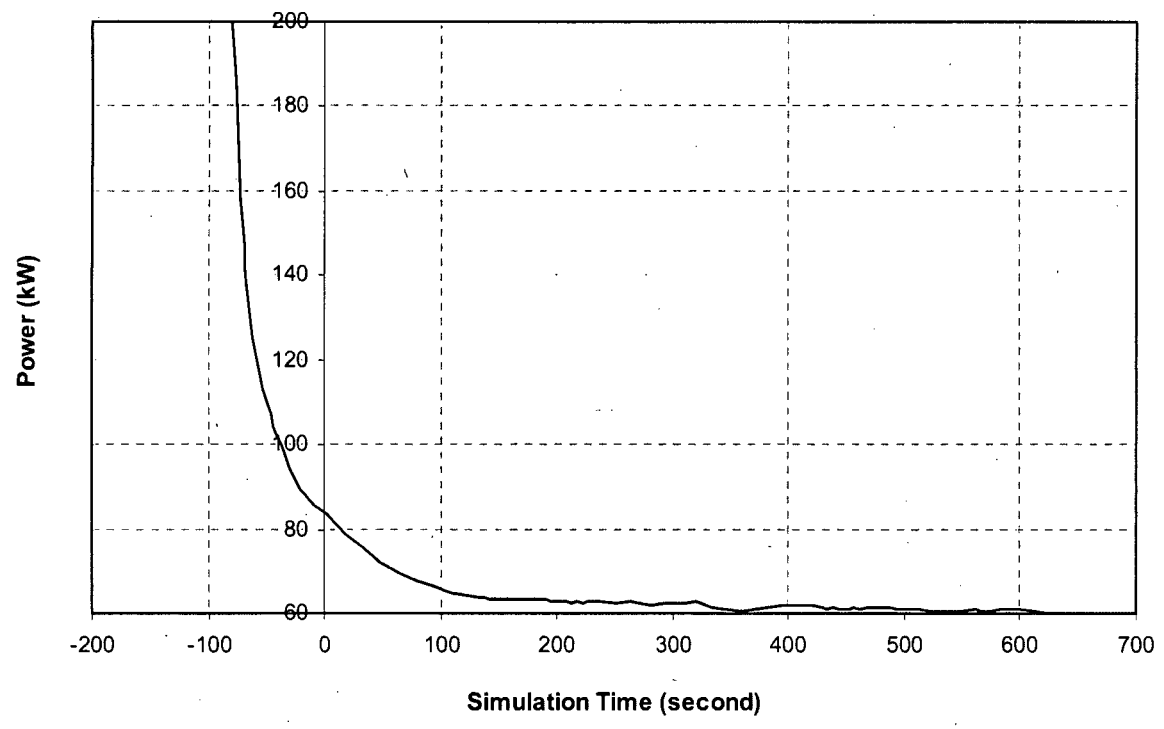
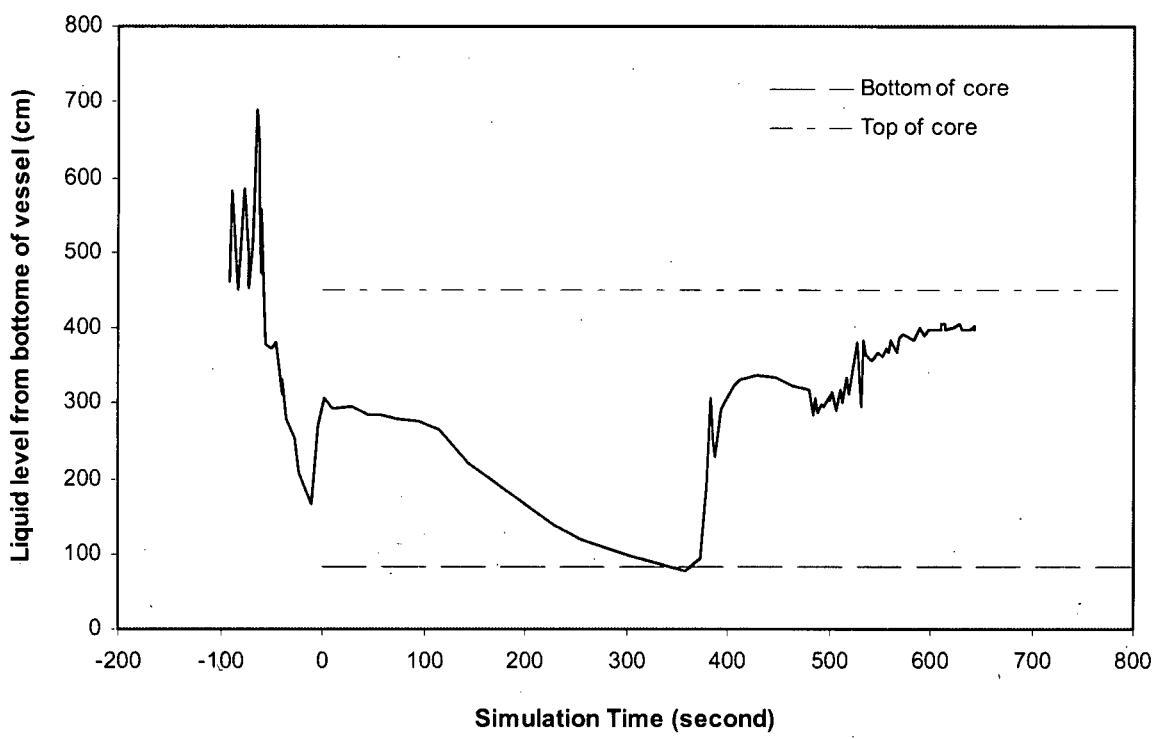
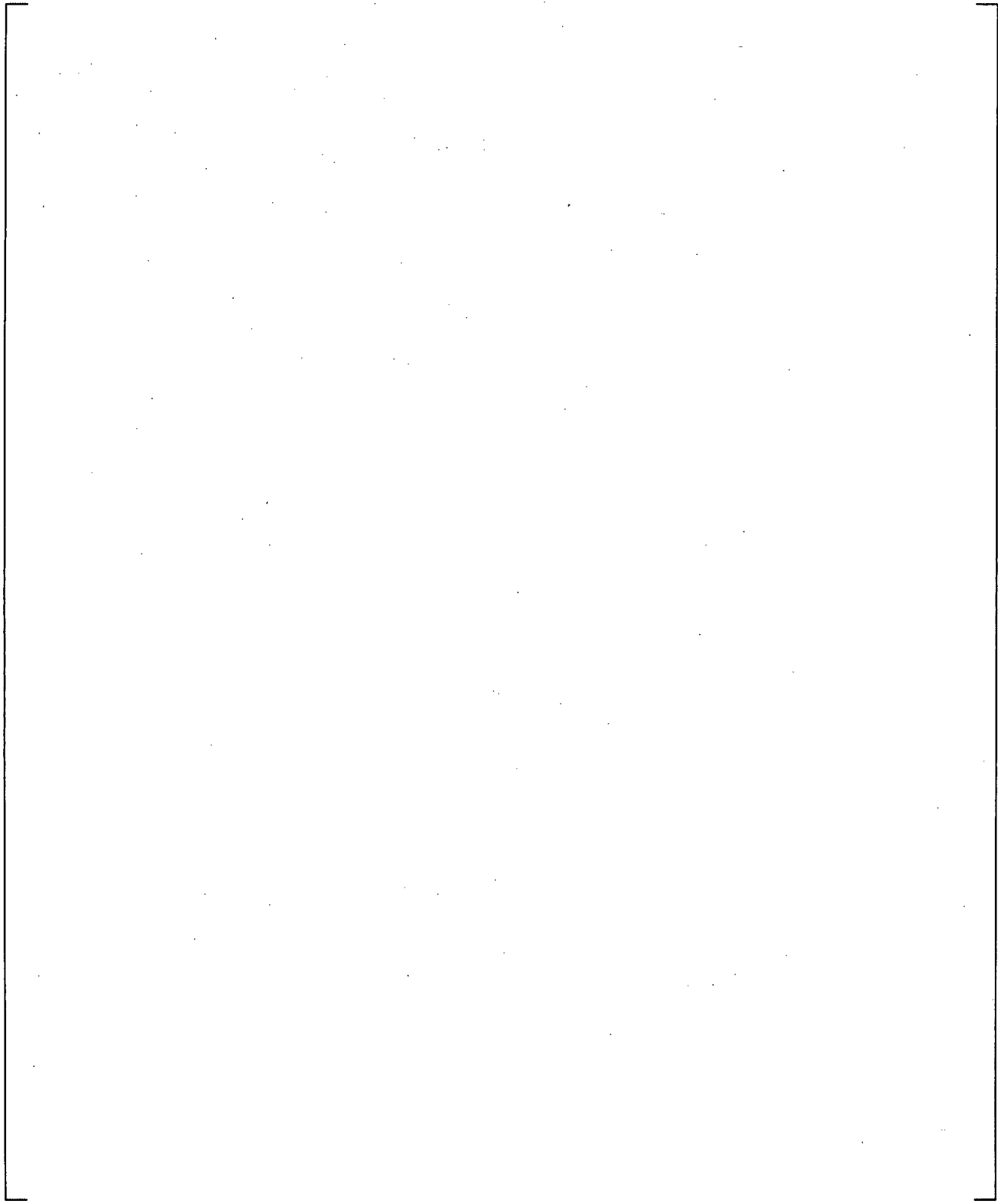


Figure 23.1.2-8 Semiscale S-07-10D Test Core Power Decay

**Semiscale S-07-10D Test - Core collapsed liquid level**  
*(DP-501-105 : dP taps are -501cm and -105cm below cold leg centerline)*



**Figure 23.1.2-9 Semiscale S-07-10D Test Core Collapsed Liquid Level**



**Figure 23.1.2-10 Density Measurement Recorded During Semiscale S-07-10D Test**

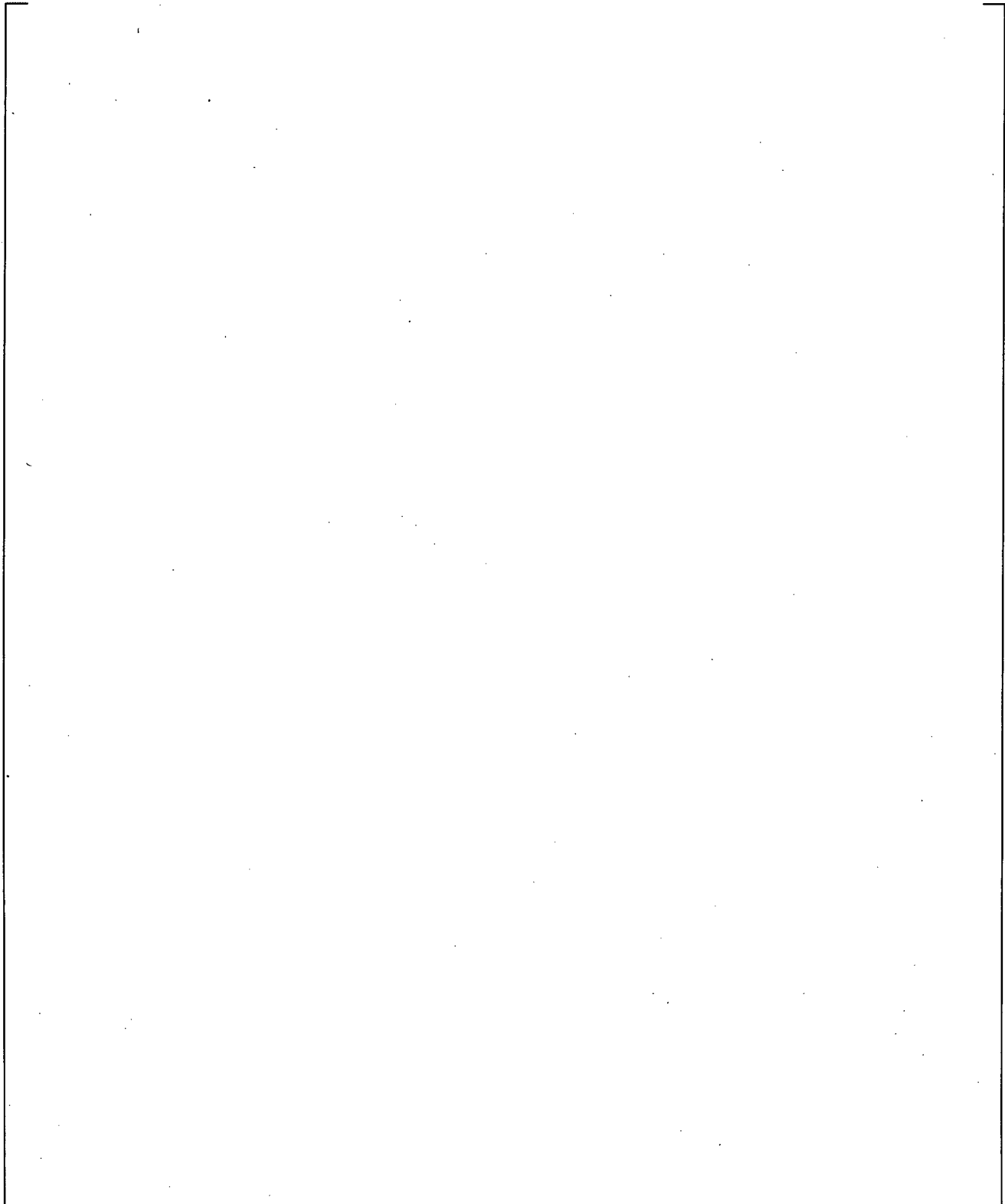


**Figure 23.1.2-11 Semiscale S-07-10D Clad Temperature at Elevation = 354 cm (from the Bottom of the Core)**

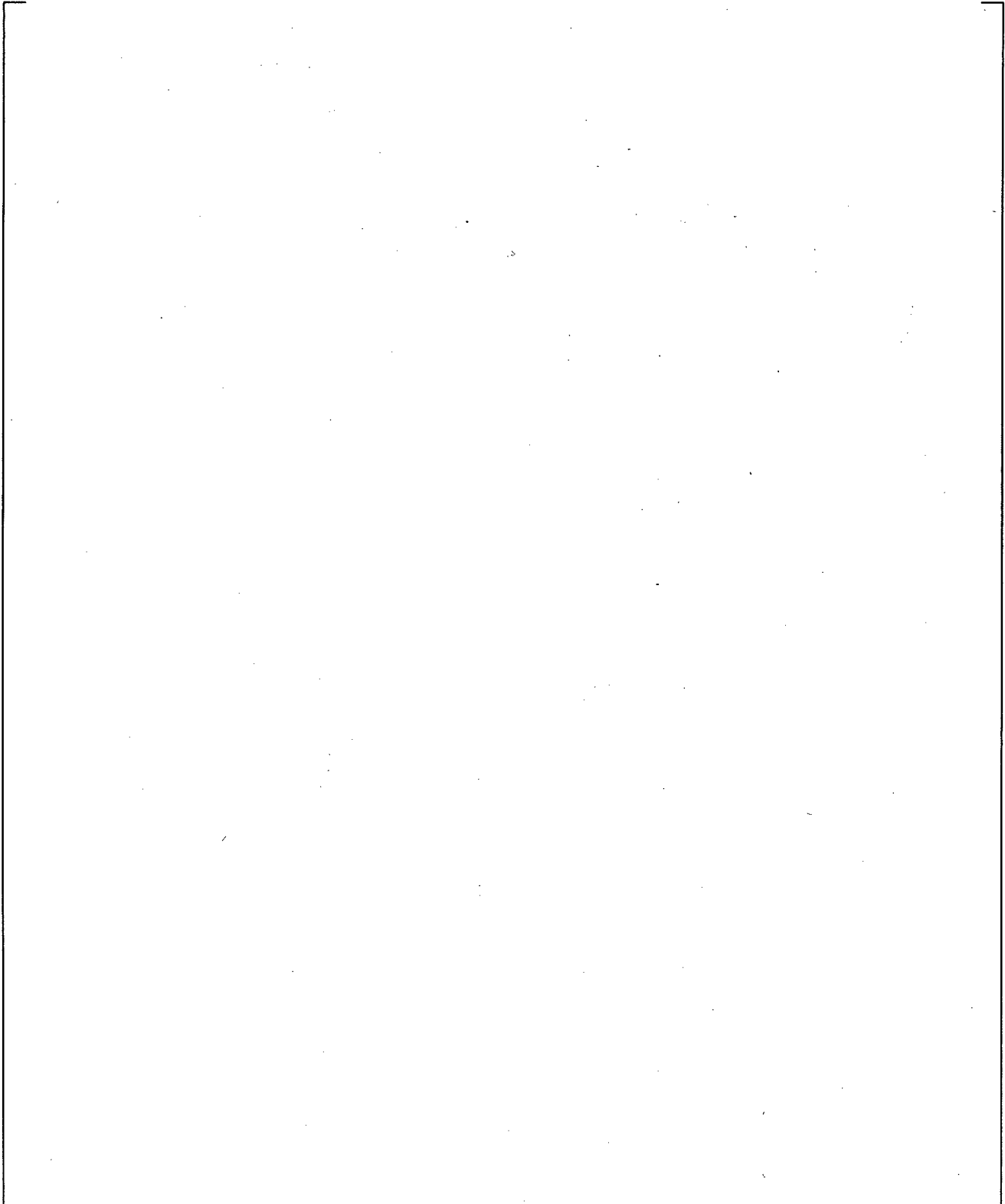


**Figure 23.1.2-12 Semiscale S-07-10D Clad Temperature at Elevation = 322 cm (from the Bottom of the Core)**

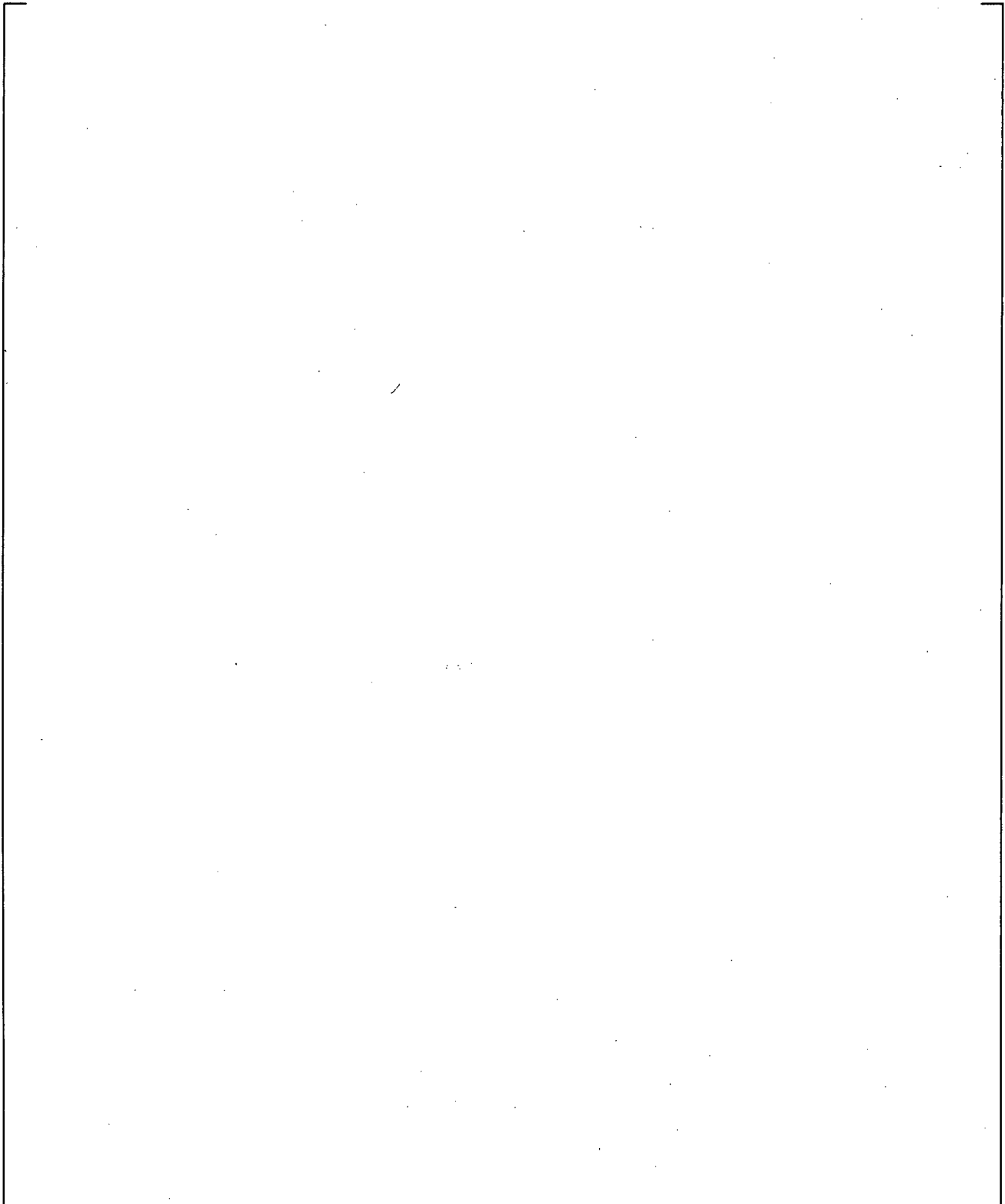


**Figure 23.1.2-13 Semiscale S-07-10D Clad Temperature at Elevation = 277 cm (from the Bottom of the Core)**

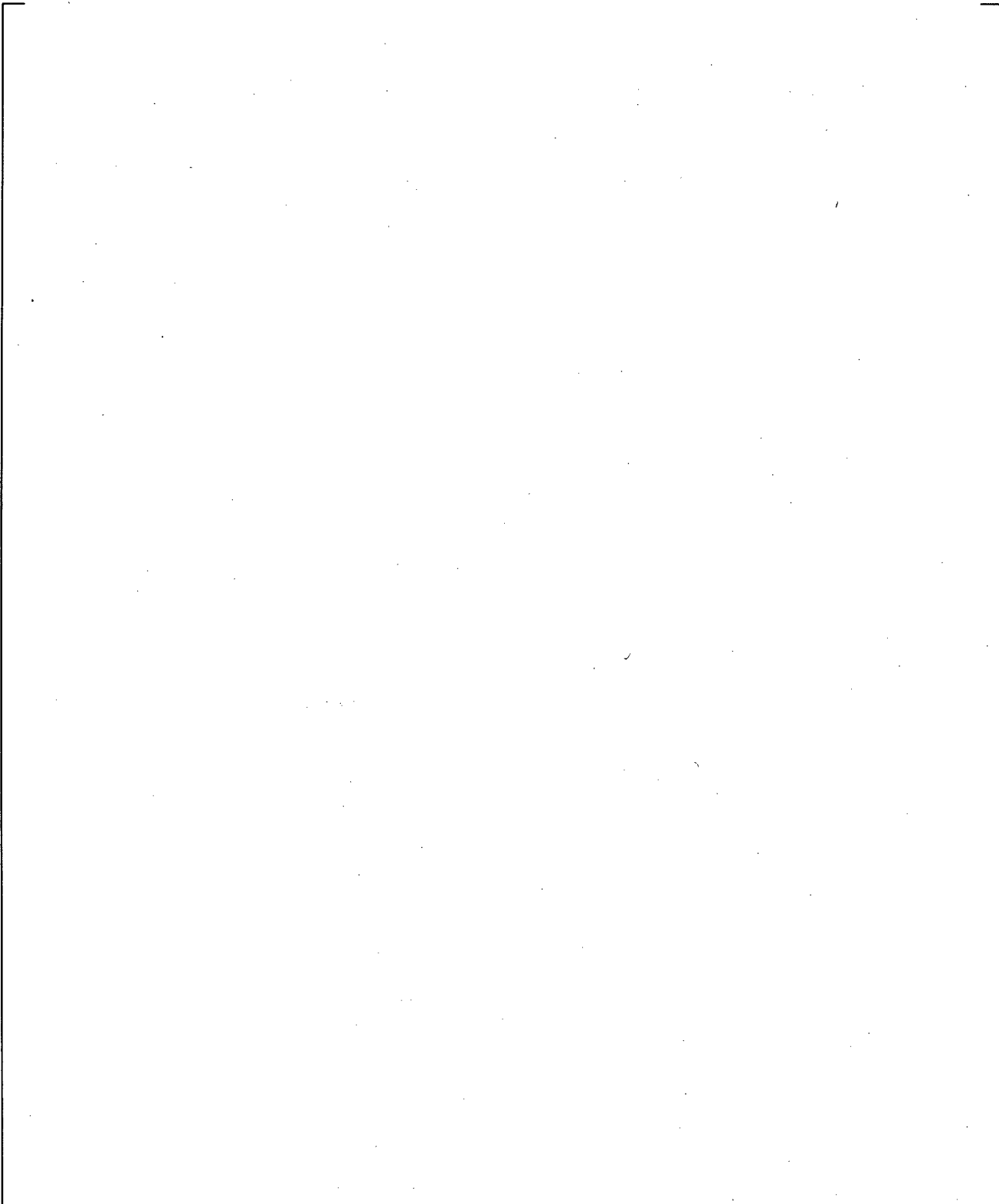


**Figure 23.1.2-14 Semiscale S-07-10D Clad Temperature at Elevation = 254 cm (from the Bottom of the Core)**

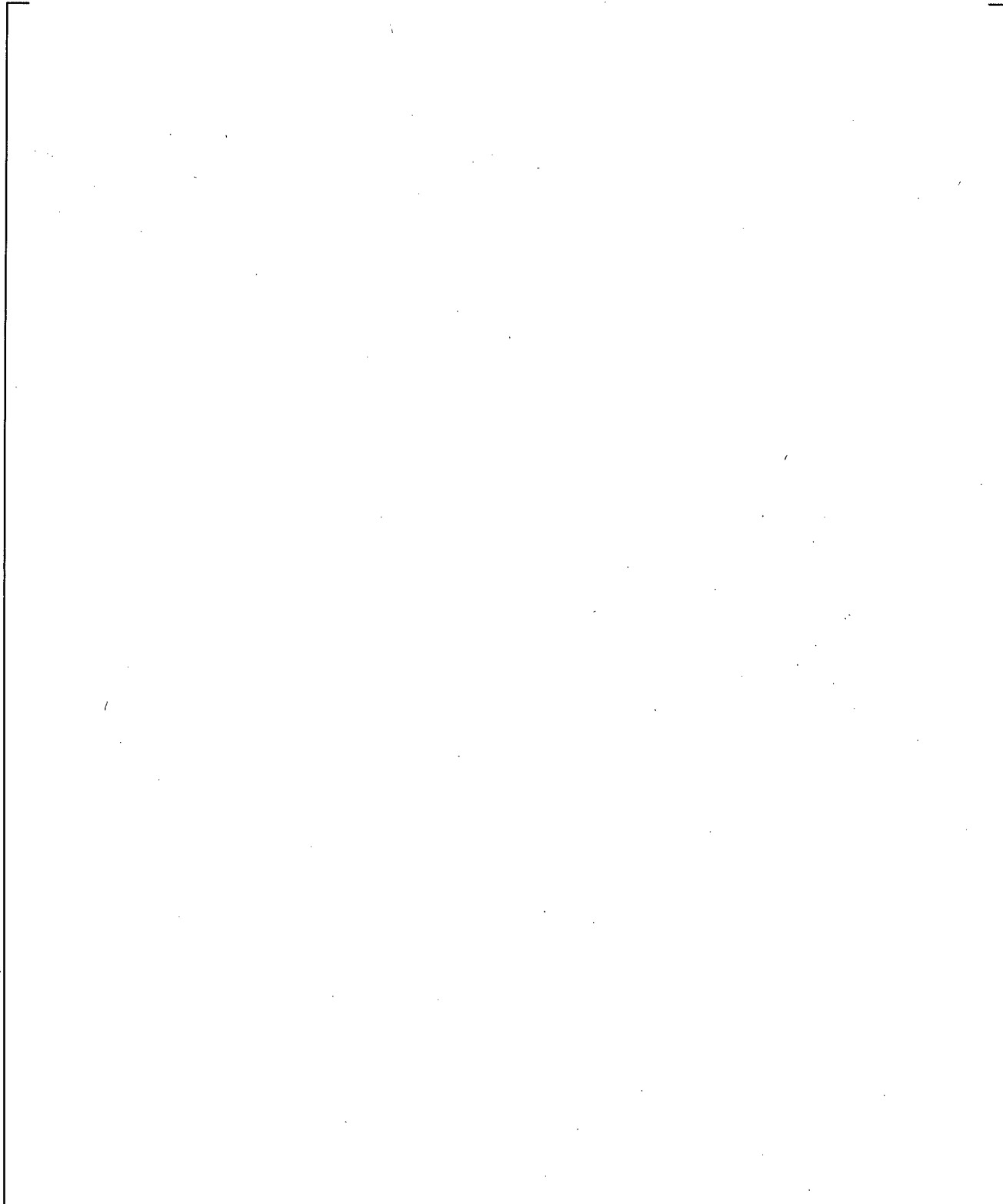


**Figure 23.1.2-15 Semiscale S-07-10D Clad Temperature at Elevation = 226 cm (from the Bottom of the Core)**

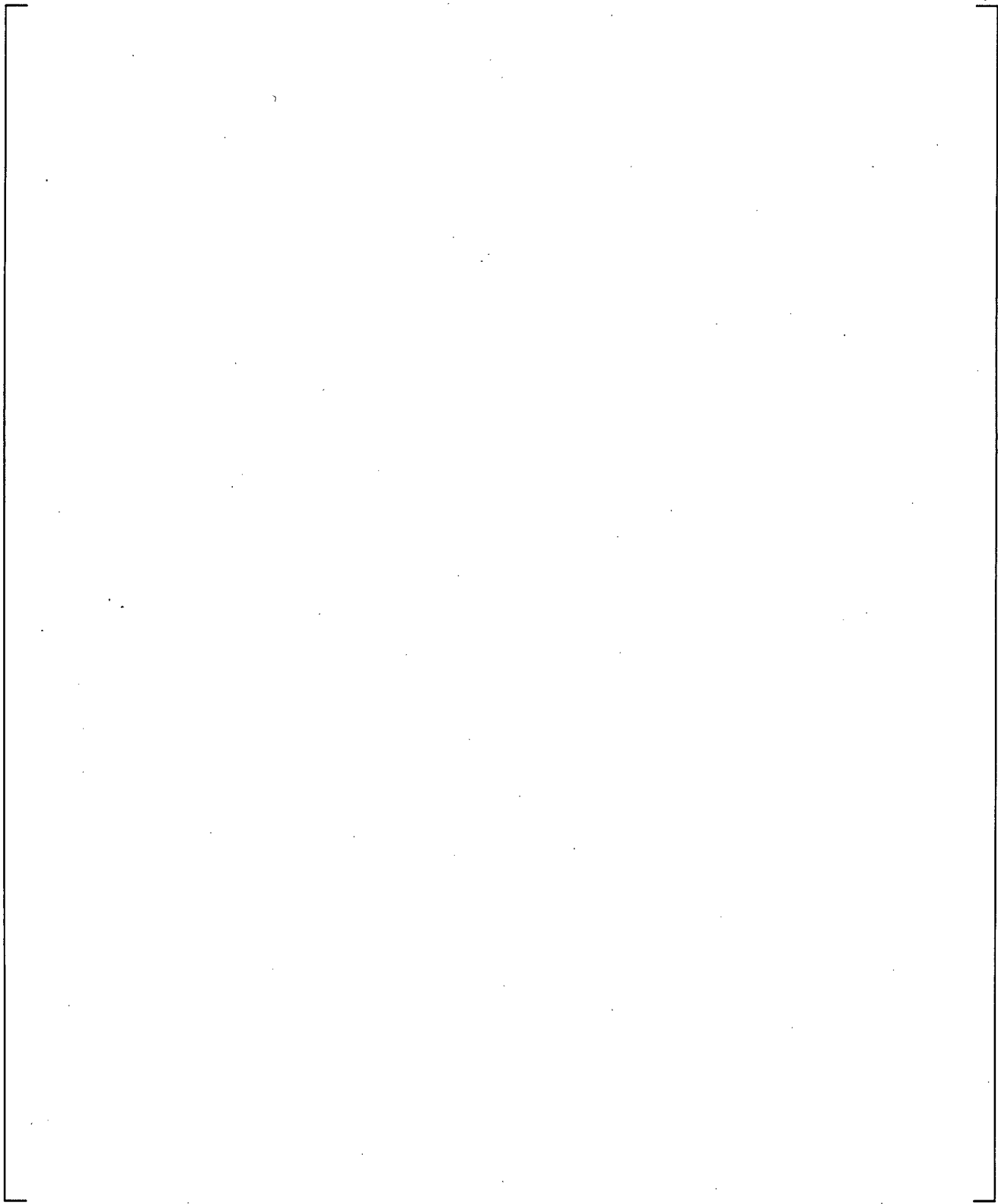


**Figure 23.1.2-16 Semiscale S-07-10D Clad Temperature at Elevation = 208 cm (from the Bottom of the Core)**

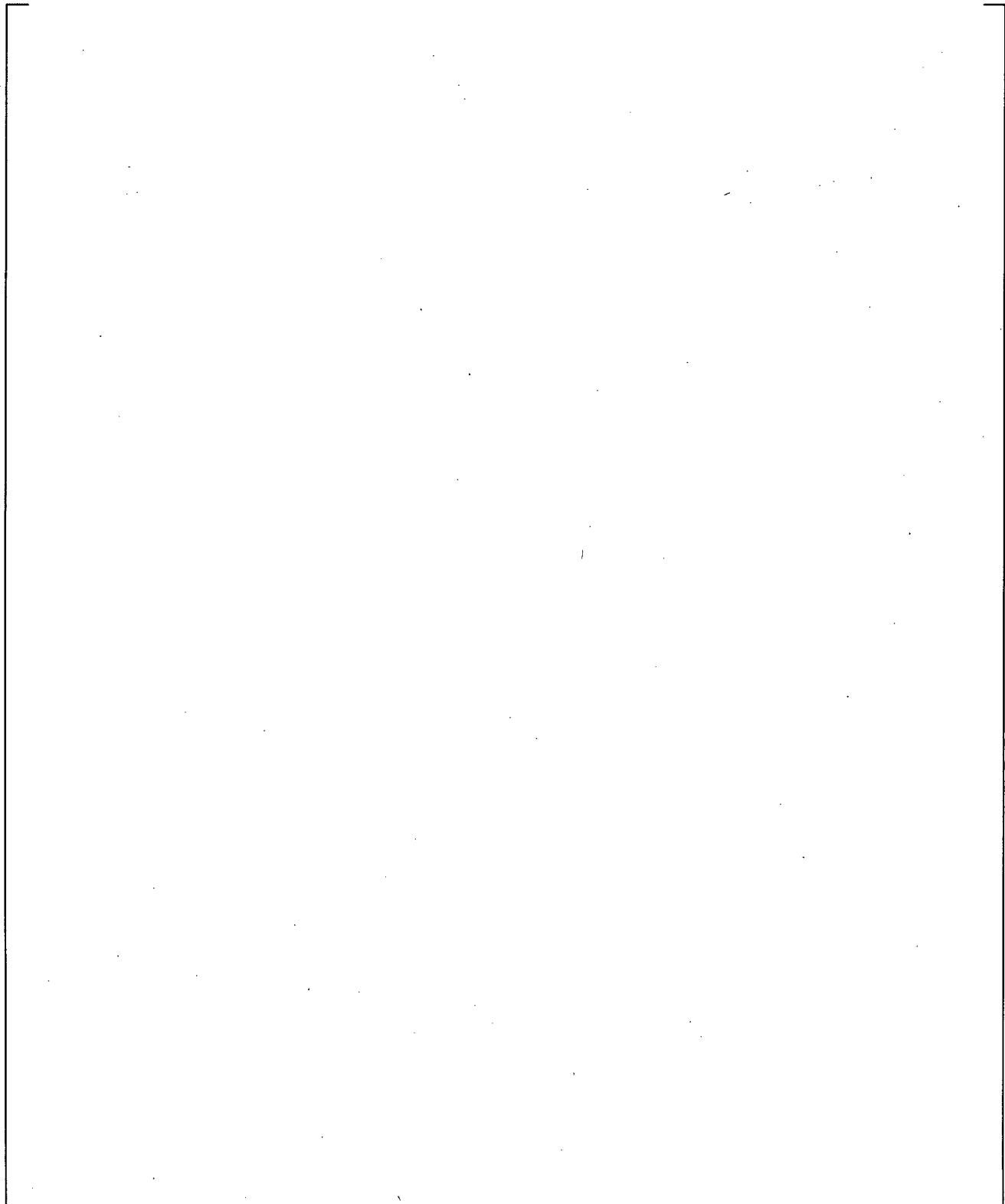


**Figure 23.1.2-17 Semiscale S-07-10D Clad Temperature at Elevation = 190 cm (from the Bottom of the Core)**

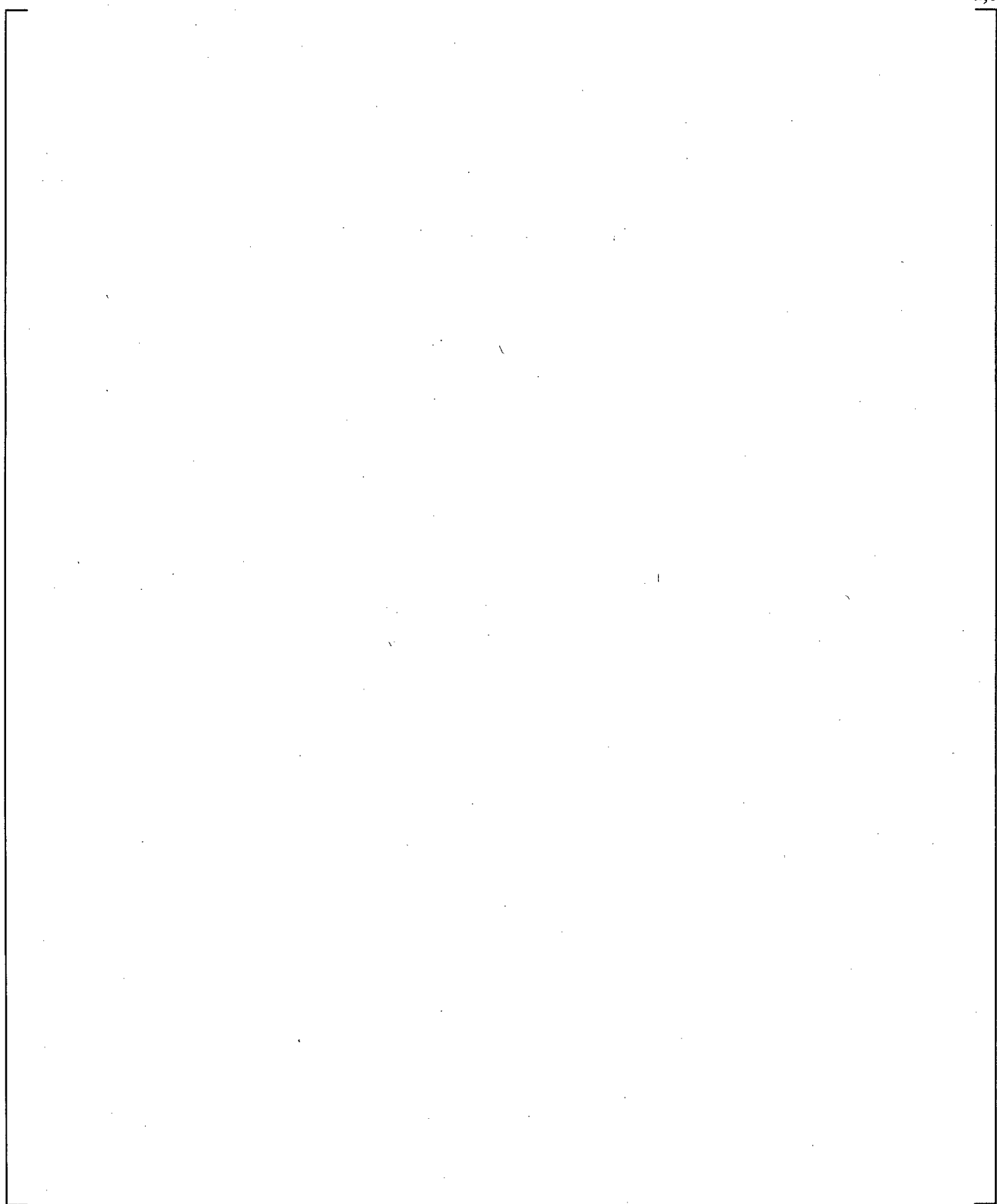


**Figure 23.1.2-18 Semiscale S-07-10D Clad Temperature at Elevation = 181 cm (from the Bottom of the Core)**

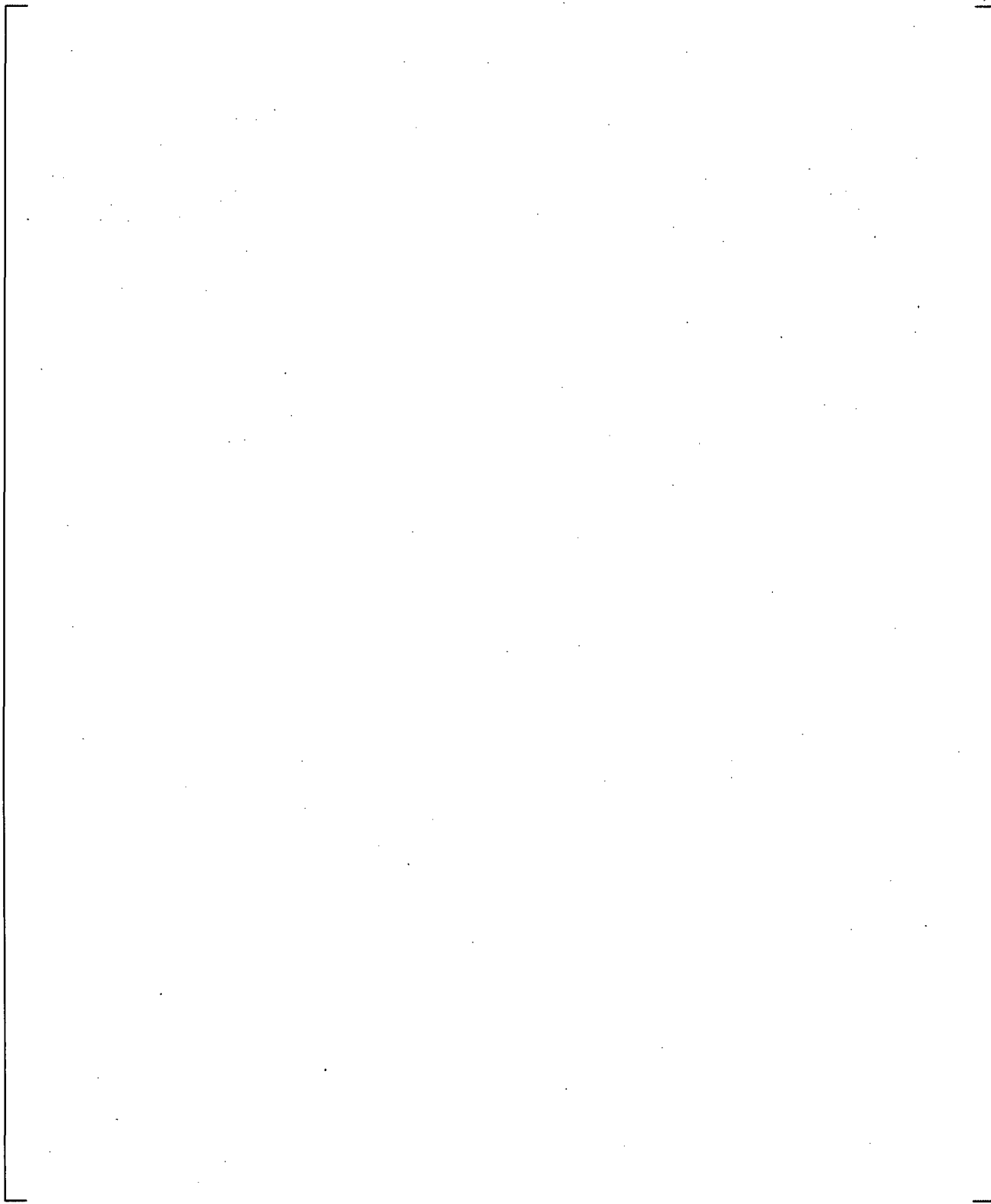


**Figure 23.1.2-19 Semiscale S-07-10D Clad Temperature at Elevation = 167 cm (from the Bottom of the Core)**

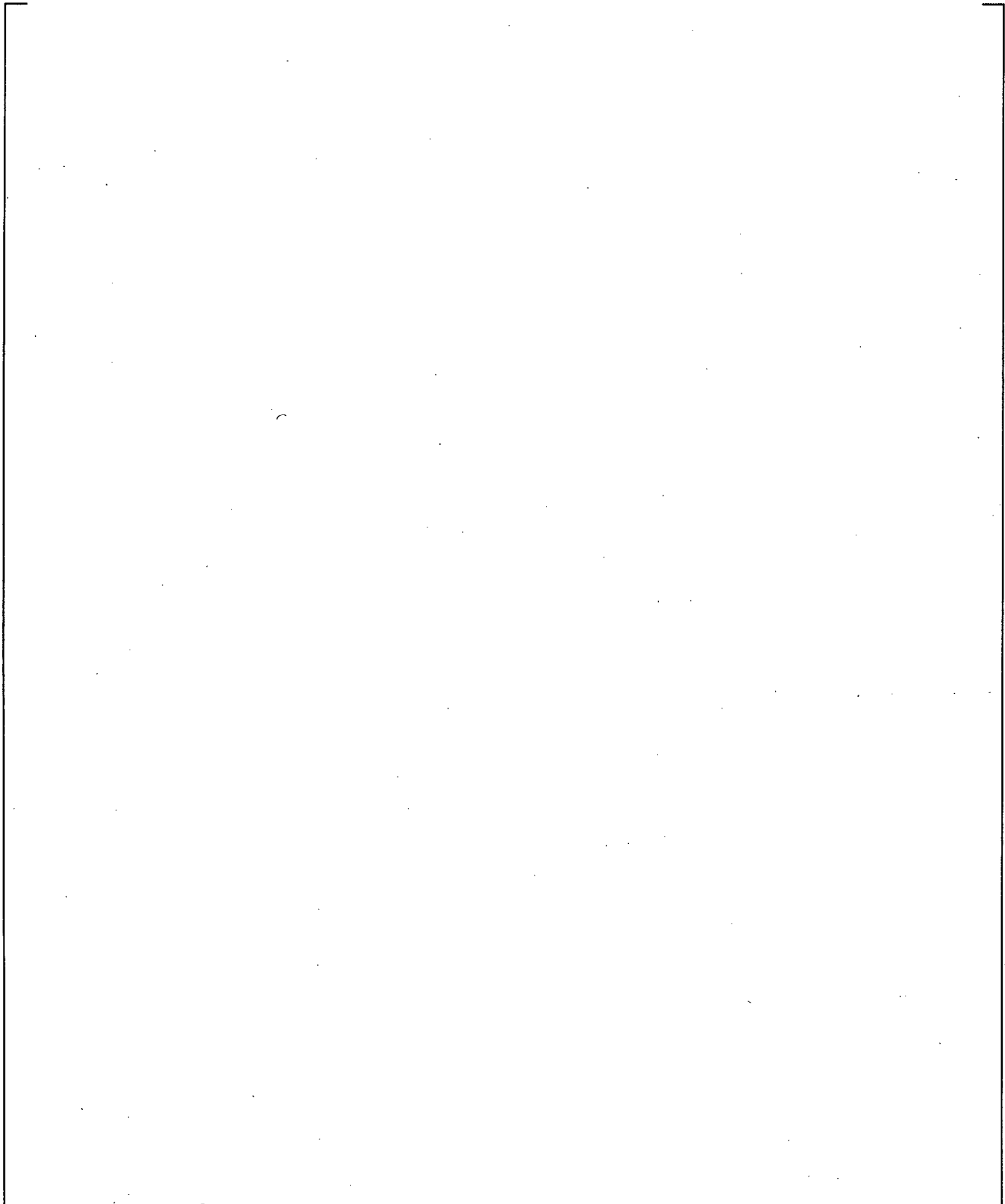


**Figure 23.1.2-20 Semiscale S-07-10D Clad Temperature Elevation = 135 cm (from the Bottom of the Core)**

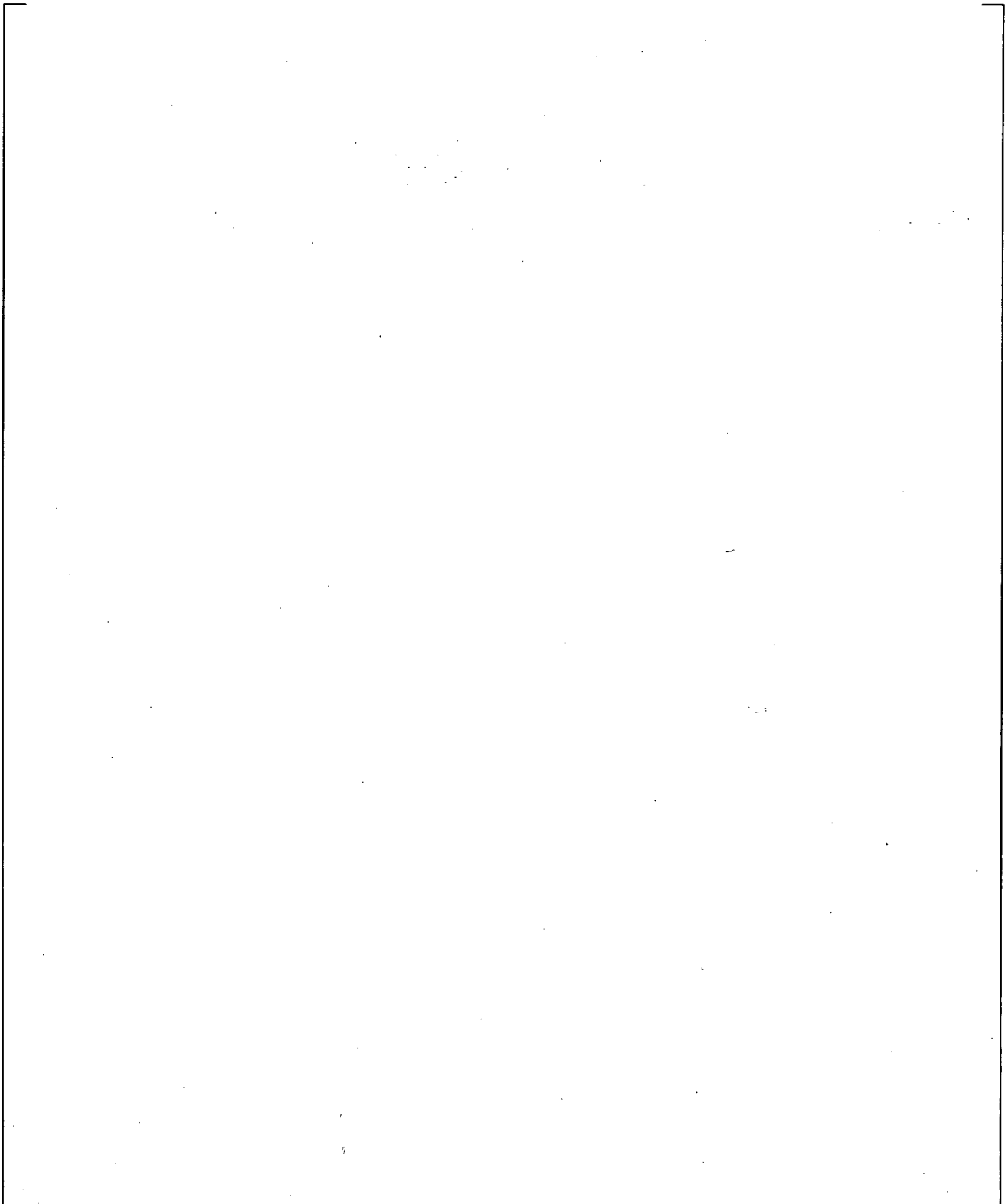


**Figure 23.1.2-21 Semiscale S-07-10D Clad Temperature at Elevation = 112 cm (from the Bottom of the Core)**

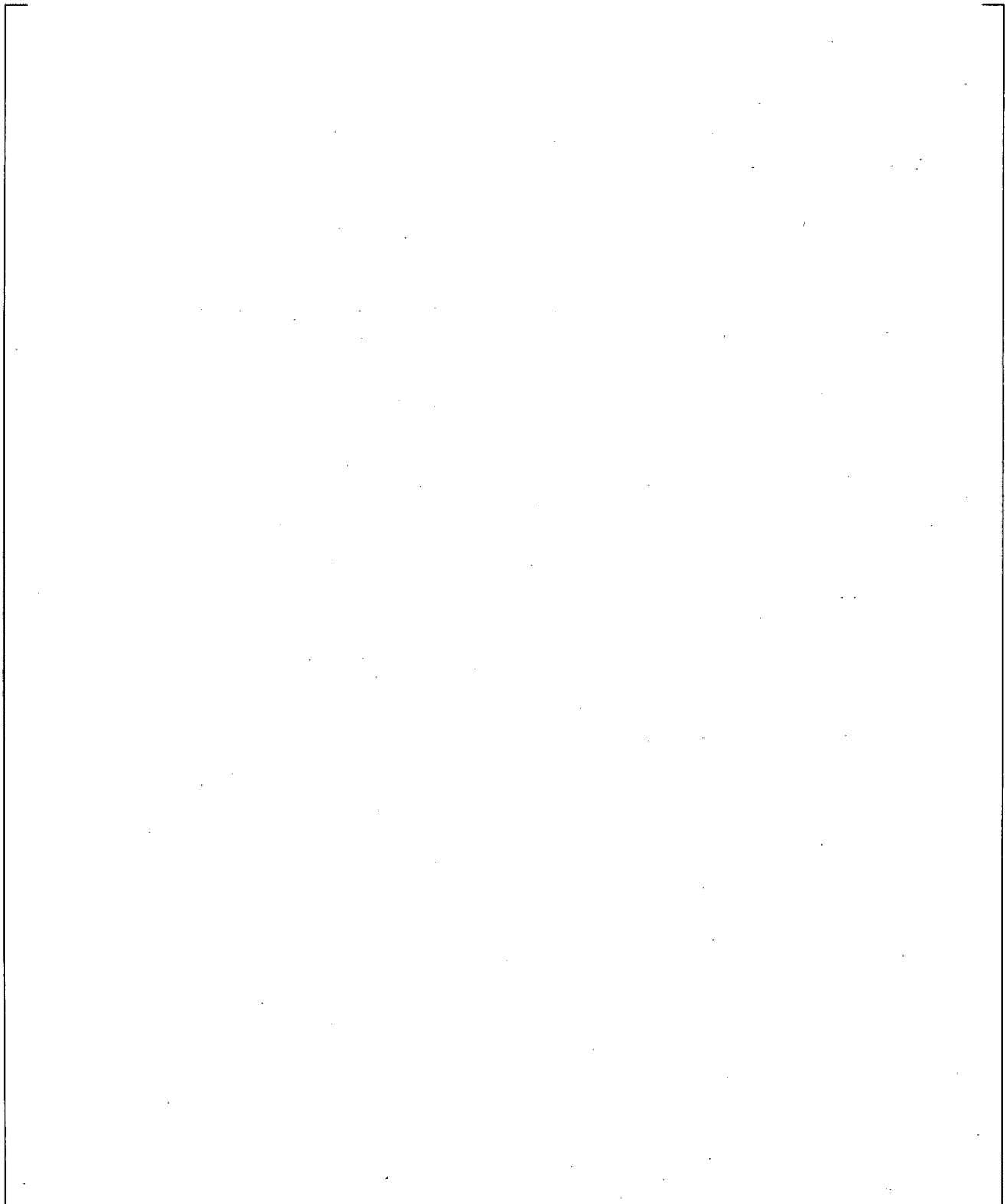


**Figure 23.1.2-22 Semiscale S-07-10D Clad Temperature at Elevation = 71 cm (from the Bottom of the Core)**

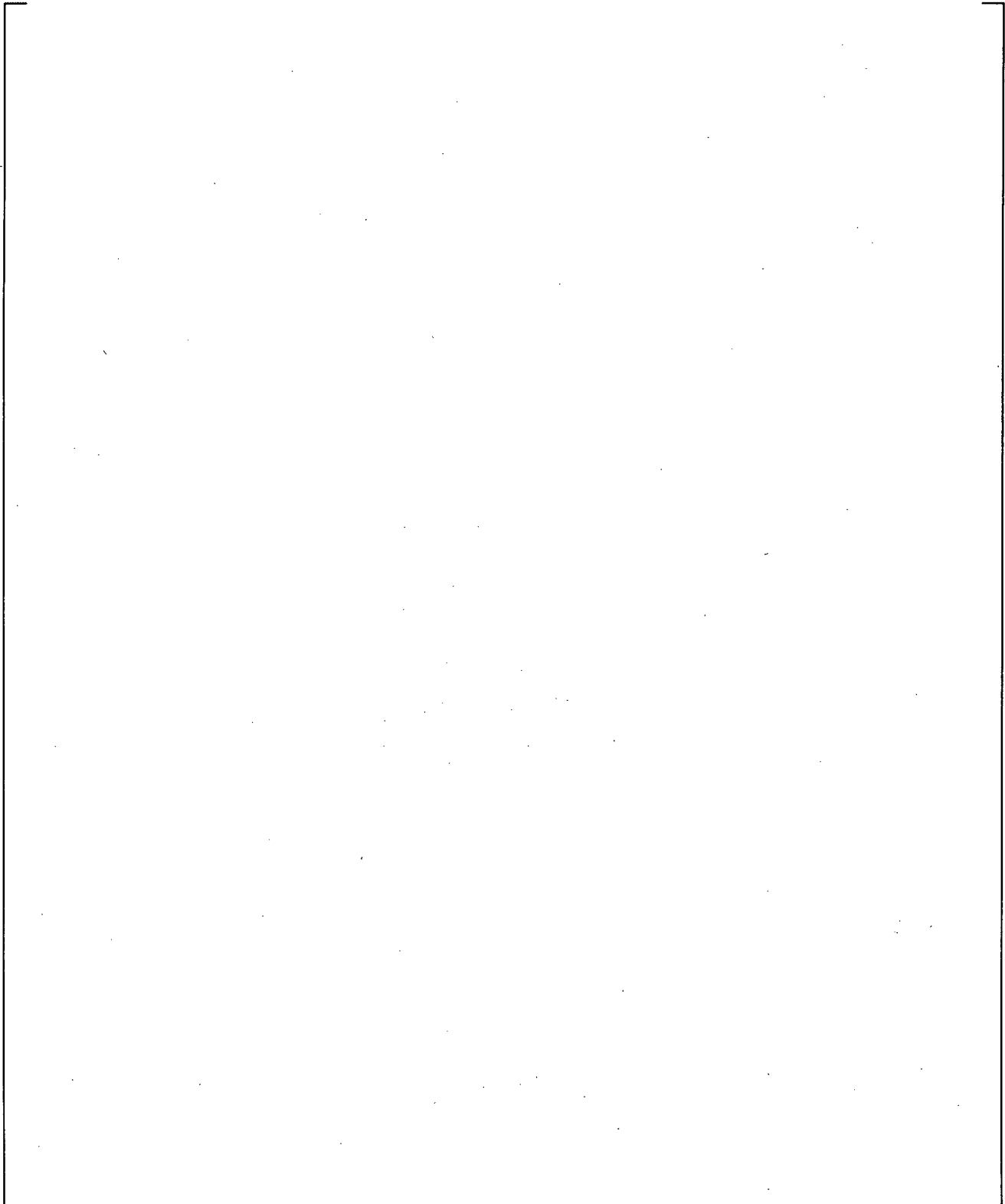


**Figure 23.1.2-23 Semiscale S-07-10D Clad Temperature at Elevation = 48 cm (from the Bottom of the Core)**

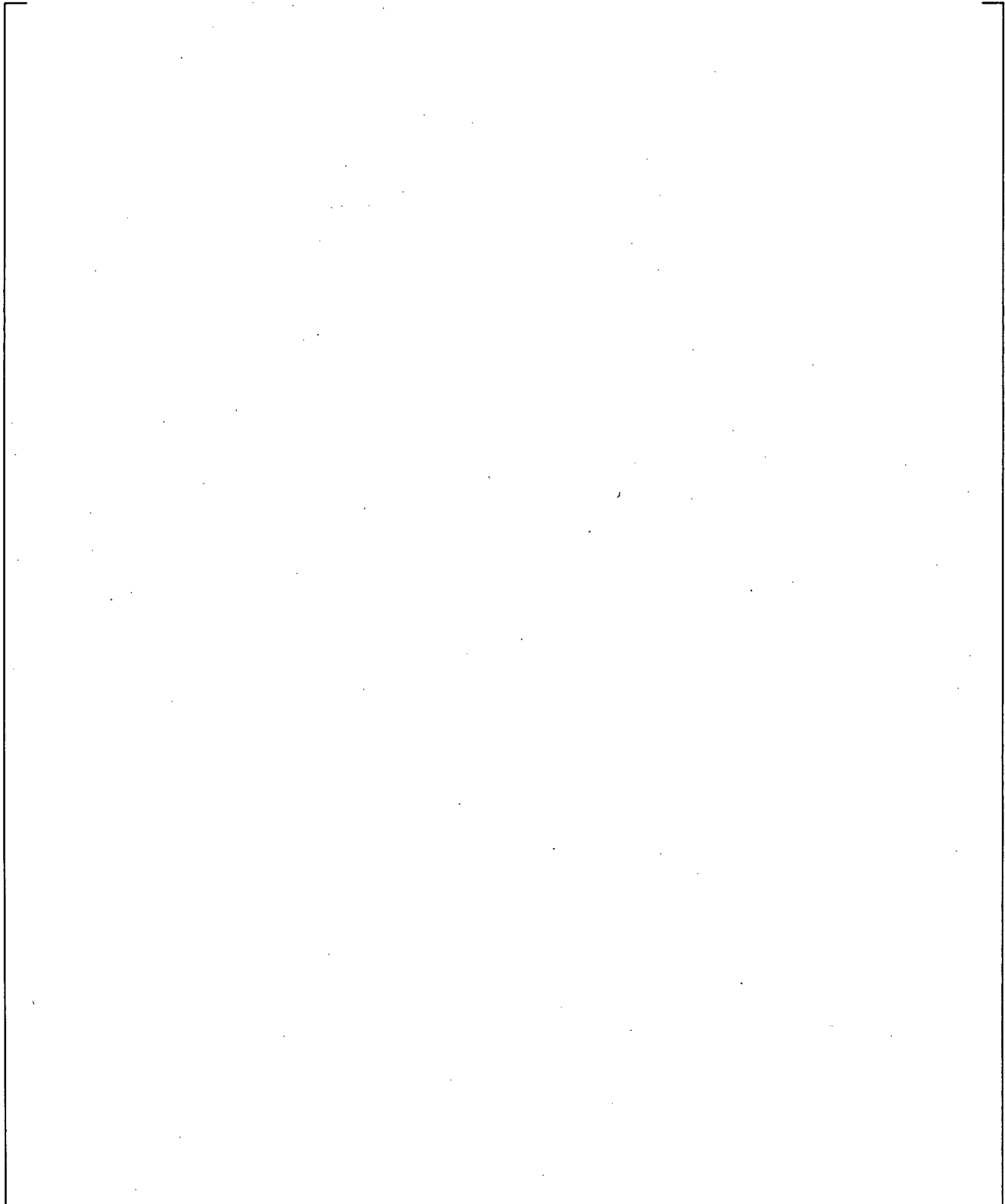


**Figure 23.1.2-24 Semiscale S-07-10D Clad Temperature at Elevation = 7 cm (from the Bottom of the Core)**

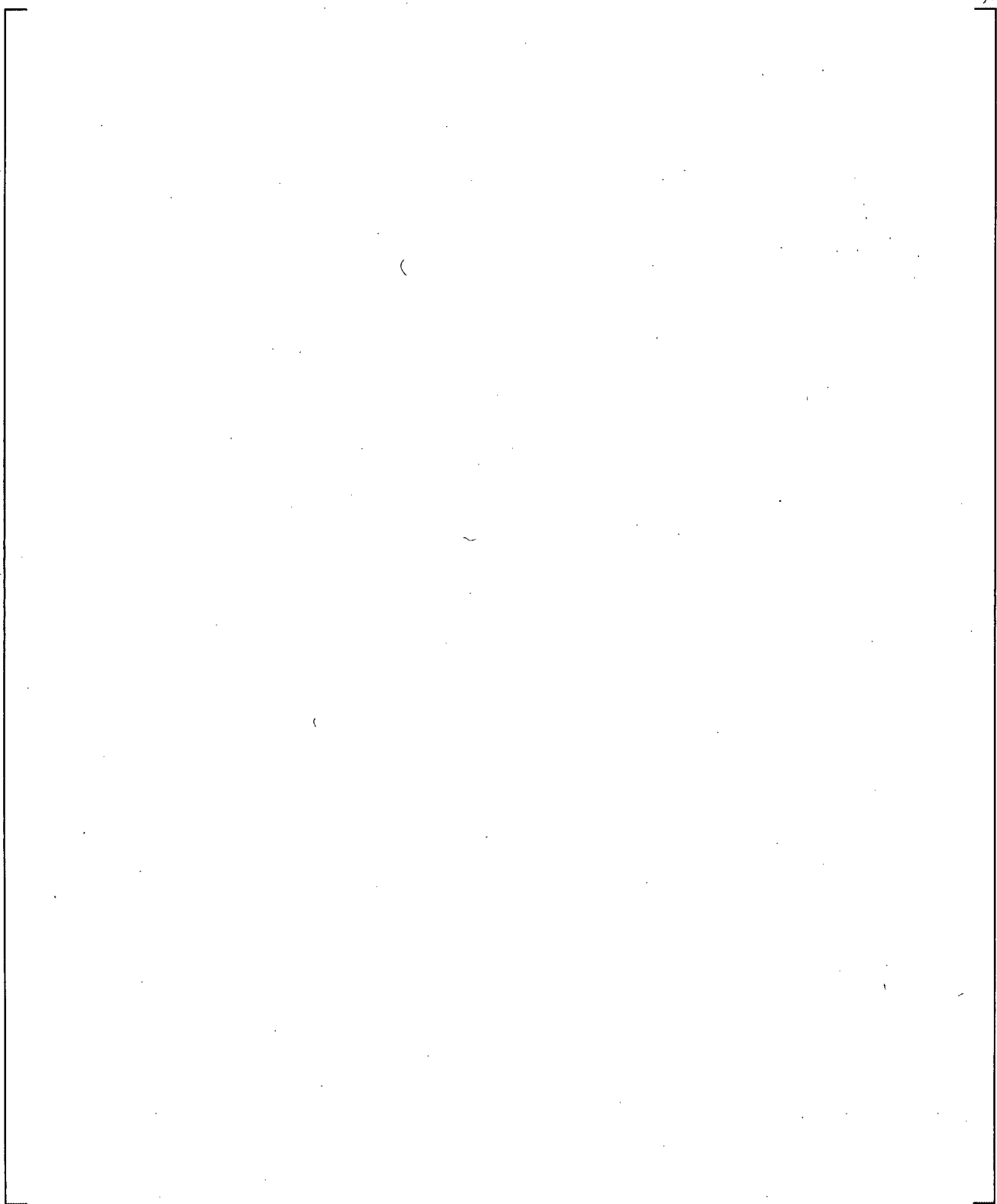


**Figure 23.1.2-25. Semiscale S-07-10D Collapsed Liquid Level**

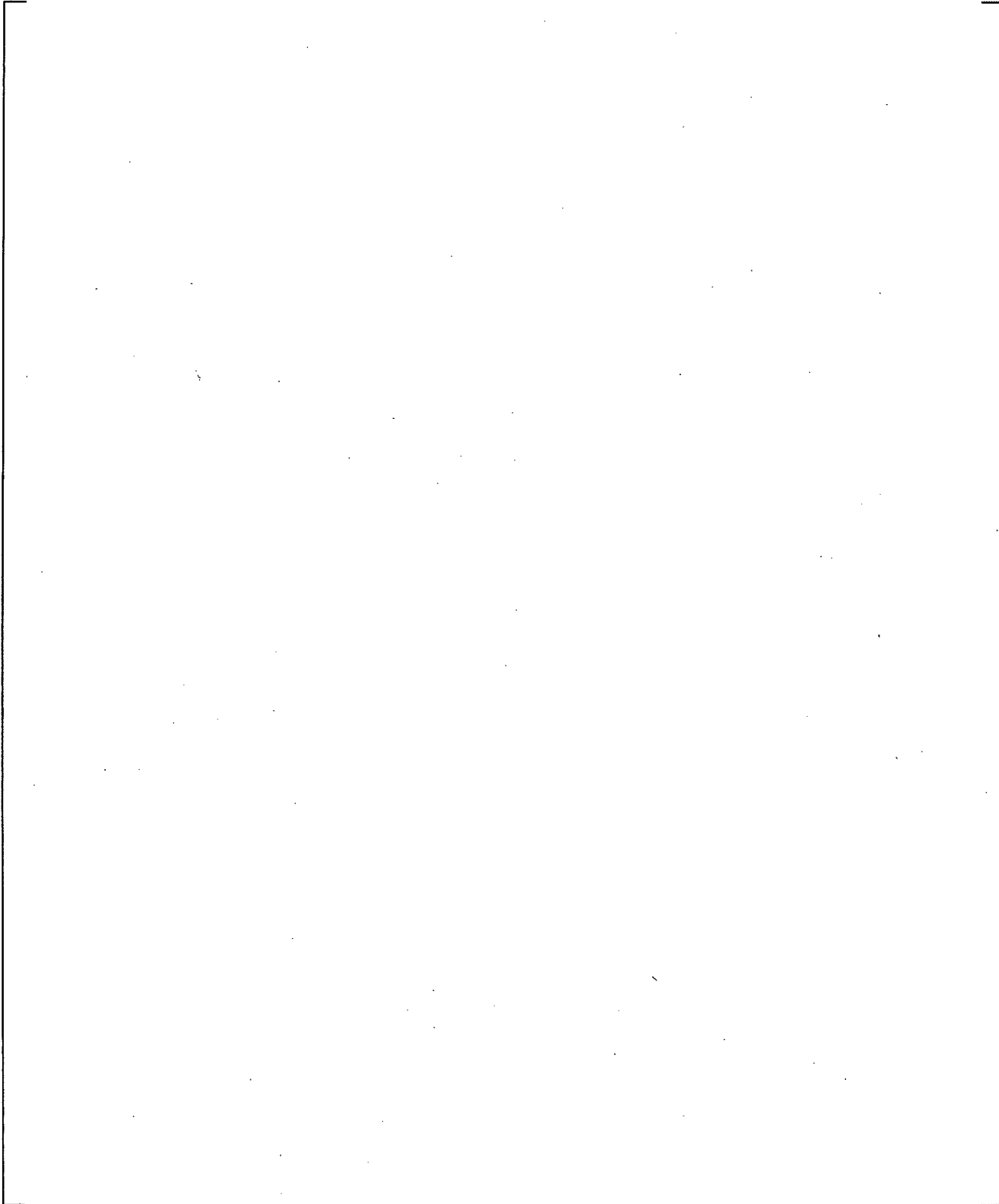


**Figure 23.1.2-26 Semiscale S-07-10D Void Fraction at Inlet of the Core (502 cm below CL Centerline)**

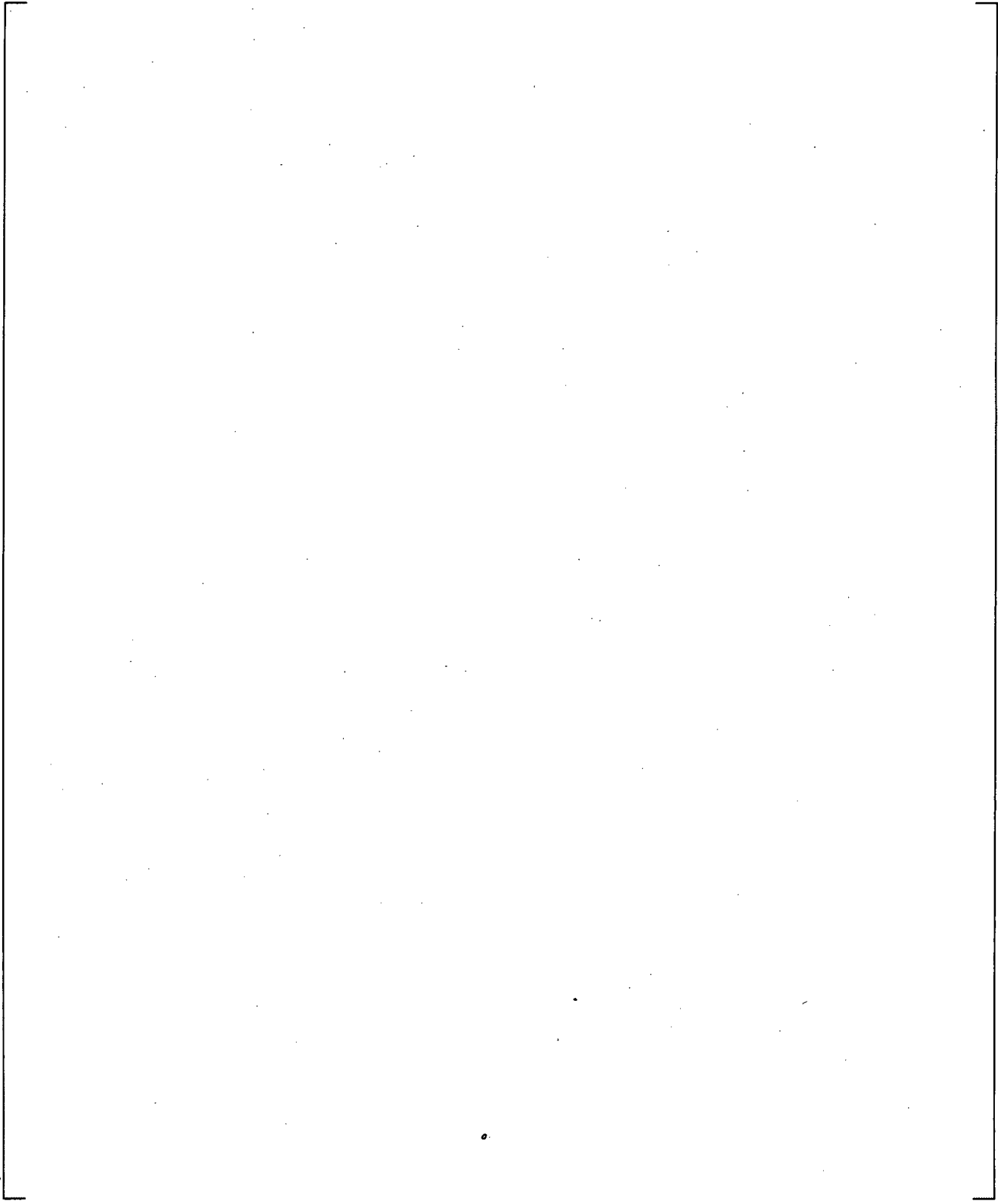


**Figure 23.1.2-27 Semiscale S-07-10D Void Fraction at 483 cm below CL Centerline**

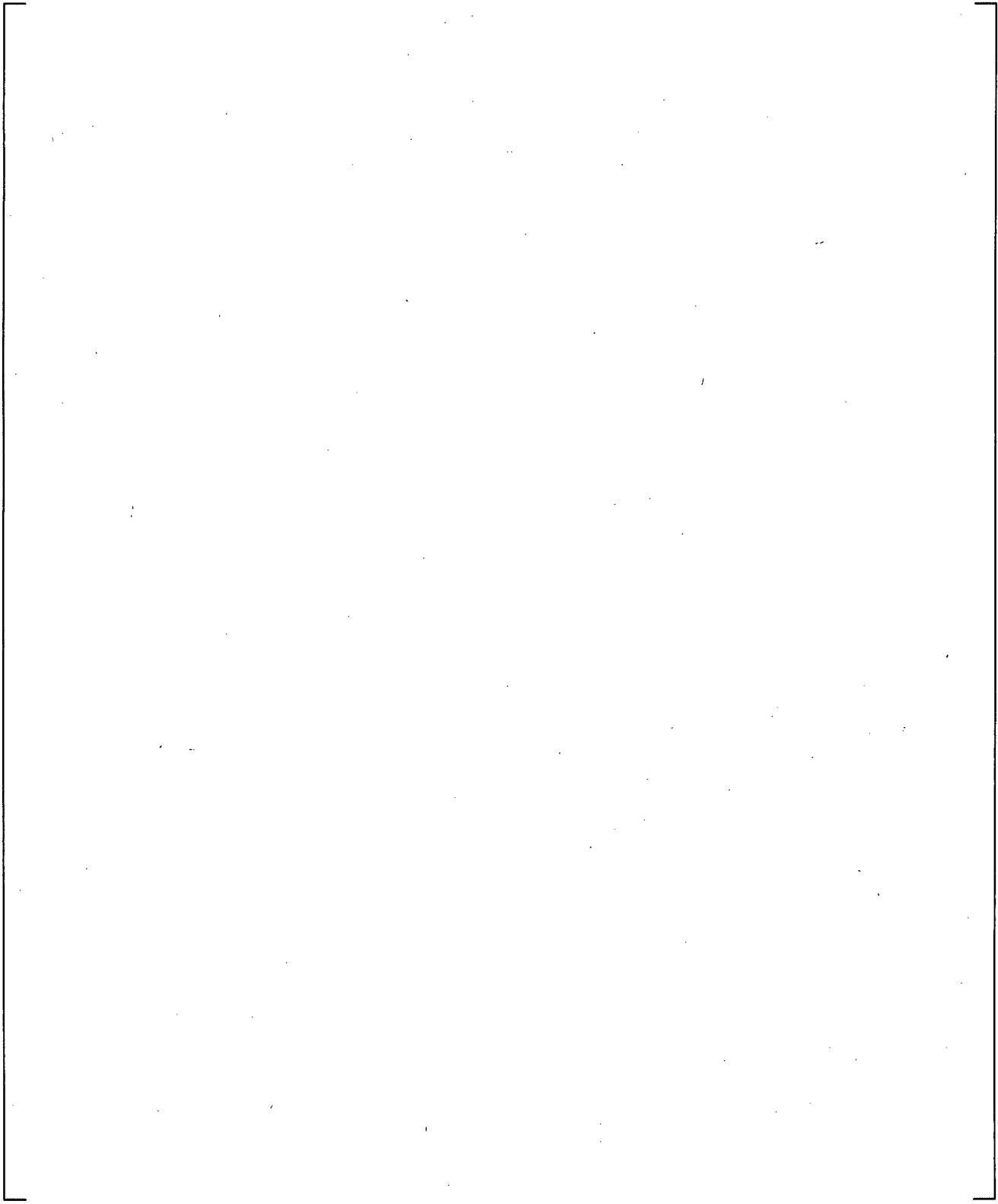


**Figure 23.1.2-28 Semiscale S-07-10D Void Fraction at 323 cm below CL Centerline**

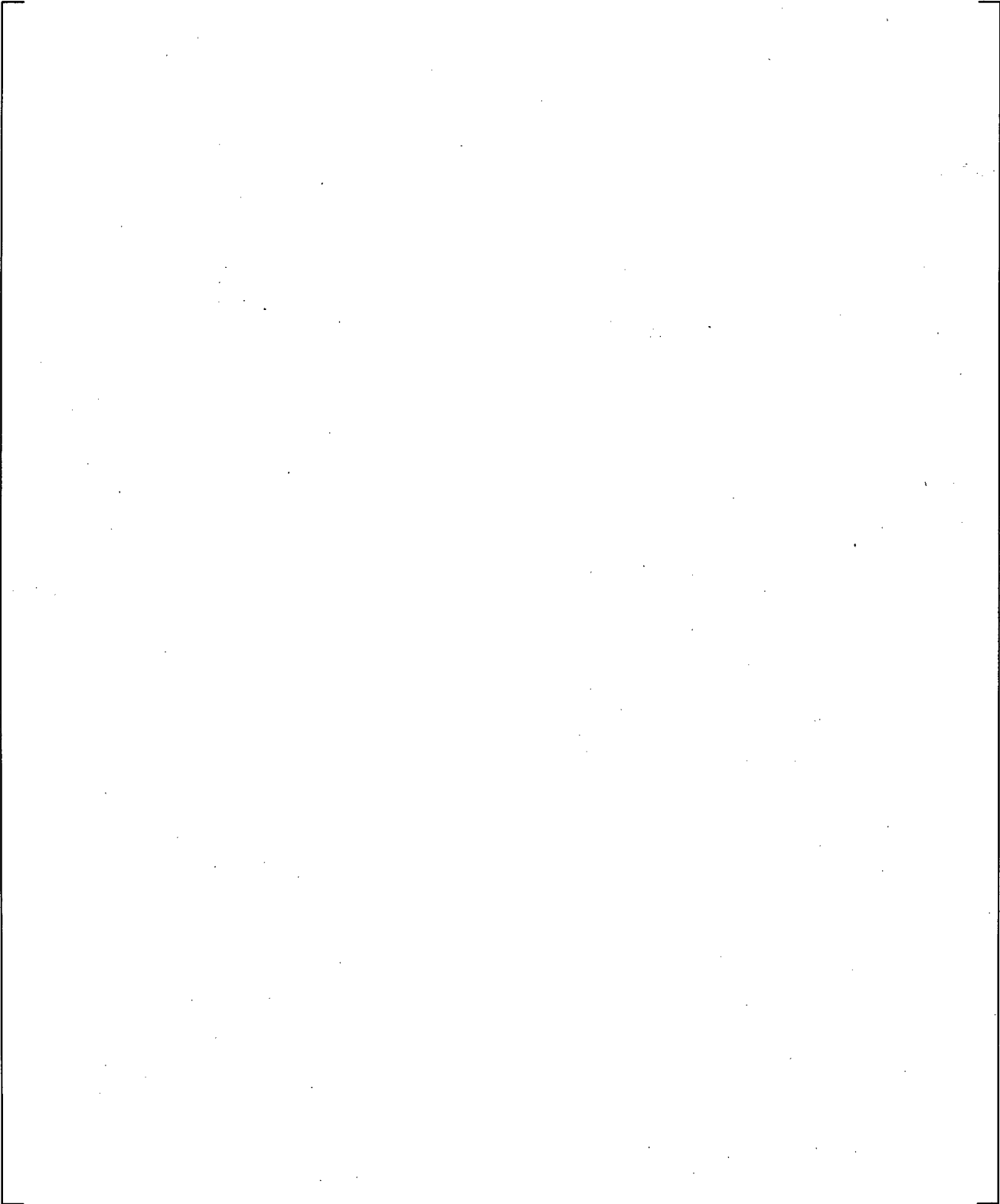


**Figure 23.1.2-29 Semiscale S-07-10D Void Fraction at 313 cm below CL Centerline**

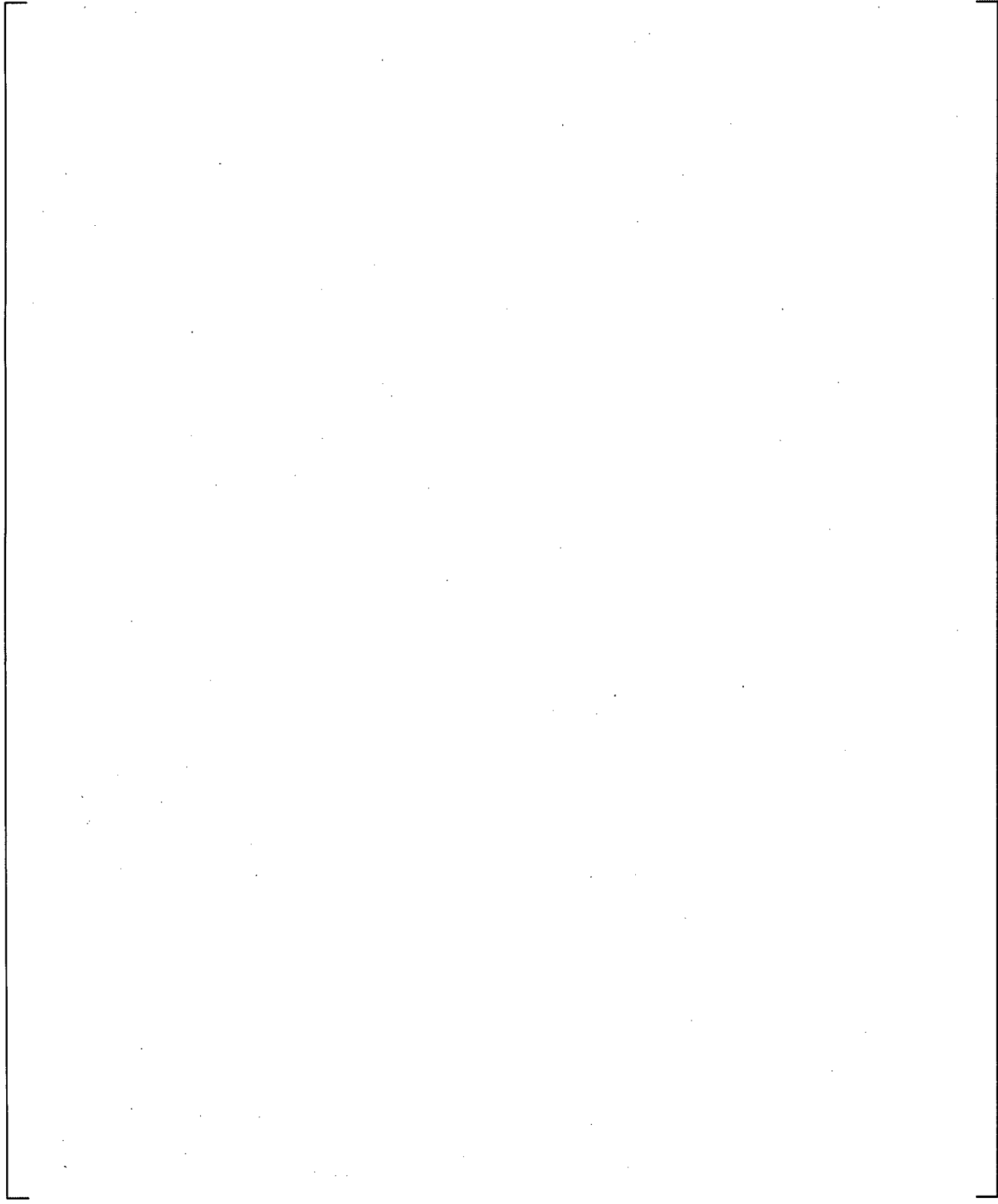


**Figure 23.1.2-30 Semiscale S-07-10D Void Fraction at 243 cm below CL Centerline**

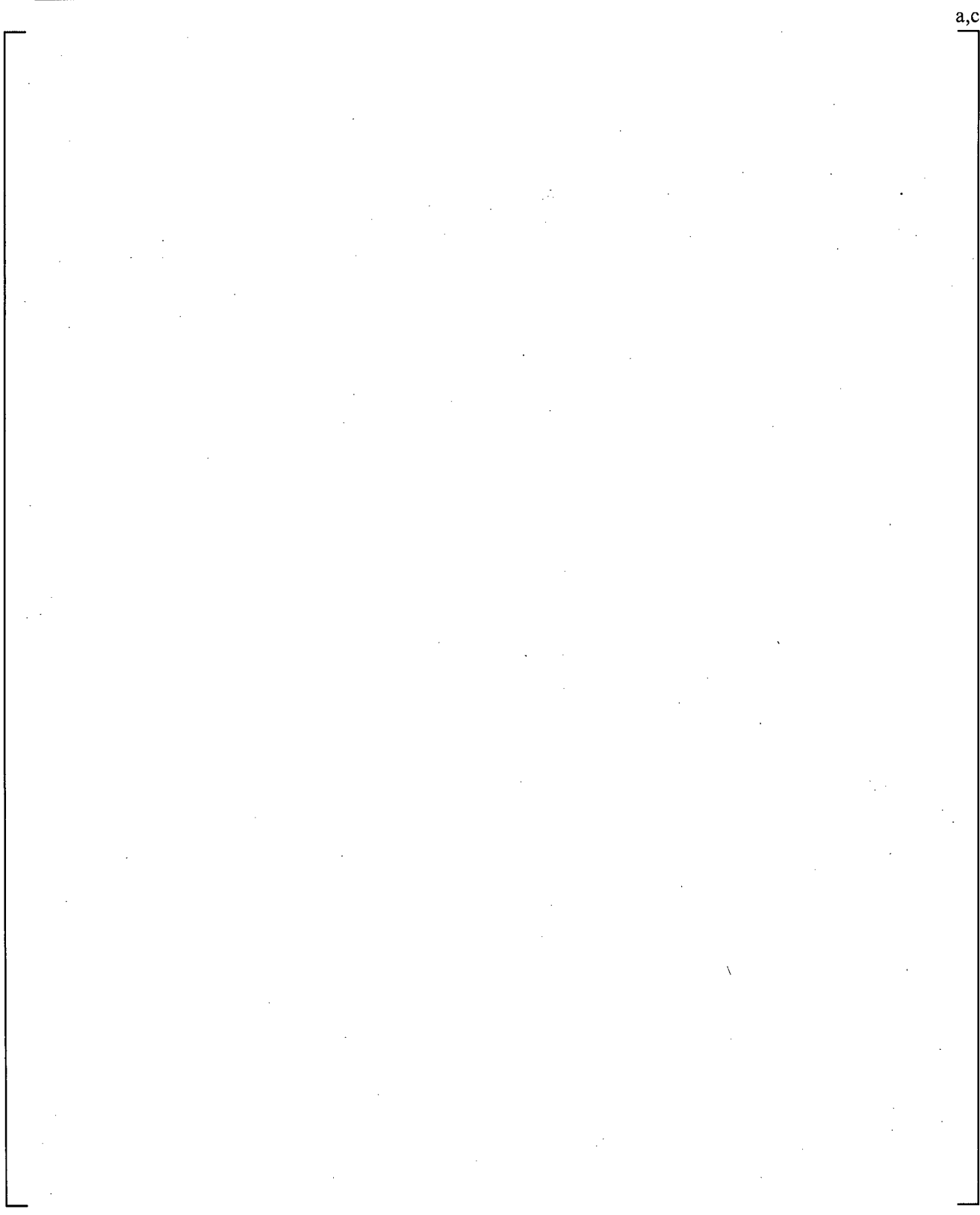


**Figure 23.1.2-31 Semiscale S-07-10D Void Fraction at 164 cm below CL Centerline**

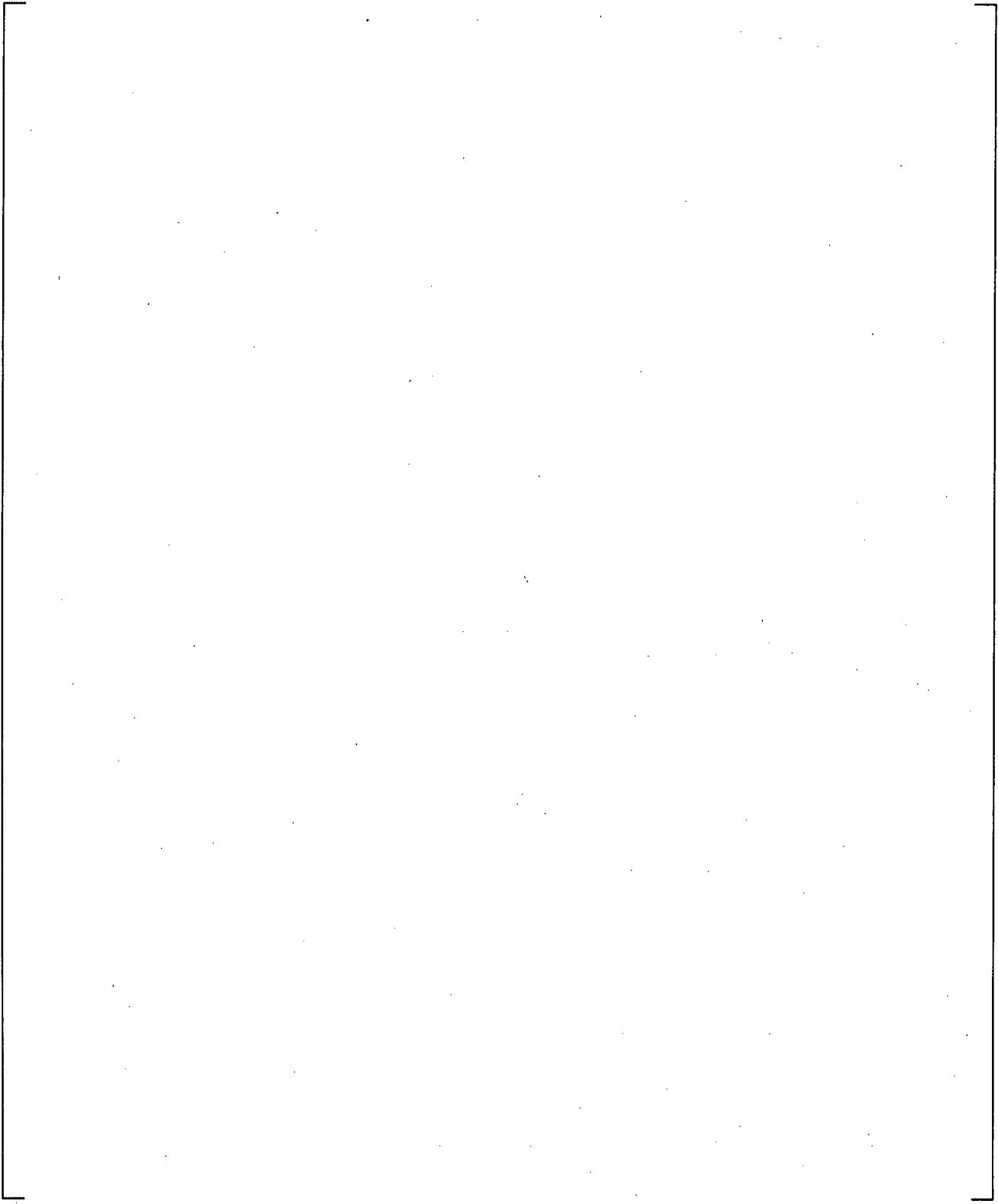


**Figure 23.1.2-32 Semiscale S-07-10D Void Fraction at Core Outlet (11 cm below CL Centerline)**

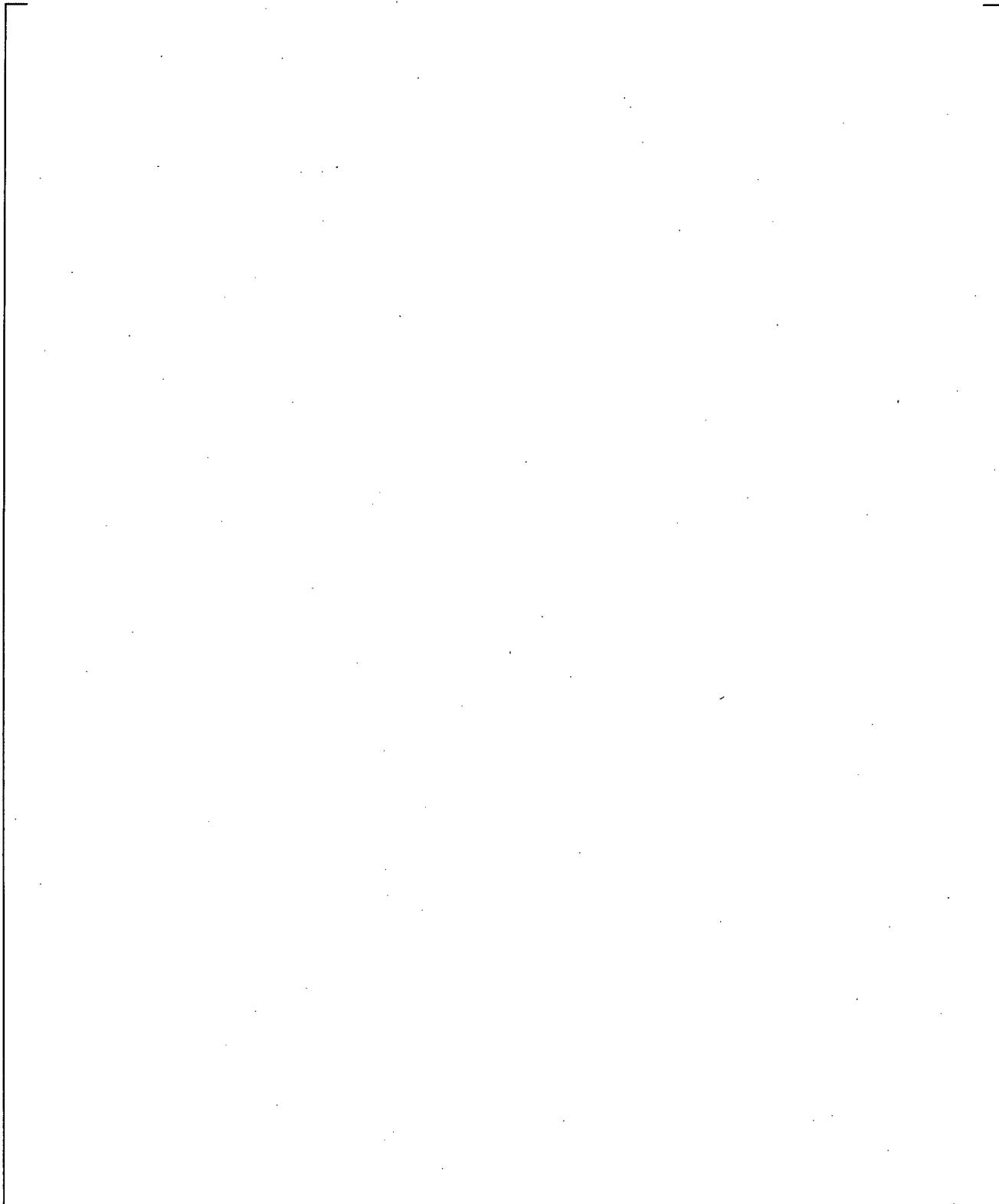


**Figure 23.1.2-33 Semiscale S-07-10D Mixture Level**

## 23.2 NUMERICAL PROBLEMS

### 23.2.1 1D PIPE Manometer Problem with Non-Condensable Gases

#### 23.2.1.1 Introduction

The objective of this problem is to test the ability of the numerical solution method to preserve system mass, which is a constant; to model the period oscillation, which is analytically known; and to evaluate the capability of the numerical discretization scheme to retain the gas-liquid interface. The problem is established as Numerical Benchmark Test No. 2.2 (NBT2.2) in (Hewitt et al., 1992).

#### 23.2.1.2 Problem Description

The apparatus consists of a 'U' tube manometer which is connected at the top, so that a closed system is formed. The system initially contains gas and liquid with the liquid forming equal collapsed liquid levels in each arm of the manometer. Further, all parts of the fluid system have a uniform velocity of 2.1 m/s but zero acceleration. Under these initial conditions, a hydrostatic pressure profile exists throughout the system. Figure 23.2.1-1 is an illustration of the initial state of the manometer system with a superimposed fixed nodalization schematic.

#### 23.2.1.3 WCOBRA/TRAC-TF2 Model

The U-tube manometer is modeled in WCOBRA/TRAC-TF2 as a 1D pipe consisting of 20 cells. The pipe junctions are connected at the top via a secondary pipe to form a closed loop. Ten of the cell interface boundaries are oriented downward, one horizontal at the bottom and the remaining 10 as upward. Each cell has a length of 1.0 m and a hydraulic diameter of 1.0 m. The initial liquid velocity in the pipe is set to 2.1 m/s as prescribed in (Hewitt et al., 1992). The top 5 cells of each leg of the pipe are initially void (vapor), whereas the remaining part is filled with subcooled liquid at 323.15K (50°C). The gas volume is filled with non-condensable gas to eliminate the complication of interfacial heat and mass transfer. The problem is assumed to be frictionless. The lower and upper limits to time step size are set to  $1.0 \times 10^{-6}$  s and  $5.0 \times 10^{-3}$  s, respectively.

#### 23.2.1.4 Numerical/Analytical Solution

In the absence of friction, the oscillating motion of a liquid in a 'U' tube obeys the following equation:

$$\frac{d^2x}{dt^2} + 2gx/L = 0$$

The problem has a solution for the velocity at the bottom of the manometer as an un-damped cosine wave with amplitude equal to the initial perturbation velocity (from Hewitt et al., 1992).

$$v = \frac{dx}{dt} + v_o \cdot \cos(2g/L)^{1/2}$$

$$\text{Period} = 2\pi \sqrt{\frac{L}{2g}} = 4.255\text{s}$$

where:

- x = elevation (position) of water level.
- L = length of the water column.
- v = velocity of the water column.
- g = acceleration due to gravity.

### 23.2.1.5 WCOBRA/TRAC-TF2 Assessment

Figure 23.2.1-2 shows the liquid velocity at the bottom of the U-tubes and Figure 23.2.1-3 shows the liquid mass in the left and right legs and the system total. The period of oscillations shows good agreement with the analytical solution ([ ]<sup>a,c</sup> compared with 4.255 seconds) and the total mass in the system is preserved. The results show that numerical viscosity has some impact, albeit small, as evidenced by the slight damping; a reduction in amplitude is observed over time.

As discussed in Section 2.2 of NBT2.2 in (Hewitt, et al., 1992), truncation errors due to finite difference equations are not necessarily zero for this problem, depending on the degree of implicitness in the mass and momentum solution. "Too implicit" schemes will cause false (numerical) damping, "too explicit" schemes will amplify the oscillations over time, and time-centered solution schemes will show no damping. Figure 23.2.1-2 shows that the 1-D module of WCOBRA/TRAC-TF2 exhibits behavior typical of a semi-implicit code, less damped than a fully implicit scheme (see Figure 3 in Section 2.2 of NBT2.2) and more damped than the undamped solution from a time-centered scheme (see Figure 5 in Section 2.2 of NBT2.2).

### 23.2.1.6 Summary and Conclusions

The U-tube manometer problem has been modeled with a 1D pipe component. Results show slight damping, indicating the presence of a small numerical viscosity (diffusion) as a result of the semi-implicit numerical scheme. However the code is in general able to resolve this problem well and good agreement is seen relative to the analytical solution, comparable to other semi-implicit codes presented in (Hewitt et al., 1992).

### 23.2.1.7 References

1. Hewitt, G.F., Delhay, J.M., Zuber, N., "Multiphase Science and Technology," Vol.6, 1992.

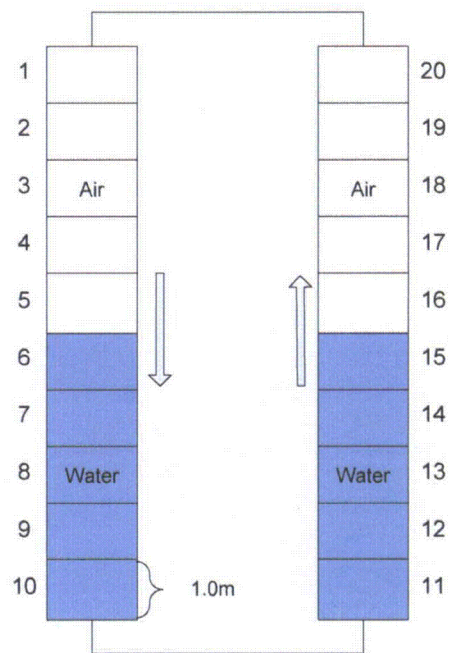
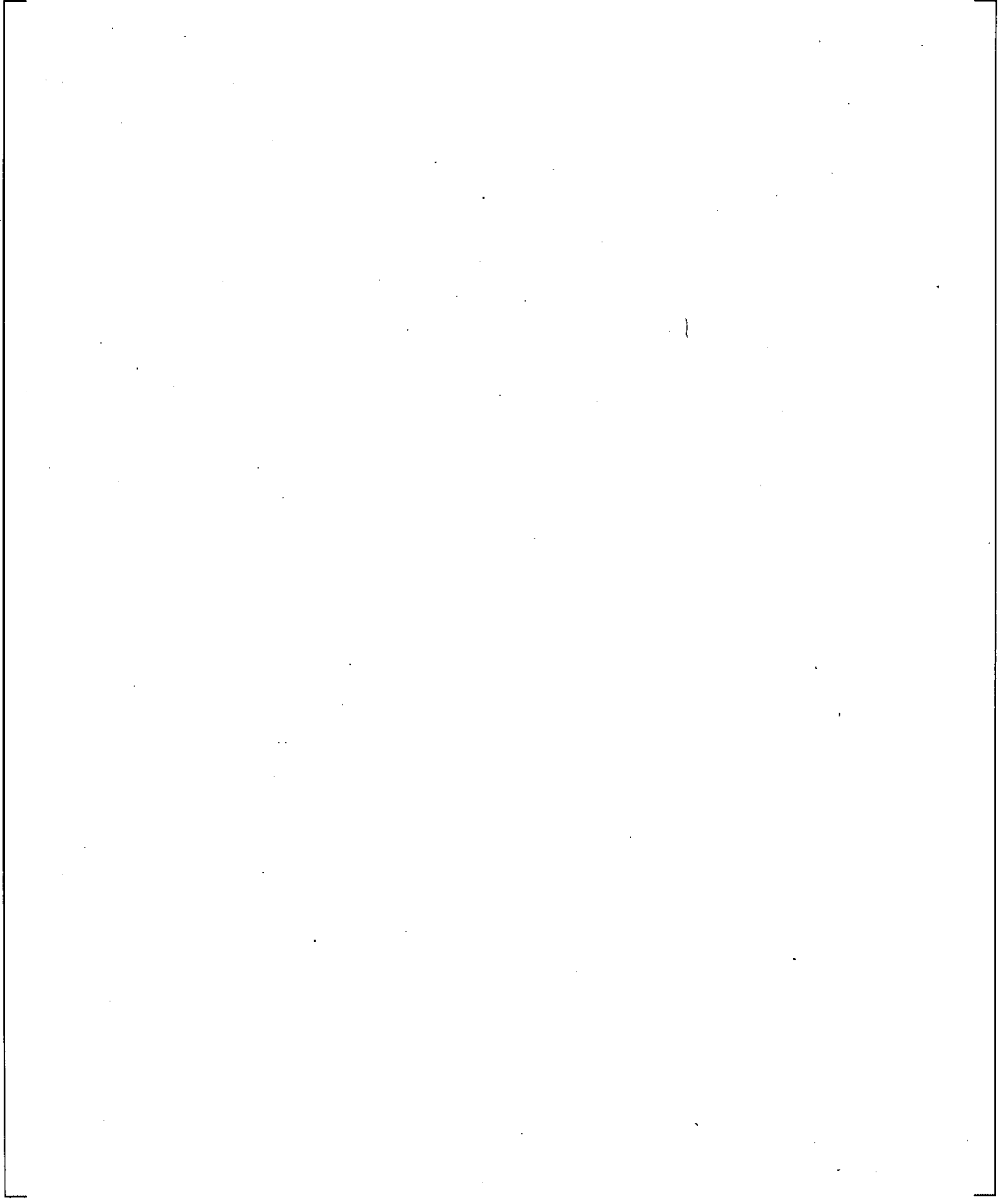


Figure 23.2.1-1

**Schematic and Nodalization Diagram for the Oscillating Manometer (note that Nodes 1 and 20 are each Connected to a PIPE Component not Depicted in the Diagram)**

a,c



**Figure 23.2.1-2 WCOBRA/TRAC-TF2 Results for Liquid Velocity at the Bottom of the Tube**

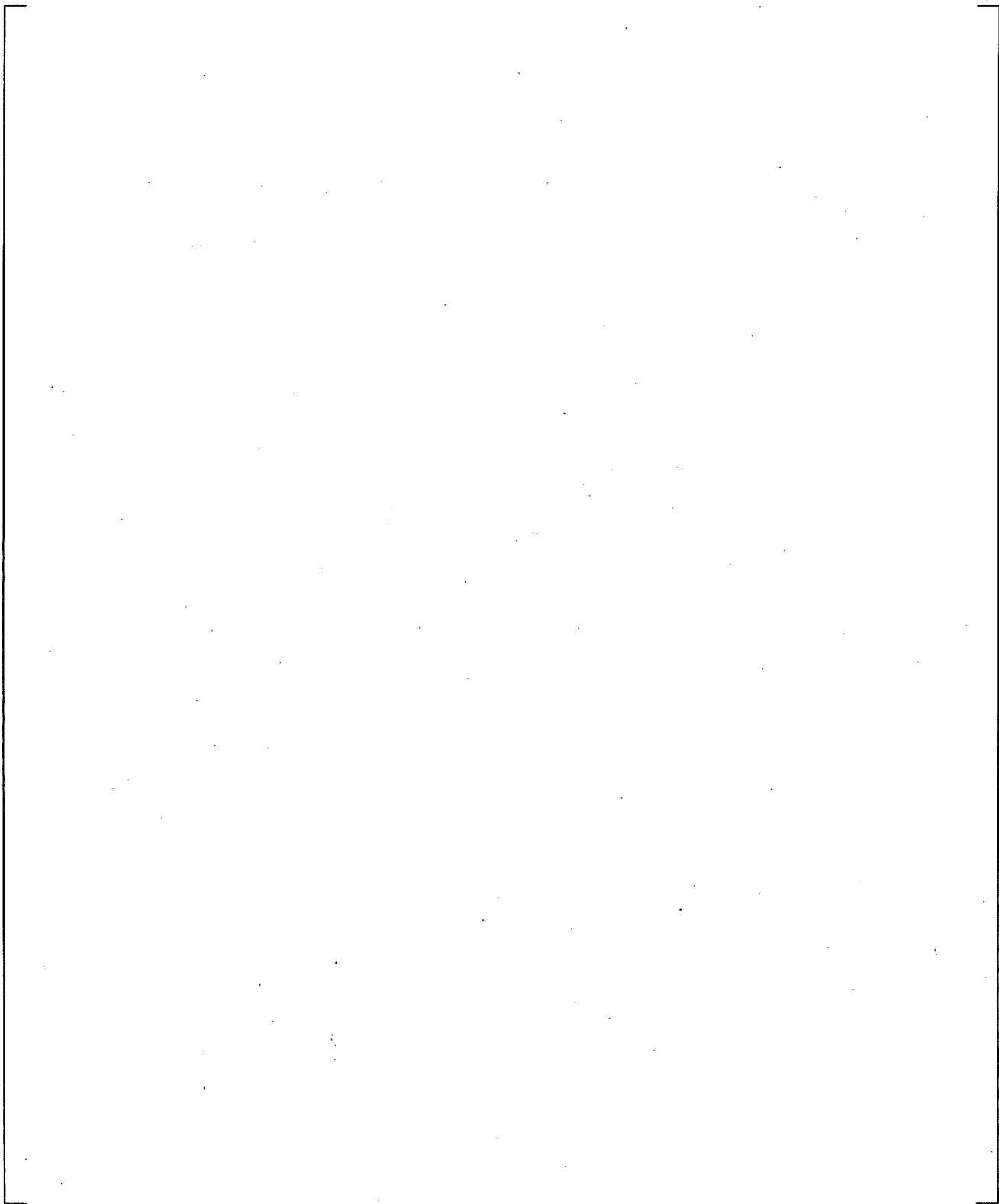


**Figure 23.2.1-3 WCOBRA/TRAC-TF2 Results for Liquid Velocity at the Bottom of the Tube**

## 23.2.2 3D VESSEL Manometer Problem with Non-Condensable Gases

### 23.2.2.1 Introduction

The objective of this problem is identical to that discussed in Section 23.2.1.1, with the only difference that the 3D VESSEL is tested here.

### 23.2.2.2 Problem Description

See Section 23.2.1.2. Here, since the VESSEL component cannot be initialized with liquid velocities, an elevation difference between the two sides of the manometer is applied at the beginning of the transient.

### 23.2.2.3 WCOBRA/TRAC-TF2 Model

The U-tube manometer is modeled in WCOBRA/TRAC-TF2 using a 2 channel VESSEL component. The channels have 10 axial nodes each, with 1.0m height and 1.0m hydraulic diameter. The channels are connected via a 1.0m long gap at the bottom. Initially, one leg of the manometer is filled with subcooled liquid up to the 7th axial node, and the other leg to the 5th. A 1D pipe is attached to the vessel component at the top of the channels providing a closed loop system. A zero velocity boundary condition is prescribed at the channel top and bottom faces. The gas volume is filled with non-condensable gas to eliminate the complication of interfacial heat and mass transfer. Figure 23.2.2-1 is an illustration of the initial state of the manometer system with a superimposed fixed nodalization schematic.

### 23.2.2.4 Numerical/Analytical Solution

See Section 23.2.1.4; the analytical solution is applicable here as well. See Section 23.2.1.5 for a discussion of the effects of the numerical solution scheme on the observed damping.

### 23.2.2.5 WCOBRA/TRAC-TF2 Assessment

Figure 23.2.2-2 shows the velocity at the bottom of 3D Vessel manometer, while Figure 23.2.2-3 shows the collapsed liquid levels in the two legs as well as the total system fluid mass. [

]<sup>a,c</sup>

As a result of the noding, shown in Figure 23.2.2-1, the flowpath of a liquid particle through the bottom of the manometer consists of a downward flow within a channel (1) to a dead-end cell, purely horizontal flow through a gap to a second channel (2), and then upward flow from a dead-end cell in the new channel (2). The deceleration of downward flow results in a calculated irreversible loss equal to the dynamic pressure, as does the acceleration to create upward flow. The implied loss coefficient is then

$$K = \frac{\Delta P}{\frac{1}{2}\rho V^2} = \frac{2 \cdot \left[ \frac{1}{2}\rho V^2 \right]}{\frac{1}{2}\rho V^2} = 2 \quad (23-1)$$

[ ]<sup>a,c</sup>

### 23.2.2.6 Summary and Conclusions

Manometric oscillations in the downcomer and core are evident during early reflood following a large break LOCA. Such is observed in integral effects tests (CCTF, see Section 19.6). Downcomer and lower plenum nodding for the plants and integral effects tests are similar to the 3-D manometer nodding in that downcomer channels are connected to the lower plenum through gaps in the lower cell(s). In the plant, external pressure forces act in addition to gravity as the liquid accumulation in the downcomer is opposed by vapor generation in the core and the consequent pressurization of the upper plenum and upper head regions. Evidenced by the CCTF simulations in Section 19.6, the oscillatory behavior in the plant case is captured adequately.

The oscillatory core injection on the reflood is expected to cause increased cooling (Oh et al., 1983). The expected improvement in cooling is [

] <sup>a,c</sup>

### 23.2.2.7 References

1. S. Oh, S. Banerjee, and G. Yadigaroglu, "The Effect of Inlet Flow Oscillations on Reflooding of a Tubular Test Section," Thermal Hydraulics of Nuclear Reactors, Volume 1, pg. 674-680. Presented at The Second International Topical Meeting on Nuclear Reactor Thermal-Hydraulics, Santa Barbara CA, USA, 1983.

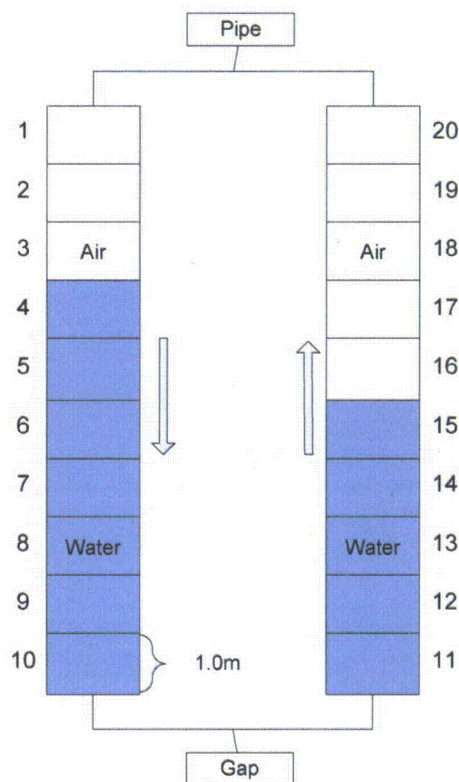
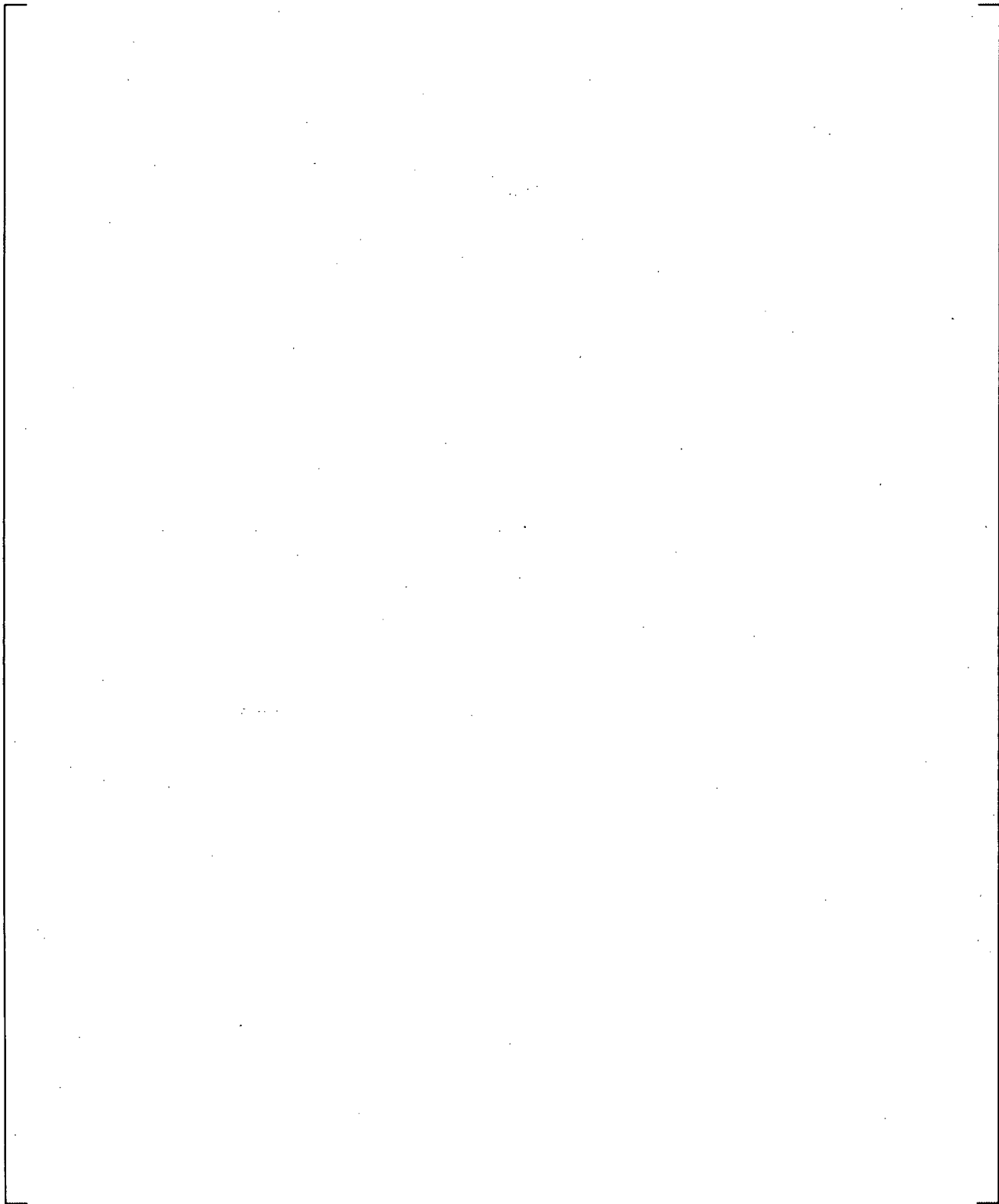
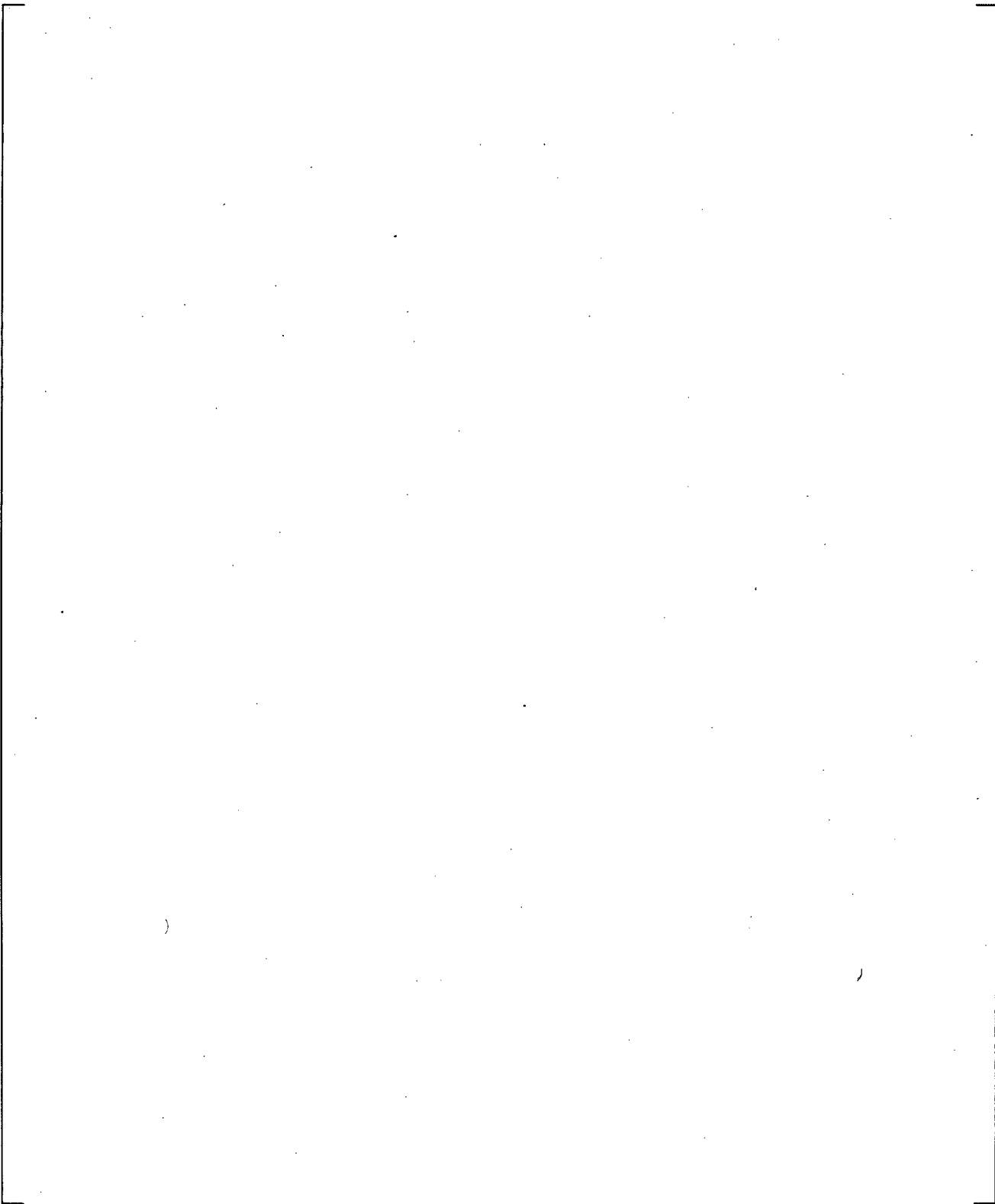


Figure 23.2.2-1

**WCOBRA/TRAC-TF2 Model of the Manometer Test Problem using the VESSEL Component**



**Figure 23.2.2-2 Velocity at the Bottom Gap of the 3D Manometer**



**Figure 23.2.2-3 Collapsed Liquid Levels and Total System Mass in the 3D Manometer**

### 23.2.3 1D PIPE Steam Expulsion Test

#### 23.2.3.1 Introduction

This problem is established as Numerical Benchmark Test No. 2.3 (NBT2.3) in (Hewitt et al., 1992).

#### 23.2.3.2 Problem Description

From (Hewitt et al., 1992):

*“The problem is formulated to test the numerical solution methods for anomalous numerical behavior associated with the mass transfer modeling that is characteristic of fixed node discretization schemes. The problem consists of, in a physical sense, a constant volume injection rate of subcooled water into a vertical tube initially filled with superheated steam and connected at the top to a constant pressure source of superheated steam.*

*“As the subcooled water is injected, condensation begins and the superheated steam is drawn into the tube. The condensation process adds energy to the injected liquid raising its temperature. In the usual fixed-mesh discretization scheme, the spatial grid spacing is too coarse to permit accurate modeling of the temperature gradient near the interface. This results in over-prediction of the condensation rate. In addition, when a node exactly fills with liquid, the condensation rate must become zero for at least one time step. This momentary numerical cessation of condensation results in a compression wave (water hammer) that propagates up the tube. The magnitude of compression depends upon the magnitude of the time step in which the condensation rate is zero.”*

#### 23.2.3.3 WCOBRA/TRAC-TF2 Model

In this test problem, a vertical tube is connected to a constant pressure source of steam at superheated and saturated conditions. Initially, the tube is filled with steam, but subcooled water is then injected from the bottom of the tube at a constant velocity 0.5 m/s. The vertical tube is 1.0 m in diameter and 3.0 m tall. The steam reservoir is held at a constant pressure of 4.0E+5 Pa and temperature of 163°C, respectively.

The steam expulsion test is modeled in WCOBRA/TRAC-TF2 as a single vertical 1D pipe, consisting of 10 cells. Each cell has a height of 0.3 m and a hydraulic diameter of 1.0 m. A BREAK component is connected at the top providing a pressure boundary condition of 4.0E+5 Pa. Two cases are modeled. In the first case, the initial pressure and temperature in the pipe is 4.0E+5 Pa and 163.0°C, representing superheated steam. In the second case, the temperature is decreased to saturation temperature of 143.6°C. A FILL component is attached to the pipe at the bottom. Subcooled liquid injection is started at the FILL with a ramp, reaching a constant 0.5 m/s steady flow in 1.s. This model is illustrated in Figure 23.2.3-1.

#### 23.2.3.4 Numerical/Analytical Solution

As described in (Hewitt et al., 1992), an exact analytical solution would require resolving the interfacial heat and mass transfer between the top of the liquid column and the vapor. This will depend on the rate of heat conduction in the liquid phase and the rate of convective heating of the interface by the steam. However, for a low filling rate of the pipe, the fill time can be estimated as slightly less than 6 sec., as a

result of liquid injection at a rate of 0.5 m/s and condensation of steam. Also the process should be continuous. The condensation rate should be very small because a layer of saturated liquid would develop at the top of the liquid column limiting the condensation.

The objective of this study is therefore to assess the fill time and analyze the effects of the spatial discretization associated with the noding scheme discussed in Section 23.2.3.3.

### 23.2.3.5 WCOBRA/TRAC-TF2 Assessment

#### 23.2.3.5.1 Superheated Steam Case

Figure 23.2.3-2 (Figure 23.2.3-3 with adjusted scale) and Figure 23.2.3-4 show the pressure and void fraction, respectively, in every two cells in the pipe, during the steam expulsion simulation. As seen in the pressure profile, [

] <sup>a,c</sup>

Other relevant plots, including liquid and vapor velocities and temperatures, are shown in Figure 23.2.3-5 through Figure 23.2.3-8. [

] <sup>a,c</sup>

The liquid temperature (Figure 23.2.3-7) is near saturation when the cell is gas filled, and drops to the liquid temperature of the cell upstream when the liquid front crosses the bottom cell boundary. The vapor in a cell is initially superheated (Figure 23.2.3-8) and quickly de-superheats as result of the interfacial heat transfer until it reaches saturation when the cell is water-packed.

#### 23.2.3.5.2 Saturated Steam Case

Figure 23.2.3-9 and Figure 23.2.3-10 show the pressure and void fraction, respectively, in every two cells in the pipe, during the steam expulsion simulation with saturated steam. As seen in the pressure profile, [

] <sup>a,c</sup> Other relevant plots, including liquid and vapor velocities and temperatures are shown in Figure 23.2.3-11 through Figure 23.2.3-14. It can be seen that the results are quite similar to the superheated steam case, [

] <sup>a,c</sup>

### 23.2.3.6 Summary and Conclusions

The steam expulsion problem is a standard numerical benchmark problem that was exercised with different codes (Hewitt et al., 1992, Pryor et al., 1978). As described in Section 3 of NBT2.3 of (Hewitt et al., 1992), the qualitative analytic solution is absent of any "spikes," although it is known that a discretized noding scheme will result in some spikes or ripples as described in Section 23.2.3.2.

[

] <sup>a,c</sup>

### 23.2.3.7 References

1. Hewitt, G.F., Delhay, J.M., Zuber, N., "Multiphase Science and Technology," Vol. 6, 1992.
2. Pryor, R.J, Liles, D.R., Mahaffy, J.H., 1978. Treatment of Water Packing Effects. Trans. ANS 30, 208-209.

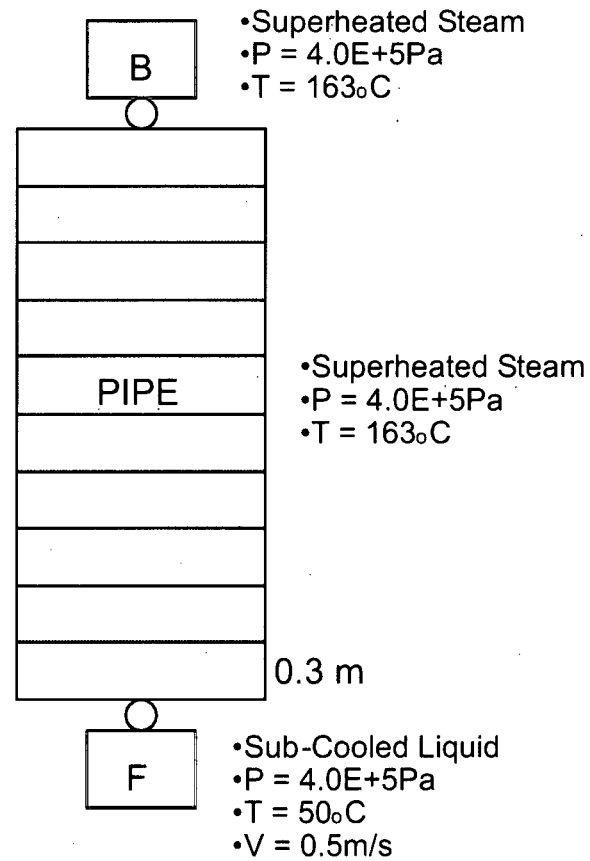
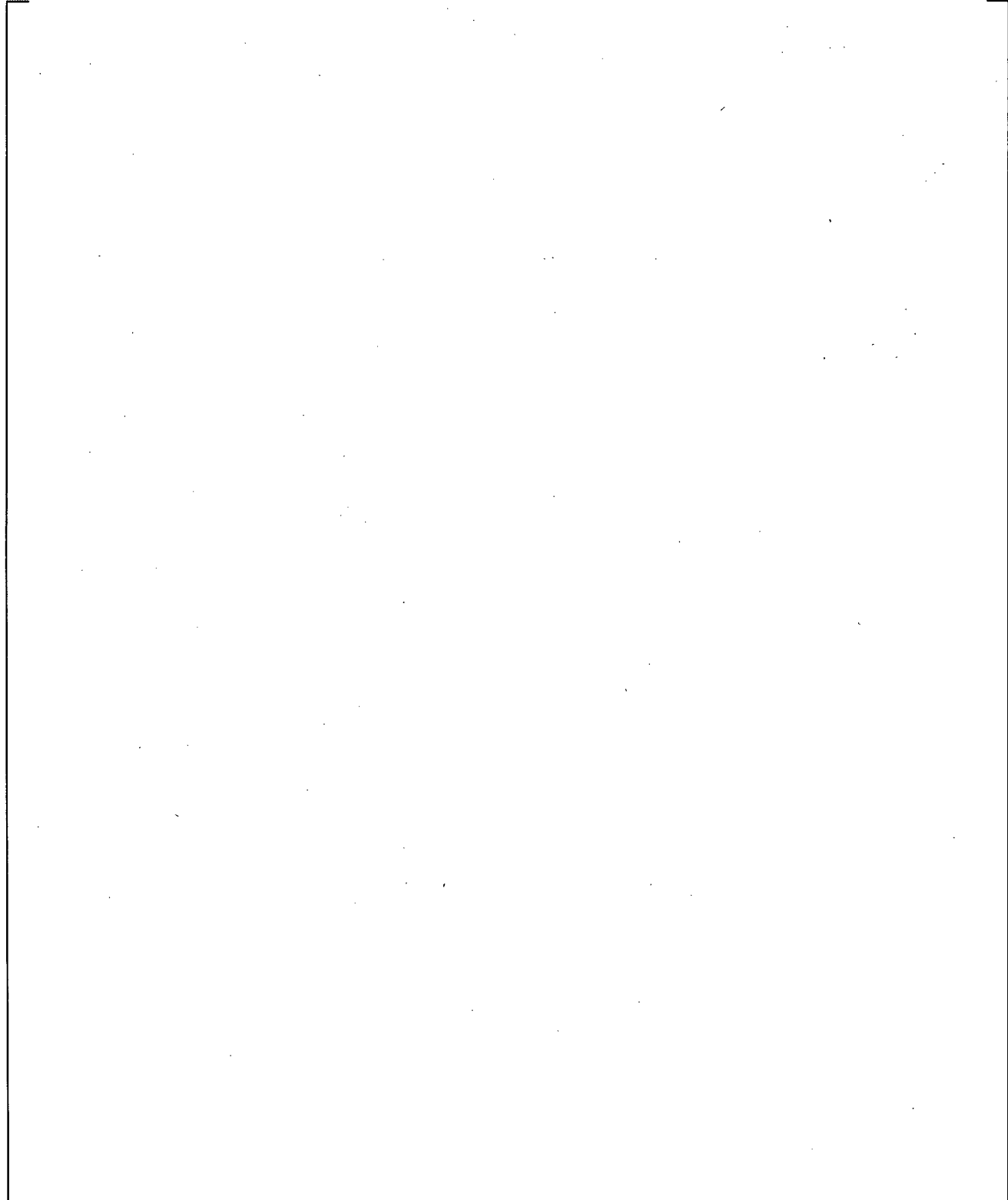
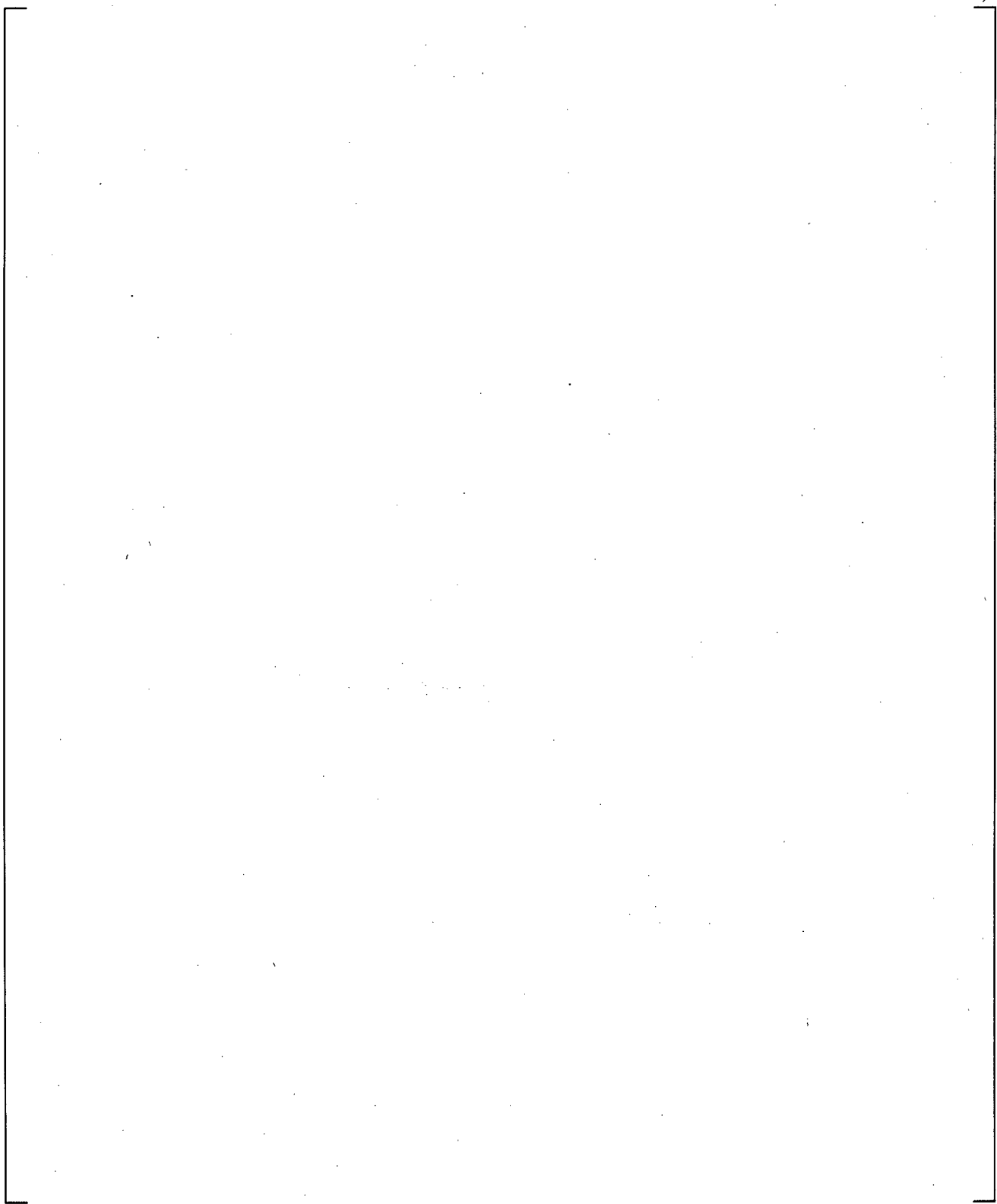


Figure 23.2.3-1 Nodalization and Schematic for Steam Expulsion Test using 1D Pipe



**Figure 23.2.3-2**

**Pressure Profile in the 1D Pipe for the Steam Expulsion Test, Superheated Steam Case**



**Figure 23.2.3-3 Pressure Profile in the 1D Pipe for the Steam Expulsion Test, Superheated Steam Case**

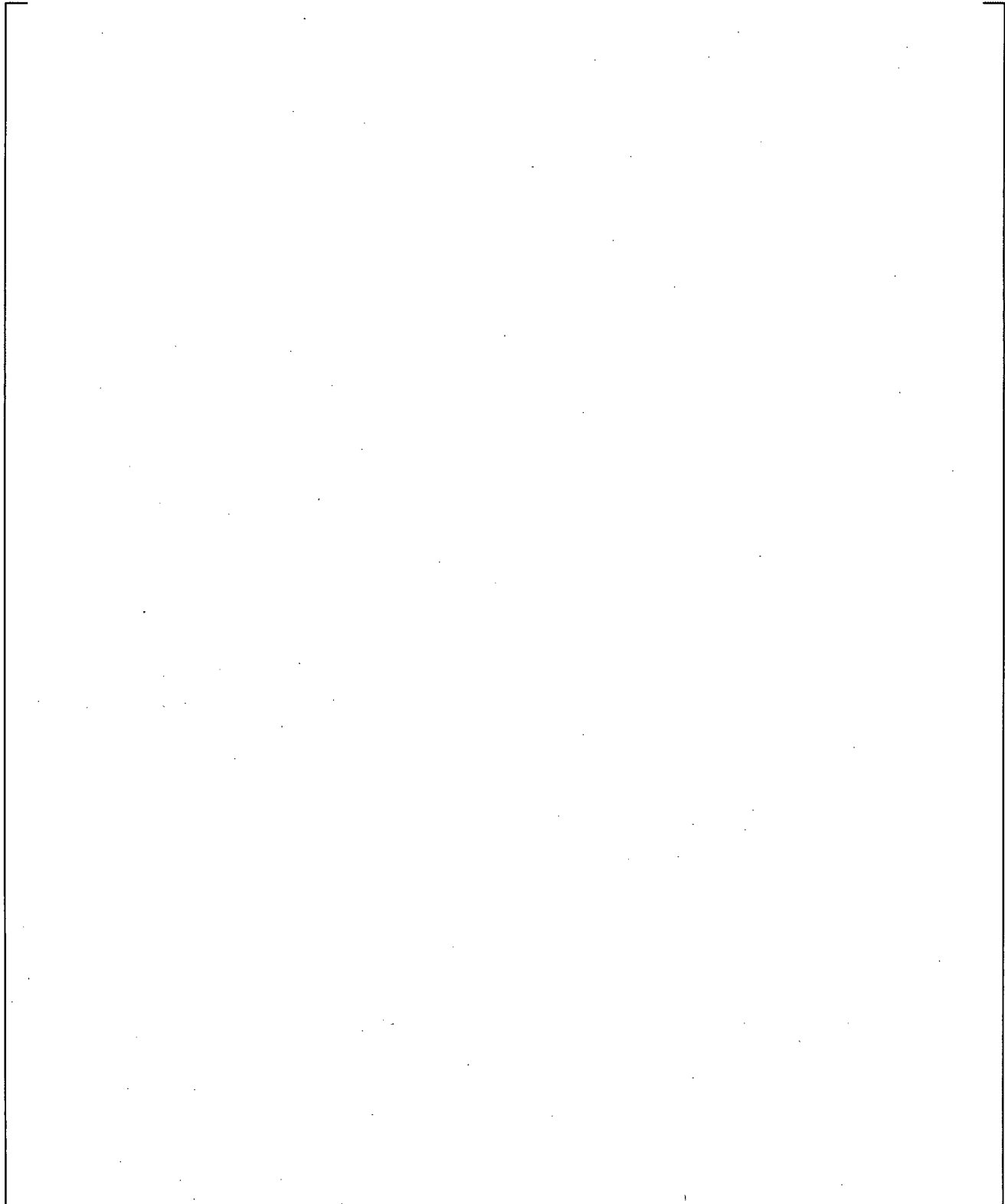


**Figure 23.2.3-4**      **Void Fraction Profile in the 1D Pipe for the Steam Expulsion Test, Superheated Steam Case**

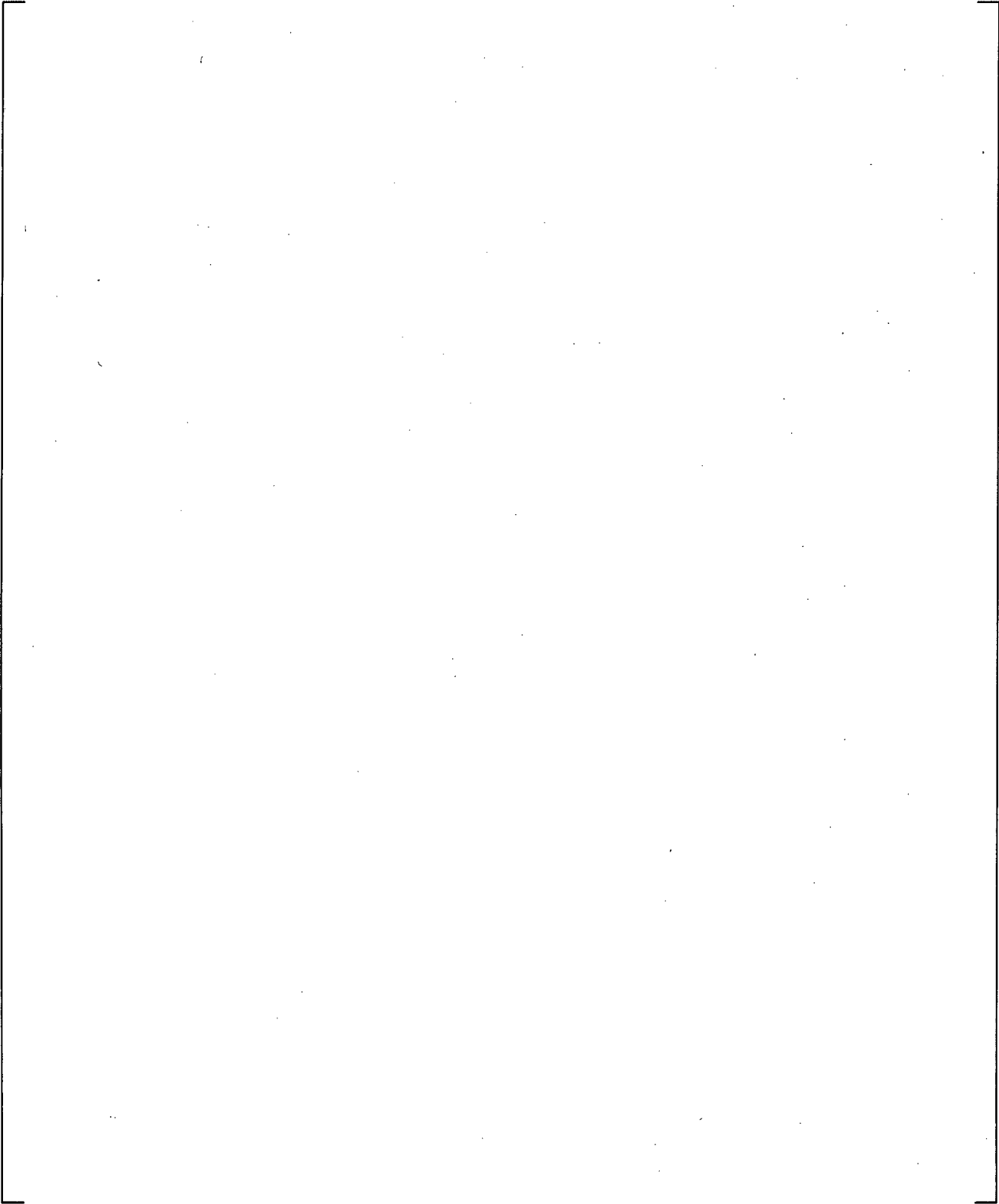


**Figure 23.2.3-5**      **Liquid Velocity Profile in the 1D Pipe for the Steam Expulsion Test, Superheated Steam Case**

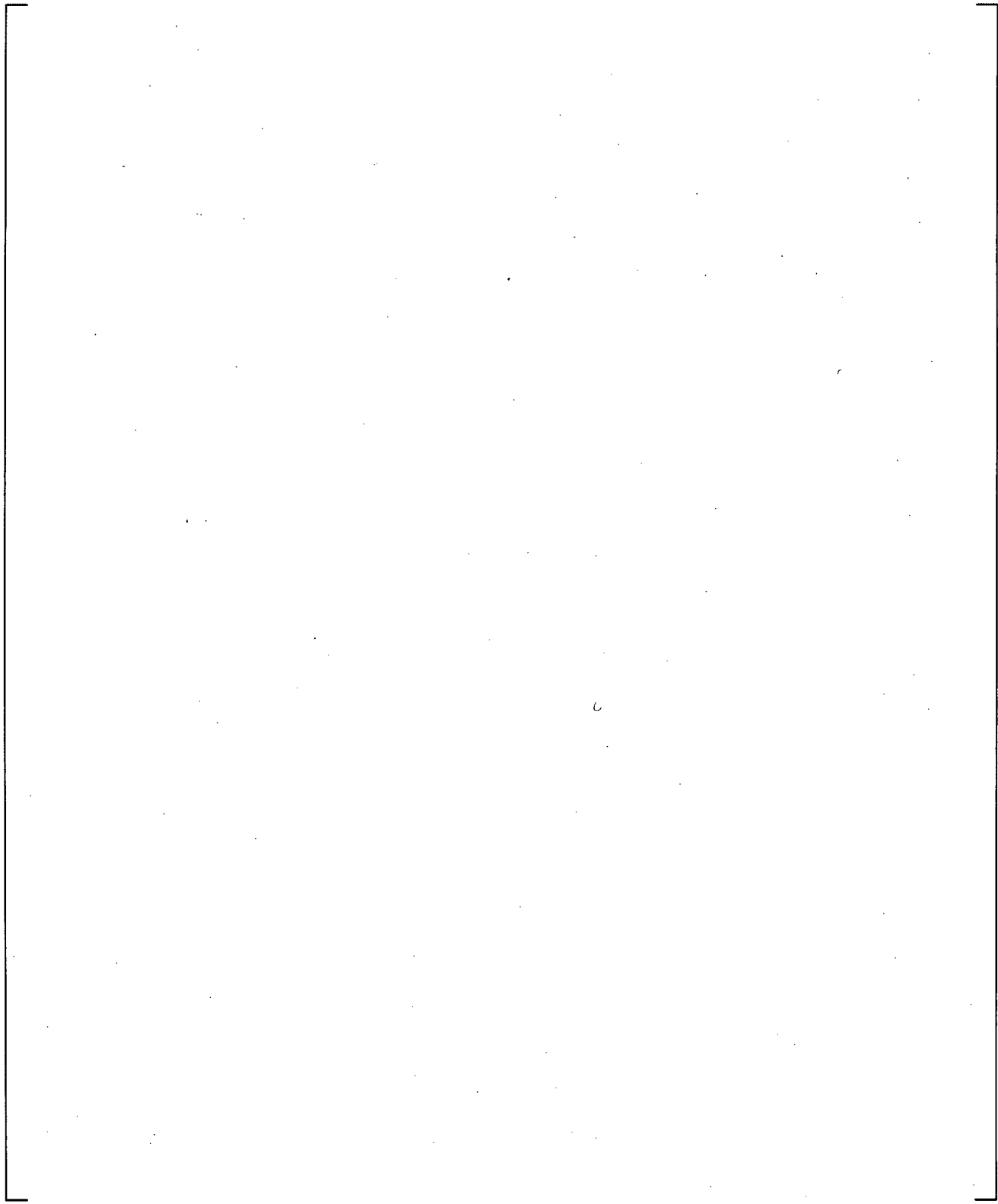


**Figure 23.2.3-6 Steam Velocity Profile in the 1D Pipe for the Steam Expulsion Test, Superheated Steam Case**

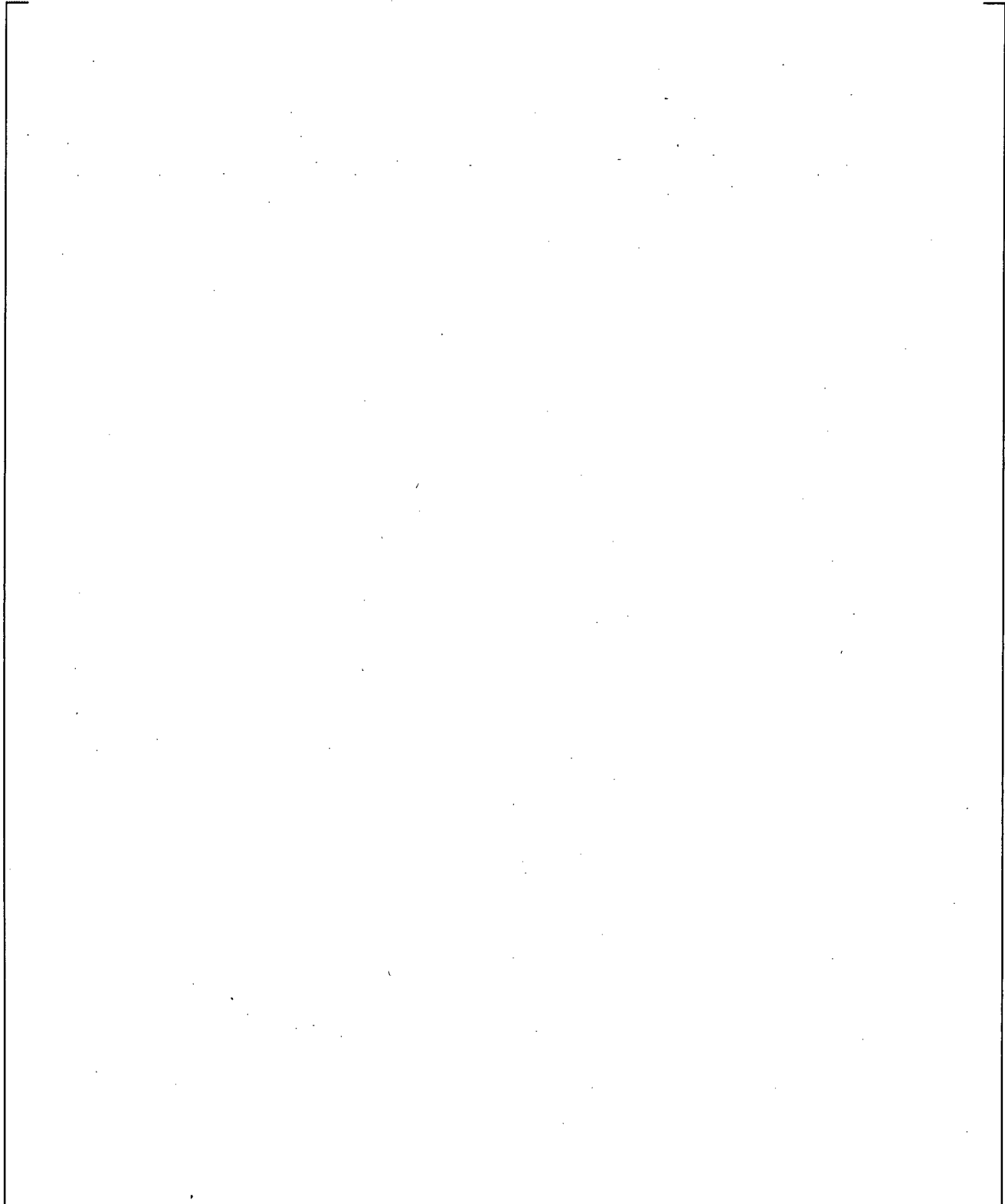


**Figure 23.2.3-7**      **Liquid Temperature Profile in the 1D Pipe for the Steam Expulsion Test, Superheated Steam Case**

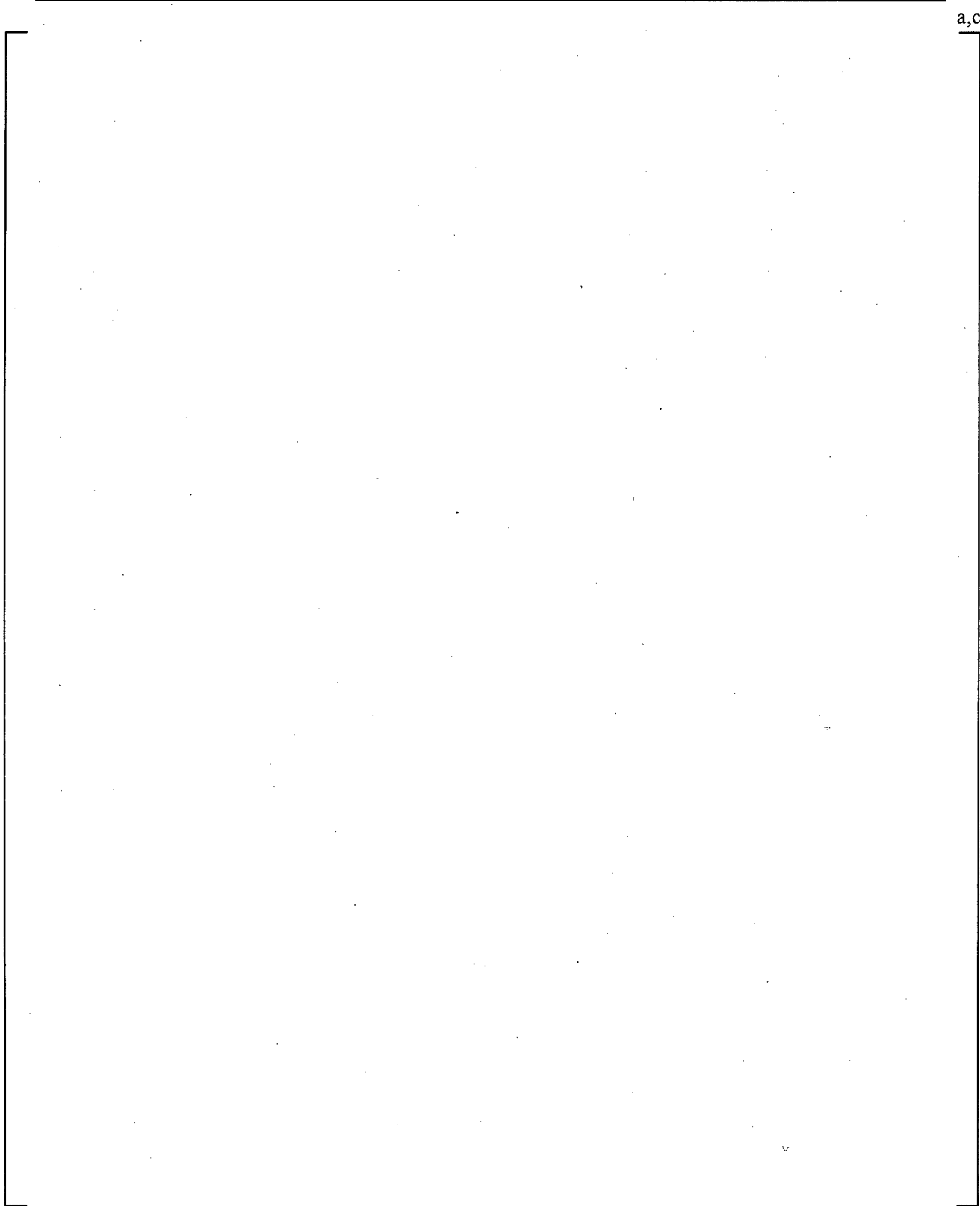


**Figure 23.2.3-8 Vapor Temperature Profile in the 1D Pipe for the Steam Expulsion Test, Superheated Steam Case**

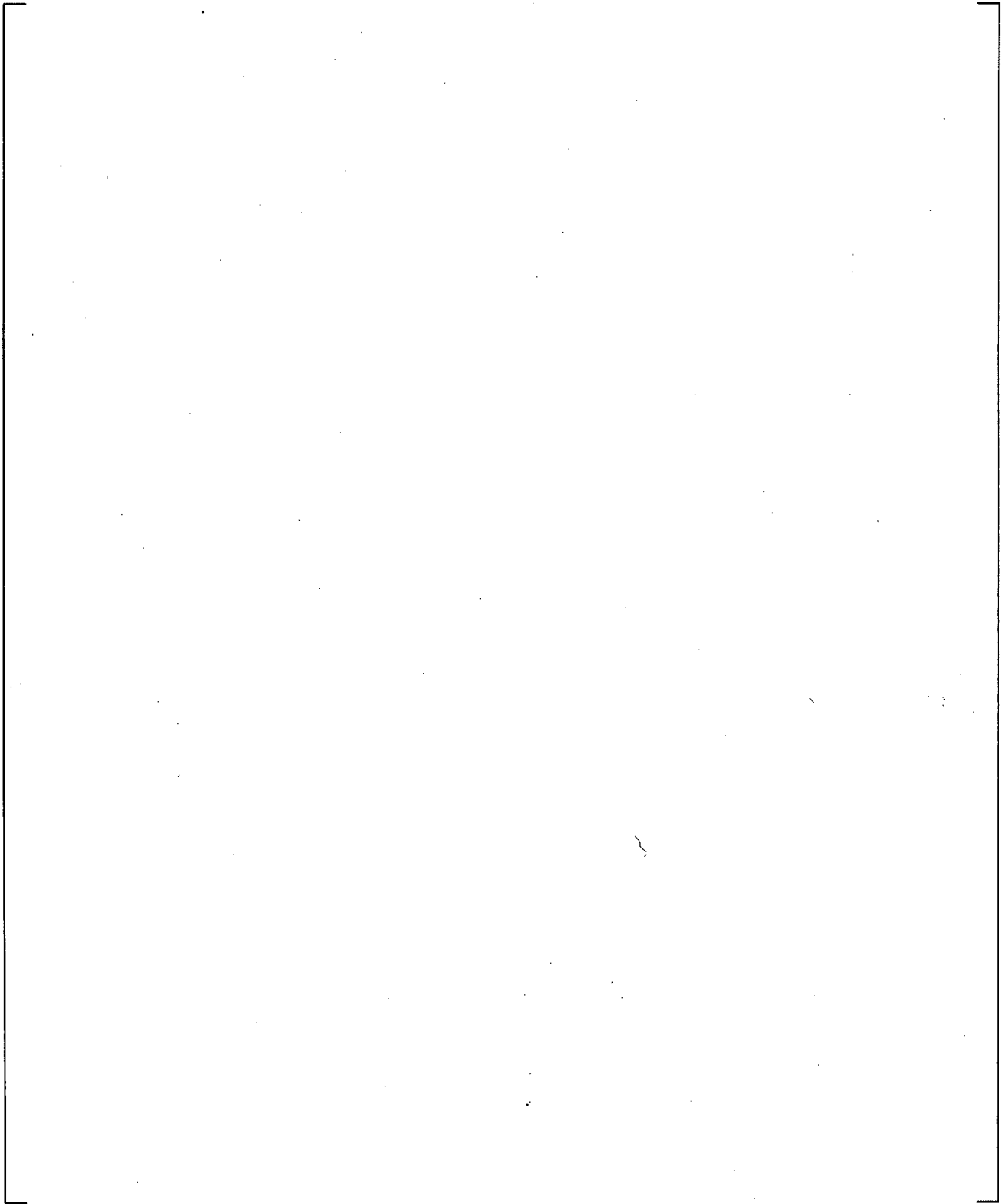


**Figure 23.2.3-9 Pressure Profile in the 1D Pipe for the Steam Expulsion Test, Saturated Steam Case**

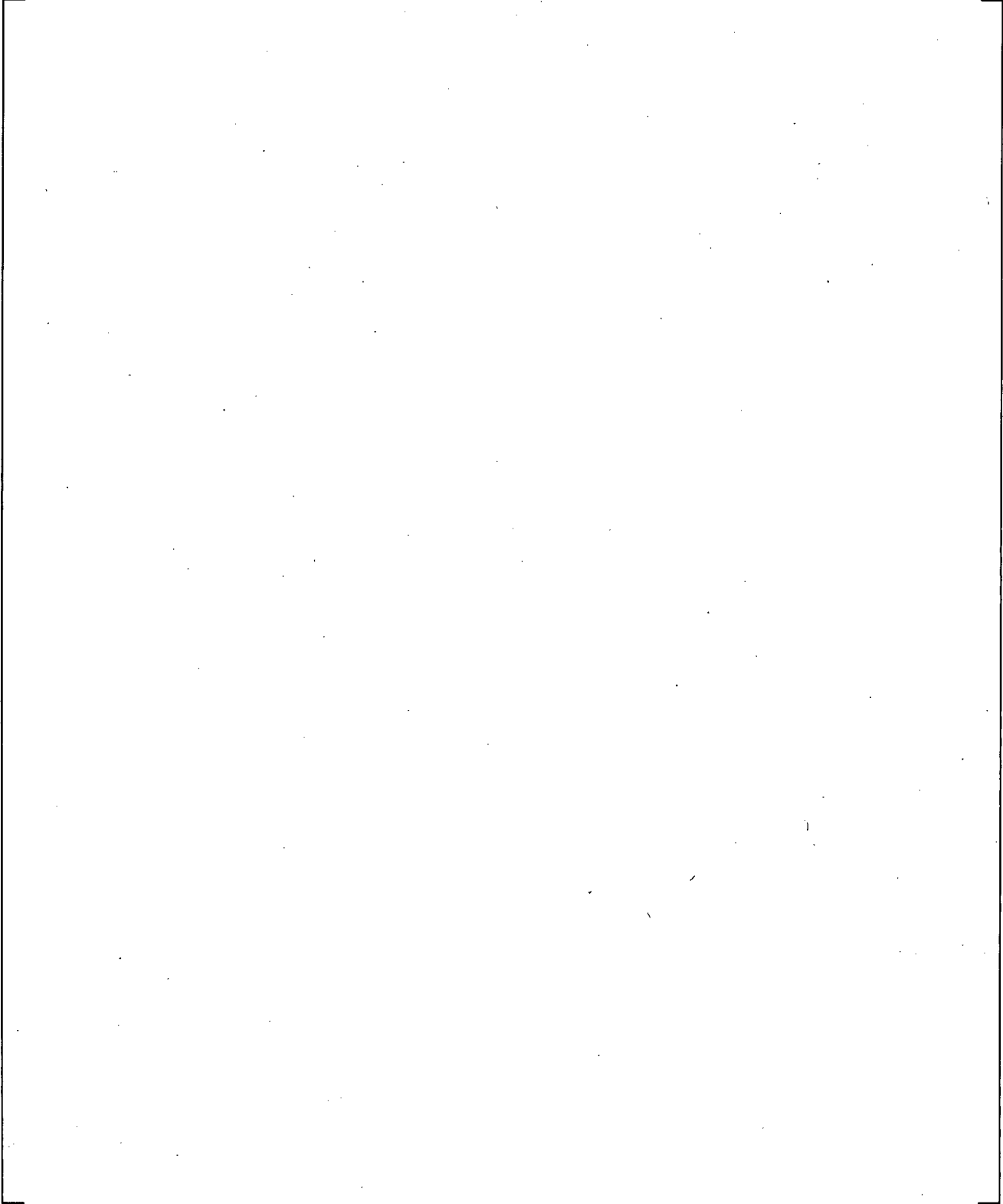


**Figure 23.2.3-10 Void Fraction Profile in the 1D Pipe for the Steam Expulsion Test, Saturated Steam Case**

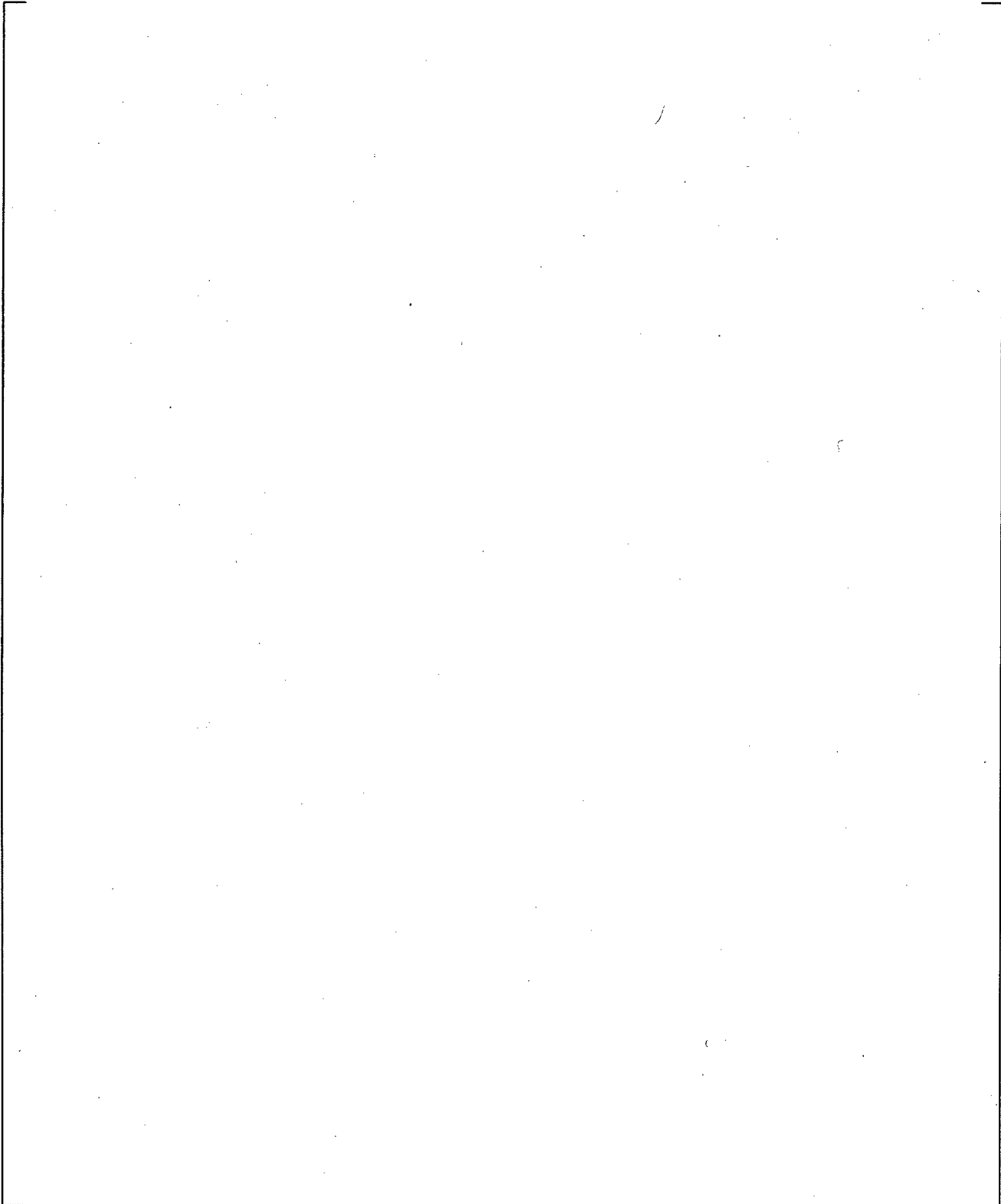


**Figure 23.2.3-11**      **Liquid Velocity Profile in the 1D Pipe for the Steam Expulsion Test, Saturated Steam Case**

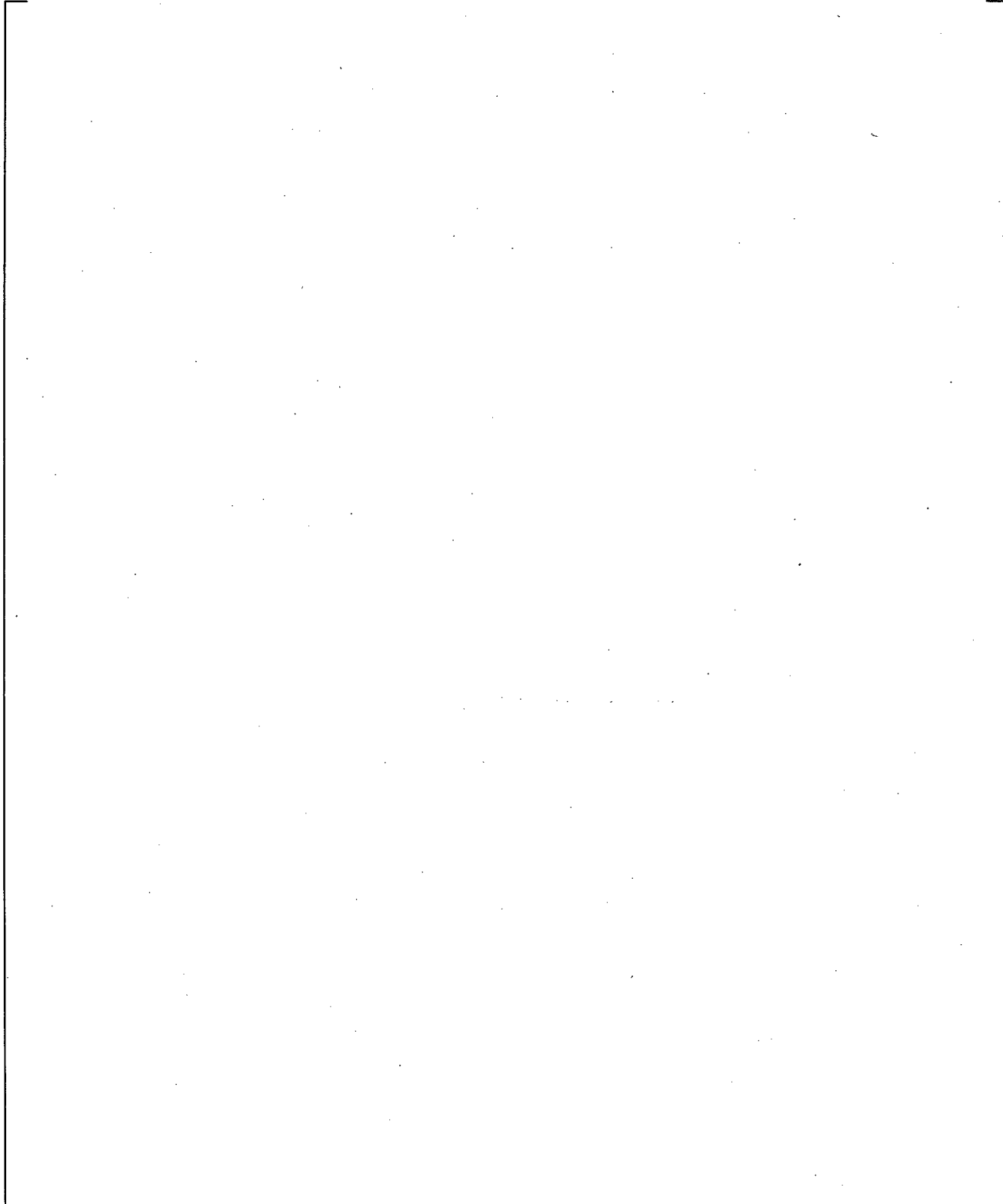


**Figure 23.2.3-12 Steam Velocity Profile in the 1D Pipe for the Steam Expulsion Test, Saturated Steam Case**

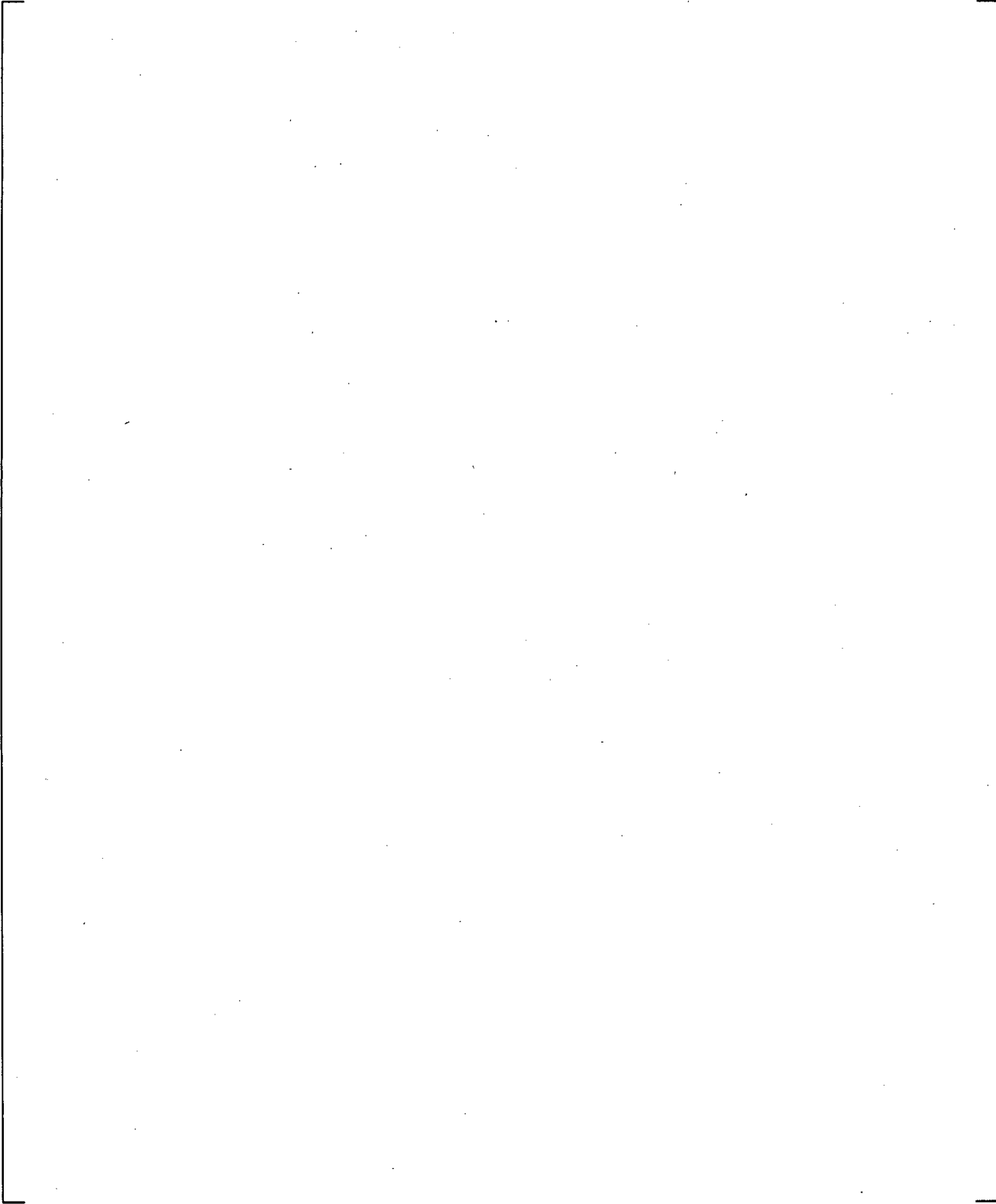


**Figure 23.2.3-13**      **Liquid Temperature Profile in the 1D Pipe for the Steam Expulsion Test, Saturated Steam Case**

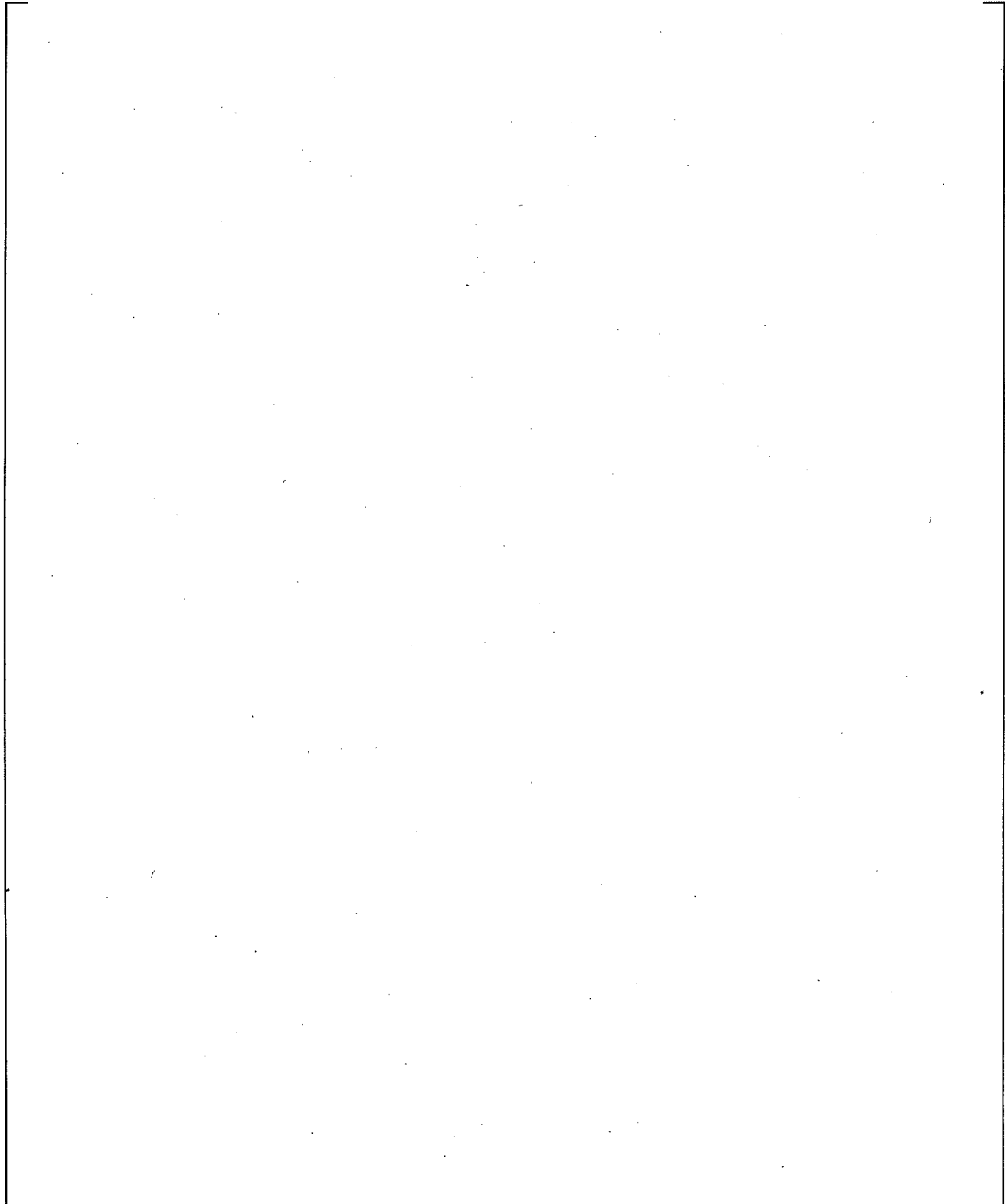


**Figure 23.2.3-14 Vapor Temperature Profile in the 1D Pipe for the Steam Expulsion Test, Saturated Steam Case**

## 23.2.4 3D VESSEL Steam Expulsion Test

### 23.2.4.1 Introduction

The steam expulsion test presented in Section 23.2.3 with a 1-D pipe is repeated here with the 3D Vessel component.

### 23.2.4.2 Problem Description

See Section 23.2.3.2.

### 23.2.4.3 WCOBRA/TRAC-TF2 Model

The steam expulsion test is modeled in WCOBRA/TRAC-TF2 as a single channel VESSEL (Figure 23.2.4-1) consisting of 10 axial nodes. Each node has a height of 0.3m and a hydraulic diameter of 1.0 m. A single cell PIPE is connected to the VESSEL at the top. A BREAK component is attached to the PIPE providing a pressure boundary condition at  $4.0E+5$  Pa. The initial pressure and enthalpy in the vessel are  $4.0E+5$  Pa and  $2.782E+6$  J/kg, respectively for the superheated steam case and  $4.0E+5$  Pa and  $2.738E+6$  J/kg in the saturated steam case. An inlet flow boundary condition is specified at the bottom of the vessel, ramping from 0.0 to 0.5 m/s in 1 s. The inlet flow is sub-cooled liquid at 50°C.

### 23.2.4.4 Numerical/Analytical Solution

See Section 23.2.3.4.

### 23.2.4.5 WCOBRA/TRAC-TF2 Assessment

#### 23.2.4.5.1 Superheated Steam Results

Collapsed liquid level in the vessel is shown in Figure 23.2.4-2. As indicated in the plot, liquid fills the vessel entirely, displacing the steam, by combination of expulsion and condensation, in about [ ]<sup>a,c</sup>. This is consistent with the expectation. Figure 23.2.4-3 and Figure 23.2.4-4 show the pressure and void fraction, respectively, in every other cell in the vessel. [

] Other relevant plots, including liquid and vapor velocities and temperatures are shown in Figure 23.2.4-5 through 23.2.4-8.

The liquid temperature (Figure 23.2.4-5) is near saturation when the cell is gas filled, and gradually drops to the liquid temperature of the cell upstream when the liquid front crosses the bottom cell boundary. The vapor in a cell is initially superheated (Figure 23.2.4-5) and gradually de-superheats as a result of the interfacial heat transfer until it reaches saturation when the cell is water-packed. The water packing results in a vapor velocity spike (Figure 23.2.4-8), forcing the vapor upward as the cell fills with liquid.

### 23.2.4.5.2 Saturated Steam Results

Collapsed liquid level in the vessel is shown in 23.2.4-9. As indicated in the plot, liquid fills the vessel entirely, displacing the steam, by combination of expulsion and condensation, in about [ ]<sup>a,c</sup>. This is consistent with the expectation.

Figure 23.2.4-10 and Figure 23.2.4-11 show the pressure and void fraction, respectively, in every two cells in the vessel. [ ]<sup>a,c</sup>

Other relevant plots, including liquid and vapor velocities and temperatures are shown in Figure 23.2.4-12 through Figure 23.2.4-15.

The only discernible difference between the case with saturated steam and that with superheated steam (Section 23.3.4.5.1) is the prediction of vapor temperature, due to the initially lower temperature of the saturated steam.

### 23.2.4.6 Summary and Conclusions

The steam expulsion problem is a standard numerical benchmark problem that was exercised with different codes (Hewitt et al., 1992, Pryor et al., 1978). As described in Section 3 of NBT2.3 of (Hewitt et al., 1992), the qualitative analytic solution is absent of any "spikes" or "ripples," although it is known that a discretized noding scheme will result in some spikes or ripples as described in Section 23.2.3.2. [ ]<sup>a,c</sup>

The fill rate is comparable to the qualitative analytic expectation, as is the general behavior regarding temperatures and pressures.

### 23.2.4.7 References

1. Hewitt, G.F., Delhay, J.M., Zuber, N., "Multiphase Science and Technology," Vol.6, 1992.
2. Pryor, R.J, Liles, D.R., Mahaffy, J.H., 1978. Treatment of Water Packing Effects. Trans. ANS 30, 208-209.

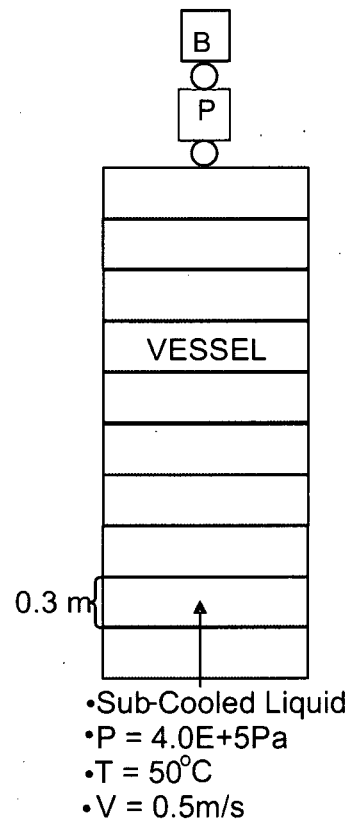
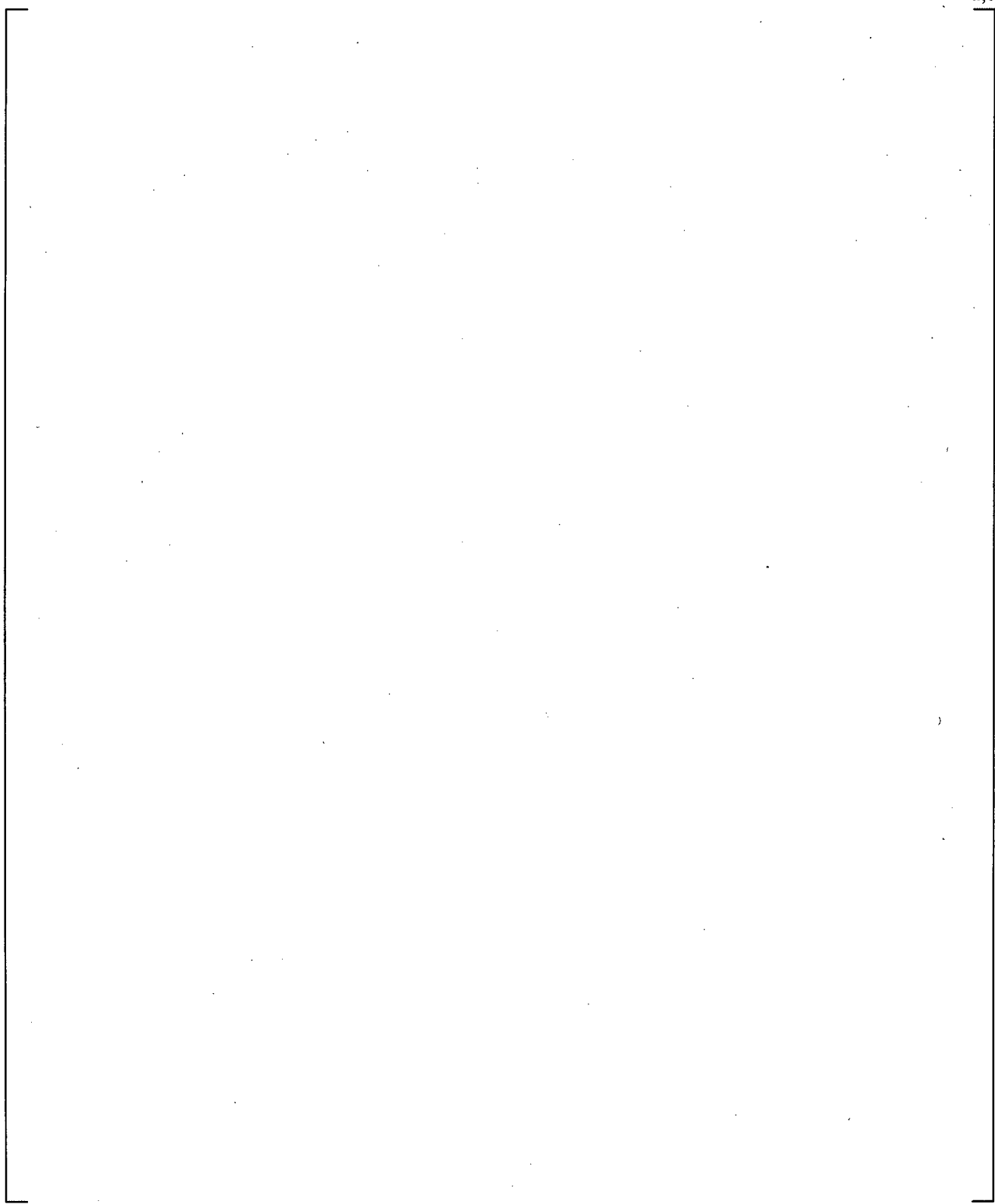
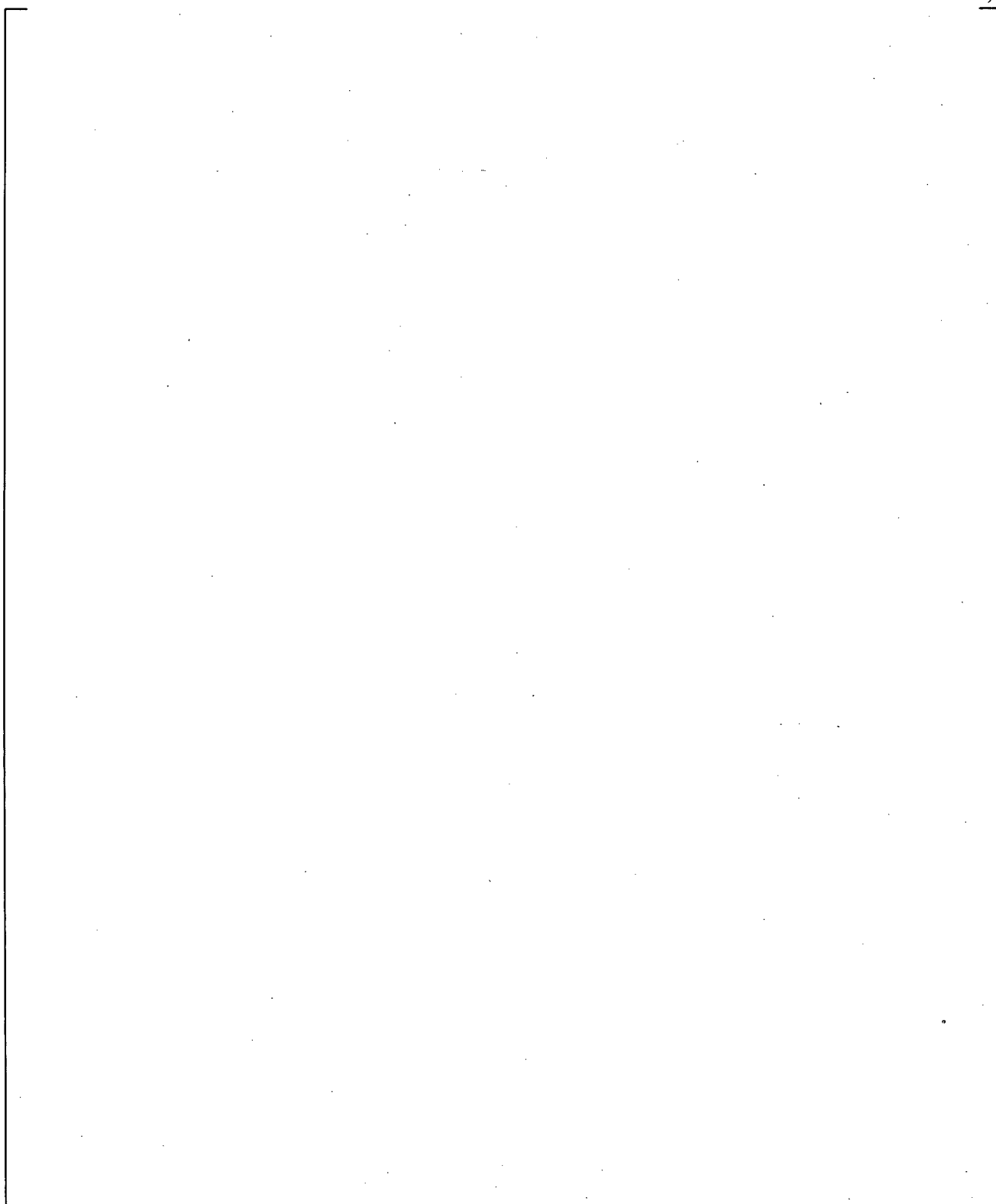


Figure 23.2.4-1 Steam Expulsion Test using 3D Vessel



**Figure 23.2.4-2**      **Collapsed Liquid Level in the Vessel for the Steam Expulsion Test, Superheated Steam Case**



**Figure 23.2.4-3 Pressure Profile in the 3D Vessel for Steam Expulsion Test, Superheated Steam Case**

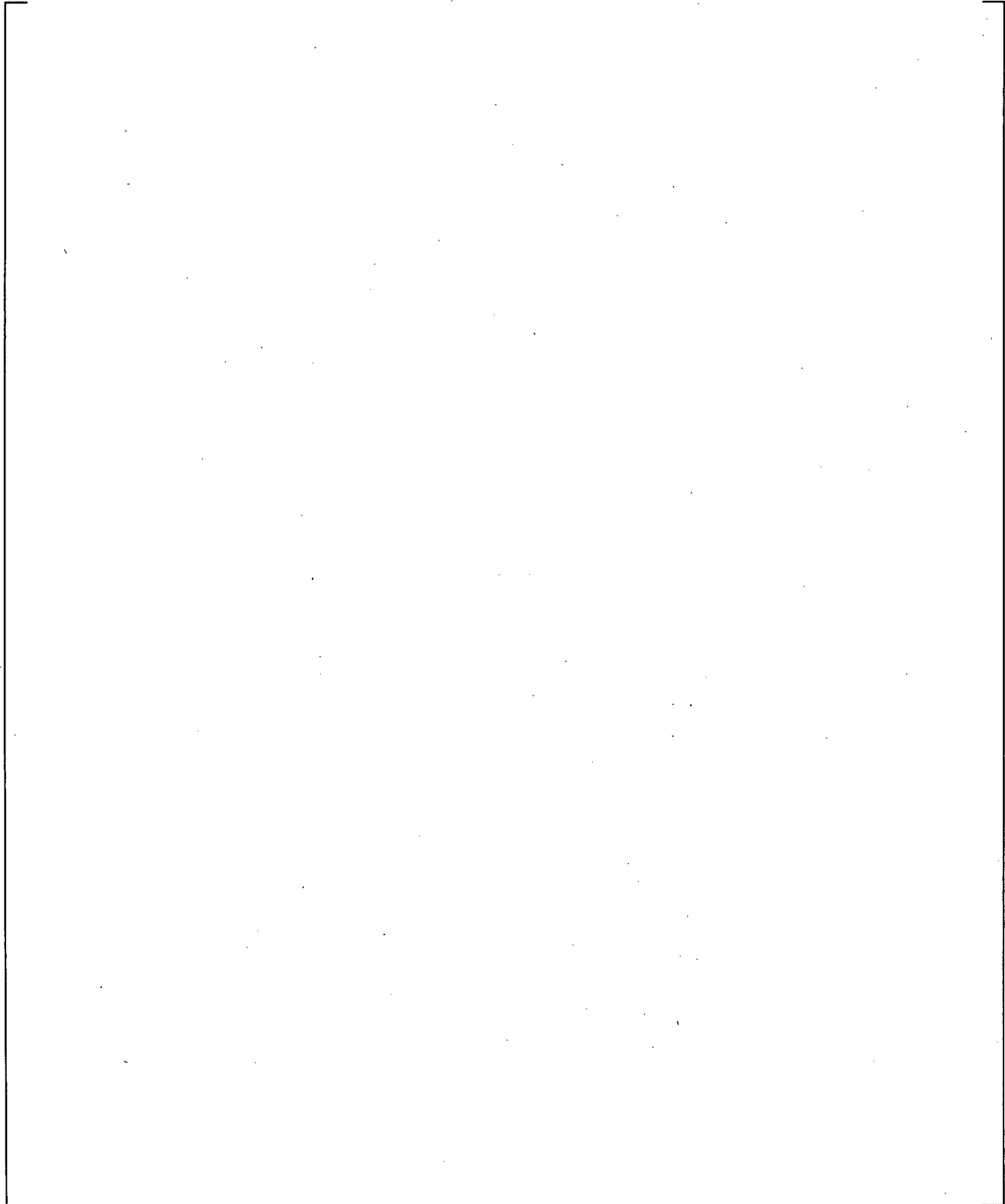


**Figure 23.2.4-4**      **Void Fraction Profile in the 3D Vessel for the Steam Expulsion Test, Superheated Steam Case**

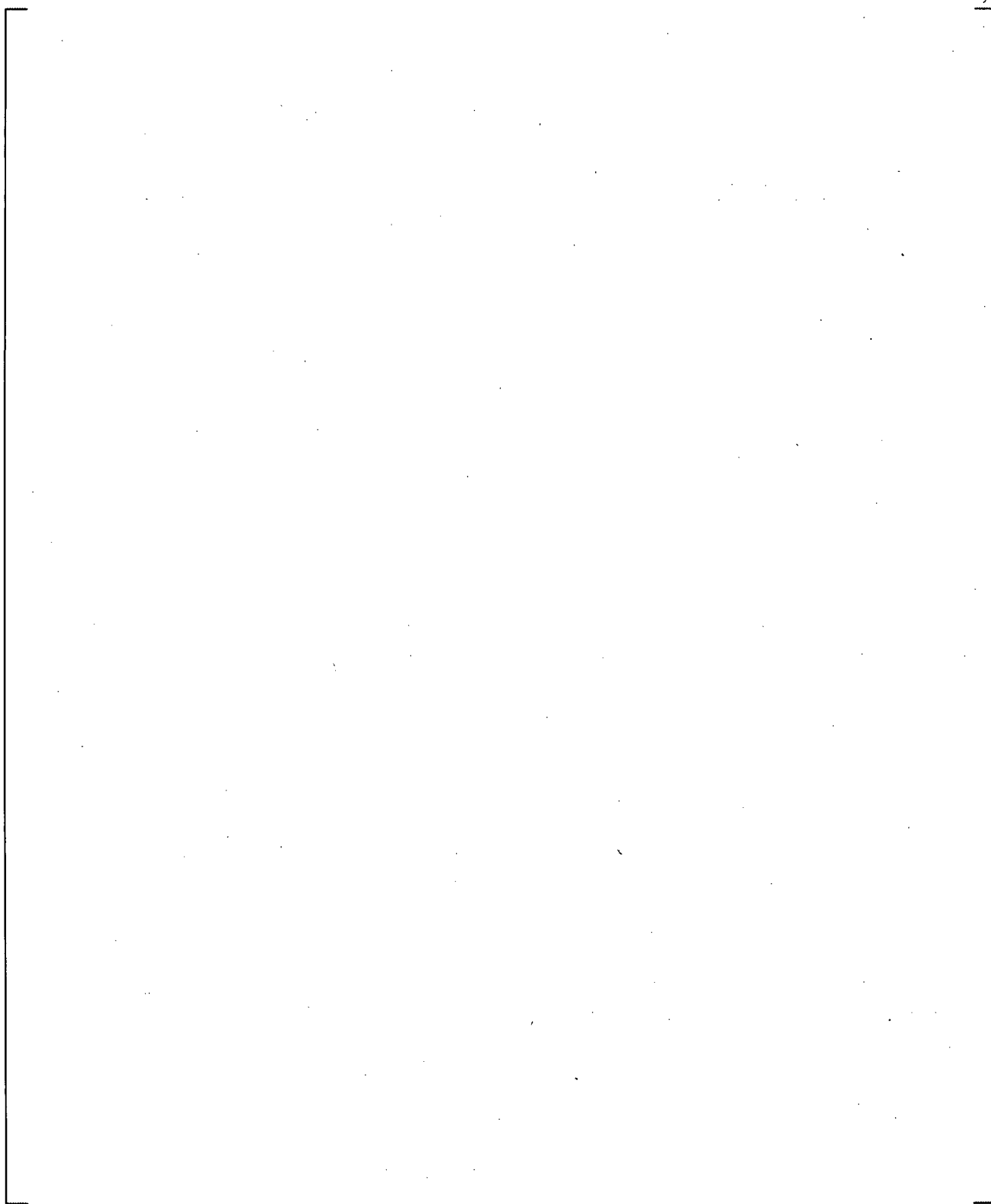


**Figure 23.2.4-5**      **Liquid Temperature Profile in the 3D Pipe for the Steam Expulsion Test, Superheated Steam Case**

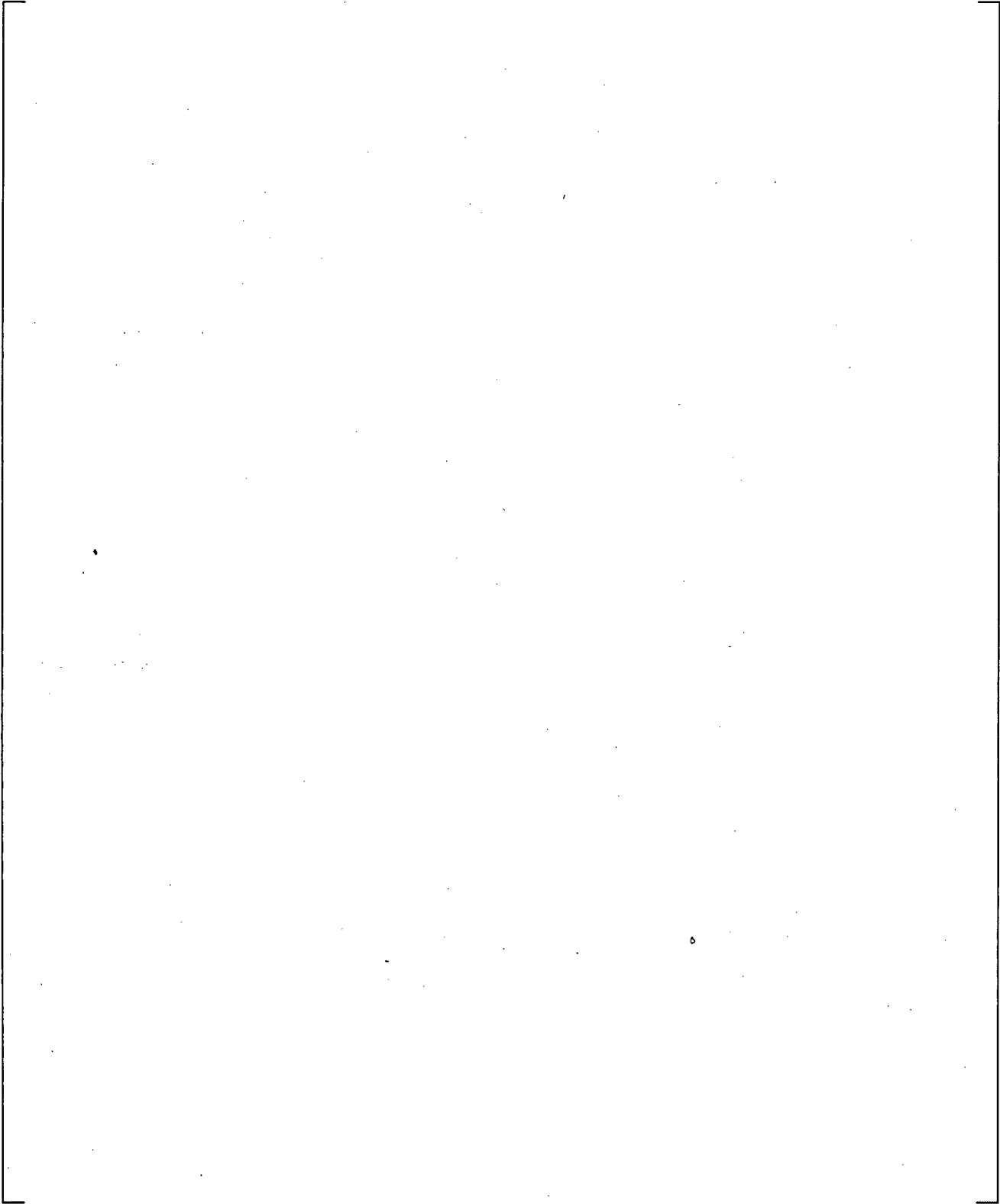


**Figure 23.2.4-6 Vapor Temperature Profile in the 3D Vessel for the Steam Expulsion Test, Superheated Steam Case**

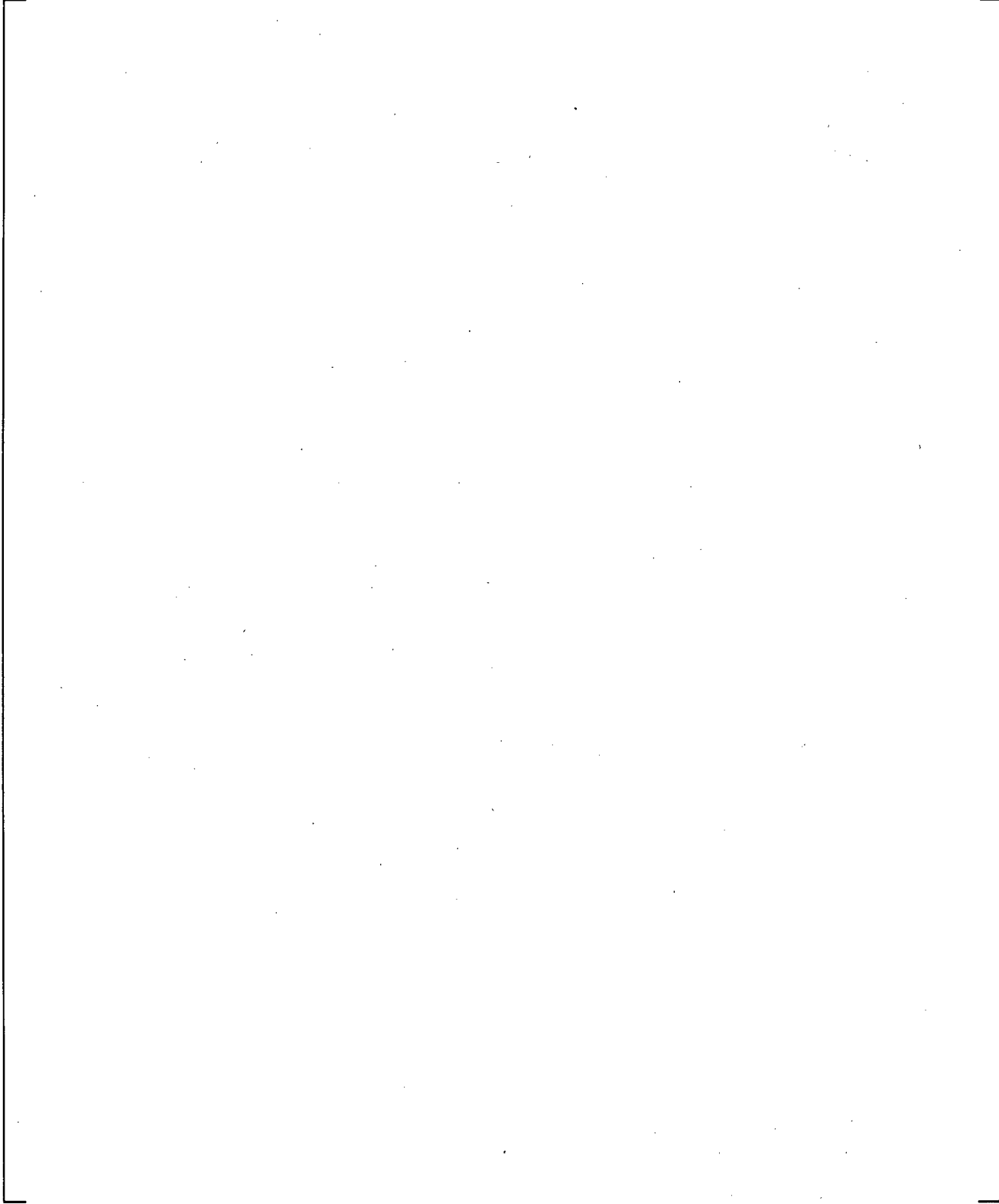


**Figure 23.2.4-7**      **Liquid Velocity Profile in the 3D Vessel for the Steam Expulsion Test, Superheated Steam Case**

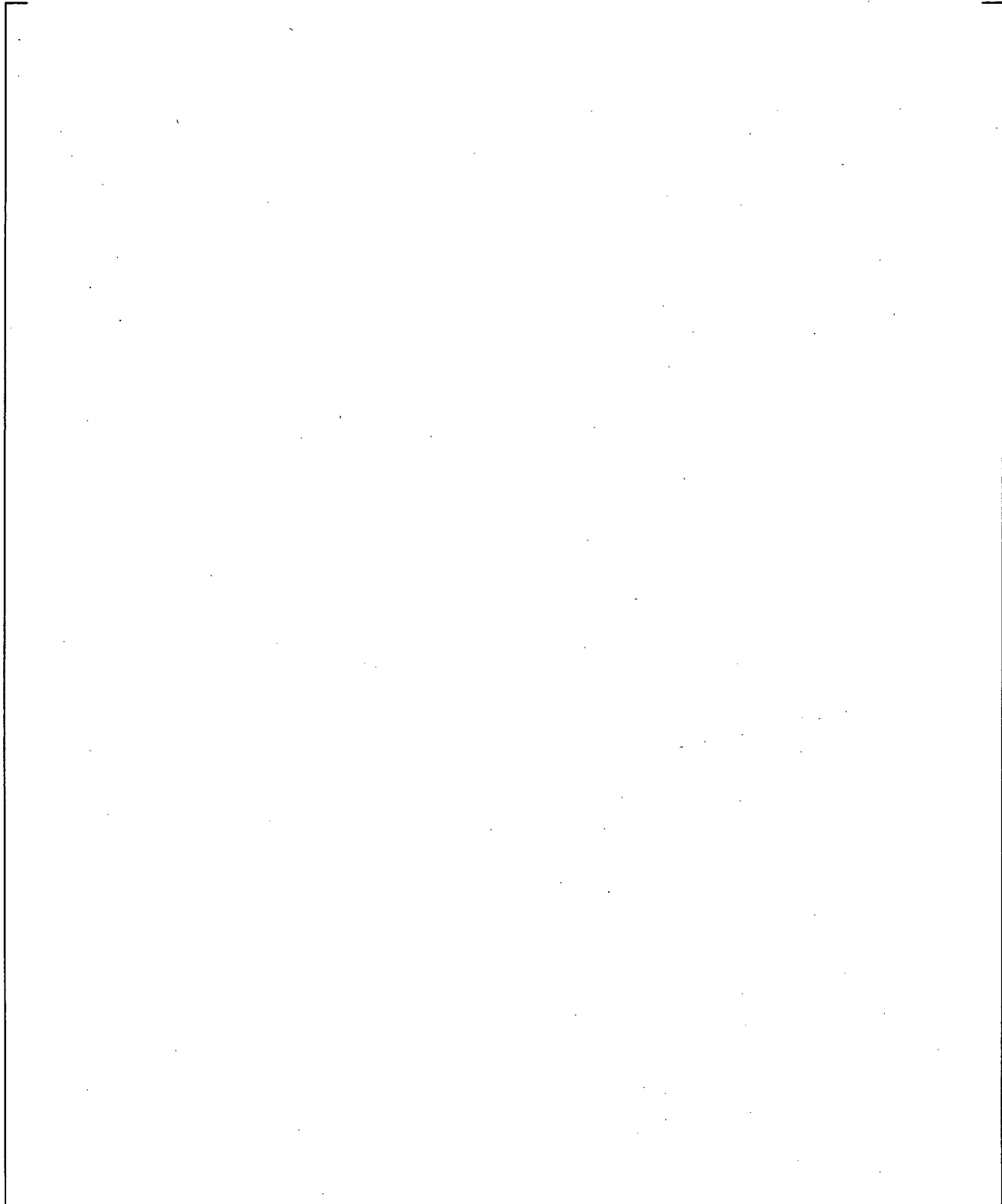


**Figure 23.2.4-8 Vapor Velocity Profile in the 3D Vessel for the Steam Expulsion Test, Superheated Steam Case, Superheated Steam Case**

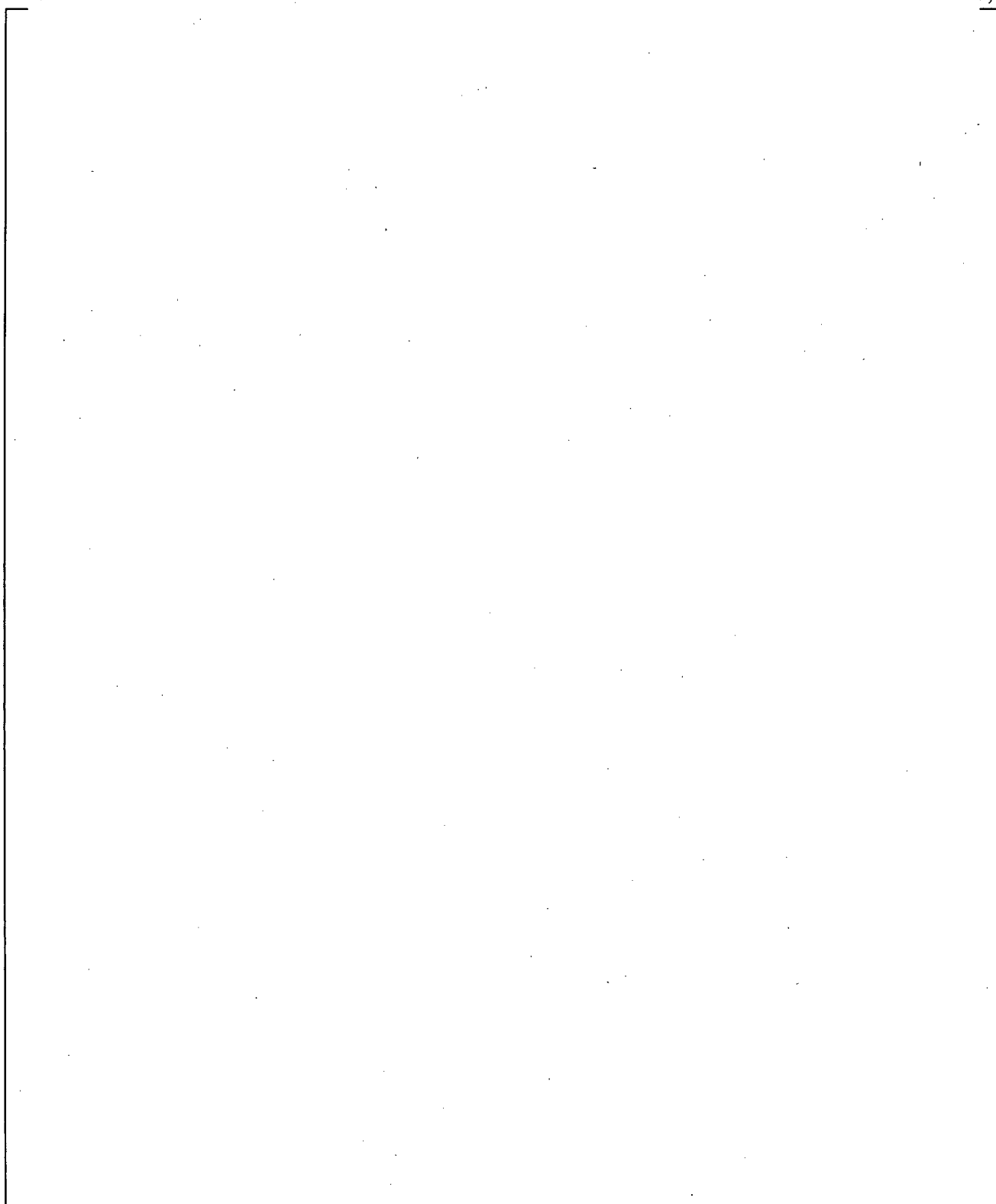


**Figure 23.2.4-9**      **Collapsed Liquid Level in the Vessel for the Steam Expulsion Test, Saturated Steam Case**

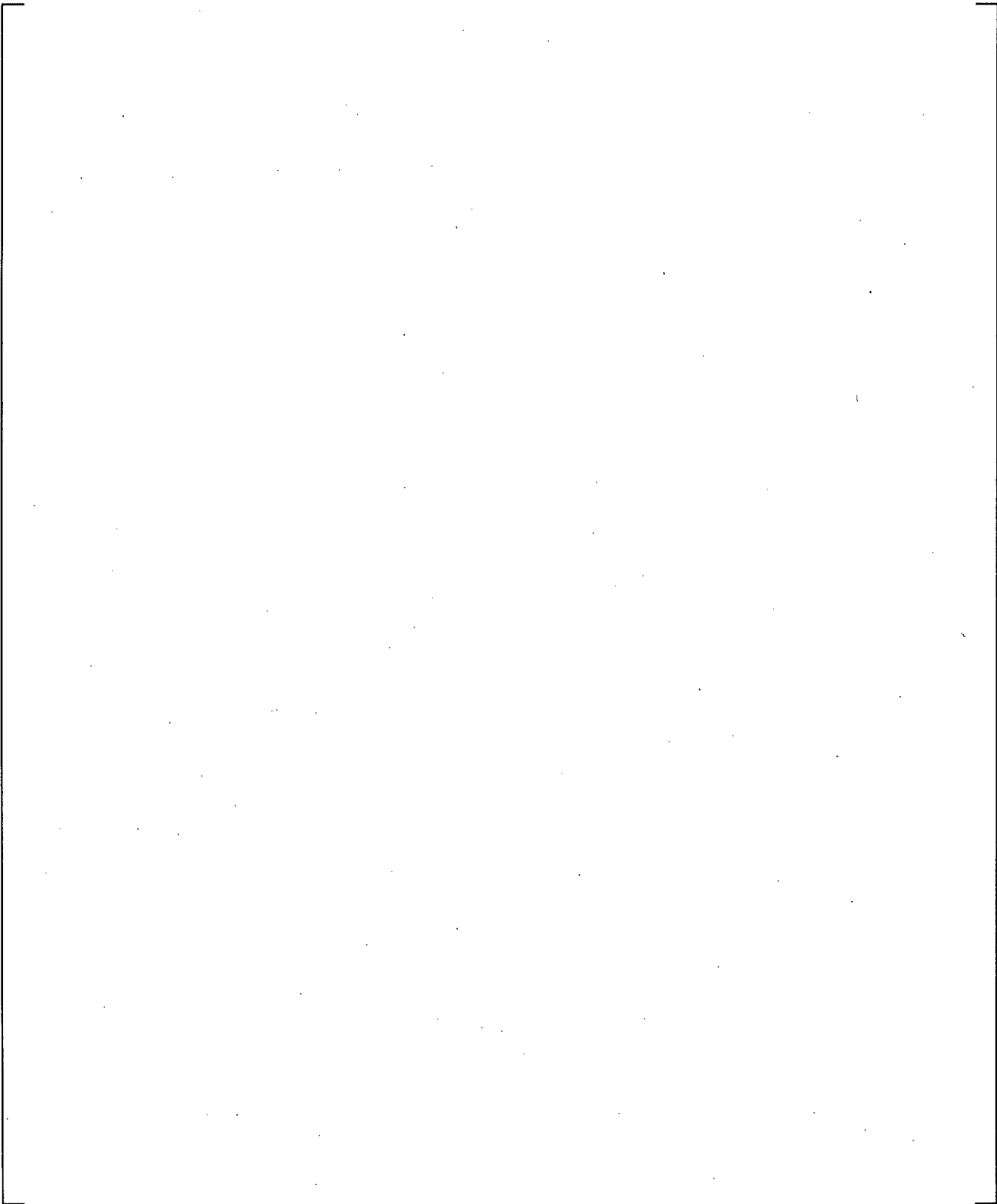


**Figure 23.2.4-10**      **Pressure Profile in the 3D Vessel for the Steam Expulsion Test, Saturated Steam Case**

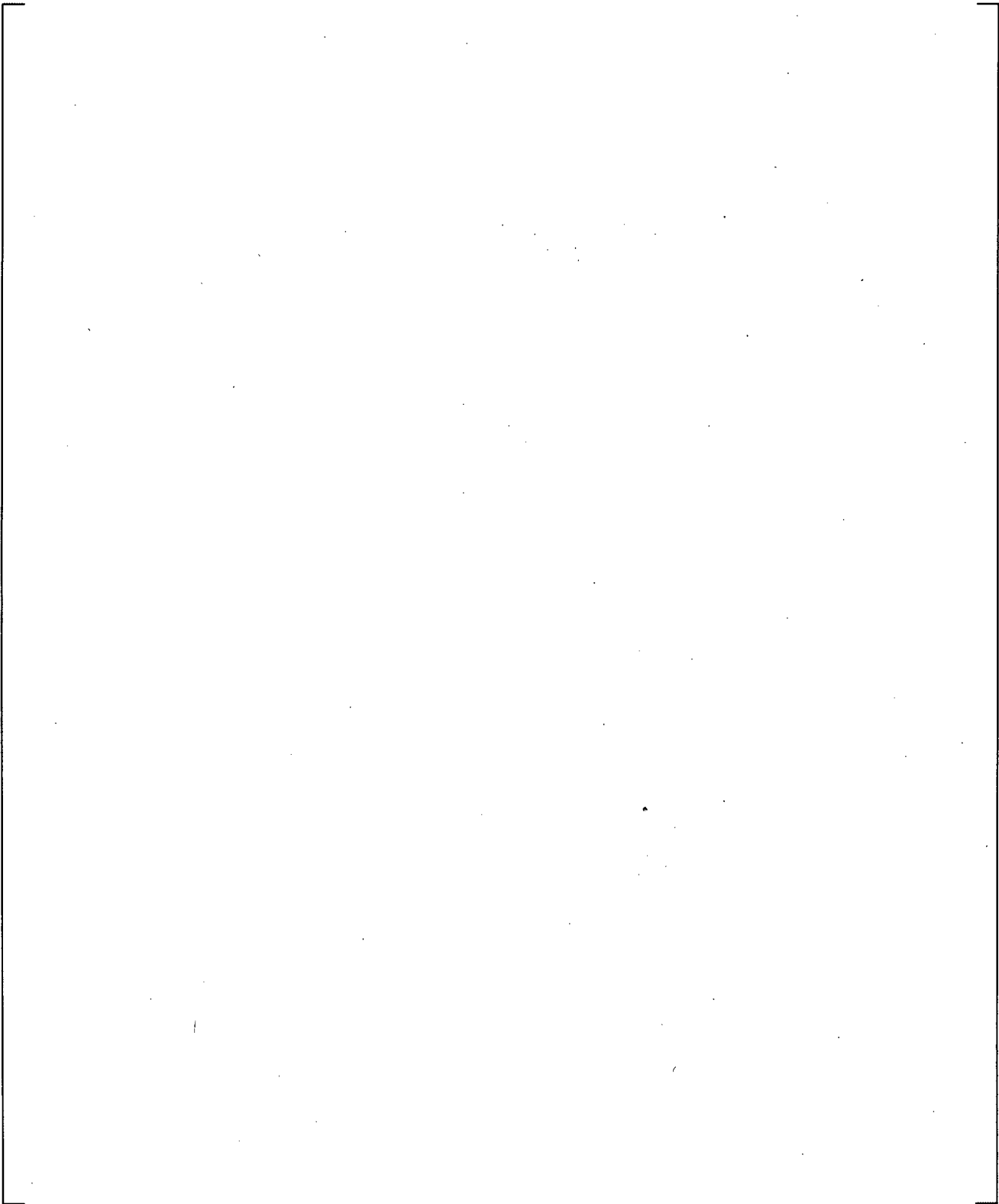


**Figure 23.2.4-11** Void Fraction Profile in the 3D Vessel for the Steam Expulsion Test, Saturated Steam Case

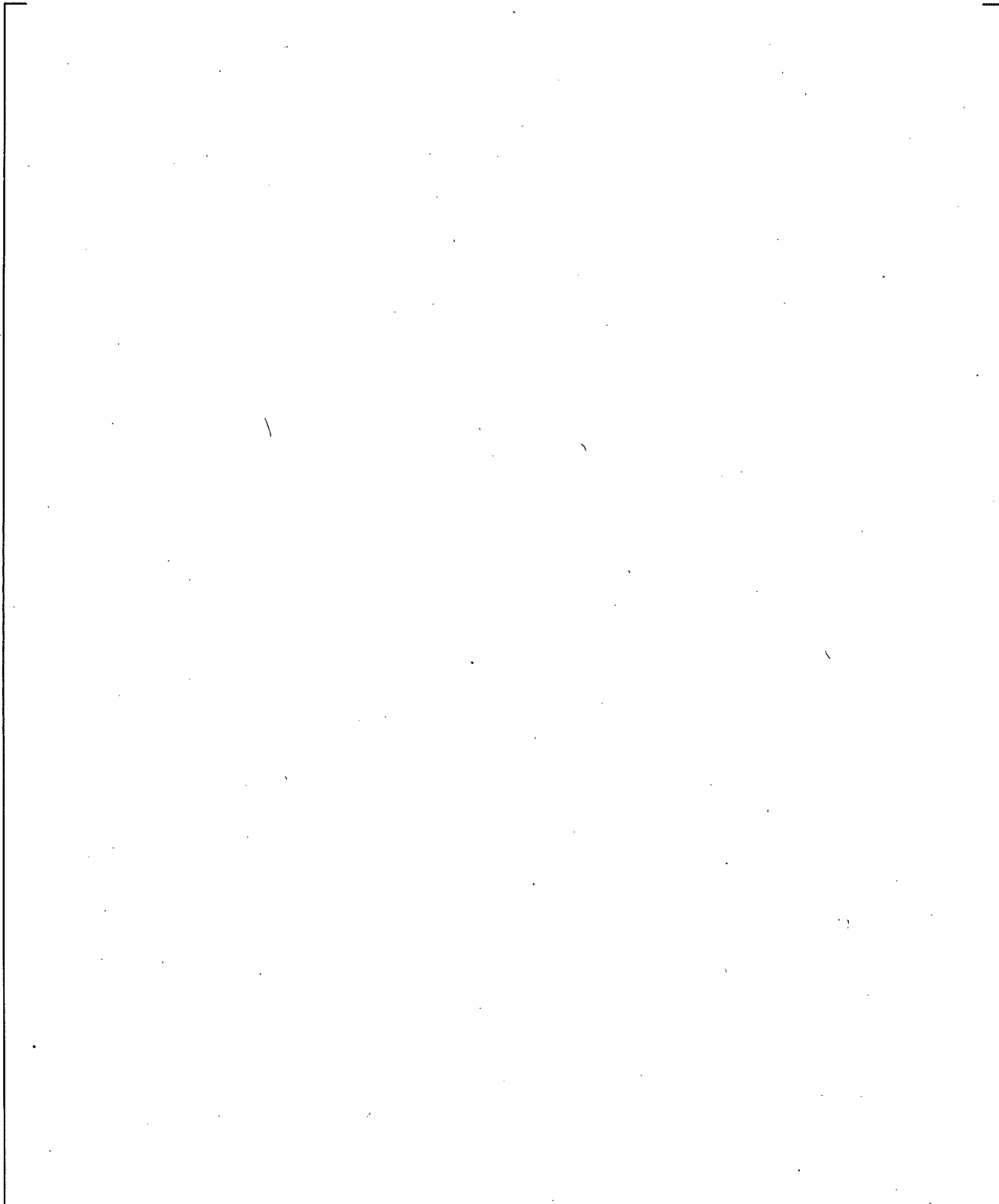


**Figure 23.2.4-12**      **Liquid Temperature Profile in the 3D Pipe for the Steam Expulsion Test, Saturated Steam Case**

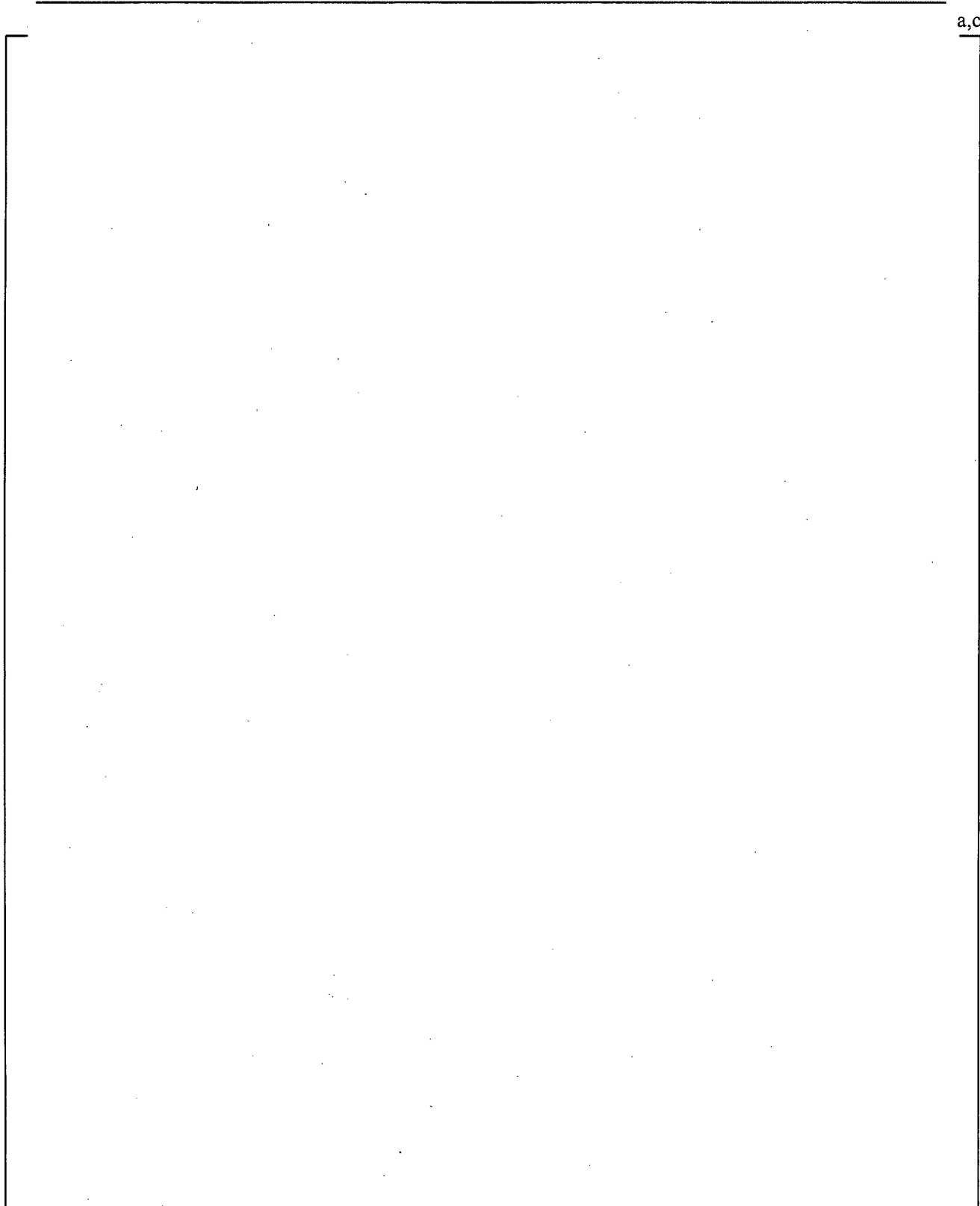


**Figure 23.2.4-13 Vapor Temperature Profile in the 3D Vessel for the Steam Expulsion Test, Saturated Steam Case**

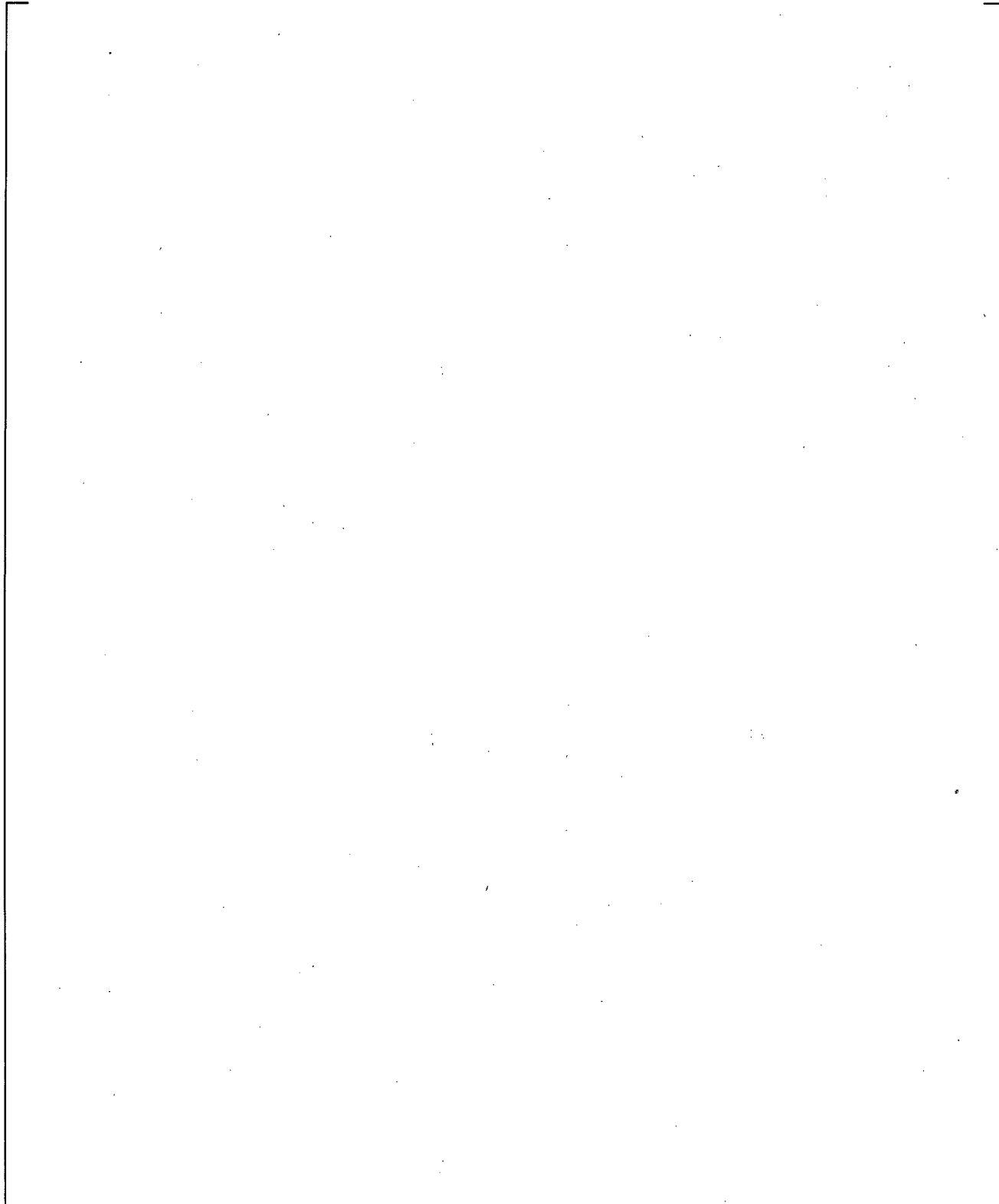


**Figure 23.2.4-14**      **Liquid Velocity Profile in the 3D Vessel for the Steam Expulsion Test, Saturated Steam Case**

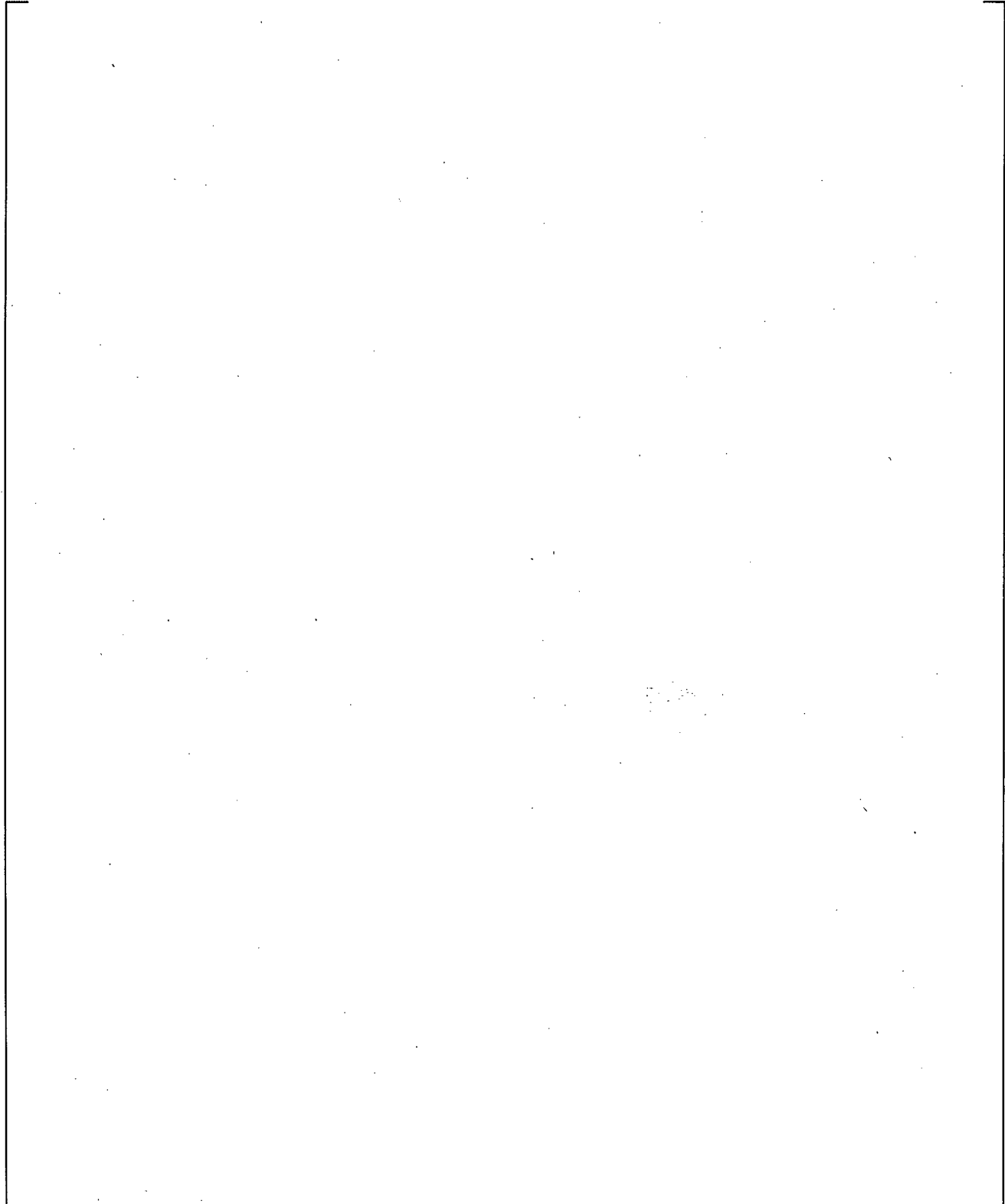


**Figure 23.2.4-15 Vapor Velocity Profile in the 3D Vessel for the Steam Expulsion Test, Saturated Steam Case**

## 23.2.5 1D PIPE Fill and Drain Test

### 23.2.5.1 Introduction

The objective of this test is to study the capability of WCOBRA/TRAC-TF2 (1D Module) of tracking a two-phase mixture level in a vertical pipe as it crosses cell boundaries. The problem is similar to the steam expulsion test, with the difference that the interfacial heat transfer is turned off, gas is injected in the liquid column and the level crosses the cell boundary in both the upward and downward direction.

The problem was first presented by Aktas and Mahaffy (1996) to evaluate a two-phase level tracking method implemented in TRAC-BWR. WCOBRA/TRAC-TF2 has no level tracking capability, however the problem provides some insights on the interfacial drag model and how it behaves in situations where a sharp void fraction gradient exists across cell boundaries. The problem was also studied in (Frepoli et al., 2003).

### 23.2.5.2 Problem Description

In this test problem, a 1D pipe is first filled and then drained to observe the mixture level crossing cell boundaries. During the first 10 seconds of the transient, a steady-state mixture level is established in the vertical pipe by injecting a constant flow of steam (0.5 m/s) at the bottom of a quiescent column of water. At 10 s, water starts to be injected at the velocity of 2.0 m/s for 5 s. At 15 s the liquid flow rate is reversed and the inlet liquid velocity is set to -2.0 m/s for another 5 s. As a result, between 10 s and 20 s, the mixture level crosses two cell boundaries in both directions. The interfacial heat transfer is turned off to focus the attention to the hydraulic behavior of the two-phase mixture. Two cases are studied:

1. Single-phase liquid column (steam flow from the bottom of the pipe is set to zero)
2. Two-phase mixture column (steam flow from the bottom of the pipe is set to 0.5 m/s)

### 23.2.5.3 WCOBRA/TRAC-TF2 (1D Module) Model

The model consists of a vertical pipe with 1.0 m<sup>2</sup> axial flow area and 10.0 m height. A TEE branch with 0.5 m<sup>2</sup> axial flow area and 3.0 m height is connected to the bottom of the pipe. Liquid water is injected, at the branch pipe of the TEE, to raise the liquid column and then withdrawn to let the level drop back to its starting point. The injection and withdrawal rate of liquid water is 2.0 m/s, subcooled at 300K, provided by the FILL attached to the branch pipe of the TEE. A second zero velocity FILL is attached to the TEE main pipe for the case without steam injection. For the steam injection case, a constant 0.5 m/s steam flow is prescribed at the FILL component. A BREAK component is attached to the top of the PIPE to maintain the system pressure at 1.0E+5 Pa. The noding diagram is shown in Figure 23.2.5-1.

### 23.2.5.4 Numerical/Analytical Solution

The solution to the problem is simply a linear increase of the water level starting as soon as liquid is injected (10 seconds). The level rises for 5 seconds, reaches the maximum elevation at 15 seconds, and then decreases for another 5 seconds returning to its starting elevation.

### 23.2.5.5 WCOBRA/TRAC-TF2 (1D Module) Assessment

#### 23.2.5.5.1 Case 1 Without Steam Injection

Figure 23.2.5-2 and Figure 23.2.5-3 show the predicted transient void fraction and pressure, respectively, in cells 5 through 8 during the time window when the level is rising and dropping (from 10 to 20 seconds). The void fraction plot shows that the liquid front moves to the next cell above, before the cell is liquid solid, therefore not resolving a perfect sharp level but diffusing the void gradient across the two cells. The liquid front is smeared over several cells. The behavior is similar during both the upward and downward movement. The predicted pressure change (Figure 23.2.5-3) [

] <sup>a,c</sup>

#### 23.2.5.5.2 Case 2 With Steam Injection

Figure 23.2.5-4 and Figure 23.2.5-5 show a similar smearing effect on the void fraction profile. This is reflected on the pressure response which [

] <sup>a,c</sup>

#### 23.2.5.6 Summary and Conclusions

The 1D Module (Loop) of WCOBRA/TRAC-TF2, although incapable of resolving a precise sharp two-phase mixture level, adequately calculates the movement of a two-phase front in a vertical pipe with pressure and void fraction effects consistent with semi-implicit numerical schemes.

#### 23.2.5.7 References

1. Aktas, Mahaffy, "A two-phase level tracking method," Nuclear Engineering and Design, 162, 1996, pp. 271-280.
2. Frepoli, Mahaffy, Ohkawa, "Notes on implementation of a fully-implicit numerical scheme for a two-phase three-field flow model," Nuclear Engineering and Design, 225, 2003, pp.191-217.

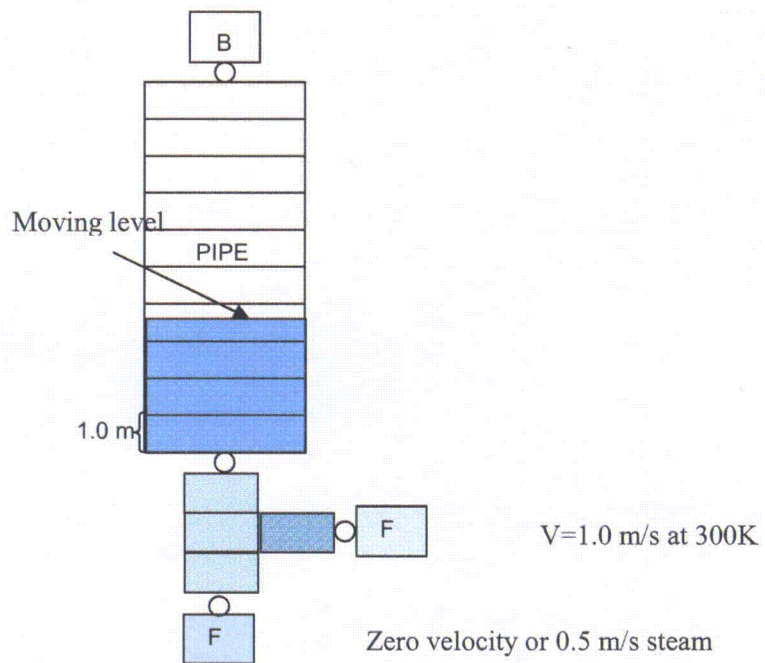
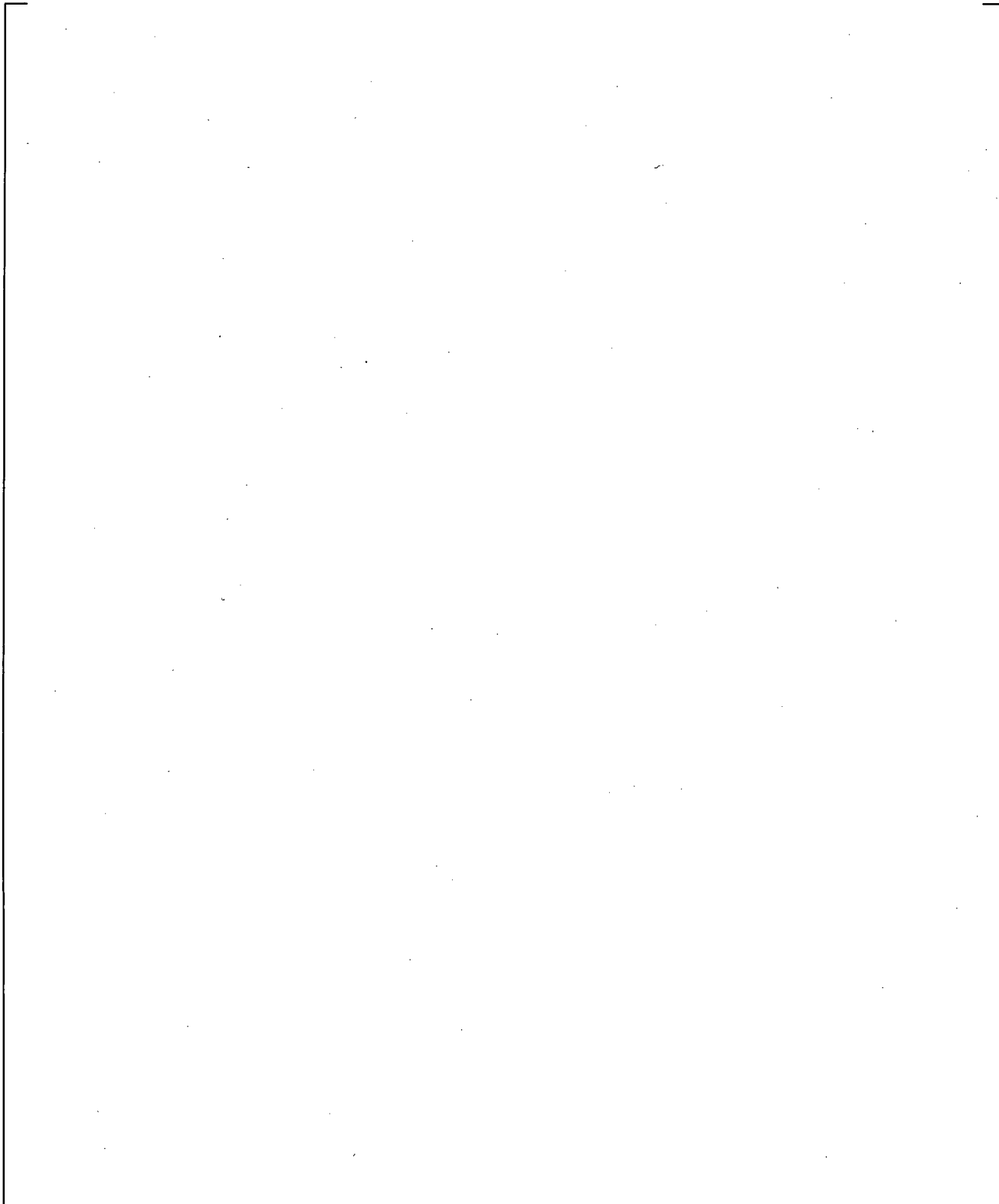
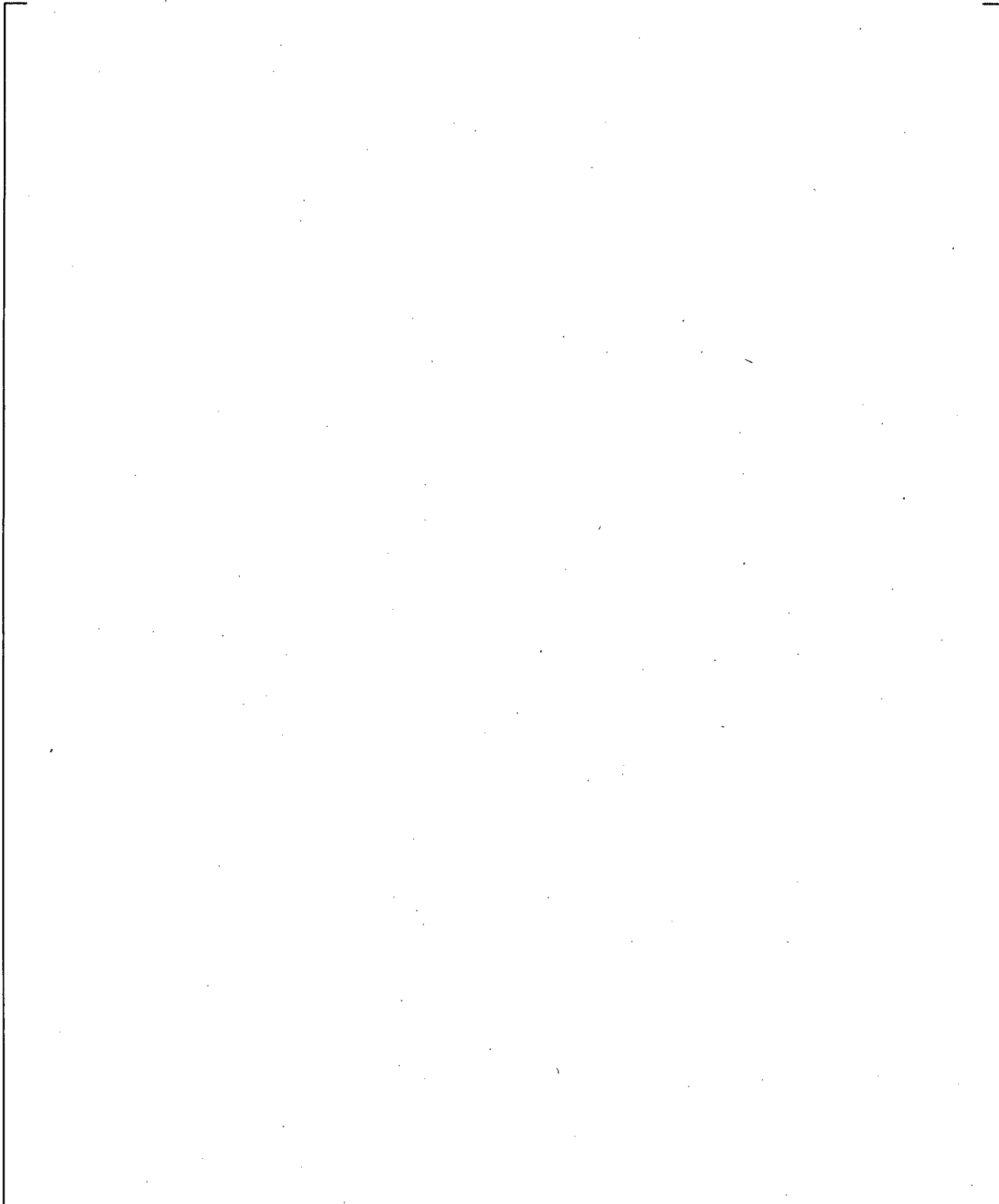


Figure 23.2.5-1 Fill and Drain Model using 1D Pipe



**Figure 23.2.5-2 Predicted Void Fraction between 10 s and 20 s in the 1D Fill and Drain Problem without Steam Injection**



**Figure 23.2.5-3 Predicted Pressure between 10 s and 20 s in the 1D Fill and Drain Problem without Steam Injection**

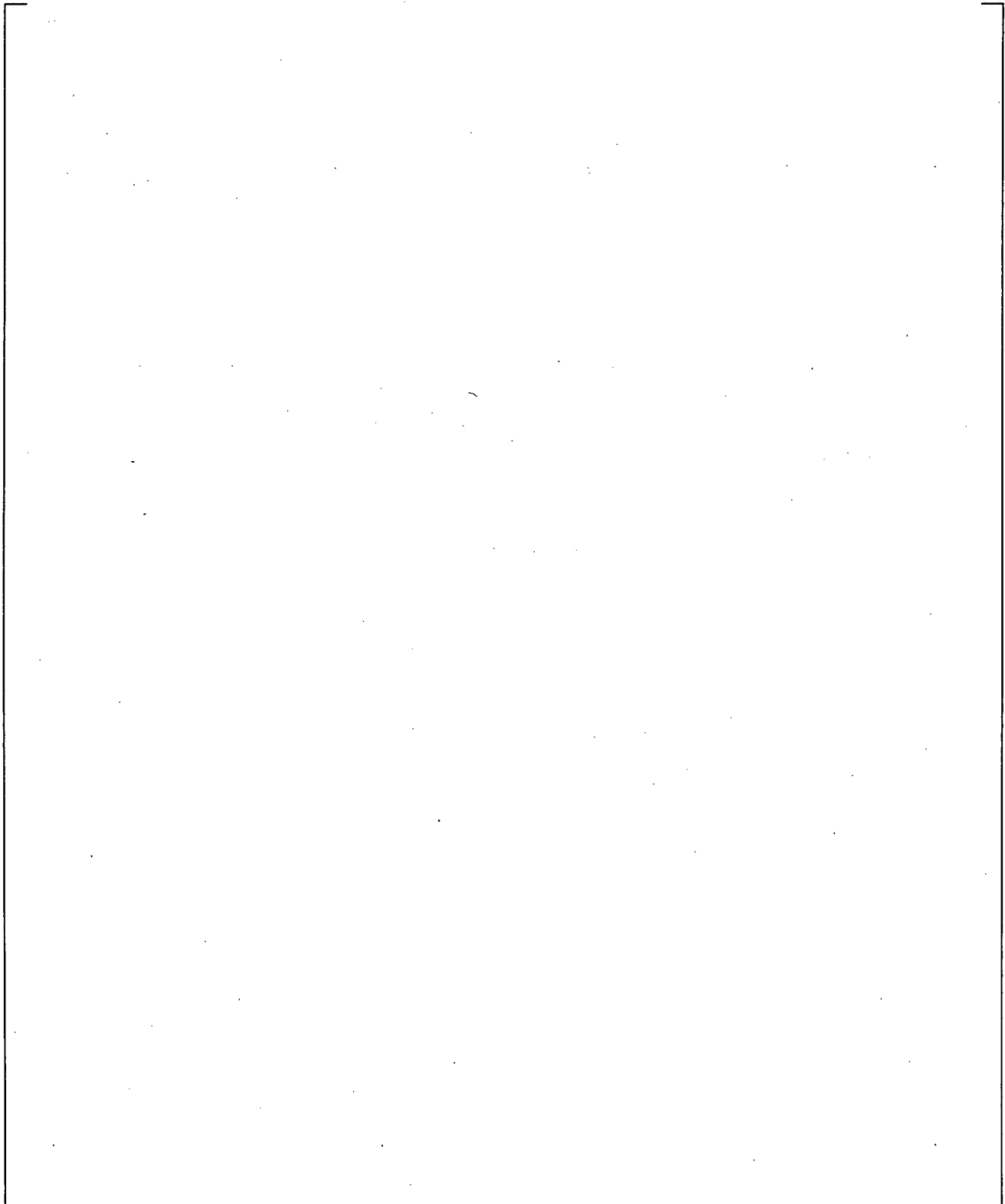


**Figure 23.2.5-4 Predicted Void Fraction between 10 s and 20 s in the 1D Fill and Drain Problem with Steam Injection**

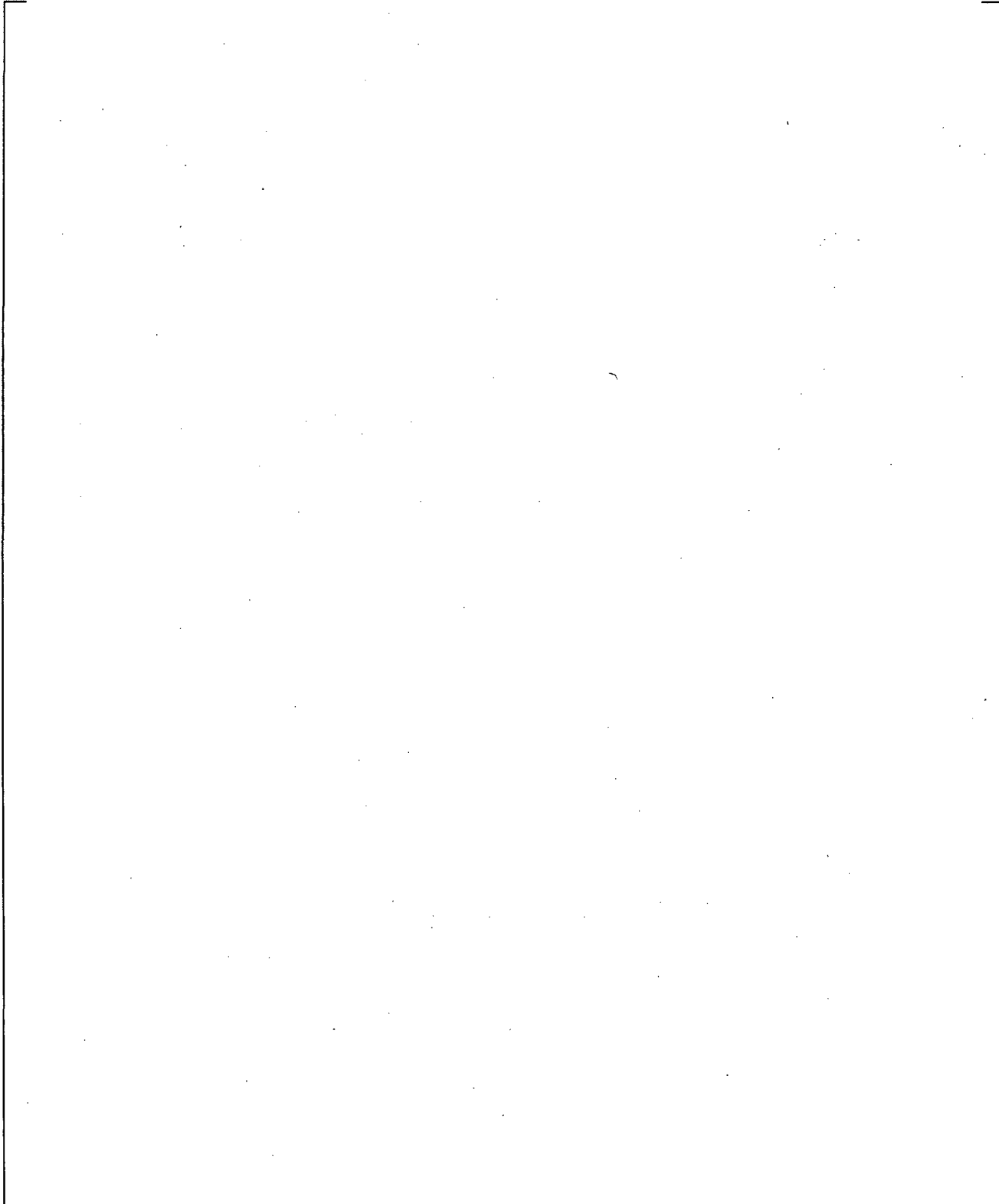


**Figure 23.2.5-5 Predicted Pressure between 10 s and 20 s in the 1D Fill and Drain Problem without Steam Injection**

## 23.2.6 3D VESSEL Fill and Drain Test

### 23.2.6.1 Introduction

The objective of this test is to study the capability of WCOBRA/TRAC-TF2 (3D Module) of tracking a two-phase mixture level in a vertical pipe as it crosses cell boundaries. The problem is identical to what was presented for the corresponding 1D case (Section 23.2.5).

### 23.2.6.2 Problem Description

See Section 23.2.5.2.

### 23.2.6.3 WCOBRA/TRAC-TF2 Model

The model consists of a single channel vessel with  $1.0 \text{ m}^2$  axial flow area and  $10.0 \text{ m}$  height. A TEE branch with  $0.5 \text{ m}^2$  axial flow area and  $3.0 \text{ m}$  height is connected to the bottom of the vessel. Liquid water is injected, at the branch pipe of the TEE, to raise the liquid column and then withdrawn to let the level drop back to its starting point. The injection and withdrawal rate of liquid water is  $2.0 \text{ m/s}$ , subcooled at  $300\text{K}$ , provided by the FILL attached to the branch pipe of the TEE. A second zero velocity FILL is attached to the TEE main pipe for the case without steam injection. For the steam injection case, a constant  $0.5 \text{ m/s}$  steam flow is prescribed at the FILL component. A short pipe and a BREAK component are attached to the top of the vessel to maintain the system pressure at  $1.0\text{E}+5 \text{ Pa}$ . The noding diagram is shown in Figure 23.2.6-1.

### 23.2.6.4 Numerical/Analytical Solution

See Section 23.2.5.4.

### 23.2.6.5 WCOBRA/TRAC-TF2 Assessment

#### 23.2.6.5.1 Case 1 Without Steam Injection

Figure 23.2.6-2 shows the predicted collapsed liquid level in the vessel. In the first  $10 \text{ s}$ , the problem reaches a steady-state. The transient starts at  $10.0 \text{ s}$ , when the liquid water starts injecting at a rate of  $2.0 \text{ m/s}$  for  $5.0 \text{ s}$ . At  $15.0 \text{ s}$ , the collapsed liquid level reaches approximately  $9 \text{ m}$ , at which point the flow is reversed, and the vessel starts draining. Similar to the 1D pipe results, the liquid front moves to the next cell before the cell is fully liquid water, as seen in the void fraction plot in Figure 23.2.6-3. [

Behavior is in general similar to the corresponding 1D case with a smaller diffusion of the void front in this case as indicated by the void fraction results in Figure 23.2.6-2. ]<sup>a,c</sup>

### 23.2.6.5.2 Case 2 With Steam Injection

Figure 23.2.6-6 shows the predicted collapsed liquid level in the vessel. In the first 10 s, the problem reaches a steady-state. The transient starts at 10.0 s, when the liquid water starts injecting at a rate of 2.0 m/s for 5.0 s. At 15.0 s, the collapsed liquid level reaches approximately 9 m, at which point the flow is reversed, and the vessel starts draining.

Results are similar to the corresponding 1D pipe results (Figure 23.2.6-7 and Figure 23.2.6-8). There is a diffusion of the void front, possibly to a lesser extent in this case.

### 23.2.6.6 Summary and Conclusions

Similar to the 1D case, the 3D Module (Vessel) of WCOBRA/TRAC-TF2, although not capable of resolving a precise sharp two-phase mixture level, calculates adequately the movement of a two-phase front in a vertical pipe with pressure and void fraction effects consistent with semi-implicit numerical schemes.

### 23.2.6.7 References

1. Aktas, Mahaffy, "A two-phase level tracking method," Nuclear Engineering and Design, 162, 1996, pp. 271-280.

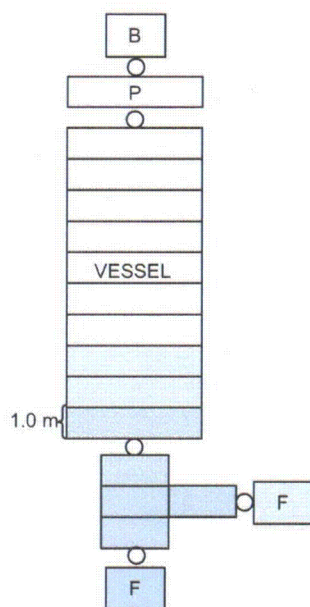
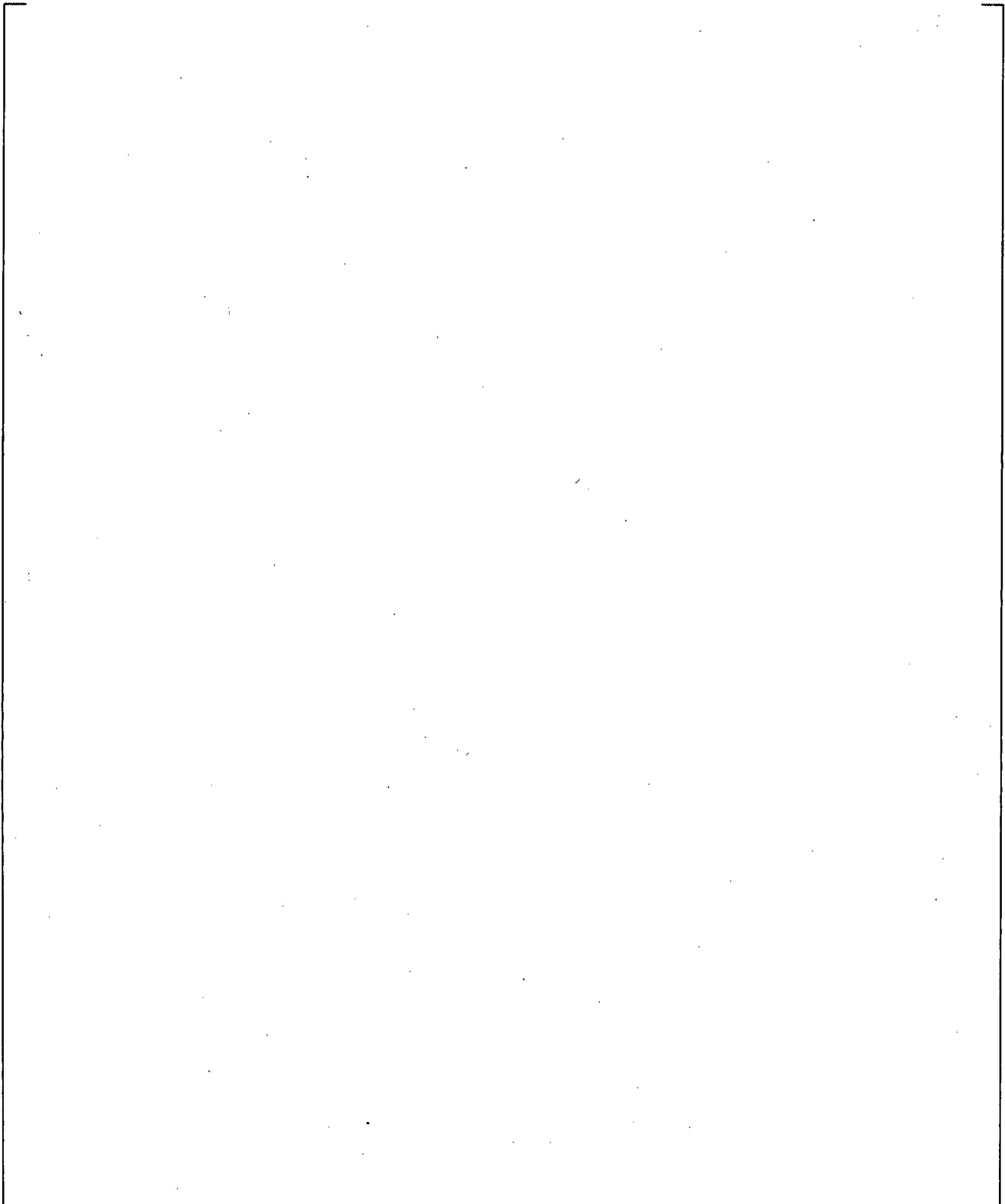


Figure 23.2.6-1 Fill and Drain Model using 3D Vessel



**Figure 23.2.6-2 Predicted Collapsed Liquid Level in the 3D Fill and Drain Problem without Steam Injection**



**Figure 23.2.6-3 Predicted Void Fraction between 10 s and 20 s in the 3D Fill and Drain Problem without Steam Injection**

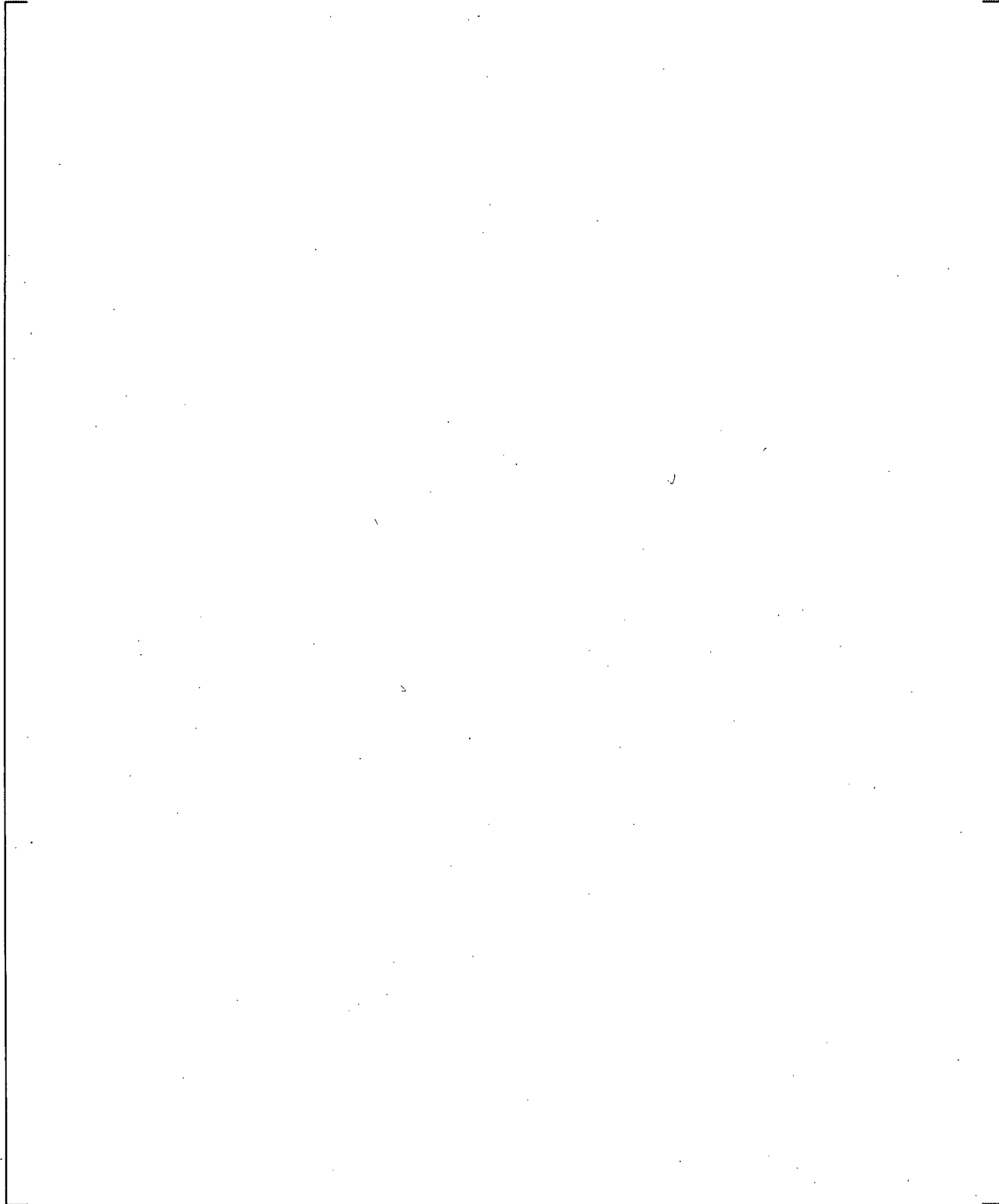


**Figure 23.2.6-4 Predicted Pressure between 10 s and 20 s in the 3D Fill and Drain Problem without Steam Injection**

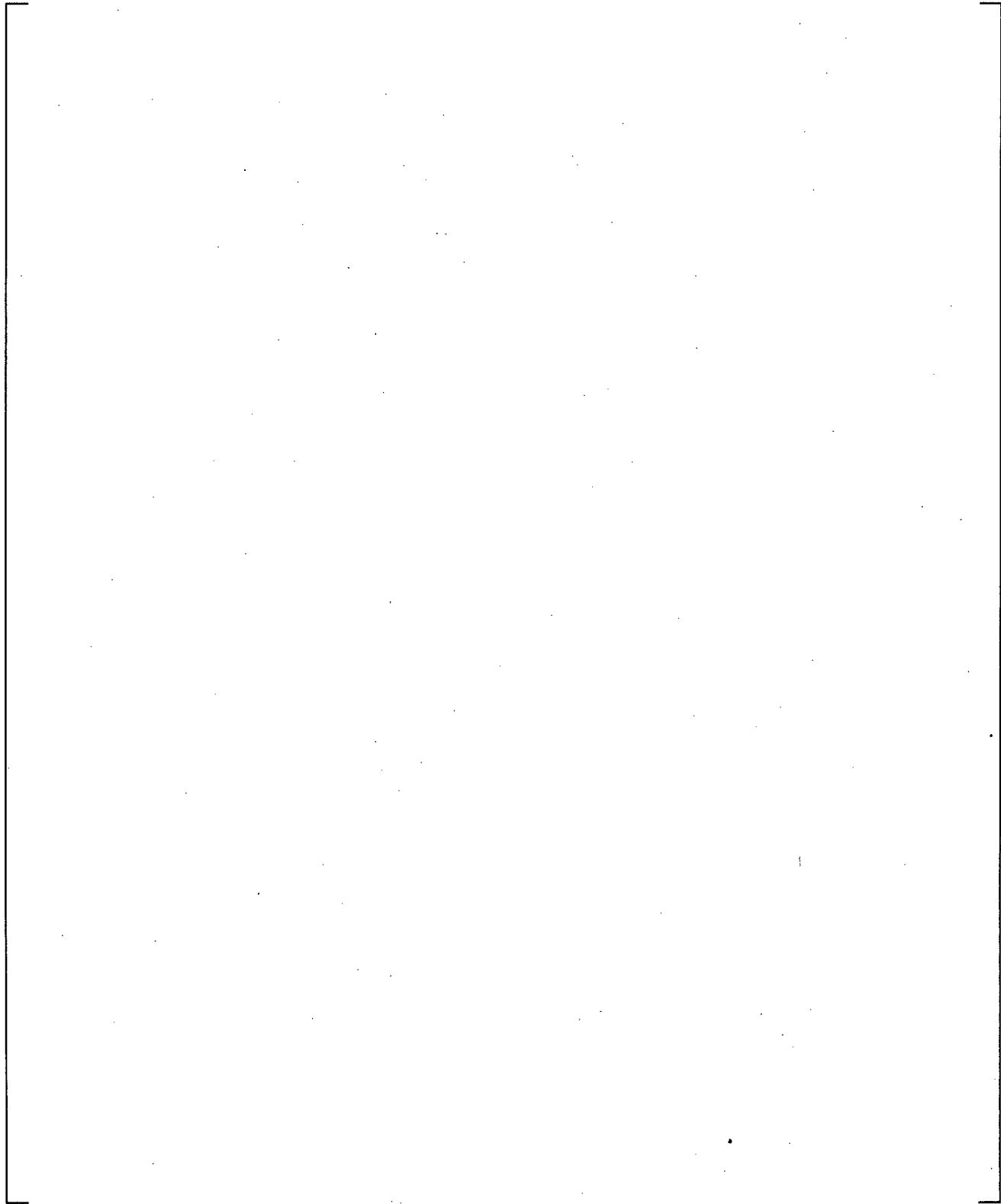


**Figure 23.2.6-5 Predicted Pressure between 10 s and 20 s in the 3D Fill and Drain Problem without Steam Injection**

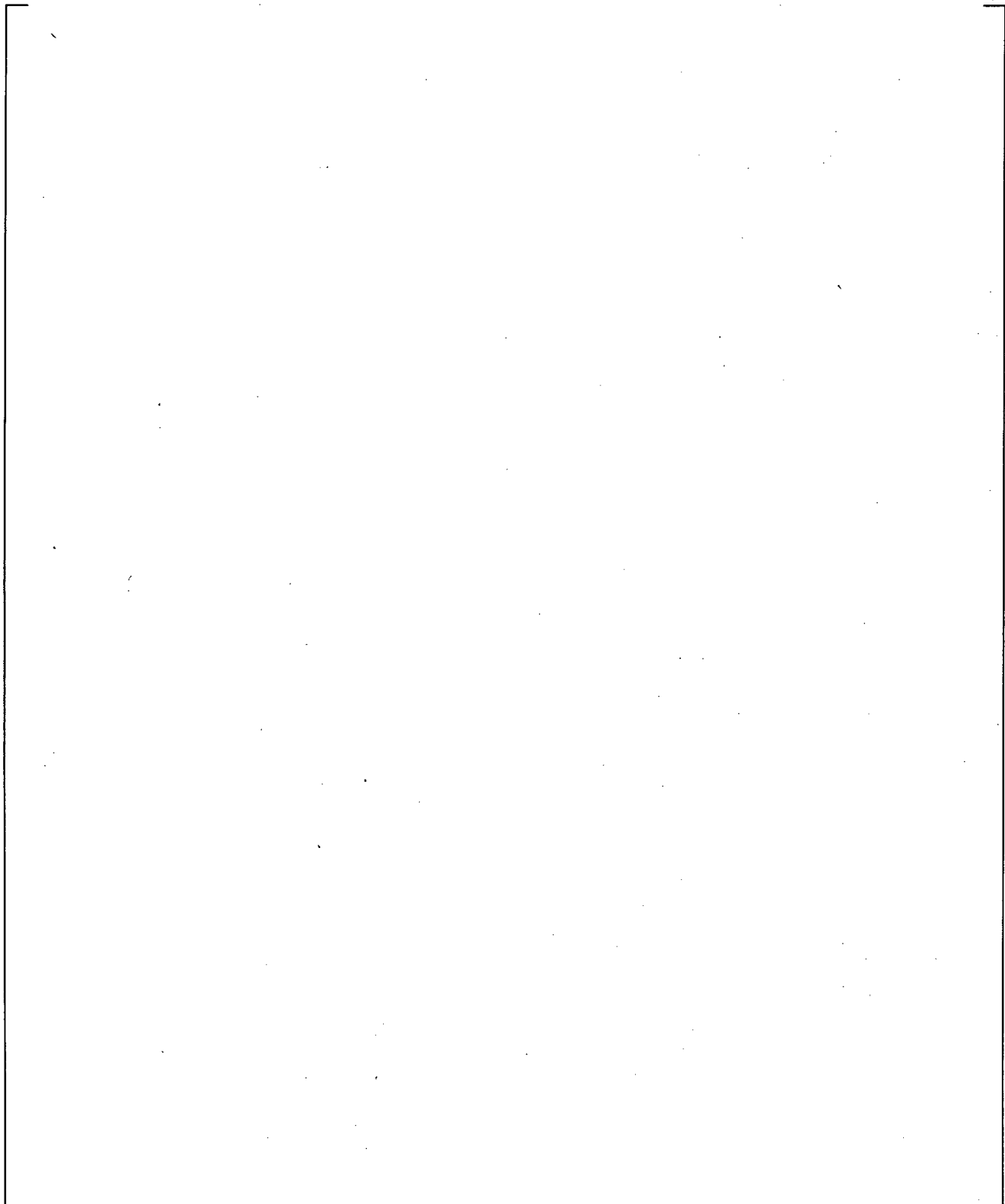


**Figure 23.2.6-6 Predicted Collapsed Liquid Level in the 3D Fill and Drain Problem with Steam Injection**

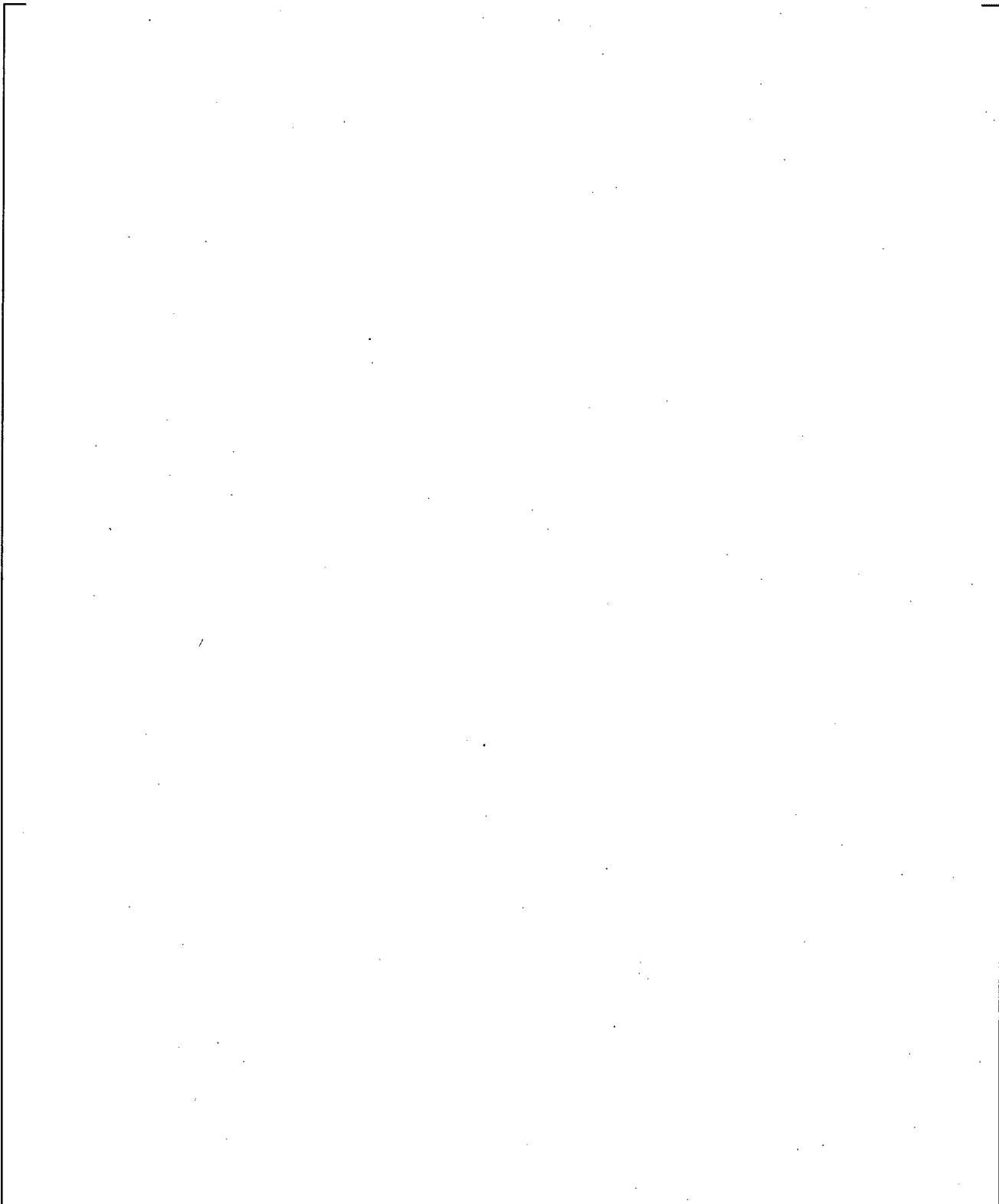


**Figure 23.2.6-7** Predicted Void Fraction between 10 s and 20 s in the 3D Fill and Drain Problem with Steam Injection

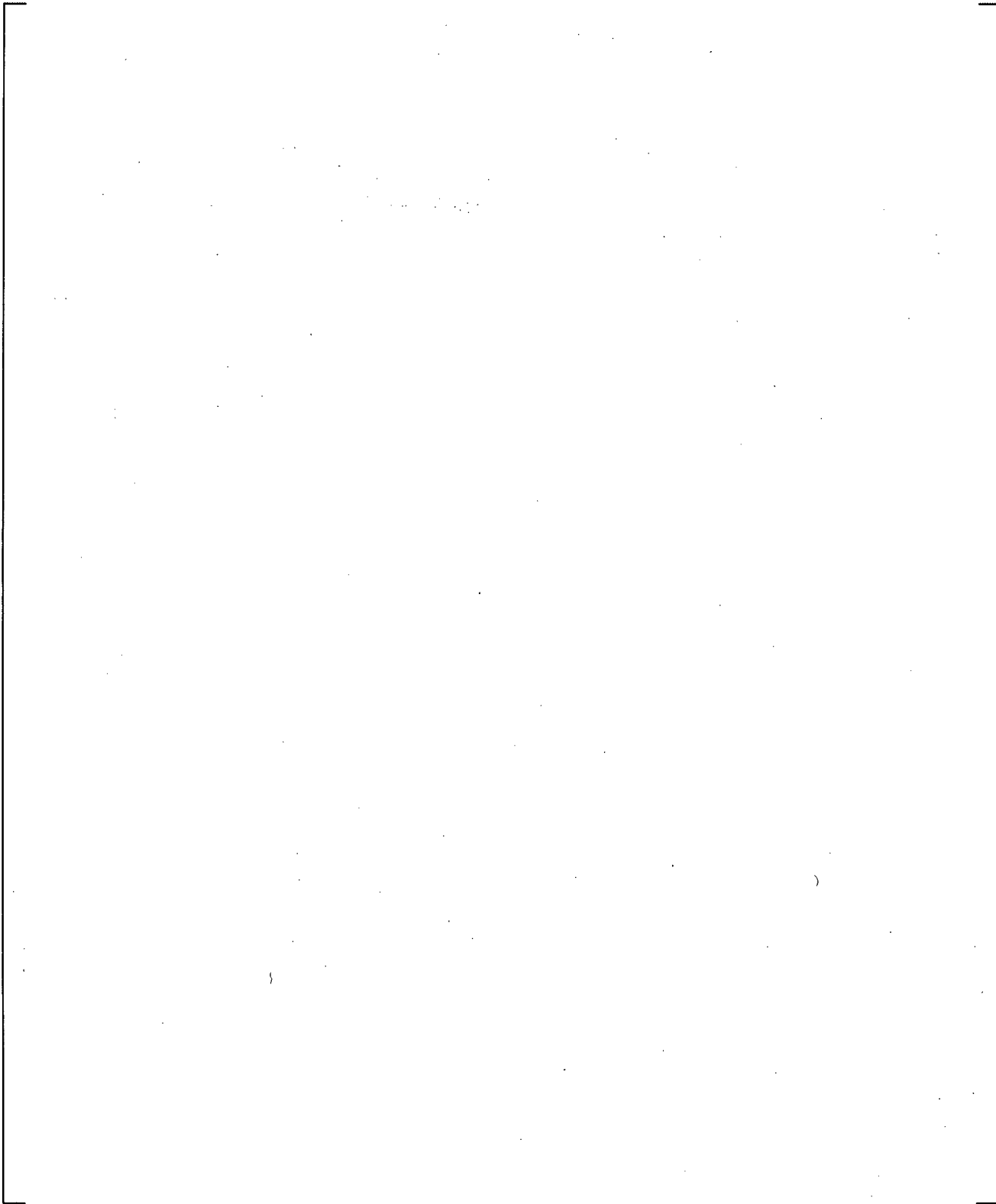


**Figure 23.2.6-8 Predicted Pressure between 10 s and 20 s in the 3D Fill and Drain Problem with Steam Injection**

## 23.2.7 Condensation Test

### 23.2.7.1 Introduction

The condensation model used in WCOBRA/TRAC-TF2 is described in Section 6 of Volume I. The objective of this Section is to assess the performance of the WCOBRA/TRAC-TF2 condensation model on simple problems, to verify that the code results are in agreement with expectations.

### 23.2.7.2 Problem Description

A vessel (1.0 ft<sup>2</sup> flow area and 1.0 ft height) is initially filled with saturated steam at 1000 psia. A heat slab is included in the vessel, which is kept at 80°F wall temperature, providing a medium for condensation. The top of the vessel is connected to a pipe, and a constant pressure of 1000 psia is maintained at the other end of the pipe. The first case analyzed does not have non-condensable gas present. In the second case, the partial pressure of non-condensable is set to 1000 psia at the outlet of the pipe. The objective is to evaluate the condensation within the vessel with and without non-condensable gas present.

### 23.2.7.3 WCOBRA/TRAC-TF2 Model

The vessel is modeled via a single channel with a 1.0 ft<sup>2</sup> flow area and 2 axial nodes, each with 1.0 ft height. The pressure boundary is maintained by a BREAK component at 1000 psia attached to the outlet pipe. A schematic of the test problem is shown in Figure 23.2.7-1.

### 23.2.7.4 Numerical/Analytical Solution

No attempt is made to develop an analytical solution of the transient for the purpose of this assessment. Results are checked against the equilibrium condition reached as a steady-state is reached. The equilibrium condition is known and is reached when all of the vapor will condense on the cold wall surface filling up the cell. Introduction of any non-condensable gases is expected to suppress the condensation.

### 23.2.7.5 WCOBRA/TRAC-TF2 Assessment

#### 23.2.7.5.1 Vapor Only Case

Saturated vapor condenses on the cold wall at the top and bottom cells and quickly forms a liquid film.  
[

] <sup>a,c</sup>

The early part of the transient is characterized by a small downward gas and liquid velocity in the bottom cell as the condensation of gas pulls saturated vapor downward. As the flow regime in the bottom cell switches to bubbly flow, the heat transfer coefficient to vapor in the top cell (Figure 23.2.7-4) and to liquid in both the bottom and top cells (Figure 23.2.7-5) increases such that the bottom cell becomes fully

liquid and the top cell undergoes condensation resulting in a void fraction near [ ]<sup>a,c</sup>. Once the bottom cell is filled with liquid, the phasic velocities become zero, resulting in negligibly small wall-fluid heat transfer and a cessation of condensation in the top cell.

#### 23.2.7.5.2 Non-Condensable Gas Case

In this test, as the saturated vapor condenses, non-condensable gas is pulled into the vessel. As the non-condensable gas enters the cell and its partial pressure increases, the relative humidity and the dew point temperature decrease, as seen in Figures 23.2.7-6, 23.2.7-7, and 23.2.7-8. Once the cell is entirely filled with liquid and non-condensables, no vapor remains for condensation and the void fraction reaches equilibrium. Since the pressure is held constant, the equilibrium solution is that the partial pressure of steam is equal to the saturation pressure at the vapor temperature. For this test, WCOBRA/TRAC-TF2 predicts a steam partial pressure of [ ]<sup>a,c</sup>, appropriate for the equilibrium vapor temperature of [ ]<sup>a,c</sup>.

#### 23.2.7.6 Summary and Conclusions

The expected outcome is achieved by the WCOBRA/TRAC-TF2 test problems: the vapor condenses on the cold wall surface filling up the cells and the introduction of non-condensable gases suppresses the condensation.

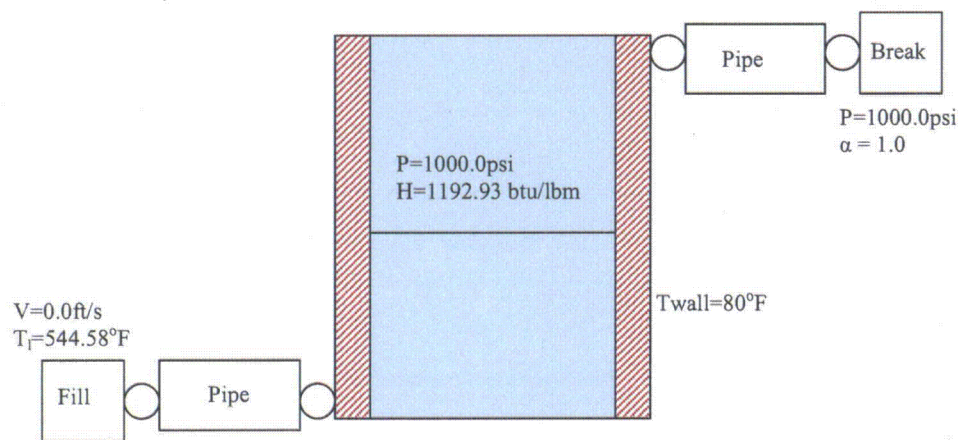
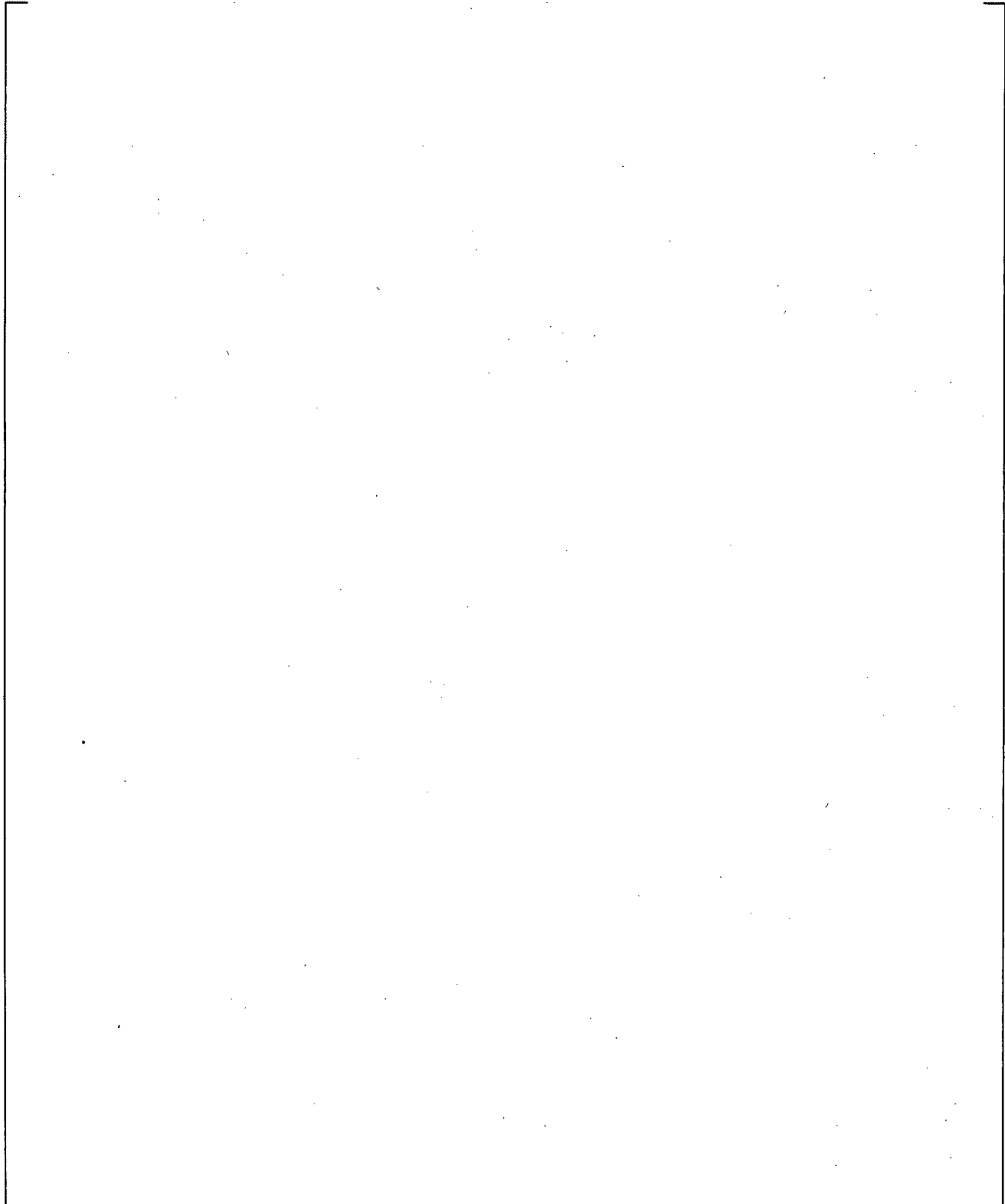
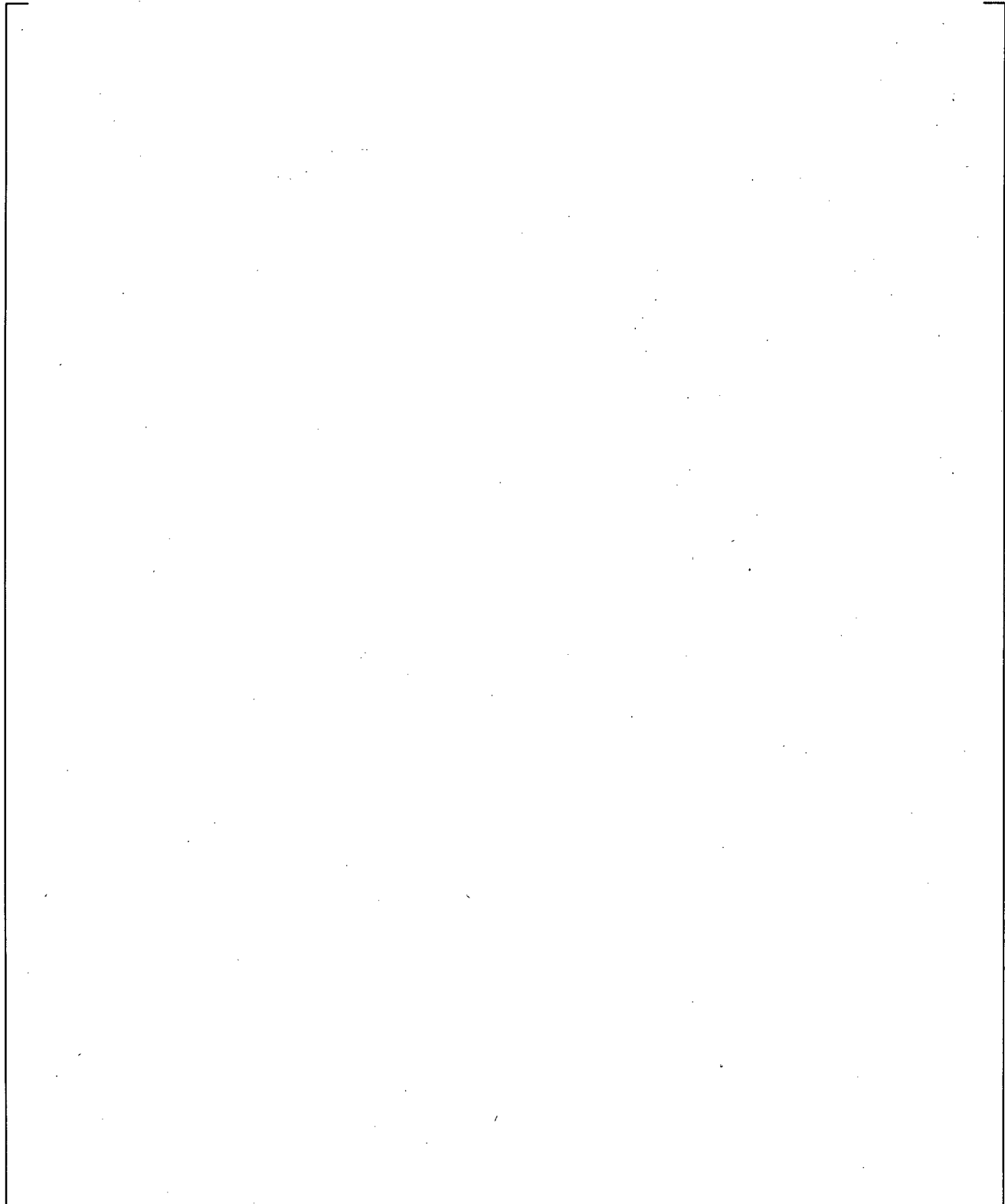


Figure 23.2.7-1 3D Vessel Model used in the Condensation Test Problem



**Figure 23.2.7-2 Void Fraction in the Condensation Test Problem, Vapor only Case**



**Figure 23.2.7-3 Flow Regime in the Condensation Test Problem, Vapor Only Case**

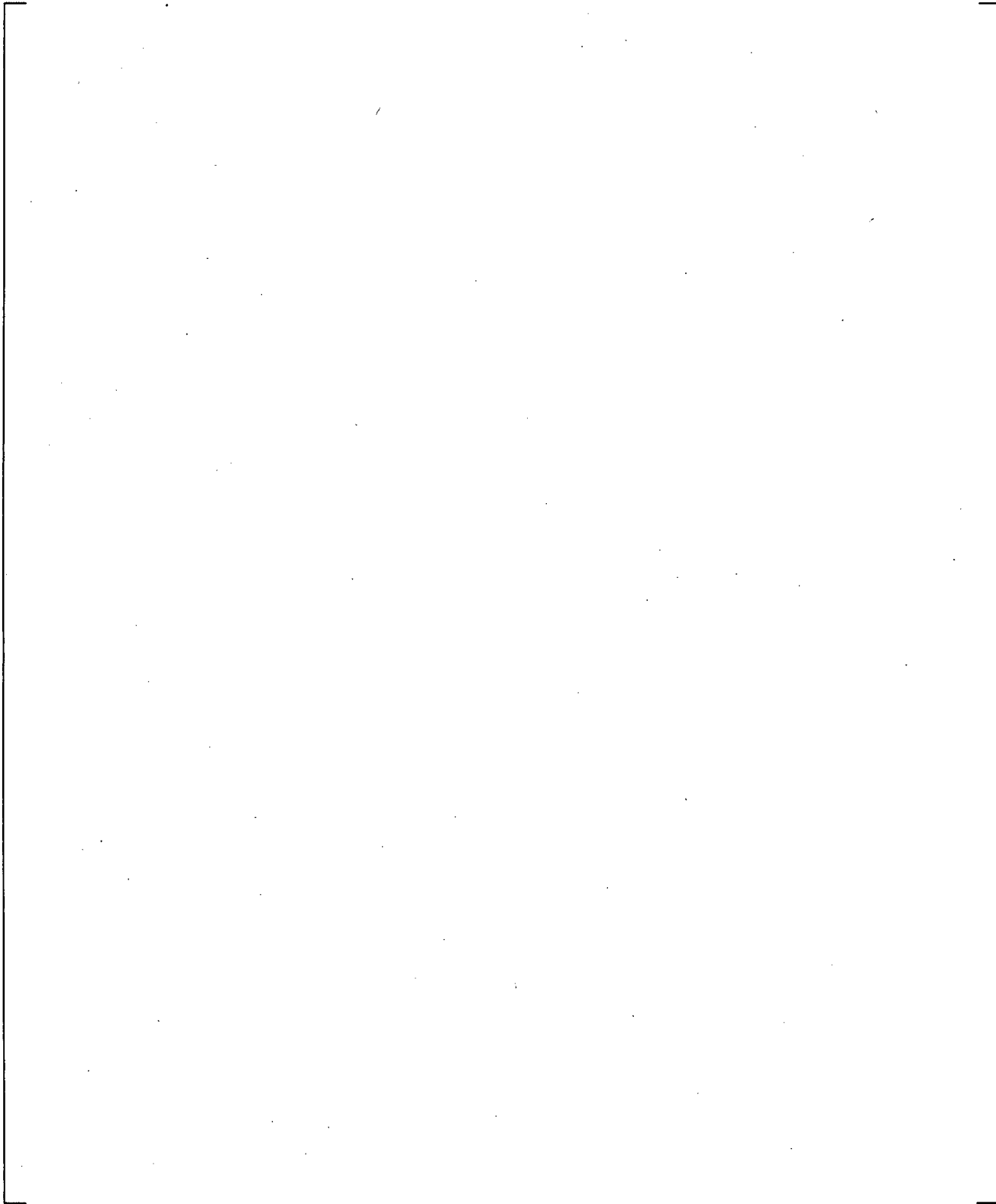


**Figure 23.2.7-4 Heat Transfer to Vapor and Vapor Velocity in the Condensation Test Problem, Vapor Only Case**

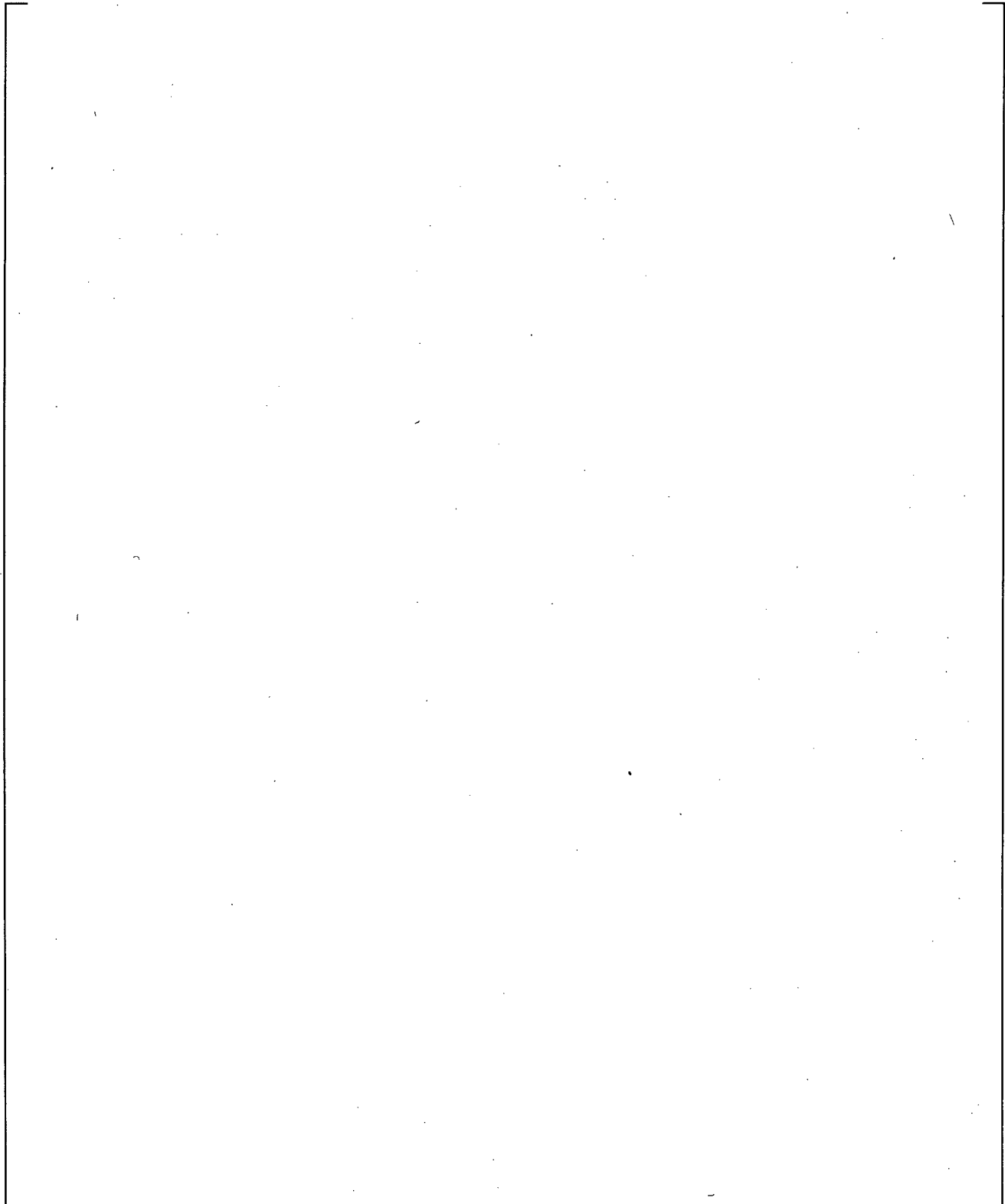


**Figure 23.2.7-5 Heat Transfer to Liquid and Liquid Velocity in the Condensation Test Problem, Vapor Only Case**

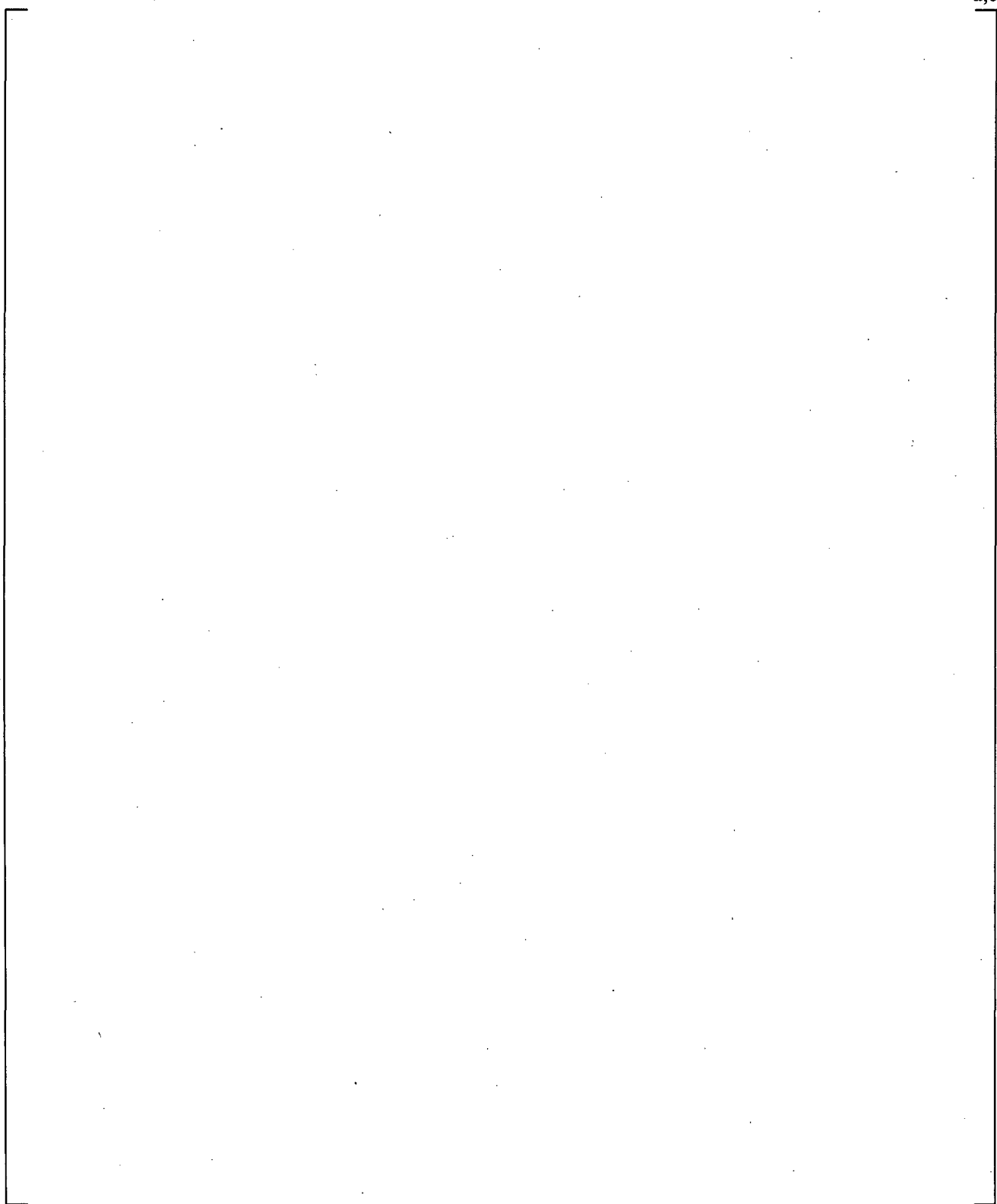


**Figure 23.2.7-6**      **Void Fraction and Relative Humidity in the Condensation Test Problem, Vapor and Non-Condensable Gas Case**

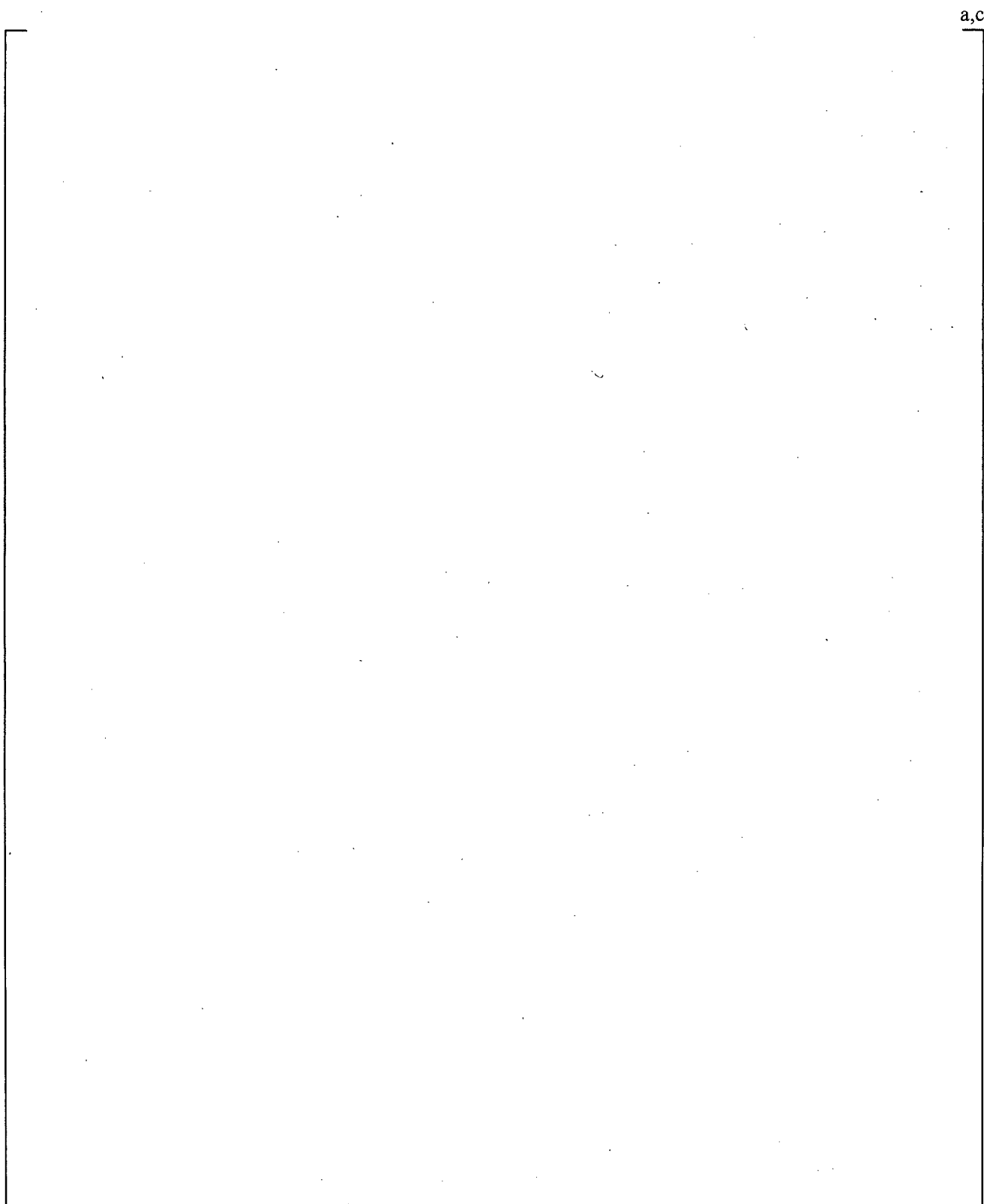


**Figure 23.2.7-7 Total, Steam, and Non-Condensable Gas Partial Pressures in the Condensation Test Problem, Vapor and Non-Condensable Gas Case**

a,c

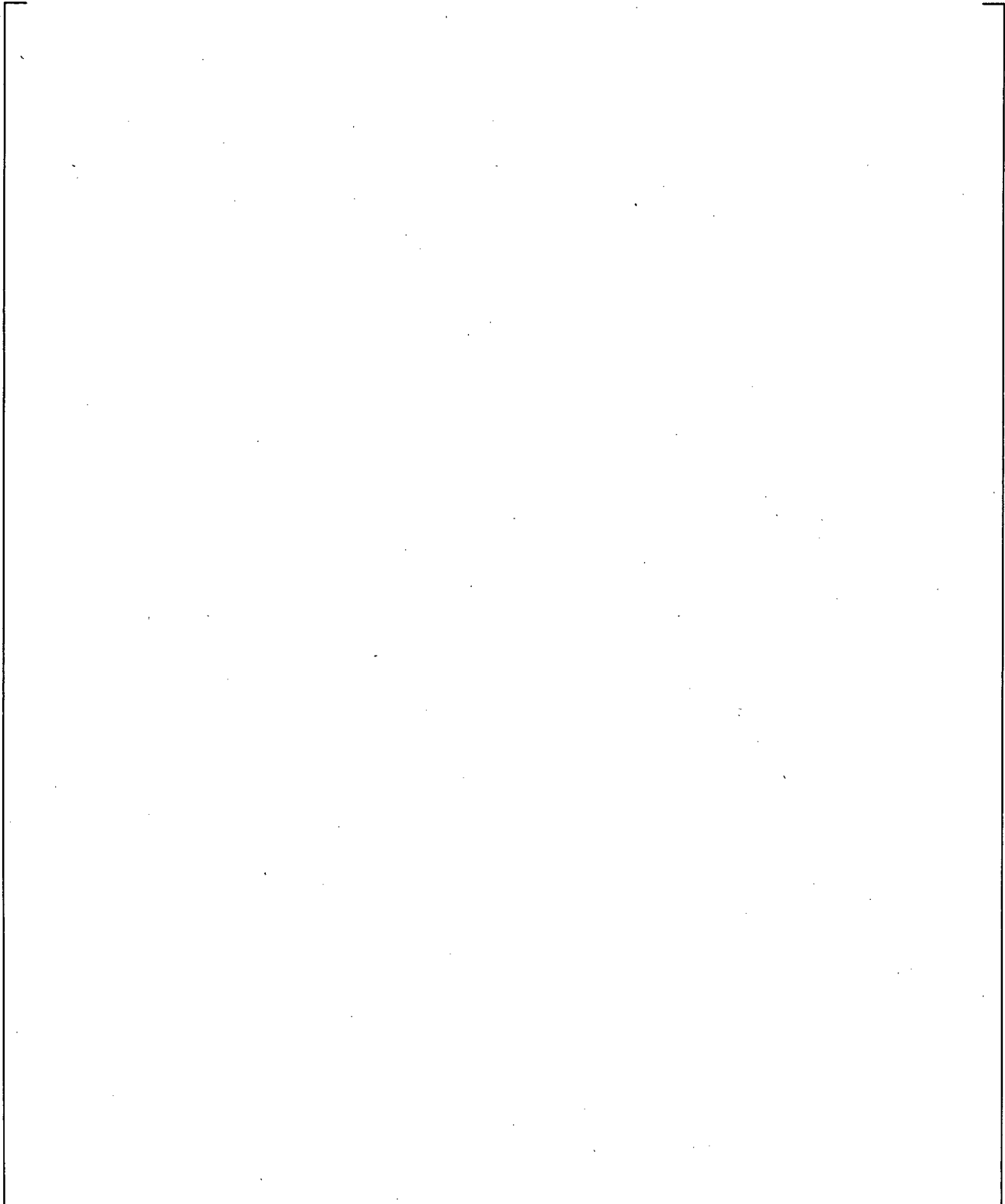


**Figure 23.2.7-8**

**Gas, Liquid, Saturation, and Dew point Temperatures in the Condensation Test Problem, Vapor and Non-Condensable Gas Case**

## 24 ASSESSMENT OF COMPENSATING ERROR IN EVALUATION MODEL USING WCOBRA/TRAC-TF2

### 24.1 INTRODUCTION

#### Compensating Errors in Simulations

In Section 1.1.2 of RG 1.203, Step 2 discusses "Figure of Merit" for the assessment, and also describes the need to consider "compensating errors" when assessing the adequacy of the code models. Section 1.1.2 states,

*"In line with the surrogate figure of merit, it is also important to consider other related performance measures in conjunction with the principle objectives. Because compensating errors in the code can unintentionally lead to correct answers, additional performance measures serve as physical tracking points and additional proof of accuracy. While the code may calculate the correct peak cladding temperature (PCT), for example, incorrect or physically impossible parameter values could evolve in other areas of the calculation."*

Compensating errors are those model errors which, when acting in combination, could result in good but misleading prediction of the phenomena or the parameter of interest for which the code is being assessed. This is especially important because most of validation tests use small scale tests, and scale impacts could magnify the code model errors of this kind. If the code contains significant compensating errors and scale test simulations appear well predicted because of the compensating errors, the accuracy of full scale transient simulations such as LOCA analysis of a PWR could be suspect.

An evaluation of the potential for the existence of compensating error in the predicted results of selected integral and separate effects tests from WCOBRA/TRAC-TF2 is performed in this section. Compensating errors are those model errors which, when operating in combination, could result in good prediction but cause improbable combination of parameters. This is a concern particularly for integral effects tests, where there are few fixed boundary conditions. For example the prediction of apparently correct heat transfer in the LOFT experiments could occur because the core flow rate was under predicted, while the heat transfer model over predicts the local heat transfer coefficient.

Not all model errors are compensating. For example, over predicting the core flow may result in over-estimating the core heat transfer. This effect would be expected if the heat transfer model was physically correct, and therefore does not point to a significant deficiency in the heat transfer model. The process of evaluation for compensating errors is briefly outlined below.

#### Identification of Possible Compensating Errors

The process of evaluation starts with the review of Highly Ranked Phenomena tabulated in Table 2-2, and WCOBRA/TRAC-TF2 Model Assessments validation matrix using Separate Effects Tests (SETs) given in Tables 2-3, 2-4 and 2-5. For each model assessment, possible compensating errors involving sub-models (or constituent models) are sought and identified. For example some models such as Post CHF Heat Transfer Model, are constructed from multiple sub-models such as the single phase vapor heat transfer,

vapor-droplet evaporation heat transfer, and the heat transfer due to droplet-wall impaction, all of which work in combination to form a heat transfer value which determines the cladding temperature which is the primary figure of merit. Because a good clad temperature prediction requires only that the sum of three models to be reasonable, there is a possibility of compensating errors where individual values may be unreasonable but the sum of three is reasonable. For all highly ranked phenomena in SETs, possibility of errors of a kind described above is examined and identified.

In Integral Effects Tests (IETs) by design, multiple physical models and components are often in competition as the transient evolves. Thus there are possible compensating errors which involve interaction of multiple models/phenomena. For example, the PCT in a SBLOCA is strongly impacted by the mixture level and the heat transfer prediction. A reasonable prediction of PCT may be obtained even when the mixture level is biased too low but the heat transfer is biased too high. For IETs of SBLOCA, IBLOCA, and LBLOCA sub-scenarios, possible occurrences of this type of compensating errors are sought and identified.

### **Evaluation of Compensating Errors in Simulations**

For selected simulations in which potential of compensating errors is identified, the simulation fidelity of parameters in addition to the main parameters of interest is evaluated for additional proof of accuracy. For example, the primary figure of merit for LOFT simulations is the PCT. But the assessment will be performed utilizing comparisons to other measured quantities such as vapor temperatures in the vicinity of core, flow, void fraction, and loop flow so that the existence or absence of significant compensating errors could be evaluated. With additional proof of accuracy the confidence that the adequacy of evaluation model using WCOBRA/TRAC-TF2 at the PWR scale would be increased.

## **24.2 IDENTIFICATION OF HIGHLY RANKED PHENOMENA AND MODEL ASSESSMENT**

Section 2 of this document discusses PIRT for the full spectrum break LOCAs. A validation test matrix for highly ranked phenomena was developed based on the high and medium ranked phenomena from the PIRT and available separate effects and integral effects tests. Tables 24.2-1 through 24.2-4 represent the validation matrix for WCOBRA/TRAC-TF2 which lists highly ranked phenomena, and SETs and IETs for LBLOCAs, SBLOCAs and IBLOCAs. The table format is altered from Tables 2-3 through 2-6 to emphasize the phenomena and supporting validation tests. For each of phenomena listed in these tables, possible compensating errors which may be present in the assessment simulations are sought and results are summarized in the subsequent sections.

<b>Phenomena</b>	<b>Test</b>	<b>Comments</b>
Critical Flow	Marviken, LOFT	High/full pressure in a full/sub scale facility
Break Resistance.	LOFT, UPTF Test 6	Loop Piping may not be prototypic, Broken cold leg nozzle.
Fuel Rod	LOFT	Blowdown heat-up
Heat Transfer	ORNL-THTF (Film Boiling Tests), W-G1 (Blowdown), LOFT	Steady State and transient DFFB tests
ECC Bypass	UPTF6, LOFT	Full scale low pressure/sub scale full pressure
SI & DC Condensation	UPTF6, UPTF8, LOFT	Full scale low pressure/sub scale full pressure

<b>Phenomena</b>	<b>Test</b>	<b>Comments</b>
Heat Transfer	W-G2 Refill/Reflood, FLECHT-LFR, FLECHT-SEASET (Reflood and Steam Cooling), FLECHT-Skewed, FEBA, Achilles, CCTF, LOFT (part length)	Full height refill/reflood bundle tests, simulated and nuclear rods (LOFT)
SI, DC Condensation	UPTF25A, LOFT	Full/sub scale tests
N2 Injection	Achilles, LOFT	L2-5 showed some impact due to N2 injection. The simulation was compared to the observation in the test.
Fuel Rod	LOFT	Not simulated. Models and correlations are judged to not contain competing effects to cause compensating errors.
Entrainment/ De-entrainment	W-G2 Reflood, FLECHT-LFR, FLECHT-SEASET, FLECHT-Skewed, FEBA, Achilles, UPTF29B, UPTF25A, CCTF, LOFT	Full height refill/reflood bundle entrainment, UP, DC entrainment

Table 24.2-3 V&V Matrix for Small Break LOCA Processes, Separate Effect Tests		
Small Break Process	Test	Comments
Critical Flow	EPRI-NP-4556 + additional Marviken Dataset represents approximately 3200 points from 53 geometries, and 10 facilities, containing data from 13 to 2500 psia.  The geometrical range: $0 < L < 2300\text{mm}$ , $0.464 < DH < 500\text{mm}$ .	Available data appears to span PWR ranges of conditions for break area, upstream subcooling, and flow quality. (V. Ilic, S. Banerjee and S. Behling, "A Qualified Database for the Critical Flow of Water," EPRI-NP-4556, May, 1986.)
Mixture Level	ORNL, W G-1 & G-2 Boiloff, TPTF, GE Blowdown, Semiscale S-7-10D (SET Mode)	Data covers PWR expected range of pressure and bundle power.
Horizontal Flow Regimes	JAERI-TPTF Horizontal Flow Tests	Horizontal stratified regime transitions predicted according to modified Taitel-Dukler/Wallis-Dobson map.
Loop Seal Clearance	UPTF Loop Seal Tests	Full scale geometry, provides information for range of Jg that covers PWRs.
Fuel Rod Models: Nuclear Rod Models ~Heat Transfer	Various sets of test data from LBLOCA, Single Phase Vapor Heat Transfer: ORNL-THTF (Uncovered Bundle Tests)	Fuel rod models were assessed and quantified for large break.  Data representative of SBLOCA conditions.
Pump Performance	Pump Specific Data from LBLOCA	Empirical pump data; assessed for large break LOCA.
SI Condensation	COSI Tests, SB-CL-05 (SET Mode)	High pressure SI condensation.
Break Flow, entrainment at Break/Offtake	TPFL	Single and two-phase critical break flow measurements available. Orientation effect.

<b>Table 24.2-4 V&amp;V Matrix for Small Break LOCA Processes, Integral Effect Tests</b>		
<b>Small Break Process</b>	<b>Test</b>	<b>Comments</b>
Break Flow, entrainment at Break	LOFT L3-1, ROSA: <u>10%</u> CL (side), <u>5%</u> CL (side), <u>2.5%</u> CL (side, top, and bottom), <u>0.5%</u> CL (top, side, and bottom)	Single and two-phase critical break flow measurements available. Orientation effect.
Mixture Level	ROSA: 10% CL, 5% CL, 2.5% CL, and 0.5% CL, L5-1	Range of break sizes. Vessel inventories and system wide mass distributions.
Steam Generator Hydraulics	ROSA NC, SB-CL series	Provides information on system wide phase separation, primary-secondary heat transfer.
Loop Seal Clearance	ROSA: 10% CL, 5% CL, 2.5% CL, 0.5% CL, and additional 5% CL with higher Core Bypass	Provides information on LSC phenomena.
Fuel Rod Models: Nuclear Rod Models: Heat Transfer:	LOFT ROSA SB-CL – series	Nuclear rods. Clad heatup & PCTs.
IBLOCAs	ROSA 10%, LOFT L5-1	A 10% cold leg break and a 14in ACC line Break

## 24.3 IDENTIFICATION OF POSSIBLE COMPENSATING ERRORS IN MODEL ASSESSMENT

### 24.3.1 Possible Compensating Errors in Separate Effects Test Simulations

#### 24.3.1.1 Delivery and Bypassing of ECC and Condensation in the Downcomer

The validation of ECC bypass model is documented in Section 19.3.5. The delivery of ECC liquid into the lower downcomer is impacted by the counter current limit in the downcomer due to high vapor flow from the core. The CCFL is affected by interfacial drag and also by condensation. CCFL conditions could be predicted well, even though under-estimating the interfacial drag (too little liquid holdup for a given steam flowrate), by under-estimating the condensation rate (too much steam flow). Therefore condensation and interfacial drag are potential source of compensating error relative to the prediction of delivery and bypass of ECC liquid.

#### 24.3.1.2 Post CHF Heat Transfer

A specific area of concern is the way in which the film boiling models are constructed in WCOBRA/TRAC-TF2. The heat transfer models are constructed as a combination of several heat transfer mechanisms. This construction is described in Section 7.2.11 of this document. In the CSAU development (Boyack et al., 1989), it was concluded that the TRAC code with the similar film boiling model with several superimposed mechanisms, could have resulted in compensating errors (i.e., too much heat transfer at moderately high liquid fractions), such that the heat transfer in some integral tests was predicted correctly because the predicted vapor fraction was too high.

Another potential compensating error is the mis-prediction of vapor temperature. The identification of evidence of non-equilibrium conditions in the core is important for post CHF heat transfer, since the heat transfer models in WCOBRA/TRAC-TF2 rely on the local vapor temperature as the heat sink. It is well known that vapor superheating significantly reduces post CHF heat transfer from high temperature fuel rods. An example of a compensating error is where the overall heat transfer is "correctly" calculated because the local heat transfer coefficient is under-predicted (due to an inappropriate model) but the temperature difference between the fuel rod and the fluid is over-predicted. Most measurements of nonequilibrium conditions, usually by thermocouples exposed to the fluid, are affected by rewet by liquid impact. However, it is believed one can safely assume that a measurement of any level of superheat above saturation temperature is a sure sign of significant non-equilibrium in the fluid, which should also be predicted by the code.

In post blowdown heat transfer, the core entrainment rate, droplet size, and interfacial drag models act in combination to predict the corresponding relative velocities, vapor fraction, and interfacial heat transfers which ultimately determine the vapor temperature and wall heat flux. Evidence of compensating error among these quantities is therefore important.

#### 24.3.1.3 Blowdown and Post Blowdown Thermal-Hydraulics/Entrainment

During blowdown, the correct prediction of mass flowrates in the broken and intact loops is important, since the core flowrate is driven by the break flowrate in the broken loop, and by the pumps in the intact

loops. An example of a compensating error would be a “correct” prediction of core flow resulting from a lucky combination of incorrect loop flows.

During reflood, the pertinent question to ask in terms of compensating errors is whether the mass flow into and out of the core is calculated correctly, and is the result of a proper balance between the driving force caused by the difference in water level between the core and the downcomer, and the pressure drop in the loops. An example of a compensating error is the situation where the core inlet flowrate is calculated “correctly” because the core level is too high (leading to a low driving force), but is compensated by a loop pressure drop which is too low.

A key aspect of the post blowdown thermal-hydraulics prediction pertaining to core cooling is the entrainment calculation; the inlet flow is controlled by the steam generation rate and liquid entrainment from the core, and by the amount of liquid which is predicted to collect in the upper plenum and hot legs.

#### **24.3.1.4 Fuel Rod Models (Oxidation, Swelling/Burst)**

Models and correlations used to calculate the oxidation and swelling/burst effects are documented in Section 8. The bias and uncertainty of the model will be accounted for in the uncertainty treatment.

#### **24.3.1.5 Break Flow**

The validation and assessment of critical flow model (Homogeneous Relaxation Model option) is documented in Section 12 of this document. [

] <sup>a,c</sup>

#### **24.3.1.6 Mixture Level/Level Swell in Simulated Core**

Prediction of mixture level inferred by the heat up location is impacted by the accuracy of interfacial drag, CHF models, nodding sizes, T/C elevations, and presence/absence of grids.

The energy equation discretization, the coarse node size and donoring scheme in the core leads to a limiting resolution of enthalpy prediction which may result in biased cladding temperature prediction.

The use of relatively coarse nodes in the core limits the accuracy of the prediction because the node average enthalpy is computed based on the heat flow in and out of the control volume. The enthalpy is computed accounting for the heat flow up to the top of the control volume. Thus in an upflow situation, the predicted enthalpy of the node corresponds to the fluid enthalpy at the top of the cell and not at the cell center point. In a downflow situation on the other hand, the predicted cell enthalpy corresponds to the fluid enthalpy at the bottom of the cell. [

] <sup>a,c</sup>

In addition to the resolution limit, in a boil-off test, a potential compensating error exists because of the process of evaporation. If the level swell is predicted high, the mixture level is high, thus more heat from the heater rods is absorbed by the liquid resulting in the higher evaporation rate which reduces the liquid inventory and subsequently the level. So the mixture level comparison may appear reasonable.

#### 24.3.1.7 Horizontally Stratified Flow Regime Transition Boundary

Prediction of horizontal stratified regime transition is impacted by the accuracy of phasic velocities, thus by the liquid level (if the total phasic flow rates are given), interfacial drag/wall drag models, also by the boundary conditions to the pipe section of interest such as the liquid level imposed at the ends.

When the level is imposed on the downstream end of pipe, and if the liquid flow is supercritical, the level is more likely determined by the wall and interfacial drag for a given  $J_G$ - $J_L$ , and if the liquid flow is subcritical, the level is determined by the downstream liquid level set by the boundary such as the downcomer liquid level. Therefore a potential compensating error exists for horizontal stratified flow test simulations. The transition to slug may be correctly predicted if the liquid level prediction is biased high and the transition criteria model is biased to high vapor flows.

#### 24.3.1.8 Steam Generator Thermal-Hydraulics

WCOBRA/TRAC-TF2's predictive capability of Steam Generator Hydraulic behavior such as the reflux condensation heat transfer and the CCFL in the tubes during and at the end of natural circulation period in SBLOCA is [

] <sup>a,c</sup>

There are multiple locations in the region between the hot leg nozzle and Steam Generator where CCFL is possible and thus limits liquid down flow from the intact steam generator prior to clearing the loopseal. Steam Generator tube inlet is one such location. [

] <sup>a,c</sup>

#### 24.3.1.9 Loop Seal Clearance

The loop seal starts to clear when the liquid level formed in the downhill side of pump suction piping reaches the top of the horizontal pipe. The onset of loop seal clearing timing is determined by the break

flow, vapor generation rate in the core, the condensation rate in the SG tubes, and the core bypass flow rate. Once the clearing commences, because of the significant volume of vapor accumulated in the inner vessel, a relatively high vapor flow is maintained for a significant time such that significant fraction or all of liquid in the loop seal is swept out of the cross-over leg and to the cold leg. At a larger break size, the vapor volumetric flow is high enough to clear loop seal in multiple loops.

The number of cleared loops is determined by the available vapor flow due to flashing from depressurization which increases with the break size, in addition to already accumulated vapor in the inner vessel, loop resistance, and the broken cold leg pressure which decreases faster as the break size increases. For a stable loop seal clearing which may include a partially cleared loop, the remaining liquid in the horizontal leg of the pump suction piping and the pressure loss through an intact loop become a factor.

The UPTF loop seal test (Leibert and Emmerling, 1998) while it is quasi-steady state, provides important full scale single loop seal clearing data in a prototypic PWR geometry, and provides  $\Delta P$  and Liquid level information for a range of  $J_g^*$  that covers conditions expected in SBLOCA in PWRs. The phenomena of loop seal clearing involves several physical models, namely the onset of slugging, entrainment in the horizontal section, the CCFL in the uphill pipe and entrainment in the vertical upflow as described in Section 18, thus there is a possibility of compensating errors.

#### 24.3.1.10 Pump Performance

There is no compensating error within the pump model. However, immediately after the break, the intact flow is still controlled by the pump which then competes against the break flow, thus impacting the core inlet flow. The interaction between the broken cold leg flow and pump creates a possibility for compensating error where the core inlet flow may be reasonably predicted when the sum total of break flow and intact pump is correct but both break flow and the pump flow may be incorrect.

#### 24.3.1.11 Safety Injection Direct Condensation in the Cold Leg

The direct condensation due to safety injection in cold legs is calculated by the use of COSI correlation which was constructed based on the 1/100 scaled cold leg SI test. Because the operation of COSI model requires the horizontally stratified or the separated flow (wavy dispersed or annular mist) in the cold leg, the model performance may be impacted by the stratified flow to slug transition criteria.

For LBLOCA application, UPTF8 (KWU, 1988) was used to assess the COSI model for the low pressure, high steam flow conditions typical for LBLOCA conditions (Section 19). [

] <sup>a,c</sup>

### **24.3.2 Possible Compensating Errors in Integral Effects Test Simulations**

In IETs, multiple physical models and components are interacting as the transient evolves which give rise to opportunities for compensating errors. Rather than identifying possible compensating errors, phenomena will be listed under the relevant sub-scenario simulations which will be used for the assessment of compensating errors.

#### **24.3.2.1 SBLOCA**

The cladding temperature could be calculated correctly if the heat transfer and the core level swell are biased in the opposite direction (higher HTC and low mixture level). Additionally the correct core mixture level could be the result of misprediction in the liquid inventory in the core and the level swell in the opposite biases (low inventory in the core and high swell). ROSA series will be used to help assess compensating errors in the areas mentioned above.

#### **24.3.2.2 IBLOCA**

Though the behavior of IBLOCA may be a combination of SB and LBLOCAs, the relative importance of observed SB and LB phenomena are different and thus the different biases in the predicted behavior are expected. SB-CL-14 (Koizumi and Tasaka, 1988) from ROSA series is a simulation of 10% cold leg break of a PWR. Minor cladding heat up was observed in this test. The test is well instrumented to allow assessing of compensating errors in TF2's simulation. Additionally LOFT intermediate break test L5-1 (Jarrell and Divine, 1981) which simulated a guillotine break of a 14 in dia. accumulator line of a 4 loop PWR, may be available to investigate the possible compensating errors although the test was conducted in a non-prototypic arrangement where there was no break in the hot leg of a "broken loop." Minor cladding heatup was observed which would enable one to assess the core mixture level prediction. In addition to a set of global parameters such as the vessel pressure and the break flow rate, there are some local measurements such as hot leg density and flow rates which allow one to evaluate the reasonableness of flow regime prediction in legs.

#### **24.3.2.3 LBLOCA**

One possible compensating error would be the blowdown cladding temperature prediction. During blowdown, the core inlet flow prediction may be impacted by compensating errors in the PUMP performance and the break flow prediction. Additionally, compensating error may be present in the cladding temperature prediction due to an interaction of the post CHF heat transfer prediction and the core flow prediction. The cladding temperature may appear reasonable when the heat transfer coefficient is biased high and the lower core flow is predicted.

### **24.4 COMPENSATING ERROR ASSESSMENT OF SELECTED HIGHLY RANKED PHENOMENA IN SETS AND IETS**

The compensating error analysis of selected highly ranked phenomena is presented in the Sections 24.5 through 24.8, where in addition to the main parameters of interest, i.e., PCT, additional parameters such as core flow and the heat transfer coefficient, which impact the computation of main parameters of interest will be compared with measurement or assessed in terms of consistency with secondary figures of merit.

For example, PCT or total heat transfer from the rod to the coolant is predicted with reasonable accuracy, but is impacted by the heat transfer coefficient and the flowrate. This exercise attempts to determine if the heat transfer is correct because both the heat transfer coefficient and the flow rate are predicted reasonably well, or the heat transfer is predicted well because these two main parameters are predicted with bias of opposite direction.

In previous sections of this document, highly ranked phenomena and models were validated for use in the LOCA analysis. Though the aspect of compensating errors in these assessments were not explicitly examined, relevant conclusions could be drawn from the assessments because of additional parametric sensitivity studies and scaling analyses that were performed, and they are summarized below.

In Section 12 the break flow model was validated and the examination of parameter impact on the prediction was conducted. The conclusion from Section 12 is that [

] <sup>a,c</sup>

Along with the heat transfer calculation, the prediction of Mixture Level/Level Swell in the Core Region was assessed in Section 13. [

] <sup>a,c</sup>

The prediction of Transition to Horizontal Stratified Flow was validated in Section 16 where the focus was the model performance in typical SBLOCA conditions. It was concluded that the model performed as expected. [

] <sup>a,c</sup>

The predicted Steam Generator Thermal-Hydraulics was examined as part of ROSA test simulations in Section 21. Section 21 confirmed that [

] <sup>a,c</sup>

The prediction of Loop Seal Clearance was the focus of Section 18 where the analysis of scaled loopseal test was presented and the full scale test simulation was used to assess the code prediction. [

] <sup>a,c</sup>

The model prediction for the Safety Injection Direct Condensation in Cold Leg was assessed in Section 17, and the model performance in the multi-component tests were assessed in Sections 19.3.8 and 19.3.11.

[

] <sup>a,c</sup>

In Sections 24.5 through 24.7, the compensating errors in phenomena associated with LBLOCA, namely the ECC bypass, Post CHF Heat Transfer, Blowdown/Post BLOWDOWN Thermal-hydraulics, are examined. The SBLOCA related phenomena are examined in Section 24.8.

## 24.5 DELIVERY AND BYPASSING OF ECC

### Summary Conclusion

Cold leg ECC injection tests, [

] <sup>a,c</sup>

### Analysis

The ECC bypass and condensation prediction in UPTF Test 6 and UPTF Test 25A test simulations were examined. The results of these simulations are documented in Section 19.3. [

] <sup>a,c</sup>

[

]^{a,c}

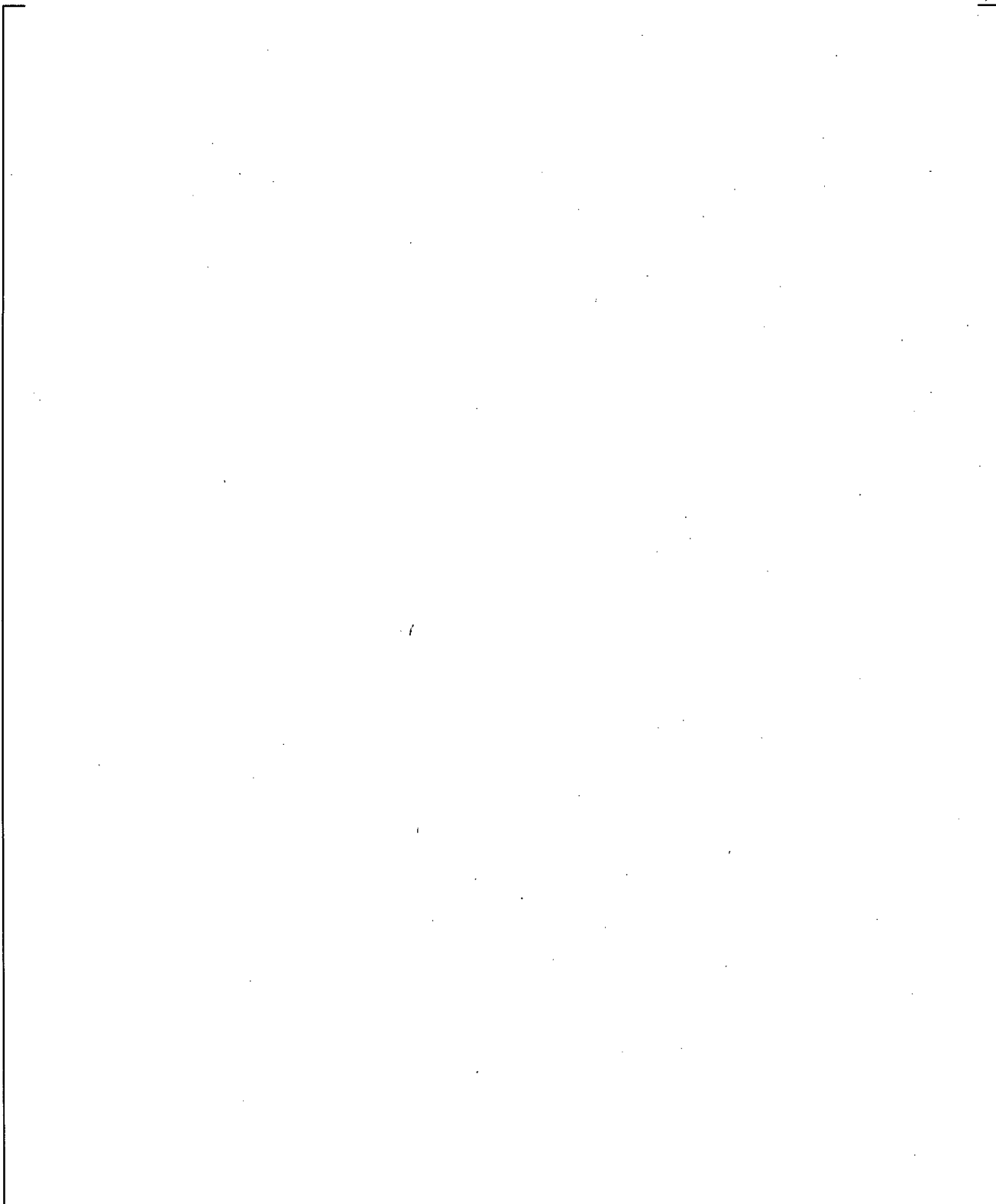


**Figure 24.5-1 Comparison of Vessel Condensation Efficiency versus Nominal Steam Flow Rate, UPTF Test 6; The Experimental Condensation Efficiency is Estimated by MPR (MPR-1163, 1990)**

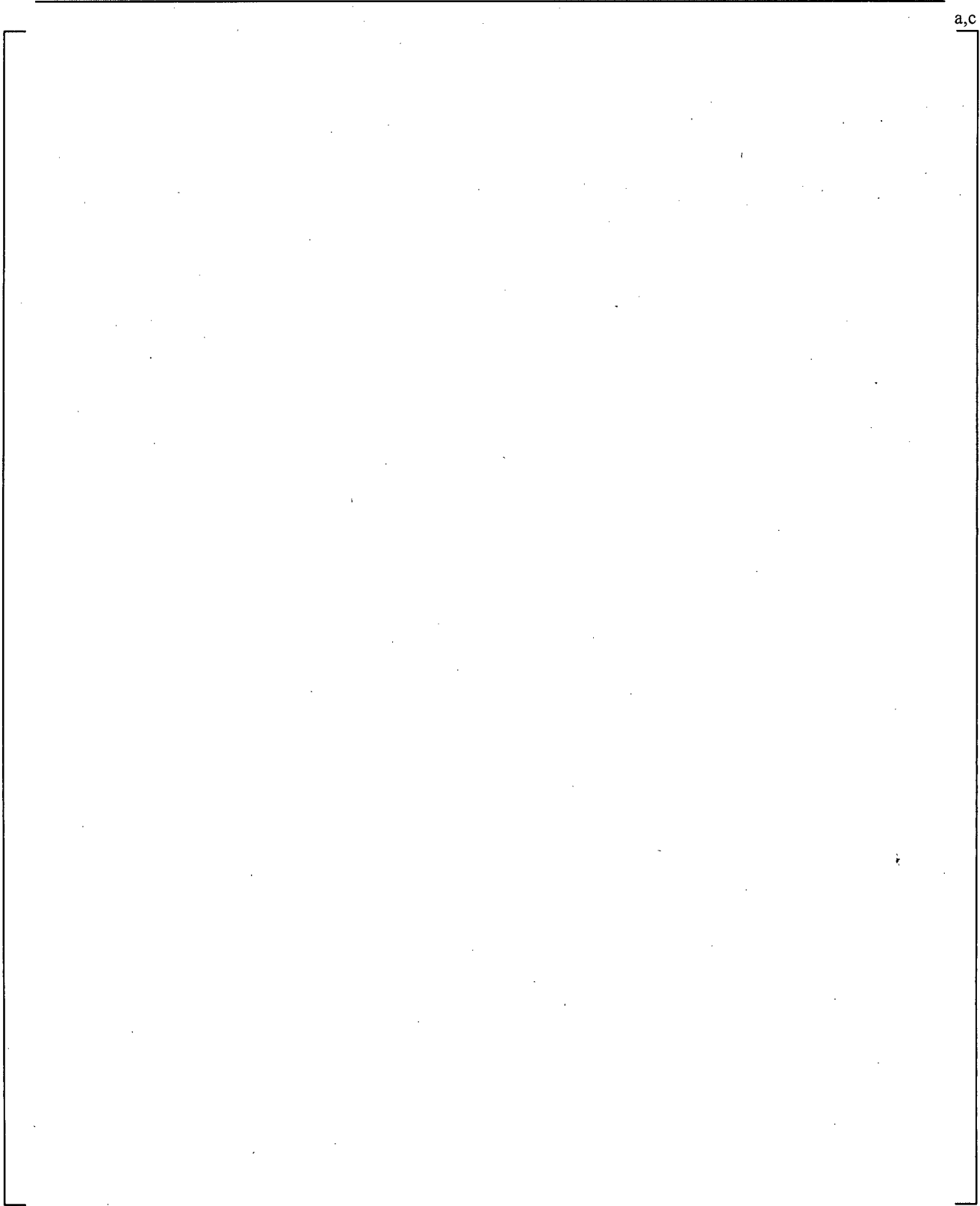


**Figure 24.5-2 ECC Liquid Temperature Comparison near Vessel Inlet**

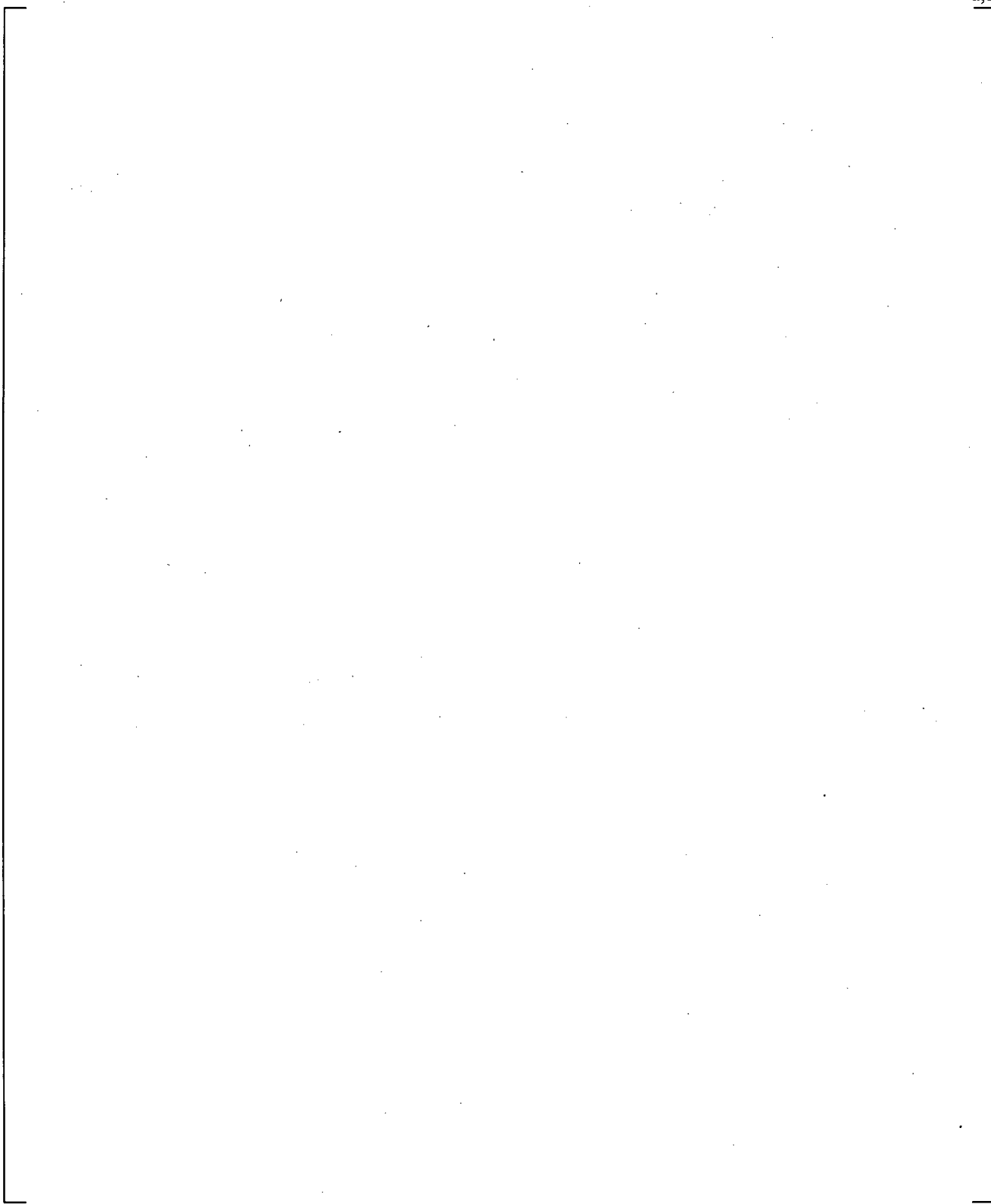


**Figure 24.5-3 Downcomer Void Height Comparison in UPTF Test 25A**

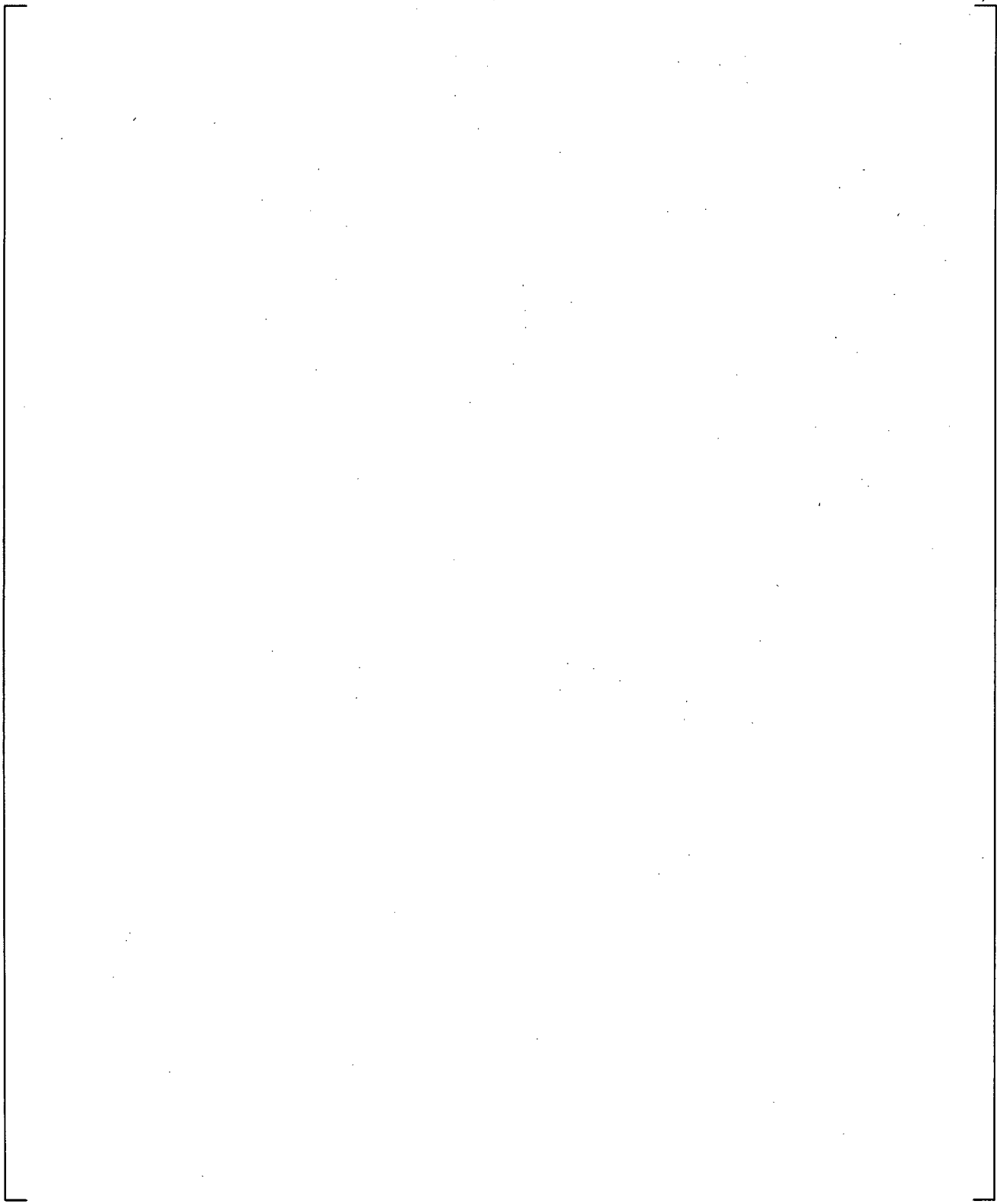


**Figure 24.5-4 Broken Loop Steam Flow Rate in UPTF Test 25A**

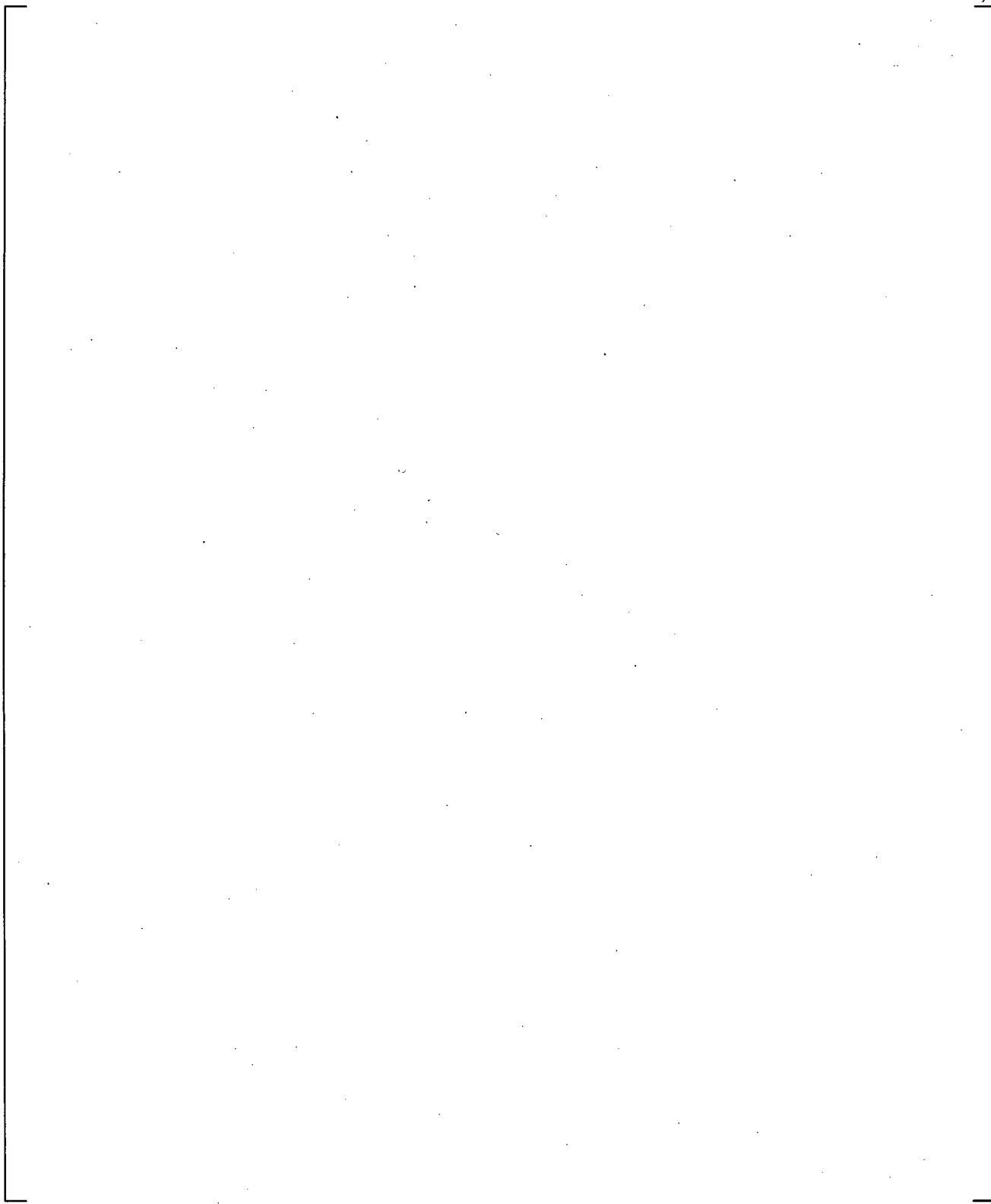


**Figure 24.5-5 Cold Leg Temperature at Exit of Cold Leg for UPTF Test 25A**

## 24.6 POST CHF HEAT TRANSFER

Potential compensating errors in the post CHF heat transfer models are investigated by first reviewing the assessment using the stand-alone heat transfer package, COBRAHT-TF2 and by examining WCOBRA/TRAC-TF2's simulation of the following test simulations:

- ORNL Uncovered Bundle Tests for Single Phase Vapor (SPV) Data (COBRAHT-TF2) (Anklam et al., 1982)
- FLECHT Steam Cooling Tests for SPV Data (COBRAHT-TF2) (Wong et al., 1981)
- ORNL high pressure Film Boiling Tests (COBRAHT-TF2 and WCOBRA/TRAC-TF2) (Mullins et al., 1982)
- G1 Blowdown Heat Transfer Tests (WCOBRA/TRAC-TF2) (Cunningham et al., 1974)
- FLECHT-SEASET forced flooding reflood tests (WCOBRA/TRAC-TF2) (Loftus et al., 1981)

### 24.6.1 Summary of Assessment with Stand-alone COBRAHT-TF2

Several tests included measurements of wall temperature, mass flux, inlet quality, and local vapor temperature. The test measurements were used to compare directly to the WCOBRA/TRAC-TF2 heat transfer package since all the required fluid parameters are available or can be estimated.

#### SPV HTC Assessment Results

The single phase vapor heat transfer was assessed in Section 15. Figures 15.4.1-1a and 15.4.1-1b in Section 15 (repeated here as Figures 24.6.1-1 and 24.6.1-2) show a comparison of the predicted heat transfer coefficient by the stand-alone WCOBRA/TRAC-TF2's heat transfer package against the high pressure measurement from ORNL-THTF uncovered bundle tests. The vapor Reynolds numbers and pressure range are appropriate to cover a range representative of blowdown period in LBLOCA, and the boil-off period in SBLOCA. Single phase vapor heat transfer in refill reflood condition was assessed against low pressure FLECHT-SEASET Steam Cooling Test Data, [

] <sup>a,c</sup>

Reynolds number dependency for the single phase vapor in the higher pressure is shown in Figure 24.6.1-2. The figure indicates that [

] <sup>a,c</sup>

### DFFB Assessment Results

The ORNL steady state tests (Yoder et al., 1982) were used to assess the Dispersed Flow Film Boiling (DFFB) model in Section 15.5. As with the assessment of SPV using the ORNL tests, the DFFB model assessment was conducted with the use of stand-alone heat transfer package extracted from WCOBRA/TRAC-TF2. Figure 24.6.1-5 shows the comparison with the ORNL steady state tests. [

] <sup>a,c</sup>

a,c



**Figure 24.6.1-1 Heat Transfer Coefficient Comparison for ORNL-THTF**

a,c



**Figure 24.6.1-2 Prediction Error as a Function of Vapor Reynolds Number**

a,c



**Figure 24.6.1-3 Heat Transfer Coefficient Comparison for FLECHT SPV Tests**

a,c



**Figure 24.6.1-4 Ratio of Measured to Predicted Heat Transfer Coefficient vs. Vapor Film Reynolds Number for FLECHT SPV Tests (from COBRAHT-TF2)**

a,c



**Figure 24.6.1-5 Average Heat Transfer Coefficient Comparison for ORNL Steady-State Film Boiling Tests**

a,c

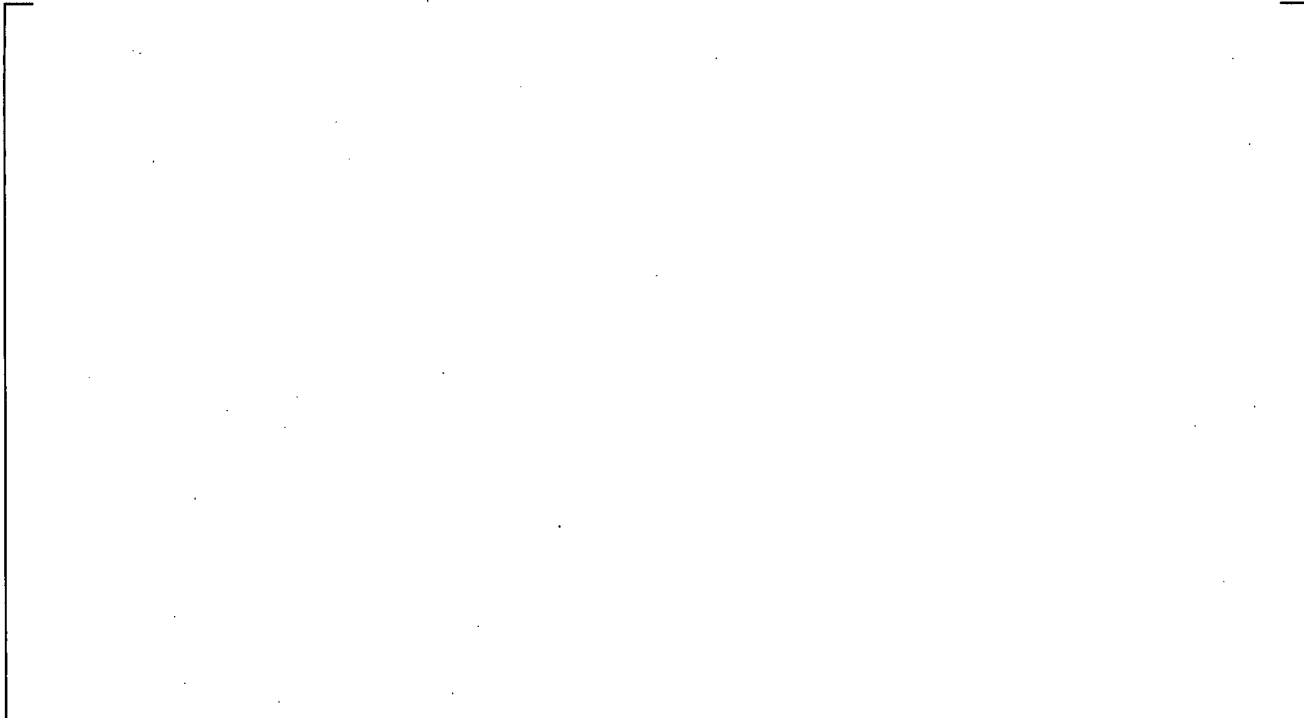


**Figure 24.6.1-6 Predicted Heat Flux Bias vs. Rev for ORNL Data**

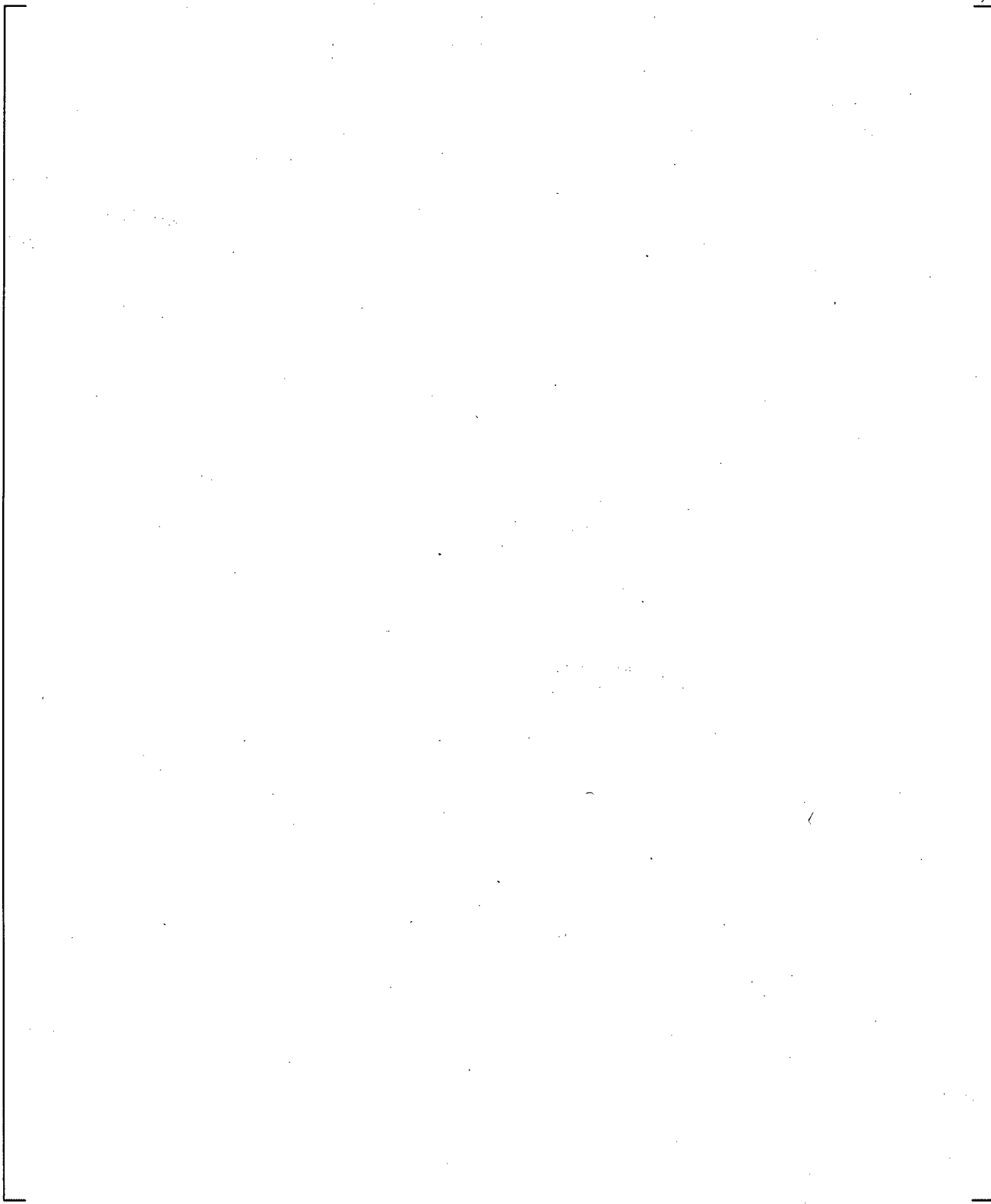


**Figure 24.6.1-7 Predicted Heat Flux Bias vs. Void Fraction for DFFB Data**

## 24.6.2 ORNL Film Boiling Test Simulation

[

] <sup>a,c</sup>

**Table 24.6.2-1 Bundle Exit Temperatures for ORNL Tests**



a,c

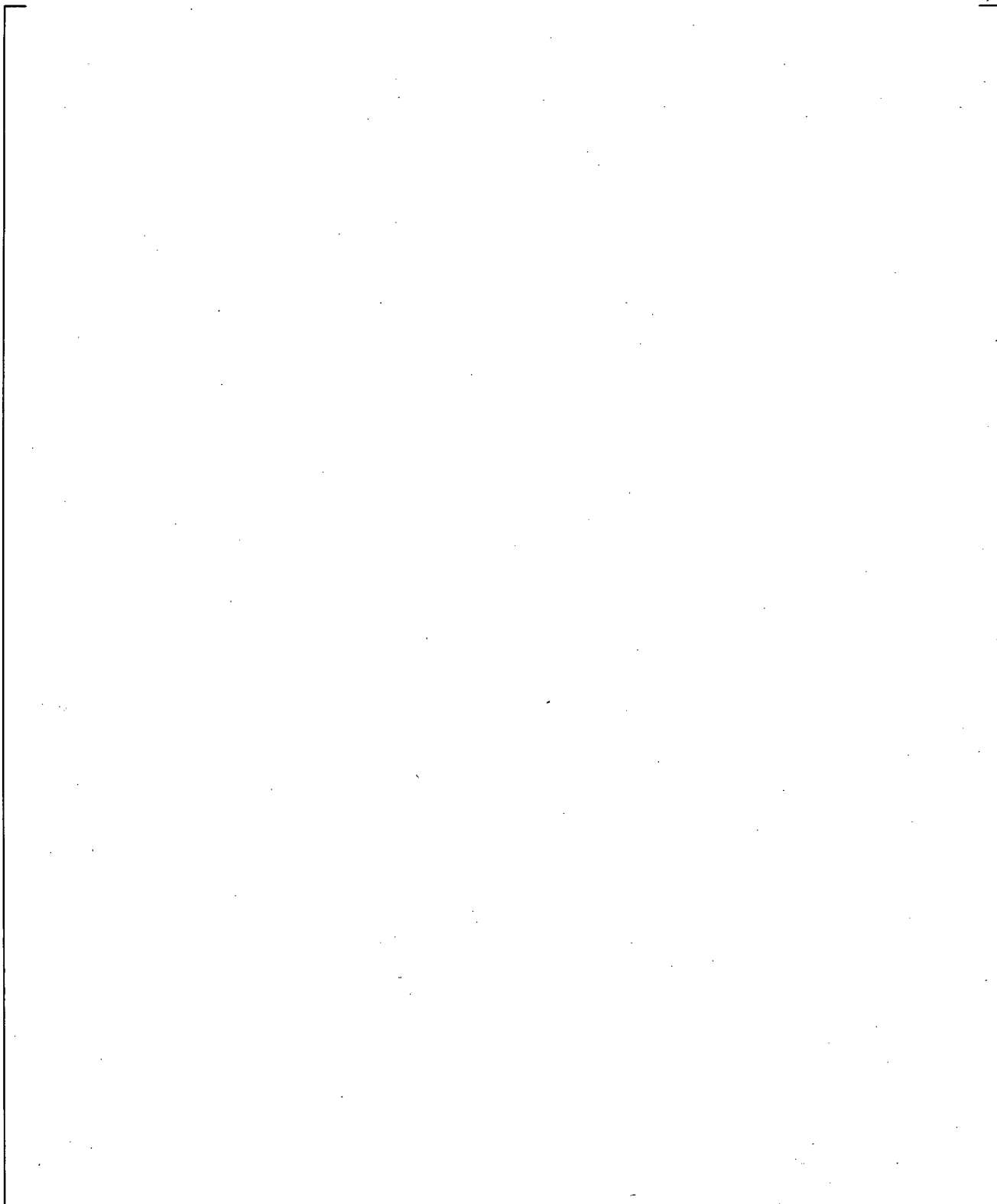


**Figure 24.6.2-1** ORNL Test 3.03.36AR – Vapor Temperature and TLIQ (=Tsat) at Bundle Exit  
Calculated by WCOBRA/TRAC-TF2

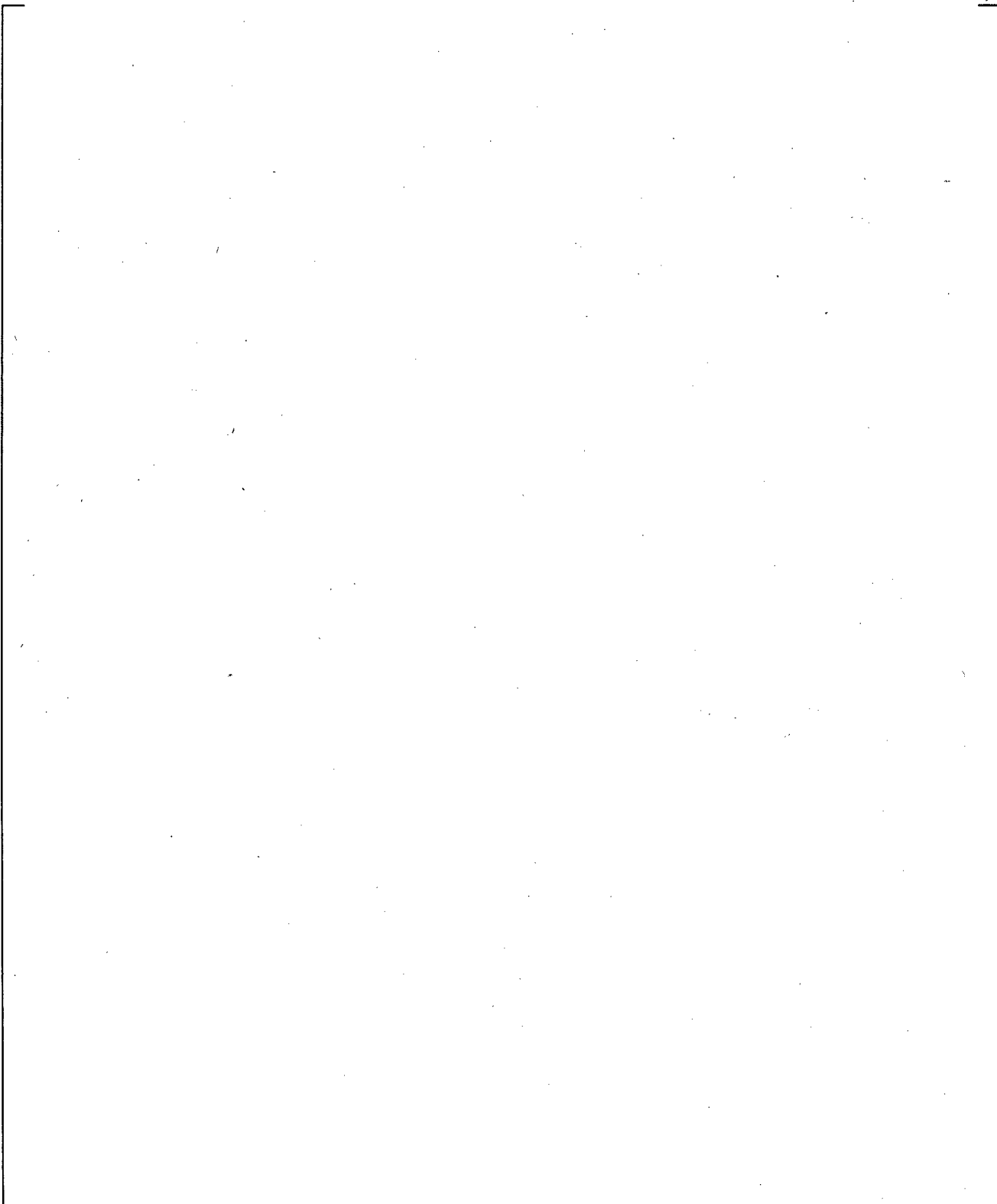


**Figure 24.6.2-2** ORNL Test 3.08.6C – Vapor Temperature and TLIQ (=Tsat) at Bundle Exit  
Calculated by WCOBRA/TRAC-TF2

### 24.6.3 G1-Blowdown Test Simulation

Figures 24.6.3-1 to 24.6.3-5 show the transient cladding temperature, mass flux, and vapor fraction at the hot spot, and axial temperature distribution at various times, for a typical three-loop plant under a LBLOCA as calculated using WCOBRA/TRAC-TF2. Three-loop plants typically have a relatively high blowdown cooling period under nominal break flow conditions. The cladding experiences substantial cooling shortly after the transient has begun (about ~7.5 seconds after the break in Figure 24.6.3-1) due to reverse (downward) core flow (Figure 24.6.3-2). As the Reactor Coolant System depressurizes and refills, the core flow is reduced and the cladding once again heats up beginning at about 35 seconds, until it reaches a maximum during reflood. The core cooling due to the reverse flow during blowdown is very important process since the highest PCT often occurs in cases with the poor blowdown cooling where the core remains in high temperature at the end of blowdown period.

The G-1 blowdown film boiling tests were performed in a 12-foot long, 480-heater rod test bundle (Section 14.2.2.2). These tests were initiated from high temperature (1500 to 1700F) and high pressure (800 psia). A simultaneous depressurization and downward flow of steam and water were imposed on the test section, simulating the core cooling phase of the blowdown transient. In some tests, the injected water was subcooled. These tests were chosen because they include all the basic features of a blowdown transient: downward flow into a hot dry bundle, two-phase inlet conditions, and depressurization.

Cladding temperatures were measured and heat transfer coefficients were inferred, using the saturation temperature as the sink temperature. No vapor temperature measurements were available. Six of these tests were modelled with WCOBRA/TRAC-TF2, ranging initial cladding temperature and inlet flowrate as shown in Table 24.6.3-1. [

] <sup>a,c</sup>

The predicted average heat transfer coefficients for these tests are compared to the measured bundle average values at several elevations in Figure 24.6.3-6. [

] <sup>a,c</sup>

Figures 24.6.3-7 to 24.6.3-12 show the axial cladding temperature distribution at various times for each test. The predicted values are the solid lines, and the measured average bundle temperatures are represented by the squares. As the inlet flow is increased, the following trends are evident.

[

] <sup>a,c</sup>

[

] <sup>a,c</sup>

There are two energy flows to the vapor which affect its temperature as it flows towards the hot spot; heat transfer to the vapor from the wall (heating the vapor), and evaporation of droplets (adding saturated vapor and cooling the vapor). The evaporation is from two sources: heat transfer from vapor to liquid, and evaporation of liquid from heat transfer directly partitioned to the liquid from the wall. Figures 24.6.4-14 to 24.6.3-19 show the WCOBRA/TRAC-TF2 calculated vapor fraction and heat flux to the vapor and liquid for Cases 1 (low flow) and 4 (high flow). The heat transfer regime map used by WCOBRA/TRAC-TF2 is shown in Figure 24.6.3-13. The calculated heat transfer regime is also shown on the figures. [

] <sup>a,c</sup>

Sensitivity studies were performed on Cases 1 and 4, [

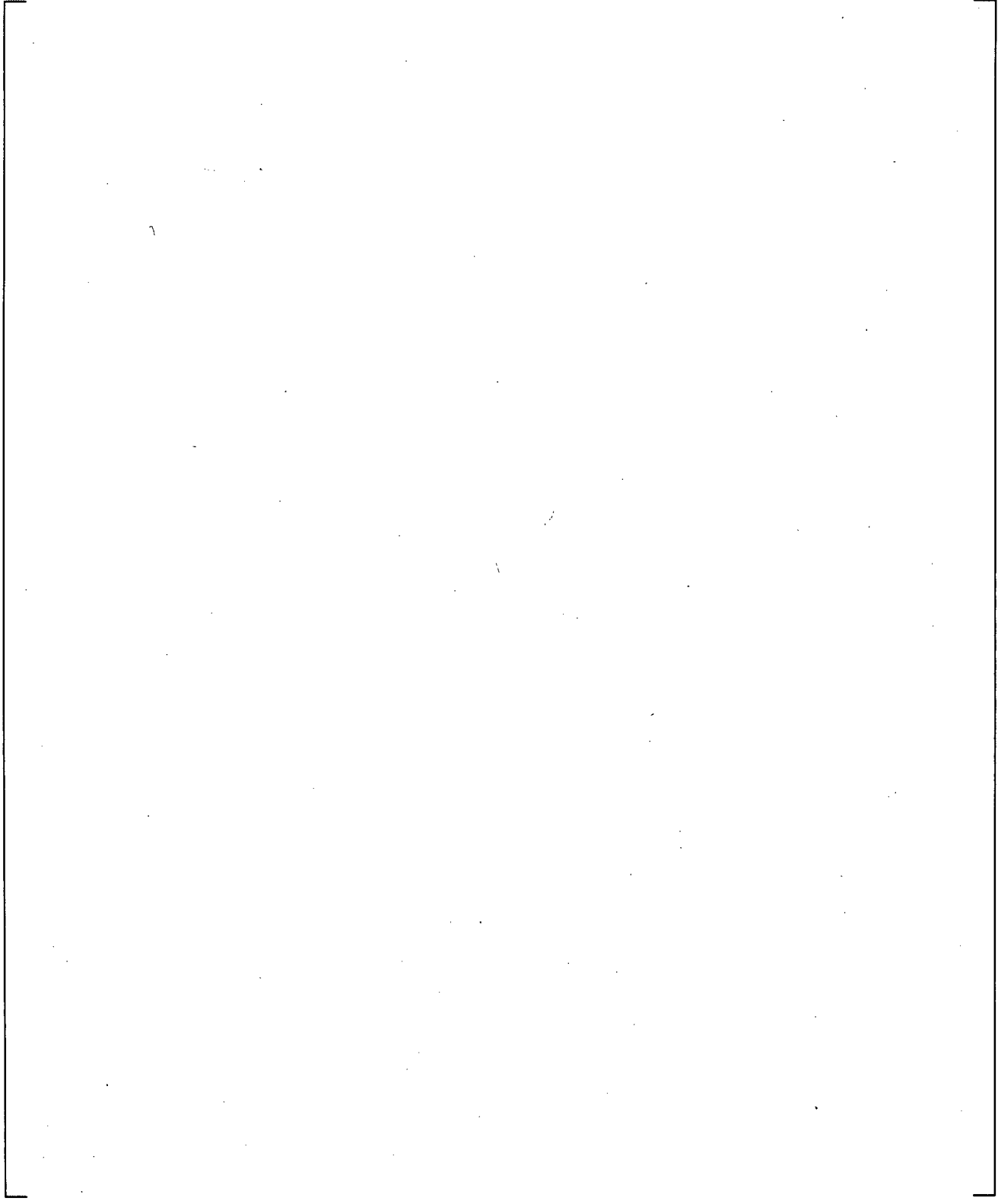
] <sup>a,c</sup> The results are shown in Figures 24.6.3-20 to 24.6.3-27 for Cases 1 and 4. These results indicate that:  
[

] <sup>a,c</sup>  
There are several models in WCOBRA/TRAC-TF2 designed to produce a reasonable drop size for blowdown conditions; the models account for the possibility of droplet break up as the liquid flows through the constricted area of the top fuel nozzle and the grids, and (through a critical Weber number), the possibility of droplet break up due to acceleration: [

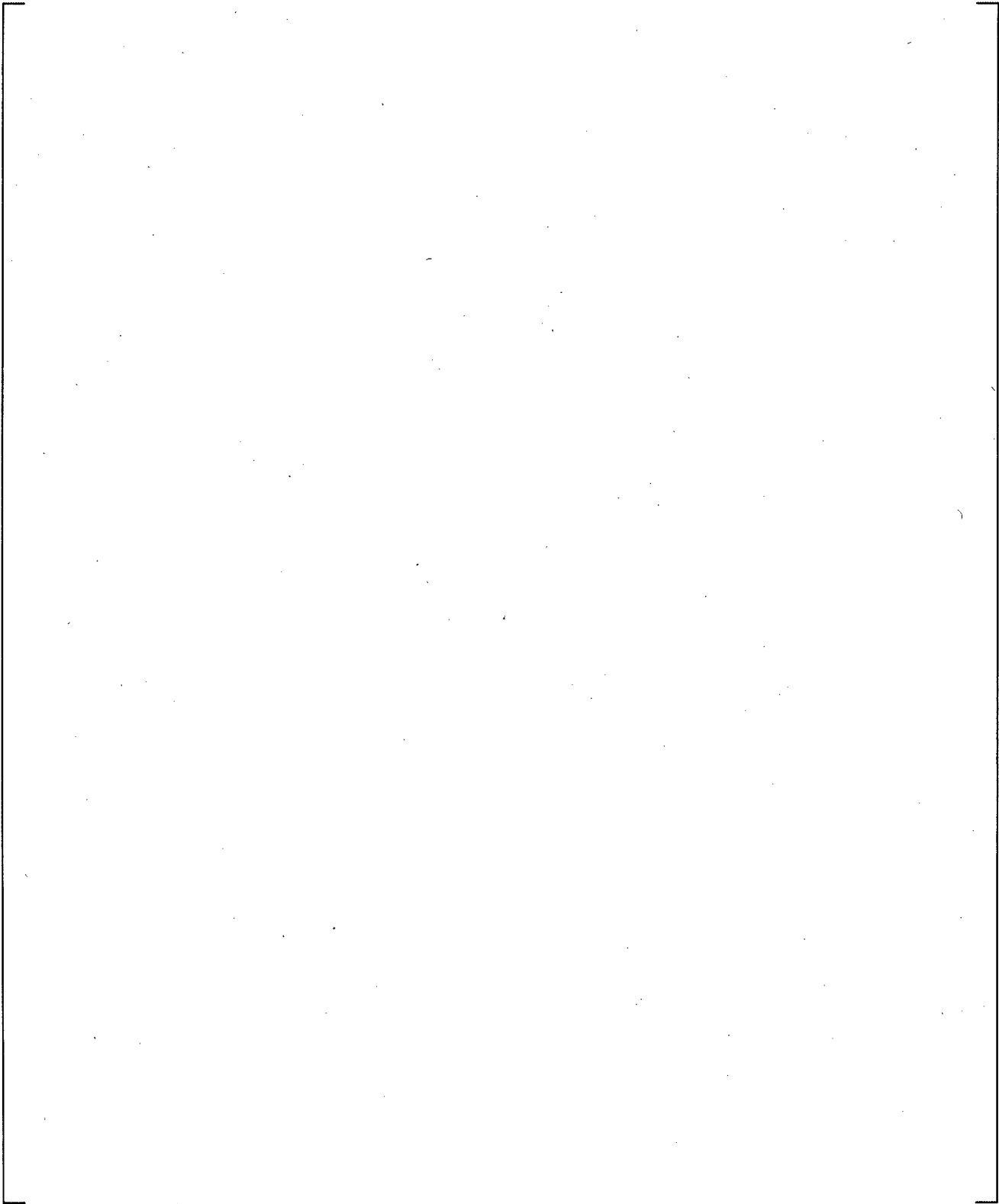
] <sup>a,c</sup>  
**Compensating Errors Found in G-1 Tests**  
[

**Table 24.4.6.3-1 G-1 Blowdown Test Conditions**

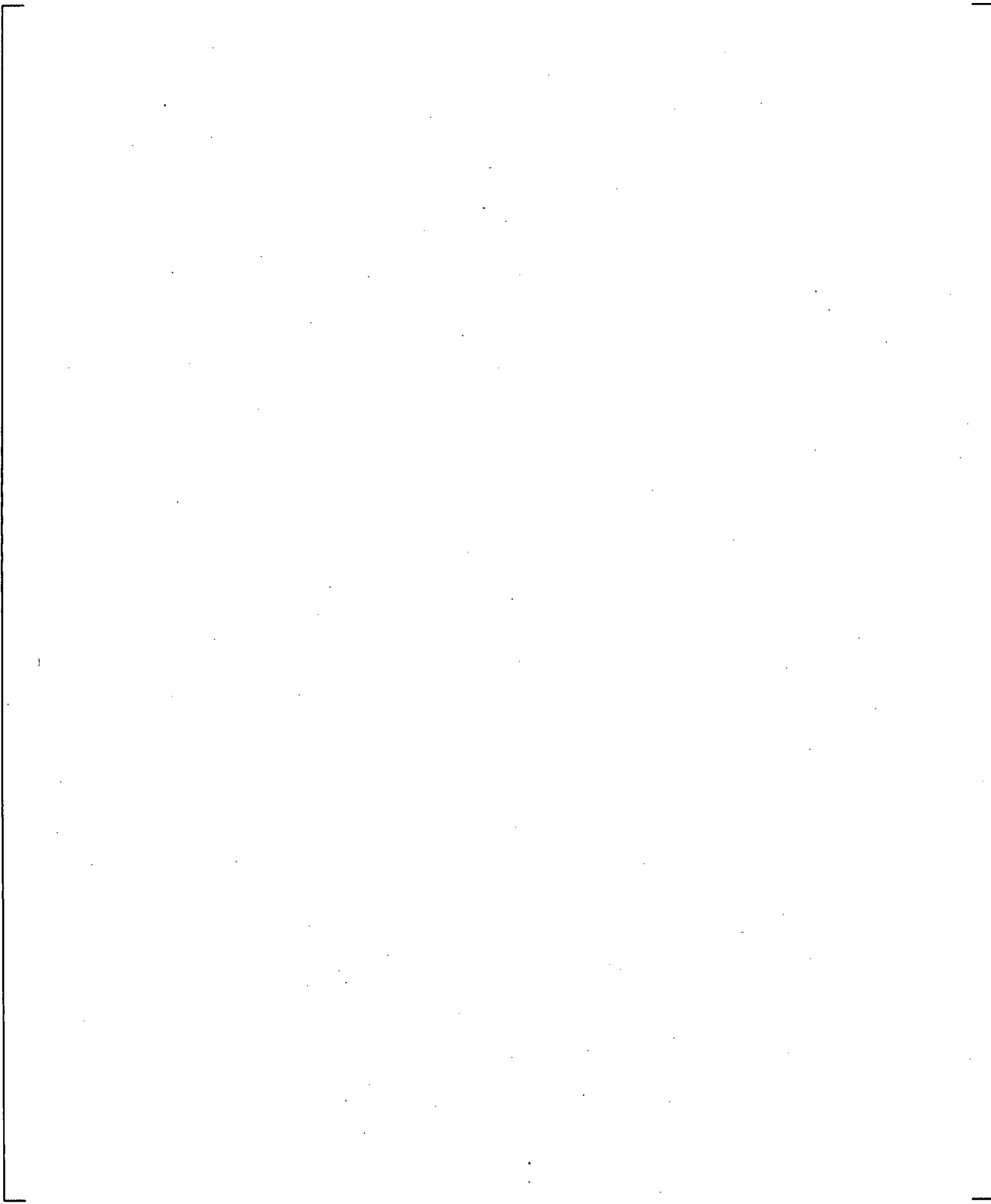
a,c.

**Figure 24.6.3-1 Cladding Temperature During LBLOCA for Three-Loop Plant**



**Figure 24.6.3-2 Mass Flux at PCT Location During Blowdown (0-30 Seconds)**



**Figure 24.6.3-3 Void Fraction at PCT Location During Blowdown (0-30 Seconds)**

**Figure 24.6.3-4 Axial Cladding Temperature Distribution at Blowdown PCT Time (7.5 Seconds after Break)**

**Figure 24.6.3-5 Axial Cladding Temperature Profile at End of Blowdown Cooling Time (11.5 Seconds after Break)**

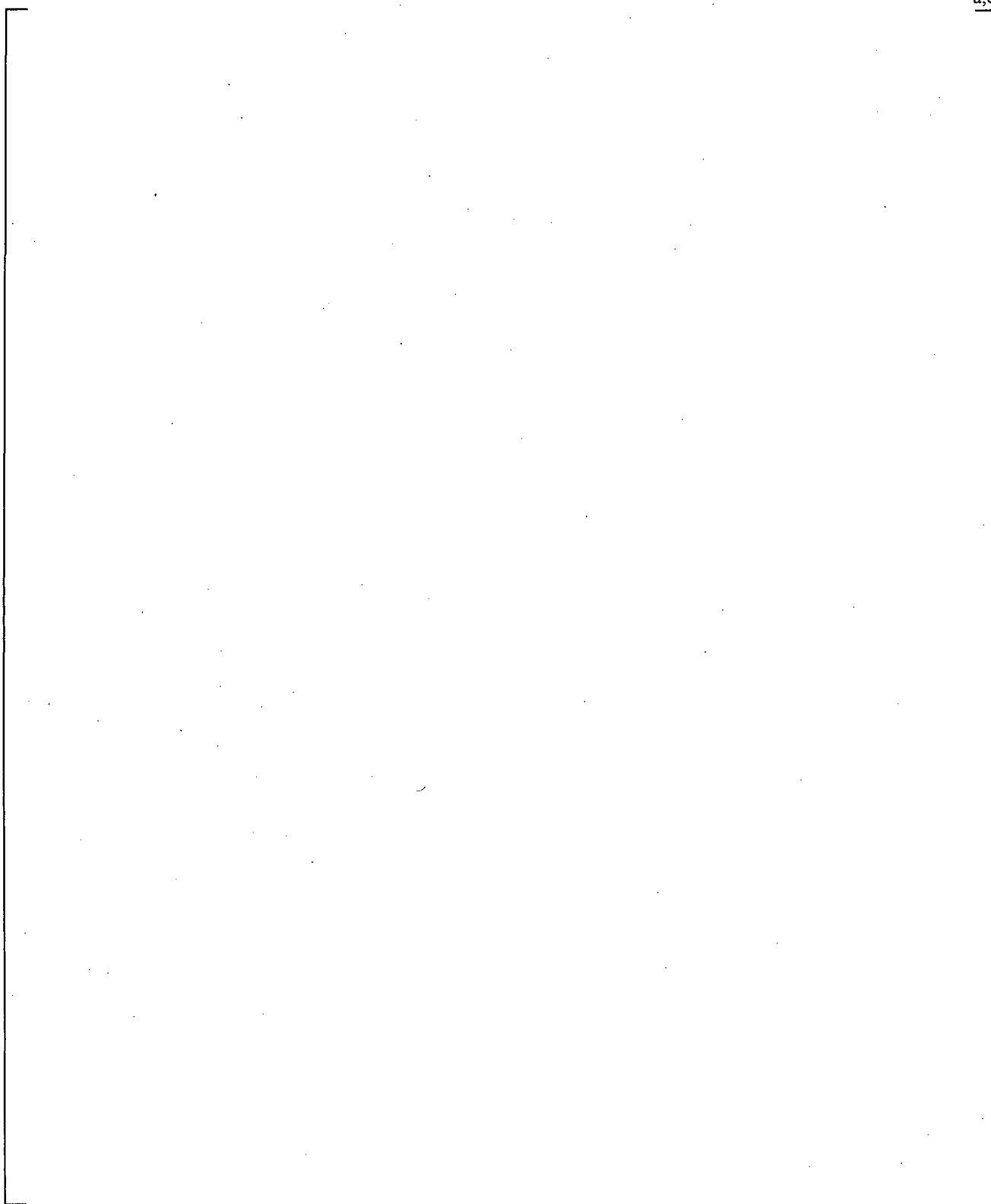


**Figure 24.6.3-6 Blowdown Cooling Rates for the G 1 Blowdown Heat Transfer Tests**

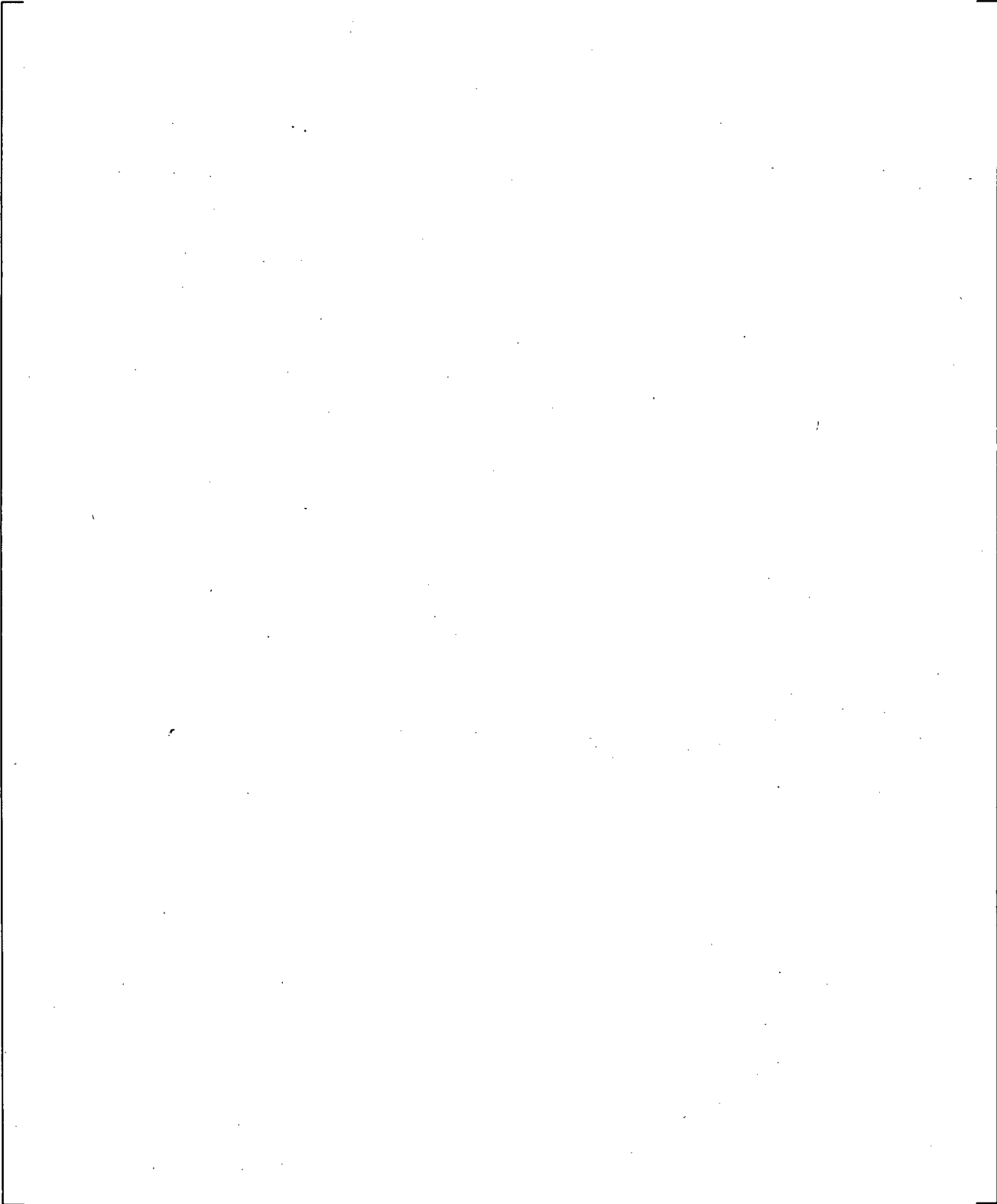


**Figure 24.6.3-7 Cladding Axial Temperature at Start of Test (6 Seconds), 15, 20, 30 Seconds for Case 1 (Test 148)**

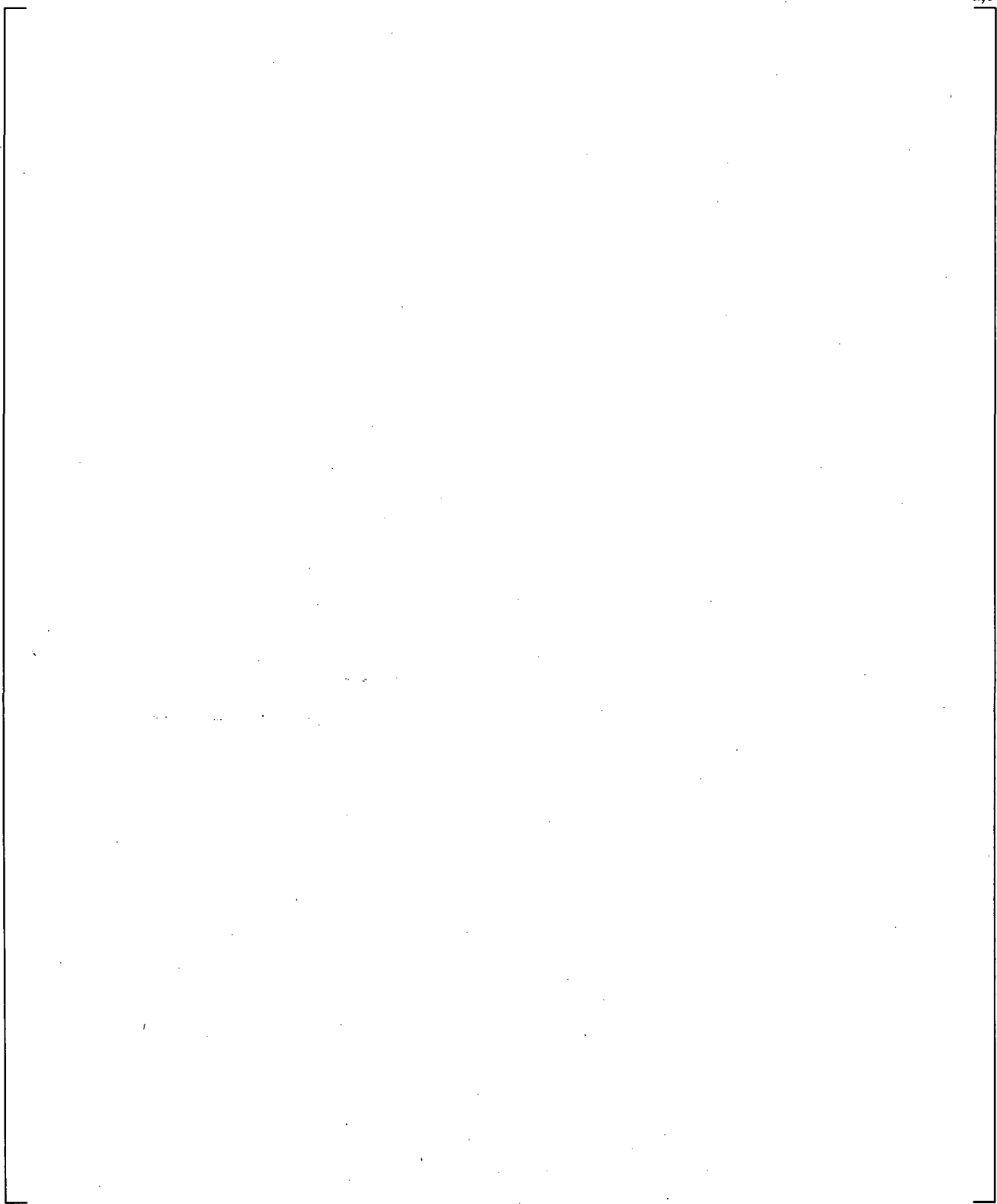


**Figure 24.6.3-8 Cladding Axial Temperature at Start of Test (6 Seconds), 15, 20, 30 Seconds for Case 2 (Test 143)**

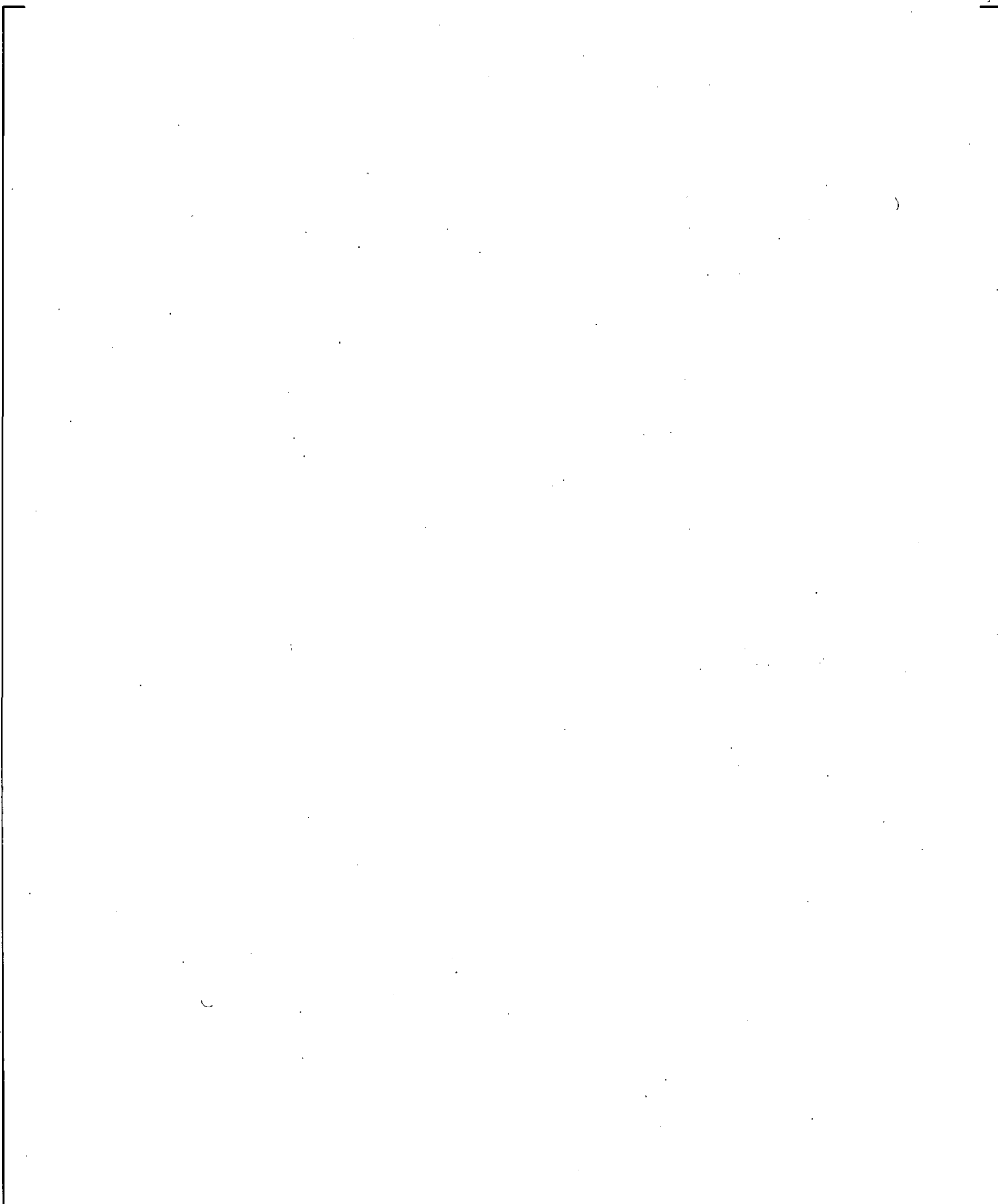


**Figure 24.6.3-9 Cladding Axial Temperature at Start of Test (6 Seconds), 15, 20, 30 Seconds for Case 3 (Test 152)**

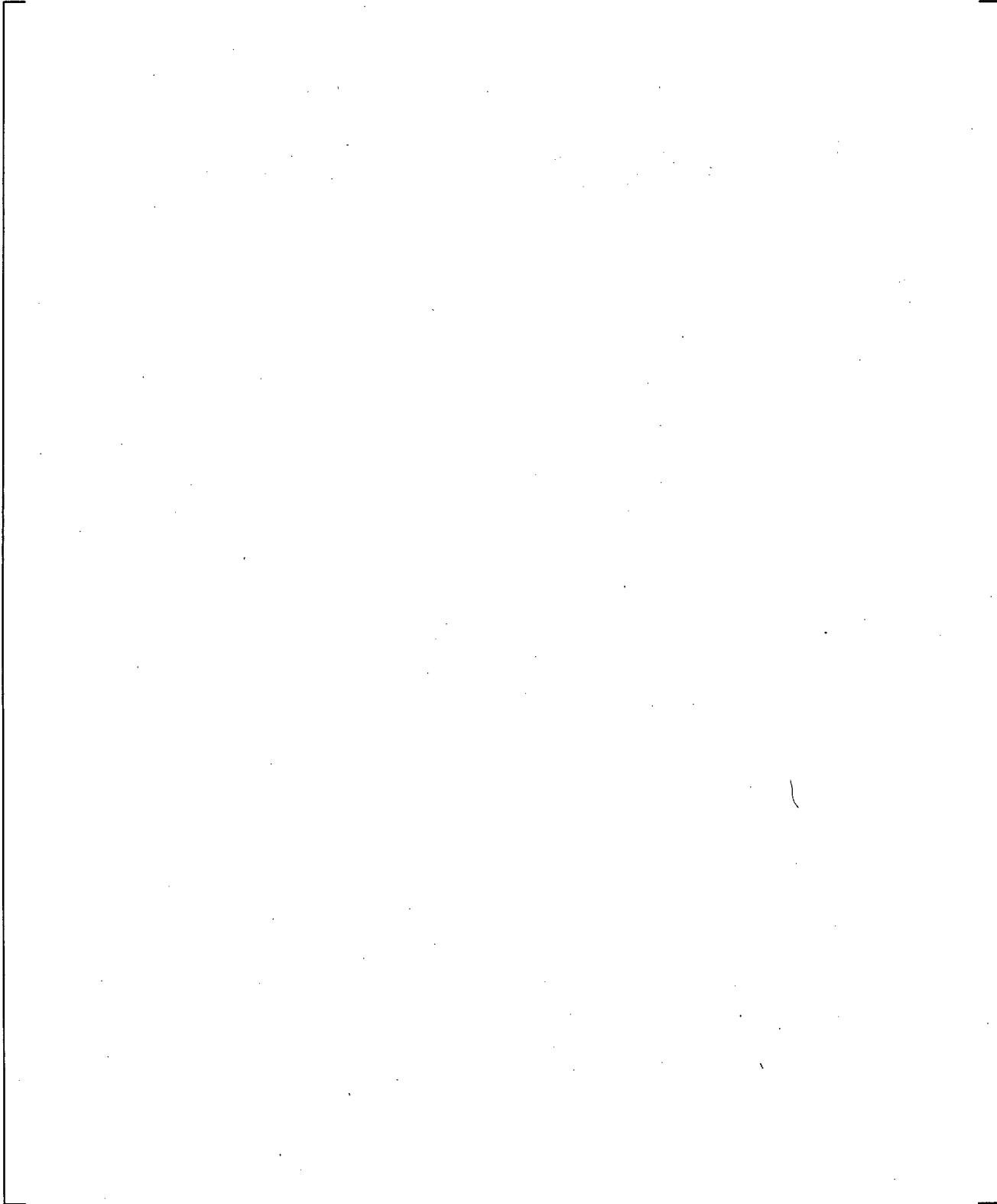


**Figure 24.6.3-10 Cladding Axial Temperature at Start of Test (6 Seconds), 15, 20, 30 Seconds for Case 4 (Test 146)**

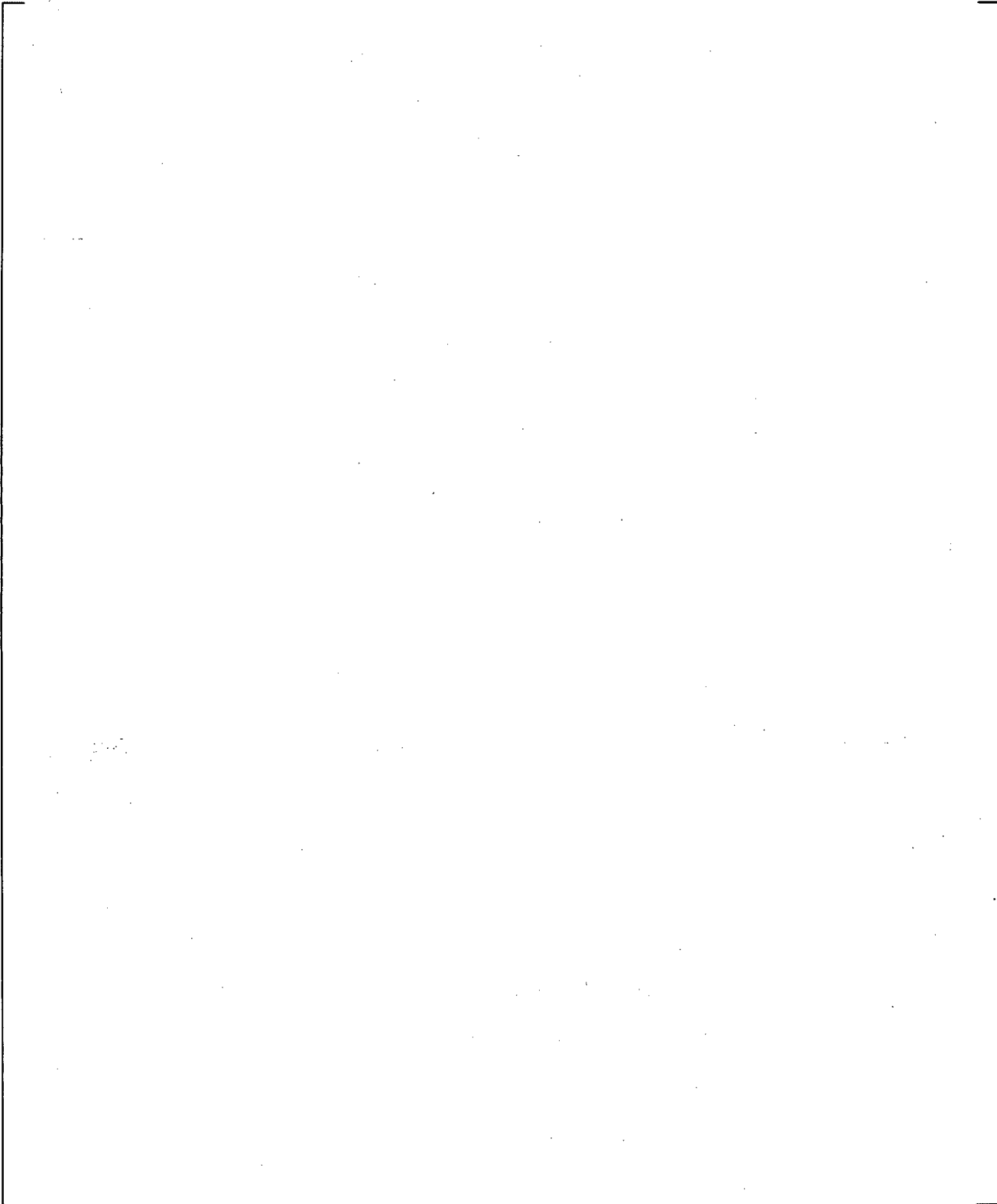


**Figure 24.6.3-11 Cladding Axial Temperature at Start of Test (6 Seconds), 15, 20, 30 Seconds for Case 5 (Test 154)**

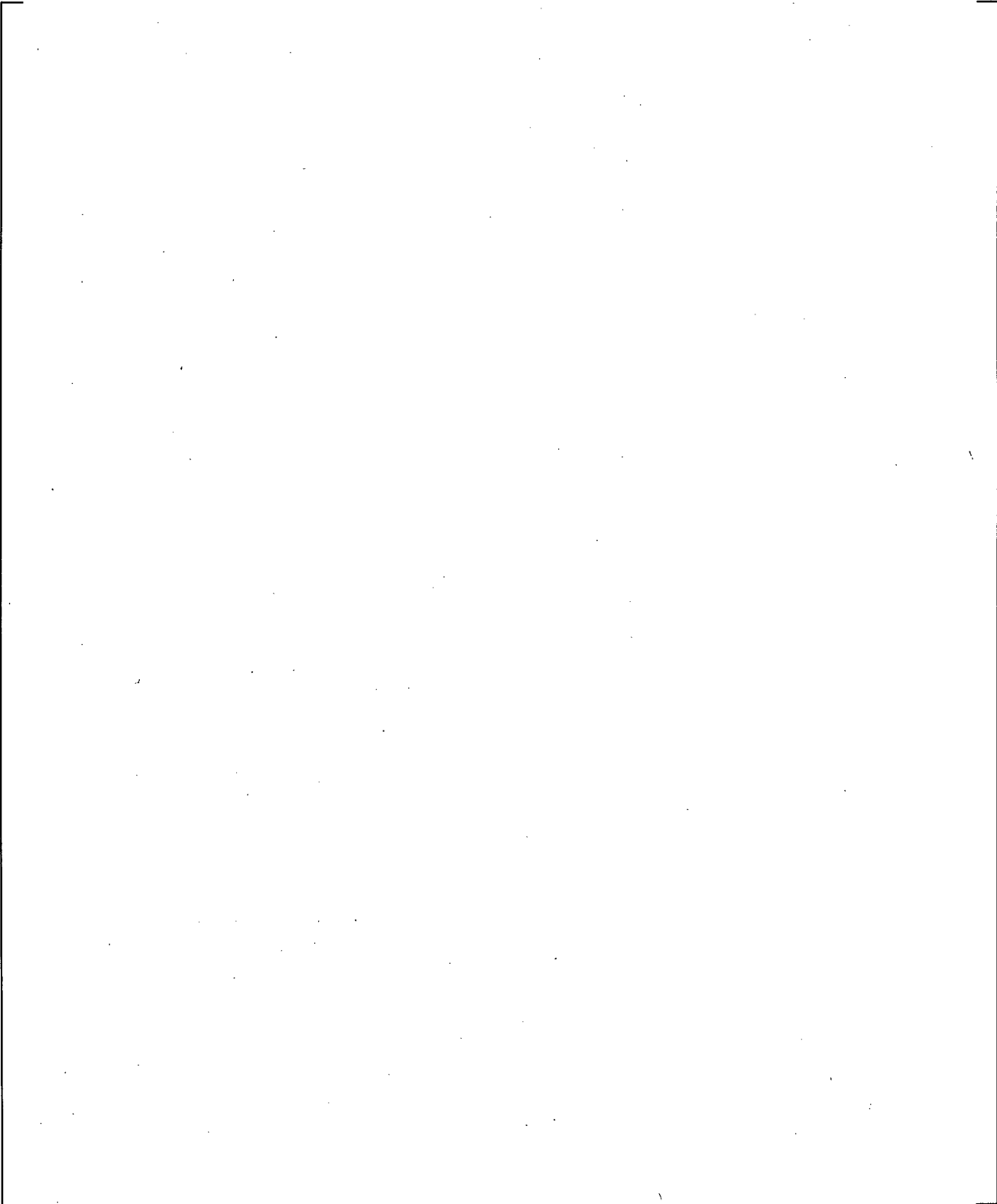


**Figure 24.6.3-12 Cladding Axial Temperature at Start of Test (6 Seconds), 15, 20, 30 Seconds for Case 6 (Test 153)**

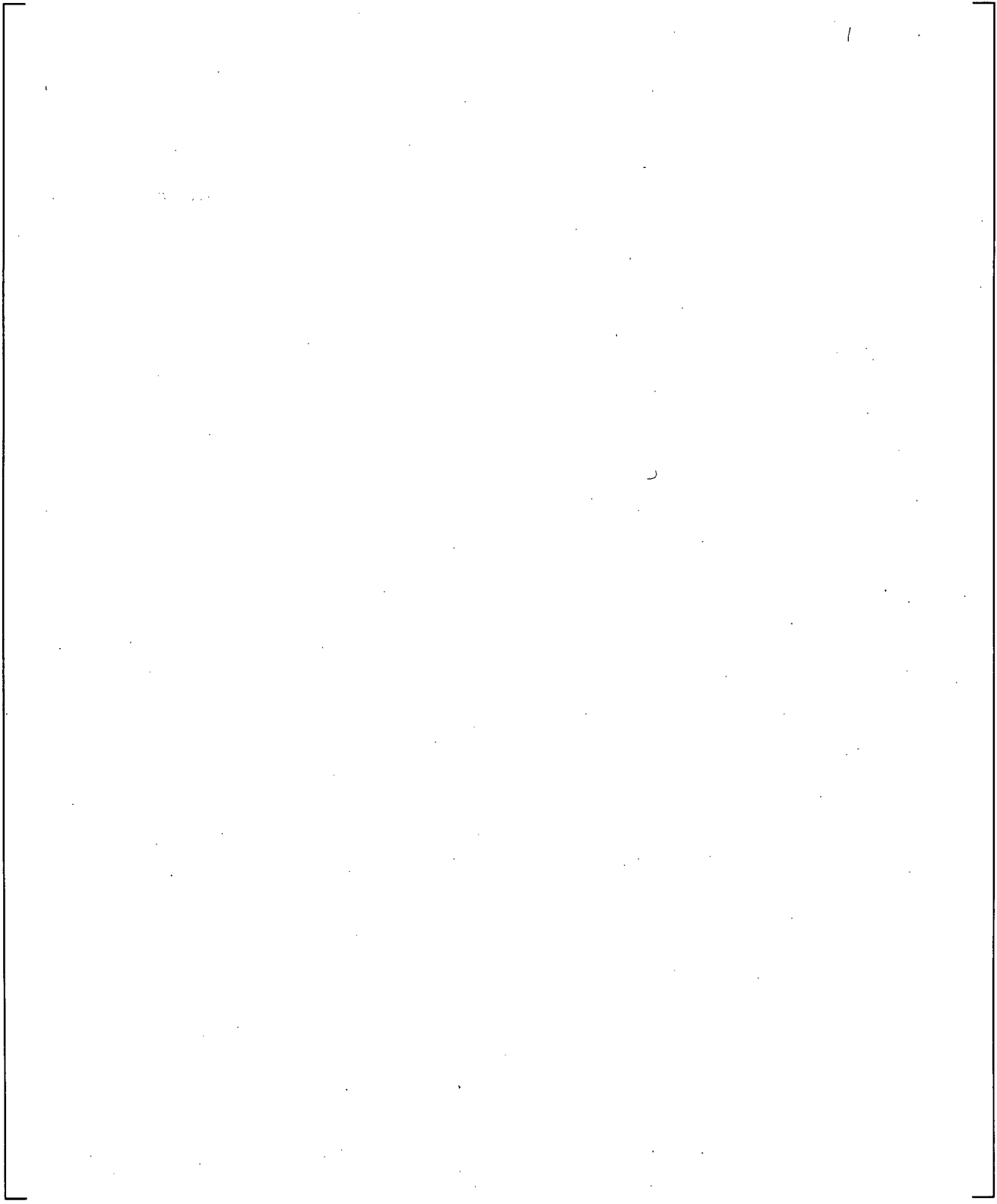
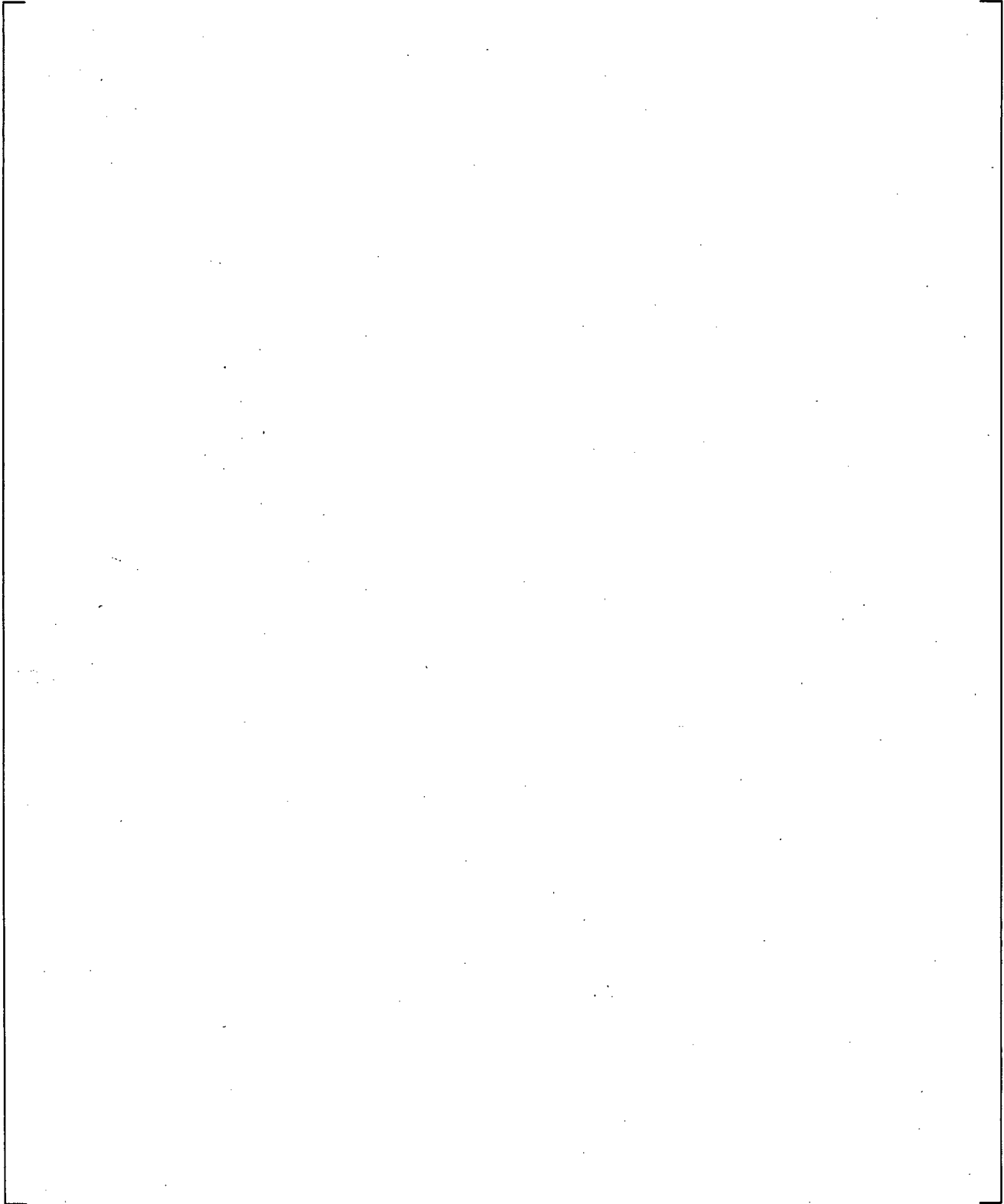
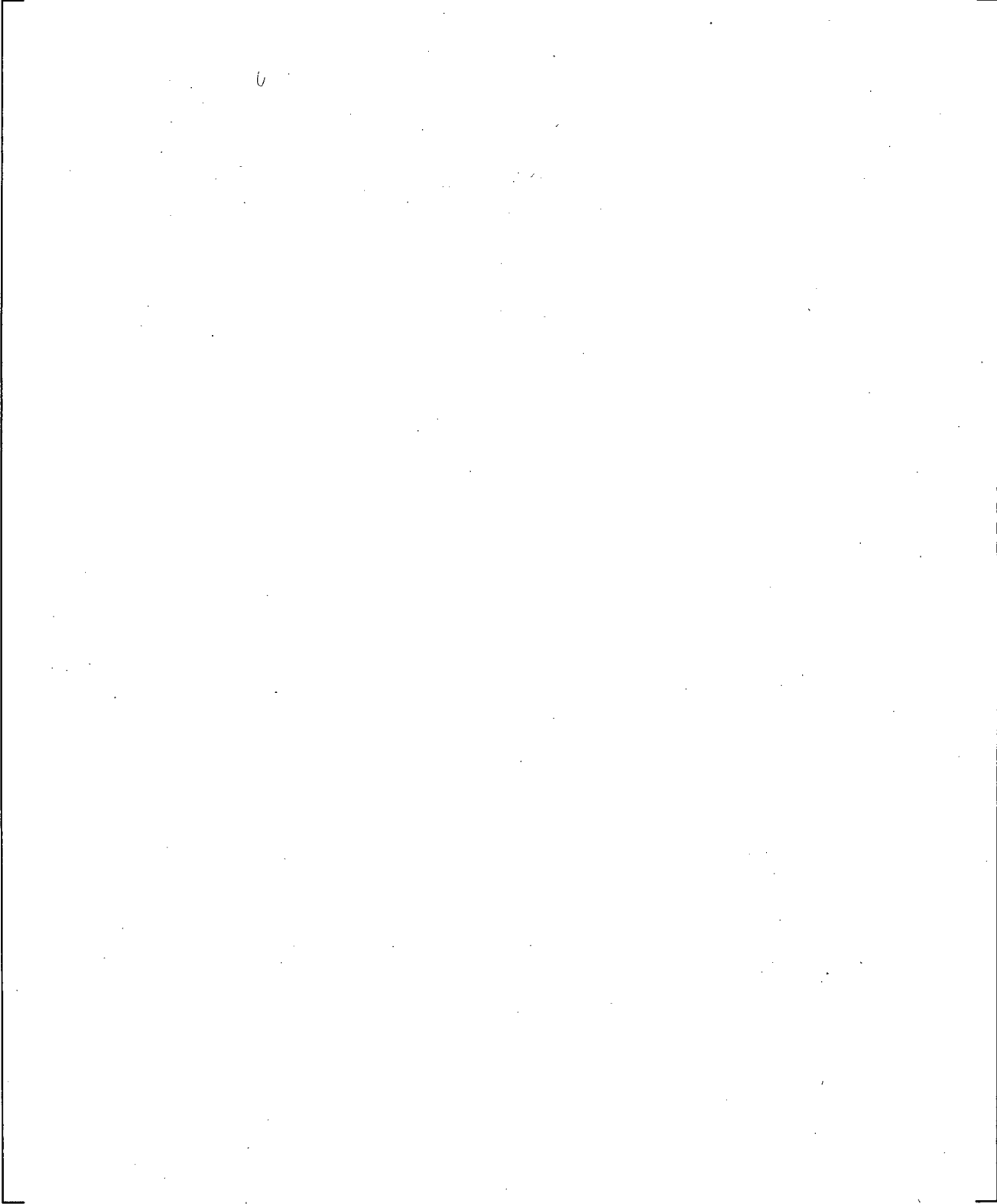


Figure 24.6.3-13 WCOBRA/TRAC-TF2 Heat Transfer Regime Map



**Figure 24.6.3-14 Vapor Fraction at 72-inch Elevation for G-1 Test 148 (Case 1)**



**Figure 24.6.3-15 Heat Flux to Vapor at 72-inch Elevation for G-1 Test 148 (Case 1)**

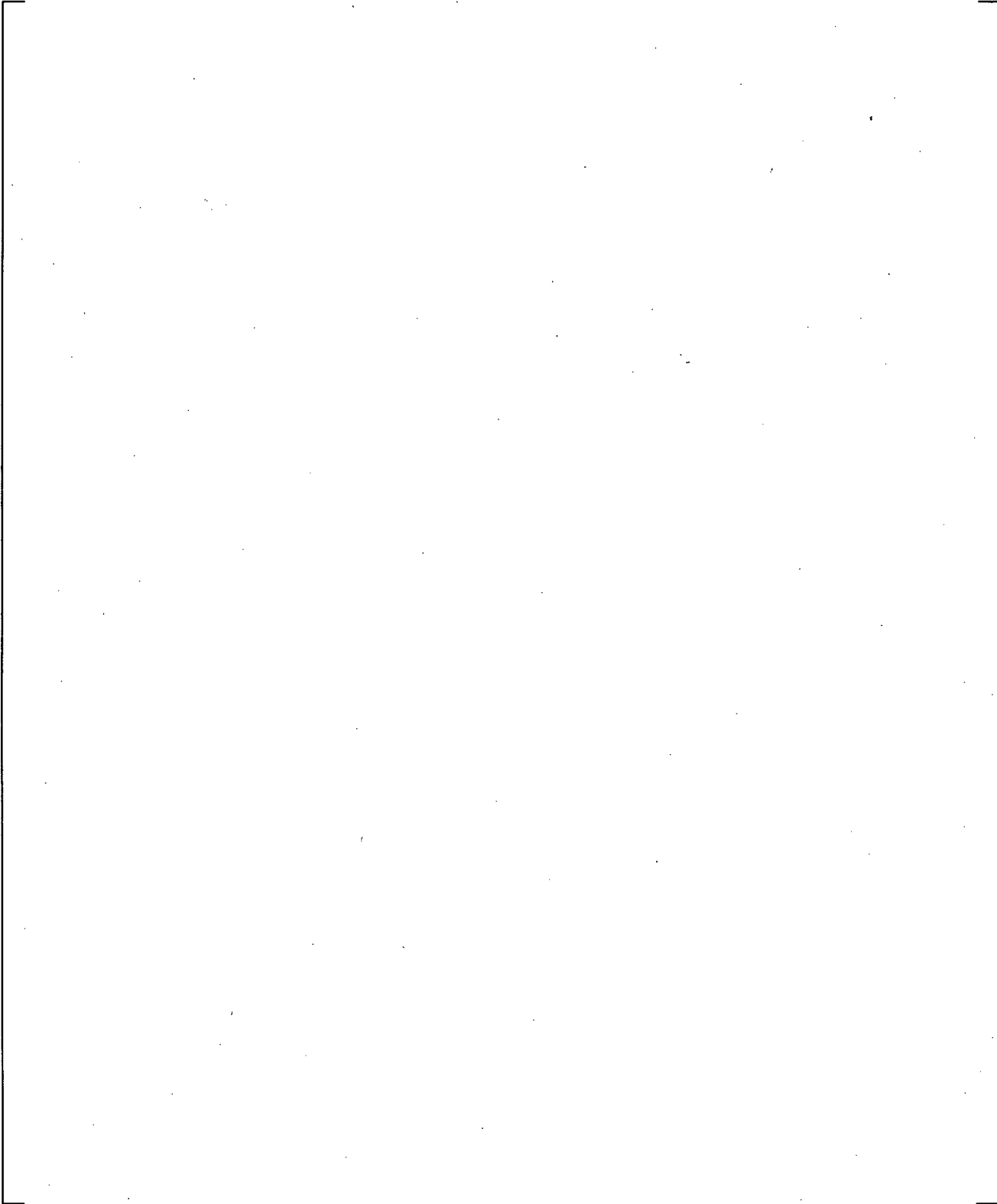


**Figure 24.6.3-16 Heat Flux to Liquid at 72-inch Elevation for G-1 Test 148 (Case 1)**

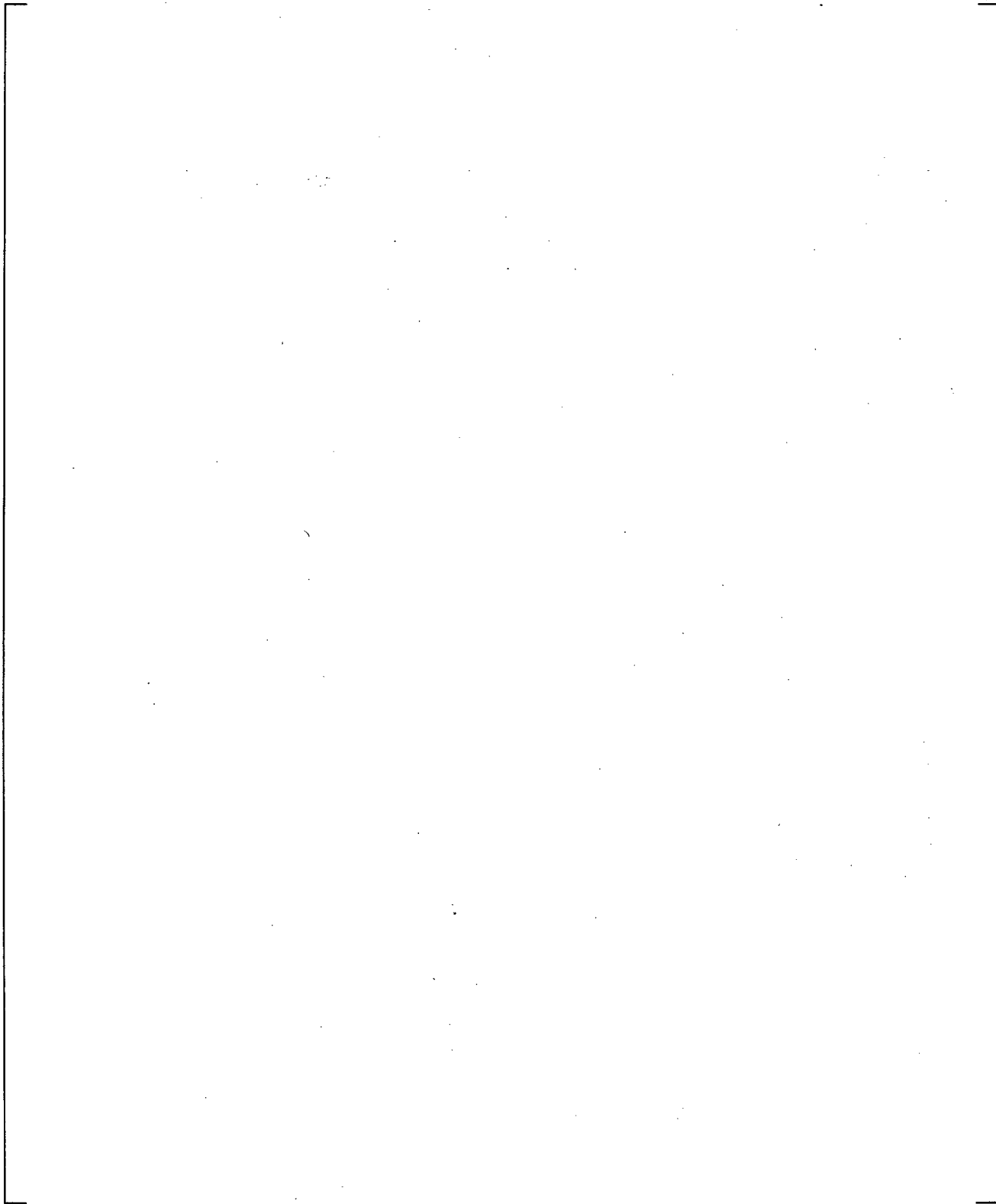


**Figure 24.6.3-17 Vapor Fraction at 72-inch Elevation for G-1 Test 146 (Case 4)**

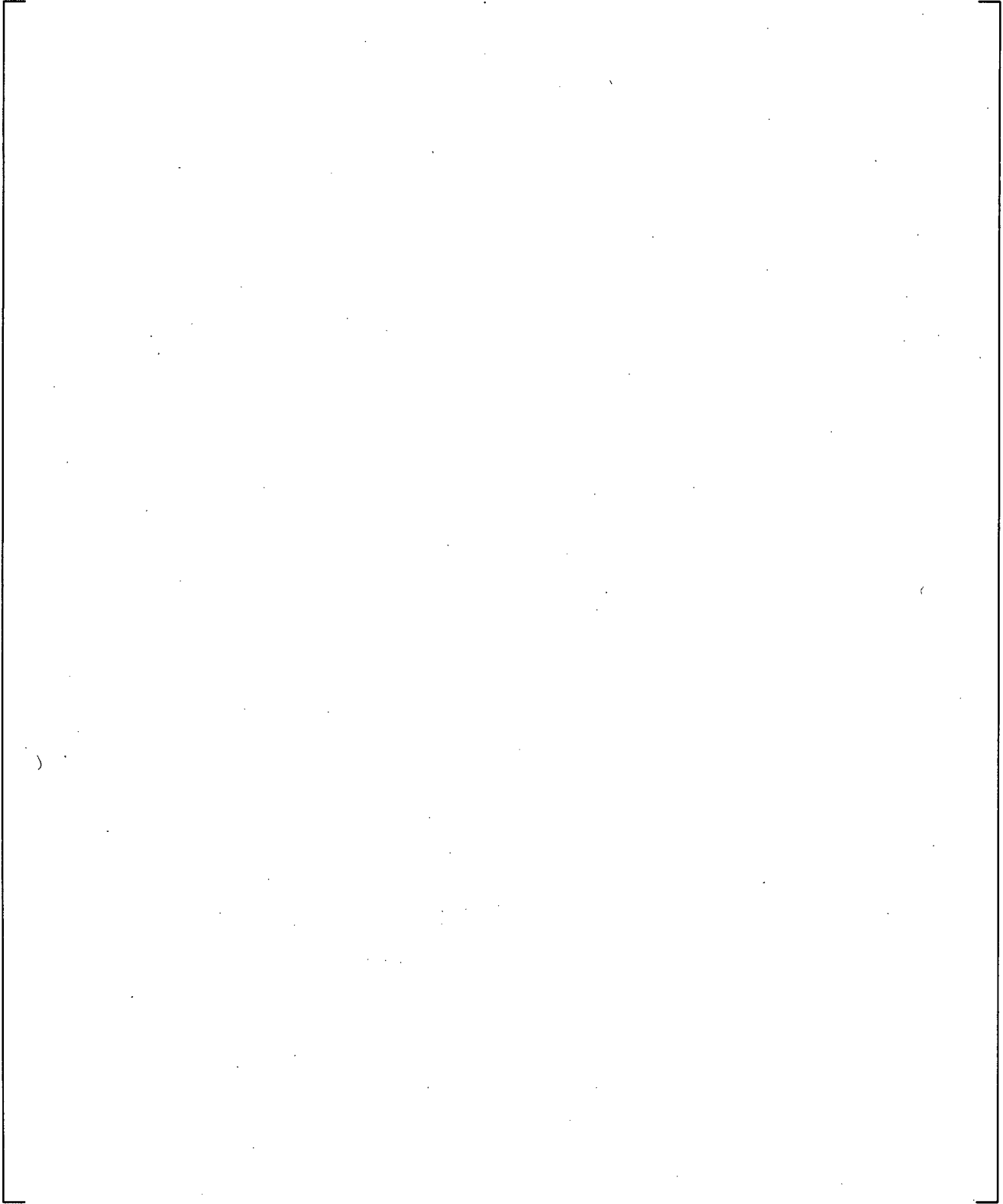


**Figure 24.6.3-18 Heat Flux to Vapor at 72-inch Elevation for G-1 Test 146 (Case 4)**

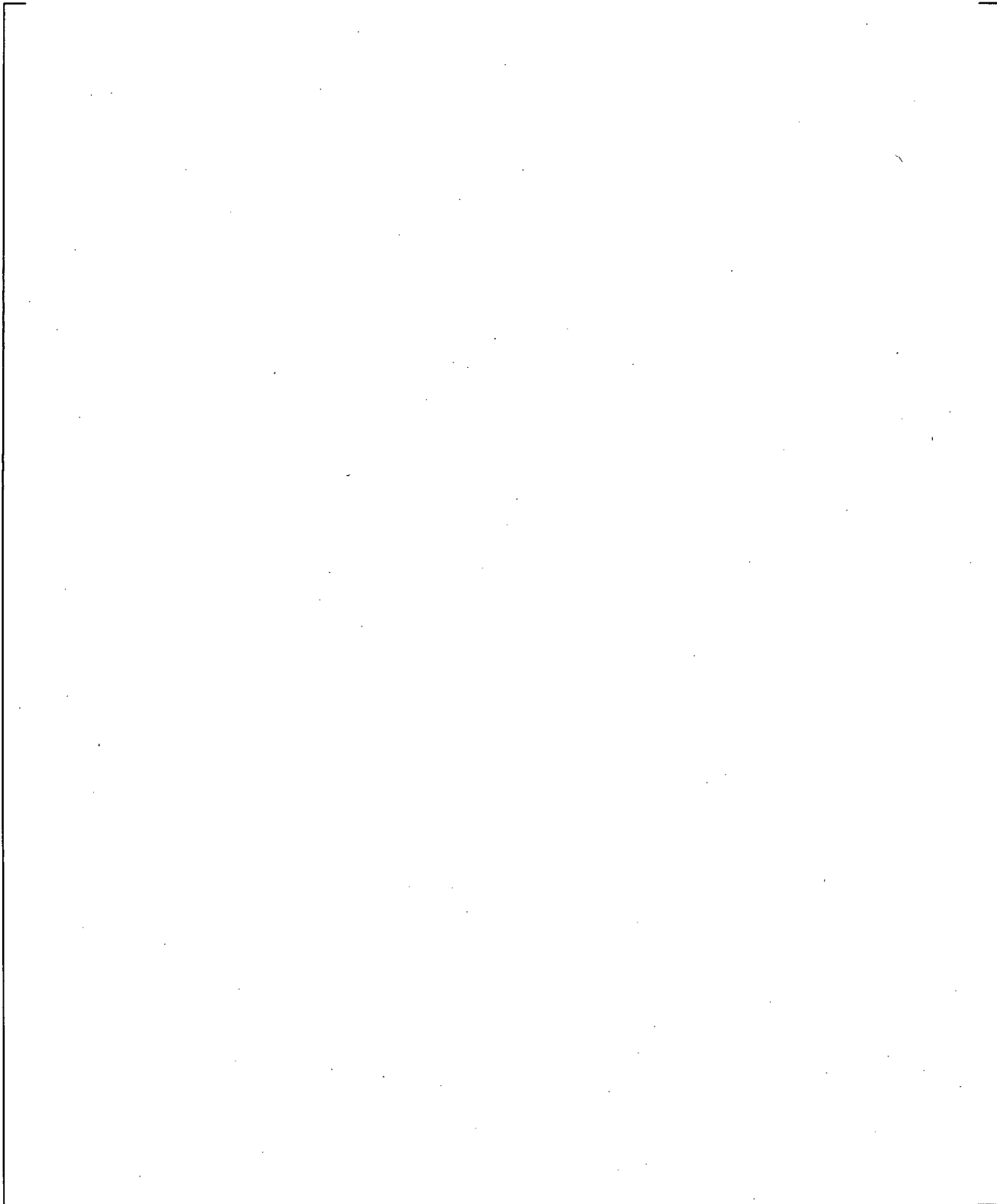


**Figure 24.6.3-19 Heat Flux to Liquid at 72-inch Elevation for G-1 Test 146 (Case 4)**

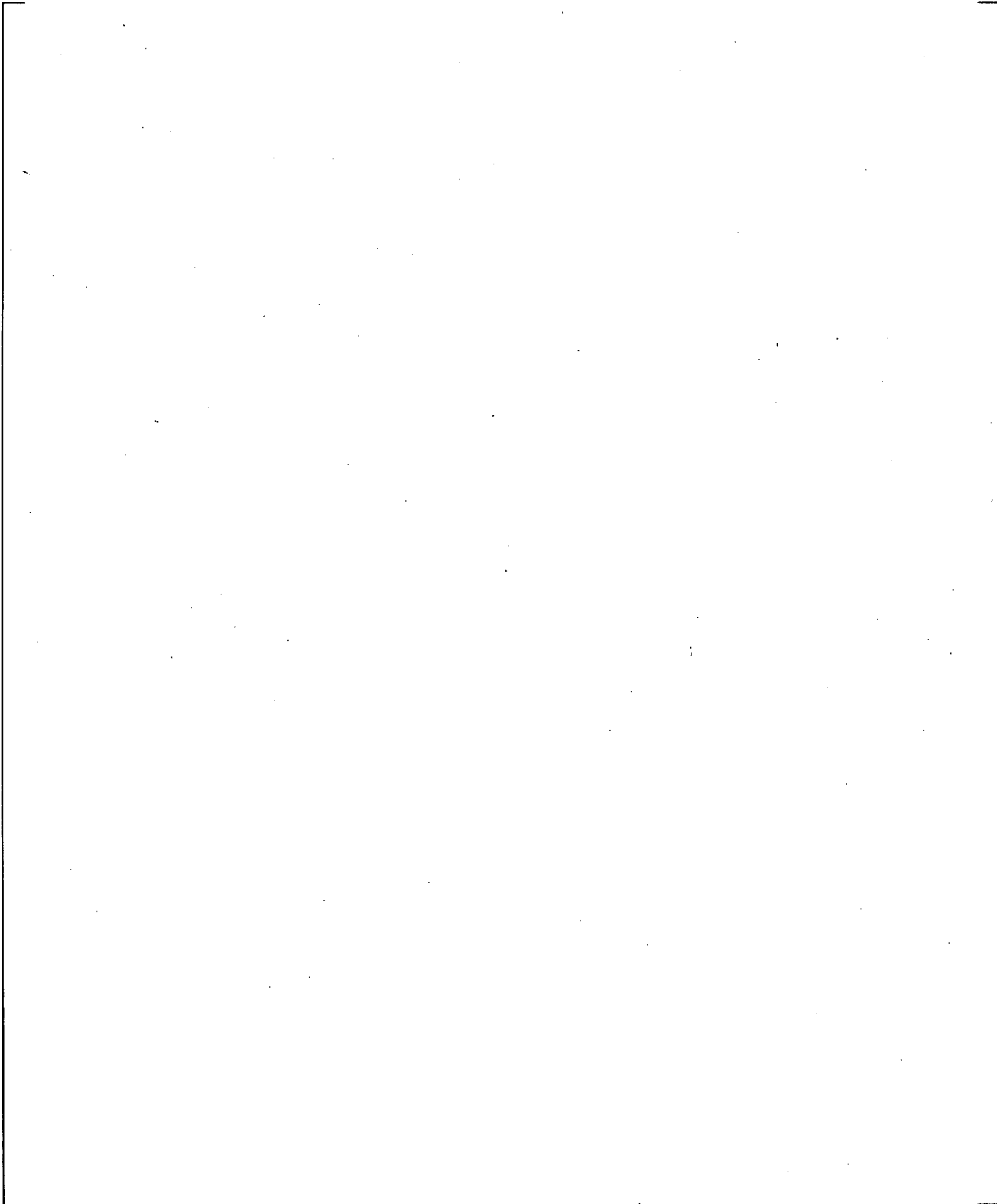


**Figure 24.6.3-20 Effect of Reduced  $T_{min}$  on Cladding Axial Temperature at 26 Seconds for Case 1 (Test 148)**

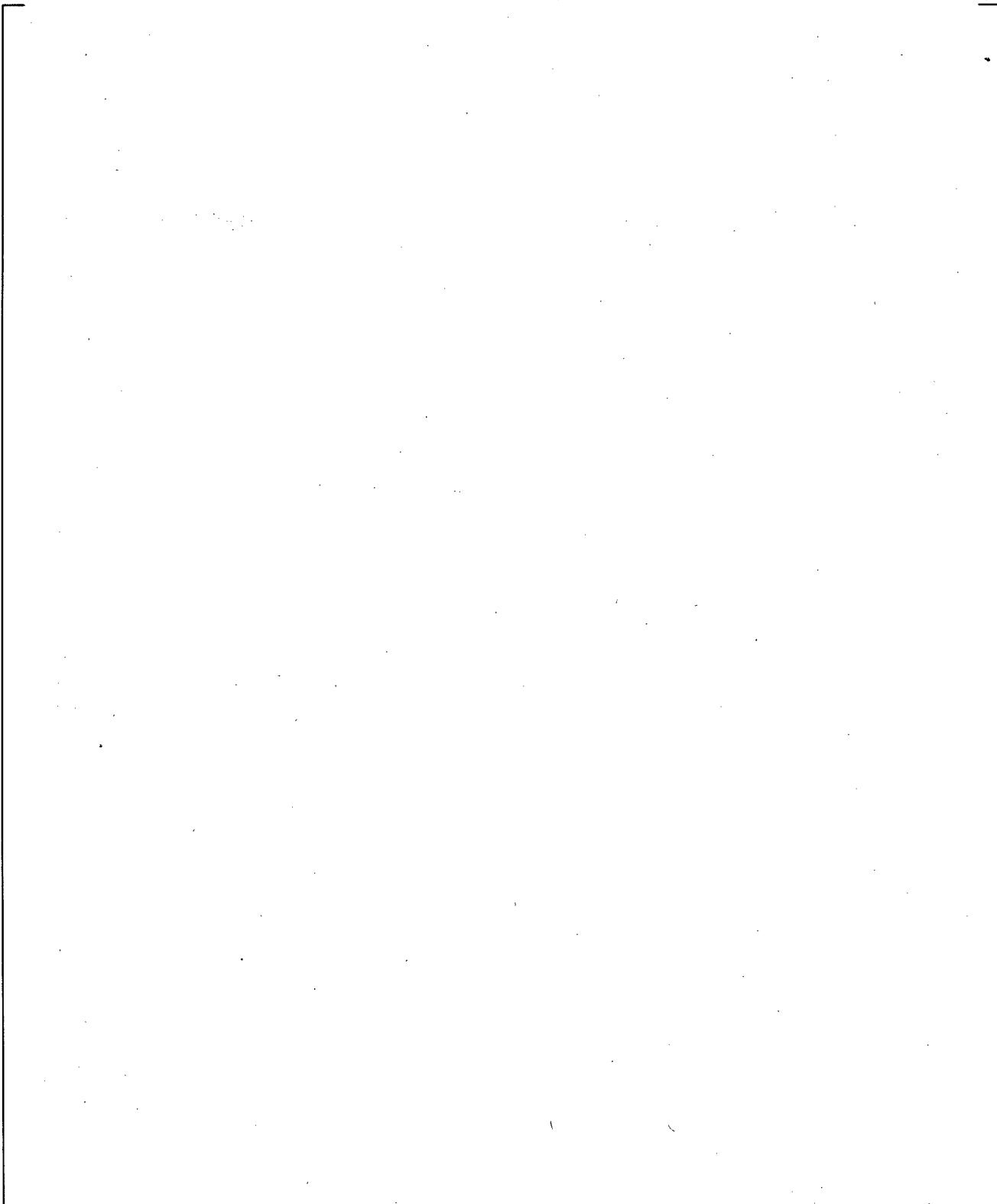


**Figure 24.6.3-21 Effect of Reduced  $T_{min}$  on Axial Vapor Temperature at 26 Seconds for Case 1 (Test 148)**

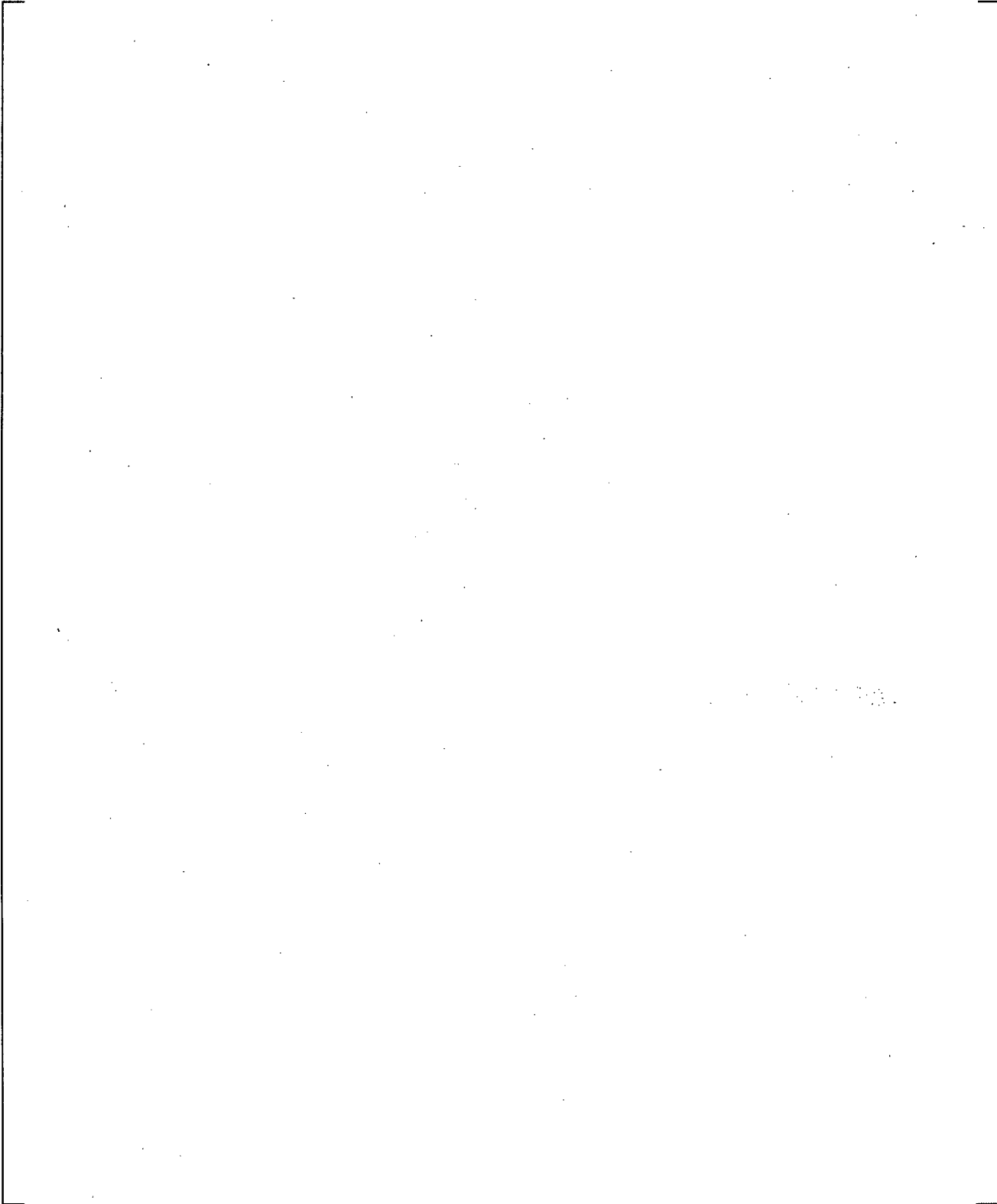


**Figure 24.6.3-22** Effect of Reduced  $D_{DROP}$  on Cladding Axial Temperature at 26 Seconds for Case 1 (Test 148)

**Figure 24.6.3-23 Effect of Reduced  $D_{DROP}$  on Axial Vapor Temperature at 26 Seconds for Case 1 (Test 148)**

**Figure 24.6.3-24 Effect of Reduced  $T_{min}$  on Cladding Axial Temperature at 22 Seconds for Case 4 (Test 146)**

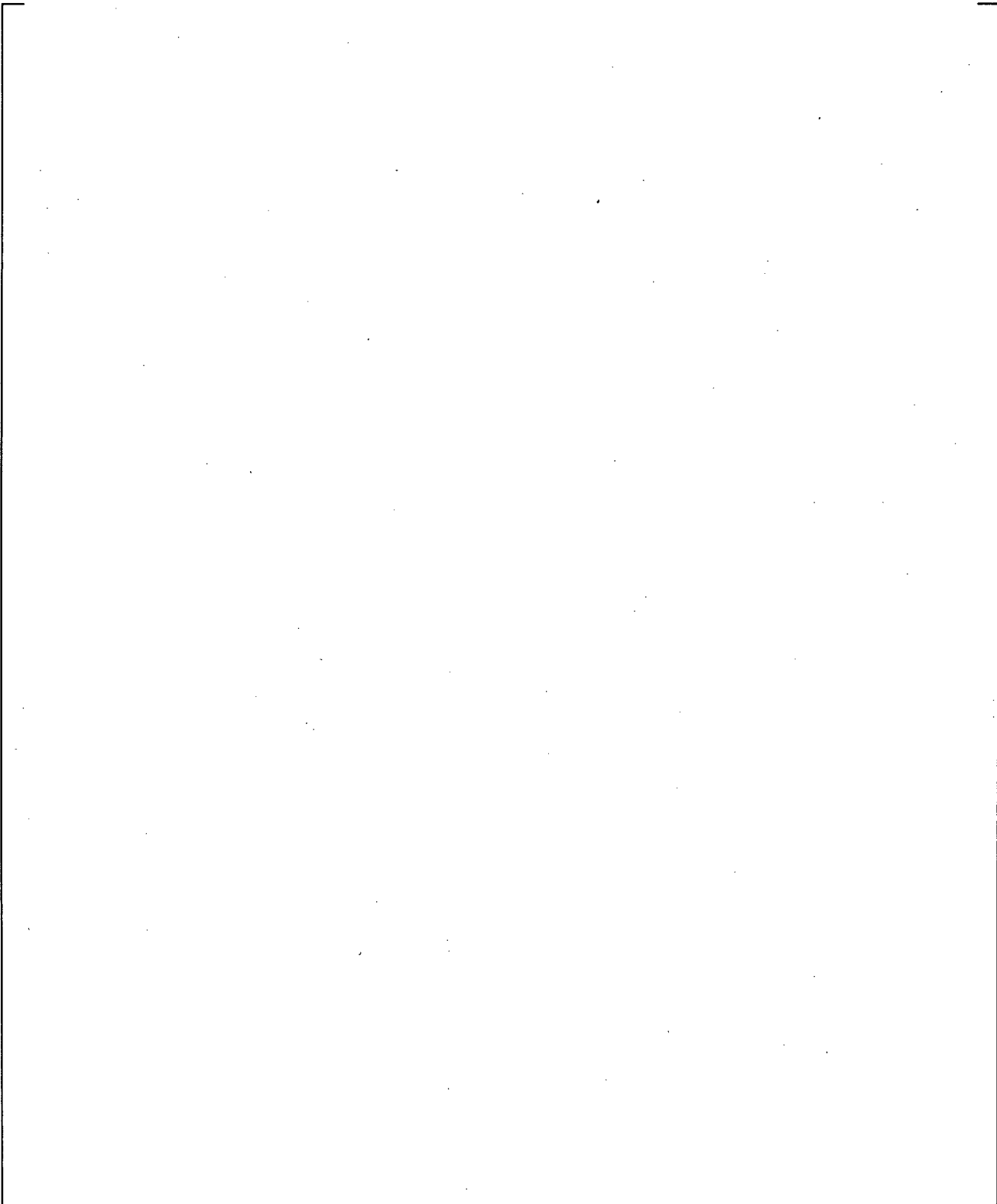


**Figure 24.6.3-25 Effect of Reduced  $T_{min}$  on Axial Vapor Temperature at 22 Seconds for Case 4 (Test 146)**

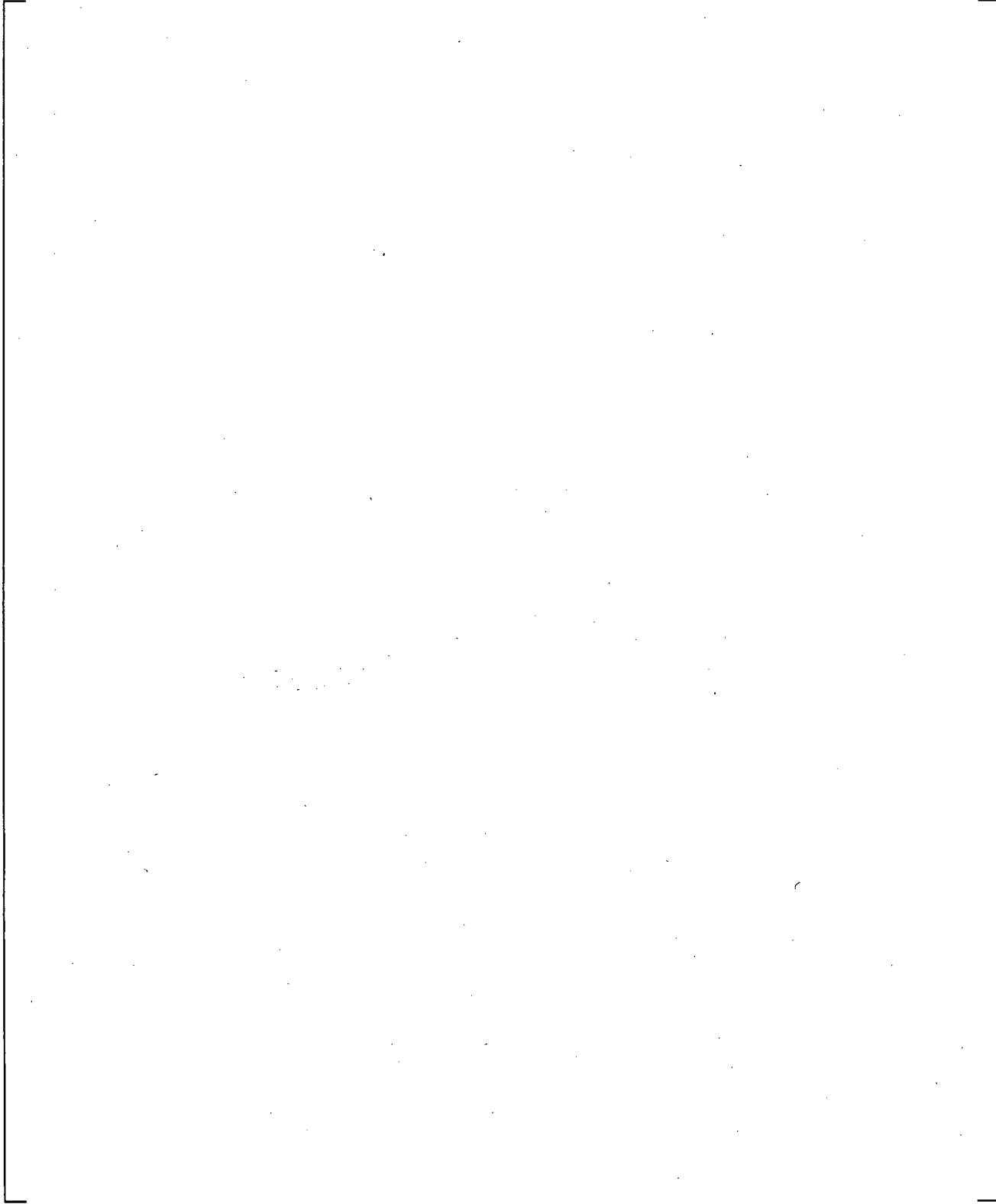


**Figure 24.6.3-26 Effect of Reduced  $D_{DROP}$  on Cladding Axial Temperature at 22 Seconds for Case 4 (Test 146)**

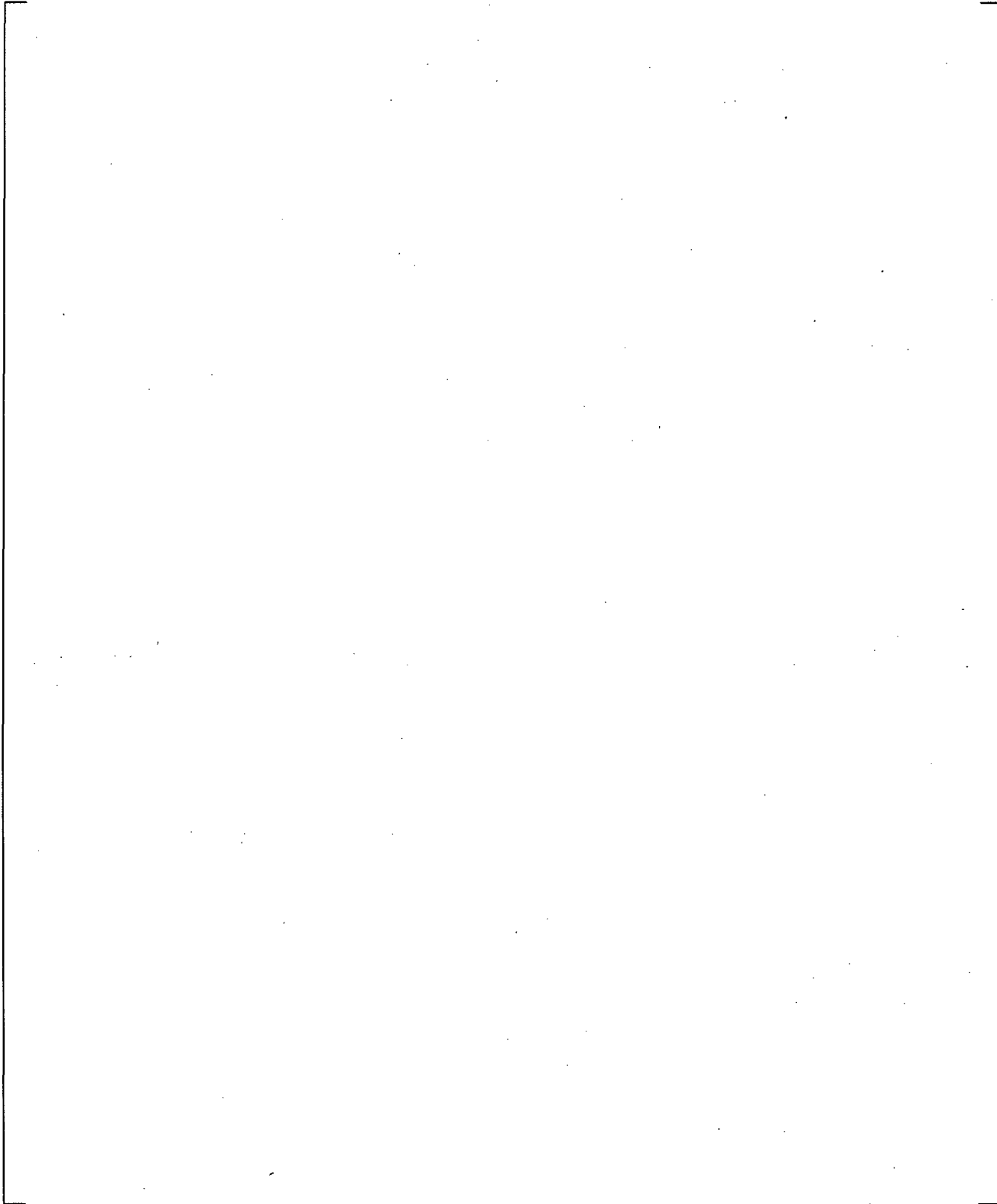


**Figure 24.6.3-27 Effect of Reduced  $D_{DROP}$  on Axial Vapor Temperature at 22 Seconds for Case 4 (Test 146)**

#### 24.6.4 FLECHT SEASET 31504 Reflood Test Simulation

FLECHT SEASET Test 31504 was evaluated for compensating error. [

] <sup>a,c</sup>

Axial profiles at [

] <sup>a,c</sup>

[

] <sup>a,c</sup>

The evaluation of FLECHT-SEASET Test 31504 showed that [

] <sup>a,c</sup>

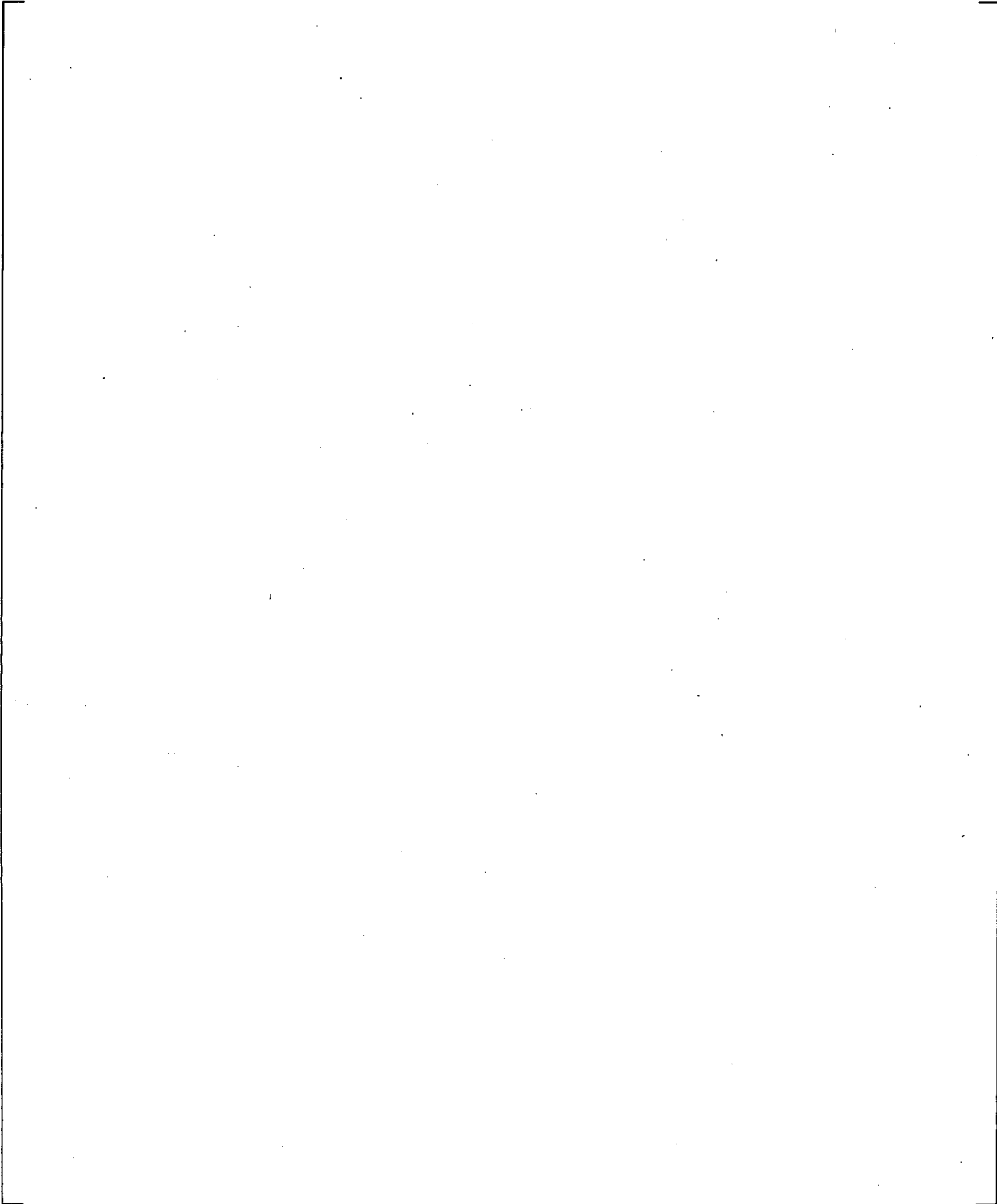


**Figure 24.6.4-1 TCLAD vs. Time at 6 ft for FLECHT-31504**

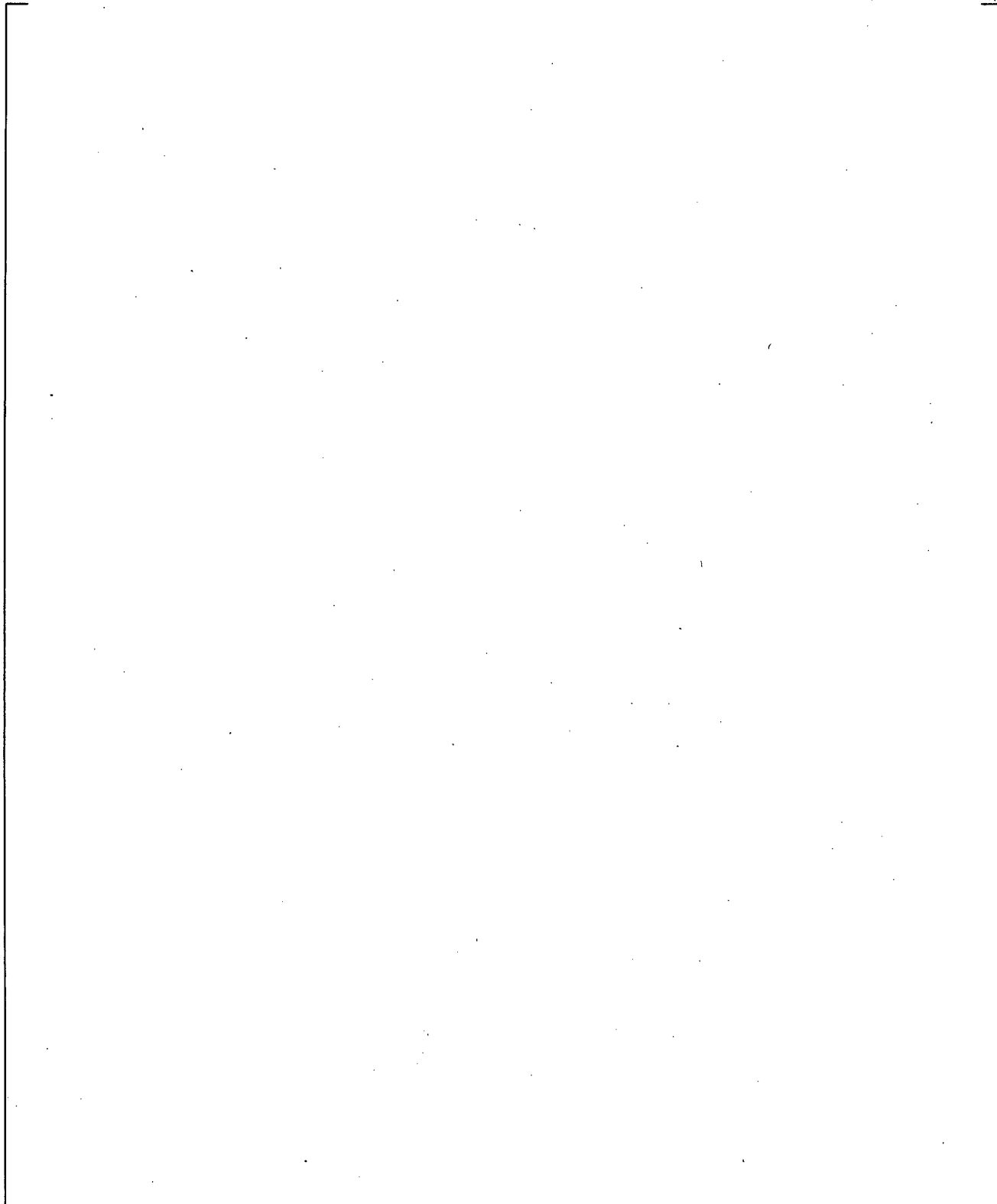


**Figure 24.6.4-2 TCLAD vs. Time at 9.3 ft for FLECHT-31504**

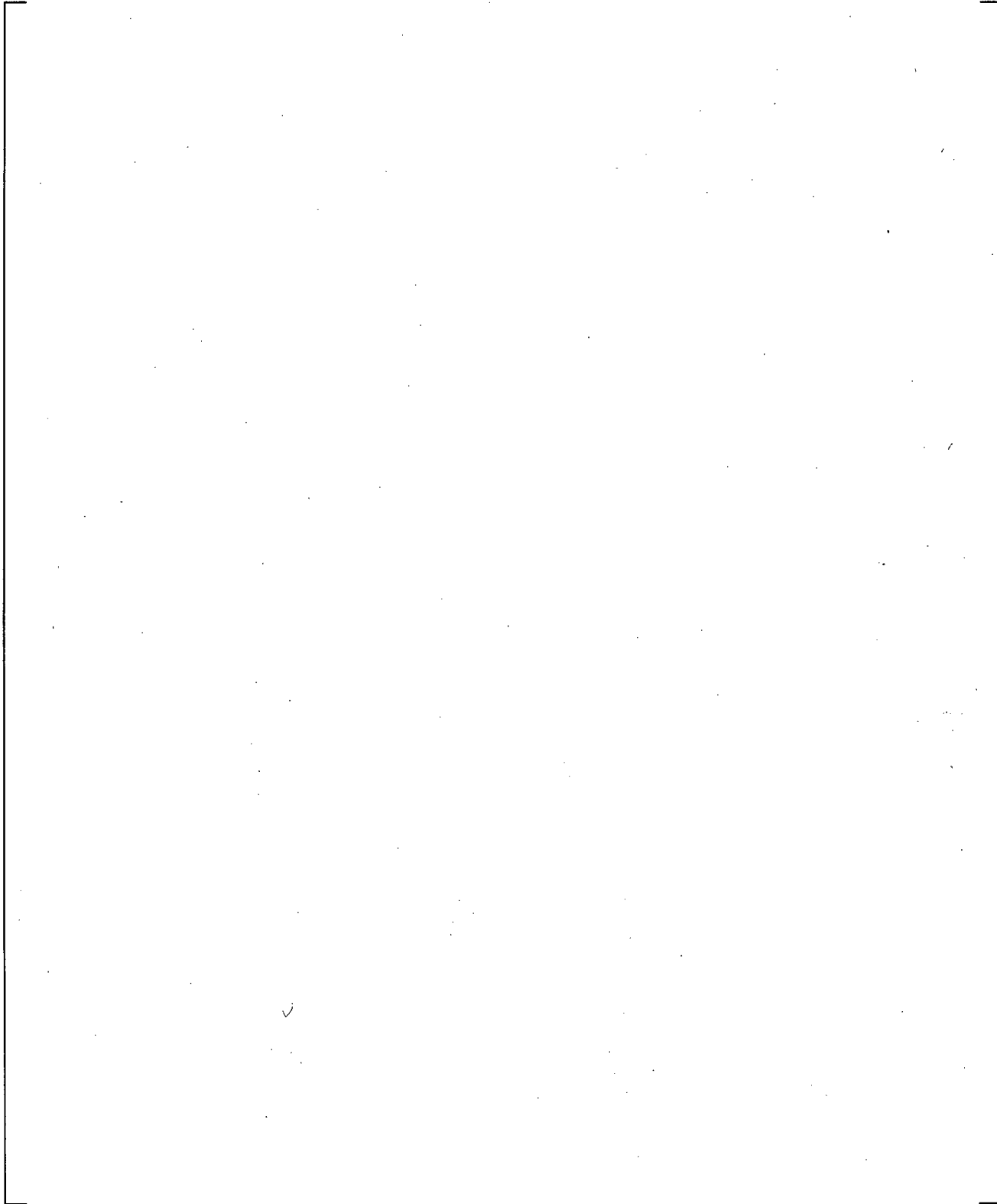


**Figure 24.6.4-3 Lower DP vs. Time for FLECHT-31504**

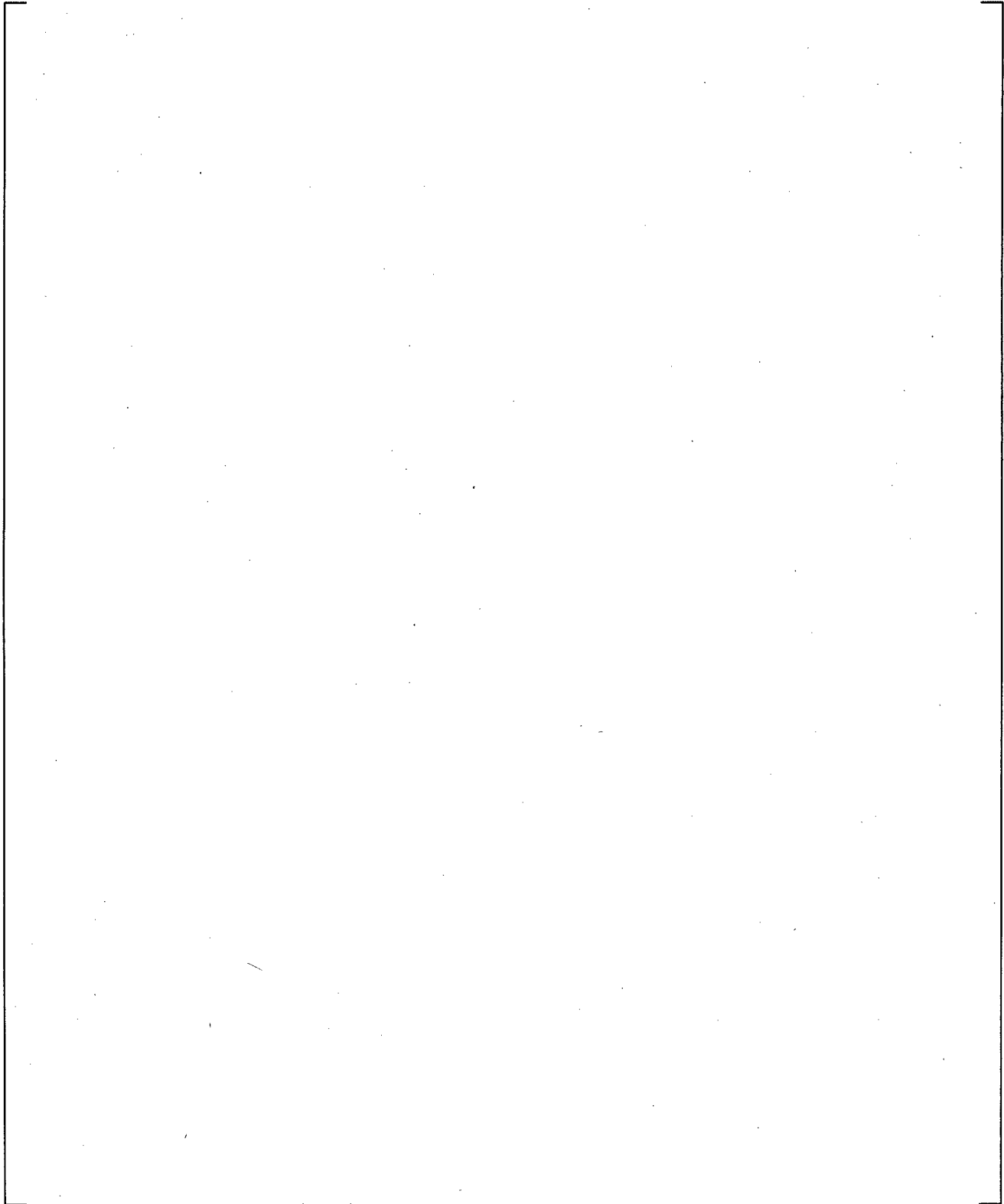


**Figure 24.6.4-4 Upper DP vs. Time for FLECHT-31504**

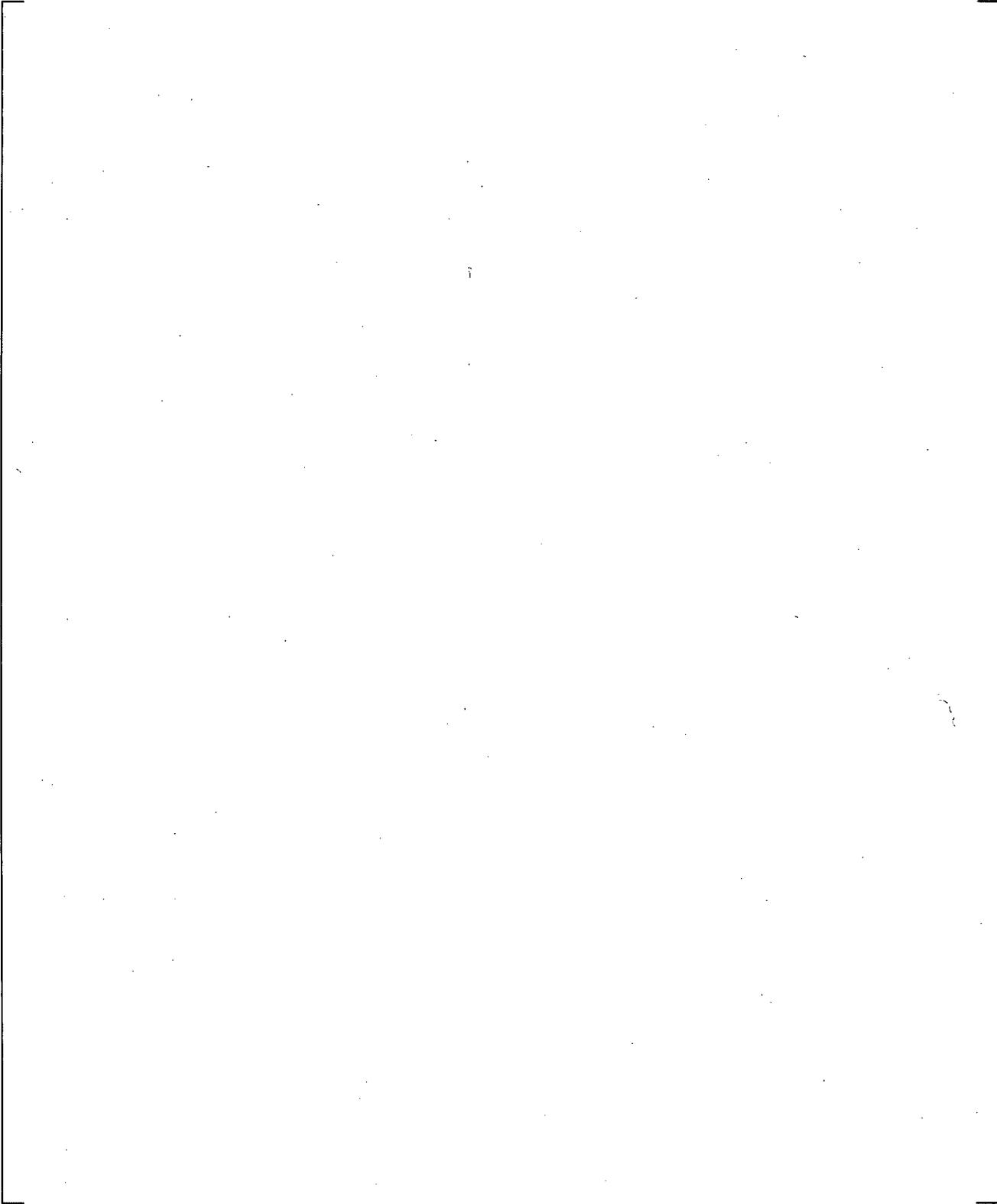


**Figure 24.6.4-5 Quench Front Elevation vs. Time for FLECHT-31504**

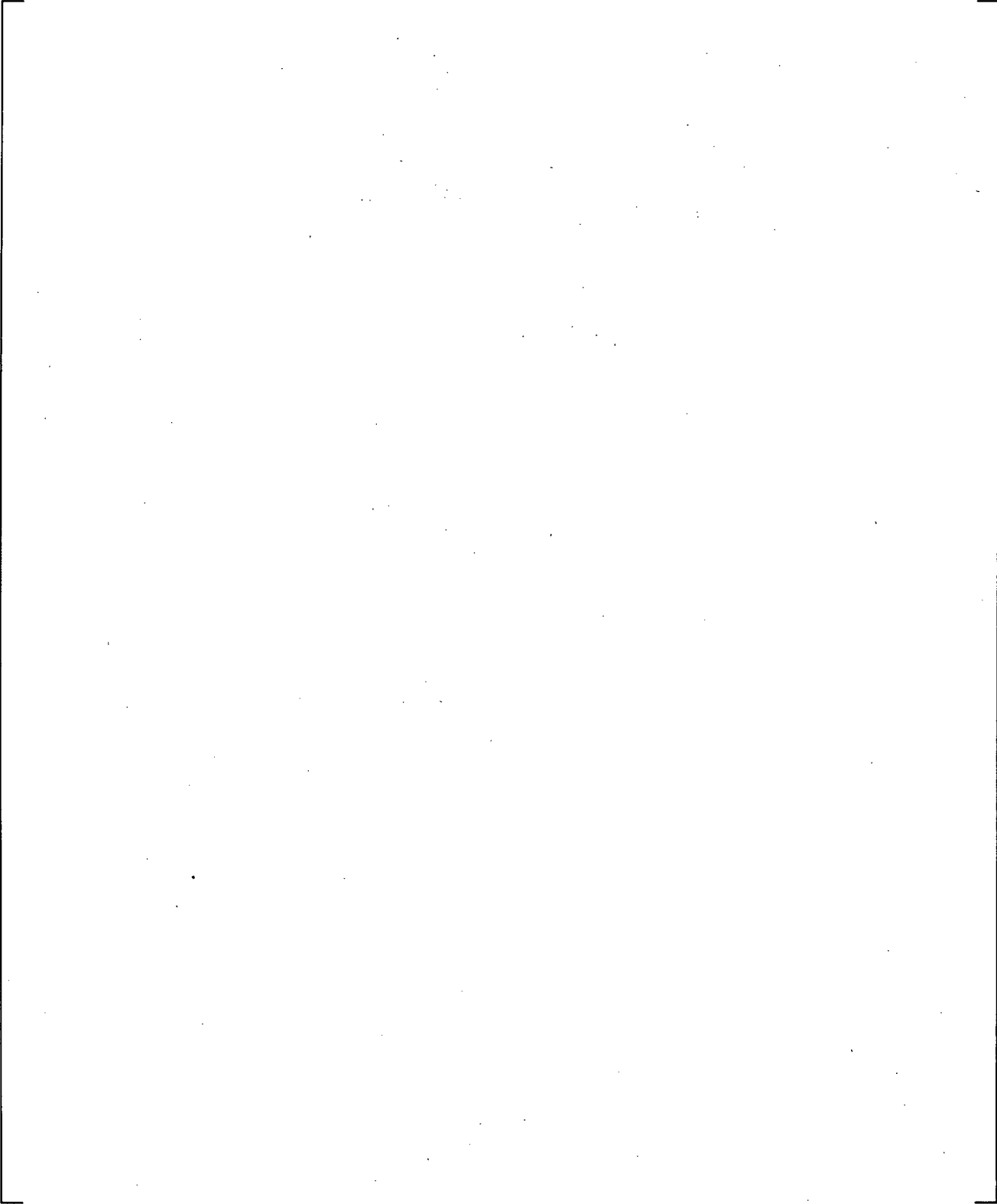


**Figure 24.6.4-6a Vapor Temperature Profile Prediction at 200 Seconds in FLECHT-31504**

**Figure 24.6.4-6b Vapor Temperature Profile Prediction at 260 Seconds Compared against Data taken at 200 Seconds**

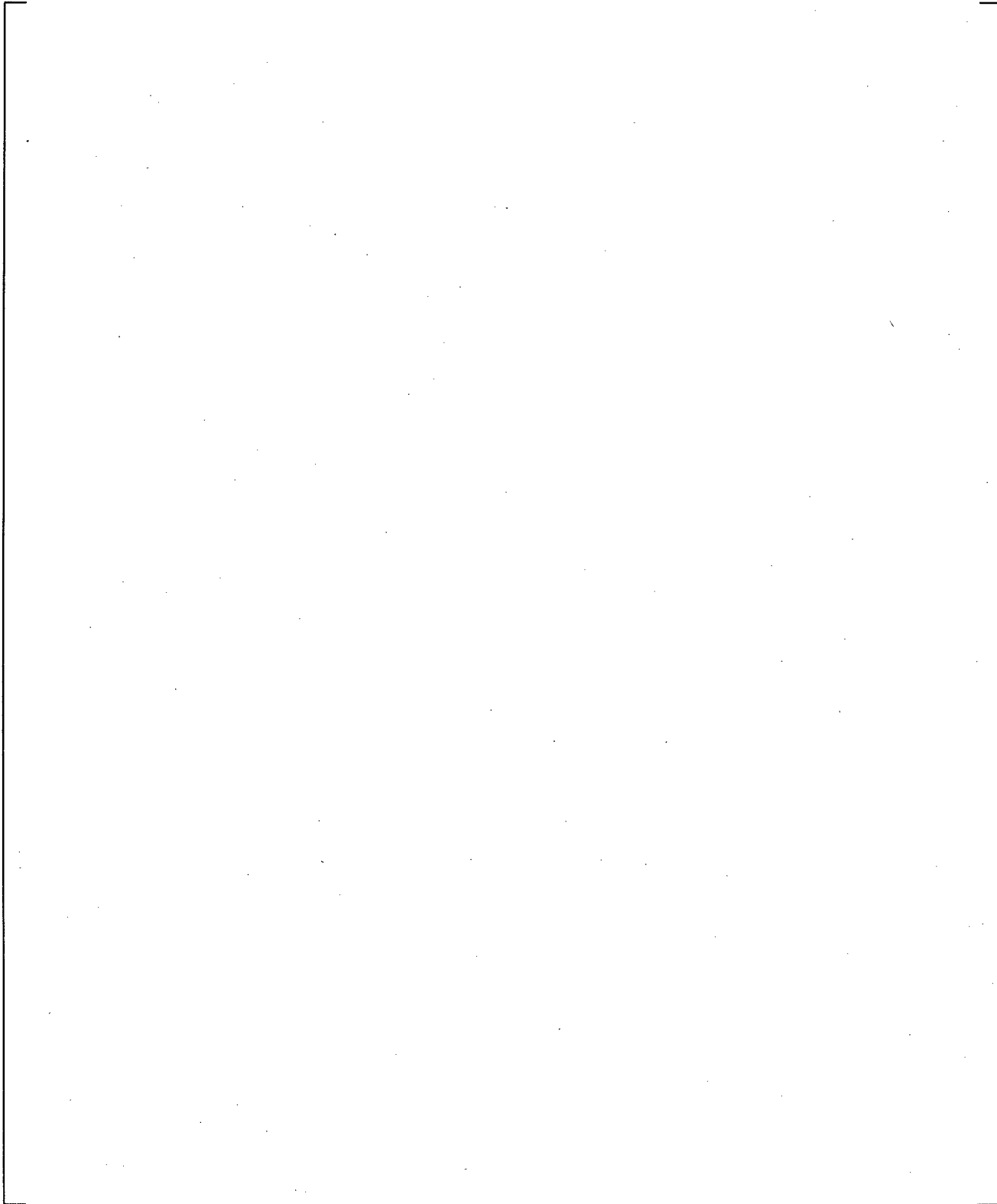


**Figure 24.6.4-7 Void Fraction Profile Comparison when the Quench Front is at 60 inches (Prediction at 260 and Data at 200 Seconds) in FLECHT-31504**

**Figure 24.6.4-8 Drop Velocity vs. Diameter Comparison at ~1ft above Quench Front (Prediction at 260 and Data at 200~206 Seconds) in FLECHT-31504**

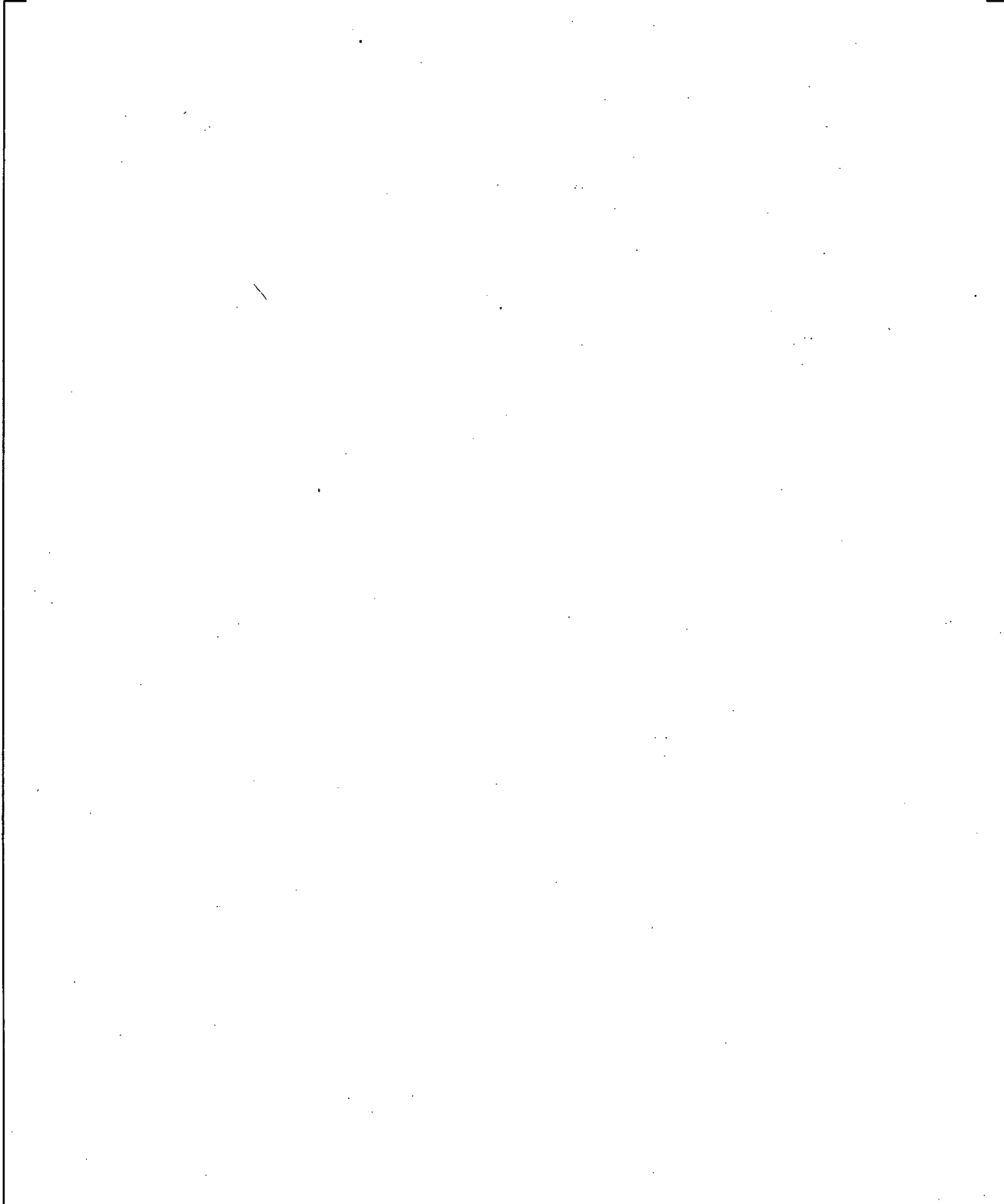


**Figure 24.6.4-9 Bundle Vapor Flow Comparison (Prediction at 260 and Data at 200 Seconds) in FLECHT-31504**

**Figure 24.6.4-10 Heat Transfer to Vapor Comparison (Prediction at 260 and Data at 200 Seconds) in FLECHT-31504**

**Figure 24.6.4-11 Heat Transfer to Liquid Comparison (Prediction at 260 and Data at 200 Seconds) in FLECHT-31504**

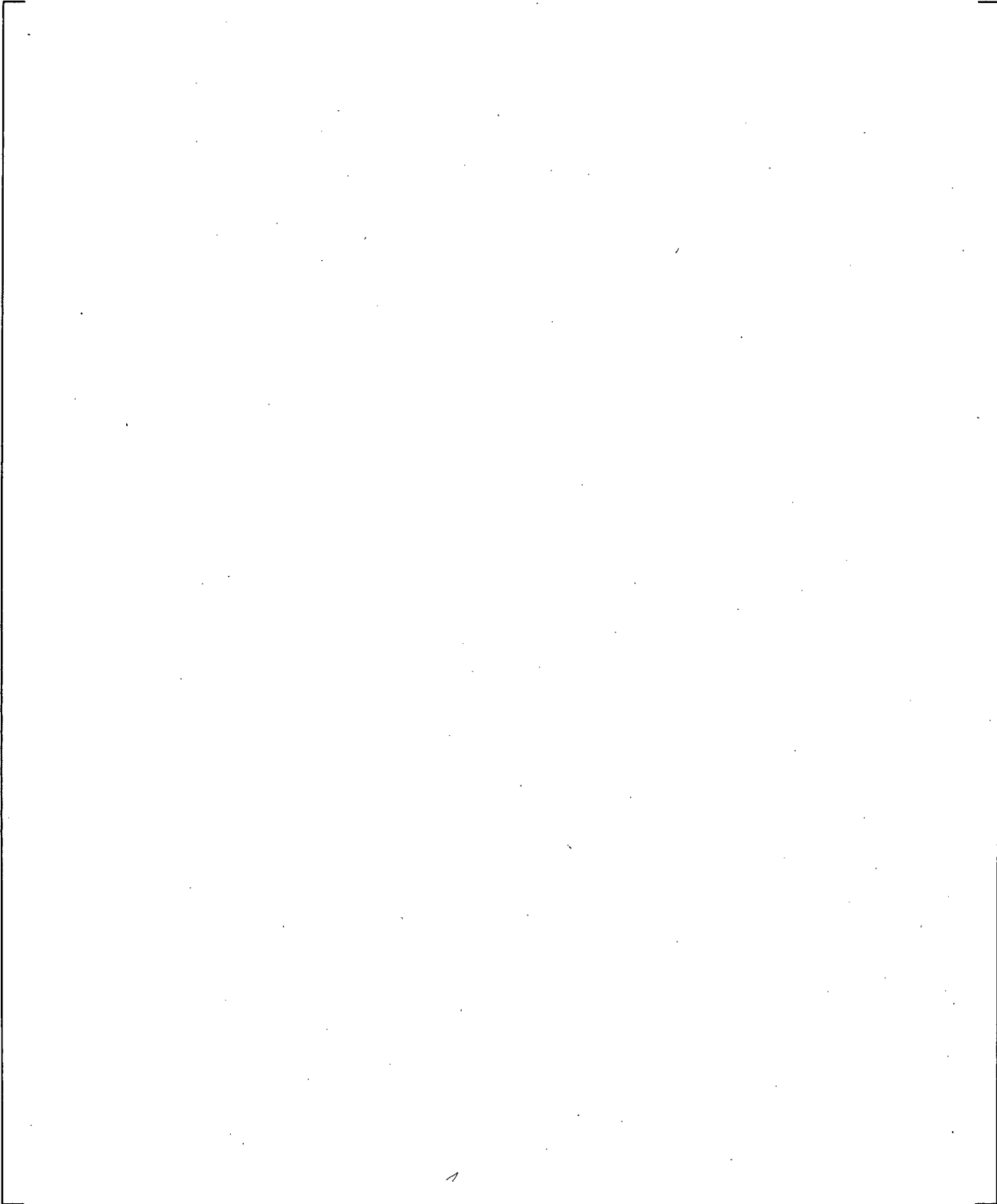


**Figure 24.6.4-12 Predicted Fraction of Heat Transfer to Liquid in FLECHT-31504**

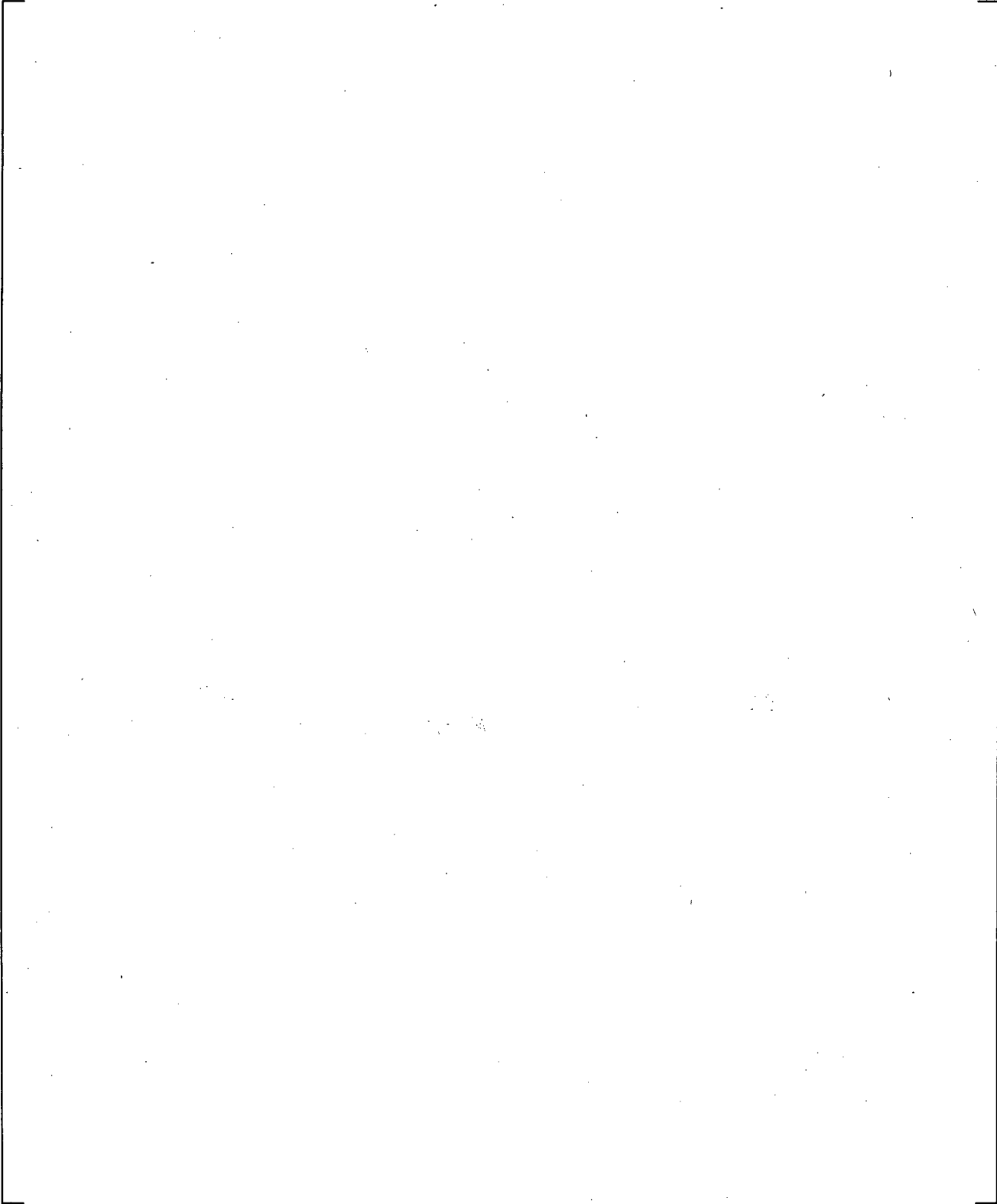


**Figure 24.6.4-13 Vapor Reynolds Number Comparison (Prediction at 260 and Data at 200 Seconds) in FLECHT-31504**

**Figure 24.6.4-14 Vapor Nusselt Number Comparison (Prediction at 260 and Data at 200 Seconds) in FLECHT-31504**

### 24.6.5 FLECHT-SEASET Test 31805

Two forced reflood tests, 31805 and 31701 are examined for the investigation of Void Fraction-Heat Transfer relation. The examination of Test 31805 is presented first. Tests 31805 had a very low flooding rate (0.81 in/sec) and 31701 had a very high flooding rate (6.1 in/sec). Figure 24.6.5-1 shows the comparison of measured void fraction profile at the PCT time. In terms of the void distribution, the tests are considerably different. Because of the low flooding rate in Test 31805, the axial void profile has a sharp gradient near the quench front while in Test 31701 there is a significant amount of liquid at all elevations. Note that in Test 31701, only 5 seconds had elapsed since the start of the reflood.

Figure 24.6.5-2 shows a comparison of the predicted and measured axial temperature profile at 100 seconds, which just precedes the PCT time of 108 seconds for the 72-inch elevation for Test 31805.

[

] <sup>a,c</sup>

The predicted and measured axial void fraction profiles at 100 seconds are compared in Figure 24.6.5-5. The agreement is good, although the prediction shows near single phase vapor condition above 8 ft. while the measurement indicates some drops at high elevations.

Next, consider the variation of clad temperatures, heat transfer coefficients, and void fraction in the vicinity of the quench front. Figure 24.6.5-6 shows the measured void fraction at the 5- to 6-ft and 6- to 7-ft elevations. [

] <sup>a,c</sup>

Figure 24.6.5-7 shows the variation of clad temperature and void fraction with time at the 6 ft. elevation based on the test data. The void fraction is the 6- to 7-ft. measurement. Figure 24.6.5-8 shows the variation in heat transfer coefficient and void fraction with time at the same elevation. The individual thermocouples (T/C) quench over a span of about 40 seconds. The heat transfer coefficients are seen to increase to values typical of nucleate boiling following the quench. Figures 24.6.5-9 and 24.6.5-10 expand the period near the quench times.

[

] <sup>a,c</sup>

Figures 24.6.5-11 and 24.6.5-12 show the corresponding behavior of clad temperature and heat transfer coefficient with void fraction based on WCOBRA/TRAC-TF2 prediction. [

] <sup>a,c</sup>

Figure 24.6.5-13 compares the predicted and measured void fraction for the 6- to 7-ft. region of the bundle. [

] <sup>a,c</sup>

Figures 24.6.5-14 through 24.6.5-17 show the variation of clad temperature and heat transfer coefficient with void fraction at the 10 ft. elevation. [

] <sup>a,c</sup> Figure 24.6.5-18 compares the predicted and measured void fraction at the 10- to 11-ft. region. [

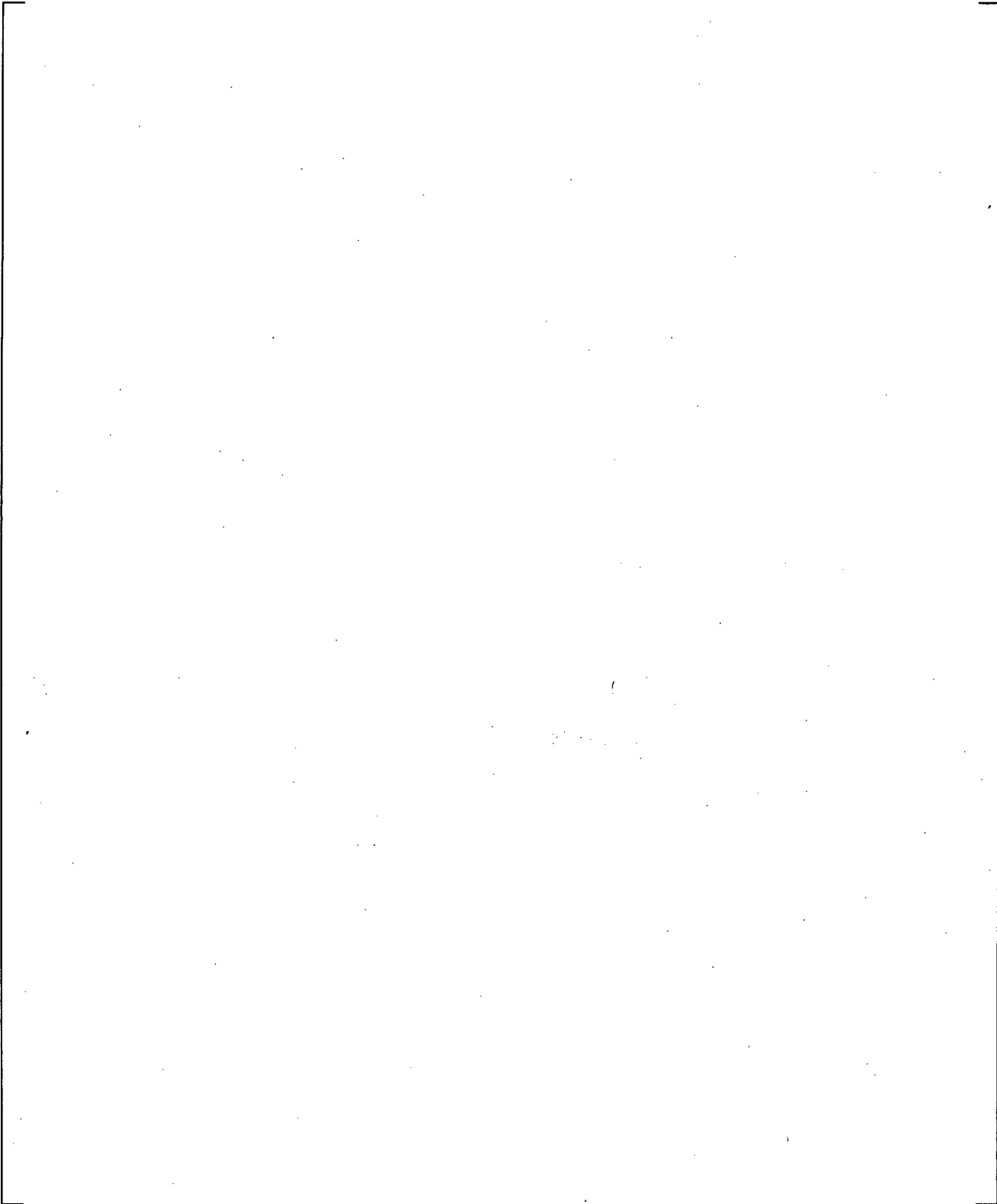
] <sup>a,c</sup>

### Level Swell Considerations

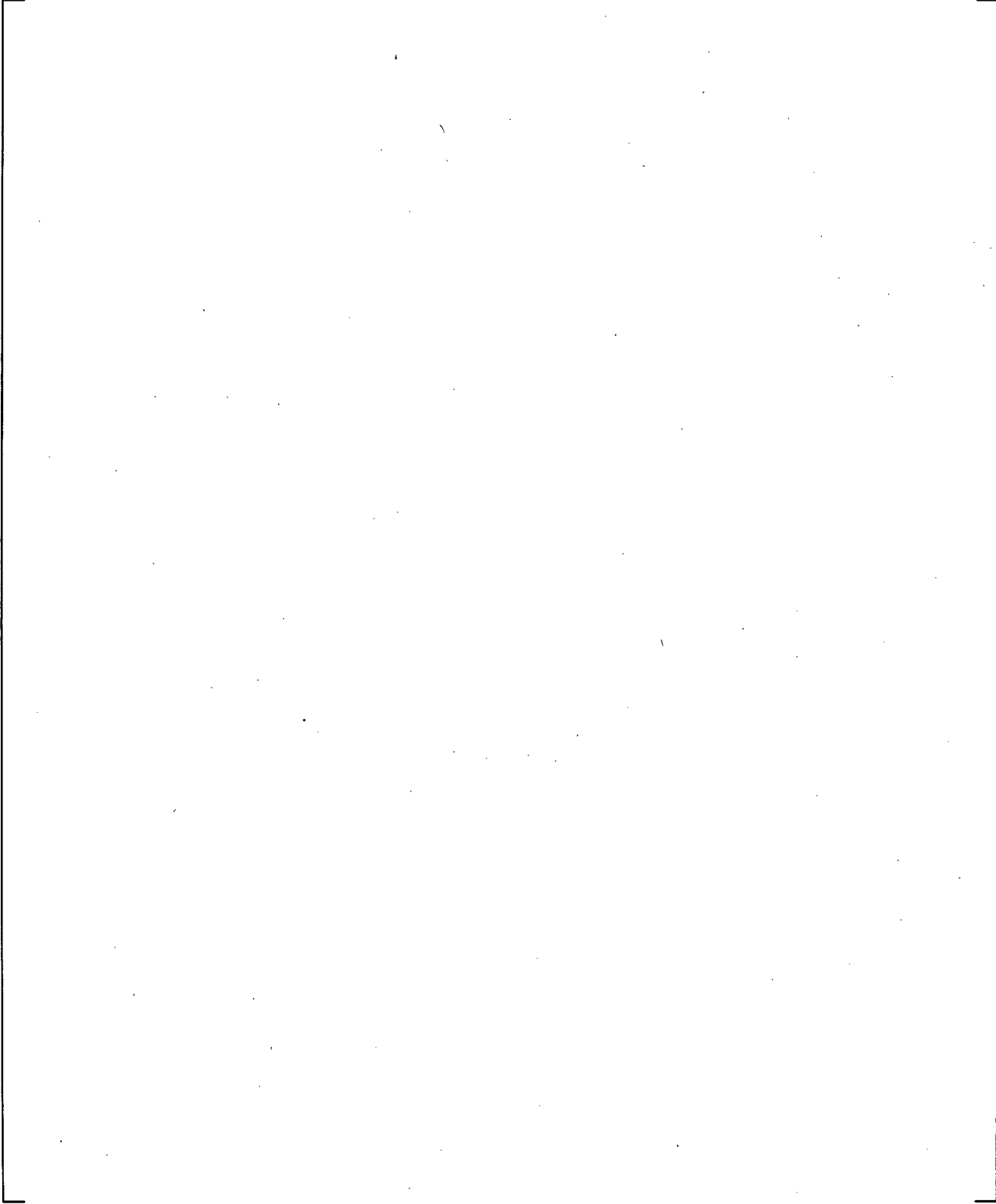
Data recording was continued in the FLECHT-SEASET tests well after bundle quench. Bundle power remained on, and although the power became low late in time, it was sufficient to maintain boiling in much of the bundle. The WCOBRA/TRAC-TF2 simulations were run past the bundle quench time (based on data), and thus simulated part of this post-quench period. A comparison of the predicted and measured void fraction distribution for this period is useful, in that it is not complicated by the entrainment process that accompanies quench.

Figure 24.6.5-19 shows a comparison of the predicted and measured [

] <sup>a,c</sup>.



**Figure 24.6.5-1 Comparison of Measured Void Fraction Distribution Reported for FLECHT-SEASET Tests 31805 and 31701**



**Figure 24.6.5-2 TCLAD Profile at 100 Seconds in FLECHT-31805**

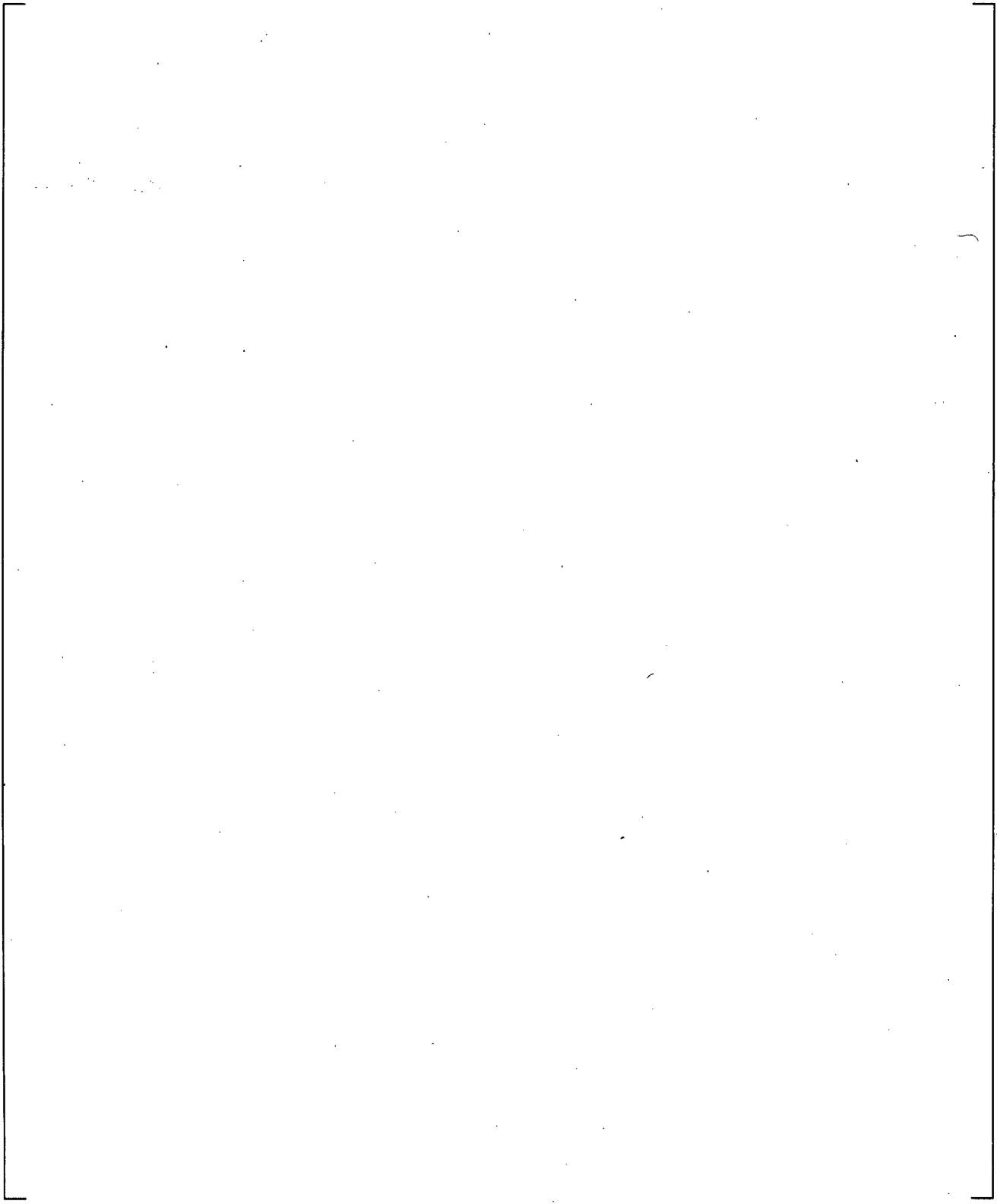


**Figure 24.6.5-3 Heat Transfer Coefficient vs. Time at ~6 ft in FLECHT-31805**

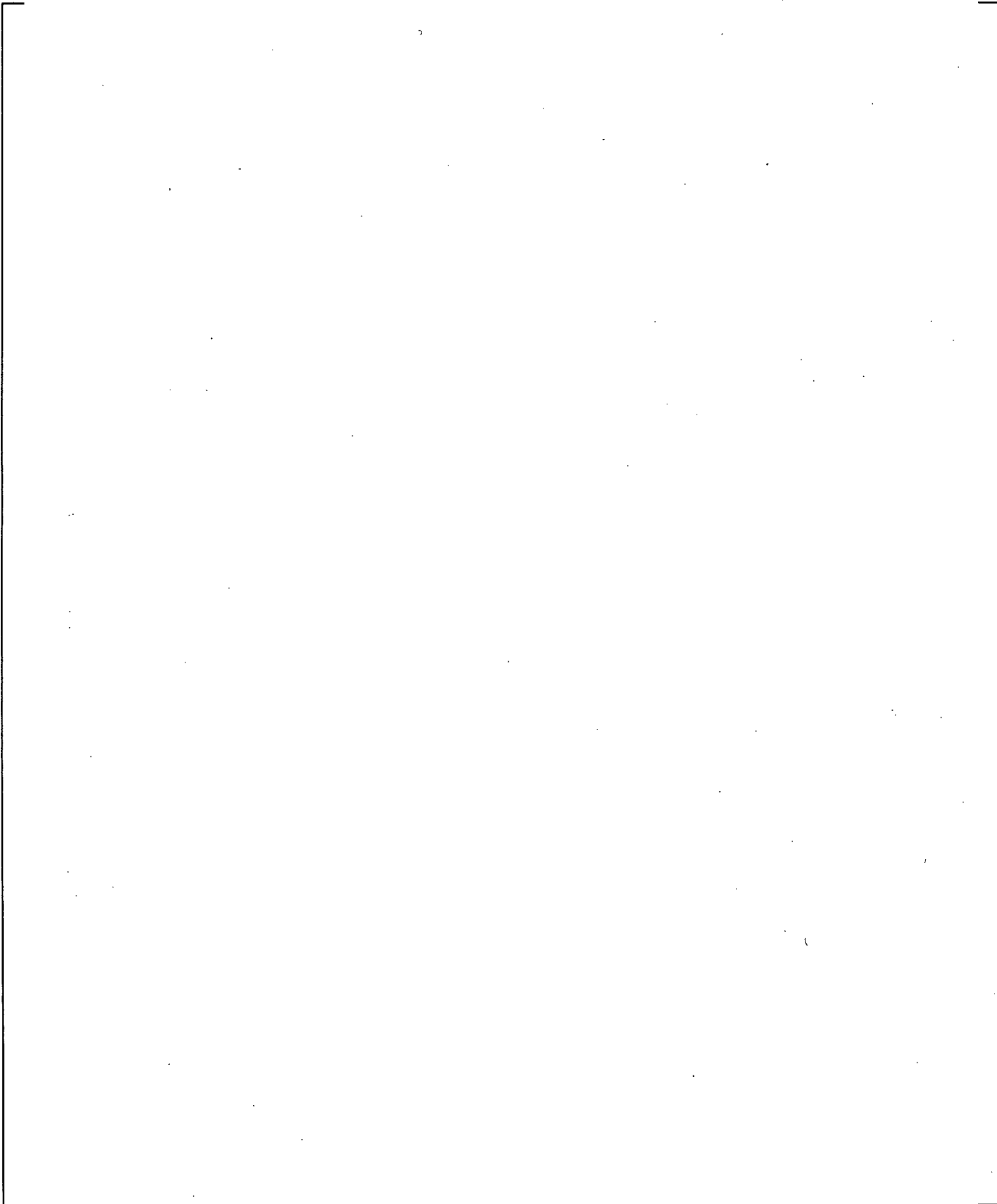


**Figure 24.6.5-4 Axial Comparison of Predicted and Measured HTC in FLECHT-SEASET 31805**

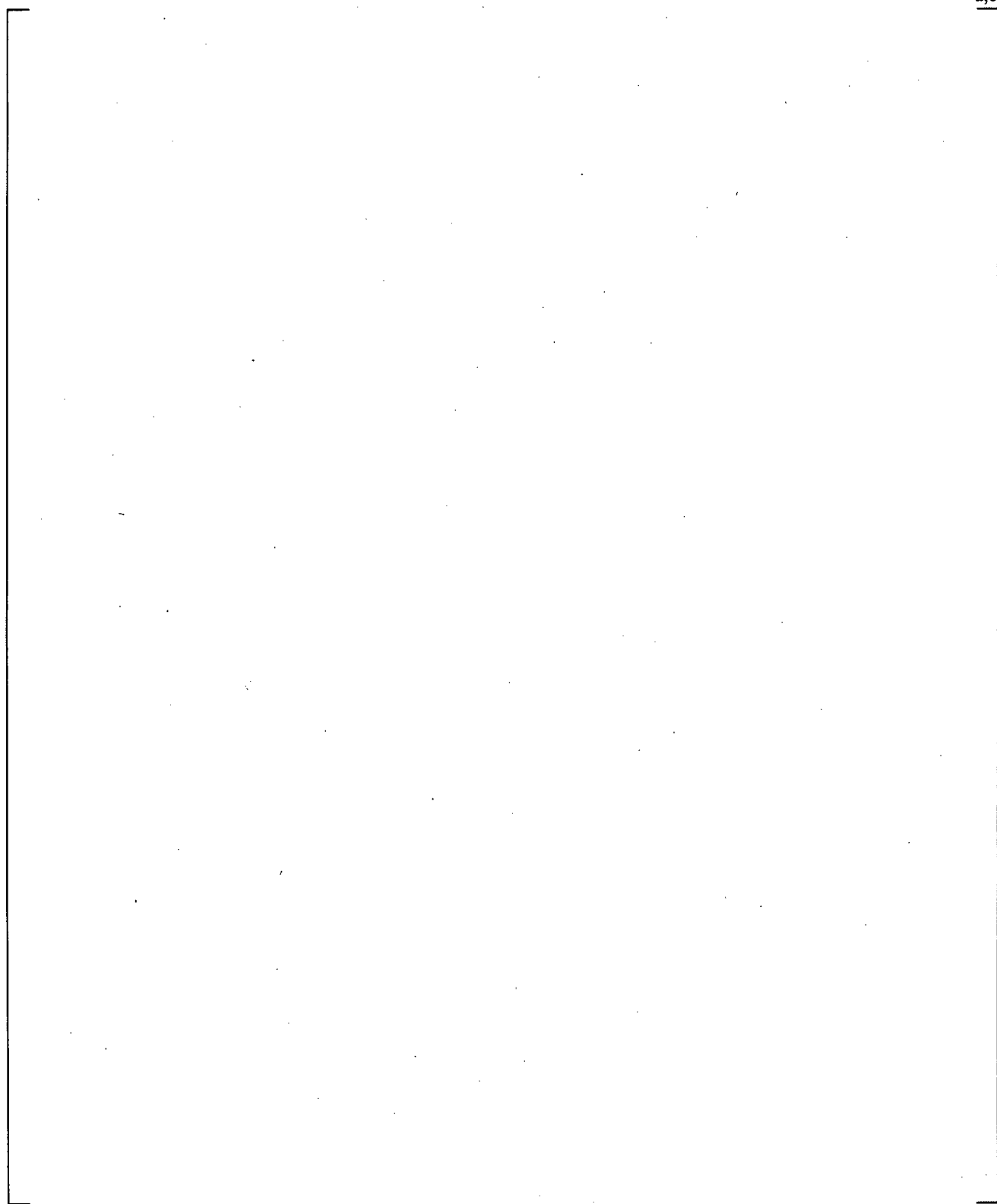


**Figure 24.6.5-5 Void Fraction Profile in FLECHT-SEASET 31805**

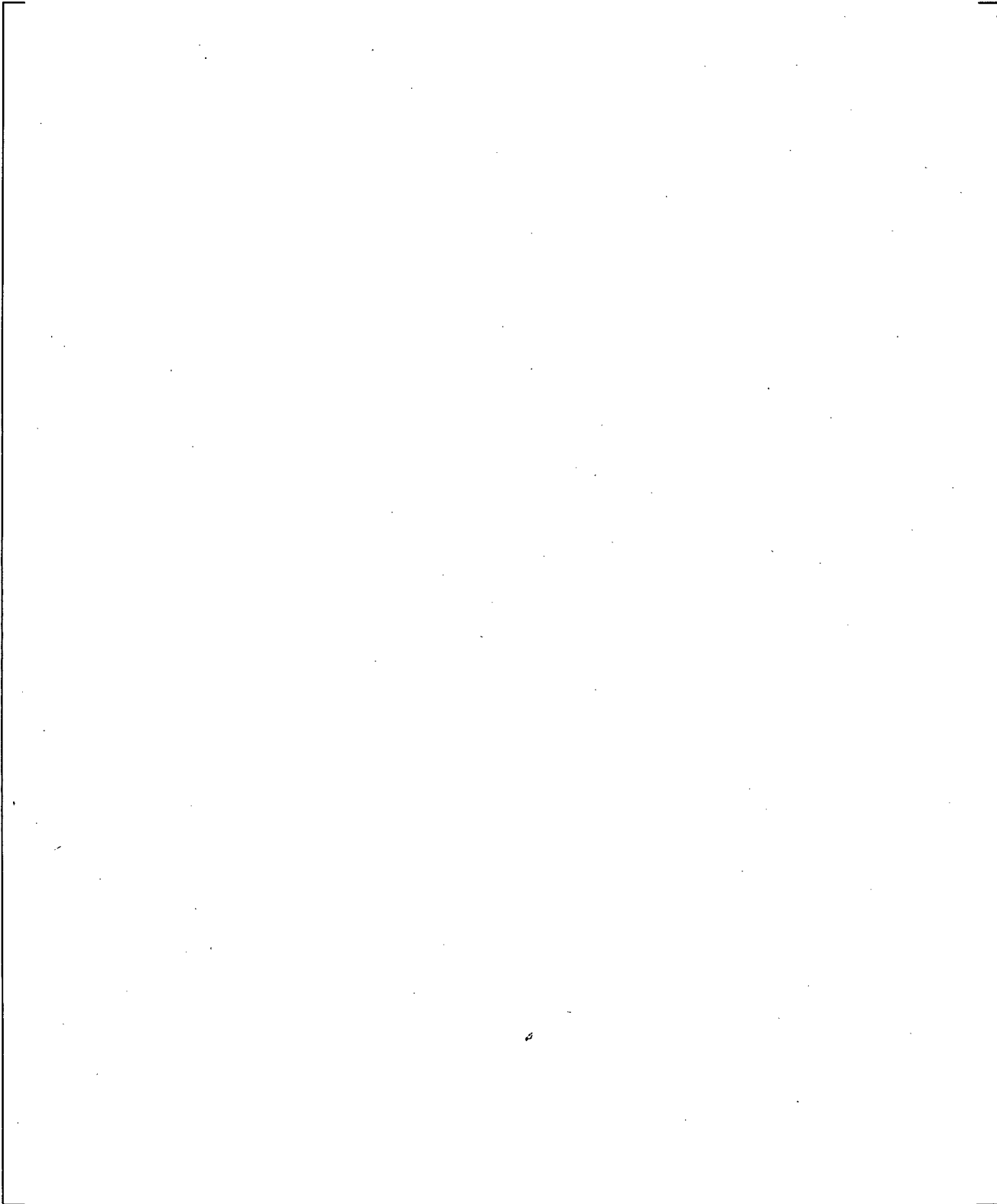


**Figure 24.6.5-6 Measured Void Fraction near 6 ft in FLECHT-SEASET 31805**

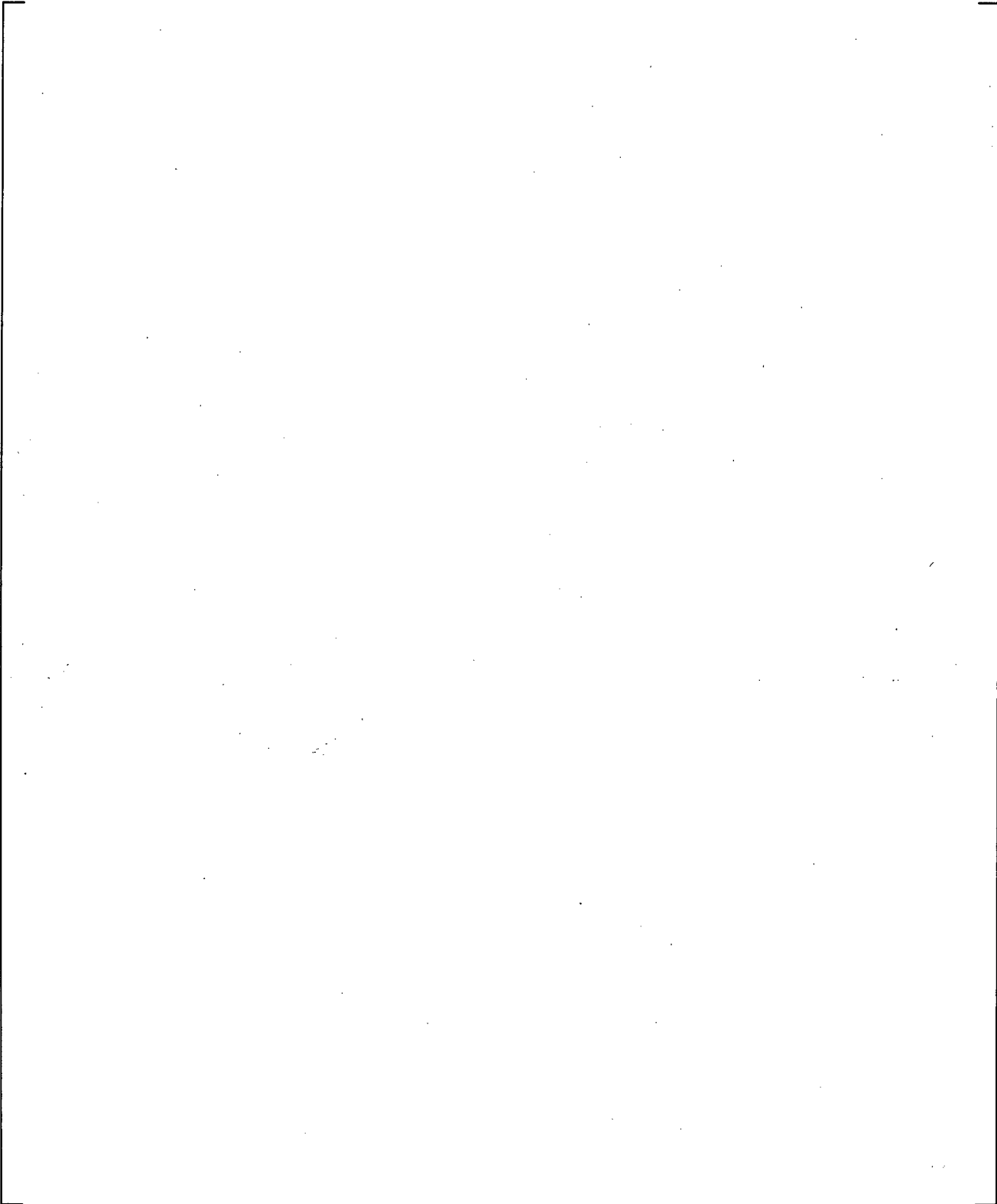


**Figure 24.6.5-7 Measured Clad Temperature, Void Fraction at 6 ft in FLECHT-SEASET 31805  
(Only one Legend is shown but all Available Thermocouples are Plotted)**

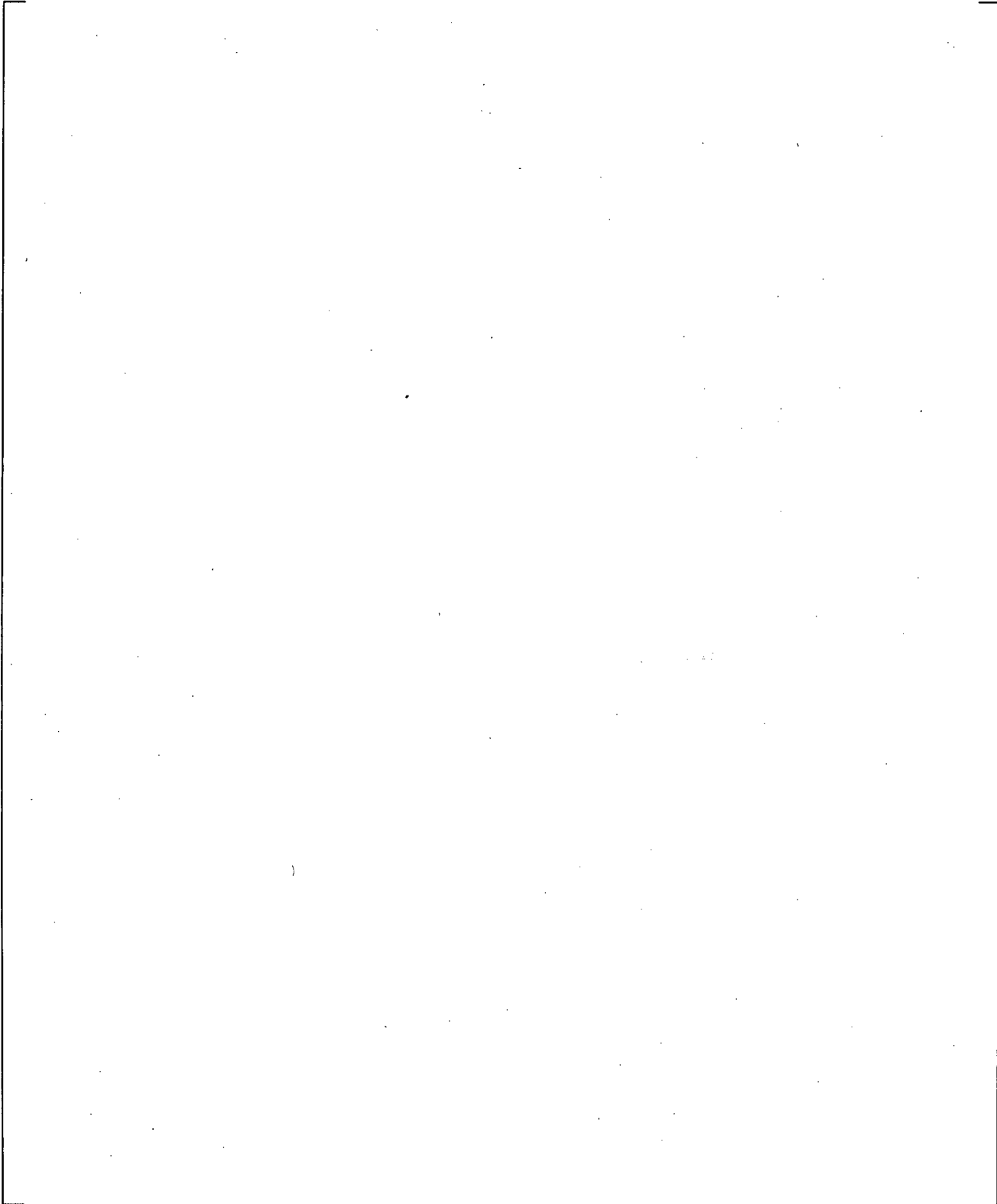


**Figure 24.6.5-8 Measured HTC, Void Fraction at 6 ft in FLECHT-SEASET 31805 (Only one Legend is shown but all Available Thermocouples are Plotted)**

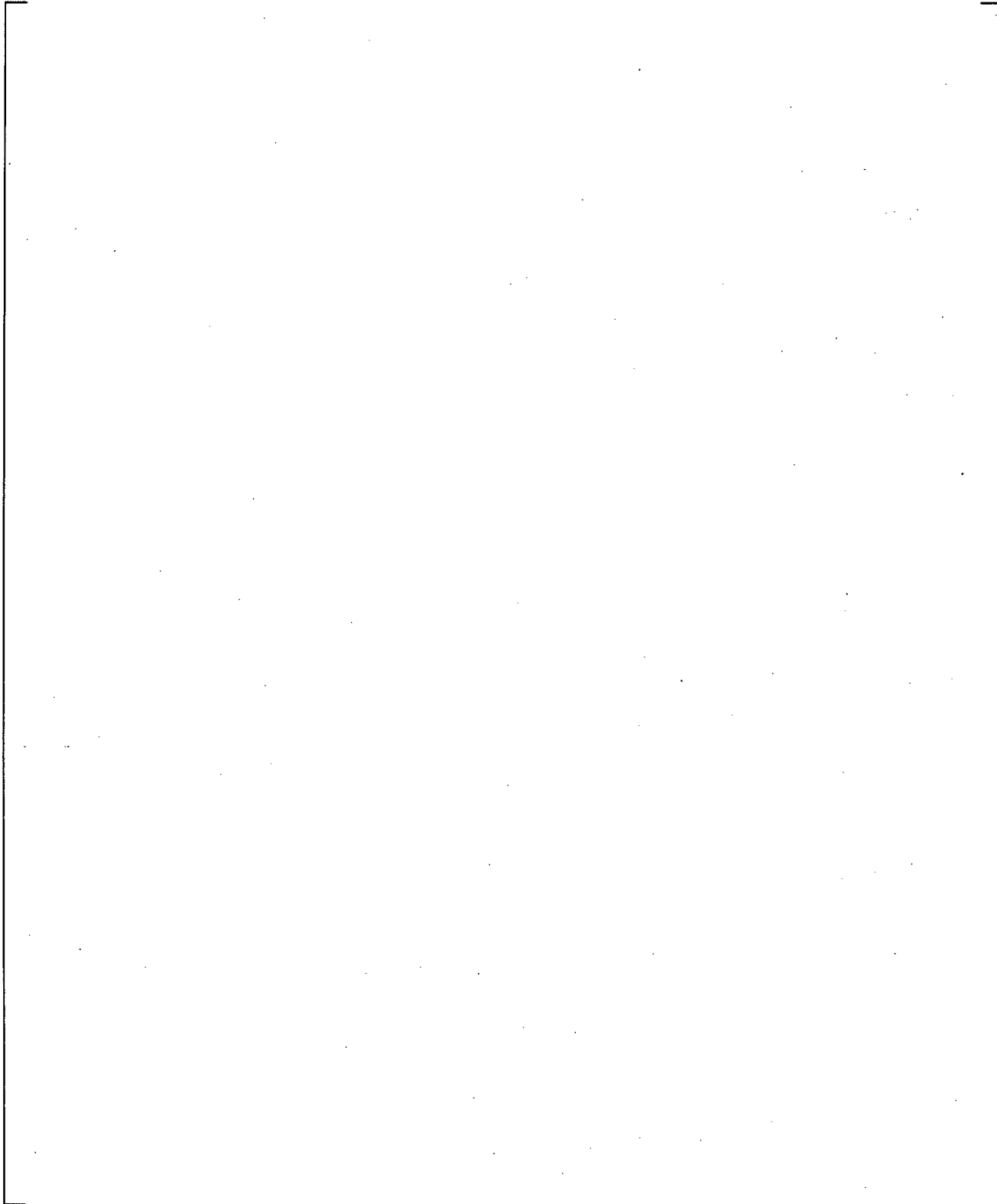


**Figure 24.6.5-9** Expanded View of Measured Clad Temperature, Void Fraction at 6 ft in FLECHT-SEASET 31805 (Only one Legend is shown but all Available Thermocouples are Plotted)

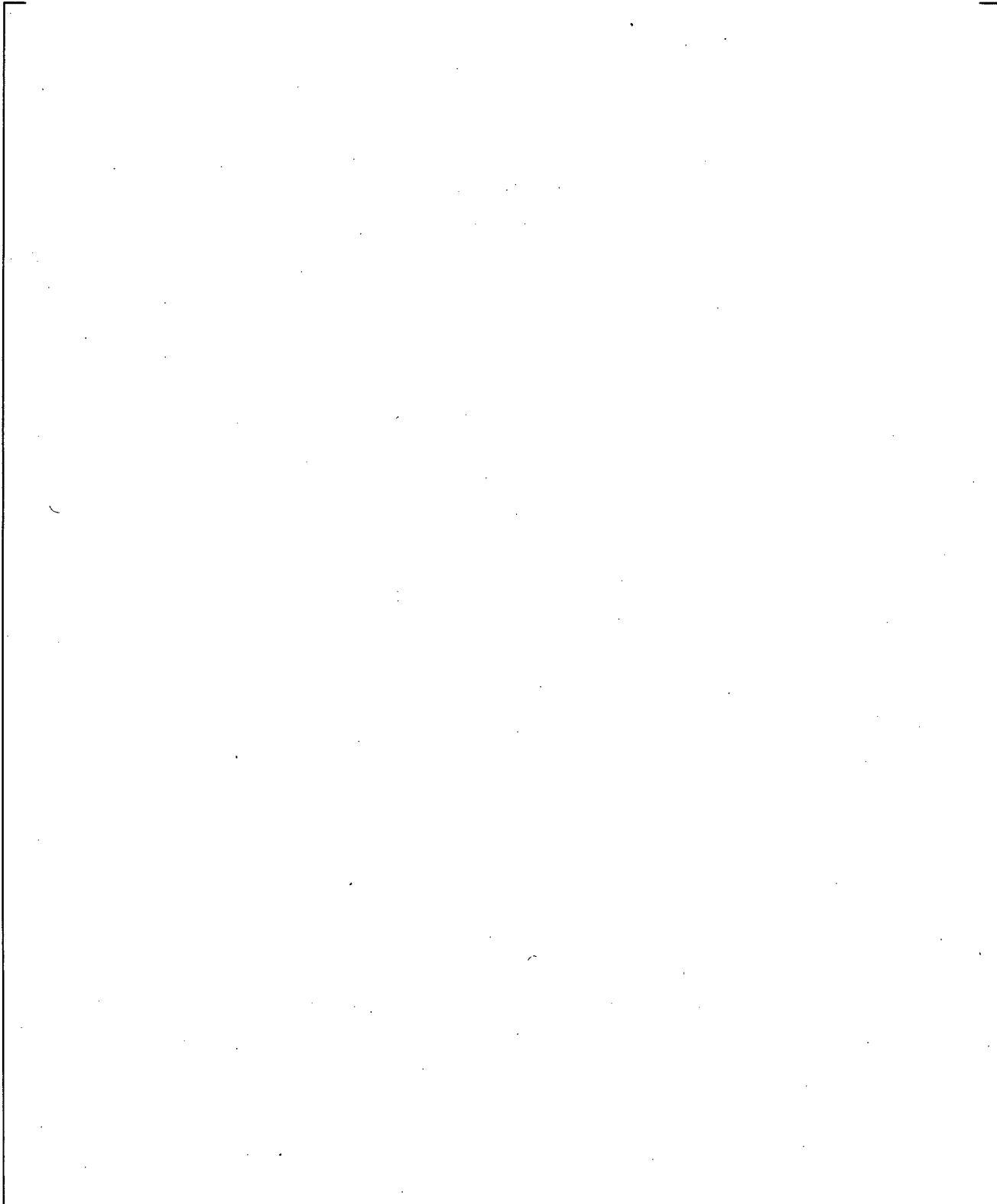


**Figure 24.6.5-10 Expanded View of Measured HTC, Void Fraction at 6 ft in FLECHT-SEASET 31805 (Only one Legend is shown but all Available Thermocouples are Plotted)**

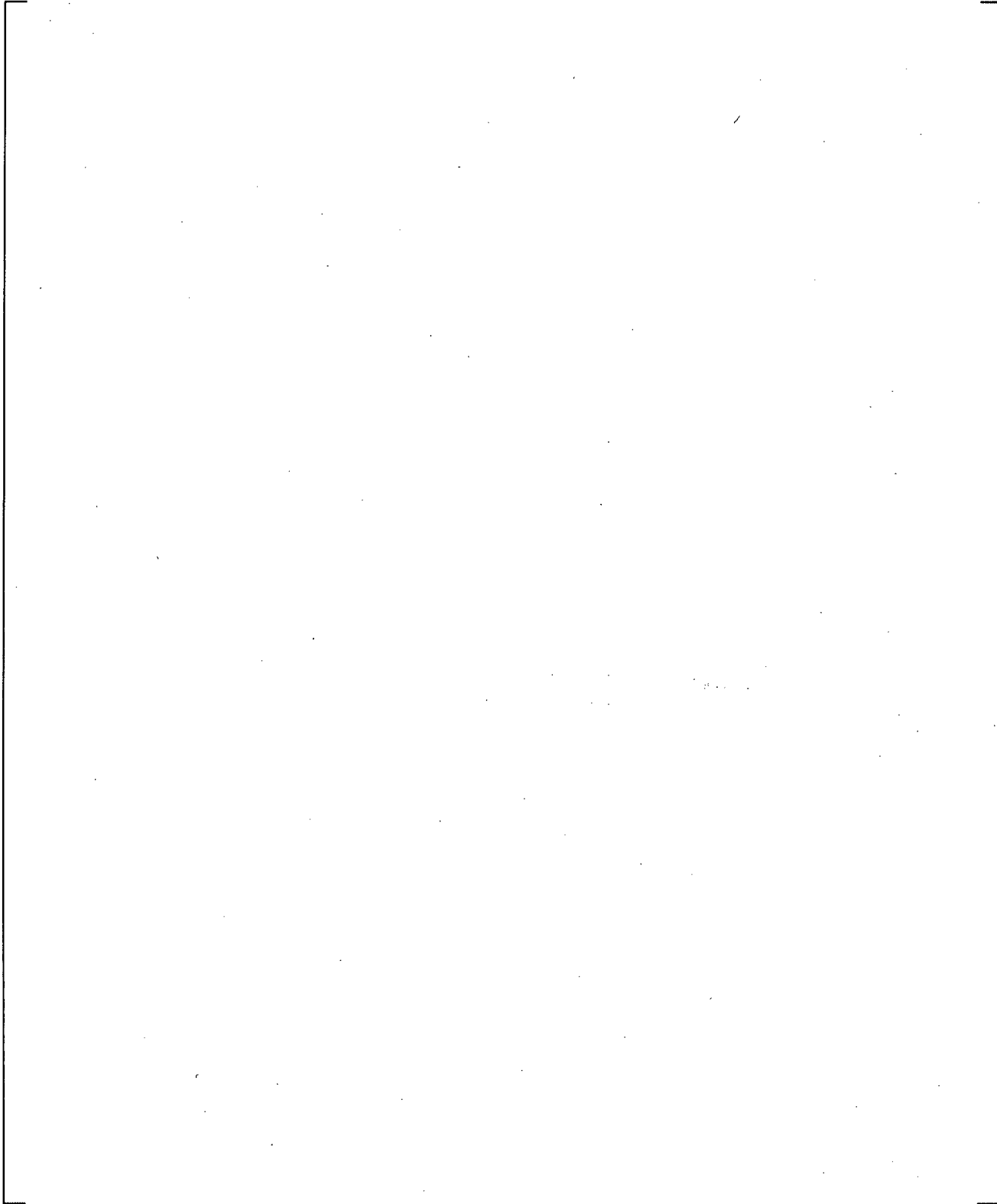


**Figure 24.6.5-11 Predicted Clad Temperature, Void Fraction at 6 ft in FLECHT-SEASET 31805**

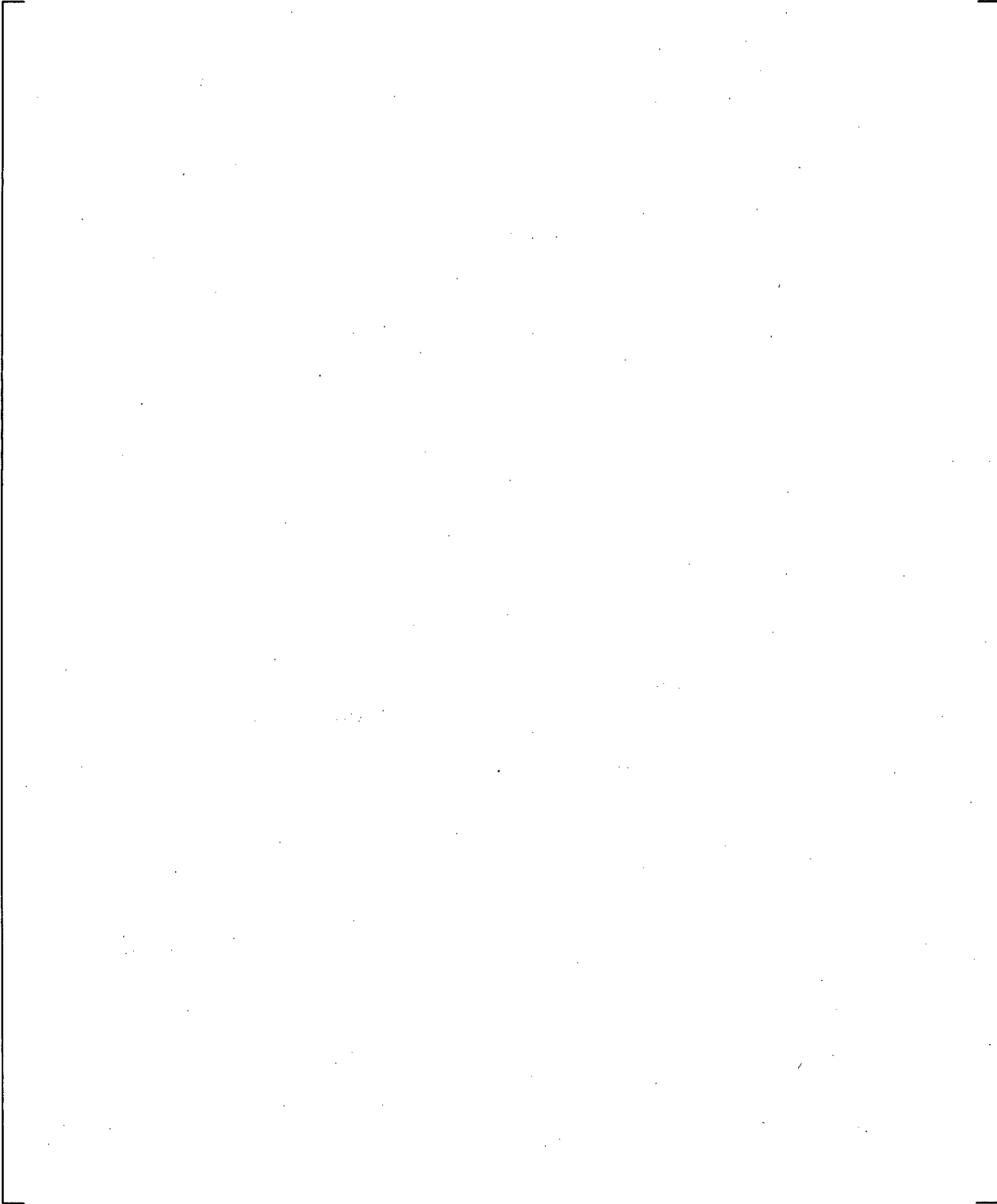


**Figure 24.6.5-12 Predicted HTC, Void Fraction at 6 ft in FLECHT-SEASET 31805**

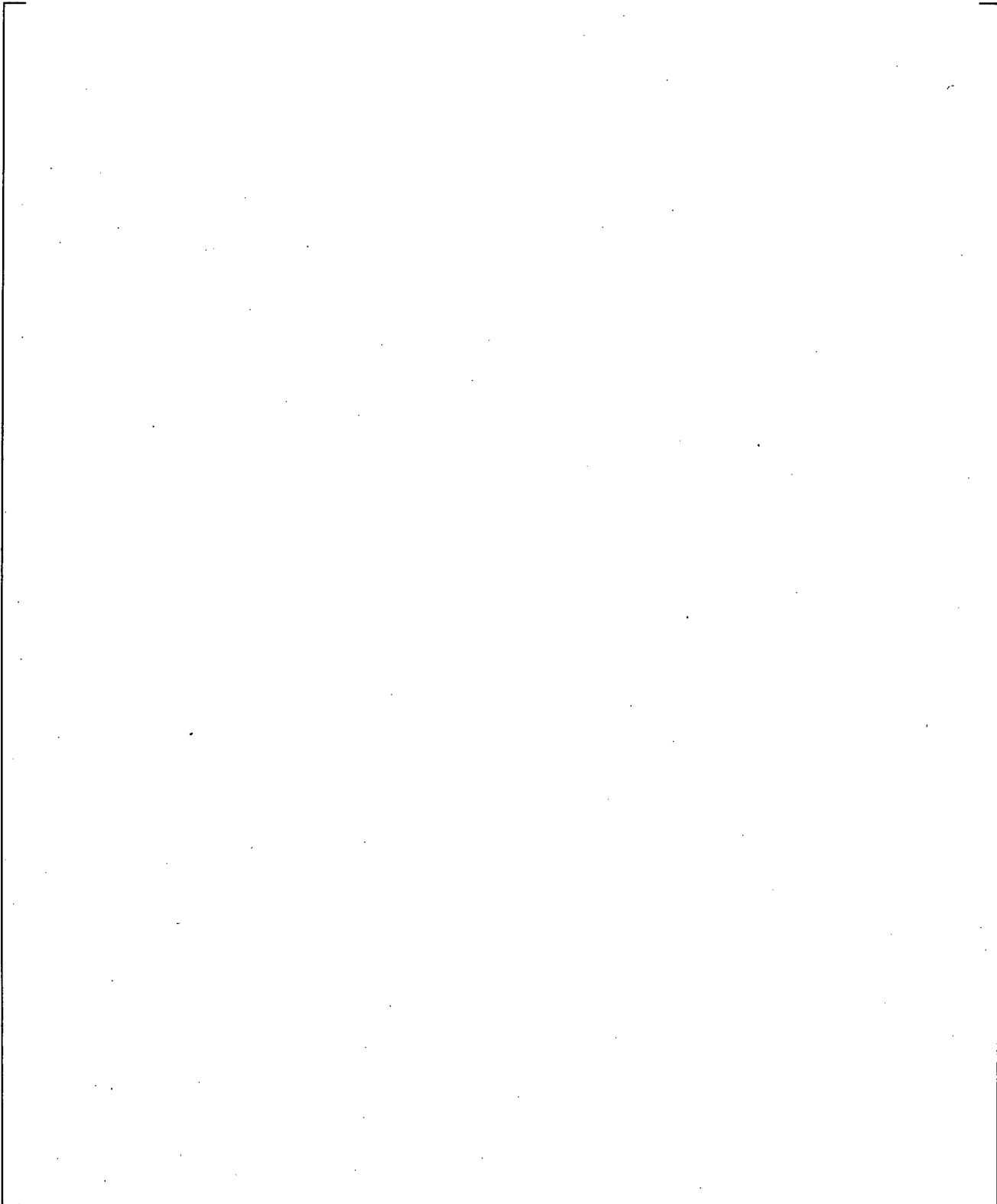


**Figure 24.6.5-13 Void Fraction Comparison at 6 ft in FLECHT-SEASET 31805**

**Figure 24.6.5-14 Measured Clad Temperature, Void Fraction at 10 ft in FLECHT-31805 (Only one Legend is shown but all Available Thermocouples are Plotted)**

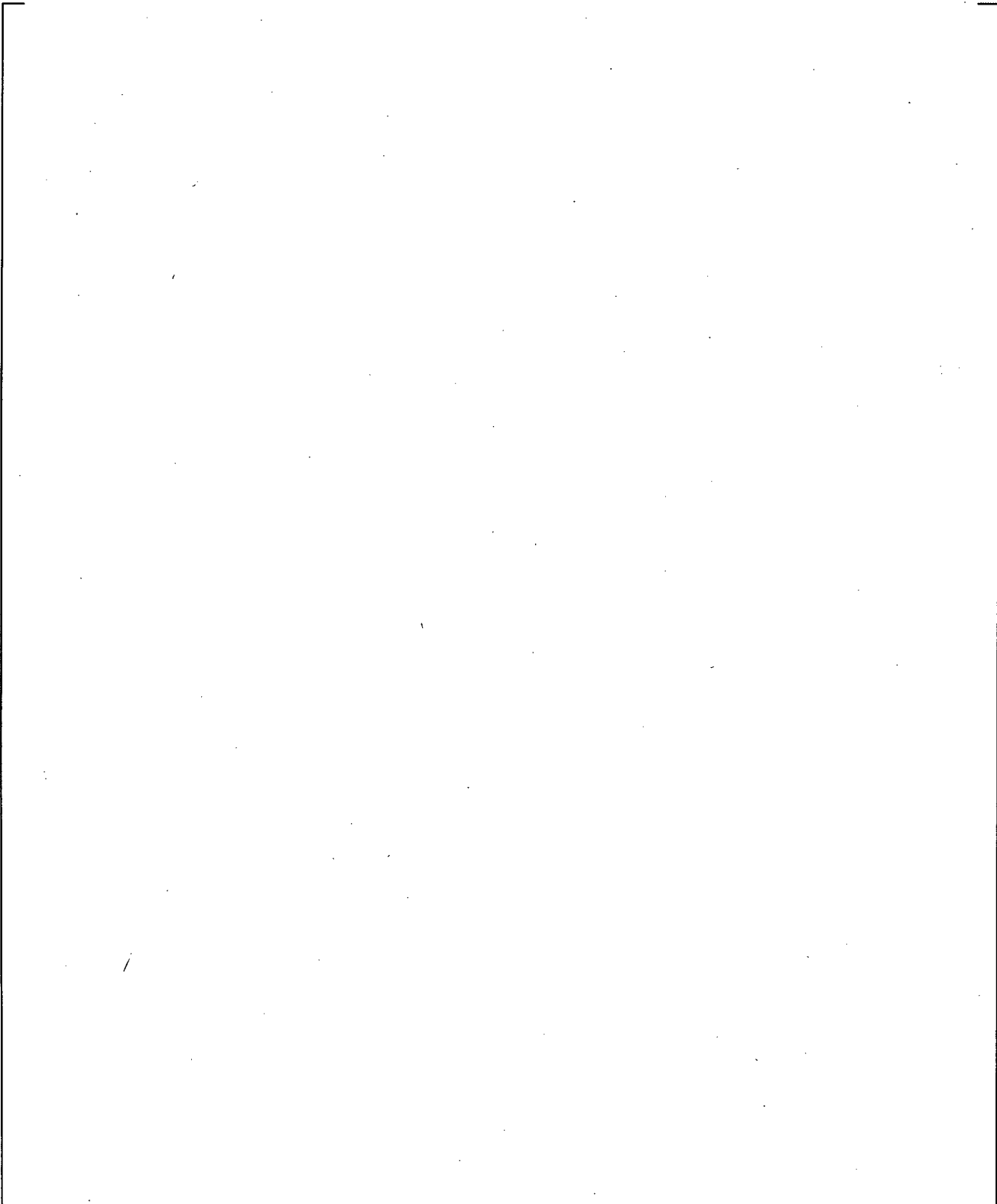


**Figure 24.6.5-15 Measured HTC, Void Fraction at 10 ft in FLECHT-SEASET 31805 (Only one Legend is shown but all Available Thermocouples are Plotted)**

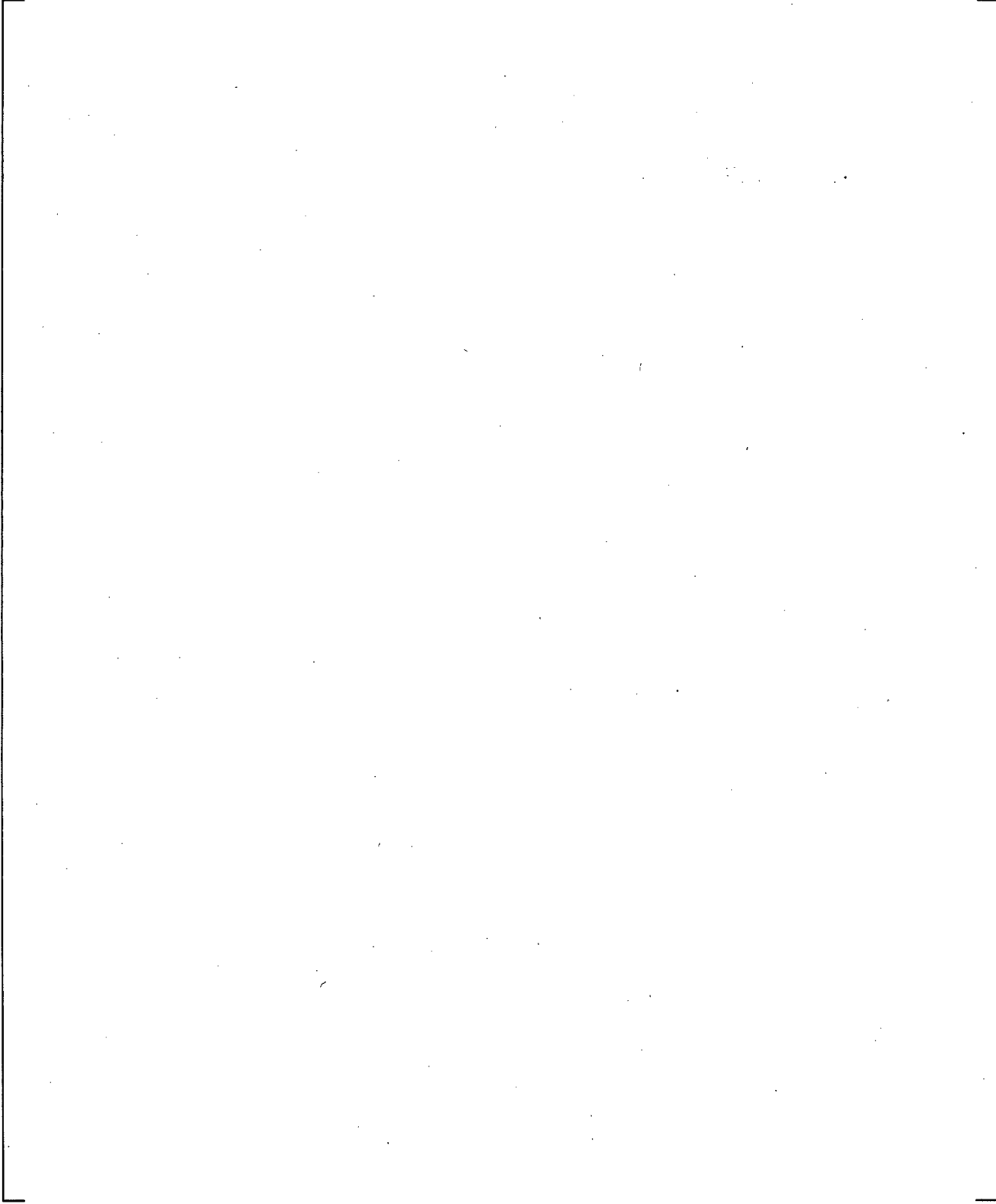


**Figure 24.6.5-16 Predicted Clad Temperature, Void Fraction at 10 ft in FLECHT-SEASET 31805**

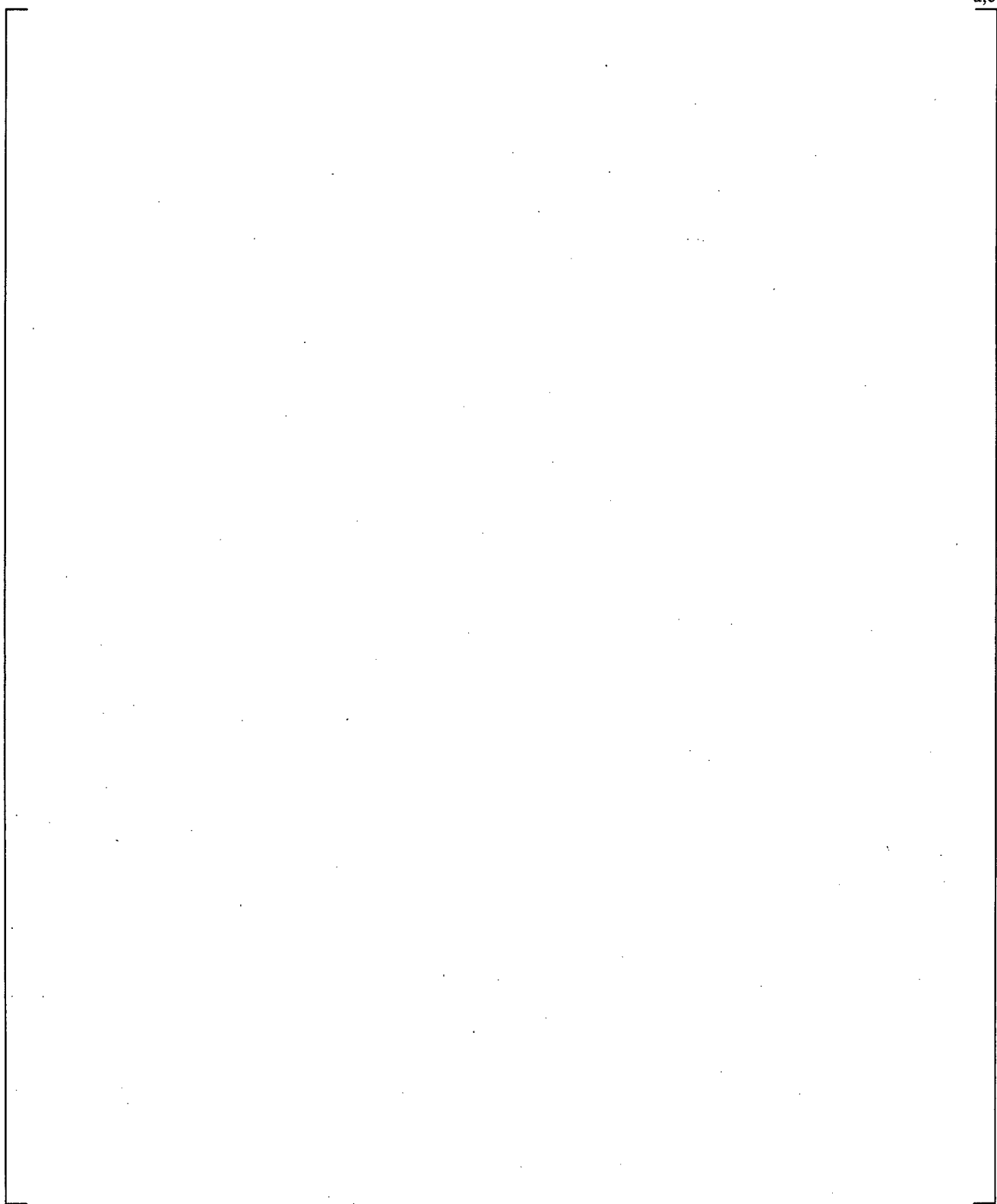


**Figure 24.6.5-17 Predicted HTC, Void Fraction at 10 ft in FLECHT-SEASET 31805**

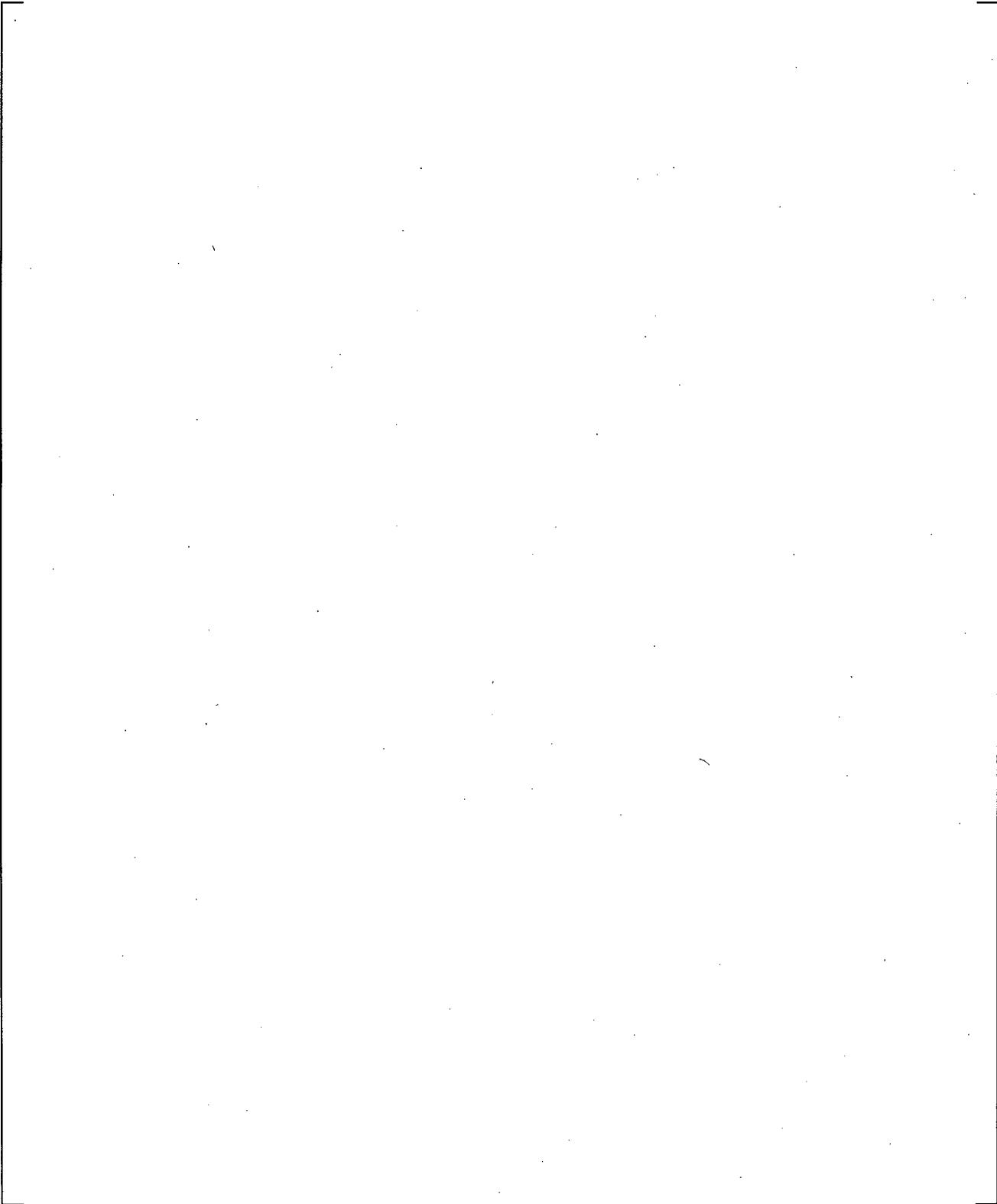


**Figure 24.6.5-18 Void Fraction Comparison at 10-11 ft in FLECHT-SEASET 31805**

a,c

**Figure 24.6.5-19 Void Fraction Axial Profile Comparison [ FLECHT-SEASET 31805**

**] a,c in**

### 24.6.6 FLECHT-SEASET Test 31701

Test 31701, because of its very high reflood rate of 6.1 in/sec, is a test that should be expected to produce an inverted annular flow over a significant region of the bundle. This is a rate sufficient to cold fill the bundle within only 24 seconds.

Figure 24.6.6-1 shows the void fractions reported for this test from the 5- to 6-ft. and the 6- to 7-ft. DP cell. [

] <sup>a,c</sup>

Figures 24.6.6-2 and 24.6.6-3 show the relation of clad temperature and heat transfer coefficient with void fraction, based on the test data. [

] <sup>a,c</sup>

Figures 24.6.6-4 and 24.6.6-5 show the clad temperature and heat transfer coefficient relationship with void fraction as predicted by WCOBRA/TRAC-TF2 for Test 31701. [

] <sup>a,c</sup>

The vertical line which appears in Figure 24.6.6-5 at [

] <sup>a,c</sup>

Figure 24.6.6-6 compares the predicted and measured void fraction for the 6- and 7-ft. region. [

] <sup>a,c</sup>

Because of the high reflood rate and rapid entrainment in Test 31701, the liquid was quickly present at the 10 ft. elevation also. As at the 6-ft. elevation, the void fraction measurements at the 9- to 10-ft. and 10- to 11-ft. elevations showed an inverse void gradient. Figure 24.6.6-7 shows the reported void fraction measurements, and an average that will be used in later plots for the 10-ft. elevation. [

] <sup>a,c</sup>

The 10-ft. elevation in Test 31701 was found to have conditions typical of an inverted annular post-CHF flow for a significant period of time. Figures 24.6.6-8 and 24.6.6-9 show the experimental relation of clad temperature and heat transfer coefficient with void fraction. [

] <sup>a,c</sup>

[

] <sup>a,c</sup>

The predicted relations of clad temperature and heat transfer coefficient with void fraction are shown in Figures 24.6.6-10 and 24.6.6-11. [

] <sup>a,c</sup>

The predicted and measured void fraction for the 10- to 11-ft. region is shown in Figure 24.6.6-12. [

] <sup>a,c</sup>

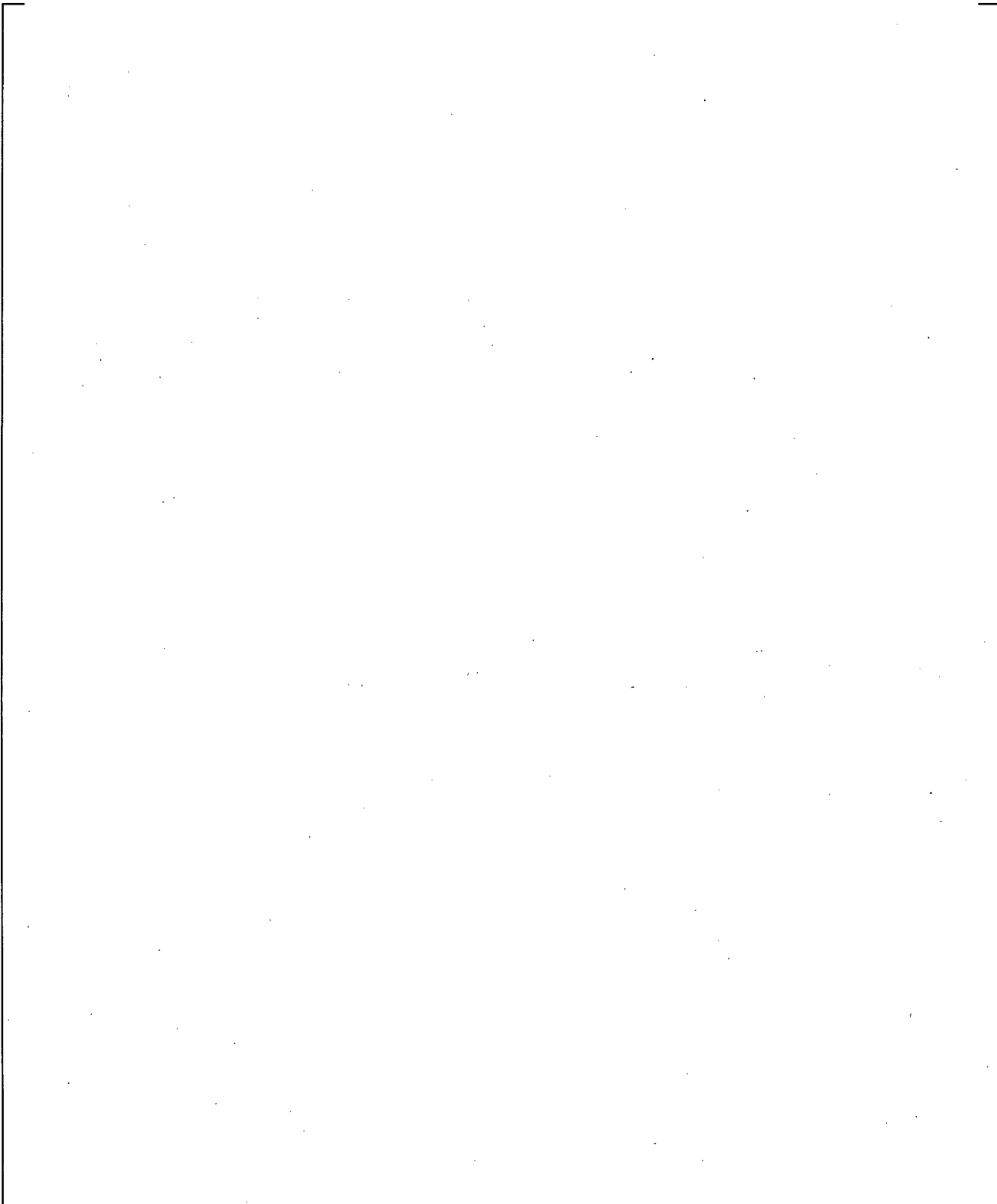


**Figure 24.6.6-1 Void Fraction Measurement at 5-7 ft for FLECHT-SEASET 31701**

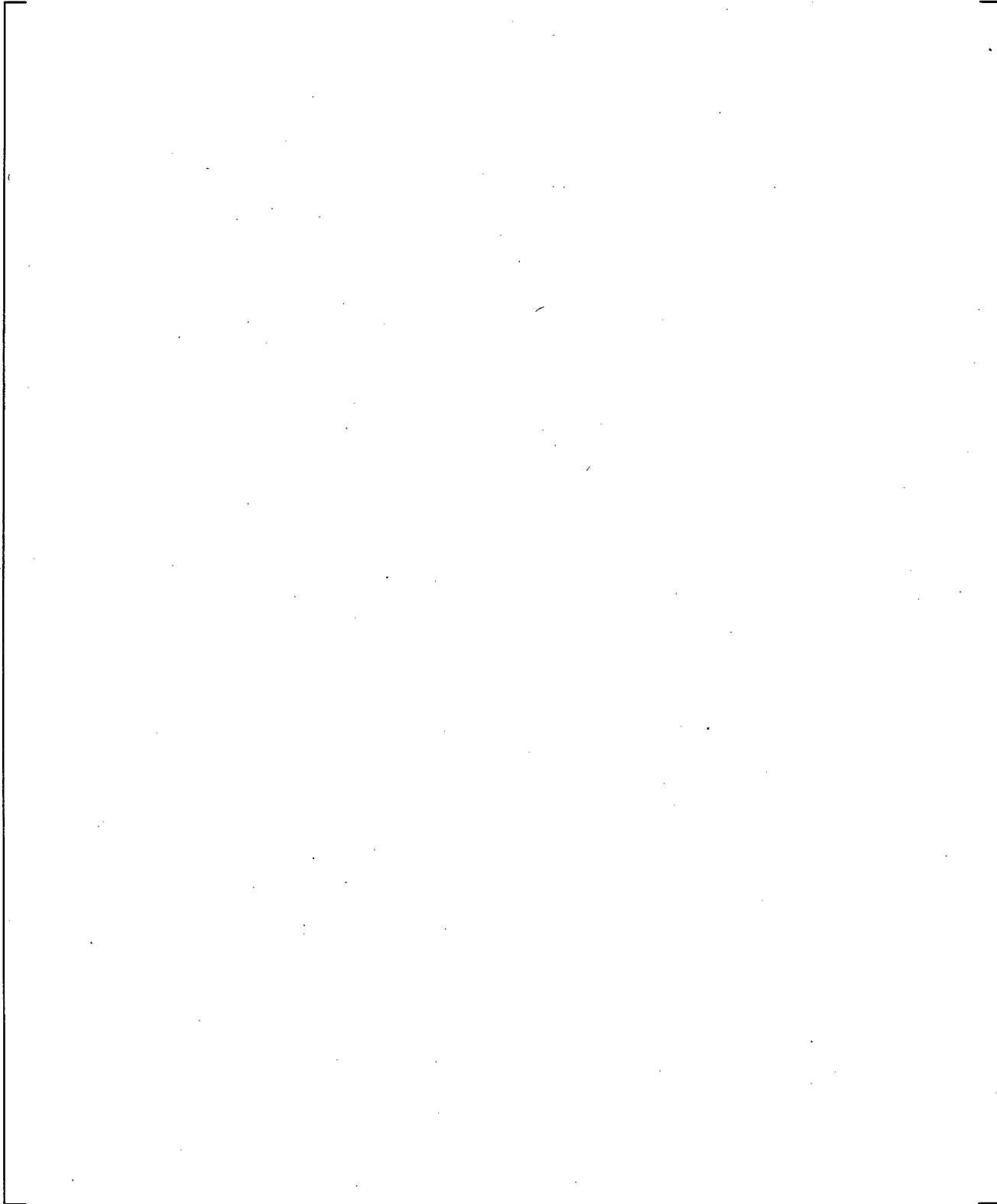


**Figure 24.6.6-2 Measured Clad Temperature, Void Fraction for FLECHT-SEASET 31701**

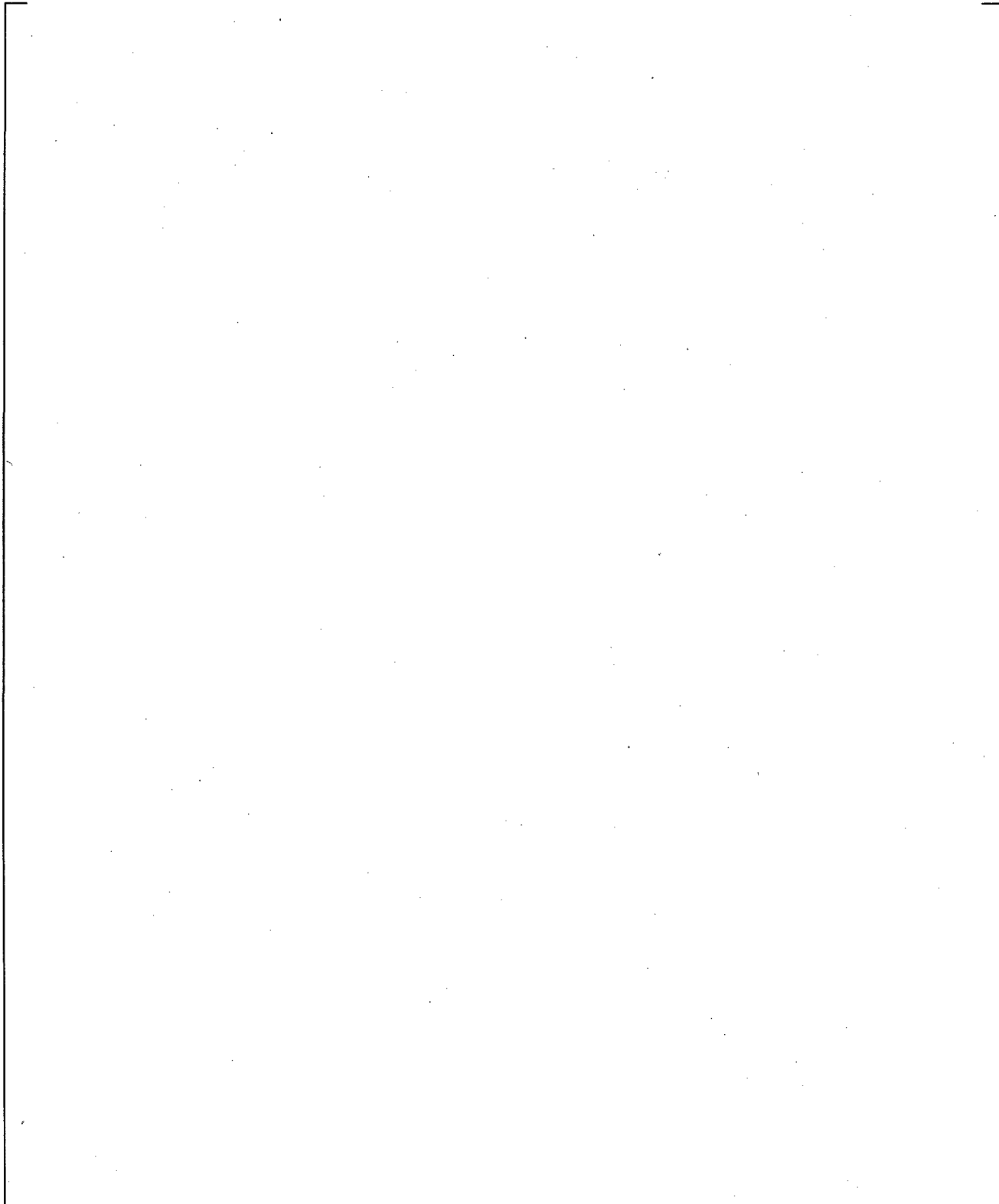


**Figure 24.6.6-3 Measured HTC, Void Fraction Relation for FLECHT-SEASET 31701**

**Figure 24.6.6-4 Predicted Clad Temperature, Void Fraction Relation at 6 ft for FLECHT-SEASET 31701**

**Figure 24.6.6-5 Predicted HTC, Void Fraction Relation at 6 ft for FLECHT-SEASET 31701**

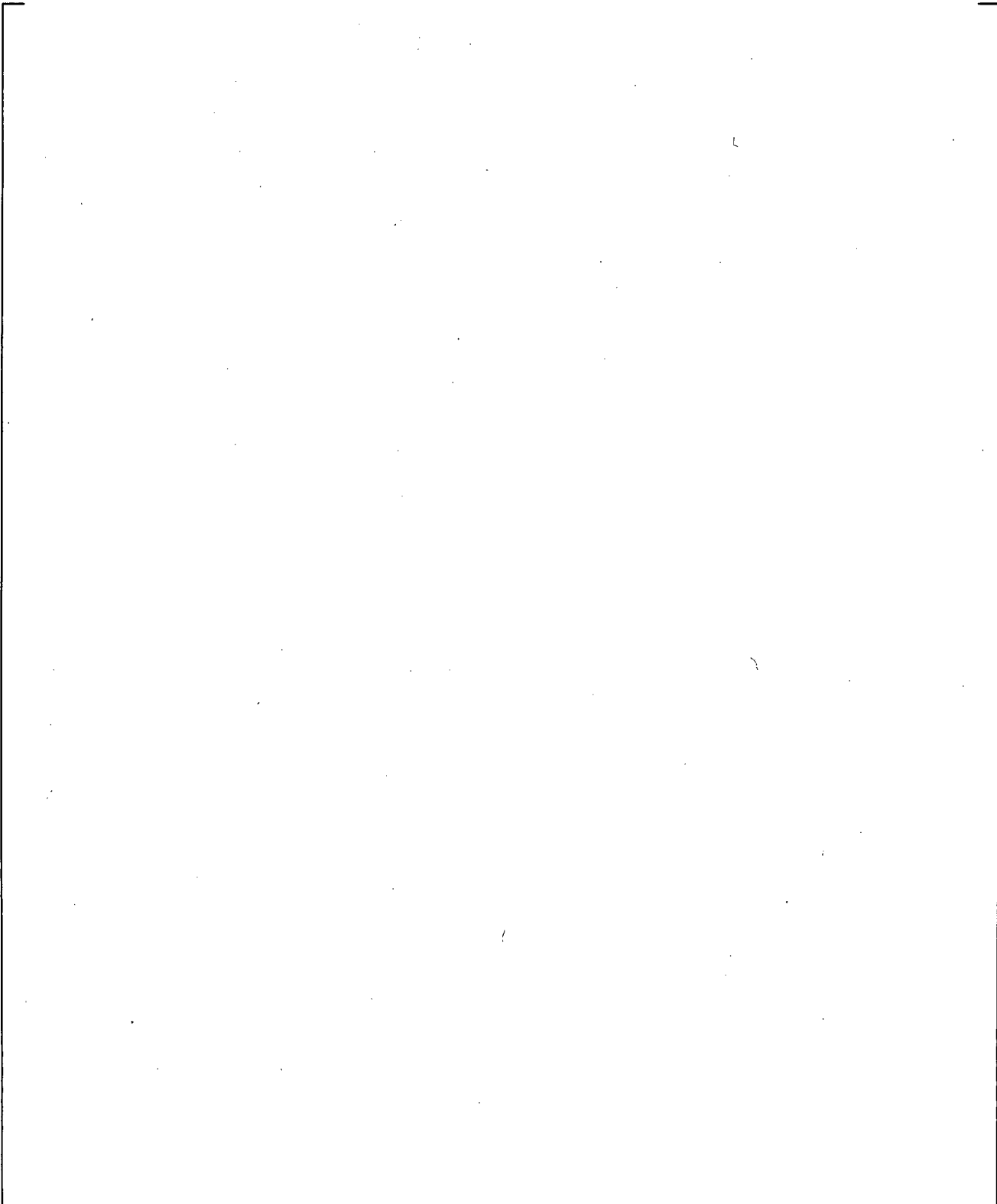


**Figure 24.6.6-6 Comparison of Predicted and Measured Void Fraction Relation at 6-7 ft for FLECHT-SEASET 31701**

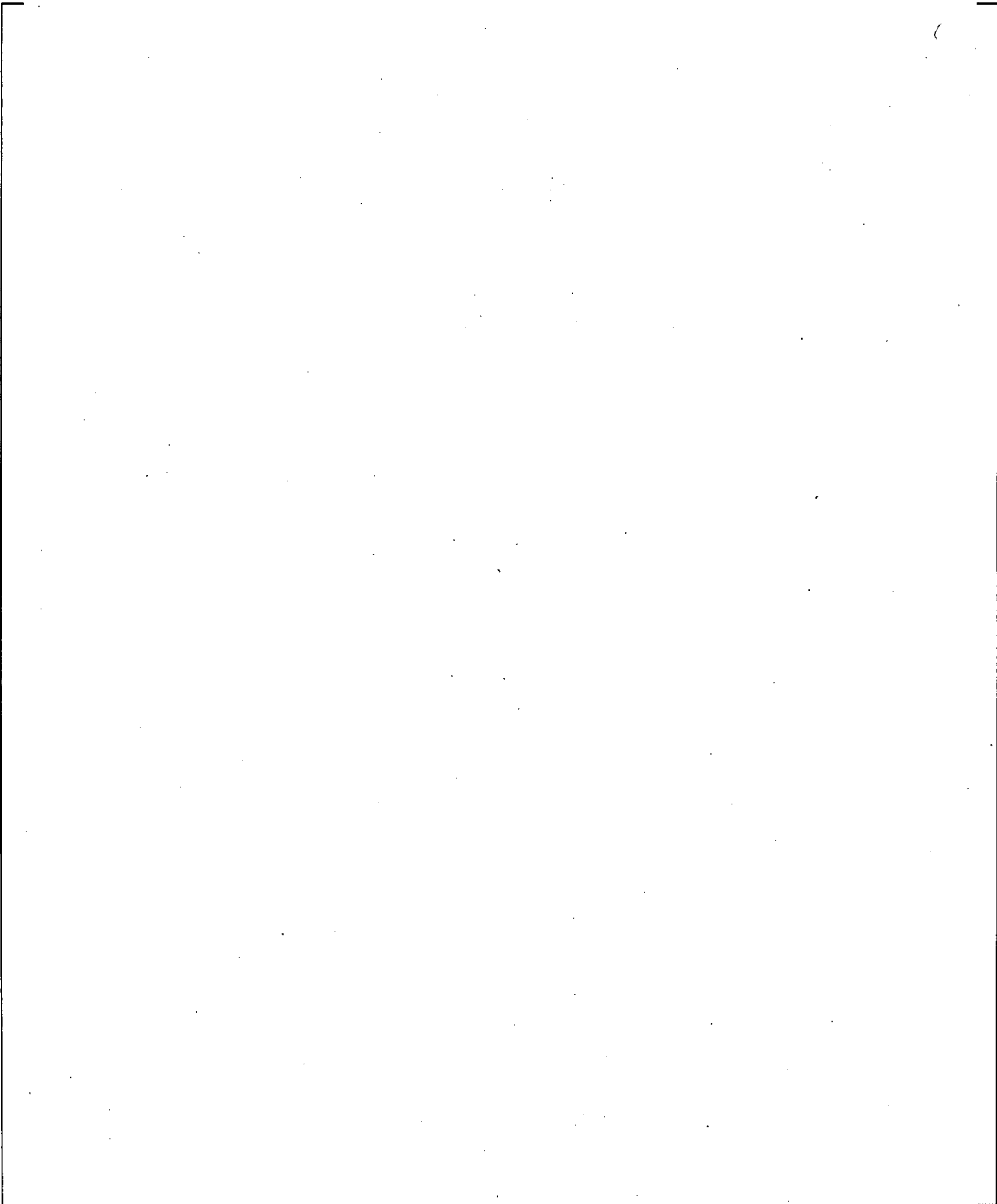


**Figure 24.6.6-7 Void Fraction Measurement at 9-11 ft for FLECHT-SEASET 31701**

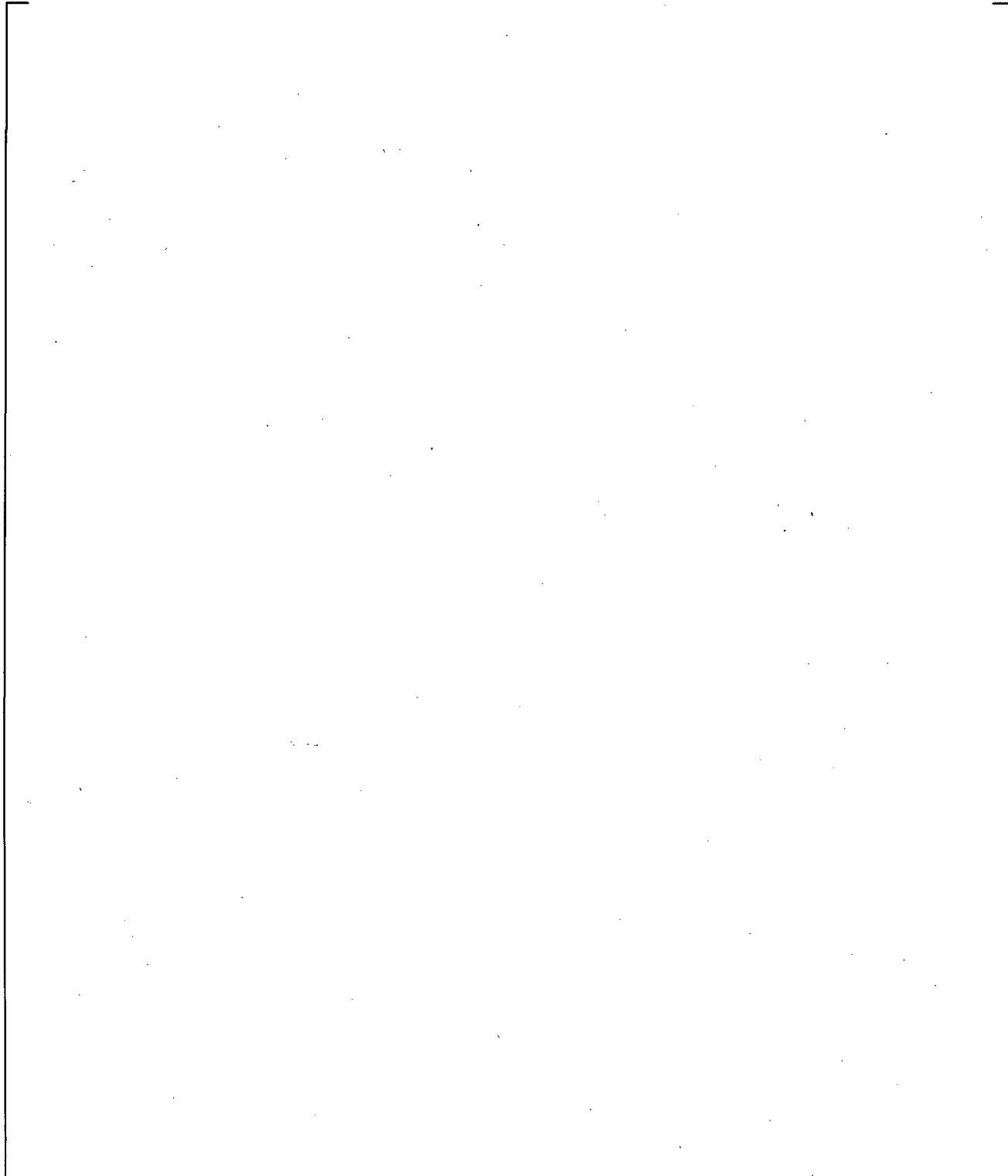


**Figure 24.6.6-8 Measured Clad Temperature, Void Fraction Relation at 10 ft for FLECHT-SEASET 31701**

**Figure 24.6.6-9 Measured HTC, Void Fraction Relation at 10 ft for FLECHT-SEASET 31701**

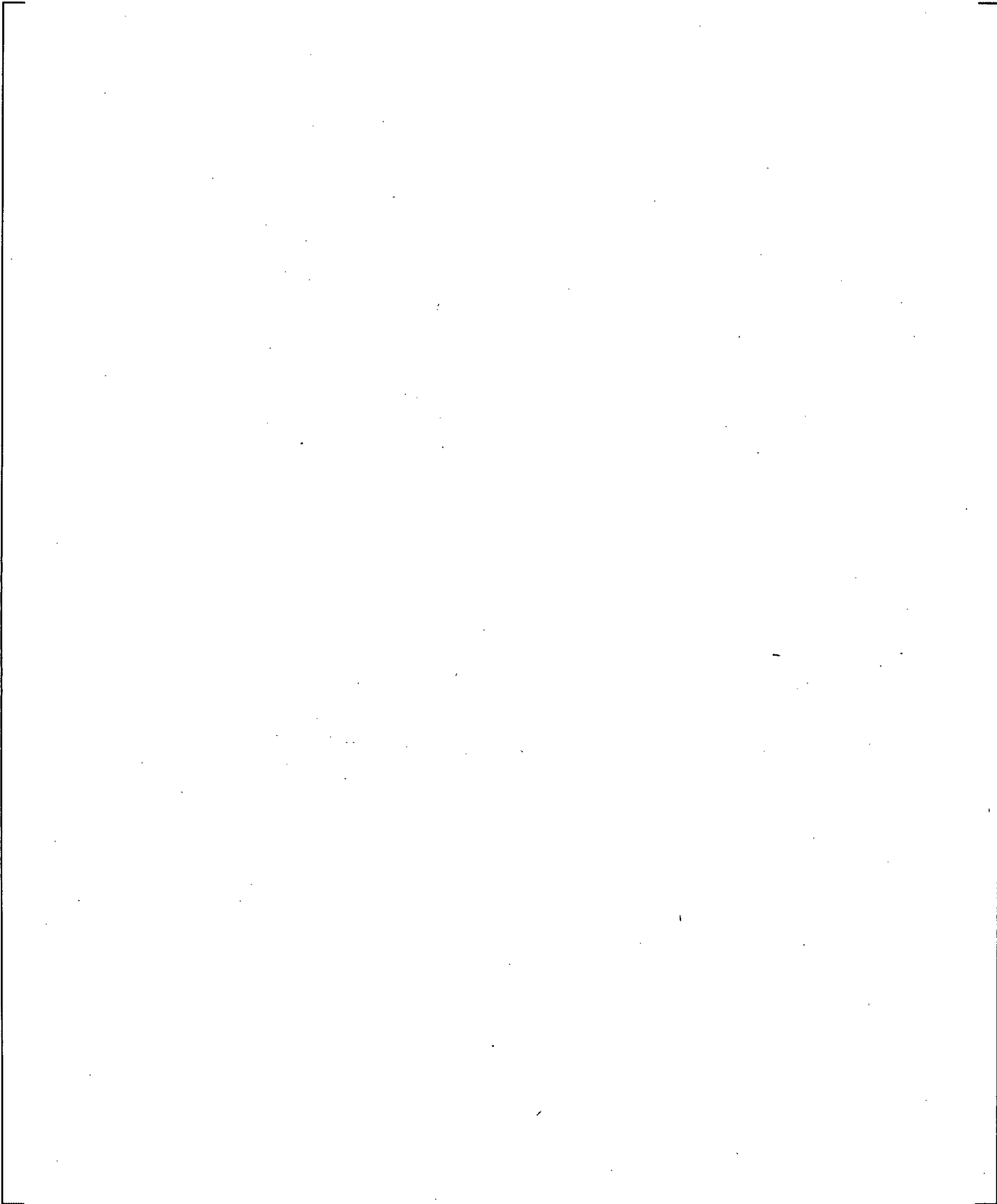


**Figure 24.6.6-10 Predicted Clad Temperature, Void Fraction Relation at 10 ft for FLECHT-SEASET 31701**

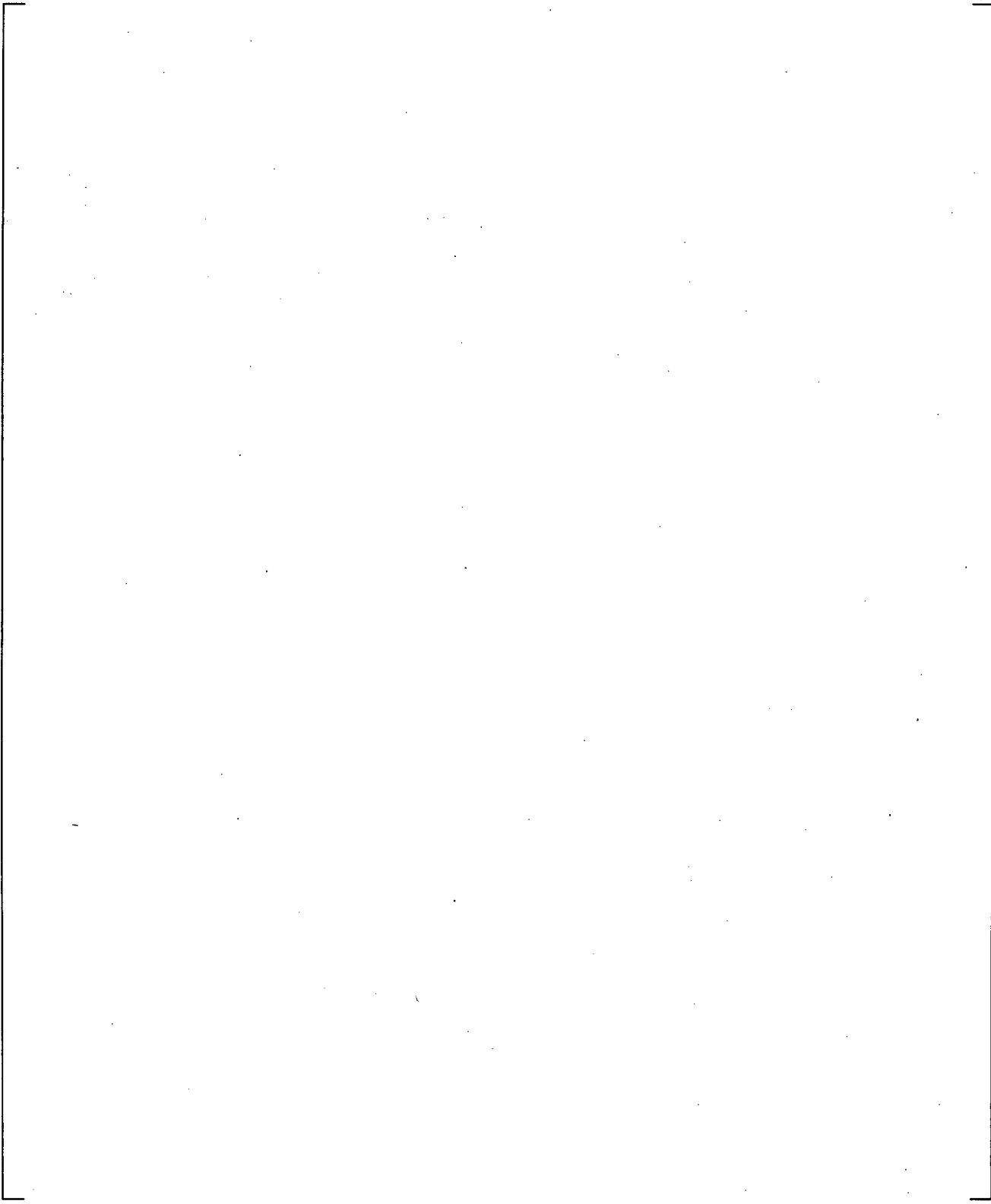


**Figure 24.6.6-11 Predicted HTC, Void Fraction Relation at 10 ft for FLECHT-SEASET 31701**

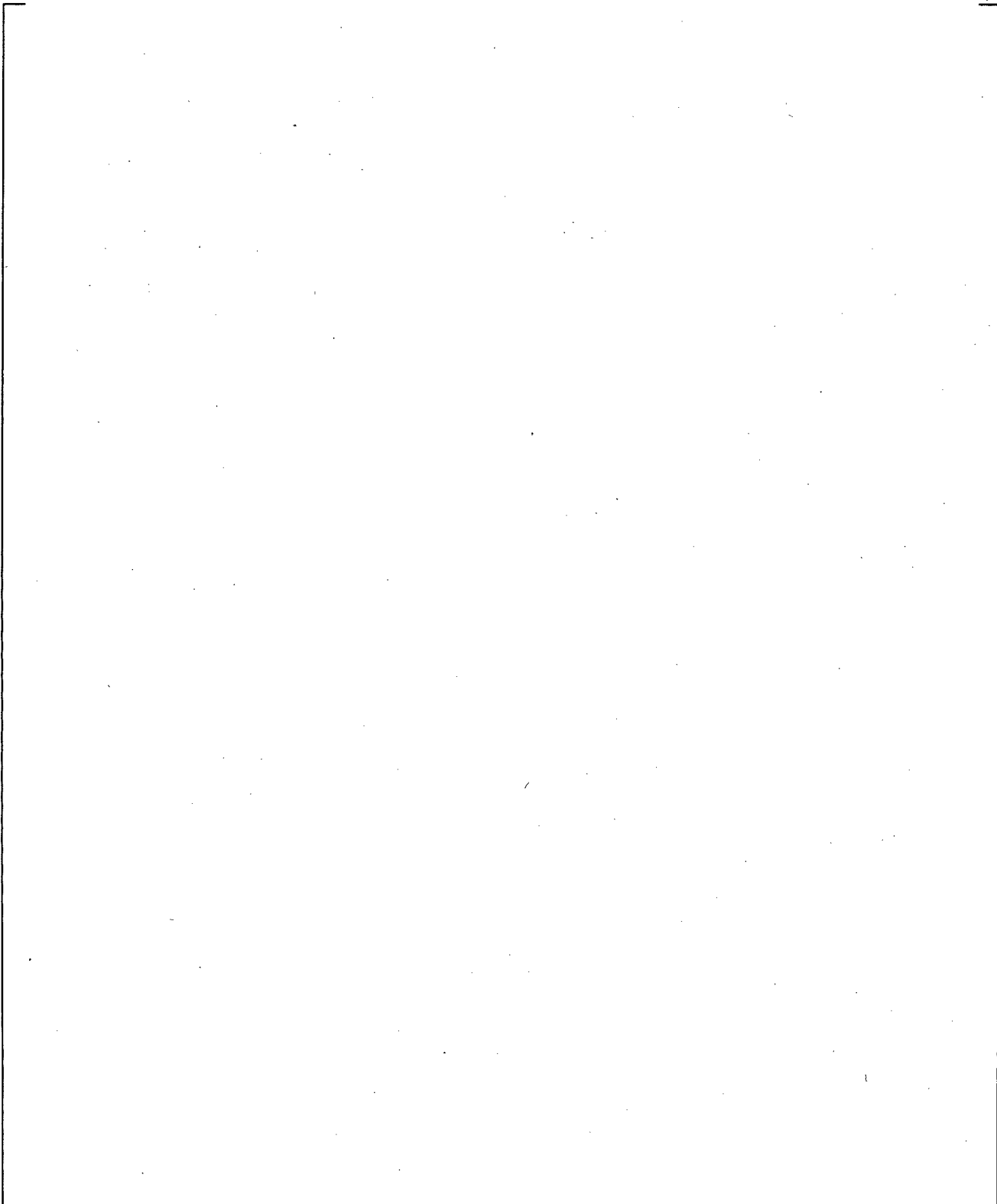


**Figure 24.6.6-12 Comparison of Measured and Predicted Void Fraction at 10 ft for FLECHT-SEASET 31701**

### 24.6.7 Conclusions

Two different FLECHT-SEASET tests were reviewed in order to identify compensating errors due to an improper coupling between heat transfer coefficient and void fraction. Both Tests 31805 and 31701 showed that [

] <sup>a,c</sup>

## 24.7 BLOWDOWN AND POST BLOWDOWN THERMAL-HYDRAULICS/ ENTRAINMENT

### 24.7.1 LOFT Test L2-3

The plots for this section are designated Figures 24.7.1-1 through 24.7.1-29. In all figures, Data legend uses the same system detector identification as in the test Data report (Prassinis, 1979) where possible (e.g., Figure 24.7.1-19 refers to DE-PC-001B). These references are to the corresponding figures in the LOFT test reports. The LOFT system is shown in Figure 24.7.1-1. LOFT Test L2-3 (Prassinis et al., 1979) was a pump-on, intermediate power test. A summary of measured event times is given below:

Event	Time (s)
Blowdown begins	0
Accumulator begins injecting	17
End of Blowdown/beginning of reflood	40
Accumulator empty (N <sub>2</sub> injection)	50-60
Core quench	55

End of blowdown is defined above as the time where system pressure levels off to a constant value, and a liquid level is detected in the core.

In addition to cladding temperature, fluid conditions at several locations in the LOFT system (Figure 24.7.1-1) were examined for compensating error.

### Core Thermal-Hydraulics

Initial blowdown heat-up and cooldown of the cladding temperatures for LOFT Test L2-3 were predicted [

] <sup>a,c</sup>

[

]a,c

**System Behavior**

The system pressure was [

]a,c

**Loop Behavior: Intact loop**

Figures 24.7.1-13 to 24.7.1-15 compared [

]a,c

[

]a,c

Figures 24.7.1-16 through 24.7.1-21 show predicated and measured trends in the [

]a,c

**Loop Behavior: Broken loop**

[

]a,c

[

]a,c

### **Sensitivity Studies**

Several studies were performed to examine what factors contribute most to the misprediction of core flow.

[

]a,c

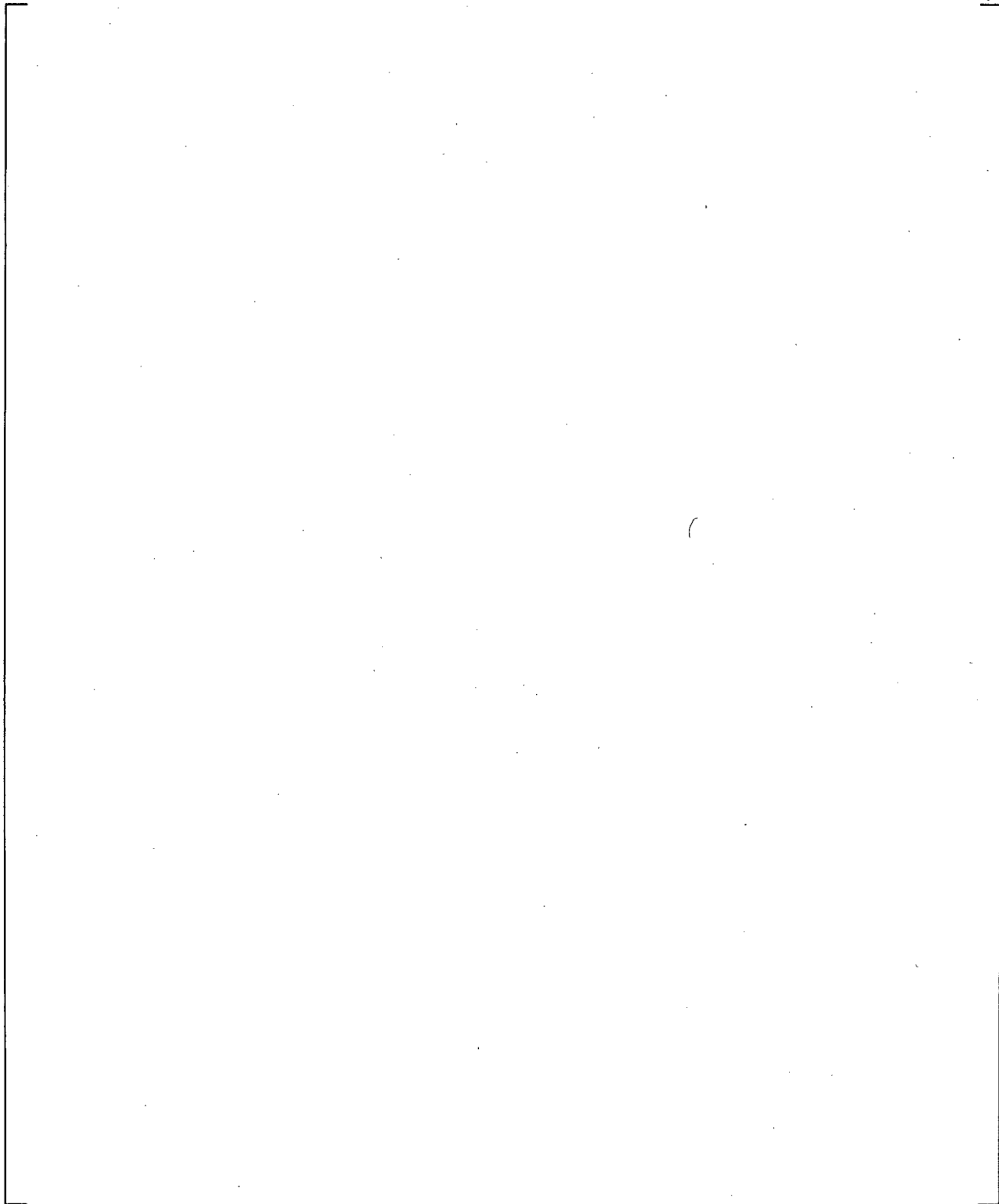


**Figure 24.7.1-1 LOFT Measurement/Prediction Locations**

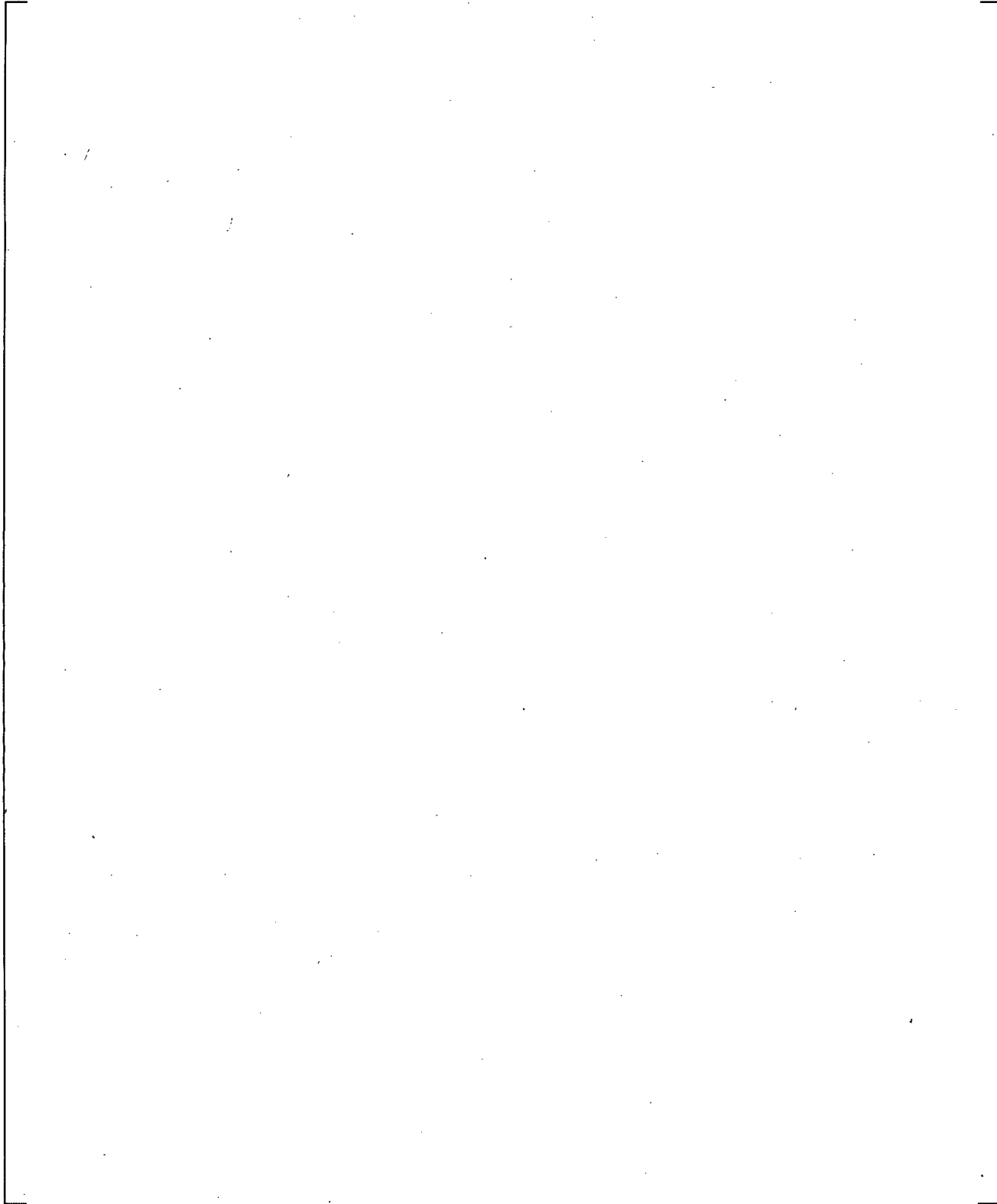


**Figure 24.7.1-2 LOFT L2-3 Data vs. Predicted Hot Rod Cladding Temperature**

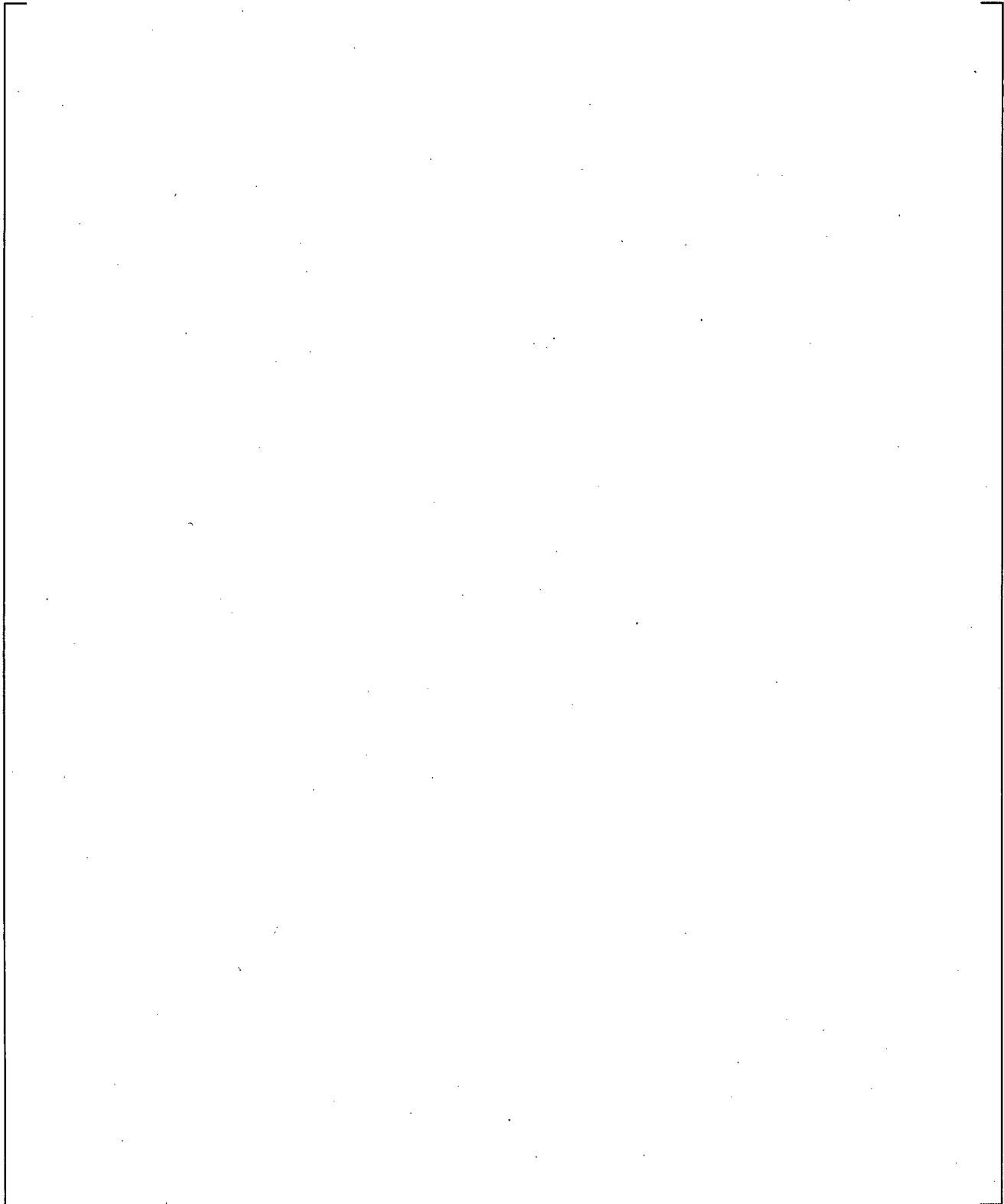


**Figure 24.7.1-3 Predicted Vapor Flowrate at Top and Bottom of Hot Assembly**

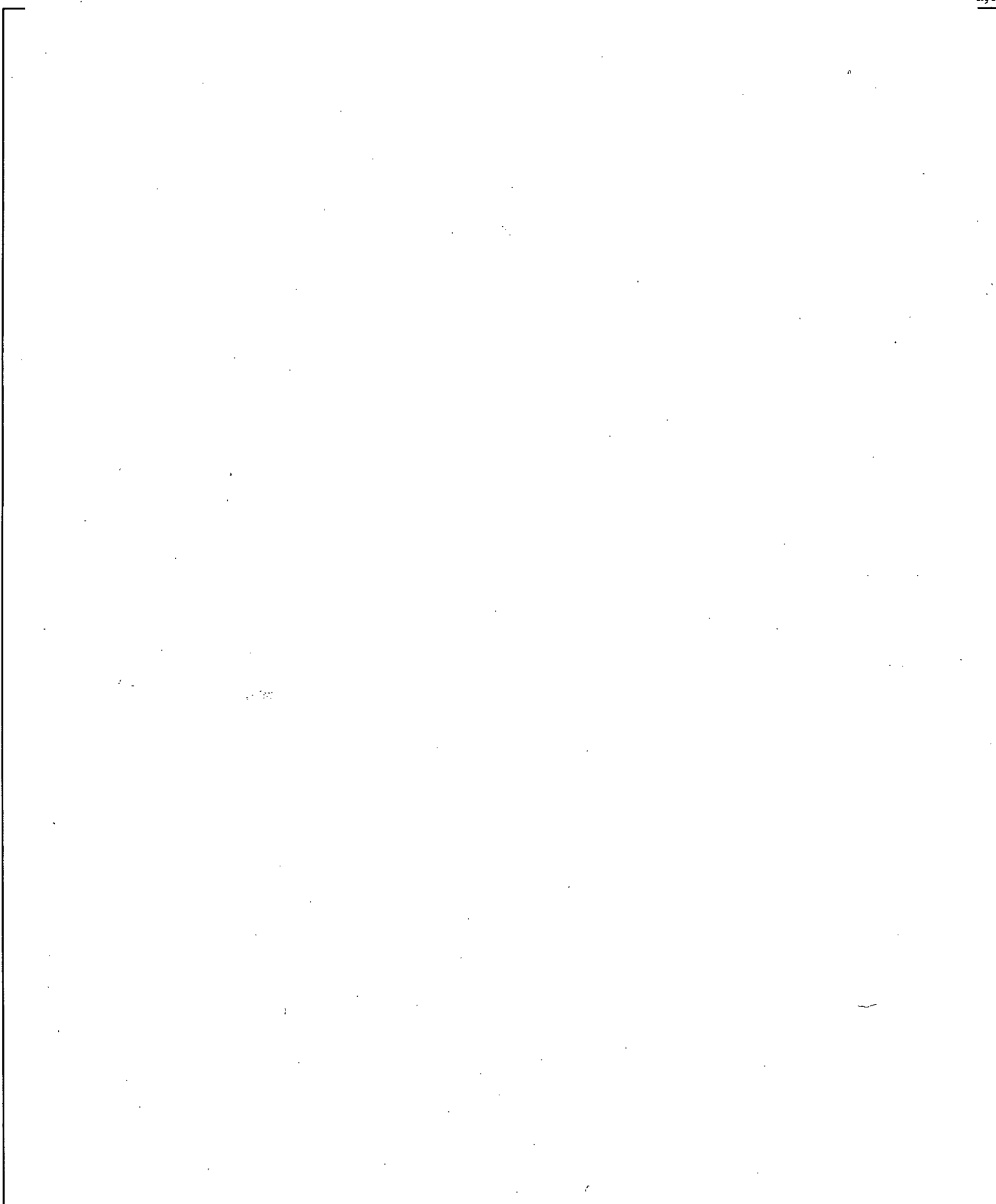


**Figure 24.7.1-4 Predicted Entrained Drop Flowrate at Top and Bottom of Hot Assembly**

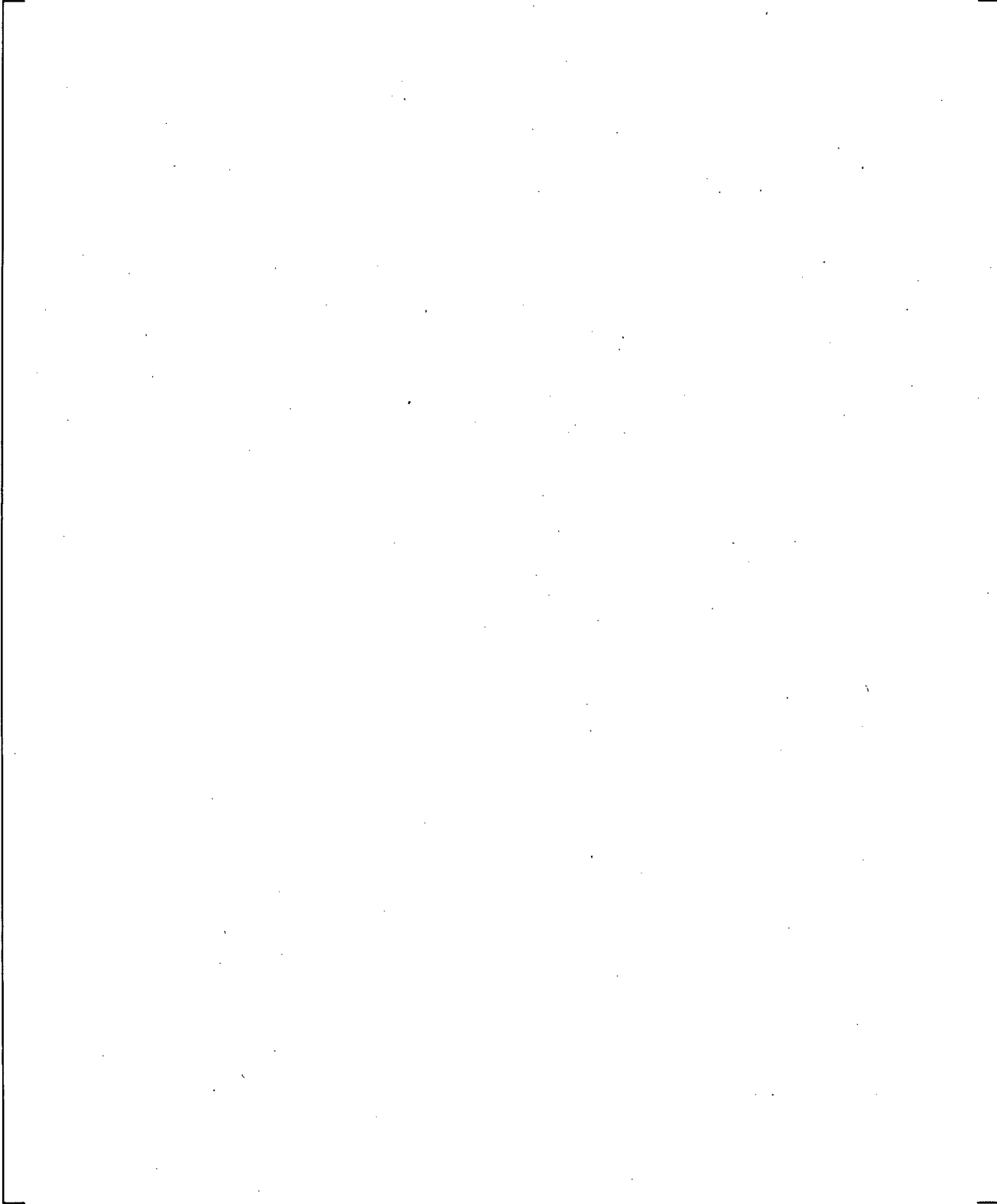


**Figure 24.7.1-5 LOFT L2-3 Data vs. Predicted Steam Temperature at Top of Hot Assembly**

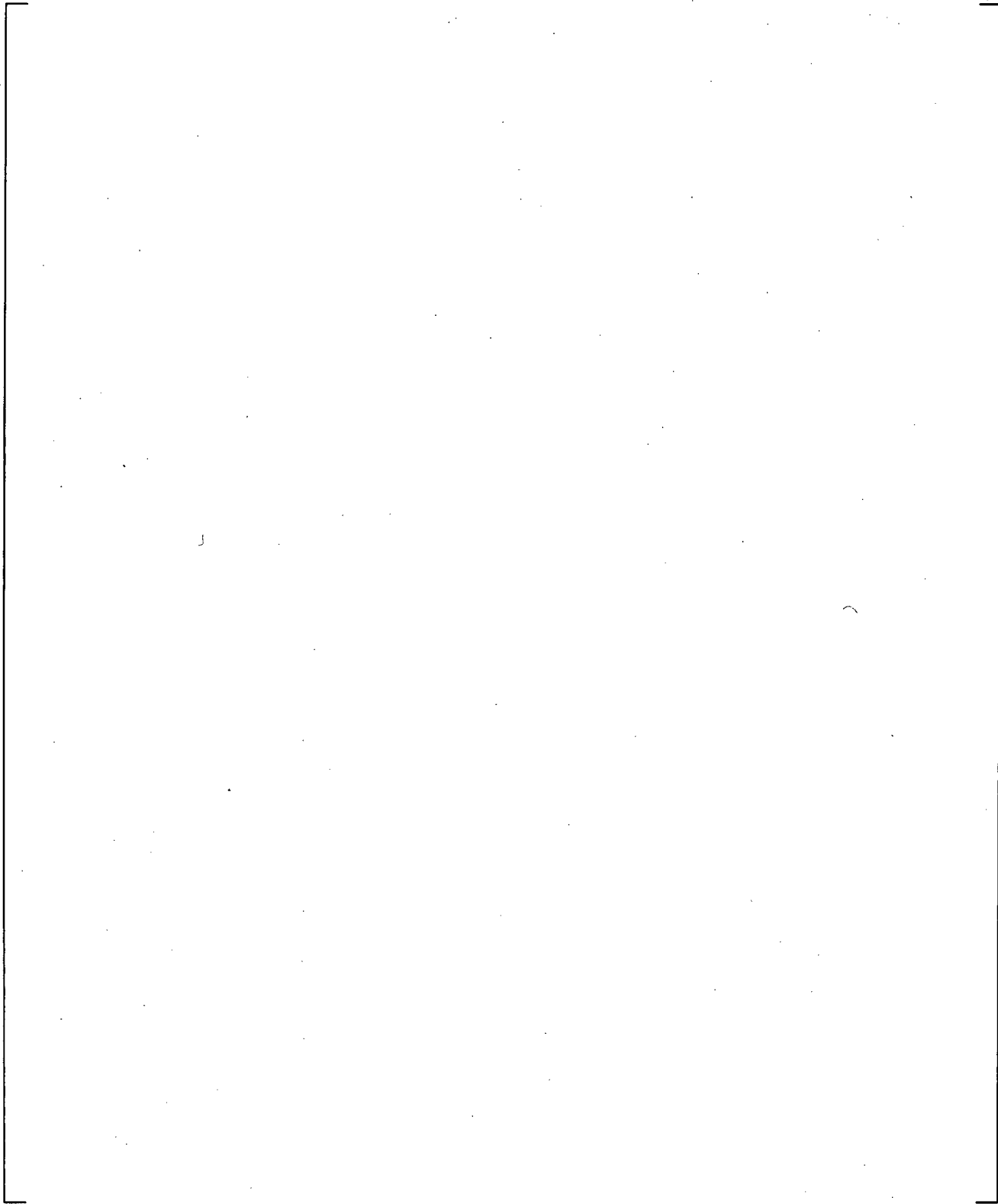


**Figure 24.7.1-6 LOFT L2-3 Data vs. Predicted Steam Temperature at Bottom of Hot Assembly**

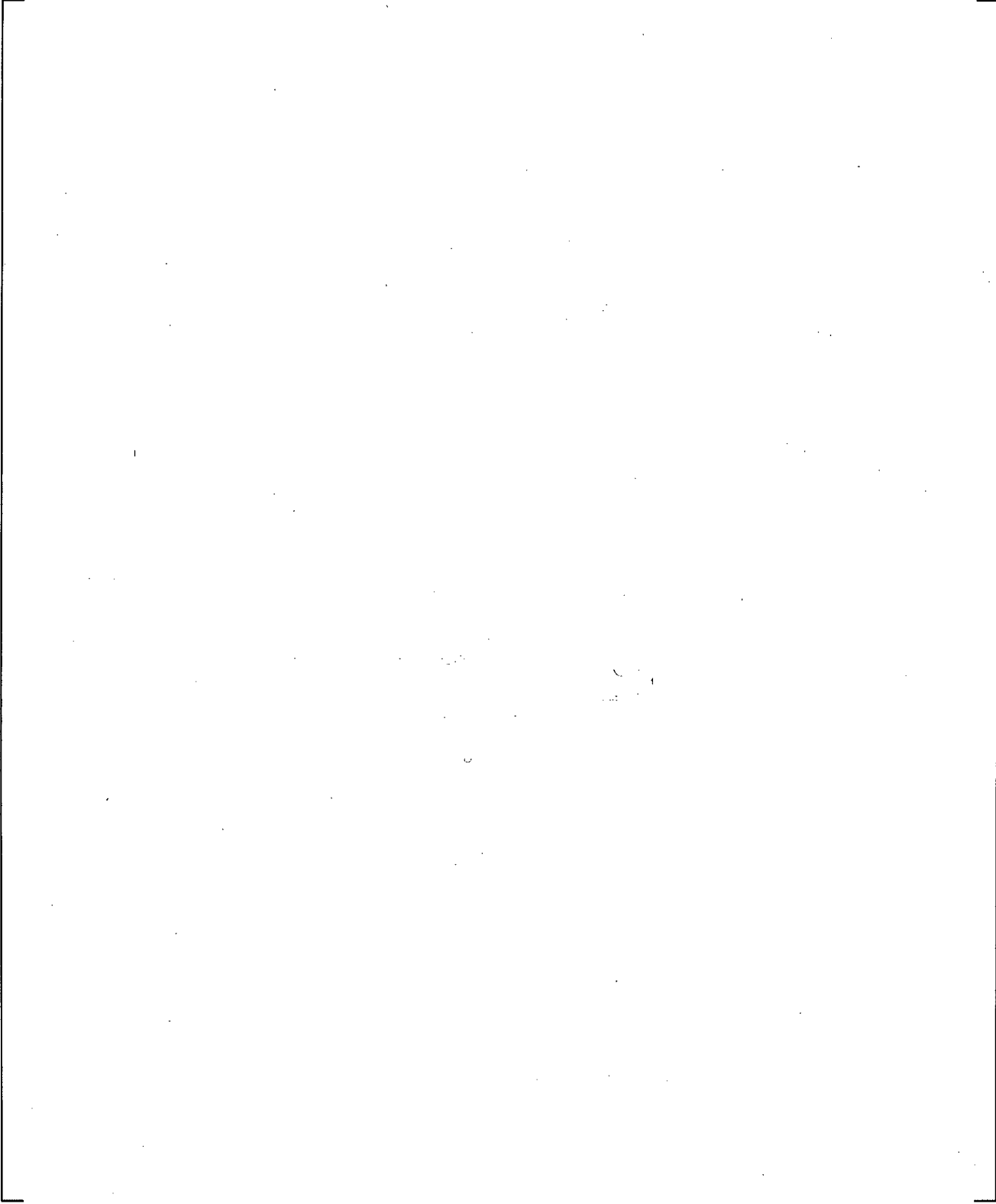


**Figure 24.7.1-7 Predicted Hot Rod Vapor Heat Transfer Coefficient at PCT Elevation**

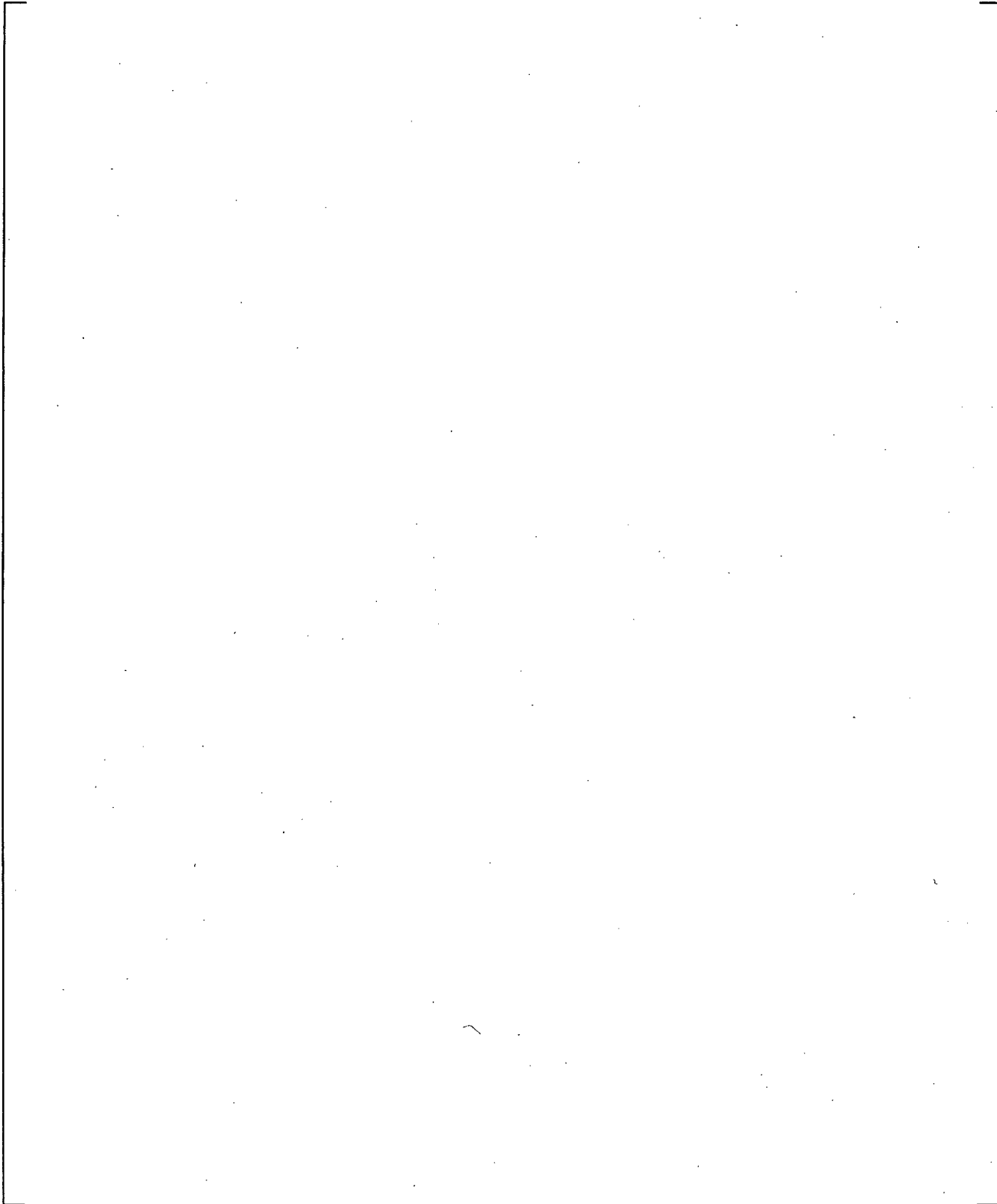


**Figure 24.7.1-8 Predicted Hot Rod Liquid Heat Transfer Coefficient at PCT Elevation**

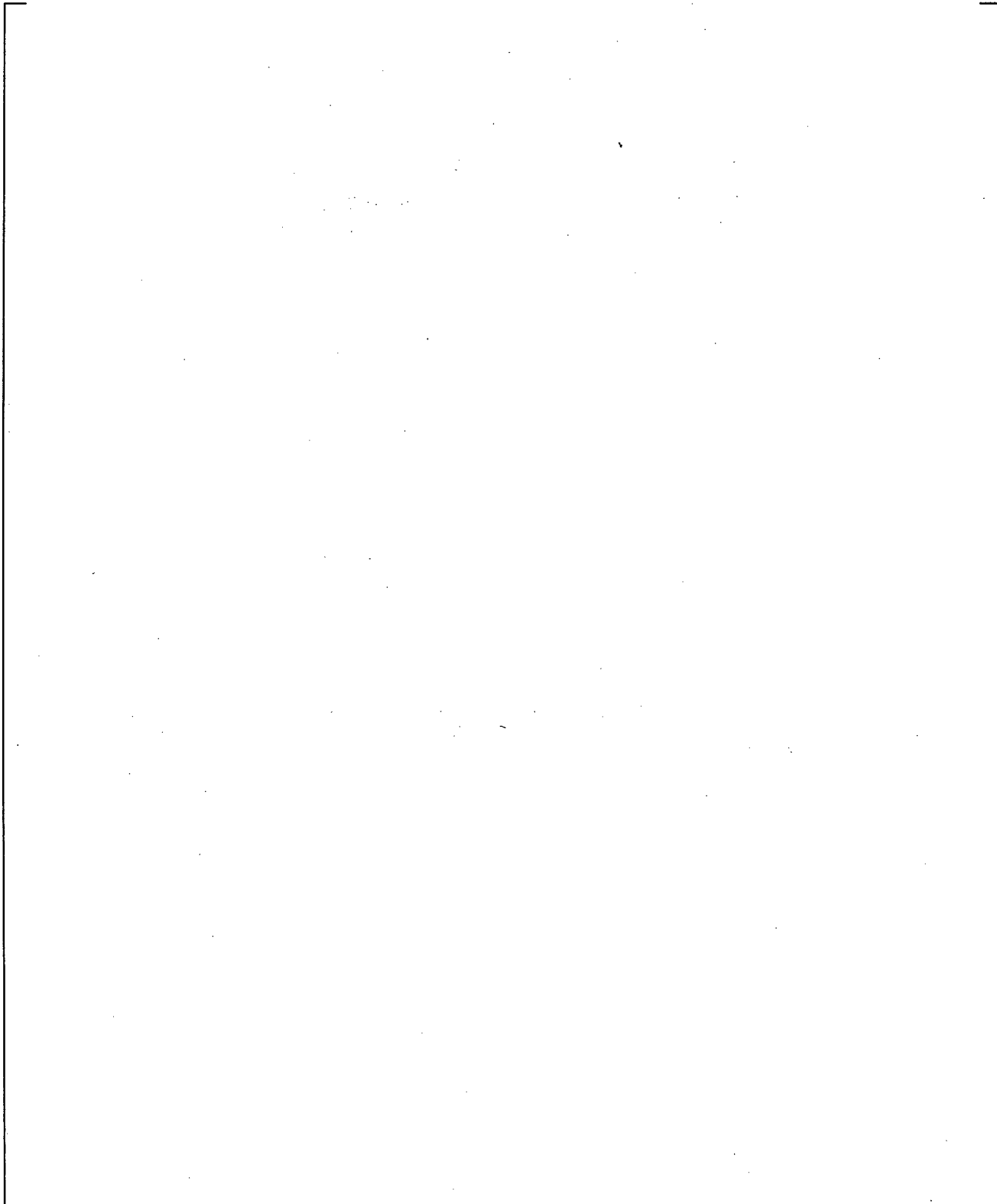


**Figure 24.7.1-8a Predicted Hot Rod Liquid Heat Transfer Coefficient at PCT Elevation  
(Expanded Scale)**

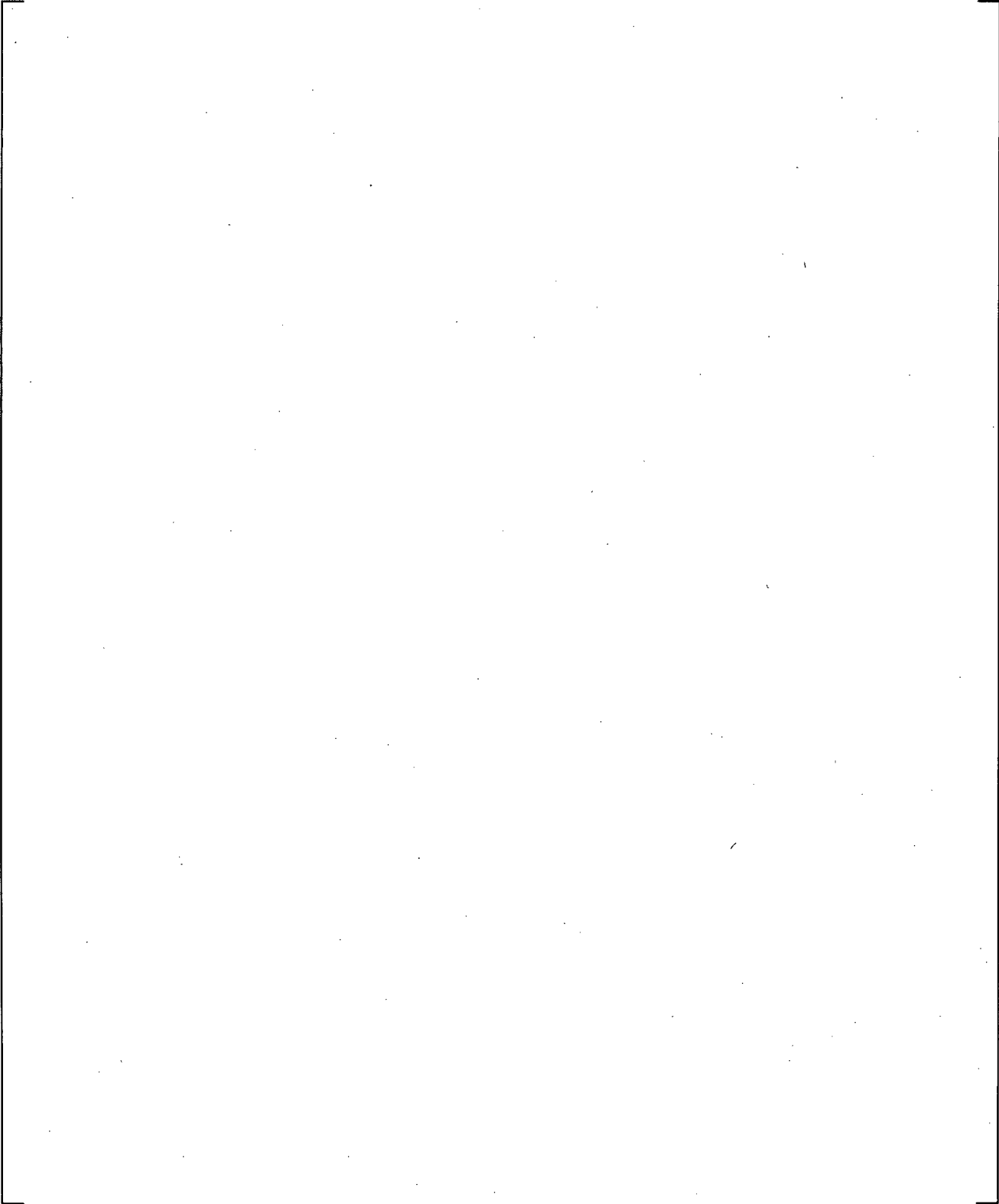


**Figure 24.7.1-9 Measured and Predicted Intact Loop Pressure**

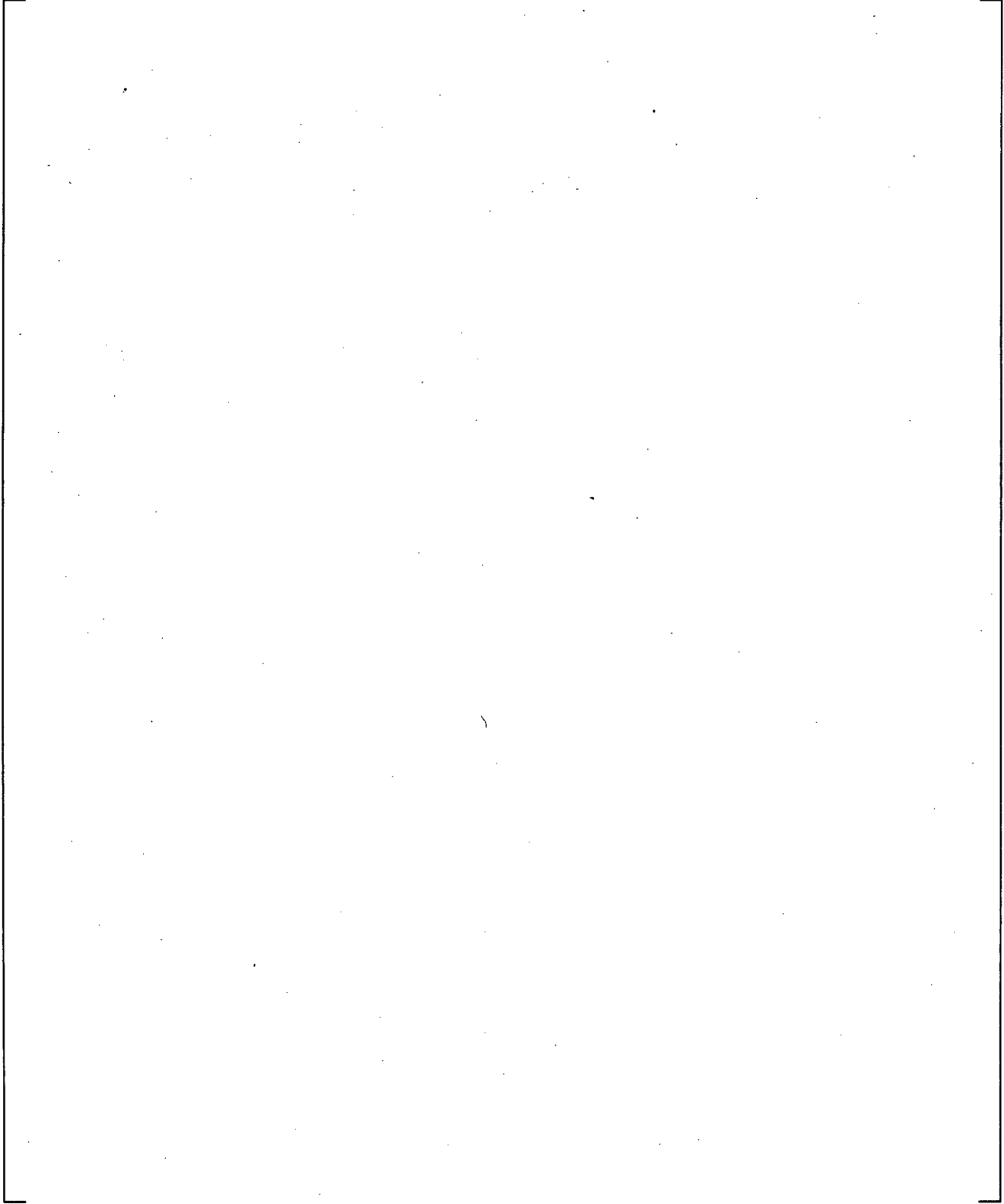


**Figure 24.7.1-10 Predicted Downcomer Collapsed Liquid Level (1- Intact, 2-Broken Side)**

**Figure 24.7.1-11 Predicted and Measured Core Collapsed Liquid Level (Line 5-Estimated from the Liquid Detector)**

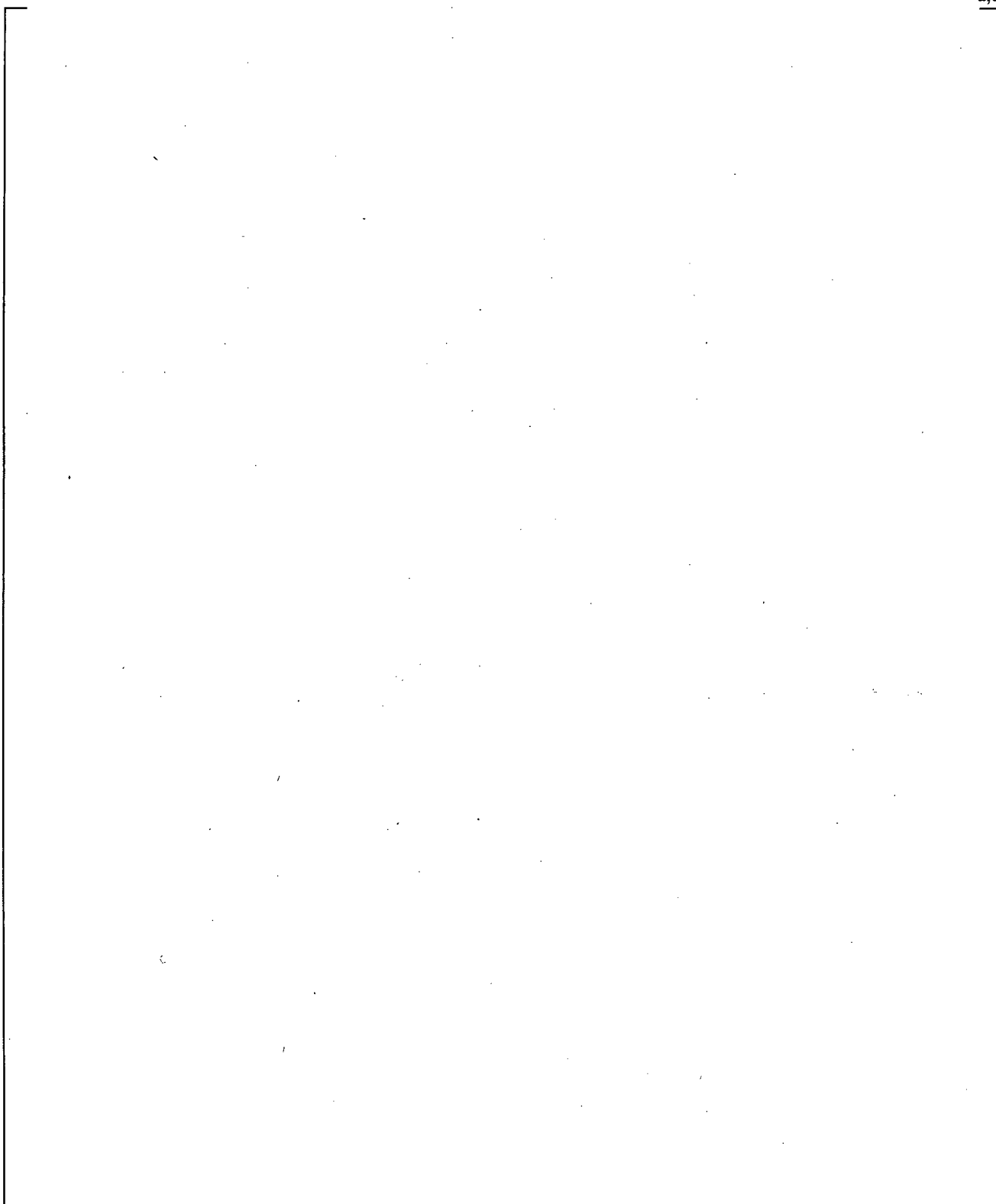


**Figure 24.7.1-12 Predicted Upper Plenum Collapsed Liquid Level**

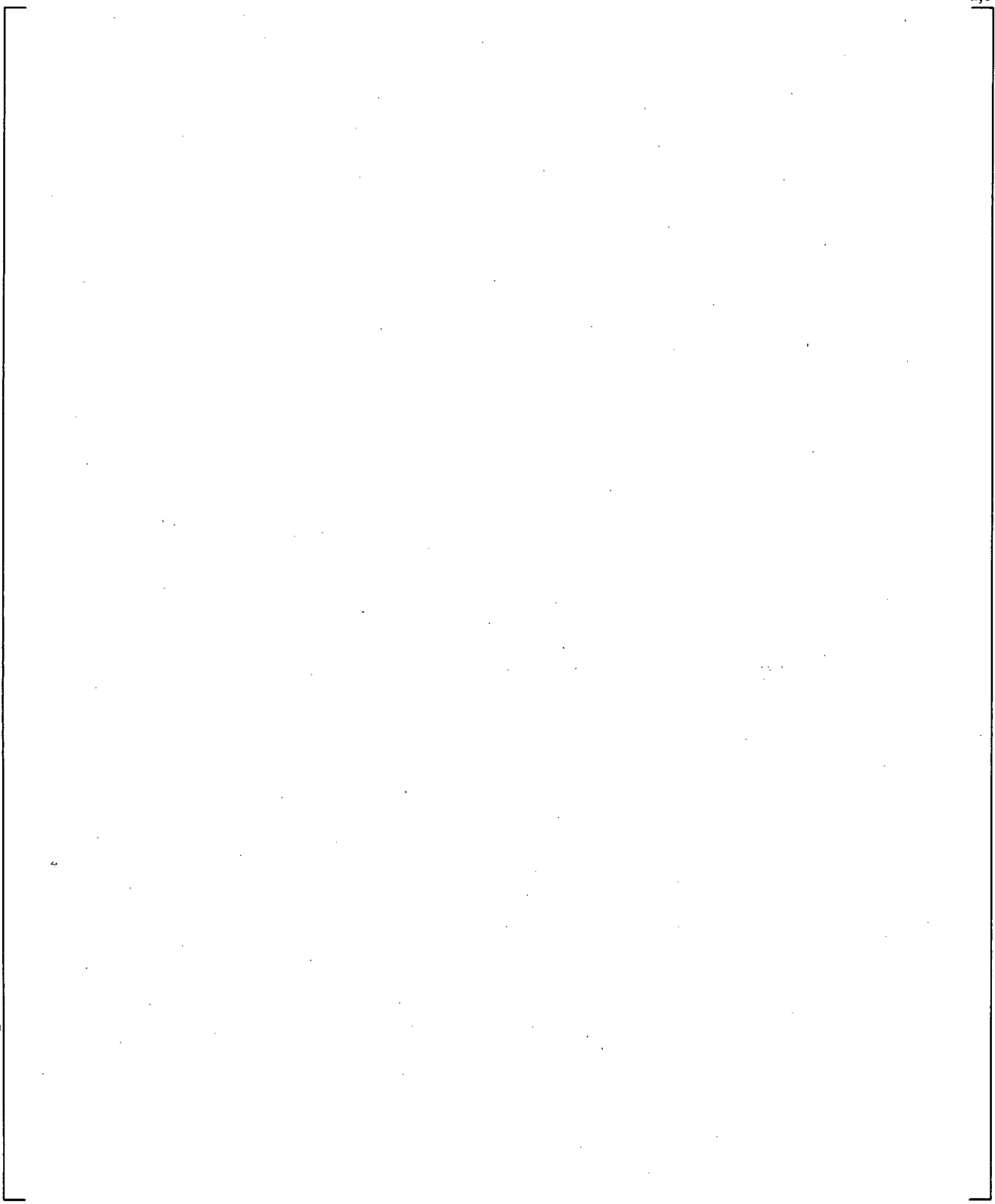


**Figure 24.7.1-13 Measured and Predicted Intact Loop Hot Leg Flowrate**

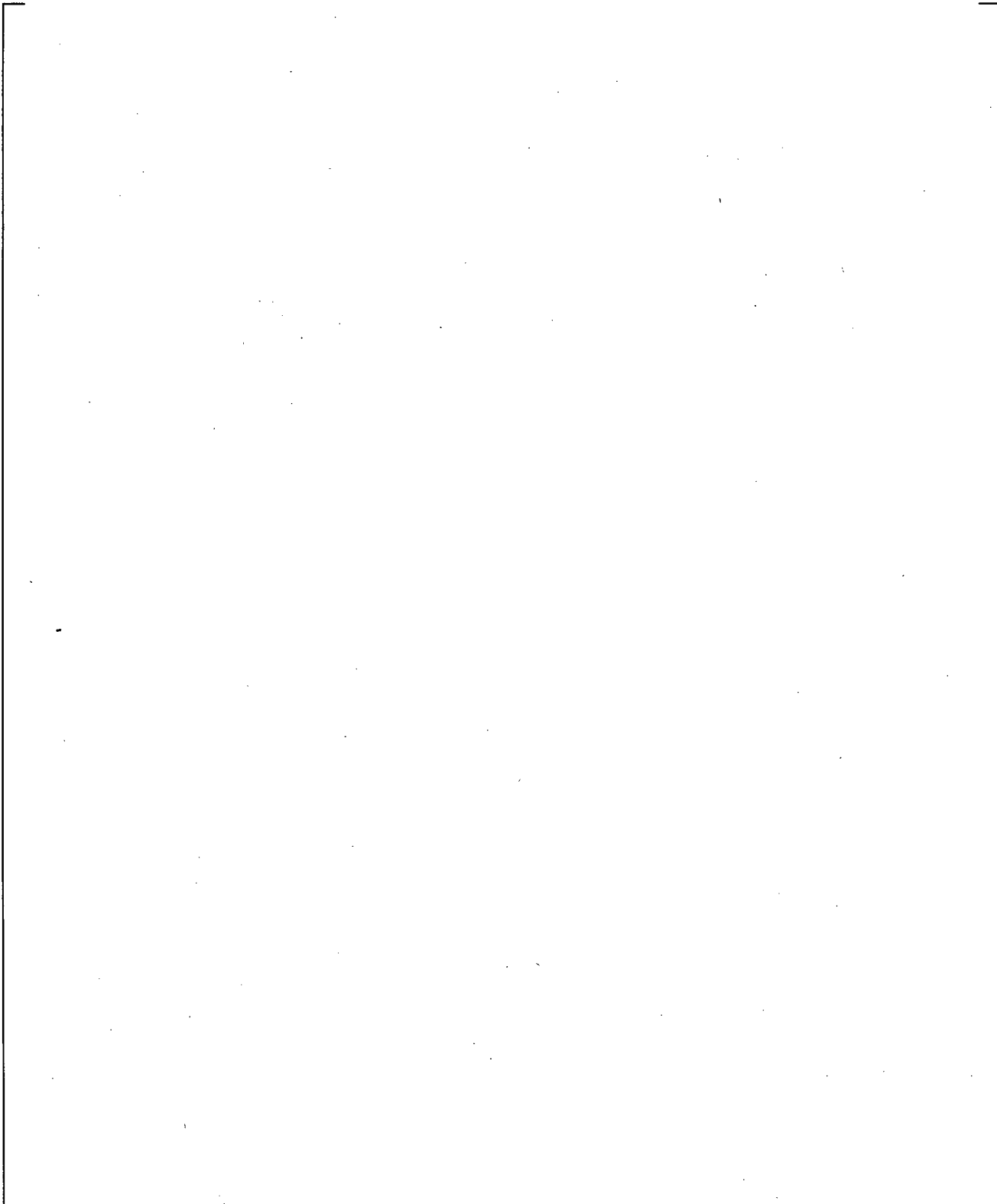


**Figure 24.7.1-14 Measured and Predicted Intact Loop Hot Leg Mixture Density**

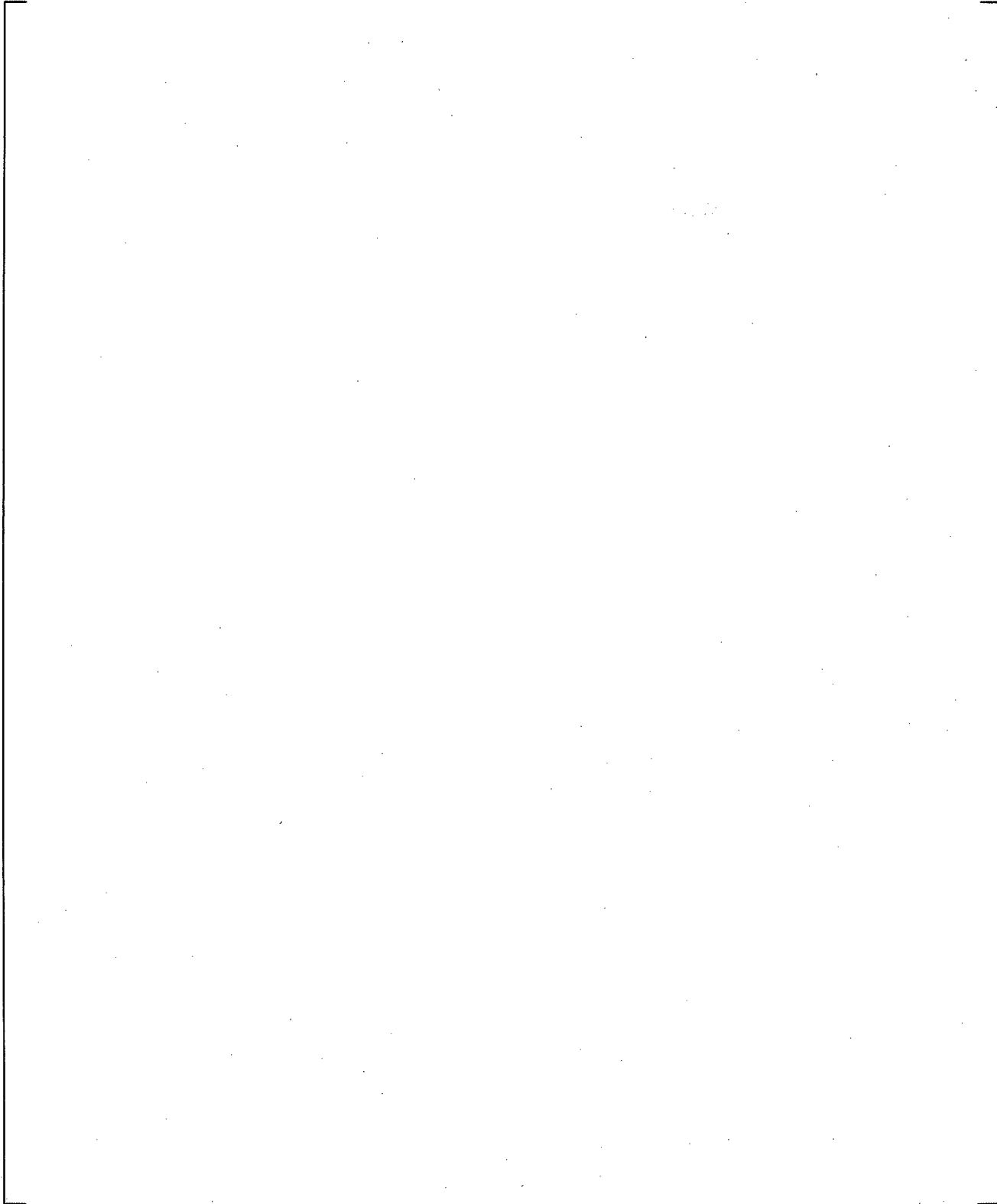


**Figure 24.7.1-15 Measured and Predicted Intact Loop Hot Leg Mixture Velocity**

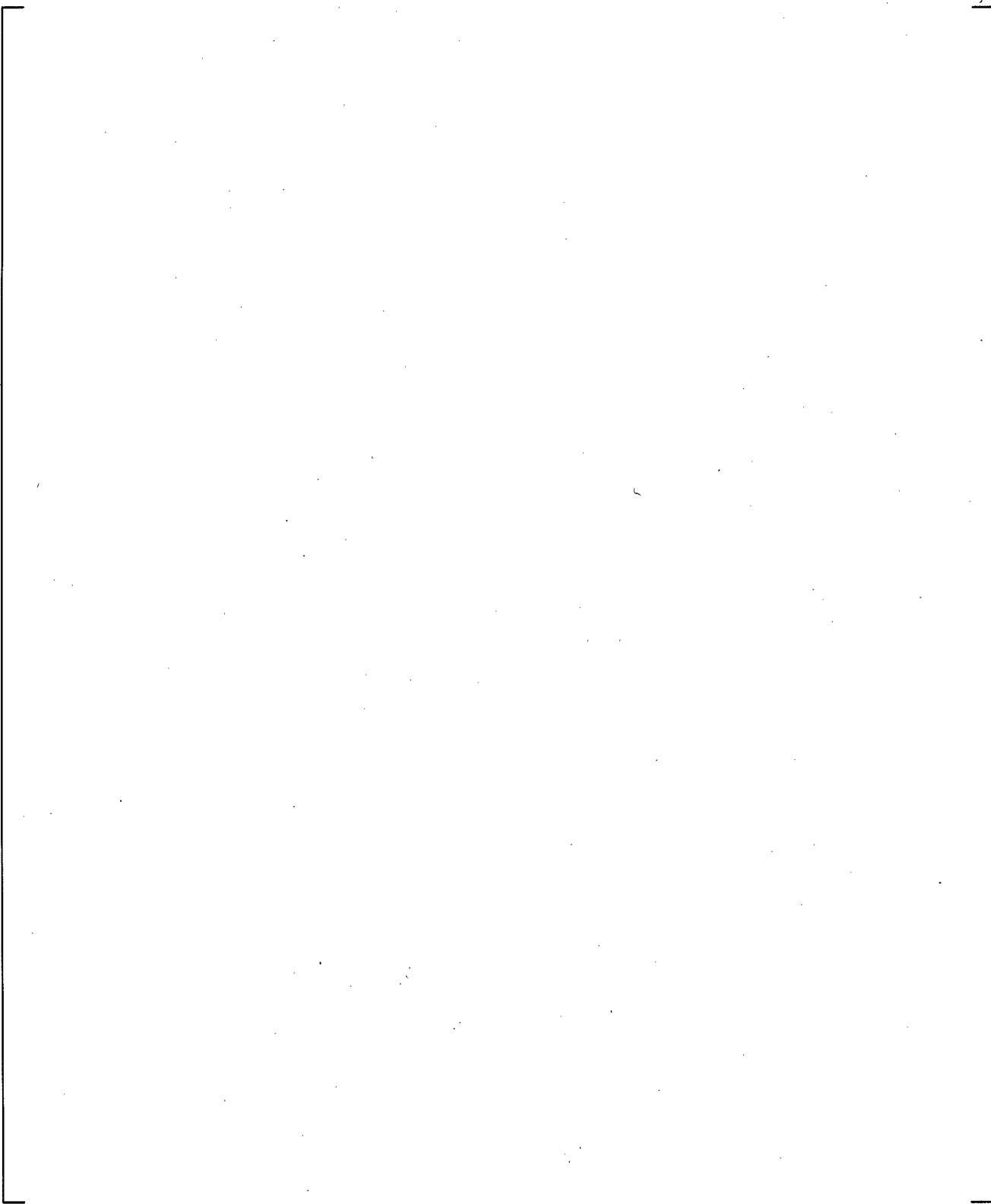


**Figure 24.7.1-15a Measured and Predicted Intact Loop Pressure Comparison**

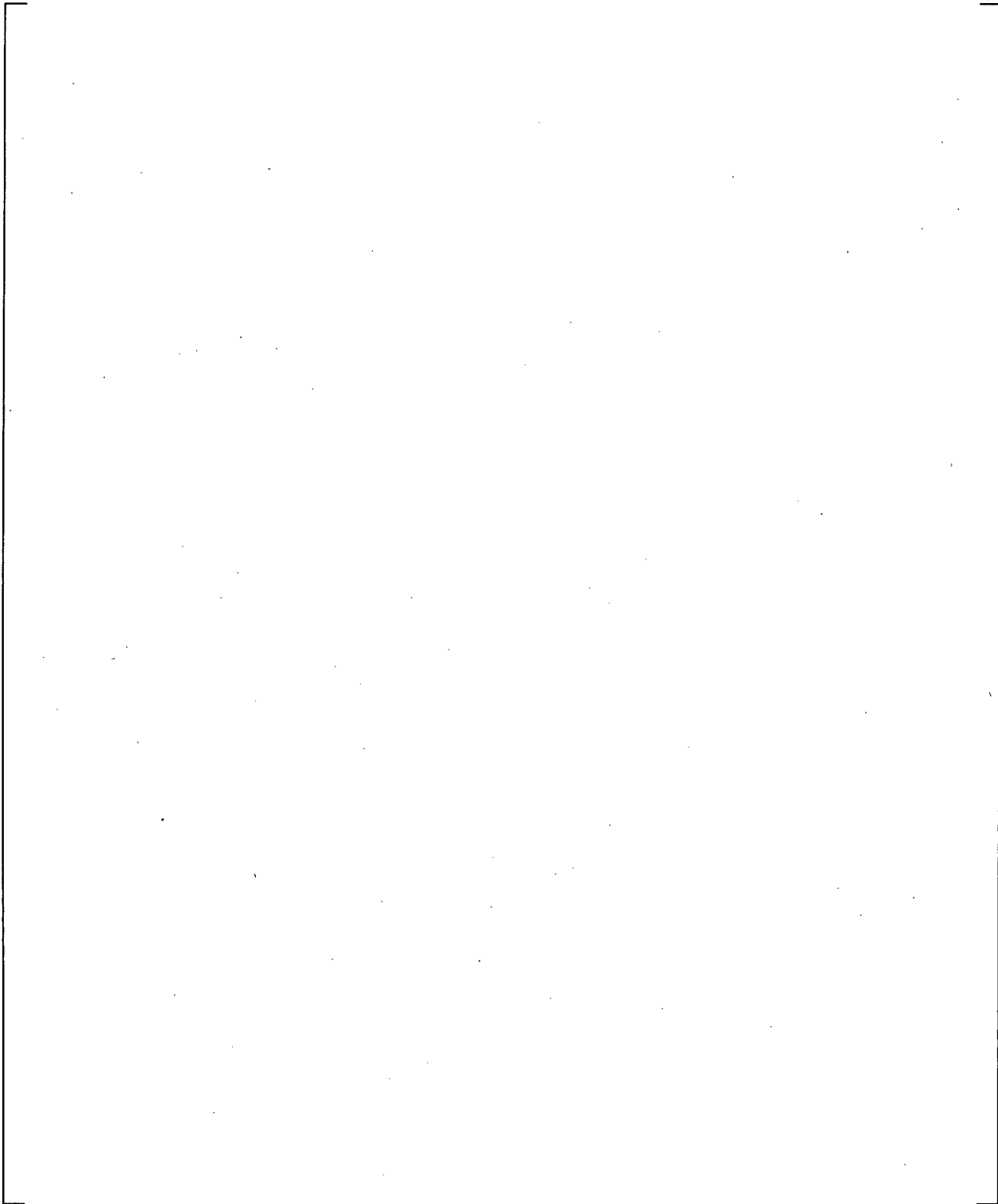


**Figure 24.7.1-16 Measured and Predicted Intact Loop Cold Leg Flowrate**

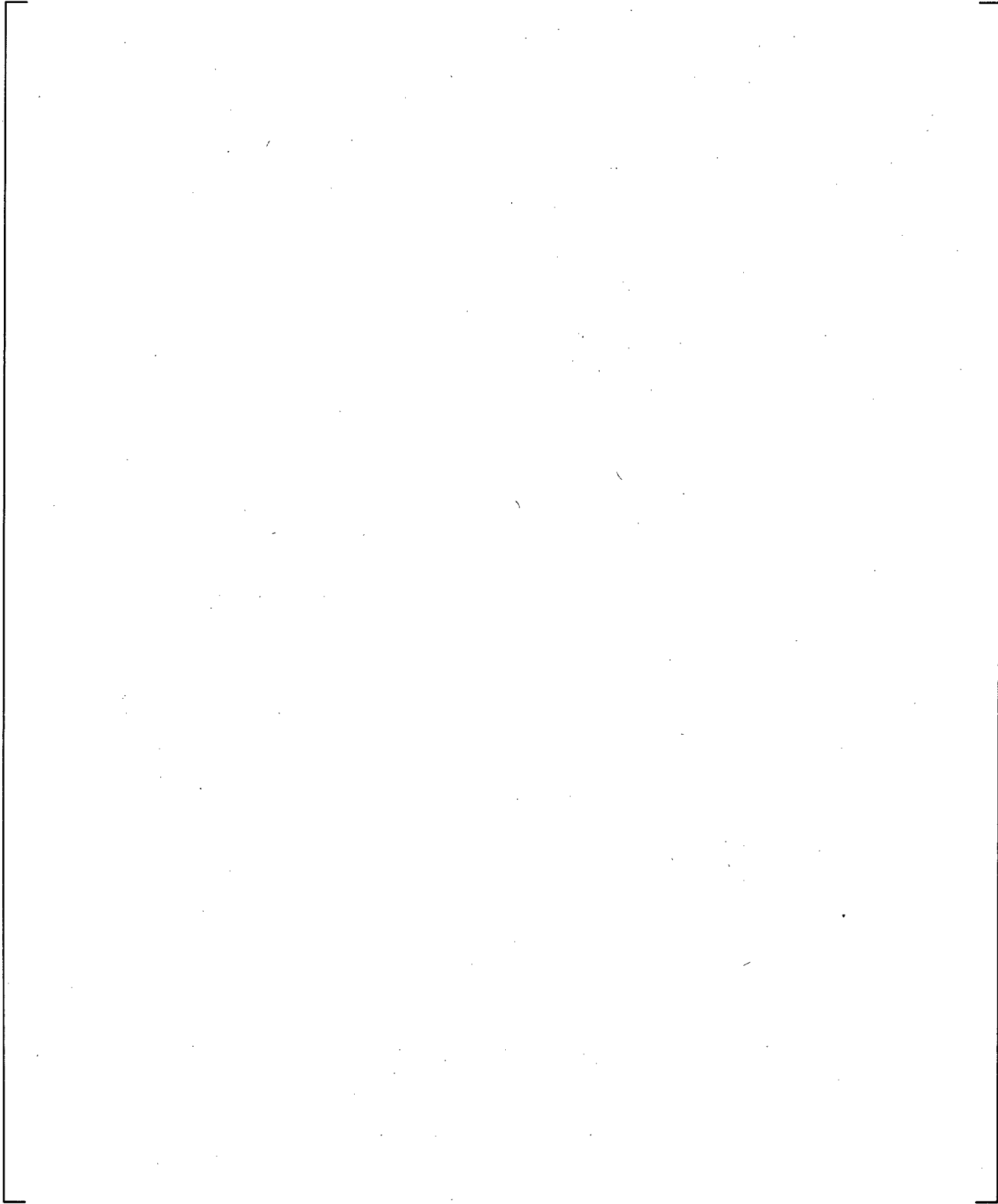


**Figure 24.7.1-17 Measured and Predicted Intact Loop Cold Leg Flowrate**

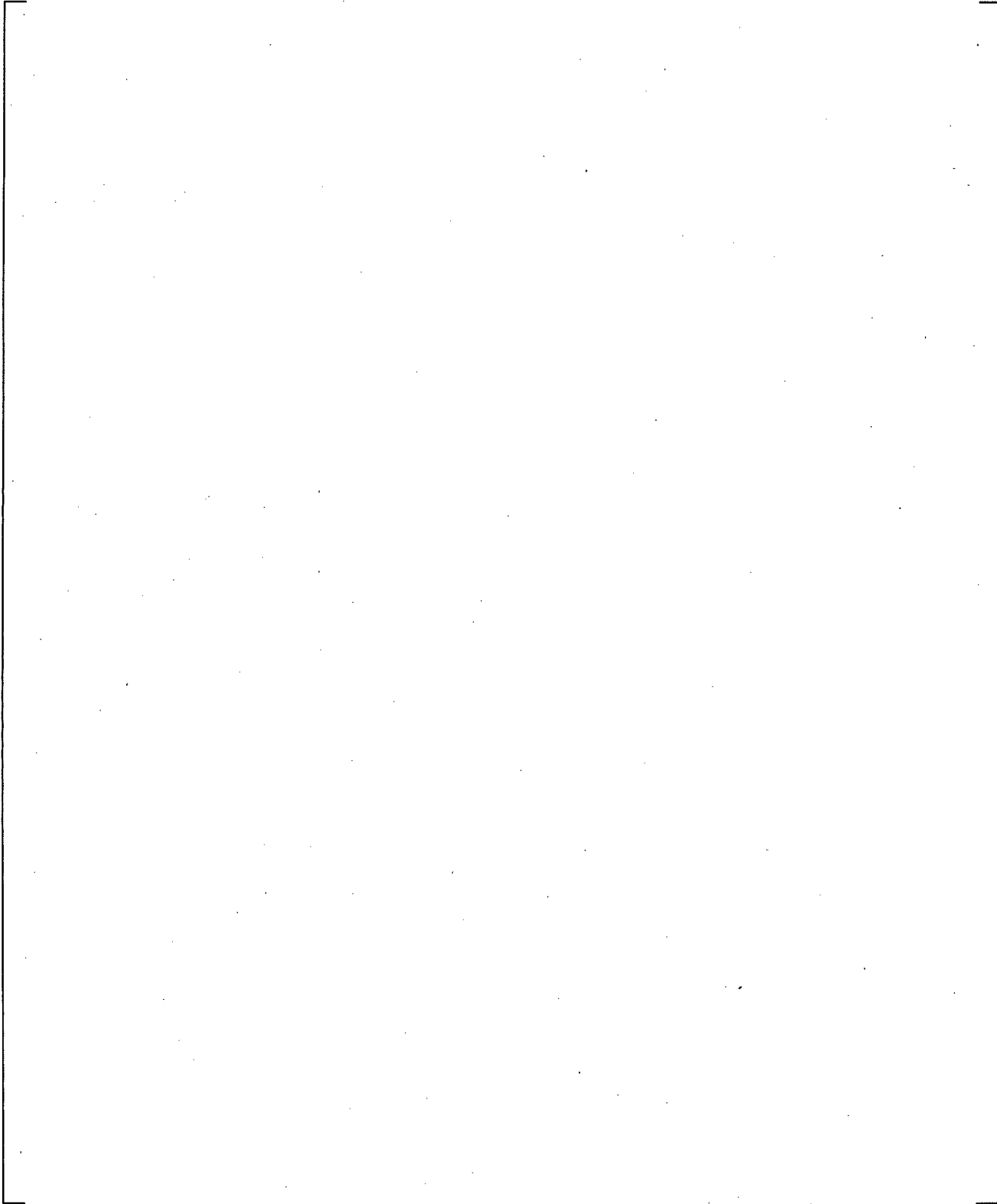


**Figure 24.7.1-18 Measured and Predicted Intact Loop Cold Leg Mixture Density**

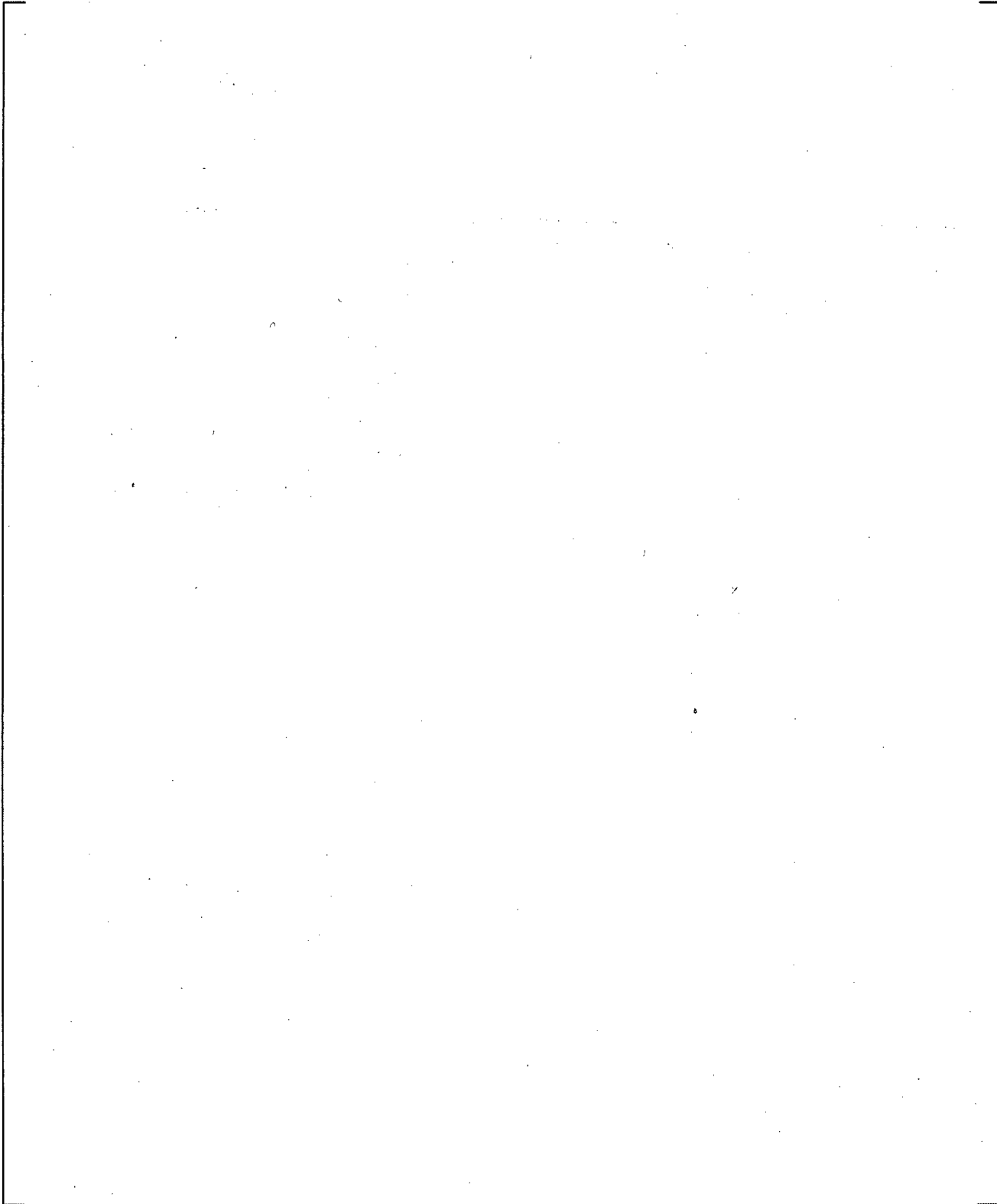


**Figure 24.7.1-19 Measured and Predicted Intact Loop Cold Leg Mixture Density**

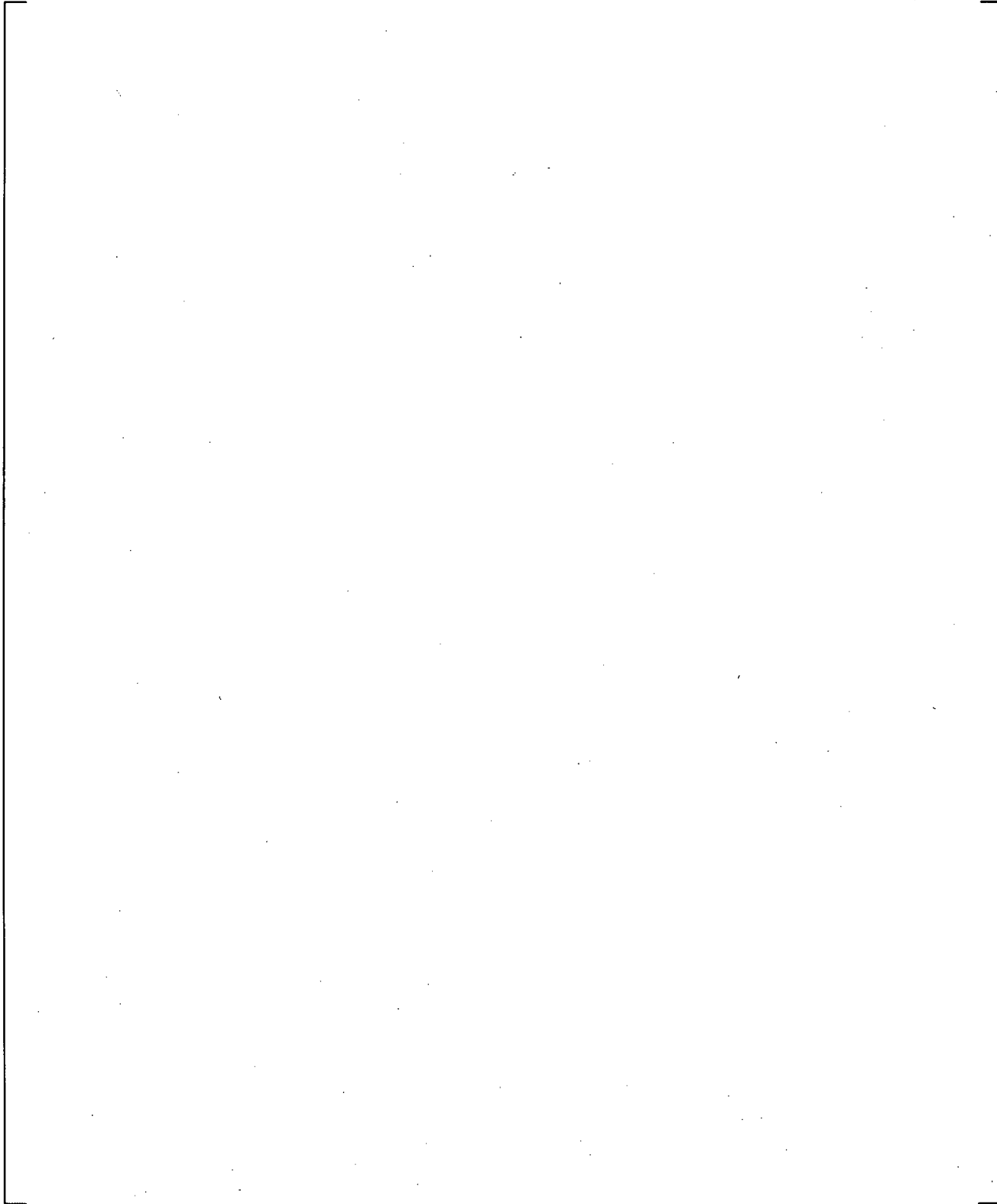


**Figure 24.7.1-20 Measured and Predicted Intact Loop Cold Leg Mixture Velocity**

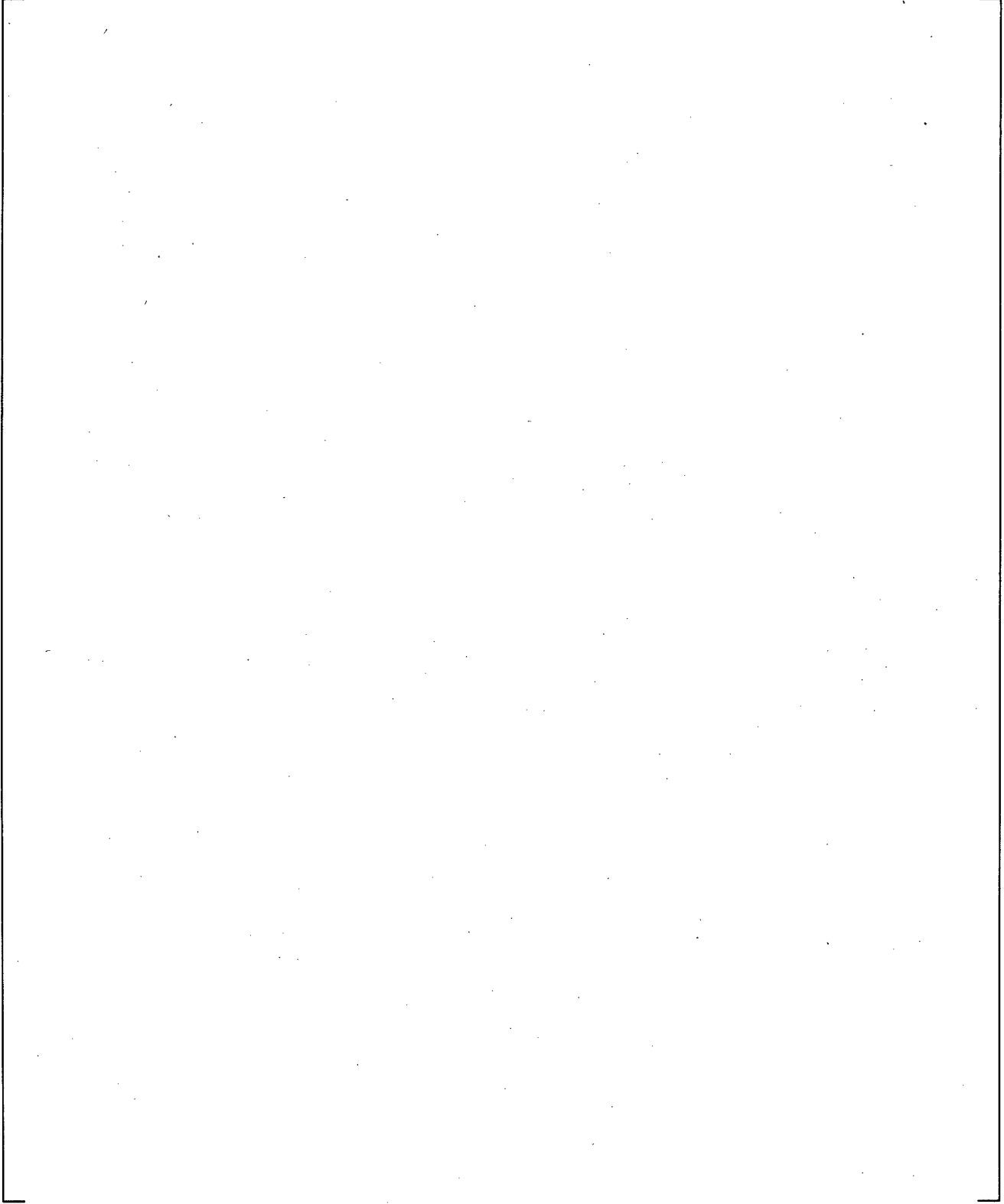


**Figure 24.7.1-21 Measured and Predicted Intact Loop Cold Leg Mixture Velocity**

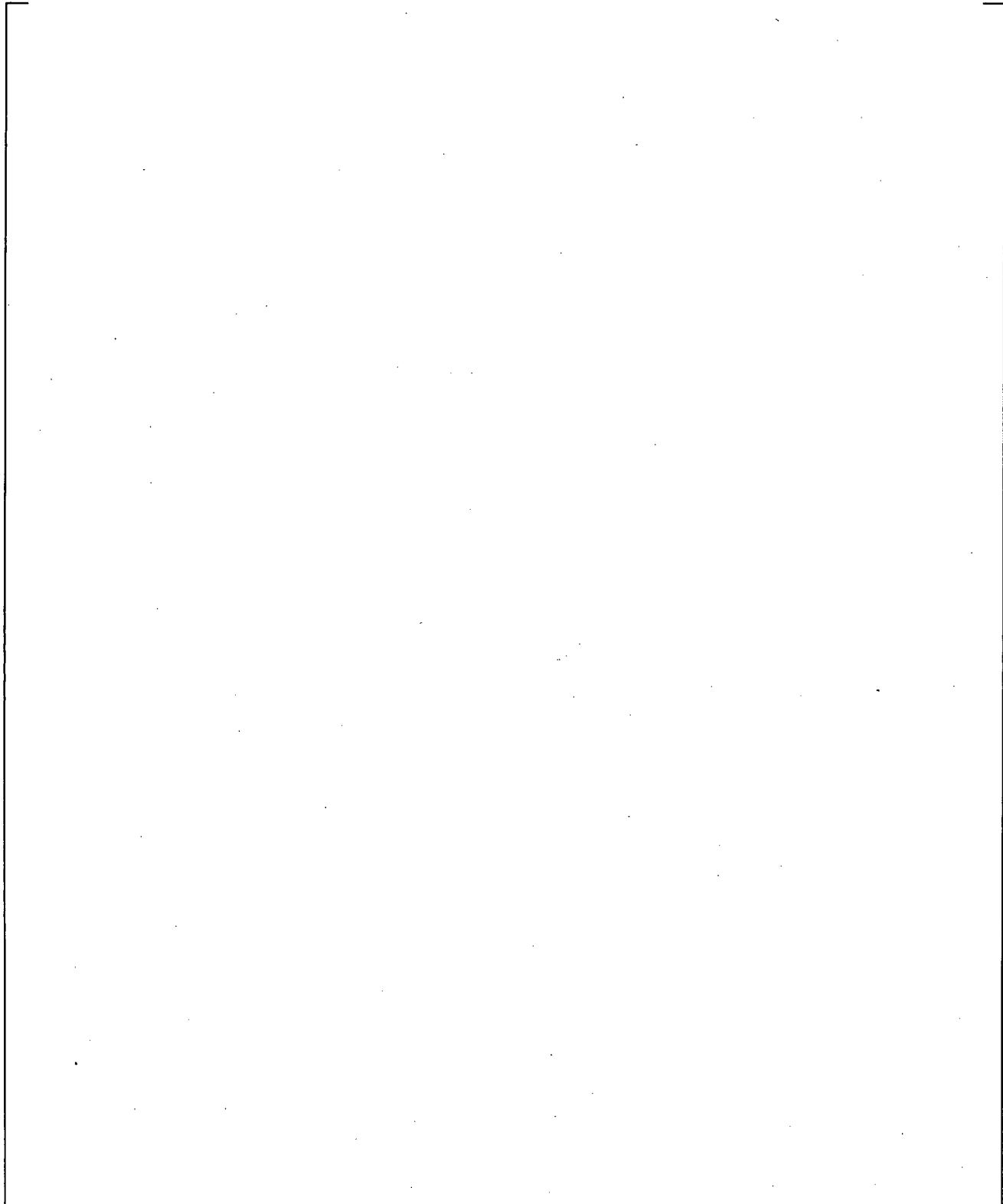


**Figure 24.7.1-22 Measured and Predicted Hot Leg Break Flowrate**

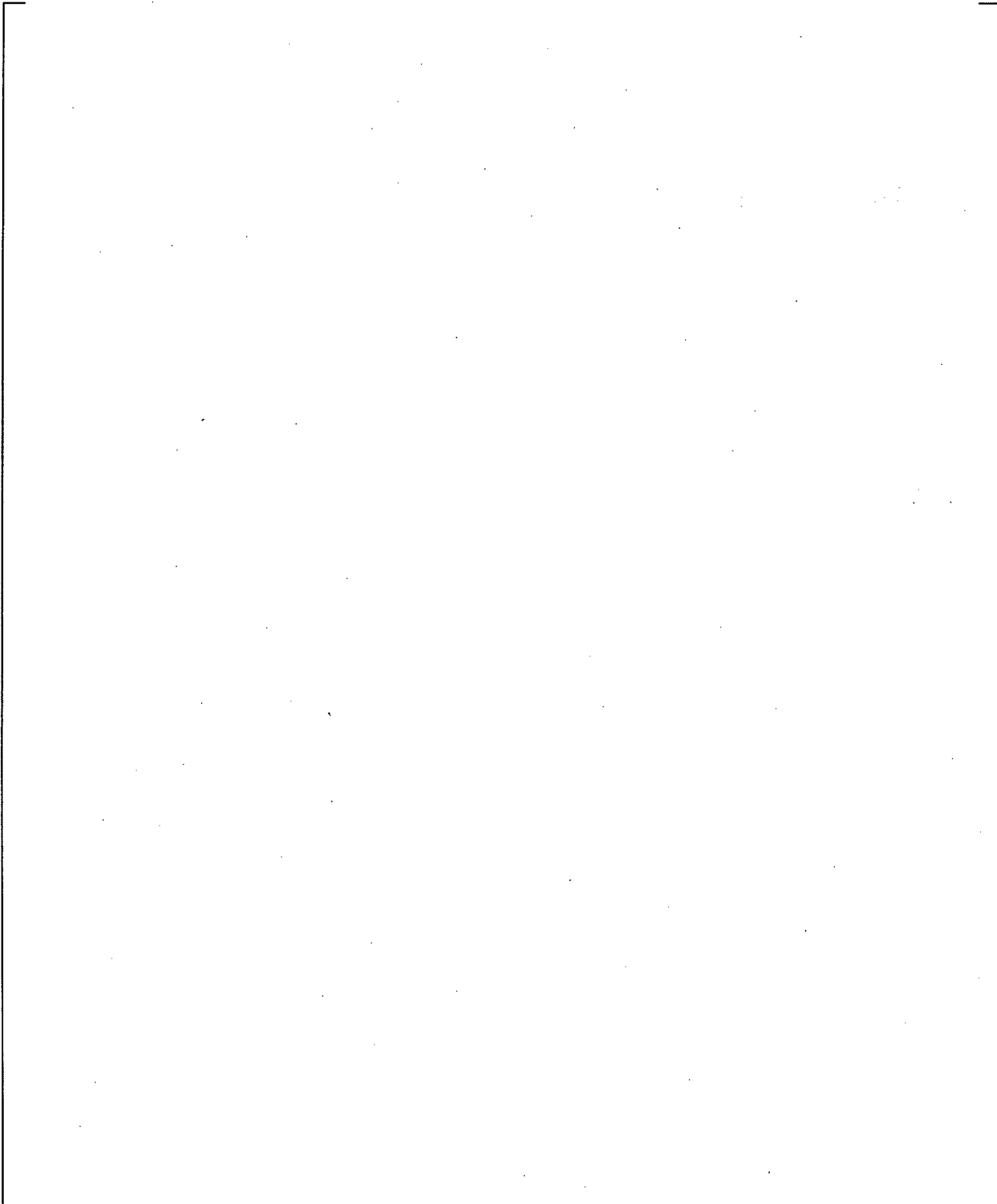


**Figure 24.7.1-23 Measured and Predicted Broken Loop Hot Leg Mixture Density**

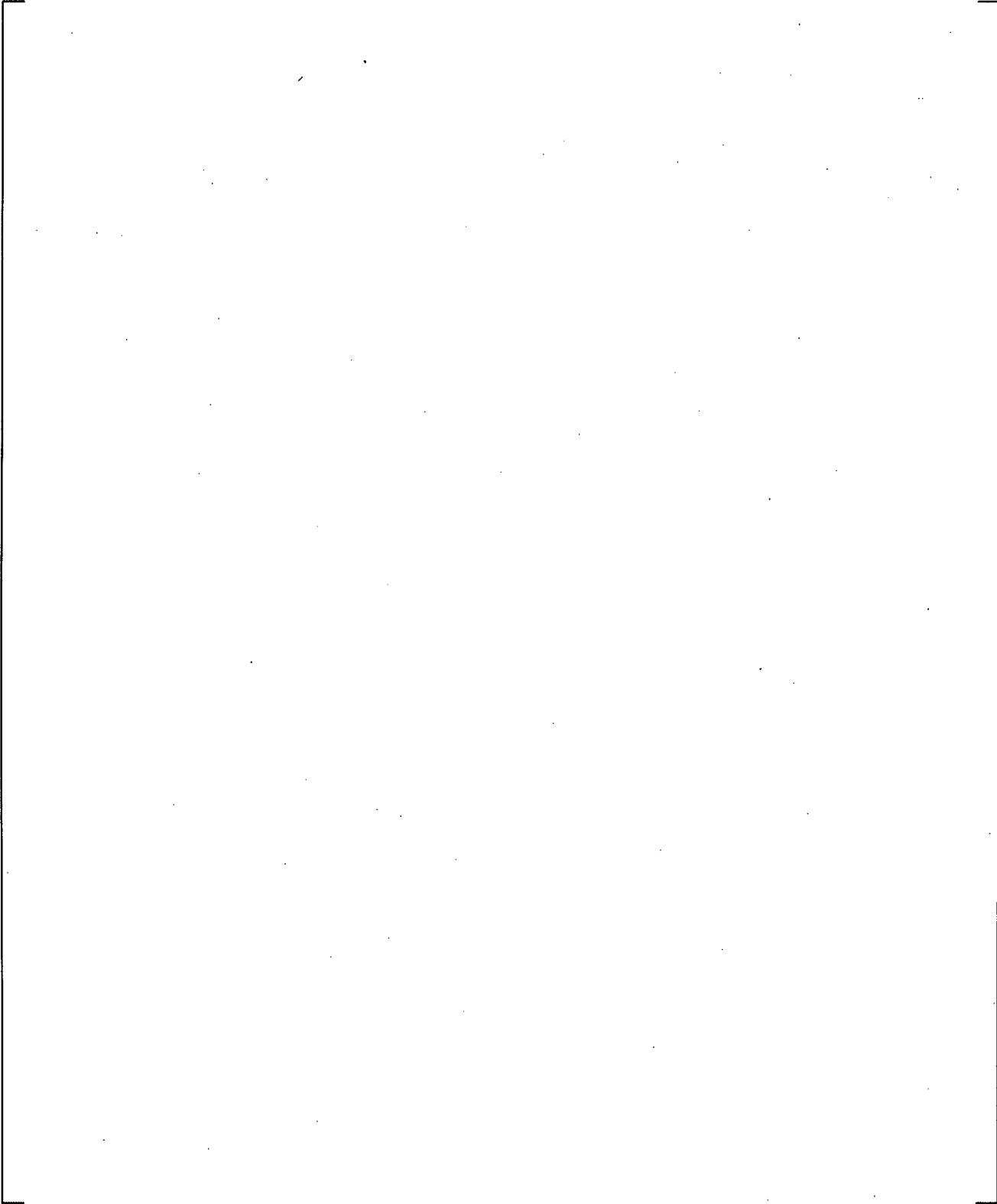


**Figure 24.7.1-24 Measured and Predicted Broken Loop Hot Leg Mixture Velocity**

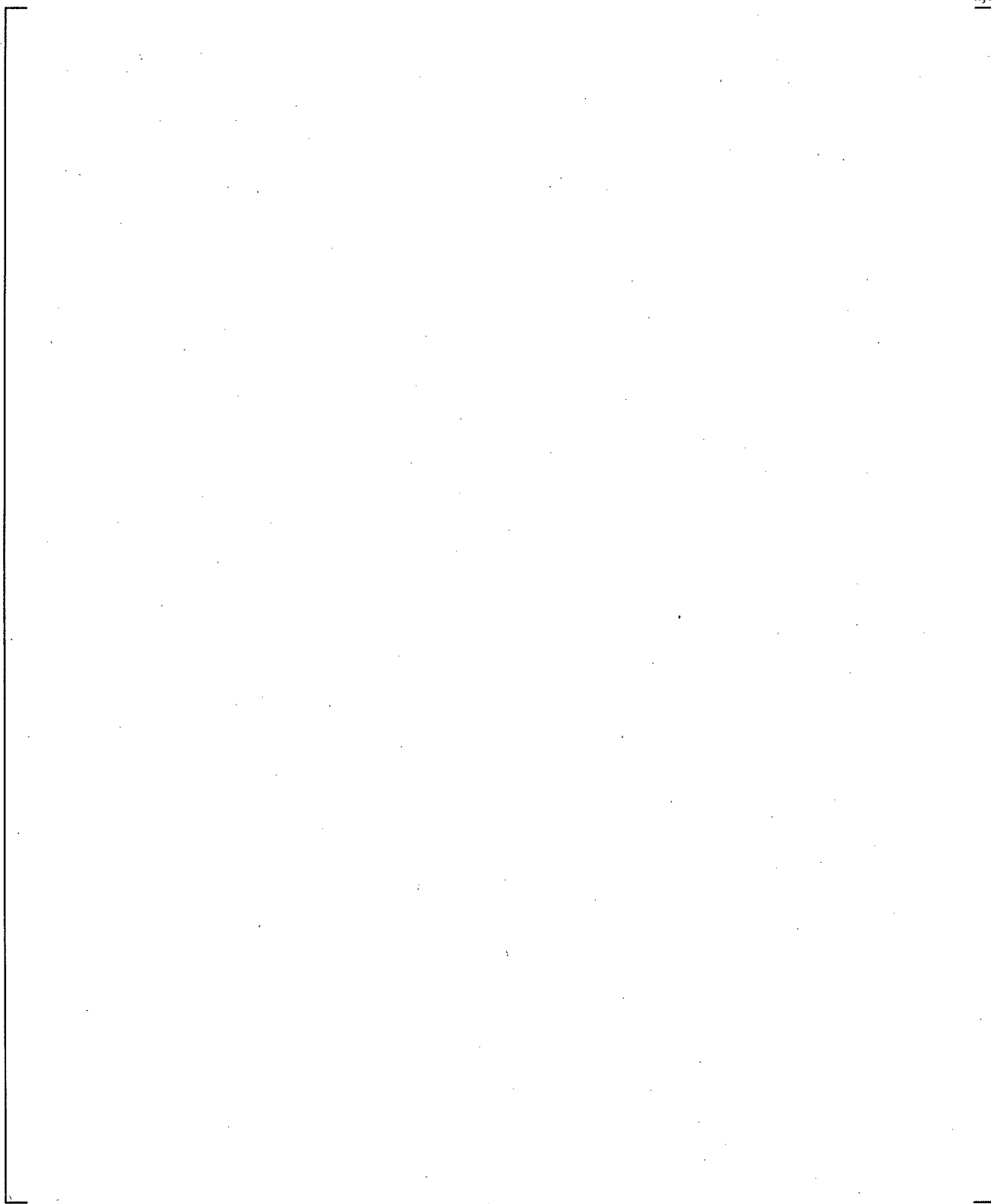


**Figure 24.7.1-25 Predicted Void Fraction in Upper Plenum at Loop Level**

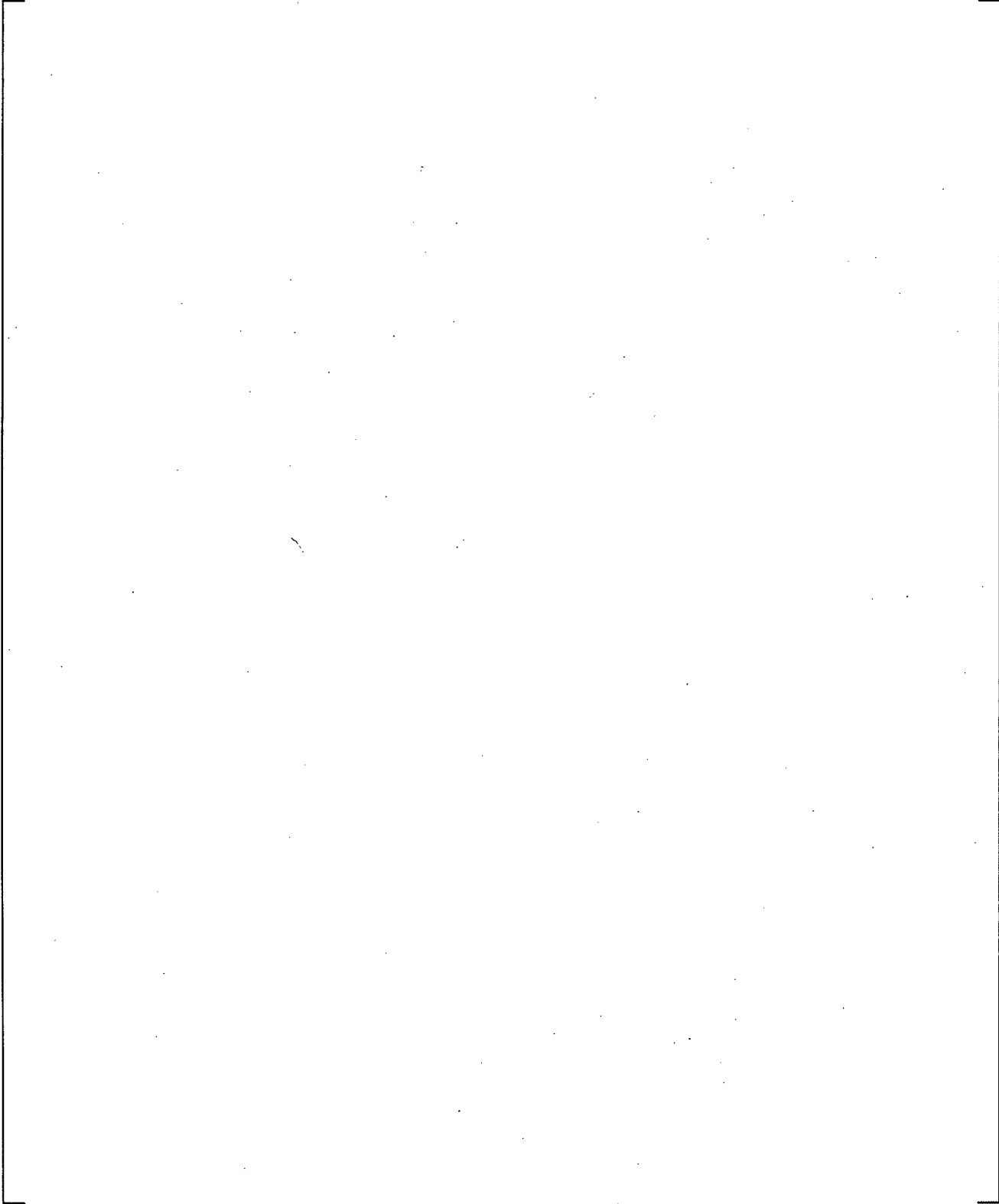


**Figure 24.7.1-26 Predicted Void Fraction in Upper Plenum above Upper Core Plate**

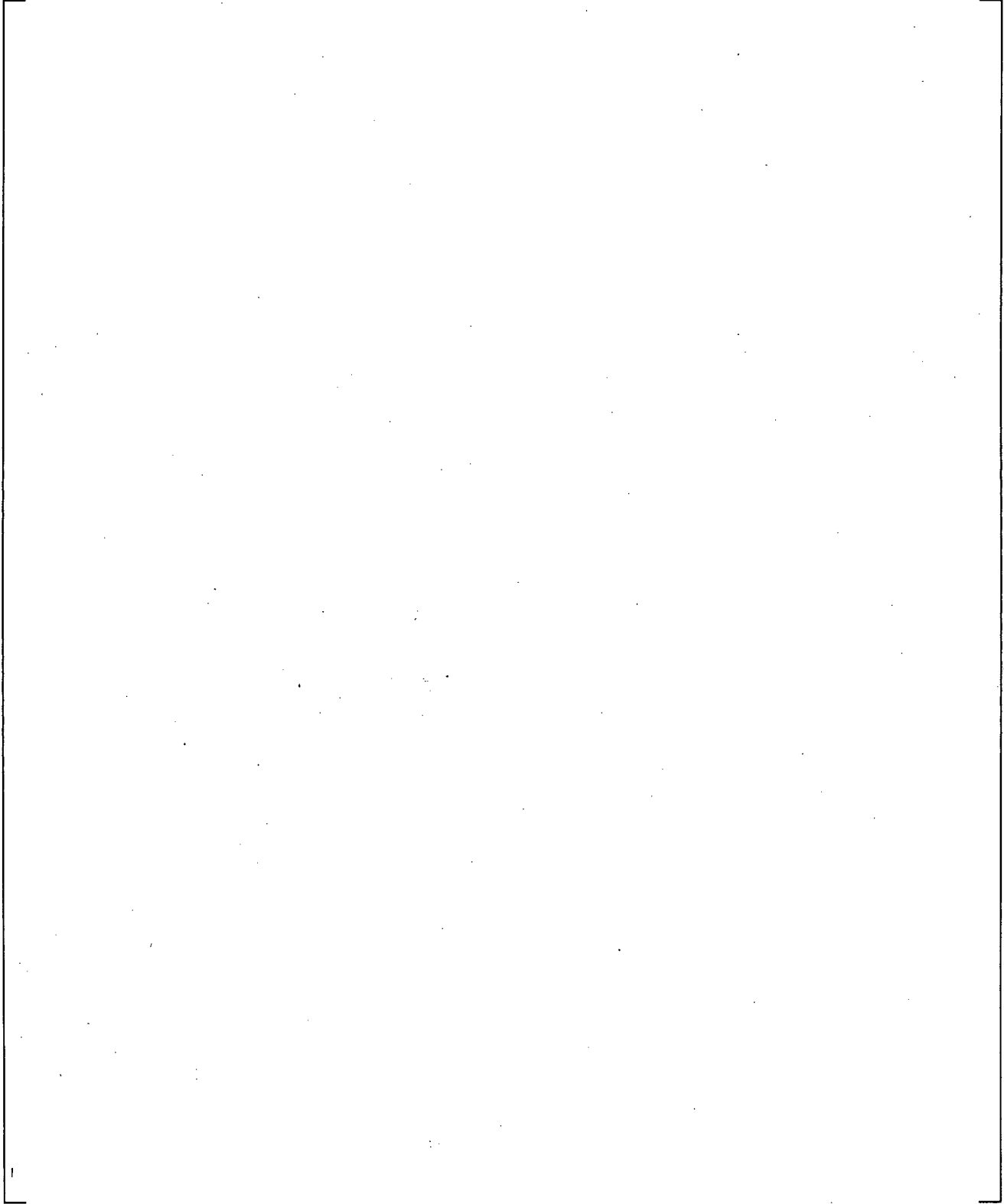


**Figure 24.7.1-27 Measured and Predicted Cold Leg Break Flowrate**

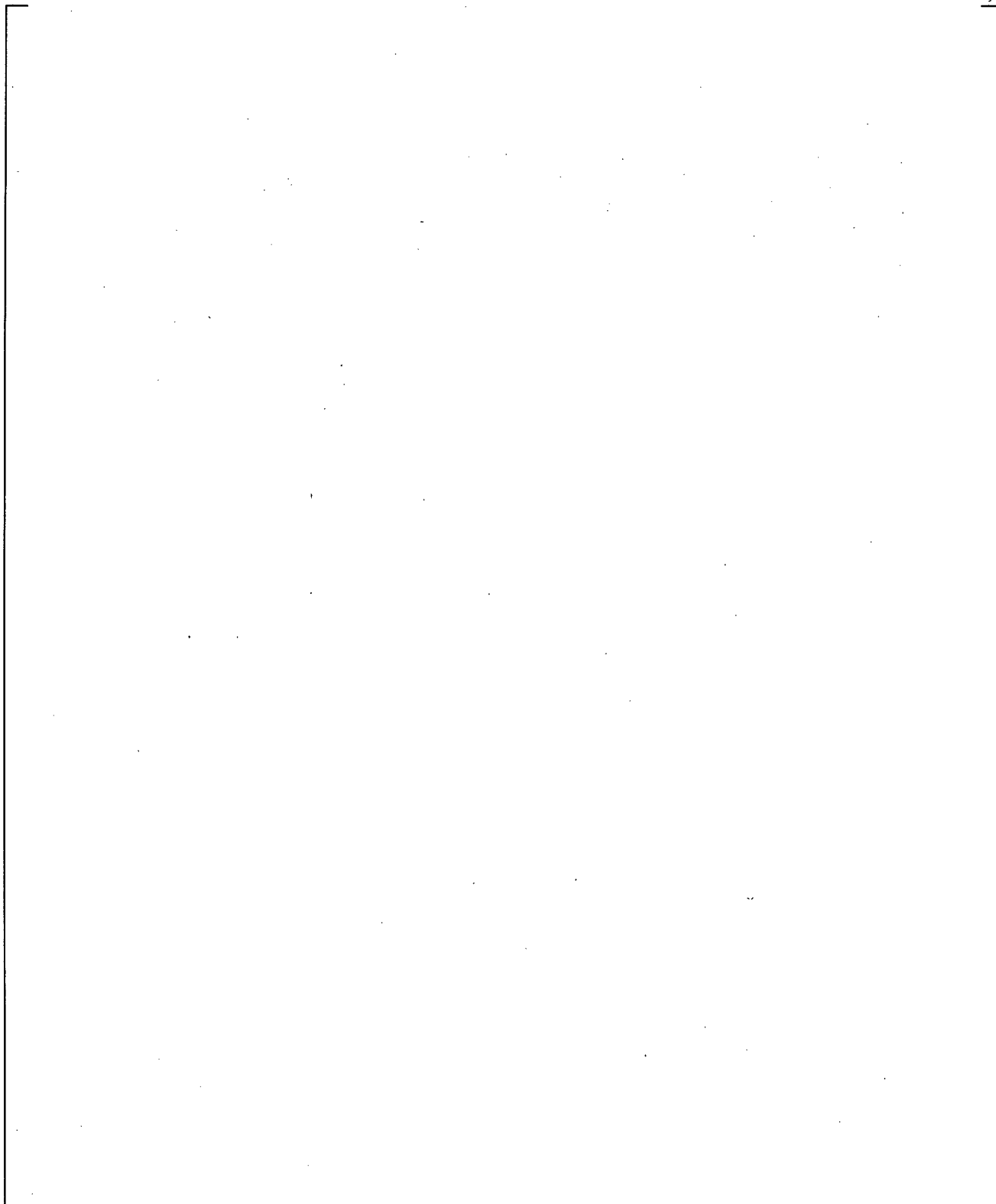


**Figure 24.7.1-28 Measured and Predicted Broken Cold Leg Mixture Density**

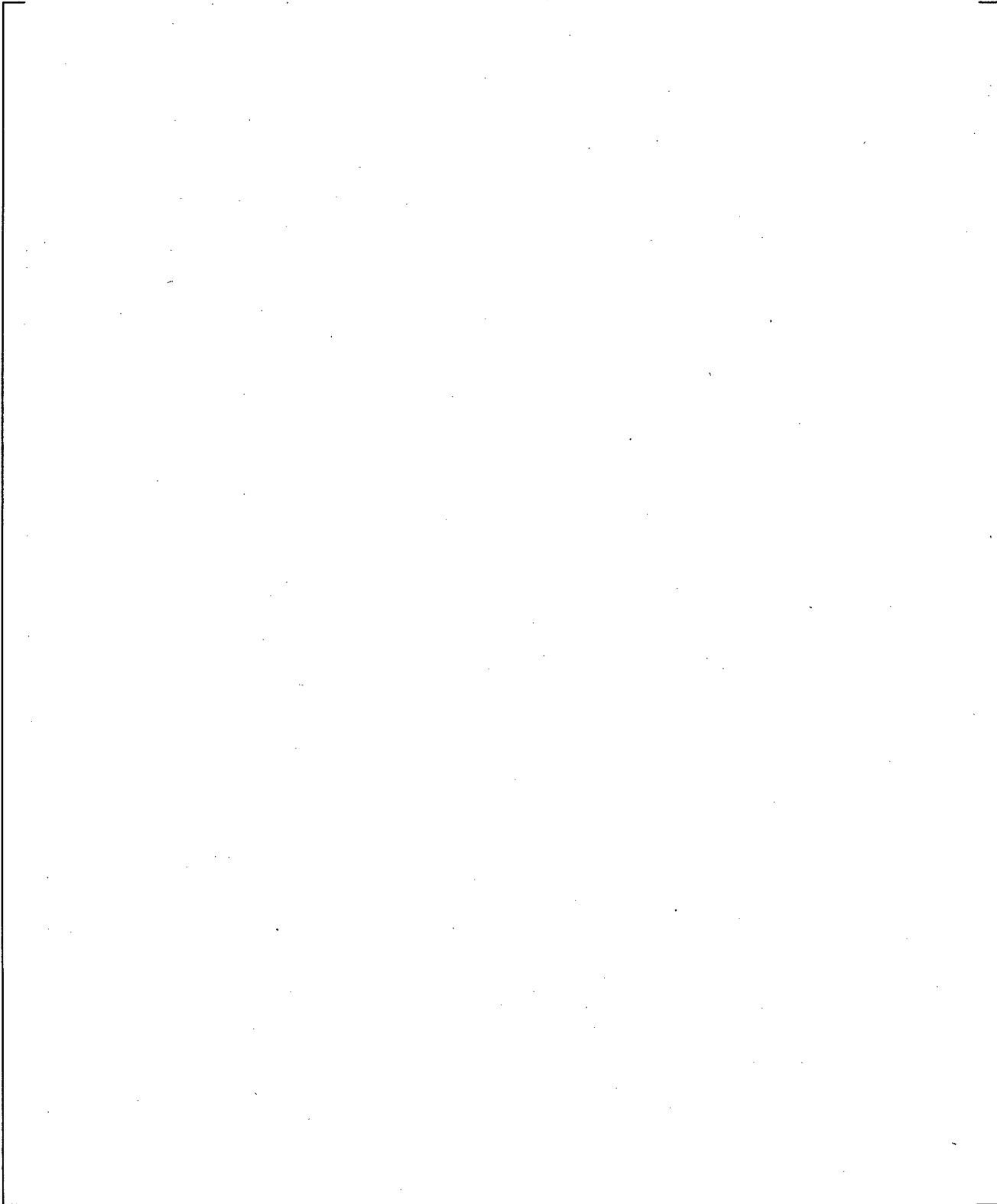


**Figure 24.7.1-29 Measured and Predicted Broken Cold Leg Mixture Velocity**

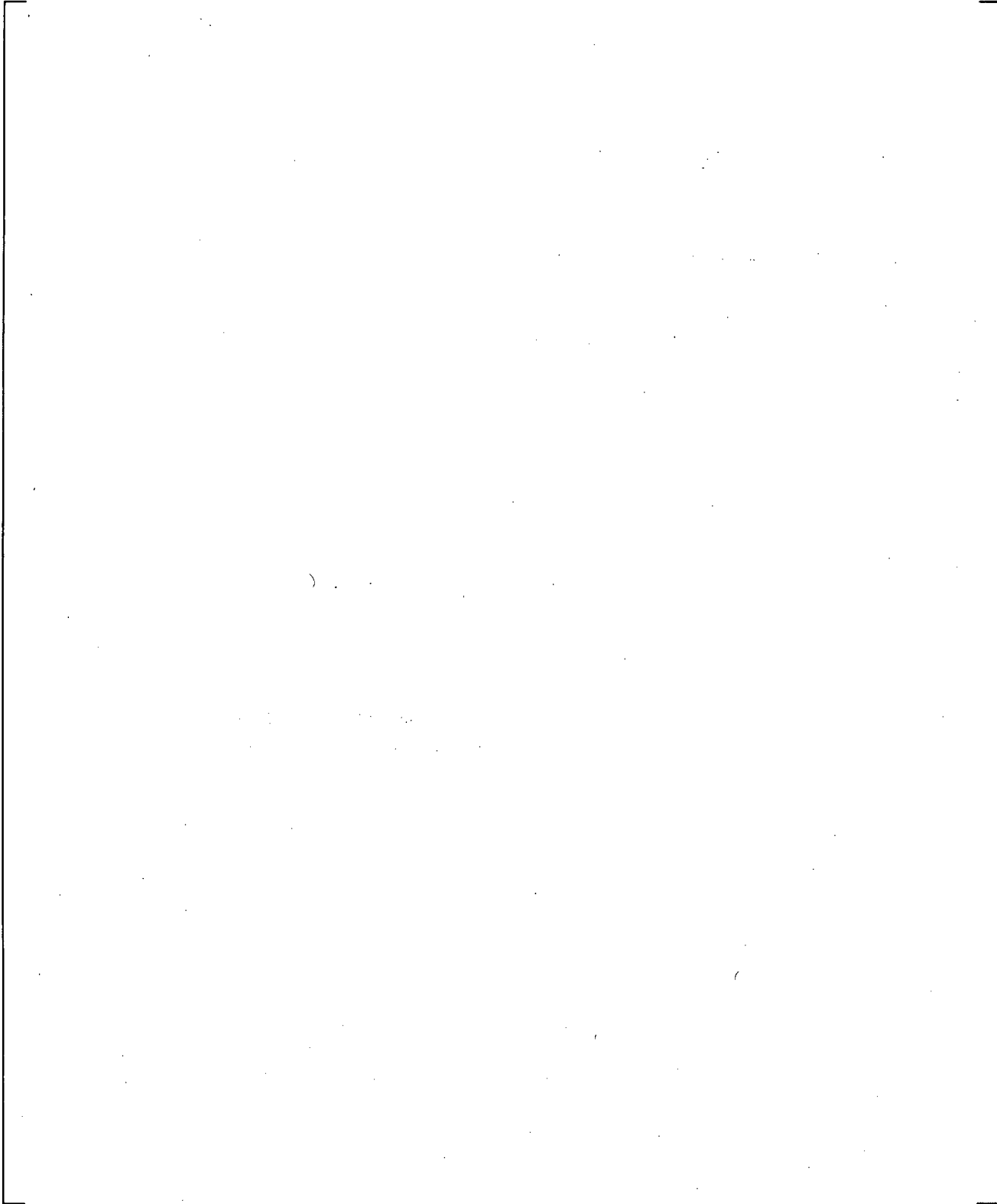


**Figure 24.7.1-30 Mid-Elevation Cladding Temperature Comparison in Sensitivity Run with CD2=1.05**

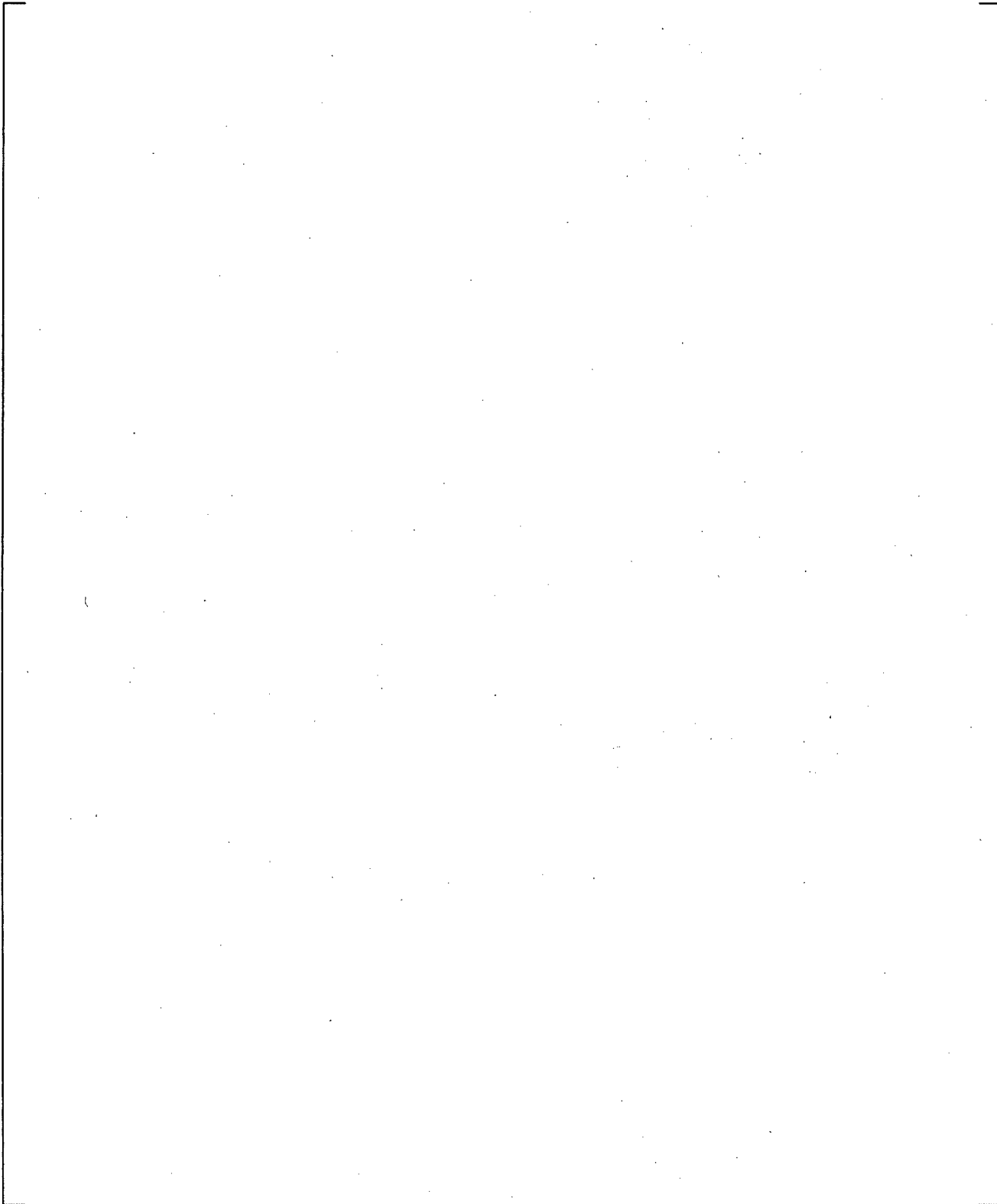


**Figure 24.7.1-31 Predicted Vapor Flowrate at Top and Bottom of Hot Assembly in Sensitivity Run with CD2=1.05**

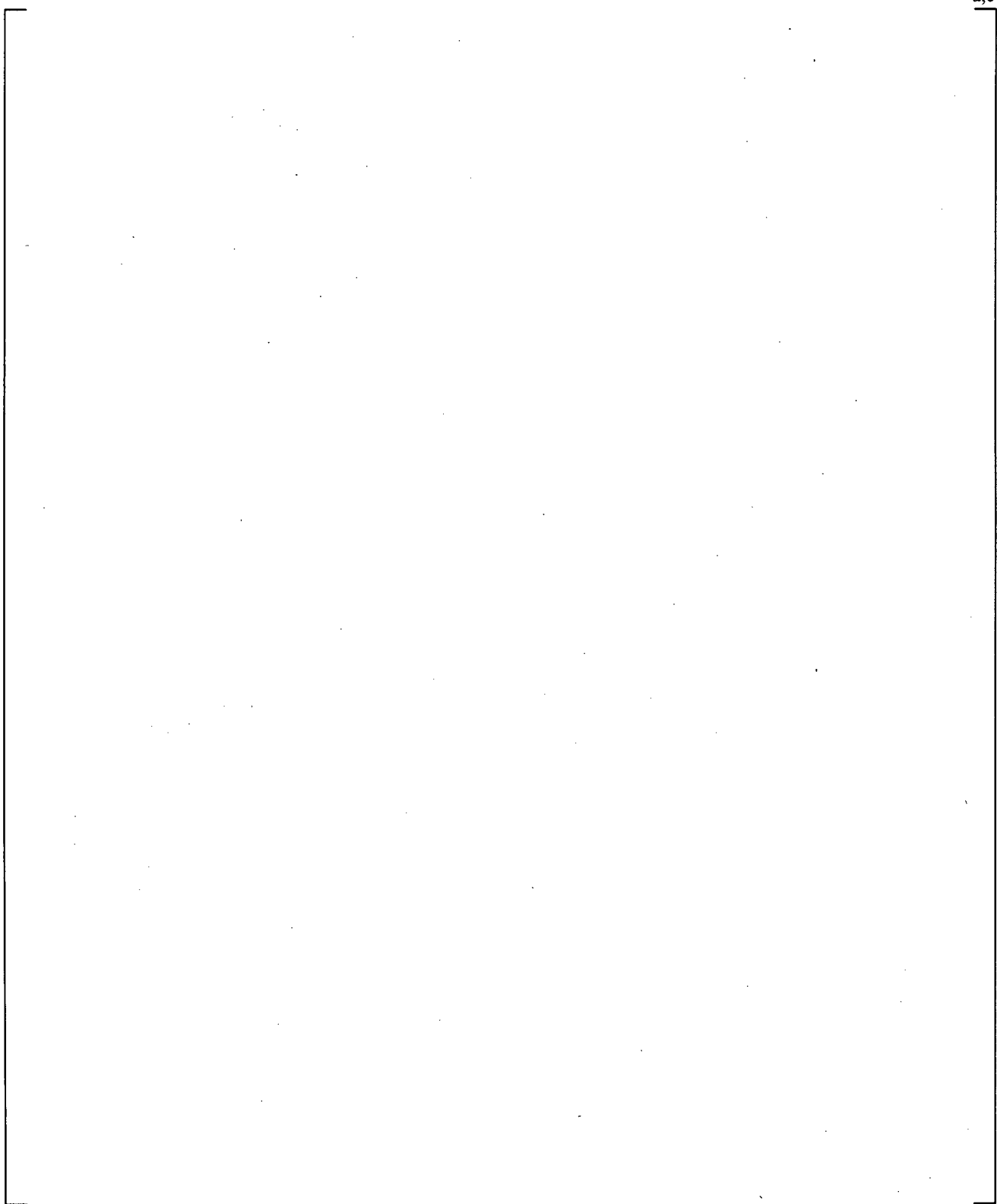


**Figure 24.7.1-32 Predicted Entrained Drop Flowrate at Top and Bottom of Hot Assembly in Sensitivity Run with CD2=1.05**

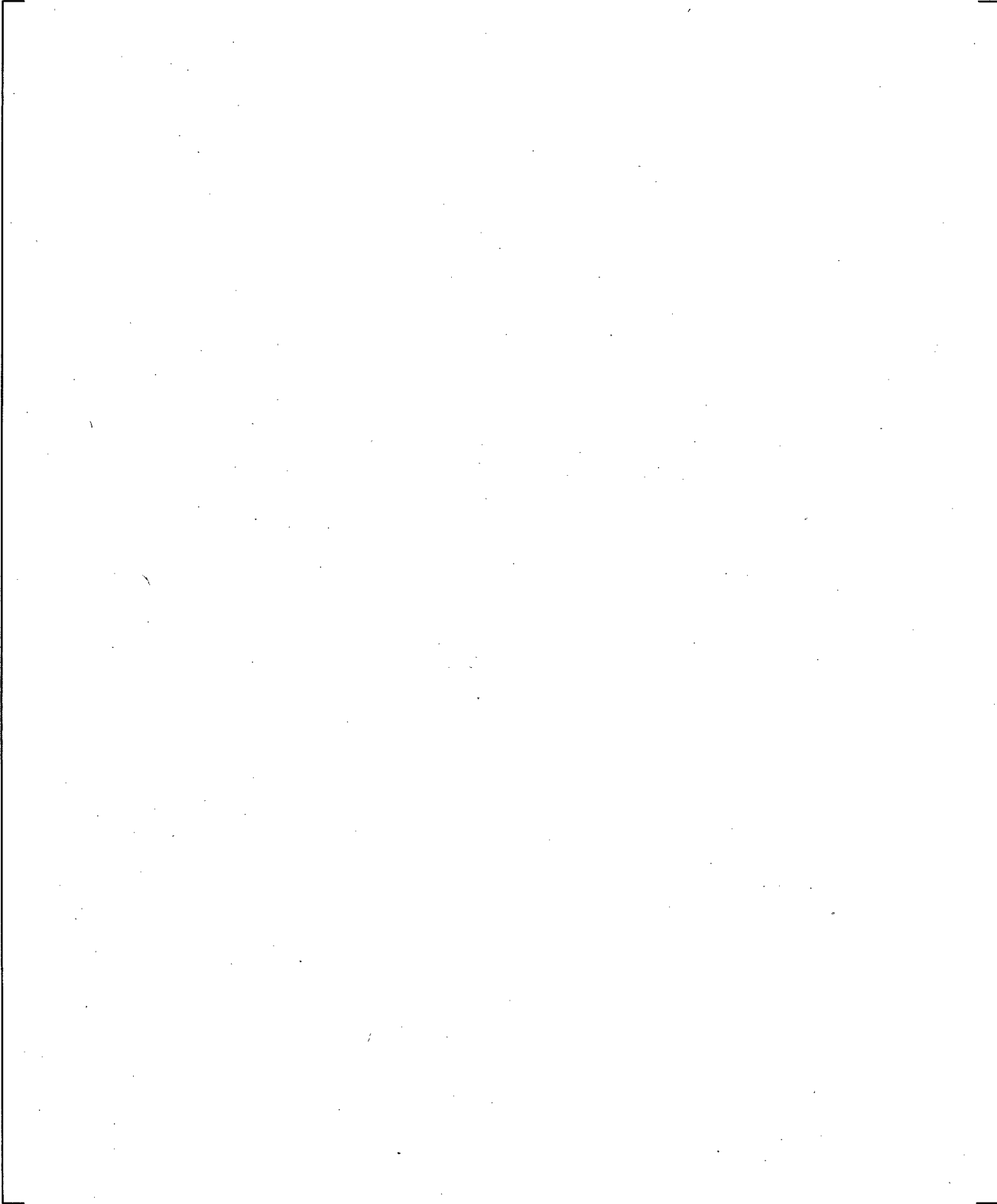


**Figure 24.7.1-33 Predicted Hot Rod Liquid Heat Transfer Coefficient at PCT Elevation in Sensitivity Run with CD2=1.05**

### 24.7.2 LOFT Test L2-5

The plots for this section are designated Figures 24.7.2-1 through 24.7.2-30. LOFT Test L2-5 (Bayless and Divine, 1982) was a pumps "off," intermediate power test. A summary of event times is given below, where end of blowdown is defined as the time when the system pressure reaches a minimum:

Event	Time (s)
Blowdown begins	0
Accumulator begins injecting	17
End of Blowdown/beginning of reflood	40
Accumulator empty (N2 injection)	50-60
Core quench	65

The prediction and data assessment will follow the same format as in LOFT Test L2-3.

#### Core Thermal-Hydraulics

The cladding temperature for LOFT Test L2-5 was [

] <sup>a,c</sup>

**System Behavior**

[

] <sup>a,c</sup>

**Loop Behavior: Intact loop**

[

] <sup>a,c</sup>

**Loop Behavior: Broken loop**

[

] <sup>a,c</sup>

[

] <sup>a,c</sup>

### **Sensitivity Studies**

Several studies were performed to examine what factors contribute most to the misprediction of core flow.

[

] <sup>a,c</sup>

[

]a,c

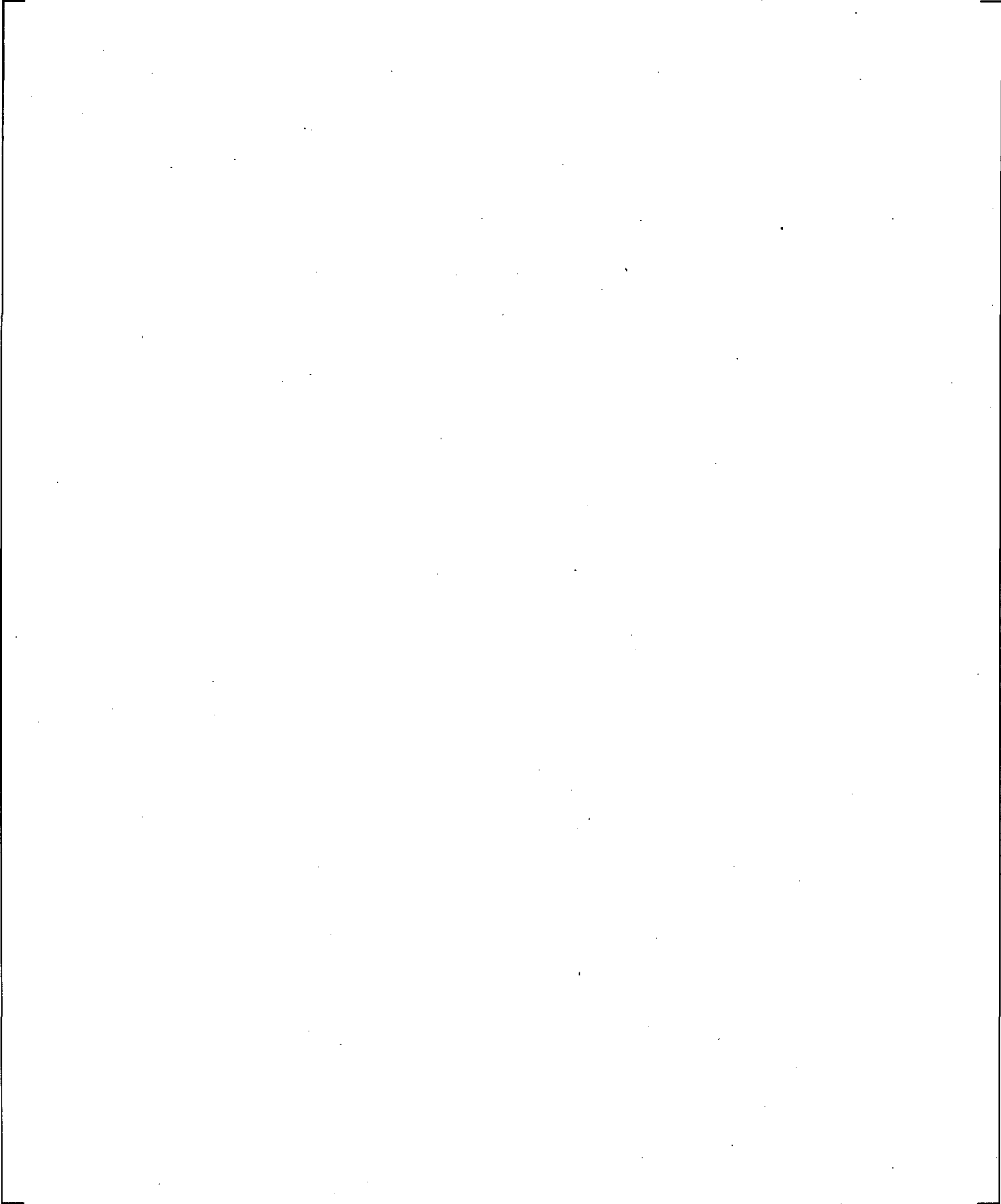


**Figure 24.7.2-1 Measured vs. Predicted Hot Rod Cladding Temperature**

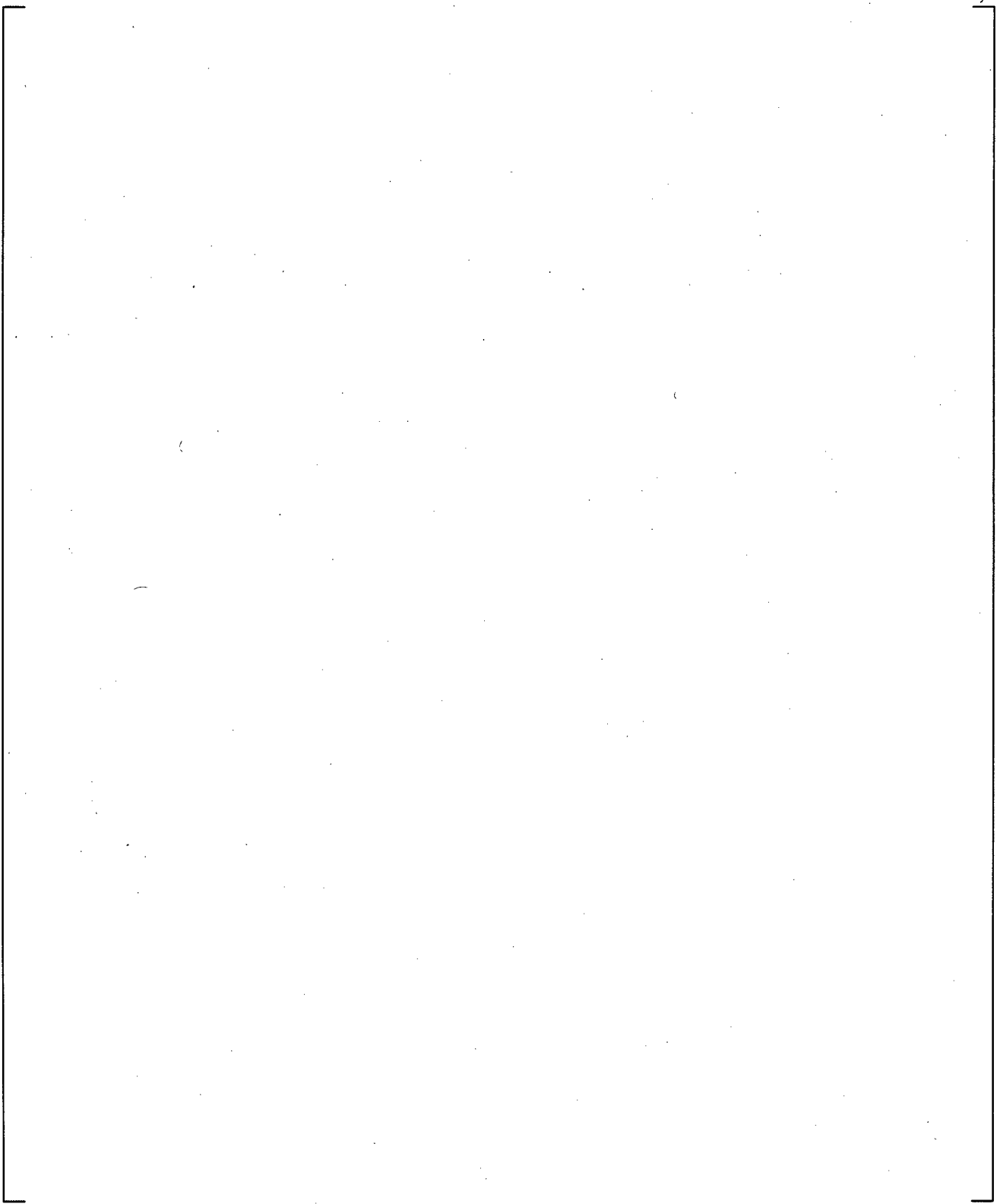


**Figure 24.7.2-2 Predicted Vapor Flowrate at Top and Bottom of Hot Assembly**

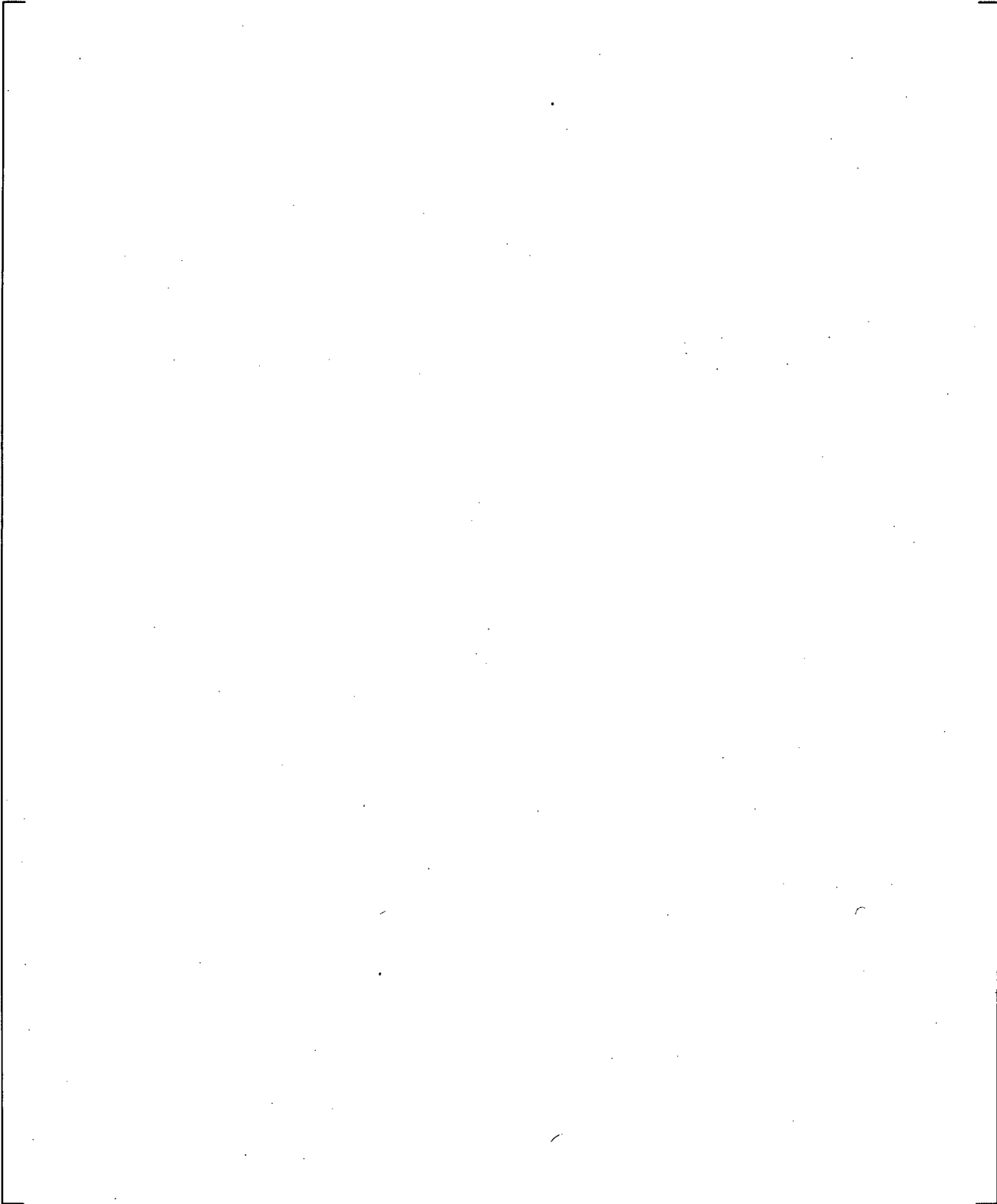


**Figure 24.7.2-3 Predicted Entrained Drop Flowrate at Top and Bottom of Hot Assembly**

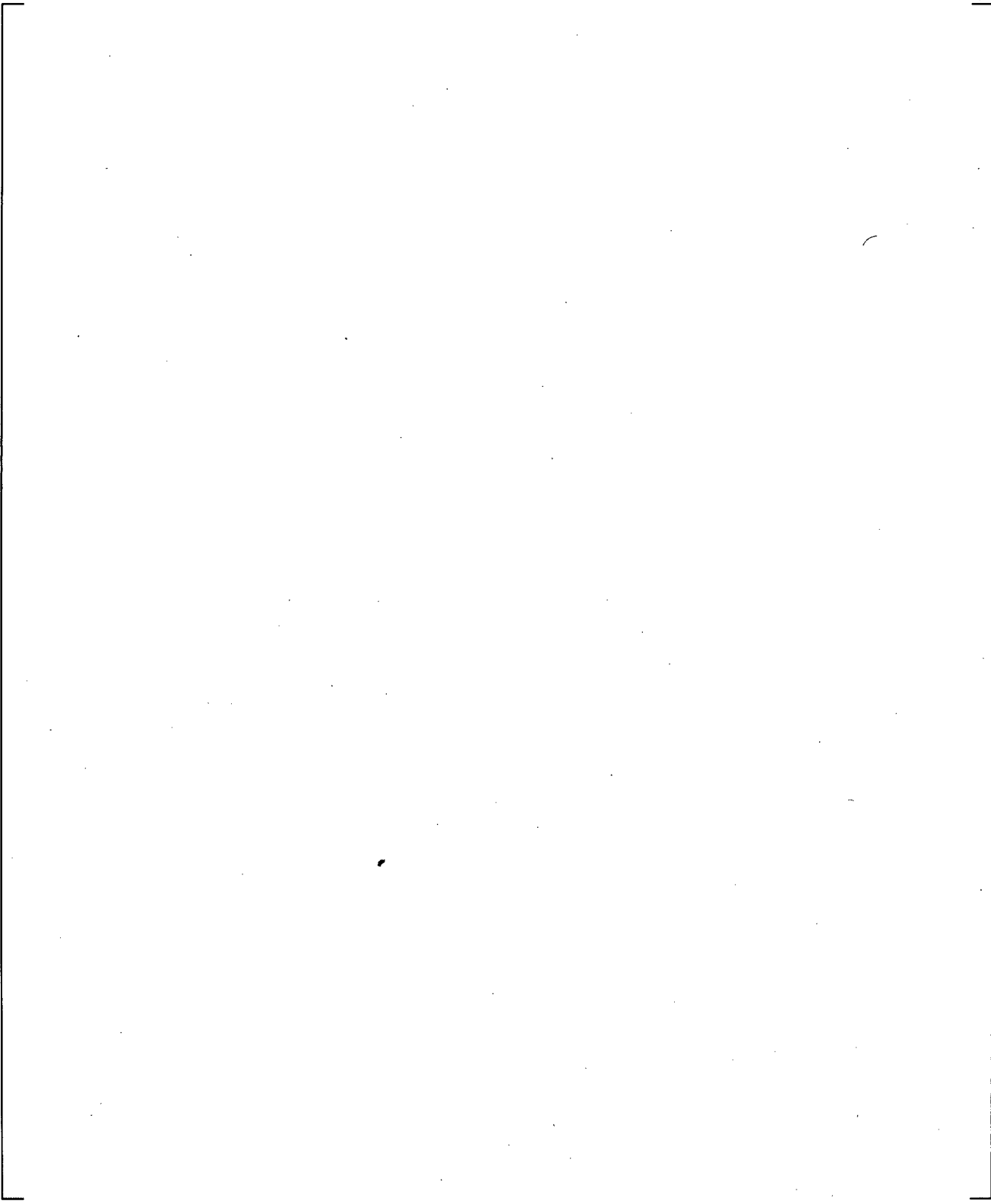


**Figure 24.7.2-4 LOFT L2-5 Data vs. Predicted Steam Temperature at Top of Hot Assembly**

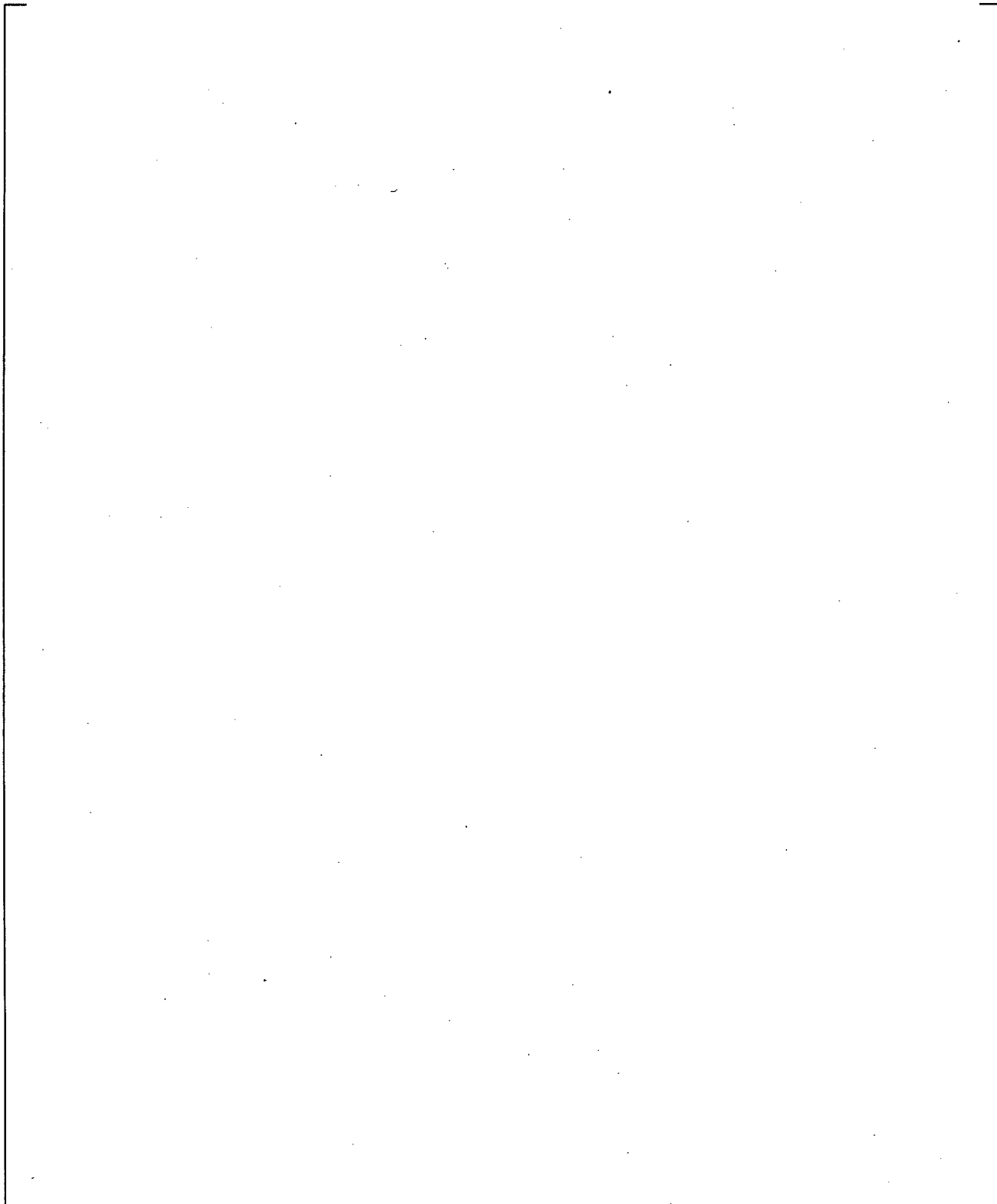


**Figure 24.7.2-5 LOFT L2-5 Data vs. Predicted Steam Temperature at Bottom of Hot Assembly**

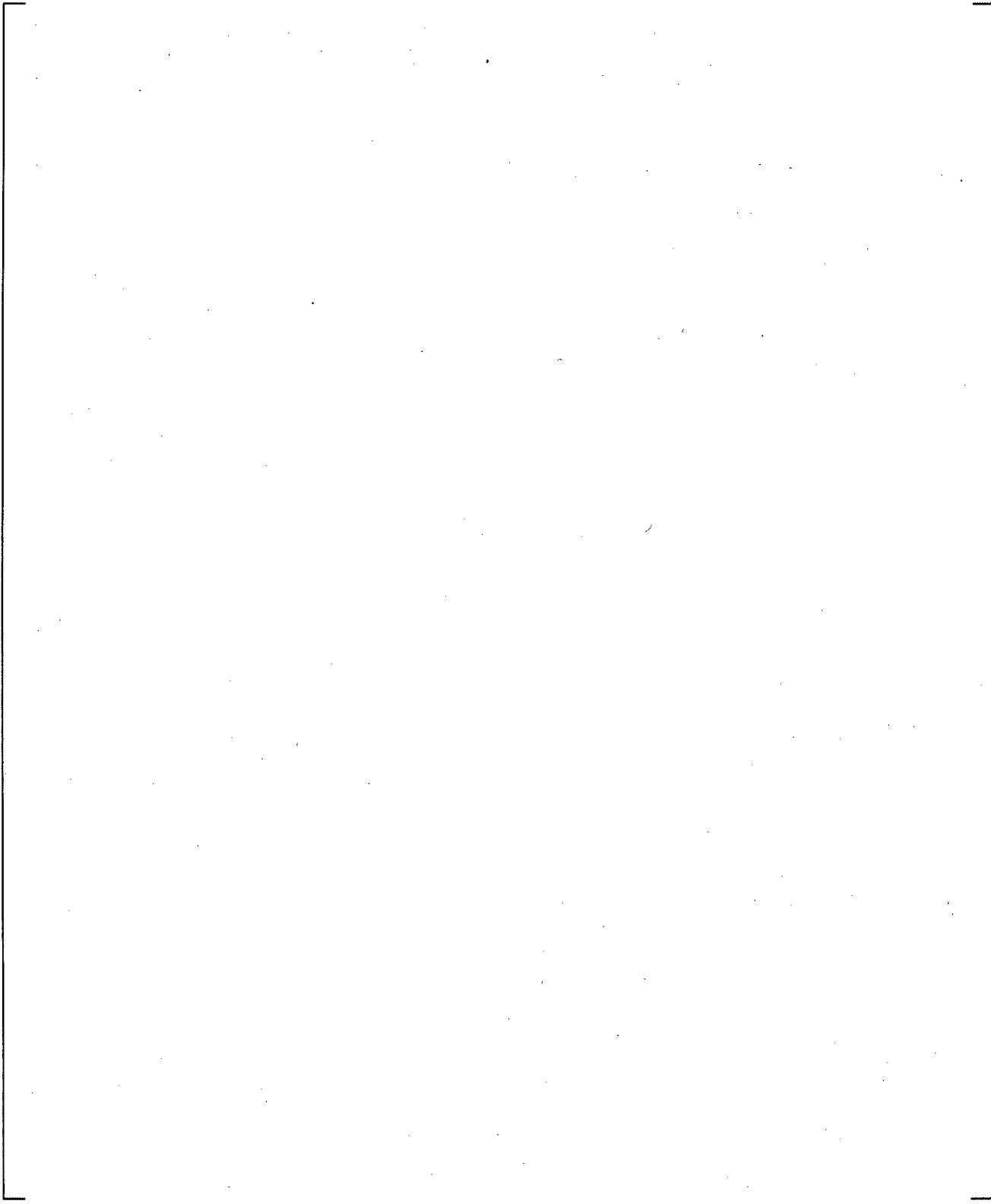


**Figure 24.7.2-6 Predicted Hot Rod Vapor Heat Transfer Coefficient at PCT Elevation**

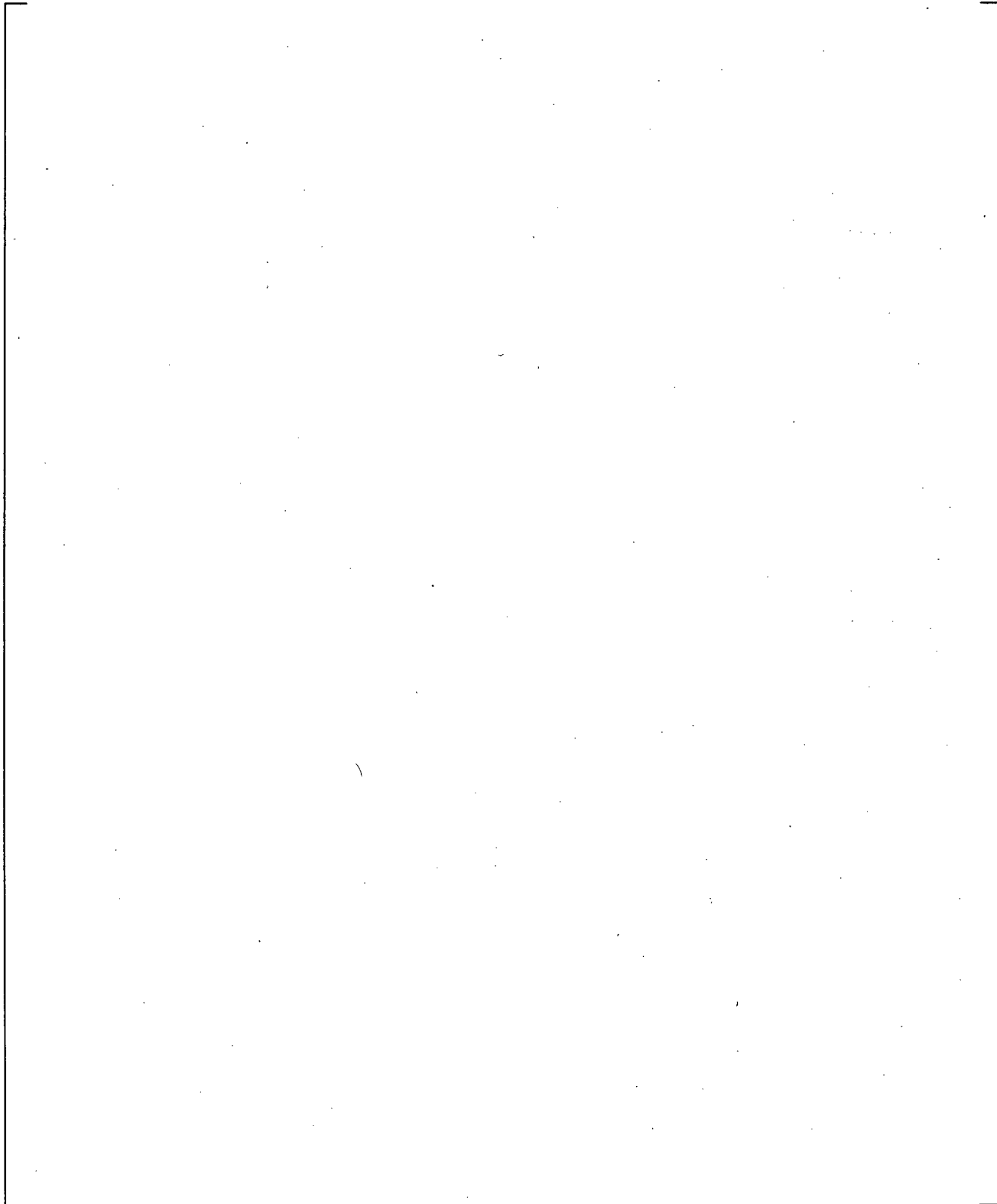


**Figure 24.7.2-7 Predicted Hot Rod Liquid Heat Transfer Coefficient at PCT Elevation**

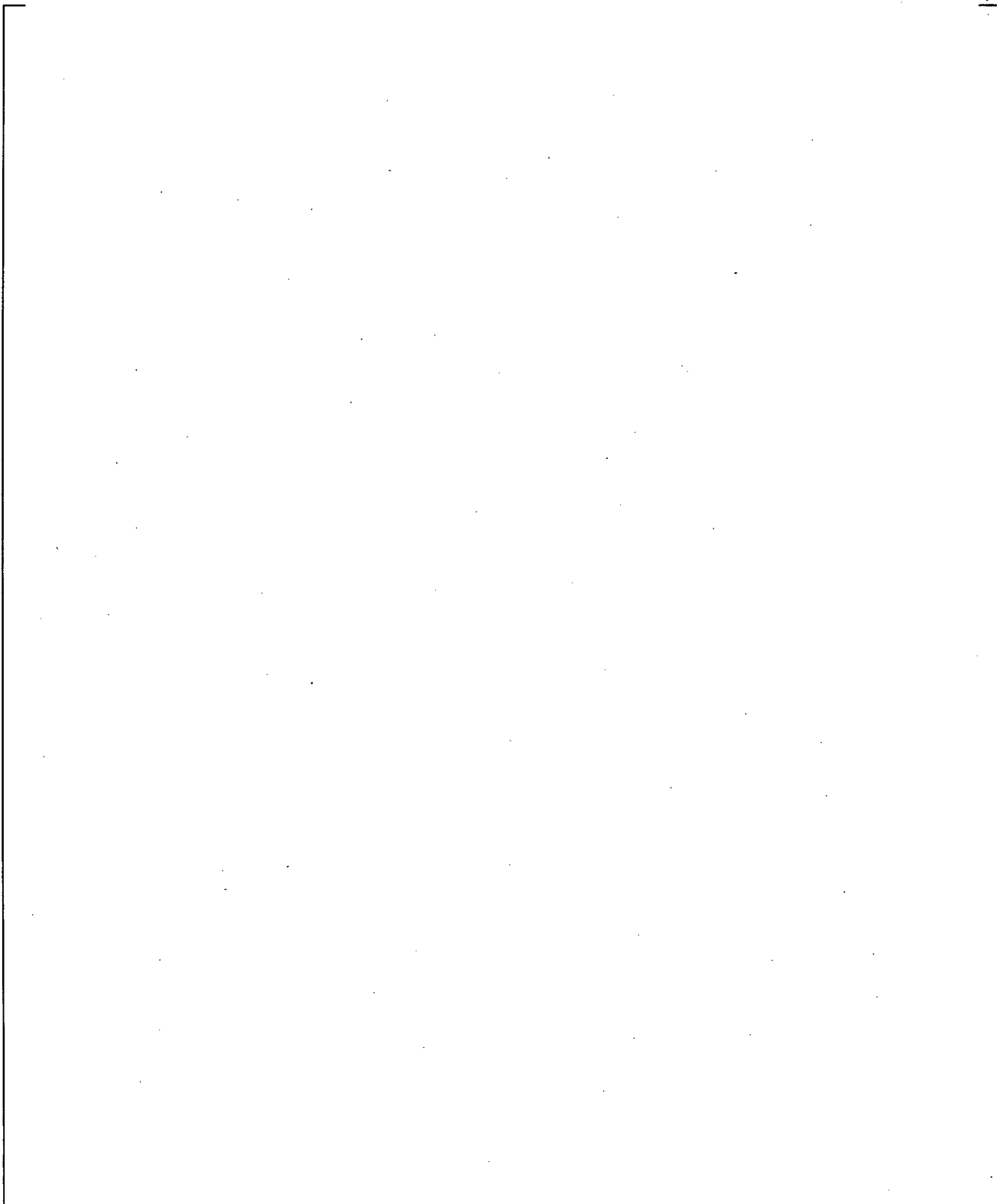


**Figure 24.7.2-7a Predicted Hot Rod Liquid Heat Transfer Coefficient at PCT Elevation (with Expanded Scale)**

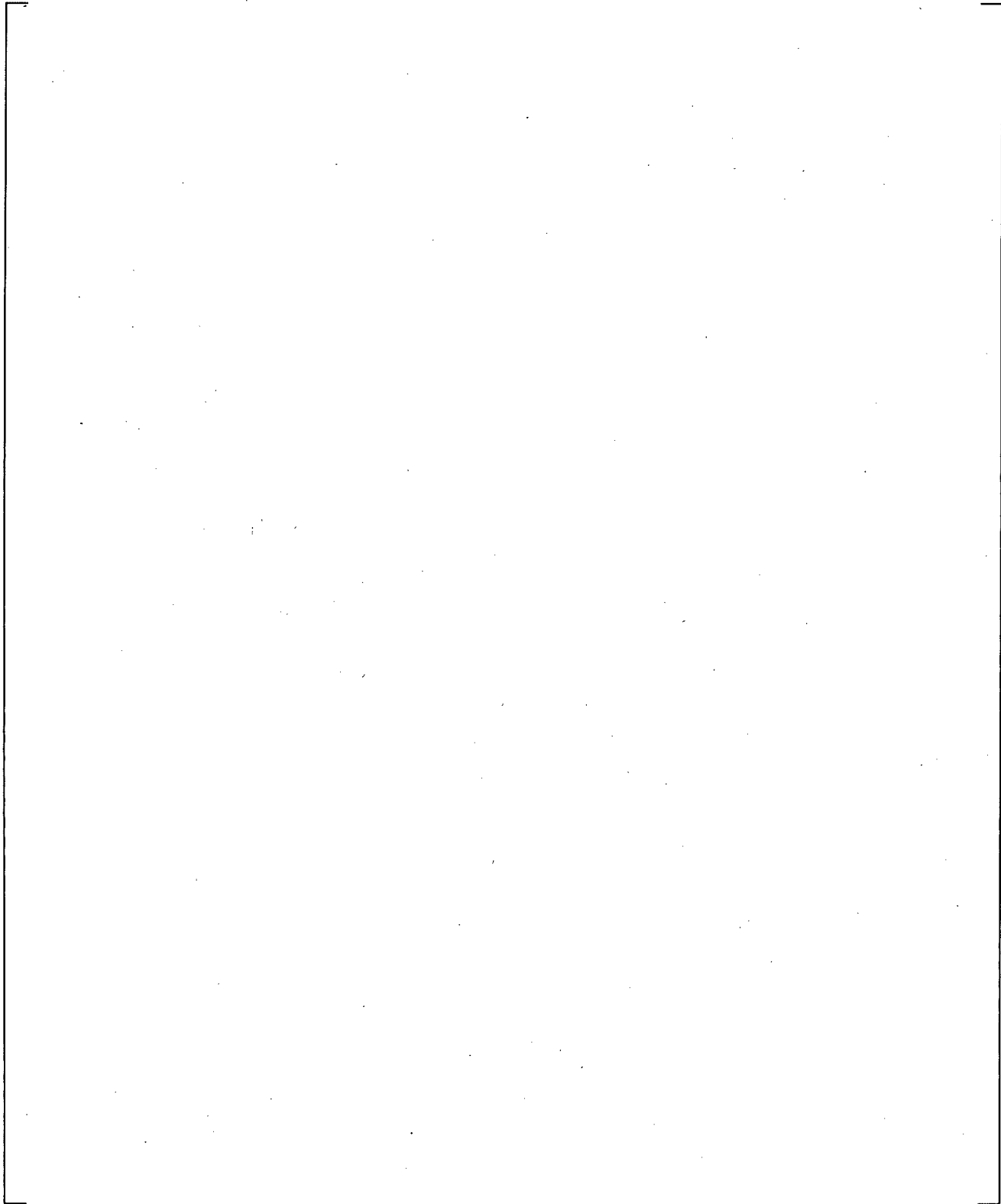


**Figure 24.7.2-8 Measured and Predicted Intact Loop Pressure**

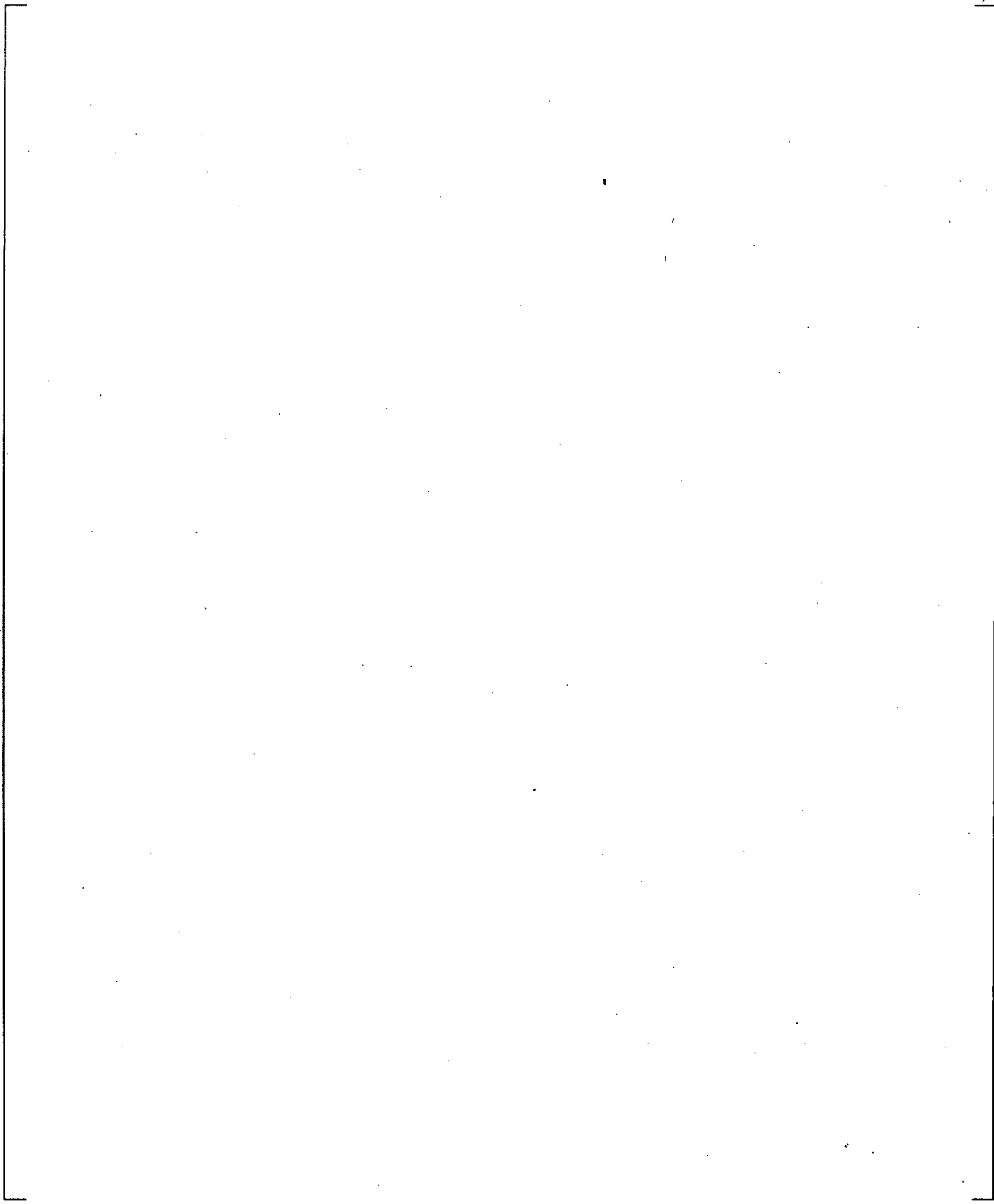


**Figure 24.7.2-9 Predicted Downcomer Collapsed Liquid Level (1- Intact, 2-Broken side)**

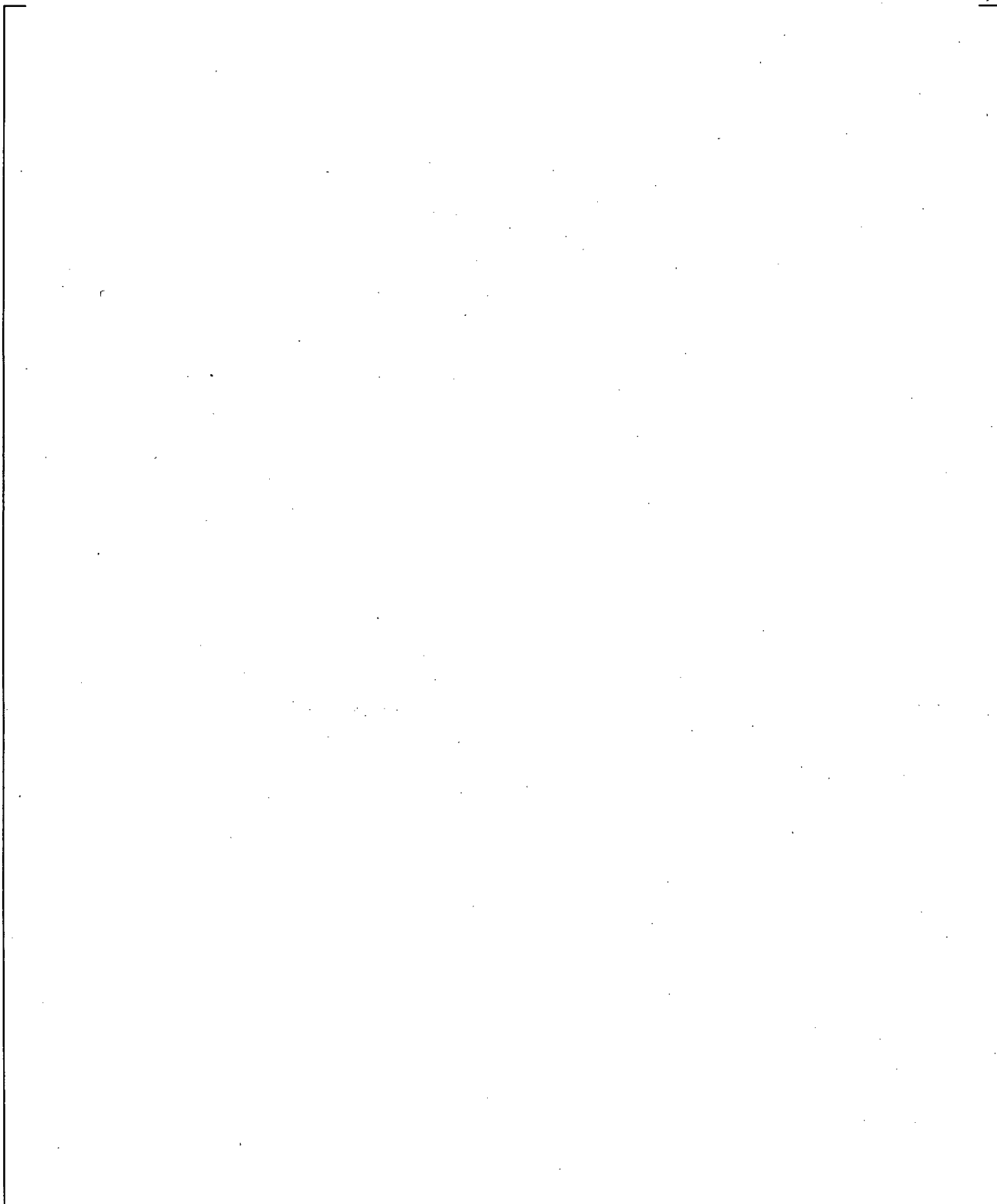


**Figure 24.7.2-10 Predicted and Measured Core Collapsed Liquid Level (Line 2-Estimated from the Liquid Detector)**

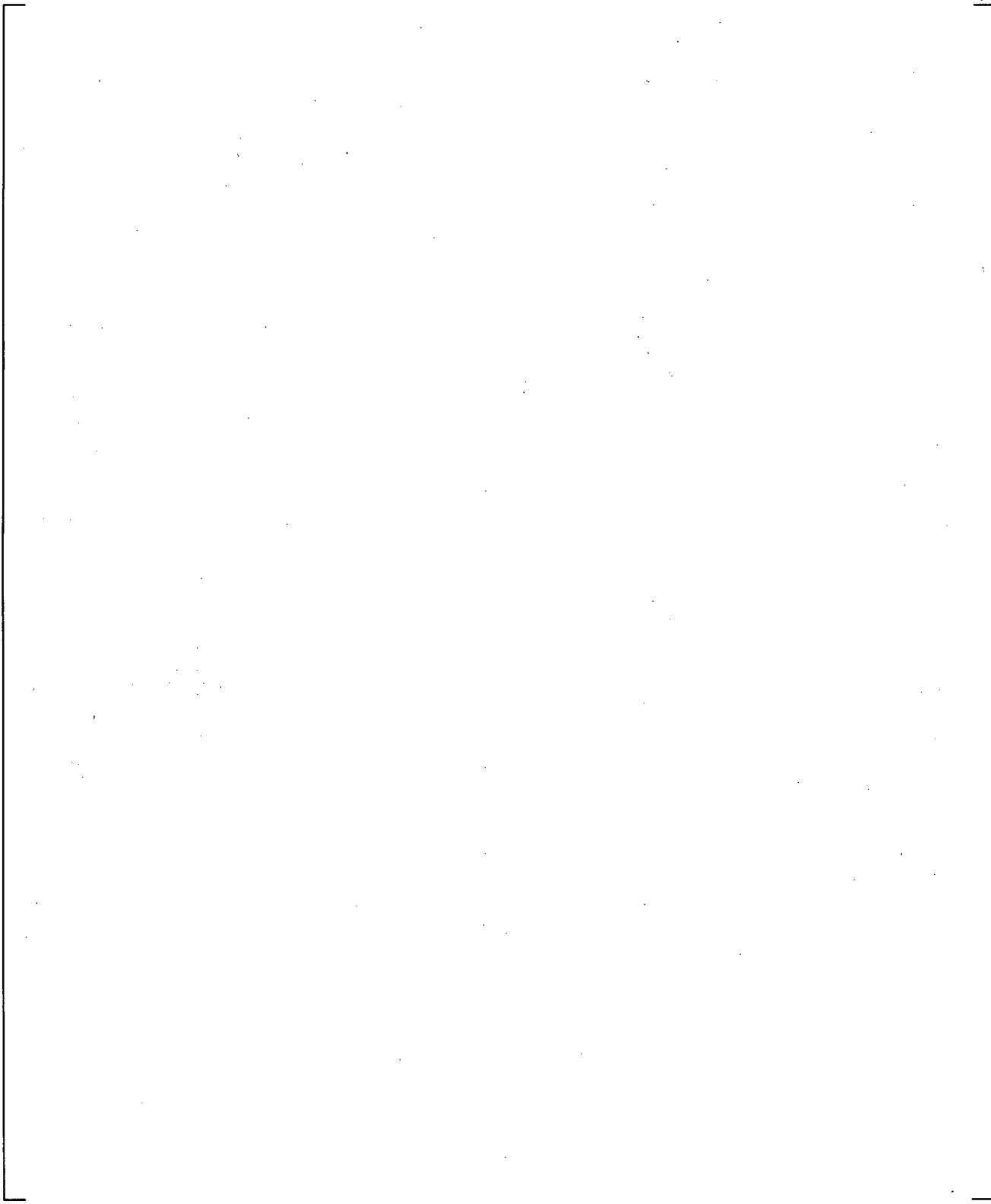


**Figure 24.7.2-11 Predicted Upper Plenum Collapsed Liquid Level**

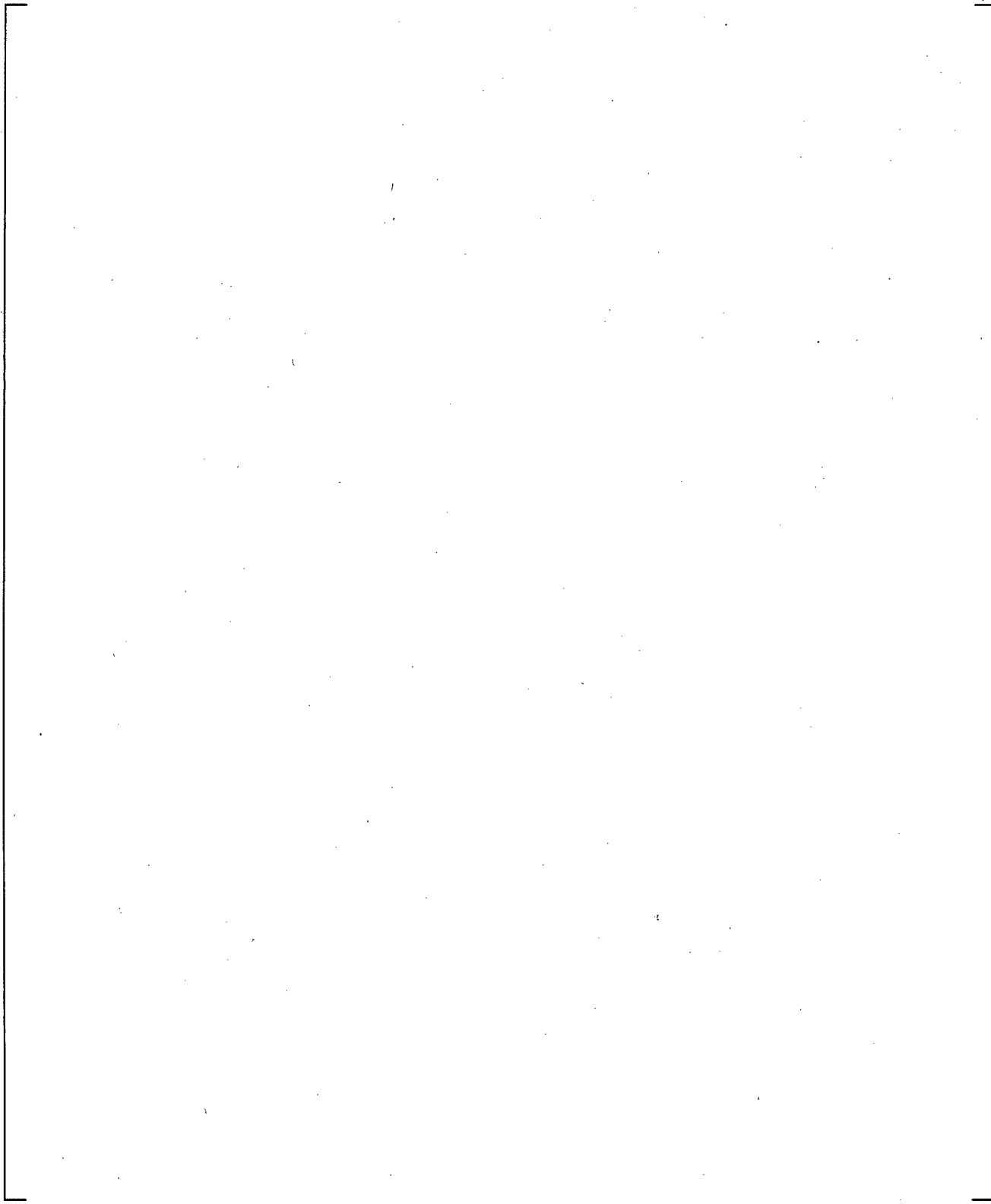


**Figure 24.7.2-12 Measured and Predicted Intact Loop Hot Leg Flowrate**

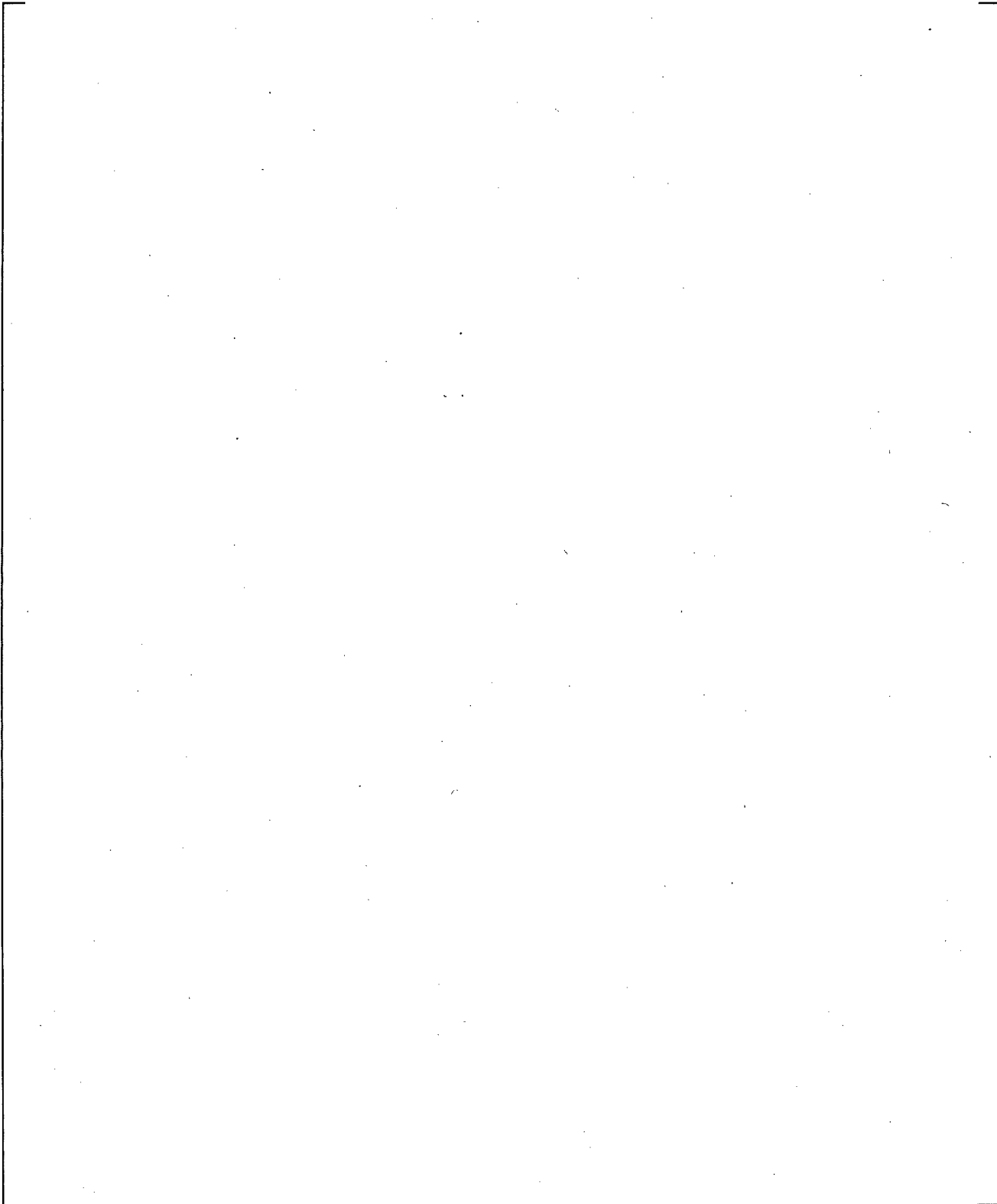


**Figure 24.7.2-13 Measured and Predicted Intact Loop Hot Leg Mixture Density**

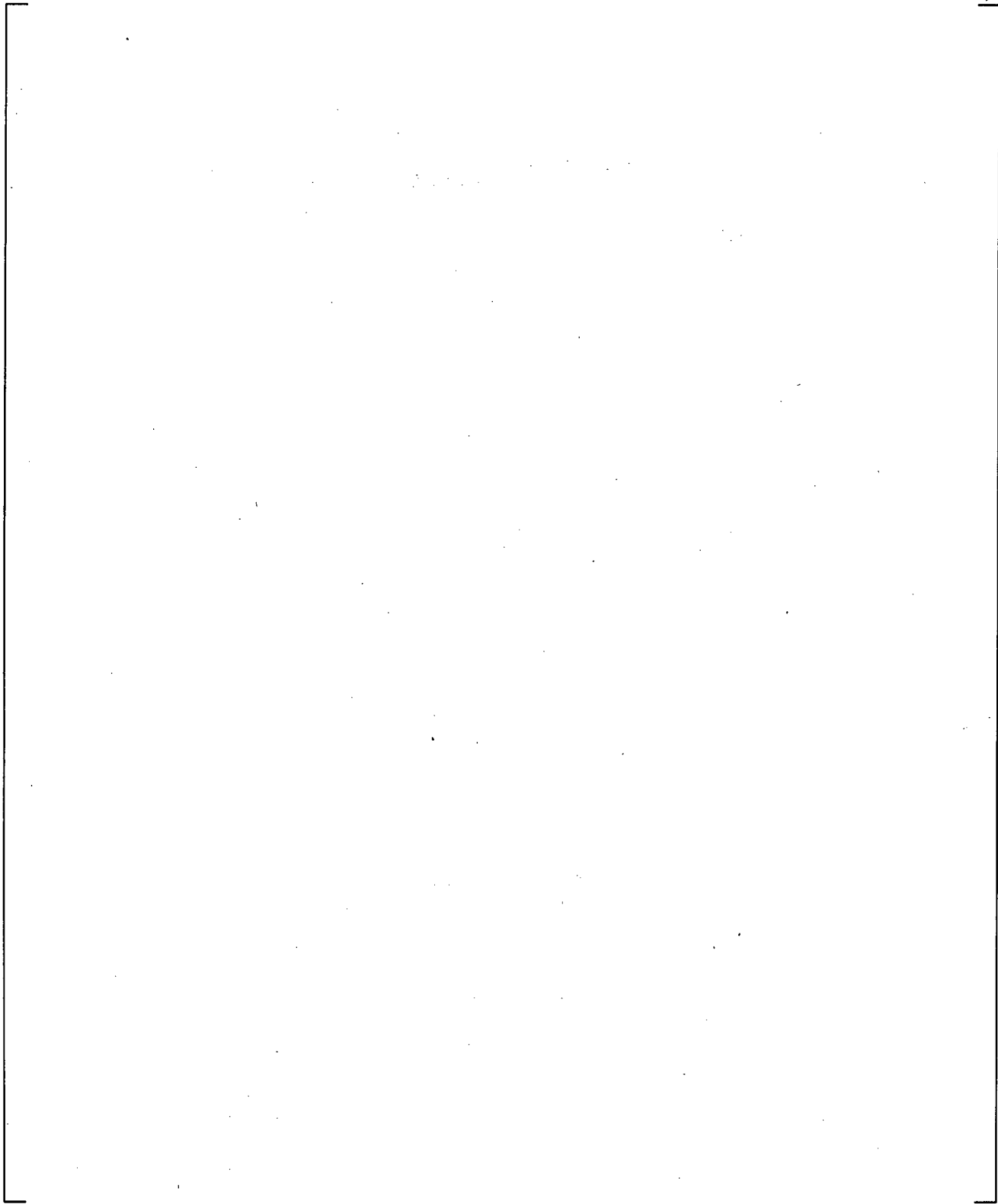


**Figure 24.7.2-14 Measured and Predicted Intact Loop Hot Leg Mixture Velocity**

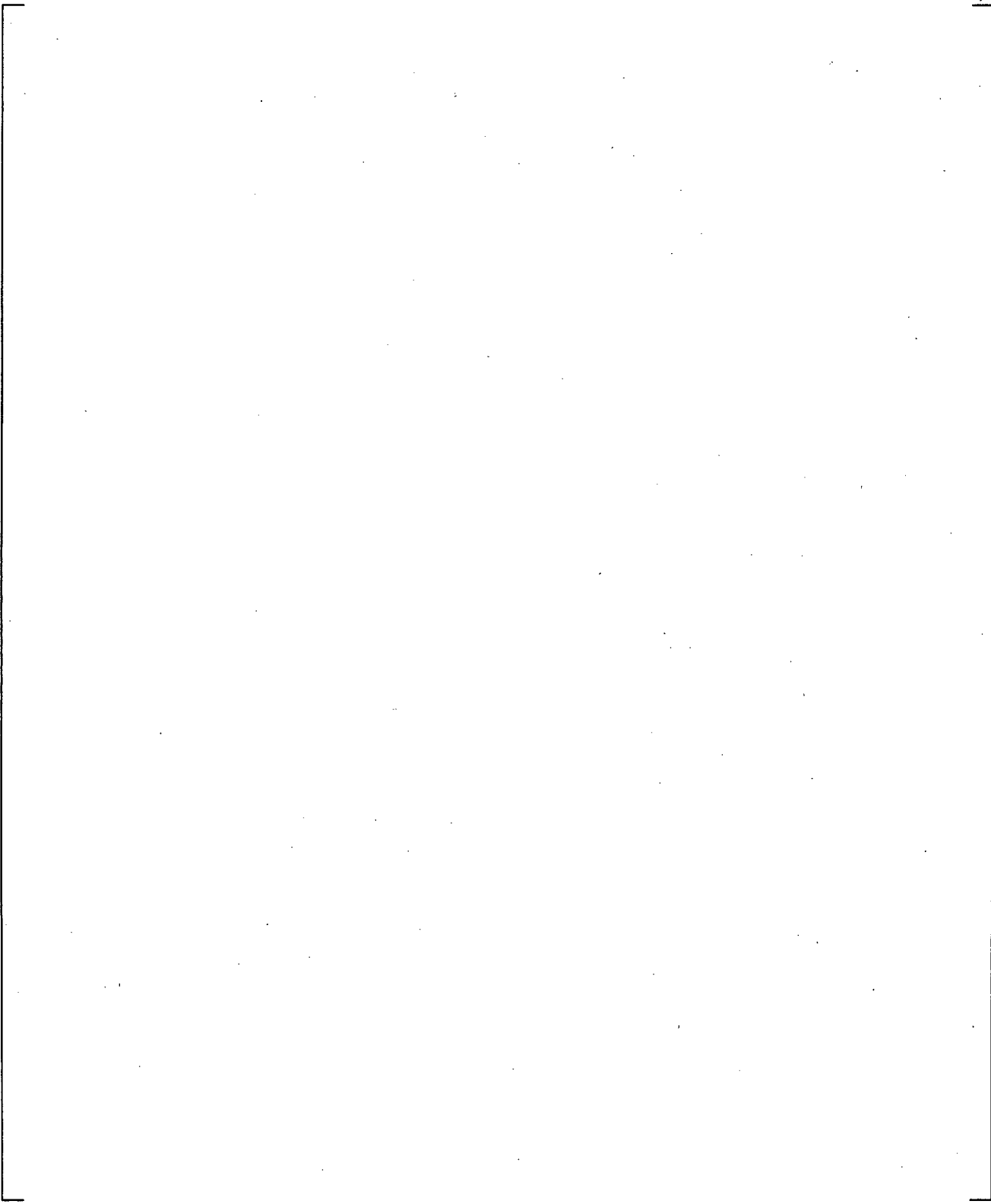


**Figure 24.7.2-15 Measured and Predicted Intact Loop Cold Leg Flowrate**

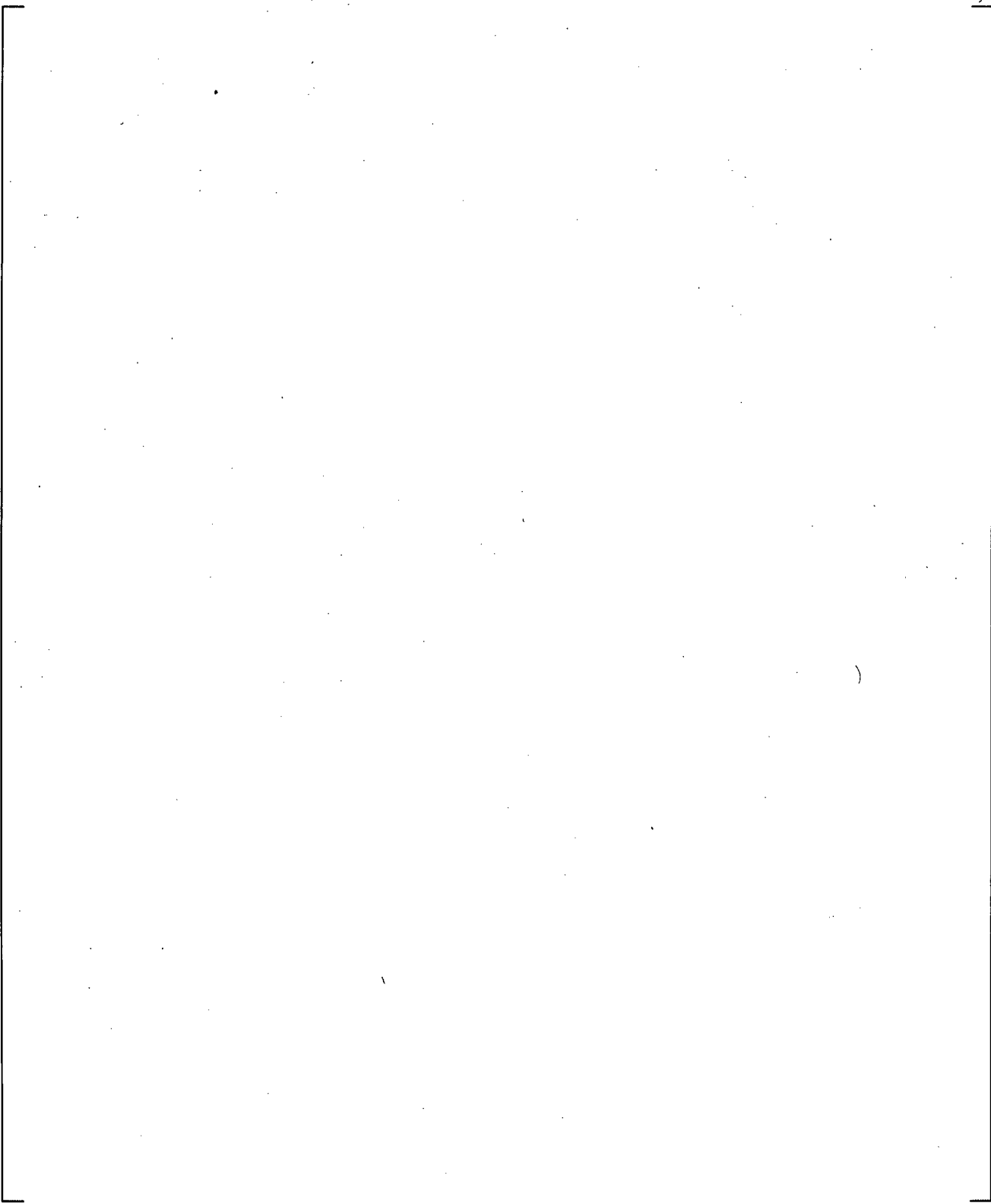


**Figure 24.7.2-16 Measured and Predicted Intact Loop Cold Leg Flowrate**

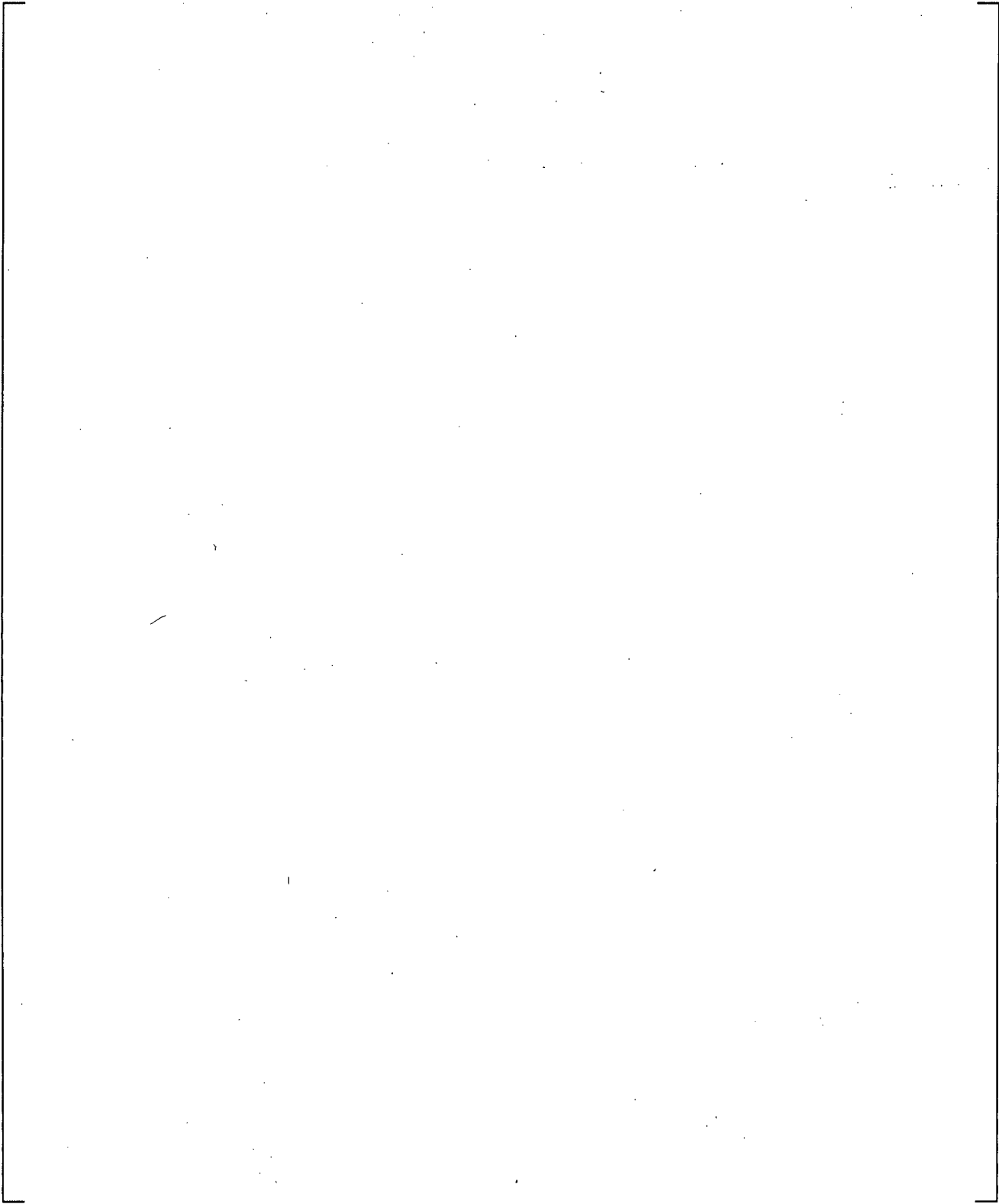


**Figure 24.7.2-17 Measured and Predicted Intact Loop Cold Leg Mixture Density**

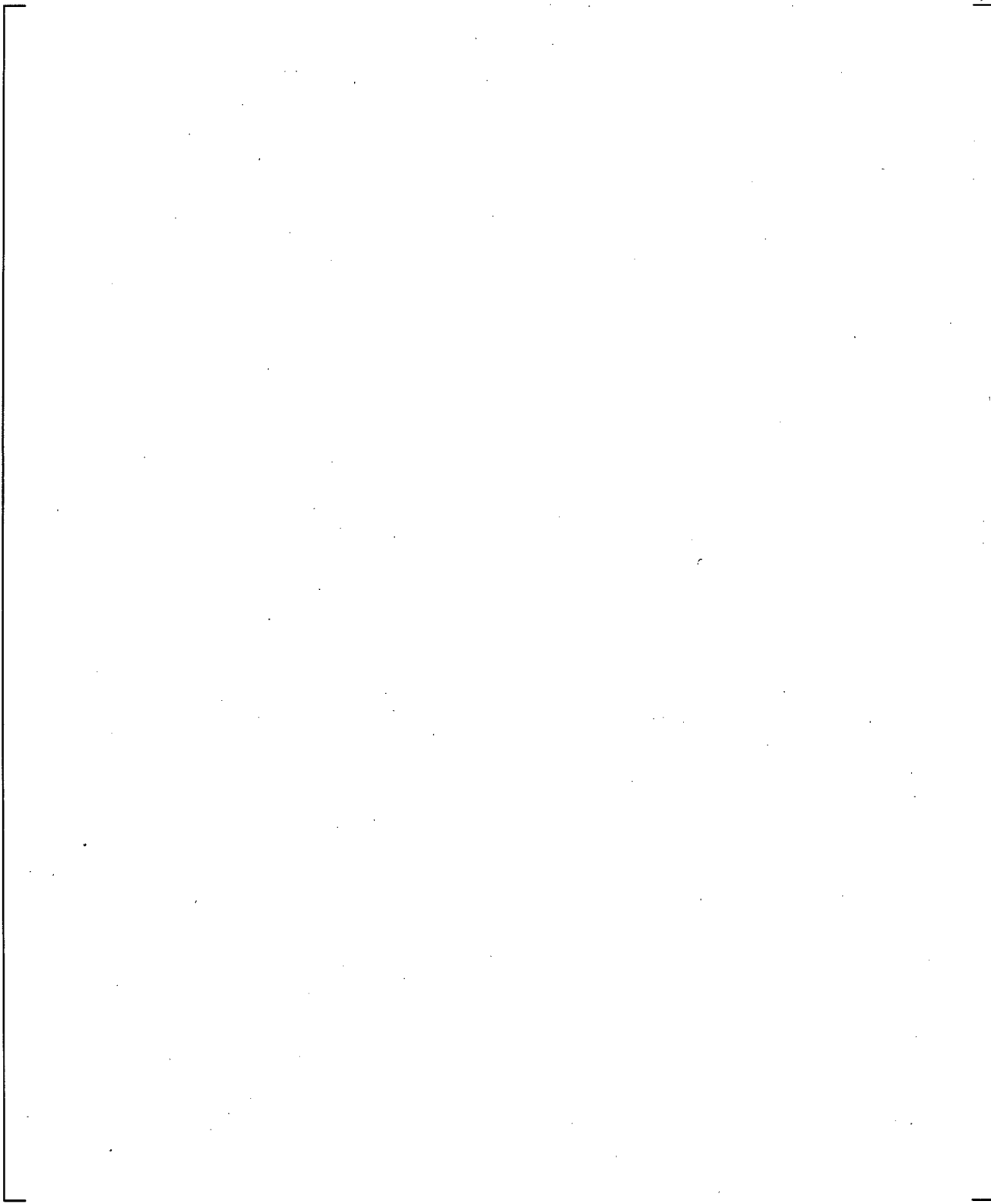


**Figure 24.7.2-18 Measured and Predicted Intact Loop Cold Leg Mixture Density**

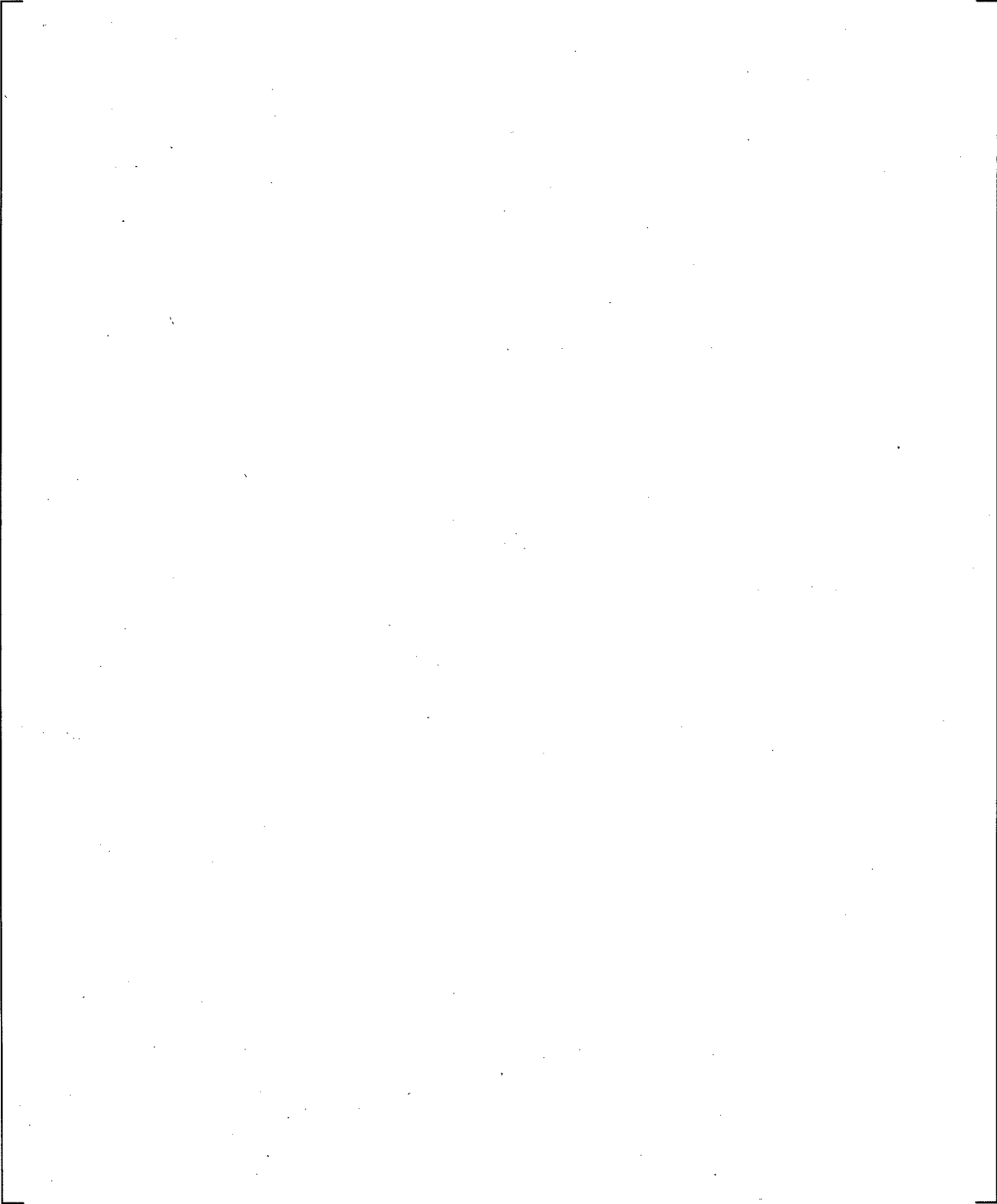


**Figure 24.7.2-19 Measured and Predicted Intact Loop Cold Leg Mixture Velocity**

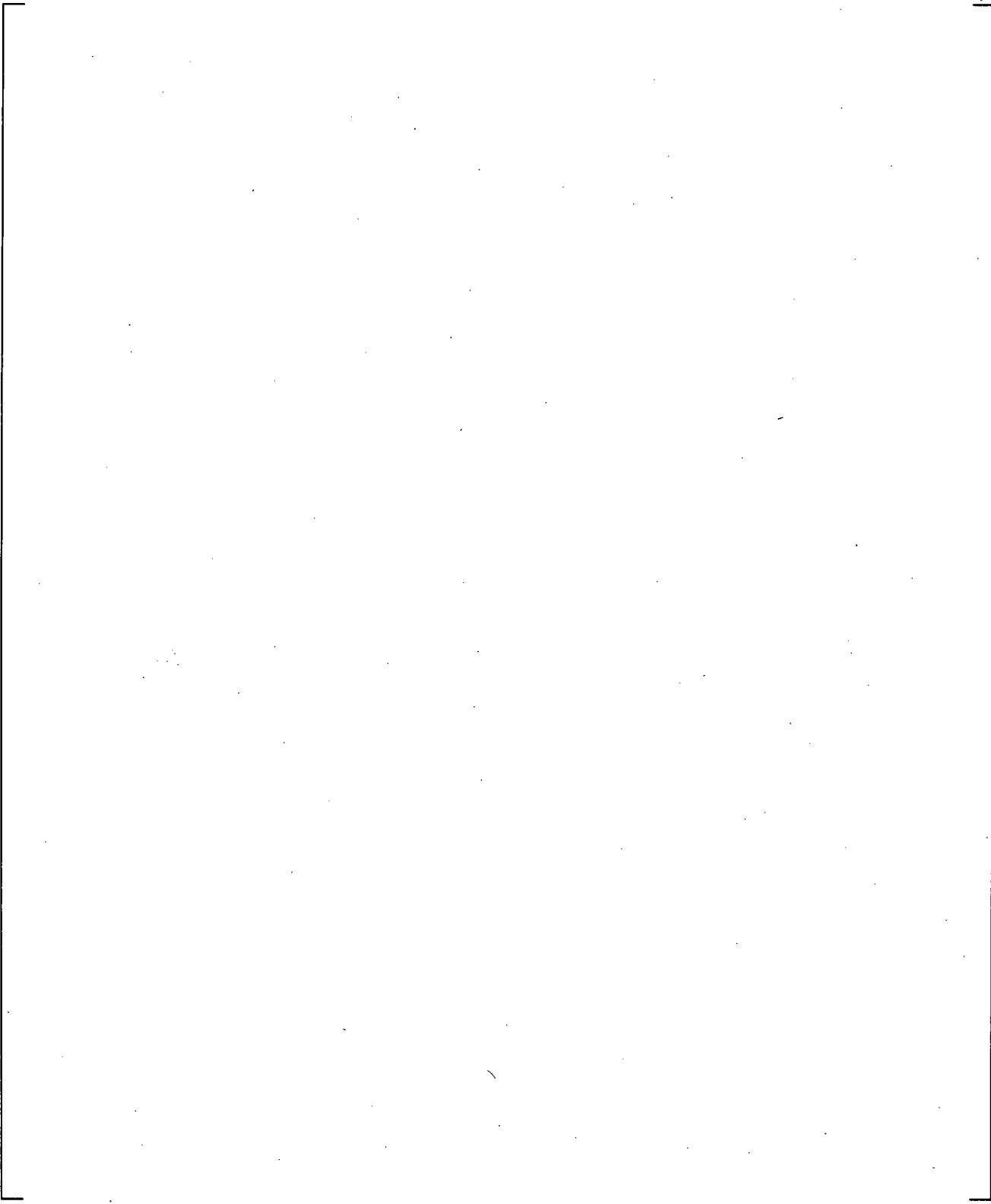


**Figure 24.7.2-20 Measured and Predicted Intact Loop Cold Leg Mixture Velocity**

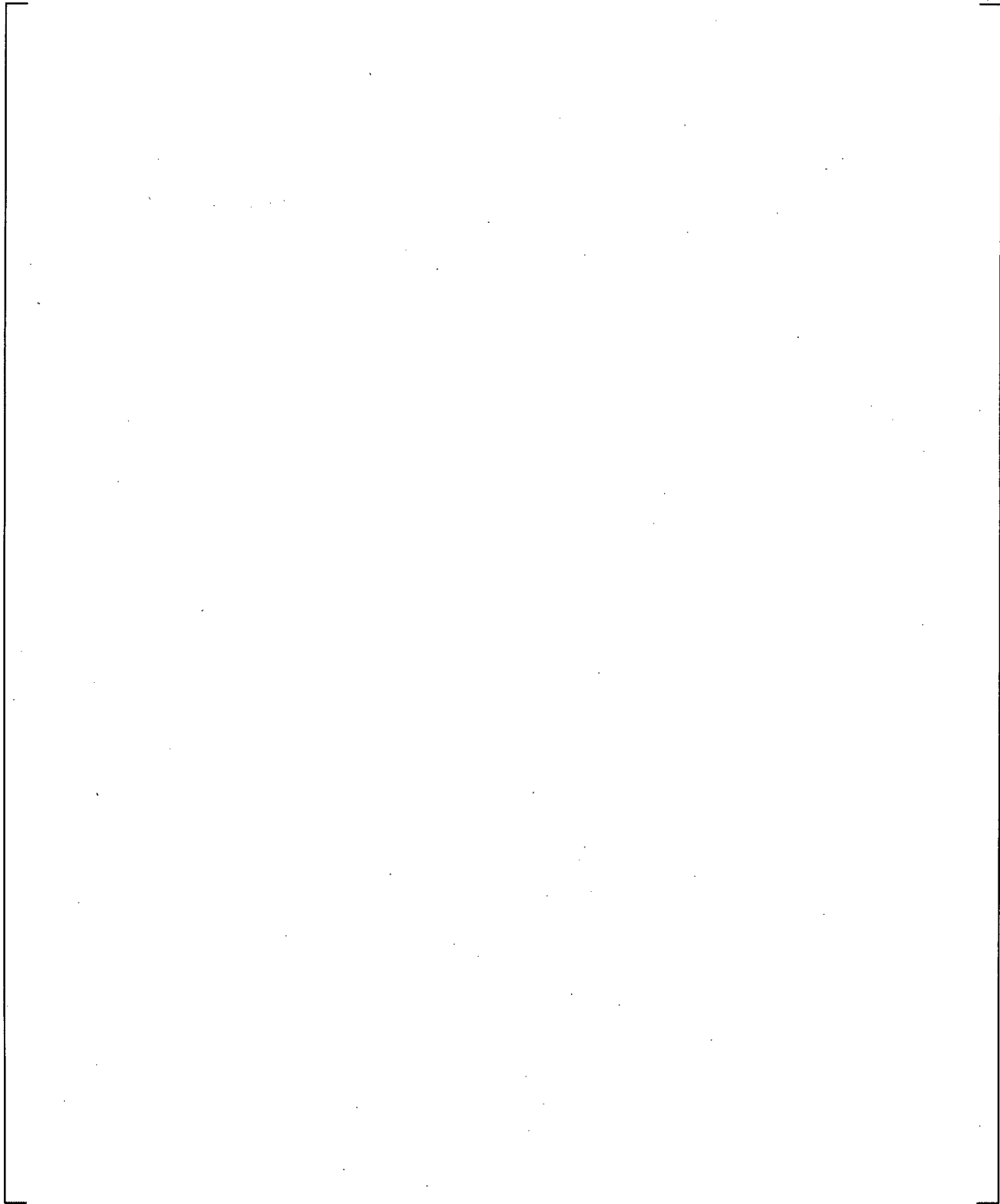


**Figure 24.7.2-21 Measured and Predicted Hot Leg Break Flowrate**

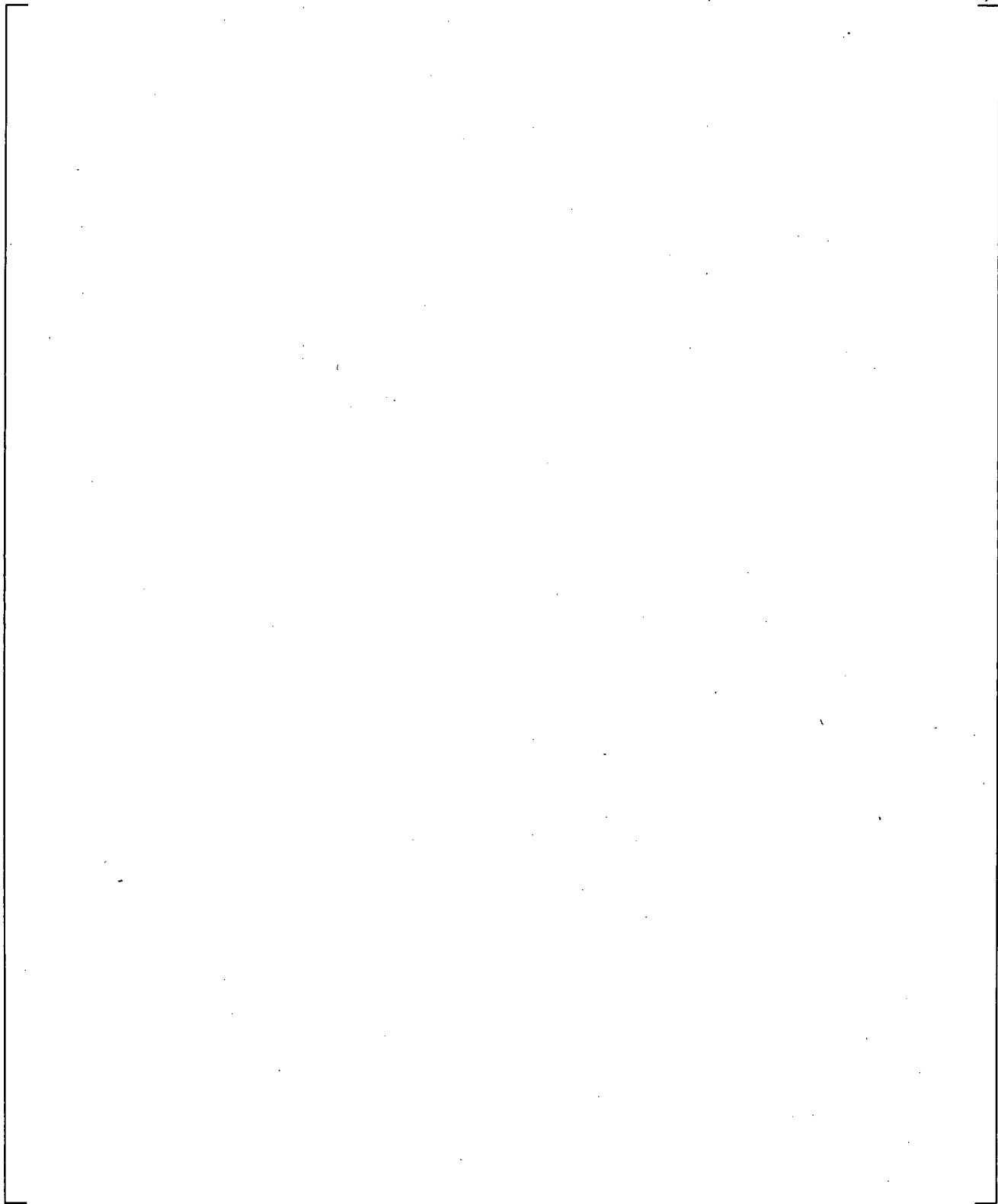


**Figure 24.7.2-22 Measured and Predicted Hot Leg Mixture Density**

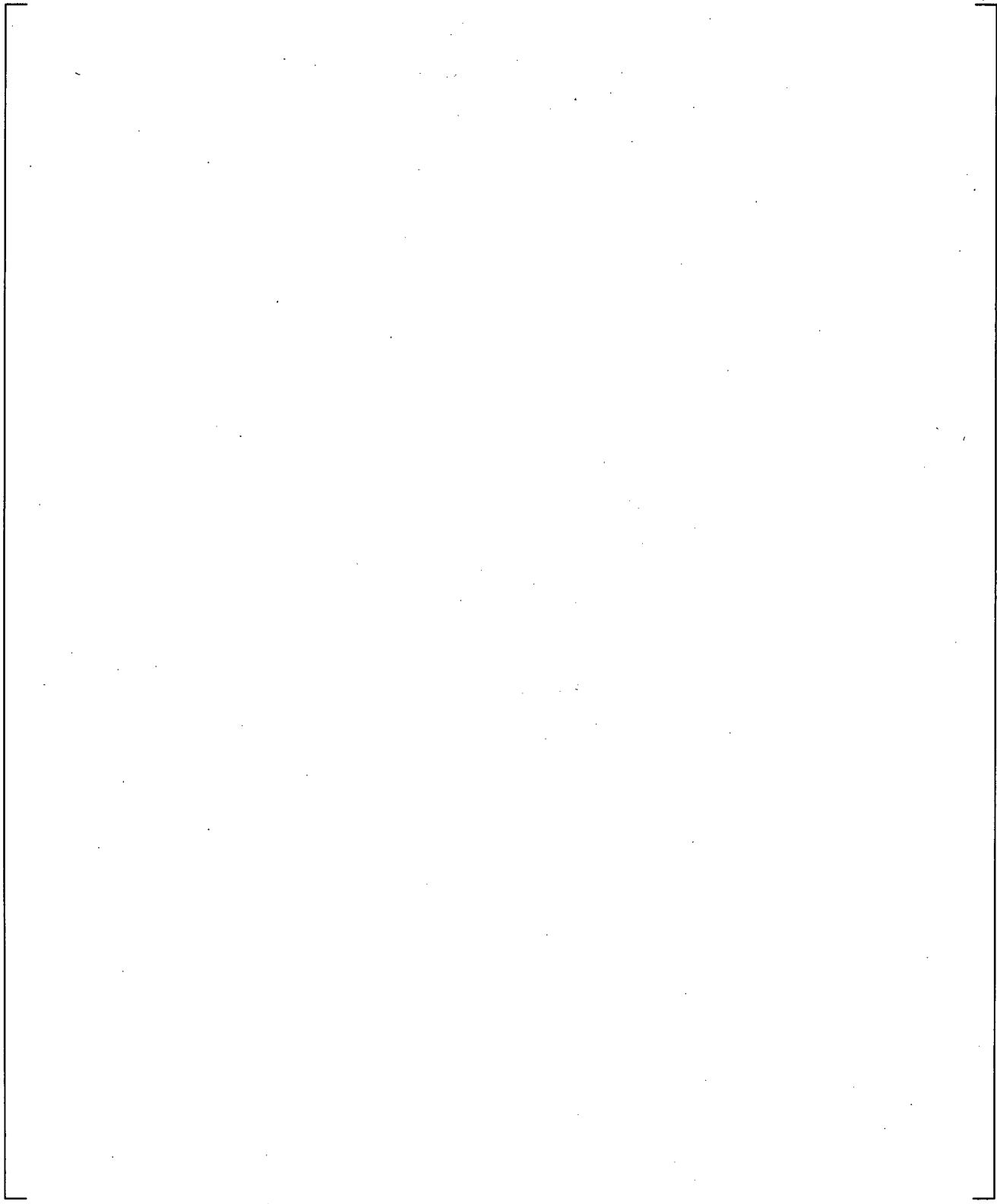


**Figure 24.7.2-23 Measured and Predicted Broken Loop Hot Leg Mixture Velocity**

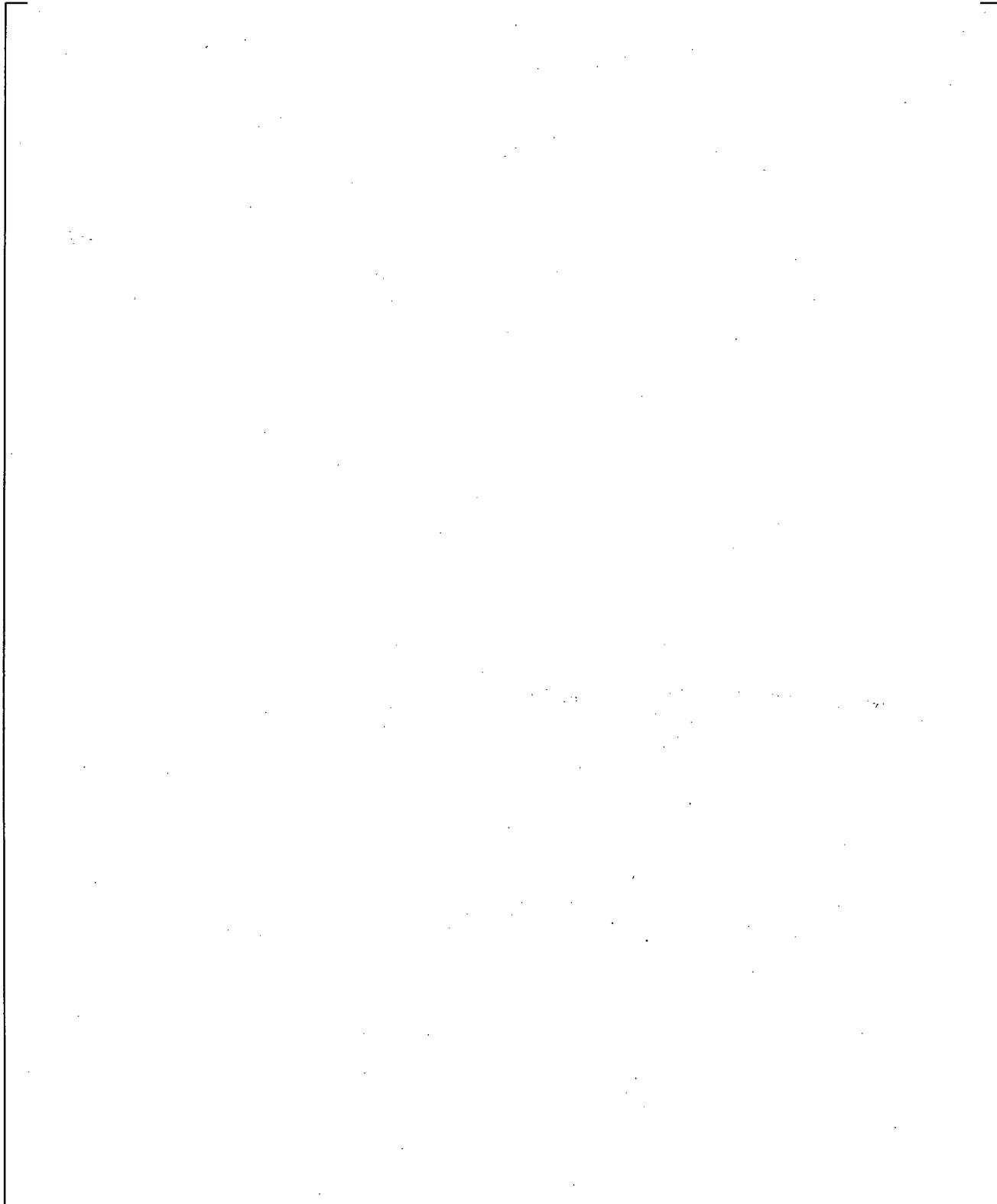


**Figure 24.7.2-24 Predicted Void Fraction in Upper Plenum at Loop Level**

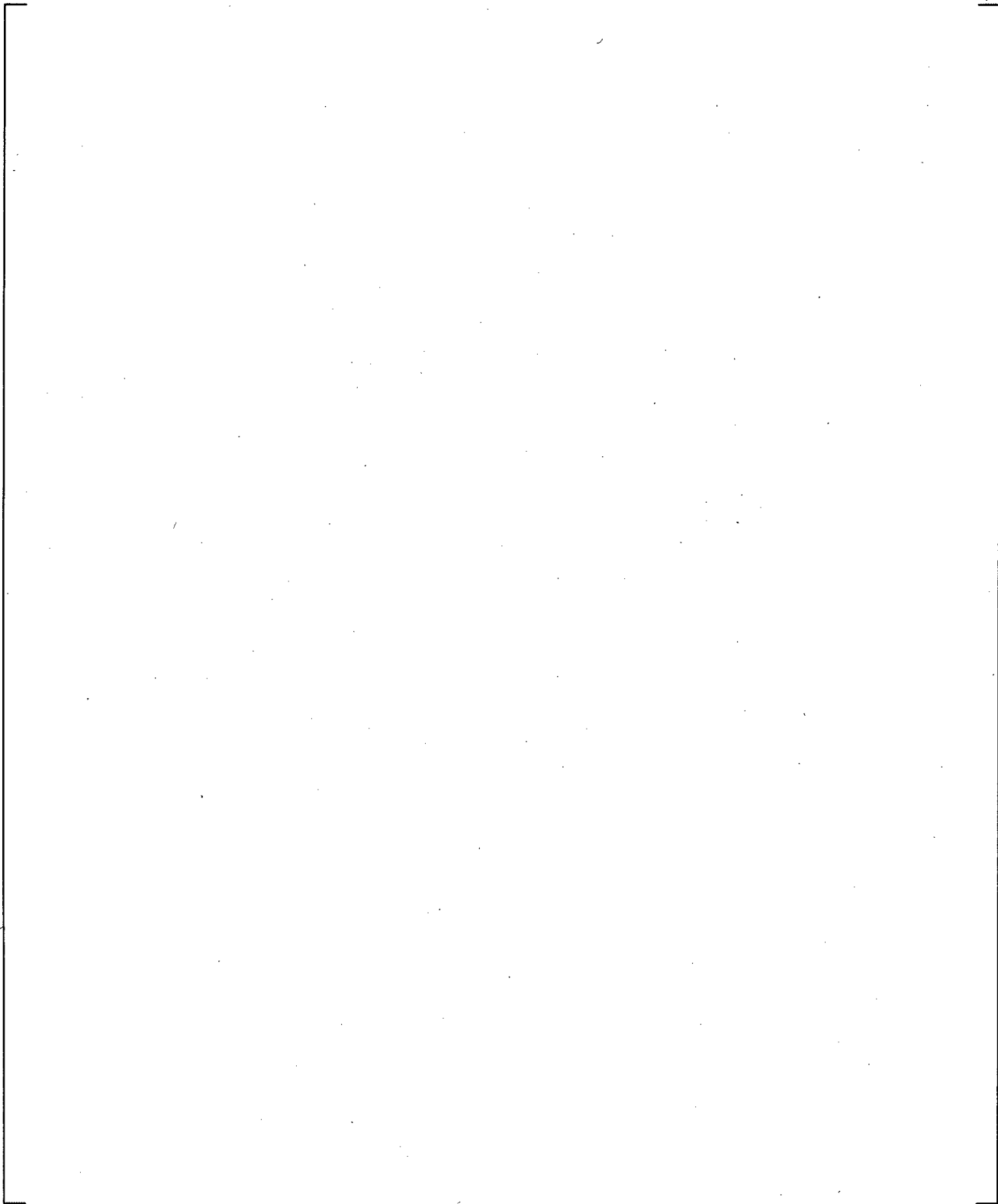


**Figure 24.7.2-25 Predicted Void Fraction in Upper Plenum at Exit of CCFL Region**

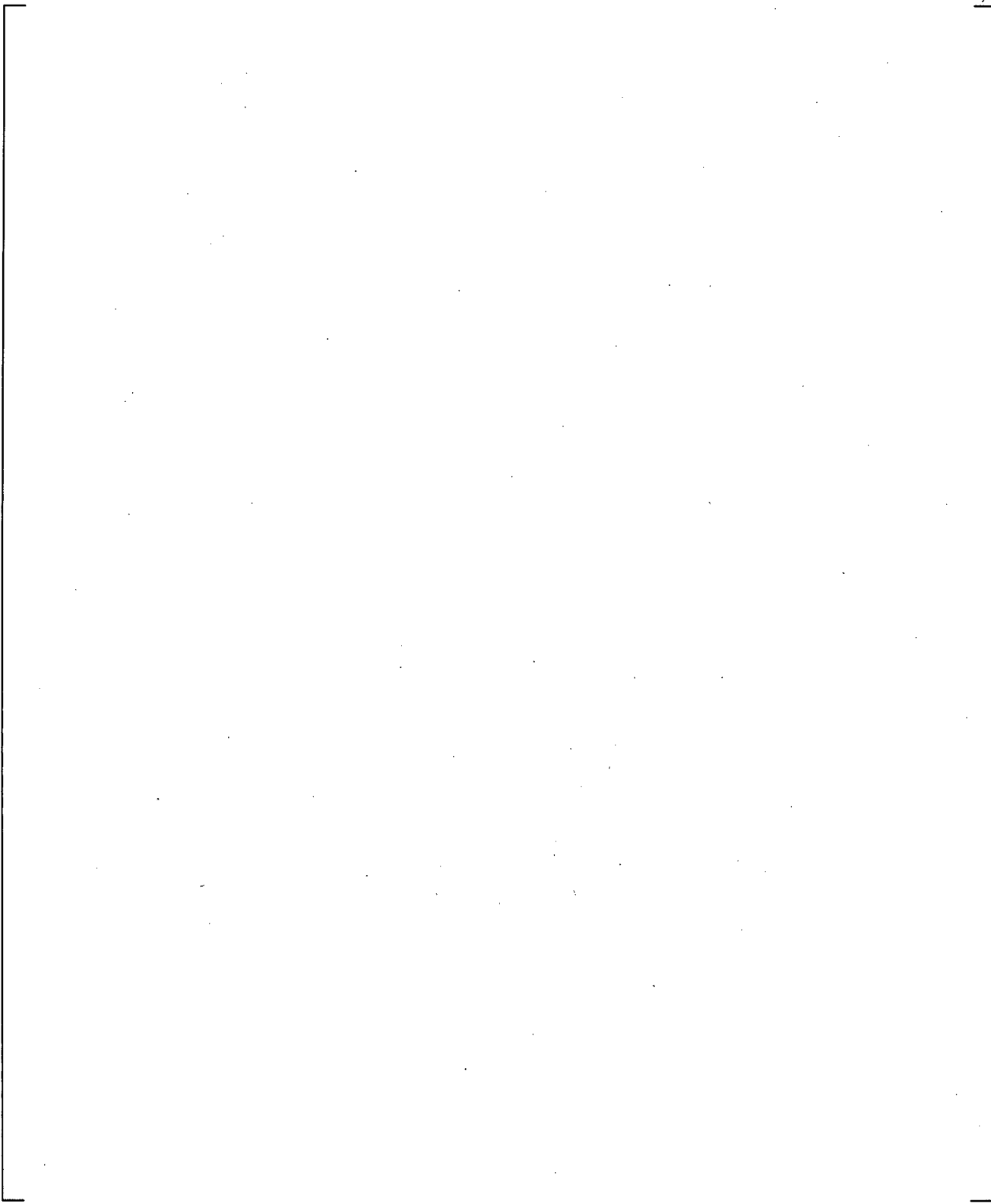


**Figure 24.7.2-26 Measured and Predicted Cold Leg Break Flowrate**

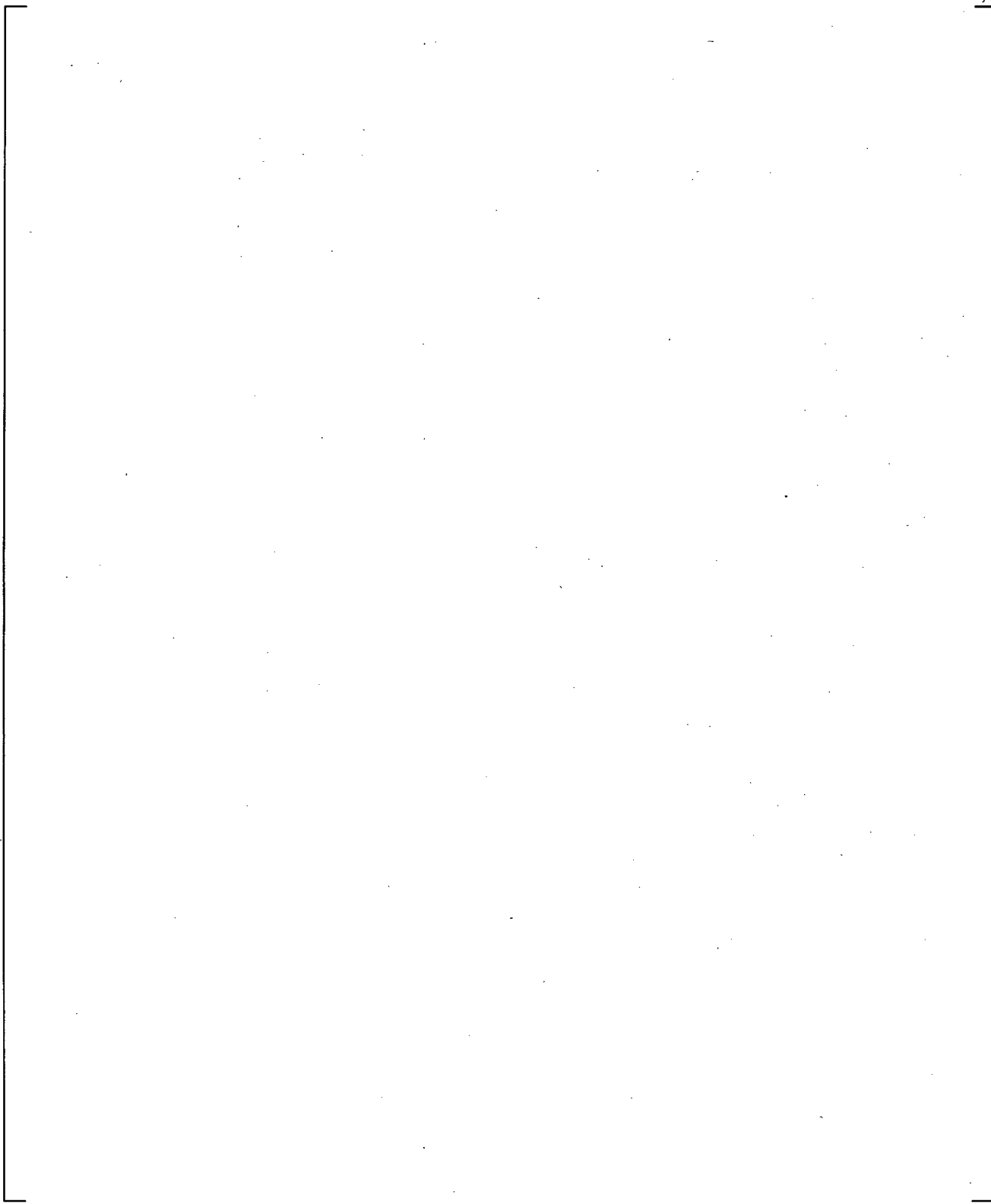


**Figure 24.7.2-27 Measured and Predicted Broken Cold Leg Mixture Density**

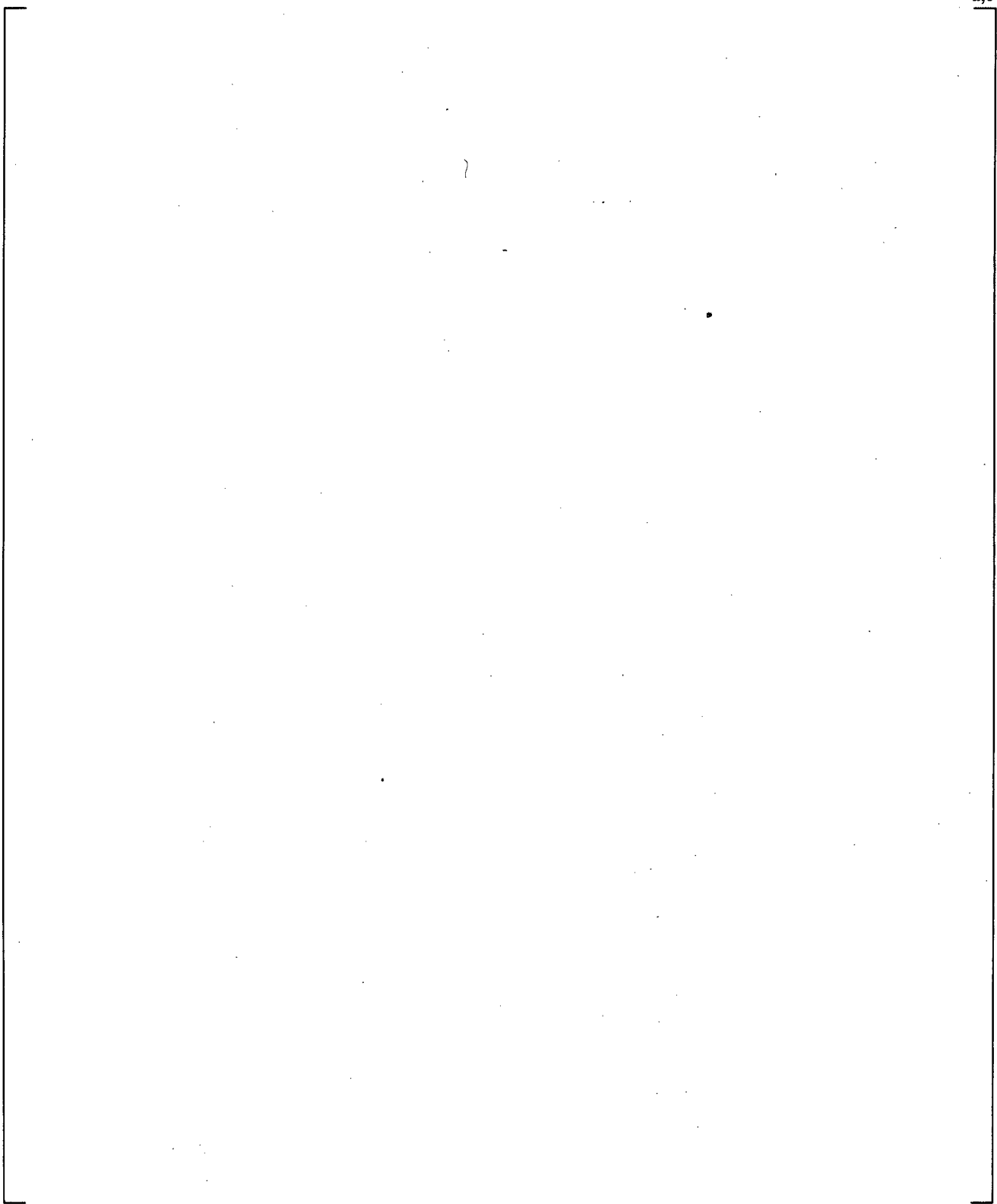


**Figure 24.7.2-28 Measured and Predicted Broken Cold Leg Mixture Velocity**

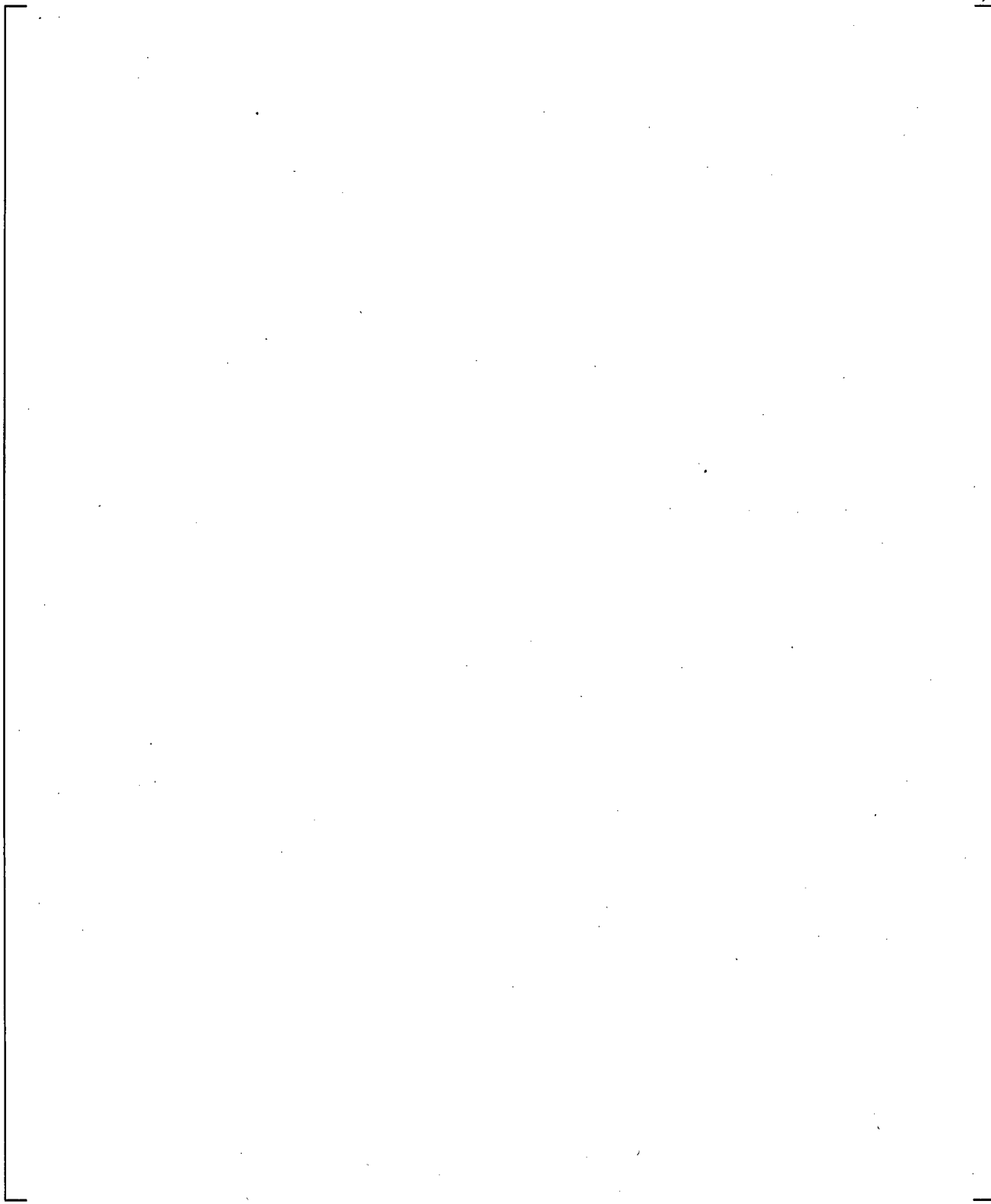


**Figure 24.7.2-29 Predicted Broken Cold Leg Nozzle DP**

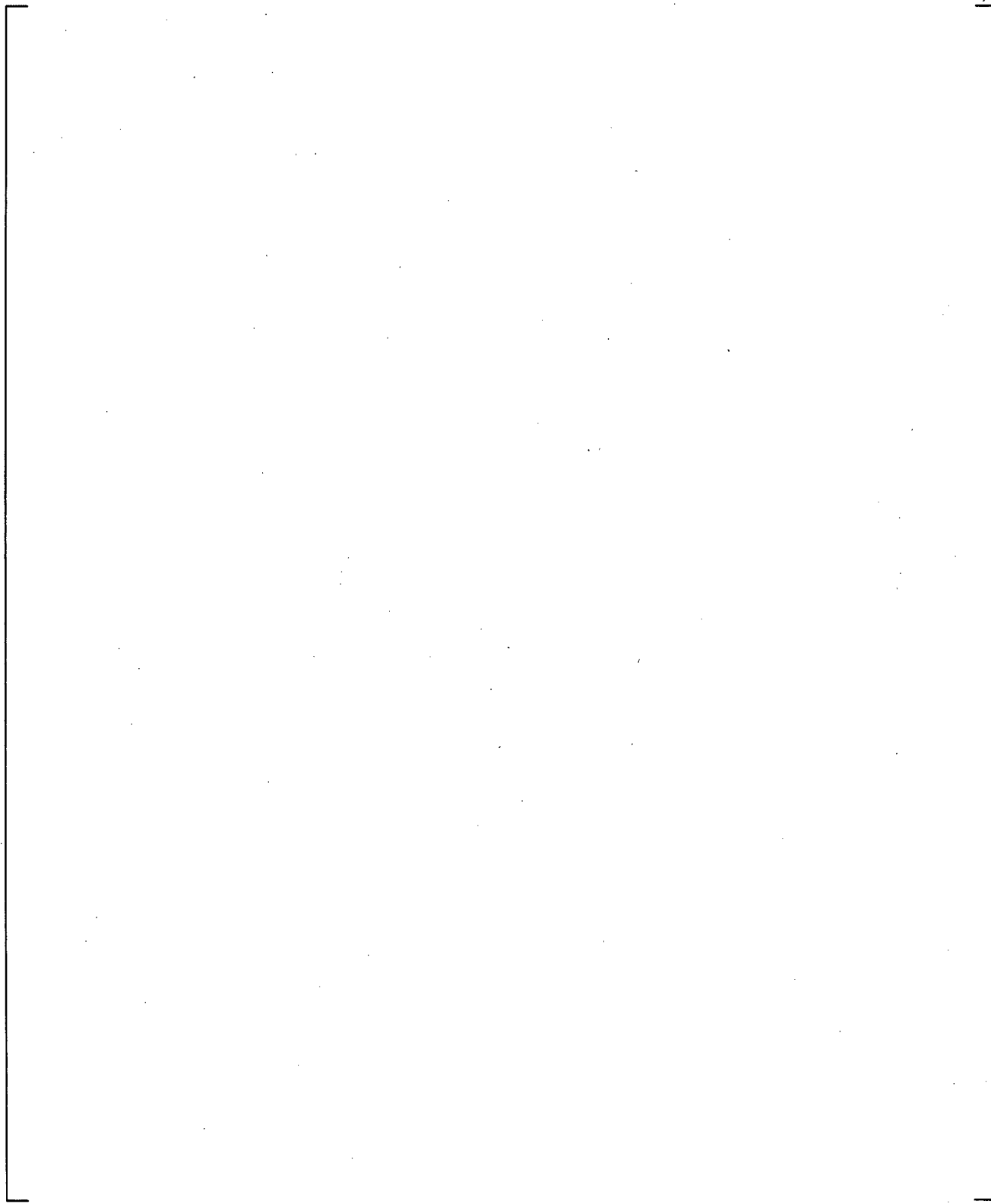


**Figure 24.7.2-30 Predicted Broken Cold Leg Pressure Drop to the Break Plane**

### 24.7.3 CCTF Run 62

CCTF Test 62 (Okubo et al., 1985) is a gravity-reflood test with initial system pressure at 29 psia. In this type of test, the predicted flow through the core depends on the prediction of hydrostatic pressure in the core and downcomer, and pressure drops through the loops. Comparisons will be made between predicted and measured cladding temperatures at the locations marked by "x" in Figure 24.7.3-1a. The pressure differences are a measure of the hydrostatic head due to liquid, as well as frictional losses. In components containing significant liquid, the pressure difference is usually a reliable indicator of collapsed liquid level or liquid fraction. [

] <sup>a,c</sup>

#### Core Thermal-Hydraulics

[

] <sup>a,c</sup>

Figures 24.7.3-10 to 24.7.3-15 compare measured and predicted average vapor fraction within the spans indicated in Figure 24.7.3-1a. [

] <sup>a,c</sup>

[

] <sup>a,c</sup>

The average vapor fraction in the upper plenum is compared in Figure 24.7.3-16. [

] <sup>a,c</sup>

### **Loop Thermal-Hydraulics**

Figure 24.7.3-19 compares the upper plenum pressure which is under-predicted. [

] <sup>a,c</sup>

Figures 24.7.3-22 to 24.7.3-26 compare the pressure difference across the intact loop [

] <sup>a,c</sup>

[

] <sup>a,c</sup>**Sensitivity Run**

Figure 24.7.3.19 (Upper Plenum Pressure) indicates [

] <sup>a,c</sup>

Figure 24.7.3.46 shows the upper plenum pressure [

] <sup>a,c</sup>

In summary, the total mass flows into the core and through the loops are predicted [

] <sup>a,c</sup>

[

]a.c

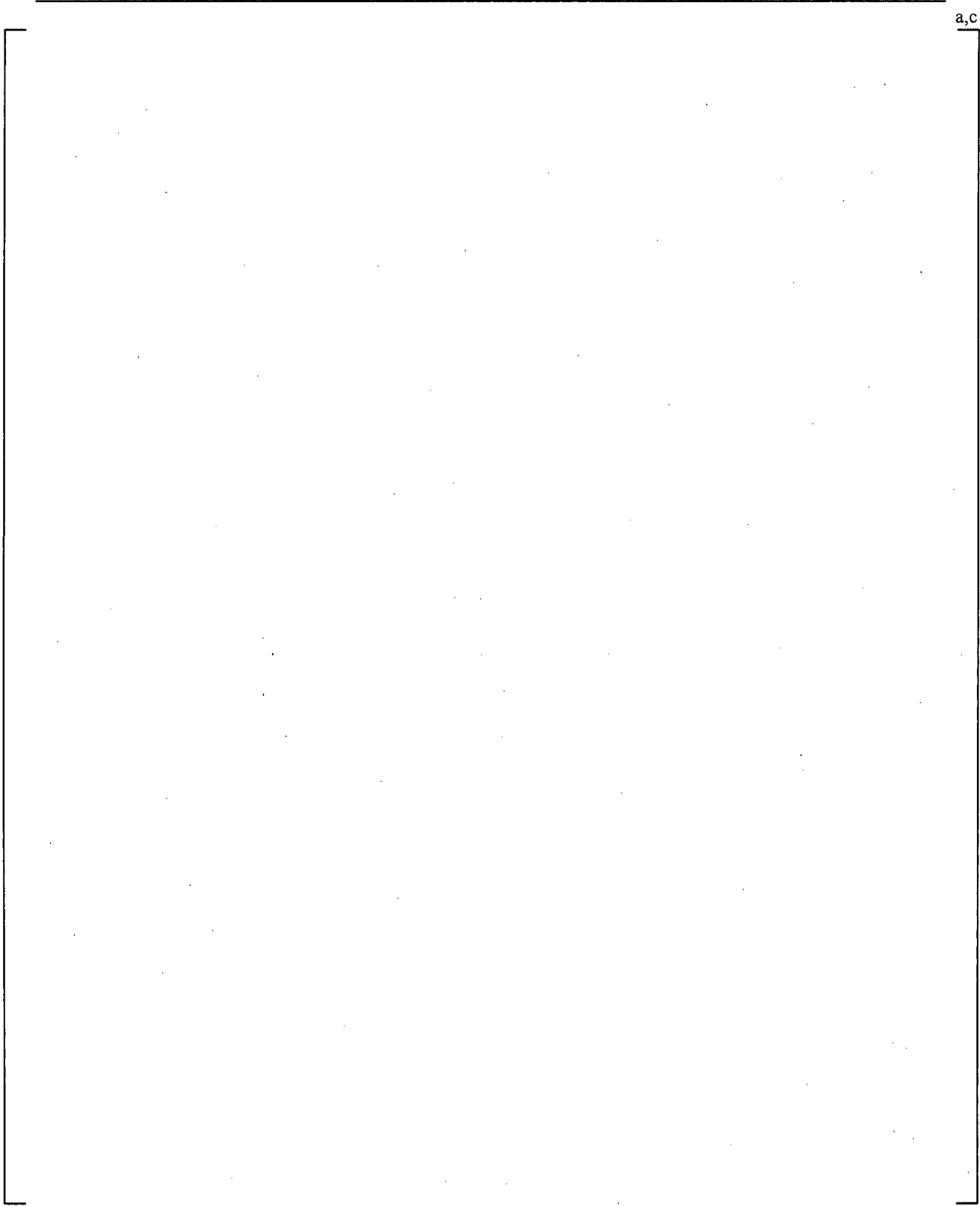


**Figure 24.7.3-1a Pressure, Differential Pressure, Liquid Level and Mass Flowrate Instrumentation Location in Pressure Vessel**

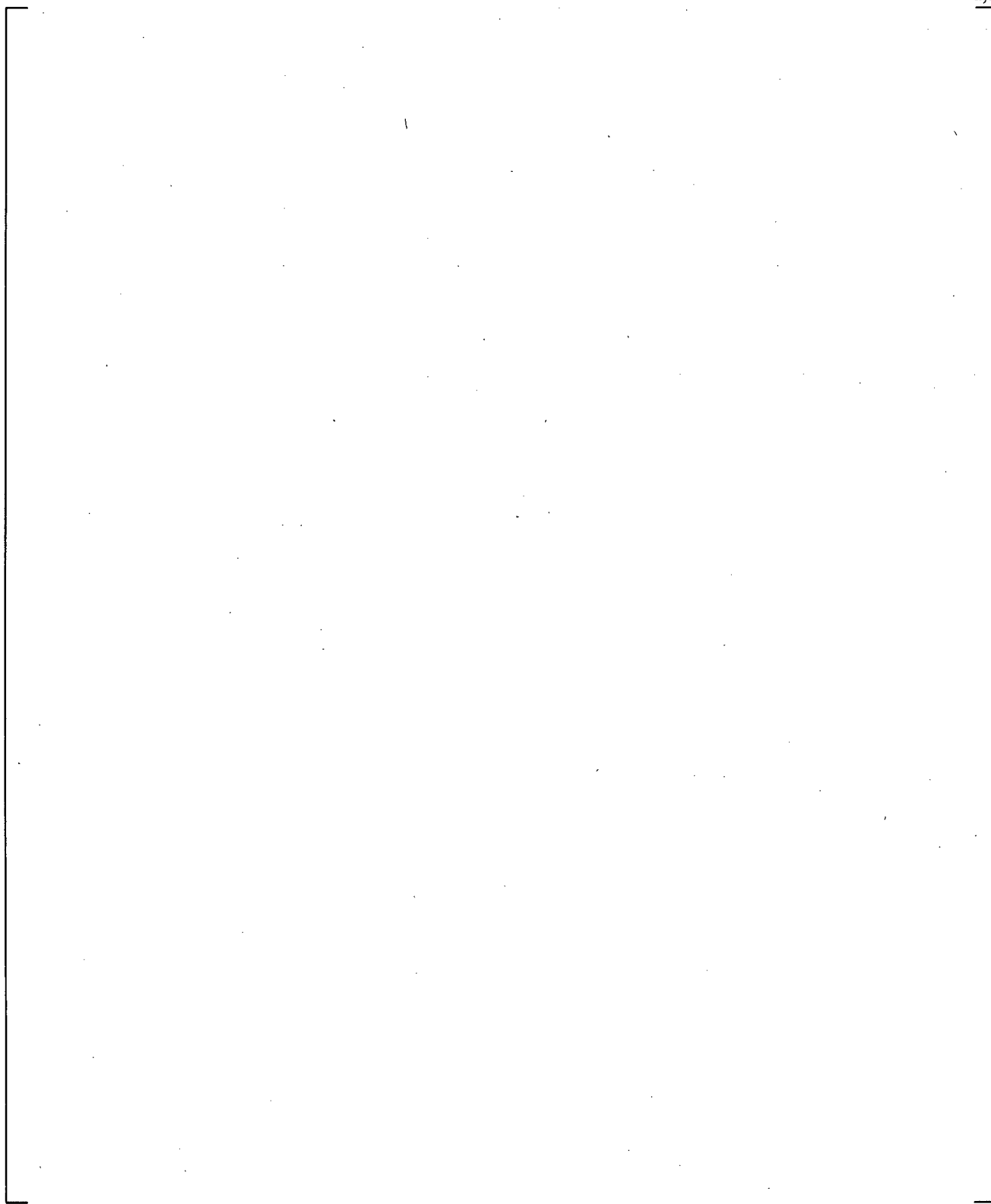


**Figure 24.7.3-1b Top View of Primary Loop Piping**

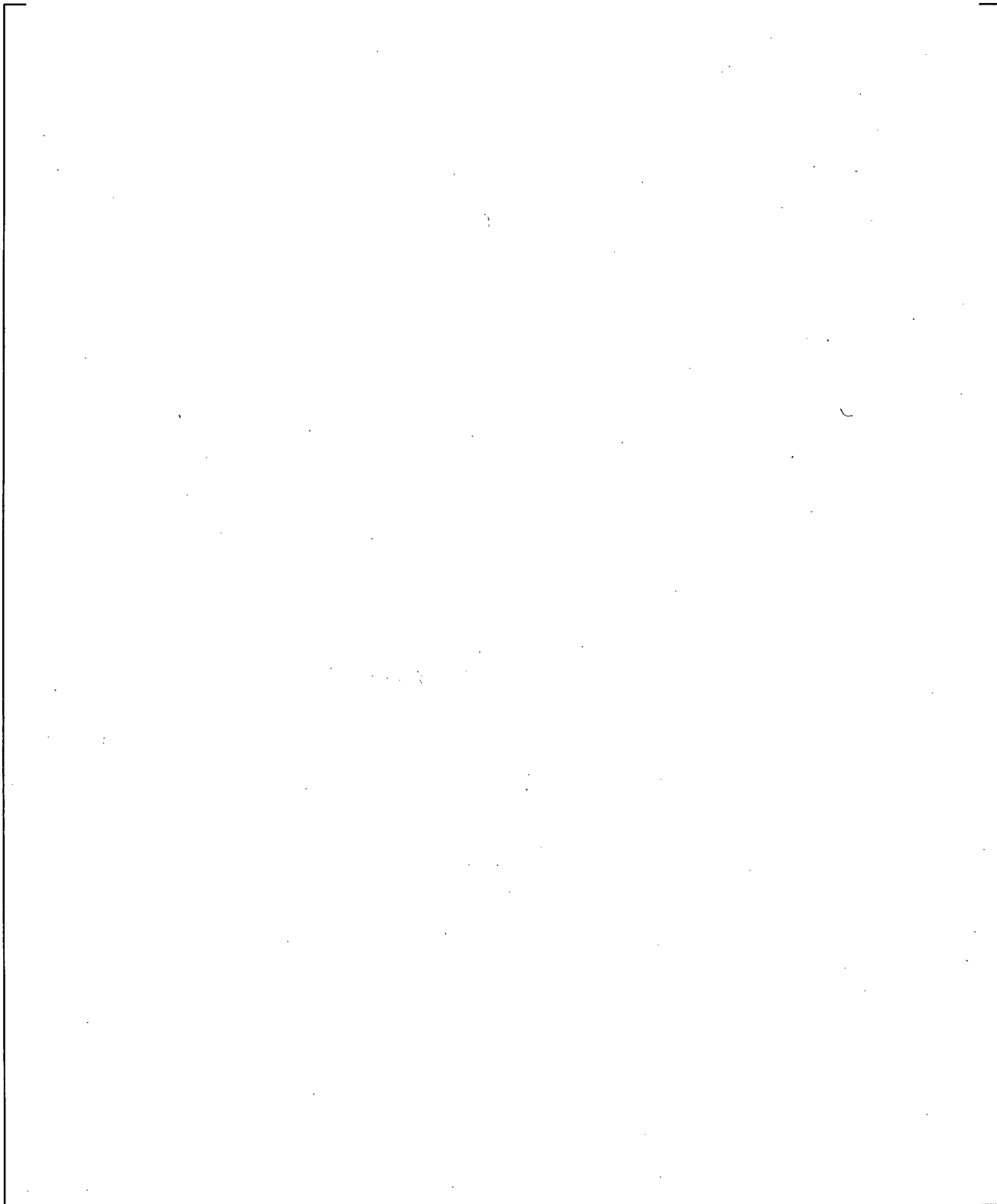


**Figure 24.7.3-2 Core Inlet Flow Comparison**

**Figure 24.7.3-3 CCTF Run 62 WCOBRA/TRAC-TF2 vs. Data – Cladding Temperature Comparison at 3.33 ft**

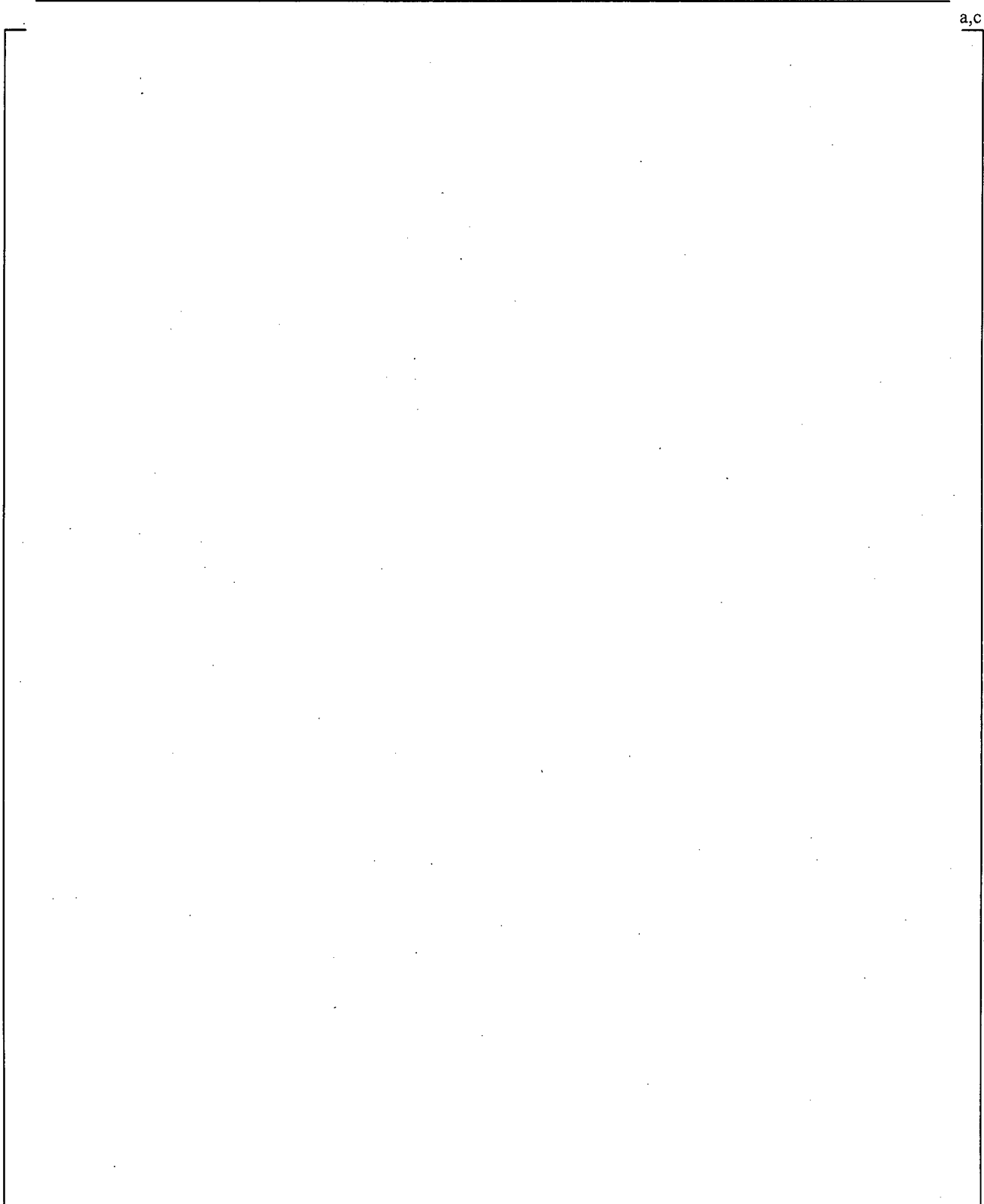


**Figure 24.7.3-4**    **CCTF Run 62 WCOBRA/TRAC-TF2 vs. Data Cladding Temperature Comparison at 6 ft**

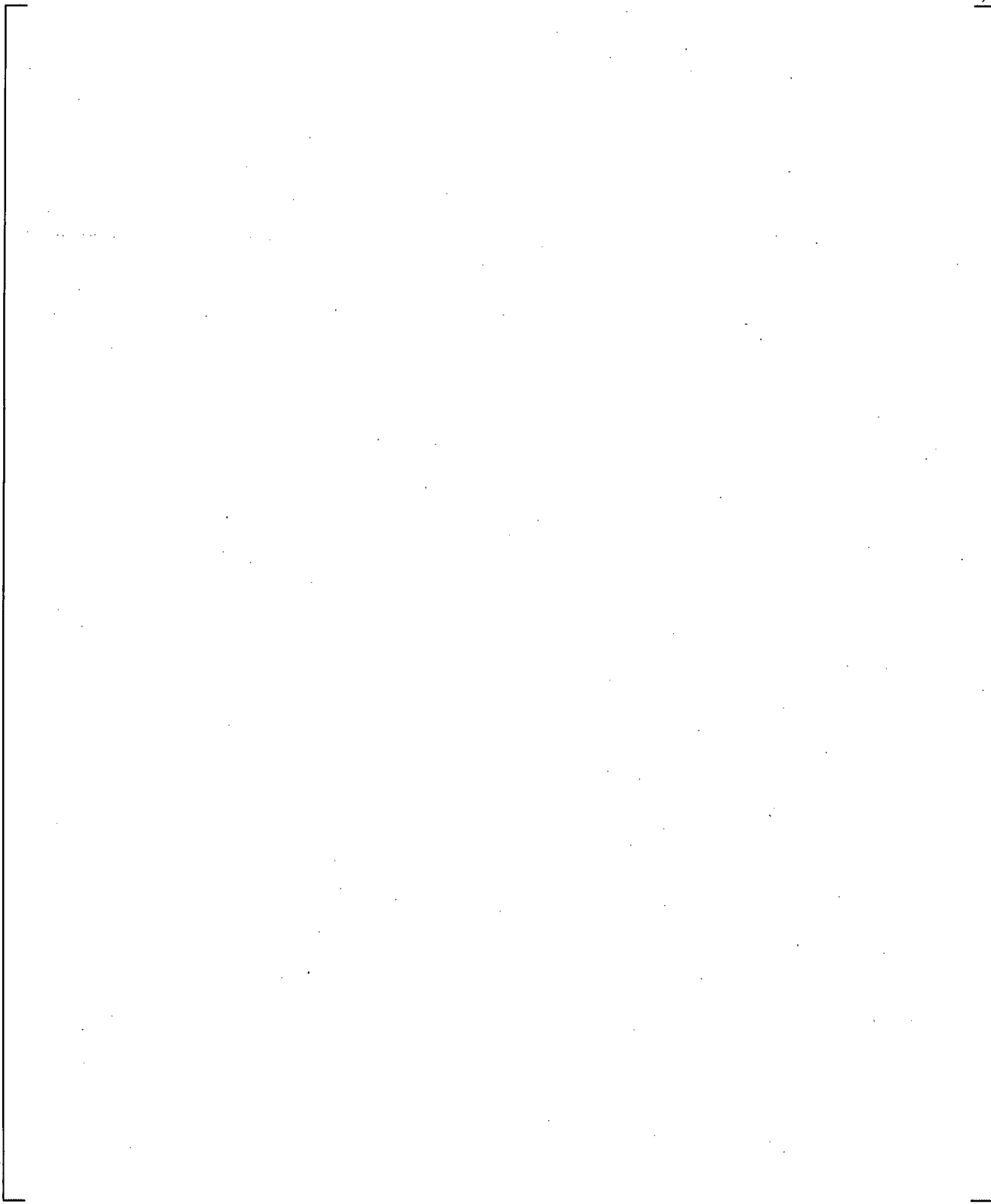


**Figure 24.7.3-5** CCTF Run 62 WCOBRA/TRAC-TF2 vs. Data Cladding Temperature Comparison at 6.68 ft

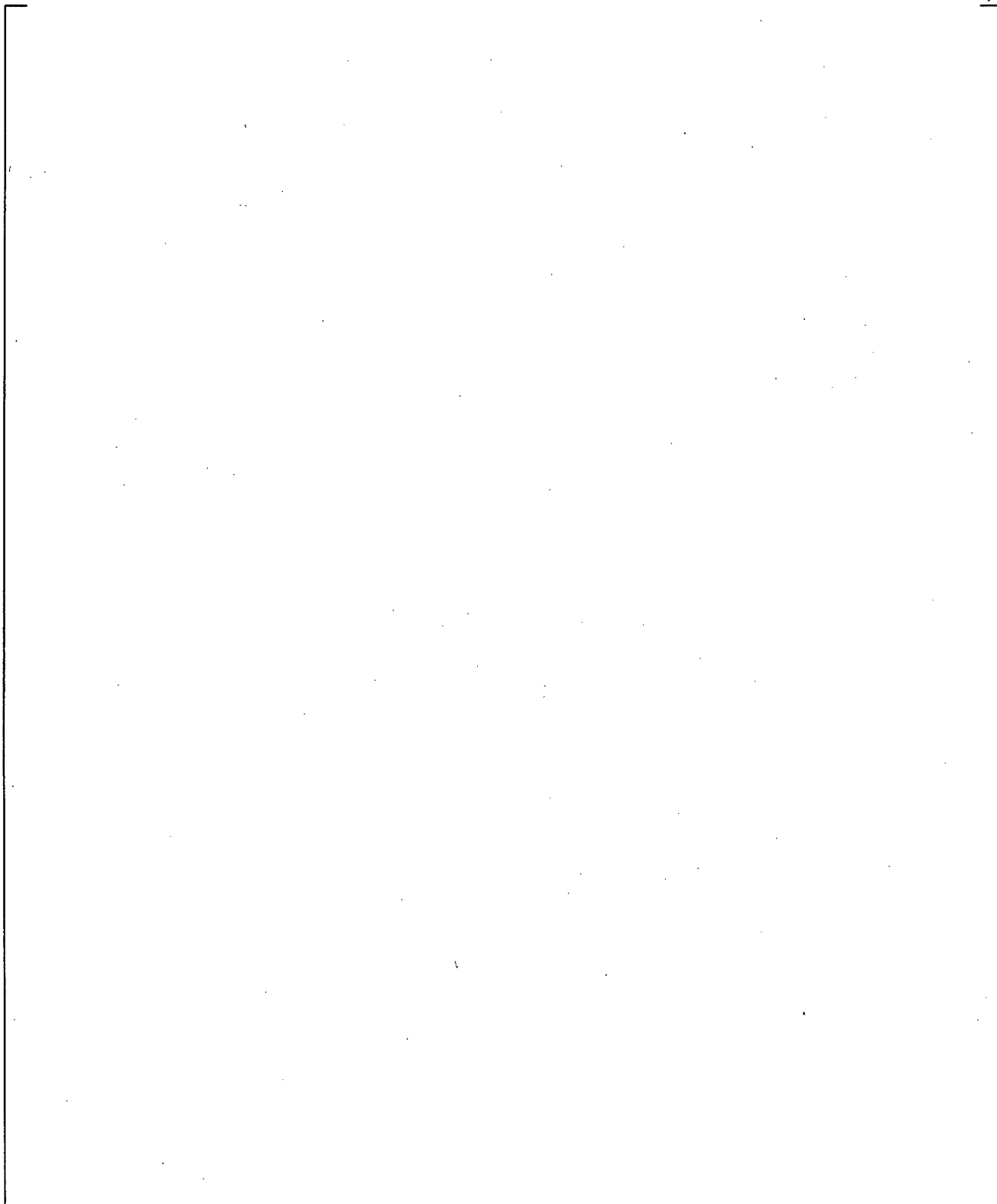


**Figure 24.7.3-6**    **CCTF Run 62 WCOBRA/TRAC-TF2 vs. Data Cladding Temperature Comparison at 8 ft**

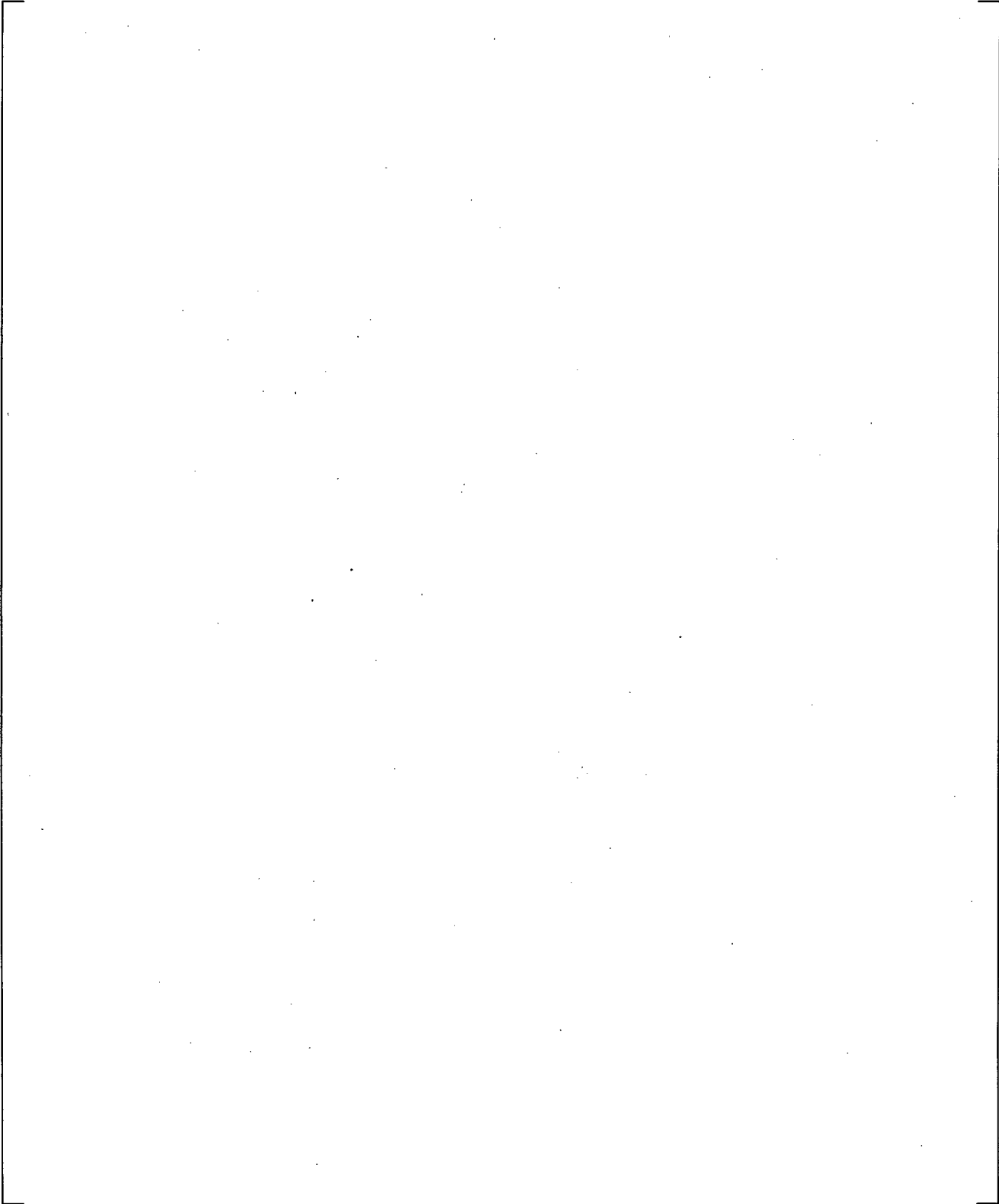


**Figure 24.7.3-7** CCTF Run 62 WCOBRA/TRAC-TF2 vs. Data Cladding Temperature Comparison at 10 ft

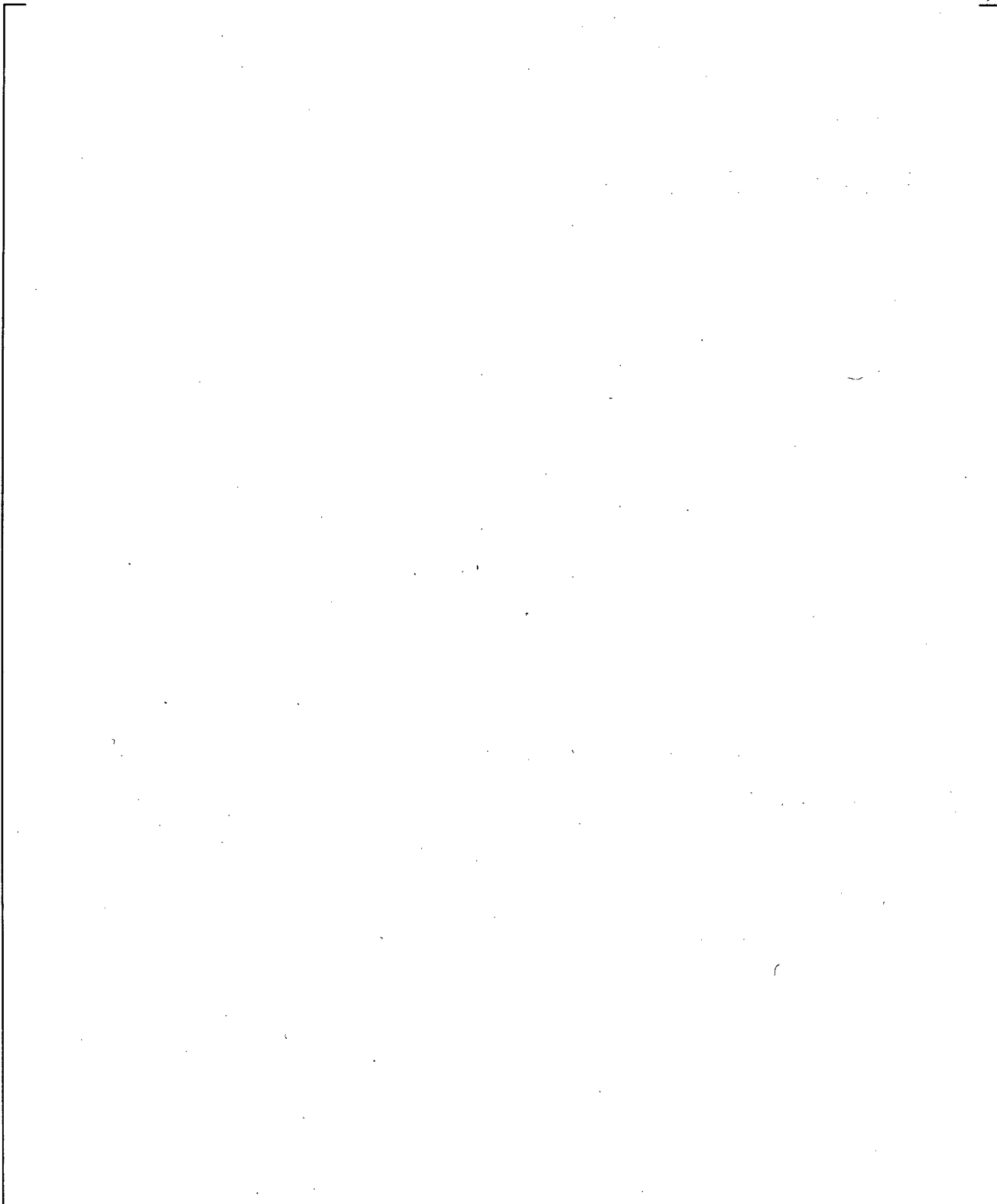


**Figure 24.7.3-8** CCTF Run 62 WCOBRA/TRAC-TF2 vs. Data Vapor Temperature Comparison at 6 ft

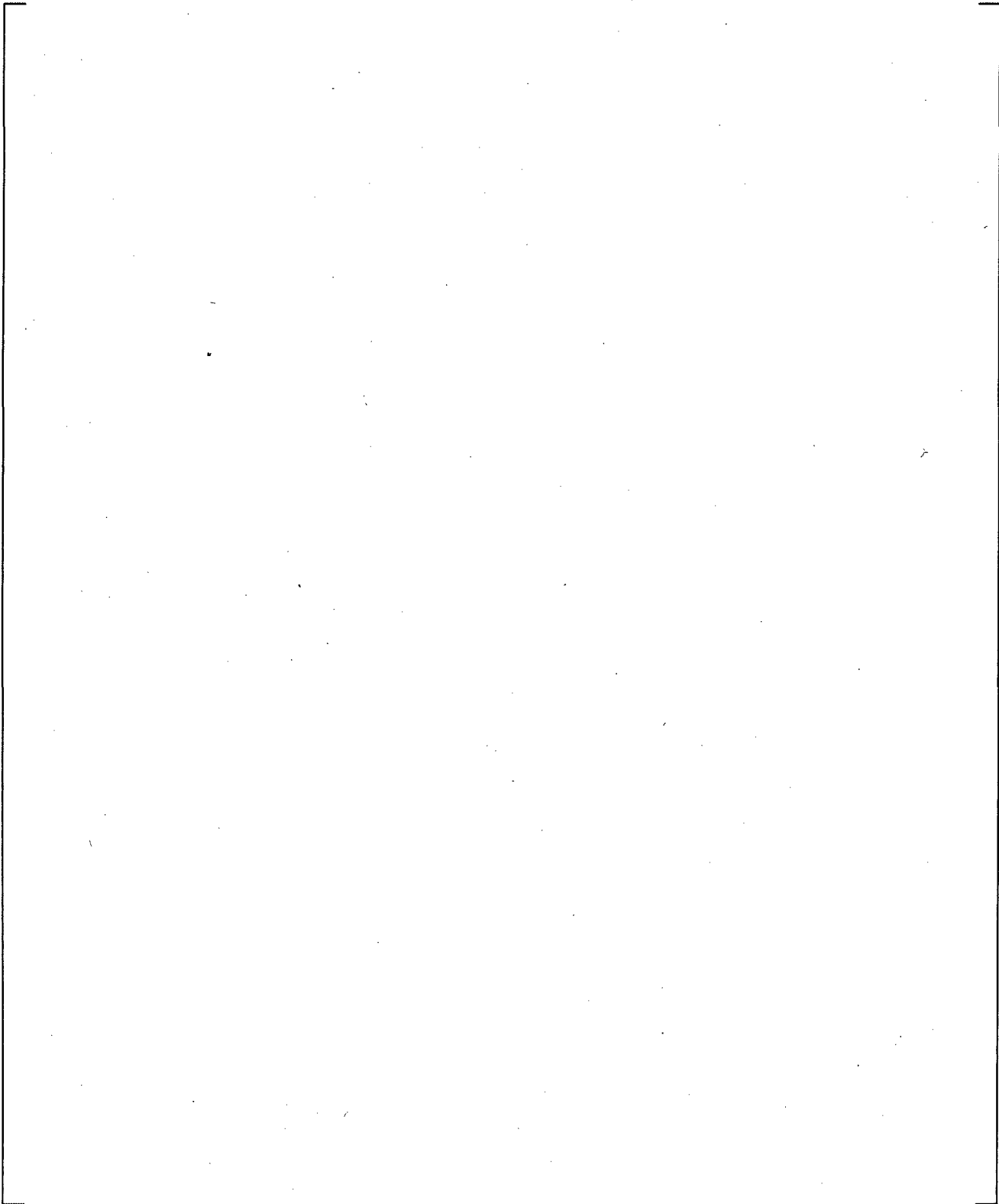


**Figure 24.7.3-9** CCTF Run 62 WCOBRA/TRAC-TF2 vs. Data Vapor Temperature Comparison at 8 ft

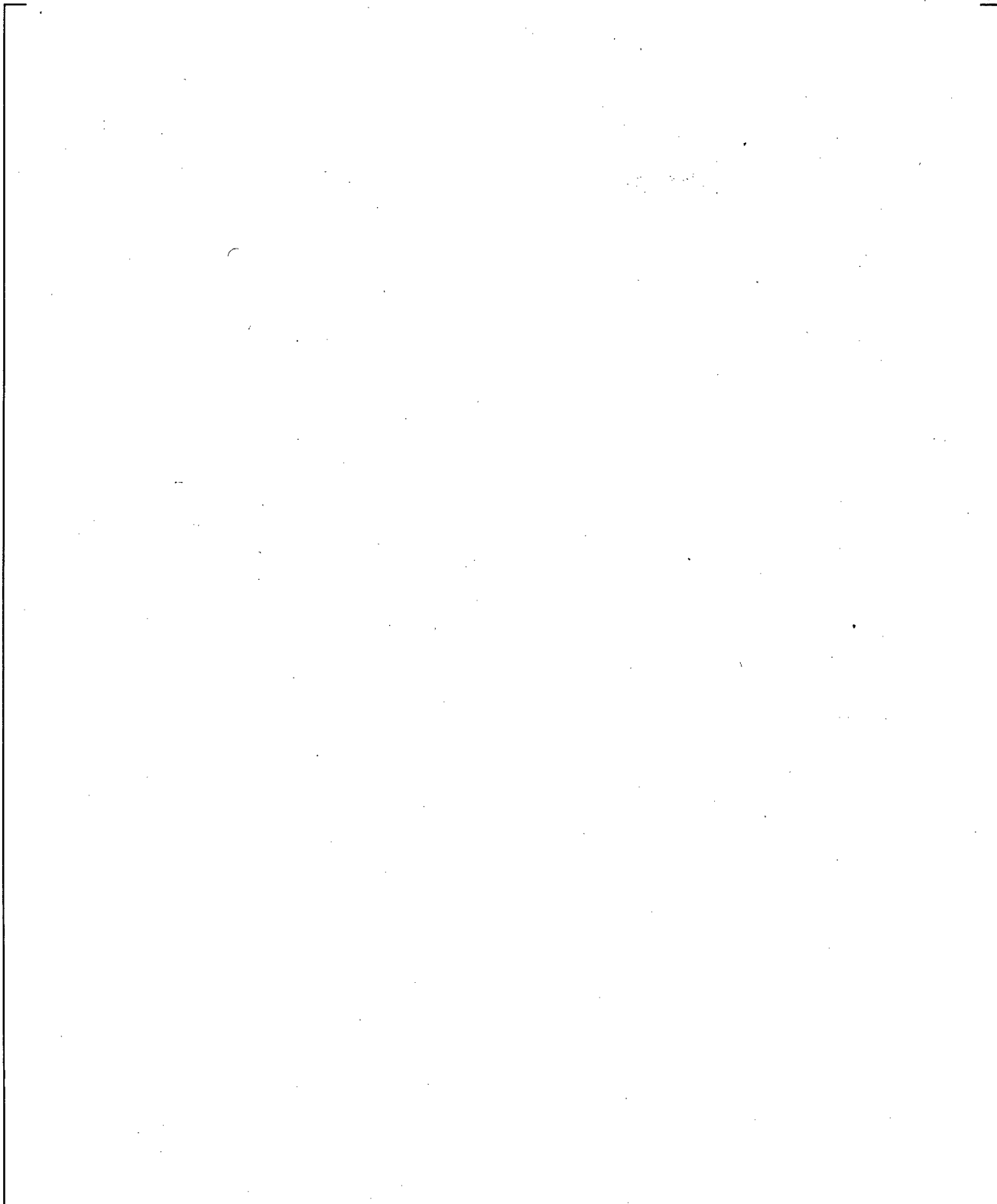


**Figure 24.7.3-10** CCTF Run 62 WCOBRA/TRAC-TF2 vs. Data Comparison Void Fraction from 2.1 to 2.71 m

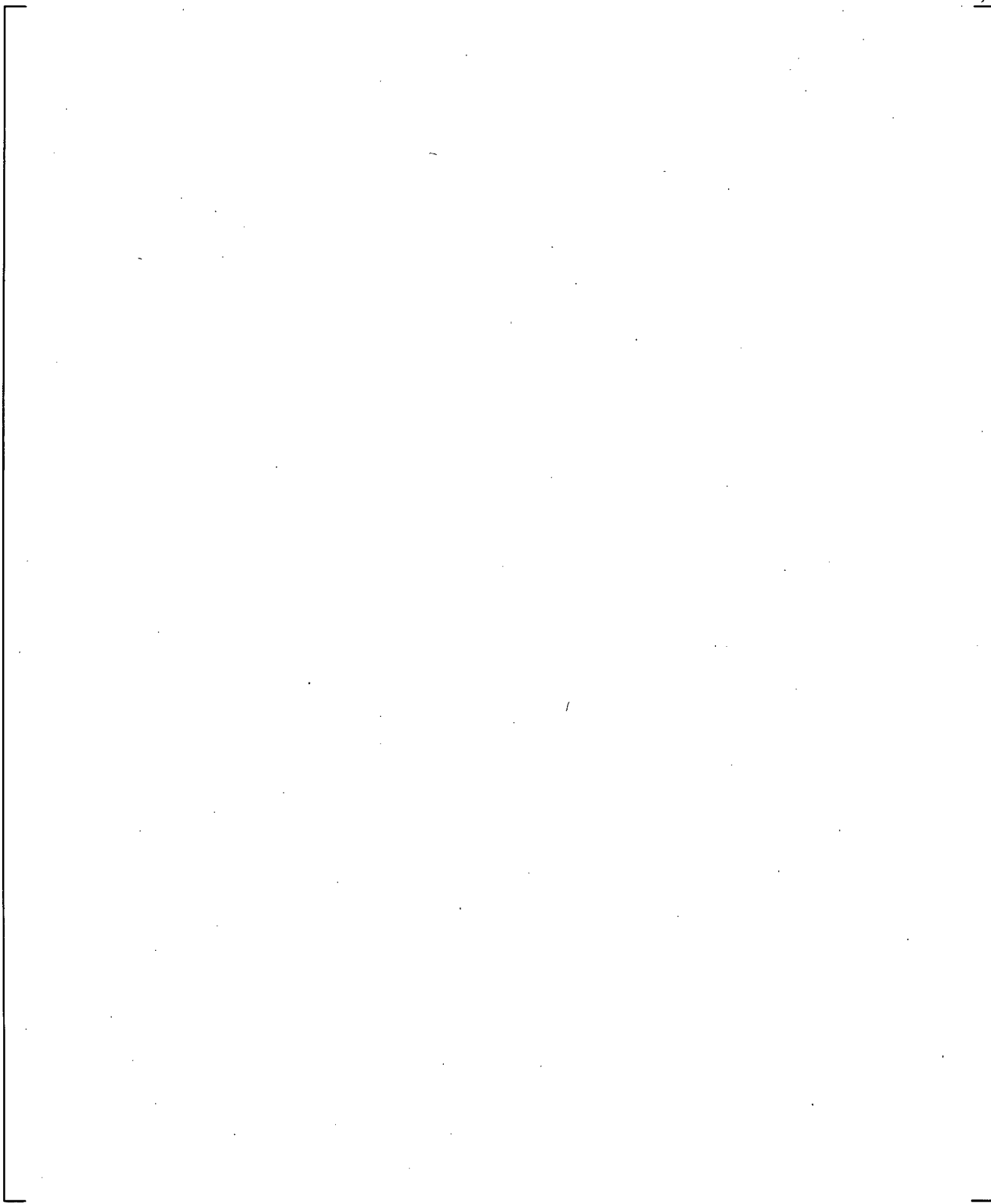


**Figure 24.7.3-11** CCTF Run 62 WCOBRA/TRAC-TF2 vs. Data Comparison Void Fraction from 2.71 to 3.32 m

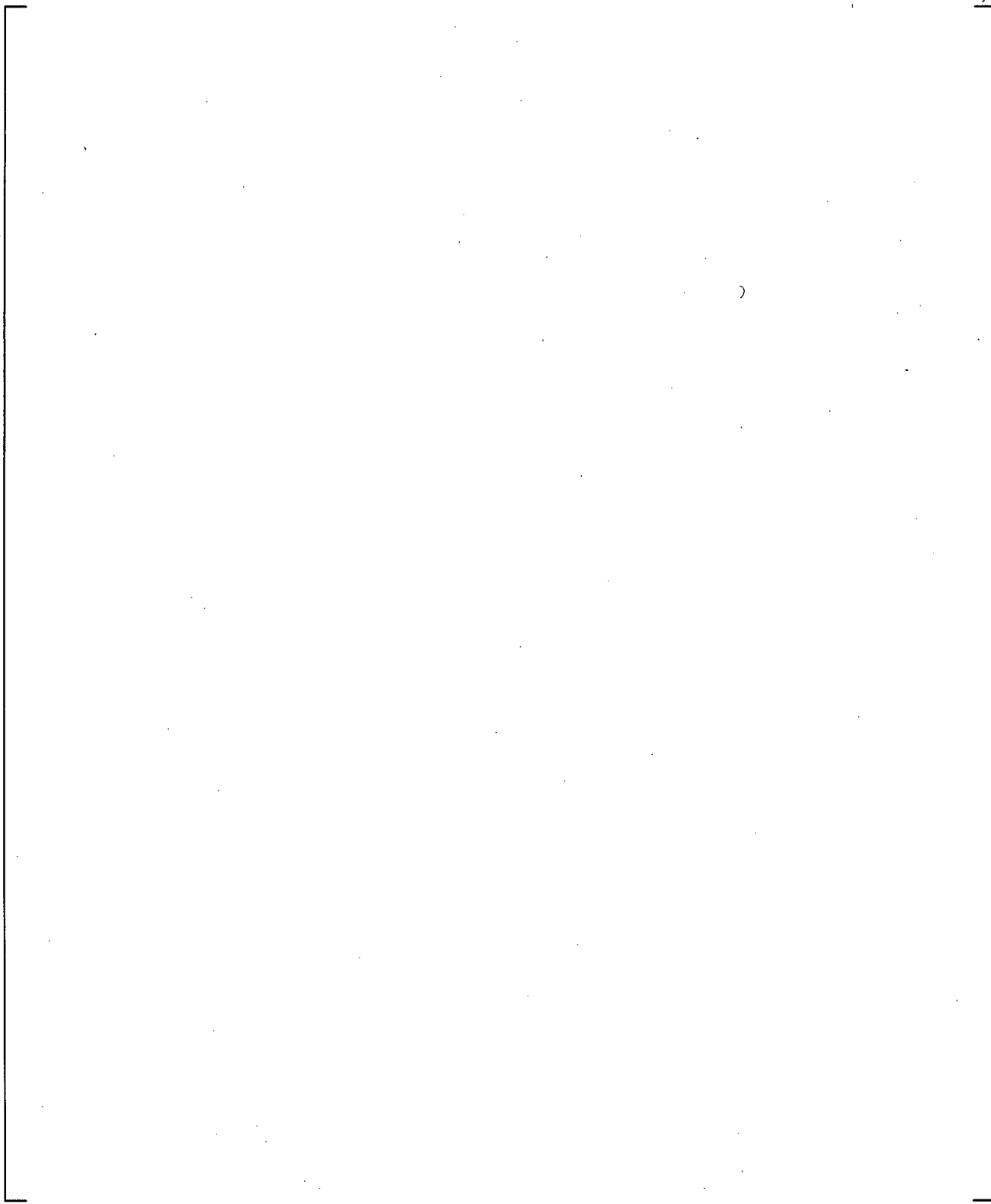


**Figure 24.7.3-12** CCTF Run 62 WCOBRA/TRAC-TF2 vs. Data Comparison Void Fraction from 3.32 to 3.93 m

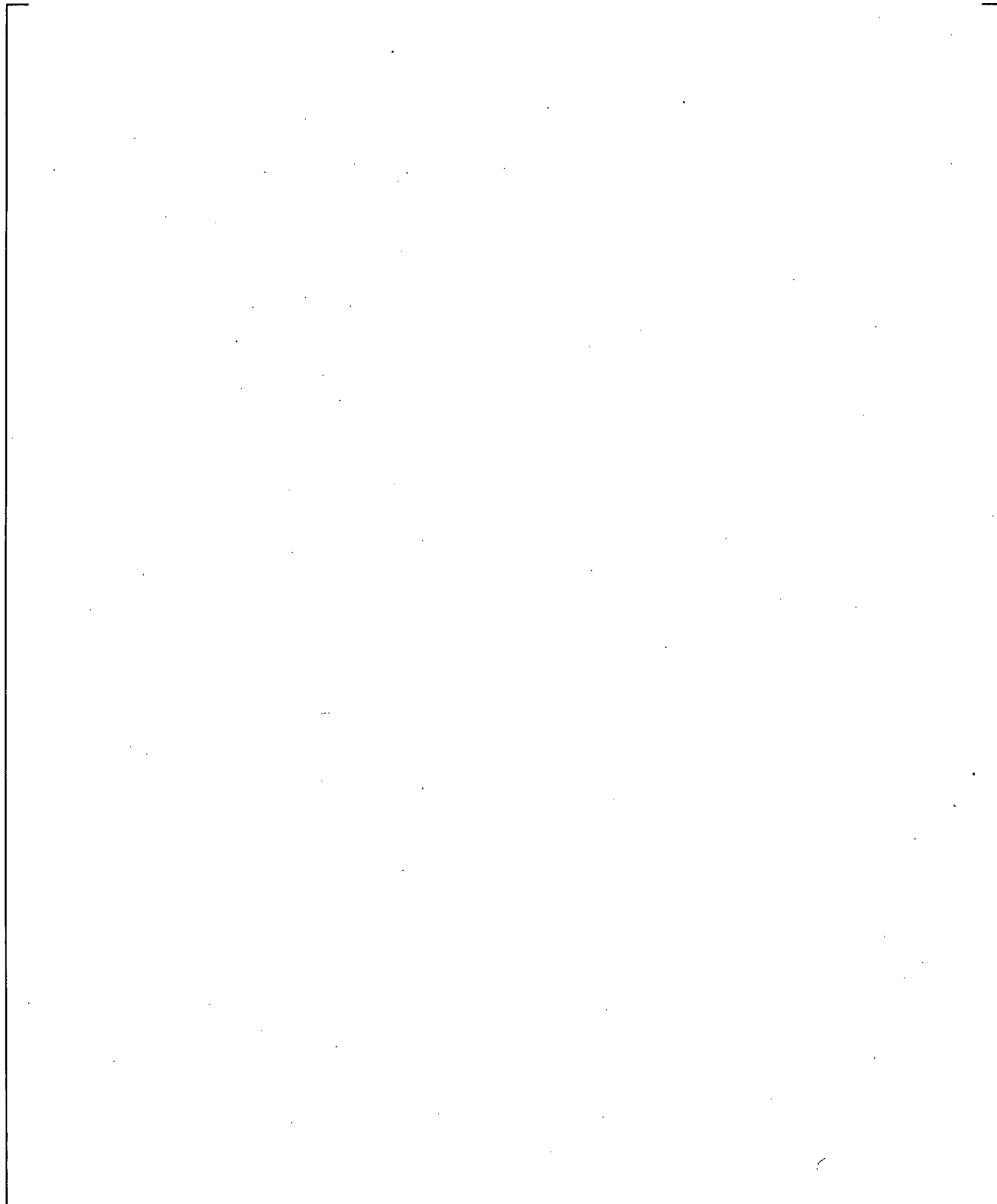


**Figure 24.7.3-13** CCTF Run 62 WCOBRA/TRAC-TF2 vs. Data Comparison Void Fraction from 3.93 to 4.54 m

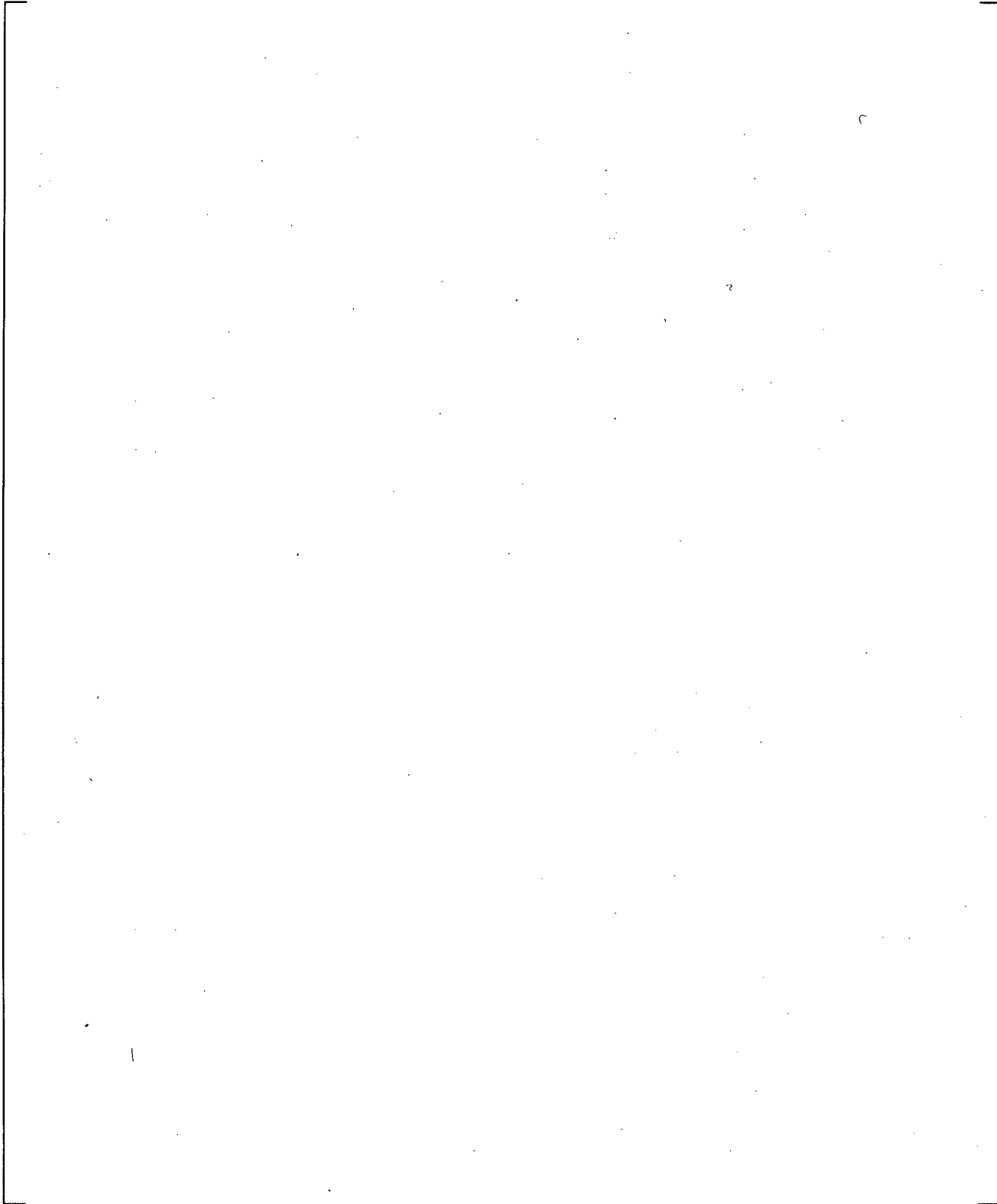


**Figure 24.7.3-14** CCTF Run 62 WCOBRA/TRAC-TF2 vs. Data Comparison Void Fraction from 4.54 to 5.15 m

**Figure 24.7.3-15** CCTF Run 62 WCOBRA/TRAC-TF2 vs. Data Comparison Void Fraction from 5.15 to 5.76 m

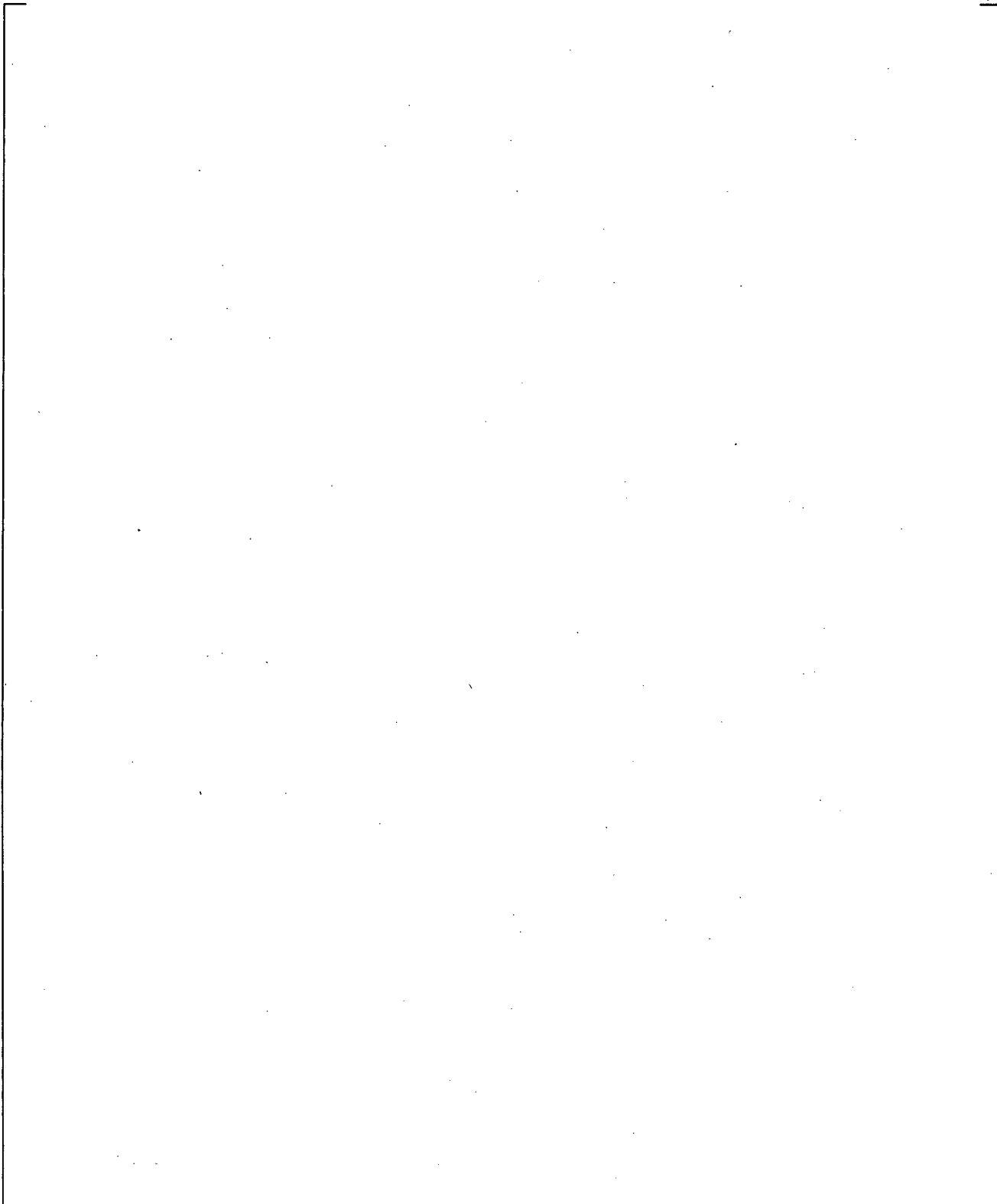


**Figure 24.7.3-16** CCTF Run 62 WCOBRA/TRAC-TF2 vs. Data Comparison Void Fraction from Top of Upper Core Plate to Bottom of Upper Support Plate

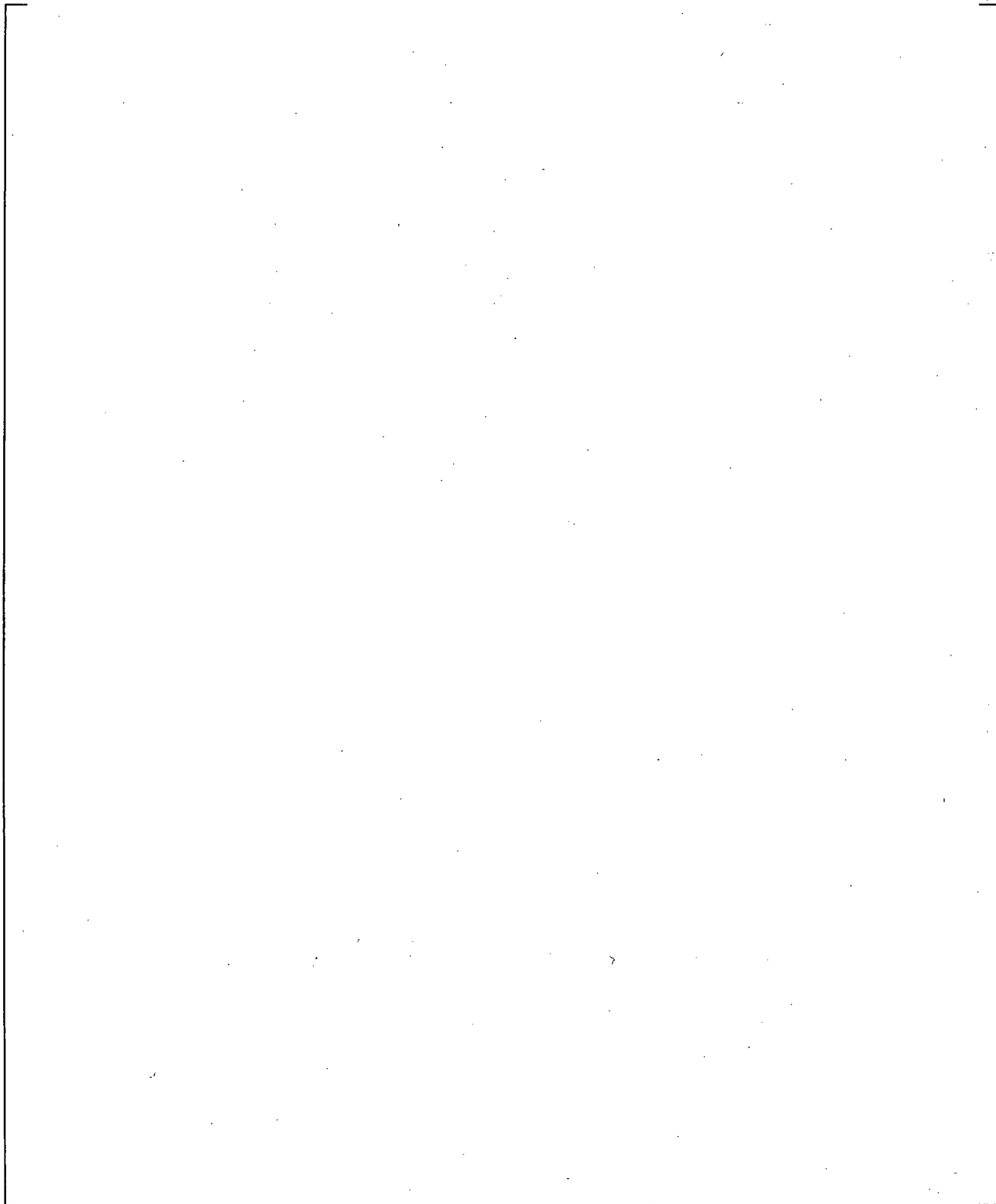


**Figure 24.7.3-17 CCTF Run 62 WCOBRA/TRAC-TF2 vs. Data Collapsed Liquid Level in Core**

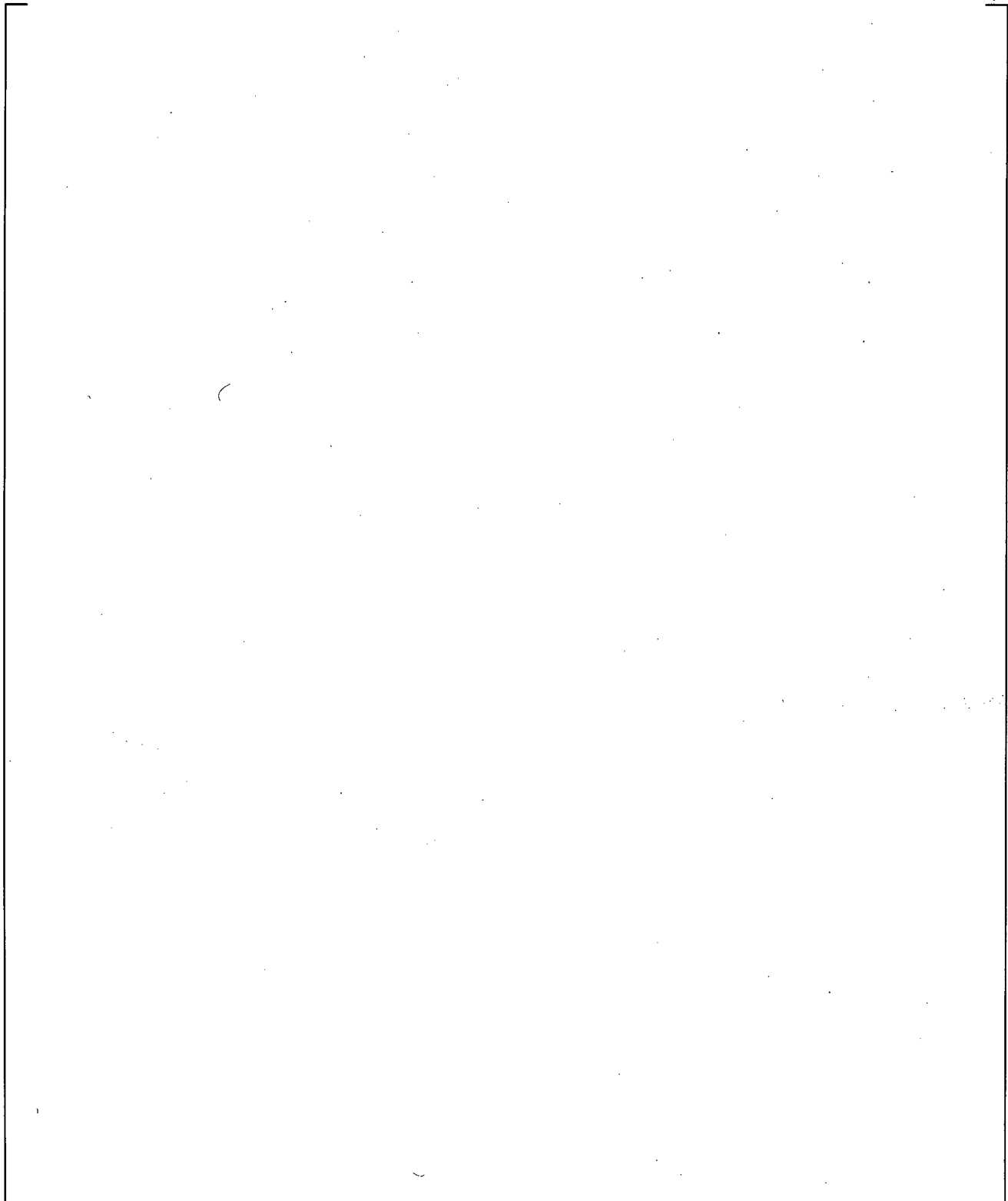


**Figure 24.7.3-18** CCTF Run 62 WCOBRA/TRAC-TF2 vs. Data Collapsed Liquid Level in Upper Plenum

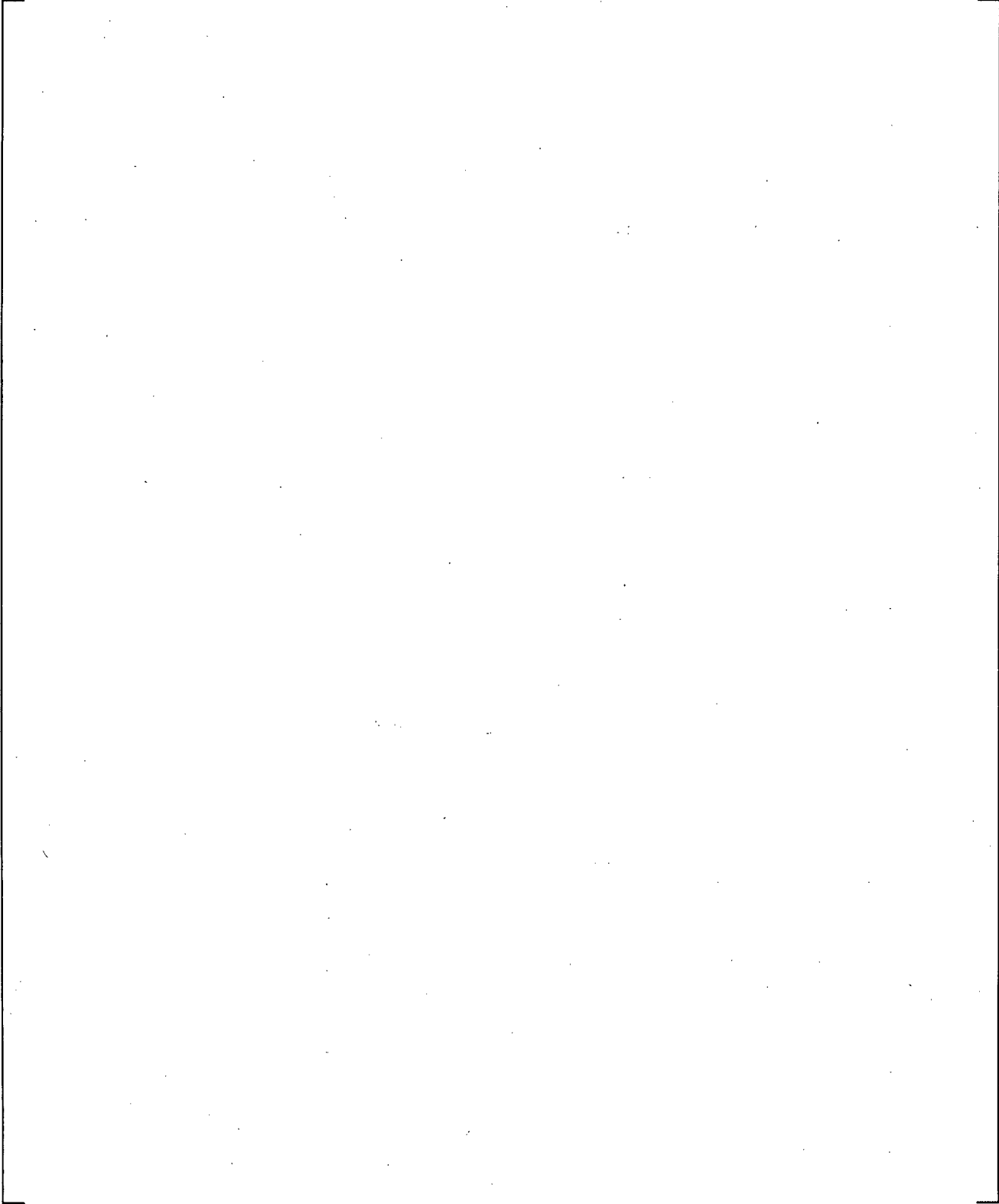


**Figure 24.7.3-19 CCTF Run 62 WCOBRA/TRAC-TF2 vs. Data Pressure in Upper Plenum**

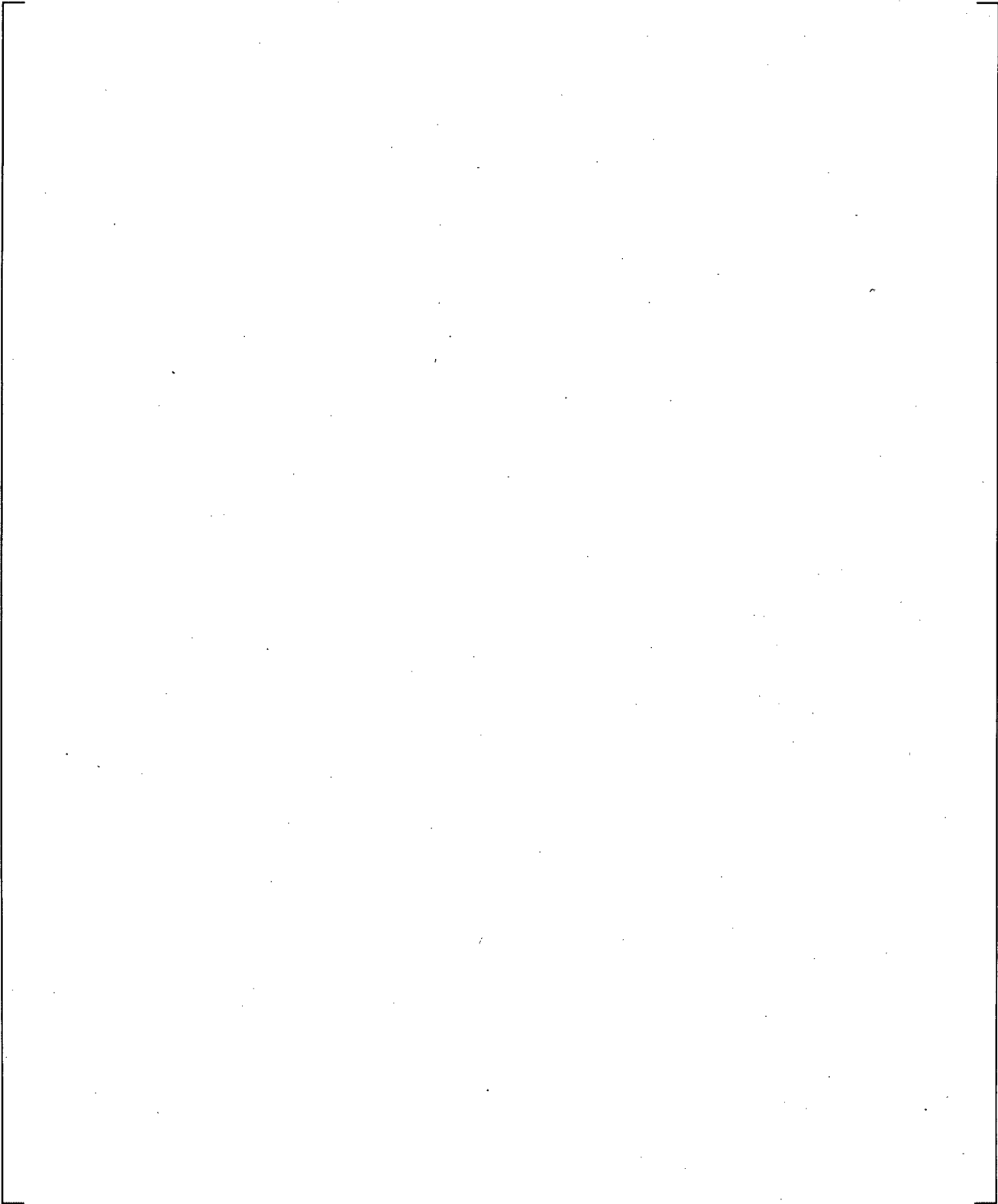


**Figure 24.7.3-20 CCTF Run 62 WCOBRA/TRAC-TF2 vs. Data Pressure Difference from Lower Plenum to Upper Plenum**

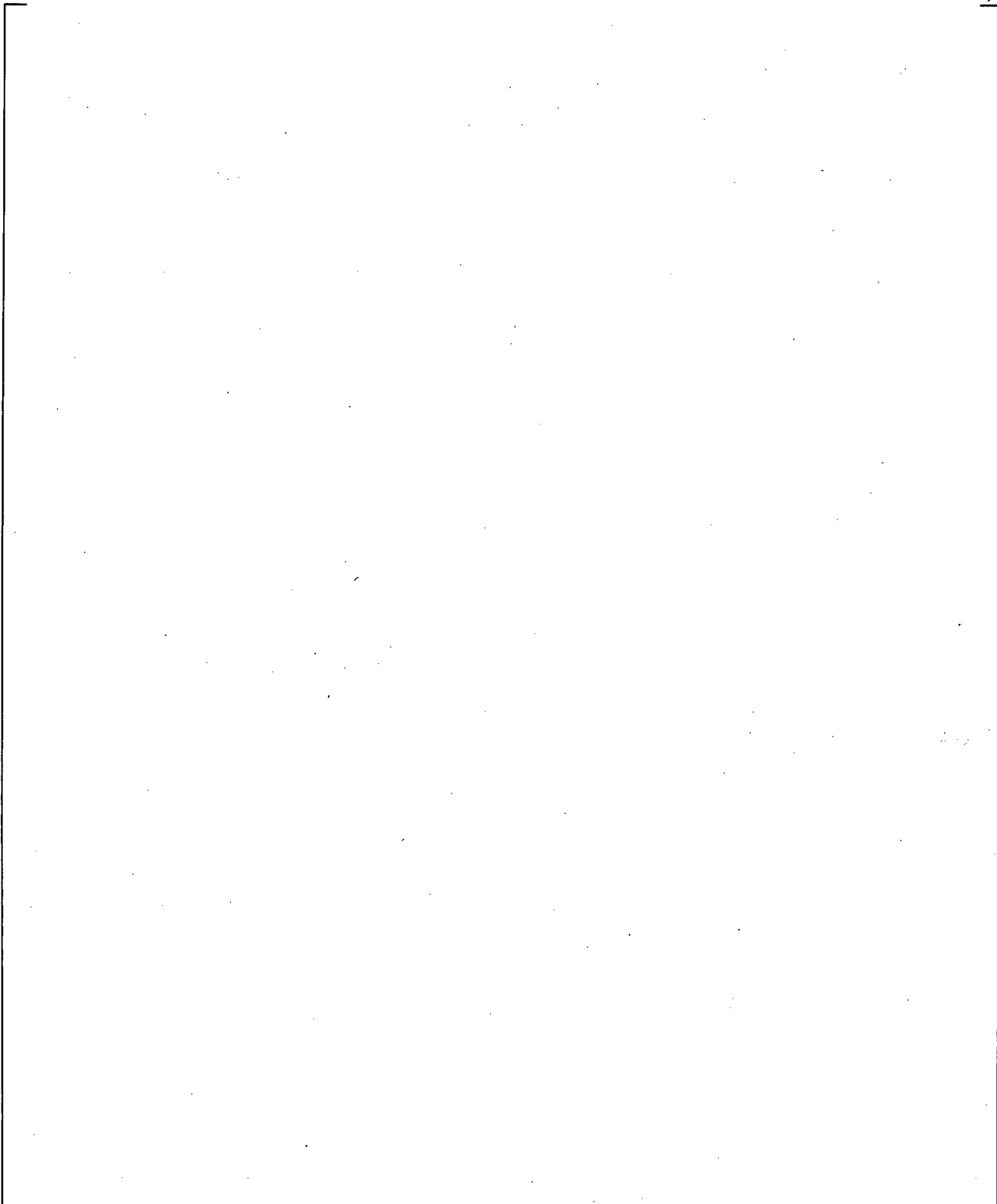


**Figure 24.7.3-21 CCTF Run 62 WCOBRA/TRAC-TF2 vs. Data Pressure Difference from Lower Plenum to Top of Downcomer**

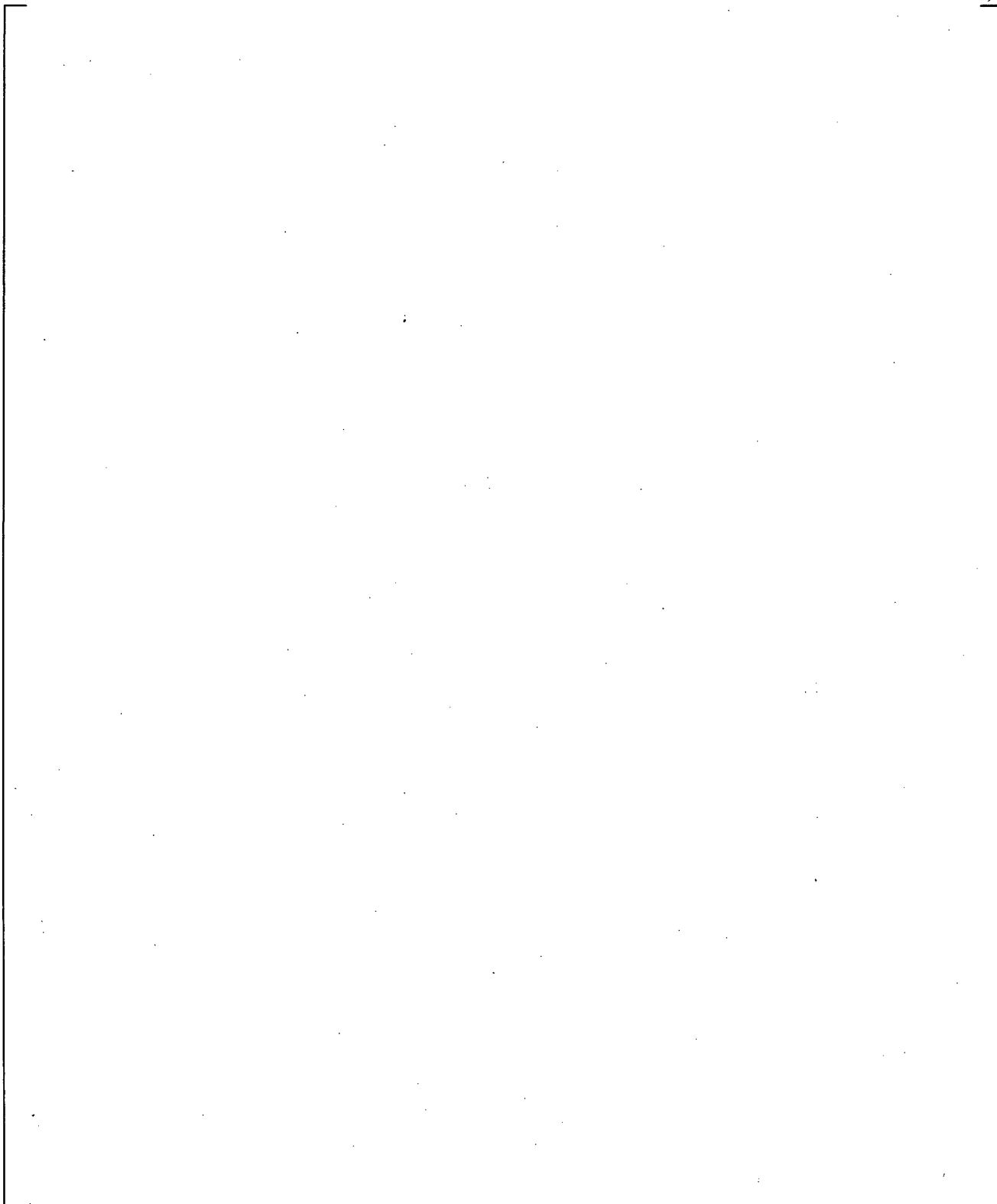


**Figure 24.7.3-22 CCTF Run 62 WCOBRA/TRAC-TF2 vs. Data Pressure Difference from Upper Plenum to Intact Cold Leg Nozzle (Intact Loop  $\Delta P$ )**

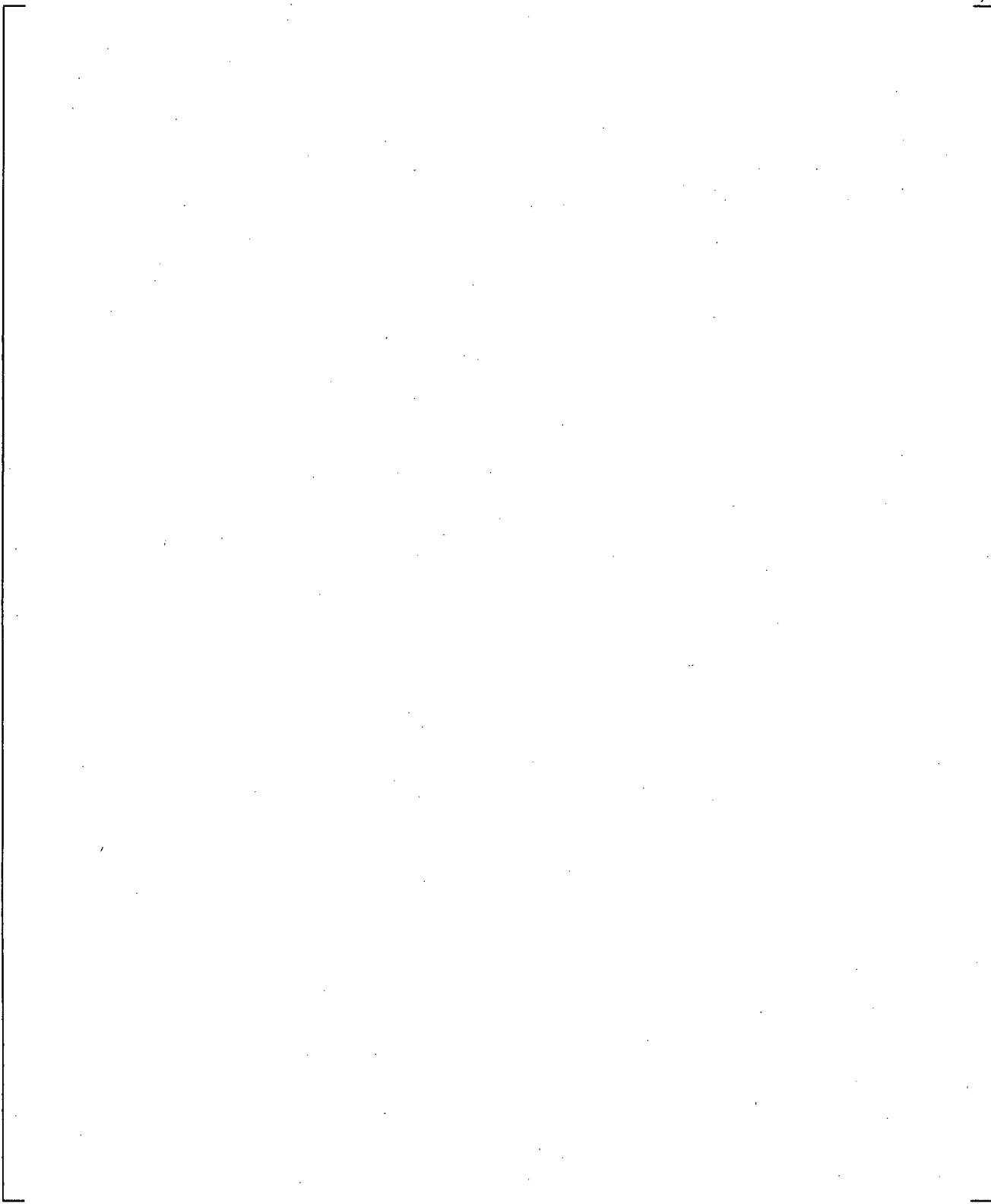


**Figure 24.7.3-23** CCTF Run 62 WCOBRA/TRAC-TF2 vs. Data Pressure Difference from Upper Plenum to Steam Generator (Intact Loop  $\Delta P$ )

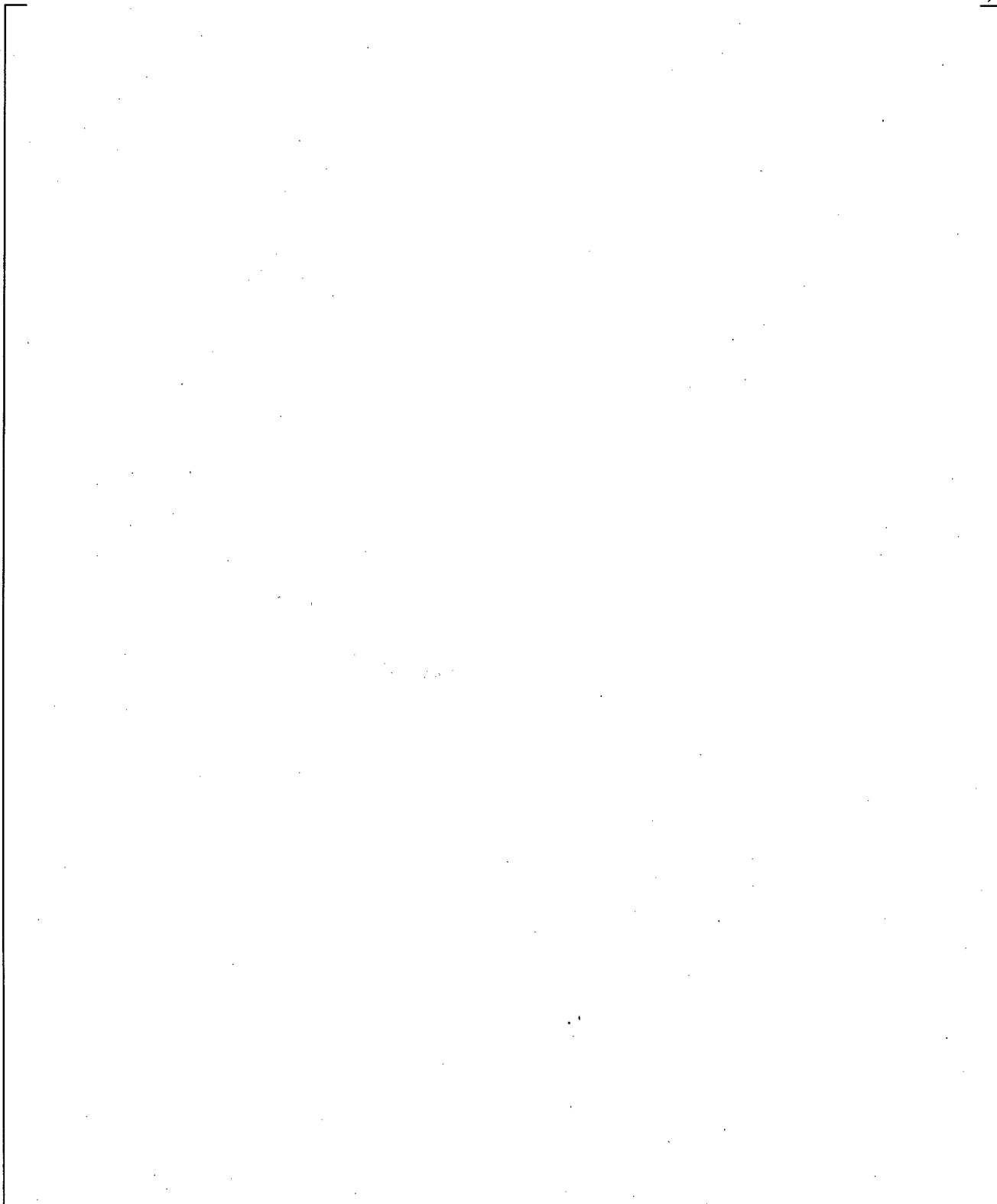


**Figure 24.7.3-24** CCTF Run 62 WCOBRA/TRAC-TF2 vs. Data Pressure Difference from Inlet to Outlet Plenum of Steam Generator (Intact Loop  $\Delta P$ )

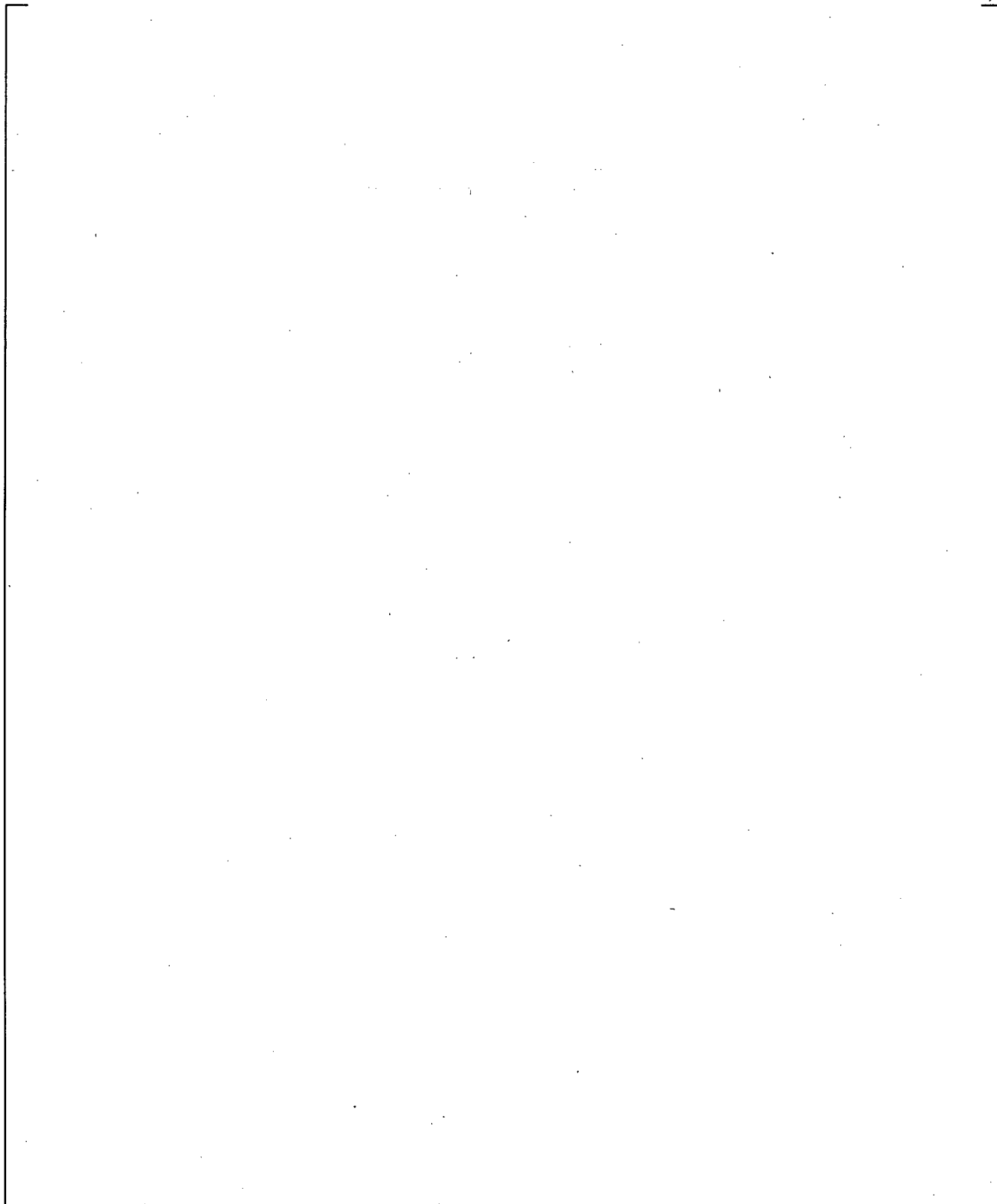


**Figure 24.7.3-25** CCTF Run 62 WCOBRA/TRAC-TF2 vs. Data Pressure Difference across RCP (Intact Loop  $\Delta P$ )

**Figure 24.7.3-26 CCTF Run 62 WCOBRA/TRAC-TF2 vs. Data Pressure Difference from RCP to Downcomer (Intact Loop  $\Delta P$ )**

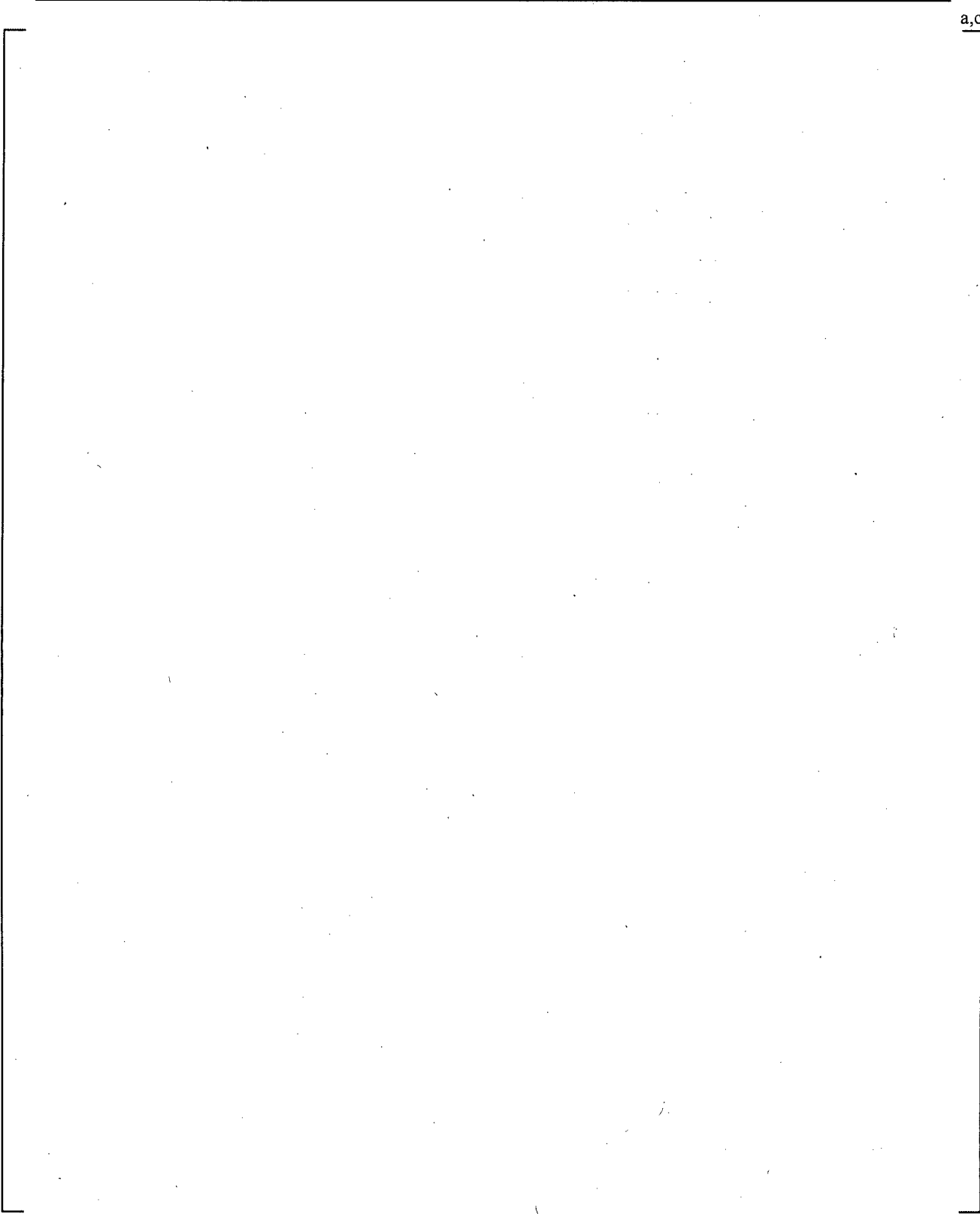


**Figure 24.7.3-27 CCTF Run 62 Pressure Difference from UP to SG**

a,c

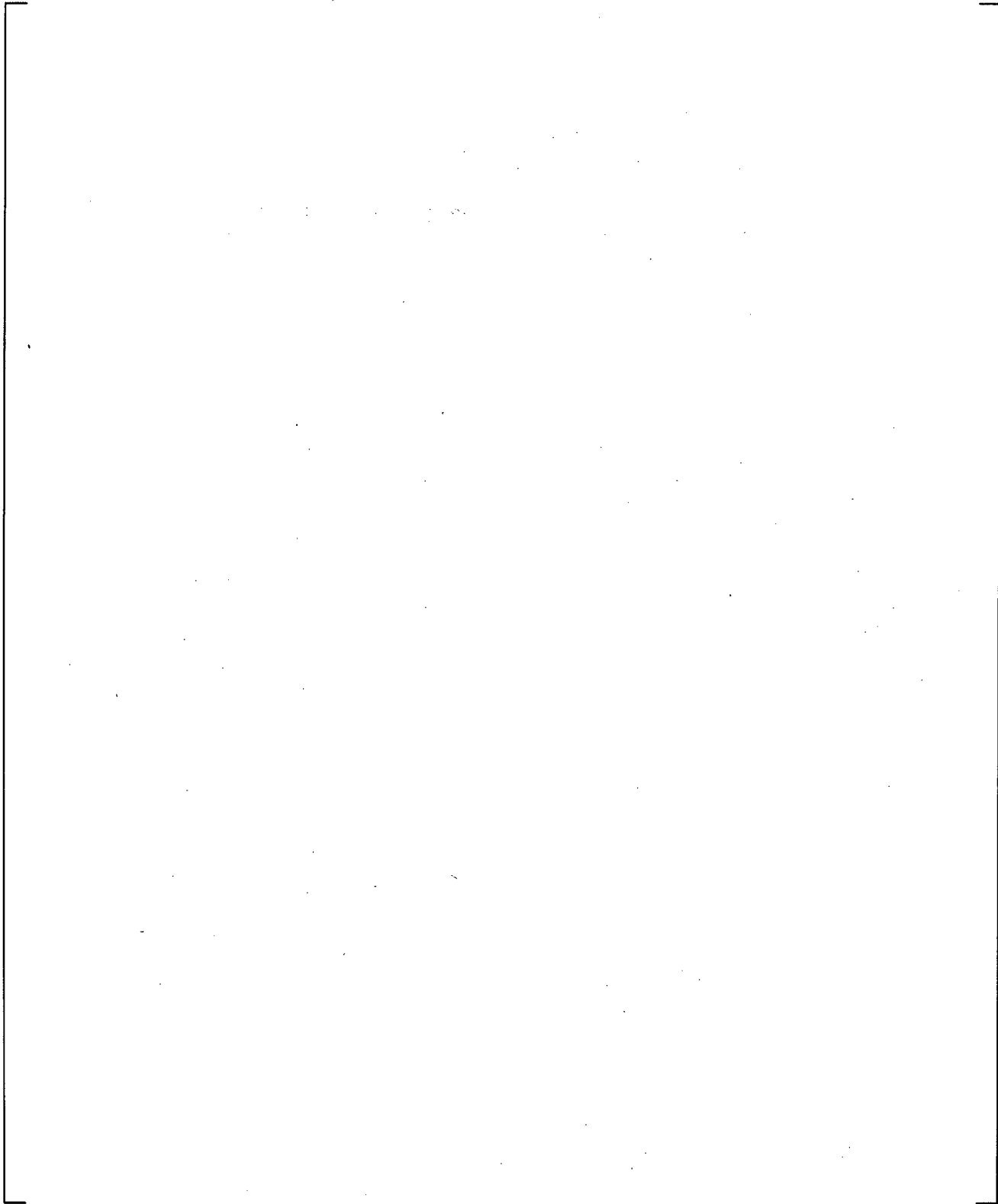


**Figure 24.7.3-28 CCTF Run 62 Pressure Difference from UP to PUMP**

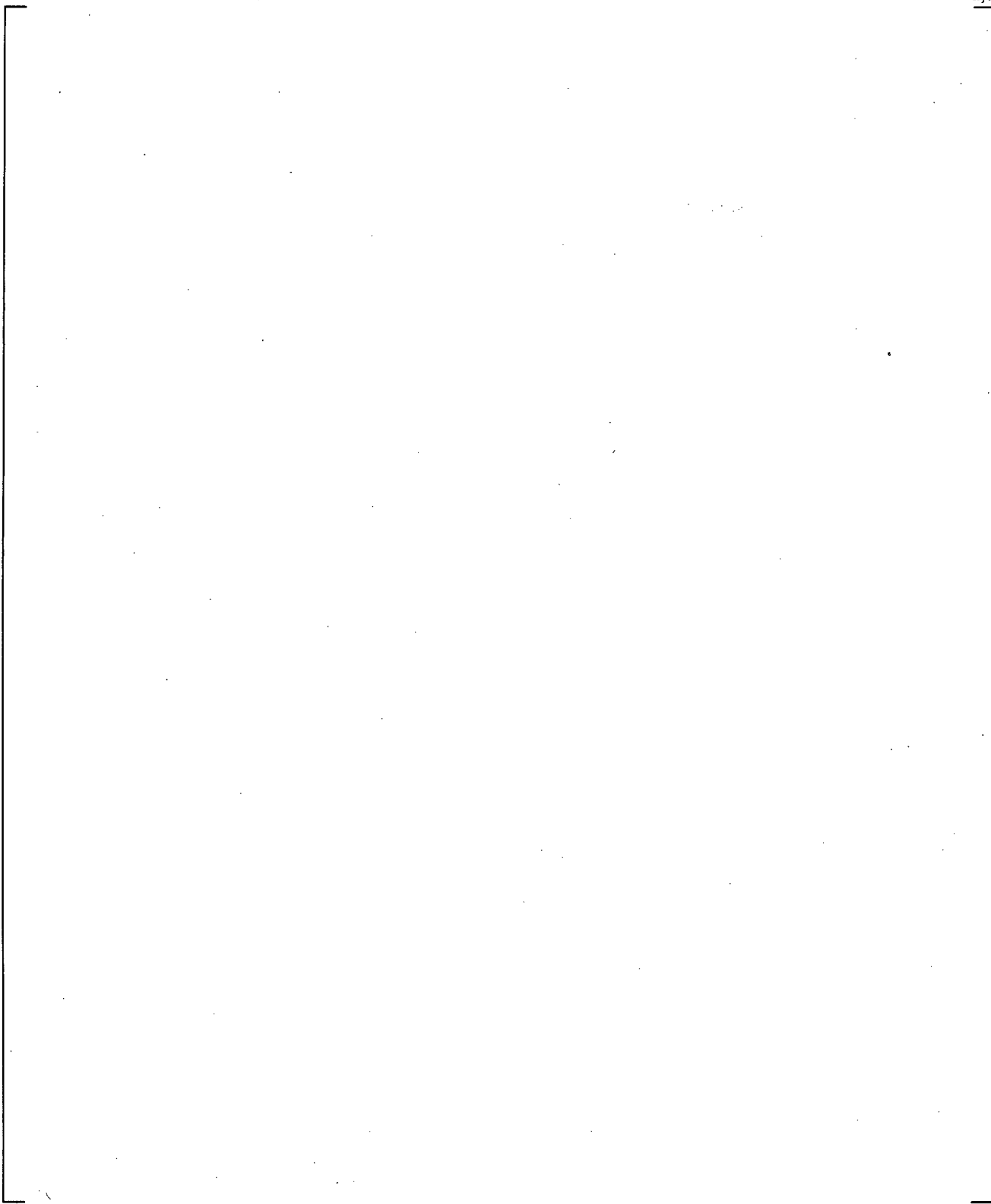


**Figure 24.7.3-29** CCTF Run 62 WCOBRA/TRAC-TF2 vs. Data Pressure Difference in Broken Loop Hot Leg (Broken Loop  $\Delta P$ )

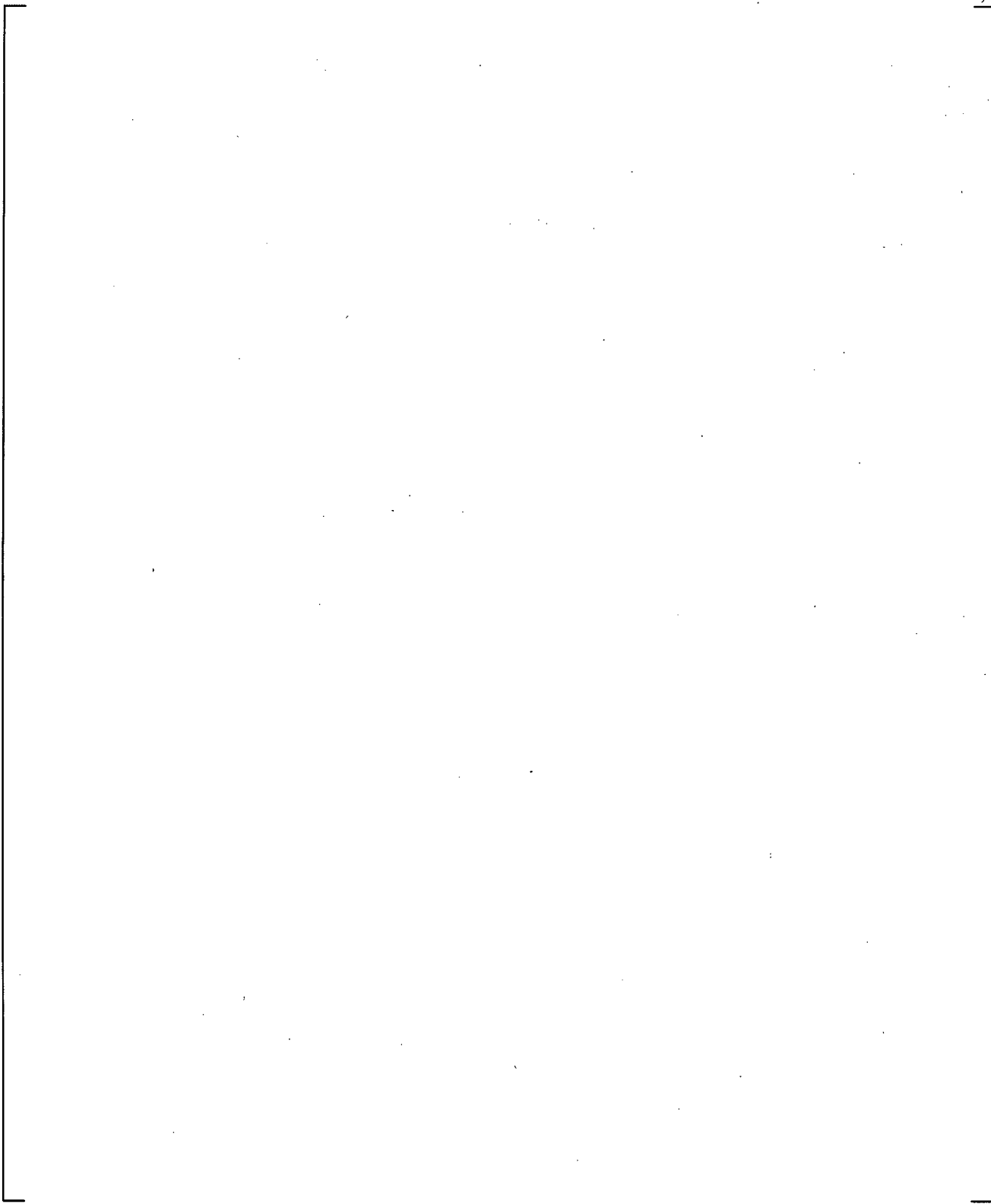


**Figure 24.7.3-30** CCTF Run 62 WCOBRA/TRAC-TF2 vs. Data Pressure Difference from Upper Plenum to Steam Generator in Broken Loop (Broken Loop  $\Delta P$ )

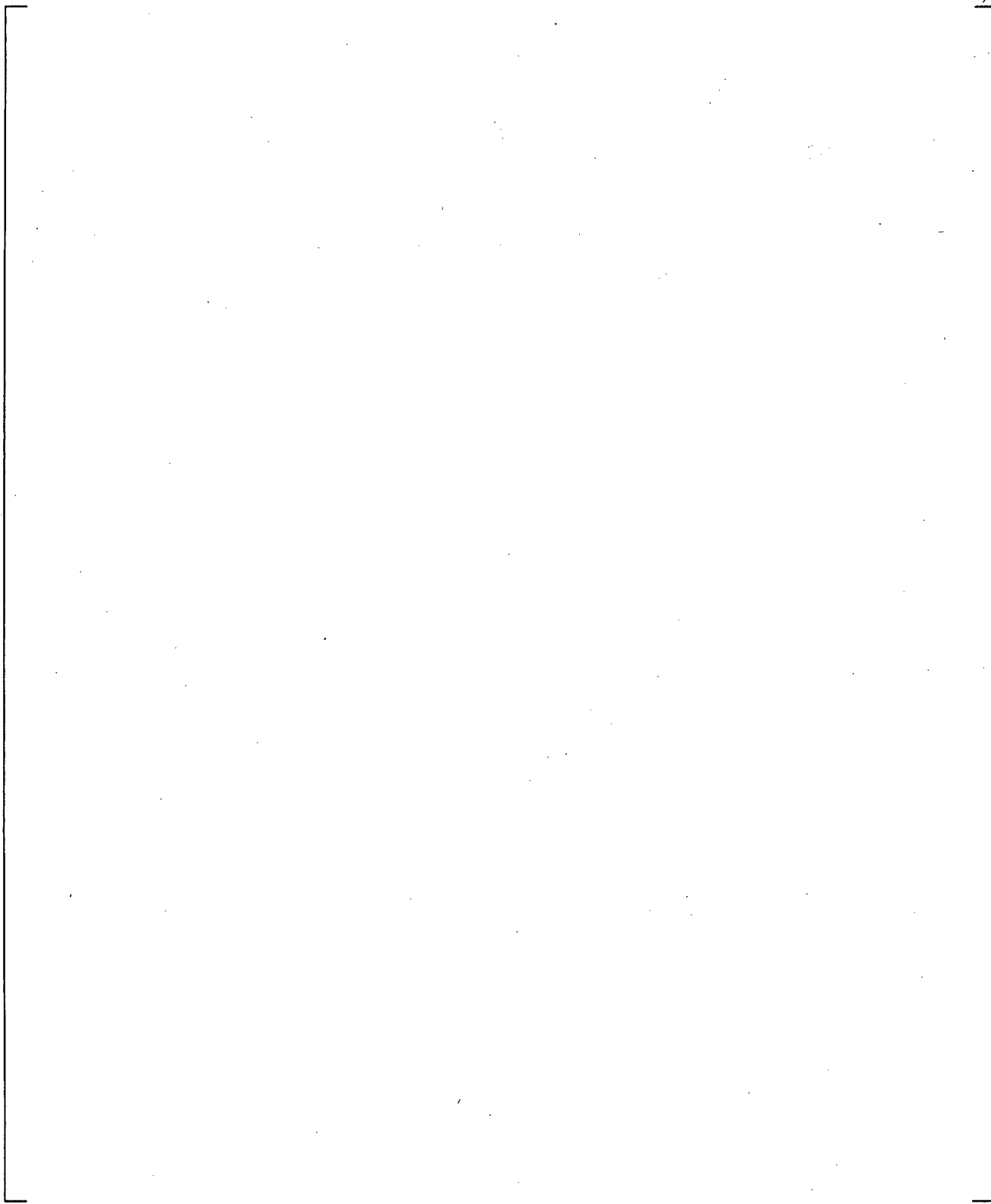


**Figure 24.7.3-31** CCTF Run 62 WCOBRA/TRAC-TF2 vs. Data Pressure Difference from Inlet to Outlet Plenum of Steam Generator in Broken Loop (Broken Loop  $\Delta P$ )

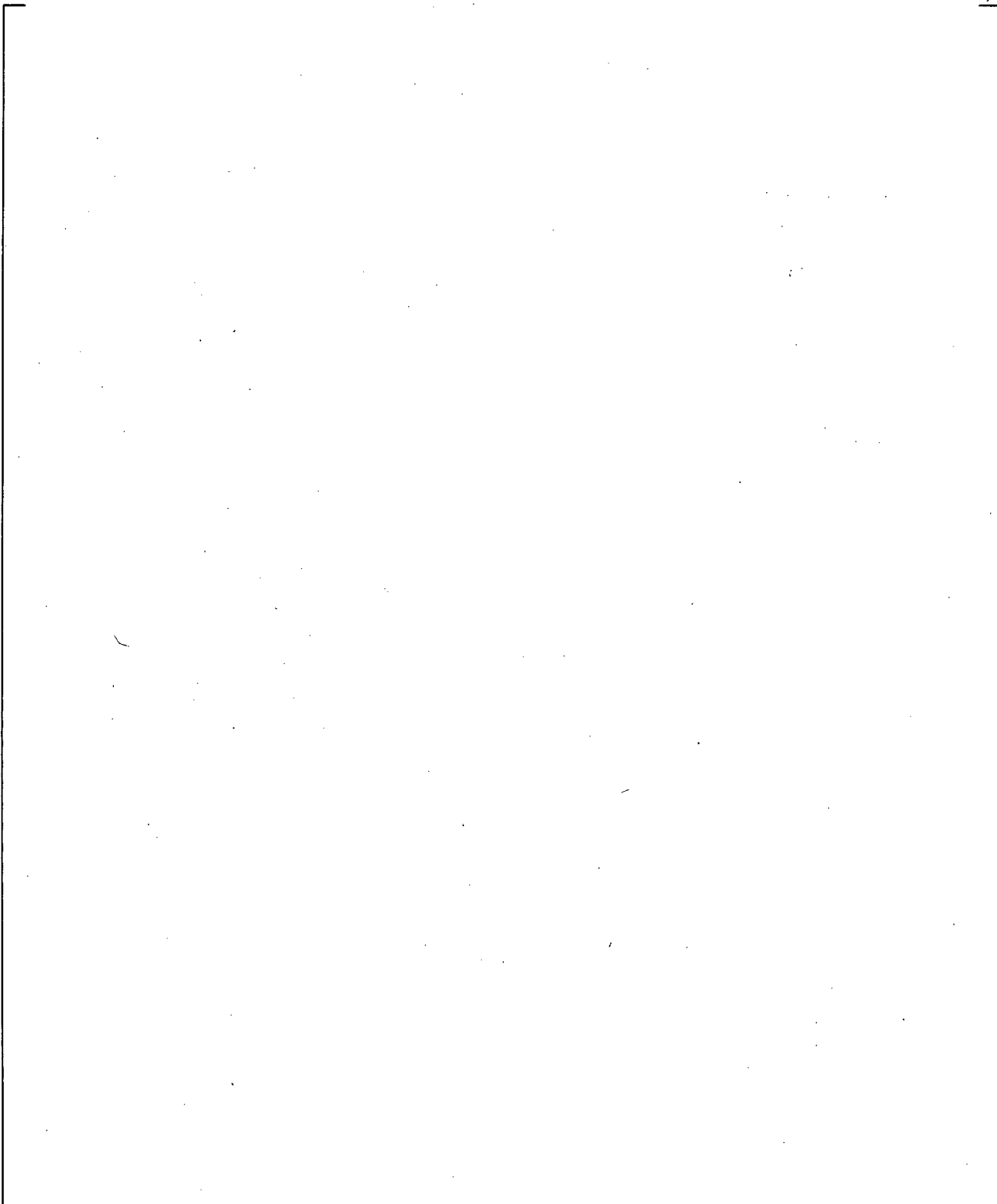


**Figure 24.7.3-32** CCTF Run 62 WCOBRA/TRAC-TF2 vs. Data Pressure Difference across RCP in Broken Loop (Broken Loop  $\Delta P$ )

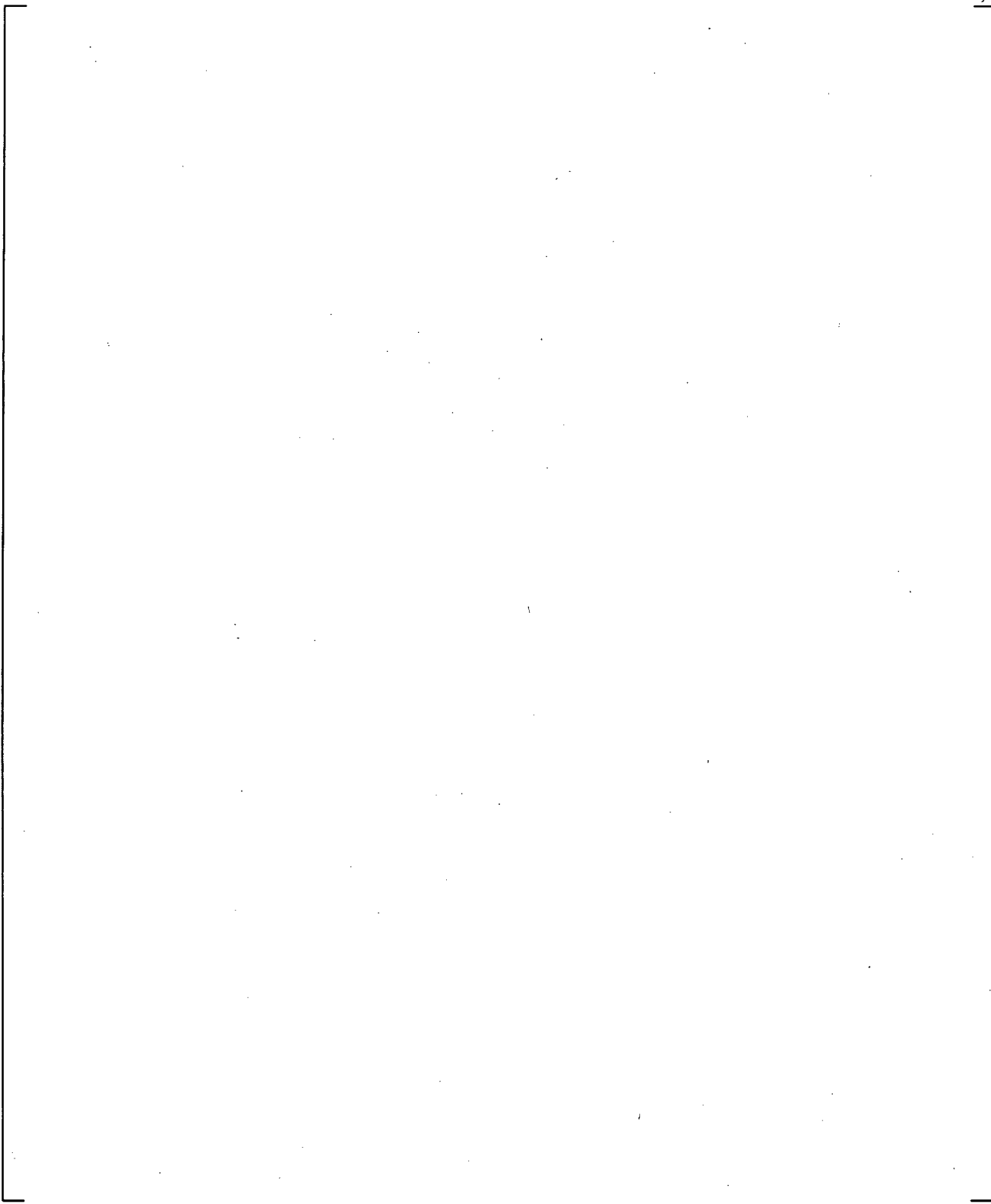


**Figure 24.7.3-33** CCTF Run 62 WCOBRA/TRAC-TF2 vs. Data Pressure Difference from RCP to CV (Broken Loop  $\Delta P$ )

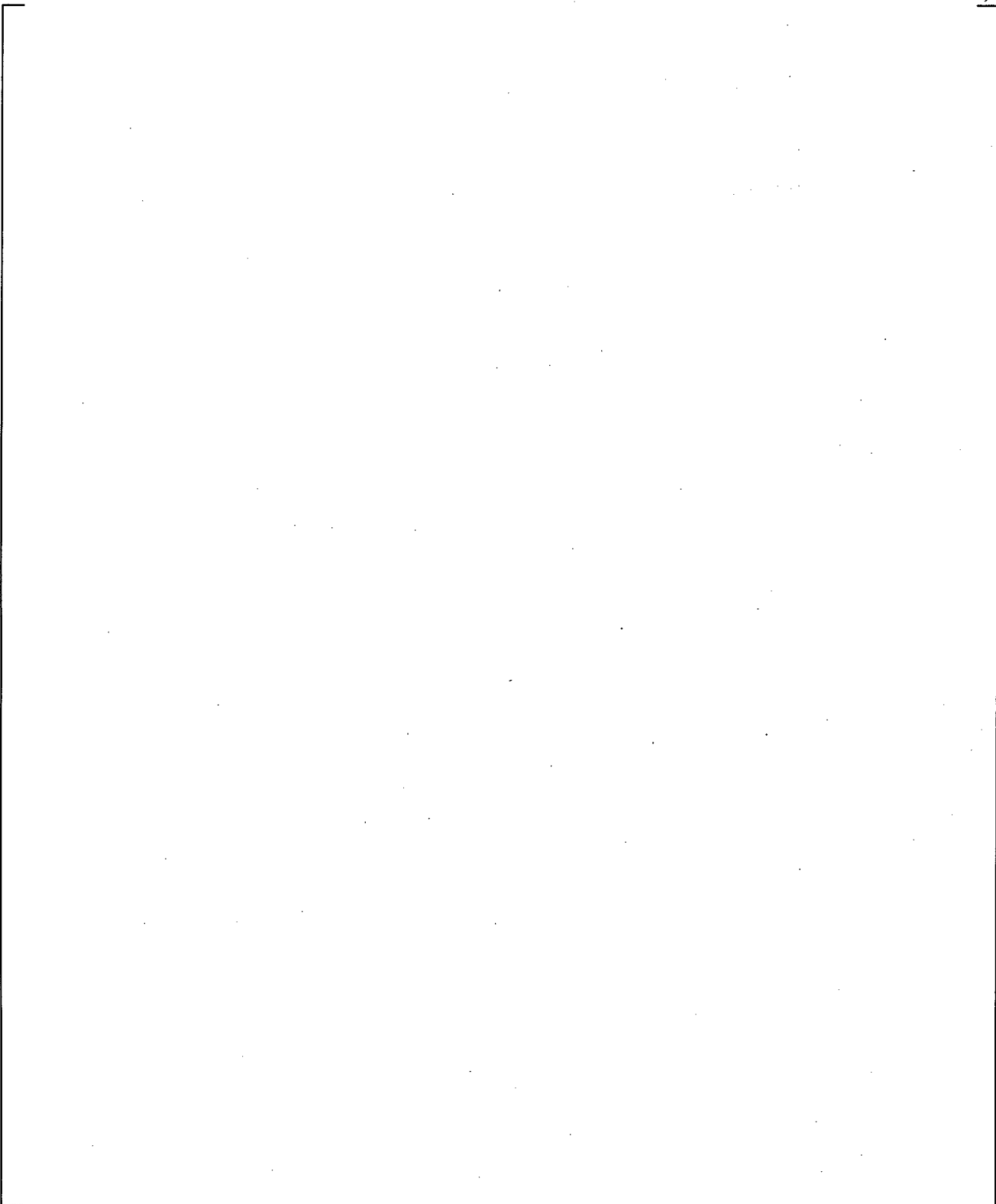


**Figure 24.7.3-34** CCTF Run 62 WCOBRA/TRAC-TF2 vs. Data Vapor Mass Flowrate in Intact Hot Leg

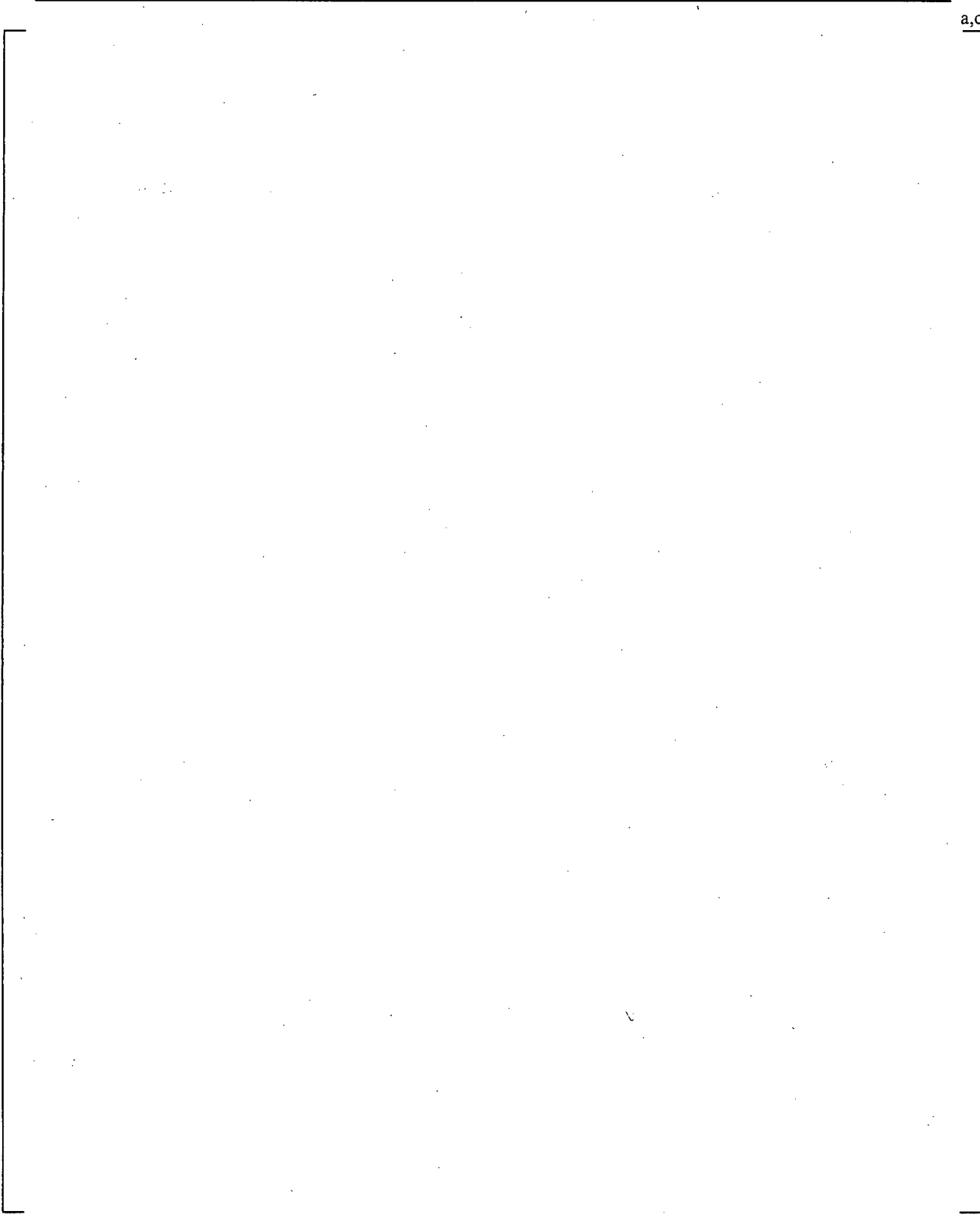


**Figure 24.7.3-35 CCTF Run 62 WCOBRA/TRAC-TF2 vs. Data Vapor Velocity in Intact Hot Leg**

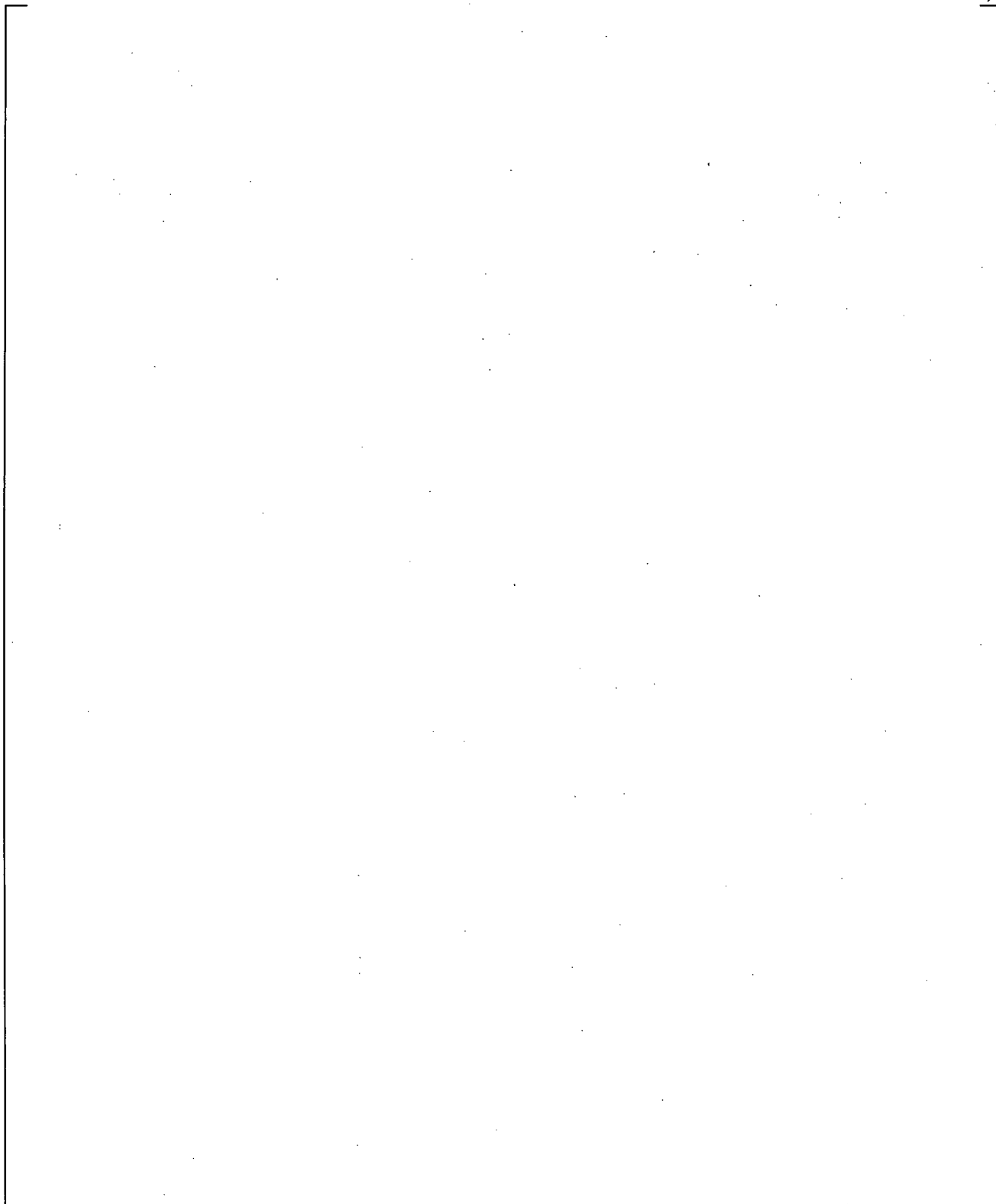


**Figure 24.7.3-36 CCTF Run 62 WCOBRA/TRAC-TF2 vs. Data Vapor Density in Intact Hot Leg**

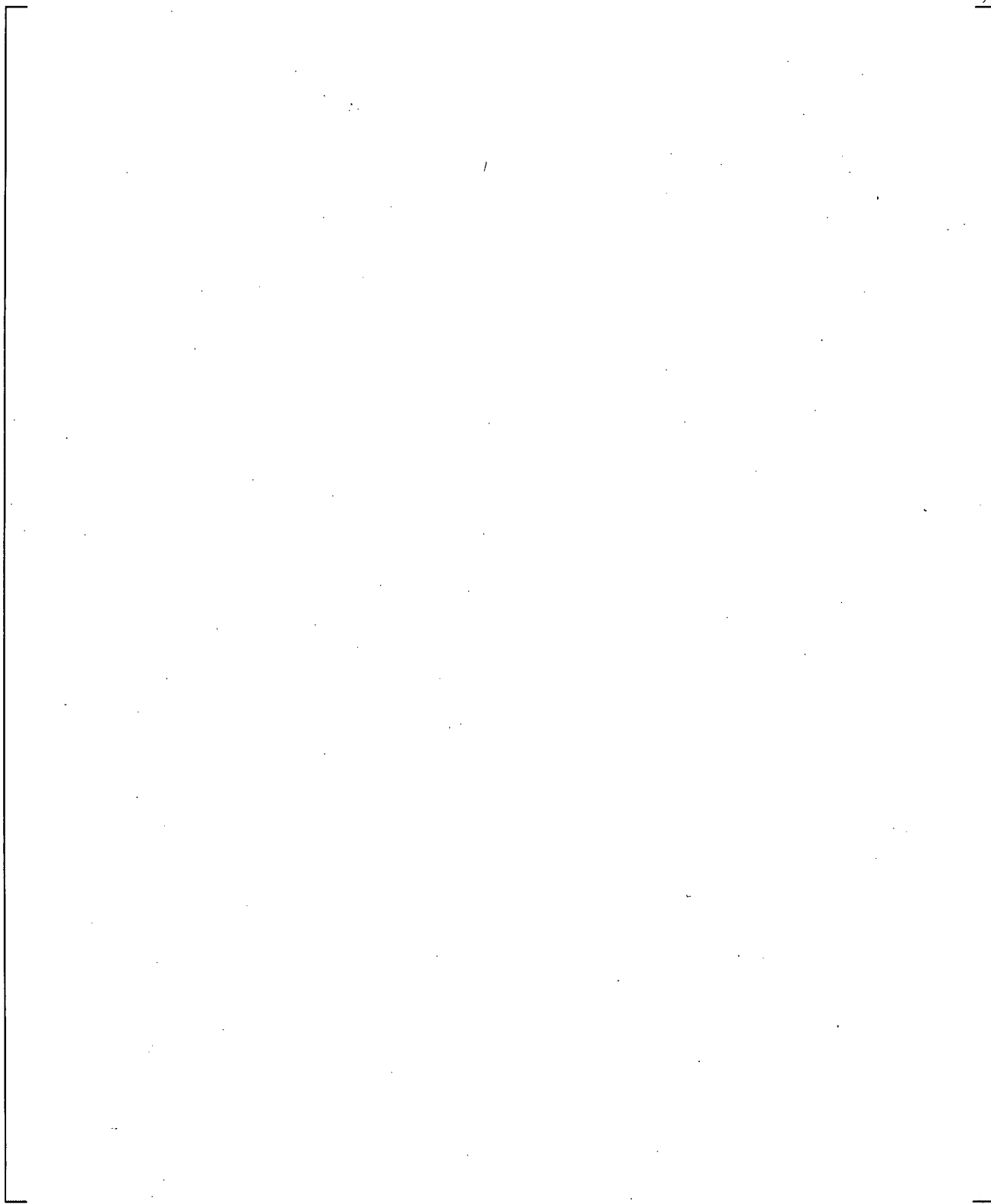


**Figure 24.7.3-37 CCTF Run 62 WCOBRA/TRAC-TF2 vs. Data Liquid Mass Flowrate in Intact Hot Leg**

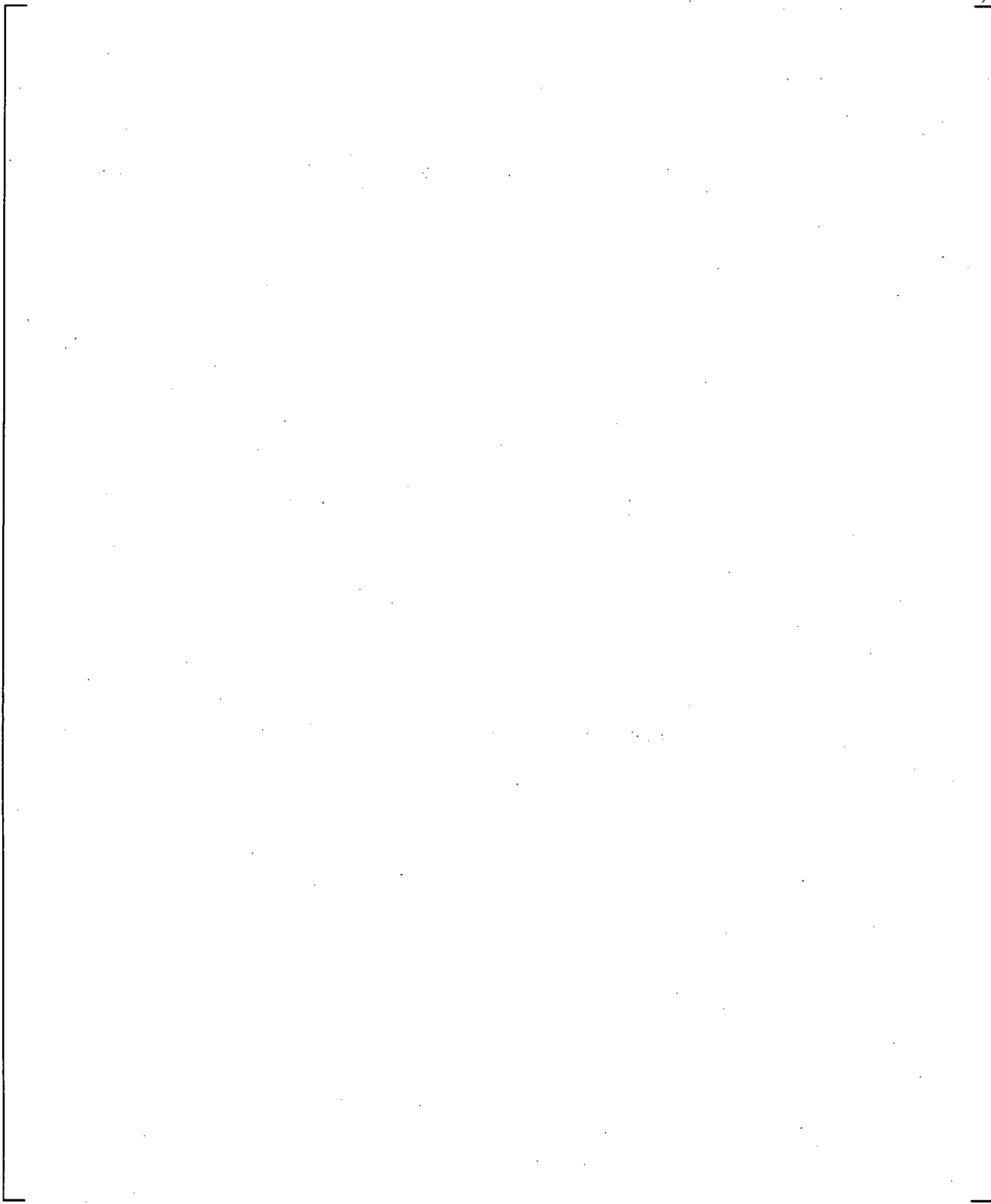


**Figure 24.7.3-38** CCTF Run 62 WCOBRA/TRAC-TF2 vs. Data Total Mass Flowrate in Intact Hot Leg

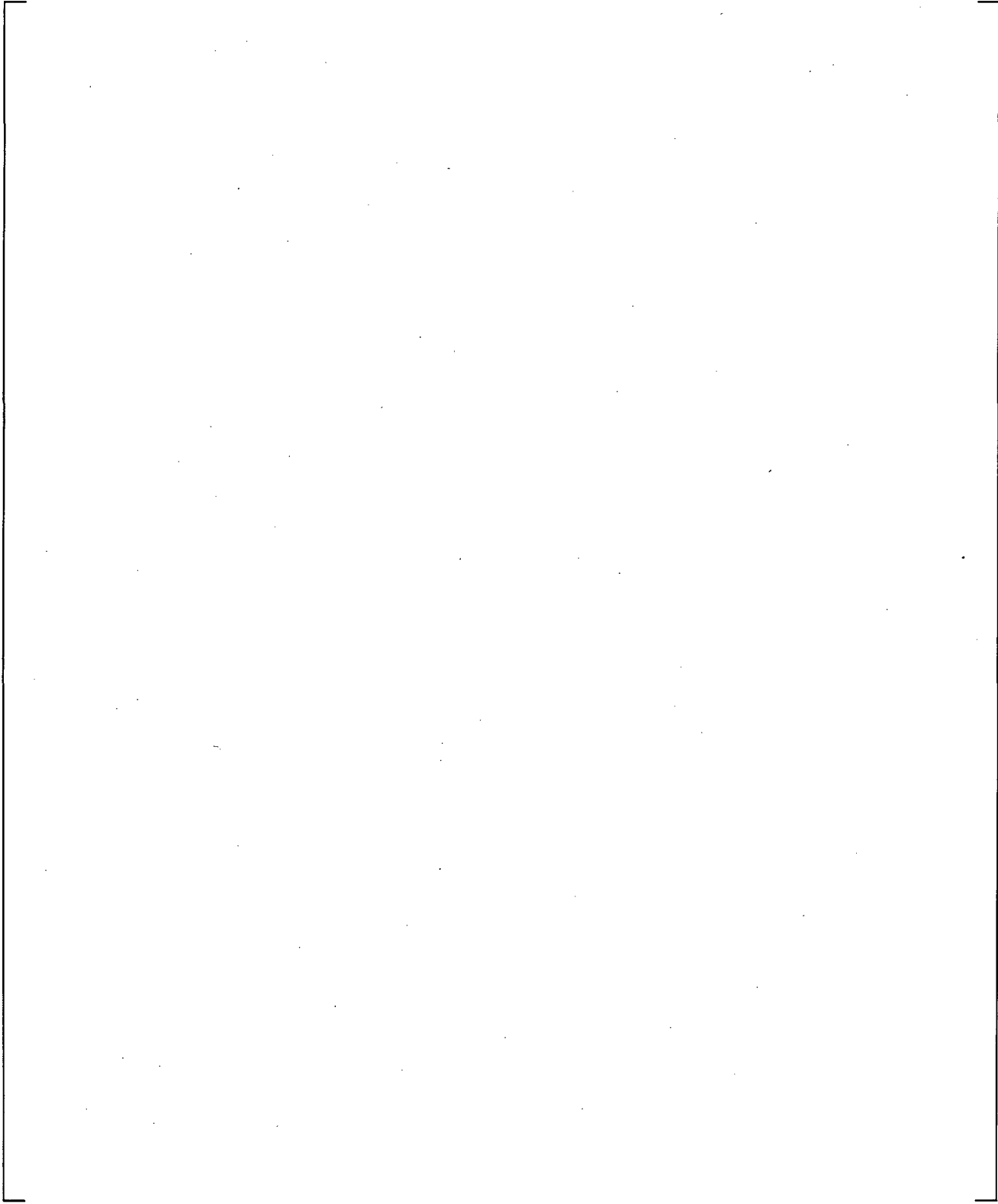


**Figure 24.7.3-39** CCTF Run 62 WCOBRA/TRAC-TF2 vs. Data Vapor Mass Flowrate in Intact Cold Leg

**Figure 24.7.3-40 CCTF Run 62 WCOBRA/TRAC-TF2 vs. Data Liquid Mass Flowrate in Intact Cold Leg**

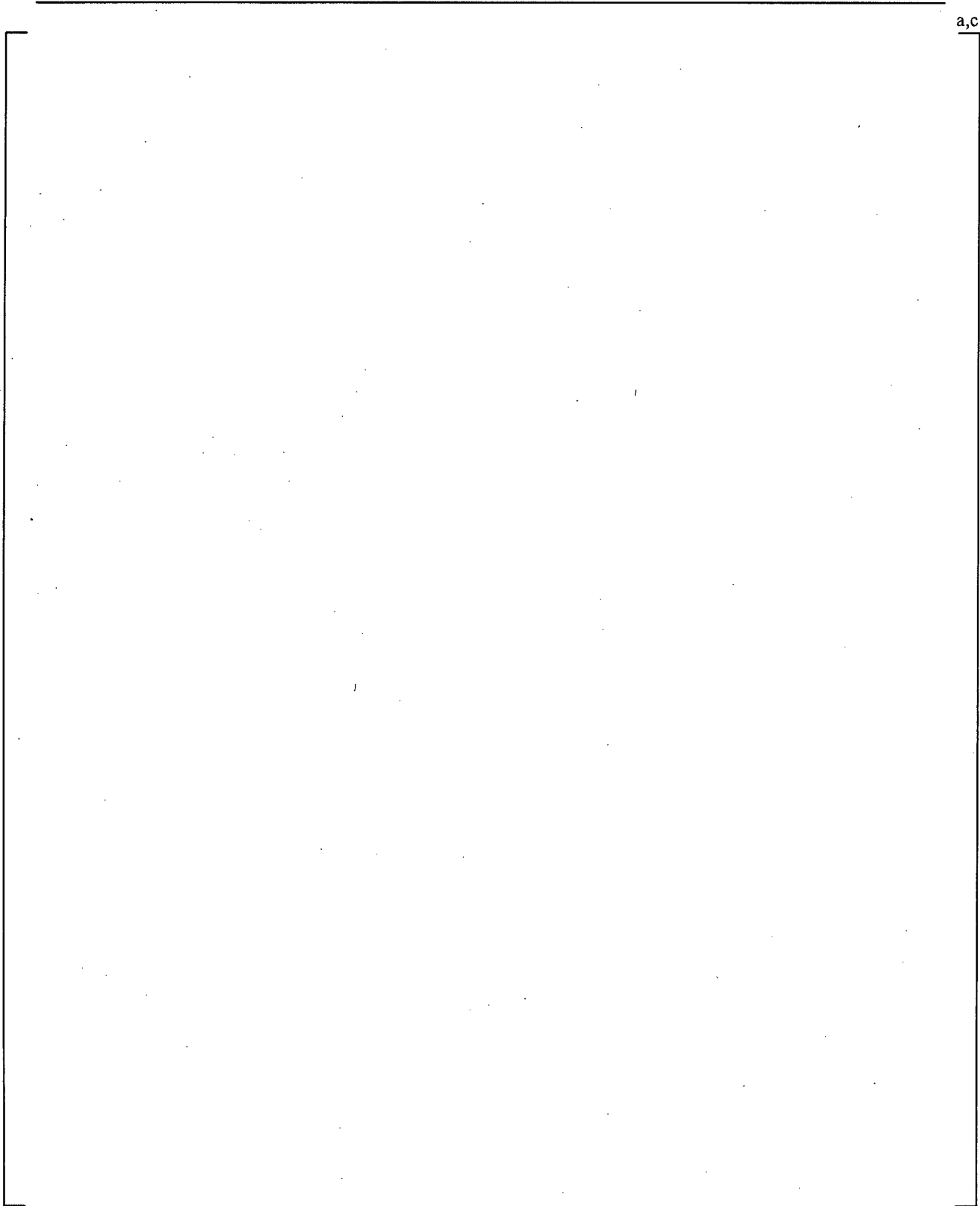
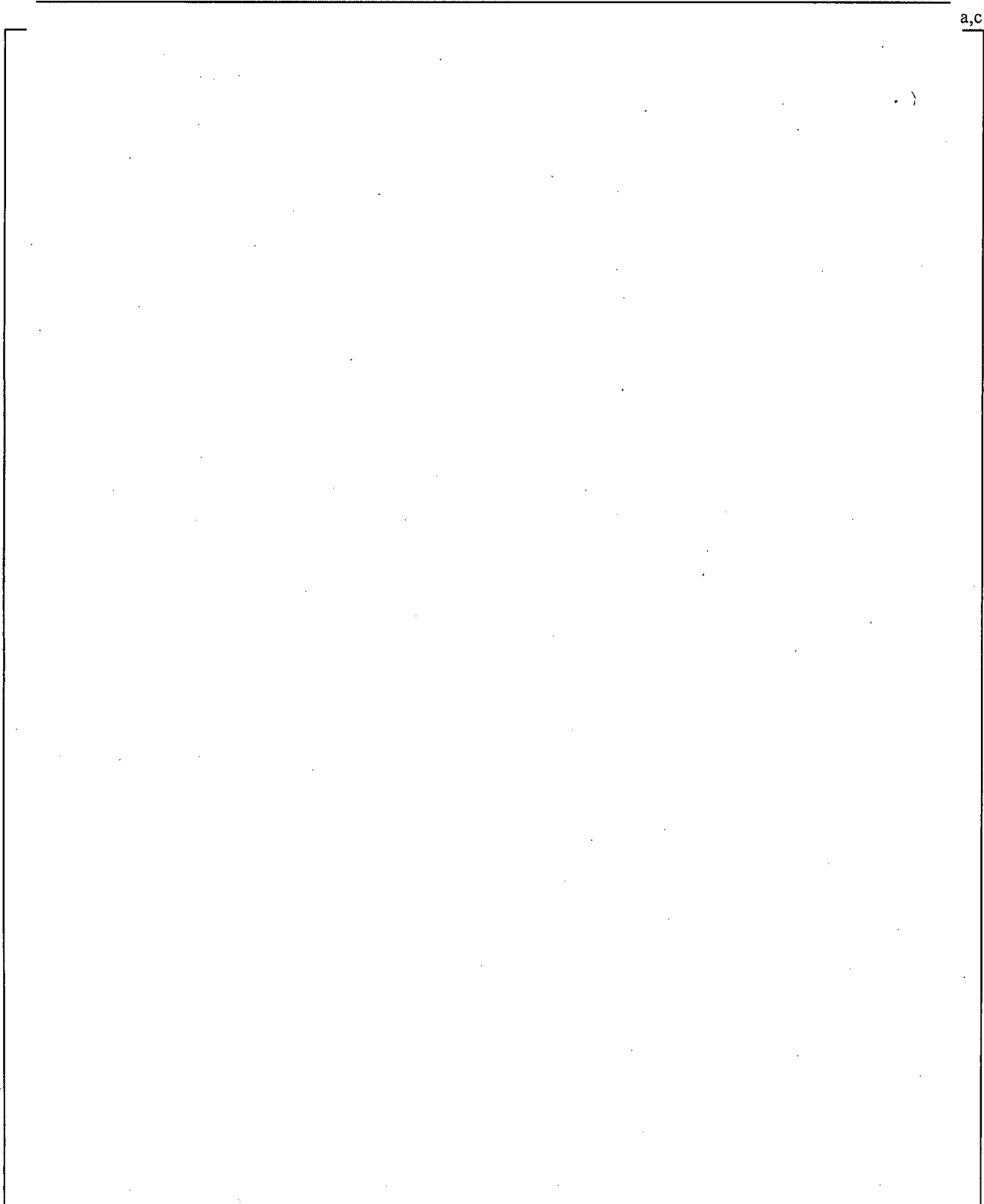
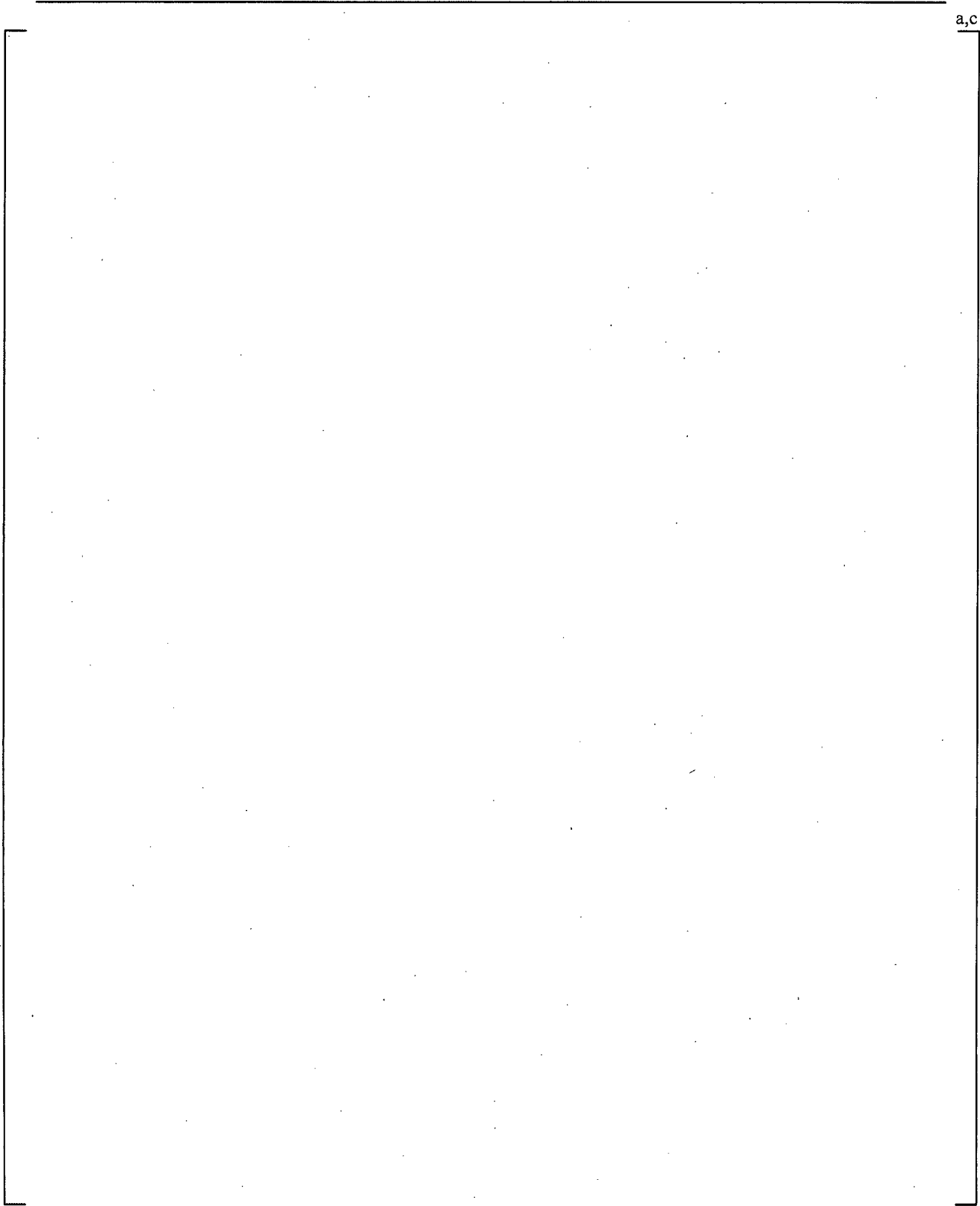


Figure 24.7.3-41 CCTF Run 62 WCOBRA/TRAC-TF2 vs. Data Total Mass Flowrate in Intact Cold Leg



**Figure 24.7.3-42** CCTF Run 62 WCOBRA/TRAC-TF2 vs. Data Liquid Mass Flowrate in Broken Hot Leg



**Figure 24.7.3-43** CCTF Run 62 WCOBRA/TRAC-TF2 vs. Data Vapor Mass Flowrate in Broken Hot Leg

**Figure 24.7.3-44** CCTF Run 62 WCOBRA/TRAC-TF2 vs. Data Total Mass Flowrate in Broken Hot Leg

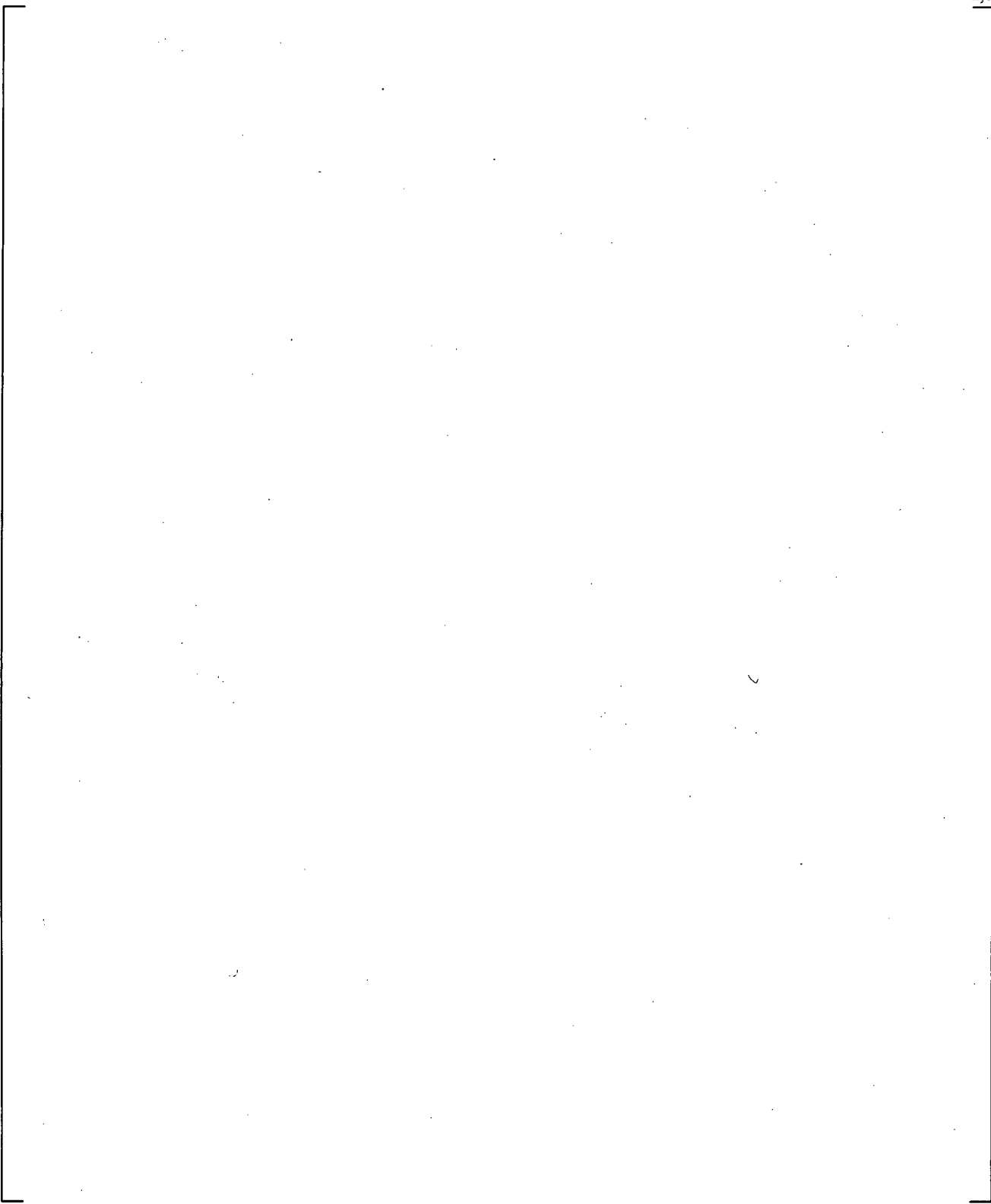


**Figure 24.7.3-45** CCTF Run 62 WCOBRA/TRAC-TF2 vs. Data Vapor Mass Flowrate in Broken Cold Leg

**Figure 24.7.3-46 CCTF Run 62 WCOBRA/TRAC-TF2 vs. Data Pressure in Upper Plenum in Higher Containment Pressure Case**

**Figure 24.7.3-47 CCTF Run 62 WCOBRA/TRAC-TF2 vs. Data Cladding Temperature Comparison at 6 ft in Higher Containment Pressure Case**

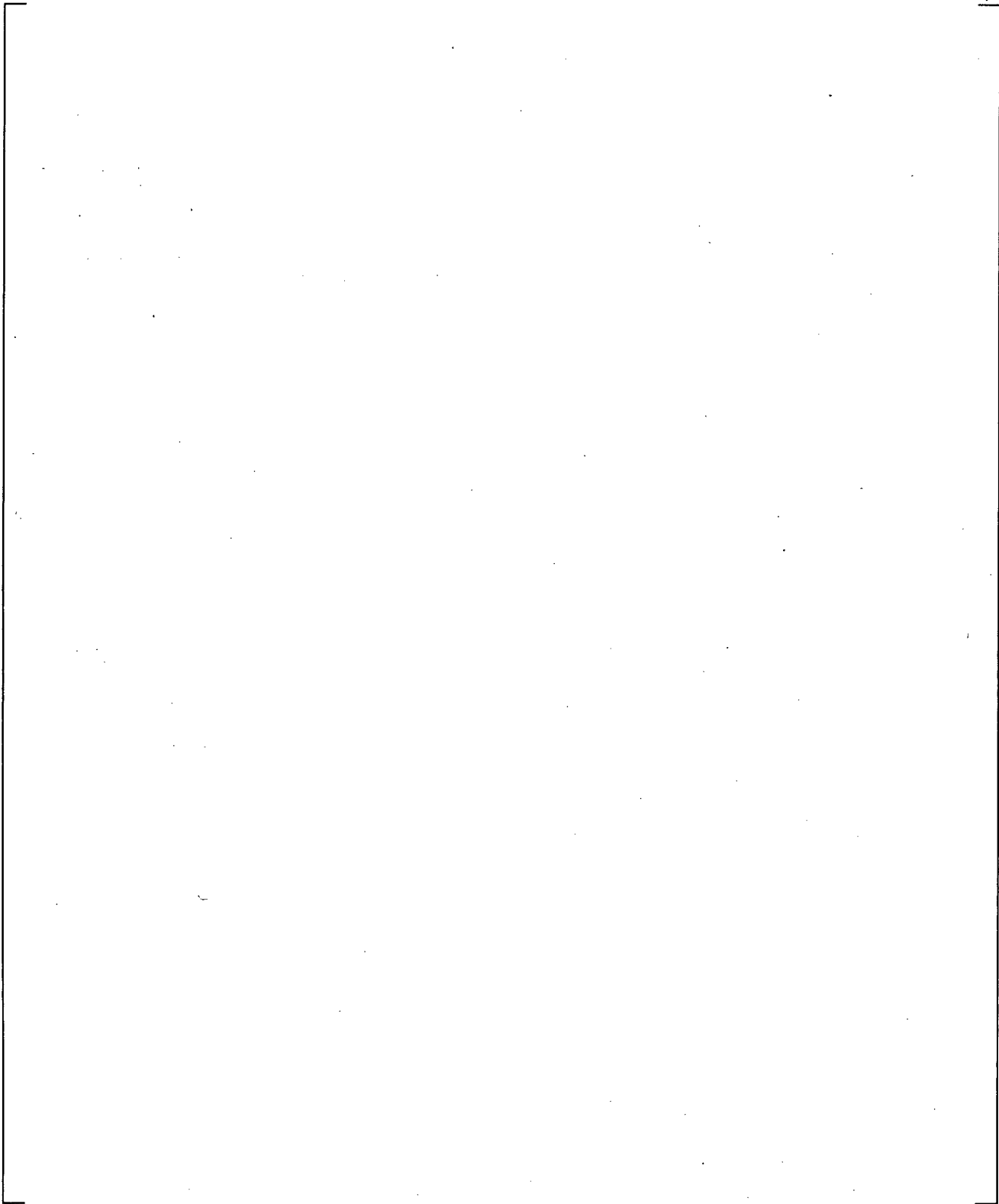


**Figure 24.7.3-48** CCTF Run 62 WCOBRA/TRAC-TF2 vs. Data Cladding Temperature Comparison at 6.68 ft in Higher Containment Pressure Case

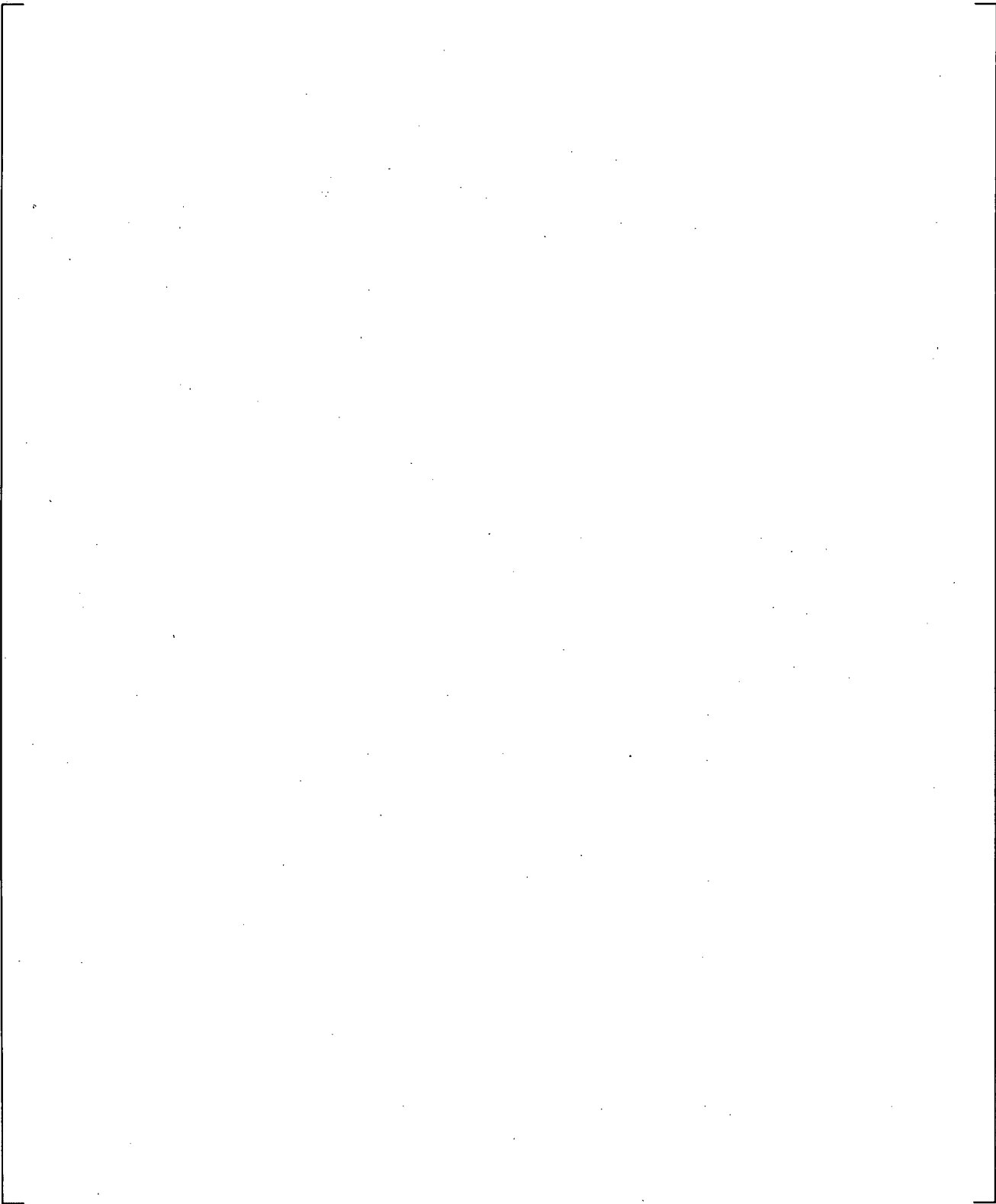


**Figure 24.7.3-49 Core Inlet Flow Comparison in Higher Containment Pressure Case**

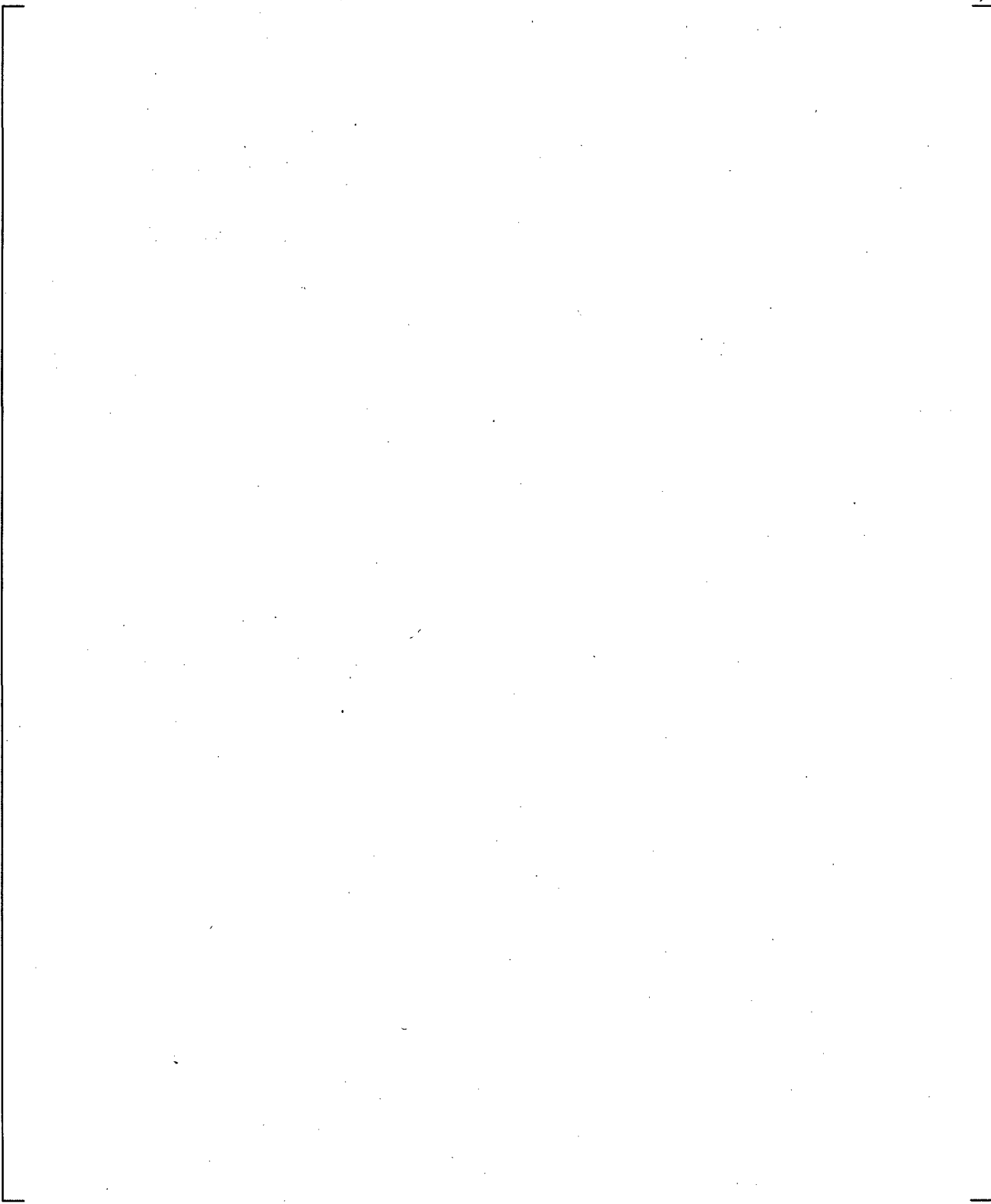


**Figure 24.7.3-50 CCTF Run 62 WCOBRA/TRAC-TF2 vs. Data Collapsed Liquid Level in Core in Higher Containment Pressure Case**

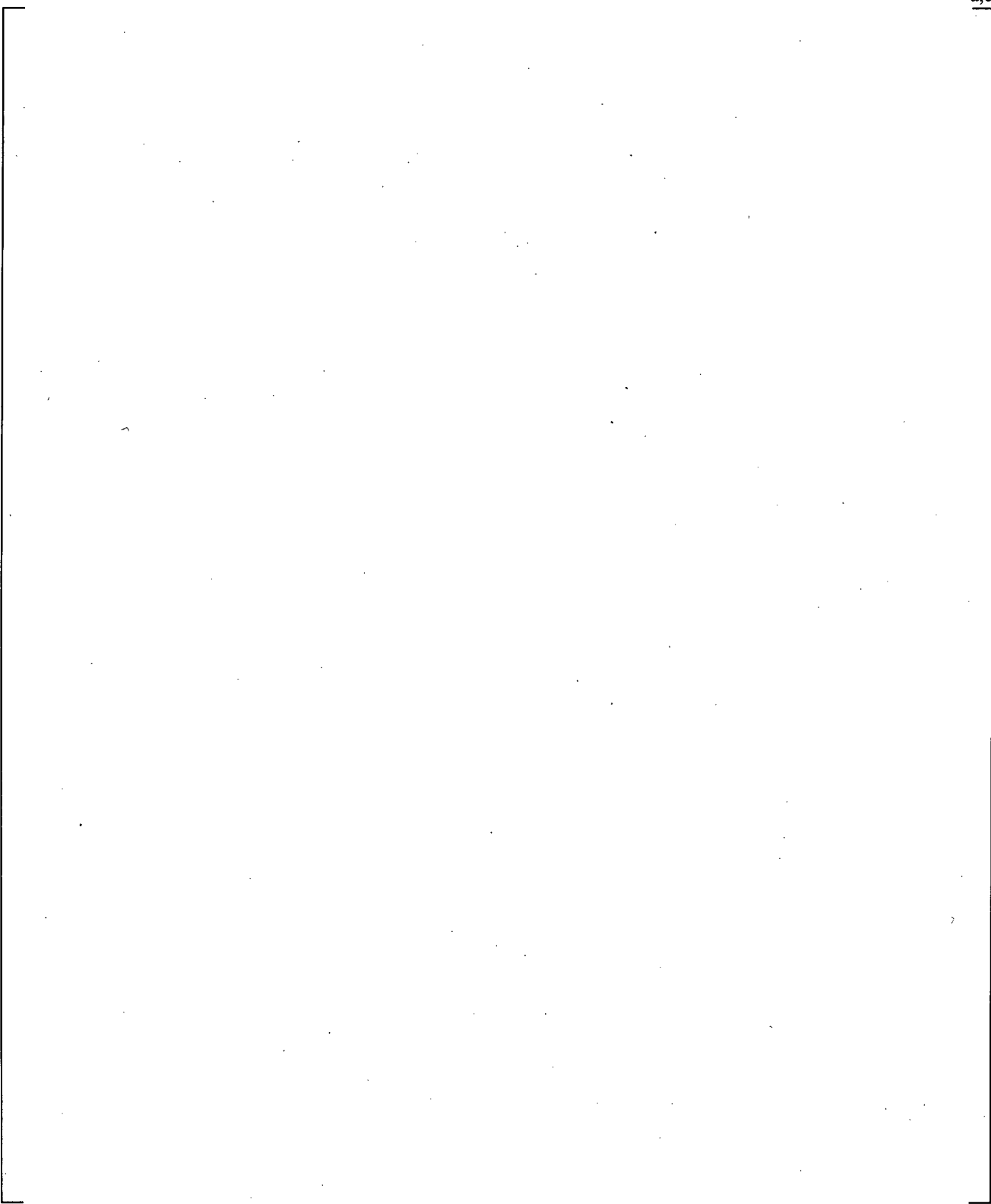


**Figure 24.7.3-51 CCTF Run 62 WCOBRA/TRAC-TF2 vs. Data Collapsed Liquid Level in Upper Plenum in Higher Containment Pressure Case**

## 24.8 CORE LEVEL PREDICTION IN SB-CL-18 TEST

In a small break LOCA, the mixture level in the core directly impacts the peak cladding temperature. In this section the predictions of mixture level seen in SB-CL-18 (Kumamaru et al., 1989) simulation (Section 21), is examined.

The predicted core DP from ROSA SB-CL-18, a 5% CL break simulation is compared against the measurement in Figure 24.8.1-1. The figure shows [

] <sup>a,c</sup> prediction is examined.

### 24.8.1 Core Collapsed Liquid Level

Comparison shows [

] <sup>a,c</sup>

#### Observed Core DP General Trend

The core DP indicates that the inventory increases initially and peaks at t=20 seconds followed by a constant decrease which slows down at t~50 seconds. The core DP continues to decrease at a relatively constant rate until t=100 seconds. The rate of DP decrease increases due to the loopseal clearance depression which according to the measurement bottoms out at t=140 seconds followed by a quick recovery due to the venting of trapped steam in the inner vessel. The core level recovers to a constant level which lasted until t=400 seconds, followed by the boil-off during which the cladding temperature increased significantly above saturation signifying the dryout condition which was terminated by the level increase at t=460 seconds due to accumulator injection.

#### Predicted Core DP Trend

The predicted core DP [

] <sup>a,c</sup>

The details of transient in terms of core DP are examined next.

#### Core DP Increase at 20 Seconds

Since the facility's power capability is 10 MW which is 14% of power required to match the scaled (1/48th) PWR's full power, the steady state loop flow is reduced to 14% of the rated flow to match the hot and cold leg temperatures of the PWR steady state. After the break at t=0 second, the pump speed is accelerated from the steady state level in order to match the expected coastdown curve from the rated

pump speed (Figure 24.8.1-2), [

] <sup>a,c</sup>

### **Core DP Increase at ~50 Seconds**

After the initial acceleration, the pump coasts down rapidly and the pump becomes [

] <sup>a,c</sup>

### **Core DP Decrease until Loopseal Clearance**

After the natural circulation driving force peaks at [

] <sup>a,c</sup>

### **Level Recovery after Loopseal Clearing**

Figure 24.8.1-11 shows that the [

] <sup>a,c</sup>

[

] <sup>a,c</sup>**Boil-off Core Level and PCT**

The predicted boil-off begins [

] <sup>a,c</sup>**Core Level Prediction at other Break Sizes**

Core DP comparison for SB-CL-01 (2.5% Cold Leg Break) (Koizumi et al., 1987) simulation is shown in Figure 24.8.1-14. The simulation of SB-CL-01 is described in Section 21. In this transient, Steam Generator drained prior to the loopseal clearance at t=300 seconds, [

] <sup>a,c</sup>

### 24.8.2 Core Mixture Level/Cladding Heat-up Elevation Prediction

The mixture level in the core region directly determines the heat-up elevation during a small break LOCA because the CHF takes place at or near where the equilibrium quality approaches unity for the heat flux range typical of a small break LOCA (Guo, Kumamaru, and Kukita, 1993). In this section, [

] <sup>a,c</sup>

### 24.8.3 Level Swell Prediction

The cladding heat-up is a result of the mixture level dropping into the core and uncovering the rod. Since at low heat flux which is the case for boil-off in SBLOCAs, [

] <sup>a,c</sup>] <sup>a,c</sup>

[

] <sup>a,c</sup>

[

]a,c

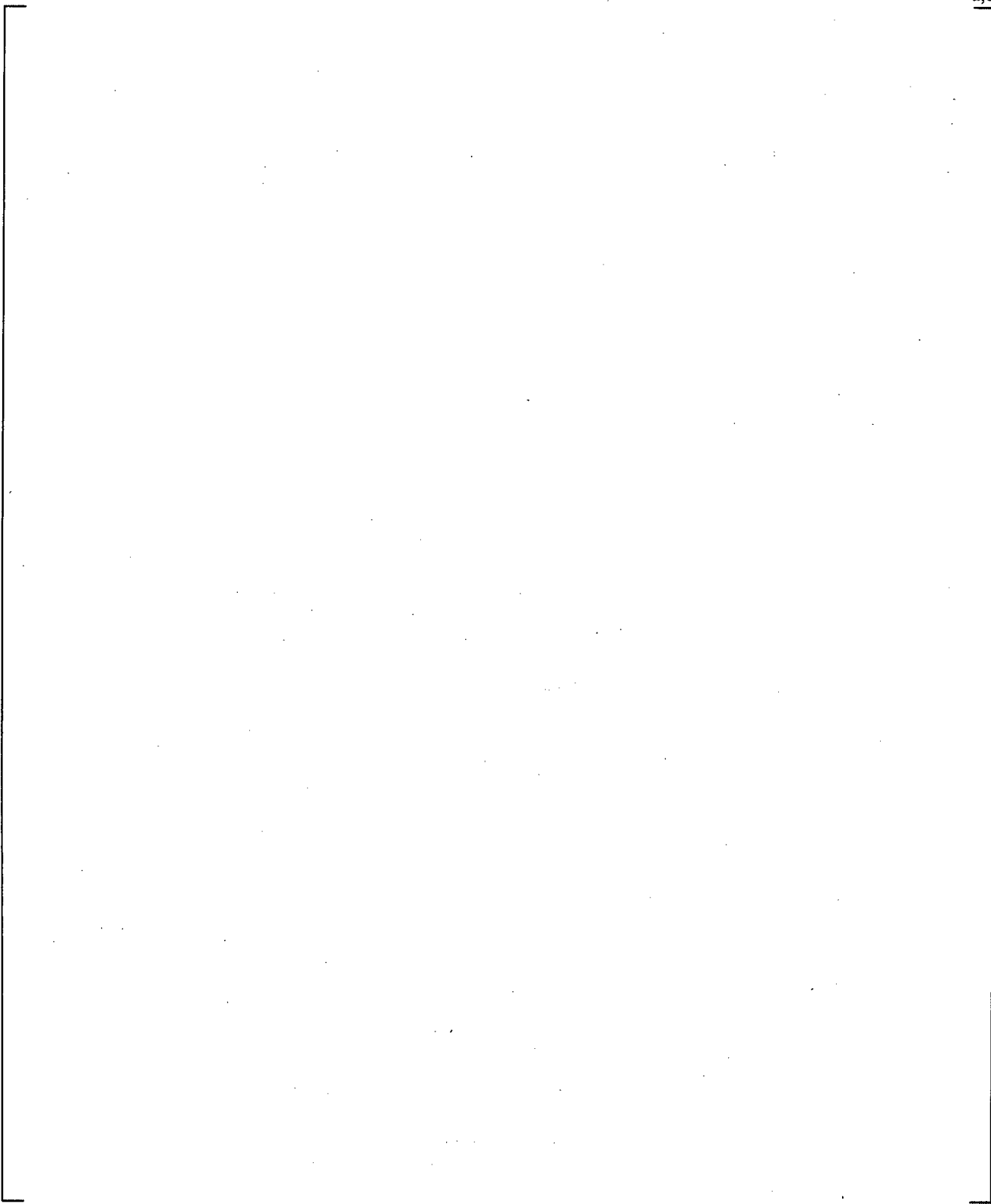


**Figure 24.8.1-1 Core DP Comparison in SB-CL-18 Simulation**

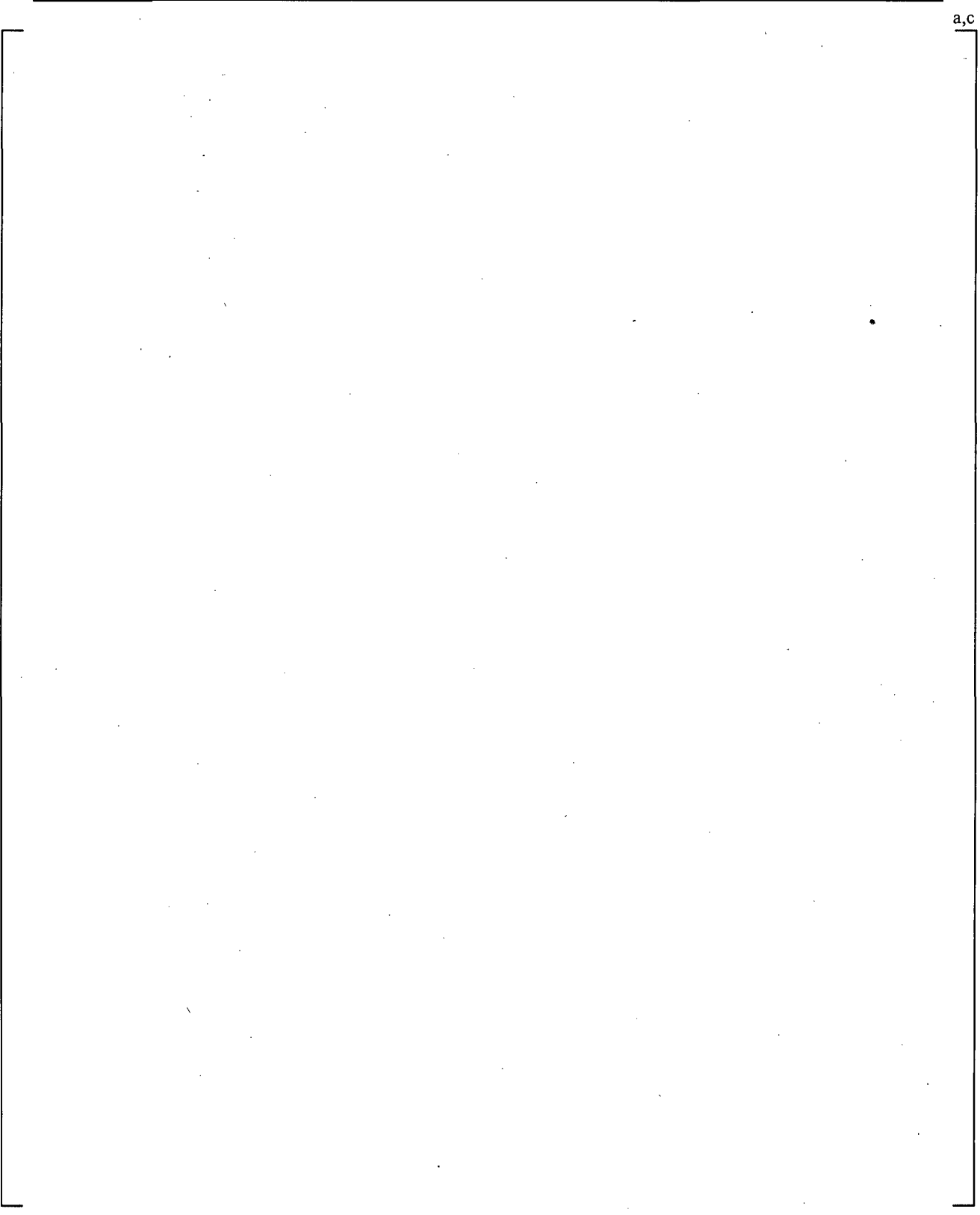


**Figure 24.8.1-2 Pump Speed used in Test and in Simulation**

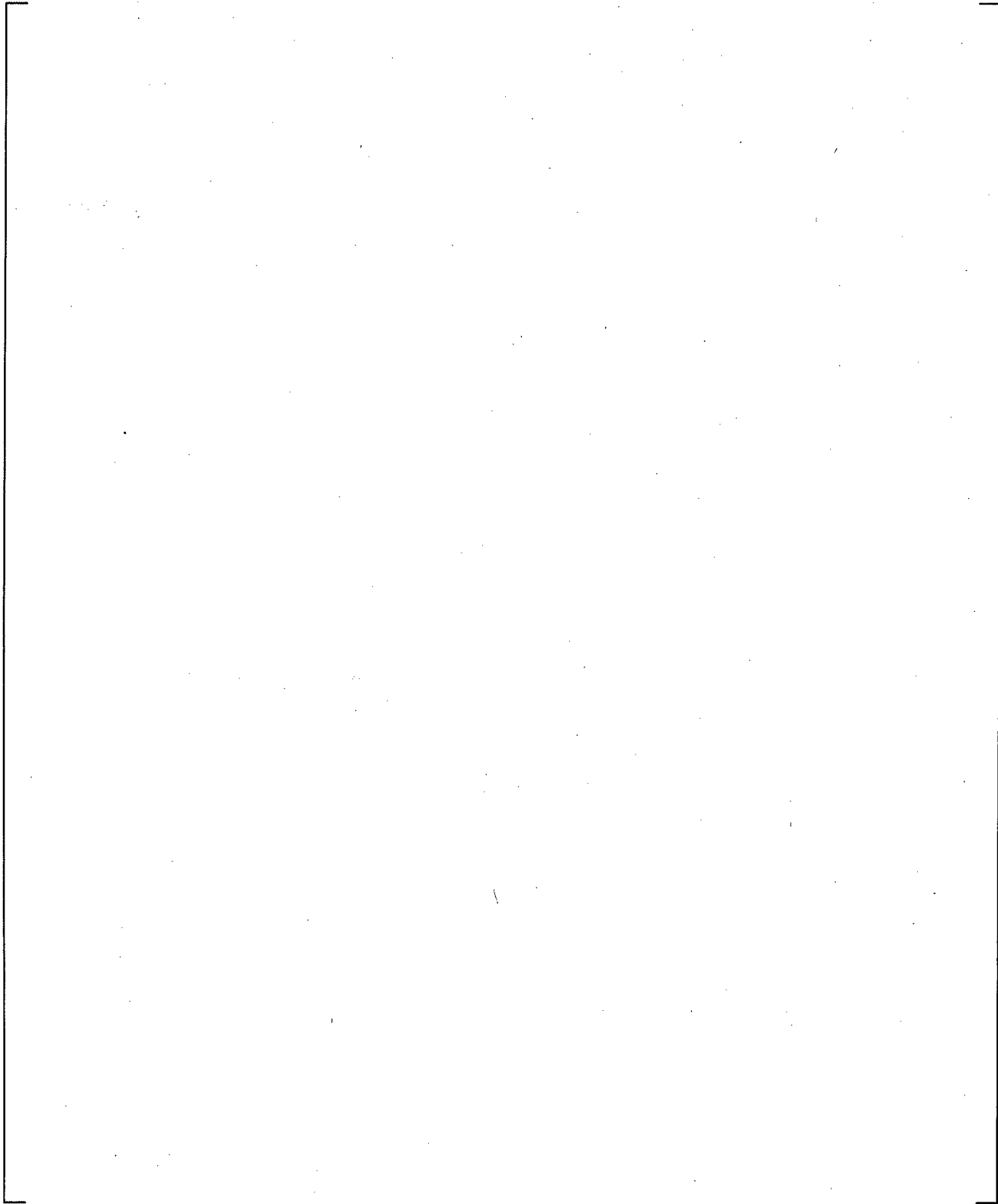


**Figure 24.8.1-3 SB-CL-18 Core DP Comparison with Core Inlet Liquid Velocity**

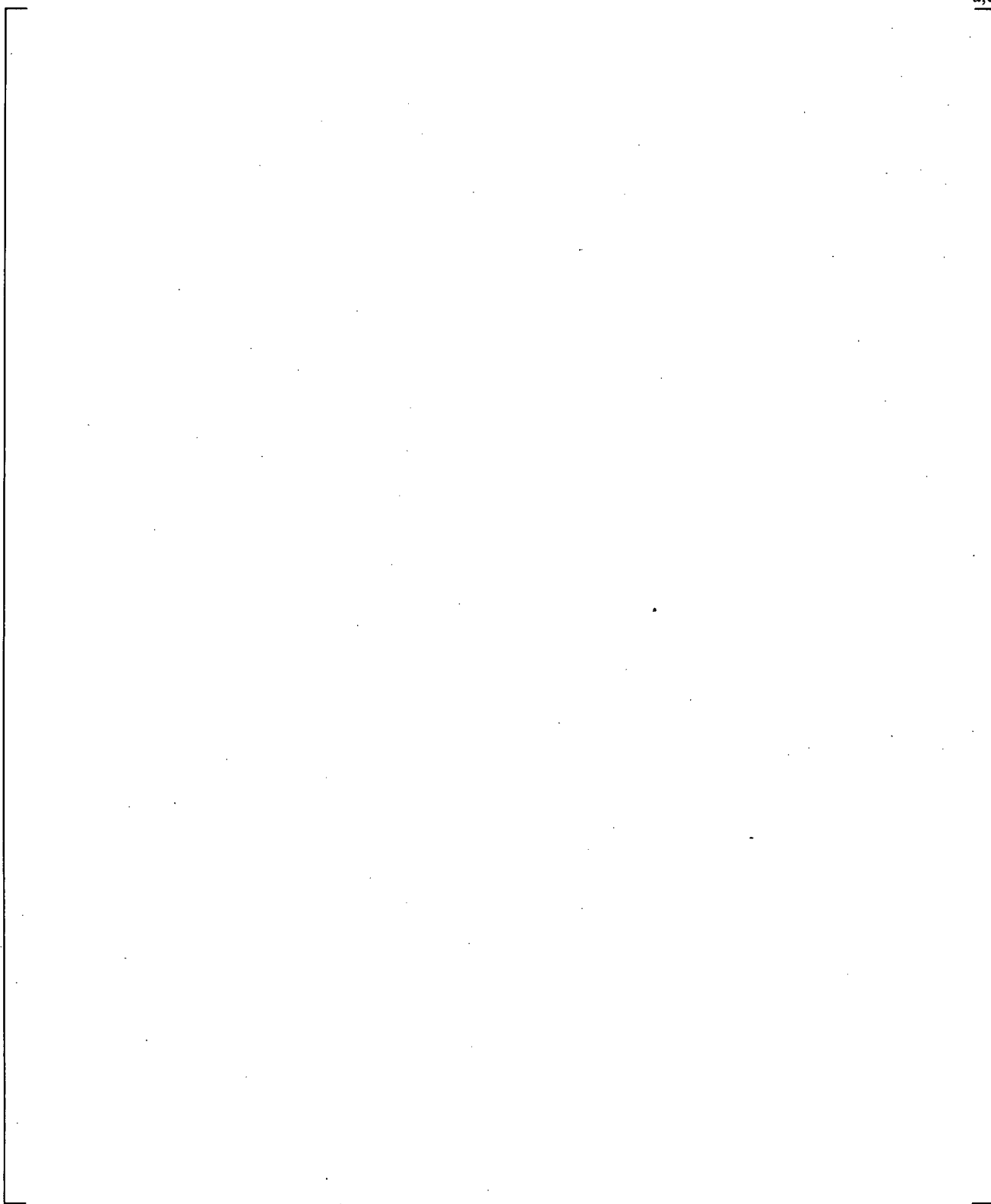


**Figure 24.8.1-4 SB-CL-18 Core DP Comparison with Pump DP in Loop A and B**

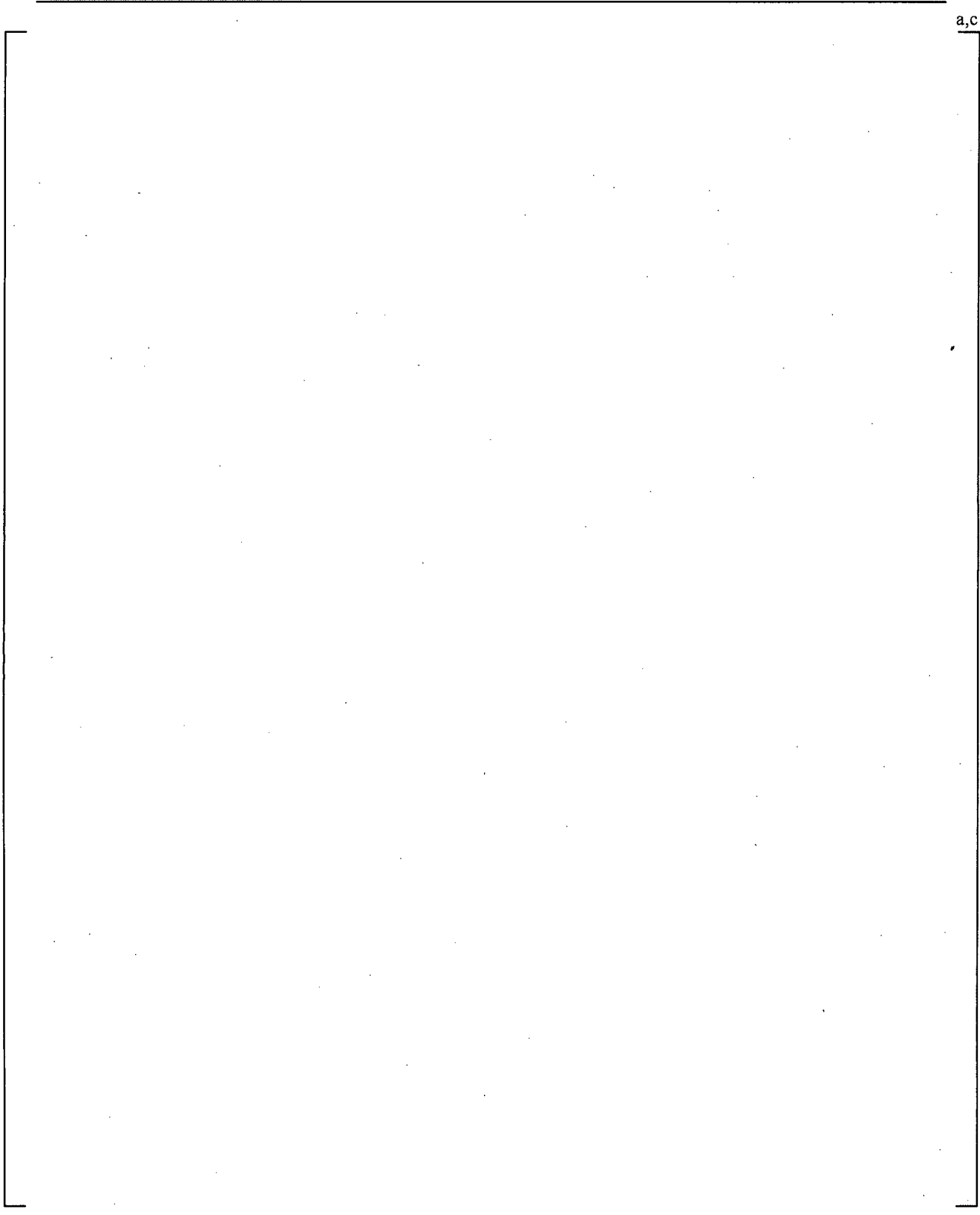


**Figure 24.8.1-5 Primary Side Circulation Flow as a Function of Primary Side Inventory**

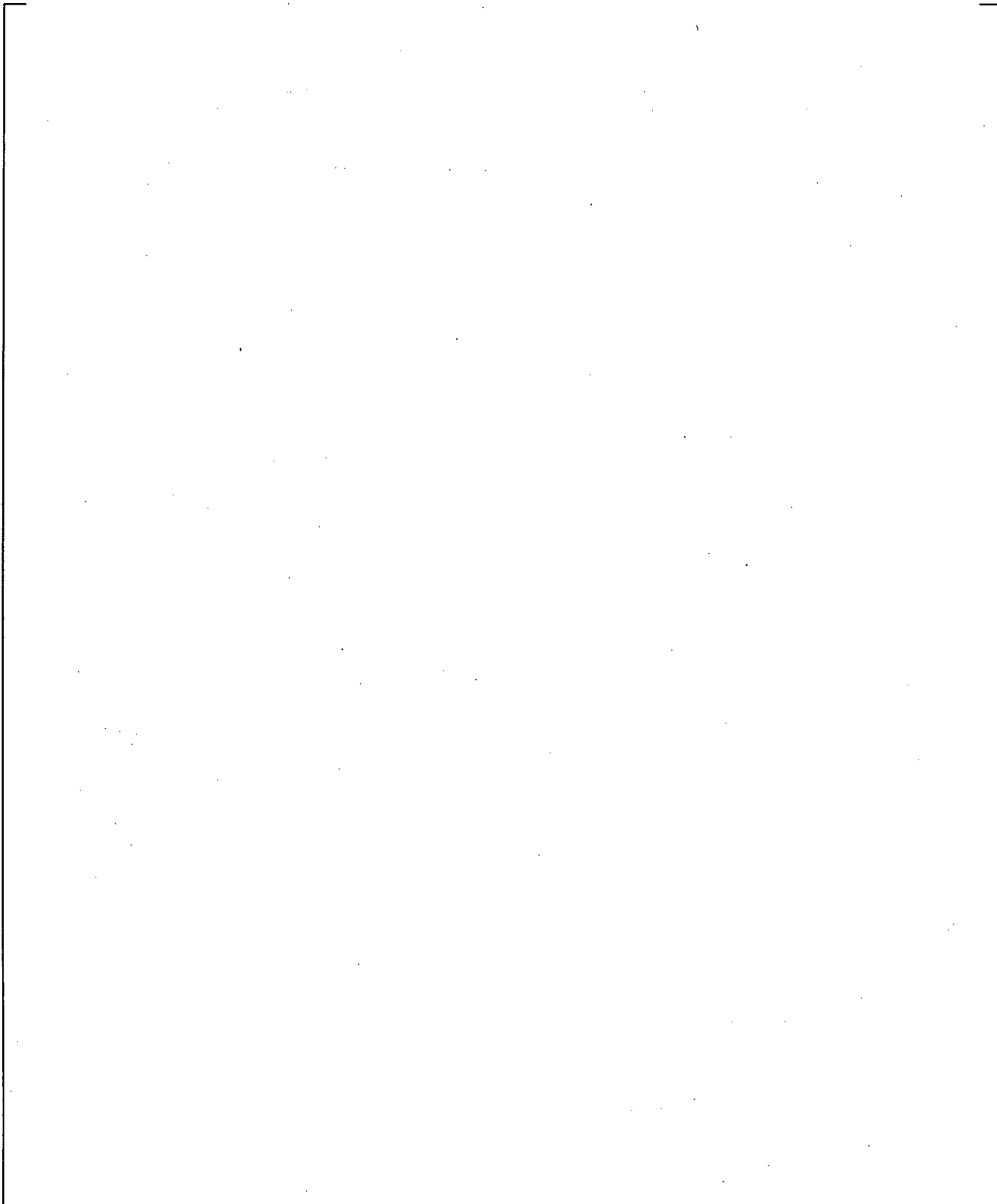


**Figure 24.8.1-6 Core DP Comparison with the Void Fraction in Downhill side on Steam Generator and Cross-over Leg**

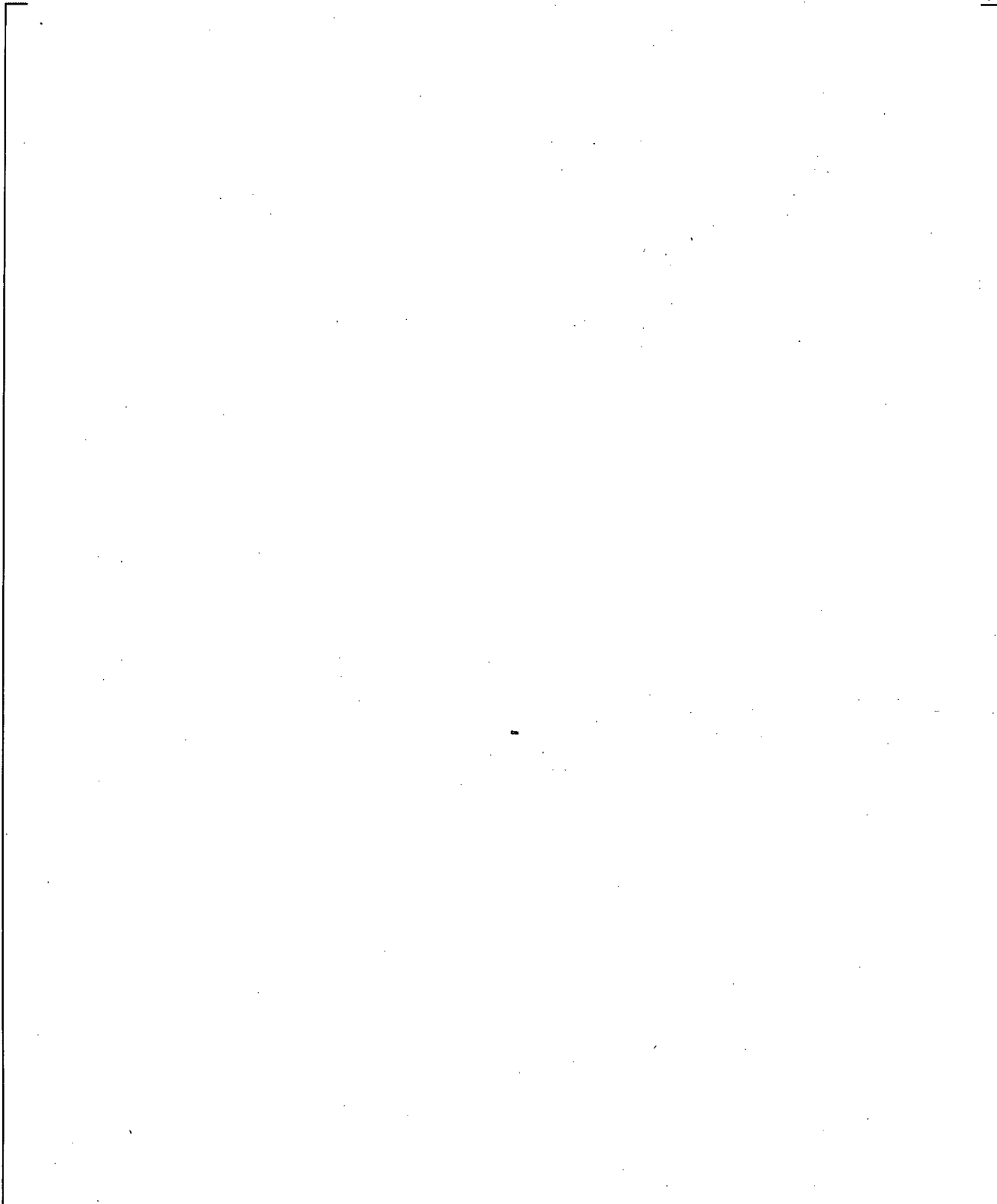


**Figure 24.8.1-7 Core DP Comparison with Axial Vapor Velocity at UCP (Curve-3=Inner High Power, Curve-4=Inner Low Power, Curve-5=Outer Low Power)**

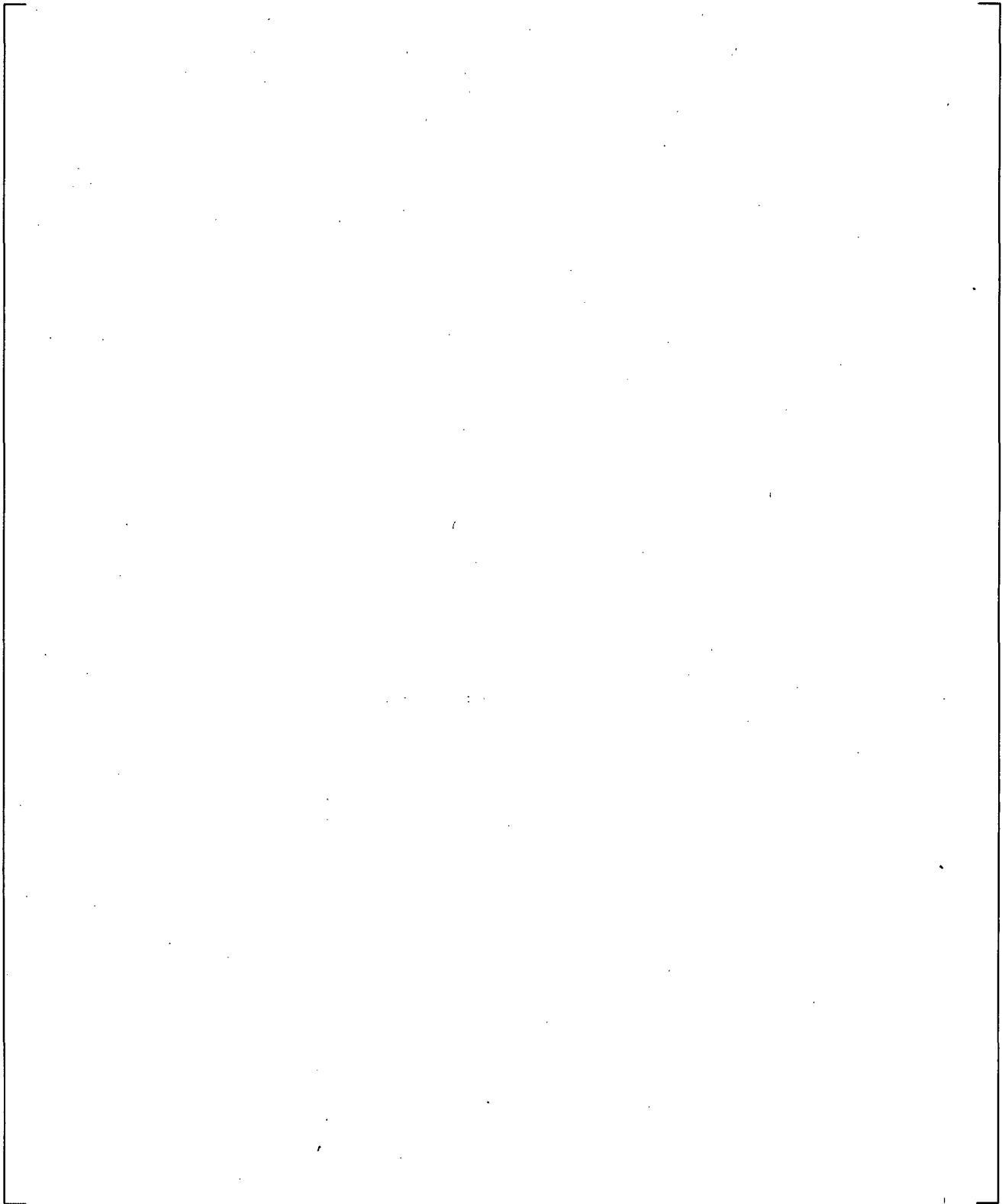


**Figure 24.8.1-8 Core DP Comparison with the Hot Leg Nozzle Liquid Flowrates**

a,c



**Figure 24.8.1-9 DP Comparison from Upper Plenum to Steam Generator Inlet**

a,c



**Figure 24.8.1-10 DP Comparison from Steam Generator Inlet to Outlet Plenum**

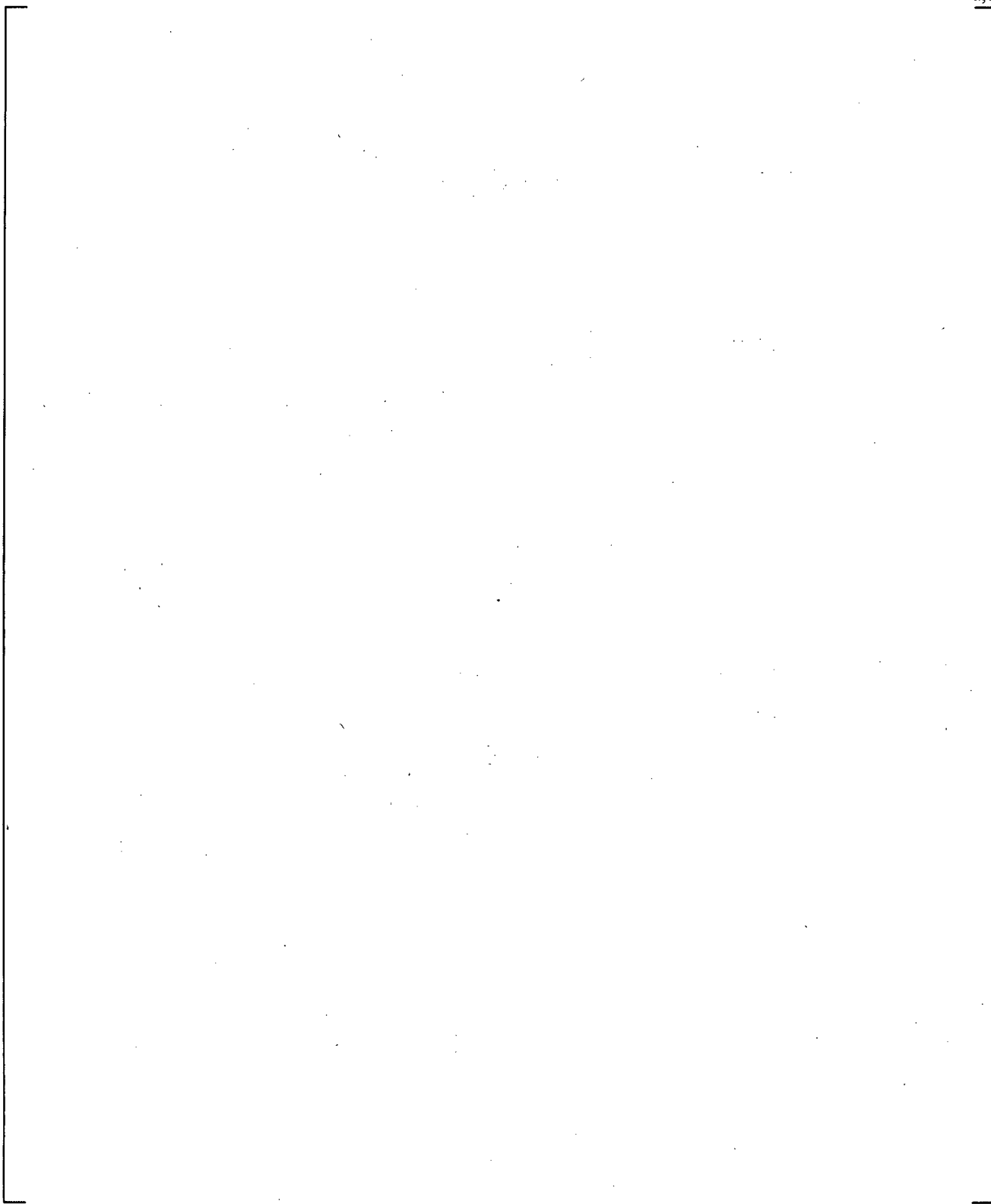


**Figure 24.8.1-11 Core DP Comparison with Void Fraction in Cross-over Leg Piping**

a,c

**Figure 24.8.1-12 Inner Vessel DP Comparison**

a,c

**Figure 24.8.1-13 Downcomer to Upper Plenum Pressure Difference**

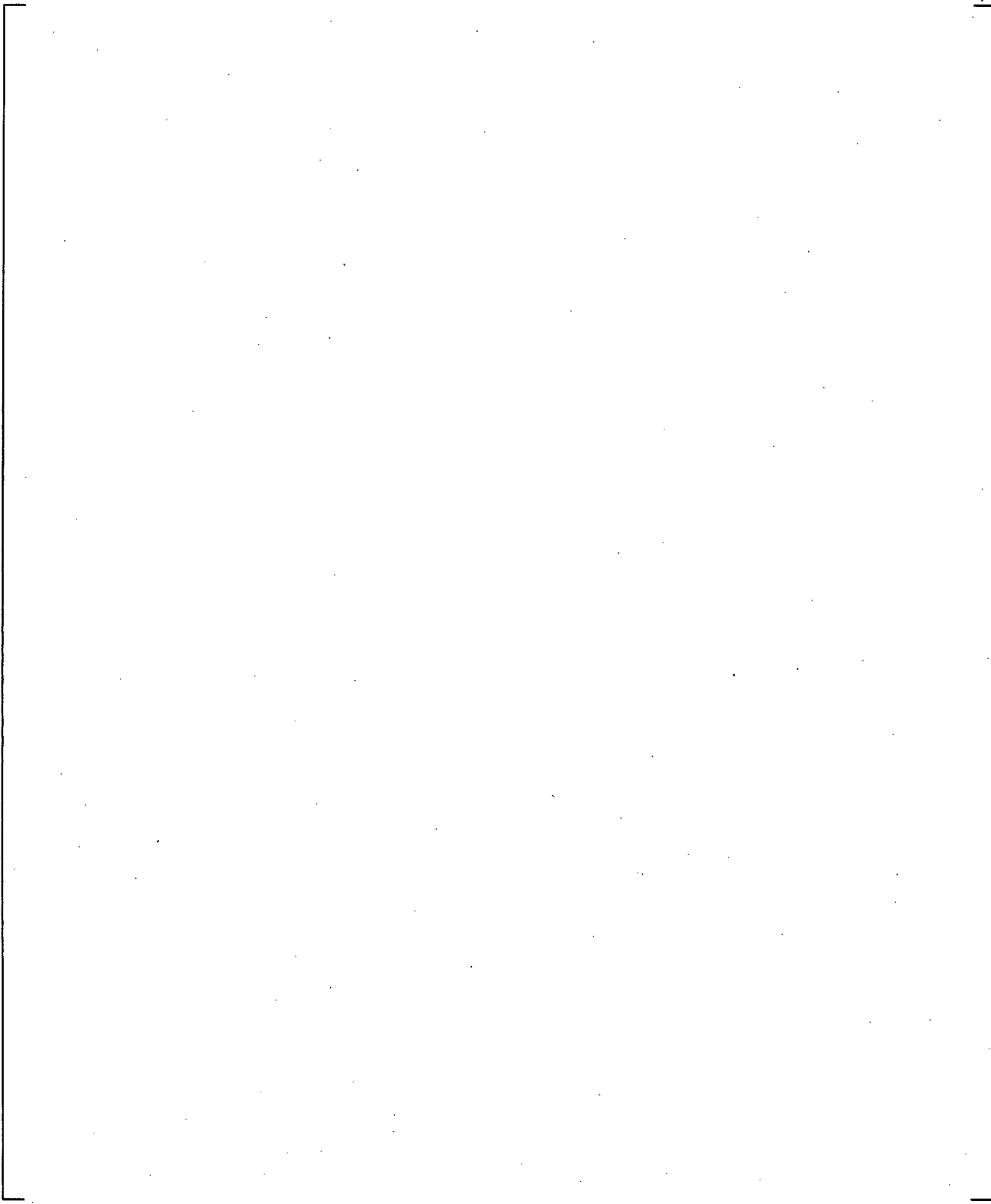


**Figure 24.8.1-14 Core DP Comparison for SB-CL-01 (2.5%)**

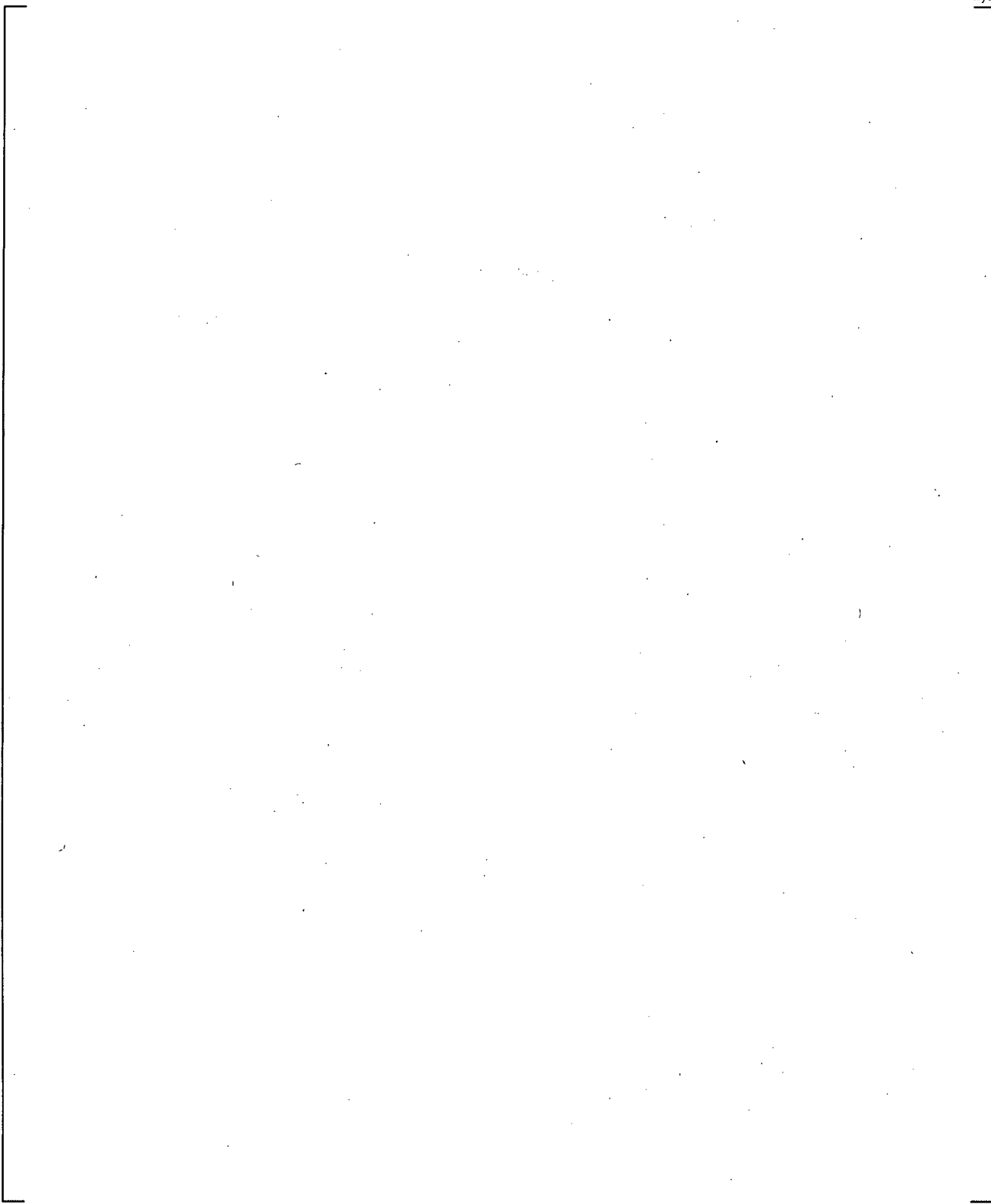


**Figure 24.8.1-15 Loop-A Loopseal Bottom to Pump DP Comparison for SB-CL-01 (2.5%)**

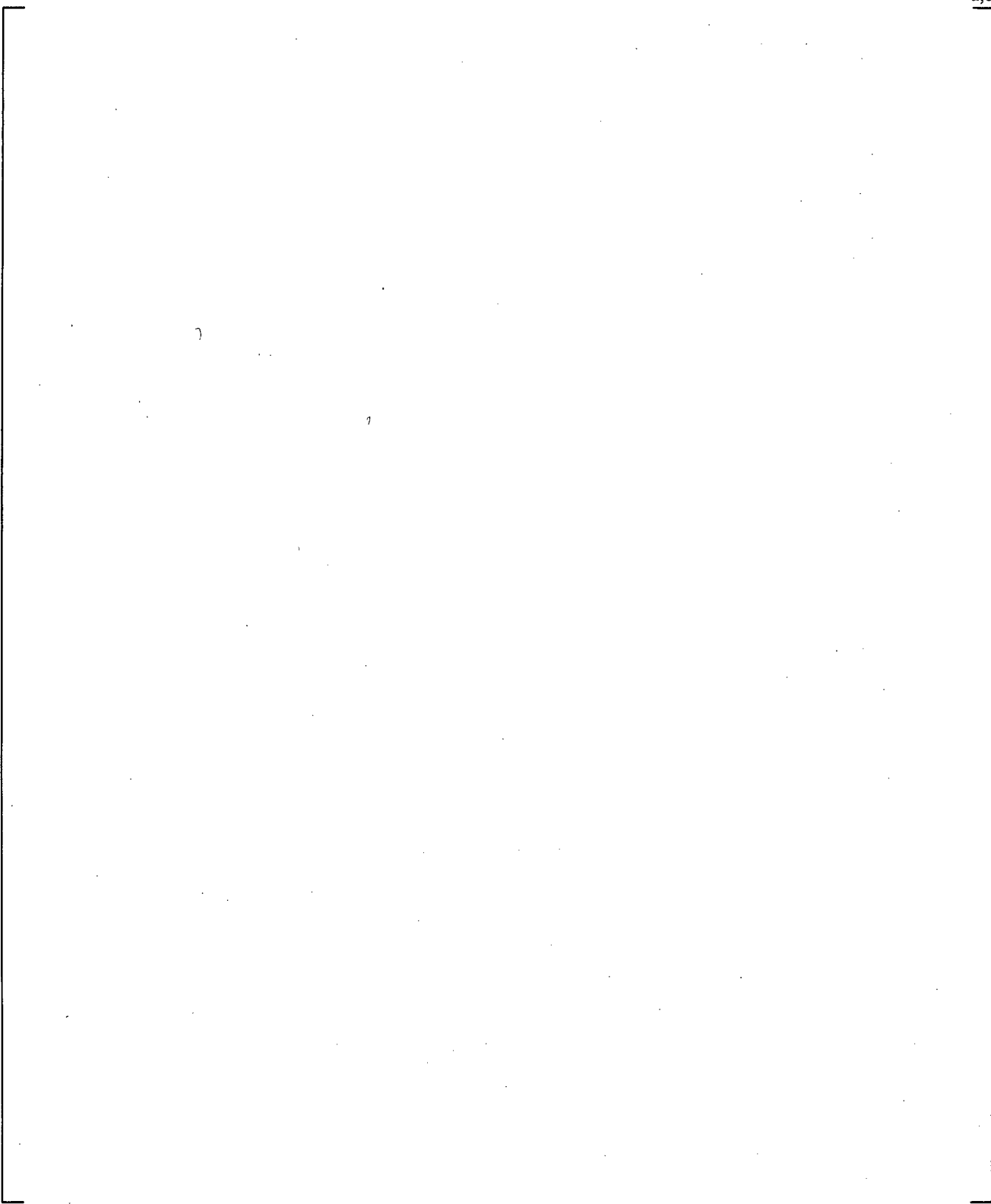


**Figure 24.8.1-16 Loop-B Loopseal Bottom to Pump DP Comparison for SB-CL-01 (2.5%)**

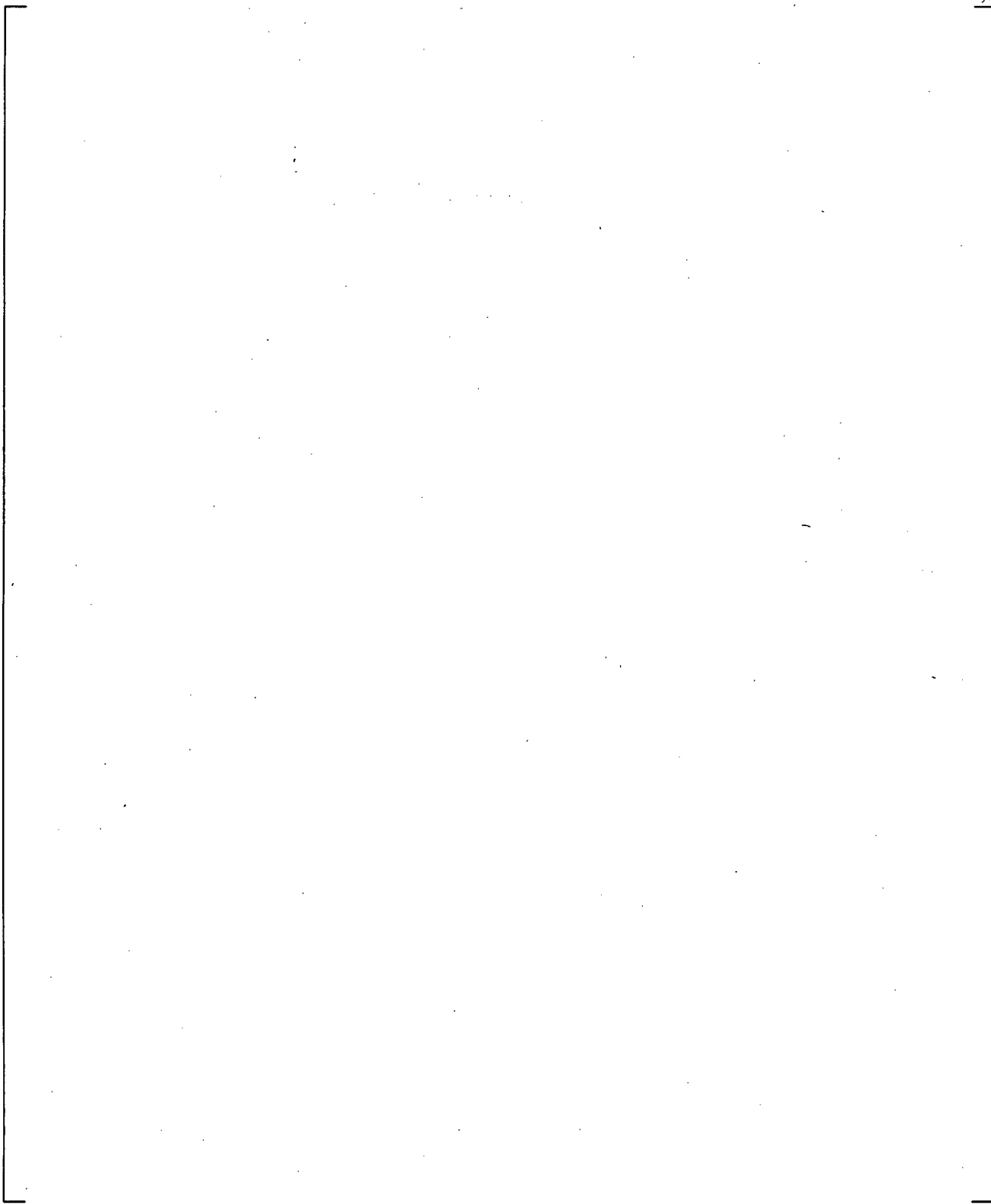


**Figure 24.8.1-17 Downcomer to Upper Plenum Pressure Difference in SB-CL-01 (2.5%)**

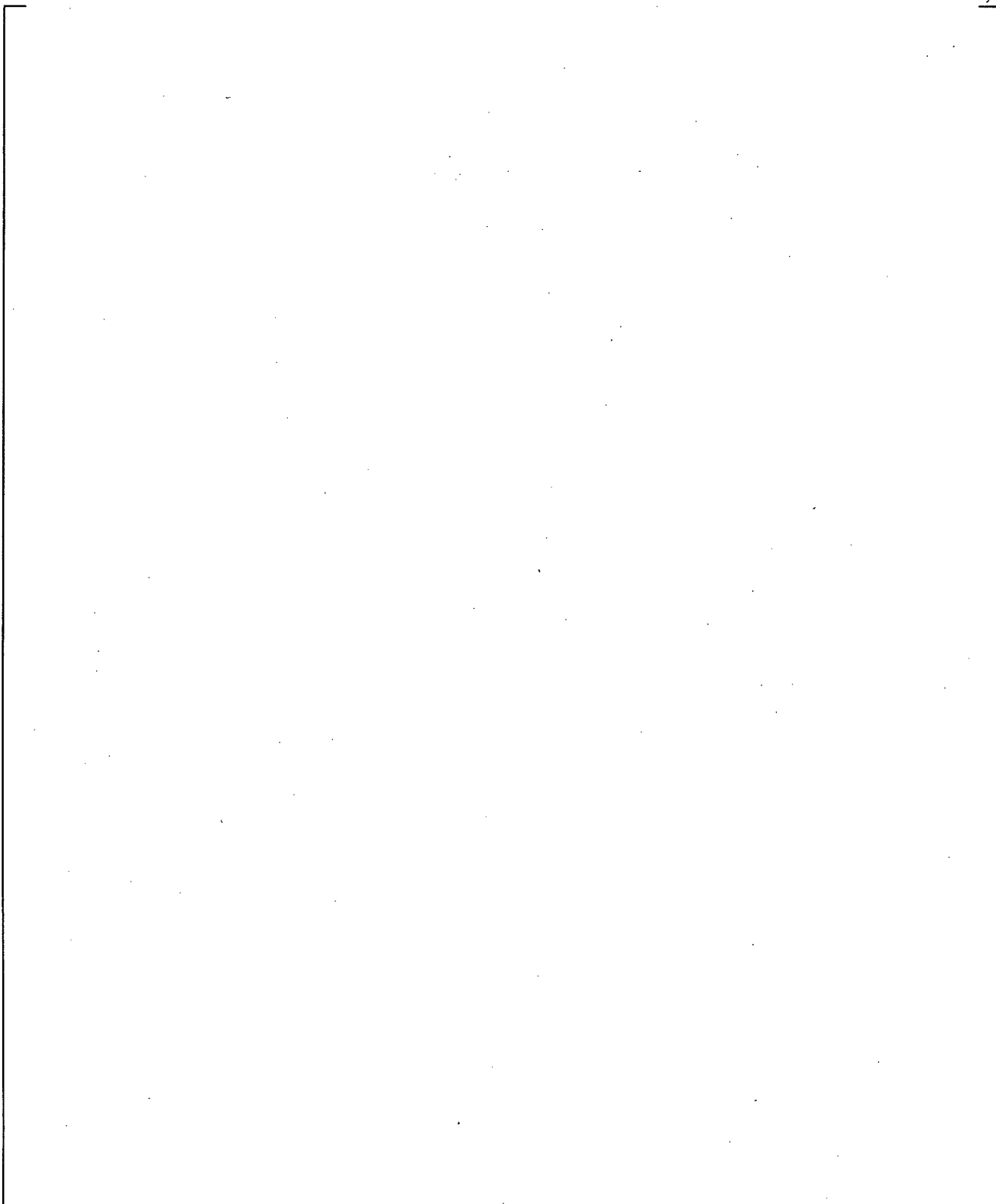


**Figure 24.8.1-18 Core Collapsed Liquid Level Comparison for SB-CL-14 (10%)**

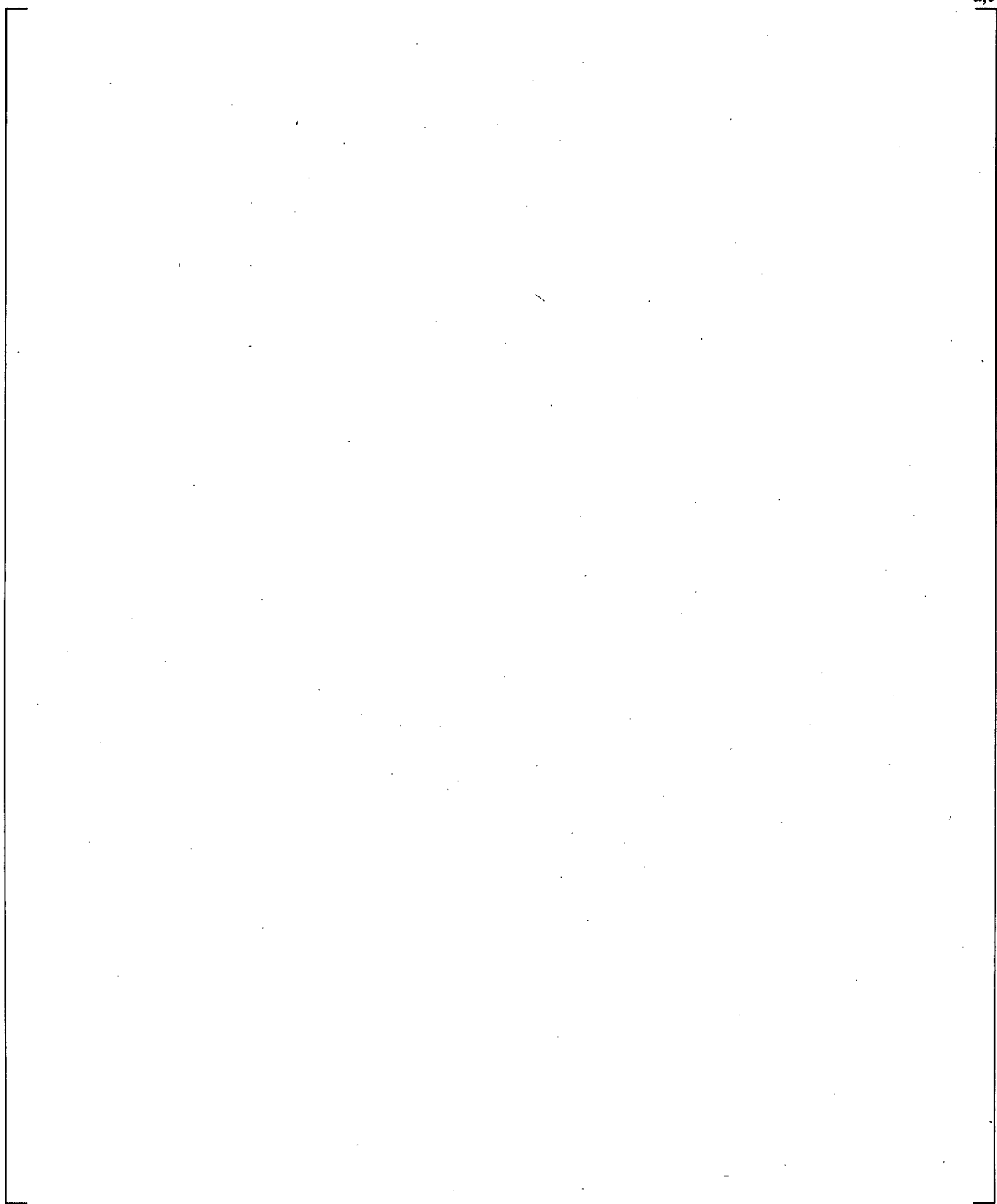


**Figure 24.8.1-19 Steam Generator Inlet to Top of Tube DP Comparison for SB-CL-14 (10%)**

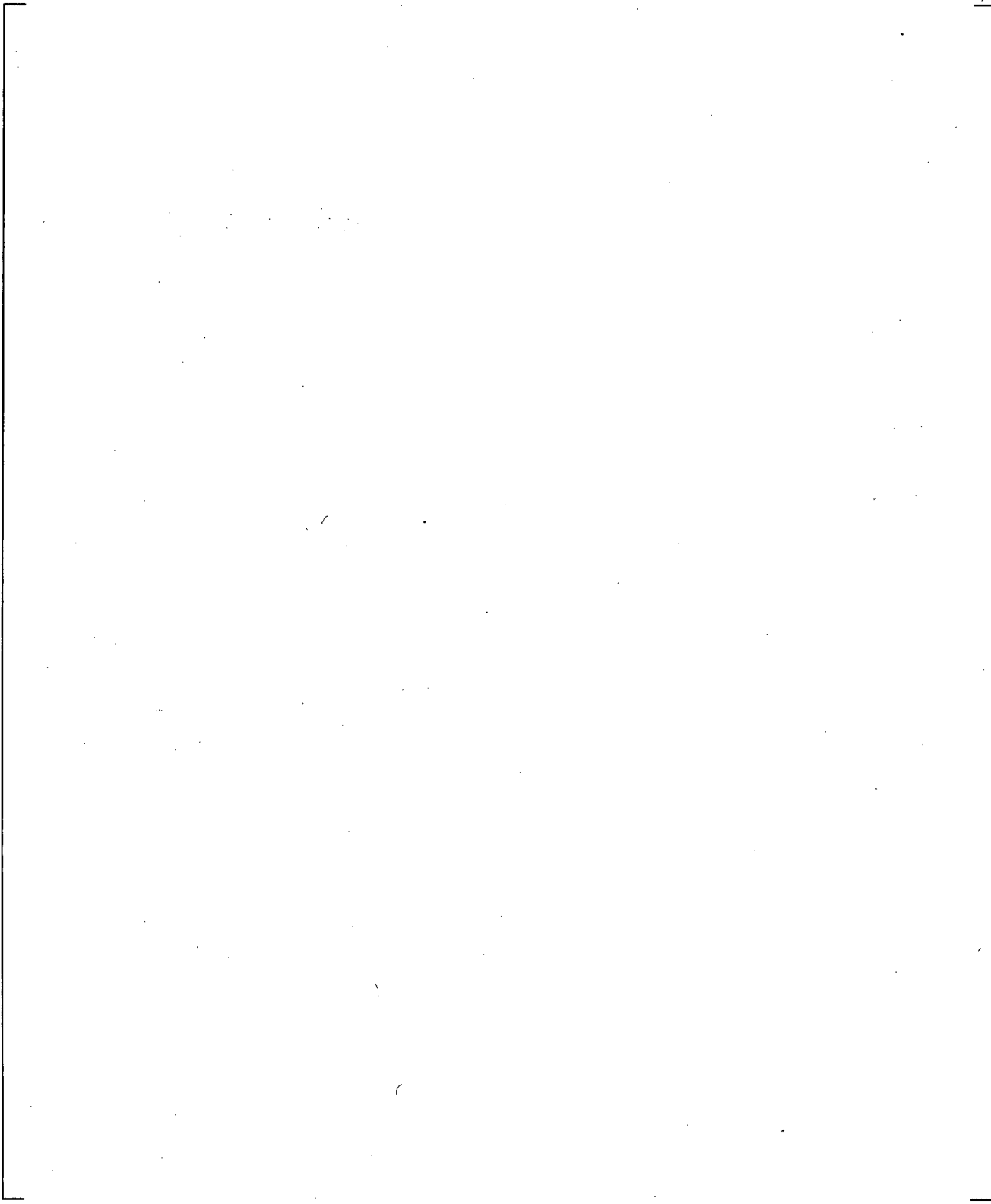


**Figure 24.8.1-20 Comparison of Loop-A Cross-Over Leg Differential Pressures**

a,c

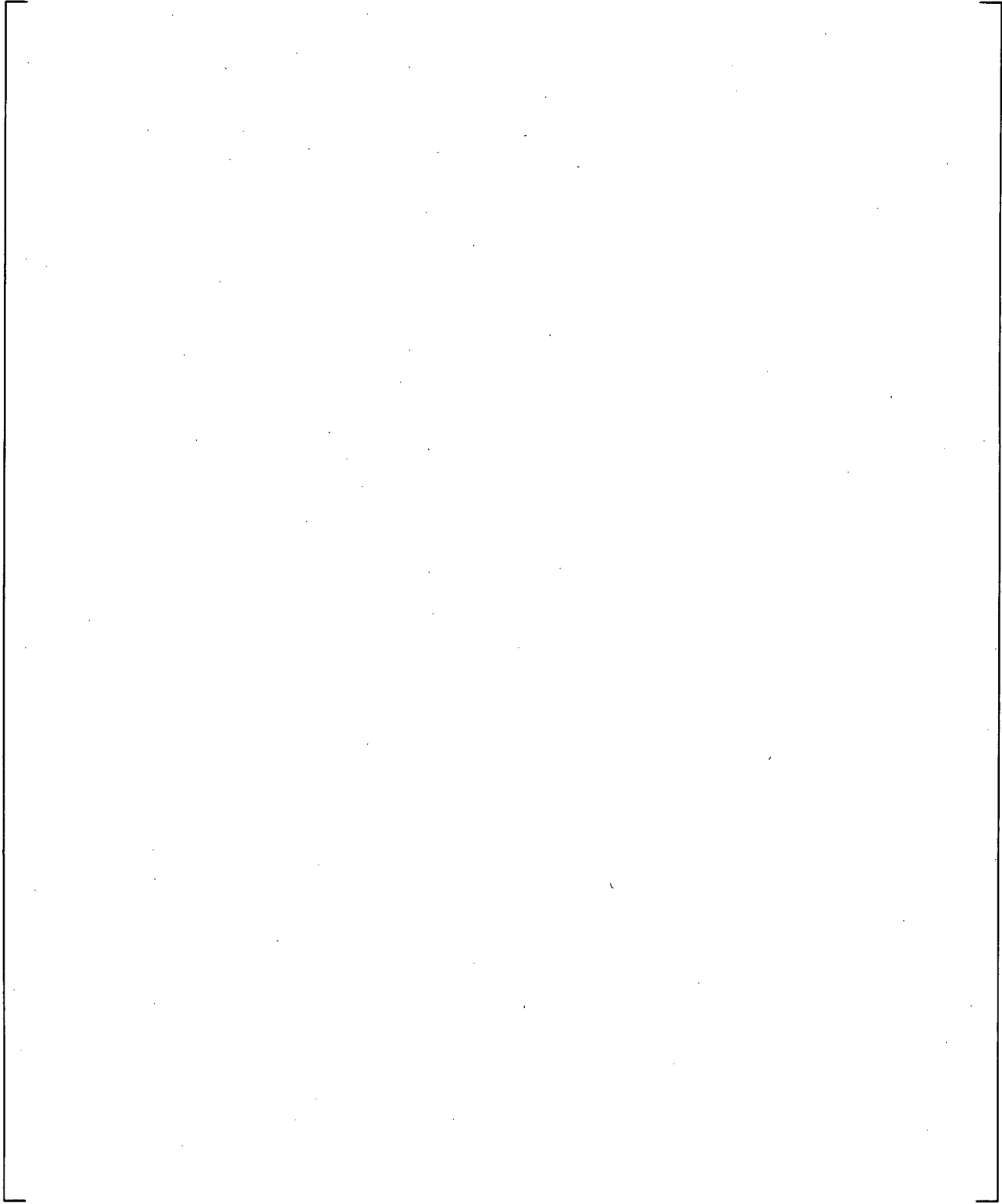


**Figure 24.8.1-21 Comparison of Loop-B Cross-Over Leg Differential Pressures**

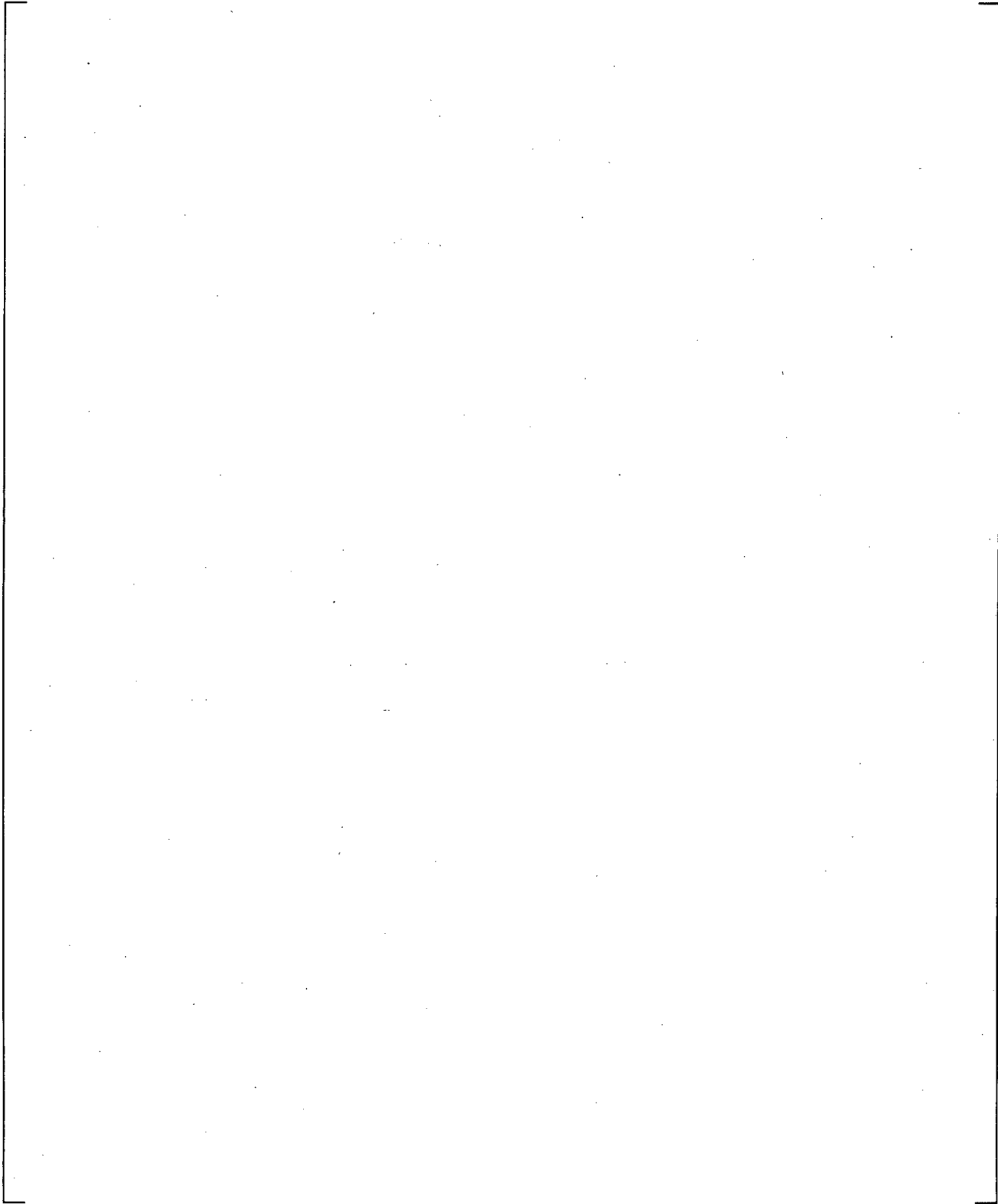


**Figure 24.8.2-1 Comparison of Predicted Mixture Level and Test Data**

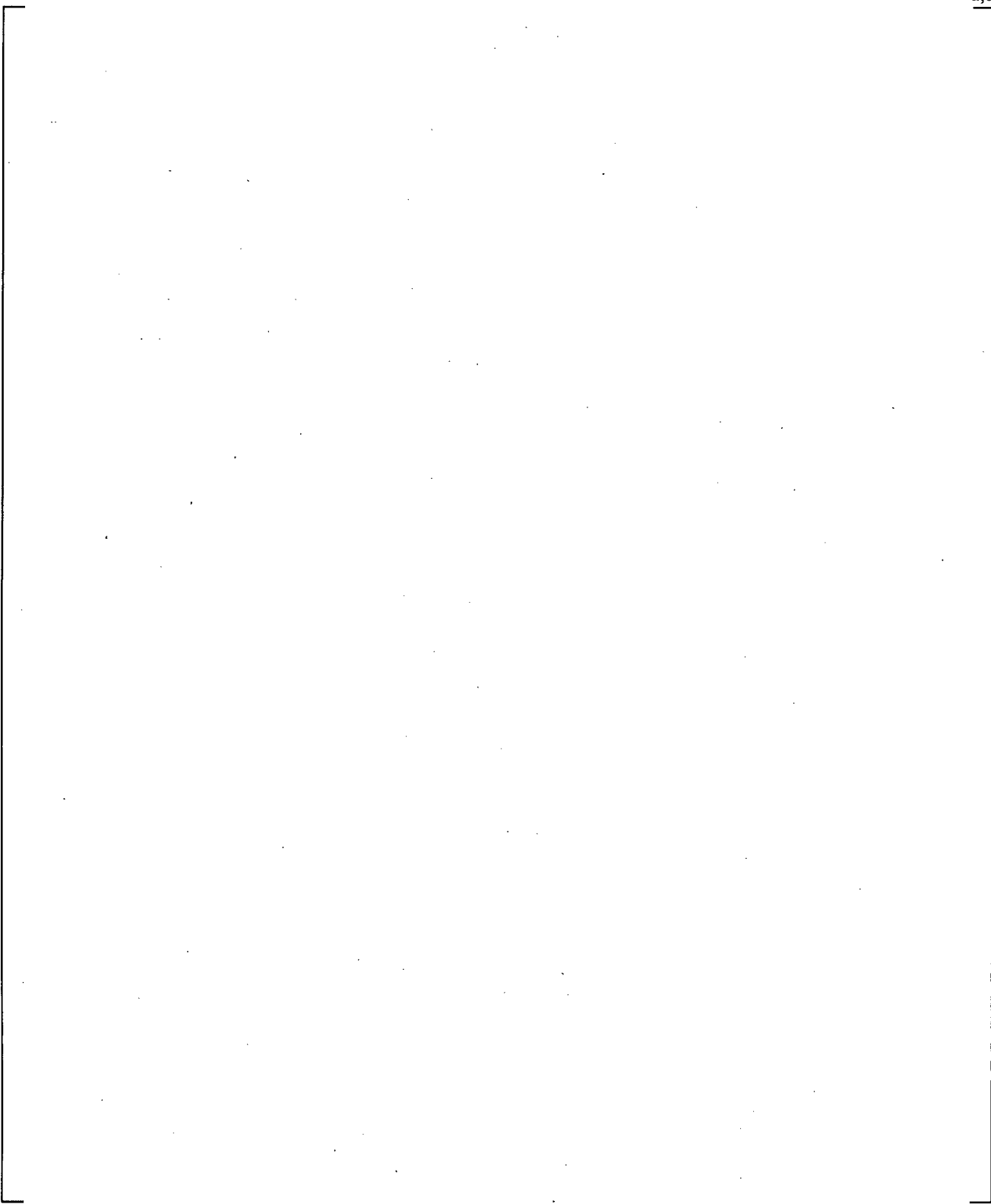


**Figure 24.8.2-2 Comparison of Predicted Mixture Level and Test Data, and YDRAG Sensitivity**

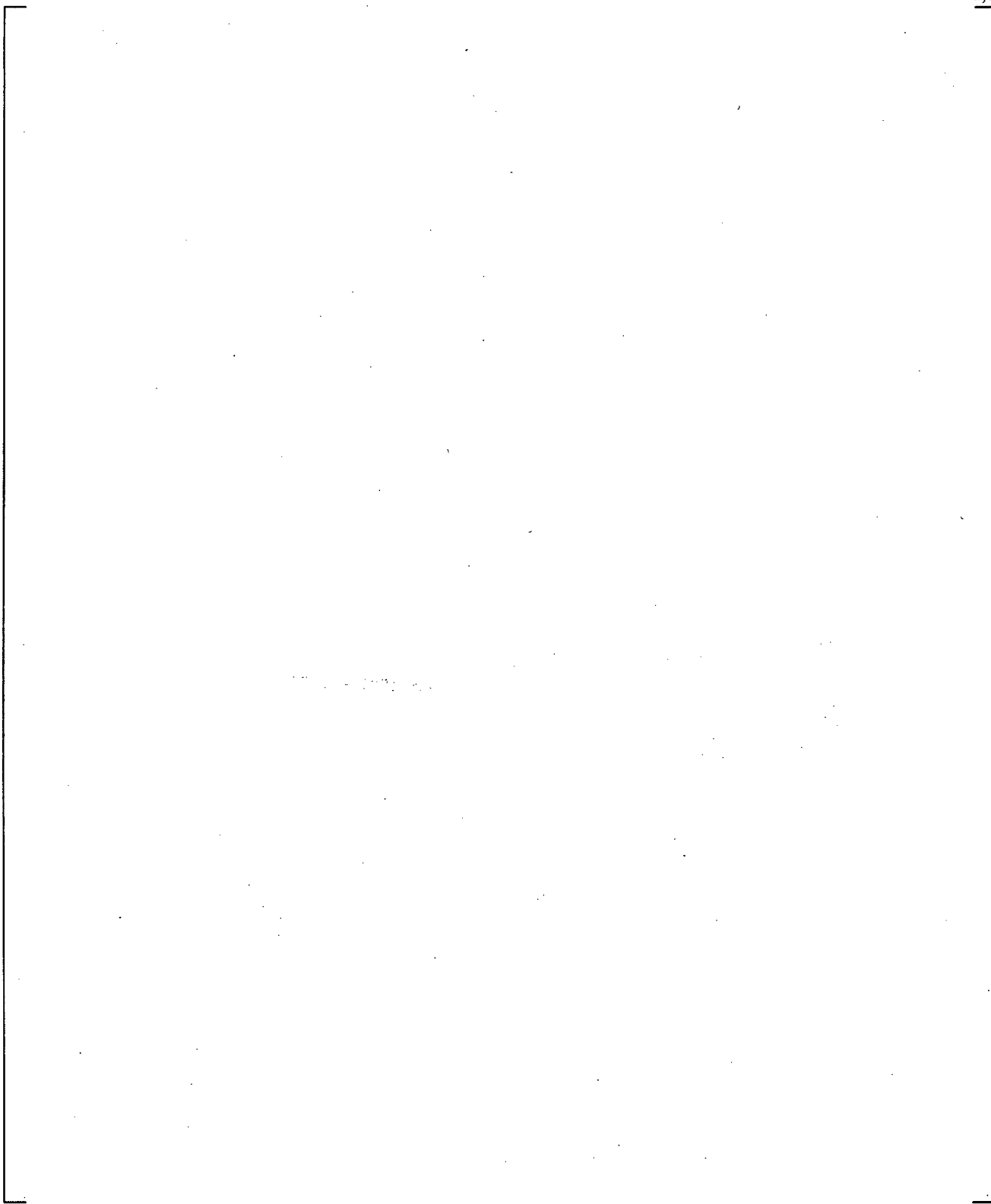


**Figure 24.8.3-1 Comparison of Predicted Level Swell against Measured**

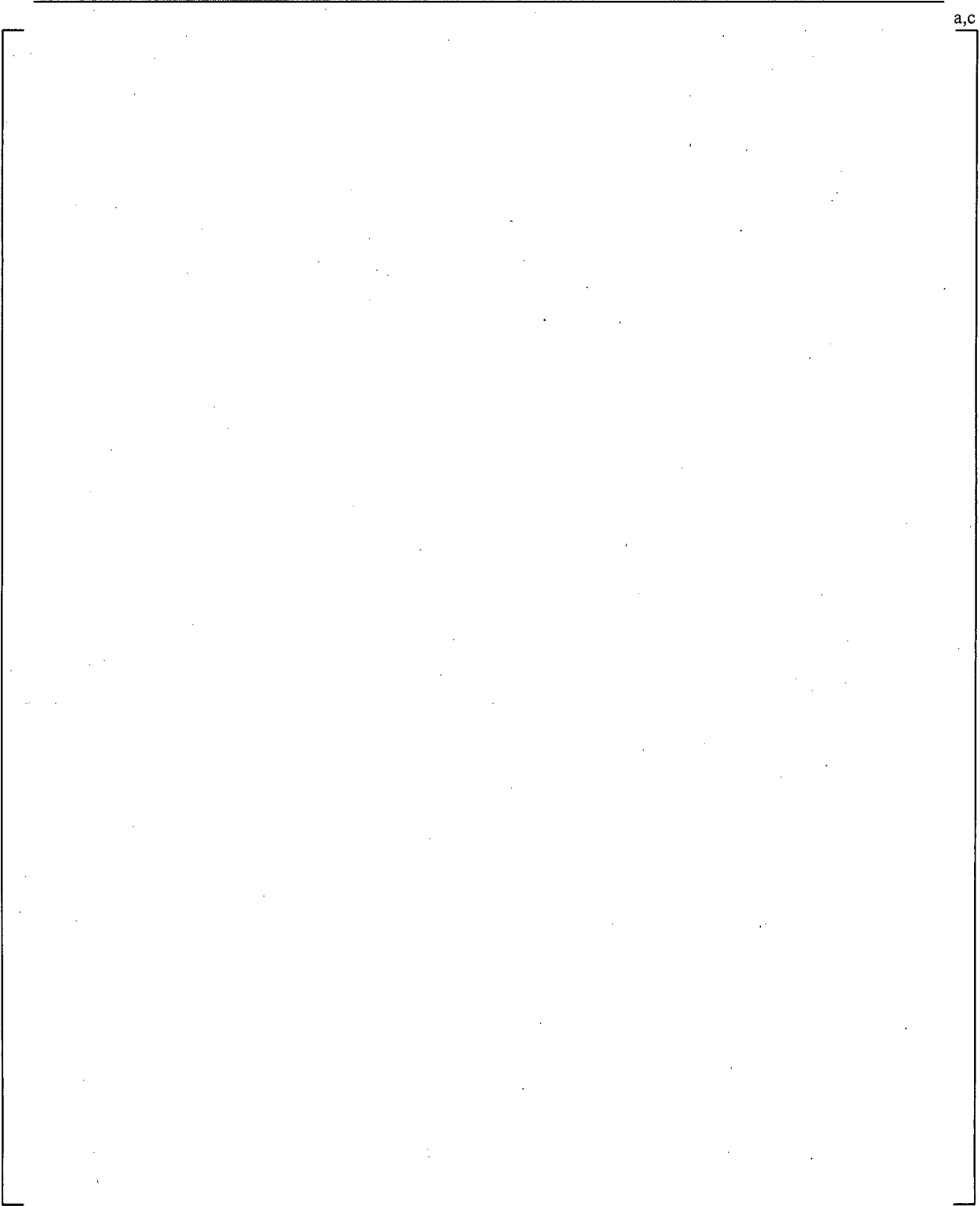


**Figure 24.8.3-2 Impact of YDRAG Variation on Predicted Level Swell**

## 24.9 SUMMARY OF COMPENSATING ERROR ASSESSMENT

The evaluations provided in this section as well as those previously performed in the model validation sections of this document give confidence that compensating errors of a nature which seriously compromise the ability of WCOBRA/TRAC-TF2 to predict conditions during a LOCA of PWR do not exist and that the [

] <sup>a,c</sup> The major finding from the analysis is tabulated below:

[

] <sup>a,c</sup>

## 24.10 REFERENCES

1. Boyack, B., et al., "Quantifying Reactor Safety Margins," NUREG/CR-5249, (1989).
2. Prassinis, P. G. et al., 1979, "Experiment Data Report for LOFT Power Ascension Experiment L2-3," NUREG/CR-0792.
3. 2D/3D Program Upper Plenum Test Facility Quick Look Report, 1989, "Test No. 6; Downcomer Countercurrent Flow Test," Siemens/KWU U9 316/89/2.
4. 2D/3D Program Upper Plenum Test Facility Experimental Data Report, 1990, "Test No. 25, Downcomer/Cold Leg Steam/Water Interaction Test," E314/90/11, KWU.
5. 2D/3D Program Upper Plenum Test Facility Experimental Data Report, 1988, "Test No. 8, Cold/Hot Leg Flow Pattern Test," U9 316/88/12, KWU.

6. Okubo, T., Iguchi, T., Okabe, K., Sugimoto, J., Akimoto, H., and Murao, Y., 1985, "Evaluation Report on CCTF Core-II Reflood Test C2-4 (Run 62)," JAERI-M 85-026.
7. Anklam, T. M., et al., 1982, "Experimental Investigations of Uncovered Bundle Heat Transfer and Two-Phase Mixture Level Swell Under High Pressure Low Heat Flux Conditions," NUREG/CR-2456.
8. Yoder, et al., 1982, "Dispersed Flow Film Boiling in Rod Bundle Geometry-Steady State Heat Transfer Data and Correlation Comparisons," NUREG/CR-2435, ORNL-5822.
9. Loftus, M. J. et al., 1981, "PWR FLECHT-SEASET Unblocked Bundle, Forced and Gravity Reflood Task Data Report," Volumes 1 and 2, NUREG/CR-1532, (WCAP-9699).
10. Wong, S. and Hochreiter, L. E., 1981, "Analysis of the FLECHT SEASET Unblocked Bundle Steam Cooling and Boiloff Tests," WCAP-9729.
11. Mullins, C. B., et al., 1982, "Thermal-Hydraulic Test Facility Experimental Data Report for Test 3.03.6AR and Test 308.6C - Transient Film Boiling in Upflow," NUREG/CR-2525, Volumes 2 and 5.
12. Bayless, P. D. and Divine, J. M., 1982, "Experiment Data Report for LOFT Large-Break Loss-of-Coolant Experiment L2-5," NUREG/CR-2826.
13. Koizumi, Y., et al., 1987, "ROSA-IV/LSTF 2.5% Cold Leg Break LOCA Experiment Data Report for Runs SB-CL-01, 02 and 03," JAERI-memo 62-399.
14. Koizumi, Y. and Tasaka, K., 1988, "Quick Look Report for ROSA-IV/LSTF 10% Cold Leg Break LOCA Test, SB-CL-14," JAERI-memo 63-262.
15. Kumamaru, et al., 1989, "ROSA-IV/LSTF 5% Cold Leg Break LOCA Experiment, Run SB-CL-18 Data Report," JAERI-M 89-027.
16. Chauliac, C. et al., JAERI-M 88-215, "Post-Test Analysis with RELAP5/MOD2 of ROSA-IV/LSTF Natural Circulation Test ST-NC-02," October 1988.
17. Liebert, J. and Emmerling, R., 1998, "UPTF Experiment Flow Phenomena During Full-Scale Loop Seal Clearing of a PWR," Nuclear Engineering and Design, Vol. 179, pp. 51-64.
18. Jarrell, Donald B. and Divine Janice M., 1981, "Experiment Data Report for LOFT Intermediate Break Experiment L5-1 and Severe Core Transient Experiment L8-2," NUREG/CR-2398.
19. Sackett, Kenneth E. and Clegg, L. Bruce, "Experiment Data Report For Semiscale MOD-3 Small Break Test S-07-10D (Baseline Test Series), December 1980, prepared for the U.S. Nuclear Regulatory Commission under Department of Energy Contract No. DE-AC07-76IDO1570.

20. MPR Associates, 1990, "Summary of Results from the UPTF Downcomer Separate Effects Tests, Comparison to Previous Scaled Tests, and Application to U.S. PWRs," MPR-1163.
21. Tolman, E. L.; Coryell, E. W., "REVIEW OF LOFT CLADDING TEMPERATURE RESPONSE FOR L2-2 & L2-3: RECOMMENDATIONS FOR IMPROVED LOFT FUEL ROD MEASUREMENTS (SYSTEMS 14 & 87)," EGG-LOFT-5244, 1980.
22. Guo, Z., Kumamaru, H., and Kukita, Y., "CRITICAL HEAT FLUX FLOW ROD BUNDLE UNDER HIGH-PRESSURE BOIL-OFF CONDITIONS," JAERI-M 930238, 1993.
23. Cunningham, J. P., Fayfich, R. R., Mandler, D. J., and Steer, R. W., "ECCS HEAT TRANSFER EXPERIMENTS WITH UPPER HEAD INJECTION, TEST FACILITY, PROCEDURE AND DATA," WCAP-8400 Volume 1, 1974.
24. Morris, D. G., Mullins, C. B., and Yoder, G. L., "An Analysis of Transient Film Boiling of High-Pressure Water in a Rod Bundle," NUREG/CR-2469, 1982.
25. Lee, N., Wong, S., Yeh, H. C., and Hochreiter, L. E., "PWR FLECHT SEASET UNBLOCKED BUNDLE, FORCED AND GRAVITY REFLOOD TASK, DATA EVALUATION AND ANALYSIS REPORT," WCAP-9891, 1981.